

RIKEN Accelerator Progress Report

2019

vol. **53**

理化学研究所 仁科加速器科学研究センター
RIKEN Nishina Center for Accelerator-Based Science



RIKEN Accelerator Progress Report 2019

vol. **53**

理化学研究所 仁科加速器科学研究センター
RIKEN Nishina Center for Accelerator-Based Science
Wako, Saitama, 351-0198 JAPAN

RIKEN Accelerator Progress Report 2019 vol.53

This is an unabridged version of the 53rd volume of RIKEN Accelerator Progress Report (hereinafter referred to as APR), the official annual report of the Nishina Center for Accelerator-Based Science.

A PDF version of APR can be downloaded from our website.
http://www.nishina.riken.jp/researcher/APR/index_e.html

Published by

RIKEN Nishina Center for Accelerator-Based Science
2-1 Hirosawa, Wako-shi, Saitama 351-0198 JAPAN

Director of RIKEN Nishina Center for Accelerator-Based Science

Hideto En'yo

Editorial Board

H. Ueno (Editor-in Chief), J. Zenihiro, T. Isobe, Y. Ichikawa, A. Kohama, E. Hiyama, T. Matsuzaki, R. Seidle, T. Doi, T. Tada, T. Tamagawa, K. Takahashi, Y. Higurashi, K. Ozeki, T. Sumikama, K. Morimoto, H. Sato, M. Watanabe, T. Ikeda, I. Watanabe, H. Haba, T. Abe, K. Tanaka, Y. Watanabe, H. Nagahama, M. Wada, Y. Tsuburai, M. Yamamoto, E. Fujino and I. Yoshida

Contact

Progress@ribf.riken.jp

All rights reserved. This report or any portion thereof may not be reproduced or used in any form, including photostatic print or microfilm, without written permission from the Publisher.
Contents of the manuscripts are the authors' responsibility. The Editors are not liable for the content of the report.

RIKEN Nishina Center for Accelerator-Based Science, September 2019

PREFACE



The RIKEN Accelerator Progress Report is the annual report of all research activities conducted in RIKEN Nishina Center for Accelerator-Based Science (RNC). This volume, No. 53, covers the activities conducted in the Japanese fiscal year of 2019 (April 2019 to March 2020).

First, March 31, 2020 was the last day for Hideto En'yo as the Director. Hideto led the RNC for a long period, since October 2009. On this occasion, all RNC members wish to express their gratitude and thank him for his management over ten and half years. During this period, one of the many excellent achievements of RNC was the discovery of Element 113, “Nihonium.” The year 2019 was designated as the International Year of the Periodic Table (IYPT). Hideto served as a member of the IYPT-Japan Committee and organized a session for the Closing Ceremony in December, Tokyo, to demonstrate the world-wide efforts in “Creation of superheavy elements,” with a focus on period-7 elements including Nihonium. In April 2019, David Morrison was appointed as the Deputy Director of

RIKEN Brookhaven Research Center.

The year 2019 was the first year of the new Japanese era “Reiwa,” which started on May 1. In RNC, this new period was celebrated with the results obtained from the first spectroscopy of ^{78}Ni , which was published in Nature, issued on the second day of Reiwa, May 2. Other selected achievements are compiled in “Highlights of the Year” in this volume, which showcase the multi-disciplinary activities of RNC in the field of science, technology, and innovation. It should be noted that these achievements were made not just by in-house researchers and engineers in RNC; for some of these projects, RNC collaborated with users at the RI Beam Factory (RIBF) and RIKEN Muon Facility at the Rutherford Appleton Laboratory.

Two excellent progresses were made in the RIBF facility. The first progress is the record breaking beam intensities achieved at the Super-conducting Ring Cyclotron (SRC); the maximum intensity achieved for ^{124}Xe was 173 pA, and that for ^{238}U was 94 pA. The excellent beams at SRC make the fast-beam programs at BigRIPS more productive, especially for the nuclear structure study in ^{100}Sn and its vicinity, and in neutron-rich nuclei produced via in-flight fission. The second progress is the intensity- and energy-upgrade of the linear accelerator RILAC, which was achieved by the recent installations of the 28-GHz ECR ion source as well as super-conducting radio-frequency cavities. The first beam with the upgraded RILAC “SRILAC” was successfully extracted at the very end of FY2019. At the same time, a new gas-filled recoil separator “GARIS-III” was installed to be coupled with SRILAC. The combination of SRILAC and GARIS-III strengthens the scientific programs focused on super-heavy elements.

Two advisory committees, Nishina Center Advisory Committee (NCAC) and RIKEN Advisory Committee (RAC), were organized. NCAC evaluated the RNC management with respect to organization, research achievement, and planning, and they suggested that the intensity upgrade of RIBF was the first priority in the coming years to be competitive with other facilities across the world. Based on the report of NCAC, RAC provided this advice to the President of RIKEN.

Since the end of FY2019, the social situation in the world has changed dramatically because of the COVID-19 pandemic. According to the measures of governments, universities, and institutes, research activities have been limited significantly. Remote-work and web-meetings using computer-network technology are highly recommended and useful for organizing discussions and collaboration works. However, the importance of face-to-face discussions and collaborations for increasing creativity has been recognized. It is hoped that research networks and relationships over the world will become more involved in future to overcome this difficult situation by sharing ideas and wisdom.

A handwritten signature in black ink, which appears to read "Hiroyoshi Sakurai". The signature is fluid and cursive.

Hiroyoshi Sakurai

Director

RIKEN Nishina Center for Accelerator-Based Science

C O N T E N T S

Page

PREFACE

I . HIGHLIGHTS OF THE YEAR

Strong one-neutron emission from two-neutron unbound states in β decays of r -process nuclei $^{86,87}\text{Ga}$	1
R. Yokoyama <i>et al.</i>	
Shell evolution towards ^{60}Ca : First spectroscopy of ^{62}Ti	2
M. L. Cortés <i>et al.</i>	
^{78}Ni revealed as a doubly magic stronghold against nuclear deformation	3
R. Taniuchi <i>et al.</i>	
Inclusive cross sections for one- and multi-nucleon removal from Sn, Sb, and Te projectiles beyond the $N = 82$ shell closure	4
V. Vaquero	
g -Factor of the ^{99}Zr isomer: monopole evolution in the shape-coexisting region	5
F. Boulay <i>et al.</i>	
Study of quasielastic barrier distributions as a step towards the synthesis of superheavy elements with hot fusion reactions	6
T. Tanaka <i>et al.</i>	
Location of the neutron dripline at fluorine and neon	7
D. S. Ahn <i>et al.</i>	
Dineutron correlation and rotational excitations in neutron-rich Mg isotopes	8
M. Yamagami	
x_F dependence of the transverse single spin asymmetry of very forward π^0 production in 510 GeV $p^\uparrow + p$ collisions	9
M. H. Kim <i>et al.</i>	
Non-evaporable getter-based differential pumping system for SRILAC	10
H. Imao <i>et al.</i>	
Calibration of the beam energy position monitor system for the RIKEN superconducting acceleration cavity	11
T. Watanabe <i>et al.</i>	
Intermediate silicon tracker development for sPHENIX experiment at RHIC	12
I. Nakagawa <i>et al.</i>	
Update of MOCO for the MPV system	13
H. Baba <i>et al.</i>	
Offline measurement of mass and correlated decay properties using radioactive ^{224}Ra source via MRTOF+ α -TOF detector	14
T. Niwase	
Offline collinear laser spectroscopy of barium II toward measurement of RIs at SLOWRI facility	15
M. Tajima <i>et al.</i>	
Angle-tunable wedge degrader for an energy-degrading RI beamline	16
J. W. Hwang <i>et al.</i>	
Effects of columnar defects introduced by 2.6 GeV U-ion irradiation on J_c characteristics of 2H-NbSe ₂	17
T. Tamegai <i>et al.</i>	
Impurity effects on magnetism of T [*] -type La _{1-x/2} Eu _{1-x/2} Sr ₃ CuO ₄	18
M. Fujita	
Size-dependent magnetic behavior of La ₂ CuO ₄ nanoparticles	19
S. Winarsih <i>et al.</i>	
Targeted alpha therapy of thyroid cancer: Evaluation of [^{211}At]NaAt treatment in the xenograft model	20
T. Watabe <i>et al.</i>	
Live mouse imaging with $^{44\text{m}}\text{Sc}$ by a multiple-isotope PET	21
T. Fukuchi <i>et al.</i>	
Production cross sections of ytterbium and thulium radioisotopes in alpha-induced nuclear reactions on natural erbium	22
M. Saito <i>et al.</i>	

Production cross sections of dysprosium-159 radioisotope from the deuteron-induced reactions on terbium-159 up to 24 MeV	23
D. Ichinkhorloo <i>et al.</i>	
Non-homologous end joining is the major repair pathway for DNA double strand breaks in human fibroblast after heavy-ion irradiation	24
M. Izumi and T. Abe	
Mutation analysis pipeline V2: an improved version of bioinformatics pipeline for plant and microbial sequencing analysis	25
H. Ichida and T. Abe	

II. RESEARCH ACTIVITIES I (Nuclear, Particle and Astro-Physics)

1. Nuclear Physics

Decay studies in the region of ^{54}Zn	27
A. Kubiela <i>et al.</i>	
Study of the β -decay of ^{70}Kr	28
A. Vitéz-Sveiczler <i>et al.</i>	
Progress on the decay spectroscopy and measurement of half-lives and P_n values in exotic nuclei near the $N = 50$ shell closure	29
C. J. Griffin <i>et al.</i>	
Total absorption gamma spectroscopy studies around ^{100}Sn	30
A. Algora <i>et al.</i>	
New and comprehensive β - and βp -decay spectroscopy results in the vicinity of ^{100}Sn	31
J. Park <i>et al.</i>	
Improved value for the Gamow-Teller strength of the ^{100}Sn beta-decay	32
T. Faestermann and D. Lubos	
β -delayed neutron emission probabilities for understanding the formation of the r -process rare-earth abundance peak (REP)	33
G. G. Kiss	
Evolution of collectivity and mirror symmetry along $N = Z$	34
K. Wimmer	
First attempt at in-beam γ -ray spectroscopy of ^{100}Sn	35
S. Chen <i>et al.</i>	
Intermediate-energy Coulomb excitation of ^{102}Sn	36
M. L. Cortés <i>et al.</i>	
In-beam γ -ray spectroscopy of ^{136}Te at relativistic energies	37
V. Vaquero	
Study of Gamow-Teller transitions from ^{11}Li	38
L. Stuhl <i>et al.</i>	
Structure of ^{13}Be probed via quasi-free scattering	39
Anna Corsi	
Overview of the experimental setup of SAMURAI11 to measure the $^{48}\text{Cr}(p, n)$ and $^{64}\text{Ge}(p, n)$ reactions in inverse kinematics	40
M. Sasano <i>et al.</i>	
Role of ^{66}Se in the rp -process nucleosynthesis in type I X-ray bursts	41
V. Panin <i>et al.</i>	
Particle identification of light charged particle by $S\pi\text{RIT-TPC}$ in Sn-Sn isotopic reactions II	42
Masanori Kaneko <i>et al.</i>	
Monte carlo simulation of collective flow analysis for $S\pi\text{RIT-TPC}$	43
M. Kurata-Nishimura <i>et al.</i>	
Measurement of the proton elastic scattering from ^{132}Sn at 300 MeV/nucleon	44
J. Zenihiro <i>et al.</i>	
TDPAD measurement for the 10^- isomer of ^{98}Y	45
J. M. Daugas <i>et al.</i>	
Investigations of magnetic moments and spin alignment in Coulomb fission reaction	46
R. Lozeva <i>et al.</i>	

Magnetic-moment measurement of the isomeric state of ^{130}Sn in the vicinity of the doubly—magic nucleus ^{132}Sn	47
G. Georgiev, Y. Ichikawa <i>et al.</i>	
Isomeric-to-ground state ratio of ^{128}Sn measured by Rare RI Ring	48
H. F. Li <i>et al.</i>	
Performance study of electron spectrometer for SCRIT experiments	49
K. Tsukada <i>et al.</i>	
Correlated measurement of mass and decay of fusion evaporation products for $^{51}\text{V}+^{159}\text{Tb}$ reactions via MRTOF+ α -TOF detector	50
T. Niwase <i>et al.</i>	
Half-life determination of nuclear excited states of ^{229}Th by the coincidence measurement between α particles and γ rays from ^{233}U	51
Y. Shigekawa <i>et al.</i>	
Mass measurements of ^{252}Cf fission fragments via MRTOF-MS	52
S. Kimura <i>et al.</i>	
In-gas-cell laser ionization spectroscopy of Os isotopes using MRTOF-MS at KISS	53
Y. Hirayama <i>et al.</i>	
Calibration and simulation of $\text{LaBr}_3:\text{Ce}$ scintillator for analyzing $^8\text{Li}(\alpha, n)^{11}\text{B}$ -reaction data	54
Y. Mizoi <i>et al.</i>	
Measurement of $^{25}\text{Al}+p$ resonant elastic scattering relevant to the astrophysical reaction $^{22}\text{Mg}(\alpha, p)^{25}\text{Al}$	55
J. Hu <i>et al.</i>	
^{26}Si beam production and thermal durability test of gas target window	56
M. J. Kim <i>et al.</i>	
Production of a high-intensity francium ion beam for the measurement of the electron electric dipole moment	57
H. Nagahama <i>et al.</i>	
Development of β -NMR with spin-aligned beam	58
H. Nishiabta <i>et al.</i>	
Production of isomers around ^{52}Fe nucleus via projectile fragmentation	59
K. Kawata <i>et al.</i>	
$^{79}\text{Se}(n, \gamma)^{80}\text{Se}$ reaction cross section through $^{77, 79}\text{Se}(d, p)^{78, 80}\text{Se}$ reactions	60
N. Imai <i>et al.</i>	
Production-cross-section measurement and new-isotope search for very neutron-deficient RIs produced from ^{78}Kr beam at 345 MeV/nucleon by BigRIPS separator	61
H. Suzuki <i>et al.</i>	
Database of radioactive isotope beams produced at the BigRIPS separator	62
Y. Shimizu <i>et al.</i>	
RI beam production at BigRIPS in 2019	63
Y. Shimizu <i>et al.</i>	
First success of RI-beam separation and particle identification for nuclei with atomic number $Z>82$ at RIKEN RI beam factory	65
T. Sumikama <i>et al.</i>	
Analysis of fake asymmetry for the MTV experiment	66
F. Goto <i>et al.</i>	
2. Nuclear Physics (Theory)	
Non-relativistic expansion of Dirac equation with spherical vector and scalar potentials	67
Y. X. Guo and H. Z. Liang	
Renormalizing random-phase approximation by using exact pairing	68
L. Tan Phuc <i>et al.</i>	
Quenching factor of Gamow-Teller and spin dipole resonances	69
Li-Gang Cao, H. Sagawa <i>et al.</i>	
Pairing in excited nuclei: a review	70
N. Quang Hung <i>et al.</i>	
Canonical base in self-consistent constrained HFB in odd-A nuclei	71
K. Sugawara-Tanabe and K. Tanabe	

S-shaped heat capacity in an odd-odd deformed nucleus	72
B. Dey <i>et al.</i>	
Evidence for three-particle correlations in nuclear matter	73
W. Bentz and I.C. Cloet	
Double charge-exchange phonon states	74
X. Roca-Maza, H. Sagawa <i>et al.</i>	
3. Nuclear Data	
EXFOR compilation of RIBF data in 2019	75
T. Tada	
4. Hadron Physics	
Unfolding the transverse momentum distribution for very forward neutron production in p Au collisions at $\sqrt{s_{NN}} = 200$ GeV	77
B. Mulilo <i>et al.</i>	
Update of single and dihadron cross sections for light hadrons in e^+e^- annihilation at $\sqrt{s} = 10.58$ GeV in Belle	78
Ralf Seidl	
Preparation status of the J-PARC E16 experiment in 2019	79
S. Yokkaichi	
Measurement of nuclear effects on anti-quarks via Drell-Yan process at FNAL-SeaQuest	80
K. Nakano <i>et al.</i>	
Progress of the polarized Drell-Yan experiment at Fermilab, SpinQuest (E1039)	81
Y. Miyachi <i>et al.</i>	
Development of zero-degree calorimeter for EIC	82
Y. Goto <i>et al.</i>	
INTT Silicon Modules and Ladders Assembly for sPHENIX Project	83
C. Miraval <i>et al.</i>	
6. Particle Physics	
Empirical formulas for the standard-model parameters	85
Y. Akiba	
Quarternion-spin-isospin model for the standard-model parameters	86
Y. Akiba	
$R = 12H_0^2$ and its implications to gravity and cosmology	87
Y. Akiba	
7. Astrophysics and Astro-Glaciology	
Experimental equipment for exploring reactions of low energy ions with an ice surface as an interstellar dust analog	89
Y. Nakai <i>et al.</i>	
Commissioning of a prototype novel laser melting sampler for analyzing ice cores with high depth resolution and high throughput	90
Y. Motizuki <i>et al.</i>	
8. Accelerator	
Reevaluation of beam orbit calculation method for the injection line of AVF cyclotron after tuning pepper-pot emittance monitor	91
Y. Kotaka <i>et al.</i>	
Non-thermal equilibrium effect on plasma window with large diameter	92
N. Ikoma <i>et al.</i>	
Status report on update of alarm system and control system of magnet power supplies for RIBF	93
M. Komiyama <i>et al.</i>	
Power supply backup system for injection and extraction magnets of cyclotrons	94
K. Kumagai and N. Fukunishi	
Improvement of beam stability by stabilizing the cooling-water temperature for the main and trim coils of IRC	95
R. Koyama <i>et al.</i>	
Interlock signal application from radiation monitoring ion chamber for SRC	96
M. Nakamura <i>et al.</i>	

Nishina RIBF water-cooling system operational report 2019 T. Maie <i>et al.</i>	97
9. Instrumentation	
Development of ZeroDegree Large Acceptance Dispersive mode H. Takeda <i>et al.</i>	99
Large-acceptance achromatic mode with mono-energetic wedge degrader for ZeroDegree spectrometer S. Chen <i>et al.</i>	100
New ion-optical operating modes of BigRIPS and ZeroDegree spectrometer for production and separation of high-quality rare isotope beams and high-resolution spectrometer experiments H. Takeda <i>et al.</i>	101
Purification of slowed-down RI beam T. Sumikama <i>et al.</i>	102
Thermal model simulation of high-power rotating target for BigRIPS separator K. Yoshida <i>et al.</i>	103
Incidents involving the DMT3 magnet in the beam transport line from SRC to BigRIPS K. Kusaka <i>et al.</i>	104
First confirmation of stopped RIs at parasitic gas cell with new approach T. Sonoda <i>et al.</i>	105
Stopping examination for high-energy RI beams in the parasitic gas cell T. Sonoda <i>et al.</i>	106
Second report on offline tests for RF carpet transportation in RF ion guide gas cell at the SLOWRI facility S. Iimura <i>et al.</i>	107
The 3rd report on offline test for RF carpet transportation in RF ion guide gas cell at the SLOWRI facility A. Takamine <i>et al.</i>	108
Battery-operated compact ion source for beam transport test T. M. Kojima <i>et al.</i>	109
Present status of ERIS at the SCRIT electron scattering facility T. Ohnishi <i>et al.</i>	110
Latest performance of FRAC at SCRIT facility S. Sato <i>et al.</i>	111
3D magnetic field measurement of the SCRIT electron spectrometer H. Wauke <i>et al.</i>	112
Measurement of the luminosity of electron scattering at SCRIT D. Taki <i>et al.</i>	113
Yield development with in-gas-jet laser ionization at KISS Y. X. Watanabe <i>et al.</i>	114
Observation of charge-stripping of 20 keV/q ions upon injection into gas cell cooler-buncher at KISS P. Schury <i>et al.</i>	115
Reliable connection methods for gas piping and signal cabling of PPAC in focal-plane vacuum chambers at BigRIPS H. Sato <i>et al.</i>	116
Performance of a none-isochronous position-sensitive detector for the Rare-RI Ring R. Crane and S. Naimi	117
Intermediate Tracker Integration in sPHENIX R. Nouicer, I. Nakagawa <i>et al.</i>	118
Assembly of Intermediate Silicon Tracker in Taiwan C. Shih <i>et al.</i>	119
Development status of long data cable for sPHENIX-INNT detector T. Hachiya <i>et al.</i>	120
Performance evaluation of a sensor module for INNT at sPHENIX A. Suzuki <i>et al.</i>	121
Sensor testing of Intermediate Silicon Tracker K. Cheng <i>et al.</i>	122
Geant4 simulation of INNT Phase-2 Test Beam at Fermilab C. Shih <i>et al.</i>	123

Development of high-resolution hard X-ray detector system by using transition-edge sensor for accelerator-based experiments.....	124
T. Isobe <i>et al.</i>	
SAMURAI DAQ speed improvement	125
J. GAO <i>et al.</i>	
High-stability high-voltage power supply for MRTOF.....	126
P. Schury <i>et al.</i>	
Eliminating mass-dependent inaccuracies in MRTOF-MS for the study of RI using arbitrary reference masses	127
M. Rosenbusch	
On-line mass measurement using multi-reflection time-of-flight mass spectrograph (MRTOF-MS) at KISS.....	128
J. Y. Moon <i>et al.</i>	
Collinear laser spectroscopy of Ba ⁺ in 6s ² S _{1/2} -6p ² P _{3/2} transition	129
Y. Sasaki <i>et al.</i>	
LIF observation of Rb atoms in superfluid helium by picosecond pulsed laser pumping	130
Y. Takeuchi <i>et al.</i>	
Measurement of stopping-position width of highly energetic Rb ion beams in liquid nitrogen	131
M. Nishimura <i>et al.</i>	
Investigation of the secondary rubidium beam profile at HIMAC towards laser spectroscopy in an optical cryostat	132
K. Tsubura <i>et al.</i>	
Degrader system for ZD-MRTOF	133
J. J. Liu <i>et al.</i>	
First test of graphenic carbon vacuum windows with heavy ions.....	134
S. Purushothaman <i>et al.</i>	
Heavy-ion irradiation test of radiochromic films	135
T. Kambara <i>et al.</i>	
Computing and network environment at the RIKEN Nishina Center	136
T. Ichihara	
CCJ operations in 2019	137
S. Yokkaichi <i>et al.</i>	

III. RESEARCH ACTIVITIES II (Material Science and Biology)

1. Atomic and Solid State Physics (Ion)

Control of electrical conductivity in diamond by boron implantation—application of high-temperature and high-pressure annealing	139
H. Yamazaki <i>et al.</i>	
Superconducting proximity effect in epitaxial Nb(110)/Au(111)/Nb(110) trilayers	140
H. Yamazaki <i>et al.</i>	
Simultaneous cluster dissociation and optical pumping of Ag in superfluid helium using a single UV laser.....	141
T. Yamamoto <i>et al.</i>	
Baseline correction system for precision measurement of the hyperfine structure of Rb atoms in superfluid helium	142
M. Doi <i>et al.</i>	
Profile measurement of laser microbeam produced by glass capillaries: tilt dependence	143
M. Mori <i>et al.</i>	

2. Atomic and Solid State Physics (Muon)

Study on magnetism of defective reduced graphene oxides	145
R. Asih <i>et al.</i>	
Magnetic ground state of $J_{\text{eff}} = 0$ Mott insulator Ag ₃ LiRu ₂ O ₆ under pressure	146
T. Takayama <i>et al.</i>	
Non-magnetic ground state of In ₂ Ru ₂ O ₇ probed by muon spin rotation	147
T. Takayama <i>et al.</i>	
Short-range magnetic order in the frustrated antiferromagnet Cu ₅ (PO ₄) ₃ (OH) ₄ (pseudomalachite).....	148
H. Kikuchi <i>et al.</i>	
μ SR investigation of spin liquid states in magnetic properties of MgTi ₂ O ₄ sample	149
U. Widyaiswari <i>et al.</i>	

Zero-point vibrational energy in the muon sites of La_2CuO_4 M. R. Ramadhan <i>et al.</i>	150
Investigations of the quantum critical behavior of the $S=1/2$ J_1 - J_2 square lattice antiferromagnets $\text{Sr}_2\text{Cu}(\text{Te}_{1-x}\text{W}_x)\text{O}_6$ Sungwon Yoon <i>et al.</i>	151
Magnetic ordering and spin dynamics of $\text{Nd}_2\text{Ru}_2\text{O}_7$ studied by μSR U. Widyaiswari <i>et al.</i>	152
Muon spin relaxation study of solute-vacancy interactions during natural aging of Al–Mg–Si–Cu alloys K. Nishimura <i>et al.</i>	153
Muon spin rotation study on the new organic spin liquid candidate λ -(STF) $_2$ GaCl $_4$ T. Minamidate <i>et al.</i>	154
Zero-field μSR on single-crystal organic superconductor λ -(BETS) $_2$ GaCl $_4$ D. P. Sari <i>et al.</i>	155
Relationship between the structure and electrical conductivity of 12-mer single-stranded polyadenine studied by scanning tunneling microscope H. Rozak <i>et al.</i>	156
Electron transfer in 12-mer double-stranded DNA by muon spectroscopy and scanning tunneling microscopy H. Rozak <i>et al.</i>	157
μSR study of the electron transfer mechanism of a blue copper protein, Pseudoazurin A. D. Pant <i>et al.</i>	158
Temperature dependence of the total muonium emission yield from silica aerogel using μSR method K. Ishida <i>et al.</i>	159
3. Radiochemistry and Nuclear Chemistry	
Relativistic density functional theory with the finite-light-speed correction for Coulomb interaction T. Naito and R. Akashi <i>et al.</i>	161
On-line anion-exchange experiment of Nb and Ta in HF/ HNO_3 mixture solution for Db chemistry S. Adachi <i>et al.</i>	162
Anion-exchange behaviour of Nb, Ta and Pa in H_2SO_4 M. Kato <i>et al.</i>	163
Anion exchange of Nb and Ta in HF/HCl mixture solution for Db chemistry T. Yokokita and H. Haba	164
Anion exchange of element 104, Rf, at 0.11 M H_2SO_4 by using batch-type solid-liquid extraction apparatus, AMBER T. Yokokita <i>et al.</i>	165
Anion exchange of Zr, Hf, and Th by the automated extraction apparatus: toward the chemical study of $_{104}\text{Rf}$ in HNO_3 E. Watanabe <i>et al.</i>	166
^{99}Ru and ^{57}Fe Mössbauer spectroscopic studies of $\text{Na}_2\text{Ru}_{1-x}\text{Fe}_x\text{O}_3$ of sodium-ion battery electrode H. Hamano <i>et al.</i>	167
Development of an RF-carpet gas cell for the chemistry of superheavy elements Y. Shigekawa <i>et al.</i>	168
An attempt to modify the membrane degasser (MDG) Y. Komori <i>et al.</i>	169
Preparation of Gd targets for in-beam fission measurements as a step towards the handling of ^{243}Am targets with ultra-thin backings T. Tanaka <i>et al.</i>	170
Preparation of [^{211}At]-labeled sodium astatide (NaAt) by reducing with ascorbic acid for the treatment of thyroid cancer Y. Shirakami	171
Development of radioimmunotherapy with astatine-211-coujugated antibodies H. Takashima <i>et al.</i>	172
Anti-cancer effect of ^{211}At -labeled antibody on xenografted mice with intravenous injection Y. Kanayama <i>et al.</i>	173
Dispersion rates of astatine-211 from aqueous solutions and chloroform A. Toyoshima <i>et al.</i>	174
Usability of ^{67}Cu as a therapeutic radioisotope for peptide receptor radionuclide therapy Y. Fujisawa <i>et al.</i>	175

Quality evaluation of RIKEN ^{67}Cu for labeling peptide compound S. Oshikiri <i>et al.</i>	176
Simultaneous imaging of Na^+/K^+ by semiconductor Compton camera GREI S. Motomura <i>et al.</i>	177
Research progress on double-photon-emission coincidence imaging with cascade gamma-ray-emitting nuclide M. Uenomachi <i>et al.</i>	178
Production of Np-236 in the $^{232}\text{Th} + ^7\text{Li}$ reaction for standard material in accelerator mass spectrometry Y. Hayakawa <i>et al.</i>	179
Excitation function measurement of the $\text{Tl}(d, \alpha)^{203}\text{Hg}$ reaction for carrier-free ^{203}Hg tracer production Y. Takahashi <i>et al.</i>	180
Activation cross sections of alpha-induced reactions on natural tungsten for ^{186}Re and ^{188}Re production N. Ukon <i>et al.</i>	181
Activation cross sections of alpha particle-induced reactions on natural hafnium up to 50 MeV S. Takacs <i>et al.</i>	182
Activation cross sections of alpha-induced reactions on natural ytterbium up to 50 MeV M. Saito <i>et al.</i>	183
Measurement of excitation functions for $^{165}\text{Ho}(\alpha, xn)^{165-168}\text{Tm}$ reactions A. R. Usman <i>et al.</i>	184
Production cross sections of (d, x) reactions on natural erbium M. U. Khandaker <i>et al.</i>	185
Activation-cross-section measurement of alpha-induced reactions on natural dysprosium T. Murata <i>et al.</i>	186
Production cross sections of ^{157}Dy in alpha-particle-induced reactions on natural gadolinium D. Ichinkhorloo <i>et al.</i>	187
Activation cross sections of alpha-particle induced nuclear reactions on natural palladium M. Aikawa <i>et al.</i>	188
Excitation function measurement for zirconium-89 and niobium-90 production using alpha-induced reactions on yttrium-89 T. Murata <i>et al.</i>	189
Production cross sections of ^{68}Ga via deuteron-induced reactions on natural zinc Ts. Zolbadral <i>et al.</i>	190
Production cross sections of ^{45}Ti via deuteron-induced reaction on ^{45}Sc Ts. Zolbadral <i>et al.</i>	191
Present status of ^{211}At production at the RIKEN AVF cyclotron Y. Wang <i>et al.</i>	192
Decontamination of Po in the $^{211}\text{Rn}/^{211}\text{At}$ generator system K. Aoi <i>et al.</i>	193
Separation and purification of ^{139}Ce tracer for metallofullerene synthesis K. Akiyama <i>et al.</i>	194
Separation of $^{121\text{m}}\text{Te}$ from antimony without redox reaction T. Kubota <i>et al.</i>	195
Chemical separation of theranostic radionuclide ^{111}Ag produced in $^{nat}\text{Pd}(d, x)^{111}\text{Ag}$ reactions K. Ooe <i>et al.</i>	196
Preliminary investigation of nanoclay-gel-based fluorescent gel dosimeters under carbon-ion beam T. Maeyama <i>et al.</i>	197
4. Radiation Chemistry and Biology	
Mutants of the ectomycorrhizal mushroom <i>Tricholoma matsutake</i> that exert detrimental effects on its symbiotic partner <i>Pinus densiflora</i> H. Murata <i>et al.</i>	199
Effect of heavy-ion-beam irradiation on mycelial growth of medicinal mushrooms M. Hatashita, K. Takagi <i>et al.</i>	200
Yield improvement of starch-degrading enzyme in fungi by ion-beam mutagenesis H. Iwahara <i>et al.</i>	201

Mutation breeding of sake yeast using heavy-ion-beam irradiation K. Baisho <i>et al.</i>	202
Isolation of morphological mutants in a bryophyte model <i>Marchantia polymorpha</i> using heavy-ion mutagenesis S. Sakai <i>et al.</i>	203
Breeding of summer-autumn-flowering small-flowered spray-type chrysanthemums cultivar ‘Nagasaki SWC1’ by heavy-ion-beam irradiation A. Hisamura <i>et al.</i>	204
Mutation induction in strawberry of original Saitama cultivar by C-ion irradiation H. Uchida <i>et al.</i>	205
Characteristics of heavy-ion mutagenesis in cultivated strawberry T. Wada <i>et al.</i>	206
Improvement of the Brix content of the sweet potato ‘Anno-Beni’ by mutation induced using heavy-ion-beam irradiation T. Hashiguchi <i>et al.</i>	207
Development of mutagenesis technique for leguminous crops using heavy-ion-beam irradiation and screening of useful mutants P. Siviengkhek <i>et al.</i>	208
Mutants of sorghum variety ‘WRAY’ induced by heavy-ion irradiation H. Cai <i>et al.</i>	209
Genetic analysis of an early flowering rice mutant induced by argon ions R. Morita <i>et al.</i>	210
Approach toward isolating early-heading mutants from Tana Toraja local aromatic rice ‘Pare Bau’ irradiated with argon- and carbon-ion beams A. M. Okasa <i>et al.</i>	211
A novel domain of <i>LONG GRAIN 1</i> in rice possesses transcriptional activation activity H. Abe <i>et al.</i>	212
Establishment of large mutant lines on rotifer using heavy-ion-beam irradiation K. Tsunezumi <i>et al.</i>	213
Contribution of multiple DNA repair pathways in <i>Arabidopsis thaliana</i> dry seeds after heavy-ion-beam irradiation K. Ishii <i>et al.</i>	214
Ion-microbeam irradiation to damage DNA in RPE cell nucleus with tapered glass capillary optics at Pelletron facility T. Ikeda <i>et al.</i>	215

IV. OPERATION RECORDS

Electric power consumption of RIKEN Nishina Center in 2019 E. Ikezawa <i>et al.</i>	217
Operation report of the ring cyclotrons in the RIBF accelerator complex N. Tsukiori <i>et al.</i>	218
RILAC operation E. Ikezawa <i>et al.</i>	219
Operation report on the RIKEN AVF cyclotron for 2019 M. Hamanaka <i>et al.</i>	220
Present status of the liquid-helium supply and recovery system T. Dantsuka <i>et al.</i>	221
Operation of the BigRIPS cryogenic plant K. Kusaka <i>et al.</i>	222
Radiation safety management at RIBF K. Tanaka <i>et al.</i>	223
Operation of the Pelletron tandem accelerator T. Ikeda <i>et al.</i>	225
Fee-based activities operated by the Industrial Application Research Team A. Yoshida <i>et al.</i>	226

V. EVENTS

Nishina School 2019	227
H. Ishiyama <i>et al.</i>	
Creation of superheavy elements highlighted at the closing ceremony of IYPT 2019	228
H. En'yo	
The 3rd "Hodan-kai" meeting for the future of exotic nuclear physics	229
W. Horiuchi <i>et al.</i>	
SHE2019—The 4th International Symposium on Superheavy Elements	230
H. Haba	
RIKEN Symposium "Trends in ion-beam breeding over the last two decades and future research"	231
T. Abe <i>et al.</i>	
RIKEN Open Day 2019	232
H. Haba and K. Takahashi	
Outreach activities outside the Wako campus	233
N. Miyauchi	

VI. ORGANIZATION AND ACTIVITIES OF RIKEN NISHINA CENTER**(Activities, Members, Publications & Presentations)**

1. Organization	235
2. Finances	236
3. Staffing	236
4. Research publication	237
5. Management	238
6. International Collaboration	241
7. Awards	243
8. Brief overview of the RI Beam Factory	245
Nuclear Science and Transmutation Research Division	
Radioactive Isotope Physics Laboratory	247
Spin isospin Laboratory	257
Nuclear Spectroscopy Laboratory	264
High Energy Astrophysics Laboratory	270
Superheavy Element Research Group	274
Superheavy Element Production Team	276
Superheavy Element Device Development Team	281
Astro-Glaciology Research Group	283
Nuclear Transmutation Data Research Group	286
Fast RI Data Team	287
Slow RI Data Team	289
Muon Data Team	290
High-Intensity Accelerator R&D Group	292
High-Gradient Cavity R&D Team	293
High-Power Target R&D Team	294
Research Facility Development Division	
Accelerator Group	295
Accelerator R&D Team	297
Ion Source Team	299
RILAC Team	300

Cyclotron Team	301
Beam Dynamics & Diagnostics Team	303
Cryogenic Technology Team	305
Infrastructure Management Team	306
Instrumentation Development Group	308
SLOWRI Team	310
Rare RI-ring Team	314
SCRIT Team	317
Research Instruments Group	320
BigRIPS Team	321
SAMURAI Team	326
Computing and Network Team	330
Detector Team	332
Accelerator Applications Research Division	
Beam Mutagenesis Group	335
Ion Beam Breeding Team	336
Plant Genome Evolution Research Team	340
RI Application Research Group	342
Nuclear Chemistry Research Team	343
Industrial Application Research Team	352
Subnuclear System Research Division	
Quantum Hadron Physics Laboratory	354
Strangeness Nuclear Physics Laboratory	358
Radiation Laboratory	361
Meson Science Laboratory	366
RIKEN BNL Research Center	371
Theory Group	372
Experimental Group	377
Computing Group	382
RIKEN Facility Office at RAL	387
Safety Management Group	391
User Liaison Group	393
RIBF User Liaison Team	394
Outreach Team	395
Office of the Center Director	396
Partner Institutions	399
Center for Nuclear Study, Graduate School of Science, The University of Tokyo	400
Wako Nuclear Science Center, IPNS (Institute of Particle and Nuclear Studies), KEK (High Energy Accelerator Research Organization)	413
Events (April 2019 — March 2020)	417
Press Releases (April 2019–March 2020)	418

VII. LIST OF PREPRINTS

List of Preprints (April 2019—March 2020)	419
---	-----

VIII. LIST OF SYMPOSIA, WORKSHOPS & SEMINARS

List of Symposia & Workshops (April 2019—March 2020)	421
List of Seminars (April 2019—March 2020)	421

I. HIGHLIGHTS OF THE YEAR

<< Selection process of highlights >>

Highlights are selected by a two-step process. In the first step, a referee who reviews a manuscript decides whether she/he would recommend it as one of the highlights.

Members of the editorial board then make additional recommendations if they think an important contribution has not been recommended by the referee.

The second step involves the editor-in-chief proposing a list of highlights based on the recommendation given above to the editorial board. After discussing the scientific merits and uniqueness of the manuscripts from viewpoints of experts/non-experts, the editorial board makes the final decision.

Strong one-neutron emission from two-neutron unbound states in β decays of r -process nuclei $^{86,87}\text{Ga}^\dagger$

R. Yokoyama,^{*1} R. Grzywacz,^{*1,*2} B. C. Rasco,^{*1,*2} N. T. Brewer,^{*1,*2} K. P. Rykaczewski,^{*2} I. Dillmann,^{*3} J. L. Tain,^{*4} and S. Nishimura^{*5} for the BRIKEN collaboration

Delayed neutron emission after β decays is found in neutron-rich nuclei in which the energy window of β^- decay (Q_β) is high enough to populate excited states of the daughter nucleus above the neutron separation energy (S_n). All of the neutron-rich nuclei on the r -process path are either one or multi- n β -delayed precursors. Delayed neutron emission shapes the final abundance pattern owing to the modification of the isotopic population through the modification of the decay path back to stability and by contributing significantly to the neutron flux after freeze-out. However, experimental data that enable the evaluation of the role of multi- n emission for the r -process nuclei are almost non-existent. Often, predictions for neutron emission probabilities are based on a simplified *cut-off* model that neglects γ -decay competition and assumes that only the higher-multiplicity neutron emission prevails in the energy regions open to multiple neutron-emission channels.

We studied neutron-rich Ga isotopes by means of β -neutron- γ spectroscopy at RIBF using the in-flight fission of a 345 MeV/nucleon $^{238}\text{U}^{86+}$ beam on a 4-mm-thick ^9Be production target. For decay measurement, 7×10^4 and 6×10^3 ions of ^{86}Ga and ^{87}Ga , respectively, were transported to the final focal plane. Double-sided silicon-strip detectors (DSSSDs), AIDA,¹⁾ WAS3ABi,²⁾ and a YSO scintillator³⁾ were employed for ion and β correlation measurements. The ^3He neutron counter array, BRIKEN,⁴⁾ was used for neutron measurement.

The half-lives and P_{xn} values were obtained through the analysis described in Ref. 6). The P_{1n} and P_{2n} values obtained in this work for ^{86}Ga are consistent with the data reported by Miernik *et al.*⁷⁾ We discovered new β -delayed two-neutron emitters, $^{84,85,87}\text{Ga}$, and measured their two-neutron branching ratio for the first time. Figure 1 shows a comparison of the experimental neutron branching ratio with shell-model calculations based on the cut-off model reported by Madurga *et al.*⁵⁾ and shell-model calculations based on the Hauser-Feshbach statistical model.⁸⁾ When comparing the new experimental results with the predictions from the shell-model calculations, we notice a discrepancy between the cut-off model and experimental data for all investigated $\beta 2n$ gallium precursors,

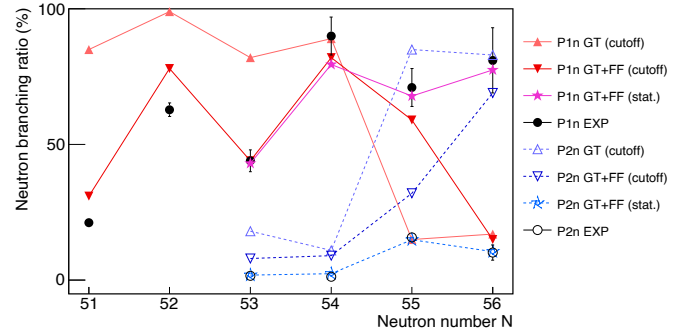


Fig. 1. Comparison of the experimental data and the predictions from the shell-model calculations by Madurga *et al.*⁵⁾ “GT” and “GT+FF” in the legend denote shell-model calculations with pure Gamow-Teller and GT + first forbidden transitions, respectively. The GT+FF predictions, when coupled with the statistical model (stat.), provide a much better agreement with the data than the cutoff model.

which is most dramatically manifested in ^{87}Ga .

In contrast to the cut-off model, the inclusion of the statistical model correctly reproduces the dominating role of one-neutron emission from two-neutron unbound states. This result is the first clear case in medium/heavy nuclei where the effects of statistical emission must be considered to model β -delayed multi-neutron emission, which is of particular importance for r -process modeling. The strong $1n$ emission from $2n$ unbound states will require more detailed studies of neutron and γ -ray spectra to establish the details of the emission process. The detection of neutron energies and γ -ray energies is required to better constrain both the strength-distribution models and statistical model parameters.

References

- 1) C. J. Griffin *et al.*, PoS **NIC XIII**, 097 (2014).
- 2) S. Nishimura *et al.*, RIKEN Accel. Prog. Rep. **46**, 182 (2013).
- 3) R. Yokoyama *et al.*, Nucl. Instrum. Methods Phys. Res. A **937**, 93–97 (2019).
- 4) A. Tarifeño-Saldivia *et al.*, J. Instrum. **12**, P04006 (2017).
- 5) M. Madurga *et al.*, Phys. Rev. Lett. **117**, 092502 (2016).
- 6) B. C. Rasco *et al.*, Nucl. Instrum. Methods Phys. Res. A **911**, 79 (2018).
- 7) K. Miernik *et al.*, Phys. Rev. Lett. **111**, 132502 (2013).
- 8) T. Kawano *et al.*, Nucl. Phys. A **913**, 51 (2013).

[†] Condensed from article Phys. Rev. C **100**, 031302(R)

^{*1} University of Tennessee, Knoxville

^{*2} Oak Ridge National Laboratory

^{*3} TRIUMF

^{*4} IFIC (CSIC, Universitat de Valencia)

^{*5} RIKEN Nishina Center

Shell evolution towards ^{60}Ca : First spectroscopy of $^{62}\text{Ti}^\dagger$

M. L. Cortés,^{*1,*2} W. Rodríguez,^{*1,*3} P. Doornenbal,^{*1} A. Obertelli,^{*4,*5} J. D. Holt,^{*6} S. M. Lenzi,^{*7} J. Menéndez,^{*8} F. Nowacki,^{*9} K. Ogata,^{*10,*11} A. Poves,^{*12} T. R. Rodríguez,^{*12} A. Schwenk,^{*5,*13,*14} J. Simonis,^{*15} S. R. Stroberg,^{*6,*16} and K. Yoshida^{*17} for the SEASTAR2017 collaboration.

The study of $N = 40$ isotones can provide insight into the mechanisms governing shell evolution. Along this isotonic chain different behaviors are observed: ^{68}Ni shows a high $E(2_1^+)$ and a low $B(E2)_{\downarrow}$.¹⁾ For Fe and Cr, a monotonous decrease of the $E(2_1^+)$ when approaching $N = 40$ has been observed,¹⁾ while the $E(2_1^+)$ of $^{58,60}\text{Ti}$ shows a moderate decrease towards $N = 40$.^{2,3)} The very exotic ^{60}Ca , where the Ca isotopic chain meets the $N = 40$ isotones, is difficult to reach experimentally and only recently its existence has been established.⁴⁾ Theoretical calculations in the shell-model framework⁵⁾ concluded that quadrupole correlations in the $N = 40$ isotopes give rise to deformed ground states dominated by intruder neutron orbits beyond the pf shell, leading to an island of inversion below ^{68}Ni . On the other hand, symmetry conserving configuration mixing calculations with the Gogny interaction predict a conservation of the $N = 40$ gap leading to spherical ^{62}Ti and ^{60}Ca .⁶⁾ In this work, the first spectroscopy of ^{62}Ti is presented.

A 345 MeV/nucleon beam of ^{70}Zn with an average intensity of 240 pnA was fragmented on a Be target to produce ^{63}V . The isotopes were identified using BigRIPS⁷⁾ and delivered to the 151.3(13) mm long liquid hydrogen target of MINOS⁸⁾ placed in front of the SAMURAI magnet. Outgoing ^{62}Ti fragments were identified using SAMURAI and associated detectors.⁹⁾ MINOS was surrounded by DALI2⁺, composed of 226 NaI(Tl) detectors.^{10,11)}

Two peaks were clearly identified in the Doppler corrected γ -spectrum, and were found to be in coincidence. Using a 2-dimensional χ^2 minimization the energies of the transitions were deduced to be 683(10) keV and 823(20) keV, which were tentatively assigned to the $2_1^+ \rightarrow 0_{\text{gs}}^+$ and $4_1^+ \rightarrow 2_1^+$ transitions, respectively. The evolution of measured $E(2_1^+)$ and $E(4_1^+)$ energies for the

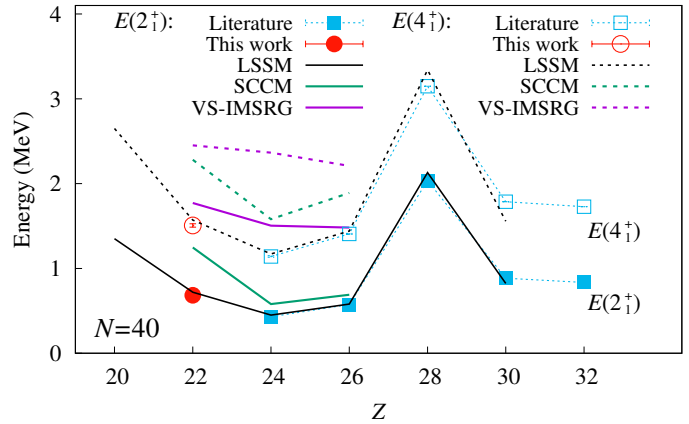


Fig. 1. Systematics of $E(2_1^+)$ and $E(4_1^+)$ for even-even $N = 40$ isotones, including the present measurement. The black, green, and purple lines represent LSSM, SCCM, and VS-IMSRG calculations, respectively.

$N = 40$ isotones between Ti and Ge¹⁾ is presented in Fig. 1. The $E(2_1^+)$ and $E(4_1^+)$ of ^{62}Ti have a similar value than the ones measured for ^{66}Fe , higher than those of ^{64}Cr . This shows the first increase of $E(2_1^+)$ along the $N = 40$ isotones towards ^{60}Ca . Large Scale Shell Model (LSSM) calculations using the LNPS interaction reproduce very accurately the data, indicating that the island of inversion in this region extends down to ^{60}Ca . Symmetry conserving configuration mixing (SCCM) calculations using the Gogny D1S effective interaction predict $E(2_1^+)$ for ^{64}Cr and ^{66}Fe which lie very close to the LSSM predictions. However, for ^{62}Ti a larger increase of the $E(2_1^+)$ is obtained. For the $E(4_1^+)$ energies, the calculations overestimate the experimental values by about 500 keV, although the minimum value for ^{64}Cr is maintained. Ab initio valence-space in-medium similarity renormalization group (VS-IMSRG) calculations overestimate the $E(2_1^+)$ and $E(4_1^+)$ excitation energies in ^{62}Ti , ^{64}Cr , and ^{66}Fe , predicting all states as spherical.

References

- 1) <http://www.nndc.bnl.gov/ensdf/>.
- 2) H. Suzuki *et al.*, Phys. Rev. C **88**, 024326 (2013).
- 3) A. Gade *et al.*, Phys. Rev. Lett. **112**, 112503 (2014).
- 4) O. B. Tarasov *et al.*, Phys. Rev. Lett. **121**, 022501 (2018).
- 5) S. M. Lenzi *et al.*, Phys. Rev. C **82**, 054301 (2010).
- 6) T. R. Rodríguez *et al.*, Phys. Rev. C **93**, 054316 (2016).
- 7) T. Kubo *et al.*, Prog. Theor. Exp. Phys. **2012**, (2012).
- 8) A. Obertelli *et al.*, Eur. Phys. J. A **50**, (2014).
- 9) T. Kobayashi *et al.*, Nucl. Instrum. Methods Phys. Res. B **317**, 294 (2013).
- 10) S. Takeuchi *et al.*, Nucl. Instrum. Methods Phys. Res. A **763**, 596 (2014).
- 11) I. Murray *et al.*, RIKEN Accel. Prog. Rep. **51**, 158 (2017).

[†] Condensed from Phys. Lett. B **800**, 135071 (2020)

^{*1} RIKEN Nishina Center

^{*2} INFN-Laboratori Nazionali di Legnaro

^{*3} Universidad Nacional de Colombia

^{*4} IRFU, CEA, Université Paris-Saclay

^{*5} Institut für Kernphysik, Technische Universität Darmstadt
^{*6} TRIUMF

^{*7} Dipartimento di Fisica e Astronomia, Università di Padova

^{*8} Center for Nuclear Study, The University of Tokyo

^{*9} IPHC, CNRS/IN2P3, Université de Strasbourg

^{*10} RCNP, Osaka University

^{*11} Department of Physics, Osaka City University

^{*12} Departamento de Física Teórica, Universidad Autónoma de Madrid

^{*13} EMMI, GSI Helmholtzzentrum für Schwerionenforschung

^{*14} Max-Planck-Institut für Kernphysik

^{*15} Institut für Kernphysik, Johannes Gutenberg-Universität

^{*16} Department of Physics, University of Washington

^{*17} Advanced Science Research Center, Japan Atomic Energy Agency

^{78}Ni revealed as a doubly magic stronghold against nuclear deformation[†]

R. Taniuchi,^{*1,*2} C. Santamaria,^{*3,*2} P. Doornenbal,^{*2} A. Obertelli,^{*3,*2,*4} and K. Yoneda^{*2}
for SEASTAR2014 Collaboration

The doubly magic character of ^{78}Ni was investigated for the first time via the in-beam γ -ray spectroscopic technique at the RIBF. Vital to the experiment was a high intensity ^{238}U primary beam, accelerated by the RIBF's cyclotron complex and followed by the BigRIPS spectrometer¹⁾ for the production of the secondary cocktail beams. BigRIPS was centered on ^{79}Cu and ^{80}Zn ions, which are bound by one and two protons more than the target isotope ^{78}Ni . Excited states of ^{78}Ni were populated by one- and two-proton knockout reactions, respectively. To produce the excited states in sufficient numbers, a new secondary target system, MINOS,²⁾ was implemented. It consisted of a 10-cm long liquid hydrogen target surrounded by a time-projection chamber to trace outgoing protons following the proton knockout reactions. Reaction residues were tagged by the ZeroDegree spectrometer¹⁾ installed behind MINOS. De-excitation γ rays emitted in prompt coincidence with the secondary reactions were detected by the large volume γ -ray scintillator array DALI2.³⁾

The γ -ray spectra of the $(p, 2p)$ and $(p, 3p)$ reactions are shown in Fig. 1. The energies of the peaks indicated in the figure were deduced by maximum-likelihood fits with simulated response functions. As a result, a clear high-energy γ -ray transition observed at 2,600(33) keV in the $(p, 2p)$ reaction illustrates the persistence of the doubly magic nature of ^{78}Ni . However, another transition at a similar energy, 2,910(43) keV observed in the $(p, 3p)$ channel, questions the stability of the proton and neutron shell closures.

The obtained levels of the excited states have been compared with several state-of-the-art calculations. Two large-scale shell-model calculations, LSSM and MCSM, employing phenomenological interactions well reproduced the experimentally observed transitions just below 3 MeV as two excited 2^+ states feeding the ground state independently. These theoretical predictions interpret the experimental result as ^{78}Ni having two coexisting shapes, spherical in the ground-state band and prolate for the excited band, respectively. Other theoretical approaches, such as the QRPA, Coupled-Cluster, and In-Medium SRG calculations, could solely reproduce the first 2^+ state at 2,600 keV as spherical shape. The absence of the second 2^+ state found at 2,910 keV is understood as due

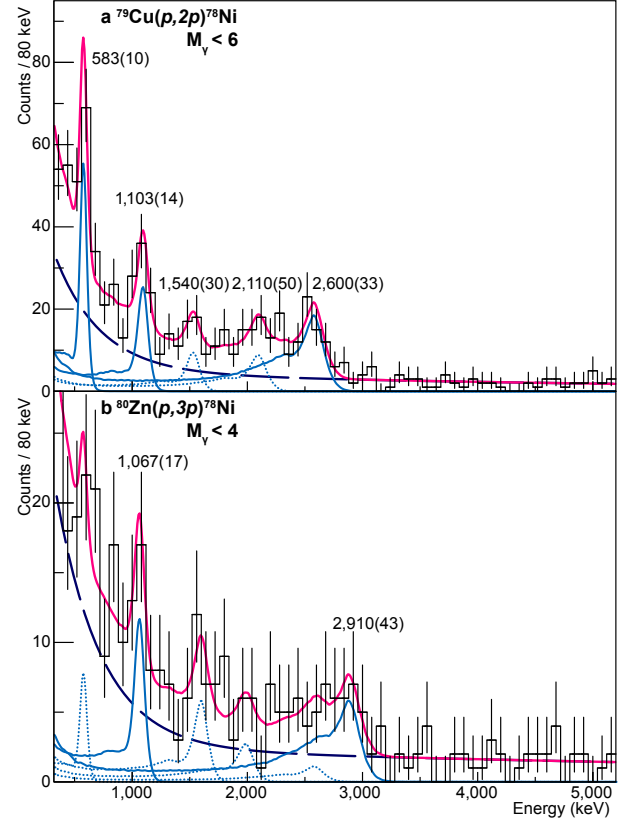


Fig. 1. Doppler-corrected γ -ray spectra of ^{78}Ni for the $(p, 2p)$ and $(p, 3p)$ channels. These histograms are fitted with simulated response functions (light blue lines) and double-exponential background curves (blue dashed line). The labels indicate the energies of the respective peaks. Solid response function lines had significance levels above 3σ , while the dotted ones did not. The magenta line in each panel shows the summed curve of the simulated functions.

to the limitations of these models such that they do not incorporate the deformed, or collective phenomena. This study suggests that the neutron-rich isotope ^{78}Ni cannot be envisaged as a simple doubly closed-shell nucleus, but rather having a competing deformed structure that prevails for more neutron-rich Ni isotopes and $N = 50$ isotones.

References

- 1) T. Kubo *et al.*, Prog. Theor. Exp. Phys. **2012**, 3C003 (2012).
- 2) A. Obertelli *et al.*, Eur. Phys. J. A **50**, 8 (2014).
- 3) S. Takeuchi *et al.*, Nucl. Instrum. Methods Phys. Res. A **763**, 596 (2014).

[†] Condensed from the article in Nature **569**, 53–58 (2019)

^{*1} Department of Physics, The University of Tokyo

^{*2} RIKEN Nishina Center

^{*3} IRFU, CEA, Université Paris-Saclay

^{*4} Institut für Kernphysik, Technische Universität Darmstadt

Inclusive cross sections for one- and multi-nucleon removal from Sn, Sb, and Te projectiles beyond the $N = 82$ shell closure[†]

V. Vaquero,^{*1} A. Jungclaus,^{*1} J. L. Rodríguez-Sánchez,^{*2} J. A. Tostevin,^{*3} P. Doornenbal,^{*4} K. Wimmer,^{*5,*4} S. Chen,^{*4,*6} E. Nácher,^{*1} E. Sahin,^{*7} Y. Shiga,^{*8} D. Steppenbeck,^{*4} R. Taniuchi,^{*4,*5} Z. Y. Xu,^{*9} T. Ando,^{*5} H. Baba,^{*4} F. L. Bello Garrote,^{*7} S. Franchoo,^{*10} A. Gargano,^{*11} K. Hadynska-Klek,^{*7} A. Kusoglu,^{*12,*13} J. Liu,^{*9} T. Lokotko,^{*9} S. Momiyama,^{*5} T. Motobayashi,^{*4} S. Nagamine,^{*5} N. Nakatsuka,^{*14} M. Niikura,^{*5} R. Orlandi,^{*15} T. Saito,^{*5} H. Sakurai,^{*4,*5} P. A. Söderström,^{*4} G. M. Tveten,^{*7} Zs. Vajta,^{*16} and M. Yalcinkaya^{*1,*12}

Inclusive one- and multi-nucleon removal cross sections have been measured for several Sn, Sb and Te isotopes just beyond the $N = 82$ neutron shell closure. The beams were produced in the projectile fission of a ^{238}U beam at the Radioactive Isotope Beam Factory at RIKEN. The experimental cross sections were compared to predictions from two different versions of the Liege intranuclear cascade (INCL) model^{1,2} as shown in Fig. 1. This figure shows an overall good agreement between the calculations and the experimental results. In particular for the $0p_{xn}$ removal from the $N = 83$ projectiles ^{133}Sn , ^{134}Sb , and ^{135}Te as well as the stable ^{112}Sn ³) both the magnitude and the gentle odd-even staggering of the cross sections is nicely reproduced by both calculations. In contrast, none of them correctly describes the measured cross sections for one- and two-neutron removal from the $N = 84$ isotones ^{134}Sn and ^{135}Sb . This failure of the INCL model could be traced to the peculiar structure of these nuclei with only a few valence neutrons above the $N = 82$ shell gap.⁴⁾

Turning now to the one-proton knockout cross sections, Fig. 1(b) clearly shows that both calculations fail to reproduce the experimental values for all three studied $N = 84$ projectiles, *i.e.* ^{134}Sn , ^{135}Sb and ^{136}Te . Note, however, that in this case the refinements, which have been introduced in the modified version of the INCL code, have a much stronger effect as compared to the case of one-neutron knockout, reducing the calculated one-proton knockout cross sections by roughly a factor of two. The underlying reasons for the overestimation of the cross section for the removal of the stronger bound nucleon species by the INCL model, which had already been recognized in the past, are still awaiting explanation.

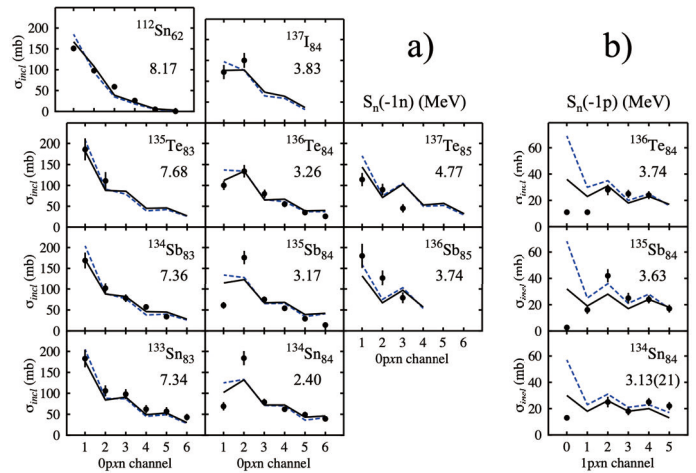


Fig. 1. Comparison between experimental inclusive removal cross sections and the results of calculations performed with two different versions (standard¹) as dashed blue and modified²) as solid black lines) of the INCL code for a) the $0p_{xn}$ and b) the $1p_{xn}$ removal channels. The experimental cross sections for $0p_{xn}$ removal from ^{112}Sn shown in a) are taken from Ref. 3).

The present data for multi-nucleon removal indicate that an ad-hoc increase of the excitation energy in the INCL model at the end of the cascade process, an approach which has been suggested to cure the incapacity of the model to correctly describe the removal of deeply bound nucleons, does not address the origin of this problem.

Finally, we mention that the experimental inclusive cross section for one-proton removal from semi-magic ^{134}Sn was also compared with calculations based on eikonal direct reaction theory with structure information from the nuclear shell model and refer to the original publication for further details.

References

- 1) D. Mancusi *et al.*, Phys. Rev. C **90**, 054602 (2014).
- 2) J. L. Rodríguez-Sánchez *et al.*, Phys. Rev. C **96**, 054602 (2017).
- 3) L. Audirac *et al.*, Phys. Rev. C **36**, 041602(R) (2013).
- 4) V. Vaquero *et al.*, Phys. Rev. Lett. **118**, 202502 (2017).

[†] Condensed from the article in Phys. Lett. B **795**, 356 (2019)

^{*1} IEM-CSIC Madrid
^{*2} Universidad de Santiago de Compostela
^{*3} University of Surrey
^{*4} RIKEN Nishina Center
^{*5} Department of Physics, University of Tokyo
^{*6} Peking University, Beijing
^{*7} University of Oslo, Oslo
^{*8} Department of Physics, Rikkyo University
^{*9} University of Hong Kong
^{*10} IN2P3-CNRS, Orsay
^{*11} INFN, Napoli
^{*12} Istanbul University
^{*13} ELI-NP, Magurele
^{*14} Department of Physics, Kyoto University
^{*15} Advanced Science Research Center, JAEA
^{*16} MTA Atomki

g -Factor of the ^{99}Zr isomer: monopole evolution in the shape-coexisting region[†]

F. Boulay,^{*1,*2,*3} G. S. Simpson,^{*4} Y. Ichikawa,^{*2} S. Kisiov,^{*5} D. Bucurescu,^{*5} A. Takamine,^{*2} D. S. Ahn,^{*2} K. Asahi,^{*2,*6} H. Baba,^{*2} D. L. Balabanski,^{*2,*7} T. Egami,^{*2,*8} T. Fujita,^{*2,*9} N. Fukuda,^{*2} C. Funayama,^{*2,*6} T. Furukawa,^{*2,*10} G. Georgiev,^{*11} A. Gladkov,^{*2,*12} M. Hass,^{*13} K. Imamura,^{*2,*14} N. Inabe,^{*2} Y. Ishibashi,^{*2,*15} T. Kawaguchi,^{*2,*8} T. Kawamura,^{*9} W. Kim,^{*12} Y. Kobayashi,^{*16} S. Kojima,^{*2,*6} A. Kusoglu,^{*11,*17} R. Lozeva,^{*11} S. Momiyama,^{*18} I. Mukul,^{*13} M. Niikura,^{*18} H. Nishibata,^{*2,*9} T. Nishizaka,^{*2,*8} A. Odahara,^{*9} Y. Ohtomo,^{*2,*6} D. Ralet,^{*11} T. Sato,^{*2,*6} Y. Shimizu,^{*2} T. Sumikama,^{*2} H. Suzuki,^{*2} H. Takeda,^{*2} L. C. Tao,^{*2,*19} Y. Togano,^{*6} D. Tominaga,^{*2,*8} H. Ueno,^{*2} H. Yamazaki,^{*2} X. F. Yang,^{*20} and J. M. Daugas^{*1,*2}

A rapid change of the ground-state shape has been known to occur in neutron-rich Zr isotopes between the spherical ^{98}Zr and deformed ^{100}Zr .¹⁾ This change has been described as a quantum phase transition (QPT) with the neutron number as a control parameter. The ^{99}Zr nucleus closest to the critical point of the QPT has an isomer ($^{99\text{m}}\text{Zr}$) with a spin parity of $7/2^+$ at 252 keV. The interaction between the $\pi g_{9/2}$ and $\nu g_{7/2}$ orbitals has been thought to be important for this QPT to occur,²⁾ and the $7/2^+$ state may be key to this mechanism. In the present study, the nature of $^{99\text{m}}\text{Zr}$ was investigated through the magnetic moment.

The magnetic-moment measurement was performed at the BigRIPS at RIBF. $^{99\text{m}}\text{Zr}$ was produced and spin-aligned via the abrasion-fission of a 345-MeV/nucleon ^{238}U beam impinging on a 100- μm -thick ^9Be target. The g -factor of $^{99\text{m}}\text{Zr}$ was measured by the time-differential perturbed angular distribution (TDPAD) method. Figure 1 shows the $R(t)$ ratio evaluated using γ rays of 130 keV and 122 keV by assuming pure $M1$ and $E2$ transitions, respectively, where a degree of spin-alignment of 1.5(4)% was extracted. The g factor of $^{99\text{m}}\text{Zr}$ determined was determined as $|g| = 0.66(4)$; thus, the magnetic moment is $|\mu| = 2.31(14) \mu_N$.

This value is far from the Schmidt value of $g_{free} = +0.425$ for the $\nu g_{7/2}$ orbital, indicating that $^{99\text{m}}\text{Zr}$ is not in a pure $(\nu g_{7/2})^1$ state. A comparison of the exper-

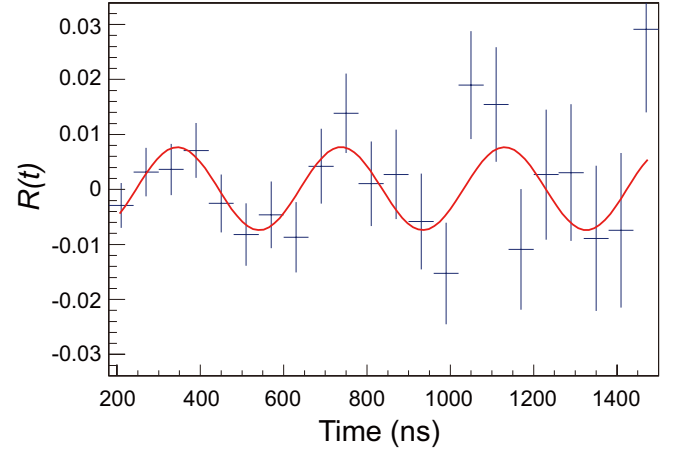


Fig. 1. $R(t)$ ratio associated with two γ rays.

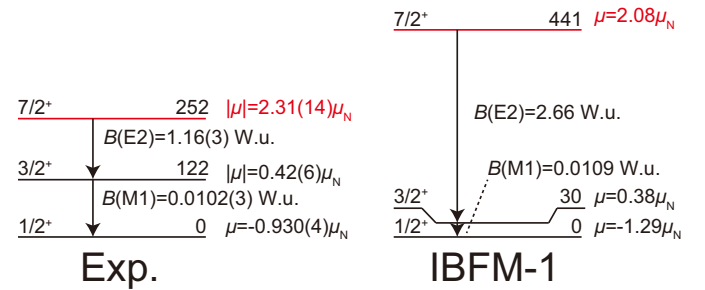


Fig. 2. Comparison between experimental and theoretical values. The IBFM-1 calculation is based on the transition probabilities among the lowest three states and the magnetic moments of the lowest two states.³⁾

imental values with the results of the interacting boson-fermion model (IBFM-1), as shown in Fig. 2, suggests that this state is strongly mixed with the main composition being $\nu d_{5/2}$. Furthermore, we found that monopole single-particle evolution changes significantly with the appearance of collective modes.^{4,5)}

References

- 1) P. Campbell *et al.*, Phys. Rev. Lett. **89**, 082501 (2002).
- 2) P. Federman, S. Pittel, Phys. Lett. B **69**, 385 (1977).
- 3) P. Spagnoletti *et al.*, Phys. Rev. C **100**, 014311 (2019).
- 4) Y. Tsunoda *et al.*, Phys. Rev. C **89**, 031301(R) (2014).
- 5) T. Togashi *et al.*, Phys. Rev. Lett. **117**, 172502 (2016).

[†] Condensed from the article in Phys. Rev. Lett. **124**, 112501 (2020)

^{*1} CEA, DAM, DIF

^{*2} RIKEN Nishina Center

^{*3} GANIL, CEA/DSM-CNRS/IN2P3

^{*4} LPSC, CNRS/IN2P3, Université Joseph Fourier Grenoble 1

^{*5} IFIN-HH

^{*6} Department of Physics, Tokyo Institute of Technology

^{*7} ELI-NP, IFIN-HH

^{*8} Department of Advanced Sciences, Hosei University

^{*9} Department of Physics, Osaka University

^{*10} Department of Physics, Tokyo Metropolitan University

^{*11} IJCLab, CNRS/IN2P3, Université Paris-Saclay

^{*12} Department of Physics, Kyungpook National University

^{*13} Department of Particle Physics, Weizmann Institute

^{*14} Department of Physics, Meiji University

^{*15} Department of Physics, University of Tsukuba

^{*16} Department of Informatics and Engineering, University of Electro-Communications

^{*17} Department of Physics, Istanbul University

^{*18} Department of Physics, University of Tokyo

^{*19} School of Physics, Peking University

^{*20} Instituut voor Kern-en Stralingsfysica, K. U. Leuven

Study of quasielastic barrier distributions as a step towards the synthesis of superheavy elements with hot fusion reactions[†]

T. Tanaka,^{*1,*2,*3} K. Morita,^{*1,*2} K. Morimoto,^{*1} D. Kaji,^{*1} H. Haba,^{*1} R. A. Boll,^{*4} N. T. Brewer,^{*4} S. Van Cleve,^{*4} D. J. Dean,^{*4} S. Ishizawa,^{*1,*5} Y. Ito,^{*1,*6} Y. Komori,^{*1} K. Nishio,^{*1,*6} T. Niwase,^{*1,*2} B. C. Rasco,^{*4} J. B. Roberto,^{*4} K. P. Rykaczewski,^{*4} H. Sakai,^{*1} D. W. Stracener,^{*4} and K. Hagino^{*7,*8,*9}

The excitation functions of quasielastic scattering cross sections for reactions relevant to the syntheses of superheavy nuclei, that is, the $^{22}\text{Ne}+^{248}\text{Cm}$, $^{26}\text{Mg}+^{248}\text{Cm}$, and $^{48}\text{Ca}+^{238}\text{U}$ systems, were measured using the gas-filled recoil ion separator GARIS to understand systematically the reaction dynamics of the hot fusion reactions. From the measured cross sections, the barrier distribution was extracted, which shows a distribution of the barrier height in the entrance channel. The experimental data were well reproduced by the coupled-channels calculations.¹⁾ The calculated results indicate that the shape of barrier distribution is affected dominantly by deformation of the actinide target nuclei, but also by vibrational/rotational excitations of the projectile nuclei as well as neutron transfer processes before capture. Contribution from each colliding angles to the barrier distribution is systematically shown in Fig. 1 (black thin solid curves) by showing the barrier distribution from each colliding-angle range with 10° interval. Here, the distribution for the side collision $80\text{--}90^\circ$ is highlighted by the red dashed curve. The total barrier distributions, which are the sum of the black thin solid curves and the red dashed curves, are also shown by the blue solid curves. The peak of the sum of the evaporation residue cross sections for Sg ($Z = 106$),^{2–6)} Hs (108),⁷⁾ Cn (112)^{8,9)} and Lv (116)^{8,10)a)} coincide not only with the barrier distribution for $80\text{--}90^\circ$, but also with that for $70\text{--}80^\circ$ etc. However, the overlap with the barrier distribution for the tip collision, such as $0^\circ\text{--}20^\circ$, is negligibly small, indicating that these hot fusion reactions take advantage of the compact collision, where the projectile approaches along the short axis of a prolately deformed nucleus, as was discussed in Refs. 11–13).

For hot fusion reactions, the optimum incident energy, at which the evaporation residue cross section

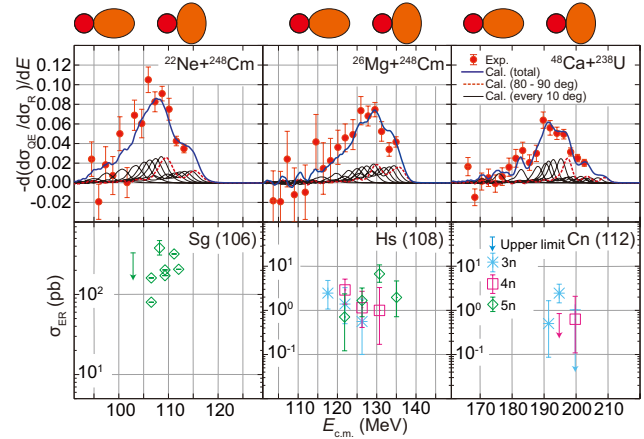


Fig. 1. A comparison between the measured quasielastic barrier distributions (the upper panels) and the evaporation residue cross sections reported at different center-of-mass energies for the syntheses of Sg, Hs, and Cn^{2–9)} (the lower panels). The red symbols indicate the experimental data from this work. The detailed explanations of the calculated results are described in main text.

is maximized, can be estimated by an experimentally determined barrier distribution, if the trend of compact collision is not changed. Importantly, it would take only about one day to measure a barrier distribution for one reaction, which is much shorter than a typical experiment to synthesize new superheavy element, *e.g.*, more than one hundred days using one μA beam. This new method will significantly contribute to future experiments to synthesize both new superheavy elements and superheavy nuclei in the island of stability.

References

- 1) K. Hagino *et al.*, *Comput. Phys. Commun.* **123**, 143 (1999).
- 2) Yu. A. Lazarev *et al.*, *Phys. Rev. Lett.* **73**, 624 (1994).
- 3) A. Türler *et al.*, *Phys. Rev. C* **57**, 1648 (1998).
- 4) R. Dressier *et al.*, *PSI Rep.* **1**, 130 (1999).
- 5) S. Hübener *et al.*, *Radiochimica Acta* **89**, 737 (2001).
- 6) H. Haba *et al.*, *Phys. Rev. C* **85**, 024611 (2012).
- 7) J. Dvorak *et al.*, *Phys. Rev. Lett.* **100**, 132503 (2008).
- 8) Y. T. Oganessian *et al.*, *Phys. Rev. C* **70**, 064609 (2004).
- 9) S. Hofmann *et al.*, *Eur. Phys. J. A* **32**, 251 (2007).
- 10) S. Hofmann *et al.*, *Eur. Phys. J. A* **48**, 62 (2012).
- 11) D. J. Hinde *et al.*, *Phys. Rev. Lett.* **74**, 1295 (1995).
- 12) K. Nishio *et al.*, *Phys. Rev. C* **62**, 014602 (2000).
- 13) T. Tanaka *et al.*, *J. Phys. Soc. Jpn.* **87**, 014201 (2018).

[†] Condensed from the article in *Phys. Rev. Lett.* **124**, 052502 (2020)

^{*1} RIKEN Nishina Center

^{*2} Department of Physics, Kyushu University

^{*3} Department of Nuclear Physics, The Australian National University

^{*4} Oak Ridge National Laboratory

^{*5} Graduate School of Science and Engineering, Yamagata University

^{*6} Advanced Science Research Center, JAEA

^{*7} Department of Physics, Tohoku University

^{*8} Research Center for Electron Photon Science, Tohoku University

^{*9} Department of Physics, Kyoto University

a) The result of $^{48}\text{Ca}+^{248}\text{Cm}\rightarrow^{296}\text{Lv}^*$ is omitted from the Fig. 1 due to the space limit. See the original article.

Location of the neutron dripline at fluorine and neon[†]

D. S. Ahn,^{*1} N. Fukuda,^{*1} H. Geissel,^{*5} N. Inabe,^{*1} N. Iwasa,^{*4} T. Kubo,^{*1,a} K. Kusaka,^{*1} D. J. Morrissey,^{*6} D. Murai,^{*3} T. Nakamura,^{*2} M. Ohtake,^{*1} H. Otsu,^{*1} H. Sato,^{*1} B. M. Sherrill,^{*6} Y. Shimizu,^{*1} H. Suzuki,^{*1} H. Takeda,^{*1} O. B. Tarasov,^{*6} H. Ueno,^{*1} Y. Yanagisawa,^{*1} and K. Yoshida^{*1}

The location of the neutron dripline has been a long-standing issue, and it is only known up to oxygen (atomic number $Z = 8$) so far. No confirmed extensions of the dripline above $Z = 8$ have been made for nearly 20 years, since ^{24}O (neutron number $N = 16$) was determined to be a dripline nucleus.

In order to investigate the neutron dripline for higher- Z elements such as fluorine ($Z = 9$), neon ($Z = 10$), and sodium ($Z = 11$), we conducted a search for the new isotopes $^{32,33}\text{F}$, $^{35,36}\text{Ne}$, and $^{38,39}\text{Na}$ at the RIKEN RIBF. We attempted to observe isotopes beyond the line of the mass number $A = 3Z + 4$, where the most neutron-rich isotopes known so far are located. The search was performed using the projectile fragmentation of an intense ^{48}Ca beam at 345 MeV/nucleon on a 20-mm-thick beryllium target. The projectile fragments were separated and identified in flight by the large-acceptance two-stage fragment separator BigRIPS.^{1,2} The ^{48}Ca -beam intensity was as high as ~ 450 particle nA ($\sim 3 \times 10^{12}$ particles/s).

Particle identification was performed at the second stage of the BigRIPS separator, relying on the combination of time of flight (TOF), magnetic rigidity ($B\rho$), and energy loss (ΔE) measurements, from which the Z and A/Z of the fragments were deduced.³ The TOF was measured between two thin plastic scintillators installed at the intermediate and final foci of the second stage. The ΔE was measured using a stack of four identical silicon semiconductor detectors installed at the final focus. The $B\rho$ was determined from a position measurement at the intermediate focus using the same plastic scintillator. The measurement was conducted with two $B\rho$ settings of the BigRIPS separator, the central particle of which was tuned to be ^{33}F and the middle of ^{36}Ne and ^{39}Na , respectively. In these settings, their neighboring isotopes also had a reasonably good transmission.

a)

After extensive running, we observed no events for $^{32,33}\text{F}$, $^{35,36}\text{Ne}$, and ^{38}Na and one event for ^{39}Na , implying that these unobserved isotopes were particle unbound. In order to assess the confidence level of the implication, production cross sections were systematically measured as a function of mass number, and the data were compared with the predictions from the EPAX 2.15

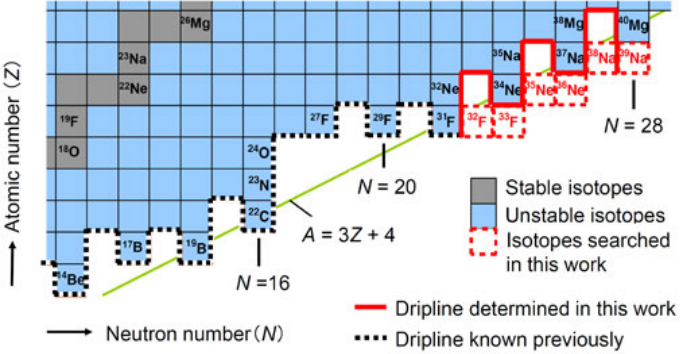


Fig. 1. Section of the nuclear chart showing the location of the neutron dripline determined in the present work.

systematics⁴) and the Qg systematics.⁵) These systematics allowed us to extrapolate the observed cross sections and, hence, estimate the expected yields of the unobserved isotopes. The comparison of no observed events with the expected yields revealed that the existence of bound $^{32,33}\text{F}$, $^{35,36}\text{Ne}$, and ^{38}Na was excluded with high confidence levels. Thus, we concluded that the most neutron-rich and heaviest bound nuclei, corresponding to the dripline nuclei, are ^{31}F and ^{34}Ne for fluorine and neon, respectively. The location of the neutron dripline has thus been extended up to $Z = 10$ for the first time in nearly 20 years, as shown in Fig. 1.

The location of the neutron dripline is sensitive to the underlying nuclear structure of neutron-rich exotic nuclei, such as the evolution of nuclear shell structure and occurrence of nuclear deformation, which are caused by the characteristic effects of complex nuclear forces.⁶⁻⁸) We compared the present results with various nuclear mass and structure models, and we found that no models could consistently account for the nuclear binding of neutron-rich nuclei in the present Z region.

The present results provide new keys to understanding the nuclear stability at extremely neutron-rich conditions and also present a new challenge to nuclear mass models as well as nuclear structure theories and calculations.

References

- 1) T. Kubo, Nucl. Instrum. Methods Phys. Res. B **204**, 97 (2003).
- 2) T. Kubo *et al.*, Prog. Theor. Exp. Phys. **2012**, 03C003 (2012).
- 3) T. Ohnishi *et al.*, J. Phys. Soc. Jpn. **77**, 083201 (2008).
- 4) K. Sümmerer, B. Blank, Phys. Rev. C **61**, 034607 (2000).
- 5) O. B. Tarasov *et al.*, Phys. Rev. C **75**, 064613 (2007).
- 6) D. S. Ahn *et al.*, Phys. Rev. Lett. **123**, 212501 (2019) and references therein.
- 7) T. Otsuka, Phys. Scr. T **152**, 014007 (2013).
- 8) T. Otsuka *et al.*, arXiv:1805.06501v5 [nucl-th] 2 Jan 2020.

[†] Condensed from the article in Phys. Rev. Lett. **123**, 212501 (2019)

^{*1} RIKEN Nishina Center

^{*2} Department of Physics, Tokyo Institute of Technology

^{*3} Department of Physics, Rikkyo University

^{*4} Department of Physics, Tohoku University

^{*5} GSI, Helmholtzzentrum für Schwerionenforschung GmbH

^{*6} National Superconducting Cyclotron Laboratory, Michigan State University

^a Corresponding author

Dineutron correlation and rotational excitations in neutron-rich Mg isotopes

M. Yamagami ^{*1}

The spatial two-neutron correlation between two weakly-bound neutrons, called dineutron correlation, is one of the unique features of nuclei around the neutron drip line. It is considered to be a universal phenomenon that appears over all mass-number regions. However, experimental probes for this phenomenon are still under intense debate, except for light-mass nuclei such as ^{11}Li . In this study, the influences of the novel pairing effect on rotational excitations in neutron-rich Mg isotopes are clarified.

The experimental moment of inertia (MOI), which can be extracted from the excitation energy $E(2_1^+)$, is smaller than the rigid-body values by a factor of 2 to 3. The most important influences in this respect are pairing correlations. I calculate the Thouless-Valatin (TV) MOI, which includes the pairing correlations and residual interactions within the framework of the quasiparticle random phase approximation (QRPA).

The Hartree-Fock-Bogoliubov (HFB) equation with the Skyrme energy density functional (EDF) is solved in the three-dimensional wave-number mesh space.¹⁾ On top of the HFB states, the QRPA equation in the A - B matrix form¹⁾ is solved for the TV MOI:

$$\mathcal{J}_{\text{TV}} = 2 \sum_{kk', ll'} (J_x)_{kk'}^* (A + B)_{kk', ll'}^{-1} (J_x)_{ll'}. \quad (1)$$

The Skyrme SkM* EDF predicts the neutron drip line at ^{44}Mg . The quadrupole deformations of $^{34}, ^{36}, ^{38}, ^{40}, ^{42}, ^{44}\text{Mg}$ are $\beta = 0.35, 0.30, 0.28, 0.28, 0.21,$

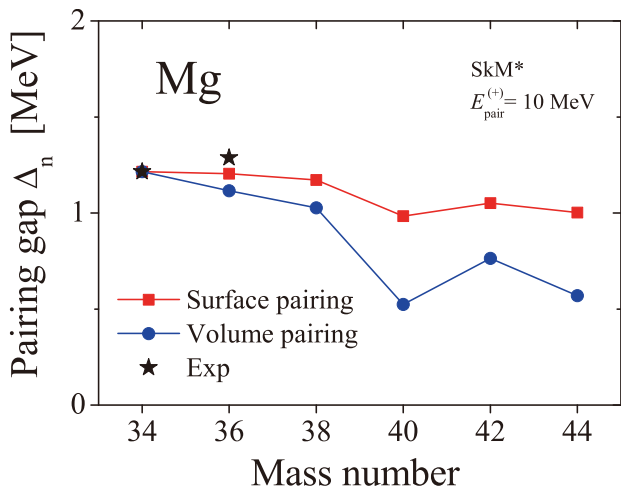


Fig. 1. Neutron pairing gaps Δ_n in neutron-rich Mg isotopes. The results obtained using the surface-type and volume-type pairing forces are compared with the experimental data.

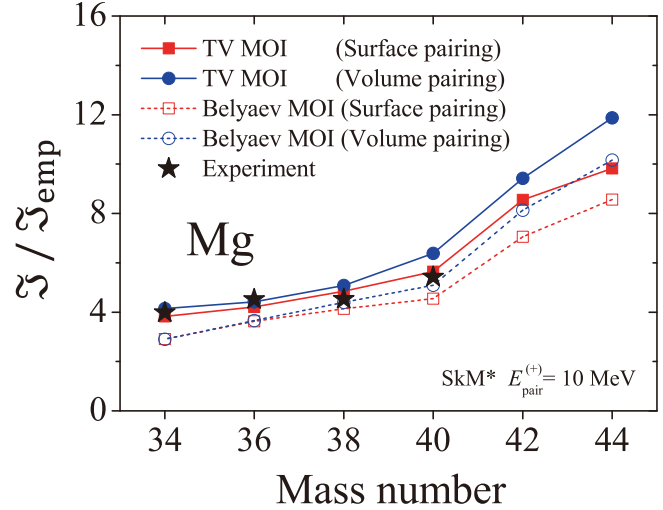


Fig. 2. Same as Fig. 1 but for the Thouless-Valatin (TV), Belyaev, and experimental MOIs. They are divided by the empirical value.

and 0.15 respectively. Figure 1 shows the neutron pairing gaps Δ_n in neutron-rich Mg isotopes. The pairing gaps Δ_n are almost constant in calculation using the surface-type pairing force. This pairing force has a strong continuum-coupling effect and creates dineutron correlation around ^{40}Mg .^{1,2)} The continuum-coupling effect is weak in the volume-type pairing force, and the neutron pairing gaps Δ_n decrease as a function of mass number A .

Figure 2 shows the TV MOIs in neutron-rich Mg isotopes. The Belyaev MOIs, in which the residual interactions in QRPA are neglected, are also shown. They are divided by the empirical value $\mathcal{J}_{\text{emp}} = \beta^2 A^{7/3} / 400$ [MeV⁻¹]. The TV MOIs using the surface-type pairing force agree well with the experimental values, whereas the Belyaev MOIs underestimate the experimental values by about 20%.

The ratios of TV MOIs $\mathcal{J}_{\text{TV}} / \mathcal{J}_{\text{emp}}$ are almost constant in Mg isotopes with $A \leq 40$, but they are substantially enhanced in $^{42}, ^{44}\text{Mg}$ owing to the weak-binding effect.

In conclusion, it is emphasized that the experimental MOIs in neutron-rich Mg isotopes are well reproduced by the TV MOIs using the surface-type pairing force, which creates dineutron correlations. The difference between the TV MOIs using the surface-type and volume-type pairing forces increases on approaching the neutron drip line, and the difference is 20.7% in ^{44}Mg .

References

- 1) M. Yamagami, Phys. Rev. C **100**, 054302 (2019).
- 2) M. Yamagami *et al.*, Phys. Rev. C **77**, 064319 (2008).

^{*1} Department of Computer Science and Engineering, University of Aizu

x_F dependence of the transverse single spin asymmetry of very forward π^0 production in 510 GeV $p^\uparrow + p$ collisions

M. H. Kim^{*1,*2} for the RHICf collaboration

The transverse single spin asymmetry, A_N , of very forward ($\eta > 6$) π^0 was first measured in the RHICf experiment¹⁾ in June, 2017 from polarized $p + p$ collisions at $\sqrt{s} = 510$ GeV. The A_N is defined as $(d\sigma_{\text{Left}} - d\sigma_{\text{Right}})/(d\sigma_{\text{Left}} + d\sigma_{\text{Right}})$, where $\sigma_{\text{Left(Right)}}$ is the particle production cross sections in the left (right) side of the polarization direction of the proton beam. The A_N of very forward π^0 is a powerful observable to investigate the contribution from the non-perturbative process to the non-zero A_N of π^0 , which has been measured in many experiments²⁻⁴⁾ thus far.

In order to measure the very forward π^0 precisely, an electromagnetic calorimeter, the RHICf detector, was installed at the zero-degree area of the STAR experiment at Relativistic Heavy Ion Collider, which was 18 m away from the beam collision point. The configuration of the RHICf detector can be found in Ref. 5). The RHICf detector has an energy resolution of 2.5–3.5% for 100–250 GeV π^0 and a transverse momentum (p_T) resolution of 0.005–0.025 GeV/ c for 0.0–0.8 GeV/ c π^0 .

The experiment was conducted for 28 h with three vertical detector positions, where the beam propagated towards the center of the large tower, center of the small tower, and a point 24 mm below the center of the small tower of the detector before the collisions. With the three detector positions, we requested radial polarization, which was the direction at an angle of 90° from the usual vertical polarization at RHIC, and a large $\beta^* = 8$ m so as to measure the wide p_T range with higher resolution. The kinematic coverage of the measured π^0 is $x_F > 0.25$ and $0.0 < p_T < 1.0$ GeV/ c , where the non-perturbative process was expected to mainly contribute to the π^0 production.

Figure 1 shows our preliminary result for the A_N of very forward π^0 as a function of x_F for five different p_T ranges. The line and box error bars represent statistical and systematic uncertainties, respectively. The estimation; of the polarization; beam center, which is defined as the extrapolated zero-degree position of the beam to the detector; and background (mostly from the two-photon coincidence of different π^0) were the three main systematic sources. See Ref. 6) for more details on the analysis procedure and systematic study.

In Fig. 1, the A_N s are consistent with zero at a very low $p_T < 0.09$ GeV/ c . However, its slope with respect to the x_F -axis becomes steeper as p_T increases. When $p_T > 0.36$ GeV/ c , the increasing A_N shows the same slope with the previous forward ($2 < \eta < 4$) π^0 measurements²⁻⁴⁾ even in the low- p_T region where only the

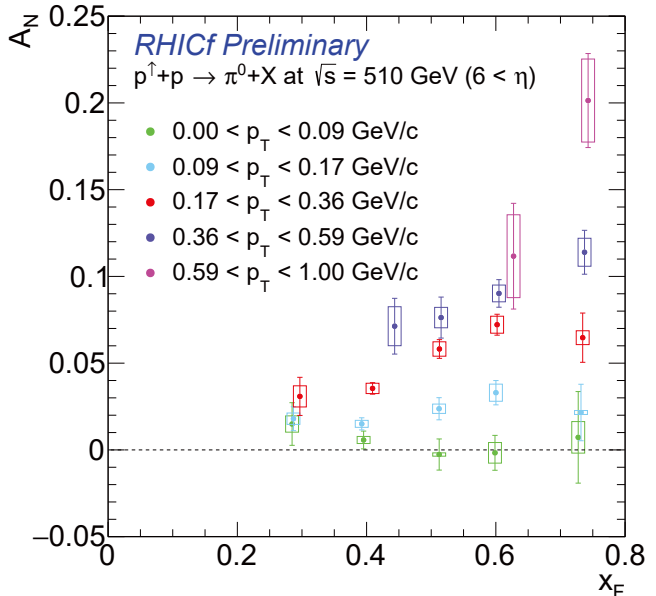


Fig. 1. Preliminary result of the A_N of very forward π^0 production as a function x_F . The five different colors correspond to different p_T ranges.

non-perturbative process is expected to be dominant. It might be possible that the non-perturbative process can contribute to the non-zero A_N of π^0 at a higher p_T .

The result also raises the necessity of further experimental efforts to compare the roles of the perturbative and non-perturbative processes in the A_N of π^0 and the measurement of the intermediate kinematic region where both processes possibly contribute ($0.8 < p_T < 2.0$ GeV/ c). Combined analysis with STAR forward and Roman pot⁷⁾ detectors is useful to separate each process by measuring the rapidity gap or tagging a proton scattered at a very low angle, which are the characteristics of the diffraction of the non-perturbative process.

References

- 1) RHICf Collaboration, arXiv: 1409.4860 [physics.ins-det].
- 2) D. L. Adams *et al.* (FNAL-E581 and E704 Collaborations), Phys. Lett. B **261**, 201 (1991).
- 3) A. Adare *et al.* (PHENIX Collaboration), Phys. Rev. D **90**, 012006 (2014).
- 4) B. I. Abelev *et al.* (STAR Collaboration), Phys. Rev. D **101**, 222001 (2008).
- 5) M. H. Kim for the RHICf Collaboration, RIKEN Accel. Prog. Rep. **52**, 83 (2019).
- 6) M. H. Kim for the RHICf Collaboration, arXiv:1902.07852 [hep-ex].
- 7) S. Bültmann *et al.* Nucl. Instrum. Methods Phys. Res. **535**, 415 (2004).

*1 Department of Physics, Korea University

*2 RIKEN Nishina Center

Non-evaporable getter-based differential pumping system for SRILAC

H. Imao,^{*1} K. Yamada,^{*1} N. Sakamoto,^{*1} T. Watanabe,^{*1} Y. Watanabe,^{*1} K. Oyamada,^{*2} A. Yusa,^{*2} and O. Kamigaito^{*1}

Upgrades of the RIKEN heavy-ion linac (RILAC) involving a new superconducting linac (SRILAC¹) are in progress. High-vacuum ($<10^{-8}$ Pa) and particulate-free conditions are strictly necessary for keeping the performance of the superconductive radio frequency (SRF) cavities of SRILAC. It is crucially important to develop neighboring warm sections to mitigate the large difference in the vacuum and clean conditions with respect to the existing old RILAC and beamlines built almost four decades ago. In the present study, a non-evaporable getter (NEG)-based differential pumping system (DPS) has been developed.

The three-stage DPS (Fig. 1) was designed to achieve a pressure reduction from the existing beamline vacuum (10^{-5} – 10^{-6} Pa) to an ultra-high vacuum of less than 10^{-8} Pa in the SRF cavities within a very limited length of only 75 cm, ensuring a beam aperture greater than 40 mm. The properties of pumps we used for the DPS are summarized in Fig. 1. Optimizations of the design were performed with Molflow+²). We measured the pressures of three stages in a prototype DPS when we leaked N_2 and H_2 with three different leak rates, respectively. The observed pressures are in good agreement with the calculated ones (Fig. 2). The DPS also has fast closing gate valve (Series 75.2; VAT Group AG) responses within 10 ms after receiving the signal of the pressure rise of three distributed cold-cathode gauges to protect the SRF systems from unexpected vacuum breaks. Compact electrostatic particle suppressors (EPSs) were equipped at the inside of the first-stage chambers of the DPSs to suppress the scattering of particles and reduce possibi-

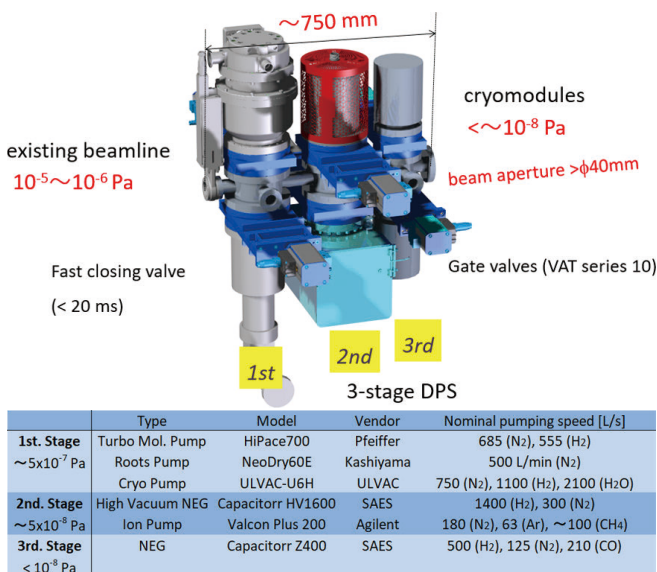


Fig. 1. Design of three-stages DPS and pump properties.

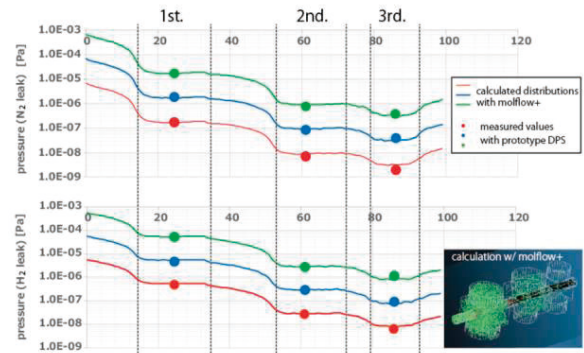


Fig. 2. Pressure distributions for N_2 and H_2 leakage.

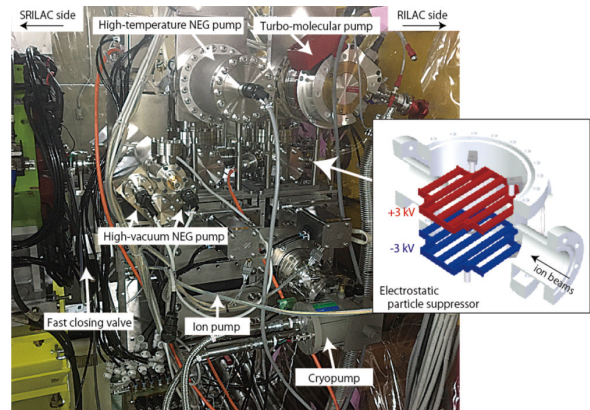


Fig. 3. Photograph of the DPS and the EPS.

ties to transport particles to the SRF cavities. The EPS consists of two electrodes, each of which consists of 6 stainless-steel bars, as shown in Fig. 3. Some particle tests with the EPS in air and vacuum were performed with a vacuum particle sensor (VACUUM PARTICLE SENSOR; Wexx Co., Ltd). Ceramic and metal particles were artificially generated by scraping blocks. The counts were significantly reduced when we applied a high voltage on the electrodes. The vacuum in the beamlines becomes an ionizing environment due to the energetic heavy ions passing during the operation. We expect that the EPS can suppress particle transport to the SRF cavities.

All components (chambers, pumps, valves, vacuum gauges, etc.) were cleaned and assembled in a clean room of ISO class 1. The installation of the pair DPSs was completed in December 2019. Some pumps are equipped in the horizontal direction to prevent particle falls (Fig. 3). We already confirmed that the desired pressure reductions were successfully achieved, and actual operations will start soon.

References

- 1) N. Sakamoto *et al.*, Proc. LINAC'18, Beijing, WE2A03 (2017).
- 2) Molflow+, <http://molflow.web.cern.ch/>.

^{*1} RIKEN Nishina Center

^{*2} Sumitomo Heavy Industries Accelerator Science Ltd.

Calibration of the beam energy position monitor system for the RIKEN superconducting acceleration cavity[†]

T. Watanabe,^{*1} H. Imao,^{*1} O. Kamigaito,^{*1} N. Sakamoto,^{*1} N. Fukunishi,^{*1} M. Fujimaki,^{*1} K. Yamada,^{*1} Y. Watanabe,^{*1} T. Toyama,^{*2} T. Miyao,^{*2} A. Miura,^{*3} K. Hanamura,^{*4} T. Kawachi,^{*4} R. Koyama,^{*5} and A. Kamoshida^{*1,*6}

Upgrades for the RIKEN Heavy-ion Linac that involve a new Superconducting Linac (SRILAC) are currently underway to promote super-heavy element searches and the radioactive isotope (RI) production of astatine (²¹¹At) for medical use.^{1,2} We have developed a beam energy position monitor (BEPM) system³) that can simultaneously measure not only the beam position but also the beam energy by measuring the time of flight of the beam. By using parabolic-shaped electrodes (Fig. 1), we realized the ideal linear response of the quadrupole moments while maintaining good linear position sensitivity. We fabricated 11 BEPMs and a position calibration system employing the wire method that we used to obtain the sensitivity and offset of the BEPMs.

Destructive monitors generate outgassing; if they are used, it becomes difficult to maintain the Q value and surface resistance of the superconducting radio frequency (SRF) cavities over a long period of time. It is, therefore, crucial to develop nondestructive beam measurement diagnostics. With the aim of measuring the beam position at an overall accuracy of ± 0.1 mm, a calibration measurement was performed at the KEK campus in Tokai.

Because there are 3 types of BEPMs for the SRILAC,³) we designed and fabricated dummy pipes that surround the wire and jigs to mechanically fit the calibration device. The calibration device is shown in Fig. 2. The BEPM to be calibrated is connected to a dummy pipe with an inner diameter equal to that of one of the BEPMs (Fig. 2(a)). The assembly is fixed to an XY stage that moves within the measurement region in 2-mm steps. A wire acting as a signal source is fixed. Round crimp terminals are attached by crimping and soldering at both

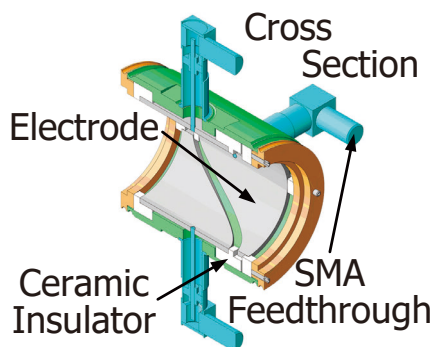


Fig. 1. Parabolic-shaped electrodes.

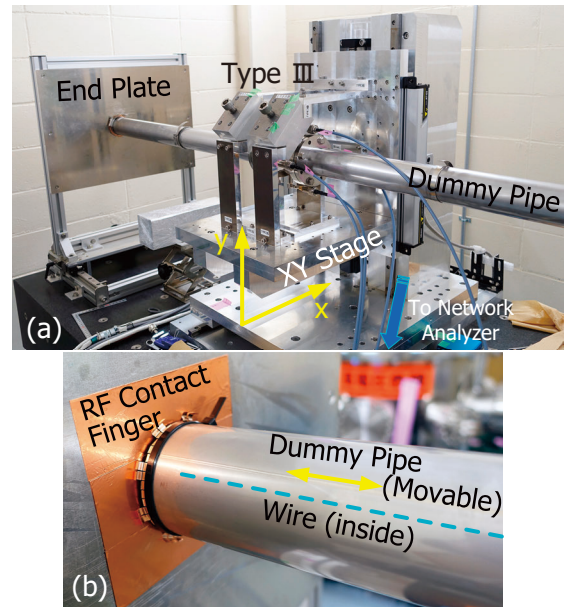


Fig. 2. Photographs of the calibration measurement device, jigs, and dummy pipes.

ends of a copper-plated piano wire. The dummy duct has a double-pipe structure that can be expanded and contracted. When the round-crimp terminals are connected to the electrode on both end plates, the inner dummy pipes are made to slide into the outer dummy pipe to provide sufficient space for the connection of the electrodes. After that operation is completed, the inner dummy pipes are restored to their original position and fixed to the double pipe by fastening bands. Adequate tension can be applied by moving one of the end plates outward with fine adjustment. The dummy pipes are connected to the end plates with an RF contact finger and are held to the ground potential (Fig. 2(b)). When the measurement was repeated, it was found that both the required electrical characteristics and flexibility could be achieved simultaneously by reducing the number of RF contact fingers and applying copper tape to the end plates. As a result, measurement errors were drastically reduced.

By using the calibration device, the calibration was completed to within ± 0.05 mm mechanical accuracy. We will continue to analyze the measurement results of all the BEPMs, which will be used to measure the beam position and energy using the calibration values when the beam is accelerated at SRILAC.

References

- 1) N. Sato *et al.*, RIKEN Accel. Prog. Rep. **50**, 262 (2017).
- 2) S. Yano *et al.*, RIKEN Accel. Prog. Rep. **50**, 263 (2017).
- 3) T. Watanabe *et al.*, Proc. 15th Ann. Meet. of Particle Accel. Soc. Jpn., Nagaoka, Japan, 2018-Aug. (2018), p. 49.

[†] Condensed from the the proceedings in 2019 International Beam Instrumentation Conference (IBIC 2019)

^{*1} RIKEN Nishina Center

^{*2} KEK/J-PARC, Tokai

^{*3} JAEA/J-PARC, Tokai

^{*4} Mitsubishi Electric System & Service Co., Ltd., Tokai

^{*5} SHI Accelerator Service Ltd., Wako

^{*6} National Instruments Japan Corporation, Tokyo

Intermediate silicon tracker development for sPHENIX experiment at RHIC

I. Nakagawa,^{*1} Y. Akiba,^{*1} D. Cacace,^{*2} K. Cheng,^{*3} E. Desmond,^{*2} T. Hachiya,^{*1,*4} S. Hasegawa,^{*5} T. Kondo,^{*6} C. Kuo,^{*3} M. Lenz,^{*2} E. Mannel,^{*2} C. Miraval,^{*2} M. Morita,^{*4} R. Nouicer,^{*2} R. Pisani,^{*2} M. Shibata,^{*4} C. Shih,^{*3} A. Suzuki,^{*4} T. Todoroki,^{*1} X. Wei,^{*7} and R. Xiao^{*7}

The construction of sPHENIX detector¹⁾ has been started since the sPHENIX was approved for the Project Decision-2/3 (corresponds to DOE's Critical Decision-2/3) in May, 2019. The subsystem detectors are now under mass production. We have been developing the one of the tracking devices of sPHENIX called INTermediate Tracker (INTT), which consisted of 2 layers of a silicon strip sensor. The INTT is the only tracker which has better than 1 beam clock resolution in sPHENIX trackers. It provides thus the timing of particle trajectories. A telescope was assembled with 3 layers of prototype ladder for the first beam test in March, 2018 at Fermilab test beam facility (FTBF). The prototype detector demonstrated satisfactory position resolution as designed and about 96% detection efficiency using well focused 120 GeV proton beam.

The design of silicon sensor and the high density interconnect readout cable were finalized after the first beam test. The next prototypes were considered as pre-production versions and new silicon ladders were assembled again to be tested in the next round beam



Fig. 1. The INTT collaboration at the Fermilab test beam facility in June 2019.

*1 RIKEN Nishina Center
 *2 Brookhaven National Laboratory
 *3 National Central University
 *4 Nara Women's University
 *5 Japan Atomic Energy Agency
 *6 Tokyo Metropolitan Industrial Technology Research Institute
 *7 Purdue University

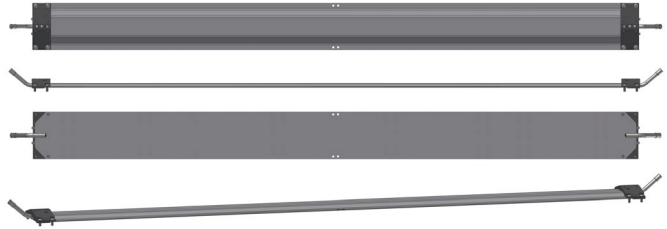


Fig. 2. The latest stave design (liquid cooling type).

test at FTBF in June, 2019. The performance of the pre-production ladders are discussed in Ref. 2). The attempt to reproduce observed performance by a GEANT MC simulation is in progress. The very first attempt was made in this beam test to accumulate data with the full chain of the INTT readout system including the 1.2 meter long bus extension cable.³⁾ Technologically, it is the most challenging R&D of the INTT project.

The stave is the support structure of the INTT module which consisted of silicon sensors and HDI. It requires not only the stiffness, but also high thermal conductivity in order to remove heat generated from the read out chips mounted on the HDI. The stave is made of a carbon fiber reinforced plastic and its prototyping has been proceeded in Asuka Co. in Japan and Lawrence Berkley National Laboratory in parallel. The latest stave is designed to be (Fig. 2) a liquid cooling type using a carbon fiber composite tube laid out in the middle of the stave. The fabrication of the latest design has been procured in Asuka Co.

The development of the INTT detector is thus in the final stage, the preparation for the mass production is in progress. Produced all silicon sensors are to be tested and evaluated in National Central University, Taiwan.⁴⁾ The ladder assembly is to be performed in both National Taiwan University⁵⁾ and BNL.⁶⁾ The mechanical design of the INTT ladders, readout chain, and support structure is discussed in Ref. 7).

References

- 1) Conceptual Design Report of sPHENIX (2018).
- 2) A. Suzuki *et al.*, in this report.
- 3) T. Hachiya *et al.*, in this report.
- 4) K. Chen *et al.*, in this report.
- 5) C. Shih *et al.*, in this report.
- 6) M. Connor *et al.*, in this report.
- 7) D. Cacace *et al.*, in this report.

Update of MOCO for the MPV system

H. Baba,^{*1} T. Ichihara,^{*1} T. Isobe,^{*1} T. Ohnishi,^{*1} K. Yoshida,^{*1} Y. Watanabe,^{*1} S. Ota,^{*2} H. Shimizu,^{*2} S. Shimoura,^{*2} S. Takeuchi,^{*2} D. Nishimura,^{*3,*2,*1} J. Zenihiro,^{*4,*1} A. O. Tokiyasu,^{*5} and R. Yokoyama^{*6}

We have been developing a data acquisition (DAQ) system. VME-bus-based DAQ systems are widely utilized in RIBF. To speed up the VME DAQ system, a mountable controller (MOCO)¹⁾ was developed and introduced in some experiments²⁾ in 2016. We could achieve very good DAQ performance; at the same time, problems on the usability and robustness were found. To establish a robust and easy-to-use system, we developed a new MOCO with parallelized VME (MPV), which is a type of parallel readout extension of VME.³⁾ The system architecture is described in Ref. 3). In this contribution, we report the update of MOCO to adopt the MPV system.

The original MOCO and new versions (prototype and production) of MOCO-MPV boards are shown in Fig. 1. In the original MOCO, trigger and data communications are performed using the LVDS I/O and USB interface. On the other hand, these communications between the MPV controller and MOCO-MPV are realized through four differential lines (LVDS I/O) that are patterned on the MOCO-MPV board. These differential lines are assigned as follows: 1) 100-MHz clock, 2) command packet, 3) data packet A, and 4) data packet B. The 100-MHz clock and the command packets are distributed from the controller. All commutations are synchronized

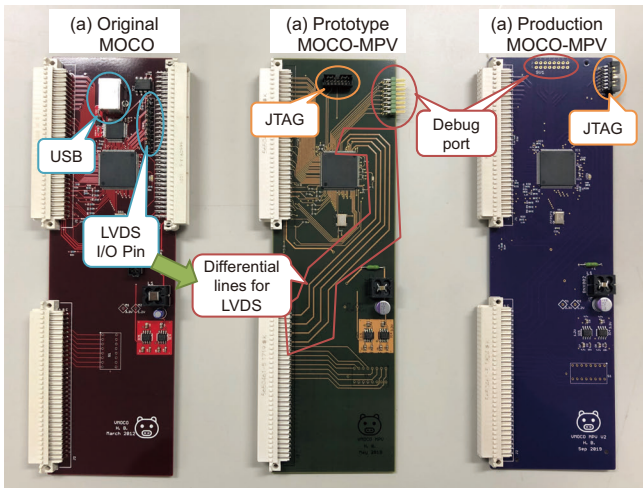


Fig. 1. Photograph of different versions of MOCO. The functionalities of the prototype and production MOCO-MPV boards are the same. However, the positions of the JTAG and debug port connectors are different.

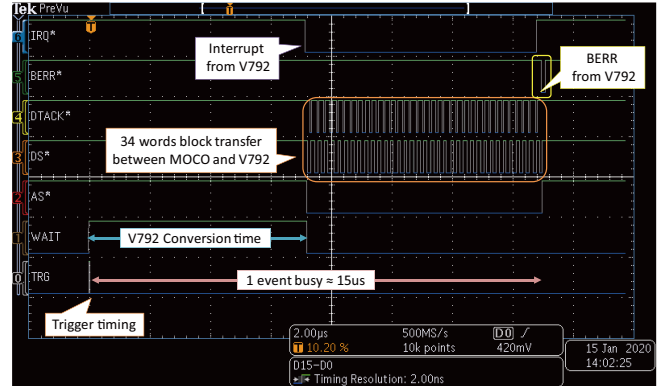


Fig. 2. Monitor signals between MOCO and CAEN V792 QDC captured by Tektronix MDO3034 through the debug port of the prototype MOCO-MPV board.

with this 100-MHz clock. MOCO-MPV sends 200-Mbps data at maximum by using two data packet lines to the controller. This 200-Mbps data throughput is sufficient because the maximum data rate of a typical 32-bit VME module is 160 Mbps (in experiments at RIBF, this data rate is usually much less than 20 Mbps per VME module). An eight-port debug interface is additionally implemented on the MOCO-MPV board to monitor the bus signals between MOCO and a VME module. Figure 2 shows the signals of MOCO-MPV reading out data from CAEN V792 QDC. MOCO-MPV waits for the interrupt signal of V792, and the block transfer is started when the interrupt signal is issued. After 34×32 -bit data read out, the BERR signal is generated from V792, following which this block transfer is terminated. Including the conversion time of V792, the duration of the one event busy is only $15 \mu\text{s}$. In the original MOCO case, DC power is supplied via the DIN41612 female connector (right-side connector) because the board is designed to place the front side of the VME backplane. In contrast, since the MOCO-MPV board is installed at the rear side, both DC power and VME bus signals pass through the DIN41612 male connectors (two left-side connectors).

The MPV system with the prototype MOCO-MPV board was successfully introduced in the NP1512-RIBF79R1-02 experiment⁴⁾ in November 2019 for the first time. Legacy VME DAQ systems in RIBF will be gradually replaced by the MPV system together with the production MOCO-MPV board.

^{*1} RIKEN Nishina Center
^{*2} Center for Nuclear Study, University of Tokyo
^{*3} Department of Natural Sciences, Tokyo City University
^{*4} Department of Physics, Kyoto University
^{*5} ELPH, Tohoku University
^{*6} Department of Physics and Astronomy, University of Tennessee

References

- 1) H. Baba *et al.*, RIKEN Accel. Prog. Rep. **45**, 9 (2012).
- 2) H. Baba *et al.*, RIKEN Accel. Prog. Rep. **50**, 224 (2017).
- 3) H. Baba *et al.*, RIKEN Accel. Prog. Rep. **52**, 146 (2019).
- 4) J. Zenihiro *et al.*, in this report.

Offline measurement of mass and correlated decay properties using radioactive ^{224}Ra source via MRTOF+ α -TOF detector

T. Niwase,^{*1,*2,*3} M. Wada,^{*3} P. Schury,^{*3} H. Haba,^{*2} S. Ishizawa,^{*5,*2,*3} Y. Ito,^{*4} D. Kaji,^{*2} S. Kimura,^{*2} H. Miyatake,^{*3} K. Morimoto,^{*2} K. Morita,^{*1,*2} M. Rosenbusch,^{*2} H. Wollnik,^{*6} T. Shanley,^{*7} and Y. Benari^{*7}

Recently, we newly developed a detector called the “ α -TOF” detector¹⁾ for the measurement of mass and correlated decay properties by using a multi-reflection time-of-flight mass spectrograph (MRTOF-MS).²⁾ We performed realistic performance tests using a ^{224}Ra source. The source, produced by a chemical separation from a ^{228}Th source,³⁾ was placed in a cryogenic gas cell.

Ions of ^{220}Rn and ^{216}Po produced by the decay of ^{224}Ra were thermalized in the gas cell and extracted using an RF carpet, transported to the MRTOF-MS preparation traps, and injected into the MRTOF-MS for the correlated measurement of the time of flight (ToF) and α -decay. ^{220}Rn and ^{216}Po have half-lives of 55.6 s and 145 ms with characteristic α -particle energies of 6.29 MeV and 6.78 MeV, respectively. During this measurement, the MRTOF was operated for only 2 laps inside the MRTOF reflection chamber. This was sufficient to unambiguously determine the A/q value with a mass resolving power of $R_m \approx 1500$ with a wide mass bandwidth.

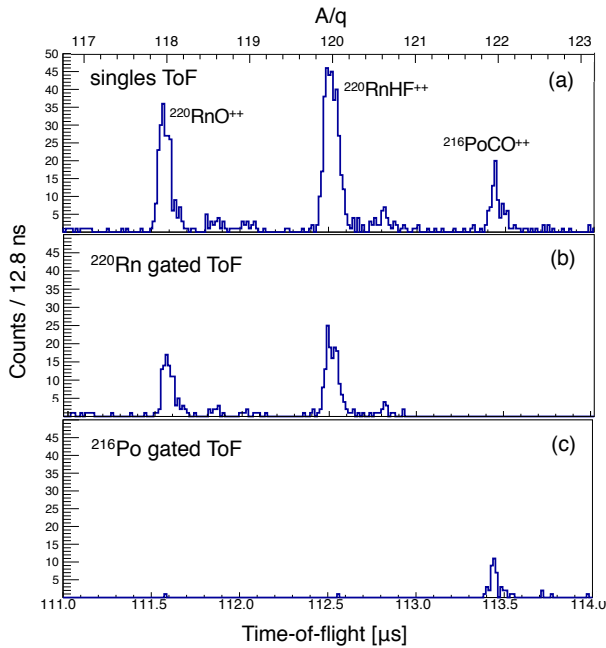


Fig. 1. (a) Singles ToF spectrum. (b) ToF spectrum in coincidence with ^{220}Rn α -decays obtained using a time gate of $T_c = 180$ s. (c) ToF spectrum in coincidence with ^{216}Po decays with $T_c = 450$ ms.

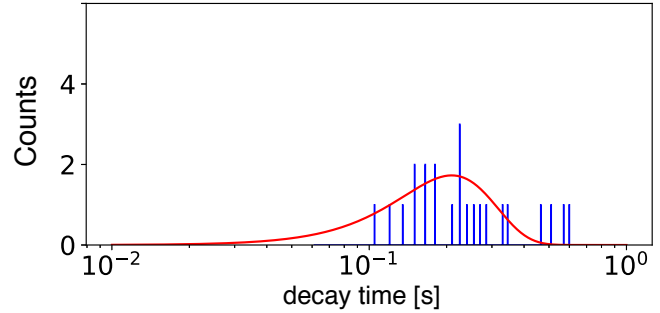


Fig. 2. Distribution of decay time of $^{216}\text{PoCO}^{++}$. The solid line indicates a distribution curve drawn with values obtained from the literature.

Figure 1 shows the ToF spectrum of ^{220}Rn and ^{216}Po . ToF and α -decay signals were recorded event by event with absolute time stamps. Figure 1(a) shows the singles ToF spectrum. By using a coincidence time gate (T_c) prior to the detection of an α -decay signal, it is possible to discriminate between ToF events corresponding to ^{220}Rn and ^{216}Po , as shown in Fig. 1(b) and (c), respectively. To identify the peak of ^{216}Po , a ± 150 keV energy gate was used for the α -decay signal at approximately 6.78 MeV with $T_c = 450$ ms corresponding to three half-life periods. To identify the peak of ^{220}Rn , a similar gate was made on the 6.29 MeV α -decay signal with $T_c = 180$ s.

Using the α -decay correlated ToF event, we determined that the ToF peak occurs at $A/q = 118$ and 120 from ^{220}Rn events and $A/q = 122$ from ^{216}Po events. The limited mass resolution of the wide mass bandwidth measurement precluded precise molecular identification. However, based on past experience, we have tentatively assigned the $A/q = 118$, 120 and 122 peaks to $^{220}\text{RnO}^{++}$, $^{220}\text{RnHF}^{++}$ and $^{216}\text{PoCO}^{++}$, respectively. In addition, by defining the decay time as the time interval between the α -signal and the ToF event, we demonstrated the ability to measure half-lives with the α -TOF detector. Figure 2 shows a plot of the measured decay time of $^{216}\text{PoCO}^{++}$ ions along with the expected decay time distribution function based on the value reported in the literature. We evaluated the half-life of ^{216}Po as $T_{1/2} = 123(22)$ ms, which is in good agreement with the literature value of 145(2) ms.

*1 Department of Physics, Kyushu University
 *2 RIKEN Nishina Center
 *3 Wako Nuclear Science Center (WNSC), KEK
 *4 Japan Atomic Energy Agency
 *5 Yamagata University
 *6 New Mexico State University
 *7 ETP Ion Detect

References

- 1) T. Niwase *et al.*, Nucl. Instrum. Methods Phys. Res. A **953**, 163198 (2020).
- 2) P. Schury *et al.*, Nucl. Instrum. Methods Phys. Res. B **335**, 39(2014).
- 3) J. Narbutt *et al.*, Appl. Radiat. Isot. **49**, 89–91(1998).

Offline collinear laser spectroscopy of barium II toward measurement of RIs at SLOWRI facility

M. Tajima,^{*1} A. Takamine,^{*1} Y. Sasaki,^{*2,*1} T. Asakawa,^{*2,*1} H. Iimura,^{*3,*1} M. Wada,^{*4} H. A. Schuessler,^{*5,*1} Y. Matsuo,^{*2,*1} and H. Ueno^{*1}

The laser spectroscopy of atomic transitions is sensitive to nuclear structures in ground or metastable states. In particular, the measurement of isotope shifts and hyperfine splittings by collinear laser spectroscopy has been a powerful tool to study RIs. Charge radii, quadrupole deformation, and electromagnetic moments have been elaborately measured at ISOL-type facilities such as ISOLDE at CERN. However, the available nuclei are limited by chemical properties and lifetime with the ISOL technique. On the other hand, the gas cell decelerator facility, SLOWRI,¹⁾ which is being developed in RIKEN, will supply low-emittance and low-energy RI beams including refractory elements and short-lived ($\gtrsim 10$ ms) nuclei, which are difficult to obtain from the ISOL-type facility. We are preparing for collinear laser spectroscopy by taking advantage of slow RI beams delivered from SLOWRI.

As a test of the system for collinear laser spectroscopy, we performed the spectroscopy of barium ions. Barium was chosen because its ion production is relatively easy and an existing dye laser is capable of inducing one of the strong transitions, $5d^2D_{5/2}-6p^2P_{3/2}$ (614 nm). A surface ionization source was constructed to obtain Ba^+ based on the design previously used at JAEA.²⁾ Barium oxide was heated up to approximately 2000 K and a few nA of Ba^+ were constantly produced. It was extracted at 10.5 keV, focused by electrostatic lenses, isotope-separated by a magnet, and focused again to enter an observation region. A continuous-wave (CW) dye laser (Coherent 899 Ring Laser) with Kiton Red pumped by a solid-state laser (Verdi V10, 6 W) was irradiated collinearly with the Ba^+ beam. The power was ~ 0.3 mW in the observation region. The laser wavelength was locked at 614.10433 nm by utilizing feedback signals from a wavelength meter (HighFinesse WS-U-10). The full width at half maximum (FWHM) of the laser frequency was ~ 5 MHz. In the observation region, the velocity of ions was changed using a set of electrodes. When the velocity was tuned according to the Doppler shift, the ion was at resonance, and spontaneous emission from $6p^2P_{3/2}$ to $6s^2S_{1/2}$ (455 nm) successively occurred. This fluorescence signal was detected by a photomultiplier (Burle 8850). The quantum efficiency of the photomultiplier was about 20% at 455 nm, but the efficiency was less than 1% at 614 nm. Therefore, this

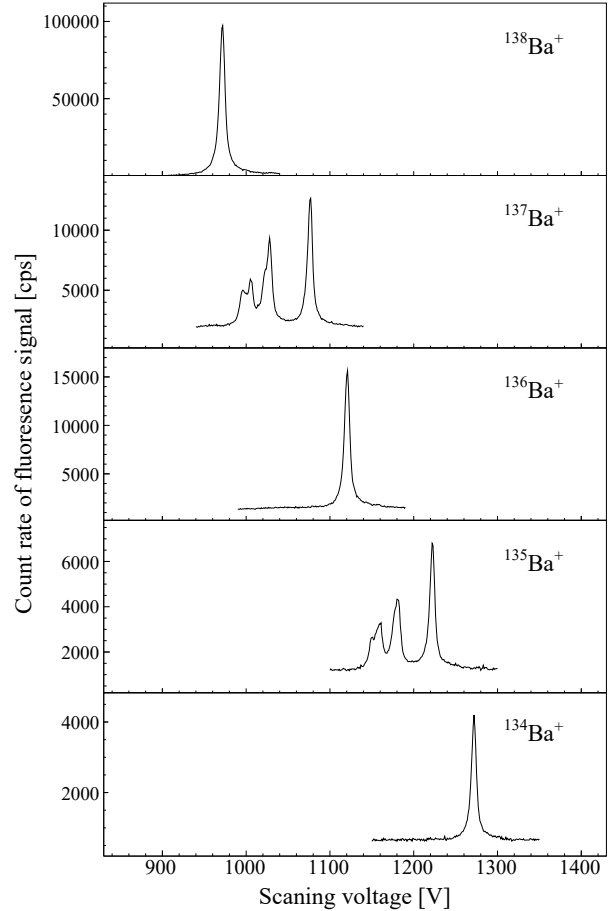


Fig. 1. Resonance spectra for the isotopes $^{134-138}Ba^+$ showing the transition $5d^2D_{5/2}-6p^2P_{3/2}$.

measurement is almost free of background counts due to stray laser light. Figure 1 shows the count rate of the fluorescence signal as a function of the voltage applied to the Doppler-shift-tuning electrodes. Isotope shifts and hyperfine splittings for $^{135,137}Ba^+$ with the nuclear spin $I = 3/2$ were successfully observed.

Trajectory simulations suggest that the resonance spectrum becomes asymmetric due to misalignment of the laser and ion beams, which can be a main systematic error. Detailed analysis is ongoing. We plan to introduce a fine-tuning system of alignment before online measurement.

References

- 1) M. Wada, Nucl. Instrum. Methods Phys. Res. B **317**, 450 (2013).
- 2) S. Ichikawa *et al.*, Nucl. Instrum. Methods Phys. Res. A **274**, 259 (1989).

^{*1} RIKEN Nishina Center

^{*2} Faculty of Science and Engineering, Hosei University

^{*3} JAEA

^{*4} Wako Nuclear Science Center, KEK

^{*5} Department of Physics and Astronomy, Texas A&M University

Angle-tunable wedge degrader for an energy-degrading RI beamline[†]

J. W. Hwang,^{*1} S. Michimasa,^{*1} S. Ota,^{*1} M. Dozono,^{*1} N. Imai,^{*1} K. Yoshida,^{*2} Y. Yanagisawa,^{*2} K. Kusaka,^{*2} M. Ohtake,^{*2} D. S. Ahn,^{*2} O. Beliuskina,^{*1} N. Fukuda,^{*2} C. Iwamoto,^{*1} S. Kawase,^{*3} K. Kawata,^{*1} N. Kitamura,^{*1} S. Masuoka,^{*1} H. Otsu,^{*2} H. Sakurai,^{*2} P. Schrock,^{*1} T. Sumikama,^{*2} H. Suzuki,^{*2} M. Takaki,^{*1} H. Takeda,^{*2} R. Tsunoda,^{*1} K. Wimmer,^{*4} K. Yako,^{*1} and S. Shimoura^{*1}

The Optimized Energy-Degrading Optics (OEDO) beamline¹⁾ was established at RIBF to produce 10–50-MeV/nucleon beams by slowing down secondary beams from the BigRIPS separator. This beamline can extend the energy range of RI beams that can be produced in RIBF to optimize nuclear reactions such as nucleon transfer and Coulomb excitation.

The angle-tunable degrader, one of the key elements in the OEDO beamline, is a monoenergetic degrader that reduces the beam energy and spread of a beam. It consists of two Al sheets with a quadratic cross section, the quadratic coefficients of which have opposite signs. While its central thickness is fixed at 3 mm, the wedge angle varies from 0 to 40 mrad according to the relative positions of the two sheets. The effective area is ± 30 mm (H) \times ± 50 mm (V), which is wide enough for the typical beam width, ± 20 mm. The average thickness deviations for sheets 1 and 2 are 33 and 58 μm , respectively. The total central thickness can be increased by introducing an additional Al flat degrader immediately behind our system.

Figure 1 shows the whole system. For parallel and separate movement of the sheets, the system includes guides for the sheets, two parallel rails, and two linear stepper motors. Each motor drives each Al sheet along the corresponding rail. Because the motors operate independently by remote control, we can optimize the wedge angle using real-time data.

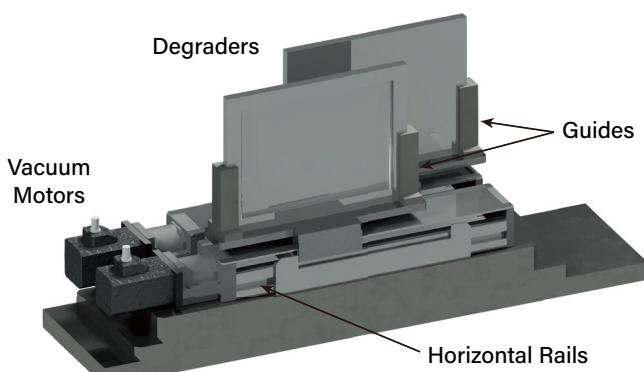


Fig. 1. 3D design of the angle-tunable degrader system.

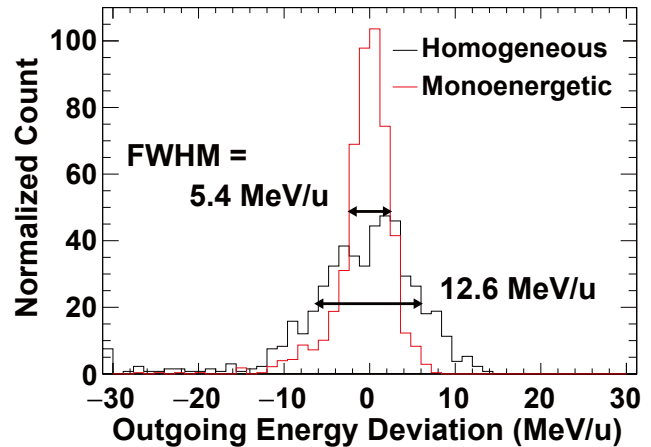


Fig. 2. Distributions of the outgoing energy spread using a homogeneous and monoenergetic degrader. All distributions were normalized to have the same number of events.

An experiment for evaluating the system performance was carried out at the OEDO beamline in RIBF. A 171-MeV/nucleon ^{79}Se beam was produced by the in-flight fission of a 345-MeV/nucleon ^{238}U beam impinging on a 5-mm-thick Be target and was transported to the OEDO beamline. The degrader system at the dispersive focus (FE9) in the OEDO beamline was optimized to obtain the 40-MeV/nucleon beam. The central thickness was set to 6 mm by placing a 3-mm-thick flat Al plate behind the system.

The performance of energy compression was evaluated by comparing the outgoing energy deviations using a monoenergetic degrader (the optimized wedge angle) to a homogeneous degrader (0 mrad setting). Figure 2 shows that the spread in the homogeneous case is 12.6 MeV/nucleon in full width at half maximum (FWHM). The monoenergetic degrader reduced the spread to 5.4 MeV/nucleon, which is similar to the estimated value of 5.2 MeV/nucleon. The performance of the system was estimated as satisfactory and its flexible wedge angle is useful to deal with many different nuclides and energies for various purposes.

Reference

- 1) S. Michimasa *et al.*, Prog. Theor. Exp. Phys. **2019**, 043D01 (2019).

[†] Condensed from the article in Prog. Theor. Exp. Phys. **2019**, 043D02 (2019), see also references therein

^{*1} Center for Nuclear Study, the University of Tokyo

^{*2} RIKEN Nishina Center

^{*3} Department of Advanced Energy Engineering Science, Kyushu University

^{*4} Department of Physics, the University of Tokyo

Effects of columnar defects introduced by 2.6 GeV U-ion irradiation on J_c characteristics of 2H-NbSe₂

T. Tamegai,^{*1} W. J. Li,^{*1} S. Pyon,^{*1} A. Takahashi,^{*1} Y. Kobayashi,^{*1} A. Yoshida,^{*2} T. Kambara,^{*2} and A. Ichinose^{*3}

One of the most salient features of superconductors is the zero-resistance state. Although the presence of such a state may be obvious in superconductors without a magnetic field, a motion of quantized vortices can destroy this useful state. The introduction of defects that function as pinning centers for vortices is known to be a practical method to restore the ideal zero-resistance state under strong magnetic fields, leading to the enhancement of the critical current density (J_c) in superconductors. The irradiation of heavy ions on superconductors can create columnar defects (CDs) by destroying the crystal structure of superconductors. CDs are ideal pinning centers for vortices because they can trap vortices along their full length. The effectiveness of CDs in enhancing J_c was demonstrated in high-temperature superconductors¹⁾ and also in iron-based superconductors.²⁾ However, the effect of heavy-ion irradiation on conventional superconductors has attracted much less attention to date. Only very recently, systematic work has been conducted on 2H-NbSe₂ irradiated at an angle of 30° from the c -axis with a dose-equivalent matching field (B_ϕ) of 3 T. In this paper, the presence of the peak effect of J_c is reported. We investigated the effect of 2.6 GeV U-ion irradiation on the J_c characteristics of 2H-NbSe₂.

Single crystals of 2H-NbSe₂ with $T_c \sim 7.2$ K were grown using the iodine transport method. 2.6 GeV U ions were irradiated on 2H-NbSe₂ at various angles, θ_{CD} , from the c -axis and at various B_ϕ values up to 16 T. The dependence of J_c on B_ϕ and θ_{CD} were studied.

Figure 1 shows scanning transmission electron microscope (STEM) image of 2H-NbSe₂ irradiated by 2.6 GeV U-ions from the directions of $\theta_{CD} = \pm 15^\circ$. It is clear that continuous CDs with diameters of ~ 7 –10 nm were created.

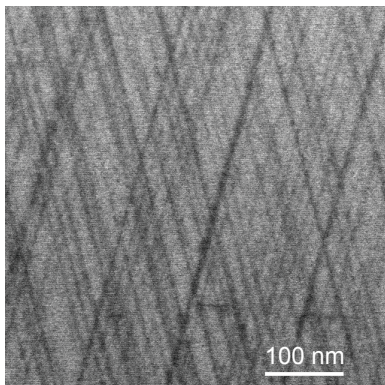


Fig. 1. Columnar defects created by 2.6 GeV U-ion irradiation ($\theta_{CD} = \pm 15^\circ$) in single-crystal 2H-NbSe₂.

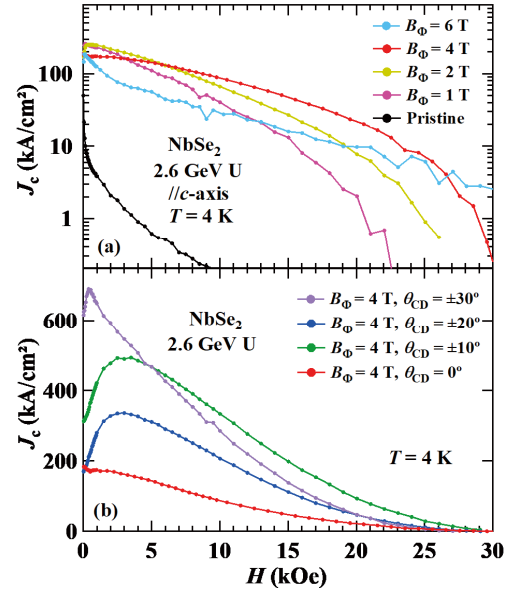


Fig. 2. Effects of 2.6 GeV U-ion irradiation on J_c - H in 2H-NbSe₂: (a) pristine and irradiated samples with $B_\phi = 1, 2, 4,$ and 6 T ($\parallel c$ -axis) and (b) samples irradiated with $\theta_{CD} = 0^\circ, \pm 10^\circ, \pm 20^\circ,$ and $\pm 30^\circ$ at $B_\phi = 4$ T.

Figure 2(a) shows J_c as a function of the magnetic field $H(\parallel c)$ at 4 K for a pristine sample of 2H-NbSe₂ and samples irradiated at $B_\phi = 1, 2, 4,$ and 6 T along the c -axis. In all cases, J_c decreases monotonically with H . Compared with the pristine sample, J_c at 1 kOe is enhanced by a factor of more than 10 even at $B_\phi = 1$ T. Figure 2(b) shows J_c as a function of H at 4 K for 2H-NbSe₂ irradiated from the directions of $\theta_{CD} = \pm 10^\circ, \pm 20^\circ,$ or $\pm 30^\circ$ at $B_\phi = 2$ T + 2 T. Shown as a reference is the sample with $B_\phi = 4$ T at $\theta_{CD} = 0^\circ$. In all cases, the magnetic field H is applied along the c -axis (the average direction of CDs). It is remarkable that, in samples irradiated with $\theta_{CD} = \pm 10^\circ$ and $\pm 20^\circ$, J_c shows a broad peak at $H = 2$ –3 kOe, which is less than 10% of the total B_ϕ . Such a peak effect is similar to the one observed in a sample with tilted CDs.³⁾ It should also be noted that similar broad peaks were observed in (Ba,K)Fe₂As₂ irradiated at $\theta_{CD} \sim \pm 15^\circ$. In this case, however, the peak appears at $H \sim 1/3 B_\phi$. At a larger $|\theta_{CD}|$, the broad peak is suppressed and replaced by a sharp drop of J_c below $H \sim 0.3$ kOe. The origin of the broad peak in J_c - H in 2H-NbSe₂ with splayed CDs is not known yet. More systematic studies on 2H-NbSe₂ with different configurations of CDs are required.

References

- 1) L. Civale *et al.*, Phys. Rev. Lett. **67**, 648 (1991).
- 2) Y. Nakajima *et al.*, Phys. Rev. B **80**, 012510 (2009).
- 3) S. Eley *et al.*, Sci. Rep. **8**, 13162 (2018).
- 4) A. Park *et al.*, Phys. Rev. B **97**, 064516 (2018).

^{*1} Department of Applied Physics, The University of Tokyo

^{*2} RIKEN Nishina Center

^{*3} Central Research Institute of Electric Power Industry

Impurity effects on magnetism of T^{*}-type La_{1-x/2}Eu_{1-x/2}Sr_xCuO₄

M. Takahama,^{*1} S. Asano,^{*1} T. Taniguchi,^{*1} I. Watanabe,^{*2} and M. Fujita^{*1}

Since superconductivity in the cation-free T^{*}-type R₂CuO₄ (R: rear-earth ion) was reported, the physical properties of cuprates have been studied in connection with the local structure around the CuO₂ plane and Cu coordination.^{1,2)} However, owing to the difficulty in detecting the variation in oxygen states through reduction annealing, the role of annealing in the mechanism of superconductivity and the genuine ground state of T^{*}-type cuprate remain controversial. To achieve progress in these issues, we newly synthesized T^{*}-type La_{1-x/2}Eu_{1-x/2}Sr_xCuO₄ (LESCO), which has a CuO₅ pyramid coordination. For the T^{*}-type cuprate, it is considered that the oxygen defect in the as-sintered (AS) non-superconducting (SC) sample is repaired by oxidation annealing.³⁾ Therefore, LESCO gives a unique opportunity to study the effect of local/global crystal structure on the physical properties.

Our previous muon spin rotation/relaxation (μ SR) measurements on LESCO clarified the existence of the disordered magnetic state in the AS sample and the absence of static magnetism in the oxidation-annealed (OA) SC sample, respectively.⁴⁾ These results demonstrate a drastic change in the magnetic state due to annealing. To gain further insight into the ground state of the T^{*}-type cuprate through the study of the magnetism, we investigated the impurity substitution effect for both AS and OA samples by μ SR measurements.

For the experiments, we prepared a pelletized sample of Zn- or Fe-substituted LESCO. The mixed powders were fired at 1050°C in air with intermediate groundings, following which a part of poly-crystals was annealed under a high oxygen pressure of 400 atm at 500°C for 60 h. Zero-field μ SR measurements were performed using a spectrometer installed at Port 2, RIKEN at Rutherford Appleton Laboratory in the UK.

Figures 1(a) and (b) show representative zero-field μ SR time spectra. In both AS and OA samples of La_{0.855}Eu_{0.855}Sr_{0.29}Cu_{0.95}Fe_{0.05}O₄, Gaussian-type depolarization changes into exponential-type depolarizing upon cooling, and a fast depolarizing component appears at low temperatures, suggesting the development of electronic magnetic correlations. The onset temperature for the appearance of the fast depolarizing component (T_m) was evaluated to be \sim 22 K for the AS sample, which is higher than T_m of \sim 7 K for the AS pristine sample with the same hole concentration. Therefore, the static (quasi-static) magnetism in the AS sample is enhanced by the impurity substitution. From a systematic measurement, we found an increase in T_m with increasing Fe concentration. Similarly, in the OA sample, the fast component develops below \sim 12 K and the

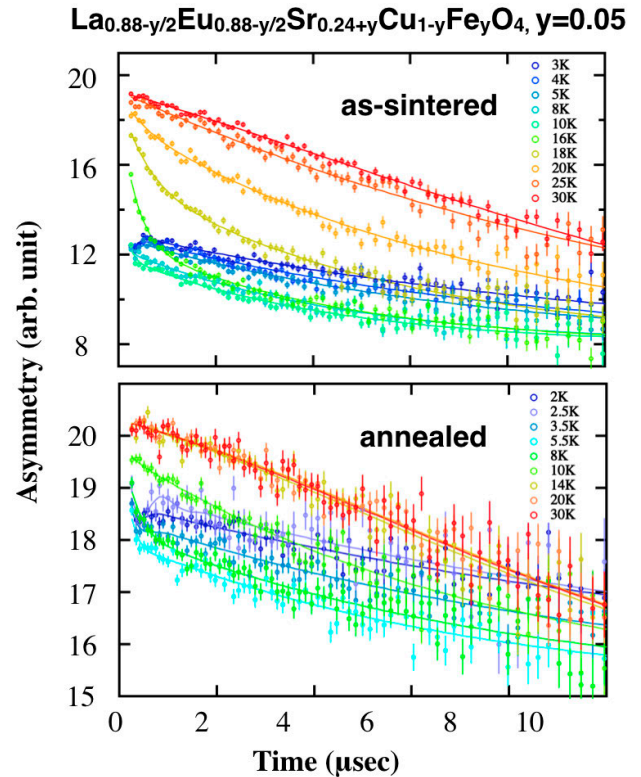


Fig. 1. The μ SR time spectra for (a) as-sintered and (b) oxidation annealed La_{0.855}Eu_{0.855}Sr_{0.29}Cu_{0.95}Fe_{0.05}O₄.

volume fraction exceeds \sim 60% at \sim 3 K, indicating that bulk static (quasi-static) magnetism is induced in the OA sample by Fe substitution.

As for the Zn substitution effect, similar results as in AS Fe-substituted samples we observed, although the enhancement of T_m by Zn substitution is weak (T_m for the 5% Zn-substituted AS $x = 0.24$ sample is \sim 9 K). However, no evidence of magnetic order was observed in the Zn substituted OA sample down to 2 K, which is quantitatively the same as the result for the pristine OA sample. Thus, the stability of magnetism induced by magnetic and non-magnetic impurity is different; that is, the magnetic impurity more effectively stabilizes/induces the static magnetism in the T^{*}-type cuprate. These results are consistent with the impurity effects reported for the optimally-doped and over-doped La_{2-x}Sr_xCuO₄, suggesting the universal nature of spin correlations in hole-doped systems. As the next step, a study of magnetic and SC properties in the under-doped region, where a strong effect of electron correlation can be expected, is important.

References

- 1) M. Naito *et al.*, Physica C **523**, 28 (2016).
- 2) C. Weber *et al.*, Nat. Phys. **6**, 574 (2010).
- 3) J. Akimitsu *et al.*, Jpn. J. Appl. Phys. **27**, L1859 (1988).
- 4) S. Asano *et al.*, J. Phys. Soc. Jpn. **88**, 084709 (2019).

^{*1} Institute for Materials Research, Tohoku University

^{*2} RIKEN Nishina Center

Size-dependent magnetic behavior of La_2CuO_4 nanoparticles

S. Winarsih,^{*1,*2} F. Budiman,^{*3,*4} H. Tanaka,^{*3,*5} T. Goto,^{*6} T. Adachi,^{*6} B. Kurniawan,^{*2} B. Soegijono,^{*2} and I. Watanabe^{*1,*2}

The study of high- T_c copper-oxide-based superconductors has been pursued for more than thirty years. The magnetic ordering of the parent compound is strongly influenced by element doping.¹⁾ The superconductivity (SC) appeared on increasing the hole-doping concentration.¹⁾ It was reported that weak magnetism appeared in the heavily doped regime for ($x \geq 0.30$).²⁾ Those results could provide valuable clarifications of the magnetic phase diagram of the high- T_c copper-oxide-based superconductors, but the correlation between spin dynamics and SC remains unclear.

In the case of nanoparticles, Néel predicted theoretically that ferromagnetic spins appear at the surface of nanoparticles.³⁾ This kind of magnetism was observed in nanogold systems and antiferromagnets such as CuO and CoO.^{4,5)} The nano-size effect also caused a reduction in magnetic transition temperature, T_N , of CuO.⁵⁾ In $\text{La}_{2-x}\text{Sr}_x\text{CuO}_4$, Yin et al. reported possible weak magnetism when the particle size was 113 nm with $0.1 \leq x \leq 0.30$.⁶⁾ With these results, the remaining problems on the magnetism and superconductivity of high- T_c superconductors become more complicated.

We aim to investigate the nano-size effect in $\text{La}_{2-x}\text{Sr}_x\text{CuO}_4$. We present the results of the parent compound, La_2CuO_4 (LCO). This report is an update to our last year's report.⁷⁾ The sol-gel method was used to produce the samples by controlling sintering temperatures and times to vary the particle size. We prepared 4 samples with different particle sizes: 24 nm, 32 nm, 52 nm, and 71 nm. The detailed sample synthesis procedure was reported in our previous paper.⁸⁾ Zero-field (ZF) muon spin relaxation (μSR) measurements of these samples were performed at the RIKEN-RAL Muon Fa-

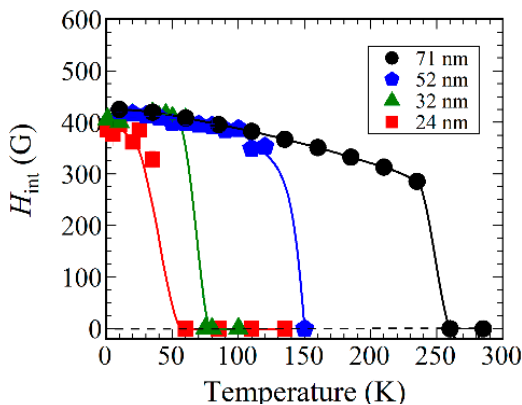


Fig. 1. Temperature dependence of the internal field at the muon site, $d H_{\text{int}}$, in La_2CuO_4 nanoparticles.

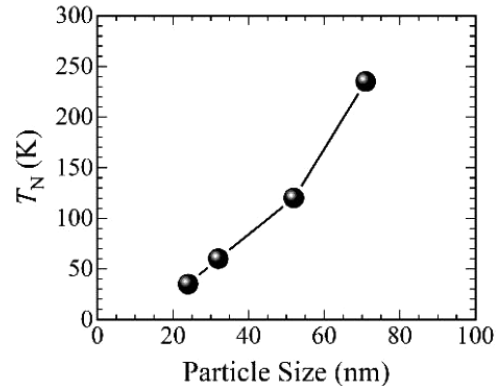


Fig. 2. Temperature dependence of the magnetic transition, T_N , of La_2CuO_4 nanoparticles.

cility, Rutherford-Appleton Laboratory, UK, by using a pulsed positive surface muon beam.

ZF- μSR time spectra of each sample were analyzed using Eq. (1). Muon spin precession, which shows the appearance of a long-range magnetically ordered state, is expressed in the first component. Slow relaxation of muon-spin polarization is expressed in the second component. From the fitting results of the time spectra, we could obtain the internal magnetic field at the muon site, H_{int} , which is shown in Fig. 1. The saturated H_{int} did not change significantly in all samples, showing a value of about 420 G. This value is identical to that observed in bulk LCO.⁹⁾

$$A(t) = A_1 e^{-\lambda_1 t} \cos(\omega t + \phi) + A_2 e^{-\lambda_2 t} \quad (1)$$

Figure 2 depicts the temperature dependence of T_N which is defined from Fig. 1. as the temperature where H_{int} suddenly drops to zero with increasing temperature. The figure shows that T_N decreases with reducing particle size. These results indicate that the particle size affects T_N without changing the saturated H_{int} . The result that the saturated $d H_{\text{int}}$ value is the same between nanoparticles of different sizes and the bulk sample implies that the magnetic moments of Cu sensed by injected muons were almost the same. The reduction in T_N might be due to the destruction of the three-dimensional exchange interaction between the spins of Cu ions, which existed in bulk LCO,¹⁰⁾ as a result of reducing the particle size. We are now summarizing these results for submission to an international journal.

References

- 1) T. P. Croft *et al.*, Phys. Rev. B **89**, 224513 (2014).
- 2) J. E. Sonier *et al.*, Proc. Natl. Acad. Sci. USA **107**, 17131 (2010).
- 3) L. Néel, Low Temperature Physics (Gordon and Breach, New York, 1962), p. 413.
- 4) Y. Yamamoto *et al.*, Phys. Rev. Lett. **93**, 116801 (2004).
- 5) X. G. Zheng *et al.*, Phys. Rev. B **72**, 014464 (2005).
- 6) Y. Yin *et al.*, J. Phys. Chem. C **117**, 328 (2013).
- 7) S. Winarsih *et al.*, RIKEN Accel. Prog. Rep. **52**, 178 (2019).
- 8) S. Winarsih *et al.*, Key. Eng. Mater. **966**, 357 (2019).
- 9) J. I. Budnick *et al.*, Europhys. Lett. **5**, 651 (1988).
- 10) R. Coldea *et al.*, Phys. Rev. Lett. **86**, 5377 (2001).

*1 RIKEN Nishina Center

*2 Department of Physics, Universitas Indonesia

*3 Department of Human Intelligence Systems, Kyushu Institute of Technology

*4 School of Electrical Engineering, Telkom University

*5 Research Center for Neuromorphic AI Hardware, Kyushu Institute of Technology

*6 Department of Engineering and Applied Sciences, Sophia University

Targeted alpha therapy of thyroid cancer: Evaluation of [^{211}At]NaAt treatment in the xenograft model[†]

T. Watabe,^{*2,*3} K. Kaneda-Nakashima,^{*3,*4} Y. Liu,^{*2} Y. Shirakami,^{*3} K. Ooe,^{*1,*2} A. Toyoshima,^{*1,*3}
E. Shimosegawa,^{*2} M. Fukuda,^{*3,*5} A. Shinohara,^{*3,*4} and J. Hatazawa^{*3,*5}

Radioactive iodine has long been used clinically for patients with differentiated thyroid cancer.¹⁾ ^{131}I is used for the ablation of thyroid remnants or treatment of metastatic thyroid cancer.¹⁾ However, some patients with multiple metastases are refractory to repetitive ^{131}I treatment, despite the targeted regions showing sufficient iodine uptake.²⁾ In such patients, beta-particle therapy using ^{131}I is inadequate, and another strategy using a more effective radionuclide targeting the sodium/iodide symporter (NIS) is required.

^{211}At is an alpha emitter with chemical properties similar to those of iodine and is used in targeted alpha therapy. In the present study, we added ascorbic acid (AA) to ^{211}At solution to increase the radiochemical purity of astatide and evaluated its efficacy against differentiated thyroid cancer, which is characterized by the expression of NIS.

Methods

^{211}At was procured from the Research Center for Nuclear Physics at Osaka University and RIKEN via the short-lived RI supply platform. Upon procurement, ^{211}At was separated and purified via dry distillation from a bismuth target and finally collected in distilled water.

Crude ^{211}At solution (AA(-) solution) and ^{211}At solution treated with AA (AA(+) solution) were prepared. Thyroid uptakes were compared between the two solutions in normal male Wistar rats ($n = 6$). Cellular uptake analysis in K1-NIS cells was performed under the AA(+) and AA(-) conditions. The AA(+) solution was injected at three doses into K1-NIS xenograft mice: 1 MBq ($n = 6$), 0.4 MBq ($n = 6$), and 0.1 MBq ($n = 6$). The vehicle was injected into control mice ($n = 6$). The treatment effects were compared among the four groups. Planar and SPECT images were acquired using a gamma camera system (E-cam, Siemens) with a low-energy all-purpose collimator.³⁾ The energy window was set at $79 \text{ keV} \pm 20\%$, targeting the X-rays emitted from the daughter nuclide of ^{211}Po .⁴⁾

All the animal experiments were performed in compliance with the guidelines of the Institute of Experimental Animal Sciences. The protocol was approved by the Animal Care and Use Committee of the Osaka University Graduate School of Medicine.

Results

Thyroid uptake was significantly enhanced in rats injected with the AA(+) solution as compared to those

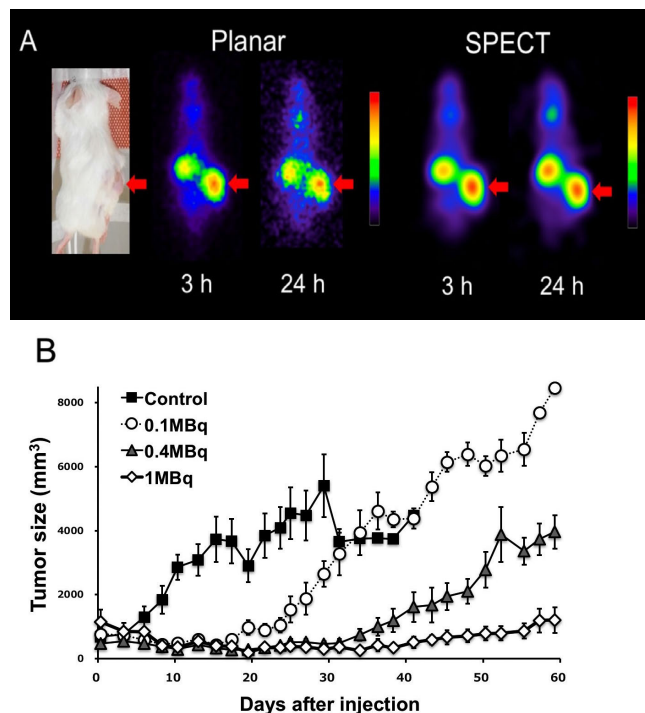


Fig. 1. (A) Planar and SPECT images of the mouse K1-NIS xenograft model after the injection of the AA(+) solution. High uptake was observed in the xenografts (arrows). (B) Change in the tumor size and body weight after the administration of AA(+) solutions.

injected with the AA(-) solution. Cellular uptake analysis showed a significantly increased uptake of ^{211}At by the K1-NIS cells under the AA(+) condition as compared to the AA(-) condition. In the mouse xenograft model, the K1-NIS tumors showed a significant accumulation of ^{211}At 3 and 24 h post administration ($22.5 \pm 10.4\%$ ID and $12.9 \pm 6.8\%$ ID, respectively). Tumor growth was immediately inhibited in a dose-dependent manner after the administration of ^{211}At . In the survival analysis, the ^{211}At groups (0.1, 0.4, and 1 MBq) showed significantly better survival than the control group.

Conclusion

The uptake of ^{211}At was enhanced in differentiated thyroid cancer cells as well as normal thyroid by using ^{211}At solution treated with AA. The solution also showed dose-dependent efficacy against the K1-NIS xenografts, suggesting its potential applicability to targeted alpha therapy.

References

- 1) T. Higashi *et al.*, *Ann. Nucl. Med.* **26**, 99 (2012).
- 2) M. Schlumberger, *J. Endocrinol. Invest.* **35**, 40 (2012).
- 3) J. T. Kuikka *et al.*, *Nucl. Med. Commun.* **19**, 457 (1998).
- 4) E. L. Johnson *et al.*, *Nucl. Med. Biol.* **22**, 45 (1995).

[†] Condensed from the article in *J. Nucl. Med.* **60**, 1301, (2019)

*1 RIKEN Nishina Center

*2 Graduate School of Medicine, Osaka University

*3 Institute for Radiation Sciences, Osaka University

*4 Graduate School of Science, Osaka University

*5 Research Center for Nuclear Physics, Osaka University

Live mouse imaging with ^{44}mSc by a multiple-isotope PET

T. Fukuchi,^{*1} M. Shigeta,^{*1} D. Mori,^{*2} T. Yokokita,^{*2} Y. Komori,^{*2} H. Haba,^{*2} and Y. Watanabe^{*1}

We have been developing a multiple-isotope positron emission tomography (MI-PET) system that can analyze the dynamics of multiple tracers. Using a positron- γ emitter, which emits de-excitation γ -ray as a tracer after the positron emission in β -decay, the MI-PET system identifies the tracer by detecting the prompt γ -ray emitted after the positron emission. Figure 1 shows a schematic illustration of the developed MI-PET prototype system. This system is composed of a PET scanner and additional γ -ray detectors.¹⁾ In this system, in addition to conventional PET imaging, coincidence among the additional detectors and the PET scanner can be performed. We expect that MI-PET will be used for drug discovery research by direct comparison between old and new drugs.

For multiple-isotope imaging using MI-PET, at least one positron- γ emitter is necessary as a tracer. Scandium-44 is one of the promising radioactive-tracer candidates for MI-PET because of its large positron and γ -ray emission ratio and moderate half-life (^{44}Sc : 3.97 h, $^{44\text{m}}\text{Sc}$: 58.61 h). In our previous work, we performed dual-isotope phantom imaging using $^{44\text{m}}\text{Sc}$ and ^{18}F (pure positron emitter) and evaluated the basic imaging performance of MI-PET for $^{44\text{m}}\text{Sc}$.²⁾

Therefore, before the future development of a $^{44\text{m}}\text{Sc}$ -labeled drug for MI-PET applications, in order to test the practical imaging ability of the MI-PET system for $^{44\text{m}}\text{Sc}$, we conducted dual-isotope live mouse imaging using $^{44\text{m}}\text{Sc}$, which is a simple substance.

Scandium-44m was produced at the RIKEN AVF cyclotron via the reaction $^{44}\text{Ca}(d, 2n)^{44\text{m}}\text{Sc}$ with a 24-MeV deuterium beam. As the irradiation target, ^{44}CaO

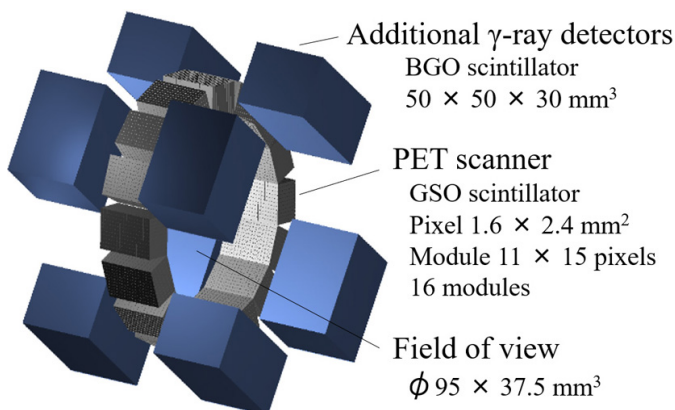


Fig. 1. Schematic illustration of the developed MI-PET prototype system.

^{*1} RIKEN Center for Biosystems Dynamics Research

^{*2} RIKEN Nishina Center

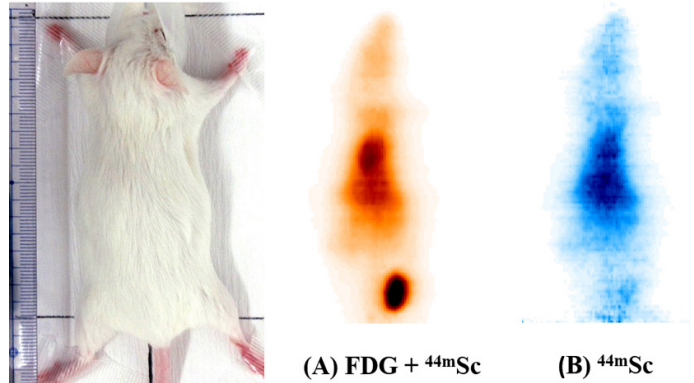


Fig. 2. Images of a live mouse with $^{44\text{m}}\text{Sc}$ and ^{18}F -FDG injections (maximum intensity projection images). The reconstructed images were acquired with the absence (A) or presence (B) of γ -ray coincidence.

(97.0% enriched ^{44}Ca isotope) powder was pressed into a disk of 10-mm diameter. The irradiated target was dissolved in 6 M HCl and purified by the chemical processes.²⁾ Finally, approximately 2 MBq of pure $^{44\text{m}}\text{Sc}$ was produced and transported to RIKEN Kobe campus for the imaging experiment. Most of the short-lived by-product, ^{44}Sc , decayed out during transportation.

In the mouse imaging experiment, 197 kBq $^{44\text{m}}\text{Sc}$ (simple substance) and 198 kBq ^{18}F -FDG were administered to an 8-week-old normal male mouse by tail-vein injection. Five minutes after administration, a 30-min whole-body scan was performed under anesthesia.

The result of dual-isotope mouse imaging is shown in Fig. 2. From the reconstructed images with the absence (A) or presence (B) of the prompt γ -ray detection, image (A) reflects the distribution of both ^{18}F -FDG and the $^{44\text{m}}\text{Sc}$ tracer, whereas image (B) reflects the isolated image of the $^{44\text{m}}\text{Sc}$ tracer. In these images, we can clearly observe the difference between ^{18}F -FDG and $^{44\text{m}}\text{Sc}$ distributions, *i.e.*, ^{18}F -FDG is distributed in the heart and urinary bladder, whereas $^{44\text{m}}\text{Sc}$ distributed in the liver.

From this experiment, we successfully demonstrated the practical feasibility of dual-isotope imaging using MI-PET with $^{44\text{m}}\text{Sc}$ as the second tracer. In the future, we will synthesize a useful MI-PET drug labeled by $^{44\text{m}}\text{Sc}$ and perform multiple-drug imaging on disease model animals.

References

- 1) T. Fukuchi *et al.*, *Med. Phys.* **44**, 2257 (2017).
- 2) T. Fukuchi *et al.*, *RIKEN Accel. Prog. Rep.* **52**, 207 (2019).

Production cross sections of ytterbium and thulium radioisotopes in alpha-induced nuclear reactions on natural erbium[†]

M. Saito,^{*1,*2} M. Aikawa,^{*1,*2,*3} M. Sakaguchi,^{*4,*5,*2} N. Ukon,^{*6,*2} Y. Komori,^{*2} and H. Haba^{*2}

Radionuclides are used in nuclear medicine for therapy and diagnosis. The production reactions of such medical radionuclides should be investigated for practical use. The best route of their production can be discussed based on cross sections of possible nuclear reactions. The radionuclide ^{169}Yb ($T_{1/2} = 32.018$ d) is a candidate of medical radionuclide. It decays with emission of Auger electrons and X-rays, which can be used for brachytherapy.¹⁾ There are several charged-particle-induced reactions to produce ^{169}Yb . In this study, we focused on alpha-induced reactions on $^{\text{nat}}\text{Er}$. Four previous studies of the $^{\text{nat}}\text{Er}(\alpha, x)^{169}\text{Yb}$ reaction²⁻⁵⁾ were found in a literature survey. However, the experimental data published earlier are rather inconsistent with each other. Therefore, we measured the excitation functions of the alpha-induced reaction on $^{\text{nat}}\text{Er}$. The cross sections of byproducts, ^{166}Yb , and $^{165, 166, 167, 168, 170, 173}\text{Tm}$, were also determined.

The experiment was performed at the RIKEN AVF cyclotron. The stacked foil activation method and gamma-ray spectrometry were used. The stacked target consisted of $^{\text{nat}}\text{Er}$ (99% purity, Goodfellow Co., Ltd., UK) and $^{\text{nat}}\text{Ti}$ (99.6% purity, Nilaco Corp., Japan). The $^{\text{nat}}\text{Ti}$ foils were used for the $^{\text{nat}}\text{Ti}(\alpha, x)^{51}\text{Cr}$ monitor reactions to assess beam parameters and target thicknesses. The sizes and weights of both foils were measured to estimate their thicknesses. The derived thicknesses of $^{\text{nat}}\text{Er}$ and $^{\text{nat}}\text{Ti}$ were 20.06 mg/cm² and 2.26 mg/cm², respectively. The measured foils were cut to 10×10 mm² to fit a target holder. The target holder also served as a Faraday cup. The stacked target was irradiated for 1 hour with a 50.9-MeV alpha-beam. The energy was measured by the time-of-flight method.⁶⁾ The energy degradation in the stacked target was calculated using stopping powers obtained with the SRIM code.⁷⁾ The beam intensity measured by the Faraday cup was 200.3 nA. These beam parameters were assessed by the $^{\text{nat}}\text{Ti}(\alpha, x)^{51}\text{Cr}$ monitor reactions. According to the comparison, we corrected the thickness of $^{\text{nat}}\text{Er}$ decreased by 1% within the uncertainty.

The cross sections of the $^{\text{nat}}\text{Er}(\alpha, x)^{169}\text{Yb}$ reaction

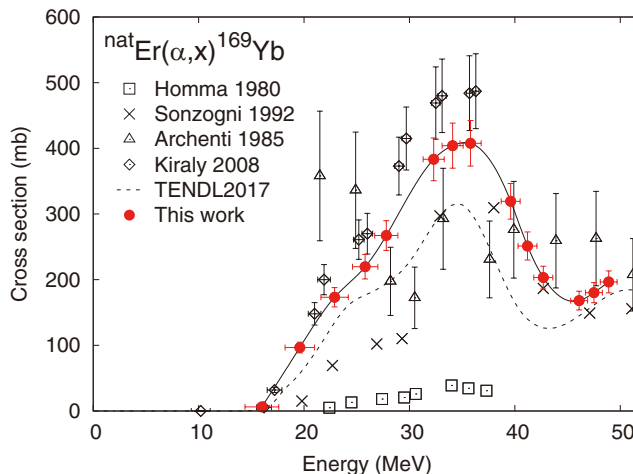


Fig. 1. Excitation function of $^{\text{nat}}\text{Er}(\alpha, x)^{169}\text{Yb}$ compared with previous data²⁻⁵⁾ and TENDL-2017.⁹⁾

were derived. The radionuclide ^{169}Yb has a metastable state with a short half-life ($T_{1/2} = 46$ s, IT: 100%), which decays only to the ground state ^{169g}Yb soon after the irradiation. The 177.21-keV gamma ($I_\gamma = 22.28\%$) associated with the decay of ^{169g}Yb was measured after a cooling time of 11 days. The cross sections were obtained from the net counts of the gamma peak and are shown in Fig. 1. The results were compared with those of previous studies²⁻⁵⁾ and the TENDL-2017 data.⁹⁾ Both data of Király *et al.* (2008) and TENDL-2017 have nearly the same peak position as ours at approximately 35 MeV while the amplitudes are different. The other experimental data differ significantly from our results in both the shape and amplitude.

This work was supported by JSPS KAKENHI Grant Number 17 K07004.

References

- 1) F. H. DeLand *et al.*, J. Nucl. Med. **12**, 683 (1971).
- 2) B. Király *et al.*, Nucl. Instrum. Methods Phys. Res. B **266**, 549 (2008).
- 3) A. A. Sonzogni *et al.*, J. Radioanal. Nucl. Chem., Letters **165**, 295 (1992).
- 4) A. Archenti *et al.*, Radiochimica Acta **38**, 65 (1985).
- 5) Y. Homma *et al.*, Int. J. Appl. Radiat. Isot. **31**, 505 (1980).
- 6) T. Watanabe *et al.*, Proc. 5th Int. Part. Accel. Conf. (IPAC2014), 3566 (2014).
- 7) J. F. Ziegler *et al.*, SRIM: the Stopping and Range of Ions in Matter, <http://www.srim.org/>.
- 8) National Nuclear Data Center, The NuDat 2 database, <http://www.nndc.bnl.gov/nudat2/>.
- 9) A. J. Koning *et al.*, Nucl. Data Sheets **113**, 2841 (2012).

[†] Condensed from the article in Appl. Radiat. Isot. **154**, 108874 (2019)

^{*1} Graduate School of Biomedical Science and Engineering, Hokkaido University

^{*2} RIKEN Nishina Center

^{*3} Faculty of Science, Hokkaido University

^{*4} School of Science, Hokkaido University

^{*5} Present address: Graduate School of Biomedical Science and Engineering, Hokkaido University

^{*6} Advanced Clinical Research Center, Fukushima Medical University

Production cross sections of dysprosium-159 radioisotope from the deuteron-induced reactions on terbium-159 up to 24 MeV[†]

D. Ichinkhorloo,^{*1,*2,*3} M. Aikawa,^{*1,*3,*4} Ts. Zolbadral,^{*4,*2,*3} Y. Komori,^{*3} and H. Haba^{*3}

Dysprosium-159 ($T_{1/2} = 144.4$ d) can be used to determine of bone mineral density.¹⁾ The dysprosium radionuclide can be produced by the charged-particle-induced reactions on the monoisotopic element terbium-159. In this work, the production cross sections of $^{157,159}\text{Dy}$ and ^{160}Tb in the deuteron-induced reactions on ^{159}Tb were studied. The results were compared with experimental data published previously^{2,3)} and TENDL-2017 data.⁴⁾

The experiment was performed at the RIKEN AVF cyclotron. The stacked foil technique, the activation method, and high-resolution γ -ray spectrometry were used to determine the activation cross sections.

The stacked target consisted of 10×10 mm² foils cut from a large Tb foil (25 μm t, 25×50 mm², 99.9% purity, Nilaco Corp., Japan) and two Ti foils (5 μm t, 50×100 mm², 99.6% purity and 20 μm , 120×100 mm², 99.5% purity, Nilaco Corp., Japan). The sizes and weights of the large foils were measured to derive the thicknesses. The thicknesses of the Tb and two Ti foils were found to be 20.56, 2.25, and 9.31 mg/cm², respectively. The Ti foils were interleaved to check the beam parameters using the $^{nat}\text{Ti}(d, x)^{48}\text{V}$ monitor reaction. The cut foils were stacked in a target holder, which also served as a Faraday cup.

The deuteron beam was accelerated to 23.9 MeV using the RIKEN AVF cyclotron. The beam energy was measured by the time-of-flight method.⁵⁾ The stacked target was irradiated by the beam for 60 min with an average intensity of 94.3 nA. The beam intensity was measured using the Faraday cup. Energy degradation in the stacked target was calculated using SRIM code.⁶⁾

The γ -rays emitted from the irradiated foils were measured using a high-resolution high-purity germanium (HPGe) detector. The γ -ray spectra were analyzed using the software Gamma Studio (SEIKO EG&G). The γ line at 58.0 keV ($I_{\gamma} = 2.27\%$) emitted with the ^{159}Dy decay ($T_{1/2} = 144.4$ d) was measured to derive the cross sections of the $^{159}\text{Tb}(d, 2n)^{159}\text{Dy}$ reaction. The measurements were performed after a cooling time of 94 days. The γ line had negligible interference with the x-ray of the lead shielding of the detector, which could be confirmed by the absence of peaks at the energy in the two foils at the downstream

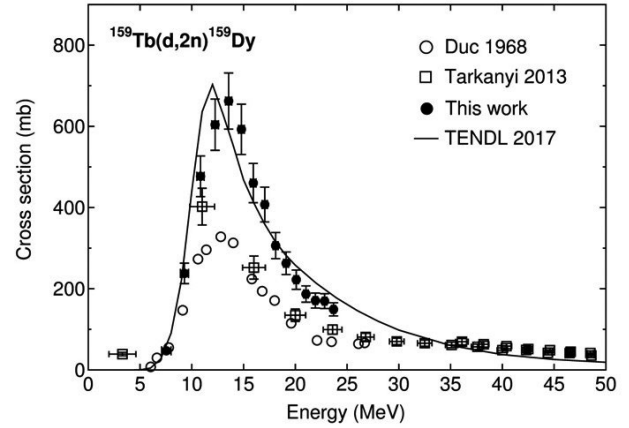


Fig. 1. Excitation function of the $^{159}\text{Tb}(d, 2n)^{159}\text{Dy}$ reaction.

of the beam. The self-absorption of the low-energy γ line in the Tb foils was considered using the mass attenuation coefficient.

The cross sections derived from the corrected activities for ^{159}Dy production are presented with previous experimental data^{2,3)} and TENDL-2017 data⁴⁾ in Fig. 1.

Our experimental data show a peak at approximately 14 MeV, which is consistent with other experimental data, while the amplitudes are substantially different. The TENDL-2017 data slightly deviate from ours.

In summary, we performed an experiment to measure the excitation functions of deuteron-induced reactions on ^{159}Tb up to 24 MeV at the RIKEN AVF cyclotron. The production cross sections of $^{157,159}\text{Dy}$ and ^{160}Tb were determined. The results were compared with previously obtained experimental data and TENDL data.

This work was supported by JSPS KAKENHI Grant Number 17K07004.

References

- 1) D. V. Rao *et al.*, *Med. Phys.* **4**, 109 (1977).
- 2) T. M. Duc *et al.*, *C. R. Acad. Sci. Ser. B* **266**, 100 (1968).
- 3) F. Tárkányi *et al.*, *Nucl. Instrum. Methods Phys. Res. B* **316**, 183 (2013).
- 4) A. J. Koning *et al.*, *Nucl. Data Sheets* **155**, 1 (2019).
- 5) T. Watanabe *et al.*, *Proc. 5th Int. Part. Accel. Conf. (IPAC 2014)*, 3566 (2014).
- 6) J. F. Ziegler *et al.*, *SRIM: the Stopping and Range of Ions in Matter*, <http://www.srim.org>.

[†] Condensed from the article in *Nucl. Instrum. Methods Phys. Res. B* **461**, 102 (2019)

^{*1} Faculty of Science, Hokkaido University

^{*2} Nuclear Research Center, National University of Mongolia

^{*3} Nishina Center for Accelerator-Based Science, RIKEN

^{*4} Graduate School of Biomedical Science and Engineering, Hokkaido University

Non-homologous end joining is the major repair pathway for DNA double strand breaks in human fibroblast after heavy-ion irradiation

M. Izumi*¹ and T. Abe*¹

Accelerated heavy-ion particles with high linear energy transfer (LET) induce complex clustered DNA damage, which are difficult to repair. Although the numbers of treatment facilities and patients undergoing heavy-ion therapy are increasing, the DNA repair mechanism caused by heavy-ion irradiation is not fully understood at the molecular level. DNA double-strand breaks (DSBs) are the most lethal damage caused by ionizing irradiation and are repaired primarily by non-homologous end joining (NHEJ) or homologous recombination (HR) in mammalian cells, whereas alternative NHEJ (alt-NHEJ) and/or single strand annealing (SSA) work only when both NHEJ and HR are impaired.

Several published results of survival assay using mammalian mutant cell lines deficient in NHEJ or HR suggest that NHEJ is inhibited after heavy-ion irradiation.^{1,2} On the other hand, studies using inhibitors and CHO mutant cell lines suggest that NHEJ is a major repair pathway after heavy-ion irradiation, although HR is more important for higher-LET radiation.^{3,4} In addition, clustered DNA damage enhances end resection, which promotes alt-NHEJ and/or SSA.⁵ Therefore, the DNA repair mechanism after heavy-ion irradiation is still controversial in higher eukaryotes.

In this study, the DSB repair mechanism after heavy-ion irradiation was examined using specific inhibitors against repair proteins. Human fibroblast NB1RGB cells were irradiated with X-ray, carbon ions, or argon ions in the presence of an NHEJ inhibitor (NU7441) or HR inhibitor (B02), as illustrated in Fig. 1. The repair efficiency was estimated by the kinetics of the phosphorylated histone H2AX foci, which reflect the presence of DSBs (Fig. 2).

The number of phosphorylated histone H2AX after X-ray irradiation decreased with similar kinetics in the

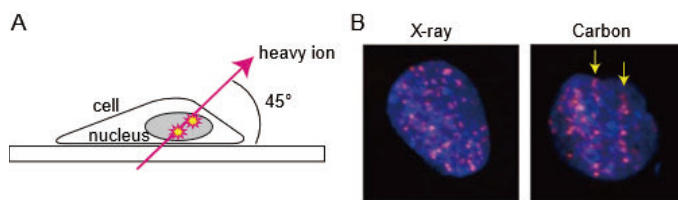


Fig. 1. A: Schematic of the irradiation. Cells were tilted at 45 degrees for heavy-ion irradiation. B: Representative immunostaining images of phosphorylated histone H2AX (red) and nuclei (blue) after 2 Gy of X-ray or carbon-ion irradiation. Arrows indicate the track of ions.

presence of NU7441 or B02, suggesting that both pathways work competitively and compensate each other. In contrast, the foci formation after heavy-ion irradiation in the presence of NU7441 was delayed and reached maximum 3 h after irradiation, probably because the histone H2AX is phosphorylated partly by DNA-PK. The foci number decreased by 30% within 5 h of heavy-ion irradiation with or without inhibitors. NU7441 inhibited DSB repair after heavy-ion irradiation at later time points (5–24 h), whereas B02 had no effect on DSB repair after heavy-ion irradiation. These results suggest that high-LET radiation induced complex damage with dirty broken ends as well as simple repairable damage. In addition, it is also suggested that NHEJ is the major repair pathway after heavy-ion irradiation and DNA damage checkpoint delays the HR kinetics after heavy-ion irradiation.

References

- 1) H. Wang *et al.*, DNA Repair **7**, 725 (2008).
- 2) S. C. Genet *et al.*, Oncology Rep. **28**, 1591 (2012).
- 3) H. Ma *et al.*, Radiat. Oncol. **10**, 225 (2015).
- 4) A. Gerelchuluun *et al.*, Rad. Res. **183**, 345–356 (2015).
- 5) H. Yajima *et al.*, DNA Repair **12**, 936 (2013).

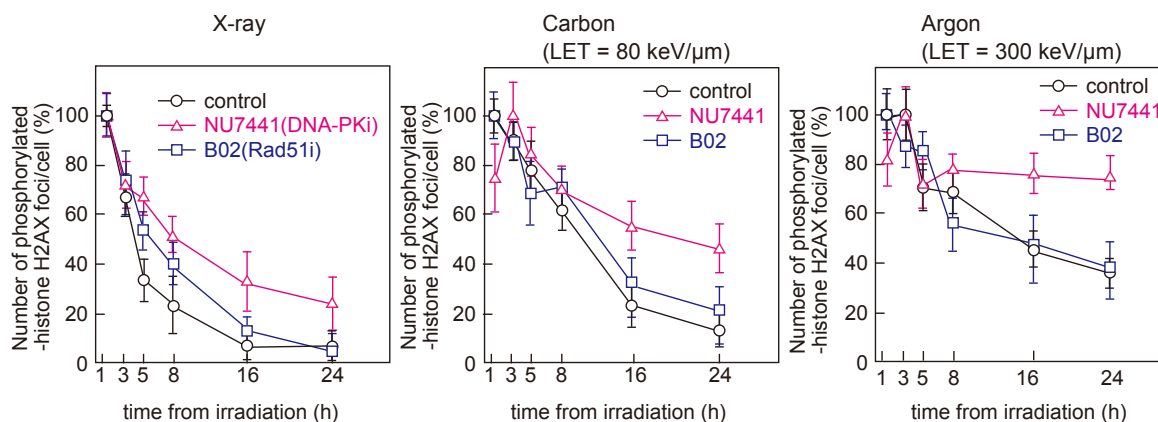


Fig. 2. Time course of phosphorylated histone H2AX foci after irradiation. NB1RGB cells were pre-treated with 3 μ M NU7441 (DNA-PK inhibitor) or 10 μ M B02 (Rad51 inhibitor) for 3 h and irradiated with 2 Gy of X-ray, carbon ions (LET = 80 keV/ μ m), or argon ions (LET = 300 keV/ μ m). The percentage of foci per cell was plotted by normalizing the numbers at the maximum time point as 100% after irradiation.

*¹ RIKEN Nishina Center

Mutation analysis pipeline V2: an improved version of bioinformatics pipeline for plant and microbial sequencing analysis

H. Ichida*¹ and T. Abe*¹

The rapid and continuous advancement in the massively parallel, “next generation” sequencing technology enabled a comprehensive analysis of genomic mutations in base-pair resolution in model species, such as rice and Arabidopsis. A commonly used state-of-the-art sequencing platform (HiSeq X, Illumina) produces roughly 2 terrabases of usable sequencing reads per run in less than 3 days. To process, analyze, and extract usable information from such large datasets, a high-throughput bioinformatics pipeline that is specialized for mutation analysis and extensively utilizes parallelization is required. Owing to such dataset volumes, it is not quite realistic to experimentally verify all mutation candidates in each dataset, although the mutation candidates must be accurate for such analysis. We have developed one such pipelines on the “HOKUSAI” parallel computing system, operated by the Advanced Center for Computing and Communication, RIKEN in 2015;¹⁾ further, we have operated and been adding continuous improvements since then. Recently, there has been a great demand to support various non-model organisms in the pipeline. Here, we present a brief description of the major updated version of our pipeline, namely, the mutation analysis pipeline V2 (MAP-V2).

The basic workflow of MAP-V2 is essentially the same as that of the previous version,²⁾ but the pipeline’s internal structure and codes have been re-designed and re-written almost from scratch. MAP-V2 runs quality checking of the input sequencing reads (by FastQC), mapping of the input sequencing reads to the reference genome, and variant calling and filtration to identify mutations induced in the genomes and filter out false positives, which are mainly derived from intra-cultivar variations. In MAP-V2, raw sequencing reads (supported for outputs from both short- and long-read sequencers) are mapped to the reference genome sequences using one of the mapping programs supported by default (BWA, minimap2, ngmlr, and BMap), sorted, and realigned, and the data are stored in the standard BAM format. Variant callings are performed with a maximum of twelve different programs (BcfTools, BedTools, BreakDancer, CNVnator, Delly, FreeBayes, GATK V4, GATK V3, Manta, Pindel, Sniffles, and Strelka) and merged into a single file. The sequence quality check, mapping, and variant calling statistics are summarized and compiled in an HTML-format report for review. MAP-V2 utilizes a modular structure in each compartment of the pipeline: new programs, workflows, and therefore new

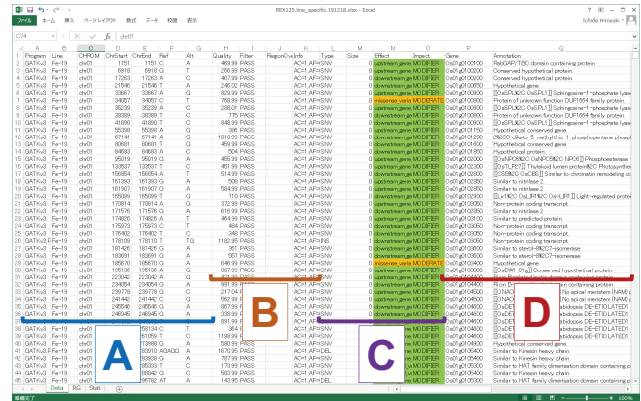


Fig. 1. An example of a MAP-V2 output. (A) Information about the mutation, (B) evaluation, (C) the type and size of the mutation, and (D) gene ID and annotation affected by the mutation.

organisms can be easily added and integrated later. It supports more programs than the previous version, but this modular structure makes it easy to further extend the pipeline to fit specific requirements for each organism and project. MAP-V2 is currently implemented and run on the HOKUSAI system, and it is capable of transfer onto private and public cloud infrastructure with minor modifications, when necessary.

The most significant change in MAP-V2 for users is the output format of the results. An example of a MAP-V2 output is shown in Fig. 1. MAP-V2 outputs native (binary) Microsoft® Excel® files instead of the tab-delimited text files in the previous version. This change enabled the simultaneous output of multiple datasets in separate worksheets. A result file contains three worksheets that include all post-filtered variants identified from the mutants analysis, mutations that possibly cause the inactivation of gene functions based on prediction from gene structures and sequence changes (candidates of responsible mutations in mutants), and statistics that summarizes identified mutations categorize in mutation types. A variety of formatting options that visually categorize the possible effects of the identified mutations are used in MAP-V2 results.

References

- 1) H. Ichida *et al.*, RIKEN Accel. Prog. Rep. **49**, 254 (2016).
- 2) H. Ichida *et al.*, Plant J. **98**, 301–314 (2019).

*1 RIKEN Nishina Center

II. RESEARCH ACTIVITIES I

(Nuclear, Particle and Astro-Physics)

1. Nuclear Physics

Decay studies in the region of ^{54}Zn

A. Kubiela,^{*1} A. A. Ciemny,^{*1} W. Dominik,^{*1} A. Giska,^{*1} Z. Janas,^{*1} C. Mazzocchi,^{*1} M. Pfützner,^{*1} M. Pomorski,^{*1} N. Sokołowska,^{*1} R. Grzywacz,^{*2} M. Madurga,^{*2} C. Thornsberry,^{*2} D. -S. Ahn,^{*3} H. Baba,^{*3} N. Fukuda,^{*3} Y. Ichikawa,^{*3} T. Kubo,^{*3} B. Mauss,^{*3} H. Nishibata,^{*3} D. Suzuki,^{*3} H. Suzuki,^{*3} Y. Shimizu,^{*3} M. Tajima,^{*3} H. Takeda,^{*3} A. Takamine,^{*3} H. Ueno,^{*3} H. Yamazaki,^{*3} K. Yoshida,^{*3} K. Kawata,^{*4,*3} Y. Takeuchi,^{*5} A. Bezbakh,^{*6} G. Kamiński,^{*6} P. Szymkiewicz,^{*6} A. Świercz,^{*6} and Ł. Janiak^{*7}

In April 2019, we performed an experiment at the RIBF facility to study the two-proton ($2p$) radioactivity of ^{54}Zn . The main goal was to measure correlations between momenta of emitted protons in order to investigate whether they can provide insight into the structure of this exotic, extremely neutron-deficient nucleus. In particular, the comparison of the measured $p-p$ correlations for ^{54}Zn with the previously established correlations for $^{45}\text{Fe}^{1)}$ could reveal the expected influence of the proton $Z = 28$ shell closure on these proton drip-line nuclei.

The nuclei of interest were produced using a ^{78}Kr primary beam at 345 MeV/nucleon impinging on a 10 mm-thick beryllium target and separated with the help of the BigRIPS separator and ZeroDegree spectrometer.²⁾ The separated ions, identified in-flight, were implanted into the Warsaw Optical Time Projection Chamber (OTPC)³⁾ mounted in the final focal plane of the ZeroDegree spectrometer (F11). In order to increase the stopping efficiency in the relatively thin gas of the OTPC, a monoenergetic degrader was installed at the F10 focal plane.

The OTPC is a gaseous detector working in the TPC mode, in which the signals are read out by means of optical methods instead of electronic ones. It can record images of tracks of charged particles, allowing their identification and the reconstruction of the decay events in three dimensions. The reconstruction is performed by combining the two-dimensional image recorded using a CCD camera with the signal from a photomultiplier recording the total light intensity as a function of time, which is related to the position in the direction perpendicular to the image via the constant drift velocity. The OTPC was filled with a gas mixture consisting of 69% Ar, 29% He, and 2% CF_4 at atmospheric pressure.

During the measurement, it was found that the production cross section for ^{54}Zn was smaller than the value predicted by the EPAX 3.1 empirical formula⁴⁾ by a factor much larger than anticipated before the experiment. Nevertheless, decays of several ions of ^{54}Zn were recorded, showing clear images of ($2p$) emission. An example of such a decay is shown in Fig. 1(a). The de-

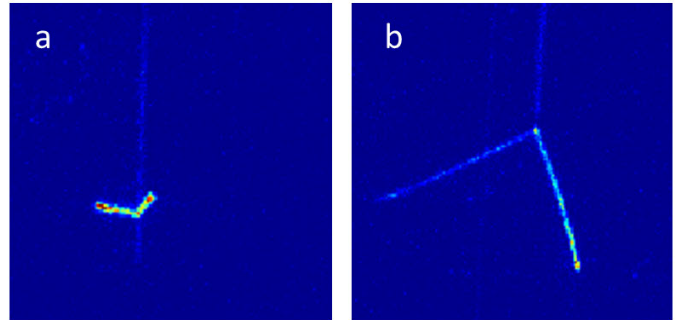


Fig. 1. Examples of CCD images showing decay events of ions stopped in the OTPC detector: (a) two-proton radioactivity of ^{54}Zn and (b) β -delayed two-proton emission from ^{55}Zn , illustrating the first observation of this channel for this nucleus.

tailed analysis of the recorded ($2p$) events is currently in progress. In addition, the collected data will be used to determine the production cross section for ^{54}Zn , which was previously unknown for the reaction used in this experiment. The cross-section systematics for neutron-deficient zinc isotopes may shed light on the puzzle of the lower-than-expected production of ^{54}Zn . Understanding the fragmentation cross sections for nuclei at the proton drip-line is of great importance for the upcoming next-generation radioactive beam facilities.

Before the final setting on ^{54}Zn was tuned, other settings of BigRIPS were optimized and calibrated. This allowed us to collect decay data for a few less-exotic nuclei in this region. According to a preliminary scan of the recorded events, approximately 50 decays of ^{55}Cu , 380 decays of ^{56}Zn , and 300 decays of ^{55}Zn were observed. Among them, the latter case is the least known: spectroscopic data for this nucleus are scarce.⁵⁾ Among the decay events of this nucleus, we observed several clear images of the β -delayed two-proton emission, a channel that has not been observed previously for this nucleus. An example of such an event is shown in Fig. 1(b). Careful analysis of all recorded decay events is in progress.

References

- 1) K. Miernik *et al.*, Eur. Phys. J. A **42**, 431 (2009).
- 2) T. Kubo *et al.*, Prog. Theor. Exp. Phys. **2012**, 03C003 (2012).
- 3) M. Pomorski *et al.*, Phys. Rev. C **90**, 014311 (2014).
- 4) K. Sümmerer, Phys. Rev. C **86**, 014601 (2012).
- 5) C. Dossat *et al.*, Nucl. Phys. A **792**, 18 (2007).

^{*1} Faculty of Physics, University of Warsaw

^{*2} Dep. of Physics and Astronomy, University of Tennessee

^{*3} RIKEN Nishina Center

^{*4} Center for Nuclear Study, University of Tokyo

^{*5} Department of Advanced Sciences, Hosei University

^{*6} Joint Institute for Nuclear Research

^{*7} National Centre for Nuclear Research

Study of the β -decay of ^{70}Kr

A. Vitéz-Sveicz, ^{*1,*2,*3} A. Algora, ^{*1,*2} A. I. Morales, ^{*1} B. Rubio, ^{*1} G. Kiss, ^{*2} J. Agramunt, ^{*1} V. Guadilla, ^{*1} A. Montaner-Pizá, ^{*1} S. E. A. Orrigo, ^{*1} A. Horváth, ^{*3} G. de Angelis, ^{*4} D. Napoli, ^{*4} F. Recchia, ^{*5} S. Lenzi, ^{*5} A. Boso, ^{*5} S. Nishimura, ^{*6} V. H. Phong, ^{*6} J. Wu, ^{*6} P. -A. Söderström, ^{*6} T. Sumikama, ^{*6} H. Suzuki, ^{*6} H. Takeda, ^{*6} D. S. Ahn, ^{*6} H. Baba, ^{*6} P. Doornebal, ^{*6} N. Fukuda, ^{*6} N. Inabe, ^{*6} T. Isobe, ^{*6} T. Kubo, ^{*6} S. Kubono, ^{*6} H. Sakurai, ^{*6} Y. Shimizu, ^{*6} C. Sidong, ^{*6} B. Blank, ^{*7} P. Ascher, ^{*7} M. Gerbaux, ^{*7} T. Goigoux, ^{*7} J. Giovannozzo, ^{*7} S. Grévy, ^{*7} T. Kurtukián Nieto, ^{*7} C. Magron, ^{*7} W. Gelletly, ^{*1,*8} Zs. Dombrádi, ^{*7} Y. Fujita, ^{*9} M. Tanaka, ^{*9} P. Aguilera, ^{*10} F. Molina, ^{*10} J. Eberth, ^{*11} F. Diel, ^{*11} D. Lubos, ^{*12} C. Borcea, ^{*13} E. Ganioglu, ^{*14} D. Nishimura, ^{*15} H. Oikawa, ^{*15} Y. Takei, ^{*15} S. Yagi, ^{*15} W. Korten, ^{*16} G. de France, ^{*17} P. Davies, ^{*18} J. Liu, ^{*19} J. Lee, ^{*19} T. Lokotko, ^{*19} I. Kojouharov, ^{*20} N. Kurz, ^{*20} and H. Shaffner ^{*20}

In this contribution, we present the preliminary results of the analysis of the experiment NP1112-RIBF93 related to our study of the β -decay of ^{70}Kr . The main goal of the experiment was to study p - n pairing and isospin-related effects in the structure of $^{70,71}\text{Kr}$ using their β -decays as a probe.

^{70}Kr nuclei were produced employing the fragmentation of a ^{78}Kr primary beam with an energy of 345 MeV/nucleon and average beam currents around 40 pA. The primary beam impinged on a 5 mm thick Be target to produce a cocktail radioactive beam. The nuclear species of interest were then separated and selected using the BigRIPS separator. The nuclei were then implanted in the WAS3ABi active stopper, surrounded by the EURICA γ -ray spectrometer¹⁾ for the study of their beta decay.

The level scheme of states in ^{70}Br populated in the beta decay of ^{70}Kr has been deduced recently. Gamma rays associated to the decay were identified using conventional β - γ and β - γ - γ coincidence techniques similarly to the procedure followed in Ref. 2). A primary assignment of gamma rays was based on the determination of the half-lives obtained from implant- β - γ correlations and their comparison with the half-life deduced from with implant- β correlations for the decay. Then γ - γ coincidences and gamma intensities were employed to fix their position in the decay level scheme. Previous to our work, only the half-life of the decay

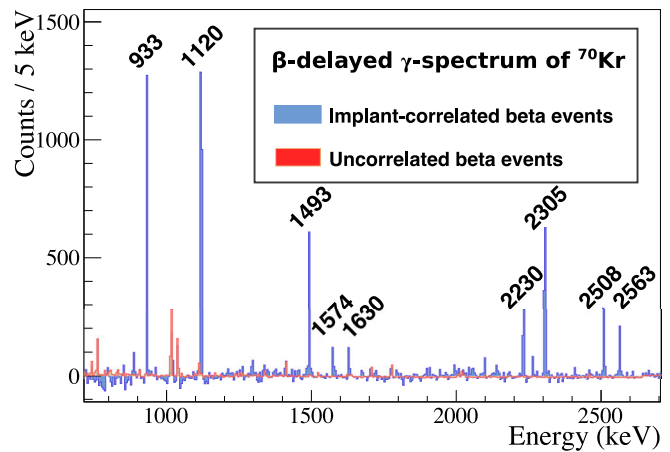


Fig. 1. Strongest identified gamma rays in the beta decay of ^{70}Kr . The spectrum is generated by requesting a condition of gamma coincidences with beta transitions correlated to ^{70}Kr implants in the analysis. Transitions tagged with negative implant- β time correlations are shown in red.

was known with lower precision and no gamma rays were associated to the decay.³⁾ From the result of our analysis fifteen gamma rays were identified for the first time and placed in the decay level scheme.⁴⁾ In Fig. 1 we present the gamma spectrum generated in coincidence with beta transitions correlated to ^{70}Kr implants (in blue), that shows the most intense gamma rays. Also for comparison, the gamma spectrum generated in coincidence with background implant-beta correlations is given (in red). Presently, a comparison of the experimental results with theoretical calculations⁵⁾ is performed in preparation for a publication.⁶⁾

References

- 1) S. Nishimura, Prog. Theor. Exp. Phys. **2012**, 03C006 (2012).
- 2) A. I. Morales *et al.*, Phys. Rev. C **95**, 064327 (2017).
- 3) G. Gürdal, E. A. Mccutchan, Nuclear Data Sheets **136**, 1 (2016).
- 4) A. Vitéz-Sveicz *et al.*, Acta Phys. Polonica B **51**, 587 (2020).
- 5) P. Sarriguren, private communication.
- 6) A. Vitéz-Sveicz *et al.*, in preparation.

*1 IFIC, CSIC-Univ. Valencia

*2 MTA ATOMKI

*3 ELTE-Budapest

*4 INFN-Legnano

*5 INFN-Padova

*6 RIKEN Nishina Center

*7 CEN Bordeaux-Gradignan

*8 Department of Physics, Surrey University

*9 Osaka University

*10 CCHEN

*11 Institute of Nucl. Physics, Universität zu Köln

*12 Physik Department, Technische Universität München

*13 IFIN-HH, Bucarest

*14 Department of Physics, University of Istanbul

*15 Tokyo Univ. Sci.

*16 IRFU, CEA, Universit Paris-Saclay

*17 GANIL-Caen

*18 Department of Physics, York University

*19 Department of Physics, University of Hong Kong

*20 GSI, Germany

Progress on the decay spectroscopy and measurement of half-lives and P_n values in exotic nuclei near the $N = 50$ shell closure

C. J. Griffin,^{*1} R. Caballero-Folch,^{*1} L. Sexton,^{*1,*2} I. Dillmann,^{*1} R. K. Grzywacz,^{*3} K. P. Rykaczewski,^{*4} J. L. Tain,^{*5} J. Agramunt,^{*5} A. Algora,^{*5} H. Baba,^{*6} S. Bae,^{*7} N. T. Brewer,^{*4} C. G. Bruno,^{*8} F. Calvino,^{*9} T. Davinson,^{*8} A. Estrade,^{*10} S. Go,^{*6} J. Ha,^{*7} O. B. Hall,^{*8} L. J. Harkness-Brennan,^{*11} T. Isobe,^{*6} D. Kahl,^{*8} M. Karny,^{*12} L. H. Khiem,^{*13} G. G. Kiss,^{*6} A. Korgul,^{*12} S. Kubono,^{*6} J. Liang,^{*14} J. Liu,^{*15} G. Lorusso,^{*2,*6,*16} K. Matsui,^{*6,*17} K. Miernik,^{*12} F. Montes,^{*18} A. I. Morales,^{*5} N. Nepal,^{*3} S. Nishimura,^{*6} V. H. Phong,^{*6,*19} B. C. Rasco,^{*4,*3} Y. Saito,^{*1} D. W. Stracener,^{*4} T. Sumikama,^{*6} A. Tarifeño-Saldivia,^{*9} A. Tolosa-Delgado,^{*5} M. Wolinska-Cichocka,^{*20} P. J. Woods,^{*8} X. X. Xu,^{*15} and R. Yokoyama^{*3} for the BRIKEN Collaboration^{*21}

β -delayed single- and multi-neutron emission is found in neutron-rich nuclei in which β decay populates states above the neutron separation energy (S_n) in the daughter nucleus. New generations of radioactive ion beam facilities will be able to produce thousands of currently inaccessible neutron-rich nuclei. Delayed neutron emission is expected to be the dominant decay process for these nuclei, with recent papers detailing the importance of β -delayed neutron emission for the r -process.^{1,2)}

In 2016, the BRIKEN collaboration constructed and commissioned the world's largest and most efficient β -delayed neutron detector^{3,4)} at RIBF to conduct a wide-ranging and systematic study into the decay properties of hundreds of the most exotic neutron-rich nuclei currently available. The BRIKEN detector consists of 140 ^3He tubes within a HDPE moderator surrounding the highly-segmented active stopper AIDA and two HPGe clover detectors in close geometry.

The NP1412-RIBF127R1 experiment implemented the BRIKEN detector to measure β -delayed neutron emission probabilities and half-lives, as well as conduct decay spectroscopy studies, around the $N = 50$ shell closure near the doubly-magic ^{78}Ni . This is a region highlighted as sensitive to β -decay properties.⁵⁾ In one of the first papers published from this experiment,^{6,7)} R. Yokoyama *et al.* observed two neutron emission in

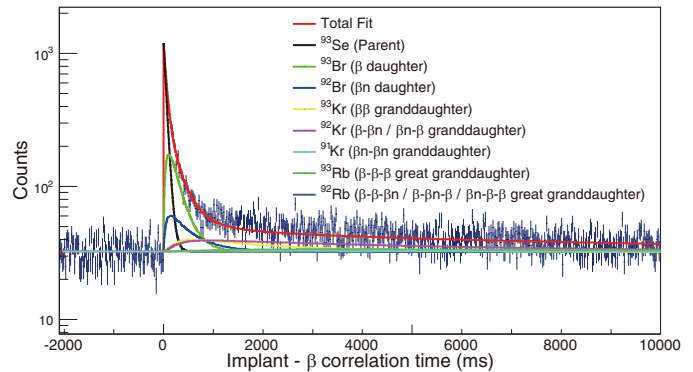


Fig. 1. Preliminary half-life analysis of ^{93}Se , showing the contributions to the total fit from the parent and daughter isotopes.

$^{84,85,87}\text{Ga}$ for the first time, and detailed dominating one-neutron emission from two-neutron unbound states in $^{86,87}\text{Ga}$.

The analysis efforts based at TRIUMF focus on the $^{91-95}\text{Se}$ and $^{94-97}\text{Br}$ isotopes. From these isotopes, half-lives and P_n values are expected to be measured for $^{92-95}\text{Se}$ and $^{95-97}\text{Br}$ for the first time. An example decay half-life Bateman fit, considering the contributions to the total fit from each of the daughter nuclei along the decay chain, is shown in Fig. 1. Decay spectroscopy information in the neutron-rich region around $A \sim 90-100$ is sparse and this analysis will allow the extraction of the first decay spectroscopy data for multiple nuclei in this region.

Further analysis of the data is ongoing and expected to yield multiple new P_n values and half-lives. Early publications highlight the potential of the highly efficient BRIKEN detector to expand the systematics of β -decay in exotic neutron-rich nuclei, vital in developing accurate r -process nucleosynthesis models.

References

- 1) A. Arcones, F. Montes, *Astrophys. J.* **731**, 5 (2011).
- 2) M. R. Mumpower *et al.*, *Phys. Rev. C* **85**, 045801 (2012).
- 3) A. Tarifeño-Saldivia *et al.*, *J. Instrum.* **12**, P04006 (2017).
- 4) A. Tolosa-Delgado *et al.*, *Nucl. Instrum. Methods Phys. Res. A* **925**, 133 (2019).
- 5) T. Shafer *et al.*, *Phys. Rev. C* **94**, 055802 (2016).
- 6) B. C. Rasco *et al.*, *Nucl. Instrum. Methods Phys. Res. A* **911**, 79 (2018).
- 7) R. Yokoyama *et al.*, *Phys. Rev. C* **100**, 031302(R) (2019).

*1 Physical Sciences Division, TRIUMF
 *2 Dept. of Physics, University of Surrey
 *3 Dept. of Physics and Astronomy, University of Tennessee
 *4 Oak Ridge National Laboratory
 *5 Instituto de Física Corpuscular (IFIC)
 *6 RIKEN Nishina Center
 *7 Dept. of Physics and Astronomy, Seoul National University
 *8 School of Physics and Astronomy, University of Edinburgh
 *9 Universitat Politècnica de Catalunya (UPC)
 *10 Dept. of Physics, Central Michigan University
 *11 Dept. of Physics, University of Liverpool
 *12 Faculty of Physics, University of Warsaw
 *13 Institute of Physics, Vietnam Academy of Science and Technology
 *14 Dept. of Physics and Astronomy, McMaster University
 *15 Dept. of Physics, University of Hong Kong
 *16 National Physical Laboratory (NPL)
 *17 Dept. of Physics, University of Tokyo
 *18 National Superconducting Cyclotron Laboratory (NSCL), Michigan State University
 *19 Faculty of Physics, VNU University of Science
 *20 Heavy Ion Laboratory, University of Warsaw
 *21 www.wiki.ed.ac.uk/display/BRIKEN/Home

Total absorption gamma spectroscopy studies around ^{100}Sn

A. Algora,^{*1,*2} J. A. Victoria,^{*1} B. Rubio,^{*1} J. L. Tain,^{*1} A. Tolosa,^{*1} J. Agramunt,^{*1} E. Nacher,^{*1} S. E. A. Orrigo,^{*1} V. Guadilla,^{*3} G. Kiss,^{*2} D. Sohler,^{*2} I. Kuti,^{*2} T. Davinson,^{*4} O. B. Hall,^{*4} D. M. Kahl,^{*4} C. G. Bruno,^{*4} C. J. Appleton,^{*4} P. J. Woods,^{*4} S. Nishimura,^{*5} N. Fukuda,^{*5} H. Suzuki,^{*5} D. S. Ahn,^{*5} H. Baba,^{*5} Y. Shimizu,^{*5} H. Takeda,^{*5} D. Nishimura,^{*5} T. Isobe,^{*5} M. Kaneko,^{*5} S. Kubono,^{*5} H. Sakurai,^{*5} H. Shimizu,^{*5} T. Sumikama,^{*5} P. Doornenbal,^{*5} M. L. Cortes,^{*6} Zs. Podolyak,^{*7} W. Gelletly,^{*7} E. Ganioglu,^{*8} Y. Fujita,^{*9} F. Molina,^{*10} J. Liu,^{*11} J. Lee,^{*11} K. P. Rykaczewski,^{*12} M. Wolinska-Cichocka,^{*13} M. Labiche,^{*14} C. J. Griffin,^{*15} S. Bae,^{*16} J. Ha,^{*16} and Y. Litvinov^{*17}

The region around ^{100}Sn in the nuclide chart is considered of great interest. There are several reasons for that: the shell structure of nuclei in the vicinity of the $Z = N = 50$ doubly-closed shell, the possibility of studying the heaviest accessible particle bound $N = Z$ nucleus ^{100}Sn , the study of the quenching of the Gamow-Teller resonance^{1,2)} and the astrophysical relevance of decays in this region for the rapid proton-capture process (see^{3,4)} and references therein).

Among the studied nuclei in the region, ^{100}Sn plays a key role. The beta decay of this nucleus and that of nuclei located south east of ^{100}Sn is dominated by the single particle Gamow-Teller transition of $\pi g_{9/2} \rightarrow \nu g_{7/2}$, which is expected to be accessible inside the Q_β window of the decay. This can provide a clear case for studying the origin of the quenching of the Gamow-Teller strength ($B(\text{GT})$), a topic that has attracted considerable attention over many years.^{1,2,5,6)}

For these kind of studies it is mandatory to use a technique that provides beta decay data that do not suffer from the Pandemonium effect.⁷⁾ This is the main motivation of the NP1612-RIBF147 experiment in which we used the total absorption spectrometer DTAS⁸⁾ developed for DESPEC (FAIR) for measurements in combination with the implantation detector AIDA.⁹⁾

The beta decay of ^{100}Sn has been previously studied using high resolution experiments at GSI and at RIKEN,^{10,11)} showing that it has the largest $B(\text{GT})$ value measured in the nuclide chart. The limited statistics and the probable presence of a low-energy gamma ray not identified in previous experiments constrain the reliability of the determination of the excitation energy of the 1^+ state in ^{100}In , the state that should be mainly

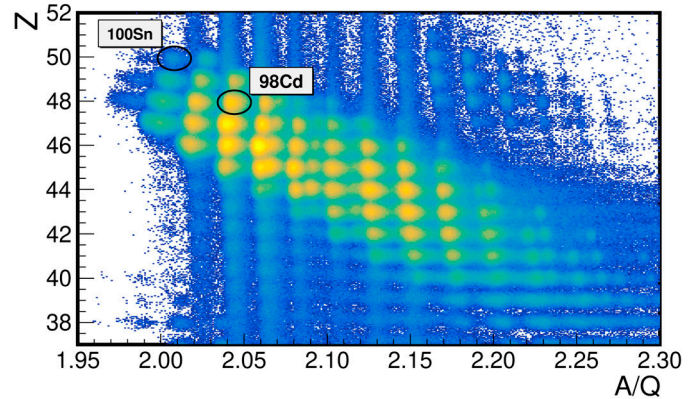


Fig. 1. Particle ID in BigRIPS from the experiment.

populated in the beta decay of ^{100}Sn . The excitation energy of this state, as well as the β end-point energy of this transition is crucial for the determination of the $B(\text{GT})$ value. The high efficiency of DTAS and its granularity can contribute to solve this question as shown by Monte Carlo simulations. In this experiment we will also have access to exotic decays that were not previously studied with the total absorption technique at the Mass Separator (MSEP) at GSI because of the limited production. In Fig. 1 we show the particle identification in BigRIPS obtained during our experiment. Due to technical problems we were able to run only 4 days from a total of 10 approved days. The continuation of the experiment is expected in 2020. The analysis of the partial set of data is on going.

References

- 1) I. Hamamoto *et al.*, Phys. Rev. C **48**, R960 (1993).
- 2) B. Alex Brown *et al.*, Phys. Rev. C **50**, R2270 (1994).
- 3) T. Faestermann *et al.*, Prog. Part. Nucl. Phys. **69**, 85 (2013).
- 4) P. Sarriguren, Phys. Rev. C **83**, 025801 (2011).
- 5) P. Gysbers *et al.*, Nat. Phys. **15**, 428 (2019).
- 6) L. Batist *et al.*, Eur. Phys. J. A **46**, 45 (2010).
- 7) J. C. Hardy *et al.*, Phys. Lett. B **71**, 307 (1977).
- 8) J. L. Tain *et al.*, Nucl. Instrum. Methods Phys. Res. A **803**, 36 (2015).
- 9) C. J. Griffin *et al.*, Proc. XIII Nuclei in the Cosmos 1, (Debrecen, Hungary, 2014) p. 97.
- 10) C. B. Hinke *et al.*, Nature **486**, 341 (2012).
- 11) D. Lubos *et al.*, Phys. Rev. Lett. **122**, 222502 (2019).

*1 IFIC, CSIC-Univ. Valencia

*2 MTA ATOMKI

*3 SUBATECH

*4 School of Physics and Astronomy, University of Edinburgh

*5 RIKEN Nishina Center

*6 INFN-Legnaro

*7 Department of Physics, Surrey University

*8 Department of Physics, University of Istanbul

*9 Osaka University

*10 CCHEN

*11 Department of Physics, University of Hong Kong

*12 Oak Ridge National Laboratory

*13 Heavy Ion Laboratory, Warsaw University

*14 STFC Daresbury Laboratory

*15 Physical Sciences Division, TRIUMF

*16 Dept. of Physics and Astronomy, Seoul National University

*17 GSI

New and comprehensive β - and βp -decay spectroscopy results in the vicinity of $^{100}\text{Sn}^\dagger$

J. Park,^{*1} R. Krücken,^{*2} D. Lubos,^{*3} R. Gernhäuser,^{*3} M. Lewitowicz,^{*4} S. Nishimura,^{*5} and H. Sakurai^{*6} for the EURICA Collaboration

The doubly magic nucleus ^{100}Sn and other nuclei with similar mass and atomic numbers possess various nuclear structure and astrophysical properties of importance.¹⁾ It is one of the few regions in the nuclear chart where experimental observables to be compared to nuclear shell model (SM) and ab-initio theories were scarce, due to the low production cross section. However, a high radioactive isotope beam production rate at RIBF enabled a decay spectroscopy experiment on ^{100}Sn and other $N \approx Z \approx 50$ nuclei, which featured WAS3ABI²⁾ and EURICA³⁾ detectors for heavy ion implantation, charged particle decay correlation and γ -ray spectroscopy.

The database on β -decay and βp -decay half-lives ($T_{1/2}$) and branching ratios (b_β , $b_{\beta p}$) of these proton-rich nuclei was greatly expanded, with new or more precise values. Several nuclei and isomers experienced notable revisions on their $T_{1/2}$ and $b_{\beta p}$. β -decay endpoint measurements yielded ground-state to ground-state energy differences for 8 proton-rich nuclei, as well as the excitation energies of 3 isomeric states (see Fig. 1). The results were consistent with AME2016,⁴⁾ mass models and SM calculations. Energy spectra of βp decays were produced with new, comparable or higher statistics in relation to the available literature.

From EURICA data, 25 new γ rays were observed and assigned to 10 new states in multiple nuclei, with guidance from empirical SM⁵⁾ in the ($p_{1/2}$, $g_{9/2}$) proton and neutron orbitals above the ^{76}Sr core. One example is the β -decay and βp decay of $^{98\text{m}}\text{In}$, where the first observation of βp -delayed γ rays from this isomer could be assigned to excited states in ^{97}Cd (see Fig. 2). As for ^{97}Cd itself, a new isomer with $J^\pi = (1/2^-)$ was proposed based on a new β -delayed γ ray with $E_\gamma = 1245$ keV, whose associated β -decay half-life was 0.73(7) s.

A systematic evaluation of the assignment of new excited states to tentative spins and parities was carried out by comparing the energies of the corresponding states, between their experimental and theoretical values. The energy discrepancies were less than 300 keV and/or 20% relative to the experimental excitation energy.

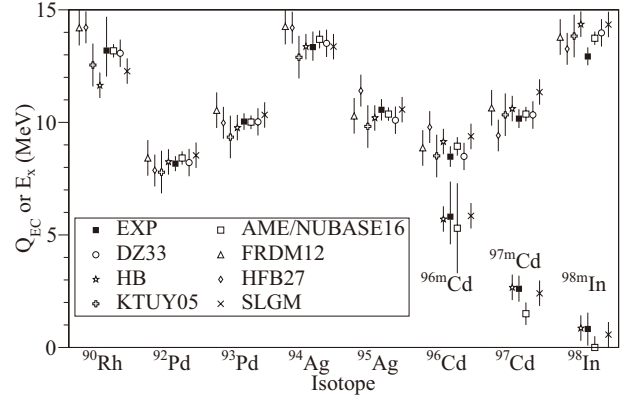


Fig. 1. Ground-state to ground-state energy differences and excitation energies of isomers deduced from β -decay endpoint energy measurements. The reader is advised to refer to the original article for references of the different mass models and SM calculations.

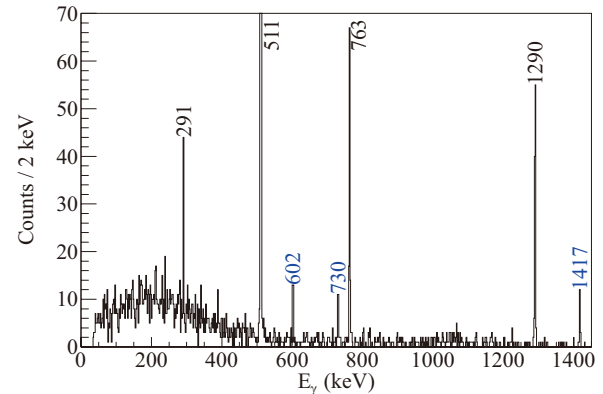


Fig. 2. γ -ray spectrum with EURICA, correlated to the βp decay of $^{98\text{m}}\text{In}$. Except for the 511-keV annihilation γ ray, the peaks labeled in black correspond to known γ rays in ^{97}Cd . Those labeled in blue were assigned as de-excitation transitions from new excited states in the same nucleus.

[†] Condensed from the article in Phys. Rev. C **99**, 034313 (2019)

^{*1} Department of Physics, Lund University

^{*2} TRIUMF

^{*3} Physik Department, Technische Universität München

^{*4} Grand Accélérateur National d'Ions Lourds (GANIL)

^{*5} RIKEN Nishina Center

^{*6} Department of Physics, University of Tokyo

References

- 1) T. Faestermann, M. Górska, H. Grawe, Prog. Part. Nucl. Phys. **69**, 85 (2013).
- 2) S. Nishimura, Prog. Theor. Exp. Phys. **2012**, 03C006 (2012).
- 3) P. -A. Söderström *et al.*, Nucl. Instrum. Methods Phys. Res. B **317**, 649 (2013).
- 4) M. Wang *et al.*, Chin. Phys. C **41**, 030003 (2017).
- 5) F. J. D. Serduke, R. D. Lawson, D. H. Gloeckner, Nucl. Phys. A **256**, 45 (1976).

Improved value for the Gamow-Teller strength of the ^{100}Sn beta-decay[†]

D. Lubos,^{*1,*2} J. Park,^{*3} T. Faestermann,^{*1} R. Gernhäuser,^{*1} R. Krücken,^{*4} M. Lewitowicz,^{*5} S. Nishimura,^{*2} and H. Sakurai^{*6} for the EURICA collaboration

The main aim of experiment NP0702-RIBF09 was to improve the value for the Gamow-Teller strength of the ^{100}Sn beta-decay. This is important because ^{100}Sn is the heaviest self-conjugate doubly-magic nucleus. The data have now been evaluated and published.

With about 2500 nuclei the number of detected ^{100}Sn nuclei was about ten times higher than in previous experiments and new isotopic species towards the proton dripline were discovered at the RIKEN Nishina Center.¹⁾

Decay spectroscopy has been performed with the high-efficiency detector arrays WAS3ABi and EURICA. The half-life of ^{100}Sn was measured more precisely than the literature values²⁾ using two methods: a) β -decays correlated with identified mother nuclei and b) correlated β -decays were in coincidence one of the known γ -rays following the beta-decay was observed. Both results agreed yielding an average of $T_{1/2} = 1.18 \pm 0.08$ s. This value agrees with and has about half the error compared to the average of the previous values.

Similarly, the β -decay endpoint energy was determined for two data sets, the β -spectrum after a ^{100}Sn implantation and by requiring, in addition, a γ -ray from the decay. The method was tested by analyzing also the ^{98}Cd decay Q-value. Both ^{100}Sn data sets yielded consistent results which give as average $Q_\beta = 3.91 \pm 0.15$ MeV. This value is more precise and larger than the best previous result²⁾ by about twice the summed error bars. This discrepancy may be due to unaccounted systematic uncertainties in either measurement.

The value and the uncertainty of the resulting strength for the pure $0^+ \rightarrow 1^+$ Gamow-Teller decay is improved to $B_{\text{GT}} = 4.4^{+0.9}_{-0.7}$. In Fig. 1 we compare a number of theoretical calculations of BGT with experimental values: an extrapolation of the B_{GT} -values of the heavier even-even Sn isotopes (the error bar seems too small) and the values measured in the two previous experiments at GSI. Of all theories the chiral effective field theory seems to describe the data best.

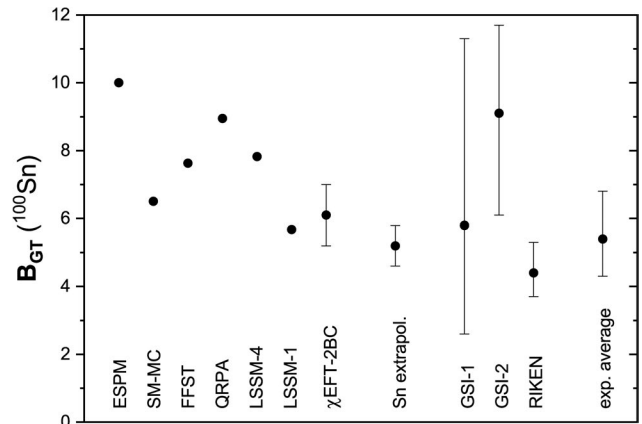


Fig. 1. Comparison of experimental and predicted GT transition strengths of ^{100}Sn . The theoretical values on the left side are from: Extreme Shell Model,³⁾ Shell Model - Monte Carlo,⁴⁾ Finite Fermi Systems and Quasiparticle Random Phase Approximation,⁵⁾ Large Scale Shell Model with transitions to the four and one lowest 1^+ -states,²⁾ the range of recent work explaining GT-quenching with calculations using Effective Field Theory combined with 2-Body Currents.⁶⁾ Experimental values are: an extrapolation from heavier even Sn isotopes,⁷⁾ first⁸⁾ and second²⁾ GSI experiment, the present result and the average of all available experimental data. For the weighted average of Q_β its error has been inflated by a factor 1.8 to account for the too large χ^2 .

References

- 1) I. Celikovic *et al.*, Phys. Rev. Lett. **116**, 162501 (2016).
- 2) C. B. Hinke *et al.*, Nature **486**, 341 (2012), and Suppl. Info.
- 3) A. de Shalit, I. Talmi, *Nuclear Shell Theory* (Academic Press, New York and London, 1963).
- 4) D. Dean, S. Koonin, T. Kuo, K. Langanke, P. Radha, Phys. Lett. B **367**, 17 (1996).
- 5) A. Bobyk, W. Kaminski, Acta Phys. Pol. B **31**, 953 (2000).
- 6) P. Gysbers *et al.*, Nature Phys. **15**, 428 (2019).
- 7) L. Batist *et al.*, Eur. Phys. J. A **46**, 45 (2010).
- 8) T. Faestermann *et al.*, Eur. Phys. J. A **15**, 185 (2002).

[†] Condensed from the article in Phys. Rev. Lett. **122**, 222502 (2019)

*1 Technische Universität München

*2 RIKEN Nishina Center

*3 Lund University

*4 TRIUMF

*5 GANIL, CEA/DSM-CNRS/IN2P3

*6 University of Tokyo

β -delayed neutron emission probabilities for understanding the formation of the r -process rare-earth abundance peak (REP)

G. G. Kiss,^{*1} A. Tarifeño-Saldivia,^{*2} J. L. Tain,^{*3} A. Estrade,^{*4} S. Nishimura,^{*5} J. Agramunt,^{*3} A. Algorta,^{*3} N. T. Brewer,^{*6} R. Caballero-Folch,^{*7} F. Calvino,^{*2} T. Davinson,^{*8} I. Dillmann,^{*7} N. Fukuda,^{*5} R. K. Grzywacz,^{*9} O. Hall,^{*6} A. I. Morales,^{*3} A. Navarro,^{*2} N. Nepal,^{*5} B. C. Rasco,^{*6} K. P. Rykaczewski,^{*6} N. T. Szegedi,^{*1} A. Vitéz-Sveiczner,^{*1} A. Tolosa-Delgado,^{*3} P. Vi,^{*10} R. Yokoyama,^{*9} M. Wolinska-Cichocka,^{*11} and P. Woods^{*8} for the BRIKEN collaboration^{*12}

The abundance distribution of the rapid-neutron capture (so-called r -) process is characterized by two large maxima at masses of $A \sim 130$ and $A \sim 195$, which are related to the flow of matter through the neutron shell closures at $N = 82$ and $N = 126$. However, there is an additional, relatively small—but distinct—peak around $A \sim 160$, which corresponds to the region of the rare-earth elements. In contrast to the main abundance maxima that form during the $(n, \gamma) \leftrightarrow (\gamma, n)$ equilibrium, the rare-earth abundance peak (REP) originates later, after neutron exhaustion, thus representing a unique opportunity to study the late-time environmental conditions of the r -process.¹⁻³⁾ Several different peak-production mechanisms were suggested, but experimental data—masses, β -decay parameters, and neutron capture rates—are clearly needed to evaluate the different astrophysical scenarios. The most influential nuclei to the REP formation, located in the $A \sim 160$, $55 \leq Z \leq 64$ neutron-rich region, have been identified by sensitivity studies.³⁾

The aim of the NP1612-RIBF148 experimental program is to measure the β -decay parameters, half-lives, and delayed-neutron-emission probabilities (P_n values) of these species using the BRIKEN array, which is the largest and most efficient β -delayed neutron detector built.^{4,5)} It consists of 140 ^3He gas-filled proportional counters embedded in a high-density polyethylene moderator. The neutron detector and two CLARION-type clover high purity germanium detectors are placed around the AIDA DSSSD array⁶⁾ which contains six layers of highly segmented Si detectors for the detection of implantations and β electrons.

The study was conducted at the Radioactive Isotope Beam Factory. A 60-pnA intensity ^{238}U beam

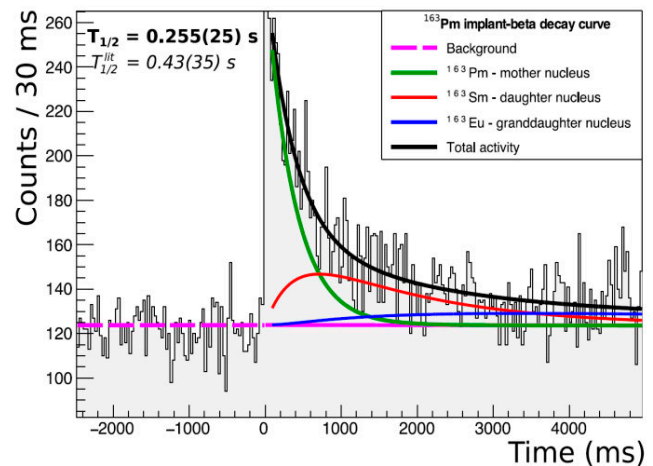


Fig. 1. Preliminary half-life analysis for ^{163}Pm isotopes, showing the contributions to the total fit from the parent, daughter, and granddaughter isotopes. Our $T_{1/2}$ result is compared to the existing data⁷⁾ (bold and slanted characters, respectively).

was accelerated up to an energy of 345 MeV/nucleon before incidence on a 4-mm thick Be target to produce radioactive secondary beams by in-flight fission. The nuclei of interest were separated and identified in the BigRIPS spectrometer, transported through the ZeroDegree spectrometer, and implanted in the AIDA array. Figure 1 shows the results of the preliminary half-life analysis of the ^{163}Pm isotope. Although some half-lives in this region have already been measured⁷⁾ our experiment will not only provide a large number of new P_n values⁸⁾ and half-lives but also considerably improve the precision of the available data.

References

- 1) R. Surman *et al.*, Phys. Rev. Lett. **79**, 1809 (1997).
- 2) A. Arcones, G. Martinez Pinedo, Phys. Rev. C **83**, 045809 (2011).
- 3) R. M. Mumpower *et al.*, Prog. Part. Nucl. Phys. **86**, 86 (2016).
- 4) A. Tarifeño-Saldivia *et al.*, J. Instrum. **12**, P04006 (2016).
- 5) A. Tolosa-Delgado *et al.*, Nucl. Instrum. Methods Phys. Res. **925**, 133 (2019).
- 6) C. Griffin *et al.*, Proc. Sci. **NIC-XIII**, 097 (2014).
- 7) J. Wu *et al.*, Phys. Rev. Lett. **118**, 072701 (2017).
- 8) A. Tarifeño-Saldivia *et al.*, RIKEN Accel. Prog. Rep. **52**, 39 (2019).

^{*1} Institute for Nuclear Research (Atomki)
^{*2} Universitat Politècnica de Catalunya (UPC)
^{*3} Instituto de Física Corpuscular (IFIC)
^{*4} University College of Science and Engineering, Central Michigan University (CMU)
^{*5} RIKEN Nishina Center
^{*6} Oak Ridge National Laboratory
^{*7} Physical Sciences Division, TRIUMF
^{*8} School of Physics and Astronomy, University of Edinburgh
^{*9} Department of Physics and Astronomy, University of Tennessee
^{*10} Faculty of Physics, VNU University of Science
^{*11} HIL, University of Warsaw
^{*12} www.wiki.edu.ac.uk/display/BRIKEN/Home

Evolution of collectivity and mirror symmetry along $N = Z$

K. Wimmer,^{*1,*2} T. Hüyük,^{*1} F. Browne,^{*3} P. Doornenbal,^{*3} T. Koiwai,^{*2,*3} H. Sakurai,^{*2,*3} T. Arici,^{*4} M. Bentley,^{*5} M. L. Cortés,^{*6} N. Imai,^{*7} A. Jungclaus,^{*1} N. Kitamura,^{*7} S. Lenzi,^{*8,*6} B. Longfellow,^{*9} R. Lozeva,^{*10} B. Mauss,^{*3} D. Napoli,^{*6} M. Niikura,^{*2} X. Pereira-Lopez,^{*5} F. Recchia,^{*8,*6} P. Ruotsalainen,^{*11} R. Taniuchi,^{*2,*3} S. Uthayakumar,^{*5} V. Vaquero,^{*1} R. Wadsworth,^{*5} and R. Yajzey^{*5,*12}

Unlike any other physical system the nucleus represents a unique dual quantum many-body system. Its constituents, the protons and neutrons, are assumed to be identical, except for their electric charge. They can be seen as two representations of the nucleon, with isospin components $t_z = \pm 1/2$ for neutrons and protons, respectively. Under the assumption of charge independence of the strong interaction, hence invariance under rotation in the isospin space, the properties of mirror nuclei should be identical.

Mirror symmetry is typically studied through energy differences between excited states of mirror nuclei or isospin triplets. Measurements of $B(E2; 0_{gs}^+ \rightarrow 2_1^+)$ values for $T = 1$ isospin triplets allow to extract information on the proton and neutron matrix elements and to test isospin symmetry.¹⁾ The proton and neutron multipole matrix elements can be written in isospin representation

$$M_{n/p} = \frac{1}{2} (M_0(T_z) \pm M_1(T_z)) \quad (1)$$

where $M_0(T_z)$ is the isoscalar and $M_1(T_z)$ the isovector multipole matrix element. Assuming isospin conservation the proton matrix elements of isobars are a linear function of T_z only, *i.e.* $M_0(T_z) = M_0$ and $M_1(T_z) = M_1 \cdot T_z$, with constant $M_{0/1}$ for all T_z . The linearity provides a direct test of the isospin purity of the states. So far this has been tested for light nuclei, mostly in the sd shell, the heaviest case where the $B(E2; 0_{gs}^+ \rightarrow 2_1^+)$ values of all three members are measured is the $A = 46$ system.²⁾

In order to test this relation in heavier nuclei we have studied the Coulomb excitation of $A = 62$ nuclei. All three nuclei were studied under identical experimental conditions to reduce the statistical and theoretical uncertainties. The ^{62}Zn , ^{62}Ga , and ^{62}Ge beams were produced by the fragmentation of a 345 AMeV primary ^{78}Kr beam provided by the SRC. Unique particle identification in BigRIPS and the ZeroDegree Spectrome-

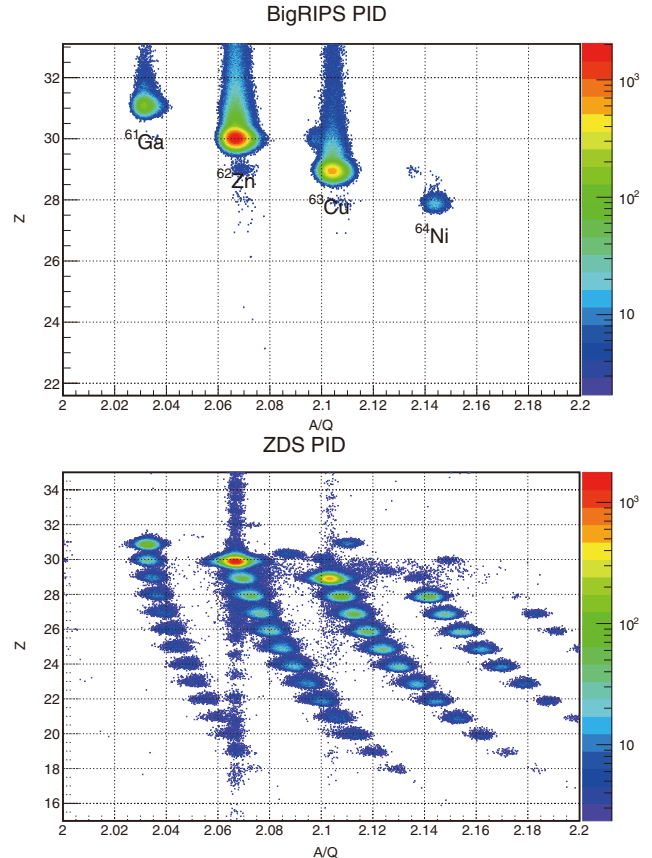


Fig. 1. Particle identification plots for the ^{62}Zn beam impinging on the Be target.

ter was achieved by means of ΔE - $B\rho$ -TOF measurements. Secondary Be and Au targets were used to determine the $B(E2; 0_{gs}^+ \rightarrow 2_1^+)$ values. The particle identification plots for the ^{62}Zn beam impinging on the Be target is shown in Fig. 1.

The beams impinged on secondary targets located at the F8 focus. γ rays from excited states were detected in the DALI2+ array. Sufficient statistics for all three members of the $A = 62$ multiplet were collected to determine the linearity of the proton multipole matrix elements with a precision of about 5%. Additionally new states were observed in nuclei beyond the $N = Z$ line. The results will shed new light on the evolution of collectivity along the $N = Z$ line and provide one of the most stringent tests of isospin symmetry.

References

- 1) A. M. Bernstein, V. R. Brown, V. A. Madsen, Phys. Rev. Lett. **42**, 425 (1979).
- 2) A. Boso *et al.*, Phys. Lett. B **797**, 134835 (2019).

*1 IEM-CSIC

*2 Department of Physics, The University of Tokyo

*3 RIKEN Nishina Center

*4 GSI Helmholtzzentrum für Schwerionenforschung

*5 Department of Physics, University of York

*6 INFN-Laboratori Nazionali di Legnaro

*7 Center for Nuclear Study, The University of Tokyo

*8 Department of Physics, University of Padova

*9 NSCL, Michigan State University

*10 CSNSM, Université Paris-Sud

*11 Department of Physics, University of Jyväskylä

*12 Physics Department, Jazan University

First attempt at in-beam γ -ray spectroscopy of ^{100}Sn

S. Chen,^{*1} J. Lee,^{*1} A. Corsi,^{*2} K. Wimmer,^{*3} P. Doornenbal,^{*4} F. Browne,^{*4} M. L. Cortés,^{*5} T. Koiwai,^{*3,*4} H. Sakurai,^{*3,*4} A. Algora,^{*6} D. Brugnara,^{*5,*7} J. Cederkäll,^{*8} J. Gerl,^{*9} M. Górska,^{*9} G. Haefner,^{*10} K. Kokubun,^{*3} P. Koseoglou,^{*11,*9} S. Kubono,^{*4} P. Li,^{*1} P. Liang,^{*1} J. Liu,^{*1} Z. Liu,^{*12} T. Lokotko,^{*1} J. Park,^{*8} L. G. Sarmiento,^{*8} R. Taniuchi,^{*4,*13} W. Xian,^{*1} and I. Zanon^{*5}

The study of the heaviest self-conjugate exotic doubly magic nucleus ^{100}Sn and the single-particle nature of its neighboring nuclei are of great importance to the fundamental understanding of nuclear structure and the astrophysical rp -process path. Owing to the low production rate, no spectroscopic information, except β -decay, has been measured for ^{100}Sn so far. As one of the first observables for nuclear structure, we aim at the measurement of the first 2^+ state of ^{100}Sn , which indicates the strength of the $N = Z = 50$ shell closures. A proposal was made to populate the excited states from neutron-removal reactions of heavier Sn isotopes to perform an in-beam γ -ray spectroscopy measurement.¹⁾ In order to properly estimate the beam time required, the production cross sections for ^{100}Sn through secondary fragmentation reactions need to be known. We performed an experiment with a beam time of 4 days to measure the production cross sections of ^{100}Sn produced in neutron-removal reactions from $^{101,102}\text{Sn}$.

A ^{124}Xe primary beam at 345 MeV/nucleon was provided by SRC with an average intensity of ~ 140 pA. The beam impinged on a 5-mm-thick ^9Be target to produce radioactive beams containing neutron-deficient Sn isotopes with the BigRIPS separator. It was tuned to center on ^{101}Sn nuclei while accepting ^{102}Sn simultaneously. Average beam intensities in front of the secondary targets were 2 pps and 27.5 pps for $^{101,102}\text{Sn}$. A 5-mm-thick CH_2 target and a 3-mm-thick C target were used to induce the $1n$ - and $2n$ -removal reactions of $^{101,102}\text{Sn}$ on C and H. The beam particles and reaction products were identified with the BigRIPS and ZeroDegree spectrometers, respectively, via the measurements of $B\rho$, ΔE , and ToF on an event-by-event basis. The beam energies were measured to be ~ 173 MeV/nucleon in BigRIPS and only ~ 98 MeV/nucleon in ZeroDegree. The DALI2⁺ high-efficiency γ -detection array²⁾ was employed to detect

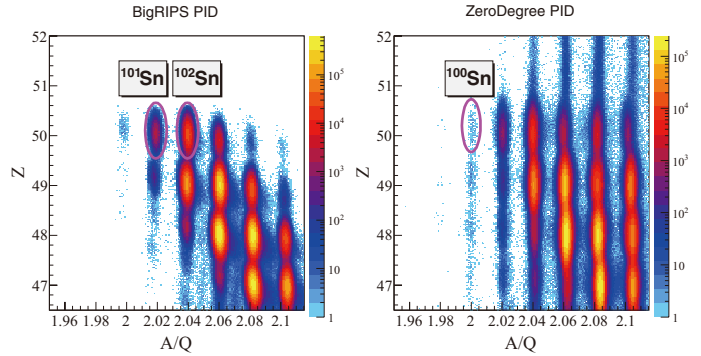


Fig. 1. BigRIPS particle identification (left) and ZeroDegree particle identification (right). The isotopes $^{101,102}\text{Sn}$ are selected in BigRIPS, while ^{100}Sn is selected in ZeroDegree.

Table 1. Number of identified events and rates.

	5 mm CH_2	3 mm C
$-1n: ^{101}\text{Sn} \rightarrow ^{100}\text{Sn}^{50+}$	53 (1.3/h)	40 (1.0/h)
$-2n: ^{102}\text{Sn} \rightarrow ^{100}\text{Sn}^{50+}$	42 (1.0/h)	30 (0.8/h)

the γ rays emitted in flight from reaction products in the vicinity of ^{100}Sn .

The particle identification plots of BigRIPS and ZeroDegree are shown in Fig. 1. Data were accumulated for 41 h on a CH_2 target and 38 h on a C target. The total numbers and counting rates of fully stripped ^{100}Sn produced by $1n$ - and $2n$ -removal reactions are summarized in Table 1.

The cross sections on the C target were determined from the number of incident projectiles, the number of reaction products identified in ZeroDegree, the atom number in the target, as well as the ZeroDegree transmission and acceptance measured in the same setting. The cross sections on H were determined using the data with the CH_2 target, subtracting the contribution measured on the C target, after normalization. To maximize the statistics, hydrogen-like charge states of ^{100}Sn in the ZeroDegree were considered to be used in $1n$ -removal reactions. Preliminary values for cross sections have been obtained. Several new γ transitions were also observed in this region. Detailed analyses for cross sections and γ spectroscopy are ongoing.

References

- 1) J. Lee, A. Corsi, K. Wimmer, RIKEN Proposal (2016).
- 2) S. Takeuchi *et al.*, Nucl. Instrum. Methods Phys. Res. A **763**, 596 (2014).

*1 Department of Physics, The University of Hong Kong

*2 IRFU, CEA, Université Paris-Saclay

*3 Department of Physics, University of Tokyo

*4 RIKEN Nishina Center

*5 INFN-LNL

*6 IFIC Valencia

*7 University of Padova

*8 Department of Physics, Lund University

*9 GSI Helmholtzzentrum Darmstadt

*10 Université Paris-Saclay, CNRS/IN2P3, IJCLab

*11 Institut für Kernphysik, Technische Universität Darmstadt

*12 Institute of Modern Physics, Chinese Academy of Sciences

*13 Department of Physics, University of York

Intermediate-energy Coulomb excitation of ^{102}Sn

M. L. Cortés,^{*1,*2} F. Browne,^{*2} P. Doornenbal,^{*2} S. Chen,^{*3} A. Corsi,^{*4} T. Koiwai,^{*5,*2} J. Lee,^{*3} H. Sakurai,^{*2,*5} K. Wimmer,^{*5} A. Algora,^{*6} D. Brugnara,^{*1} J. Cederkäll,^{*7} J. Gerl,^{*8} M. Gorska,^{*8} G. Haefner,^{*9} K. Kokubun,^{*5} P. Koseoglou,^{*10} S. Kubono,^{*2} P. Li,^{*3} P. Liang,^{*3} J. Liu,^{*3} Z. Liu,^{*11} T. Lokotko,^{*3} J. Park,^{*7} L. G. Sarmiento,^{*7} R. Taniuchi,^{*12} W. Xian,^{*3} and I. Zanon^{*1}

Being presumably the heaviest, particle-bound, doubly magic $N = Z$ nucleus, ^{100}Sn offers a fundamental testing ground for nuclear theories. Experimental signatures of shell structure can be provided by the 2_1^+ energies as well as by the reduced transition probabilities, $B(E2; 0_{\text{gs}}^+ \rightarrow 2_1^+)$. In the Sn isotopes between the $N = 50$ and $N = 82$ shell closures, the 2_1^+ energies are well established and show an almost constant value,¹⁾ as expected in the generalized seniority scheme. Within the same framework, the $B(E2)\uparrow$ values should resemble an inverted parabola peaking at mid-shell. However, measurements in the most proton-rich Sn isotopes,²⁻⁴⁾ have shown a clear deviation from the expected behavior.

Different calculations based on the large-scale shell model as well as on the relativistic quasi-particle random-phase approximation have been performed in order to give an account of the measured $B(E2)\uparrow$ values.⁵⁾ Although the calculations tend to agree on the neutron-rich side of the chain, significant differences are observed on the proton-rich side. This is particularly true for ^{102}Sn , where the difference between the predictions amounts to almost a factor of 3, making this isotope a good candidate for the investigation of the effects driving the nuclear structure in the vicinity of ^{100}Sn . In order to elucidate the nuclear structure underlying the measured $B(E2)\uparrow$ values, the first Coulomb excitation measurement of ^{102}Sn was performed at the RIBF.⁶⁾

A 345 MeV/nucleon beam of ^{124}Xe with an average intensity of 120 pnA was fragmented on a 5 mm thick Be target at the entrance of the BigRIPS separator⁷⁾ to produce ^{102}Sn . Within the same experimental setting, ^{100}Cd was also transmitted. The isotopes of interest were identified on an event-by-event basis using the $B\rho\text{-}\Delta E\text{-}B\rho$ technique. Figure 1a) shows the particle identification obtained in BigRIPS, where ^{102}Sn and ^{100}Cd are clearly visible. A 0.5 mm Au target placed at F8 was used to induce Coulomb ex-

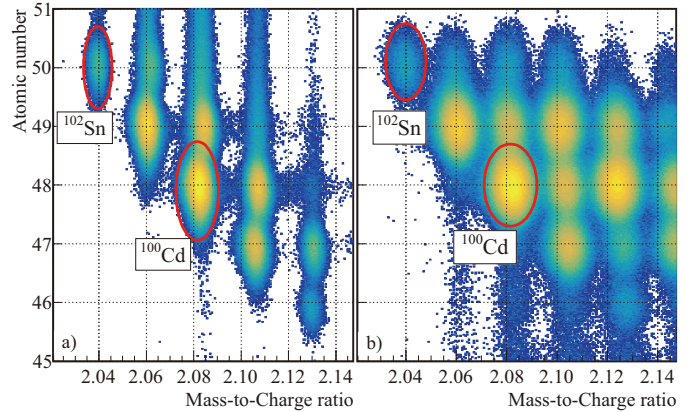


Fig. 1. Particle identification in a) BigRIPS, and b) Zero degree. In both cases ^{102}Sn and ^{100}Cd are clearly identified.

citation. In addition, measurements with a 3 mm C target were performed to obtain the nuclear contribution to the cross section. Outgoing fragments were identified using the ZeroDegree spectrometer, as shown in Fig. 1b). The target was surrounded by the high-efficiency DALI2⁺ γ -detector array, composed of 226 NaI(Tl) detectors.^{8,9)} The average beam intensities before the secondary target were 90 pps and 4200 pps for ^{102}Sn and ^{100}Cd , respectively, with an energy around 177 MeV/nucleon.

As part of the experiment, the incoming beam was implanted into a plastic target at F7 for 1 h, and data on the γ rays emitted following the decay of the isomer were collected using a HPGe detector. By combining the information on the number of ions implanted and the total γ rays observed, the isomeric ratio of the beam can be obtained. This quantity is fundamental for the correct determination of the cross section from the Coulomb excitation measurement. Finalization of the outgoing particle identification and further analysis on the in-beam γ -ray spectra of ^{102}Sn and ^{100}Cd is ongoing.

References

- 1) <http://www.nndc.bnl.gov/ensdf/>.
- 2) G. Guastalla *et al.*, Phys. Rev. Lett. **110**, 172501 (2013).
- 3) V. M. Bader *et al.*, Phys. Rev. C **88**, 051301(R) (2013).
- 4) P. Doornenbal *et al.*, Phys. Rev. C **90**, 061302(R) (2014).
- 5) T. Togashi *et al.*, Phys. Rev. Lett. **121**, 062501 (2018).
- 6) M. L. Cortés, Experiment NP1612-RIBF153R1.
- 7) T. Kubo, *et al.*, Prog. Theor. Exp. Phys. **2012** (2012).
- 8) S. Takeuchi *et al.*, Nucl. Instrum. Methods Phys. Res. A **763**, 596 (2014).
- 9) I. Murray *et al.*, RIKEN Accel. Prog. Rep. **51**, 158 (2017).

*1 INFN-Laboratori Nazionali di Legnaro

*2 RIKEN Nishina Center

*3 Department of Physics, The University of Hong Kong

*4 IRFU, CEA, Université Paris-Saclay

*5 Department of Physics, The University of Tokyo

*6 IFIC Valencia

*7 Department of Physics, Lund University

*8 GSI Helmholtzzentrum für Schwerionenforschung

*9 Université Paris-Saclay, CNRS/IN2P3, IJCLab

*10 Institut für Kernphysik, Technische Universität Darmstadt

*11 Institute of Modern Physics, Chinese Academy of Sciences

*12 Department of physics, University of York

In-beam γ -ray spectroscopy of ^{136}Te at relativistic energies[†]

V. Vaquero,^{*1} A. Jungclaus,^{*1} P. Doornenbal,^{*2} K. Wimmer,^{*3,*2} A. M. Moro,^{*4} K. Ogata,^{*5} T. Furumoto,^{*6} S. Chen,^{*2,*7} E. Nácher,^{*1} E. Sahin,^{*8} Y. Shiga,^{*9} D. Steppenbeck,^{*2} R. Taniuchi,^{*2,*3} Z. Y. Xu,^{*10} T. Ando,^{*3} H. Baba,^{*2} F. L. Bello Garrote,^{*8} S. Franchoo,^{*11} K. Hadynska-Klek,^{*8} A. Kusoglu,^{*12,*13} J. Liu,^{*10} T. Lokotko,^{*10} S. Momiyama,^{*3} T. Motobayashi,^{*2} S. Nagamine,^{*3} N. Nakatsuka,^{*14} M. Niikura,^{*3} R. Orlandi,^{*15} T. Saito,^{*3} H. Sakurai,^{*2,*3} P. A. Söderström,^{*2} G. M. Tveten,^{*8} Zs. Vajta,^{*16} and M. Yalcinkaya^{*12}

The reduced transition probability $B(E2; 0_1^+ \rightarrow 2_1^+)$ to the first excited 2^+ state of the neutron-rich nucleus ^{136}Te , with two protons and two neutrons outside the doubly-magic ^{132}Sn core, has been measured via Coulomb excitation at relativistic energies at the RIKEN Radioactive Isotope Beam Factory. A value of $B(E2) = 0.191(26) e^2b^2$ was extracted from the measured inelastic scattering cross section on a Au target taking into account the contributions from both Coulomb and nuclear excitations. This value is compared to previous experimental results reported in the literature and various theoretical calculations in Fig. 1. Our measurement, performed at relativistic energies, agrees with the large value which has recently been obtained in Coulomb excitation at safe energies at Oak Ridge.¹⁾ It is, however, in conflict with the low-energy Coulomb excitation measurement of Refs. 2–3) and the preliminary result of the experiment using the fast timing technique reported by Fraile *et al.*⁴⁾ For a detailed discussion of the comparison to theory we refer the reader to the original publication.

The high statistics gathered in the present experiment allowed for the first time to evaluate in detail the validity of the approach employed in the analysis of Coulomb excitation experiments at beam energies around 150 MeV/nucleon and to estimate the systematic uncertainties involved in the different steps of the analysis. In this publication, a detailed discussion of the analysis procedure is provided so that it can serve as guideline for the analysis of future experiments using the same technique but accumulating less statistics. In particular, the correct determination of the

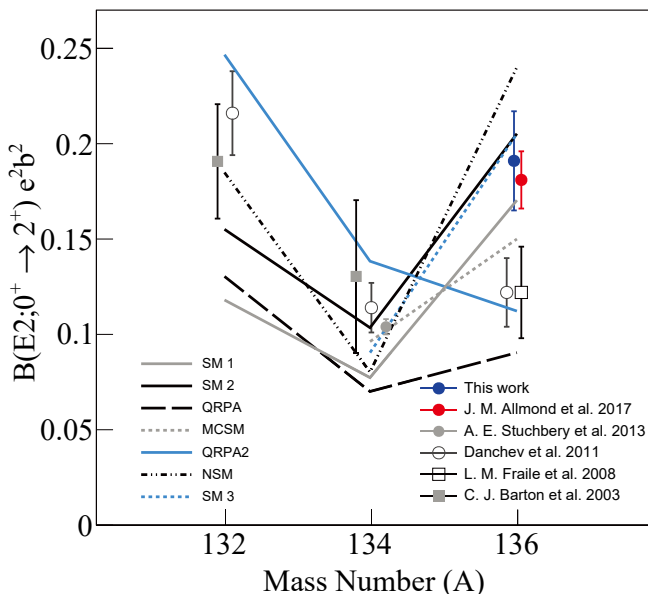


Fig. 1. Comparison of the experimental $B(E2; 0_1^+ \rightarrow 2_1^+)$ value for ^{136}Te determined in the present work to literature values for the $^{132}, ^{134}, ^{136}\text{Te}$ isotopes and different theoretical calculations (for details see the original publication).

exclusive scattering cross section to the 2_1^+ state, taking into account the scattering-angle dependent losses due to the limited acceptance of the ZeroDegree spectrometer and losses due to reactions which take place on any material in the beam line between the identifications in BigRIPS and the ZeroDegree spectrometer, is discussed in detail. The other important part of the analysis concerns the determination of a $B(E2)$ value from the measured exclusive cross section, which requires a consistent description of both nuclear and electromagnetic excitations. In the present case, the code FRESKO^{5,6)} was employed for this purpose.

References

- 1) J. M. Allmond *et al.*, Phys. Rev. Lett. **118**, 092503 (2017).
- 2) D. C. Radford *et al.*, Phys. Rev. Lett. **88**, 222501 (2002).
- 3) M. Danchev *et al.*, Phys. Rev. C **84**, 061306(R) (2011).
- 4) L. M. Fraile *et al.*, Nucl. Phys. A **805**, 218 (2008).
- 5) I. J. Thompson, Comput. Phys. Rep. **7**, 3 (1988).
- 6) <http://fresco.org.uk>.

[†] Condensed from the article in Phys. Rev. C **99**, 034306 (2019)

*1 IEM-CSIC Madrid

*2 RIKEN Nishina Center

*3 Department of Physics, University of Tokyo

*4 Universidad de Sevilla, Sevilla

*5 Research Center for Nuclear Physics, Osaka University

*6 Graduate School of Education, Yokohama National University

*7 Peking University, Beijing

*8 University of Oslo, Oslo

*9 Department of Physics, Rikkyo University

*10 University of Hong Kong

*11 IN2P3-CNRS, Orsay

*12 Istanbul University, Istanbul

*13 ELI-NP, Magurele

*14 Department of Physics, Kyoto University

*15 Advanced Science Research Center, JAEA, Tokai

*16 MTA Atomki, Debrecen

Study of Gamow-Teller transitions from ^{11}Li

L. Stuhl,^{*1,*2,*10} M. Sasano,^{*2} J. Gao,^{*2,*3} Y. Hirai,^{*4} K. Yako,^{*1} T. Wakasa,^{*4} D. S. Ahn,^{*2} H. Baba,^{*2} A. I. Chilug,^{*5,*2} S. Franchoo,^{*6} Y. Fujino,^{*7} J. Gibelin,^{*8} I. S. Hahn,^{*9} Z. Halász,^{*10} T. Harada,^{*11} M. N. Harakeh,^{*12,*13} D. Inomoto,^{*4} T. Isobe,^{*2} H. Kasahara,^{*4} D. Kim,^{*14} G. G. Kiss,^{*10} T. Kobayashi,^{*15} Y. Kondo,^{*16} Z. Korkulu,^{*2,*10} S. Koyama,^{*17} Y. Kubota,^{*2} A. Kurihara,^{*16} H. N. Liu,^{*18} M. Matsumoto,^{*16} S. Michimasa,^{*1} H. Miki,^{*16} M. Miwa,^{*19} T. Motobayashi,^{*2} T. Nakamura,^{*16} M. Nishimura,^{*2} H. Otsu,^{*2} V. Panin,^{*2} S. Park,^{*9} A. T. Saito,^{*16} H. Sakai,^{*2} H. Sato,^{*2} T. Shimada,^{*16} Y. Shimizu,^{*2} S. Shimoura,^{*1} A. Spiridon,^{*5} I. C. Stefanescu,^{*5} X. Sun,^{*2,*3} Y. L. Sun,^{*18} H. Suzuki,^{*2} Y. Togano,^{*7} T. Tomai,^{*16,*2} L. Trache,^{*5} D. Tudor,^{*5,*2} T. Uesaka,^{*2} H. Yamada,^{*16} M. Yasuda,^{*16} K. Yoneda,^{*2} K. Yoshida,^{*2} J. Zenihiro,^{*2} and N. Zhang^{*20,*1}

The studies of dynamic properties of exotic nuclei such as giant resonances, which are manifested at high excitation energies ($>10\text{--}15$ MeV), are in the very early stage. No data are available on spin-isospin collectivity for nuclei with large isospin asymmetry factors, where $(N - Z)/A > 0.25$.¹⁾

In the SAMURAI30 experiment, we studied the most basic nuclear collectivity, the Gamow-Teller (GT) giant resonance, in the drip-line nucleus ^{11}Li at 181 MeV/nucleon. The charge-exchange (CE) (p, n) reactions in inverse kinematics are efficient tools to extract the $B(\text{GT})$ strengths of unstable isotopes up to high excitation energies, without Q -value limitation.²⁾

The combined setup of Particle Analyzer Neutron Detector Of Real-time Acquisition (PANDORA)³⁾ low-energy neutron counter and the SAMURAI magnetic spectrometer,⁴⁾ together with a thick liquid hydrogen target allowed us to perform such measurements with high luminosity. In this setup, PANDORA is used for the detection of the recoil neutrons. The neutron kinetic energies are deduced by the time-of-flight technique, and SAMURAI is used for tagging the decay channel of the reaction residues. Many relevant decay channels after the CE reaction can be measured in a single magnetic rigidity setting owing to the large acceptance of SAMURAI. Such a setup was already successfully used in our first (p, n) experiment on ^{132}Sn .⁵⁾ It was proven that we can obtain information about the strength distribution of isovector spin-flip giant resonances of unstable nuclei with quality comparable to those on stable nuclei.⁵⁾

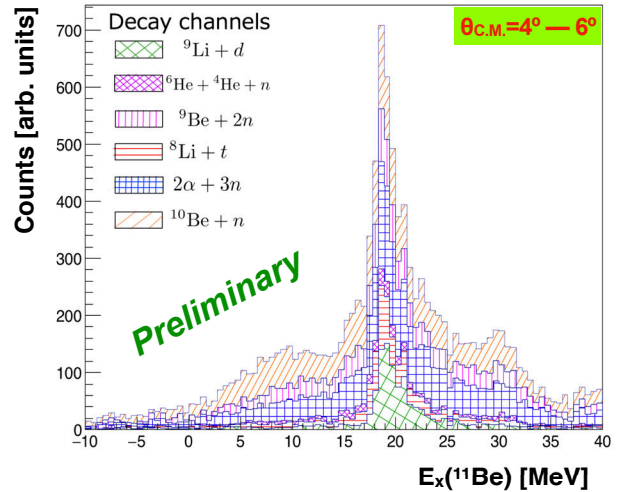


Fig. 1. Preliminary excitation energy spectrum in the $4^\circ\text{--}6^\circ$ center-of-mass system. The contributions of different decay channels are presented.

In our $^{11}\text{Li}(p, n)^{11}\text{Be}$ measurement, we successfully identified clear kinematical correlations⁶⁾ between the neutron energy and laboratory scattering angle for the different decay channels of ^{11}Be : $^{10}\text{Be}+n$, $^9\text{Be}+2n$, $\alpha+^6\text{He}+n$, $2\alpha+3n$, $^8\text{Li}+t$, and $^9\text{Li}+d$.

The reconstruction of the excitation-energy spectrum up to about 40 MeV, including the giant resonance region, is ongoing. Figure 1 presents preliminary results of the excitation energy spectra in the daughter nucleus ^{11}Be . The background subtraction and correction for the detection efficiency and acceptance are ongoing. We will derive the excitation energy spectra for $\theta_{C.M.} = 1^\circ\text{--}10^\circ$ from all decay channels. The forward scattering peaks in the $0^\circ\text{--}8^\circ$ center-of-mass system, suggest a strong GT transition at approximately 18 MeV, in agreement with previous beta-decay studies.⁷⁾

References

- 1) K. Nakayama *et al.*, Phys. Lett. B **114**, 217(1982).
- 2) M. Sasano *et al.*, Phys. Rev. Lett. **107**, 202501 (2011).
- 3) L. Stuhl *et al.*, Nucl. Instrum. Methods Phys. Res. A **866**, 164 (2017).
- 4) T. Kobayashi *et al.*, Nucl. Instrum. Methods Phys. Res. B **317**, 294 (2013).
- 5) J. Yasuda *et al.*, Phys. Rev. Lett. **121**, 132501 (2018).
- 6) L. Stuhl *et al.*, Nucl. Instrum. Methods Phys. Res. B **463**, 189 (2020).
- 7) R. Raabe *et al.*, Phys. Rev. Lett. **101**, 212501 (2008).

*1 Center for Nuclear Study, University of Tokyo, Japan
 *2 RIKEN Nishina Center, Japan
 *3 School of Physics, Peking University, China
 *4 Department of Physics, Kyushu University, Japan
 *5 Horia Hulubei Nat. Inst. of Phys. and Nucl. Eng., Romania
 *6 Inst. de Physique Nuclaire, Univ. Paris-Saclay, France
 *7 Department of Physics, Rikkyo University, Japan
 *8 LPC CAEN, France
 *9 Department of Physics, Ewha Womans University, Korea
 *10 ATOMKI, Institute for Nuclear Research, HAS, Hungary
 *11 Department of Physics, Toho University, Japan
 *12 KVI - CART, University of Groningen, The Netherlands
 *13 GSI Helmholtzzentrum für Schwerionenforschung, Germany
 *14 Department of Physics, Korea University, Korea
 *15 Department of Physics, Tohoku University, Japan
 *16 Dept. of Physics, Tokyo Institute of Technology, Japan
 *17 Department of Physics, University of Tokyo, Japan
 *18 Dépt. Physique Nucl., CEA, Univ. Paris-Saclay, France
 *19 Dept. of Physics, Saitama University, Saitama, Japan
 *20 Institute of Modern Physics, Chinese Acad. of Sci., China

Structure of ^{13}Be probed via quasi-free scattering

A. Corsi,^{*1} Y. Kubota,^{*2,3} G. Authelet,^{*1} H. Baba,^{*2} C. Caesar,^{*4} D. Calvet,^{*1} A. Delbart,^{*1} M. Dozono,^{*3} J. Feng,^{*5} F. Flavigny,^{*6} J.-M. Gheller,^{*1} J. Gibelin,^{*7} A. Giganon,^{*1} A. Gillibert,^{*1} K. Hasegawa,^{*8,2} T. Isobe,^{*2} Y. Kanaya,^{*9,2} S. Kawakami,^{*9,2} D. Kim,^{*10,2} Y. Kiyokawa,^{*3} M. Kobayashi,^{*3} N. Kobayashi,^{*11} T. Kobayashi,^{*8,2} Y. Kondo,^{*12,2} Z. Korkulu,^{*2} S. Koyama,^{*11,2} V. Lapoux,^{*1,2} Y. Maeda,^{*9} F. M. Marqués,^{*7} T. Motobayashi,^{*2} T. Miyazaki,^{*11} T. Nakamura,^{*12,2} N. Nakatsuka,^{*14,2} Y. Nishio,^{*15,2} A. Obertelli,^{*3,2} A. Ohkura,^{*15,2} N. A. Orr,^{*7} S. Ota,^{*3} H. Otsu,^{*2} T. Ozaki,^{*12,2} V. Panin,^{*2} S. Paschalis,^{*4} E. C. Pollacco,^{*1} S. Reichert,^{*16} J.-Y. Roussé,^{*1} A. T. Saito,^{*12,2} S. Sakaguchi,^{*15,2} M. Sako,^{*2} C. Santamaria,^{*1,2} M. Sasano,^{*2} H. Sato,^{*2} M. Shikata,^{*12,2} Y. Shimizu,^{*2} Y. Shindo,^{*15,2} L. Stuhl,^{*2} T. Sumikama,^{*8,2} M. Tabata,^{*15,2} Y. Togano,^{*12,2} J. Tsubota,^{*12,2} T. Uesaka,^{*2} Z. H. Yang,^{*2} J. Yasuda,^{*15,2} K. Yoneda,^{*2} J. Zenihiro,^{*2} J. Casal,^{*17} M. Gómez-Ramos,^{*18} and A. M. Moro^{*18}

Several experiments have attempted to study the spectroscopy of the unbound isotope ^{13}Be via both the missing-mass and invariant-mass technique using charge exchange, fragmentation, proton removal from ^{14}B , and neutron removal from ^{14}Be . Even when considering only the results obtained with the last method,¹⁻⁴⁾ interpretation of the excitation spectrum is sparse.

We performed a new measurement of neutron removal from ^{14}Be at the RIBF facility using the SAMURAI spectrometer⁵⁾ and its standard detectors, in addition to the MINOS target-tracker system⁶⁾ surrounded by gamma detectors from the DALI2 array. For the interpretation of the invariant mass spectrum of ^{13}Be , we adopted a novel method, proposed in Ref. 7), which uses consistent three- and two-body models for ^{14}Be and ^{13}Be , respectively, and can provide predictions for the absolute cross sections, including the positions and weights of the structures of the spectrum, thus reducing ambiguities in the analysis. A part of the complexity of the ^{13}Be continuum spectrum stems from the admixtures of single-particle structures with core-excited components. In this experiment, we were able to measure with high statistics the possible $^{12}\text{Be}(2^+, 1^-)$ core excited component that decays via gamma rays.

The relative energy spectrum of ^{13}Be is shown in Fig. 1. The absolute cross section is determined taking into account the efficiency for invariant-mass measurement and fragment transmission. The spectrum

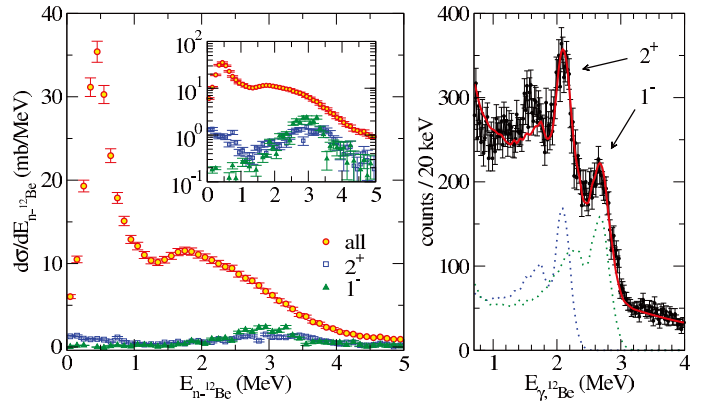


Fig. 1. Left: relative energy spectrum of ^{13}Be and contributions from core excited components. Right: gamma spectrum of ^{12}Be . The two transitions are reproduced by the sum of an exponential background and the response functions (dashed curves) of the DALI2 detector obtained via a GEANT4 simulation.

is characterized by a prominent peak with a maximum at ~ 0.48 MeV and a broader structure, peaked at ~ 2.3 MeV, extending from ~ 1 MeV to ~ 5 MeV. The contribution corresponding to $^{12}\text{Be}(2^+)$ and $^{12}\text{Be}(1^-)$ core excited states has been fixed via coincidences with 2.1 and 2.7 MeV gamma transitions, respectively, and is shown for comparison after correcting for gamma-detection efficiency.

The interpretation of the relative energy and transverse momentum spectrum, described more thoroughly in Ref. 8), permitted to pin down the dominant $\ell = 1$ contribution of the resonant peak observed in the low-lying spectrum, in agreement with²⁾ and at variance with the conclusions of Refs. 3-4), which assigned a dominant $\ell = 0$ content to this peak.

References

- 1) H. Simon *et al.*, Nucl. Phys. A **791**, 267 (2007).
- 2) Y. Kondo *et al.*, Phys. Lett. B **690**, 245 (2010).
- 3) Y. Aksyutina *et al.*, Phys. Lett. B **718**, 1309 (2013).
- 4) Y. Aksyutina *et al.*, Phys. Rev. C **87**, 064316 (2013).
- 5) T. Kobayashi *et al.*, Nucl. Instrum. Methods Phys. Res. B **317**, 294 (2013).
- 6) A. Obertelli *et al.*, Eur. Phys. J. A **50**, 8 (2014).
- 7) M. Gómez-Ramos *et al.*, Phys. Lett. B **772**, 115, (2017).
- 8) A. Corsi *et al.*, Phys. Lett. B **797**, 134843 (2019).

*1 CEA, Université Paris-Saclay
 *2 RIKEN Nishina Center
 *3 Center for Nuclear Study, University of Tokyo
 *4 Department of Physics, Technische Universität Darmstadt
 *5 Department of Physics, Peking University
 *6 IPN Orsay
 *7 LPC Caen
 *8 Department of Physics, Tohoku University
 *9 Department of Applied Physics, University of Miyazaki
 *10 Department of Physics, Ehwa Womans University
 *11 Department of Physics, University of Tokyo
 *12 Department of Physics, Tokyo Institute of Technology
 *14 Department of Physics, Kyoto University
 *15 Department of Physics, Kyushu University
 *16 Department of Physics, Technische Universität München
 *17 Dipartimento di Fisica e Astronomia, Università di Padova and INFN
 *18 Departamento de Física Atómica, Molecular y Nuclear, Facultad de Física, Universidad de Sevilla

Overview of the experimental setup of SAMURAI11 to measure the $^{48}\text{Cr}(p, n)$ and $^{64}\text{Ge}(p, n)$ reactions in inverse kinematics

M. Sasano,^{*1} J. Gao,^{*1,*3} L. Stuhl,^{*2} Y. Hirai,^{*4} T. Wakasa,^{*4} D. S. Ahn,^{*1} J. K. Ahn,^{*13} H. Baba,^{*1} K. Chae,^{*20} A. Chilug,^{*5,*1} K. Cook,^{*15} Y. Fujino,^{*7} N. Fukuda,^{*1} B. Gao,^{*19} S. Goto,^{*4} I. S. Hahn,^{*8} Y. Hamano,^{*4} Z. Halász,^{*9} T. Harada,^{*10} S. Hong,^{*20} S. Huang,^{*1,*3} N. Inabe,^{*1} D. Inomoto,^{*4} T. Isobe,^{*1} H. Kasahara,^{*4} D. Kim,^{*8} T. Kobayashi,^{*14} Y. Kondo,^{*15} Z. Korkulu,^{*1} A. Krasznahorkai,^{*9} H. Miki,^{*15} K. Miki,^{*14} S. Mitsumoto,^{*4} M. Miwa,^{*18} T. Motobayashi,^{*1} T. Nakamura,^{*15} M. Nishimura,^{*1} H. Oshiro,^{*4} H. Otsu,^{*1} V. Panin,^{*1} S. Sakaguchi,^{*4} D. Sakai,^{*14} H. Sakai,^{*1} S. Sakaki,^{*4} H. Sato,^{*1} T. Shimada,^{*15} Y. Shimizu,^{*1} B. Sun,^{*21} X. Sun,^{*1,*3} H. Suzuki,^{*1} J. Tanaka,^{*1} Y. Togano,^{*7} T. Tomai,^{*15,*1} T. Uesaka,^{*1} Y. Utsuki,^{*14} H. Wang,^{*15} X. Xu,^{*19} K. Yako,^{*2} A. Yasuda,^{*15} K. Yoneda,^{*1} K. Yoshida,^{*1} Y. Yoshitome,^{*15} and J. Zenihiro^{*1}

In this report, we provide an overview of the setup used in the SAMURAI11 experiment performed at the RI Beam Factory (RIBF) of RIKEN Nishina Center in the spring of 2019.

The experiment was performed to measure the (p, n) reaction on ^{48}Cr and ^{64}Ge . For each of ^{48}Cr and ^{64}Ge , a secondary cocktail beam was produced via the fragmentation reaction of a 345 MeV/nucleon ^{78}Kr primary beam on a 3 mm-thick ^9Be target installed at the F0 focal plane of the BigRIPS separator. The purity of ^{48}Cr (^{64}Ge) was 75.9% (58.3%) for a total beam intensity of 1.5×10^5 (1.4×10^5) particle/s.

The SAMURAI spectrometer¹⁾ was used as the key device to tag the (p, n) reaction channel through the particle identification of residual beam nuclei. The large acceptance of the SAMURAI spectrometer was crucial to detect a wide range of residual nuclei with different masses and proton numbers in the same setup.

Figure 1 shows a schematic view of the experimental setup around the SAMURAI spectrometer. Two thin plastic scintillators (SBT1,2) were installed downstream of STQ25 for the detection of beam particles. Two multi-wire drift chambers were installed (BDC1,2) to tune the beam focus. The secondary beam was transported onto a liquid hydrogen (Liq. H) target with a thickness and diameter of 10 and 60 mm, respectively, at the secondary target position of SAMURAI (F13).

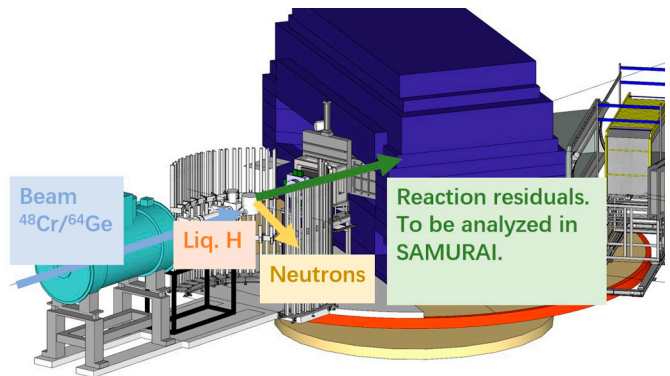


Fig. 1. Schematic view of the experimental setup around the SAMURAI spectrometer.

The PANDORA neutron detector setup consisted of 37 plastic scintillators and was placed on the left and right sides of the Liq. H target. The neutron-gamma pulse-shape discrimination (PSD) capability of PANDORA in combination with a new DAQ system based on digitizers enables the reduction of the gamma-ray background originating from the environment as well as from the beam.²⁾ PANDORA was optimized to detect neutrons with a kinetic energy of 0.1–5 MeV. The reaction residues entered SAMURAI after passing through the forward drift chambers, FDC0 and FDC1. The magnetic field of the spectrometer was set to 1.45 (1.36) T for the ^{48}Cr (^{64}Ge) beam. At the focal plane of SAMURAI, the beam residue particles were tracked by FDC2K/3K drift chambers, followed by plastic scintillator walls HODS. In this experiment, a high rate of accepted triggers of approximately 5 kHz was achieved by employing a new method.³⁾

We are grateful to the RIKEN accelerator staff and CNS, University of Tokyo, for their continuous efforts to accomplish this stable beam acceleration.

References

- 1) T. Kobayashi, *et al.*, Nucl. Instrum. Methods Phys. Res. B **317**, 294 (2013).
- 2) L. Stuhl, *et al.*, Nucl. Instrum. Methods Phys. Res. A **866**, 164–172 (2017).
- 3) J. Gao *et al.*, in this report.

^{*1} RIKEN Nishina Center, Japan
^{*2} Center for Nuclear Study, University of Tokyo, Japan
^{*3} School of Physics, Peking University, China
^{*4} Department of Physics, Kyushu University, Japan
^{*5} Horia Hulubei Nat. Inst. of Phys. and Nucl. Eng., Romania
^{*7} Department of Physics, Rikkyo University, Japan
^{*8} Department of Physics, Ewha Womans University, Korea
^{*9} ATOMKI, Institute for Nuclear Research, HAS, Hungary
^{*10} Department of Physics, Toho University, Japan
^{*11} KVI - CART, University of Groningen, The Netherlands
^{*12} GSI Helmholtzzentrum für Schwerionenforschung, Germany
^{*13} Department of Physics, Korea University, Korea
^{*14} Department of Physics, Tohoku University, Japan
^{*15} Dept. of Physics, Tokyo Institute of Technology, Japan
^{*16} Department of Physics, University of Tokyo, Japan
^{*18} Dept. of Physics, Saitama University, Saitama, Japan
^{*19} Institute of Modern Physics, Chinese Acad. of Sci., China
^{*20} Department of Physics, Sungkyunkwan University, Korea
^{*21} School of Physics and Nuclear Engineering, Beihang University, China

Role of ^{66}Se in the rp -process nucleosynthesis in type I X-ray bursts

V. Panin,^{*1} A. Chilug,^{*2} A. Saastamoinen,^{*3} Z. Halasz,^{*4} D. S. Ahn,^{*1} A. Al-Adili,^{*5} H. Baba,^{*1} K. Cook,^{*6} C. Dósa,^{*4} Z. Elekes,^{*4} N. Fukuda,^{*1} J. Gao,^{*1} J. Gibelin,^{*7} K. Hahn,^{*8} G. Hegyesi,^{*4} T. Isobe,^{*1} D. Kim,^{*8} T. Kobayashi,^{*1} Y. Kondo,^{*6} A. Kurihara,^{*6} I. Kuti,^{*4} H. Miki,^{*6} K. Miki,^{*9} T. Motobayashi,^{*1} H. Otsu,^{*1} M. Sasano,^{*1} H. Sato,^{*1} T. Shimada,^{*6} Y. Shimizu,^{*1} L. Sobotka,^{*10} I. Stefanescu,^{*2} L. Stuhl,^{*1} H. Suzuki,^{*1} H. Takeda,^{*1} Y. Togano,^{*11} T. Tomai,^{*6} L. Trache,^{*2} D. Tudor,^{*2} T. Uesaka,^{*1} Y. Utsuki,^{*9} H. Wang,^{*6} A. Yasuda,^{*6} K. Yoneda,^{*1} and Y. Yoshitome^{*6}

The important role of ^{66}Se in the dynamics of the rp -process occurring in type I X-ray bursts was pointed out by several theoretical studies.^{1,2} The resonant proton capture reaction $^{65}\text{As}(p, \gamma)^{66}\text{Se}$ can provide a potential breakout path from the waiting-point nucleus ^{64}Ge . Theoretical variations of the rate of this reaction predict a dramatic effect on the resulting chemical abundances and light curves of the X-ray bursts, while the experimental constraints have not yet been well established.

The experiment NP1406-SAMURAI24 was conducted in March 2019 to measure the time-reversal process, namely one- and two-proton emission from the unbound states of ^{66}Se populated by neutron removal from a ^{67}Se projectile at 250 MeV/nucleon in a carbon target. A secondary beam of ^{67}Se was obtained by the fragmentation of the primary ^{78}Kr beam at 345 MeV/nucleon from SRC in a 2 mm Be target. The secondary ^{67}Se beam intensity at the end of BigRIPS was on the order of 10^3 pps with a purity of approximately 10%.

A schematic of the experimental setup at SAMURAI is shown in Fig. 1. Two carbon targets with thicknesses

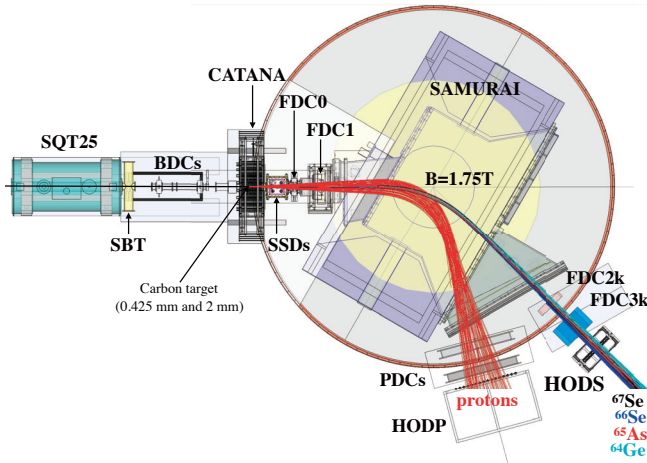


Fig. 1. The experimental setup in NP1406-SAMURAI24.

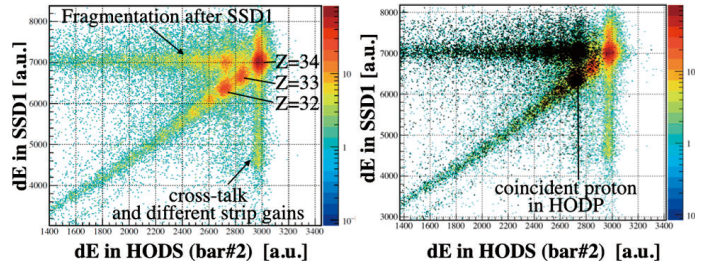


Fig. 2. Charge identification of outgoing fragments in the first SSD and in HODS.

of 0.425 mm and 2 mm were used inside the CATANA gamma detector³) followed by an array of GLAST-type⁴) silicon-strip detectors (SSDs) for coincident measurements of the forward-focused protons and heavy fragments. The SSDs are equipped with dedicated dual-gain ASIC preamplifiers.^{5,6}) In addition, two drift chambers (FDC0 and FDC1) are placed behind the SSDs for tracking the fragments. The SAMURAI spectrometer is used to separate the reaction products and direct them into corresponding tracking systems. Protons are measured by two drift chambers (PDCs) and a hodoscope (HODP), and heavy fragments are measured by two other drift chambers (FDC2k and FDC3k) and a hodoscope (HODS).

Figure 2 shows an example of coincident charge identification of the heavy fragments in the first SSD behind the target and in one scintillating bar of HODS with a cut on the ^{67}Se projectile. Secondary fragmentation occurring in the beamline materials downstream of the target can be clearly identified. The events on the diagonal line indicate the reactions that occur in the target. The right panel of Fig. 2 shows the overlap of the same correlation plot with an additional condition on the coincident proton signal in HODP (black dots). Further analysis of the experimental data is ongoing.

References

- 1) A. Parikh *et al.*, Prog. Part. Nucl. Phys. **69**, 225 (2013).
- 2) Y. H. Lam *et al.*, arXiv:1505.02275v1 (2015).
- 3) Y. Togano *et al.*, Nucl. Instrum. Methods Phys. Res. B, **463**, 195 (2020).
- 4) C. Sgrò *et al.*, Nucl. Instrum. Methods Phys. Res. A, **583**, 9 (2007).
- 5) V. Panin *et al.*, RIKEN Accel. Prog. Rep. **49**, 164 (2016).
- 6) V. Panin *et al.*, RIKEN Accel. Prog. Rep. **51**, 148 (2018).

*1 RIKEN Nishina Center

*2 IFIN-HH, Bucharest-Magurele

*3 Texas A&M University

*4 MTA Atomki, Debrecen

*5 Uppsala University

*6 Department of Physics, Tokyo Institute of Technology

*7 LPC Caen

*8 Ewha Woman's University, Seoul

*9 Department of Physics, Tohoku University

*10 Washington University in St. Louis

*11 Department of Physics, Rikkyo University

Particle identification of light charged particle by S π RIT-TPC in Sn-Sn isotopic reactions II

M. Kaneko,^{*1,*2} J. Barney,^{*2,*3} G. Cerizza,^{*2,*3} J. Estee,^{*2,*3} W. G. Lynch,^{*3} T. Isobe,^{*2} G. Jhang,^{*2,*3} M. Kurata-Nishimura,^{*2} P. Lasko,^{*5,*2} J. Łukasik,^{*5} T. Murakami,^{*1,*2} P. Pawłowski,^{*5,*2} C. Santamaria,^{*2,*7} M. B. Tsang,^{*3} J. W. Lee,^{*4,*2} and Y. Zhang^{*6,*2} for the S π RIT collaboration

The main focus of the S π RIT-TPC⁽¹⁾ project is to constrain the high-density nuclear equation of state by using heavy-ion reactions. S π RIT-TPC is designed to measure charged pions as well as light charged particles from central collisions, which have been predicted to be sensitive probes of dense nuclear matter.^(2,3) This report describes particle identification (PID) in TPC based on the last report⁽⁵⁾ and the preliminary spectra of protons and deuterons in $^{132}\text{Sn}+^{124}\text{Sn}$ reactions.

The PID in TPC relies on two measured observables, namely, the magnetic rigidity and energy deposit per unit length (dE/dx). The truncated-mean method was applied for the dE/dx measurement, which was found to depend on the emission angles. To calibrate the angle dependence of dE/dx , tracks were classified by their pitch (Θ^{Pitch}) and yaw (Θ^{Yaw}) angles, and their origins are set to the beam-axis direction. Figure 1 shows dE/dx vs magnetic rigidity plots in two different angular regions of pitch and yaw angles. The loci of protons, deuterons, and tritons were simultaneously fitted by the simplified Bethe-Bloch formula⁽⁴⁾ for each region. As explained in Ref. 5), the mass was calculated from given dE/dx and rigidity values with fitting parameters. Then, the angle-calibrated observable is obtained.

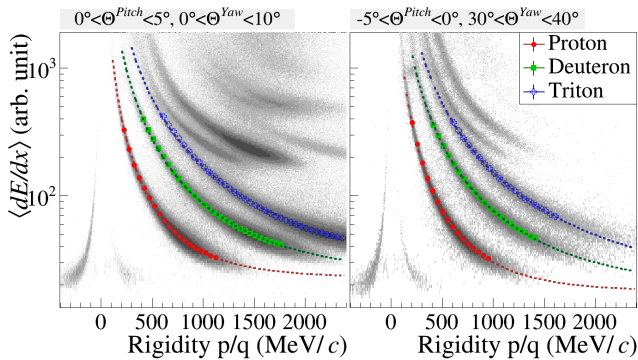


Fig. 1. Particle identification spectra for different emission angles. Overdrawn markers and dotted lines are the Gaussian-fitted mean dE/dx values in each 50 MeV/c rigidity bin and the results of a simultaneous fit, respectively.

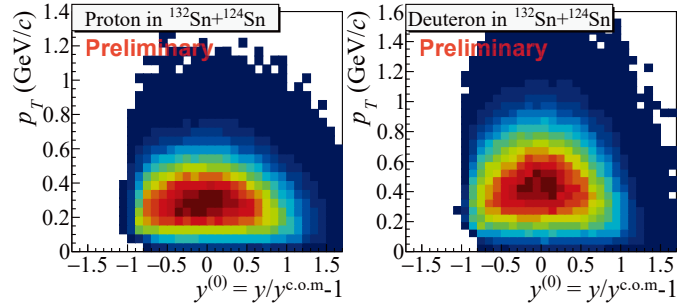


Fig. 2. Transverse momentum and normalized rapidity spectra of protons and deuterons in central $^{132}\text{Sn}+^{124}\text{Sn}$ reactions without efficiency corrections.

Figure 2 presents preliminary spectra of the transverse momentum p_T vs normalized rapidity $y^{(0)}$ without detection-efficiency corrections for protons and deuterons in $^{132}\text{Sn}+^{124}\text{Sn}$ reactions. The rapidity was normalized by the center-of-mass rapidity of the reaction system ($y^{\text{c.o.m}}$) and shifted by -1 . A higher track multiplicity cut, $M_{\text{TPC}} \geq 55$, was applied for selecting central collisions. Protons and deuterons were identified using the angle-dependent mass described above. The value $y^{(0)} = -1$ corresponds to the perpendicular emissions, and it is close to the acceptance limit of the TPC. At $y^{(0)} \geq -0.5$, approximately symmetric distributions centered at the mid-rapidity, $y^{(0)} = 0$, were obtained, which is reasonable as the kinematics of heavy-ion reactions. To extract physics information and to compare with model predictions, efficiency correction is necessary, which is currently being evaluated by Monte Carlo simulations.

This work is supported by the Japanese MEXT KAKENHI Grant No. 24105004; the U.S. DOE under Grant Nos. DE-SC0004835, DE-SC0014530, and DE-NA0002923; the U.S. NSF Grant No. PHY-1565546; and the Polish NSC Grant Nos. UMO-2013/09/B/ST2/04064 and UMO-2013/10/M/ST2/00624. The computing resources were provided by the HOKUSAI system at RIKEN.

References

- 1) R. Shane *et al.*, Nucl. Instrum. Methods Phys. Res. A **784**, 513 (2015).
- 2) M. B. Tsang *et al.*, Phys. Rev. C **95**, 044614 (2017).
- 3) N. Ikeno *et al.*, Phys. Rev. C **97**, 069902 (2018).
- 4) A. A. Mudrokh, A. I. Zinchenko, J. Phys. Conf. Ser. **798**, 012071 (2017).
- 5) M. Kaneko *et al.*, RIKEN Accel. Prog. Rep. **52**, 36 (2019).

*1 Department of Physics, Kyoto University

*2 RIKEN Nishina Center

*3 NSCL and Dept. of Phys. & Ast., Michigan State University

*4 Department of Physics, Korea University

*5 Institute of Nuclear Physics, PAN, Kraków, Poland

*6 Department of Physics, Tsinghua University

*7 Lawrence Berkeley National Laboratory, UC Berkeley

Monte carlo simulation of collective flow analysis for S π RIT-TPC

M. Kurata-Nishimura,^{*1} J. Barney,^{*2,*1} G. Cerizza,^{*2,*1} J. Estee,^{*2,*1} B. Hong,^{*3} T. Isobe,^{*1} G. Jhang,^{*2,*1} M. Kaneko,^{*4,*1} H. S. Lee,^{*7} J. W. Lee,^{*3,*1} J. Łukasik,^{*5} W. G. Lynch,^{*2} A. B. McIntosh,^{*8} T. Murakami,^{*4,*1} P. Pawłowski,^{*5,*1} H. Sakurai,^{*1} C. Santamaria,^{*2,*1} R. Shane,^{*2} D. Suzuki,^{*1} M. B. Tsang,^{*2} and S. J. Yennello^{*8} for S π RIT Collaboration

The SAMURAI Pion-Reconstruction and Ion-Tracker-Time-Projection Chamber (S π RIT-TPC)¹⁾ project aims to constrain the nuclear equation of state (EoS) at supra-saturation density using heavy ion collisions.

In heavy ion collision, the corrective flow, which is one of sensitive probes to the nuclear EoS, characterized by asymmetric azimuthal emission amplitude, v_1 and v_2 with respect to a reaction plane orientation, Ψ ,

$$\frac{2\pi}{N} \frac{dN}{d(\phi - \Psi)} = 1 + 2v_1 \cos(\phi - \Psi) + 2v_2 \cos(2(\phi - \Psi)). \quad (1)$$

The Ψ is determined from an azimuthal angle distribution of charged particles event by event. In S π RIT-TPC experiment, the Ψ is calculated summing up unit vectors of transverse momentum for $Z = 1$ and 2 particles.²⁾ The detector bias on the Ψ caused by its rectangular shape and a limited acceptance was corrected using shifting and flattening methods.³⁾ The coefficients, v_1 and v_2 , were obtained after correcting with a reaction plane resolution⁴⁾ which depends on the laboratory azimuthal angle.

A Monte Carlo simulation was performed to validate our analysis method. Configurations of the generated events were chosen to reproduce distributions of real data as listed in Table 1. Two acceptance setting for the S π RIT-TPC and 4π (full) coverage were compared

Table 1. Configurations in the Monte Carlo simulation.

The center of mass rapidity normalized with the beam rapidity was defined as $y_{nrm} \equiv y_{cm}/y_{beam}$. The transverse momentum $u_t (= \beta_t \gamma_t)$ was utilized.

Particle	proton
Multiplicity	40
dN/dy_{nrm}	$\exp(-0.5 * (y_{nrm}/0.78)^2)$
dN/du_t	$\exp(-0.1u_t)$
v_1	$0.52y_{nrm} - 0.18y_{nrm}^3$, const. in u_t
v_2	$-0.08 + 0.1y_{nrm}^2 - 0.02y_{nrm}^4$, const. in u_t
Acceptance	(A) S π RIT-TPC/(B) Full

^{*1} RIKEN Nishina Center

^{*2} NSCL and Dept. of Phys. & Ast., Michigan State University

^{*3} Department of Physics, Korea University

^{*4} Department of Physics, Kyoto University

^{*5} IFJ PAN, Kraków

^{*6} Faculty of Physics, Astronomy and Applied Computer Science, Jagiellonian University, Kraków

^{*7} Rare Isotope Science Project, Institute for Basic Science

^{*8} Cyclotron Institute, Texas A&M University

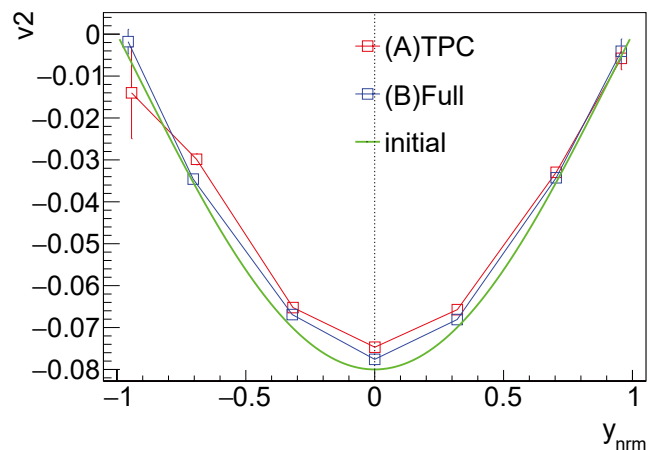


Fig. 1. The v_2 simulated with (A) S π RIT-TPC and (B) Full acceptance. A green line shows the initial function.

by analyzing through the same code developed for real data.

In Fig. 1, v_2 as a function of the center of mass rapidity were shown for (A)S π RIT-TPC and (B)full acceptance. The rapidity was normalized by the beam rapidity, $y_{nrm} (\equiv y_{cm}/y_{beam})$. As a result, both of them almost reproduce the initial function (green line). It indicates that the correction for the detector bias was done properly. However, the absolute v_2 are $\sim 6\%$ smaller at $y_{nrm} = 0$, whereas v_1 reproduces the initial value. This discrepancy should be taken into account as a systematic error.

This work is supported by the U.S. Department of Energy under Grant Nos. DE-SC0004835, DE-SC0014530, DE-NA0002923, US National Science Foundation Grant No. PHY-1565546, the Japanese MEXT KAKENHI (Grant-in-Aid for Scientific Research on Innovative Areas) grant No. 24105004, and the Polish National Science Center (NCN), under contract Nos. UMO- 2013/09/B/ST2/04064 and UMO-2013/10/M/ST2/00624.

References

- 1) R. Shane *et al.*, Nucl. Instrum. Methods Phys. Res. A **784**, 513 (2015).
- 2) M. Kurata-Nishimura *et al.*, RIKEN Accel. Prog. Rep. **62**, 37 (2019).
- 3) J. Barrette *et al.*, Phys. Rev. C **56**, 3254 (1997).
- 4) A. M. Poskanzer, S. A. Voloshin, Phys. Rev. C **58**, 1671 (1998).

Measurement of the proton elastic scattering from ^{132}Sn at 300 MeV/nucleon

J. Zenihiro,^{*1} T. Harada,^{*2,*3} N. Aoi,^{*4} H. Baba,^{*2} M. Dozono,^{*5} F. Endo,^{*5} S. Enyo,^{*1} Y. Fujikawa,^{*1}
S. Hanai,^{*5} Y. Hijikata,^{*1} J. Hwang,^{*5} N. Imai,^{*5} K. Inaba,^{*1} S. Ishida,^{*6} T. Isobe,^{*2} T. Kawabata,^{*7}
S. Kiyotake,^{*8} A. Kohda,^{*4} R. Kojima,^{*5} R. Maeda,^{*6} Y. Maeda,^{*8} Y. Matsuda,^{*6} S. Matsumoto,^{*1}
R. Matsumura,^{*2,*3} B. Mauss,^{*2} S. Michimasa,^{*5} D. Nishimura,^{*9} T. Nishimura,^{*8} K. Nosaka,^{*6} S. Ota,^{*5}
H. Sakaguchi,^{*4} K. Sakanashi,^{*7} H. Shimizu,^{*5} D. Suzuki,^{*2} J. Tanaka,^{*2} S. Terashima,^{*10} R. Tsunoda,^{*5} and
T. Uesaka^{*2}

The “neutron skin” structure is an important phenomenon in finite nuclei and is known to be strongly related with the properties of nuclear matter. In neutron-rich nuclei, excess neutrons are pushed out to the surface region, evolving the “neutron skin” structure. Many mean-field predictions indicate that the thickness of the neutron skin (Δr_{np}), which is defined as the difference in root-mean-square radii between the proton and neutron, is strongly correlated with the equation of state (EOS) of the neutron matter. Neutron-rich doubly magic ^{208}Pb is a benchmarking nucleus for EOS studies. Thus far, many theoretical and experimental studies on the Δr_{np} of ^{208}Pb have been conducted.

Proton elastic scattering is a powerful tool to extract density information and Δr_{np} . In the case of stable nuclei, we have established the method to determine neutron density distributions from proton elastic scattering at 300 MeV.¹⁾ It is natural to expand this study to the unstable region, where large Δr_{np} values are expected because of the large isospin asymmetry. To apply our method to unstable nuclei, we started a new project to measure the elastic scattering of protons with RI beams (ESPRI) based on missing mass spectroscopy in inverse kinematics. We developed a new device, recoil particle spectrometer (RPS), which consists of a 1-mm-thick solid hydrogen target (SHT),²⁾ two multi-wire drift chambers (MWDCs), two plastic scintillators, and fourteen NaI(Tl) calorimeter rods. RPS covers a wide range of momentum transfers ($0.5\text{--}2.5\text{ fm}^{-1}$) corresponding to $10^\circ\text{--}35^\circ$ in the c.m. scattering angles. We successfully performed ESPRI measurements with RPS for several light unstable nuclei.³⁾ We also developed a new method to determine the proton and neutron density distributions from two-energy proton elastic scattering data at 200 and 300 MeV/nucleon. Usually, the proton density distributions can be derived from the nuclear charge distributions determined by electron elastic scattering,⁴⁾ but at present, little information is avail-

able on the charge distributions of unstable nuclei. This method is based on the different energy dependences between pp and pn interactions, which was demonstrated by the proton elastic scattering data of Zr isotopes at 200 and 300 MeV/nucleon.¹⁾

^{132}Sn is another benchmarking nucleus, which has a larger isospin asymmetry than that of ^{208}Pb . In November 2019, we successfully completed the ESPRI experiment for ^{132}Sn at 300 MeV/nucleon (NP1512-RIBF79R1). The first part of this experiment at 200 MeV/nucleon was already completed in 2016.⁵⁾ A secondary beam around ^{132}Sn at 300 MeV/nucleon was produced by fission fragmentation with a ^{238}U beam at 345 MeV/nucleon. In this experiment, the purity of ^{132}Sn was $\sim 20\%$, and the total intensity of the cocktail beam was ~ 700 kcps. Since high-intensity and heavy RI beams cause critical radiation damage to and/or low efficiencies of detectors such as plastic scintillators, delay-line parallel-plate avalanche counters (DL-PPACs), and ion chambers, in place of the standard ones at BigRIPS, we have used new detectors with good radiation hardnesses and fast timing responses, namely, diamond detectors, MWDCs, strip-readout PPACs (SR-PPACs), and Xe gas scintillators.⁶⁾ The secondary beam particles were transported to F8 and finally to the SHT at F12, where RPS was installed. At F8, a CNS active target (CAT) was also installed for measurement at a forward scattering angle around $7^\circ\text{--}10^\circ$ in the c.m. angles. A new high-speed DAQ system, MOCO with parallelized VME (MPV),⁷⁾ was introduced for the first time, and it worked with a good live-time ratio under a high-data-rate condition. During the measurement, we clearly identified elastic events from the correlation of recoil proton energies and angles.

References

- 1) H. Sakaguchi *et al.*, Prog. Part. Nucl. Phys. **97**, 1 (2017).
- 2) Y. Matsuda *et al.*, Nucl. Instrum. Methods. Phys. Res. A **643**, 6 (2011).
- 3) Y. Matsuda *et al.*, Phys. Rev. C **87**, 034614 (2013).
- 4) H. De Vries *et al.*, At. Data Nucl. Data Tables **36**, 495 (1987).
- 5) J. Zenihiro *et al.*, RIKEN Accel. Prog. Rep. **50**, 54 (2017).
- 6) J. Zenihiro *et al.*, RIKEN Accel. Prog. Rep. **51**, 156 (2018).
- 7) H. Baba *et al.*, in this report.

^{*1} Department of Physics, Kyoto University

^{*2} RIKEN Nishina Center

^{*3} Department of Physics, Toho University

^{*4} RCNP, Osaka University

^{*5} CNS, University of Tokyo

^{*6} CYRIC, Tohoku University

^{*7} Department of Physics, Osaka University

^{*8} Department of Applied Physics, Miyazaki University

^{*9} Department of Natural Sciences, Tokyo City University

^{*10} School of Physics, Beihang University

TDPAD measurement for the 10^- isomer of ^{98}Y

J. M. Daugas,^{*1,*2,*3} F. Boulay,^{*1,*2,*4} Y. Ichikawa,^{*2} A. Takamine,^{*2} D. S. Ahn,^{*2} K. Asahi,^{*2,*5} H. Baba,^{*2} D. L. Balabanski,^{*2,*6} T. Egami,^{*2,*7} T. Fujita,^{*2,*8} N. Fukuda,^{*2} C. Funayama,^{*2,*5} T. Furukawa,^{*2,*9} G. Georgiev,^{*10} A. Gladkov,^{*2,*11} M. Hass,^{*12} K. Imamura,^{*2,*13} N. Inabe,^{*2} Y. Ishibashi,^{*2,*14} T. Kawaguchi,^{*2,*7} T. Kawamura,^{*8} W. Kim,^{*11} Y. Kobayashi,^{*15} S. Kojima,^{*2,*5} A. Kusoglu,^{*10,*16} R. Lozeva,^{*10} S. Momiyama,^{*17} I. Mukul,^{*12} M. Niikura,^{*17} H. Nishibata,^{*2,*8} T. Nishizaka,^{*2,*7} A. Odahara,^{*8} Y. Ohtomo,^{*2,*5} D. Ralet,^{*10} T. Sato,^{*2,*5} G. S. Simpson,^{*18} Y. Shimizu,^{*2} T. Sumikama,^{*2} H. Suzuki,^{*2} H. Takeda,^{*2} L. C. Tao,^{*2,*19} Y. Togano,^{*5} D. Tominaga,^{*2,*7} H. Ueno,^{*2} H. Yamazaki,^{*2} and X. F. Yang^{*20}

A time-differential perturbed angular distribution (TDPAD) measurement was performed for the 10^- isomer $^{98\text{m}}\text{Y}$. The first aim of this experiment was to investigate the single-particle structure and on the wave functions of $^{98\text{m}}\text{Y}$, which is located in a region with a rapid change of the ground-state nuclear shape, through the magnetic moment. The second aim was to measure the amount of spin alignment of the isomeric states produced by the abrasion-fission reaction.

Neutron-rich $N = 59$ isotones were produced by the abrasion-fission reaction of a primary ^{238}U beam at 345 MeV/nucleon incident on a 100- μm -thick ^9Be target. A thin target was used to avoid the mixing of different momentum distributions if the reaction occurred at the entrance or exit of the target. Figure 1 shows the three selections in the momentum distribution of ^{98}Y

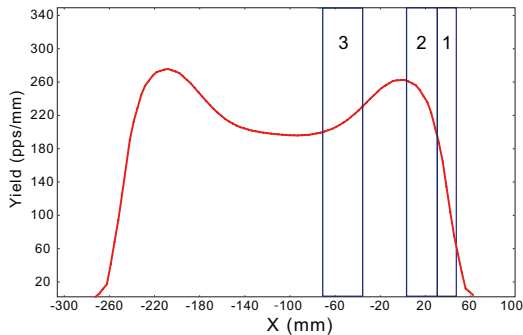


Fig. 1. Selections in the momentum distribution of ^{98}Y . The distribution shape was estimated by LISE++.

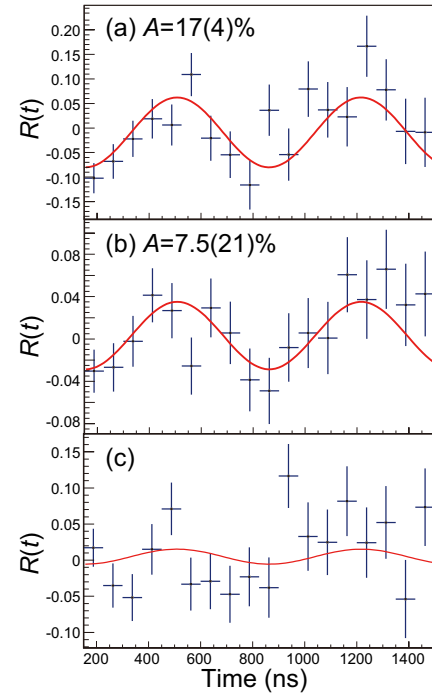


Fig. 2. (a), (b), and (c) represent the $R(t)$ ratio of $^{98\text{m}}\text{Y}$ for selections 1, 2, and 3, respectively. See Refs. 1–2) for the definition of $R(t)$.

at F1. The selected isotones were implanted in a non-perturbing copper host at F8. The TDPAD apparatus located at F8 was same as in Refs. 1–2), and an external magnetic field of 0.250 T was applied.

Figures 2 (a), (b), and (c) show the TDPAD spectra with respect to the momentum distribution, where the highest spin alignment of 17(4)% is located in its outer wing and no spin alignment exists at the center. The g -factor of $^{98\text{m}}\text{Y}$ was deduced to be $|g| = 0.36(2)$. This value is far from the one expected under the assumption of a $(\pi g_{9/2} \otimes h_{11/2})_{10^-}$ configuration, where the additivity rules give $g = +0.517$ considering the g -factors of the $9/2^+$ and the $11/2^-$ isomers of ^{97}Y and ^{99}Mo , respectively.^{3,4)} The interpretation of this result needs improvement in theoretical calculations for the odd-odd mass isotopes in this interesting region.

References

- 1) Y. Ichikawa *et al.*, Nature Phys. **15**, 321 (2019).
- 2) F. Boulay *et al.*, Phys. Rev. Lett. **124**, 112501 (2020).
- 3) B. Cheal *et al.*, Phys. Lett. B **645**, 133 (2007).
- 4) J. M. Daugas, private communication.

*1 CEA, DAM, DIF
 *2 RIKEN Nishina Center
 *3 LCM, LNE-CNAM
 *4 GANIL, CEA/DSM-CNRS/IN2P3
 *5 Department of Physics, Tokyo Institute of Technology
 *6 ELI-NP, IFIN-HH
 *7 Department of Advanced Sciences, Hosei University
 *8 Department of Physics, Osaka University
 *9 Department of Physics, Tokyo Metropolitan University
 *10 IJCLab, CNRS/IN2P3, Université Paris-Saclay
 *11 Department of Physics, Kyungpook National University
 *12 Department of Particle Physics, Weizmann Institute of Science
 *13 Department of Physics, Meiji University
 *14 Department of Physics, University of Tsukuba
 *15 Department of Informatics and Engineering, University of Electro-Communication
 *16 Department of Physics, Istanbul University
 *17 Department of Physics, University of Tokyo
 *18 LPSC, CNRS/IN2P3, Université Grenoble Alpes
 *19 School of Physics, Peking University
 *20 Instituut voor Kern- en Stralingsfysica, K. U. Leuven

Investigations of magnetic moments and spin alignment in Coulomb fission reaction

R. Lozeva,^{*1} G. Häfner,^{*1,*2} M. Si,^{*1} Y. Ichikawa,^{*3} H. Ueno,^{*3} D. S. Ahn,^{*3} K. Asahi,^{*3} T. Asakawa,^{*3,*4} H. Baba,^{*3} A. Esmaylzadeh,^{*2} N. Fukuda,^{*3} A. Gladkov,^{*3} K. Imamura,^{*3} N. Inabe,^{*3} K. Kawata,^{*3,*5} L. Knafila,^{*2} A. Kusoglu,^{*6} M. Niikura,^{*7} Y. Sasaki,^{*3,*4} H. Sato,^{*3} Y. Shimizu,^{*3} H. Suzuki,^{*3} M. Tajima,^{*3} A. Takamine,^{*3} H. Takeda,^{*3} Y. Takeuchi,^{*3,*4} Y. Yanagisawa,^{*3} H. Yamazaki,^{*3} and K. Yoshida^{*3}

As one of the most accurate probes of the nuclear wave-functions, the magnetic moments of excited states in nuclei are both important and interesting. Their measurement has several difficulties and particularities. One of the most crucial ones is the spin alignment of the nuclear ensemble which is produced in the reaction populating the nucleus of interest. In such an experiment we have investigated the Coulomb fission reaction, which was not previously studied, aiming to probe the nuclear alignment through the measurement of magnetic moments.

Nuclei around ^{132}Sn form a key region of the nuclear chart from astrophysics and nuclear structure point of view. In particular, below ^{132}Sn , several isomeric structures emerge as for example in the $^{124,125}\text{Ag}$ isotopes, which have interesting behaviour of the three proton holes below $Z = 50$ closed-shell coupled to even or odd amount of neutron holes from predominantly the last three $\nu h_{11/2}$, $d_{3/2}$ and $s_{1/2}$ neutron orbitals below $N = 82$.¹⁾ Measuring nuclear moments of such excited isomeric states allows to find what type of configurations are formed in these nuclei, and at the same time, investigate unknown properties of the fission reaction mechanism.

The experiment was carried out in December 2019 at the RIBF using the BigRIPS spectrometer. Primary ^{238}U beam with an energy of 345 MeV/nucleon and an intensity of the order of 100 pnA was used to induce Coulomb fission onto a thin ^{184}W production target. This very thin foil of only 0.1 mm was used for the first time in our experiment and performed well at the used very high flux. The isotopes of interest produced in the reaction were separated, transported and identified using the standard methods for BigRIPS and using Al wedges at the F1 and F5 focal planes of 7 mm and 1 mm, respectively. Our detection setup was placed at the F8 focal plane where the beam was stopped in a sandwich of 2 mm thick plastic and 3 mm thick Cu host.

The momentum distribution for ions produced in the fission reaction is generally wide and it is only partially accepted (*e.g.* $\pm 3\%$) by the BigRIPS spectrometer.²⁾

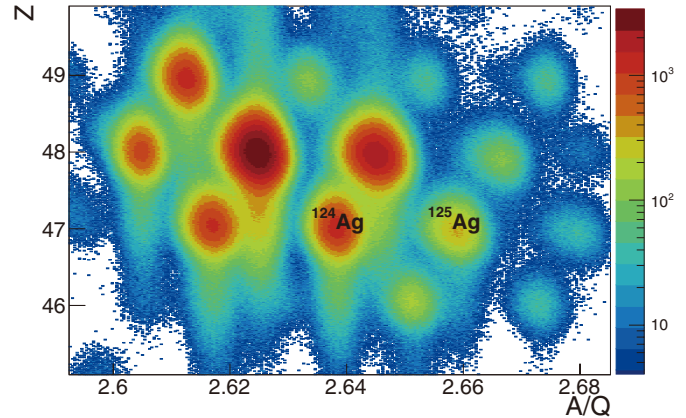


Fig. 1. Particle-identification for the central setting.

In addition, in order to select certain parts of this momentum we have performed F1 slit cuts by accepting only the high or only the low part of momentum distribution for the ions of interest.

Typical particle-identification spectrum from this experiment for the central selection is shown in Fig. 1 for about 10% of the collected data. Similar statistics was obtained also for the wing setting. For the measurement of the nuclear moments we have employed the well-known TDPAD method, applied successfully at RIBF.^{3,4)} We used four HpGe detectors at 90° with respect to each other and two LaBr_3 detectors of 1.5×1.5 in. They were all placed in a horizontal plane, while the magnetic field used to induce the precession of the nuclear spins was provided by a compact electromagnet and applied in a vertical direction.

Data analysis for the oscillation pattern and magnetic moment for the nuclei of interest are currently in progress.

References

- 1) S. Lalkovski *et al.*, Phys. Rev. C **87**, 034308 (2013).
- 2) T. Kubo *et al.*, Nucl. Instrum. Methods Phys. Res. B **204**, 97 (2003).
- 3) Y. Ichikawa *et al.*, Nat. Phys. **15**, 321 (2019).
- 4) F. Boulay *et al.*, Phys. Rev. Lett. **124**, 112501 (2020).

*1 Université Paris-Saclay, CNRS/IN2P3, IJCLab

*2 IKP, University of Cologne

*3 RIKEN Nishina Center

*4 Department of Advanced Sciences, Hosei University

*5 Center for Nuclear Study, University of Tokyo

*6 Department of Physics, Istanbul University

*7 Department of Physics, University of Tokyo

Magnetic-moment measurement of the isomeric state of ^{130}Sn in the vicinity of the doubly—magic nucleus ^{132}Sn

G. Georgiev,^{*1,*2,*3} Y. Ichikawa,^{*1} D. S. Ahn,^{*1} T. Asakawa,^{*4} K. Asahi,^{*1} H. Baba,^{*1} K. Doi,^{*4} N. Fukuda,^{*1} A. Gladkov,^{*1,*5} T. Gray,^{*3} G. Häfner,^{*2,*6} K. Kawata,^{*1,*7} W. Kobayashi,^{*4} A. Kusoglu,^{*8} G. J. Lane,^{*1,*3} R. L. Lozeva,^{*2} C. Mihai,^{*9} R. Mihai,^{*9} Y. Nakamura,^{*10} M. Niikura,^{*11} H. Nishibata,^{*1} A. Odahara,^{*12} S. Pascu,^{*9} M. Sanjo,^{*4} Y. Sasaki,^{*4} T. Sato,^{*1} Y. Shimizu,^{*1} E. Simpson,^{*3} C. Sotty,^{*9} A. Stuchbery,^{*3} T. Sumikama,^{*1} H. Suzuki,^{*1} M. Tajima,^{*1} A. Takamine,^{*1} H. Takeda,^{*1} Y. Takeuchi,^{*4} A. Toda,^{*5} A. Turturica,^{*9} H. Ueno,^{*1} and H. Yamazaki^{*1}

The region around ^{132}Sn has attracted much experimental and theoretical interest recently due to its doubly—magic character. A microsecond isomeric state has been observed experimentally in $^{130}\text{Sn}^{1-3}$ ($t_{1/2} = 1.6 \mu\text{s}$). Its tentative spin-parity assignment of 10^+ suggests a neutron $h_{11/2}^2$ configuration, which, due to its high spin, is expected to have a very pure wavefunction configuration. A magnetic moment study on this isomeric state should be able to shed light on the robustness of the double shell closure ($Z = 50$ and $N = 82$) at ^{132}Sn .

The NP1712-RIBF143R1 experiment was performed in December 2018 at the BigRIPS separator at RIBF. A two-step fragmentation scheme⁴ was employed to produce a spin-aligned ^{130}Sn beam. A secondary beam of ^{132}Sn was produced following the fission of a 345 MeV/nucleon ^{238}U beam on a 6 mm ^9Be target at F0. A wedge-shaped aluminium degrader (having a mean thickness of 6 mm), positioned at the F1 dispersive focal plane, was used for the secondary-beam purification. The momentum acceptance was restricted to $\pm 1.4\%$ using the F1 momentum slits. A tertiary beam of ^{130}Sn was produced with a wedge-shaped (2 mm) aluminium secondary target placed at the F5 momentum-dispersive focal plane. A two-neutron (2n) removal reaction mechanism was used to populate the 10^+ isomeric state of interest. Special care was taken to match the momentum dispersion between F5 and F7 to that between F3 and F5. The momentum slits at F7 were set to ± 9 mm, which corresponds to $\pm 0.26\%$ momentum selection. A beam intensity of 30 pps, with a purity of $\sim 20\%$, was obtained for ^{130}Sn .

The isomeric states of interest were implanted in a 3 mm Cu host positioned between the poles of an electro-magnet in the center of the time-differential perturbed angular distribution (TDPAD) apparatus at

the F12 focal plane.

Four Ge and two LaBr₃ detectors, positioned 7 cm from the host in a horizontal plane around the magnet, were used to monitor the γ -rays from the decay of the isomeric state. The dipole magnet provided a static magnetic field of $B = 0.150$ T in the vertical direction. A 0.1 mm plastic scintillator, placed upstream of the stopper, provided the $t = 0$ signal for isomeric-decay measurement. The TDPAD technique entails observing the modulation of the angular distribution of the isomeric γ -rays due to the rotation of the nuclear spin ensemble in the magnetic field with the Larmor frequency $\omega_L = g\mu_N B/h$. This is realized by constructing a ratio function ($R(t)$), which combines detectors positioned at 90° with respect to each other. Provided that the magnetic field at the nuclear site is well known, one can readily determine the g factor of the state of interest from the oscillation pattern in the $R(t)$ function.

Two γ -rays (97 keV and 391 keV) were observed from the decay of the isomeric state, as expected from the previously known decay scheme. Their lifetimes, determined from the time spectra, were in agreement with the previously observed lifetime of the isomeric state. An oscillation pattern with a statistical significance of 2.7σ was observed during the analysis of the ratio function. It indicates a gyromagnetic factor very close to the free-nucleon Schmidt limit, in contrast with the g factors of other $h_{11/2}$ states in the region, for which a reduction of about 30% of the free-nucleon g factors ($g_s^{\text{eff}} = 0.7 \times g_s^{\text{free}}$) is observed. This very small reduction of the g factor compared to the Schmidt-limit indicates a very robust double—shell closure at ^{132}Sn . Following this observation, a new proposal has been submitted to the RIKEN NP PAC in December 2019. It aims at confirming this very intriguing indication with a higher statistical significance.

*1 RIKEN Nishina Center

*2 CSNSM, CNRS/IN2P3, Université Paris-Saclay

*3 Department of Physics, Australian National University

*4 Department of Advanced Sciences, Hosei University

*5 Department of Physics, Kyungpook National University

*6 Department of Physics, University of Cologne

*7 Center for Nuclear Study, University of Tokyo

*8 ELI-NP, IFIN-HH

*9 NIPNE, IFIN-HH

*10 Department of Physics, Meiji University

*11 Department of Physics, University of Tokyo

*12 Department of Physics, Osaka University

References

- 1) R. L. Lozeva *et al.*, Phys. Rev. C **77**, 064313 (2008).
- 2) D. Kameda *et al.*, Phys. Rev. C **86**, 054319 (2012).
- 3) S. Pietri *et al.*, Phys. Rev. C **83**, 044328 (2011).
- 4) Y. Ichikawa *et al.*, Nat. Phys. **8**, 918 (2012).

Isomeric-to-ground state ratio of ^{128}Sn measured by Rare RI Ring

H. F. Li,^{*1,*2,*3} S. Naimi,^{*1} D. Nagae,^{*1} Y. Abe,^{*1} F. Suzuki,^{*1} Y. Yamaguchi,^{*1} M. Wakasugi,^{*1} S. Omika,^{*4} K. Inomata,^{*4} H. Arakawa,^{*4} S. Hosoi,^{*4} K. Nishimuro,^{*4} Y. Inada,^{*4} T. Kobayashi,^{*4} D. Kajiki,^{*4} D. Hamakawa,^{*4} W. B. Dou,^{*4} T. Yamaguchi,^{*5} M. Mukai,^{*5} T. Moriguchi,^{*5} R. Kagesawa,^{*5} D. Kamioka,^{*5} A. Ozawa,^{*5} S. Suzuki,^{*2} Z. Ge,^{*2} C. Y. Fu,^{*2} Q. Wang,^{*2} M. Wang,^{*2} S. Ota,^{*6} S. Michimasa,^{*6} N. Kitamura,^{*6} S. Masuoka,^{*6} D. S. Ahn,^{*1} H. Suzuki,^{*1} N. Fukuda,^{*1} H. Takeda,^{*1} Y. Shimizu,^{*1} Y. A. Litvinov,^{*7} G. Lorusso,^{*8} and T. Uesaka^{*1}

The excitation energy of the isomeric state and the isomeric-to-ground state ratios are very important to understand the nuclear structure and reactions. Direct mass measurement can be used for measuring the excitation energy of the long-lived isomeric state and determining the isomeric-to-ground state ratio simultaneously. Rare RI Ring (R3) is an isochronous mass spectrometer in RIBF. The principle of the mass measurement at R3 is described by the following equation:

$$\frac{m_1}{q_1} = \frac{m_0}{q_0} \frac{T_1^{corr}}{T_0} = \frac{m_0}{q_0} \frac{1}{T_0} T_1 \sqrt{1 + \frac{1 - \left(\frac{T_0}{T_1}\right)^2}{\left(\frac{m_0/q_0}{B\rho_1} c\right)^2}}, \quad (1)$$

where T_1 and T_0 are the time-of-flight (TOF) of the nucleus of interest and reference nucleus, respectively, and $B\rho_1$ is the magnet rigidity of the nucleus of interest.¹⁾ The unknown mass m_1 is determined relative to the mass of the isochronous reference nucleus m_0 . $B\rho$ tagging is performed at the momentum-dispersive focal plane F5 of BigRIPS by measuring the horizontal position with two parallel-plate avalanche counters (PPACs). The TOF of the nuclei in R3 was measured using the E-MCP detector²⁾ at S0 of SHARAQ and a plastic scintillator placed

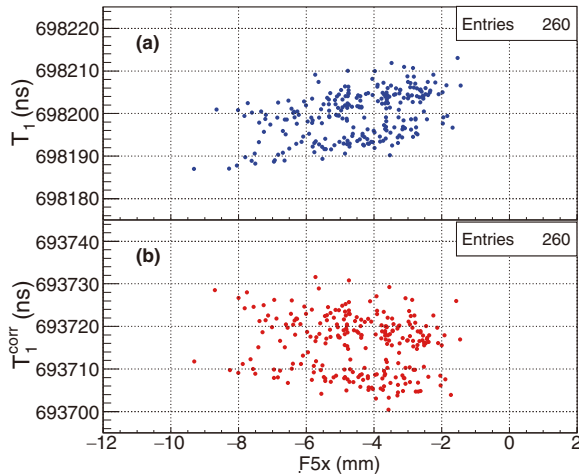


Fig. 1. (a), (b) Correlations between T_1 and T_1^{corr} , respectively, and the F5 position for ^{128}Sn .

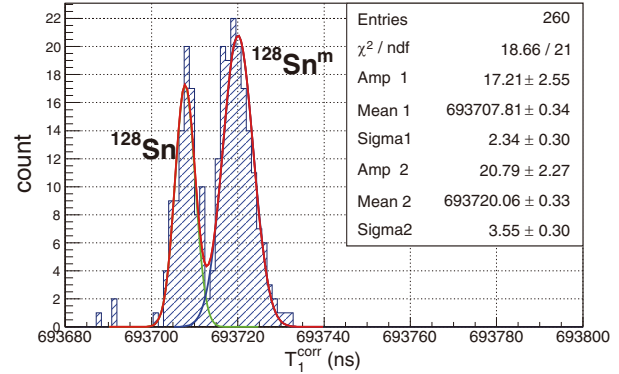


Fig. 2. T_1^{corr} spectrum of ^{128}Sn ; two Gaussian functions were used to fit the histogram.

behind R3.

In the autumn of 2018, the first mass measurement campaign was conducted at R3. To measure the mass of ^{125}Ag and ^{124}Pd , 3 neighbor isotones, ^{126}Cd , ^{127}In , and ^{128}Sn , were injected in R3 as reference nuclei to determine the mean $B\rho$ value of R3.³⁾ The first isomeric state of ^{128}Sn , the excitation energy and half-life of which are about 2091.5 keV and 6.5 s,⁵⁾ respectively, was produced and observed during this experiment. The TOF in R3 for each particle was normalized to the same turn numbers⁴⁾ to determine T_1 . The correlation between the T_1 of ^{128}Sn and the F5 position is shown in Fig. 1(a). After event-wise correction with $B\rho$, T_1^{corr} 's dependence on the F5 position is shown in Fig. 1(b). The isomeric state and ground state of ^{128}Sn can be well resolved in the spectrum of T_1^{corr} , as shown in Fig. 2. The left peak is the ground state of ^{128}Sn , and the right one is the isomeric state. A function composed of the sum of two Gaussian functions was used to fit this spectrum.

The mass resolving power of R3 can be given by

$$R = m/\Delta m = T_1^{corr} / \Delta T_1^{corr}, \quad (2)$$

which is derived from Eq. (1). The full width at half maximum of the achieved mass resolving power is about 125,000 from the ground-state peak. The isomeric-to-ground state ratio for ^{128}Sn is 1.8(4), which is determined by the integral values' ratio of the fitting functions.

References

- 1) A. Ozawa *et al.*, Prog. Theor. Exp. Phys. **2012**, 03C009 (2012).
- 2) Y. Abe *et al.*, JPS Conf. Proc. **1**, 013059 (2014).
- 3) S. Naimi *et al.*, RIKEN Accel. Prog. Rep. **52**, 102 (2019).
- 4) H. F. Li *et al.*, RIKEN Accel. Prog. Rep. **52**, 52 (2019).
- 5) G. Audi *et al.*, Chin. Phys. C **41**, 030001 (2017).

*1 RIKEN Nishina Center
 *2 Institute of Modern Physics, Chinese Academy of Sciences
 *3 University of Chinese Academy of Sciences
 *4 Department of Physics, Saitama University
 *5 Institute of Physics, University of Tsukuba
 *6 Center for Nuclear Study, University of Tokyo
 *7 GSI Helmholtzzentrum für Schwerionenforschung
 *8 NPL, University of Surrey

Performance study of electron spectrometer for SCRIT experiments

K. Tsukada,^{*1,*2} A. Enokizono,^{*2} Y. Honda,^{*1,*2} K. Kurita,^{*3} H. Ohnishi,^{*2} S. Sato,^{*3} T. Suda,^{*1,*2} S. Takagi,^{*4}
D. Taki,^{*1,*2} T. Tamae,^{*1,*2} M. Watanabe,^{*2} M. Wakasugi,^{*2,*4} and H. Wauke^{*1,*2}

We constructed the Self-Confining Radioactive Ion Target (SCRIT) electron scattering facility¹⁾ to perform electron scattering experiments for short-lived unstable nuclei. Such experiments have been long desired but unrealized thus far because of the difficulties in preparing a thick target from such short-lived nuclei. SCRIT is a novel technique to achieve a sufficiently high luminosity to perform electron scattering experiments by trapping the target ions along the electron beam. After successful commissioning experiments with stable targets,²⁾ we started to prepare for an experiment with an unstable nuclear target.

The SCRIT electrode was replaced with a new one that has a larger cross section and less material around the trapping region, in addition to providing a much more uniform electric potential. Simultaneously, three identical carbon foils with a thickness of 35 μm were installed as fixed targets at the center and both edges of the SCRIT electrodes, respectively, to evaluate the performance of the electron spectrometer, window-frame spectrometer for electron scattering (WiSES). The carbon targets can be moved out of the electron-beam axis when they are not in use. For WiSES, the drift chamber in front of the spectrometer magnet was replaced with a new one with both vertical and horizontal wires to reconstruct the horizontal and vertical trajectory information of scattered electrons simulta-

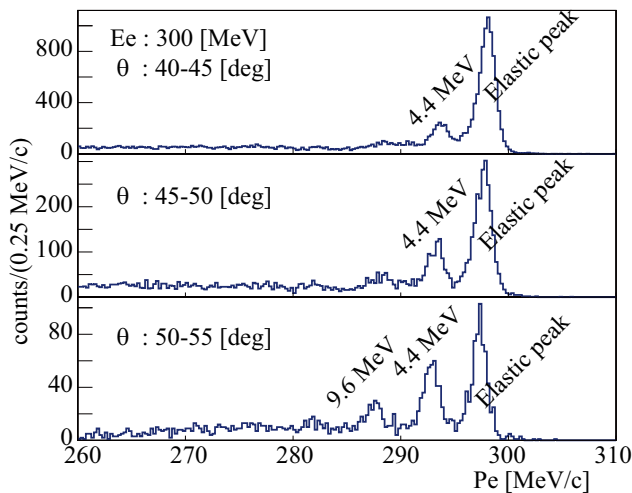


Fig. 1. Reconstructed momentum spectra of scattered electrons for different scattering-angle regions.

*1 ELPH, Tohoku University

*2 RIKEN Nishina Center

*3 Department of Physics, Rikkyo University

*4 Institute for Chemical Research, Kyoto University

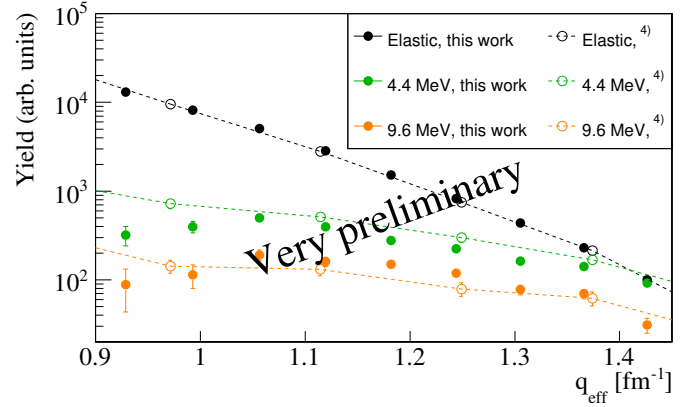


Fig. 2. Yield distributions with varying effective momentum transfer after acceptance corrections. Filled circles indicate preliminary results from this work. Opened circles are from Ref. 4).

neously. In addition, a magnetic-field measurement was performed to study the momentum resolution of WiSES.

In 2019, we performed a series of electron-scattering experiments with carbon targets to evaluate the acceptance and momentum resolution of the spectrometer after the measurement of the magnetic-field distribution of the spectrometer magnet. The status of the field measurement is reported elsewhere.³⁾

Figure 1 shows reconstructed momentum spectra from the center of targets for an electron beam energy of 300 MeV and three scattering angle regions: 40°–45°, 45°–50°, and 50°–55°. One elastic peak and two inelastic peaks are clearly observed. Figure 2 shows yield distributions with varying effective momentum transfer after acceptance corrections. In the present analysis, only the radiation tail from the elastic peak is taken into account for counting the yields. Moreover, the acceptances for the elastic and inelastic events are assumed to be the same. Although the distributions of the elastic events are consistent between this work and a previous experiment,⁴⁾ those of the inelastic events show finite discrepancies.

Further analysis is ongoing to evaluate the performance of the spectrometer.

References

- 1) M. Wakasugi *et al.*, Phys. Rev. Lett. **100**, 164801 (2008).
- 2) K. Tsukada *et al.*, Phys. Rev. Lett. **118**, 262501 (2017).
- 3) H. Wauke *et al.*, in this report.
- 4) J. H. Fregeau *et al.*, Phys. Rev. **104**, 225 (1956).

Correlated measurement of mass and decay of fusion evaporation products for $^{51}\text{V} + ^{159}\text{Tb}$ reactions via MRTOF + α -TOF detector

T. Niwase,^{*1,*2,*3} M. Wada,^{*3} P. Schury,^{*3} Y. Ito,^{*4} S. Kimura,^{*2} D. Kaji,^{*2} M. Rosenbusch,^{*2} Y. X. Watanabe,^{*3} Y. Hirayama,^{*3} H. Miyatake,^{*3} J. Y. Moon,^{*9} H. Ishiyama,^{*2} K. Morimoto,^{*2} H. Haba,^{*2} T. Tanaka,^{*7} S. Ishizawa,^{*5,*2,*3} P. Brionnet,^{*2} S. Iimura,^{*8,*2,*3} A. Takamine,^{*2} K. Morita,^{*1,*2} and H. Wollnik^{*6}

The SHE-Mass-II facility¹⁾ is a system with a multi-reflection time-of-flight mass spectrograph (MRTOF-MS²⁾) coupled with the gas-filled recoil ion separator GARIS-II³⁾ in the E6 experimental room for the mass measurement of fusion evaporation products, such as very low yield nuclei in the superheavy region.

Recently, we developed and installed a novel detector named α -TOF⁴⁾, which simultaneously records the time-of-flight (TOF) signal and successive α -decay. The α -TOF detector has the capability to significantly reduce the background level.

The experiment was performed using $^{51}\text{V} + ^{159}\text{Tb}$ reactions. A ^{51}V beam was accelerated up to 6.0 MeV/nucleon by RRC. The beam energy on the target was reduced by an aluminum degrader to approximately 4.8 MeV/nucleon. A 460- $\mu\text{g}/\text{cm}^2$ -thick ^{159}Tb

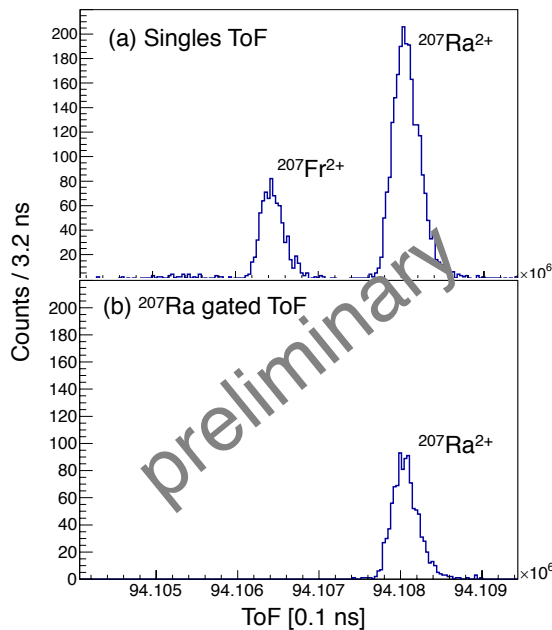


Fig. 1. (a) Singles TOF spectrum. (b) TOF spectrum in coincidence with ^{207}Ra α -decays obtained using a time gate of 5s.

^{*1} Department of Physics, Kyushu University
^{*2} RIKEN Nishina Center
^{*3} Wako Nuclear Science Center (WNSC), KEK
^{*4} Japan Atomic Energy Agency
^{*5} Graduate School of Science and Engineering, Yamagata University
^{*6} Department of Chemistry and Biochemistry, New Mexico State University
^{*7} Department of Nuclear Physics, The Australian National University
^{*8} Department of Physics, Osaka University.
^{*9} Institute for Basic Science

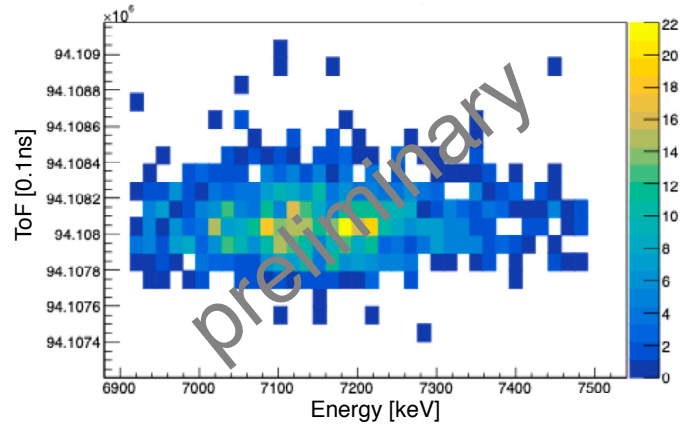


Fig. 2. Two-dimensional mapping of TOF versus correlated α -decay energies.

target was prepared by a sputtering method on a 3.0 μm Ti backing foil.

The fusion evaporation residues (ERs) were separated from the primary beam and efficiently transported using GARIS-II. After decelerating ERs using a Mylar foil, the ERs were captured in a cryogenic high-purity He gas catcher, and the thermalized ions were extracted by an RF-carpet and transported to the MRTOF-MS via multiple RF ion traps. We observed the $^{206,207}\text{Fr}$, $^{206,207}\text{Ra}$ and ^{204}Rn isotopes extracted as doubly charged ions. In this measurement, we focused on $^{206,207}\text{Ra}$ isotopes having relatively short half-lives, *i.e.*, $T_{1/2} = 240$ ms for ^{206}Ra and $T_{1/2} = 1.38$ s for ^{207}Ra .

Figure 1 shows a part of the TOF spectrum at $A = 207$. When we gated the ToF spectrum by the α -ray energy of ^{207}Ra with a coincident time of 5 s (3.5 half-lives), we clearly discriminated the decay-correlated TOF events (Fig. 1(b)).

Figure 2 shows a part of the two-dimensional spectrum for TOF and the correlated α -decay energies. From the correlation mapping, we obtained the information of TOF, as well as decay properties such as α -energy and decay time, atom by atom. Further analysis is in progress.

References

- 1) M. Wada *et al.*, RIKEN Accl. Prog. Rep. **52**, 136 (2019).
- 2) P. Schury *et al.*, Nucl. Instrum. Methods Phys. Res. B, **335**, 39 (2014).
- 3) D. Kaji *et al.*, Nucl. Instrum. Methods Phys. Res. B, **317**, 311 (2013).
- 4) T. Niwase *et al.*, Nucl. Instrum. Methods Phys. Res. A, **953**, 163198 (2020).

Half-life determination of nuclear excited states of ^{229}Th by the coincidence measurement between α particles and γ rays from ^{233}U

Y. Shigekawa,^{*1,*2} A. Yamaguchi,^{*3} K. Suzuki,^{*4} H. Haba,^{*1} T. Hiraki,^{*4} H. Kikunaga,^{*5} T. Masuda,^{*4}
S. Nishimura,^{*1} N. Sasao,^{*4} A. Yoshimi,^{*4} and K. Yoshimura^{*4}

Studying the nuclear structure of ^{229}Th is important in that reflection-symmetric and reflection-asymmetric shapes are expected to coexist¹⁾ and the first nuclear excited isomeric state of ^{229}Th ($^{229\text{m}}\text{Th}$) has an extremely low energy of 8.3 eV,²⁾ which would enable the development of nuclear laser spectroscopy and an ultraprecise nuclear clock. In this study, we measured the half-lives of nuclear excited states of ^{229}Th , populated through the alpha decay of ^{233}U , for further understanding of the nuclear properties of ^{229}Th . This work was also aimed at determining the half-life of the 29.2-keV state (Fig. 1). This half-life was one of the key parameters for exciting ^{229}Th from the ground state to the 29.2-keV state with synchrotron radiation to actively produce $^{229\text{m}}\text{Th}$, which was recently realized by our group.³⁾

For the half-life determination, we performed a coincidence measurement between α particles and γ rays from a ^{233}U source prepared by electrodeposition. The ^{233}U source was placed inside a vacuum chamber enclosed by 5-cm Pb blocks for background γ -ray reduction. Emitted α particles from the source were measured with a passivated implanted planar silicon detector mounted inside the chamber, and γ rays that were emitted from the source and passed through a polyimide window out of the vacuum were measured with a $\text{LaBr}_3(\text{Ce})$ scintillator and photomultiplier. After amplification, α -particle

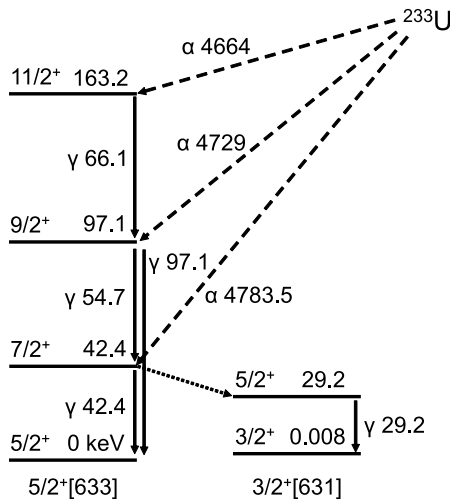


Fig. 1. Excited states of ^{229}Th the half-lives of which were determined, and α and γ transitions used for determining the half-lives (unit: keV).

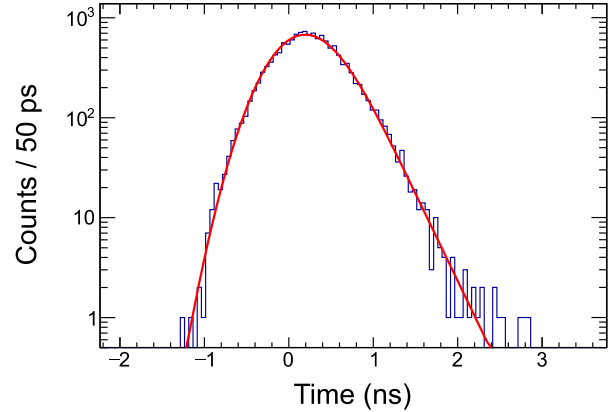


Fig. 2. Time spectrum of γ -ray signals following α -particle signals for 4783.5-keV α particles and 42.4-keV γ rays (histogram). A single exponential decay function convoluted with a Gaussian function is fitted to the data (curve).

and γ -ray signals were recorded with Computer-Aided Measurement And Control (CAMAC) modules to obtain time spectra of γ -ray signals following α -particle signals for each combination of α -particle and γ -ray energies.

Figure 2 shows a time spectrum for 4783.5-keV α particles and 42.4-keV γ rays. The half-life obtained from the fitting of a single exponential decay function convoluted with a Gaussian function was almost the same as the reference value (172(6) ps).⁴⁾ From a time spectrum for 4783.5-keV α particles and 29.2-keV γ rays, we obtained the half-life of the 29.2-keV state, which is consistent with that obtained from our synchrotron excitation of ^{229}Th (82(4) ps).³⁾ These coincidences with the previous results indicate that our experiments and data analysis were correctly performed. The half-life of the 97.1-keV state was obtained from γ rays of 54.7 and 97.1 keV detected in coincidence with 4729-keV alpha particles. The obtained half-life was seemingly shorter than the reference value (147(12) ps).⁴⁾ This may be because our measurement has better and time resolutions than the previous measurement.⁴⁾

We could clearly observe the peak of 66.1-keV γ rays by gating the γ -ray spectrum with α particles of approximately 4664 keV, which allowed us to obtain the half-life of the 163.2-keV state for the first time. We will continue detailed analysis to precisely determine each half-life and discuss the nuclear properties of ^{229}Th based on the half-lives determined in this study.

*1 RIKEN Nishina Center

*2 Graduate School of Science, Osaka University

*3 Quantum Metrology Laboratory, RIKEN

*4 Research Institute for Interdisciplinary Science, Okayama University

*5 Research Center for Electron Photon Science, Tohoku University

References

- 1) G. A. Leander *et al.*, Nucl. Phys. A **413**, 375 (1984).
- 2) B. Seiferle *et al.*, Nature **573**, 243 (2019).
- 3) T. Masuda *et al.*, Nature **573**, 238 (2019).
- 4) H. Ton *et al.*, Nucl. Phys. A **155**, 245 (1970).

Mass measurements of ^{252}Cf fission fragments via MRTOF-MS

S. Kimura,^{*1} M. Wada,^{*2} H. Haba,^{*1} S. Ishizawa,^{*1,*3,*2} T. Niwase,^{*1,*4,*2} M. Rosenbusch,^{*2} and P. Schury^{*2}
for the SHE-Mass Collaboration

The rapid neutron-capture (r -) process path is governed by the balance between the β^- -decay rate and neutron-capture rate. Masses of nuclei involved in the r -process path play a crucial role in determining the final isotopic abundance. It is difficult to access the r -process nuclei due to their locations far from stability; thus, theoretical predictions are needed to obtain the final isotopic abundances. However, in the region where there are no experimental data on nuclear masses, the predicted mass values show a large variance.¹⁾ Thus, accurate and precise mass data of neutron-rich nuclei are required.

Here, we report mass measurements of the neutron-rich nuclei produced by the spontaneous fission ^{252}Cf with multi-reflection time-of-flight mass spectroscopy (MRTOF-MS).²⁾ The MRTOF-MS system consists of a cryogenic gas cell (GC) with a $0.5\ \mu\text{m}$ Mylar window, an ion transport system having two linear RF quadrupole traps, and an ejection system to the MRTOF device. A $350\ \text{kBq}$ ^{252}Cf source (SF: 3.09%) with $6\ \mu\text{m}$ Ti degrader was installed in front of the GC window. Throughout the measurements, the GC was cryogenically cooled below 70 K while the He gas pressure was regulated to maintain a density equivalent to 150 mbar at room temperature.

The measurement results are summarized in Fig. 1. In the present study, we observed 78 isotopes from iodine ($Z = 53$) to europium ($Z = 63$) in the TOF spectra. The masses of the observed isotopes were

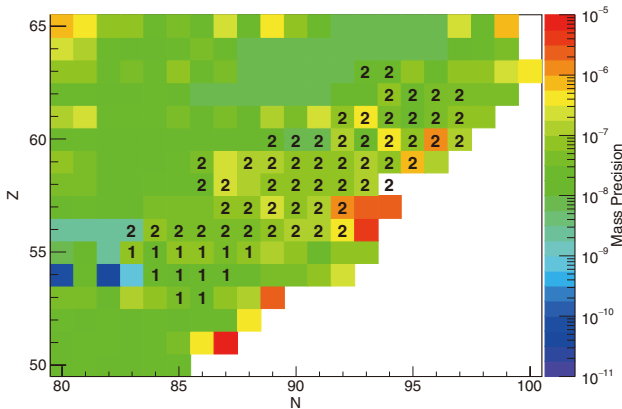


Fig. 1. Location of the observed isotopes on the nuclear chart. The numbers, 1 or 2, indicate the observed charge state. The color bar represents the precision of experimental mass data taken from the 2016 Atomic Mass Evaluation (AME16).

^{*1} RIKEN Nishina Center

^{*2} WNSC, IPNS, KEK

^{*3} Department of Physics, Yamagata University

^{*4} Department of Physics, Kyushu University

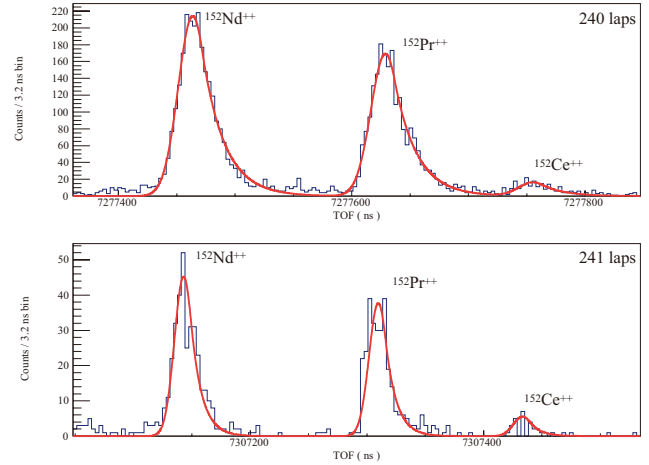


Fig. 2. TOF spectra of doubly charged $A = 152$ series. The red line indicates a fit obtained using an exponential-Gaussian hybrid function.³⁾

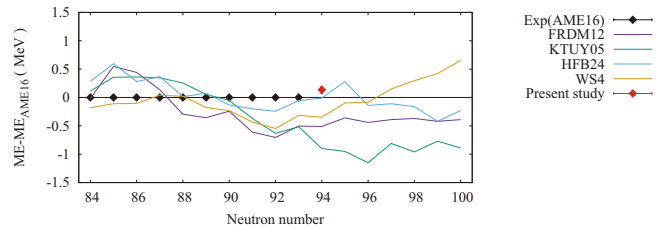


Fig. 3. Neutron-number dependence of cerium-isotope mass excess. Each line indicates a theoretical prediction. In the region of $N > 93$, the zero line corresponds to the extrapolated masses listed in AME16.

determined by a single reference method.³⁾ A typical measurement achieved a relative precision of $\delta m/m \sim 10^{-7}$. Figure 2 shows TOF spectra of the doubly charged $A = 152$ series with different numbers of laps. As the relative position and intensity remain constant when the number of laps is varied, we can infer that the three peaks are isobaric. In this case, ^{152}Nd was used as a mass reference, and we experimentally determine the mass of ^{152}Ce for the first time. The measured mass excess of ^{152}Ce is $ME = -58845(61)\ \text{keV}$ and indicated in Fig. 3 with several theoretical predictions. This result shows that the ground state of ^{152}Ce is less bound than all the predictions listed in Fig. 3.

References

- 1) M. R. Mumpower *et al.*, Prog. Part. Nucl. Phys. **86**, 86 (2016).
- 2) P. Schury *et al.*, Nucl. Instrum. Methods Phys. Res. B **335**, 39 (2014).
- 3) Y. Ito *et al.*, Phys. Rev. C **88**, 011306(R) (2013).

In-gas-cell laser ionization spectroscopy of Os isotopes using MRTOF-MS at KISS

Y. Hirayama,^{*1} H. Choi,^{*2} J. Y. Moon,^{*3} T. Hashimoto,^{*3} M. Mukai,^{*4} T. Niwase,^{*5} M. Oyaizu,^{*1} M. Rosenbusch,^{*1} P. Schury,^{*1} A. Taniguchi,^{*6} M. Wada,^{*1} Y. X. Watanabe,^{*1} and H. Miyatake^{*1}

We developed the KEK Isotope Separation System (KISS)¹⁾ to study the nuclear properties of neutron-rich isotopes with neutron numbers around $N = 126$. To study the nuclear structures at KISS, we measured the hyperfine structure (HFS) of ^{194}Os ($I^\pi = 0^+$, $T_{1/2} = 6.0$ y) and ^{196}Os ($I^\pi = 0^+$, $T_{1/2} = 34.9$ m) to determine the change in charge radius using the in-gas-cell laser ionization spectroscopy technique²⁾ assisted by the multi-reflection time-of-flight mass spectrograph (MRTOF-MS). The MRTOF-MS installed at KISS can successfully identify isotopes from mass-dependent time-of-flight (TOF) spectra.³⁾

We measured the HFS of short-lived ($T_{1/2} \sim 30$ min) isotopes by detecting the β - and γ -rays at KISS, and it is difficult to measure the HFS of isotopes with $T_{1/2} > 1$ h by detecting the decay radiations in a limited beam time. However, we can efficiently measure the HFS of these isotopes through ion counting using the MRTOF-MS without waiting for the radiation decays. Here, we report the HFS measurement of ^{194}Os using the MRTOF-MS.

The ^{194}Os isotopes were produced in multi-nucleon transfer reactions by using a stable ^{136}Xe beam (50 pA) with an energy of approximately 10 MeV/nucleon impinging on a ^{198}Pt target (12.5 mg/cm², enriched to 91% with about 3% each of $^{194}, ^{195}, ^{196}\text{Pt}$). Singly charged isotopes, produced by the in-gas-cell laser ionization technique, with an energy of 20 keV were extracted from the KISS gas cell for the HFS measurements. The extracted isotopes were injected into a helium gas cell for thermalization. Doubly charged ions were primarily produced by the charge exchange reaction with helium atoms in

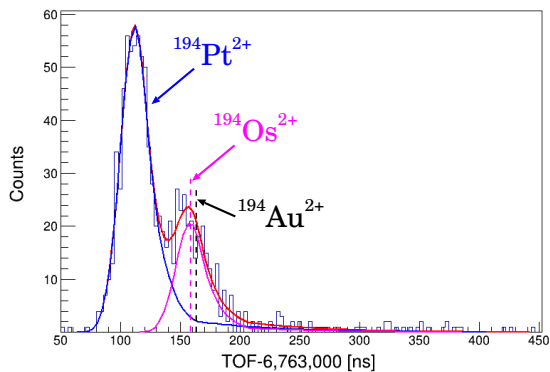


Fig. 1. Measured TOF spectrum of $^{194}\text{Os}^{2+}$.

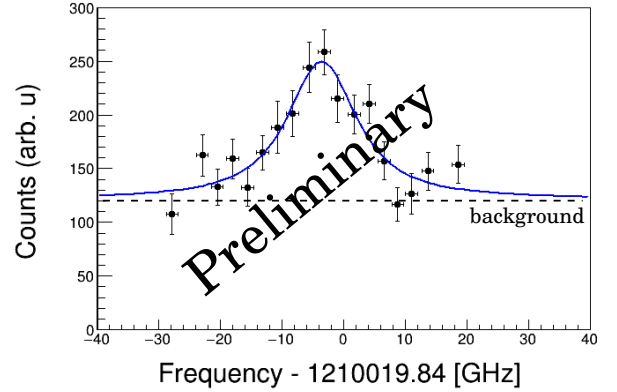


Fig. 2. Measured HFS spectrum of ^{194}Os ($I^\pi = 0^+$). Horizontal uncertainty estimated from the accuracy of a wavemeter.

the stopping process, and they were extracted from the helium gas cell. Subsequently, the bunched isotopes were injected into the MRTOF-MS for particle identification. The details of the MRTOF-MS system are reported in Ref. 3).

Figure 1 shows the TOF spectrum of $^{194}\text{Os}^{2+}$ measured using the MRTOF-MS at KISS. We can clearly identify the $^{194}\text{Os}^{2+}$ isotope with a contaminant peak of $^{194}\text{Pt}^{2+}$ ions, which were emitted through elastic events from the production target and transported to the MRTOF-MS as survived ions. By fitting the TOF spectrum, we can deduce the number of ions extracted from the KISS gas cell. The HFS spectrum, as shown in Fig. 2, was obtained by measuring the number of laser-ionized ^{194}Os isotopes as a function of the laser wavelength. There appears one resonance peak stemming from one atomic transition of ^{194}Os due to $I^\pi = 0^+$. The constant background (dashed line) in Fig. 2 indicates the contaminant at the $^{194}\text{Os}^{2+}$ peak, which corresponds to $^{194}\text{Au}^{2+}$ transported as survived ions. The expected TOF peak position of $^{194}\text{Au}^{2+}$ indicated by the black dotted line in Fig. 1 deviates by about 4 ns from the $^{194}\text{Os}^{2+}$ peak. To evaluate the extraction yields of $^{194}\text{Os}^{2+}$ accurately, we fit the spectrum by omitting the $^{194}\text{Au}^{2+}$ peak because of the closeness of the peak positions. However, we could clearly deduce the resonance peak of ^{194}Os and the amount of ^{194}Au as the constant background, as shown in Fig. 2. From the peak position, we can determine the isotope shift value of ^{194}Os to deduce the change in the charge radius and discuss the nuclear deformation. Further analysis is in progress.

References

- 1) Y. Hirayama *et al.*, Nucl. Instrum. Methods Phys. Res. **B412**, 11 (2017).
- 2) Y. Hirayama *et al.*, Phys. Rev. C **96**, 014307 (2017).
- 3) J. Y. Moon *et al.*, in this report.

^{*1} Wako Nuclear Science Center (WNCS), Institute of Particle and Nuclear Studies (IPNS), High Energy Accelerator Research Organization (KEK)

^{*2} Seoul National University

^{*3} Institute for Basic Science (IBS)

^{*4} Department of Physics, University of Tsukuba

^{*5} Department of Physics, Kyushu University

^{*6} Institute for Integrated Radiation and Nuclear Science, Kyoto University (KURNS)

Calibration and simulation of LaBr₃:Ce scintillator for analyzing ⁸Li(α , n)¹¹B-reaction data

Y. Mizoi,^{*1,*2,*3} H. Baba,^{*3} A. Bracco,^{*4,*5} F. Camera,^{*4,*5} S. M. Cha,^{*6} K. Y. Chae,^{*6} S. Cherubini,^{*3,*7,*8} H. S. Choi,^{*9} N. N. Duy,^{*6} T. Fukuda,^{*3,*10} S. Hayakawa,^{*2} Y. Hirayama,^{*11} N. Imai,^{*2} H. Ishiyama,^{*3} A. Kim,^{*12} D. H. Kim,^{*6} N. Kitamura,^{*2} S. Kubono,^{*2,*3} M. S. Kwag,^{*6} S. Michimasa,^{*2} M. Mihara,^{*3,*13} H. Miyatake,^{*11} S. Ota,^{*2} R. G. Pizzone,^{*7} H. Shimizu,^{*2,*3} N. K. Uyen,^{*6} R. Wakabayashi,^{*3,*13} Y. X. Watanabe,^{*11} O. Wieland,^{*4} H. Yamaguchi,^{*2} L. Yang,^{*2} N. Zhang,^{*2,*14} and Z. C. Zhang^{*14}

We performed an experiment¹⁾ using LaBr₃:Ce scintillators²⁾ at CRIB in 2018 for investigating controversial large differences among the previously reported³⁻⁹⁾ cross-section data of the ⁸Li(α , n)¹¹B reaction. In order to resolve the discrepancies among them, it is essential to obtain an accurate γ -ray spectrum of ¹¹B; therefore, accurate energy calibration and precise efficiency estimation play a crucial role. We performed off-line measurements for energy calibration using radiation sources, as listed in Table 1. Figure 1 presents the calibration plot, in which the horizontal and vertical axes correspond to the time-to-digital converter (TDC) channel reduced by a charge-to-time converter (QTC) and the expected γ -ray energy, respectively; the plot shows sufficiently good linearity. On-line measurements using ¹⁶N beams were also performed at CRIB. In the studied reaction, ¹⁶N decays to ¹⁶O*, which emits γ -rays with $E_\gamma = 6130$ keV. GEANT4 simulations were also performed for each type of γ -rays. One example is shown in Fig. 2, which is the preliminary result of the γ -ray energy spectrum of ¹⁶N($\beta\gamma$). The histogram with error bars and filled histogram are measured and simulated spectra, respectively. The measured peaks of full energy,

single escape and double escape are consistent with the simulated ones. By applying the results of our precise energy calibration, we can proceed to the data analysis for solving the discrepancies among the previous results.

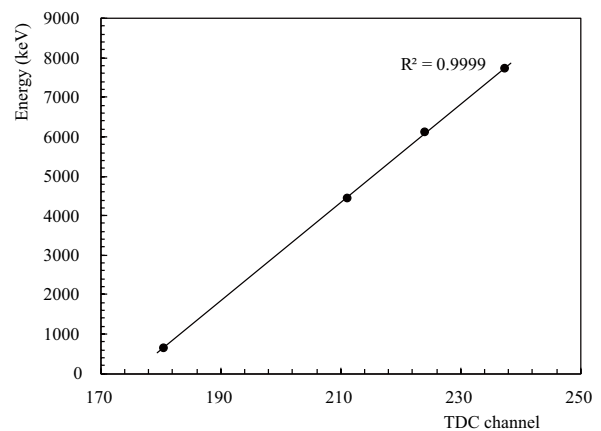


Fig. 1. Calibration plot obtained by off-line measurements.

Table 1. Gamma-ray sources used for off-line calibration and their energies.

Source	Energy (keV)
¹³⁷ Cs	662
Am/Be(¹² C*)	4440
Cm/C(¹⁶ O*)	6130
Am/Be+Al	7724

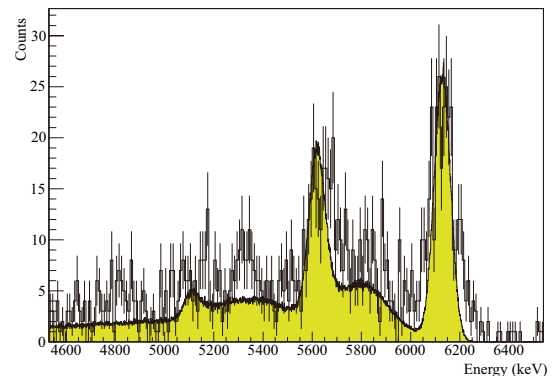


Fig. 2. Energy spectrum of γ -rays from ¹⁶N($\beta\gamma$).

*1 Center for Physics and Mathematics, Institute for Liberal Arts and Sciences, Osaka Electro-Communication University
 *2 Center for Nuclear Study, the University of Tokyo
 *3 RIKEN Nishina Center
 *4 INFN - Sezione di Milano
 *5 Dipartimento di Fisica dell'Università degli Studi di Milano
 *6 Department of Physics, Sungkyunkwan University
 *7 INFN - Laboratori Nazionali del Sud (LNS)
 *8 Dipartimento di Fisica ed Astronomia, Università di Catania
 *9 Department of Physics and Astronomy, Seoul National University
 *10 RCNP, Osaka University
 *11 Wako Nuclear Science Center (WNSC/IPNS), KEK
 *12 Department of Physics, Ewha Womans University
 *13 Department of Physics, Osaka University
 *14 IMP, Chinese Academy of Science (CAS)

References

- 1) Y. Mizoi *et al.*, RIKEN Accel. Prog. Rep. **52**, 58 (2019).
- 2) A. Gaiz *et al.*, Nucl. Instrum. Methods Phys. Res. A **729**, 910 (2013).
- 3) R. N. Boyd *et al.*, Phys. Rev. Lett. **68**, 1283 (1992).
- 4) X. Gu *et al.*, Phys. Lett. B **343**, 31 (1995).
- 5) Y. Mizoi *et al.*, Phys. Rev. C **62**, 065801 (2000).
- 6) S. Cherubini *et al.*, Eur. Phys. J. **20**, 355 (2004).
- 7) H. Ishiyama *et al.*, Phys. Lett. B **640**, 82 (2006).
- 8) M. La Cognata *et al.*, Phys. Lett. B **664**, 157 (2008).
- 9) S. K. Das *et al.*, Phys. Rev. C **95**, 055805 (2017).

Measurement of $^{25}\text{Al}+p$ resonant elastic scattering relevant to the astrophysical reaction $^{22}\text{Mg}(\alpha, p)^{25}\text{Al}$

J. Hu,^{*1} H. Yamaguchi,^{*2} S. W. Xu,^{*1} N. T. Zhang,^{*1} S. B. Ma,^{*1} L. H. Ru,^{*1} E. Q. Liu,^{*1} T. Liu,^{*1} S. Hayakawa,^{*2} L. Yang,^{*2} H. Shimizu,^{*2} D. Kahl,^{*3} C. B. Hamill,^{*3} A. Murphy,^{*3} J. Su,^{*4} X. Fang,^{*5} K. Chae,^{*6} M. Kwag,^{*6} S. Cha,^{*6} N. N. Duy,^{*6} N. K. Uyen,^{*6} D. Kim,^{*6} G. Pizzone,^{*7} M. L. Cognata,^{*7} S. Cherubini,^{*7} S. Romano,^{*7} A. Tumino,^{*7} J. Liang,^{*8} A. Psaltis,^{*8} M. Sferrazza,^{*8} D. H. Kim,^{*9} and S. Kubono^{*10}

Type-I X-ray bursts are the most frequently observed thermonuclear explosions in nature.¹⁾ They occur on the surface of accreting neutron stars in low-mass X-ray binary systems. The investigation of X-ray bursts can help us understand the properties of a neutron star and the underlying physics.

The bursts are driven by the tripe- α reaction, the αp -process, and the rp -process. After breakout from the hot CNO cycle, the nucleosynthesis path is characterized by the αp -process.²⁾ The αp -process is a sequence of α - and proton-induced reactions that transport nuclear material from the CNO cycle toward the region of heavier proton-rich nuclei.

The X-ray light curve is the main direct observable of X-ray bursts and could be affected significantly by the αp -process. According to a recent sensitivity study by Cyburt,³⁾ the $^{22}\text{Mg}(\alpha, p)^{25}\text{Al}$ reaction is thought to be the most sensitive one during the αp -process and may have a prominent impact on the burst light curve. However, with scarce experimental information on this reaction, the reaction rate in the calculations of X-ray bursts is estimated based on statistical models.

A measurement of $^{25}\text{Al}+p$ resonant elastic scattering has been performed to experimentally examine the $^{22}\text{Mg}(\alpha, p)^{25}\text{Al}$ reaction rates. The experiment was performed using the CNS radioactive ion beam separator (CRIB),⁴⁾ installed by the Center for Nuclear Study (CNS), University of Tokyo, in the RIKEN Accelerator Research Facility. A primary beam of $^{24}\text{Mg}^{8+}$ was accelerated up to 8.0 MeV/nucleon by the AVF cyclotron with an average intensity of 1 e μ A. The primary beam bombarded a liquid-nitrogen-cooled D₂ gas target to produce a secondary ^{25}Al beam via the $^{24}\text{Mg}(d, n)^{25}\text{Al}$ reaction in inverse kinematics. The ^{25}Al beam was separated by the CRIB separator. The ^{25}Al beam, with an average energy of 5.68 MeV/nucleon and an average intensity of 2.0×10^5 pps, was then delivered to the F3 experimental chamber, where it bom-

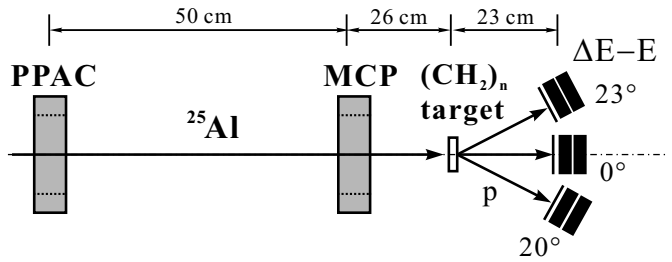


Fig. 1. Schematic diagram (top view) of the experimental setup at the F3 chamber.

barded a 13.95-mg/cm²-thick $(\text{CH}_2)_n$ target and a 18.02-mg/cm²-thick C target in which the beam was stopped. The C target was used to evaluate the background contributions. After passing through a Wien filter, the ^{25}Al beam purity can be up to 80%.

The setup at the F3 experimental chamber is shown in Fig. 1. A parallel-plate avalanche counter (PPAC) and a micro channel plate (MCP) were used for measuring the time and position information of the beam particles. The beam particles were identified in an event-by-event mode using the abscissa of MCP and the time of flight between MCP and the RF signal provided by the cyclotron.

The recoiling light particles from the $^{25}\text{Al}+p$ reaction were measured using three sets of Si telescopes at average angles of $\theta_{lab} \approx 0^\circ$, 20° , and 23° , respectively. Each telescope consisted of a 65- μm -thick double-side-strip (16×16 strips) silicon detector and two 1500- μm -thick pad detectors. The recoiling particles were clearly identified using the ΔE -E method. An array of ten NaI(Tl) detectors was mounted directly above the target and used to detect the γ rays from the decay of the excited states in ^{25}Al . The data analysis is in progress.

References

- 1) W. H. G. Lewin, J. V. Paradijs, R. E. Taam, *Space Science Reviews* **62**, 223 (1993).
- 2) R. K. Wallace, S. E. Woosley, *Astrophys. J. Suppl.* **45**, 389 (1981).
- 3) R. H. Cyburt *et al.*, *Astrophys. J. Suppl.* **830**, 55 (2016).
- 4) Y. Yanagisawa *et al.*, *Nucl. Instrum. Methods Phys. Res. A* **539**, 74 (2005).

*1 Institute of Modern Physics, Chinese Academy of Sciences
 *2 Center for Nuclear Study, University of Tokyo
 *3 School of Physics & Astronomy, University of Edinburgh
 *4 College of Nuclear Science and Technology, Beijing Normal University
 *5 School of Physics, Sun Yet-sen University
 *6 Department of Physics, Sungkyunkwan University
 *7 INFN-LNS, Laboratori Nazionali del Sud
 *8 Department of Physics & Astronomy, McMaster University
 *9 Department of Physics, Ewha Womans University
 *10 RIKEN Nishina Center

^{26}Si beam production and thermal durability test of gas target window

M. J. Kim,^{*1} K. Y. Chae,^{*1} S. Hayakawa,^{*2} S. M. Cha,^{*1} N. N. Duy,^{*1} G. M. Gu,^{*1} M. S. Kwag,^{*1} N. R. Ma,^{*2} N. K. Uyen,^{*1} H. Shimizu,^{*2} and H. Yamaguchi^{*2}

The study of the αp process is important for understanding nucleosynthesis in x-ray burst. The process, which is composed of alternating (α, p) and (p, γ) reactions, is considered the bridge between the CNO cycle and rp process. Owing to technical issues, most of the astrophysical (α, p) reactions on radioactive isotopes are less understood experimentally, including the $^{26}\text{Si}(\alpha, p)^{29}\text{P}$ reaction. The energy levels of ^{30}S falling in the Gamow window of the reaction at x-ray burst temperatures ($T = 1 - 3$ GK, $E_x = 10 - 14$ MeV) are crucial for the $^{26}\text{Si}(\alpha, p)^{29}\text{P}$ reaction rate. Many energy levels were identified through previous works,¹⁾ but the spins of levels above $E_x = 10$ MeV are not constrained in many cases. Additionally, no energy levels above $E_x = 12.4$ MeV have been measured so far. Thus, we thus plan to measure the $^{26}\text{Si}(\alpha, \alpha)^{26}\text{Si}$ elastic resonant scattering. We simultaneously expect that the $^{26}\text{Si}(\alpha, p)^{29}\text{P}$ reaction is also directly observable, which requires a rather high-intensity ^{26}Si beam. The primary beam intensity is, however, limited to only approximately 200 pA to prevent the deposited heat from breaking the F0 gas target window (Havar foil). Therefore, other types of foils were tested during the beam time.

We took 1.5 days out of the approved 12 days of beamtime to test the ^{26}Si beam production at the Center for Nuclear Study Radioactive Ion Beam Separator (CRIB)²⁾ of the University of Tokyo in December 2019. A primary beam of $^{24}\text{Mg}^{8+}$ was accelerated by the AVF cyclotron at 7.5 MeV/nucleon and with a maximum intensity of 400 pA, bombarding the cryogenic ^3He gas target of 0.94 mg/cm². The ^3He gas was confined with windows of 3- μm -thick Ti foil ($\phi = 20$ mm), which has a lower thickness and higher heat conductivity than the commonly used Havar foil, with the expectation of a higher injecting beam intensity. The beam of the radioactive isotope ^{26}Si was produced by the $^3\text{He}(^{24}\text{Mg}, ^{26}\text{Si})n$ reaction. We installed a 0.2-mg/cm²-thick carbon foil as a charge stripper to obtain a higher population of the highest charge state $^{26}\text{Si}^{14+}$. The magnetic rigidity was set to 0.61208 Tm to select the desired beam energy of 5.2 MeV/nucleon. The voltage of the subsequent Wien filter was ± 85.5 kV. A ^{26}Si purity of 59% and a beam intensity of about 4.7×10^4 particles per second were achieved at the F3 focal plane, which are much higher than those of the previously produced ^{26}Si beam at CRIB.³⁾ The particle identification plot at F3 is shown in Fig. 1. This improvement may be attributed to the higher primary beam intensity, the thinner gas target window foil, the newly installed charge stripper, and the higher Wien filter voltage.

We also investigated the thermal durability of other

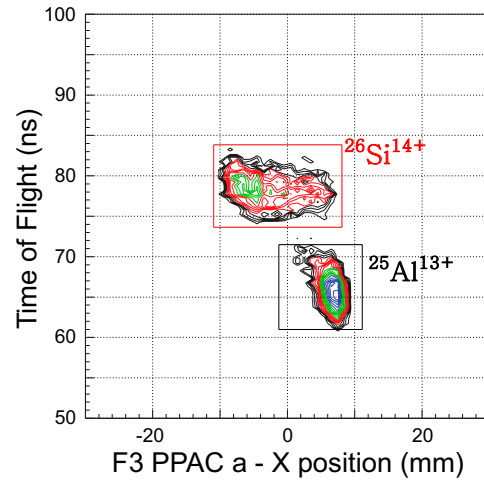


Fig. 1. Particle identification spectrum obtained at the F3 focal plane. The ^{26}Si beam is clearly separated from other beam particles.

materials of the gas target window through primary beam injection. We installed Mo (100% molybdenum, thickness: 3 μm , thermal conductivity: 138 W/m/K, melting point: 2896 K), Ti (100% titanium, thickness: 3 μm , thermal conductivity: 21.9 W/m/K, melting point: 1941 K), Havar (thickness: 2.5 μm , thermal conductivity: 13 W/m/K, melting point: 1753 K) and CuBe (98% copper, 2% beryllium, thickness: 3 μm , thermal conductivity: 105 W/m/K, melting point: 1143 K) foils held by copper frames on a rotating wheel⁴⁾ in the F0 chamber. The temperature of each window was monitored by thermography. The foils were exposed to a $^{24}\text{Mg}^{8+}$ primary beam up to an intensity of about 2800 enA, at which all the foils were pin-holed on the beam-spot position but the Mo foil endured. The typical beam size is measured to be about 2 mm. We also tested those foils mounted on the gas-filled target cell with liquid-nitrogen cooling-except the CuBe foil. We exposed the Ti foil to a 2600 enA $^{24}\text{Mg}^{8+}$ beam and the Havar and Mo foils to 1800 enA beams. The result shows that only the Mo foil resisted breakage, suggesting that it is the most durable material. This is consistent with the highest thermal conductivity and melting point among the tested materials. We will determine the upper limit of the heat deposition rate through further investigation. We anticipate that a higher intensity of the secondary ^{26}Si beam could be realized when Mo foils are used at the F0 gas cell.

References

- 1) S. Almaraz-calderon *et al.*, Phys. Rev. C **86**, 065805 (2012).
- 2) Y. Yanagisawa *et al.*, Nucl. Instrum. Method Phys. Res. A **539**, 74 (2005).
- 3) H. S. Jung *et al.*, Phys. Rev. C **85**, 045802 (2012).
- 4) D. Kahl, Master's thesis, McMaster University (2008).

^{*1} Department of Physics, Sungkyunkwan University

^{*2} Center for Nuclear Study, University of Tokyo

Production of a high-intensity francium ion beam for the measurement of the electron electric dipole moment

H. Nagahama,^{*1} K. Nakamura,^{*1} N. Ozawa,^{*1} Y. Kotaka,^{*1} H. Haba,^{*2} T. Hayamizu,^{*2} M. Ohtsuka,^{*2,*3} K. S. Tanaka,^{*4} H. Ueno,^{*2} Y. Ichikawa,^{*2} and Y. Sakemi^{*1}

The striking imbalance between matter and anti-matter observed in the universe is known to be one of the biggest mysteries in modern physics. For decades, physicists have been attempting to investigate CP (C: charge conjugation, P: parity transformation) violations for different physical systems, which could lead to the discovery of the fundamental reasons for this mystery. One of these intriguing systems is the electric dipole moment of an electron (eEDM). The existence of an absolute value of the eEDM implies that CP symmetry has been violated. At the same time, this would also reveal the existence of a new theory beyond the standard model of particle physics.

Since the eEDM is expected to be small,¹⁾ it is necessary to adopt a system that enhances the eEDM to a sufficiently large value. For this purpose, we have chosen francium. Francium has an eEDM enhancement factor of approximately 10^3 , which is known to be the largest among any ground-state atom.²⁾ The ideal environment for Ramsey spectroscopy to measure the eEDM using francium atom is one in which a large amount of francium atoms are trapped in a tiny volume where the interactions with other particles are highly suppressed. To this end, we are planning to develop a three-dimensional optical lattice to confine laser-cooled francium atoms.

In this study, we constructed a surface ionizer to create a high-intensity francium ion beam. The surface ionizer consists of a vacuum chamber, a gold target, deflection electrodes, and an infrared radiation heater, as shown in Fig. 1. An $^{18}\text{O}^{6+}$ beam (6.28 MeV/nucleon) provided by the AVF cyclotron in RIKEN RIBF will be irradiated on the gold target to induce the following fusion reactions inside the gold: $^{197}\text{Au}(^{18}\text{O}, xn)^{215-x}\text{Fr}$. By heating up the target using the infrared heater, the thermal diffusion process of the franciums will occur, and some fractions will reach the surface. Most of the franciums at the surface will be ionized according to the Saha-Langmuir equation³⁾ and, subsequently, thermally released into the vacuum. Since high voltages are applied to the target (~ 1000 V) as well as to the deflection electrodes (~ 930 V), the thermal francium ions will experience the electric-field gradient and be transported as a secondary beam (~ 1 keV), which will be guided at an angle of 45° with respect to the $^{18}\text{O}^{6+}$ beam. The francium ion beam generated will finally

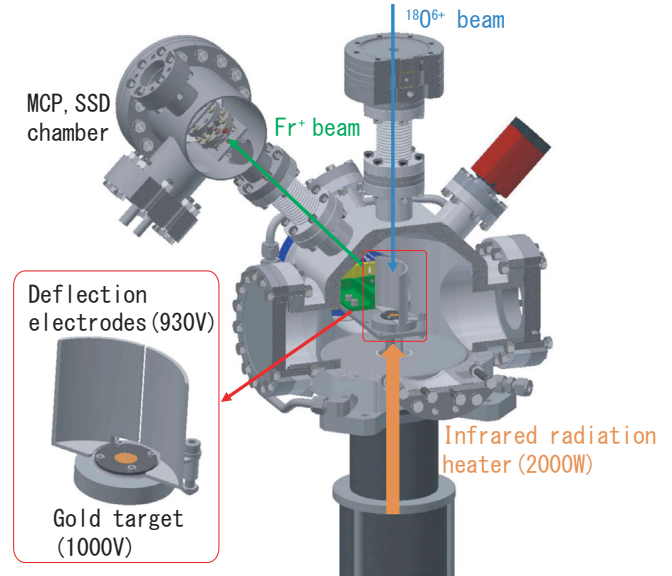


Fig. 1. Schematic of the experimental apparatus to produce a high-intensity francium ion beam.

be monitored using a beam diagnostic system. The beam diagnostic system consists of a micro-channel plate (MCP) to monitor the beam's characteristics and a silicon semiconducting detector (SSD) to observe α radiation caused by the α decay of the franciums. An α radiation source (Am) is placed near the SSD to calibrate the energy of the α radiation.

In September 2019, we constructed this experimental apparatus and performed an offline test. During the offline test, we heated up the target to $400 \sim 800^\circ\text{C}$ using the infrared heater and thermally ionized particles already existing on the surface. These ionized particles were monitored by the MCP, which allowed us to optimise the voltages applied to the target and the deflection electrodes. We have confirmed that the optimised voltages are consistent with our previous simulation using SIMION 8.1. After the offline test, we performed online experiments on October 25, 2019 and November 22, 2019. Through data analysis, we verified that we had succeeded in producing a $^{210}\text{Fr}^+$ beam with an intensity of $1.3 \times 10^6/\text{s}$.

References

- 1) M. S. Safronova *et al.*, Rev. Mod. Phys. **90**, 025008 (2018).
- 2) J. S. M. Geinges, V. V. Flambaum, Phys. Rep. **397**, 63 (2004).
- 3) M. J. Dresser, J. Appl. Phys. **39**, 338 (1968).

*1 Center for Nuclear Study, the University of Tokyo

*2 RIKEN Nishina Center

*3 Waseda University Honjo Senior High School

*4 Cyclotron and Radioisotope Center, Tohoku University

Development of β -NMR with spin-aligned beam

H. Nishibata,^{*1,*2} A. Gladkov,^{*1} H. Ueno,^{*1} Y. Ichikawa,^{*1} A. Takamine,^{*1} H. Yamazaki,^{*1} M. Tajima,^{*1} K. Kawata,^{*1,*3} M. Mihara,^{*4} T. Sato,^{*1} K. Doi,^{*1,*5} W. Kobayashi,^{*1,*5} M. Sanjo,^{*1,*5} T. Asakawa,^{*1,*5} Y. Sasaki,^{*1,*5} T. Yada,^{*1,*5} and K. Asahi^{*1}

Nuclear electromagnetic moments, namely magnetic dipole (μ) and electric quadrupole (Q) moments, are one of the most sensitive probes to address a single-particle configuration and nuclear deformation, respectively. So far, nuclear moments for ground states have been measured by the method of β -ray-detected nuclear magnetic resonance (β -NMR) combined with a spin-polarized radioactive beam. However, it is difficult to apply β -NMR to far-unstable nuclei produced by BigRIPS because the spin polarization is significantly reduced for reactions with the removal of many nucleons and/or with a beam energy >100 MeV/nucleon. In order to overcome this difficulty, we have been developing a new method that combines the β -NMR technique and highly spin-aligned beam production with the two-step fragmentation method by using BigRIPS.¹⁾ This report presents the recent results of a demonstration experiment using spin-aligned ^{13}B ($T_{1/2} = 17.3$ ms, $I^\pi = 3/2^-$) with the known ground-state μ and Q moments.³⁾

The experiment was performed at the Heavy Ion Medical Accelerator in Chiba (HIMAC). A primary ^{15}N beam with an energy of 100 MeV/nucleon was accelerated by the synchrotron. The beam irradiation time was 20 ms in every 3.3 s. A radioactive ^{13}B beam was produced by the two-proton-removal reaction of ^{15}N with a 1-mm-thick Be target, which was located at the entrance of the secondary beamline SB2. The ^{13}B beam was separated by two dipole magnets and a wedge-type energy degrader (3-mm thickness, 6° angle) at the dispersive focal plane F1. The spin alignment was obtained by selecting a moment off the center of the momentum distribution by -4 – -3% . Subsequently, the spin-aligned ^{13}B beam was delivered to the end of the beamline F3, where the β -NMR apparatus is located, and was implanted to a TiO_2 single crystal.

Since the Q moment of the implanted ^{13}B interacts with an electric field gradient at the implantation site in the crystal and causes unequal Zeeman splitting between the individual sub-levels, a partial spin reversal using the adiabatic fast passage (AFP) method²⁾ becomes possible and convert the spin alignment of the implanted ^{13}B into the spin polarization. Consequently, the angular distribution of the emitted β rays becomes anisotropic. For the AFP method, a static

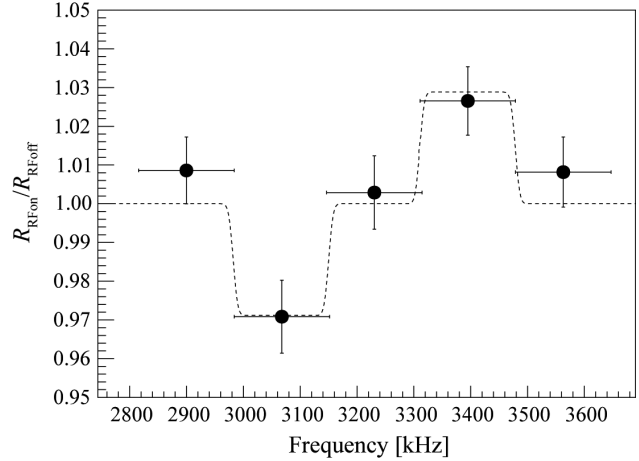


Fig. 1. Obtained NMR spectrum for spin-aligned ^{13}B . The ordinate of this spectrum shows the double ratio $R_{\text{RFon}}/R_{\text{RFoff}}$, where R_{RFon} (R_{RFoff}) is the ratio of the β -ray counts detected by the 0° and 180° telescopes with (without) the oscillating magnetic field. The dotted line is the spectrum expected from the literature values of $\mu = +3.1778(5) \mu_{\text{N}}$ and $Q = +36.6(8) \text{ mb}^3$ assuming a spin alignment of 4.5%.

magnetic field of 0.2 T was applied to the crystal perpendicular to the beam axis in the horizontal plane, and an oscillating magnetic field was applied by a pair of coils perpendicular to the static magnetic field. The β rays from the β decay of ^{13}B were detected by two telescopes placed at 0° and 180° with respect to the direction of the static magnetic field. Each telescope consists of two 1.0-mm-thick plastic scintillators.

Figure 1 shows the obtained NMR spectrum for spin-aligned ^{13}B . The resonances were observed at 3067 ± 84 kHz and 3394 ± 84 kHz, which correspond to the transitions between the Zeeman sub-levels with $m = -3/2$ and $-1/2$, $+1/2$, and $+3/2$, respectively. From these values, the moments of $^{13}\text{B}_{\text{g.s.}}$ were deduced to be $|\mu| = 3.18(9) \mu_{\text{N}}$ and $|Q| = 36(9) \text{ mb}$, which are consistent with the literature values of $\mu = +3.1778(5) \mu_{\text{N}}$ and $Q = +36.6(8) \text{ mb}$.³⁾ We have successfully demonstrated our new method of β -NMR with a spin-aligned beam.

References

- 1) Y. Ichikawa *et al.*, Nat. Phys. **8**, 918 (2012).
- 2) A. Abragam, *The Principles of Nuclear Magnetism*, (Clarendon, Oxford, 1961).
- 3) T. Nagatomo *et al.*, Nucl. Phys. A **746**, 509c (2004).

*1 RIKEN Nishina Center

*2 Department of Physics, Kyushu University

*3 Center for Nuclear Study, University of Tokyo

*4 Department of Physics, Osaka University

*5 Department of Physics, Hosei University

Production of isomers around ^{52}Fe nucleus via projectile fragmentation

K. Kawata,^{*1,*2} S. Ota,^{*2} J. Zenihiro,^{*1} C. Iwamoto,^{*2} N. Kitamura,^{*2} H. Sakai,^{*2} S. Masuoka,^{*2} S. Michimasa,^{*2} K. Yako,^{*2} T. Harada,^{*2} H. Nishibata,^{*2} R. Tsunoda,^{*2} N. Imai,^{*2} J. Hwang,^{*2} N. Zhang,^{*4} and F. Endo^{*5}

The nuclear responses of isomeric high-spin states are attractive topics. A recent theoretical study on the spin-isospin response of the 12^+ isomeric state in ^{52}Fe showed that the widths of the GT strength distributions from the ground and isomeric states may differ from each other due to the different collectivities,¹⁾ which may call for the modification of a simple Brink hypothesis. To perform nuclear reactions on such isomers, isomeric nuclear beams should be prepared since the isomers are still short-lived nuclei.

Projectile fragmentation is a popular method to produce short-lived nuclei. In order to prepare the isomer beam, it is necessary to understand the production mechanism of isomers through the projectile fragmentation process. We studied the isomer ratios in the vicinity of ^{52}Fe as a function of the linear momentum transfer. Although the ratios are conventionally described by a classical model assuming the contribution of the angular momentum transfers during the projectile fragmentation process,²⁾ it is still not clear how the angular momentum is transferred to the fragmented particles. To learn the role of the angular momentum transfer, we studied not only the isomer ratio but also the momentum distribution of the isomeric state of the fragmentation process. In this paper, we report a new systematic measurement of production cross sections of the isomers $^{52}\text{Fe}(12^+)$, $^{53}\text{Fe}(19/2^-)$, $^{54}\text{Co}(7^+)$, and $^{54}\text{Fe}(10^+)$ by primary beams of $^{58}\text{Ni}(0^+)$ and $^{59}\text{Co}(7/2^-)$.

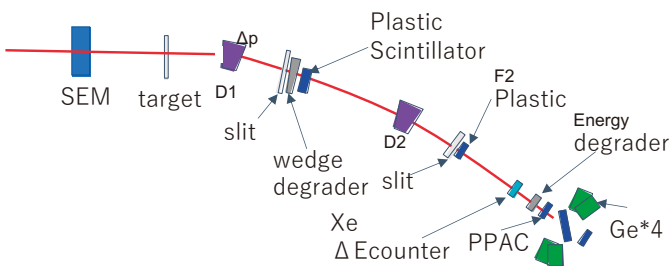


Fig. 1. Experimental setup in the SB2 course (16H362).

The number of primary beams was counted by a secondary emission monitor (SEM), which consists of a thin Cu film. We identified the fragment by using the ToF- ΔE method. ToF was measured from F2 to F3, and ΔE was measured by a Xe scintillation detector. The number of isomers was counted by a Ge detector.

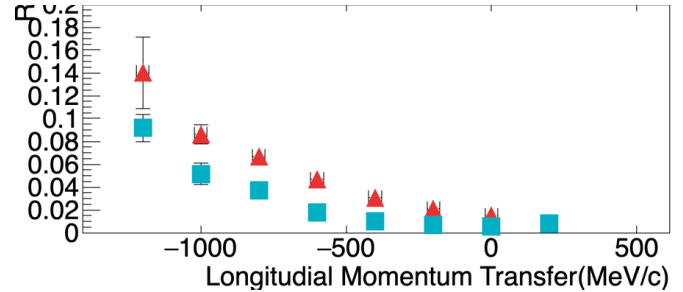


Fig. 2. Isomer ratio of $^{52}\text{Fe}(12^+)$. Red triangles show the result from the $^{59}\text{Co}(7/2^-)$ beam, and the blue squares show the result from the $^{58}\text{Ni}(0^+)$ beam.

The experiment was performed at the SB2 course in HIMAC, a synchrotron facility in Chiba. Figure 1 shows the experimental setup at the SB2 course. The primary beams of ^{58}Ni and ^{59}Co at 350 MeV/nucleon bombarded a 14-mm-thick ^9Be production target. The fragments are separated and momentum analyzed by a fragment separator consisting of two dipole magnets and quadrupole magnets. In order to obtain isomer ratios, the number of fragments and γ rays from the isomers were counted. A Xe scintillator was used for counting the fragment, and four Ge detectors were used for detecting γ rays. The isomer ratio of a certain fragment nucleus is the ratio of the number of emitted gamma rays obtained after correcting for the efficiency to the number of fragments.

When the velocity of the fragment is the same as that of the projectile, no momentum is transferred to the fragment.

Figure 2 shows the preliminary result of the isomer ratio of $^{52}\text{Fe}(12^+)$. The momentum-transfer dependence of the isomer ratio is clearly observed. The isomer ratio with the $^{59}\text{Co}(7/2^-)$ beam at each momentum is larger than that with the $^{58}\text{Ni}(0^+)$ beam. It is inferred that the initial angular momentum of the projectile has a significant effect on isomer production.

The data analysis is ongoing. The difference between the momentum distributions of isomers and non-isomers will be investigated in order to clarify the role of angular momentum transfer from the viewpoint of the correlation between the linear momentum transfers and angular momentum transfers.

*1 RIKEN Nishina Center

*2 Center for Nuclear Study, University of Tokyo

*3 Toho University

*4 Institute of Modern Physics

*5 Tohoku University

References

- 1) H. Z. Liang *et al.*, Phys. Rev. C **98**, 014311 (2018).
- 2) W. -D. Schmidt *et al.*, Z. Phys. A **350**, 215 (1994).

$^{79}\text{Se}(n, \gamma)^{80}\text{Se}$ reaction cross section through $^{77, 79}\text{Se}(d, p)^{78, 80}\text{Se}$ reactions

N. Imai,^{*1} M. Dozono,^{*1} S. Michimasa,^{*1} T. Sumikama,^{*2} S. Ota,^{*1} S. Hayakawa,^{*1} K. Iribe,^{*2,*3} C. Iwamoto,^{*1} S. Kawase,^{*4} K. Kawata,^{*1,*2} N. Kitamura,^{*1} S. Masuoka,^{*1} K. Nakano,^{*4} P. Schrock,^{*1} D. Suzuki,^{*2} R. Tsunoda,^{*1} K. Wimmer,^{*2,*5} D. S. Ahn,^{*2} O. Beliuskina,^{*1} N. Chiga,^{*2} N. Fukuda,^{*2} E. Ideguchi,^{*2,*6} K. Kusaka,^{*2} H. Miki,^{*2,*7} H. Miyatake,^{*8} D. Nagae,^{*2} M. Nakano,^{*2,*9} S. Ohmika,^{*2} M. Ohtake,^{*2} H. Otsu,^{*2} H. J. Ong,^{*2,*6} S. Sato,^{*2,*9} H. Shimizu,^{*1} Y. Shimizu,^{*2} H. Sakurai,^{*2,*5} X. Sun,^{*2} H. Suzuki,^{*2} M. Takaki,^{*1} H. Takeda,^{*2} S. Takeuchi,^{*2,*7} T. Teranishi,^{*2,*3} Y. Watanabe,^{*4} Y. X. Watanabe,^{*8} H. Yamada,^{*2,*7} H. Yamaguchi,^{*1} L. Yang,^{*1} R. Yanagihara,^{*6} K. Yoshida,^{*2} Y. Yanagisawa,^{*2} and S. Shimoura¹

^{79}Se is one of the long-lived fission products (LLFPs) of nuclear waste. To design a facility to transmuted the nucleus, a neutron-capture cross section on the nucleus was conceptualized. However, because both the neutron and LLFPs are unstable, the measurement of neutron-induced cross section is quite challenging. Alternatively, the reaction cross section can be indirectly determined through a surrogate reaction.

It is generally accepted that the (n, γ) cross section is composed of two parts: the formation of a compound state and the subsequent decay. The first term can be calculated using optical-model potentials with global parameter sets. In contrast, theoretical estimates of the second process is quite challenging owing to its high level density and complicated decay scheme, and it needs to be evaluated experimentally.¹⁾ The present work aims to determine the γ emission probability, P_γ , as a function of the excitation energy from the unbound states of ^{80}Se populated by the (d, p) reaction. In the surrogate method, the P_γ from the transfer reaction is used to determine the (n, γ) cross section. However, it is known that a mismatch in the angular-momentum transfer between the transfer reaction and capture reaction leads to a large cross section. To compensate for the mismatch, a surrogate ratio method is often used, where the (n, γ) cross section of interest is normalized using a pair of (n, γ) and transfer reactions of the neighboring nucleus. We deduce the $^{79}\text{Se}(n, \gamma)^{80}\text{Se}$ reaction by employing cross sections of $^{77}\text{Se}(n, \gamma)^{78}\text{Se}^{2)}$ and $^{77}\text{Se}(d, p)^{78}\text{Se}$ reaction.

The experiment was performed using the OEDO beam line³⁾ as one of the first physics experiments. $^{77, 79}\text{Se}$ beams produced by BigRIPS were energy-degraded at F5, and the beam was spatially focused on a 4-mg/cm² thick polyethylene deuteride target by OEDO. The beam energy was adjusted to 20 MeV/nucleon at the target. The recoiled particles were identified by employing a six-

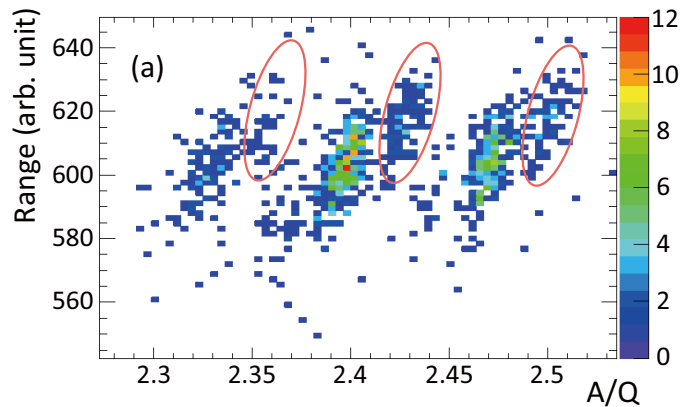


Fig. 1. Mass of the outgoing reaction residue as a function of their A/Q measured at the S1 focal plane. The events circled were $^{80}\text{Se}^{34+}$, $^{80}\text{Se}^{33+}$, $^{80}\text{Se}^{32+}$, respectively. See the text for details.

SSD-CsI(Tl) array called TiNA, which covered an angular range of 100°–150° in the laboratory frame. The excitation energies of the state populated in ^{78}Se (^{80}Se) were determined using TiNA and the incident beam momentum. The momenta of the outgoing nuclei were analyzed by the first half of the SHARAQ spectrometer.

In the correlation between the excitation energy and the mass-to-charge ratio (A/Q), which we presented in the last report, $^{80}\text{Se}^{33+}$ ($A/Q = 2.42$) was not clearly separated from $^{78}\text{Se}^{32+}$ ($A/Q = 2.44$). However, in Fig. 1, which presents the mass as a function of the A/Q ratio of ^{80}Se , they are separated well. Here, the mass was deduced from the analysis of the Bragg curve in the ionization chamber installed at the SHARAQ focal plane. Analysis has almost been finalized. The manuscript will be submitted soon.

This work was funded by the ImPACT Program of Council for Science, Technology and Innovation (Cabinet Office, Government of Japan).

References

- 1) J. E. Escher *et al.*, Rev. Mod. Phys. **84**, 353 (2012).
- 2) S. Kawada, M. Igashira, T. Katabuchi, M. Mizumoto, J. Nucl. Sci. Tech. **47**, 643 (2010).
- 3) S. Michimasa *et al.*, Prog. Theor. Exp. Phys. **2019**, 043D01 (2019).

^{*1} Center for Nuclear Study, University of Tokyo
^{*2} RIKEN Nishina Center
^{*3} Department of Physics, Kyushu Univ.
^{*4} Department of Advanced Energy Engineering Science, Kyushu Univ.
^{*5} Department of Physics, Univ. of Tokyo
^{*6} RCNP, Osaka University
^{*7} Department of Physics, Tokyo Institute of Technology
^{*8} WNSC, IPNS, KEK
^{*9} Department of Physics, Rikkyo University

Production-cross-section measurement and new-isotope search for very neutron-deficient RIs produced from ^{78}Kr beam at 345 MeV/nucleon by BigRIPS separator

H. Suzuki,^{*1} N. Fukuda,^{*1} H. Takeda,^{*1} Y. Shimizu,^{*1} D. S. Ahn,^{*1} T. Komatsubara,^{*1} N. Inabe,^{*1} K. Kusaka,^{*1} Y. Yanagisawa,^{*1} M. Ohtake,^{*1} H. Sato,^{*1} and K. Yoshida^{*1}

We performed production-cross-section measurements and new-isotope searches around the proton drip-line with the atomic numbers $Z = 22\text{--}30$. Proton-rich radioactive isotopes (RIs) were produced by the projectile fragmentation of a 270-pnA ^{78}Kr beam at 345 MeV/nucleon impinged on a 5-mm-thick Be production target in the BigRIPS separator.¹⁾ Particle identification based on the TOF- $B\rho$ - ΔE method²⁾ was performed in the second stage of BigRIPS. The production rates and momentum distributions of the RIs were measured.

The production cross sections were deduced from the measured production rates and their transmission efficiencies in BigRIPS, which were simulated with LISE⁺⁺ calculation code.^{3,4)} In the LISE⁺⁺ simulation, a parameter “coef,” which controls the slopes of exponential low-momentum tails in the momentum distribution of the RIs, was adjusted to reproduce the measured distribution. The tails observed in the experiments fell off faster than those calculated using LISE⁺⁺ with the original parametrization. Momentum-peak shifts between the simulations and experimental results were also taken into account in the calculation by tuning the $B\rho$ values of the dipoles. The tuned $B\rho$ values in the calculation were typically $\sim 1\%$ higher than the experimental ones. The parameters of the angular distribution were not changed in the code.

Figure 1 shows the production cross sections of RIs obtained in the ^{78}Kr -beam campaign in 2019 (open circles) and 2015 (open squares) with measurements by B. Blank *et al.*⁵⁾ (filled triangles). The solid lines in Fig. 1 show the cross sections predicted from the empirical formula EPAX3.1a.⁶⁾ The measured cross sections of RIs with a wide range of Z are fairly well reproduced by EPAX3.1a, except in a region around the proton drip-line. There are discrepancies between the cross sections measured by B. Blank *et al.*⁵⁾ and the ones in 2019 for Ti and Cr isotopes. It may have been caused by insufficient tunings in the calculation in our preliminary analysis.

No new isotopes were discovered in our measurement for Cr nor Ti isotopes. From the lack of observation of ^{41}Cr and ^{39}Ti and their expected yields, the upper limits of their half-lives were preliminarily estimated to be 70 ns and 90 ns, respectively.

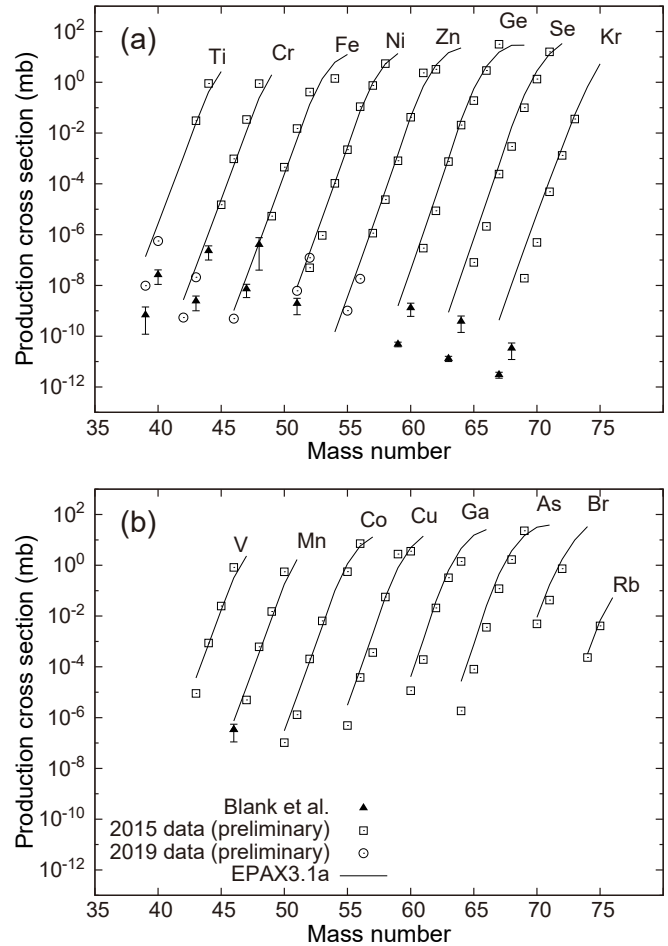


Fig. 1. Production cross sections of RIs produced in the $^{78}\text{Kr} + \text{Be}$ reaction at 345 MeV/nucleon. (a) Results for even- Z isotopes. (b) Results for odd- Z isotopes. Filled triangles, open squares, and open circles show the data measured by Blank *et al.*,⁵⁾ data measured in 2015, and data measured in 2019, respectively. Solid lines show the values predicted using the EPAX3.1a formula.⁶⁾

References

- 1) T. Kubo, Nucl. Instrum. Methods Phys. Res. B **204**, 97 (2003).
- 2) N. Fukuda *et al.*, Nucl. Instrum. Methods Phys. Res. B **317**, 323 (2013).
- 3) O. B. Tarasov, D. Bazin, Nucl. Instrum. Methods Phys. Res. B **266**, 4657 (2008) (references therein; LISE⁺⁺ site, <http://lise.nscl.edu,MichiganStateUniversity>).
- 4) O. B. Tarasov, Nucl. Phys. A **734**, 536 (2004).
- 5) B. Blank *et al.*, Phys. Rev. C **93**, 061301(R) (2016).
- 6) K. Sümmer, Phys. Rev. C **86**, 014601 (2012).

^{*1} RIKEN Nishina Center

Database of radioactive isotope beams produced at the BigRIPS separator[†]

Y. Shimizu,^{*1} N. Fukuda,^{*1} H. Takeda,^{*1} H. Suzuki,^{*1} D. S. Ahn,^{*1} N. Inabe,^{*1} K. Kusaka,^{*1} M. Ohtake,^{*1}
Y. Yanagisawa,^{*1} K. Yoshida,^{*1} T. Sumikama,^{*1} and T. Kubo^{*1,*2}

Many studies on exotic nuclei far from stability have been conducted at the RIKEN RIBF¹⁾ since 2007, taking advantage of the high intensity and large isotope variety of RI beams produced by the superconducting in-flight separator BigRIPS.²⁾ Neutron-rich RI beams in a very wide range of the nuclear chart have been produced utilizing the in-flight fission of a ^{238}U beam and the projectile fragmentation of ^{18}O , ^{48}Ca , and ^{70}Zn beams. Furthermore, a wide range of proton-rich RI beams have also been produced utilizing the projectile fragmentation of ^{78}Kr and ^{124}Xe beams. The systematically measured production cross sections and other related data are important to provide accurate production-yield information for planning rare-isotope experiments and to improve models and formulae to predict the cross section. Therefore, we have organized the data concerning the RI beam production and constructed a database to compile them.

The measured production cross sections and yields have been registered in the RI-beam database,³⁾ along with other data sets such as the setting of the BigRIPS separator and particle-identification information. We constructed such a relational database based on Microsoft Access 2010. Table 1 summarizes the structure of the database, which consists of five tables named “settings,” “yields,” “isomers,” “experiments,” and “papers.”

The graphical user interface of the RI-beam database was developed as a web application using PHP. As illustrated in Fig. 1, the web interface of the RI-beam database graphically represents a nuclear chart based on the KTUY05 formula.⁴⁾ In the nuclear chart, RI

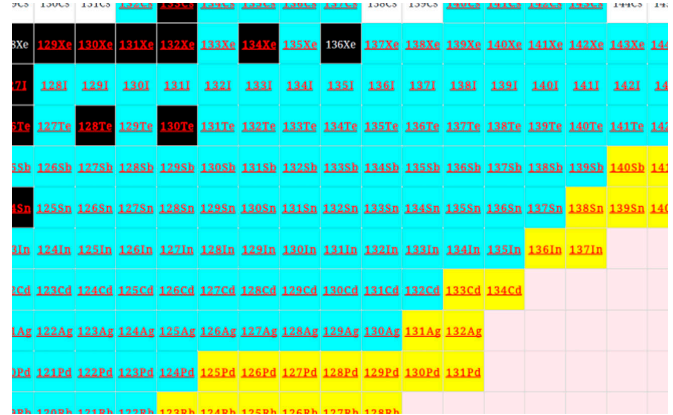


Fig. 1. Web interface. Cyan and yellow indicate nuclei and new isotopes produced at the BigRIPS separator, respectively. Pink indicates the nuclei predicted by KTUY05.⁴⁾ The production cross section and production yield for a nucleus of interest can be accessed through the hyperlinked site.

beams produced with the BigRIPS separator are indicated by red letters. The production cross section and production yield for a nucleus of interest can be accessed through the hyperlinked site.

The RI-beam database and its web interface allow efficient RI-beam production at the BigRIPS separator. The database stores the RI-beam and related information obtained for more than 1,600 RI beams produced using BigRIPS. This system is a powerful tool for planning RI-beam production procedures, optimizing BigRIPS settings, and implementing particle identification and isotope separation. However, the present database system was developed with a focus on the use of the production yields and cross sections measured under various experimental conditions; currently, other information such as RI beam purity is not included. In the future, we plan to improve the system so that such information can be stored as well. This would further aid researchers in designing a more accurate experimental plan.

References

- 1) Y. Yano, Nucl. Instrum. Methods Phys. Res. B **261**, 1009 (2007).
- 2) T. Kubo, Nucl. Instrum. Methods Phys. Res. B **204**, 97 (2003).
- 3) *Database of radioactive isotope beams produced at the BigRIPS separator*. Available at <https://ribeam.riken.jp/> (Accessed 1 Apr. 2019).
- 4) H. Koura *et al.*, Prog. Theor. Phys. **113**, 305 (2006).

Table 1. Structure of RI-beam database system as of December 2018.

table	contents
settings	settings_id, experimental conditions (beam, target, degraders, slit openings, $B\rho_s$, detectors)
yields	RI, yield, cross section, settings_id
isomers	RI, γ -ray energy, half-life, intensity, level energy, spectrum of γ -ray energy
experiments	proposal number, spokesperson, date, beam, course, delivered RIs
papers	title, doi, first author, delivered RIs

[†] Condensed from the article in Nucl. Instrum. Methods Phys. Res. B **463**, 158 (2020)

^{*1} RIKEN Nishina Center

^{*2} Facility for Rare Isotope Beams

RI beam production at BigRIPS in 2019

Y. Shimizu,^{*1} N. Fukuda,^{*1} H. Takeda,^{*1} H. Suzuki,^{*1} D. S. Ahn,^{*1} N. Inabe,^{*1} K. Kusaka,^{*1} M. Ohtake,^{*1}
Y. Yanagisawa,^{*1} T. Komatsubara,^{*1} H. Sato,^{*1} K. Yoshida,^{*1} and T. Uesaka^{*1}

The radioactive isotope (RI) beam production at the BigRIPS fragment separator¹⁾ in 2019 is reported here. Table 1 summarizes the experimental programs that involved the use of the BigRIPS separator during this period and the RI beams produced for each experiment.

In the spring beam time, a ^{78}Kr beam campaign was conducted with eight experiments. A ^{67}Se beam was delivered to the SAMURAI spectrometer to study the proton-unbound state of ^{66}Se relevant to the rp -process. A PALIS experiment was performed to confirm the practical feasibility using the same settings as for the ^{67}Se beam. A ^{62}Zn beam and, thereafter, a cocktail beam of ^{62}Ga and ^{62}Ge were produced to measure the Coulomb excitation of the $A = 62$ isospin triplets and to extract the $B(E2)$ values as well as proton and isoscalar multipole matrix elements. A ^{56}Zn beam was produced to perform the first γ -ray spectroscopy of the $T_Z = -2$ nucleus ^{56}Zn to investigate the mass dependence of the isospin-breaking effects. ^{48}Cr and ^{64}Ge beams were produced to study Gamow-Teller transitions via the (p, n) reaction on the $N = Z$ unstable nuclei ^{48}Cr and ^{64}Ge . The BigRIPS group measured the production cross sections of the proton-

rich nuclei around ^{54}Zn and ^{43}Cr regions, and searched the new isotopes for $^{37,38}\text{Ti}$ and ^{47}Cr .²⁾

After the ^{78}Kr beam campaign, a ^{124}Xe beam campaign was conducted with four experiments. A ^{101}Sn beam was produced to measure the energy of the first 2^+ state in ^{100}Sn . A ^{102}Sn beam was produced to study the $E2$ transition strength of ^{102}Sn . An experiment with the DTAS setup was performed to measure the probability of beta decay to excited states populated in the decay of ^{100}Sn using a cocktail beam of nuclei around ^{100}Sn .

In the autumn beam time, a ^{238}U beam campaign was conducted with six experiments. A ^{132}Sn beam was produced to study the ground-state properties of ^{132}Sn using proton elastic scattering with the ESPRI setup. A PALIS experiment was performed to study the extraction efficiency using alpha emitters around the ^{208}Rn region. A cocktail beam of ^{127}Sn and ^{128}Sn was delivered to F8 for the magnetic moment measurement using the time-differential perturbed angular distribution method. Three machine studies³⁻⁵⁾ were performed to develop the production of the neutron-rich nuclei with $N = 126$, the production of a slowed-down RI beam using momentum-compressed optics, and the

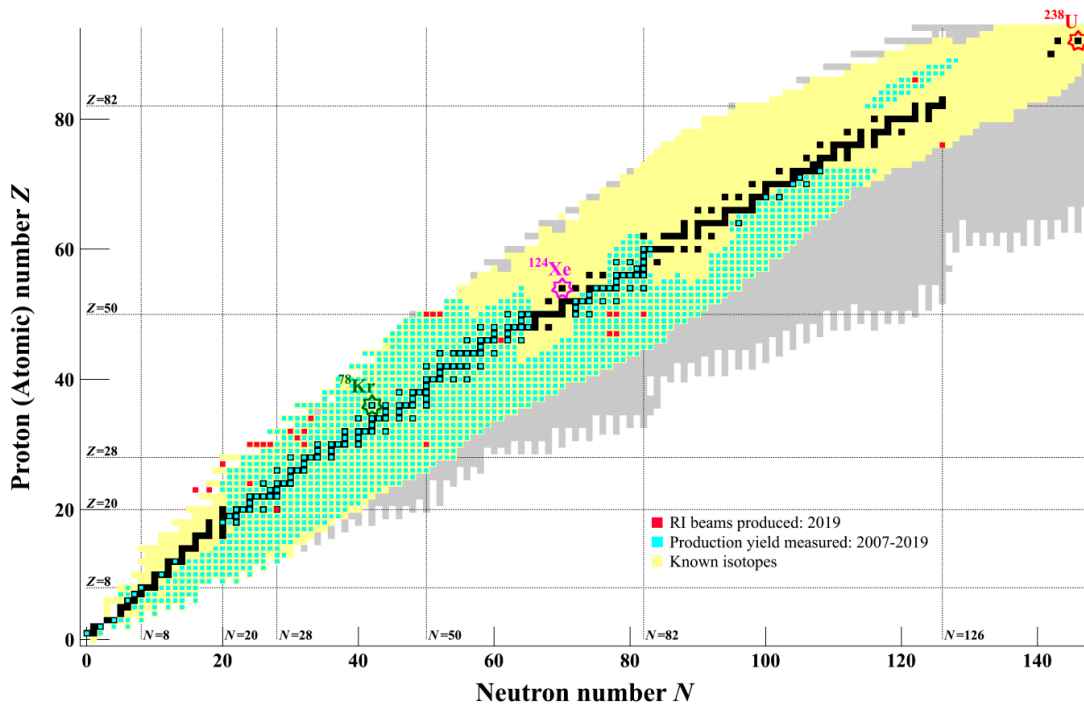


Fig. 1. RI beams produced in 2019 and the production yield measured from March 2007 to December 2019 at the BigRIPS separator.

^{*1} RIKEN Nishina Center

ion optics of the large-acceptance-dispersive mode for the ZeroDegree spectrometer.

The number of experiments using RI beams at the BigRIPS separator is tallied in Table 2 for various primary beams in each year. A total of 191 experiments have been performed so far. Figure 1 shows the RI beams produced in 2019 at the BigRIPS separator on the table of nuclides with red squares. The production yields for 1608 RI beams have been measured from March 2007 to December 2019, and they are indicated with cyan squares.

References

- 1) T. Kubo, Nucl. Instrum. Methods Phys. Res. B **204**, 97 (2003).
- 2) H. Suzuki *et al.*, in this report.
- 3) N. Fukuda *et al.*, in this report.
- 4) T. Sumikama *et al.*, in this report.
- 5) H. Takeda *et al.*, in this report.

Table 1. List of experimental programs and RI beams produced at the BigRIPS separator in 2019.

Primary beam (Period)	Proposal No.	Course	RI beams
^{78}Kr 345 MeV/nucleon (Mar. 19 – Apr. 18)	NP1406-SAMURAI24	SAMURAI	^{67}Se , ^1H
	NP1712-RIBF166-01	PALIS	^{67}Se
	NP1712-RIBF151R1	ZeroDegree	$^{62}\text{Ge}/^{62}\text{Ga}$, ^{62}Zn
	NP1712-RIBF145R1	ZeroDegree	$^{56}\text{Zn}/^{57}\text{Zn}$
	MS-EXP19-01	ZeroDegree	^{54}Zn , $^{41}\text{V}^\#$
	NP1612-SAMURAI11R1-01/02	SAMURAI	^{48}Cr , ^{64}Ge
	NP1512-RIBF104R1 DA19-01-01	ZeroDegree BigRIPS	$^{54,55,56}\text{Zn}$ $^{47}\text{Co}^\#$, $^{39}\text{V}^\#$
^{124}Xe 345 MeV/nucleon (May 29 – Jun. 18)	NP1612-RIBF146	ZeroDegree	^{101}Sn
	NP1612-RIBF153R1	ZeroDegree	^{102}Sn
	NP1612-RIBF147	ZeroDegree	^{100}Sn
	PE19-01	BigRIPS	
^{238}U 345 MeV/nucleon (Nov. 18 – Dec. 6)	NP1512-RIBF79R1	F12	^{132}Sn , ^{48}Ca
	NP1712-RIBF166-02	PALIS	^{208}Rn
	MS-EXP19-06	BigRIPS	^{202}Os
	MS-EXP19-04	ZeroDegree	^{107}Pd
	MS-EXP19-05	ZeroDegree	^{80}Zn
	NP1712-RIBF157	F8	$^{124}\text{Ag}/^{125}\text{Ag}$, $^{127}\text{Sn}/^{128}\text{Sn}$

[#] assumed RI beam for the BigRIPS spectrometer

Table 2. Number of experiments performed using RI beams in each year.

Year	^{238}U	^{124}Xe	^{86}Kr	^{78}Kr	^{70}Zn	^{48}Ca	^{18}O	^{16}O	^{14}N	^4He	^2H	Yearly total
2007	4		1									5
2008	2					4						6
2009	3					3			3	1		10
2010						10	1		2		1	14
2011	4	2					2					8
2012	6	3			1	4	6					20
2013	4	2					3					9
2014	11				1	3		1			1	17
2015	15			6		4					1	26
2016	13	1				6	2					22
2017	13				4	2	3					22
2018	7						7					14
2019	6	4		8								18
Total	88	12	1	14	6	36	24	1	5	1	3	191

First success of RI-beam separation and particle identification for nuclei with atomic number $Z > 82$ at RIKEN RI beam factory[†]

T. Sumikama,^{*1} T. Kubo,^{*1,*2} N. Fukuda,^{*1} D. S. Ahn,^{*1} H. Takeda,^{*1} Y. Shimizu,^{*1} H. Suzuki,^{*1} N. Inabe,^{*1} D. Murai,^{*1,*3} H. Sato,^{*1} K. Kusaka,^{*1} Y. Yanagisawa,^{*1} M. Ohtake,^{*1} and K. Yoshida^{*1}

The separation of heavy RI beams is difficult at RIKEN RIBF, because the charge state Q of ions frequently changes in certain materials including a wedge degrader used for the RI-beam separation. In an earlier study,¹⁾ a large amount of in-flight fission fragments prevented the good separation of heavy RI beams. In the present study, the charge-state change in the wedge degrader was taken into consideration in terms of the RI-beam purification. We found that a ^{208}Rn beam can be well separated from the fission fragments when He-like and fully-stripped ions are selected at the first and second dipole magnets, respectively. Figure 1 shows the selected isotopes when an aluminum degrader with a thickness of 2 mm is used at F1 of the BigRIPS separator.²⁾ This is an extension of a figure for the full-strip ions for both dipole magnets given in Ref. 3). The fission fragments with atomic numbers between 25 and 65 are required to have Li-like or Be-like ions at the first dipole. The probabilities of Li-like and Be-like ions for ^{160}Tb was estimated using the

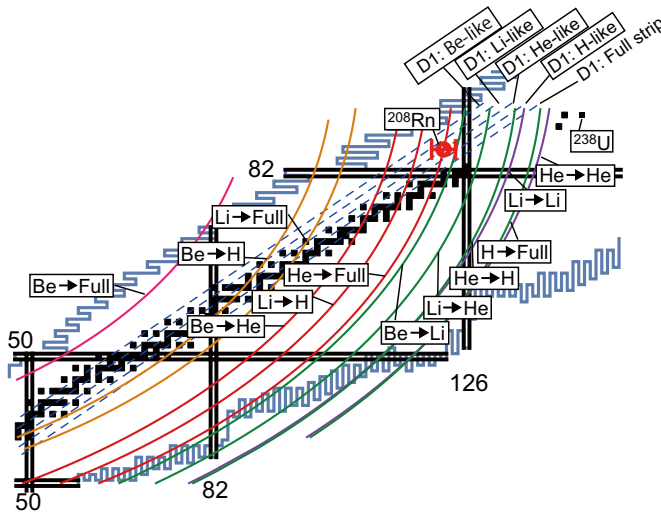


Fig. 1. RI-beam separation scheme at the first stage of the BigRIPS separator in the case of a 2-mm-thick aluminum degrader. The purple, green, red, orange, and pink solid lines show the selected RI beams for the charge-state change $\Delta Q_{F1} = 0, +1, +2, +3,$ and $+4$ at F1, respectively. The blue dashed lines show nuclei having the same A/Q as ^{208}Rn with $Q = 84$.

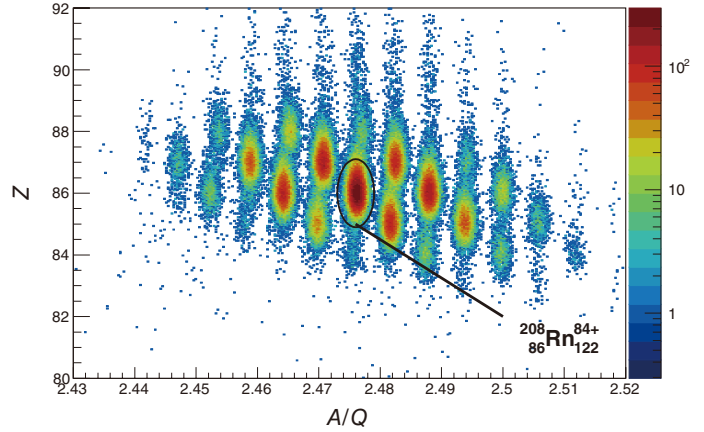


Fig. 2. Particle-identification plot of the RI beams, which was obtained by applying software gates of $-5 < x < 5$ mm on the F3 and F7 positions.

Global code⁴⁾ to be 4.7×10^{-4} and 1.8×10^{-6} , respectively. Because of these low probabilities, the fission fragments are expected to be well eliminated.

An experiment to produce a ^{208}Rn beam was performed at RIKEN RIBF. The 3-mm-thick beryllium was used as the production target. The thickness of the aluminum wedge degraders at F1 and F5 were 2 and 1 mm, respectively. The He-like and fully-stripped ions were chosen at the first and second halves of the first stage of BigRIPS, respectively. The He-like ions were chosen at the second stage of BigRIPS. To compare the separated RI beams with those in Fig. 1, a wide slit setting of ± 20 mm was applied at the achromatic foci F2 and F7. The fission fragments were not transported to the second stage of BigRIPS even for the wide slit. Software gates were applied to the positions measured at F3 and F7 to simulate the RI beams with a narrow slit setting. Figure 2 shows a particle-identification plot with gates of $-5 < x < 5$ mm at F3 and F7. The purity of ^{208}Rn reached 25%. Therefore, RIKEN RIBF is now ready for user experiments in this region of the nuclear chart.

References

- 1) N. Inabe *et al.*, RIKEN Accel. Prog. Rep. **48**, 73 (2015).
- 2) T. Kubo, Nucl. Instrum. Methods Phys. Res. B **204**, 97 (2003).
- 3) J. P. Dufour *et al.*, Nucl. Instrum. Methods Phys. Res. A **248**, 267 (1986).
- 4) C. Scheidenberger *et al.*, Nucl. Instrum. Methods Phys. Res. B **142**, 441 (1998).

[†] Condensed from the article in Nucl. Instrum. Methods Phys. Res. B **463**, 237 (2020)

^{*1} RIKEN Nishina Center

^{*2} FRIB/NSCL, MSU

^{*3} Department of Physics, Rikkyo University

Analysis of fake asymmetry for the MTV experiment

F. Goto,^{*1,*2} H. Baba,^{*2} J. A. Behr,^{*3} T. Kajihara,^{*4} H. Kawamura,^{*5} M. Kitaguchi,^{*1} C. D. P. Levy,^{*3} H. Masuda,^{*4} Y. Nakaya,^{*4} K. Ninomiya,^{*4} J. Onishi,^{*4} R. Openshaw,^{*3} S. Ozaki,^{*4} M. Pearson,^{*3} Y. Sakamoto,^{*4} H. M. Shimizu,^{*1} Y. Shimizu,^{*4} R. Takenaka,^{*4} K. Tamura,^{*4} S. Tanaka,^{*4} R. Tanuma,^{*4} Y. Totsuka,^{*4} E. Watanabe,^{*4} Y. Yamamoto,^{*4} Y. Yamawaki,^{*4} M. Yokohashi,^{*1} and J. Murata⁴

The Mott polarimetry for T-Violation (MTV) experiment aims to search for a large time-reversal symmetry violation (T-violation) in polarized ^8Li β decay. This experiment was conducted at the TRIUMF Isotope Separator and Accelerator (TRIUMF-ISAC). T-Violation may arise in triple-vector correlation (R-correlation) in beta decay. R-correlation causes electron transverse polarization and it can be measured by detecting the angle symmetry of electron Mott scattering using a cylindrical drift chamber (CDC). Figure 1 shows a schematic of how β rays are detected. A ^8Li beam is stopped at the beam stopper placed at the center of CDC, and an electron is emitted. CDC can detect the track of the electron scattered on an analyzer foil.

The electron emission distribution of β^- decay, ω , is expressed as¹⁾

$$\omega dE_e d\Omega_e \propto 1 + R\vec{\sigma} \cdot \left[\frac{\langle \vec{J} \rangle}{J} \times \frac{\vec{p}_e}{E_e} \right] + A \frac{\langle \vec{J} \rangle}{J} \cdot \frac{\vec{p}_e}{E_e} + \dots \quad (1)$$

The definition of R -correlation can be found in this function, where \vec{J} is the spin polarization of the parent nuclei and $\vec{\sigma}$, \vec{p}_e , and E_e are the spin polarization, momentum, and electron energy, respectively. A -correlation is the anisotropy of β -ray emission. In the case of ^8Li , $A = -\frac{1}{3}$. Both A - and R -correlation terms are proportional to the parent nuclei's polarization. Therefore, we adopt R -asymmetry (Mott Scattering angle asymmetry) divided by A -asymmetry (β ray emission rate asymmetry) as a scale of coefficient R .

In our previous studies, we recognized a systematic effect that causes a large fake R -asymmetry. It is estimated that the source of this systematic effect is accidental coincidence, and it shows an obvious dependence on the width of the coincidence window and beam intensity.²⁾ We assume an evaluation model function of

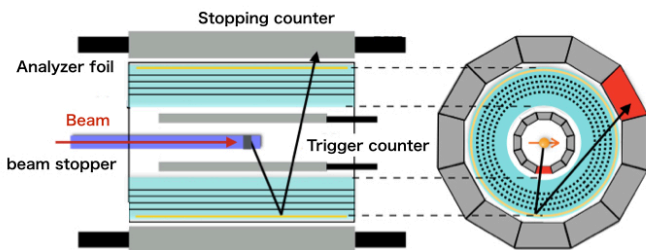


Fig. 1. Schematic of CDC.

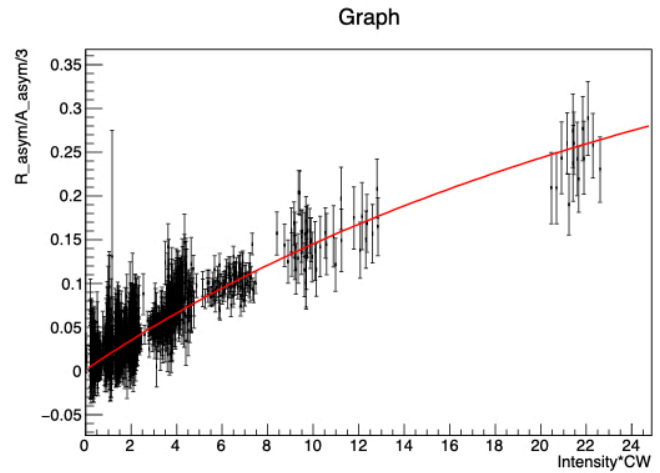


Fig. 2. Beam-intensity and coincidence-window dependence of Mott scattering asymmetry. The red line indicates fitting with Eq. (2).

fake asymmetry $Asym(x)$. The variable x is presented as a product of the beam intensity and the width of the coincidence window in arbitrary units.

$$Asym(x) = \frac{a}{1 + \frac{b}{x}} + \frac{c}{1 + \frac{x}{b}}. \quad (2)$$

The parameter a represents fake asymmetry caused by accidental coincidence, b/x represents the ratio of the number of real Mott scattering events to accidental coincidence events, and c is the asymmetry of real Mott scattering events. The limit of $Asym(x)$ as x approaches 0 is c . This means that the y-intercept of this function is the coefficient R , which we want to know. Figure 2 shows 1183 measured asymmetry data points acquired in 2017. The measurement time was 400 s per plotted data point. The beam intensity was about 10^{5-7} pps, and the coincidence window varies from 100 ns to 3000 ns. This shows that our model is suitable for evaluating the scale of fake asymmetry as a function of the product of beam intensity and the width of the coincidence window.

The accidental coincidence model we use is assumed with consideration of the double coincidence of β rays, but there can be triple or more coincidence events. Multiple coincidence could cause other effects of fake asymmetry. We need to evaluate this factor to draw a conclusion from our data.

References

- 1) J. D. Jackson, S. B. Treiman, H. W. Wyld Jr., Phys. Rev. **106**, 517 (1957).
- 2) J. Murata *et al.*, Hyperfine Interact. **237**, 125 (2016).

*1 Department of Physics, Nagoya University

*2 RIKEN Nishina Center

*3 TRIUMF

*4 Department of Physics, Rikkyo University

*5 Cyclotron and Radioisotope Center, Tohoku University

2. Nuclear Physics (Theory)

Non-relativistic expansion of Dirac equation with spherical vector and scalar potentials[†]

Y. X. Guo^{*1,*2,*3} and H. Z. Liang^{*2,*1}

Since the 1970s, the density function theory (DFT) in both the non-relativistic and relativistic frameworks has succeeded in microscopically describing the ground-state and excited-state properties of thousands of nuclei in a self-consistent manner. However, the connection between these two frameworks remains unclear. The non-relativistic expansion of the Dirac equation is considered to be a potential bridge connecting these two frameworks.^{1,2)}

In 2012, Guo³⁾ first applied the similarity renormalization method (SRG)^{4,5)} to perform the non-relativistic expansion of the Dirac equation. By using SRG, the Dirac Hamiltonian can be transformed into a diagonal form after infinite steps of unitary transformations, *i.e.*, the eigenequations for the upper and lower components of the Dirac spinors can be decoupled. Furthermore, the Hamiltonian \mathcal{H} thus obtained was expanded in powers of $1/M$ (with M being the bare mass of the nucleon).

The results up to the $1/M^3$ order were calculated.³⁾ However, the differences between the corresponding results and the exact ones were still approximately 1 MeV. Therefore, it is necessary to include higher-order corrections. In this work, the results up to the $1/M^4$ order are calculated, and the differences between the calculated and exact values are less than 0.2 MeV for all states.

From a simple observation, some geometric progressions are determined in the results of the conventional SRG method. This observation is reminiscent of the idea of resummation. In the reconstituted SRG method, replacing M with the Dirac mass $M^* = M + S$ (with S being the scalar potential) not only yields the non-relativistic expansion up to a certain order, but also sums up the terms that belong to their families up to infinite order. Consequently, the convergence of the reconstituted SRG is much faster than that of the conventional SRG. The spectrum of the Hamiltonian $\tilde{\mathcal{H}}$ thus obtained is shown in Fig. 1.

The Foldy-Wouthuysen (FW) transformation⁶⁻⁹⁾ is another non-relativistic expansion method that has been widely used. Both the FW transformation and SRG method provide a systematic way to perform the non-relativistic expansion of the Dirac equation up to an arbitrary order. Thus, we also apply the FW transformation to a general case of the covariant DFT. In

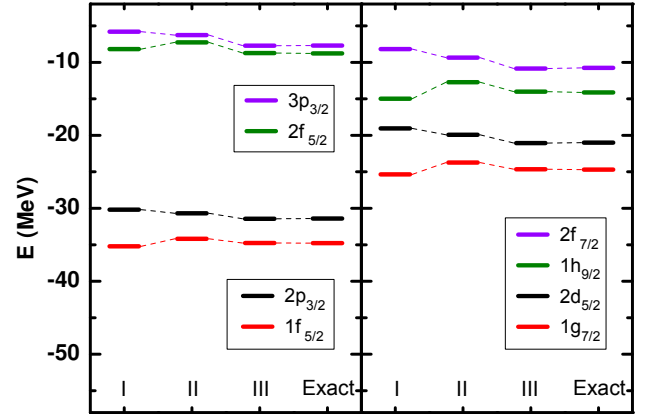


Fig. 1. Energy spectrum of $\tilde{\mathcal{H}}$ for the four pseudospin partners calculated using the reconstituted SRG method. The first, second, and third columns show the single-particle energies up to the first, second, and third orders, respectively. The last column, labeled “Exact,” shows the eigenenergies of the Dirac equation.

this work, the results with the FW transformation have also been obtained up to the $1/M^4$ order and compared with the corresponding results obtained using conventional SRG method. It seems that the FW transformation and the conventional SRG method produce the same results up to the second order, but they show differences from the third order. By introducing a block-diagonal transformation Ξ , we determined that the results obtained using the conventional SRG method are equal to those obtained using the FW transformation with an additional unitary transformation Ξ . Consequently, the spectrum of the single-particle energy obtained using the FW transformation is identical to that obtained using the SRG method.

With the applications of the SRG method and FW transformation, the bridge connecting the DFT in the relativistic and non-relativistic frameworks is now conceivable.

References

- 1) P. G. Reinhard, Rep. Prog. Phys. **52**, 439–514 (1989).
- 2) M. Bender, P. H. Heenen, P. G. Reinhard, Rev. Mod. Phys. **75**, 121–180 (2003).
- 3) J. Y. Guo, Phys. Rev. C **85**, 021302 (2012).
- 4) F. Wegner, Ann. Phys. Berlin **506**, 77–91 (1994).
- 5) A. B. Bylev, H. J. Pirner, Phys. Lett. B **428**, 329–333 (1998).
- 6) M. H. L. Pryce, Proc. Royal Soc. A **195**, 62–81 (1948).
- 7) L. L. Foldy, S. A. Wouthuysen, Phys. Rev. **78**, 29–33 (1950).
- 8) S. Tani, Prog. Theor. Phys. **16**, 267–285 (1951).
- 9) L. L. Foldy, Phys. Rev. **87**, 688–693 (1952).

[†] Condensed from the articles in Phys. Rev. C **99**, 054324 (2019) and Chin. Phys. C **43**, 114105 (2019)

^{*1} Department of Physics, The University of Tokyo

^{*2} RIKEN Nishina Center

^{*3} Department of Modern Physics, University of Science and Technology of China

Renormalizing random-phase approximation by using exact pairing[†]

L. Tan Phuc,^{*1} N. Quang Hung,^{*1} and N. Dinh Dang^{*2}

The random-phase approximation (RPA) is a popular theoretical method to study the low-lying excitations and high-lying giant resonances in nuclei. The excited states of RPA are built on the particle-hole (ph) components, which are represented by the ph pairs operators: B_{ph} and B_{ph}^\dagger . Because of the unknown of the RPA ground state $|RPA\rangle$, the quasi-boson approximation (QBA), which assumes a ph pair as a boson and $|RPA\rangle \sim |HF\rangle$, is used to derive the RPA expectation value, namely $\langle RPA|[B_{ph}, B_{p'h'}^\dagger]|RPA\rangle \sim \langle HF|[B_{ph}, B_{p'h'}^\dagger]|HF\rangle = \delta_{pp'}\delta_{hh'}$.¹⁾ Using QBA within RPA leads to a basic drawback that is the violation of Pauli principle because the nucleons are fermions instead of boson as the assumption of QBA.

To overcome this problem, the ground-state correlations (GSC) factor D_{ph} are taken into account to renormalize the residual interaction of RPA (RRPA). The RPA expectation value becomes $\langle RPA|[B_{ph}, B_{p'h'}^\dagger]|RPA\rangle \simeq D_{ph} \equiv f_p - f_p$, where f_p and f_h are p and h occupation numbers.²⁾ Although the RRPA restored the Pauli principle, the energy-weighted sum rule (EWSR) was violated.³⁾ Therefore, another technique was developed to fix this drawback, namely the pp and hh correlations were added in the ph RRPA matrix to fulfill the EWSR.³⁾ However, this way doubled the matrix size of RPA equations and lead to time-consuming. On the other hand, the RRPA does not include superfluid pairing. Therefore, we propose a method to overcome all these shortcomings. In particular, by using the Hartree-Fock mean field plus exact pairing solution (HFEP),⁴⁾ we can supply a good set of initial inputs for RPA. The GSC factor D_{ph} , which is used to renormalize the residual interactions, is calculated directly from exact pairing (EP). These are expected to preserve both Pauli principle and EWSR without adding any pp and hh correlations that make time-consuming.

The proposed approach is applied for the dipole case in several light-, medium-, and heavy-mass nuclei, namely $^{22,24,28}\text{O}$, ^{60}Ni , and ^{90}Zr . The calculations are performed within the conventional RPA, HFEP+RPA (HFEP+RPA) and self-consistent HFEP+RPA (SC-HFEP+RPA). The E1 EWSR will be compared with the model independent sum rule such as the Thomas-Reich-Kuhn (TRK) sum rule. Our approach shows that the drawback of the ph RRPA is removed, namely the EWSR are fulfilled without adding any pp and hh configurations, hence the extension of RPA matrices and time-consuming calculations are avoided. As compared to the RPA results, the effects

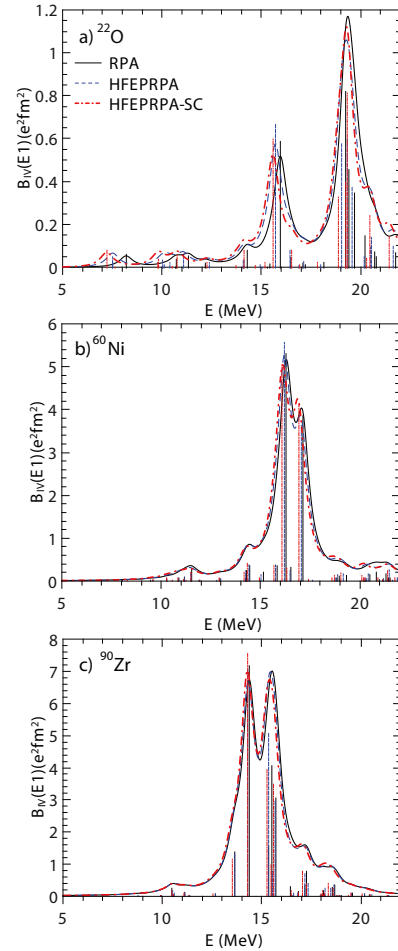


Fig. 1. The Isovector dipole transition probabilities of ^{22}O (a), ^{60}Ni (b) and ^{90}Zr (c) obtained within different approaches. The sticks and lines represent to the probabilities $B(E1, 0 \rightarrow 1^-)$ and strength functions $S(E)$.

of GSC and EP in the renormalization are significant in light nuclei and small in medium and heavy nuclei (see the shift of $S(E)$ in Fig. 1(a)–(c)). The antipairing effect is observed for the first time within the SC-HFEP+RPA, which reduces the pairing energy from more than 10% up to around 30% in the neutron-rich ^{22}O nucleus. This shows the contribution from the mutual effect of the short-range pairing and long-range ph residual interaction to the mean field. The PDR is also found to be enhanced in neutron-rich nuclei because of the pairing effect.

References

- 1) P. Ring, P. Schuck, *The Nuclear Many-Problem* (Springer, 2004).
- 2) F. Catara, N. D. Dang, M. Sambataro, Nucl. Phys. A **579**, 1 (1994).
- 3) N. Q. Hung, N. D. Dang, T. V. N. Hao, L. T. Phuc, Phys. Rev. C **94**, 064312 (2016).
- 4) L. T. Phuc, N. Q. Hung, N. D. Dang, Phys. Rev. C **97**, 024331 (2018).

[†] Condensed from the article in Phys. Rev. C **99**, 064322 (2019)

^{*1} Duy Tan University

^{*2} RIKEN Nishina Center

Quenching factor of Gamow-Teller and spin dipole resonances[†]

L. -G. Cao,^{*1} S. -S. Zhang,^{*2} and H. Sagawa^{*3,*4}

Spin-isospin excitations provide a unique opportunity to study the spin correlations in nuclei. The Gamow-Teller (GT) transition is the simplest with both spin and isospin transfers by one unit. The next simplest is spin-dipole (SD) excitations, which involve the orbital angular momentum transfer by one unit together with spin and isospin transfer. The quenching of the total GT strength from the model-independent sum rule has prompted theoretical studies of possible mechanisms, ranging from conventional configuration mixing to an admixture of Δ -hole states. Experimental investigations of the (p, n) and (n, p) reactions using the multipole decomposition (MD) technique have identified not only the GT strength but also a considerable amount of broadly distributed $L = 1$ SD strength at excitation energies beyond the GT peak.

We study GT and SD states in four doubly magic nuclei ^{48}Ca , ^{90}Zr , ^{132}Sn , and ^{208}Pb by using the self-consistent Hartree-Fock+random-phase approximation (RPA) model with/without tensor interactions. We adopt the modern energy density functions (EDFs) SAMi and SAMi-T for the theoretical study. The latter has tensor terms determined from Bruckner HF calculations with the AV18 interaction.

The GT strength is shown in Fig. 1 for the t_- channel of ^{48}Ca . The main experimental GT resonance was found experimentally at $E_x \sim 10$ MeV, in addition to a small peak at $E_x = 3$ MeV in ^{48}Ca . The results calculated with SAMi reproduce well the main peak, but the low-energy strength is predicted 1 MeV lower than the experimental one. SAMi-T gives essentially the same results for the main peak, but reproduces better the excitation energy for the small lower energy peak. The integrated GT strength from $E_x = 0 \rightarrow 25$ MeV is 15.3, which is 64% of the GT sum rule. The calculated results exhaust almost 100% of the sum rule up to $E_x = 20$ MeV. The quenching factor for the transition strength is defined as

$$qf = \frac{\sum_{E_x=0}^{E_x(max)} B(GT : E_x)_{exp}}{\sum_{E_x=0}^{E_x(max)} B(GT)_{cal}},$$

where $E_x(max)$ is taken to be 30 MeV in the GT case. The quenching factor $qf = 0.64$ corresponds to a renormalization factor of $q_{RF} = 0.80$ for the GT transition operator to retain the empirical sum rule value.

The calculated SD strength for ^{48}Ca is shown in Fig. 1.

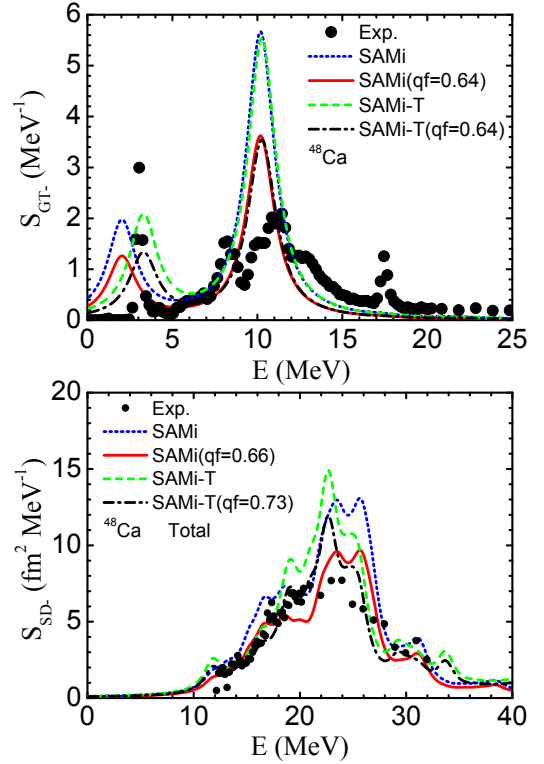


Fig. 1. RPA strength functions of ^{48}Ca for the t_- channel of GT and SD resonances. The solid circles are the experimental data taken from Ref. 1). The short-dotted (short-dashed) and solid (dashed-dotted) lines are the theoretical results without and with a quenching factor given by the SAMi (SAMi-T) EDF, respectively.

The tensor interactions have substantial effects on the SD response, and the effect is different for each multipole. As a net effect, the main peak at $E_x \sim 23$ MeV is shifted to a lower energy by 1 MeV by the tensor effect, which provides a better description of the experimental strength distributions of SD for ^{48}Ca .

The quenching effect is modest for the SD strength. In ^{48}Ca , the qf value is 0.66 (0.73) for the SD with the SAMi (SAMi-T) EDF. In ^{90}Zr , the GT needs $qf = 0.7$, while the SD shows $qf = 0.8$. The feature of quenching is the same for ^{208}Pb ; $qf = 0.65$ for the GT and $qf = 0.78(0.80)$ for the SD with the SAMi (SAMi-T) EDF.

In conclusion, the quenching effect is modest for the SD strength with the quenching factor $qf \sim 0.8$ compared with that for GT, for which $qf \sim (0.55 - 0.69)$, which is consistent with the quenching value obtained from the GT beta decay processes in nuclei with $A < 50$. This difference in the effective quenching factors between GT and SD should be implemented in future theoretical studies of double beta decay probabilities.

Reference

- 1) K. Yako *et al.*, Phys. Rev. Lett. **103**, 012503 (2009) and private communications.

[†] Condensed from the article in Phys. Rev. C **100**, 054324 (2019)

^{*1} School of Mathematics and Physics, North China Electric Power University

^{*2} School of Physics and Nuclear Energy Engineering, Beihang University

^{*3} RIKEN Nishina Center

^{*4} Center for Mathematics and Physics, University of Aizu

Pairing in excited nuclei: a review[†]

N. Quang Hung,^{*1} N. Dinh Dang,^{*2} and L. G. Moretto^{*3}

The present review summarizes the recent progress in the study of pairing properties in excited nuclei and their analogy to those appeared in other finite systems including superconductors, metallic nano sized clusters/grains, and solid-state materials such as ferromagnets. The review consists of four parts.

The first part discusses the treatment of pairing within a uniform model based on the BCS Hamiltonian within the grand canonical ensemble.

The second part focuses on the grandcanonical treatment of pairing within the Hartree-Fock-Bogoliubov theory and finite-temperature pairing reentrance phenomenon in superconducting ultrasmall metallic grains as well as in even-even and odd nuclei.

The third part presents the results obtained from the treatment of nuclear pairing within the canonical and microcanonical ensembles, from which the effect caused by the finite size of the systems is highlighted. Different approaches to canonical and microcanonical ensembles including particle-number projection, particle-number projection plus static path approximation, solutions of BCS with Lipkin-Nogami particle-number projection incorporating the self-consistent quasiparticle random-phase approximation embedded into the canonical and microcanonical ensembles, shell model Monte Carlo method at finite temperature, and exact solutions of the pairing problems, which are embedded into the canonical and microcanonical ensembles, are introduced.

In the fourth part, the first experimental evidence of the pairing reentrance phenomenon in a warm rotating ^{104}Pd nucleus, which was observed via the local enhancement of nuclear level density at low temperature and high angular momentum extracted from the reaction $^{12}\text{C} + ^{93}\text{Nb}$ at the incident energy of 40–50 MeV, is analyzed and discussed within the framework of the finite-temperature BCS (FTBCS), which includes the quasiparticle-number fluctuations (FTBCS1) at angular momentum J (Fig. 1). The similar behavior of pairing reentrance observed in the condensed-matter counterpart such as metallic compound of $\text{Eu}_{0.75}\text{Sn}_{0.25}\text{Mo}_6\text{S}_{7.2}\text{Se}_{0.8}$ and heavy-fermion cubic system of CePb_3 , quasi-2D organic conductor $\kappa\text{-(BETS)}_2\text{FeCl}_4$, and ferromagnetic superconductor of URhGe under the strong magnetic field is also summarized.

It has been found that, by applying the BCS theory

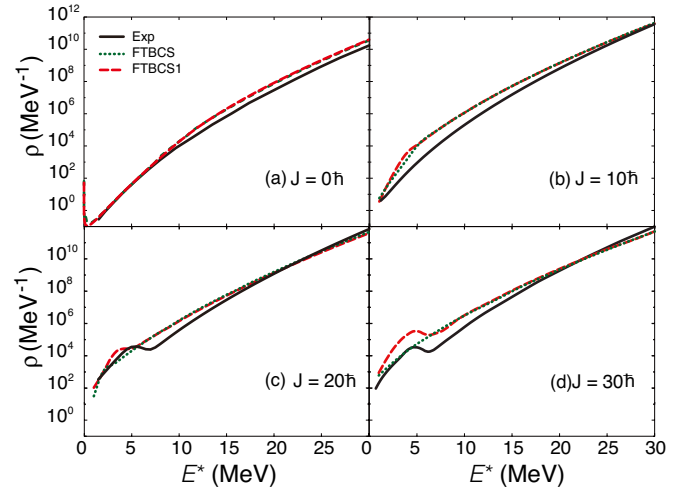


Fig. 1. Level densities for ^{104}Pd as function of excitation energy E^* at the quadrupole deformation parameter $\beta_2 = 0.276$ and different values of total angular momentum J . The dotted and dashed lines stand for the FTBCS and FTBCS1 results, respectively. The solid lines are the experimentally extracted level densities.

at finite temperature and angular momentum to the uniform nuclear model, for which the analytic solutions of the BCS equation can be obtained, one is able to study the appearance of the first-order and second-order phase transitions in finite nuclear systems when either the total angular momentum or the number of quasiparticles or the total energy of the system is fixed. However, it has also been pointed out that these shape phase transitions are simply an artifact caused by the application of the BCS theory to finite nuclei, neglecting all the thermal fluctuations. In fact, strong thermal fluctuations in finite systems smooth out all the phase transitions, leading to different behaviors of nuclear thermodynamic quantities. For example, the fluctuations of the quasiparticle number are one of the microscopic origins caused the nonvanishing nuclear pairing gaps at finite temperature, resulting in the smoothing of the superfluid-normal (second-order) phase transition. This finding is important in the sense that thermal fluctuations should always be considered whenever the statistical methods are applied to finite systems.

[†] Condensed from the article in Rep. Prog. Phys. **82**, 056301 (2019)

^{*1} Duy Tan University

^{*2} RIKEN Nishina Center

^{*3} University of California at Berkeley and Lawrence Berkeley National Laboratory

Canonical base in self-consistent constrained HFB in odd-A nuclei[†]

K. Sugawara-Tanabe^{*1,*2} and K. Tanabe^{*3}

We developed a program for solving the self-consistent Hartree-Fock-Bogoliubov (CHFHB) equation under four constraints, one each on the total angular-momentum I , proton number Z_+ in the + parity proton shell (p^+), proton number Z_- in the - parity proton shell (p^-), and neutron number N , so that it reproduces the $11/2^-$ band in ^{135}Pr . We choose the signature-invariant base C_k and $C_{\hat{k}}$, where \hat{k} is the time-reversed level of k , and adopt a Hamiltonian with spherical single-particle energies plus the residual quadrupole-quadrupole, monopole-pairing, and quadrupole-pairing interactions. In this signature-invariant base, the generalized density matrix $K (= K^2)$ is expressed in terms of $\rho_{kl}^{1c} = \langle C_l^\dagger C_k \rangle$, $\rho_{\hat{k}l}^{2c} = \langle C_l^\dagger C_{\hat{k}} \rangle$ and $\kappa_{\hat{k}l} = \langle C_l C_{\hat{k}} \rangle$, where the state $| \rangle$ is the quasiparticle vacuum. The CHFHB equation is given as Eq. (1) in Ref. 1). After rendering the dangerous term zero through the iteration procedure, we can transform the elements in K to the canonical forms, *i.e.*, $(F^1)_{km}^{-1} \rho_{mn}^1 F_{nk}^1 \equiv \rho_{kk}^{1c}$ and $(F^2)_{\hat{k}m}^{-1} \rho_{\hat{m}n}^2 F_{\hat{n}\hat{k}}^2 \equiv \rho_{\hat{k}\hat{k}}^{2c}$; thus $(F^2)_{\hat{k}m}^{-1} \kappa_{\hat{m}n} F_{nk}^1 \equiv \kappa_{\hat{k}k}^c$. In other words, K is transformed to K_c , and the relation $K_c^2 = K_c$ follows. Subsequently, we obtain $\rho^{1c} = \rho^{2c}$. If we apply the same transformation to the CHFHB matrix (see Eq. (1) in Ref. 1)), we obtain

$$\rho_{ii}^{1c} = \rho_{ii}^{2c} = \frac{1}{2} \left(1 - \frac{(\xi_{ii}^1 + \xi_{ii}^2)/2}{\sqrt{(\Delta_{ii}^c)^2 + ((\xi_{ii}^1 + \xi_{ii}^2)/2)^2}} \right), \quad (1)$$

where $\xi^1 = (F^1)^{-1}(h^1 - \omega j_x)F^1$, $\xi^2 = (F^2)^{-1}(h^2 + \omega j_x)F^2$, and $\Delta^c = (F^2)^{-1}\Delta F^1$. Here h^1 , h^2 , and Δ are defined in Eq. (1) in Ref. 1). In Fig. 1, we compare the CHFHB solution under three constraints for $I = 31/2$, $Z = Z_+ + Z_-$, and N (open squares and open circles) with the CHFHB solution under four constraints (filled squares and filled circles). Here, the circles correspond to the p^+ shell, and squares correspond to the p^- shells. The quantities represented by the red filled square under the constraint $Z_- = 17$ and the red open square under $Z = 31$ are composed of the contribution mainly from the $h_{11/2}$ level with $j_z = 5/2$. The number $Z = 31$ corresponds to the proton number outside core 28 for ^{135}Pr . As shown in (A) of Fig. 1, $\rho^{1c} = \rho^{2c} \sim 1/2$, *i.e.*, $1/2 \times 2 = 1$ in the p^- shell, we confirm that the solution certainly describes the negative parity band in the odd- Z nucleus ($11/2^-$ band in

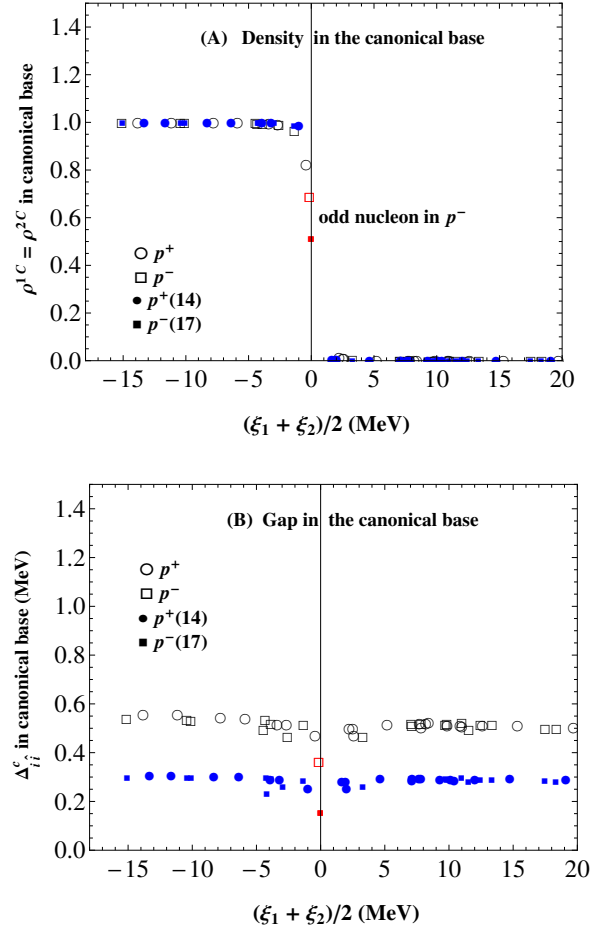


Fig. 1. (A) $\rho^{1c} = \rho^{2c}$ in the canonical base as a function of $(\xi^1 + \xi^2)/2$ at the $I = 31/2^-$ state. (B) Δ^c in the canonical base as a function of $(\xi^1 + \xi^2)/2$ at the $I = 31/2^-$ state. In both figures, filled circles represent the proton levels in the p^+ shell with $Z_+ = 14$, and filled squares represent the proton levels in the p^- shell with $Z_- = 17$. Open circles and open squares indicate the CHFHB solution under $Z = 14+17 = 31$. The red filled-square level with $Z_- = 17$ and the red open-square level with $Z = 31$ are mainly from $h_{11/2}$. See the text for further details.

^{135}Pr). In (B) of Fig. 1, we compare Δ_{ii}^c between the CHFHB solution under three constraints and the CHFHB solution under four constraints. The blocking effect is clearly indicated by the red filled or open squares because these gap values are much smaller than those for the other levels.

Reference

- 1) K. Sugawara-Tanabe, K. Tanabe, RIKEN Accel. Prog. Rep. **52**, 1148 (2019).

[†] Condensed from the talk at the autumn meeting of Japan Physical Society, Yamagata University, Sept. 18th (2019)

*1 RIKEN Nishina Center

*2 Department of Information Design, Otsuma Women's University

*3 Department of Physics, Saitama University

S-shaped heat capacity in an odd-odd deformed nucleus[†]

B. Dey,^{*1} N. Quang Hung,^{*2} D. Pandit,^{*3} S. Bhattacharya,^{*4} N. Dinh Dang,^{*5} L. T. Quynh Huong,^{*6}
D. Mondal,^{*3} S. Mukhopadhyay,^{*3} S. Pal,^{*3} A. De,^{*7} and S. R. Banerjee^{*7}

A long-standing problem in nuclear physics is the experimental observation of the pairing phase transition in atomic nuclei. Thermodynamic properties such as superfluidity and pairing phase transition are well-established facts in infinite nuclear matter.¹⁾ However, these properties digress from infinite nuclear matter to finite nuclei owing to statistical fluctuations in the order parameter. Therefore, the gradual transition from strongly correlated paired states to unpaired ones in atomic nuclei may not be as evident as in infinite matter.¹⁾ This induces a high degree of interest in the study of nuclear thermodynamics, especially in the energy domain of neutron binding.

The study of thermodynamics of finite nuclei involves the reliable extraction of experimental nuclear level density (NLD). The experimental determination of NLDs has been difficult in the past owing to the absence of suitable experimental techniques. Recently, the thermal properties of different nuclei were measured by the Oslo group using a new technique, called the Oslo method, and the S -shaped canonical heat capacity was extracted, signaling the pairing phase transition around the critical temperature $T_c = 0.5\text{--}1.0$ MeV.^{2,3)} However, this method is limited to a low excitation energy E^* (below the particle threshold) and angular momentum J (only a few multiples of \hbar). This limitation in E^* and J has recently been overcome by measuring the NLD from the evaporated particle spectra in compound nuclear reactions.³⁾ In addition, thus far, most of the thermal properties have been studied in nuclei where the shell effect (δS) is very small (less than ~ 1 MeV). The mass region exhibiting a large shell effect ($\delta S \sim 10$ MeV) has rarely been studied; and thus, it is very important to investigate how the thermodynamic properties behave because of the large effect of nuclear shells. In this work, the NLDs and, consequently, the nuclear thermodynamic quantities (TQs) for four different nuclei, ^{184}Re , ^{200}Tl , ^{211}Po , and ^{212}At , are estimated to understand the shell and deformation effects on the TQs.

Figure 1 shows the free energy F , average energy \bar{E} , entropy S , and heat capacity C as functions of T . F and \bar{E} behave smoothly with varying T for all the nuclei. However, S and C show different variations with T . The difference in entropy appears primarily because of

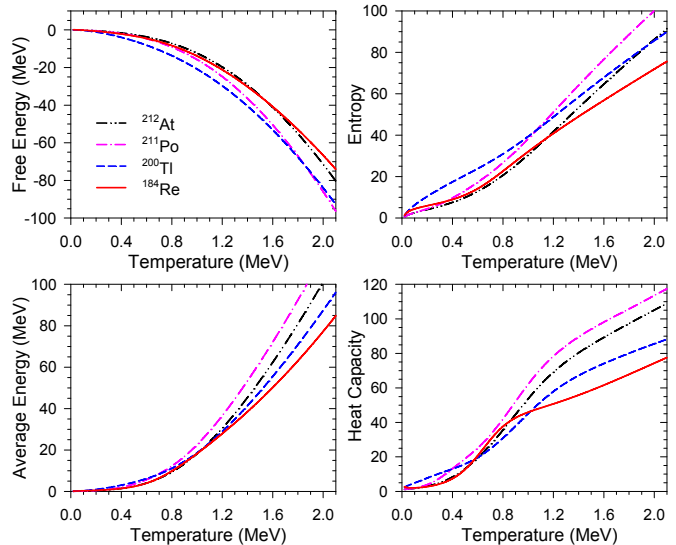


Fig. 1. TQs as functions of temperature obtained using the EP+IPM level densities for $J = 12 \hbar$.

the different shell structures of the nuclei at low T since they show a smooth variation at higher T (above $T = 1.6$ MeV), where the shell structures are predicted to be melted. Most noteworthy is the nature of the heat capacity of ^{184}Re , which is completely different from those of the other three nuclei. There is a pronounced bump (S -shape) in the heat capacity of ^{184}Re at $T \sim 0.8$ MeV, which is close to the critical temperature T_c , where the pairing gap collapses, as predicted by the conventional BCS theory. This S -shape in the heat capacity is interpreted as a fingerprint for a pairing transition in nuclei. The heat capacities of ^{211}Po , ^{212}At , and ^{200}Tl do not show the pronounced S -shape structure, as expected for odd-odd and odd-even nuclei. In order to understand the S -shaped heat capacity in such odd-odd deformed nuclei, the exact neutron and proton pairing gaps have been calculated as functions of T , as discussed in detail in Ref. 4). It has been shown that S -shape of the heat capacity observed in the odd-odd deformed ^{184}Re nucleus at $J = 12 \hbar$ is only due to the change in pairing gaps caused by the change in deformation.

The authors are very grateful to Dr. Pratap Roy, VECC, Kolkata for providing experimental neutron energy spectra.

References

- 1) A. Belic *et al.*, Nucl. Phys. A **731**, 381 (2004).
- 2) E. Melby *et al.*, Phys. Rev. Lett. **83**, 3150 (1999).
- 3) B. Dey *et al.*, Phys. Rev. C **96**, 054326 (2017) and references therein.
- 4) B. Dey *et al.*, Phys. Lett. B **789**, 634 (2019).

[†] Condensed from the article in Phys. Lett. B **789**, 634 (2019)

^{*1} Bankura University

^{*2} Institute of Fundamental and Applied Sciences, Duy Tan University

^{*3} Variable Energy Cyclotron Centre

^{*4} Dept. of Phys., Barasat Govt. College

^{*5} RIKEN Nishina Center

^{*6} Department of Natural Science and Technology, University of Khanh Hoa

^{*7} Dept. of Phys., Raniganj Girls' College

Evidence for three-particle correlations in nuclear matter[†]

W. Bentz^{*1} and I. C. Cloët^{*2}

The properties of infinite nuclear matter have been the subject of intensive investigations for many decades, mainly because of the wide range of applications, including the properties of heavy nuclei, supernova explosions, and neutron stars. In particular, studies on three-particle correlations have a long history, beginning with the pioneering work of Bethe in 1965.¹⁾ In this paper we focus our attention on the skewness of nuclear matter and its implications for three-particle correlations. Skewness is defined as $J = 27\rho^3 (d^3E_A/d\rho^3)$ at $\rho = \rho_0$, where E_A is the energy per nucleon in isospin symmetric nuclear matter, and ρ_0 is the saturation density. Recently, empirical values of J have been extracted in Ref. 2) from heavy ion collisions and neutron star observations, and the following range was deduced:

$$-0.50 \text{ GeV} < J < -0.01 \text{ GeV}. \quad (1)$$

By using the theoretical framework of the Landau-Migdal theory, we will show that those empirical values provide us with information on three-particle correlations in nuclear matter.

Extending Landau's basic formula³⁾ for the variation of the energy density of nuclear matter to include the third order term, which involves the totally symmetric spin-isospin averaged three-particle forward scattering amplitude $h(\mathbf{k}_1, \mathbf{k}_2, \mathbf{k}_3)$, we are able to derive the following exact expression for J :

$$J = -9K + \frac{9p_F^2}{M^{*2}} \times \left(-\frac{1}{3} + 3\frac{M - M^*}{M} - \frac{4}{3}\frac{p_F}{M^*} \frac{dM^*}{dp_F} + (H_0 - H_1) \right), \quad (2)$$

where K is the incompressibility, p_F the Fermi momentum, $M^* \equiv M^*(k = p_F)$ the Landau effective mass at the Fermi surface, $\frac{dM^*}{dp_F} = \frac{dM^*(k)}{dk}|_{k=p_F}$ the slope of $M^*(k)$ at the Fermi surface, and the dimensionless three-particle interaction parameters H_ℓ ($\ell = 0, 1$) are defined by

$$H_\ell = \left(\frac{2p_F M^*}{\pi^2} \rho_0 \right) h_\ell, \quad (3)$$

where $h_\ell = h_\ell(k_1 = k_2 = k_3 = p_F)$ is given by the angular average

$$\frac{1}{2\ell + 1} h_\ell(k_1, k_2, k_3)$$

$$= \int \frac{d\Omega_2}{4\pi} \int \frac{d\Omega_3}{4\pi} (\hat{\mathbf{k}}_1 \cdot \hat{\mathbf{k}}_2)^\ell h(\mathbf{k}_1, \mathbf{k}_2, \mathbf{k}_3). \quad (4)$$

By using empirically and theoretically obtained ranges for the incompressibility,²⁾ the effective mass M^* ,⁴⁾ and its slope at the Fermi surface,^{5,6)} we can deduce the following inequality from (1) and (2):

$$\frac{M}{M^*} (H_0 - H_1) > 1.24 \quad (5)$$

The three-particle amplitudes H_ℓ satisfy a Faddeev equation in the medium, with a 1-particle reducible driving term (first diagram in Fig. 1), and genuine three-particle correlations, which start with the second diagram in Fig. 1. The driving term can be easily estimated by using effective contact interactions of the Landau-Migdal type, and give a contribution between 0.75 and 1.23 to Eq. (5). (Here we used the Landau-Migdal parameters obtained from Skyrme interactions⁷⁾ and chiral effective field theory.⁸⁾ This gives us an important hint that two-particle correlations alone cannot satisfy the inequality Eq. (5), and three-particle correlations processes are needed to explain the skewness of nuclear matter.

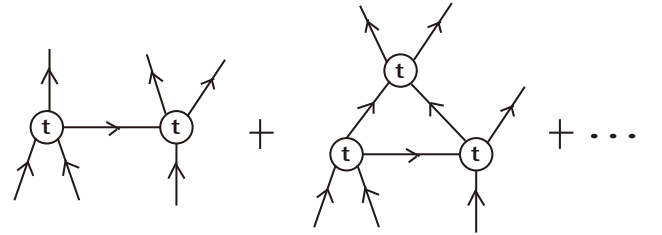


Fig. 1. The first two terms in the Faddeev series of the three-particle amplitudes. Genuine three-particle correlations start with the second diagram. The circles represent two-body t -matrices.

References

- 1) H. A. Bethe, Phys. Rev. B **138**, 804 (1965).
- 2) B. -A. Li, B. -J. Cai, L. -W. Chen, J. Xu, Prog. Part. Nucl. Phys. **99**, 29 (2018).
- 3) J. Negele, H. Orland, *Quantum Many-particle systems* (Springer, 1980).
- 4) C. Mahaux, P. F. Bortignon, R. A. Broglia, C. H. Dasso, Phys. Rep. **120**, 1 (1985).
- 5) J. P. Blaizot, B. L. Friman, Nucl. Phys. A **372**, 69 (1981).
- 6) E. N. E. van Dalen, C. Fuchs, A. Faessler, Phys. Rev. C **72**, 065803 (2005).
- 7) Z. Zhang, L. -W. Chen, Phys. Rev. C **94**, 064326 (2016).
- 8) J. W. Holt, N. Kaiser, T. R. Whitehead, Phys. Rev. C **97**, 054325 (2018).

[†] Condensed from an article by W. Bentz and I. C. Cloët, Phys. Rev. C **100**, 014303 (2019).

^{*1} Department of Physics, Tokai University

^{*2} Physics Division, Argonne National Laboratory

Double charge-exchange phonon states[†]

X. Roca-Maza,^{*1,*2} H. Sagawa,^{*3,*4} and G. Colò^{*1,*2}

The possibility of inducing double charge-exchange excitations by heavy-ion beams at intermediate energies has recently fostered interest in new collective excitations such as double isobaric analog states (DIAS) and double Gamow-Teller giant resonances (DGT). We present some formulas to evaluate different combinations of the average excitation energies of DIAS and DGTR by using commutator relations.

The expectation value for the energy of the DIAS (DGT) is defined as

$$E_{\text{DIAS(DGT)}} \equiv \langle \text{DIAS(DGT)} | \mathcal{H} | \text{DIAS(DGT)} \rangle - \langle 0 | \mathcal{H} | 0 \rangle. \quad (1)$$

Here $|0\rangle$ represents the ground state, and

$$|\text{DIAS(DGT)}\rangle \equiv \frac{O_- |\text{IAS(GT)}\rangle}{\langle \text{IAS(GT)} | O_+ O_- | \text{IAS(GT)} \rangle^{1/2}} \quad (2)$$

is the definition of the DIAS (DGT) state in terms of the IAS (GT), which can be written as

$$|\text{IAS(GT)}\rangle \equiv \frac{O_- |0\rangle}{\langle 0 | O_+ O_- | 0 \rangle^{1/2}}. \quad (3)$$

The operators $O_{\pm} = T_{\pm} \equiv \sum_i^A t_{\pm}(i)$ are the isospin raising and lowering operators for IAS and DIAS. For GT and DGT, $O_{\pm} = G_{\pm} \equiv \sum_i^A \sigma_z(i) t_{\pm}(i)$. Starting from Eq. (1), one may write the excitation energy of the DIAS (DGT) as

$$E_{\text{DIAS(DGT)}} = \frac{\langle 0 | [O_+^2, [\mathcal{H}, O_-^2]] | 0 \rangle}{\langle 0 | O_+^2 O_-^2 | 0 \rangle}, \quad (4)$$

assuming that the ground state has good isospin, that is, there is no isospin mixing and $T_+ |0\rangle = 0$. Within the same approximation, $E_{\text{IAS(GT)}}$ reads

$$E_{\text{IAS(GT)}} = \langle \text{IAS(GT)} | \mathcal{H} | \text{IAS(GT)} \rangle - \langle 0 | \mathcal{H} | 0 \rangle = \frac{\langle 0 | [O_+, [\mathcal{H}, O_-]] | 0 \rangle}{\langle 0 | O_+ O_- | 0 \rangle}. \quad (5)$$

One can write the energies for DIAS and DGT as

$$E_{\text{DIAS(DGT)}} = 2E_{\text{IAS(GT)}} + \frac{\langle 0 | [O_+, [O_+, [[\mathcal{H}, O_-], O_-]]] | 0 \rangle}{2(N-Z)(N-Z-1)}. \quad (6)$$

The denominator of Eq. (4) is evaluated to be $\langle 0 | O_+^2 O_-^2 | 0 \rangle = 2(N-Z)(N-Z-1)$. The second term

on the right-hand side in Eq. (6) could be different from zero only for the isospin symmetry breaking (ISB) terms in \mathcal{H} because they contribute to E_{IAS} [cf. Eq. (5)]. In other words, the IAS and DIAS energies are a special filter for the terms in the Hamiltonian that break isospin symmetry (Coulomb and the small contributions from the strong force), while the isospin-conserving part of \mathcal{H} does not contribute.

In order to evaluate the quartic and double commutators, we take the Hamiltonian

$$\mathcal{H} = \mathcal{H}_0 + V + V_C + V_{\text{ISB}}, \quad (7)$$

where V is the spin- and isospin-dependent interaction, V_C is the Coulomb interaction, and V_{ISB} is an ISB effective interaction originating from the nuclear strong force. From Eq. (6), we can derive the relation between the DGTR and DIAS energies as,

$$E_{\text{DGTR}} - E_{\text{DIAS}} = \frac{\langle 0 | [G_+^2, [V, G_-^2]] | 0 \rangle}{2(N-Z)(N-Z-1)}, \quad (8)$$

since $[G_+^2, [V_C + V_{\text{ISB}}, G_-^2]] = [T_+^2, [V_C + V_{\text{ISB}}, T_-^2]]$. In order to evaluate the energy difference between E_{DGTR} and E_{DIAS} , we adopt the separable interaction¹⁾

$$V = \sum_i^A \kappa_{ls} \mathbf{l}(i) \cdot \mathbf{s}(i) + \frac{1}{2} \frac{\kappa_{\tau}}{A} \sum_{i \neq j}^A \tau(i) \cdot \tau(j) + \frac{1}{2} \frac{\kappa_{\sigma\tau}}{A} \sum_{i \neq j}^A (\sigma(i) \cdot \sigma(j)) (\tau(i) \cdot \tau(j)), \quad (9)$$

where κ_{ls} is the one-body spin-orbit coupling strength, while κ_{τ} and $\kappa_{\sigma\tau}$ are the coupling strengths of the residual two-body interactions in the isospin and spin-isospin channels, respectively. The average energy of the GTR minus that of the IAS is expressed as

$$E_{\text{GT}} - E_{\text{IAS}} = \frac{\langle 0 | [G_+, [V, G_-]] | 0 \rangle}{(N-Z)} = -\frac{4}{3} \frac{\kappa_{ls}}{N-Z} \left\langle 0 \left| \sum_i^A \mathbf{l}(i) \cdot \mathbf{s}(i) \right| 0 \right\rangle + 2(\kappa_{\sigma\tau} - \kappa_{\tau}) \frac{N-Z}{A}.$$

The energy difference between DGTR and DIAS (8) is expressed in a similar manner as

$$E_{\text{DGTR}} - E_{\text{DIAS}} = \left(1 + \frac{N-Z}{N-Z-1} \right) (E_{\text{GT}} - E_{\text{IAS}}) = \frac{4}{3} \frac{\kappa_{ls}}{(N-Z)(N-Z-1)} \left\langle 0 \left| \sum_i^A \mathbf{l}(i) \cdot \mathbf{s}(i) \right| 0 \right\rangle - 6(\kappa_{\sigma\tau} - \kappa_{\tau}) \frac{1}{A} \frac{N-Z}{N-Z-1}.$$

Quantitative discussions of the above formulas are reported elsewhere.

Reference

- 1) A. Bohr, B. R. Mottelson, *Nuclear Structure Vol.I* (World Scientific, 1975).

[†] Condensed from the article in Phys. Rev. C **101**, 014320 (2020)

^{*1} Dipartimento di Fisica ‘‘Aldo Pontremoli,’’ Universit  degli Studi di Milano

^{*2} INFN, Sezione di Milano

^{*3} RIKEN Nishina Center

^{*4} Department of Physics, Omsk University

3. Nuclear Data

EXFOR compilation of RIBF data in 2019

T. Tada,^{*1} S. Imai,^{*2} D. Ichinkhorloo,^{*3} M. Kimura^{*3,*4} M. Aikawa,^{*3,*5} and N. Otuka^{*5,*6}

Nuclear-reaction data support the most essential part of nuclear technologies (*e.g.*, nuclear power production, nuclear fuel cycles, environmental monitoring, dosimetry, radiation safety, radioisotope production, radiotherapy, and medical diagnostics) and sciences (*e.g.*, nuclear physics, nuclear chemistry, geophysics, and astrophysics). Nuclear databases play a vital role in providing the best estimate for nuclear reactions to a wide range of data users in various scientific fields and related areas. One of the largest global nuclear reaction databases open to the public is the EXFOR library (EXchange FORmat for experimental nuclear reaction data).¹⁾ The EXFOR library is a universal common repository for nuclear reactions established in 1967. The International Network of Nuclear Reaction Data Centres (NRDC) maintains the EXFOR library under the auspices of the International Atomic Energy Agency (IAEA).²⁾ The scope of the EXFOR library covers a wide range of nuclear reactions such as neutron-, charged-particle-, and photon-induced reactions.

Our group, the Hokkaido University Nuclear Reaction Data Centre (JCPRG),³⁾ was founded in 1973 and joined the NRDC as the first Asian member in 1975. We are responsible for the compilation of charged-particle-, and photon-induced nuclear reactions measured at facilities in Japan.⁴⁾ Our contributions to the EXFOR database account for $\sim 10\%$ of the complete database. The database compilation process involves the scanning of peer-reviewed journals for published papers within the EXFOR scope. A unique entry number is given to each selected paper to be compiled for the EXFOR library. We extract information from the bibliography, experimental setup, measured physical quantities, measured numerical data, and uncertainties. The information is input in a single entry of EXFOR. During this process, we contact the corresponding authors with questions on the contents of the papers and requests for numerical data.

JCPRG has been cooperating with the RIKEN Nishina Center since 2010 for the compilation of data obtained by RIBF, which aims at the enhancement of the availability of the RIBF data. Our activities related to the RIBF experiments are as follows. We have compiled 48 new articles produced at Japanese facilities and modified 42 old entries. This includes 10

articles from RIKEN, 6 new articles, and 4 old entries. The compiled data are accessible by the entry numbers listed in Table 1. The status of those compilations is periodically reported via Nishina Center News.

We acknowledge that collaboration with RIKEN is a great help for us to establish an effective procedure for the compilations. Most of the RIKEN data are very quickly compiled after publication, and the end users can access them smoothly. We also thank all the authors of the RIKEN articles who kindly provided numerical data. This greatly helps increase the accuracy and quality of the database.

Table 1. Entry numbers with references compiled from RIBF data in 2019.

	Entries		
New	E2553 ⁵⁾	E2583 ⁶⁾	E2584 ⁷⁾
	E2586 ⁸⁾	E2590 ⁹⁾	E2592 ¹⁰⁾
Revised	E2430 ¹¹⁾	E2434 ¹²⁾	E2493 ¹³⁾
	E2539 ¹⁴⁾		
Total	10		

We would like to take this opportunity to express our gratitude to the authors of these papers for their kind cooperation with the EXFOR compilation process.

References

- 1) N. Otuka *et al.*, Nucl. Data Sheets **120**, 272 (2014).
- 2) <https://www.nds.iaea.org/>.
- 3) Hokkaido University Nuclear Reaction Data Centre, <http://www.jcprg.org/>.
- 4) M. Kimura, AAPPS Bulletin **28**, 24 (2018).
- 5) S. Momiyama *et al.*, Phys. Rev. C **96**, 034328 (2017).
- 6) D. Kahl *et al.*, Phys. Rev. C **97**, 015802 (2018).
- 7) M. L. Cortés *et al.*, Phys. Rev. C **97**, 044315 (2018).
- 8) O. B. Tarasov *et al.*, Phys. Rev. Lett. **121**, 022501 (2018).
- 9) M. Yoshie, I. Kohno, Sci. Pap. Inst. Phys. Chem. Res. **69**, 63 (1975).
- 10) T. Murata *et al.*, Appl. Radiat. Isot. **144**, 47 (2019).
- 11) A. K. Kurilkin *et al.*, Phys. Rev. C **87**, 051001(R) (2013).
- 12) L. Y. Zhang *et al.*, Phys. Rev. C **89**, 015804 (2014).
- 13) H. Wang *et al.*, Phys. Lett. B **754**, 104 (2016).
- 14) S. Kawase *et al.*, Prog. Theor. Exp. Phys. **2017**, 093D03 (2017).

*1 Graduate School of Science, Hokkaido University

*2 Institute for the Advancement of Higher Education, Hokkaido University

*3 Faculty of Science, Hokkaido University

*4 Research Center for Nuclear Physics (RCNP), Osaka University

*5 RIKEN Nishina Center

*6 NDS, IAEA

4. Hadron Physics

Unfolding the transverse momentum distribution for very forward neutron production in $p\text{Au}$ collisions at $\sqrt{s_{NN}} = 200$ GeV

B. Mulilo^{*1,*2} for the PHENIX collaboration

The PHENIX collaboration measured that when a transversely polarized proton with spin up collides with unpolarized proton at $\sqrt{s} = 200$ GeV, they generate neutrons predominantly to the right.¹⁾ In 2011, theorists explained this result in terms of the interference of pion and a_1 reggeon exchanges.²⁾ But in 2015 using run 15 pAu data, we observed that when a polarized proton collides with a gold nucleus at $\sqrt{s_{NN}} = 200$ GeV, they generate more neutrons to the left³⁾ contrary to theoretical predictions.²⁾ This nuclear dependence of the asymmetry (A_N) has, therefore, attracted a massive interest in nuclear physics.

We are now studying A_N as a function of the transverse momentum (Pt). We begin with an understanding that our measurements are limited by known effects such as the detector resolution and detection efficiency among others. Our technique is, therefore, to employ a method known as unfolding to remove these known effects and recover the distribution.

We proceed by parametrizing measurement effects using the response matrix in Fig. 1 from Monte Carlo.⁴⁾ What this matrix does is to map the binned true spectrum in the magenta line onto the smeared spectrum in the green line of Fig. 2. For the smeared and true distribution bins R_i and T_j , respectively, the smearing matrix element S_{ij} gives the fraction of entries from bin T_j that end up being reconstructed in bin R_i .

The unfolding has been performed using the singular value decomposition method⁵⁾ contained in CERN's ROOT toolkit. Since our smearing matrix is not perfectly diagonal, we unfolded with a parameter, alias Kreg,⁵⁾ which determines the regularization of the unfolding. The unfolded spectrum is the distribution corresponding to an optimum regularization parameter, Kreg = 6 as depicted in Fig. 2.

We are now optimizing and extending the ideas of the one dimensional unfolding to two dimensional unfolding of transverse momentum (Pt) in azimuthal angle (Φ). The transverse single spin asymmetry (A_N) for very forward neutron production will then be calculated as a function of the unfolded Pt distribution.

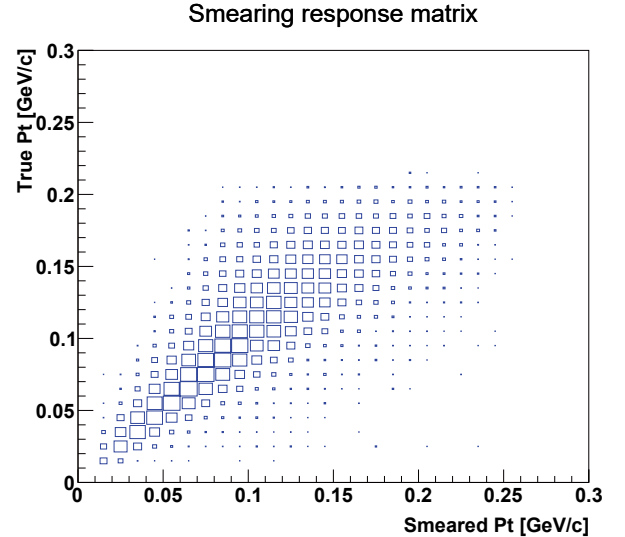


Fig. 1. Smearing response matrix mapping the binned true Pt spectrum to the smeared Pt spectrum.

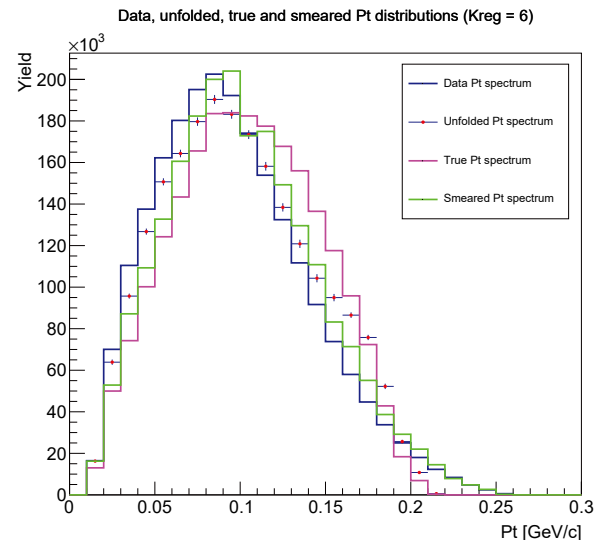


Fig. 2. Superposition of the experimental data, unfolded, true and smeared Pt distributions. The Pt distribution in the green line is smeared from Monte Carlo while that in the dark blue line is the experimental data. The Pt distribution in the magenta line is generated using Monte Carlo event generator.⁴⁾

References

- 1) A. Adare *et al.*, Phys. Rev. D **88**, 032006 (2013).
- 2) B. Z. Kopeliovich *et al.*, Phys. Rev. D **84**, 114012 (2011).
- 3) A. Aidala *et al.*, Phys. Rev. Lett. **120**, 022001 (2018).
- 4) G. Mitsuka, Phys. Rev. C **95**, 044908 (2017).
- 5) Nucl. Instrum. Methods Phys. Res. A **372**, 469 (1996).

^{*1} RIKEN Nishina Center

^{*2} Department of Physics, Korea University

Update of single and dihadron cross sections for light hadrons in e^+e^- annihilation at $\sqrt{s} = 10.58$ GeV in Belle[†]

R. Seidl^{*1}

The fragmentation process describes the formation of final-state hadrons from initial high-energetic partons such as quarks and gluons. Due to the strength of the coupling of the strong interaction, described by quantum chromodynamics, QCD, this process is obtained only experimentally and parameterized in fragmentation functions, FFs. FFs are universal and factorize for most relevant processes and FF types. They therefore serve as an important tool in the study of the spin, momentum and flavor structure of the nucleon or other bound states of QCD. Its universality can be used to extract them in one process, such as electron-positron annihilation where no hadrons exist in the initial state, and apply it to semi-inclusive deep-inelastic lepton nucleon scattering SIDIS or hadron-hadron scattering.

In the Belle experiment at the KEKB accelerator, a large amount of data exists that can be analyzed to extract various hadronic cross sections as a function of the fractional energy the hadrons carry relative to the initial parton energies, as well as their spin and transverse momentum dependence.

The extraction of the flavor dependence of fragmentation functions from electron-positron annihilation is not as easy since the cross sections are a sum over all accessible flavors, at Belle energies up, down, strange and charm quarks. To gain some sensitivity the extraction of cross sections for two hadrons in the final state have been published a few years ago,^{1,2)} where the flavor dependence of each of two single hadron fragmentation functions can be used together. However, the interpretation via single hadron fragmentation functions is only possible when both hadrons appear in opposite hemispheres which in turn can only be ensured via additional quantities. Such variables are difficult to treat theoretically, so in an update two different fractional-energy definitions were used and compared to the conventional one.

Both definitions contain scalar products between the two hadron's four-momenta and therefore only have sizable fractional energies when both hadrons are far separated without the need of an explicit hemisphere assignment. The cross section ratios for pion pairs can be seen in Fig. 1 relative to the default definition. The first definition is actually the oldest one suggested for dihadrons³⁾ which is meant to also be able to interpret the dihadron cross sections at higher orders of the strong coupling. The second definition is similar, but stresses the transverse momentum in the two-hadron

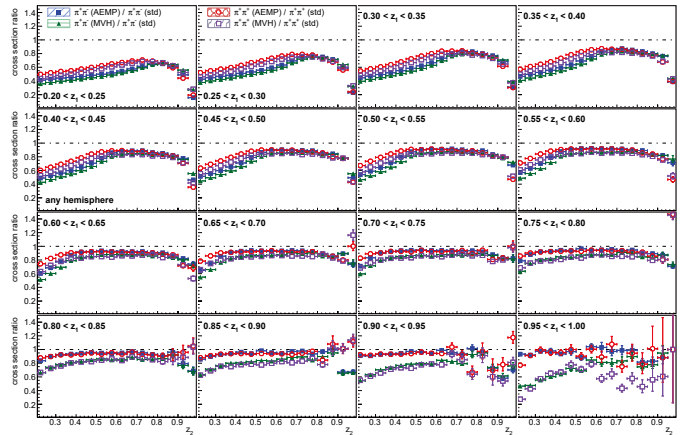


Fig. 1. Dipion cross section ratios as a function of fractional energy z_2 in bins of z_1 relative to the conventional fractional energy definitions. The opposite sign pairs are displayed in blue squares and green triangles for the AEMP and MVH definitions while the same sign pairs are displayed by red circles and purple squares, respectively.

system.⁴⁾ As can be seen, at very high fractional energies all three definitions are similar as both hadrons need to be nearly back-to-back and no phase space for transverse momentum remains. At low fractional momenta the cross sections using the alternative definitions are far smaller since the same-hemisphere hadron pairs would appear at much smaller fractional energies due to the scalar product.

In addition to these updated dihadron cross sections, also single hadron cross sections were updated. The difference to previously published single hadron cross sections for pions, kaons and protons^{2,5)} (as well as for dihadrons using the default fractional energy definitions) is an improved initial state radiation correction as well as the separation of correlated and uncorrelated systematic uncertainties.

References

- 1) R. Seidl *et al.*, Phys. Rev. D **96**, 032005 (2017).
- 2) R. Seidl *et al.*, Phys. Rev. D **92**, 092007 (2015).
- 3) G. Altarelli, R. K. Ellis, G. Martinelli, S. Y. Pi, Nucl. Phys. B **160**, 301 (1979). doi:10.1016/0550-3213(79)90062-2
- 4) P. J. Mulders, C. Van Hulse, Phys. Rev. D **100**, 034011 (2019).
- 5) M. Leitgab, *et al.*, Phys. Rev. Lett. **111**, 062002 (2013).

[†] Condensed from Phys. Rev. D **101**, 092004 (2020)

^{*1} RIKEN Nishina Center

Preparation status of the J-PARC E16 experiment in 2019

S. Yokkaichi*¹ for the J-PARC E16 Collaboration

We have proposed the experiment E16¹⁾ to measure the vector meson decays in nuclei in order to investigate the chiral symmetry restoration in dense nuclear matter. The experiment will be performed at the J-PARC Hadron Experimental Facility. The high-momentum beamline, where the experiment will be conducted, is being constructed by KEK. Its scientific (“stage-1”) approval was granted to the experiment E16 by PAC in March 2007. For the full (“stage-2”) approval, a technical design report was submitted to PAC in May 2014, and reviewed for the experimental and budgetary feasibility. In the PAC meeting held in Jul. 2017, the stage-2 approval for 40 shifts (320 hours) of a commissioning run was granted. In this run, the background measurement at the new beamline is required. The construction of the beamline and our spectrometer is on schedule for completion in Feb. 2020. Only 20 shifts are allocated in Feb.–Mar. 2020, and another 20 shifts are planned in early 2021.

This experiment aims to systematically study the spectral modification of vector mesons in nuclei, particularly the ϕ meson, using the e^+e^- decay channel with statistics that are two orders larger in magnitude than those of the precedent E325²⁾ experiment performed at KEK-PS. In other words, it aims to accumulate 1×10^5 to 2×10^5 events for each nuclear target (H, C, Cu, and Pb) and deduce the dependence of the spectral modification on the size of matter and meson momentum.

Our proposed spectrometer has 26 modules. Owing to budget limitations, our first goal of staged construction plan is to construct eight modules, as shown in Fig. 1. With the eight-module configuration, we proposed a physics run, Run-1, with 160 shifts (1280 hours), as described in the previous APR.³⁾

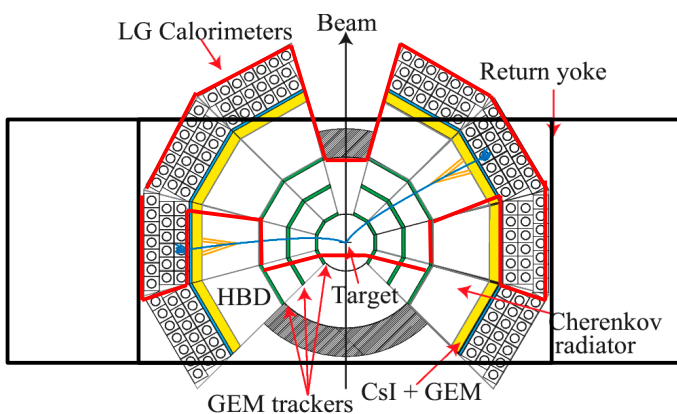


Fig. 1. Plan view of the proposed E16 Spectrometer in the eight-module configuration. The red line shows the constructed parts for the commissioning run in Feb. 2020. The SSD located in the innermost layer is not shown.



Fig. 2. Photograph of the E16 Spectrometer, which is under construction.

The development of detectors and front-end modules has been completed. Field mapping for the spectrometer magnet was performed in Jun.–Jul. 2019. We installed the detectors in the spectrometer magnet in Jul. 2019–Jan. 2020, including three layers of GEM Trackers (GTR) for tracking,⁴⁾ Hadron Blind Čerenkov detectors (HBD),⁵⁾ and Lead-Glass calorimeters (LG) for electron identification. We joined the RD51⁶⁾ collaboration in CERN that aims to develop multi-pixel gas detectors including GEM. One layer of Solid-State Detector (SSD) is introduced between GTR and the target in order to help the tracking under the huge background. The last part of development of trigger electronics,⁸⁾ namely, the amp-shaper-discriminator boards to generate the trigger signal at GTR and HBD, were completed in 2019.

We will start the commissioning run with 6 SSD, 6 GTR, 4 HBD, and 6 LG modules, out of eight modules each, as shown in Fig. 1. The installation of detectors has been completed, and shakedown is underway as of Jan. 2020, as shown in Fig. 2.

References

- 1) S. Yokkaichi *et al.*, J-PARC proposal No. 16, (http://j-parc.jp/researcher/Hadron/en/pac_0606/pdf/p16-Yokkaichi_2.pdf); Y. Komatsu *et al.*, JPS Conf. Proc. **12**, (2017), p. 020005; S. Ashikaga *et al.*, JPS Conf. Proc. **26**, (2019), p. 024005.
- 2) R. Muto *et al.*, Phys. Rev. Lett. **98**, 042501 (2007).
- 3) S. Yokkaichi, RIKEN Accel. Prog. Rep. **52**, 90 (2019).
- 4) W. Nakai *et al.*, RIKEN Accel. Prog. Rep. **49**, 195 (2015).
- 5) K. Kanno *et al.*, Nucl. Instrum. Methods Phys. Res. A **819**, 20 (2016).
- 6) <http://rd51-public.web.cern.ch/RD51-Public/>.
- 7) <https://www.psi.ch/drs/drs-chip/>.
- 8) T. N. Takahashi *et al.*, J. Phys. Conf. Ser. **664**, 082053 (2015); M. Ichikawa *et al.*, IEEE Trans. Nucl. Sci. **66**, 2022 (2019).

*¹ RIKEN Nishina Center

Measurement of nuclear effects on anti-quarks via Drell-Yan process at FNAL-SeaQuest

K. Nakano,^{*1,*2} Y. Goto,^{*2} Y. Miyachi,^{*3} K. Nagai,^{*4} S. Sawada,^{*2,*5} and T. -A. Shibata^{*2,*6}
for the E906/SeaQuest Collaboration

The nuclear effects on the partonic structure of nucleons signify that the distribution of partons in a nucleon bound inside a heavy nucleus changes from that in a free nucleon. It was first discovered by the EMC collaboration in 1983¹⁾ and is being studied using various measurements and theories to understand its mechanism. Most measurements made use of deep inelastic scattering (DIS), which does not differentiate between quarks and anti-quarks. The E772 experiment utilized the Drell-Yan process to extract the nuclear effects on anti-quarks.²⁾ It indicates that the effects are smaller than those observed in DIS, although the statistical precision was limited. If the difference between quarks and anti-quarks in the nuclear effects is confirmed, it will be a strong constraint in understanding the mechanism because it contradicts, for example, the conventional nuclear model.³⁾ A number of theoretical models were proposed to reproduce the measured difference.⁴⁾

The E906/SeaQuest experiment at Fermilab aims to study the anti-quark distributions in the nucleon and nuclei. It utilizes the 120-GeV proton beam from the Fermilab Main Injector ($\sqrt{s} = 15$ GeV). It employs liquid hydrogen (LH₂), liquid deuterium (LD₂), carbon, iron, and tungsten as targets to measure the Drell-Yan process in $p + p$, $p + d$, and $p + A$ reactions. In the Drell-Yan process, a quark in one hadron and an anti-quark in the other hadron are annihilated to produce a virtual photon, which then decays into a lepton pair: $q + \bar{q} \rightarrow \gamma^* \rightarrow l^+ + l^-$. When it is measured at forward rapidity ($x_F \gg 0$), an anti-quark nearly always originates from the target-side hadron. Therefore, the ratios of per-nucleon cross sections of two targets, $R(A/D) \equiv (\sigma_{p+A}/A) / (\sigma_{p+d}/2)$, are sensitive to the nuclear effects on anti-quarks.

The SeaQuest spectrometer⁵⁾ detects the final-state muon pair of the Drell-Yan process. SeaQuest acquired physics data from November 2013 to July 2017 with a summer accelerator shutdown each year. It has recorded 1.4×10^{18} beam protons on targets and analyzed approximately 40% of the recorded data. We selected dimuons with the invariant mass larger than 4.2 GeV, for which the Drell-Yan events are dominant. The dimuon yields have been corrected for track-reconstruction efficiency and background dimuons by using the extrapolation method.⁶⁾

*1 School of Science, Tokyo Institute of Technology

*2 RIKEN Nishina Center

*3 Faculty of Science, Yamagata University

*4 Institute of Physics, Academia Sinica, Taiwan

*5 Institute of Particle and Nuclear Studies, KEK

*6 College of Science and Technology, Nihon University

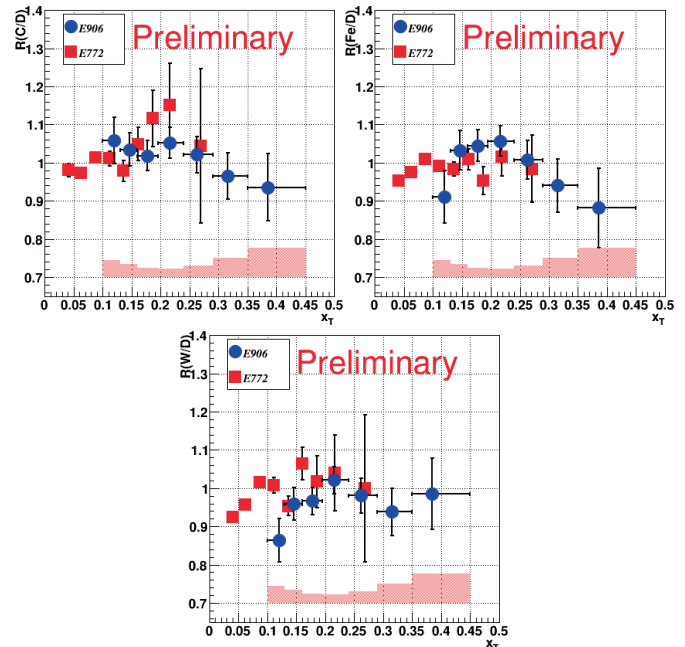


Fig. 1. Ratios of per-nucleon cross sections of C, Fe, and W to D versus the Bjorken x of target-side partons (x_T). The SeaQuest preliminary result is drawn with blue circles, and the E772 result is drawn with red squares.

Figure 1 shows the preliminary result of $R(A/D)$ measured using SeaQuest, together with the result obtained using E772 for comparison. The systematic uncertainty arises mostly from the fitting shape used in the extrapolation method. SeaQuest is consistent with E772 in the commonly measured region, $x_T \sim 0.2$, with better accuracy at higher x_T . It favors the observation by E772 that the nuclear effects on anti-quarks differ from those on quarks. Improvements in the measured precision and comparisons to theoretical models in order to finalize the result are ongoing.

References

- 1) J. J. Aubert *et al.*, Phys. Lett. **B123**, 275 (1983).
- 2) D. M. Alde *et al.*, Phys. Rev. Lett. **64**, 2479 (1990).
- 3) E. L. Berger, F. Coester, Phys. Rev. D **32**, 1071 (1985).
- 4) A. E. L. Dieperink, C. L. Korpa, Phys. Rev. C **55**, 2665 (1997).
- 5) C. A. Aidala *et al.*, Nucl. Instrum. Methods Phys. Res. A **930**, 49 (2019).
- 6) K. Nagai *et al.*, 2RIKEN Accel. Prog. Rep. **52**, 86 (2019).

Progress of the polarized Drell-Yan experiment at Fermilab, SpinQuest (E1039)

Y. Miyachi,^{*1} Y. Goto,^{*2} K. Nagai,^{*2,*3} K. Nakano,^{*2,*4} G. Nukazuka,^{*1} S. Sawada,^{*2,*5} and T. -A. Shibata^{*1,*6} for the SpinQuest Collaboration

SpinQuest is a polarized fixed-target Drell-Yan experiment using a 120 GeV proton beam from Main Injector at Fermilab. The primary goal of SpinQuest is to measure the Sivers asymmetries, aiming to obtain a hint for the following fundamental question: “Do the light sea quarks contribute to the intrinsic spin of the nucleon via their orbital angular momentum?” The Sivers asymmetry was first introduced to explain the unexpected, large, transverse, single-spin asymmetries observed in hadron scattering. Non-zero values of the Sivers asymmetry have been measured in the Semi-Inclusive Deep-Inelastic Scattering (SIDIS) experiments. The correlation between the transverse momentum of a quark and the spin of the parent nucleon, represented by the Sivers function, is a source of the asymmetry. The Sivers functions for u and d quarks were determined to be similar in size but with the opposite signs.^{2,3)} As no results for the Sivers functions for sea quarks are available, SpinQuest can help determine them for \bar{u} and \bar{d} , through the measurement of the Sivers asymmetries in the Drell-Yan process using the transversely polarized proton and deuteron targets, for the first time.

NH_3 and ND_3 are used as the polarized proton and deuteron target material. The target polarization is obtained with dynamic nuclear polarization, which requires a low temperature of 1 K, strong magnetic field of 5 T, and 140 GHz microwave radiation. Under the greatest instantaneous luminosity of any previous evaporation refrigerator system, with a beam intensity of 3×10^{12} protons/s for 5 s, a high-cooling-power ^4He evaporation refrigerator connected to a large pump system (14,000 m^3/h) successfully maintains the target material temperature at 1 K. The longest (along with the beam-line) target cell to date for an evaporation refrigerator requires a unique microwave distributing horn. Three NMR coils installed for the target cell reduce systematic uncertainties in the polarization measurement.

The SpinQuest experiment inherits the spectrometer from the SeaQuest experiments,¹⁾ which measured the flavor asymmetry in the light quark sea, \bar{d}/\bar{u} . It covers the kinematic region where target sea quarks dominate the Drell-Yan process: u or d quarks in the beam are annihilated with \bar{u} or \bar{d} anti-quarks in the target, re-

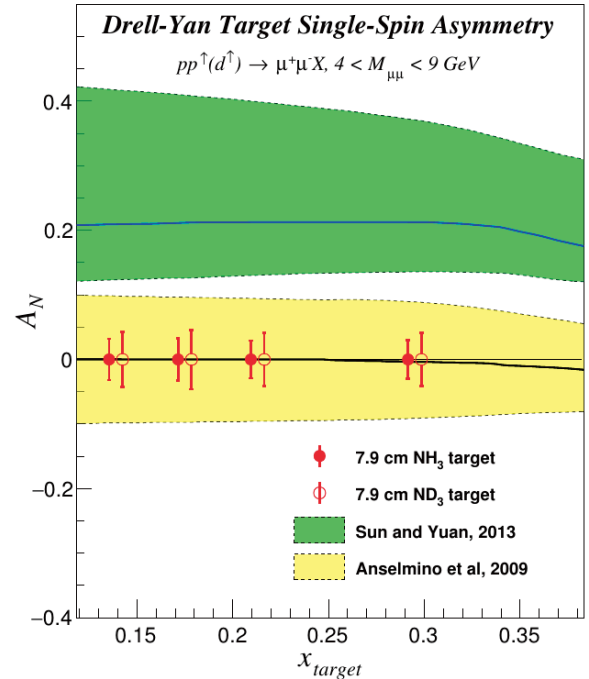


Fig. 1. Projected sensitivities of the single spin asymmetries at SpinQuest.

spectively. Because SpinQuest probes a lower x_{target} than SeaQuest, the target position has been moved further upstream of the beam dump to increase acceptance in the low x_{target} range, as well as to improve separation for target and dump events. At present, the commissioning of the target and spectrometer is ongoing. The beam time is expected to begin in early 2020.

Figure 1 shows the expected sensitivities of SpinQuest on the single spin asymmetries, A_N , after two years of combined operation on the NH_3 and ND_3 targets. The error bars are statistical only. A relative systematic uncertainty of 0.04 is expected. The bands represent theoretical predictions based on the Sivers functions^{2,3)} extracted from the present available SIDIS data. A comparison between the NH_3 and ND_3 results could also be sensitive to the flavor dependence of the sea-quark Sivers function.

References

- 1) C. A. Aidala *et al.*, [SeaQuest Collaboration], Nucl. Instrum. Methods Phys. Res. A **930**, 49 (2019).
- 2) M. Anselmino *et al.*, Eur. Phys. J. A **39**, 89 (2009).
- 3) P. Sun, F. Yuan, Phys. Rev. D **88**, 034016 (2013).

^{*1} Faculty of Science, Yamagata University

^{*2} RIKEN Nishina Center

^{*3} Institute of Physics, Academia Sinica, Taiwan

^{*4} School of Science, Tokyo Institute of Technology

^{*5} Institute of Particle and Nuclear Studies, KEK

^{*6} College of Science and Technology, Nihon University

Development of zero-degree calorimeter for EIC

Y. Goto,^{*1} T. Chujo,^{*2} Y. Itow,^{*3} J. H. Lee,^{*4} H. Menjo,^{*5} Y. Miyachi,^{*6} I. Nakagawa,^{*1} K. Nakano,^{*1,*7}
T. Sako,^{*1,*8} R. Seidl,^{*1} T. -A. Shibata,^{*1,*7,*9} K. Tanida,^{*1,*10} and Y. Yamazaki^{*11}

We propose the development of zero-degree apparatus in the Electron-Ion Collider (EIC) experiment. Zero-degree detectors play critical roles in a number of important physics topics at EIC.¹⁾ We will study the requirements and technologies of zero-degree detectors and mainly develop a position-sensitive zero-degree calorimeter (ZDC).

In electron + nucleus collisions, exclusive vector meson production in a diffractive process is one of the key measurements at EIC. For the coherent process in which the nucleus remains intact, the cross section dependent on the momentum transfer (t) can be translated to the transverse spatial distribution of gluons in the nucleus and is thus considered to be directly sensitive to the gluon saturation. This requires accurate determination of the coherence of the reaction, which must be determined by identifying the breakup of the excited nucleus. Evaporated neutrons from the breakup in the diffraction process can be used to separate the coherence with the highest probability ($\sim 90\%$). In addition, photons from the de-excitation of the excited nucleus signal incoherence in the absence of evaporated neutrons. This leads to a requirement to measure neutrons and photons precisely at near zero degree to complete the coverage of coherence tagging in a wide t range.

Collision geometry is an important measure in electron + nucleus collisions for an event-by-event characterization. It has been proposed that collision geometries can be tagged through forward neutron multiplicities emitted at near zero degree.²⁾ Constraining collision geometry quantities such as the “traveling length” of the struck parton in the nucleus, which is correlated with the impact parameter of the collision, is very meaningful in studies of nuclear medium effects. With the determination of collision geometry in these measurements, higher-precision constraints can be achieved to enhance our understanding of the nuclear structure.

In electron + deuteron and helium-3 collisions at

EIC, physics programs require the tagging of forward neutrons as spectators to identify the target nucleon. It constrains kinematics for studies of the short-range correlation (SRC). The SRC is a nucleon-nucleon interaction at a very short distance. It shows how nucleons form a nucleus, and has a deep connection to how the quark-gluon structure of a nucleon in a nucleus is modified, which is a phenomenon known as the EMC effect.³⁾ Experiments have shown it is universal that $\sim 20\%$ of nucleons are in SRC pairs. These SRC pairs have high momentum and are spatially very close to each other. Almost all of these SRC pairs are found to be similar to a quasi-deuteron at its high-momentum tail. In addition to the SRC study in electron + nucleus collisions, we will be able to understand the deuteron as a baseline of the SRC pair in electron + deuteron collisions at zero degree.

In electron + proton collisions, the leading proton and neutron productions in DIS were measured, and their production mechanisms were studied at HERA by comparison with the fragmentation process and one-pion exchange (OPE) process. The results support that the OPE process dominates the production, but there are still tension in detailed understanding of the mechanism and comparison between ZEUS⁴⁾ and H1⁵⁾ data. In addition to the production cross section measurement, the spin asymmetry measurement of the leading baryons in polarized electron + proton collisions will give us useful additional information for the study of the production mechanism. The data will also be used to understand the energy flow and development of the event generator, and applied for understanding the air shower evolution of high-energy cosmic rays and the neutrino interaction.

We will conduct the following studies in the future; 1) a photon detector study at a low energy < 300 MeV, 2) a prototype study of ZDC with position sensitivity, and 3) a radiation hardness study of scintillators. We would like to maximize the physics capability by studying detector design, development, and simulation.

^{*1} RIKEN Nishina Center

^{*2} Tomonaga Center for the History of the Universe, University of Tsukuba

^{*3} Institute for Space-Earth Environmental Research, Nagoya University

^{*4} Physics Department, Brookhaven National Laboratory

^{*5} Graduate school of Science, Nagoya University

^{*6} Department of Physics, Yamagata University

^{*7} Department of Physics, Tokyo Institute of Technology

^{*8} Institute for Cosmic Ray Research, University of Tokyo

^{*9} College of Science and Technology, Nihon University

^{*10} Advanced Science Research Center, Japan Atomic Energy Agency

^{*11} Graduate School of Science, Kobe University

References

- 1) A. Accardi *et al.*, Eur. Phys. J. A **52**, 268 (2016) [arXiv:1212.1701 [nucl-ex]].
- 2) L. Zheng, E. C. Aschenauer, J. H. Lee, Eur. Phys. J. A **50**, 189 (2014) [arXiv:1407.8055 [hep-ex]].
- 3) B. Schmookler *et al.*, [CLAS Collaboration], Nature **566**, 354 (2019).
- 4) S. Chekanov *et al.*, [ZEUS Collaboration], Nucl. Phys. B **776**, 1 (2007) [hep-ex/0702028].
- 5) F. D. Aaron *et al.*, [H1 Collaboration], Eur. Phys. J. C **68**, 381 (2010) [arXiv:1001.0532 [hep-ex]].

INTT Silicon Modules and Ladders Assembly for sPHENIX Project

C. Miraval,^{*2} Y. Akiba,^{*1} K. Cheng,^{*3} E. Desmond,^{*2} T. Hachiya,^{*1,*4} T. Kondo,^{*5} C. Kuo,^{*3} M. Lenz,^{*2} E. Mannel,^{*2} D. Cacace,^{*2} M. Morita,^{*4} I. Nakagawa,^{*1} R. Nouicer,^{*2} R. Pisani,^{*2} M. Shibata,^{*4} C. Shih,^{*3} A. Suzuki,^{*4} T. Todoroki,^{*1} X. Wei,^{*6} and R. Xiao^{*6}

The INTermediate silicon strip Tracker (INTT) barrel is comprised of several ladders tangentially arranged in layers around the RHIC beam pipe.¹⁾ Each ladder assembly has two high-density interconnects (HDI) that are epoxied to a carbon fiber stave support. The two HDIs collectively host 52 FPHX chips and 4 silicon sensors. The sensors and the chips are glued to pads on the HDIs, wire-bonded, and then encapsulated.

The assembly process consists of multiple steps (cf. Fig. 1). During the inspection step of assembly, the carbon fiber staves are measured for flatness on BNL's OGP Smartscope Flash 500. The OGP is a top-down laser optical measurement system with a potential Z accuracy of 2 microns. Qualified carbon fiber staves are placed on the assembly fixture (cf. Fig. 2) and HDIs are installed and epoxied using glue masks.

Glue masks are placed in order to accurately epoxy to the chip pads on the HDIs. Chips are then precisely located and placed with acrylic vacuum fixtures that interface with the main assembly fixture (cf. Figs. 3–5). After the chips are epoxied, they are wire-bonded to the HDIs and then electronically tested.

In the same fashion that the chips were installed, the silicon sensors are placed on epoxied locations along the HDIs using vacuum fixtures. The sensor's vacuum fixture (cf. Figs. 4 and 5) has micro adjusters allowing the sensor's position to be perfected before the epoxy cures. Small marks are referenced on the HDI and the silicon sensors using the OGP machine. These marks are used for live alignment checks while adjusting the positions of the sensors. After the epoxy is cured, a final wire-bond job is performed and the full assembly is then electrically tested.

Currently, all assembly fixtures have been designed, fabricated, and received; permitting us to begin prototype production. Additional fixtures used in transportation and wire-bonding/encapsulation are designed and being sent for fabrication. The transportation container doubles as a safe storage and testing fixture, as the electronic connectors and the cooling pipe can be accessed from outside the transportation container without putting the delicate sensors and chips at risk. Specific fixtures were necessary for the

wire-bonding and encapsulation machines so that multiple staves can be produced in the same exact manner every time, streamlining production.

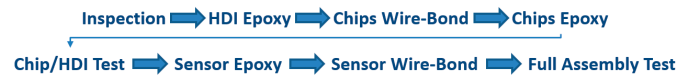


Fig. 1. Assembly Steps.

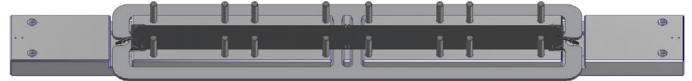


Fig. 2. Assembly Fixture.

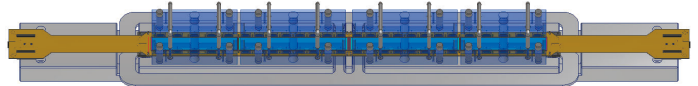


Fig. 3. Chip Placement Tools on Assembly.

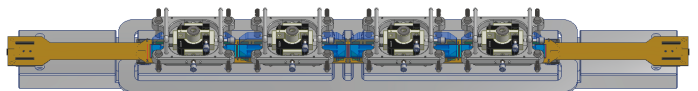


Fig. 4. Sensor Placement Tools on Assembly.

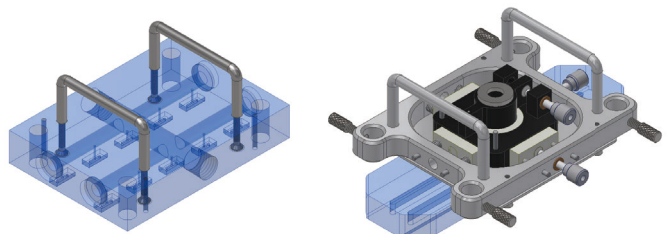


Fig. 5. Chip Placement Tool and Sensor Placement Tool

^{*1} RIKEN Nishina Center

^{*2} Brookhaven National Laboratory

^{*3} National Central University

^{*4} Nara Women's University

^{*5} Tokyo Metropolitan Industrial Technology Research Institute

^{*6} Purdue University

Reference

- 1) Conceptual Design Report of sPHENIX (2018).

6. Particle Physics

Empirical formulas for the standard-model parameters

Y. Akiba,*¹

In my previous article,¹⁾ I reported empirical formulas of the masses of the elementary particles in the standard model (SM), namely, charged leptons (e, μ, τ), quarks (t, c, u, b, s, d), gauge bosons (Z, W), and the Higgs boson (H). Each of these formulas yields the ratio μ_p/M_{pl} of the mass of particle p to the Planck mass $M_{pl} = 1.220910 \pm 0.000029 \times 10^{19}$ GeV in terms of a dimensionless constant $\epsilon_0 = 2 \times (6\pi)^{-48}$. There is no adjustable parameter in the formulas.

Here, I report similar formulas for the mass of neutrinos, Cabibbo-Kobayashi-Masukawa (CKM) quark mixing parameters, and neutrino mixing parameters. Table 1 lists mass formulas including neutrinos. The neutrino masses calculated from the formulas are $m_1 = 2.70 \times 10^{-3}$ eV, $m_2 = 9.01 \times 10^{-3}$ eV, and $m_3 = 5.09 \times 10^{-2}$ eV. Table 2 shows the formulas for the CKM matrix elements and their calculated values. Table 3 lists the formulas of the neutrino mixing parameters and their calculated values.

Table 1. Formulas for the masses of the SM particles.

particle p	formula ($\mu_p = m_p/M_{pl}$)
e	$\frac{1}{12\pi^2} \epsilon_0^{1/3} \left(1 + \frac{1}{4} \frac{1}{(6\pi)^2}\right)^{-1}$
μ	$\frac{3}{2} \epsilon_0^{1/3} \left(1 - \frac{3}{6\pi} + \frac{27}{4} \frac{1}{(6\pi)^2}\right)^{-1}$
τ	$9\pi \epsilon_0^{1/3} \left(1 - \frac{3}{4} \frac{1}{6\pi} + \frac{5}{4} \frac{1}{(6\pi)^2}\right)^{-1}$
ν_1	$\frac{2}{3} \epsilon_0^{1/2} \left(1 + \frac{1}{6\pi}\right)^{-1}$
ν_2	$2\epsilon_0^{1/2} \left(1 - \frac{1}{6\pi}\right)^{-1}$
ν_3	$4\pi \epsilon_0^{1/2} \left(1 + \frac{1}{6\pi}\right)^{-1}$
t	$8(6\pi)^2 \epsilon_0^{1/3}$
c	$12\epsilon_0^{1/3}$
u	$8(6\pi)^{-2} \epsilon_0^{1/3}$
b	$3(6\pi) \epsilon_0^{1/3} \left(1 + \frac{3}{2} \frac{1}{6\pi} + \frac{27}{4} \frac{1}{(6\pi)^2}\right)^{-1}$
s	$\epsilon_0^{1/3}$
d	$(6\pi)^{-1} \epsilon_0^{1/3} \left(1 + \frac{1}{6\pi}\right)^{-1}$
Z	$\frac{1}{(8\pi^2)} \epsilon_0^{1/4} \left(1 + \frac{1}{12} \frac{1}{6\pi} + \frac{1}{12} \frac{1}{(6\pi)^2}\right)^{-1/2}$
W	$\frac{2^{-1/4}}{(8\pi^2)} \epsilon_0^{1/4} \left(1 - \frac{3}{2} \frac{1}{6\pi} - \frac{9}{4} \frac{1}{(6\pi)^2}\right)^{-1/2}$
H	$\frac{2^{1/2}}{8\pi^2} \epsilon_0^{1/4} \left(1 + \frac{3}{2} \frac{1}{6\pi} - \frac{9}{2} \frac{1}{(6\pi)^2}\right)^{-1/2}$

*¹ RIKEN Nishina Center

Table 2. Formulas of the CKM matrix elements V_{us}, V_{cb}, V_{ub} , and the CP-violation parameter $\bar{\eta}$.

	formula	calculated
V_{us}	$\left(\frac{1}{6\pi} \left(1 + \frac{1}{6\pi}\right)^{-1}\right)^{1/2}$	0.22445
V_{cb}	$\left(\frac{2}{3}\right)^{1/2} \frac{1}{6\pi}$	0.04332
V_{ub}	$\frac{4}{3} \frac{1}{(6\pi)^2}$	0.003753
$\bar{\eta}$	$\left(1 + \frac{3}{2} \frac{1}{6\pi} + \frac{27}{4} \frac{1}{(6\pi)^2}\right) \frac{1}{\pi}$	0.3497

Table 3. Formulas of the neutrino-mixing matrix.

	formula	calculated
s_{12}	$\left(\frac{1}{3} \left(1 - \frac{1}{6\pi}\right) \left(1 + \frac{1}{6\pi}\right)^{-1}\right)^{1/2}$	0.547
s_{23}	$\left(\frac{3}{2\pi} \left(1 + \frac{1}{6\pi}\right) \left(1 - \frac{1}{6\pi}\right)^{-1}\right)^{1/2}$	0.729
s_{13}	$\left(\frac{1}{12\pi}\right)^{1/2} \left(1 - \frac{1}{6\pi}\right) \left(1 + \frac{1}{6\pi}\right)^{-1}$	0.146

The values calculated from these formulas all agree with experimental data within the uncertainty of the data.

There are 25 free parameters in the SM. These formulas yield 22 out of the 25 parameters. The remaining 3 parameters are the fine structure constant α , the strong coupling constant α_s , and the neutrino CP violation parameter δ_{CP} . Both α and α_s are scale dependent, and δ_{CP} is the only unmeasured parameter in the SM.

Note that the value of ϵ_0 is consistent with the product of the Hubble constant H_0 and the Planck time $t_{pl} = 1/M_{pl}$:

$$H_0 \times t_{pl} = (1.211 \pm 0.014) \times 10^{-61}.$$

$$\epsilon_0 \equiv 2 \times (6\pi)^{-48} = 1.220608 \times 10^{-61}.$$

Here, the Wilkinson Microwave Anisotropy Probe (WMAP) nine-year value of H_0 is used. This suggests that the masses of elementary particles are related to the expansion of spacetime.

A model to explain these formulae is reported in the next article,²⁾ and implications to gravity and cosmology are reported in the article appearing after that.³⁾

References

- 1) Y. Akiba, Accel. Prog. Rep. **52**, 98 (2019).
- 2) Y. Akiba, in this report.
- 3) Y. Akiba, in this report.

Quarternion-spin-isospin model for the standard-model parameters

Y. Akiba ^{*1}

In the preceding article,¹⁾ empirical formulas of the parameters of the standard model (SM) of particle physics are presented. Here, I report a model that can produce these formulas. We call the model the “Quarternion-spin-isospin model” since it is based on operators that are products of the quarternion bases I^μ , spin operator σ^ν , and (weak) isospin operator τ^a . In the model, the Planck time $\tau_{pl} = 1/M_{pl} = 5.3912 \times 10^{-44}$ s is the minimum duration of time. A term of the Lagrangian density \mathcal{L}_i of a particle is an “oriented product” of 48 “normalized primordial actions” (NPAs) that are selected from the following 64 NPAs.

$$\left\{ \frac{I^\mu \sigma^\nu \tau^a}{6\pi}, \frac{i}{3\pi}, \frac{\tau^3}{3\pi}, \frac{I^c \tau^3}{3\pi}, \frac{-I^c}{2\pi}, \frac{-i}{\pi}, i, I^c, -2, 2, 1 \right\}$$

The oriented product operator \vee has the following reduction rules:

$$\hat{\alpha} \vee \hat{\beta} = \begin{cases} \hat{\alpha}\hat{\beta}, & (\text{if } \hat{\alpha}\hat{\beta} = -\hat{\beta}\hat{\alpha}) \\ 0, & (\text{if } \hat{\alpha}\hat{\beta} = \hat{\beta}\hat{\alpha}) \end{cases}$$

$$\hat{\alpha} \vee \hat{\beta} \vee \hat{\gamma} = \begin{cases} \hat{\alpha}\hat{\beta}\hat{\gamma}, & (\text{if } \hat{\alpha}\hat{\beta} = -\hat{\beta}\hat{\alpha}, \hat{\beta}\hat{\gamma} = -\hat{\gamma}\hat{\beta}, \hat{\gamma}\hat{\alpha} = -\hat{\alpha}\hat{\gamma}) \\ 0, & (\text{otherwise}) \end{cases}$$

$$s \vee \hat{\alpha} = s\hat{\alpha}, \quad s_1 \vee s_2 = 0, \quad \hat{\alpha} \vee s \vee \hat{\beta} = s\hat{\alpha}\hat{\beta}.$$

Here, s is a scalar. Following these rules, a 48 \vee product of NPAs, $dS = \hat{s}_{i_1} \vee \cdots \vee \hat{s}_{i_{48}}$, is reduced to a value in the form of $\pm m(6\pi)^n i^s (\tau^3)^{s'} \epsilon_0$, where $\epsilon_0 = 2 \times (6\pi)^{-48}$, $s \in \{0, 1\}$, $s' \in \{0, 1\}$, $m \in \{1, \pm 2, \pm 3, \pm 4, \pm 6, \pm 8, \pm 12, \pm 18, \pm 24\}$, and $n \in \{0, 1, 2\}$. The values of s, s', n , and m are determined by the selection of the subset $\{\hat{s}_1, \cdots, \hat{s}_{48}\}$ from S_{NPA} . Due to the calculation rules of the \vee product, only a limited number of 48 products have a non-zero reduced value. We call these non-zero 48 product the “elementary action” (EA). An EA corresponds to a term of Lagrangian density \mathcal{L} of an elementary particle, *e.g.*, the electron.

We found 48 EAs that correspond to the elementary particles of the SM, which are summarized in Table 1. In the table, U and D denote U -type and D -type quarks, respectively, when their masses are ignored.

The mass of particles can be obtained from Table I. In the following, I show how the mass formula of the electron can be obtained from the table as an example.

The Lagrangian of the electron is a sum of three EAs.

$$\hat{\mathcal{L}}_e = 4(6\pi)^2 i \epsilon_0 \tau^3 + i \epsilon_0 i \tau^3 + 3\epsilon_0.$$

Each EA can then be written as a product of the following “operators.”

Table 1. Elementary actions.

	$(6\pi)^2 \epsilon_0$		$(6\pi) \epsilon_0$				ϵ_0		
	$i\tau^3$	i	$i\tau^3$	i	τ^3	1	$i\tau^3$	i	1
g_{3D}									3
g_{2D}									2
G^{ab}									-24
e	4								3
μ	4		-12						3
τ	4		-3		3				1+4
ν_1		12		12					2
ν_2		-4	4						2
ν_3		12		12	-2	2			
U	-12								2
u	4								8
c	4								24
t	4								8
D	-12								1
d	-12		-12		3				
s	-12								3
b	4		6		3				27 18
Z		12	1						1 18
H	-4		6						18
W		12		-18					-27 18

$$\hat{\partial}_{16} = \epsilon_0^{1/3} (1 + i\sigma^1 + i\sigma^2 + i\sigma^3),$$

$$\hat{\psi}_{15}^+ = |\psi_{15}| \tau^+ (u_1^+ \sigma^1 + u_2^+ \sigma^2 + u_3^+ \sigma^3),$$

$$\hat{\psi}_{15}^- = |\psi_{15}| \tau^- (u_1^- \sigma^1 + u_2^- \sigma^2 + u_3^- \sigma^3),$$

$$\hat{A}_{18} = (6\pi)^{-2} \epsilon_0^{1/3} (1 + i\sigma^1 + i\sigma^2 + i\sigma^3).$$

Here, $|\psi_{15}| = (6\pi)\epsilon_0^{1/3}$ and the 3D vectors $u^+ = (u_1^+, u_2^+, u_3^+)$ and $u^- = (u_1^-, u_2^-, u_3^-)$ satisfy $u^+ \times u^- = (-1, -1, -1)$ and $u^+ \cdot u^- = 1$. The operators $\hat{\partial}_{16}$ and $\hat{\psi}_{15}^\pm$ correspond to the differential operator $i\sigma^\mu \partial_\mu$ and the electron field operator, and ψ_{15}^+ corresponds to its conjugate. One can show

$$\hat{\mathcal{L}}_e = \left(1 + \frac{1}{4} \frac{1}{(6\pi)^2} \right) \left(\hat{\partial}_{16} \hat{\psi}_{15}^+ \hat{\psi}_{15}^- + \mu_e |\psi_{15}|^2 \right),$$

$$\mu_e = \left(1 + \frac{1}{4} \frac{1}{(6\pi)^2} \right)^{-1} \frac{1}{12\pi^2} \epsilon_0^{1/3}.$$

Similarly, all of the 22 formulas of the SM parameters presented in the preceding article are derived. The model also predicts 100% CP violation in the neutrino sector and that the product of the Hubble constant H_0 and the Planck time t_{pl} is $H_0 t_{pl} = 2 \times (6\pi)^{-48}$.

Reference

- 1) Y. Akiba, in this report.

^{*1} RIKEN Nishina Center

$R = 12H_0^2$ and its implications to gravity and cosmology

Y. Akiba ^{*1}

In the preceding article,¹⁾ I report a model (QST model) that can yield the formulas of the standard model (SM) parameters. The model implies that the product of the Hubble constant H_0 and the Planck time t_{pl} is $H_0 t_{pl} = 2 \times (6\pi)^{-48} = \epsilon_0$. This relation is derived as follows.

In general relativity, the action is written as

$$S = \int \mathcal{L} \sqrt{-g} dx^4 = \int \mathcal{L} \sqrt{\det(g_{\mu\nu})} d^4x,$$

where $g_{\mu\nu}$ is the metric and \mathcal{L} is the Lagrangian density of the system.

In the QST model, this is expressed as

$$(1 + \hat{\mathcal{L}}) \sqrt{-g} = 1 + \hat{\mathcal{L}} + \hat{\mathcal{L}}_{g3D}$$

where $\hat{\mathcal{L}}$ is the elementary action (EA), and $\hat{\mathcal{L}}_{g3D} = 3\epsilon_0$ is the EA corresponding to the gravity.

$$\sqrt{-g} = 1 + \hat{\mathcal{L}}_{g3D} = 1 + 3\epsilon_0$$

Now the spacetime metric of the Hubble expansion is

$$ds^2 = -dt^2 + e^{2H_0 t} (dx^2 + dy^2 + dz^2).$$

For $t = t_{pl}$, we have $\sqrt{-g} = e^{3H_0 t} = 1 + 3H_0 t_{pl}$. From the comparison, we have $H_0 t_{pl} = \epsilon_0$. The Ricci scalar curvature R and the 3D curvature K of this metric are

$$\begin{aligned} R &= 12H_0^2, \\ K &= 0. \end{aligned}$$

Since $H_0 = \epsilon_0/t_{pl}$ is a constant, R is also a constant in the QST model.

Now, we generalize the metric to allow local changes of the scale with a constraint that Ricci curvature should remain constant.

$$\begin{aligned} ds^2 &= -e^{2u(x,y,z)} dt^2 + e^{2H_0 t} (dx^2 + dy^2 + dz^2), \\ R &= 12H_0^2. \end{aligned}$$

The Ricci curvature of this metric is

$$R = -2(\Delta u + (\nabla u)^2) e^{-2H_0 t} + 12H_0^2 e^{-2u} = 12H_0^2.$$

We can show that Coulomb gravity can be derived from this metric. When we take the approximation $H_0 \simeq 0$, we have

$$R = -2(\Delta u + (\nabla u)^2) = 0.$$

Now, we define $\phi = e^u$; thus, we have

$$\Delta \phi = \Delta(e^u) = (\Delta u + (\nabla u)^2) \phi = 0,$$

which means that ϕ satisfies the Laplace equation. The general solution of ϕ is

$$\phi(\vec{r}) = 1 - \sum_i \frac{r_s^i}{|\vec{r} - \vec{r}_i^s|}.$$

We note that $\phi^2 = e^{2u} = -g_{00}$. In general relativity, $g_{00} \simeq -1 - 2\phi_G$, where ϕ_G is the gravitational potential. This means that $\phi = \phi_G$. Thus, the relation $R = 0$ implies the Coulombic gravitational potential.

If we take into account the fact that $H_0 \neq 0$, the potential equation for gravity becomes non-linear.

$$\Delta \phi + 6H_0^2 e^{2H_0 t} (\phi - 1/\phi) = 0.$$

One may question the validity of the QST model, since the model implies that the Hubble constant is a constant, which would mean that spacetime expands exponentially at a constant rate. This contradicts standard Big Bang cosmology. In the Big Bang theory, H_0 is not constant, and the scale of the universe is zero at the Big Bang, which supposed to have occurred 13.8 billion years ago.

We note that there is no direct evidence that the Big Bang occurred 13.8 billion years ago, because the absolute scale of the time coordinate in the past is impossible to determine. The distance to an object far away can only be measured by the red shift z . The value of z is then translated to the time based on standard cosmology by using the Friedmann equations. However, there is no experimental method to verify that the translation from z to t is correct.

The cosmic microwave background (CMB) is usually considered as the direct evidence of the Big Bang. I argue that it is not. CMB is definitive evidence that there was an era of $z = 1100$ when the spacetime scale is 1/1100 of the present one and the temperature of the Universe was 3000 K. In the standard cosmology, $z = 1100$ translates to 13.8 billion years ago and 380,000 years after the Big Bang. However, the only basis for this time scale is the Friedmann equations. If we assume that H_0 is constant, the only change is that the time of CMB formation becomes about 1 trillion years ago instead of 13.8 billion years ago.

The agreement between the abundance of ^4He and the Big Bang nucleosynthesis (BBN) model is considered another evidence of the Big Bang. In standard cosmology, BBN occurred 3 minutes after the Big Bang. However, it is impossible to determine the absolute time when BBN occurred. There is no observation that contradicts with the assumption that H_0 is constant.

References

- 1) Y. Akiba, in this report.

^{*1} RIKEN Nishina Center

7. Astrophysics and Astro-Glaciology

Experimental equipment for exploring reactions of low energy ions with an ice surface as an interstellar dust analog

Y. Nakai,^{*1} H. Hidaka,^{*2} and N. Watanabe^{*2}

An understanding of the synthesis of interstellar molecular evolution is indispensable for understanding various chemical aspects in the universe, *e.g.*, the origin of life. Various kinds of molecules have been found even in molecular clouds in the first stage of star formation, despite their very low temperature. Gas-phase ion-molecule reactions have been always considered to play an important role in the chemical evolution in molecular clouds. Reactions of neutral radicals with neutral species on an icy grain surface have been also proposed as other pathways, the importance of which has been confirmed for the production of hydrogen molecules, water molecules, methanol molecules, and so on.¹⁾ Recently, the reactions of very-low-energy (eV order) ions with an icy surface have been theoretically proposed to be new non-negligible reaction pathways. In most of the proposed pathways, neutral species and H_3O^+ ions are produced on the surface through reactions involving multiple water molecules.^{2,3)} These reactions are extremely complicated compared with gas-phase reactions. In addition, an actual icy surface probably has more variety and complexity than the theoretical assumptions. Therefore, experimental investigations are crucial to confirm theoretical predictions and explore such reactions more deeply. However, no experiments have been reported to our knowledge. Thus, we have started developing an experimental apparatus. In this report, we will provide an overview of our apparatus under development.

Figure 1 shows a schematic of our experimental equipment. An amorphous solid water (ASW) film is made on an aluminum substrate mounted on the cold head of a He refrigerator at a low temperature ($\sim 10\text{--}50$ K) by introducing water vapor of $\sim 1 \times 10^{-5}$ Pa into the vacuum chamber. The thickness of the ASW film is estimated from its infrared absorption intensity, which is measured using Fourier-transform infrared spectroscopy (FTIR). After the introduction of water vapor is stopped, the ASW surface is irradiated with low-energy atomic/molecular ions using the ion source located at the front of the substrate (low-energy ion source in Fig. 1). This ion source consists of an electron-impact ionizer, a Wien filter in which the ions are mass-analyzed, and a deceleration lens system to decelerate and focus ions on the substrate. In the test of the ion source using a N_2^+ beam, we obtained an intensity of ~ 2.8 nA with an energy of ~ 3 eV and an energy spread of approximately ± 2 eV on the substrate.

^{*1} RIKEN Nishina Center

^{*2} Institute of Low Temperature Science, Hokkaido University

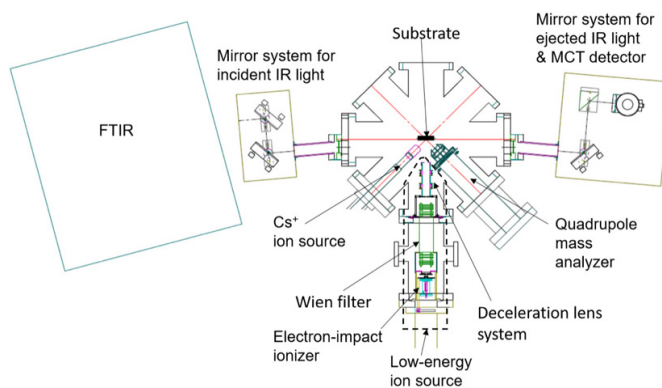


Fig. 1. Schematic drawing of the experimental setup.

Our apparatus has another ion source (Cs^+ ion source in Fig. 1) for detecting reaction products by the irradiation of low-energy atomic/molecule ions. The detection method is based on reactive ion scattering (RIS) and low-energy ion sputtering (LES) by Cs^+ ions with a kinetic energy of a few or several tens of eV, which has been mainly developed as a detection method for neutral and/or ionic species on metal and ice surfaces at temperatures higher than ~ 70 K.⁴⁾ When Cs^+ ions collide with an ice surface, a part of them pick up neutral species including water molecules on the surface and scattered composite ions of CsM^+ (RIS), where M is a picked-up neutral species. We can obtain a mass of M from the mass analysis of scattered CsM^+ ions. Moreover, we can obtain the masses of ionic species on the surface through the mass analysis of ions sputtered by Cs^+ (LES). A quadrupole mass analyzer is used for these mass analyses. At present, we performed isolated tests of the RIS method using a pristine ASW film at 30 K and could detect $\text{Cs}(\text{H}_2\text{O})^+$ ions from the RIS process. However, the detection sensitivity will be further improved for our purpose.

We are now continuing development of the low-energy ion source and the RIS-LES method for the ASW surface at low temperature, aiming for better performances.

References

- 1) N. Watanabe, A. Kouchi, *Prog. Surf. Sci.* **83**, 439 (2008).
- 2) D. Woon, *Astrophys. J.* **728**, 44 (2011).
- 3) E. J. McBride *et al.*, *J. Phys. Chem. A* **118**, 6991 (2014).
- 4) H. Kang, *Bull. Korean Chem. Soc.* **32**, 389 (2011).

Commissioning of a prototype novel laser melting sampler for analyzing ice cores with high depth resolution and high throughput

Y. Motizuki,^{*1} Y. Nakai,^{*1} M. Yumoto,^{*2} M. Maruyama,^{*2} K. Takahashi,^{*1} K. Kase,^{*2} S. Wada,^{*2} J. Hirose,^{*1} and Y. Yano^{*1}

A new facility for analyzing ice cores is being developed jointly by the Astro-Glaciology Research Group (AGRG) of RIKEN Nishina Center and the Photonics Control Technology Team of RIKEN Center for Advanced Photonics in a room (50 m²) at Wako Campus. The mission of this facility is to analyze ice cores with high depth (temporal) resolution and high throughput to obtain concentration profiles of various isotopes such as ¹⁸O/¹⁶O and various ions such as SO₄²⁻ and NO₃⁻.

The ice cores that we study have been drilled by the Japanese Antarctic Research Expedition (JARE) around Dome Fuji (DF) station in East Antarctica, and the current JARE project to obtain the third Japanese deep ice core, which is expected to contain information up to more than a million years ago, has been approved and is in progress. We aim at investigating the long-term history of climate change from the viewpoints of the relation with solar activities and volcanic eruptions. We also seek traces of supernovae in our galaxy and its explosion rate as our final goal.

In our facility, a low-temperature (LT) room, *i.e.*, a prefabricated freezer container (3 m wide × 5 m long × 3 m high), has been installed, and its inside has been kept at -20°C. Outside the LT room, *two* sets of isotope analyzers have been equipped at room temperature; we plan to add the newest ion chromatography system here in the near future.

The application of the laser melting method on ice cores to obtain samples is the first in the world. Figure 1 depicts a schematic of the prototype laser melting sampler. The sampler consists of a continuous-wave fiber laser ($\lambda = 1.55 \mu\text{m}$), an optical fiber (core diameter = 200 μm , our originally designed nozzle (2 mm outer ϕ), a sampling buffer system with an electromagnetic valve, and a computer that controls the positions of the sampling nozzle and the motorized stage on which an ice core is placed. This system makes it possible to analyze ice cores at a high depth resolution of ~ 2 mm scale, which corresponds to a temporal resolution of ~ 1 month in the case of a DF ice core. Our system is also applicable to a 1-year resolution (~ 3 cm) when sampling is performed in the direction of core depth.

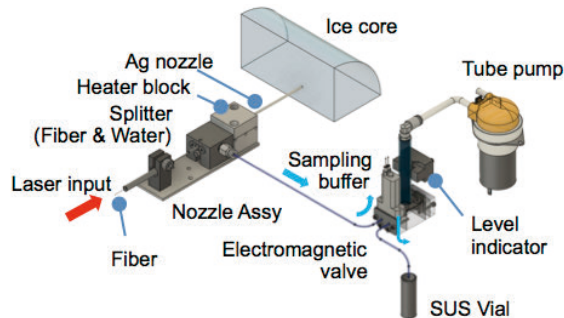


Fig. 1. Schematic of the ice-core laser melting sampling system.

^{*1} RIKEN Nishina Center

^{*2} RIKEN Center for Advanced Photonics



Fig. 2. Left figure shows a photo of melting ice with the nozzle intruding the dummy ice (bottom right) and the inside buffer being filled (bottom left). The right shows a filled vial.

In Fig. 1, the laser beam delivered by the optical fiber irradiates the target ice-core surface, and 1.5 mL of melted water (sufficient volume for our precision analysis) is sucked up through the nozzle and transported into our original SUS vial bottle by a peristaltic tube pump at a pressure drop of 1 atm. The nozzle and tube are kept above 0°C by the heaters installed inside the nozzle assembly.

We succeeded in continuous sampling into the vials using this prototype sampler. Figure 2 shows the result: the holes were vertically made as small as 2 mm ϕ on a dummy ice block ($\rho = 0.9 \text{ g/cc}$) by laser melting. For this purpose, a laser beam with a power of $\sim 1.3 \text{ W}$ was irradiated, and the nozzle intruding speed was set to 0.40 mm/s. The efficiency of collecting melted water was estimated to be $\sim 100\%$. As the first step, we set our target sampling time for a vial to 20 min, which was determined in concordance with the measurement time of *one* sample by *a single* isotope analyzer using the AGRG protocol developed based on our isotope measurements. By choosing optimum apparatus parameters and by using an automated *multi-nozzle* system that has already been equipped in our system, we plan to attain a higher throughput to handle many sample vials.

Our new technique has some advantages in comparison with the standard heater-melting continuous flow analysis method.¹⁾ They are as follows: 1) sampling zones are discrete to avoid mixing with each other, 2) the amount of sampling ice can be adequately minimized, and 3) fragile low-density ice cores are also applicable because the portion of a core is placed horizontally (Fig. 1). Making the most of these merits, we have started to perform our first application on Antarctic ice to study if there appear seasonal variations in the well-established temperature proxy (¹⁸O/¹⁶O) for the first time in the past ~ 30 years for direct comparison with the temperature measured in the area.

We are grateful to Michio Sakashita for supporting us with laser fiber treatment and Yu Vin Sahoo for preparing clear dummy ice blocks suitable for our experiments.

Reference

- 1) *e.g.*, R. Dallmayr *et al.*, Bull. Glaciol. Res. **34**, 11 (2016).

8. Accelerator

Revaluation of beam orbit calculation method for the injection line of AVF cyclotron after tuning pepper-pot emittance monitor

Y. Kotaka,^{*1} Y. Ohshiro,^{*1} H. Yamaguchi,^{*1} N. Imai,^{*1} Y. Sakemi,^{*1} T. Nagatomo,^{*2} T. Nakagawa,^{*2} M. Kase,^{*2} J. Ohnishi,^{*2} A. Goto,^{*2} K. Hatanaka,^{*3} H. Muto,^{*4} and S. Shimoura^{*1}

We developed a calculation method for the beam orbit from the Hyper ECR ion source to the AVF cyclotron using the 4D emittance measured by a pepper-pot emittance monitor¹⁾ named PEM_IH10^{2,3)} and evaluated it with the degree of fit, which is χ^2 divided by the degree of freedom (DOF) between two projections to an arbitrary coordinate axis made from both the measurement of other diagnostics and the beam orbit calculation. However, the dispersion of χ^2 is assumed to be the square of 10% of the highest value of the measurement. Subsequently, the method of processing the beam image on the fluorescent plate of PEM_IH10 recorded by a digital camera was improved.⁴⁾ This report is a summary of Ref. 4).

This year, as it was found that the degree of fit varied at different thicknesses of the fluorescent agent, the variation of the degree of fit was examined while varying the combination of the exposure time and gain and the thickness. The results of beam orbit calculations are compared with the beam profile monitor (BPM), which measures 3 axes of profiles set 867 mm behind PEM_IH10 using the 23.6-keV $^4\text{He}^{2+}$ ion beam of 100 μA . In this test, the degree of fit is defined by dividing the sum of 3 axes of χ^2 by the sum of 3 axes of DOF. The thickness is defined by dividing the weight by the area and density. The upper and lower tables of Fig. 1 show the degree of fit obtained from thickness of 1.9 and 34.6 μm , respectively. From these results, irrespective of the thickness, the measurement of PEM_IH10 can be homogenized if the gain and exposure time are optimized.

In order to revalue the beam orbit calculation method after the optimization with respect to the thickness of the he fluorescent agent, the degree of fit is examined using 4 beam intensities (124, 187, 196, and 308 μA) of 15.4 keV

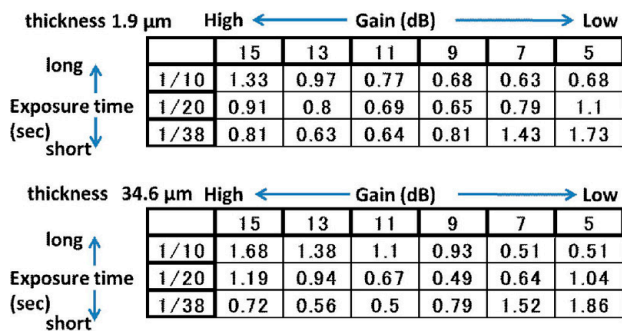


Fig. 1. Degree of fit compared with BPM when the thickness of the fluorescence agent and the exposure time and gain of the digital camera are varied. (top) thickness = 1.9 μm ; (bottom) thickness = 34.6 μm .

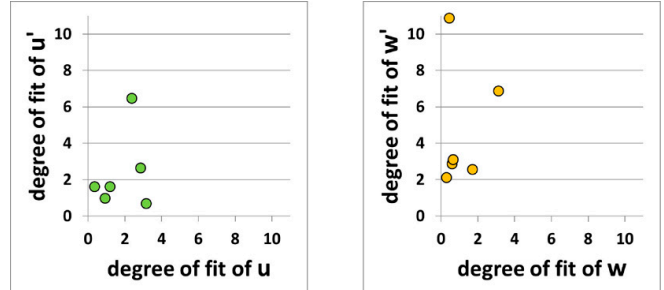


Fig. 2. Scatter plots showing the degree of fit of (left) (u, u') and (right) (w, w') compared with EM_I36.

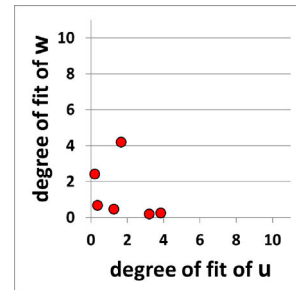


Fig. 3. Scatter plot showing the degree of fit of (u, w) compared with a BPM set 107.5 mm behind EM_I36.

$^4\text{He}^{2+}$, 100 μA of 12.6 keV $^2\text{H}^+$, and 214 μA of 12.8 keV $^2\text{H}^+$ by comparing the measurement of a 2D emittance monitor⁵⁾ (EM_I36) set 6.2 m behind PEM_IH10 with u and w coordinate axes perpendicular to the beam direction. The angles of u and w are indicated by u' and w' , respectively. The left and right of Fig. 2 show the scatter plot of the degree of fit of (u, u') and (w, w') of EM_I36, respectively. The u or w values of all samples are less than 4. However, 3 samples showed u' or w' values are greater than 6, and their widths of angular distributions from the beam orbit calculations were all smaller than those from the measurements for both u and w .

On the contrary, Fig. 3 shows the scatter plot of degree of fit of (u, w) of BPM set 107.5 mm behind EM_I36. It is found that all the degrees of fit are less than 4.2. This reason is not clear yet. We will check the tendency with more data. On the whole, the results of beam orbit calculation using 4D emittance measured by PEM_IH10 agree with real beam orbit so that they are useful for analysing real beam orbits.

References

- 1) T. Hoffmann *et al.*, AIP Conf. Proc. **546**, 432 (2000).
- 2) Y. Kotaka *et al.*, Proc. 13th Annual Meeting of PASJ, (2016), pp. 1072–1075.
- 3) Y. Kotaka *et al.*, Proc. 14th Annual Meeting of PASJ, (2017), pp. 1118–1122.
- 4) Y. Kotaka *et al.*, Proc. 16th Annual Meeting of PASJ, (2019), pp. 1109–1113.
- 5) Y. Kotaka *et al.*, RIKEN Accel. Prog. Rep. **41**, 96 (2008).

^{*1} Center for Nuclear Study, University of Tokyo
^{*2} RIKEN Nishina Center
^{*3} RCNP, Osaka University
^{*4} Center of General Education, Tokyo University of Science, Suwa

Non-thermal equilibrium effect on plasma window with large diameter

N. Ikoma,^{*1,*2} Y. Miyake,^{*1} M. Takahashi,^{*1} H. Okuno,^{*1} S. Namba,^{*3} K. Takahashi,^{*2} T. Sasaki,^{*2} and T. Kikuchi^{*2}

The disposal of high-level radioactive waste (HLW) is a serious social problem. To address it, a transmutation scheme of long-lived fission products (LLFP) employing a high-power accelerator, which provides deuteron beams of 400 MW, was proposed in the ImPACT Fujita program.¹⁾ In such a system, a beam window, which separates the accelerator and target region, is considered one of the key issues. A plasma window (PW),²⁾ which exploits a large pressure gradient generated by an arc plasma filling the discharge channel, is considered a promising candidate. However, the first PW invented by Hershcovitch²⁾ had an aperture of 2.36 mm, while the beam-spot size required in our case is 100 mm or larger.

Therefore, we developed a PW with a maximum diameter of 20 mm, as shown in Fig. 1, and demonstrated conductance reduction by the PW.³⁾ Furthermore, a comparison between the achieved cell pressure P_{cell} and the pressure estimated from Eq. (1)^{4,5)} suggested that the gas (or heavy-particle) temperature T_h was lower at larger diameters due to the low-input power density.³⁾

$$P_{cell} \simeq \sqrt{\frac{16\eta k T_h}{\pi m_h}} \frac{\sqrt{QL}}{r^2}, \quad (1)$$

where η , k , m_h , Q , r , and L are the viscosity of the gas, Boltzmann constant, mass of gas particles, mass flow rate, channel radius, and channel length, respectively.

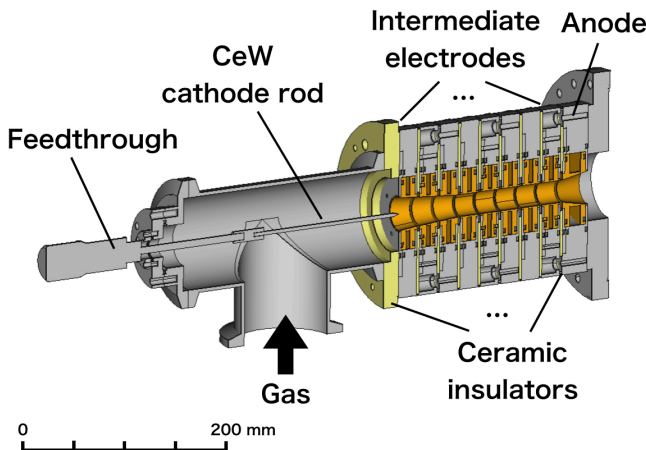


Fig. 1. Structure of the PW developed in this study.

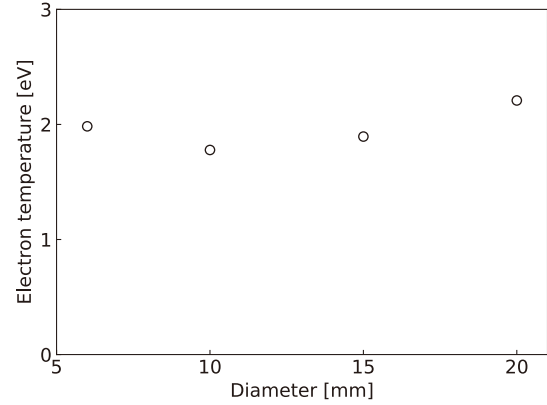


Fig. 2. T_e vs. PW diameter.

In this paper, the typical electron temperature T_e was estimated based on the report that the axial electron temperature variation in cascade arc devices is small.^{6,7)} The T_e is described by the Spitzer formula:

$$T_e \approx \left(\frac{\ln \Lambda}{2 \times 10^4 \sigma} \right)^{2/3}, \quad (2)$$

where σ is the average electrical conductivity of the plasma obtained from discharge current, voltage, and geometry of the channel, assuming a uniform cylinder. The Coulomb logarithm $\ln \Lambda$ was assumed as 10.

In contrast with the tendency of the heavy-particle temperature,³⁾ the estimated T_e shown in Fig. 2 was almost constant regardless of the diameters. This may indicate that the temperatures of electrons and heavy particles attain a non-equilibrium state as the diameter increases. Because T_h is the most important factor in the performance of the PW as described by Eq. (1), the non-equilibrium effect will be discussed with the conductance-reduction effect of plasma ignition.

This work was supported by RIKEN Junior Research Associate Program. Furthermore, this work was funded by ImPACT Program of Council for Science, Technology and Innovation (Cabinet Office, Government of Japan).

References

- 1) H. Okuno *et al.*, Proc. Jpn. Acad. Ser. B **95**, 430 (2019).
- 2) A. Hershcovitch, J. Appl. Phys. **78**, 5283 (1995).
- 3) N. Ikoma *et al.*, Plasma Fusion Res. **14**, 1206148 (2019).
- 4) W. A. J. Vijvers *et al.*, Phys. Plasmas **15**, 093507 (2008).
- 5) S. Huang *et al.*, Phys. Plasmas **21**, 123511 (2014).
- 6) J. J. Beulens *et al.*, Phys. Fluids B **3**, 2548 (1991).
- 7) J. J. Beulens *et al.*, Plasma Sources Sci. Technol. **2**, 180 (1993).

*1 RIKEN Nishina Center

*2 Graduate School of Engineering, Nagaoka University of Technology

*3 Graduate School of Engineering, Hiroshima University

Status report on update of alarm system and control system of magnet power supplies for RIBF

M. Komiyama,^{*1} A. Uchiyama,^{*1} M. Fujimaki,^{*1} M. Hamanaka,^{*2} M. Nishimura,^{*2} and N. Fukunishi^{*1}

We report the following two improvements of the RIBF control system. The first is the update of an alarm system, which supports the stability of beam delivery. The second is an improvement of the performance of the new module for the control system of magnet power supplies: NIO-C developed as a programmable logic controller (PLC) module.

In the RIBF facility, an alarm system has been operated along with the beam interlock system (BIS).¹⁾ We have applied an alarm system mainly to signals indicating abnormal conditions of hardware of the accelerator facility that may adversely affect accelerator tuning. We are monitoring the status of the following equipment with an alarm system now:

- (1) Vacuum pumps and valves associated with the pump system, such as the on/off status of turbo molecular pumps on beamline.
- (2) Vacuum pressure at the cyclotrons and beamline.
- (3) Various devices in the AVF cyclotron and its ion sources, such as the on/off status of the radio frequency (RF) system and status of current from the magnet power supply for the main coil.

The numbers of signals from the equipment listed above are 198, 74, and 18, respectively.

The alarm system has been operated using a tool in the Control System Studio (CSS)²⁾ and the Best Ever Alarm System Toolkit (BEAST).³⁾ The BEAST is a distributed alarm system consisting of Alarm Server, a CSS user interface (UI) for viewing current alarms, and a relational database for configuration and logging. The BEAST was first introduced in the RIBF control system in 2012, and it has been actively used in recent times at the AVF console in the RIBF control room. As the AVF console was moved to a new location in the summer of 2019, we updated the platform that operates the Alarm Server and relational database from a dedicated PC to a server running CentOS 7 in a virtual machine to ensure its stable operation. The BEAST was also updated to the latest version. The latest version of the CSS software has undergone major improvements over the previous version in the connection method for experimental physics and industrial control system (EPICS)⁴⁾ process variables (PVs). We newly employed CSS version 4.5.0 for the Alarm Server and PostgreSQL version 9.2.24 for the relational database, and CSS version 4.5.8 was newly installed on client PCs. In addition, with reference to the case of KEK, EPICS PVs dedicated to the alarm system are created separately from the EPICS PV used to control the equipment. They are operated on the EPICS input-output controller (IOC) dedicated to the alarm system. Changing the EPICS PV often

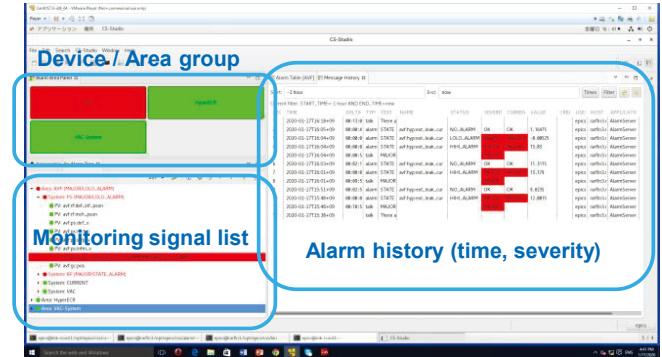


Fig. 1. Sample of the CSS UI for the BEAST operated at the RIBF control system. A green signal indicates normal operation, whereas red-highlighted signals are currently outputting an alarm (except for the alarm history part).

requires a restart of the EPICS IOC, which may affect beam delivery. The new system allows changing alarm conditions during beam delivery without affecting the beam delivery.

The second is related to the NIO-C successor developed as a PLC module in 2016.⁵⁾ We reported in Ref. 5) that we could successfully control 34 magnet power supplies by using the NIO-C successor in the same manner as the existing system, which uses the NIO-C developed based on the Versa Module Eurocard (VME) bus. However, it became clear that the command processing time of the NIO-C successor is longer with higher fluctuation than that of VME-based NIO-C. While the command processing time for one NIO-S was 11.8 ms on average and fluctuated in the range of 11.7–11.9 ms in the VME-based NIO-C system, the NIO-C successor system took 18.3 ms on average and fluctuated in the range of 4–37 ms. The speed is too slow in actual accelerator operation. After investigation, we found that the slow speed is caused by a logic of polling performed by NIO-C, which is one of the important functions of the NIO system. By improving the logic, the average command processing time was shortened to 7 ms on average, and the fluctuation range was narrowed down to 2.7–12.2 ms. The next step is to determine whether the new system shows the same performance in an actual operating environment, in which several NIO-Ss are connected to one NIO-C.

References

- 1) M. Komiyama *et al.*, RIKEN Accel. Prog. Rep. **39**, 239 (2006).
- 2) <http://controlsystemstudio.org/>.
- 3) <https://github.com/ControlSystemStudio/cs-studio/wiki/BEAST>.
- 4) <https://epics.anl.gov/>.
- 5) M. Komiyama *et al.*, Proc. PCaPAC2018, pp. 66–68.

^{*1} RIKEN Nishina Center

^{*2} SHI Accelerator Service Ltd.

Power supply backup system for injection and extraction magnets of cyclotrons

K. Kumagai*¹ and N. Fukunishi*¹

A large number of electromagnets are used to accelerate ion beams in the RIBF¹⁾. For example, in the case of the uranium-beam machine time, there are 500 electromagnets from RILAC2 to the end of SRC through RRC, fRC, and IRC, each of which is excited by a DC power supply with high current stability. As a high-quality beam cannot be emitted unless all power supplies are available, it is important to perform the regular maintenance of power supplies and to consider how to handle them if a failure occurs. In particular, in the case of a failure during the machine time, it is necessary to restore the power supply as quickly as possible to minimize downtime.

If any power supply fails, we attempt to repair it first. However, if the defective part cannot be identified immediately, the part is estimated to take time to repair, or a replacement is not at hand, it is necessary to consider whether another power supply can be used. As power supplies with relatively low output current, such as those for quadrupole magnets and steering magnets, have relatively small chassis and are easy to handle, it is easy to replace them with the same type of power supply used for other beam courses. Since the output current of the power supply for the trim coil and the dipole is not very large, about 500 A at maximum, it is possible to substitute a power supply for other courses. On the other hand, the main coil power supply for the four cyclotrons (RRC, fRC, IRC, and SRC) typically has an output of several hundred to several thousand amperes and several hundred volts, and no power supply can be replaced. Therefore, in the event of a failure, it is necessary to repair this power supply; therefore, we prepare as many spare parts as possible.

Each cyclotron has 4 to 5 injection magnets and 3 to 5 extraction magnets. These magnets require extremely high current of approximately 1000 A to 3500 A and various voltages ranging from 20 V to 120 V. Despite the large number of power supplies, the power supply chassis are large and need many thick output-current cables; therefore, it is difficult to relocate the power supply after a failure occurs. Therefore, a plan has been considered in which a power supply that can be replaced in the event of a failure is arranged at an appropriate place and used as a replacement for as many injection/extraction power supplies as possible by adding partial temporary wiring.

The fRC-EBM power supply, a power supply for the fRC Extraction Bending Magnet manufactured in 2012, was designed to be operated in the dual pattern of large current-low voltage (2800 A–65 V) and medium current-medium voltage (1500 A–100 V) in anticipation of use as an alternative power supply. The thyristor rectification part of the power supply is equipped with two units, which can be connected in parallel or series, and

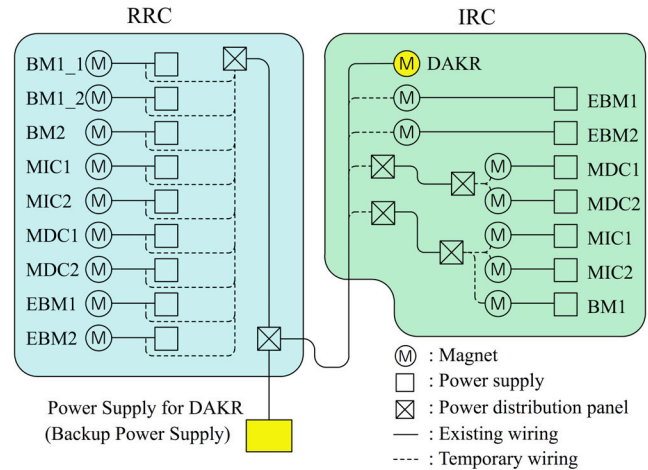


Fig. 1. Wiring layout of the backup power supply for the injection/extraction magnets of RRC and IRC.

the voltage-current ratio can be changed. In addition, the transistor driver is prepared in two patterns having different control constants. In 2014, we reassigned the power supply as that for the DAKR magnet on the IRC-E5 beam line, which is operated several times a year, and wired it so that it could be used as an alternative power supply for injection and extraction magnets of the RRC cyclotron (hereafter referred to as “backup power supply”). In 2019, the wiring was extended so that it could be used as a substitute for the power supply for injection and extraction magnets of the IRC cyclotron if a failure occurs. Figure 1 shows the current wiring layout of the backup power supply.

A malfunction of the RRC-EBM1 power supply occurred on November 13, 2019 during a preparation period for uranium machine time. It was caused by the failure of a shunt made of zeranin, a low-resistance alloy for high-precision current detection, immersed in cooling water and had been used since the power supply was manufactured in 1985. It was expected that it would take about a week to remove the failed shunt, install the DCCT, replace the accompanying control boards, and make overall adjustments. Therefore, we immediately decided against repairing, switched the RRC-EBM1 magnet to the backup power supply, and resumed operation on the same day.

In addition, to enable the immediate use of the alternative power supply in case of trouble, we installed AC 400 V power receiving equipment, cooling water piping for the alternative power supply, and wiring for the DC current output in various places. In this manner we are preparing to maintain the machine time.

Reference

- 1) Y. Yano, Proc. PAC07, TUYKI02, **700** (2007).

*¹ RIKEN Nishina Center

Improvement of beam stability by stabilizing the cooling-water temperature for the main and trim coils of IRC

R. Koyama,^{*1,*2} T. Maie,^{*1} K. Kumagai,^{*1} and N. Fukunishi^{*1}

Thermal stability is highly important for the stable operation of RIBF with a high-intensity beam. It makes the beam trajectory in a cyclotron stable and thereby reduces the heat load due to beam loss on the septum of the electrostatic deflection channel (EDC), especially of SRC. Consequently, the beam-tuning for obtaining a high-intensity beam is facilitated.

The periodic fluctuation of the heat load on SRC-EDC has been observed with high-intensity beams such as 345 MeV/nucleon ^{238}U since 2017. It has been the fastest and most effective method to adjust the rf voltage and/or phase of RRC and/or fRC to suppress the increase in heat load, but such an adjustment has a negative impact on the improvement of overall beam-transmission efficiency.

An investigation performed at the end of 2018 clarified that the period of such heat-load fluctuations is synchronized with the fluctuation period of the cooling-water temperature for the main and trim coils of IRC (upstream cyclotron of SRC). This synchronization is caused by the periodic movement of the temperature-regulating valves for the secondary cooling water of these coils with 0–100% opening, which results from some kind of failure of the temperature control system.

In a 2019 operation of a 345 MeV/nucleon ^{238}U , the temperature of both the primary and secondary cooling water of the main and trim coils of IRC were drastically

stabilized by fixing the valve openings to 50%, and the resulting extraction beam from IRC was stabilized.

The correlation between the values before and after improvement are shown in the left and right part of Fig. 1, respectively, where the details are as follows (the itemization corresponds to that in Fig. 1):

- Temperature of the primary cooling water for the main and trim coils of IRC. The fluctuation ranges of both were improved from $\sim 6^\circ\text{C}$ to 0.2°C .
- Rising temperature of SRC-EDC due to the beam loss. It was improved from $8 \pm 1^\circ\text{C}$ to $6 \pm 0.5^\circ\text{C}$.
- Opening of temperature-regulating valves for the secondary cooling water of the main and trim coils of IRC. They were fixed to 50% for stabilization.
- e) Stability of the beam intensity and phase observed by the phase probe K01 (~ 5 m downstream from IRC). The fluctuation range of beam intensity is improved from 8% to 3% and that of beam phase is improved from 0.1 ns to 0.01 ns.

The improvement of the thermal stability of IRC made the extraction beam from IRC and the beam trajectory in SRC stable, and thereby, a tuning procedure for the suppression of heat load on SRC-EDC consistent with the overall beam-transmission efficiency has been facilitated. Consequently, we achieved the highest intensity thus far of 94 particle nA for 345 MeV/nucleon ^{238}U which is also attributed to other continuous efforts.

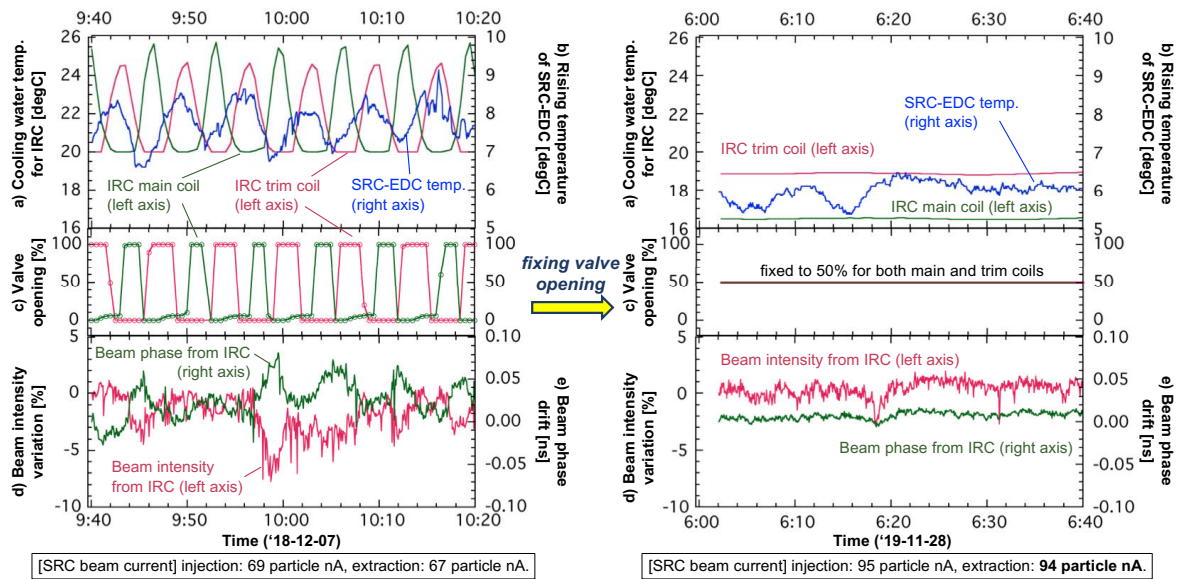


Fig. 1. Stabilizing effect of cooling-water temperature for the main and trim coils of IRC in a 345 MeV/nucleon ^{238}U operation. The data acquired before and after stabilization are indicated on the left and right part, respectively.

^{*1} RIKEN Nishina Center

^{*2} SHI Accelerator Service Ltd.

Interlock signal application from radiation monitoring ion chamber for SRC

M. Nakamura,^{*1} K. Yamada,^{*1} A. Uchiyama,^{*1} H. Okuno,^{*1} and M. Kase^{*1}

Recently, we attempted to monitor the radiation due to beam loss in the RIBF using ionization chambers (ICs).^{1,2)} Usually, we investigate the radiation from the electrostatic deflection channels (EDC) at RRC, fRC, IRC, and SRC.³⁾ On the other hand, the intensities of the ion beams generated by RIBF increase in every year. Accordingly, the management of the beam loss at important positions in RIBF is increasingly important for safe and efficient operation of RIBF. In this study, we investigated the IC signal near the EDC of SRC and attempted to input the alarm signal from this IC to the beam interlock system (BIS) of RIBF in the user time of a $^{238}\text{U}^{86+}$ beam.

Usually, the alarm levels of the ICs are determined by comparing the signals from the ICs with those from thermocouples set at the septum of the EDC of SRC.⁴⁾ Hence, the temperatures of the first septum were compared with the signals of the IC set near the EDC of SRC from October 15 to December 10 in 2018. The results are shown in Fig. 1. The data demonstrated little dispersion, and we can obtain a calibration curve (red line). From this curve, we can recognize that the voltage of the IC became approximately 1.1 V when the temperature of the first septum became 42°C .⁴⁾

From November 12 to December 6 in 2019, the $^{238}\text{U}^{86+}$ ion beam was accelerated to 345 MeV/nucleon. Before this acceleration time, we set the alarm level of IC at 1.1 V to the BIS.

Investigations were performed during this term by inputting the alarm signal to the BIS. However, in this

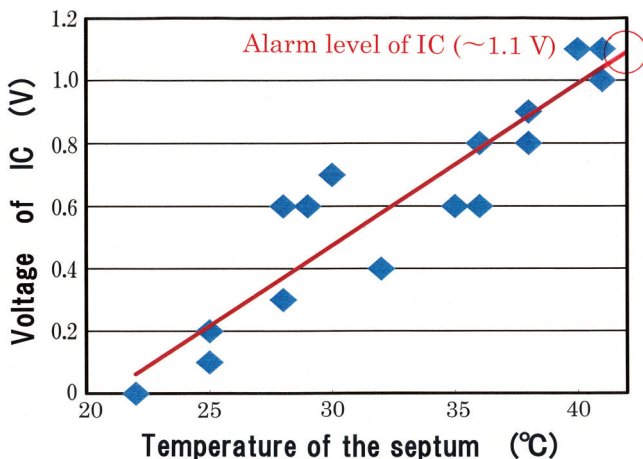


Fig. 1. Correlation between the IC voltage and the temperature of the first septum of EDC.

Table 1. Frequencies of troubles for which the BIS was engaged during the acceleration of the $^{238}\text{U}^{86+}$ beam in 2019.

SRC-EDC-ARC	1080
RF-Tr	450
PS-Tr	375
BF-Tr	282
Others	1614
Total	3801

term, we could not observe signals stronger than 1.1 V, which was the estimated alarm level. Consequently the BIS from IC near the EDC did not act in this time. From these results, we could consider that the operation of the SRC in this term was completed favorably.

Subsequently, we investigated the frequency at which the BIS of all RIBF systems was engaged from October 23 to December 10 in 2018. In this term, BIS was engaged 19049 times. This result shows that BIS was engaged about 389 times per day. On the other hand, from November 12 to December 6 in 2019, BIS was engaged 3801 times. This result shows that BIS was engaged about 152 times per day. By comparing these two results, we could recognize that the operations of RIBF in 2019 were completed more safety and efficiently than in 2018.

Next, we investigated the type of alarm signals put into BIS during the acceleration of the $^{238}\text{U}^{86+}$ beam in 2019. BIS engagement via arc discharge at the EDC of SRC (SRC-EDC-ARC) was observed most frequently. BIS engagement due to a trouble of RF (RF-Tr) had the second-highest frequency. BIS engagement due to troubles of a power supply in RIBF (PS-Tr) and due to troubles of baffles (BF-Tr) were also frequently observed. The frequencies of these troubles are listed in Table 1.

Considering these results, we will investigate the correlation of the IC voltage and the conditions under which the arc discharge at the EDC of SRC is generated in the next step. Subsequently, we will re-examine the alarm level of IC.

References

- 1) M. Nakamura *et al.*, RIKEN Accel. Prog. Rep. **52**, 114 (2018).
- 2) M. Nakamura *et al.*, RIKEN Accel. Prog. Rep. **51**, 139 (2017).
- 3) M. Nakamura *et al.*, RIKEN Accel. Prog. Rep. **50**, 152 (2016).
- 4) M. Nakamura *et al.*, RIKEN Accel. Prog. Rep. **49**, 146 (2015).

*1 RIKEN Nishina Center

Nishina RIBF water-cooling system operational report 2019

T. Maie,*¹ K. Kusaka,*¹ Y. Watanabe,*¹ E. Ikezawa,*¹ M. Oshima,*² H. Shiraki,*² H. Hirai,*² K. Kobayashi,*³ and J. Shibata*³

Operation condition

In 2019, the cooling systems of Nishina and RIBF were operated for a slightly longer period than the accelerators. Excluding some installation that was run continuously, RIBF's cooling systems were operated for approximately four months. Furthermore, Nishina's cooling systems AVF-standalone, AVF+RRC, AVF+RRC+IRC, and RI-LAC II+RRC+GARIS-II were operated for approximately eight months.

No huge troubles that could cause the long-term interruption of accelerator operation occurred, and the cooling systems operated stably with the exception of some minor problems.

Trouble report

Many issues occurred because of the cooling systems, and all of the inverters were unexpectedly renewed owing to these issues. There was a malfunction of the bearing of the cooling water pump motor, an issue with the control valve of cooling water for stable supply, and a failure of the inverter for the cooling-water pump due to aging.

Periodic maintenance

- (1) Cleaning of the cooling towers
- (2) Inspection and overhauling of the cooling-water pumps
- (3) Inspection of the inverter for the RIBF cooling-water pumps
- (4) Replacement of some superannuated hoses, joints and valves used in the system
- (5) Cleaning of the strainers and filters used in the deionized water production system
- (6) Extension of the sensing wires of the water-leakage alarm to floors of new areas
- (7) Flushing work of the cooling-water pipe that was blocked by dirt

New installations and improvements

The cooling systems for the superconducting RI-LAC, which had been constructed in the previous year, started operation for commissioning. In addition, new cooling systems, which were built for increasing the



Photograph of the RRC Cooling capacity augment equipment

cooling capacity of RRC and for stabilizing the cooling-water temperature of RRC was safely completed in March 2019. While the implementation of new systems has not started yet, reasonable data could be obtained during the trial operation. It is expected that a progress report concerning implementation will be available in the next year.

References

- 1) T. Maie *et al.*, RIKEN Accel. Prog. Rep. **51** (2017).
- 2) T. Maie *et al.*, RIKEN Accel. Prog. Rep. **52** (2018).

*¹ RIKEN Nishina Center

*² Nippon Air Conditioning Service Co., Ltd.

*³ SHI Accelerator Service Co., Ltd.

9. Instrumentation

Development of ZeroDegree Large Acceptance Dispersive mode

H. Takeda,^{*1} N. Fukuda,^{*1} H. Suzuki,^{*1} Y. Shimizu,^{*1} D. S. Ahn,^{*1} T. Komatsubara,^{*1} N. Inabe,^{*1} K. Yoshida,^{*1} S. Chen,^{*2,*3} M. Wada,^{*3} A. Takamine,^{*1} P. Doornenbal,^{*1} and R. Tsunoda^{*4}

The ZeroDegree spectrometer¹⁾ is an RI-beam delivery line following the BigRIPS separator.²⁾ Four operating modes are provided: two achromatic and two dispersive modes with different momentum resolutions and acceptances. Among them, the Large Acceptance Achromatic (LAA) mode is the standard one, and most experiments have been conducted in this mode so far.

A parasitic experiment is proposed using ZeroDegree, where the online commissioning of a SLOWRI gas catcher and a multi-reflection time-of-flight mass spectrograph (MRTOF-MS) located at the final focal plane F11 will be performed symbiotically with other ZeroDegree experiments. For this purpose, mono-energetic beams are desired to improve the stopping efficiency because the material thickness of a gas cell is very thin.

In order to realize such beams, a straight-forward solution is to employ a mono-energetic wedge degrader at the dispersive focal plane (F9 or F10) in the standard LAA mode. However, transmission loss due to the degrader may be a problem. Another option is to use a dispersive mode of ZeroDegree with a mono-energetic degrader located immediately before the gas cell to minimize the transmission loss. Both the previously prepared dispersive modes (MRD and HRD¹⁾) are undesirable because they have a smaller acceptance compared to the LAA mode as a result of aiming at a high momentum resolution. Thus, a new dispersive mode with a larger acceptance, named the Large Acceptance Dispersive (LAD) mode, was developed. Figure 1 shows the first-order ion optics in the LAD mode of ZeroDegree. The horizontal acceptance and momentum resolution $p/\Delta p$ are ± 35 mrad and 2100, respectively, while they are ± 20 mrad and 4200 for the MRD mode and ± 10 mrad and 6500 for the HRD mode, respectively.

A machine study with a ^{80}Zn beam produced by the in-flight fission of a ^{238}U beam at 345 MeV/nucleon with a 4 mm-thick Be target was conducted to examine the

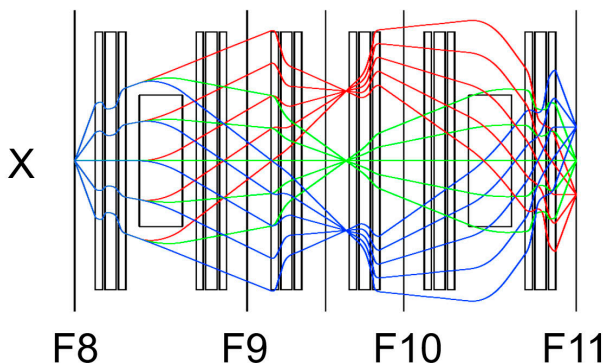


Fig. 1. First-order ion optics in the LAD mode of ZeroDegree in the horizontal (X) plane. Red, green, and blue curves correspond to the momentum deviation $\delta = -1.5$, 0 , and 1.5% , respectively.

Table 1. Measured (Exp.) and designed (COSY) F8-F11 first-order transfer matrix elements in the LAD mode. The units are mm, mrad, and % in x , a , and δ , respectively.

	$(x x)$	$(x a)$	$(a x)$	$(a a)$	$(x \delta)$	$(a \delta)$
Exp.	1.02	0.27	-0.35	0.89	20.3	-5.49
COSY	1.0	0.0	0.0	1.0	21.0	0.0

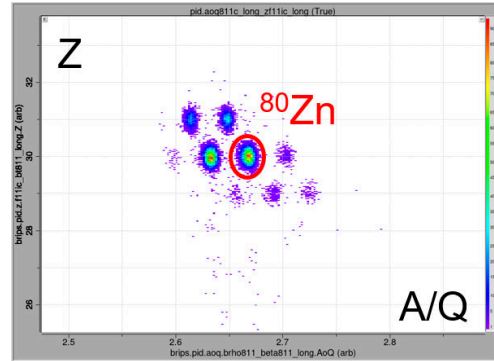


Fig. 2. Z versus A/Q plot measured in the ZeroDegree LAD mode. The ^{80}Zn beam is clearly separated.

LAD mode. The LAA mode with a mono-energetic degrader (LAAmono mode) was also tested³⁾ in the same machine study. We report the results for the LAD mode here.

The RI beam was identified and tagged⁴⁾ in the BigRIPS separator and delivered to the ZeroDegree spectrometer. We first measured the transfer matrix elements in the LAD mode. The results are summarized in Table 1 and compared with the designed values calculated by COSY INFINITY. The main features are well reproduced.

By using these matrix elements, particle identification was performed independently in the ZeroDegree spectrometer. The measured Z versus A/Q particle identification plot is shown in Fig. 2. The A/Q resolution was measured at narrow ($\pm 0.1\%$) and wide ($\pm 3\%$) momentum slit settings. The results were 0.15% and 0.17% in σ , respectively. Higher-order aberration correction is required to reach an expected value of 0.05% estimated from detector resolutions and ion-optical parameters. Analysis is in progress.

The transmission efficiency was also measured by comparing the number of ^{80}Zn with BigRIPS and ZeroDegree. The results were 85.5% (narrow) and 70.2% (wide). The transmission losses mainly occur at F10, where the beam spreads for a large momentum deviation (δ) (see Fig. 1). The readjustment of ion optics is necessary to reduce the beam spread.

References

- 1) T. Kubo *et al.*, Prog. Theor. Exp. Phys. **2012**, 03C003 (2012).
- 2) T. Kubo, Nucl. Instrum. Methods Phys. Res. B **204**, 97 (2003).
- 3) S. Chen *et al.*, in this report.
- 4) N. Fukuda *et al.*, Nucl. Instrum. Methods Phys. Res. B **317**, 323 (2013).

*1 RIKEN Nishina Center

*2 Department of Physics, The University of Hong Kong

*3 KEK Wako Nuclear Science Center

*4 Center for Nuclear Study, the University of Tokyo

Large-acceptance achromatic mode with mono-energetic wedge degrader for ZeroDegree spectrometer

S. Chen,^{*1,*2} H. Takeda,^{*3} M. Wada,^{*2} P. Doornenbal,^{*3} D. S. Ahn,^{*3} N. Fukuda,^{*3} S. Imura,^{*3} H. Ishiyama,^{*3} J. Liu,^{*1,*2} M. Rosenbusch,^{*2} P. Schury,^{*2} Y. Shimizu,^{*3} H. Suzuki,^{*3} A. Takamine,^{*3} and K. Yoshida^{*3}

An experiment was proposed to achieve the online commissioning of the SLOWRI gas catcher and multi-reflection time-of-flight (MRTOF) mass measurements symbiotically with in-flight experiments using the ZeroDegree spectrometer.¹⁾ A 50-cm-long cryogenic He gas cell will be placed downstream of the F11 chamber to provide low-energy radioactive isotopes from the energetic radioactive isotope (RI) beams of ZeroDegree. For ZeroDegree, the typically used large-acceptance achromatic (LAA) mode provides beams with a large energy spread at the F11 focal plane, resulting in a relatively low stopping efficiency ($\sim 1\%$) in the gas cell. In order to improve the stopping efficiency, mono-energetic beams are preferred. Two ion optic settings were proposed to make such beams: the large-acceptance dispersive (LAD) mode²⁾ and the LAA mode with a mono-energetic wedge degrader (LAAmono). The transmission efficiencies and particle identification resolutions were investigated for both modes. Herein, we report the results of the LAAmono mode.

A test was performed with a typical experimental con-

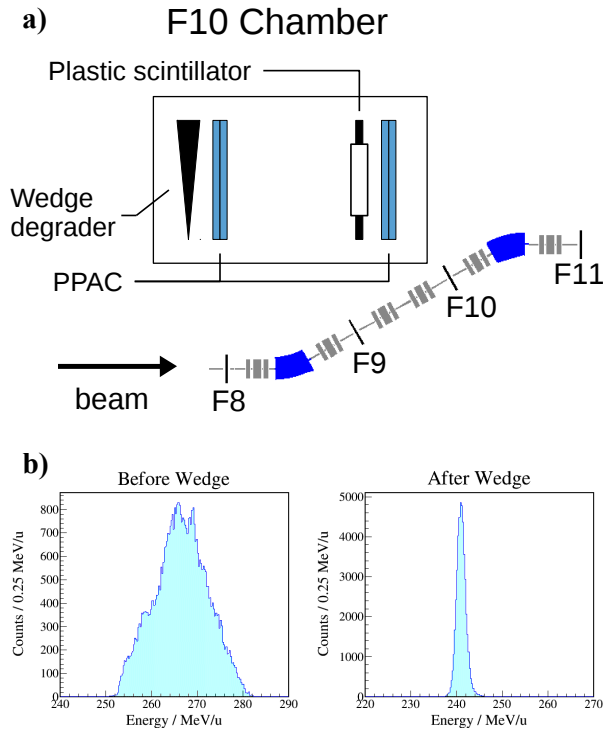


Fig. 1. (a) ZeroDegree setup for the LAAmono mode. (b) Energy distributions of ^{80}Zn before (left) and after (right) the F10 wedge degrader.

^{*1} Department of Physics, The University of Hong Kong
^{*2} KEK Wako Nuclear Science Center
^{*3} RIKEN Nishina Center

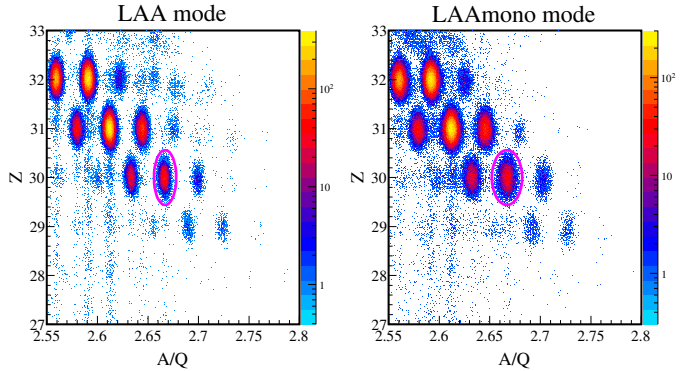


Fig. 2. Particle identification plots from the LAA mode (left) and LAAmono mode (right). The ^{80}Zn isotopes are indicated by the red ellipse in both plots.

dition for an in-beam gamma-ray experiment. A combination of a 345 MeV/nucleon ^{238}U primary beam and a 4-mm-thick ^9Be target was used to produce radioactive beams around ^{79}Cu at ~ 270 MeV/nucleon. Both BigRIPS and ZeroDegree were tuned for the ^{80}Zn isotopes. The LAA and LAAmono mode were applied in turns for the ZeroDegree spectrometer. In the LAAmono mode, an Al wedge degrader with an angle of 20.8 mrad and a center thickness of 2.85 mm was employed at the momentum-dispersive focal plane (F10) of the standard LAA mode, as shown in Fig. 1(a). The energy distribution of ^{80}Zn isotopes after the wedge degrader [Fig. 1(b) right] shows a good mono-energetic property. A stopping efficiency of $\sim 5\%$ in the gas cell was estimated from this distribution.

The particle identification (PID) for both modes was performed using the time of flight from F8 to F11, reconstructed $B\rho$ between F8 and F10, $B\rho$ between F10 and F11, and ΔE measured using the F11 ionization chamber. The PID plots from both modes are shown in Fig. 2. The one from the LAAmono mode exhibits a resolution slightly worse than the one from the LAA mode, but the resolution was sufficient to separate all the different isotopes well. The transmission efficiencies of ZeroDegree were studied by comparing the statistics of the ^{80}Zn isotopes in BigRIPS and ZeroDegree PID plots. The LAAmono mode keeps 95% efficiency in comparison with the standard LAA mode in this test experiment. This efficiency is consistent with the value estimated from LISE++ calculations, which suggests that the main loss originates from the reaction losses in the wedge degrader.

References

- 1) M. Wada, RIKEN Proposal NP1912-RIBF176.
- 2) H. Takeda, in this report.

New ion-optical operating modes of BigRIPS and ZeroDegree spectrometer for production and separation of high-quality rare isotope beams and high-resolution spectrometer experiments[†]

H. Takeda,^{*1} Y. K. Tanaka,^{*2} H. Suzuki,^{*1} D. S. Ahn,^{*1} B. Franczak,^{*2} N. Fukuda,^{*1} H. Geissel,^{*2} E. Haettner,^{*2} N. Inabe,^{*1} K. Itahashi,^{*1} T. Komatsubara,^{*1} T. Kubo,^{*1,*3} K. Kusaka,^{*1} S. Y. Matsumoto,^{*4} D. Murai,^{*1} T. Nishi,^{*1} M. Ohtake,^{*1} C. Scheidenberger,^{*2} Y. Shimizu,^{*1} T. Sumikama,^{*1} H. Ueno,^{*1} T. Uesaka,^{*1} Y. Yanagisawa,^{*1} and K. Yoshida^{*1}

BigRIPS¹⁾ is a powerful two-stage in-flight separator that has been used for frontier experiments with exotic nuclei for more than a decade. The ion-optical system is very versatile owing to the multi-stage structure of BigRIPS combined with the ZeroDegree spectrometer²⁾ or the Superconducting Ring Cyclotron (SRC). Various optical modes can be flexibly realized according to the purpose of experiments. Two categories of developments are presented here.

One is a new operating mode of BigRIPS aiming at a higher ion-optical resolving power. BigRIPS itself has a two-stage structure consisting of F0-F2 and F3-F7 with a matching section F2-F3 in between. In each stage, the isotopic separation of projectile fragments at an overall achromatic focus is performed in the $B\rho$ - ΔE - $B\rho$ operation with an achromatic energy degrader positioned in a dispersive focal plane. In principle, the two stages act independently and their isotopic separation powers can be added or subtracted depending on the sign of the optical magnification in the matching section F2-F3. In the standard operating mode of BigRIPS, the two spatial separations with energy degraders are subtractive. The ion-optical solution for adding the $B\rho$ - ΔE - $B\rho$ separation power (the additive mode) is obtained by adding an x -focus at F2.5. The spatial-separation performance of the standard and additive modes of BigRIPS is demonstrated in the simulation with different combinations of achromatic F1- and F5-degraders. With the resulting increased spatial separation power, the isotopic background can be substantially reduced. On the other hand, the standard mode has a slightly better overall transmission and is superior in providing an isotope cocktail focused on a small-area detector or a secondary target. One can favorably use either the standard or the new additive mode depending on the experimental requirements and priorities.

Higher ion-optical resolving powers of the first and second BigRIPS stages are also investigated with the goals of further reducing the background and yielding

access to new isotopes of heavier elements. First, the resolving power of the second stage was doubled (the high-resolution Ddouble mode³⁾). Improved particle identification was confirmed by the first test experiments. The simulation of a test case indicated that the increased resolving power of both the first and second stages in the additive mode can reduce the background to a large extent. The actual use of the proposed and prepared additive, standard, and higher-resolution ion-optical modes primarily depends on the detailed goals of future BigRIPS experiments.

The other development is a dispersion-matched system with BigRIPS for high-resolution spectrometer experiments. The BigRIPS and ZeroDegree spectrometer are presently two independent, coupled achromatic systems. A new dispersion-matched mode of BigRIPS and ZeroDegree will enable novel experiments. In this experimental scenario, the F8 focal plane is dispersive and accommodates the secondary target. The secondary target can be viewed, *e.g.*, by the γ -ray detector array, and thus, high-resolution momentum measurements after a removal reaction can be performed at F11 in coincidence with γ -spectroscopy.

For high-resolution spectroscopy experiments with high-intensity light projectiles, SRC and BigRIPS can be operated as a dispersion-matched system. In this mode, the dispersive beamline from SRC to F0 and the BigRIPS stages up to F5 form an overall achromatic system. The momentum spread of high-intensity primary beams from the SRC is canceled in the position spectra at F5, for instance, in the experiments studying pionic states. The first experimental tests of the proposed ion-optical mode have been successfully performed.

The described different ion-optical developments will be a base for novel BigRIPS experiments with exotic nuclei and mesic atoms, and thus, contribute to a better understanding of the strong interaction and properties of hadronic matter.

References

- 1) T. Kubo, Nucl. Instrum. Methods Phys. Res. B **204**, 97 (2003).
- 2) T. Kubo *et al.*, Prog. Theor. Exp. Phys. **2012**, 03C003 (2012).
- 3) H. Suzuki *et al.*, RIKEN Accel. Prog. Rep. **46**, 155 (2013).

[†] Condensed from the article in Nucl. Instrum. Methods Phys. Res. B **463**, 515 (2020)

^{*1} RIKEN Nishina Center

^{*2} GSI Helmholtzzentrum für Schwerionenforschung GmbH

^{*3} Facility for Rare Isotope Beams and National Superconducting Cyclotron Laboratory, Michigan State University

^{*4} Department of Physics, Kyoto University

Purification of slowed-down RI beam

T. Sumikama,^{*1} D. S. Ahn,^{*1} N. Fukuda,^{*1} N. Inabe,^{*1} T. Komatsubara,^{*1} K. Kusaka,^{*1} M. Ohtake,^{*1} H. Sakurai,^{*1} Y. Shimizu,^{*1} H. Suzuki,^{*1} H. Takeda,^{*1} Y. Yanagisawa,^{*1} K. Yoshida,^{*1} M. Dozono,^{*2} N. Imai,^{*2} S. Michimasa,^{*2} R. Tsunoda,^{*1,*2} Y. X. Watanabe,^{*3} M. Hausmann,^{*4} and O. Tarasov^{*1,*5}

The purity of a slowed-down RI beam at the second stage of the BigRIPS separator¹⁾ is important for particle identification (PID) under the condition of a total rate of 10^5 pps or higher.²⁾ High-purity slowed-down RI beams are desirable for experiments at BigRIPS and the OEDO beamline.³⁾ A high-intensity purified slowed-down exotic RI beam (HIPSER) concept is proposed to obtain high-intensity and high-purity RI beams using two-stage separation with two thick wedge degraders before measurement using beamline detectors for PID. The HIPSER concept consists of three technical components:

- (1) purification of the RI beam using the two-stage separation,
- (2) two-step momentum compression, and
- (3) transport of three charge states coupled with PID using a time-of-flight (TOF) measurement after the purification.

In this report, we focus on the RI-beam purification.

An experiment to verify the HIPSER concept was performed using a ^{107}Pd beam produced with the BigRIPS separator at RIKEN RIBF. The ^{107}Pd beams were separated at the first stage of BigRIPS using a

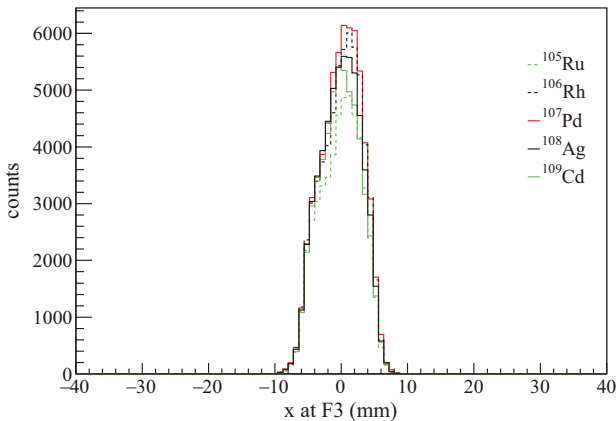


Fig. 1. Horizontal-position distributions of ^{107}Pd and its isotones at F3. The results of ^{105}Ru , ^{106}Rh , ^{107}Pd , ^{108}Ag , and ^{109}Cd are shown by the green-dashed, black-dashed, red-solid, black-solid, and green-solid lines, respectively.

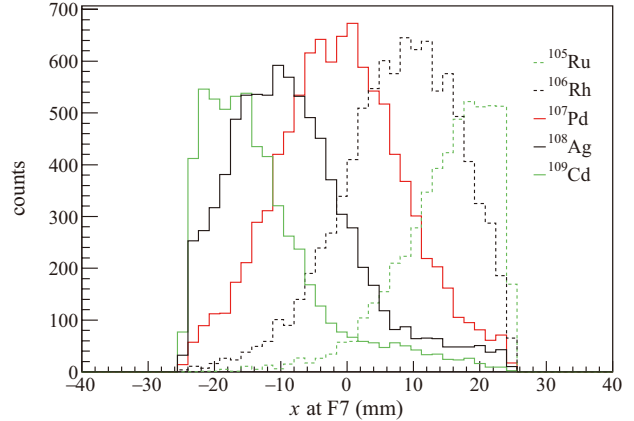


Fig. 2. Same as Fig. 1 but for the positions at F7.

wedge degrader with a thickness of 4.5 mm at F1 and the F2 slit with a ± 5 -mm setting. The thickness-to-range ratio (d/R) was 0.47. The energy was slowed down from 254 to 174 MeV/nucleon. The contaminants at F2 were isotones of ^{107}Pd , since the horizontal position x_{F2} of ^{107}Pd at F2 were the same as those of the isotones. Figure 1 shows x_{F3} distributions of ^{105}Ru , ^{106}Rh , ^{107}Pd , ^{108}Ag , and ^{109}Cd beams measured at F3. The positions at F2 and F3 show the relation, $x_{F3} = -x_{F2}$. The central values of the x_{F3} distribution for these RI beams were the same.

With a thicker wedge degrader at F5, the ^{107}Pd beam could be separated from its isotones.^{1,2)} The second wedge degrader at F5 had a thickness of 3.5 mm ($d/R = 0.69$). The F7 position x_{F7} of the ^{107}Pd beam was separated from the isotones, as shown in Fig. 2. By setting the F7 slit as $-10 \text{ mm} < x_{F7} < +5 \text{ mm}$, the purity of ^{107}Pd was obtained as 32%. The beam energy between F5 and F7 was 78 MeV/nucleon. The TOF measurement for the three charge states was performed at the ZeroDegree spectrometer. The charge-state separation at the ZeroDegree spectrometer, influence of higher-order aberration, and beam-energy broadening due to energy-loss straggling will be investigated in a future analysis.

References

- 1) T. Kubo, Nucl. Instrum. Methods Phys. Res. B **204**, 97 (2003).
- 2) T. Sumikama *et al.*, Nucl. Instrum. Methods Phys. Res. B **376**, 180 (2016).
- 3) S. Michimasa *et al.*, Prog. Theor. Exp. Phys. **2019**, 043D01 (2019).

^{*1} RIKEN Nishina Center

^{*2} Center for Nuclear Study, University of Tokyo

^{*3} Wako Nuclear Science Center, KEK

^{*4} FRIB, MSU

^{*5} NSCL, MSU

Thermal model simulation of high-power rotating target for BigRIPS separator

K. Yoshida,^{*1} Z. Korkulu,^{*1} Y. Yanagisawa,^{*1} and T. Kubo^{*1}

A realistic thermal-model simulation is particularly important to evaluate the beam-power tolerance of the high-power rotating target system of BigRIPS separator,^{1,2)} which has been successfully operating at RIBF since 2007. The target system was designed to withstand a beam power of 82 kW, which corresponds to the goal beam intensity of 1 particle μA ($\text{p}\mu\text{A}$) for a ^{238}U beam at 345 MeV/nucleon. The available beam intensity at RIBF was 13 kW so far, less than 20% of the goal. Therefore, thermal-model simulations were utilized to estimate the thermal behavior of the target system for high-intensity beams from the observation at lower beam intensities.

Many efforts¹⁻⁵⁾ have been devoted to the thermal model simulations of the target systems with finite-element ANSYS code. In the simulations, the rotating target was modeled using a mass transport option of ANSYS⁶⁾ to describe the rotating motion. The model worked fine at the design stage⁴⁾ but has been less usable because a recent version of ANSYS limits the use of mass transport only for motion slower than the thermal diffusion speed. Since the rotating target distributes the heat load by a fast rotating motion, the restriction prevents the simulation in the operational condition of the rotating target.

A new model of the rotating target was developed to avoid the restrictions. In the new model, the target itself is fixed, and a heat source moves along the circumference of the target. As shown in Fig. 1, many heat sources with a square shape of 1 mm by 1 mm were defined along the circle of the beam trajectory, and each source was excited by a heat load at a slightly different timing along the trajectory. Thus, the rotation of the heat source was successfully accounted for in the transient thermal calculation of ANSYS. In order to obtain the temperature distribution of a rotating target at the steady state, we have

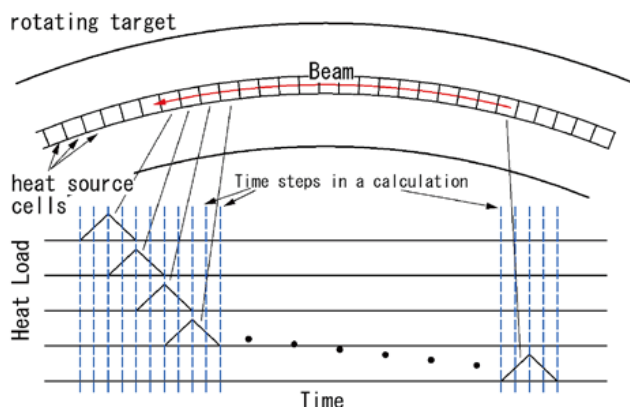


Fig. 1. Model of the rotating target. Graphs are the time structure of heat loads applied to heat source cells.

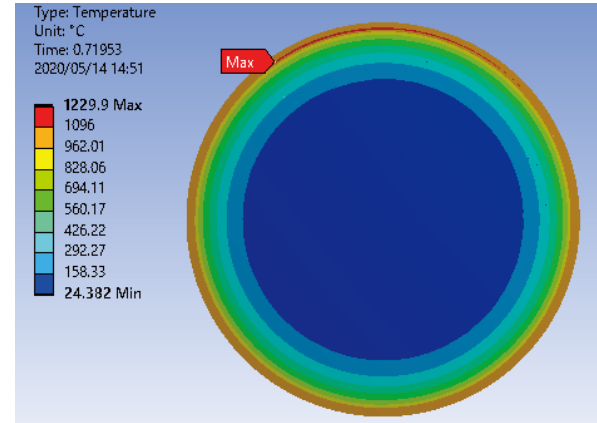


Fig. 2. Temperature distribution of the rotating target for irradiation with a ^{238}U beam at 345 MeV/nucleon, 1 $\text{p}\mu\text{A}$.

to simulate whole thermal equilibration process starting with the room-temperature target. More than 400 rotations of a spot heat source were necessary to obtain the saturation of the temperature. This process can be shortened by starting with the temperature distribution of a time-averaged heat source, which was calculated by steady-state thermal calculations with a time-averaged circular heat source. A nearly steady temperature distribution was obtained after 3–4 rotations of the spot heat source in this case.

A simulation for the case of a ^{238}U beam at an energy of 345 MeV/n and 1 $\text{p}\mu\text{A}$ impinging on a 2-mm-thick Be target was performed, and the resulting temperature distribution is shown in Fig. 2. Heat transfer coefficients of 10.5 and 3 $\text{kW}/\text{m}^2\text{K}$ were used for thermal contacts between the cooling water and cooling disk and between the cooling disk and Be target, respectively. As shown in Fig. 2, the highest temperature of 1230°C indicated by the “Max” label was obtained at the beam spot. Starting at the beam spot, the high-temperature region was spread along the beam trajectory. The calculation shows that the Be target does not melt in the heat of the beam since the melting point of Be is 1287°C. The maximum temperature of the calculation for ^{238}U beam at 30 pA was 66°C, which is consistent with the measured temperature of 63.6°C at RIBF. Thermo-mechanical calculations are in progress to check the thermal deformation or destruction of the target.

References

- 1) A. Yoshida *et al.*, Nucl. Instrum. Methods Phys. Res. A **521**, 65 (2004).
- 2) A. Yoshida *et al.*, Nucl. Instrum. Methods Phys. Res. A **590**, 204 (2008).
- 3) A. Yoshida *et al.*, RIKEN Accel. Prog. Rep. **35**, 152 (2002).
- 4) A. Yoshida *et al.*, RIKEN Accel. Prog. Rep. **37**, 295 (2004).
- 5) Z. Korkulu *et al.*, RIKEN Accel. Prog. Rep. **52**, 132 (2019).
- 6) ANSYS. Inc Product Release 19.

^{*1} RIKEN Nishina Center

Incidents involving the DMT3 magnet in the beam transport line from SRC to BigRIPS

K. Kusaka,*¹ K. Yoshida,*¹ M. Ohtake,*¹ and Y. Yanagisawa*¹

After the October 2017 incident, wherein the lower correction coil in the DMT3 magnet in the “T-course” beam line was damaged,¹⁾ a new lower correction coil was fabricated at Toshiba and installed in DMT3 in March 2018. In addition to repairing the correction coil, we renewed its water-cooling channels such that the cooling-water lines of correction-coil pancakes are independent from those of the main-coil pancakes. The DMT2 magnet, which is a “2-Tesla” resistive-type dipole magnet identical to DMT3, was also improved in the water-cooling design. A ¹⁸O beam at 230 MeV/nucleon and ²³⁸U beam at 345 MeV/nucleon were safely transported to the BigRIPS target via the “T-course” beam line with the DMT2 and DMT3 magnets in 2018.

When we improved the cooling-water piping, we flushed all the cooling channels in DMT2 and DMT3 coils. Every pancake of the main and the correction coils was flushed with compressed air and water. We found a considerable amount of black powdery impurities in the water that rinsed all the cooling channels. The composition of the impurities was analyzed using an electron probe micro analyzer (EPMA), and we found that the impurity was mostly copper-oxide crystals. The amount of the impurities we extracted from the non-damaged upper correction coil of the DMT3 magnet was 0.8 g.

We investigated the cooling-water channel in the damaged correction coil by cutting the coil conductor. We cut the damaged coil into 11 pieces. Figure 1 shows, as an example, a cross section of the correction coil cut at a saddle-shaped coil end. Although we found no notable evidence of blockage by impurities, it is likely that a shortage of heat removal due to poor cooling-water flow in the correction coil damaged the epoxy isolation.

A ⁷⁸Kr beam and ¹²⁴Xe beam at 345 MeV/nucleon were transported and RI beam experiments were successfully performed in the early summer 2019. However, at the beginning of the uranium beam time in November 2019, we again faced a similar incident, wherein the upper correction coil in the DMT3 magnet was damaged. The DMT2 and DMT3 magnets were excited with currents of 596 A and 594 A, respectively. However, the total excitation voltage of the DMT3 magnet was

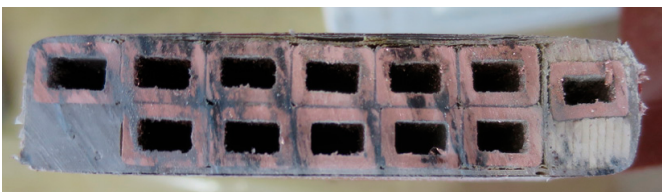


Fig. 1. Cross section of the damaged lower correction coil at the saddle-shaped coil end.



Fig. 2. Damaged upper correction coil of the DMT3 magnet.

131.6 V, which was about 10 V lower than the voltage of the DMT2 magnet (141.2 V). Furthermore, the temperatures of the cooling-water outlet of the upper and lower correction coils of the DMT3 magnet were 20.5°C and 40.1°C, respectively. We concluded that the upper correction coil in the DMT3 magnet was short-circuited.

In order to complete the beam service successfully, we isolated the upper correction coil from the excitation circuit, as we had done in 2017. The DMT3 magnet was re-excited while monitoring the voltage of each coil pancake.

Furthermore, we introduced an additional auxiliary DC power supply in the DMT3 excitation circuit in a parallel connection. Water-cooled protection diodes were also used for safety. We excited the DMT3 magnet using two power supplies with currents of 110 A and 536 A so that the uranium beam was safely transported to the BigRIPS target from SRC. After 2 days of beam-time suspension, scheduled experiments were performed till December 6. At the end of the beam time, we tested the transportation of the uranium beam using the DMT3 magnet without correction coils. We excited only the main coils of DMT3 magnet using two power supplies with currents of 110 A and 563 A. We confirmed that the uranium beam focused on the BigRIPS target well and the main coils were well cooled with a sufficient water flow.

We investigated the upper correction coil by inserting a fiberscope CCD camera into the space between the main coils of the DMT3 magnet after the beam time. Damage was found at the position of the second coil support from the beam exit side. Figure 2 shows the damage on the outer circumference of the upper correction coil. The origin of the incident is under investigation.

Reference

1) K. Kusaka *et al.*, RIKEN Accel. Prog. Rep. **51**, 173 (2018).

*¹ RIKEN Nishina Center

First confirmation of stopped RIs at parasitic gas cell with new approach

T. Sonoda,^{*1} I. Katayama,^{*1} M. Wada,^{*2} H. Imura,^{*3} V. Sonnenschein,^{*4} S. Imura,^{*1} A. Takamine,^{*1} M. Rosenbusch,^{*2} T. M. Kojima,^{*1} D. S. Ahn,^{*1} N. Fukuda,^{*1} T. Kubo,^{*1} S. Nishimura,^{*1} Y. Shimizu,^{*1} T. Sumikama,^{*1} H. Suzuki,^{*1} H. Takeda,^{*1} M. Tanigaki,^{*5} H. Tomita,^{*4} K. Yoshida,^{*1} and H. Ishiyama^{*1}

We are developing a scheme of parasitic low-energy RI-beam production (PALIS)¹⁾ in the second focal chamber (F2) of BigRIPS to establish the effective utilization of rare isotopes and to perform comprehensive measurements of the physical properties of exotic nuclei.

From previous experimental results,²⁾ we figured out that very intense radiation stays around the high-energy beam passage in F2. Under an intense radiation environment, a strong plasma can easily be created inside the PALIS gas cell, which prevents the stopped RIs from proper extraction. Therefore, we applied a new approach to transport the stopped RIs from the strong plasma via a long gas tube towards a lower-radiation environment. This concept is similar to the “helium-jet” technique, but the present approach does not use aerosols. In this beam time, we investigated the feasibility of this new approach by using alpha emitters produced by projectile fragmentation via a uranium beam and beryllium target.

Figure 1 shows a schematic of the experimental setup.

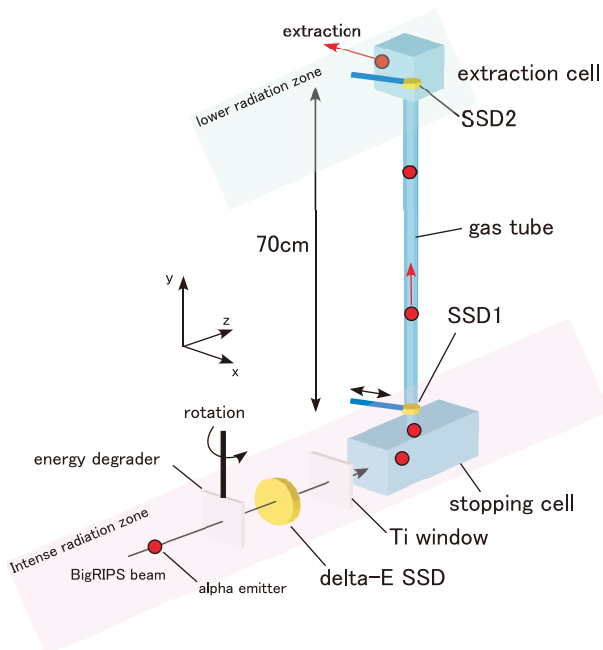


Fig. 1. Experimental setup.

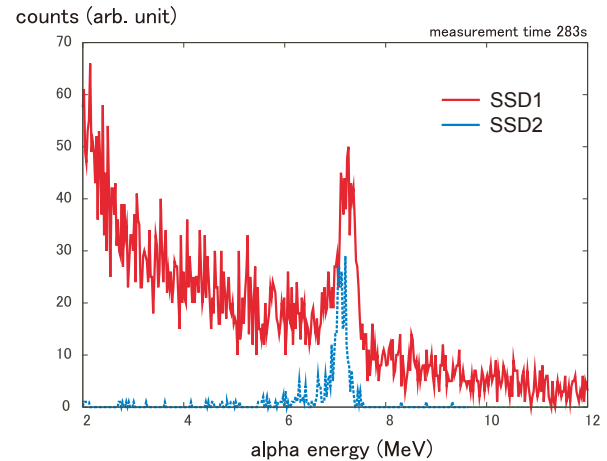


Fig. 2. Alpha spectra observed by SSD1 and SSD2.

The gas cell is separated into two parts: a stopping cell and an extraction cell which are joined with a 70-cm-long and thin gas tube. High-energy alpha-emitter beams were introduced to the stopping cell. The BigRIPS optical parameters were set to those in Sumikama *et al.*'s experiment.³⁾ Firstly, we confirmed alpha rays created via decays from the alpha emitters that were stopped in the delta-E SSD by adjusting the energy degrader. By decreasing the degrader thickness, those observed alpha emitters were stopped inside the gas cell filled with argon gas at 0.5 to 1 atm. The alpha emitters stopped in the stopping cell were transported to the extraction cell by a gas jet, where the radiation intensity is at least 100 times lower than in the stopping cell. We observed a part of the alpha emitters that were accidentally incident on the silicon pin-diode (SSD1) surface facing the flow path at the entrance of the gas tube. Finally, we could confirm the alpha emitters by inserting another silicon pin-diode (SSD2) in the flow path at the end of the gas tube. Figure 2 shows the alpha spectra observed at SSD1 and SSD2.

The feasibility of the new gas cell structure was verified for the first time. In the next beam time, we will evaluate the extraction efficiency and apply laser ionization for those alpha emitters.

References

- 1) T. Sonoda *et al.*, Prog. Theor. Exp. Phys. **2019**, 113D02 (2019).
- 2) T. Sonoda *et al.*, RIKEN Accel. Prog. Rep. **51**, 171 (2017).
- 3) T. Sumikama *et al.*, Nucl. Instrum. Methods Phys. Res. B **463**, 237 (2020).

*1 RIKEN Nishina Center
 *2 High Energy Accelerator Research Organization, KEK
 *3 Japan Atomic Energy Agency, JAEA
 *4 Faculty of Engineering, Nagoya University, Nagoya
 *5 Institute for Integrated Radiation and Nuclear Science, KURNS

Stopping examination for high-energy RI beams in the parasitic gas cell†

T. Sonoda,*¹ I. Katayama,*¹ M. Wada,*² H. Imura,*³ V. Sonnenschein,*⁴ S. Imura,*¹ A. Takamine,*¹ M. Rosenbusch,*² T. M. Kojima,*¹ D. S. Ahn,*¹ N. Fukuda,*¹ T. Kubo,*¹ S. Nishimura,*¹ Y. Shimizu,*¹ H. Suzuki,*¹ H. Takeda,*¹ M. Tanigaki,*⁵ H. Tomita,*⁴ K. Yoshida,*¹ and H. Ishiyama*¹

We are developing a scheme of parasitic low-energy RI-beam production (PALIS)¹⁾ to establish the effective utilization of rare isotopes and to perform comprehensive measurements of physical properties of exotic nuclei. So far, we spent totally about two days of on-line commissioning beam time from 2015,^{2,3)} thanks to the RIBF MT committee. However, as the beam time is insufficient to optimize the new device, we requested the PAC committee for authentic beam time in 2017, and 3 days of beam time was approved. Our plan in this formally provided beam time consists of 3 stages: 1) stopping examination for high-energy RI beams in the parasitic gas cell, 2) an extraction test for stopped RIs and efficiency evaluation, and 3) the demonstration of physical spectroscopy using a low-energy RI beam. Here we report the results of the 12 h of on-line experiment in the first stage.

A schematic of the experimental setup is shown in Fig. 1.

Two silicon surface barrier Detectors (SSDs) were installed inside the BigRIPS F2-chamber and used for examining the ΔE - E relation. The first detector (ΔE -SSD) was mounted immediately after the (glass) energy degrader, and the second (E-SSD) was mounted inside the gas cell. A radioactive ⁶⁷Se beam was introduced to this setup as the main secondary beam, which was produced by projectile fragmentation via ⁷⁸Kr (340 MeV/nucleon) and a beryllium target. We confirmed that each isotone beam with the same neutron number (N) = 31, 32, and 33 was well separated energetically after the energy degrader. Here, the $N = 33$ isotone-beam, consisting of ⁶⁷Se, ⁶⁶As, ⁶⁵Ge, and ⁶⁴Ga, was adjusted to maximize

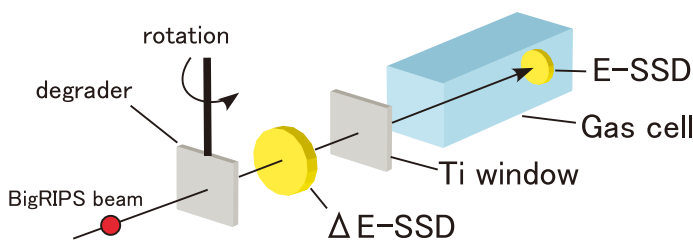


Fig. 1. Experimental setup.

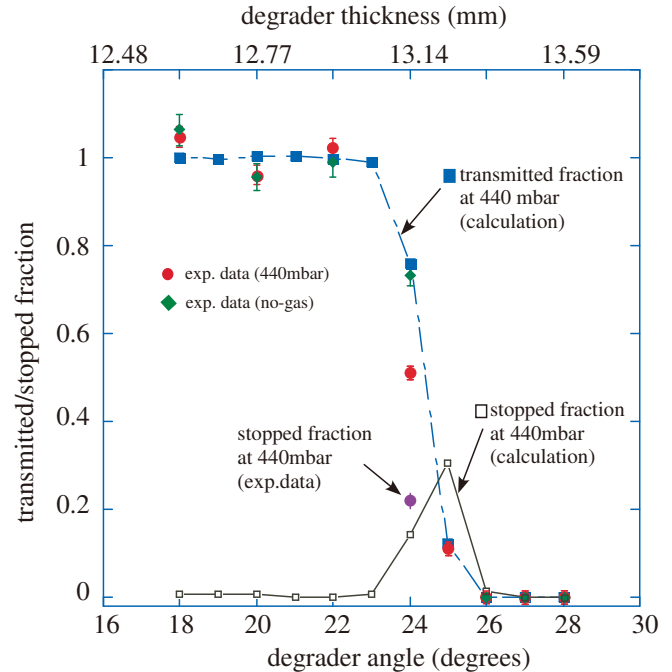


Fig. 2. Normalized transmitted and estimated stopped fractions as functions of the degrader angle.

the stopping efficiency in the gas. The effective thickness of the energy degrader was varied by adjusting its rotation using a stepping motor. Energy-loss spectra were obtained with ΔE -SSD and E-SSD as the angle of the glass degrader was varied from 18 to 28 degrees.

The normalized transmitted fraction at E-SSD and expected stopped fractions in the gas cell are plotted in Fig. 2 as functions of the degrader angle for the cases of no-gas (green rhombuses) and 440 mbar argon (red circles) in the gas cell. The experimental data at 440 mbar were well reproduced by LISE⁺⁺ calculations. In addition, the expected stopped fraction in the gas was estimated by comparing the transmitted fractions with and without gas. In this experiment, we confirmed that approximately 30% of the ensemble of $N = 33$ isotone beams were stopped in 440 mbar argon at the optimum degrader angle.

As a next step, we will establish the extraction technique of stopped RIs for low-energy RI-beams.

References

- 1) T. Sonoda *et al.*, Prog. Theor. Exp. Phys. **2019**, 113D02 (2019).
- 2) T. Sonoda *et al.*, RIKEN Accel. Prog. Rep. **49**, 16 (2015).
- 3) T. Sonoda *et al.*, RIKEN Accel. Prog. Rep. **51**, 169 (2017).

† Condensed from the article in Prog. Theor. Exp. Phys. **2019**, 113D02 (2019)

*¹ RIKEN Nishina Center

*² IPNS, High Energy Accelerator Research Organization

*³ Applied Nuclear Physics Laboratory, Japan Atomic Energy Agency

*⁴ Faculty of Engineering, Nagoya University, Nagoya

*⁵ Institute for Integrated Radiation and Nuclear Science

Second report on offline tests for RF carpet transportation in RF ion guide gas cell at the SLOWRI facility

S. Iimura,^{*1,*2,*3} A. Takamine,^{*1} M. Rosenbusch,^{*3} M. Wada,^{*3} S. Chen,^{*4} J. Liu,^{*4} P. Schury,^{*3} T. Sonoda,^{*1} T. M. Kojima,^{*1} Y. X. Watanabe,^{*3} A. Odahara,^{*2} and H. Ishiyama^{*1}

We are developing a radio frequency carpet (RFCP)-type ion guide¹⁾ gas catcher cell (RFGC) at the SLOWRI facility. In the previous version,²⁾ we could achieve a transport efficiency of $\sim 60\%$ only in 133 mbar helium gas on the first carpet from offline measurements. In these developments, to improve the transport efficiency, we changed the carpet pitch (the distance between the center of neighboring RF electrodes) from 0.32 mm to 0.25 mm.

In our offline measurements, we evaluated the transport efficiency of the RFGC using a surface ionization Cs ion source placed at the inner wall of the gas cell. Firstly, we measured the ion reaching onto the 1st RFCP by using it as a Faraday cup. Subsequently, we used the 2nd RFCP as a Faraday cup to measure ions transported by the 1st RFCP after applying appropriate RF and DC fields. The efficiency was defined by the current measured at the 2nd RFCP divided by that measured at the 1st RFCP.

Figure 1 shows the result of the obtained transport efficiency as a function of the RF voltages applied to the 1st RFCP in three different helium gas pressures. The transport efficiency reached $\sim 80\%$ at each pressure, which is ~ 1.3 times greater than in the previous measurements.²⁾

In an online experiment, the total extraction efficiency is determined by the product of stopping, ion survival,

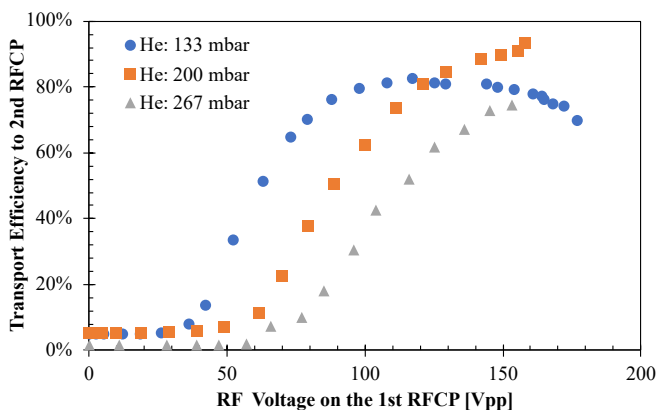


Fig. 1. 1st RFCP transportation test results in three different helium gas pressures: 133 mbar, 200 mbar, and 267 mbar. In this test, the drag dc field on the 1st RFCP, the extraction DC field between the 1st and 2nd RFCPs, and each RF frequency were 4 V/cm, 20 V/cm, and ~ 5 MHz, respectively.

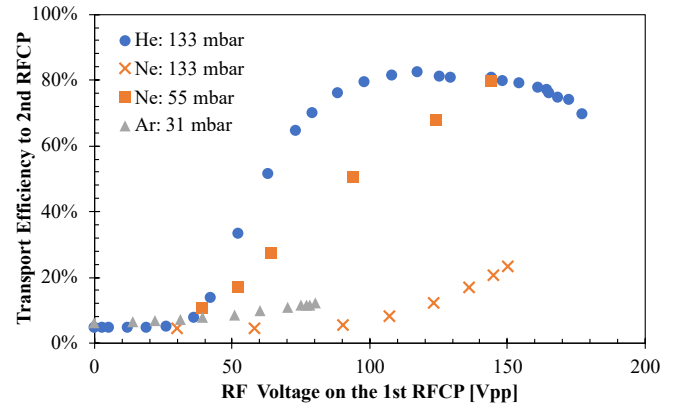


Fig. 2. 1st RFCP transportation test results for three kinds of gases: helium, neon, and argon. The DC fields condition and RF frequency were the same as in the previous tests.

and transport efficiencies. In order to enable more efficient stopping, heavier species of buffer gas have been investigated. Figure 2 shows the result of the measured transport efficiency for three kinds of buffer gases. The gas pressures of neon (55 mbar) and argon (31 mbar) were adjusted so that the beam would be stopped with the same efficiency as that achieved for 133 mbar of helium. It was found that helium (133 mbar) and neon (55 mbar) gases gave comparable transport efficiencies. On the other hand, with a higher pressure for neon, *i.e.*, equal to the helium pressure, the transport in neon gas was observed to be four times less efficient. In addition to these results, considering that the ion survival probability in helium is 1.3 times higher than that in neon, as shown previously,³⁾ the total efficiency in helium gas may be the best performance.

We will keep testing the RFCP to search for the optimum conditions, especially for the parameters of the 2nd RFCP. Furthermore, the ion-guide system to be placed behind the 2nd RFCP is under assembly; it consists of a quadrupole ion beam guide and an ion trapping system. After that, we can provide a low-energy RI beam to a multi-reflection time-of-flight mass spectrograph (MRTOF-MS), which is under preparation. We plan to start online commissioning of the RFGC and the MRTOF-MS in spring FY2020 at the downstream of the ZeroDegree Spectrometer.

References

- 1) M. Wada *et al.*, Nucl. Instrum. Methods Phys. Res. B **204**, 570 (2003).
- 2) A. Takamine *et al.*, RIKEN Accel. Prog. Rep. **52**, 139 (2019).
- 3) P. Dendooven *et al.*, Nucl. Instrum. Methods Phys. Res. A **558**, 580 (2006).

^{*1} RIKEN Nishina Center

^{*2} Department of Physics, Osaka University

^{*3} Wako Nuclear Science Center (WNSC), IPNS, KEK

^{*4} Department of Physics, The University of Hong Kong

The 3rd report on offline test for RF carpet transportation in RF ion guide gas cell at the SLOWRI facility

A. Takamine,^{*1} S. Imura,^{*1} M. Rosenbusch,^{*2} M. Wada,^{*2} S. Chen,^{*3} J. Liu,^{*3} P. Schury,^{*2} T. Sonoda,^{*1}
T. M. Kojima,^{*1} I. Katayama,^{*1} Y. X. Watanabe,^{*2} H. Ueno,^{*1} and H. Ishiyama^{*1}

A gas catcher cell using a radio-frequency (RF) ion guide method¹⁾ is being developed to provide ultra-slow RI beams at the SLOWRI facility. We built a gutter-structure ion guide gas cell, which consists of two-stage RF carpets (RFCPs).²⁾ We previously used strip electrodes with a pitch of 0.32 mm (electrode width of 0.16 mm and spacing of 0.16 mm) for the 1st RFCP. The transport efficiency was limited to $\approx 60\%$ in 133 mbar of He gas and even lower in a higher pressure gas. We replaced the 1st RFCP with a finer pitch of 0.25 mm (electrode width of 0.1 mm and spacing of 0.15 mm) to improve the performance. However, finer-pitch RF electrodes have a larger capacitance, which would practically limit the RF resonance frequency for the RFCP. Therefore, we conducted an offline test to investigate the RF transport performance on the new 1st RFCP at different RFs by changing the resonance coil of the resonant circuit.

The offline test was performed using surface-ionization ion sources of Cs and K which were placed at the inner wall of the gas cell. The setup is shown in a figure in Ref. 2). The ions produced from the ion sources were collected onto the 1st RFCP, transported on the 1st RFCP, and collected onto the 2nd RFCP. We measured the ion currents, I_1 , on the 1st RFCP and those on the 2nd RFCP, I_2 , by a pA meter using each of the RFCPs as a Faraday cup. The transported efficiency was defined as I_2/I_1 . It should be noted that for the measurements of I_1 , the DC potential distribution was slightly different from that in the case of I_2 because we could apply a DC gradient on the on the 1st RFCP only for the measurements of I_2 .

Figure 1 shows the test results in 133 mbar of He gas for (a) Cs⁺ ions and (b) K⁺ ions at different RF frequencies. The drag DC field on the 1st RFCP was 4 V/cm, and the extraction DC field on 2nd RFCP was 20 V/cm. We achieved a higher transport efficiency compared with the previous RFCP,²⁾ although we found that it requires a correction to the efficiencies by a factor of not more than ~ 0.9 , which results from the DC-field distribution difference mentioned above. The results indicate that an RF frequency of ~ 6 MHz was sufficient for Cs⁺ ($m/q = 133$), although it did not saturate the K⁺ ($m/q = 39$) transport efficiency. According to the results, we will operate the RF ion guide gas cell at 7–8 MHz in the commissioning at the end of the ZeroDegree beam line in spring FY2020.

The plots clearly show that higher RF voltages are required to transport the lighter ions at a similar RF fre-

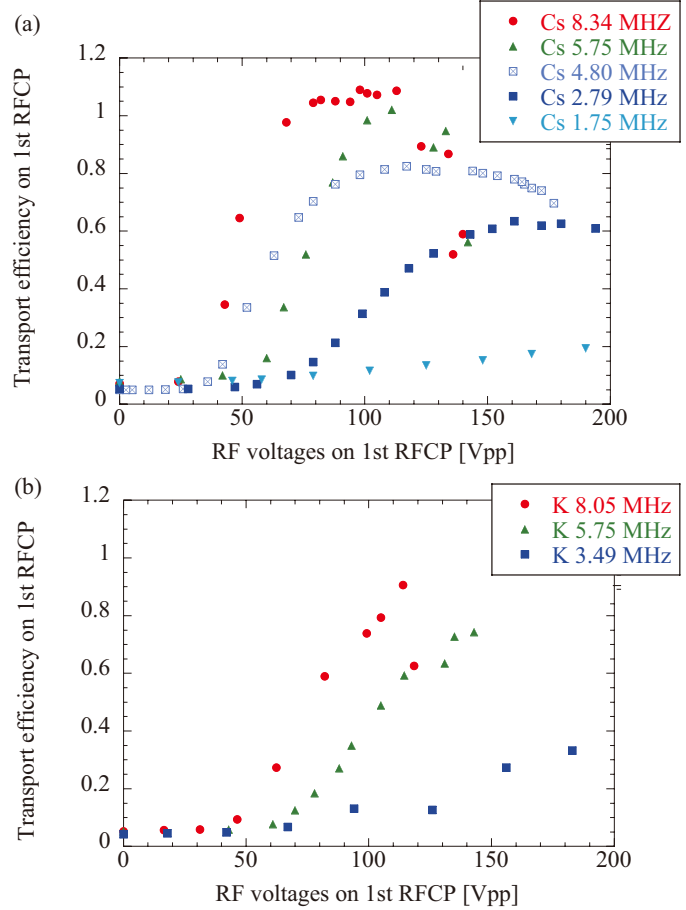


Fig. 1. RF voltage dependence of the RF transportation efficiencies for (a) Cs⁺ and (b) K⁺.

quency, which can be straightforwardly interpreted from the expression of the RF repelling force.¹⁾ The plot (a) also shows that there exist RF voltages maximizing the transport efficiency for each RF frequency. We observed some discharge-like ion currents at a higher voltage than the efficiency peak points; consequently, the discharge seemingly disturbed the ion transport. However the transport efficiency would be different depending on the position in an RFCP stability diagram,³⁾ defined by the RF and DC voltage values, which has a possibility to explain this result. An attempt at quantitative interpretation is underway.

References

- 1) M. Wada *et al.*, Nucl. Instrum. Methods Phys. Res. B **204**, 570 (2003).
- 2) A. Takamine *et al.*, RIKEN Accel. Prog. Rep. **52**, 139 (2019).
- 3) S. Schwarz, Int. J. Mass Spectrom. **299**, 71 (2011).

^{*1} RIKEN Nishina Center

^{*2} Wako Nuclear Science Center (WNSC), IPNS, KEK

^{*3} Department of Physics, The University of Hong Kong

Battery-operated compact ion source for beam transport test

T. M. Kojima,^{*1} T. Sonoda,^{*1} I. Katayama,^{*1} M. Wada,^{*2} and H. Ishiyama^{*1}

An ion source for a beam transport test at the SLOWRI beamline¹⁾ has been designed and assembled. The beamline was constructed to transport slow rare isotope (RI) ions extracted with an accelerating voltage of a few tens of kilovolts from the PALIS apparatus²⁾ or RF gas cell.³⁾ PALIS and the gas cell are systems used for catching, thermalizing, and accumulating RIs produced at BigRIPS. At present, neither PALIS nor the gas cell is completed, and no ion can be extracted. Instead of those systems, an ion source is necessary to examine ion transport at the SLOWRI beamline. However, there is no room for installing a usual ion source at the upstream end of the beamline, since PALIS has been already installed at that place, *i.e.*, the F2 chamber of the BigRIPS facility.

The newly designed ion source is used as a side-inserted-type device. It can be installed at any of the particular CF114 flanges for the beam-profile monitor on the duct (see Fig. 1). The system consists of an ion emitter part and extraction part. The former is biased at an accelerating voltage of a few tens of kilovolts so that it is isolated with a CF70 isolating nipple. A commercial thermal-ionization-type alkali ion emitter (Heat-Wave Labs, Model 101139 Cs⁺)⁴⁾ surrounded with a 50 mm ϕ repeller electrode is mounted at the end of the isolated rod (see Fig. 2). The emitter, which contains a heater inside, has a cylindrical shape of 6.35 mm ϕ and 9.9-mm length, and its end side is coated with alkali compounds. Note that the center hole of the repeller is 10 mm ϕ , which is slightly larger than the emitter, to avoid thermal contact. The position of the emitter is designed to be on the axis of the beamline duct. The heater power of the emitter is supplied by a lithium-ion

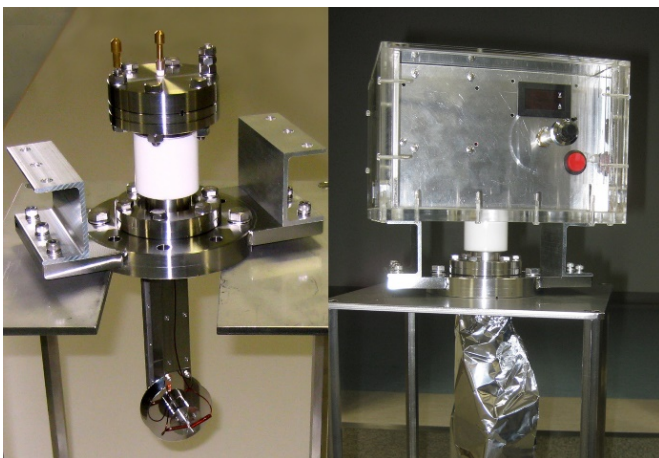


Fig. 1. Left: The assembled ion source without the heater controller. Right: The heater controller set on the top of the CF70 isolating nipple.

^{*1} RIKEN Nishina Center

^{*2} KEK Wako Nuclear Science Center

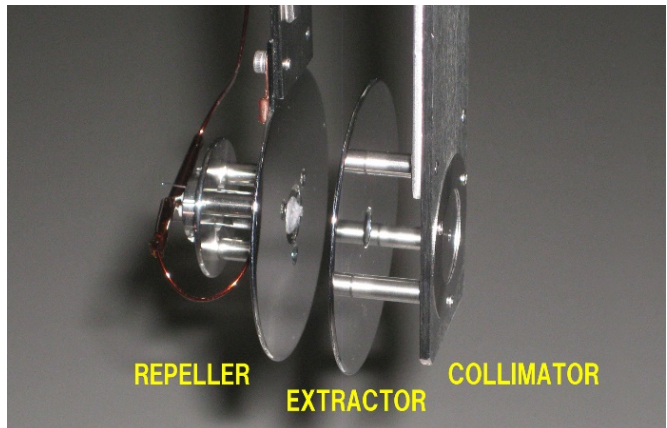


Fig. 2. Photograph of the electrode arrangement of the ion source. The coated alkali compounds of the ion emitter are seen at the center of the repeller.

battery (GlobalTech, GANGAN GT5)⁵⁾ with an output regulating circuit. The battery and circuit are housed in an acrylic box mounted on the top of the isolating nipple; thus, they are isolated from the GND potential. Therefore, it is easy to apply a high voltage bias to the ion emitter part. The battery, when fully charged, can operate the ion source for more than ten hours under usual conditions. The extraction part is assembled on the CF114 flange at the GND potential. It has two electrodes, *i.e.*, an extractor with a 6 mm ϕ aperture and a “collimator” with a replacable aperture plate. One can adjust the emittance of extracted ions by changing the aperture size of the “collimator,” though the extracted intensity decreases as the emittance decreases. A 4 mm ϕ aperture is set currently.

The ion source was tested at a very short (40 cm) region of the beamline, which includes only one 20-cm-long electrostatic quadrupole between the ion source and a Faraday cup. With 10-kV acceleration and 6.8-W heater power, the ion current extracted through the 4 mm ϕ “collimator” was about 1 nA on the Faraday cup at 40 cm downstream when the electrostatic quadrupole was optimized. The intensity is sufficient for our purpose. In addition, a higher intensity is expected with a higher power since the rated power of the heater is 11.3 W.

With this ion source, the ion-transport properties of the beamline will be examined and adjusted.

References

- 1) M. Wada *et al.*, RIKEN Accel. Prog. Rep. **47**, 203 (2014).
- 2) T. Sonoda *et al.*, Prog. Theor. Exp. Phys. **2019**, 113D02 (2019).
- 3) M. Wada *et al.*, Nucl. Instrum. Methods Phys. Res. B **204**, 570–581 (2003).
- 4) https://www.cathode.com/i_alkali.htm.
- 5) <https://g-tech.jp/gt5>. (in Japanese)

Present status of ERIS at the SCRIT electron scattering facility

T. Ohnishi,^{*1} S. Ichikawa,^{*1} A. Enokizono,^{*1} K. Kurita,^{*2} S. Sato,^{*1,*2} M. Watanabe,^{*1} and M. Wakasugi^{*1,*3}

The electron-beam-driven RI separator for SCRIT (ERIS)¹⁾ at the SCRIT electron scattering facility²⁾ is an online isotope separator system used to produce low-energy RI beams using the photofission of uranium. Recently, we developed ion-stacking and pulse-extraction systems to improve the DC-to-pulse conversion efficiency using an RFQ cooler buncher named the fringing-RF-field activated DC-to-pulse converter (FRAC).³⁾ With a surface-ionization ion source, a high conversion efficiency was obtained.⁴⁾ In the present year, we produced RI beams using the surface-ionization ion source and applied the ion-stacking and pulse-extraction systems to RI beams. In this paper, we report the results.

Details of the RI production method and the surface-ionization ion source of ERIS are reported in Refs. 4–5). In this measurement, 43 uranium-carbide disks, with a thickness of 0.8 mm and a diameter of 18 mm, were used as production targets. The total amount of uranium was about 30 g. The uranium-carbide disks were irradiated with an electron beam accelerated to 150 MeV. The electron beam power was adjusted to approximately 0.25–1 W to reduce background events. The target and ionization chamber were heated to 1500–2000°C by using resistive heating. The electric currents applied to the ionization chamber and target heater were 120 A and 900 A, respectively. Ionized RIs were extracted by the exit grid of the ionization chamber, accelerated to 10 keV, and transported to the PID system¹⁾ located at the exit of FRAC. Particle identification was performed by measuring specific γ rays corresponding to the decay of the RIs by using a Ge detector.

Each measurement was performed as follows. First, we irradiated production targets for 4 min to achieve the equilibrium state of the RI production. Next, RI beams were injected to the PID system for 1 min while continuing the target irradiation. Finally, the target irradiation was stopped, and γ rays were measured for 1 min. The rate of RI production is estimated from the observed γ -ray yield using the efficiency of the Ge detector and the half-life of the RI. For example, the rate of ^{140}Cs production is estimated as 4×10^5 atoms/s with an electron beam power of 1 W. The transmission efficiency from the ion source to the PID system was measured as 23% using a stable Cs ion beam. This low efficiency was due to the insufficient adjustment of the ion-beam optics for the injection to FRAC.

The ion stacking and pulse extraction were examined using the ^{140}Cs beam. The stacking and extrac-

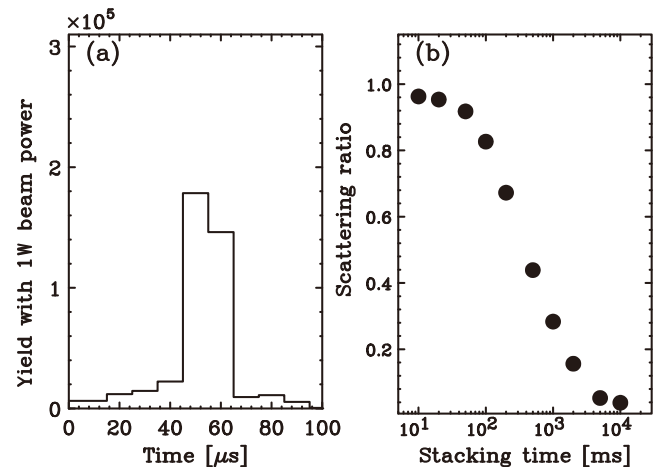


Fig. 1. (a) Pulse shape of the ^{140}Cs beam with a 100-ms stacking time and 1-W electron beam power. (b) Stacking-time dependence of the stacking ratio.

tion voltages of the exit grid were 100 and -200 V, respectively. The pulse shape of the pulsed RI beam was measured with a fixed time window, $10 \mu\text{s}$, by changing the time interval between the extraction from ERIS and the injection to FRAC. Figure 1(a) shows the time-interval dependence of the measured yield of ^{140}Cs with a 100-ms stacking time and 1-W electron beam power. RI beams were extracted within $20 \mu\text{s}$, which helps realize zero escape of stacked ions from FRAC during the injection. The stacking-time dependence of the stacking ratio is shown in Fig. 2(b). Here, the stacking ratio is the ratio of the total number of RIs measured with stacking inside the ion source to that measured without stacking. A stacking ratio of almost 0.9 was obtained at a stacking time of 100 ms, which corresponds to the cooling time inside FRAC with a relatively small amount of buffer gas ($\sim 10^{-3}$ Pa).

Considering these results, ERIS is almost ready for the first electron scattering experiment with unstable nuclei. We consider ^{137}Cs as a candidate isotope due to its high production rate. Under the condition of 100% transmission efficiency and a 10-W electron beam power, which is the present maximum beam power, the rate of ^{137}Cs is expected to be 4×10^7 atoms/s, which is sufficient for the experiment.

References

- 1) T. Ohnishi *et al.*, Nucl. Instrum. Methods Phys. Res. B **317**, 357 (2013).
- 2) M. Wakasugi *et al.*, Nucl. Instrum. Methods Phys. Res. B **317**, 668 (2013).
- 3) M. Wakasugi *et al.*, Rev. Sci. Instrum. **89**, 095107 (2018).
- 4) T. Ohnishi *et al.*, RIKEN Accel. Prog. Rep. **52**, 142 (2019).
- 5) T. Ohnishi *et al.*, RIKEN Accel. Prog. Rep. **48**, 229 (2015).

^{*1} RIKEN Nishina Center

^{*2} Department of Physics, Rikkyo University

^{*3} ICR, Kyoto University

Latest performance of FRAC at SCRIT facility

S. Sato,^{*1,*2} A. Enokizono,^{*2} T. Ohnishi,^{*2} K. Kurita,^{*1} M. Wakasugi,^{*2,*3} and M. Watanabe^{*2}

The construction of the SCRIT electron scattering facility,¹⁾ which aims to realize the world's first electron scattering experiment for unstable nuclei, enabled measurement with $\sim 10^8$ ions/s. In order to perform electron scattering with unstable nuclei at a small production rate, it is necessary to convert the ions generated continuously by the ISOL-type ion separator, Electron-beam-driven RI separator for SCRIT(ERIS),²⁾ to a pulsed beam with an efficiency as high as possible. For this purpose, we developed a dc-to-pulse converter, Fringing-Rf-field-Activated dc-to-pulse Converter(FRAC).³⁾ In 2018, the dc-to-pulse conversion efficiency was greatly improved through a modification to incorporate cooling and the 2 step-bunching method.⁴⁾ In this article, we report the optimization of the 2 step-bunching method, the latest performance, and the future plan.

In the 2 step-bunching method, pre-pulsed beams extracted from ERIS are stacked in FRAC and extracted as a high-intensity pulsed beam from FRAC. Therefore, to achieve a high dc-to-pulse conversion efficiency, the efficiencies of both ERIS and FRAC are important. The most important factor in these efficiencies is the extraction frequency of the pre-pulsed beam, f_{pre} . To determine the most appropriate f_{pre} , we performed two measurements. The first measurement was of the stacking-time dependence of the stacking efficiency of ERIS, E_{ERIS} . E_{ERIS} was $\sim 100\%$ for stacking times up to 100 ms. The details are reported in Ref. 5). The second measurement is of the cooling time. The cooling time is the time until the ions injected into FRAC are sufficiently cooled. When ^{133}Cs was used as the ion beam and Xe gas of $\sim 10^{-3}$ Pa was used as the coolant, the

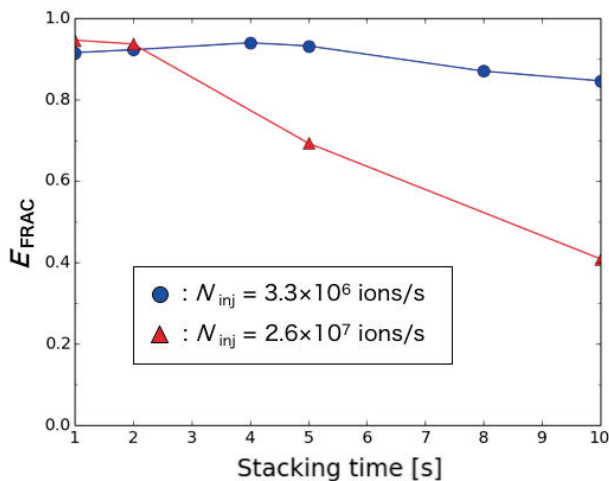


Fig. 1. Stacking-time dependence of E_{FRAC} .

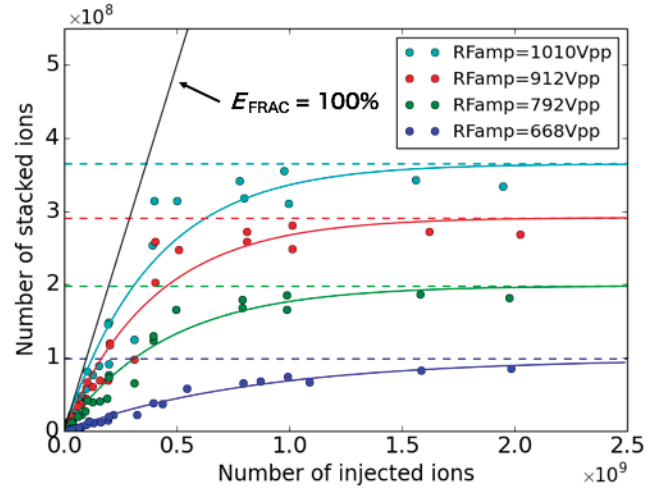


Fig. 2. RF-amplitude dependence of the number of stacked ions.

cooling time was 50 ms. From these results, the appropriate time interval for extracting the pre-pulsed beam was determined to be from 50 ms to 100 ms. Therefore, 2 step-bunching was performed at $f_{\text{pre}} = 10$ Hz.

In the measurement after the optimization of 2 step-bunching, the stacking time dependence of the efficiency of FRAC, E_{FRAC} , was measured. The measurement was performed twice while changing the number of injected ions per second, N_{inj} . Figure 1 shows the results. E_{FRAC} was constant at $\sim 90\%$ when the number of injected ions was less than 5.2×10^7 . However, E_{FRAC} decreased as the number of injected ions increased further. This is considered to be due to the shallowing of the pseudo potential created by the RF electric field, which is a result of the space charge effect of the stacked ions. The ions injected thereafter cannot be stacked further.

The pseudo potential can be deepened by increasing the RF amplitude. We measured the RF-amplitude dependence of the number of stacked ions in order to explore the possibility of improving E_{FRAC} by increasing the RF amplitude. Figure 2 shows the result. As the RF amplitude increases, the number of stacked ions increases and E_{FRAC} approaches 100%. From this result, it is concluded that increasing the RF amplitude was effective. In order to stack $\sim 10^8$ ions with a higher efficiency, we are planning to increase the RF amplitude.

References

- 1) M. Wakasugi *et al.*, Nucl. Instrum. Methods Phys. Res. B **317**, 668 (2013).
- 2) T. Ohnishi *et al.*, Nucl. Instrum. Methods Phys. Res. B **317**, 357 (2013).
- 3) M. Wakasugi *et al.*, Rev. Sci. Instrum. **89**, 095107 (2018).
- 4) S. Sato *et al.*, RIKEN Accel. Prog. Rep. **52**, 144 (2019).
- 5) T. Ohnishi *et al.*, in this report.

*1 Department of Physics, Rikkyo University

*2 RIKEN Nishina Center

*3 Institute for Chemical Research, Kyoto University

3D magnetic field measurement of the SCRIT electron spectrometer

H. Wauke,^{*1,*2} T. Aoyagi,^{*1,*2} A. Enokizono,^{*1} Y. Honda,^{*1,*2} K. Kurita,^{*1,*3} S. Sato,^{*1,*3} T. Suda,^{*1,*2} S. Takagi,^{*1,*4} S. Takayama,^{*1,*2} D. Taki,^{*1,*2} T. Tamae,^{*2} K. Tsukada,^{*1,*2} T. Ohnishi,^{*1} M. Wakasugi,^{*1,*4} and M. Watanabe^{*1}

Window-frame Spectrometer for Electron Scattering (WiSES)¹⁾ is an electron spectrometer for Self-Confining Radioactive-isotope Ion Target (SCRIT)²⁾ experiment. WiSES consists of a dipole magnet,³⁾ two drift chambers at the entrance and exit of the magnet, a helium bag installed between the two drift chambers to reduce the multiple scattering effect, and two scintillation counters used for trigger generation. The solid angle of the spectrometer is about 80 msr, covering a wide range of scattering angles, *i.e.*, from 30° to 60°. A typical momentum resolution of $\Delta p/p \sim 10^{-3}$ for an electron energy in the range of 150–300 MeV is required to separate elastic and inelastic scattering with WiSES. It was found that the momentum resolution evaluated in past elastic scattering experiments did not reach the design value. One possible cause was that the map calculated using OPERA3D to reconstruct the trajectories of the scattered electrons had not accurately reproduced the WiSES magnetic field.

The scattered electrons passing through WiSES experience strong vertical focusing due to B_z , which is a horizontal component of the fringing field.

In order to check the calculated map, we measured the 3D magnetic field of WiSES with the measured accuracy $\Delta B/B \sim 10^{-3}$. The magnetic field strength was 0.4–0.8 T, which corresponds to an electron beam energy of 150–300 MeV in the experiment. In 2018, we developed a triaxial probe made from three Hall probes to measure three field components simultaneously.⁴⁾ The measurement resolution of these probes is about 10^{-6} T. In addition, we developed a 3D driving device consisting

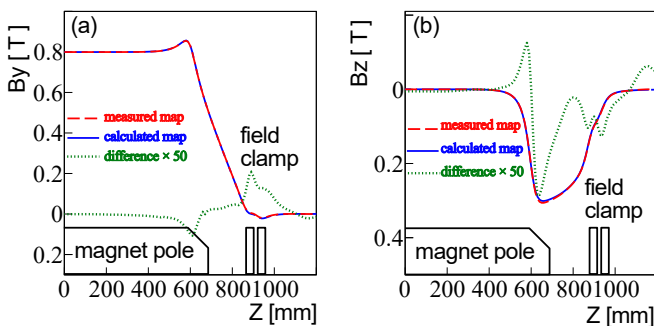


Fig. 1. Comparison between the measured map and the calculated one near the magnetic pole. The strength of the magnetic field was 0.8 T. (a) shows vertical component B_y and (b) shows horizontal component of the fringing field B_z . The red line is the measured map, blue line is the calculated one, and green line shows 50 times the difference between the two maps.

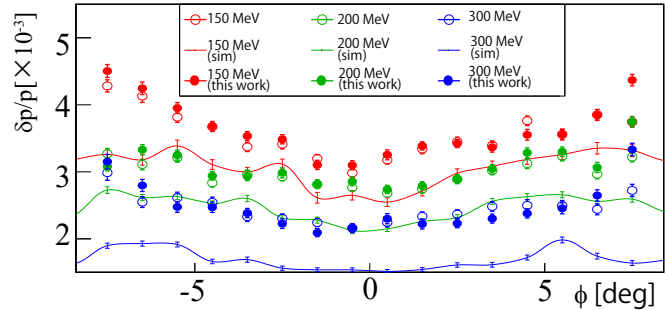


Fig. 2. Comparison of the momentum resolution between the measured map and the calculated one. The solid lines show the simulation results, the open circles show the results obtained with the calculation map, and the filled circles show the results obtained with the measured map. Red indicates the results with 150 MeV, green indicates the results with 200 MeV, and blue indicates the results with 300 MeV.

of three electric sliders that move in a large measurement area. The 3D driving device was controlled by a LabVIEW program. The program also read the field values from the Hall probes and the absolute magnetic field of the WiSES magnet from nuclear magnetic resonance (NMR).

Figure 1 shows the vertical component B_y and the horizontal component of the fringing field B_z of the measured map and the calculated one. The structure of the measured magnetic field is similar to the calculated one even at about 1 cm from the magnet pole. Over the entire measurement area, the difference between the two maps was $\sim 10^{-3}$ T for both B_y and B_z . Similar results were obtained for other magnetic field strengths.

In November 2019, an electron scattering experiment using a carbon target was conducted.⁵⁾ The momentum resolution is the width of the elastic scattering peak obtained in the experiment. The resolution was obtained using the above two maps and compared. Figure 2 shows the result. ϕ is the azimuth angle of the scattered electrons as viewed from the target. The width of the elastic scattering peak obtained in the experiment was used as the momentum resolution. At three electron energies, the momentum resolutions obtained from the measured map in this study were almost the same as that obtained from the calculated one.

We need further consideration to explain the difference of the WiSES momentum resolution between the simulated and experimental values.

References

- 1) T. Adachi *et al.*, RIKEN Accel. Prog. Rep. **45**, 144 (2012).
- 2) M. Wakasugi *et al.*, Phys. Rev. Lett. **100**, 164801 (2008).
- 3) T. Suda *et al.*, RIKEN Accel. Prog. Rep. **46**, 184 (2013).
- 4) H. Wauke *et al.*, RIKEN Accel. Prog. Rep. **52**, 144 (2018).
- 5) K. Tsukada *et al.*, in this report.

*1 RIKEN Nishina Center

*2 ELPH, Tohoku University

*3 Department of Physics, Rikkyo University

*4 Institute for Chemical Research, Kyoto University

Measurement of the luminosity of electron scattering at SCRIT

D. Taki,^{*1,*2} A. Enokizono,^{*1} K. Kurita,^{*1,*3} T. Ohnishi,^{*1} S. Sato,^{*1,*3} T. Suda,^{*1,*2} S. Takagi,^{*1,*4} S. Takayama,^{*1,*2} T. Tamae,^{*1} K. Tsukada,^{*1,*2} M. Wakasugi,^{*1,*4} M. Watanabe,^{*1} and H. Wauke^{*1,*2}

At the Self-Confining Radioactive-isotope Ion Target(SCRIT) electron scattering facility, we will measure the absolute luminosity value with a luminosity monitor (LMon),¹⁾ which consists of a CsI calorimeter array and two-dimensional fiber scintillators. Luminosity is expressed as follows:

$$L = \frac{N_{Brem.}}{\sigma_{Brem.}} \cdot \frac{1}{\varepsilon} [\text{cm}^{-2}\text{s}^{-1}], \quad (1)$$

where $N_{Brem.}$ is the number of measured bremsstrahlung photons per second, $\sigma_{Brem.}$ is the calculated bremsstrahlung cross section, and ε is transmittance efficiency estimated as the number of detected photons divided by the number of photons generated from the electron target scatterings. Because LMon is located 7 m downstream of the vertex position and there are some obstacles in between such as cryopanel and pipes, ε is as small as 0.30–0.55 depending on the electron beam energy, angle, width, and so on.²⁾ Therefore, it is important to evaluate the beam condition and corresponding ε precisely by using a detector simulation to obtain L accurately. In a previous study,³⁾ ε was derived by comparing the spatial distribution measured using the fiber scintillators with the simulated one. However, it was found that the fiber scintillators with a spatial resolution of 3 mm are inadequate to determine the beam conditions correctly. Therefore, the spatial distribution is measured with higher resolution by using a silicon strip detector (SSD) in this study.

Figure 1 shows the layout of the new LMon. The SSD has four layers (X,Y,X,Y) of silicon sensors, each of which has a sensitive area of $7.7 \times 7.7 \text{ cm}^2$ and 1536 strips with a pitch of $50 \mu\text{m}$ pitch. We use two out of the four layers of SSD to measure horizontal and vertical distributions. In addition, two plastic scintillators are used: one is used as a trigger counter, and the other is

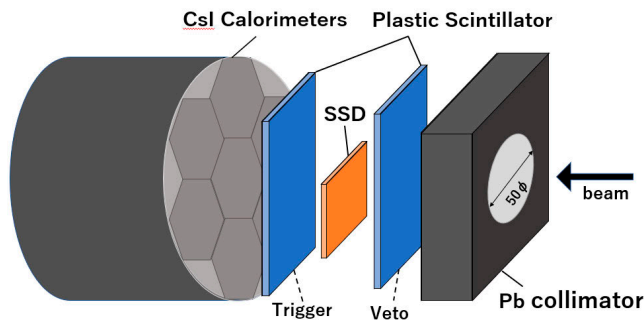


Fig. 1. Layout of the new LMon.

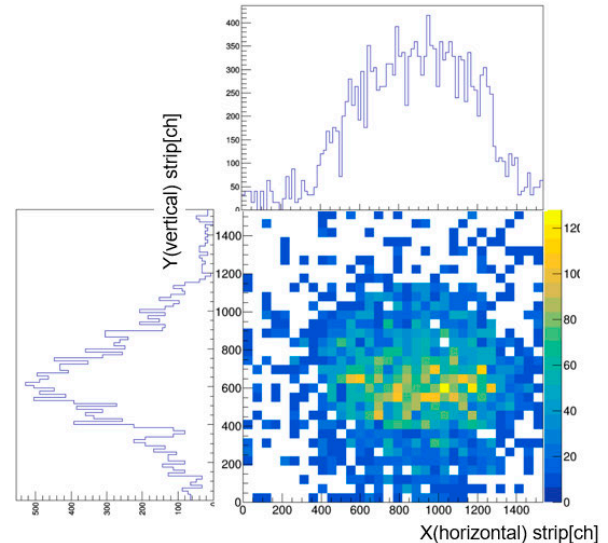


Fig. 2. X, Y and XY distributions.

used as a veto counter to remove the background electrons and positrons created upstream. The thickness of the SSD is about $300 \mu\text{m}$, and it converts bremsstrahlung into electrons and positrons for the trigger scintillator.

Figure 2 shows the measured horizontal and vertical spatial distributions of the bremsstrahlung photons together with the two-dimensional spatial distribution at a beam energy of 150 MeV. About 8000 events were accumulated within 10 min. More detailed spatial distributions than the previous study¹⁾ are obtained. Since this test experiment was performed without target ions, this distribution represents bremsstrahlung generated from residual gases throughout the straight section of the electron storage ring. As was observed in the previous study, the vertical distribution is sharper than the horizontal one due to obstacles. The spread of the beam is about 1000 ch, which coincides with 5 cm of the collimator hole.

At a next step, the spatial distributions will be measured with target ions. By comparing them with GEANT4 simulation results, a precise value of ε will be obtained. In addition, the DAQ rate must be increased by implementing the zero suppression mode. The acquisition rate is currently limited about 10 Hz at most because the information of all channels of the SSD is recorded in the current DAQ setup. Note that the beam condition and corresponding ε change every moment, and therefore, the spatial distributions have to be measured with a high DAQ rate for a short period in order to obtain accurate total luminosities.

References

- 1) S. Yoneyama *et al.*, RIKEN Accel. Prog. Rep. **48**, 227 (2015).
- 2) S. Yoneyama, Master's thesis (in Japanese), Tohoku University (2014).
- 3) T. Fujita *et al.*, RIKEN Accel. Prog. Rep. **50**, 188 (2017).

*1 RIKEN Nishina Center

*2 ELPH, Tohoku University

*3 Department of Physics, Rikkyo University

*4 Institute for Chemical Research, Kyoto University

Yield development with in-gas-jet laser ionization at KISS

Y. X. Watanabe,^{*1} Y. Hirayama,^{*1} H. S. Choi,^{*2} M. Mukai,^{*3} H. Miyatake,^{*1} S. Iimura,^{*4,*5} M. Oyaizu,^{*1} Y. Kakiguchi,^{*1} N. Ishiyama,^{*5} M. Wada,^{*1} P. Schury,^{*1} M. Rosenbusch,^{*1} A. Taniguchi,^{*6} J. H. Park,^{*7} and T. T. Yeung^{*8,*5}

We are developing the KEK Isotope Separation System (KISS)¹⁾ to perform experimental studies such as lifetime measurements, mass measurements, β - γ spectroscopy, and laser spectroscopy for neutron-rich nuclei around the closed neutron shell $N = 126$, which is relevant to r-process nucleosynthesis. KISS is an argon-gas-cell-based laser ion source, in which these neutron-rich nuclei are produced by multinucleon transfer (MNT) reactions between a ^{136}Xe beam and ^{198}Pt target.²⁾ The beam is provided by RILAC2 + RRC with an energy of 9.4 MeV/nucleon on the target, which had a thickness of 12.5 mg/cm². The reaction products ejected from the target enter the gas cell through a 5- μm polyimide window placed 10 mm downstream from the target. The gas cell is filled with 1-atm argon gas, which thermalizes and neutralizes injected reaction products. They are transported to the exit of the gas cell by laminar gas flow. In or out of the gas cell, these neutral atoms are irradiated by lasers for laser resonance ionization. Two lasers are used: one is for excitation, while the other is for ionization. One specific element can be selected for ionization by tuning the wavelength of the excitation laser. These ions are transported by radio frequency (RF) ion guides and accelerated by a high voltage of 20 kV followed by a dipole electromagnet for mass separation.

Since the neutron-rich nuclei of interest around $N = 126$ are produced in rare channels of MNT reactions, their efficient extraction is essential for their measurements. Thus far, in-gas-cell laser ionization has been used, in which two lasers are irradiated into the gas cell. Recently, KU Leuven group demonstrated in-gas-jet laser ionization with efficiency more than 10 times that of in-gas-cell ionization.³⁾ In-gas-jet laser ionization uses two lasers, which are irradiated on a gas jet formed by a de Laval nozzle attached at the exit of the gas cell. Low-temperature and low-pressure conditions in the supersonic jet could reduce the loss of ions caused by their collisions with dense gas atoms. For yield development at KISS, we introduced an in-gas-jet

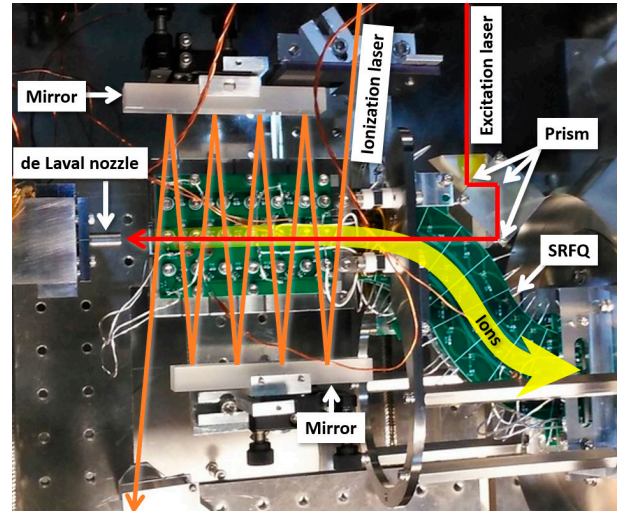


Fig. 1. KISS setup for in-gas-jet laser ionization.

laser ionization setup, as shown in Fig. 1. In order to sufficiently irradiate two lasers on the neutral atoms of interest in the supersonic jet, the overlap among them are optimized by arranging the excitation laser collinearly with the gas jet, and the ionization laser is perpendicularly reflected several times by two mirrors. An S-shaped RF quadrupole ion guide (SRFQ) was introduced to enable the collinear injection of the excitation laser. The SRFQ was segmented along the ion transportation to apply an increasing electric potential from the upstream to the downstream because a simulation with the SIMION code for the ion transportation indicated that ions stopped in the absence of such an electric-potential gradient. The on-line experiment did not show increased extraction yields with in-gas-jet laser ionization. When the same SRFQ was used with in-gas-cell ionization, the count rates of extracted ions were the same between extraction with and without the electric-potential gradient. This result indicates that the initial ion velocities obtained from the gas jet are not correctly evaluated in the simulation. We will further investigate the SRFQ design for yield development with in-gas-jet laser ionization through a more realistic simulation.

References

- 1) Y. Hirayama *et al.*, Nucl. Instrum. Methods Phys. Res. B **412**, 11 (2017).
- 2) Y. X. Watanabe *et al.*, Phys. Rev. Lett. **115**, 172503 (2015).
- 3) R. Ferrer *et al.*, Nat. Commun. **8**, 14520 (2017).

*1 Wako Nuclear Science Center (WNSC), Institute of Particle and Nuclear Studies (IPNS), High Energy Accelerator Research Organization (KEK)

*2 Department of Physics and Astronomy, Seoul National University

*3 Department of Physics, University of Tsukuba

*4 Department of Physics, Osaka University

*5 RIKEN Nishina Center

*6 Institute for Integrated Radiation and Nuclear Science, Kyoto University (KURNS)

*7 Rare Isotope Science Project (RISP), Institute for Basic Science (IBS)

*8 Department of Physics, The University of Hong Kong

Observation of charge-stripping of 20 keV/ q ions upon injection into gas cell cooler-buncher at KISS

P. Schury,^{*1} T. Hashimoto,^{*1,*3} Y. Ito,^{*4} H. Miyatake,^{*1} J. -Y. Moon,^{*1,*3} T. Niwase,^{*1,*5} Y. Hirayama,^{*1} M. Rosenbusch,^{*1} M. Wada,^{*1} X. Y. Watanabe,^{*1} and H. Wollnik^{*1,*2}

At the KISS facility, rare isotopes are produced in-flight by multi-nucleon transfer (MNT) reactions. They are then stopped and neutralized in high pressure argon gas and transported by gas flow to an exit nozzle. Atoms of rare isotopes are then re-ionized in an element-selective manner by use of a 2-step laser excitation; the method can only produce singly-charged ions. The gas cell system floats on a 20 kV bias, thereby producing 20 keV/ q ions. A magnetic separator with $R_m \approx 900$ ensures only a single isobar chain is transported downstream to the experimental apparatuses.

One of the primary experimental devices at KISS is multi-reflection time-of-flight mass spectrograph (MRTOF). The MRTOF, however, requires very low-energy ions. To make the 20 keV/ q KISS beam useable by the MRTOF, a gas cell cooler-buncher (GCCB)¹ has been constructed. This device is similar in construction to a small rf carpet gas cell,²⁾ but is windowless and pressurized to only 1 mbar. The beam from KISS stops in the GCCB, and is then extracted to vacuum and transferred to the MRTOF. The MRTOF makes rapidly interleaved time-of-flight measurements of analyte (the beam from GCCB) and reference ions.

In the initial test of the GCCB, a 20 keV/ q beam of $^{198}\text{Pt}^+$ was delivered from KISS. Figure 1 shows a time-of-flight spectra measured during that study. It was presumed that the peak at $A/q = 99$ was $^{198}\text{Pt}^{++}$ and a high-resolution follow-up measurement confirmed as much.

There are two ion traps between the GCCB and MRTOF. While the first of these has a very broadband response, the second trap (referred to as “flat trap”) is somewhat mass selective. The amplitude of the flat trap was systematically varied to determine the probability of conversion to a doubly-charged state. A time-of-flight spectrum was measured at each amplitude, and the number of singly- and doubly-charged $A = 198$ ions was recorded. The result, shown in Fig. 2, indicates that $\approx 80\%$ of incoming Pt ions were converted to the doubly-charged state.

From the occurrence of such charge-stripping reactions we presume the GCCB will also be highly effective at breaking molecular contaminants which are a common problem for gas cell based studies. We hope to report on such an effect in the near future.

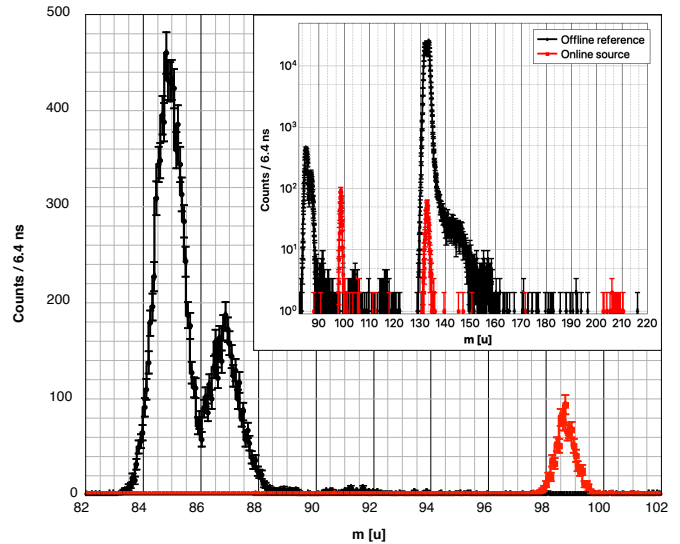


Fig. 1. Time-of-flight spectra from offline test of KISS gas cell cooler-buncher (GCCB) using a 20 keV/ q beam of $^{198}\text{Pt}^+$. The black spectrum shows the reference ions, $^{85,87}\text{Rb}^+$ and $^{133}\text{Cs}^+$. The red spectrum shows the ions delivered from the GCCB, dominantly $A/q = 99$.

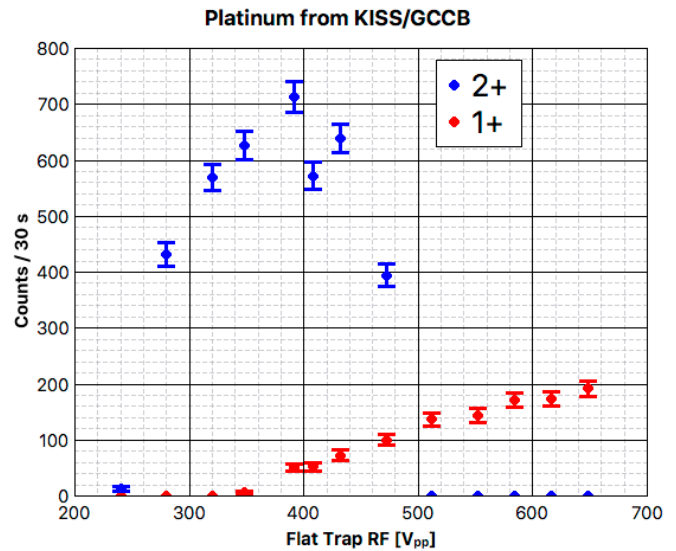


Fig. 2. Effect of varying the RF amplitude of the final preparation trap before the MRTOF, indicating that $\approx 80\%$ of the incoming beam is converted to a doubly-charged state.

*1 KEK Wako Nuclear Science Center
 *2 New Mexico State University, USA
 *3 Institute for Basic Science, Korea
 *4 Japan Atomic Energy Agency
 *5 Kyushu University

References

- 1) Y. Ito *et al.*, JPS Conf. Proc. **6**, 030112 (2015).
- 2) Y. Ito *et al.*, RIKEN Accel. Prog. Rep. **49**, 183 (2016).

Reliable connection methods for gas piping and signal cabling of PPAC in focal-plane vacuum chambers at BigRIPS

H. Sato,^{*1} D. S. Ahn,^{*1} N. Fukuda,^{*1} T. Komatsubara,^{*1} Y. Shimizu,^{*1} H. Suzuki,^{*1} H. Takeda,^{*1} and K. Yoshida^{*1}

Two sets of parallel-plate avalanche counters (PPACs) are installed in each focal-plane vacuum chamber at the BigRIPS and ZeroDegree separators.¹⁾ For replacing the PPACs in a short time without any trouble, we introduced reliable connection methods for gas piping and signal cabling inside the chamber: a quick coupling and a multipole connector, respectively.

The PPAC is filled with 10 Torr of gaseous isobutane when in operation. The gas introduced from outside of the chamber is transferred to the PPAC through two Teflon tubes (for the inlet and outlet), and each tube is inserted into a Wilson seal connector on the PPAC. Because of the bad working environment due to the narrow space of the chamber, a defect in the fitting of the Wilson seal may occur, causing gas leakage. To avoid this, Full Flow Quick-Connects (Swagelok SS-QF4-B-6M0 and SS-QF4-S-6M0) were adopted for easy coupling (Fig. 1). The stems and bodies of the Quick-Connects are attached to the PPAC and Teflon tubes, respectively. A leakage test of the PPAC with the Quick-Connects was performed by filling 10 Torr of isobutane, and we observed no leakage in a vacuum of 5.5×10^{-5} Pa. In addition, no degradation of the vacuum occurred during the up-and-down motion of the

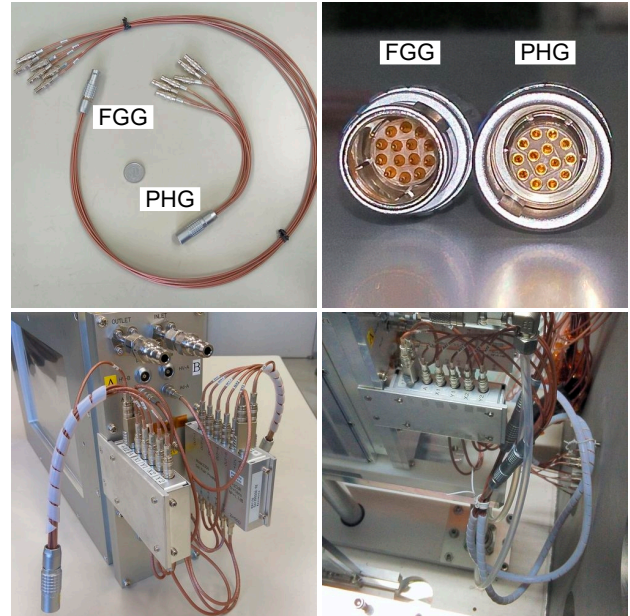


Fig. 2. Images of signal cables with multipole connectors. The shorter (200 mm) cables are connected to the PPAC, and the longer (800 mm) cables are connected to the chamber.

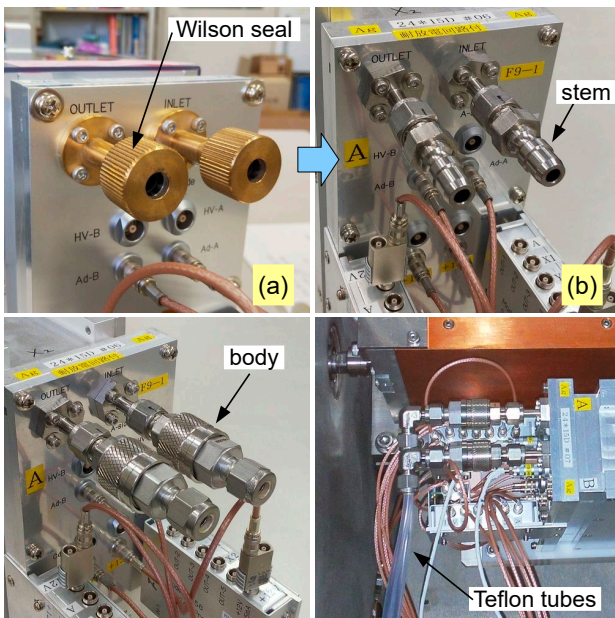


Fig. 1. Images of the Quick-Connects. (a) Ordinary gas ports with Wilson seals. (b) New gas ports with the stems of Quick-Connects.

PPAC. We applied the Quick-Connects to the PPACs in the F2, F3, F5, F7, F8, F9, F10, F11, and F12 chambers during the autumn beam time in 2019.

For signal readouts, five coaxial cables (for anode, x1, x2, y1, and y2) are independently connected to the output ports of the preamplifier of the PPAC. In addition, another cable for supplying a DC 12 V to the preamplifier is connected. For easy and error-free connection, 14-pin multipole connectors (LEMO FGG.1B.314.CLAD76 and PHG.1B.314.CLAD76) were adopted (Fig. 2). Six coaxial cables (RG178B/U) are soldered to one multipole connector. We performed the noise-level testing of the signal from the PPAC with the multipole connectors by using an alpha source ^{241}Am . As a result, the noise level of the signal was the same as that obtained with ordinary cabling. We applied the multipole connectors to the PPACs in the F3, F5, F7, and F8 chambers during the spring beam time in 2019.

We will finish the introduction of these two improvements to all the PPACs in 2020.

Reference

- 1) N. Fukuda *et al.*, Nucl. Instrum. Methods Phys. Res. B **317**, 323 (2013).

^{*1} RIKEN Nishina Center

Performance of a none-isochronous position-sensitive detector for the Rare-RI Ring

R. Crane,^{*1} S. Naimi,^{*1} S. Hosoi,^{*2} M. Mukai,^{*3} H. F. Li,^{*1,*4} Y. Abe,^{*1,*5} D. Nagae,^{*1,*6} D. Hamakawa,^{*2} Y. Inada,^{*2} D. Kajiki,^{*2} M. Sakaue,^{*2} W. B. Tou,^{*2} and K. Yokota^{*2}

We have developed a large area position-sensitive detector with a thin foil to be used for mass measurement with the Rare-RI Ring.¹⁾ The principle of the detector operation is shown in the bottom of Fig. 1. When high energy beam passes through the thin foil, secondary electrons (SEs) are released and reflected by the outer and inner mirror grids potential. The SEs energy is determined by the acceleration grid placed after the foil. The beam position is inferred from SEs position measurement with the delay line MCP placed 45° from the foil. To minimize the effect of the SEs initial velocity, the detector has an isochronous design,²⁾ which is achieved by careful choice of geometry and potentials: $D/(L_1 + L_2) = 0.236U_{mir}/U_{acc}$, where U_{mir} and U_{acc} are the acceleration and mirror potentials, respectively, D , L_1 and L_2 are dimensions of detector as shown in Fig. 1. We have designed the detector to be operated in the isochronous condition and also in the none-isochronous condition, simply by modifying the distance D between the inner and outer mirror grid. In the isochronous detector operation $D = 28$ mm, while for the none-isochronous operation $D = 8$ mm.

We have tested the detector at HIMAC with 200 MeV/nucleon ^{84}Kr beam in both isochronous (Iso) and none-isochronous (None-Iso) operation. For the Iso detector we tested the performance for a grid pitch of 1 mm, while for the None-Iso detector 1 mm and 2 mm pitch were tested. The test results are summarized in Table 1. The detector position accuracy is determined by the deviation from the foil image reconstructed by two PPACs. The position resolution is determined from a 2 mm diameter gate on the reconstructed foil image. For the mass measurement with the Rare-RI Ring the accuracy and resolution of the horizontal position are critical. The horizontal resolution of the None-Iso is better than the Iso detector. The position accuracy of the None-Iso detector with 2 mm grid pitch is best, because we introduced a calibration mask in front of the foil to correct for any misalignment between the PPACs and the detector that could result in a compromised position accuracy.

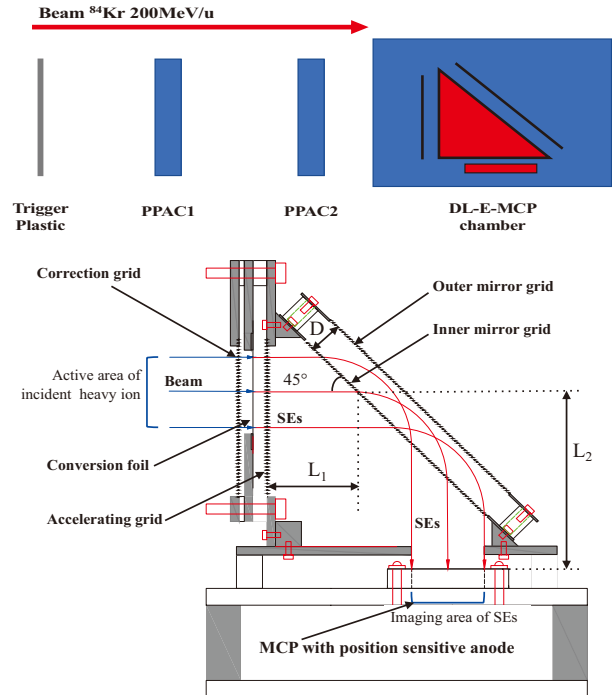


Fig. 1. (Top) Experimental setup at HIMAC consisting of a trigger plastic scintillator, two PPACs and a vacuum chamber containing the DL-E-MCP. (Bottom) Side view of the DL-E-MCP detector, where the beam passage through the foil generates secondary electrons that are reflected to the MCP with position-sensitive delay line anode.

Table 1. The detector position accuracy $A_{x,y}$ and resolution in sigma ($\sigma_{x,y}$) are shown for both horizontal (x) and vertical (y) beam positions for different detector operation; Isochronous (Iso.) and none-isochronous (None-Iso.). The performance of the latter is shown for two different grid pitch of 1 mm and 2 mm. The results are shown for the same acceleration potential and different optimized mirror potential in each configuration.

	Iso.	None-Iso.	None-Iso.
	1 mm pitch	1 mm pitch	2 mm pitch
A_x [mm]	+4.0	+1.5	-0.8
A_y [mm]	-0.1	0.0	+0.6
σ_x [mm]	3.5	2.4	2.9
σ_y [mm]	2.2	2.9	4.5

*1 RIKEN Nishina Center

*2 Department of Physics, Saitama University

*3 Department of Physics, University of Tsukuba

*4 IMP, CAS

*5 National Institute of Radiological Sciences (NIRS), QST

*6 Faculty of Sciences, Kyushu University

References

- 1) Z. Ge *et al.*, RIKEN Accel. Prog. Rep. **50**, (2017).
- 2) N. Nankov *et al.*, Wiss. Tech. Berichte (Annual Report 2004) **FZR-423**, 25 (2005).

Intermediate Tracker Integration in sPHENIX

D. Cacace,^{*2} Y. Akiba,^{*1} K. Cheng,^{*3} E. Desmond,^{*2} T. Hachiya,^{*1,*4} T. Kondo,^{*5} C. Kuo,^{*3} M. Lenz,^{*2} E. Mannel,^{*2} C. Miraval,^{*2} M. Morita,^{*4} I. Nakagawa,^{*1} R. Nouicer,^{*2} R. Pisani,^{*2} M. Shibata,^{*4} C. Shih,^{*3} A. Suzuki,^{*4} T. Todoroki,^{*1} X. Wei,^{*6} and R. Xiao^{*6}

The sPHENIX collaboration at RHIC is constructing a major upgrade to the PHENIX detector, consisting of an entirely new spectrometer based on the former BaBar solenoid magnet and the PHENIX facilities and infrastructure.¹⁾ The upgrade will allow for an in depth jet and beauty quarkonia physics program to address the fundamentals of strongly coupled quark-gluon plasma. The solenoid magnet is sandwiched by hadronic calorimeters (HCal) followed by an electromagnetic calorimeter (EMCal). Inward of the EMCal is a time projection chamber (TPC), INTermediate silicon strip Tracker (INTT) and MAPS-based VerTeX detector (MVTX) composing the sPHENIX tracking system. All of the subsystems have their challenges when coalescing with one another, but the INTT is of particular interest in terms of integration considerations.

The INTT design, constrained by its neighbors, has been heavily influenced by the other sPHENIX tracking components. The MVTX's active region has an outer diameter of 10.5 cm and has a service cone longitudinally starting at 25 cm from the vertex and grows to a diameter of 21.5 cm. The TPC has an inner diameter of 40 cm that spans a length of 117 cm from the vertex in both directions. The INTT has to fit between these envelopes. The INTT detector itself consists of three main components each consisting of several sub-components as seen in Fig. 1.

The first main component is the active region containing the silicon sensors. Four sensors are wire bonded to 52 FPHX chips¹⁾ which are wire bonded and epoxied to two high-density interconnects (HDI) and both are epoxied to a stave for structural support. This assembly, known as a ladder, as seen in Fig. 2, covers an acceptance of pseudorapidity of ± 1.1 . Several ladders arranged tangentially to a circle around the vertex compose what is referred to as a barrel. The active area of the sensors is approximately half the width of the HDI, which lends itself to a configuration where two barrels are required to obtain hermetic 2π azimuthal coverage, referred to as one layer. The detector consists of four barrels or two layers at approximate radial positions of 7.2, 7.7, 9.7 and 10.3 cm from the beam axis. The layers are held in position

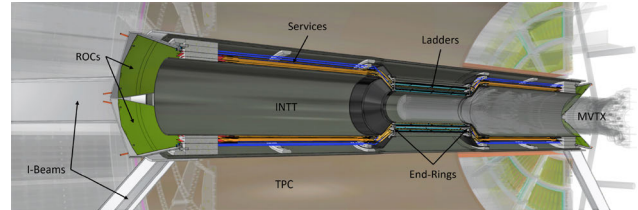


Fig. 1. INTT in sPHENIX 3D model cross section.

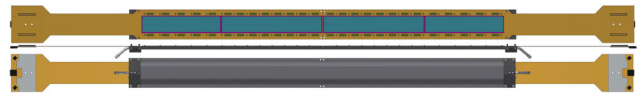


Fig. 2. INTT ladder 3D model.

with a series of stave end-caps and end-rings.

The end-rings also attach the barrels to the second main component, the service barrel. The service barrel, consisting of two carbon fiber tubes and miscellaneous brackets, carries the services (cables, cooling, nitrogen, *etc.*) from the ladders to beyond the TPC volume. The cables terminate just beyond the TPC and connect to the readout cards (ROC). The cooling and nitrogen connect to manifolds beyond the TPC. From there all the services are routed to the respective racks and/or infrastructure facilities. The outside of the service barrel also has features that allow for the detector and service barrel to be installed as a singular unit.

Lastly, the third main component of the INTT is its support structure. Consisting of a carbon fiber tube and aluminum I-beams, the support structure facilitates the installation and operation of the INTT and all of its services. The I-beams connect the carbon fiber tube to the inner HCal creating a direct load path for the detector and direct service routing to the INTT's racks. The I-beams also support the ROCs at an appropriate location for the HDI extension cables that have a maximum length of 120 cm.

Prototype ladders are being produced to verify the design and assembly fixtures for production.²⁾ Prototype end-rings will be produced in conjunction with the ladders to verify the barrel configurations. The service barrel and support structure designs are far along and are continuously being verified that they properly integrate with the surrounding sPHENIX detectors.

^{*1} RIKEN Nishina Center

^{*2} Brookhaven National Laboratory

^{*3} National Central University

^{*4} Nara Women's University

^{*5} Tokyo Metropolitan Industrial Technology Research Institute

^{*6} Purdue University

References

- 1) sPHENIX Conceptual Design Report (2018), https://indico.bnl.gov/event/4625/attachments/18432/23516/sphenix-conceptual-design_051918.pdf.
- 2) C. Miraval *et al.*, in this report.

Assembly of Intermediate Silicon Tracker in Taiwan

C. Shih,^{*3} Y. Akiba,^{*1} D. Cacace,^{*2} K. Cheng,^{*3} E. Desmond,^{*2} T. Hachiya,^{*1,*4} S. Hasegawa,^{*5} T. Kondo,^{*6} C. Kuo,^{*3} M. Lenz,^{*2} E. Mannel,^{*2} C. Miraval,^{*2} M. Morita,^{*4} I. Nakagawa,^{*1} R. Nouicer,^{*2} R. Pisani,^{*2} M. Shibata,^{*4} A. Suzuki,^{*4} T. Todoroki,^{*1} X. Wei,^{*7} and R. Xiao^{*7}

The INtermediate Tracker (INTT) is the tracker system between the Time Projection Chamber (TPC) and the MAPS-based Vertex Detector (MVTX). INTT makes up the gap between TPC and MVTX, it can precisely reconstruct the track of charge particles. One INTT ladder consists of 59 components, 1 stave, 2-high density interconnects (HDIs), 52 readout chips and 4 silicon sensors. All the components will be fixed by glue and screws. A ladder assembly is performed in the following sequence. 1), Fix the readout chip on HDI by silver epoxy with 26 chips per HDI. 2), Bond the readout chips to HDI using a bonding machine and check the response to slow control commands in a test bench. 3), assemble HDI with readout chips onto stave by thermal glue and screws. 4), Assemble silicon sensors onto the ladder by silver epoxy. 5), Bond the silicon sensors to readout chips by a bonding machine and check the FPHX response again and also silicon sensor performance. 6), Apply an encapsulation to protect the bonding wires. The National Central University (NCU) in Taiwan is responsible for one-third of the INTT ladder production.

The assembly procedures 1) and 2) are planned to be covered by a private company in Taiwan, and the remaining procedures will be conducted in a clean-room facility at the National Taiwan University (NTU). Figure 1 shows the gantry to be used for the assembly in NTU, which consists of a large flat table with a four-dimensional robotic gantry head. The gantry head is equipped with an optical microscope, which allows a calibration error in position to be the order of $10\ \mu\text{m}$. Thus far, the assembly procedure requires 9 tools, as shown

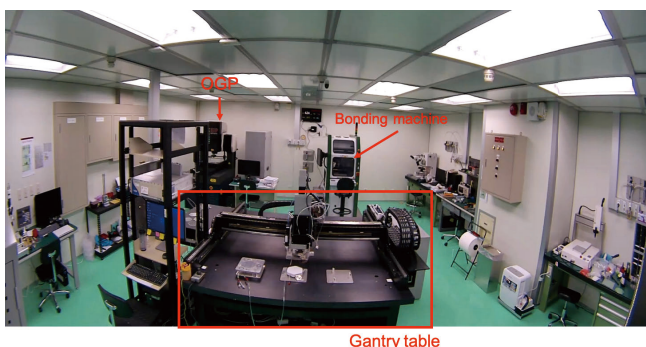


Fig. 1. Photo of the clean room in NTU. Gantry, bonding machine and optical gaging products (OGP) microscope are all available.

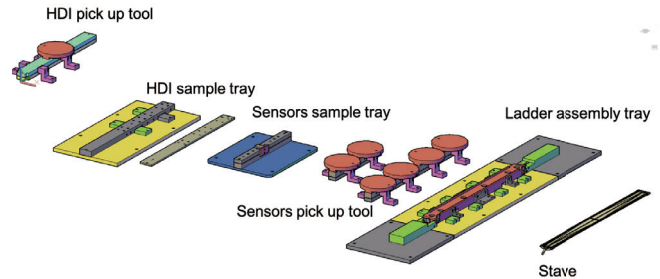


Fig. 2. The designs of the prototype of INTT ladder assembly tools, the assembly tools family.

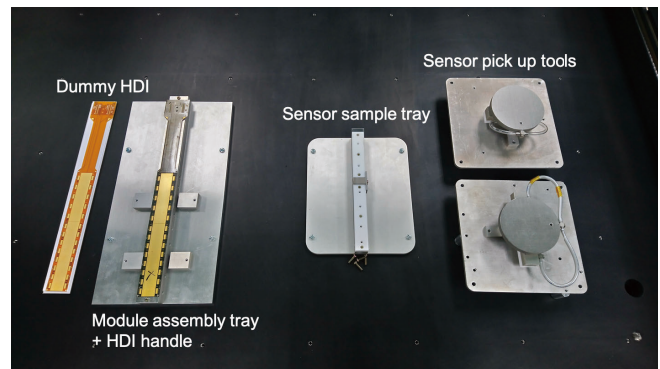


Fig. 3. Assembly tools already fabricated by AS CNC.

in Fig. 2. The assembly unit is one ladder, and the designs of all prototype assembly tools have been completed. The idea is to assemble the entire ladder on the ladder assembly tray, while HDIs and silicon sensors are placed on the HDI sample tray and sensor sample tray by hand, respectively. Pick up tools are used to pick up the HDI and silicon sensors via the vacuum system and move them to the stave by the gantry. An order for the tools has already been submitted to the Academia Sinica (AS) computer numerical control (CNC) factory. The production of 5 has been completed, as shown in Fig. 3. The assembly exercise and bonding exercise are scheduled to start simultaneously in early March. A dummy HDI, dummy silicon sensor, and dummy stave have also been produced, which are sufficient for the exercise. Two important aspects namely, the type of glue and the procedure to apply the glue, are uncertain and need to be determined. Both are expected to be finalized at the end of March. A new INTT test bench has been set up in NCU, and a few checks are to be made to be fully functional.

The conclusion for the INTT assembly in Taiwan is that we aim to provide one functional complete ladder for INTT phase - 3 Test Beam at 22th April.

References

- 1) Conceptual Design Report of sPHENIX (2018).
- 2) The PHENIX Forward Silicon Vertex Detector.

^{*1} RIKEN Nishina Center
^{*2} Brookhaven National Laboratory
^{*3} National Central University
^{*4} Nara Women's University
^{*5} Japan Atomic Energy Agency
^{*6} Tokyo Metropolitan Industrial Technology Research Institute
^{*7} Purdue University

Development status of long data cable for sPHENIX-INTT detector

T. Hachiya,^{*1,*2} Y. Akiba,^{*1} D. Cacace,^{*3} K. Cheng,^{*4} E. Desmond,^{*3} S. Hasegawa,^{*5} T. Kondo,^{*6} C. Kuo,^{*4} M. Lenz,^{*3} E. Mannel,^{*3} C. Miraval,^{*3} M. Morita,^{*2} I. Nakagawa,^{*1} R. Nouicer,^{*3} R. Pisani,^{*3} M. Shibata,^{*2} C. Shih,^{*4} A. Suzuki,^{*2} T. Todoroki,^{*2} X. Wei,^{*7} and R. Xiao^{*7}

The intermediate tracker (INTT) is a silicon strip barrel detector for the sPHENIX experiment.¹⁾ INTT requires a special extension cable for data transfer between the INTT module and readout electronics. The data cable must satisfy the following requirements to fit the tight space available for INTT at the sPHENIX detector: (1) flexibility, (2) a very long length of at least 120 cm, (3) high-density signal lines (128 lines/5 cm width), and (4) high-speed signal transfer (by LVDS).²⁾ The development of the cable is the most challenging part of the INTT project.

We performed research and development of the cable in the past two years. The design of the cable was optimized using a signal-transfer simulation with the strip-line structure. We then made a prototype of the cable using a flexible printed circuit board (FPC) with a liquid crystal polymer (LCP) as the substrate. The LCP realizes a small signal loss because of its small dielectric constant. The electrical and mechanical performance of the prototype were tested.²⁾ Based on this knowledge, we made a 120-cm-long prototype cable.

We measured the eye diagram to study the transfer performance of the cable. Figure 1 shows the input (left) and output (right) shapes of the eye diagrams. The signal height is 30% attenuated, and the waveform is rounded. This change in waveform is consistent with the expectation from simulation. We found that the eye is clearly open. To quantify the performance, we will measure the bit error rate.

In June 2019, we performed a beam test with a 120 GeV proton beam at the Fermilab Test Beam Facility (FTBF). The performance of the INTT module

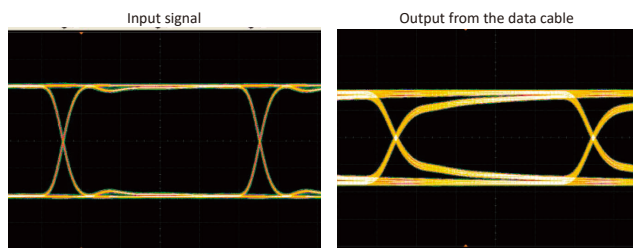


Fig. 1. Eye diagram with (right) and without (left) the cable.

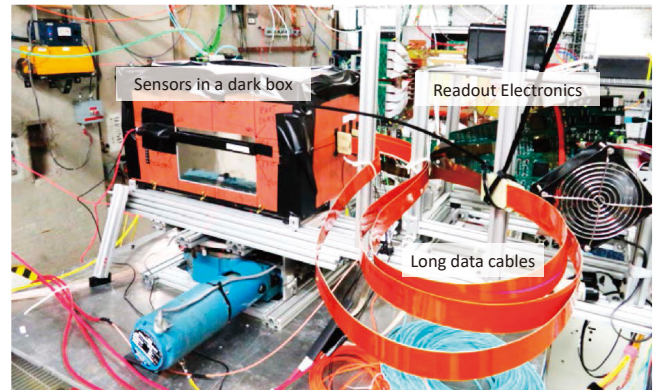


Fig. 2. Setup for testing the cable during the beam test at FTBF.

was evaluated in terms of the detection efficiency and minimum ionizing particle (MIP) peak.³⁾ In addition, the prototype cable was tested under a beam environment. The data were taken using the cable together with the INTT module and, later, readout electronics. Figure 2 shows the test setup at the beam test. The INTT modules are installed in a dark box, and the readout electronics are placed. The cable, shown as an orange flat cable that makes loops, is connected to them. This was the first attempt to take data with the full readout chain of the INTT detector. Further investigation is ongoing to quantify the performance under the beam environment.

An issue was found in the production of through holes on the cable. We found that the through holes have nodules caused by the residue of the adhesive sheet used to laminate the FPC layers. Several attempts to clean the through holes by changing the drill process and desmear process were unsuccessful. We will test new adhesive sheets from different manufacturers. These sheets are suitable for LCP according to the catalog.

In summary, the development of an extremely long and high-density cable is in progress. The production version of the cable was made and tested under a beam environment. An issue is under investigation. We will test new adhesive sheets, and a new prototype will be made using a new adhesive sheet and tested during the beam test in May 2020.

References

- 1) I. Nakagawa *et al.*, in this report.
- 2) T. Hachiya *et al.*, RIKEN Accel. Prog. Rep. **52**, 128 (2019).
- 3) A. Suzuki *et al.*, in this report.

*1 RIKEN Nishina Center

*2 Nara Women's University

*3 Brookhaven National Laboratory

*4 National Central University

*5 Japan Atomic Energy Agency

*6 Tokyo Metropolitan Industrial Technology Research Institute

*7 Purdue University

Performance evaluation of a sensor module for INTT at sPHENIX

A. Suzuki,^{*1} Y. Akiba,^{*2} D. Cacace,^{*3} K. Cheng,^{*4} E. Desmond,^{*3} T. Hachiya,^{*2,*1} S. Hasegawa,^{*5} T. Kondo,^{*6} C. Kuo,^{*4} M. Lenz,^{*3} E. Mannel,^{*3} C. Miraval,^{*3} M. Morita,^{*1} I. Nakagawa,^{*2} R. Nouicer,^{*3} R. Pisani,^{*3} M. Shibata,^{*1} C. Shih,^{*4} T. Todoroki,^{*2} X. Wei,^{*7} and R. Xiao^{*7}

The intermediate silicon strip tracker (INTT) is one of the tracking detectors of sPHENIX.¹⁾ An INTT sensor module consists of a silicon strip sensor, a read-out chip called FPHX and a high-density interconnect (HDI).²⁾ The size of the silicon strip sensor is $232.2 \times 22.5 \times 0.32 \text{ mm}^3$. FPHX is a read-out LSI chip used for PHENIX.¹⁾ One FPHX reads out 128 channels. 26 FPHXs correspond to 128×26 read-out channels. Each channel is equipped with a shaping amplifier and 3-bit ADC. HDI is a flexible PC board.

We performed a beam test using a 120 GeV proton beam in June, 2019 at Fermilab and analyzed the data to evaluate the performance of the INTT sensor module. Figure 1 shows the setup of three sensor modules and two trigger scintillators. We call the layers from the front of the beam direction L0, L1 and L2. Two scintillators are arranged to sandwich the sensor modules.

We define the efficiency of L0 by Eq. (1) and describe how to calculate the efficiency. (1) Figure 2 shows the hit channel distributions for 26 FPHXs in a layer. The beam spot was observed at chip 6, 7, 19 and 20, respectively. L1 and L2 required a single strip hit at chip 6 and $\text{ADC} > 3$ to reduce noise. An L0 hit can be multi-strip hits among several chips around the beam spot. (2) We calculate the channel difference between L1 and L2 to choose the coincident hit from the track. Figure 3(a) shows the hit correlation between L1 and L2 so that events of channels with a difference $< \pm 5$ are selected for as shown in Fig. 3(b). (3) We calculate the hit expectation of L0 using L1 and L2 hits by using Eq. (2) to search for the most probable hit at L0. (4) We search for a corresponding hit at L0 to choose the one closest to the hit expectation. L0 channels are numbered from 0 to 256 by combining two FPHX chips to cover the whole width

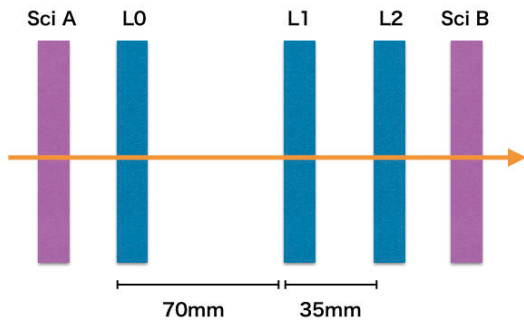


Fig. 1. Setup of ladders and scintillators in the beam test. The orange arrow indicates the beam direction.

^{*1} Nara Women's University

^{*2} RIKEN Nishina Center

^{*3} Brookhaven National Laboratory

^{*4} National Central University

^{*5} Japan Atomic Energy Agency

^{*6} Tokyo Metropolitan Industrial Technology Research Institute

^{*7} Purdue University

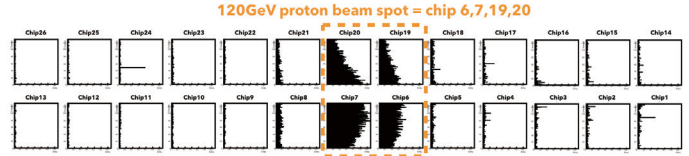


Fig. 2. Hit channel distribution of L0. X-axis: entries, Y-axis: channel number.

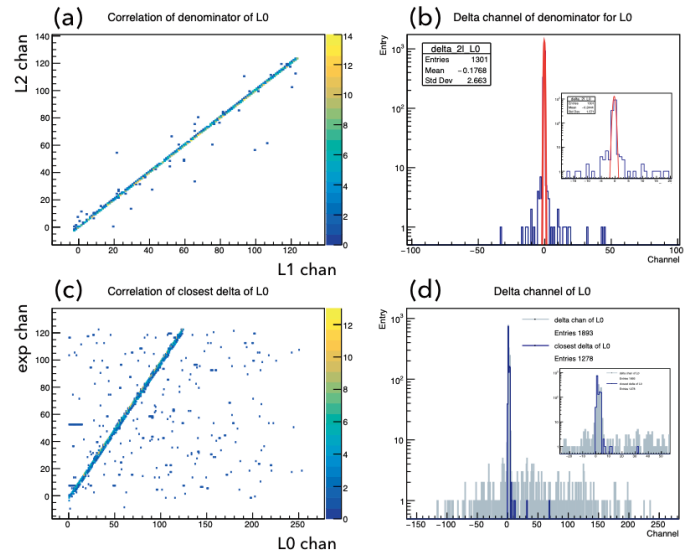


Fig. 3. (a) Hit correlation between L1 and L2. X-axis: L1 channel, Y-axis: L2 channel. (b) Difference (L1 channel - L2 channel). (c) Hit correlation between L0 and expectation. X-axis: L0 channel, Y-axis: expected channel. (d) Difference (L0 channel - expected channel).

of the sensor. Figure 3(c) shows the hit correlation of L0 with the expectation so that events of the closest hit of channels with a difference $< \pm 5$ are selected as shown Fig. 3(d). (5) The events of (2) as the denominator and (4) as the numerator for Eq. (1) are counted. The detection efficiency is evaluated as $96.0 \pm 0.5\%$, which is within the error margins of the value of $96.4 \pm 1.0\%$ obtained in the previous experiment conducted in 2018.

$$\text{L0 Efficiency} = \frac{N(\text{L0}_{\text{hit}} \cap \text{L1}_{\text{hit}} \cap \text{L2}_{\text{hit}})}{N(\text{L1}_{\text{hit}} \cap \text{L2}_{\text{hit}})}. \quad (1)$$

$$\text{L0}_{\text{exp}} = \text{L1}_{\text{chan}} \times 3 - \text{L2}_{\text{chan}} \times 2. \quad (2)$$

In summary, we analyzed the beam test data to evaluate the efficiency of the INTT sensor module. The efficiency of L0 is $96.0 \pm 0.6\%$. This result is consistent with the 2018 result.

References

- 1) I. Nakagawa *et al.*, in this report.
- 2) C. Aidata *et al.*, Nucl. Instrum. Methods Phys. Res. A **755**, 44–61 (2014).

Sensor testing of Intermediate Silicon Tracker

K. Cheng,^{*3} Y. Akiba,^{*1} D. Cacace,^{*2} E. Desmond,^{*2} T. Hachiya,^{*1,*4} T. Kondo,^{*5} C. Kuo,^{*3} M. Lenz,^{*2} E. Mannel,^{*2} C. Miraval,^{*2} M. Morita,^{*4} I. Nakagawa,^{*1} R. Nouicer,^{*2} R. Pisani,^{*2} M. Shibata,^{*4} C. Shih,^{*3} A. Suzuki,^{*4} T. Todoroki,^{*1} X. Wei,^{*6} and R. Xiao^{*6}

The Intermediate Silicon Tracker (INTT) uses a multi-channel silicon sensor to record tracks of charged particles. The characteristics of all channels should be measured to determine the performance before assembly. Some coarse quality assurances of every sensor are made by Hamamatsu Photonics K.K. before delivery, including total IV and CV measurements of combined multiple channels. Individual channels are then tested at the National Central University (NCU) in Taiwan.

A half ladder of the INTT detector has 26 chips, and each chip has 128 channels. If we use a micropositioner to touch the sensor channel by channel, the measurement time will be huge. Furthermore, in this method, it is difficult to control the touch force on AC pads, resulting in severe damage to the pads. A major scratch on an AC pad can cause a fatal problem in the wire bond to the pad in an assembly process. The best solution is to use a probe card to connect 128 channels simultaneously and then pass through the relay matrix to scan each channel. We only need to raise the voltage once in one chip and keep the voltage to measure other channels. To avoid severe scratching on bonding pads in this testing process, we employ a probe station (MPI TS200) that can control the contact force of the probe. When height is defined, the repeatability of the machine is smaller than $2\ \mu\text{m}$, and the contact force is controlled by a machine, rather than a human hand. Because INTT silicon sensors have an AC-coupling design, all of the leakage current originating from silicon will be blocked by a capacitor between silicon and the readout metal. The most important measurement is, thus, the capacitance of each channel for the AC-coupling silicon sensors. To measure the capacitance, the silicon sensor should be fully depleted.¹⁾ In the AC-coupling silicon sensor structure (Fig. 1), the AC pads and silicon are isolated; therefore,

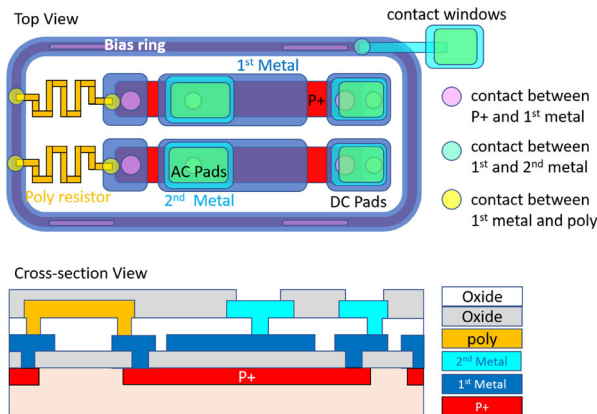


Fig. 1. Schematic of the AC coupling sensor.

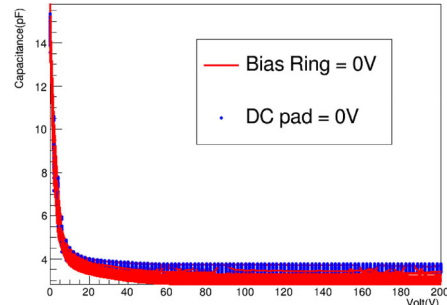


Fig. 2. CV curves of all channels in one chip. The blue markers show the result of connecting the DC pad to 0 V, and the red lines show the result of connecting the bias ring to 0 V.

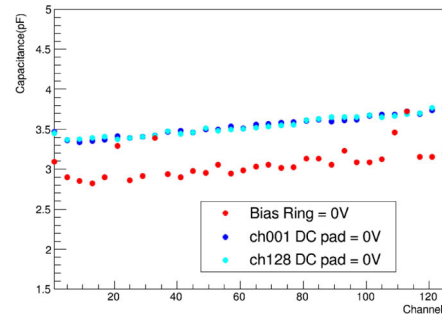


Fig. 3. Channel distribution of capacitance at full depletion. The red circles show the values obtained with the bias ring connected to 0 V, the blue and cyan circles show the value with the DC pads of channel-1 and channel-128 connected to 0 V.

we need a contacting bias ring to create a closed circuit to ensure full depletion. However, using a probe card to touch the readout pads and bias ring together is difficult because the contact window only opens at four corners of the full sensor. Therefore, the coordinates of the window are not constant for each chip. Now, we change the connection to the DC pad to 0 V create a circuit. In the first study, the capacitance difference is only 0.5 pF between the connections to the bias ring and DC pad. CV curves (Fig. 2) and the channel distribution of capacitance (Fig. 3) measured with two methods in one chip show almost the same behaviors, thus suggesting that the DC pad provides a reasonably consistent 0 V contact point as the bias ring with an extra offset of ~ 0.5 pF. Figure 3 shows that the capacitance is independent of which channel is connected to 0 V; therefore, a one-pin connection to the DC pad should be sufficient. Therefore, the probe card will have 129 pins: 128 for the measurement of the AC readout and one for the DC pad. Subsequently we can determine the existence of bad strips on the sensor and mark them.

Reference

- 1) R. Nouicer *et al.*, Nucl. Instrum. Methods Phys. Res. A **461**, 143–149 (2001).

*1 RIKEN Nishina Center
 *2 Brookhaven National Laboratory
 *3 National Central University
 *4 Nara Women's University
 *5 Tokyo Metropolitan Industrial Technology Research Institute
 *6 Purdue University

Geant4 simulation of INTT Phase-2 Test Beam at Fermilab

C. Shih,^{*3} Y. Akiba,^{*1} D. Cacace,^{*2} K. Cheng,^{*3} E. Desmond,^{*2} T. Hachiya,^{*1,*4} S. Hasegawa,^{*5} T. Kondo,^{*6}
 C. Kuo,^{*3} M. Lenz,^{*2} E. Mannel,^{*2} C. Miraval,^{*2} M. Morita,^{*4} I. Nakagawa,^{*1} R. Nouicer,^{*2} R. Pisani,^{*2}
 M. Shibata,^{*4} A. Suzuki,^{*4} T. Todoroki,^{*1} X. Wei,^{*7} and R. Xiao^{*7}

The INtermediate Tracker (INTT) is the tracker system between the Time Projection Chamber (TPC) and the MAPS - based Vertex Detector (MVTX). It makes up the gap between the TPC and the MVTX, and it can produce the track reconstruction of charged particles more precisely. To check the performance of the INTT modules, a beam test of INTT phase-2 was conducted in Fermilab in May 2019. Protons at 120 GeV were used in the test beam. Geant4 is applied to check the analysis results. The geometry of the INTT beam test in simulation is shown in Fig. 1. There are 4 layers of INTT modules, each of which is formed by 2 silicon sensors, HDI, and a cooling system. The air gap between two layers is 35 mm. The INTT modules are sandwiched by trigger scintillators, one in the front and one in the back. The readout chips and glue layers are not considered in the simulation.

The beam is set to be perpendicular to the modules in the first simulation. To be consistent with the actual data analysis of the beam test, only events that fire a single strip in layer 1 were selected in MC. A comparison of energy deposit distributions is shown in Fig. 2. The horizontal scale for MC is adjusted to match the MIP peak position. The result shows that MC is wider than the data. In order to investigate the discrepancy, the injection angle theta of the beam is scanned from 0 to 2.81 degree with 0.01 degree step in the second simulation. For most cases, the distribution of energy deposit is similar to that of the first simulation. However, we found that the shape of the distribution changes once the an-

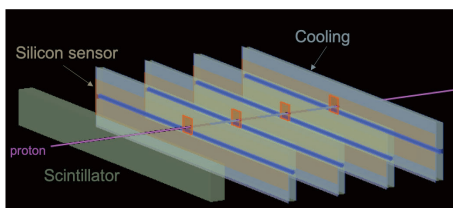


Fig. 1. Geometry of INTT Test Beam in simulation.

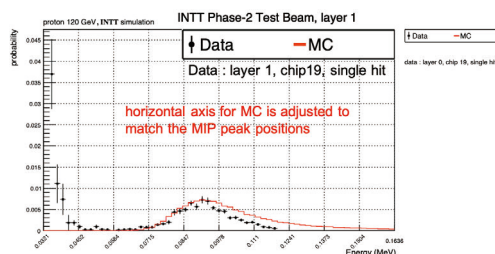


Fig. 2. Distribution of energy deposit, the beam direction is set to be perpendicular to modules.

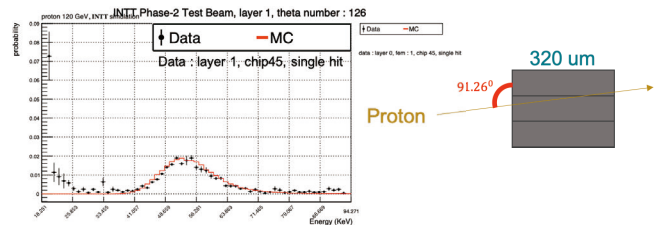


Fig. 3. Left: Distribution of energy deposit, beam theta angle is 1.26 degree. Right: the schematic of event display.

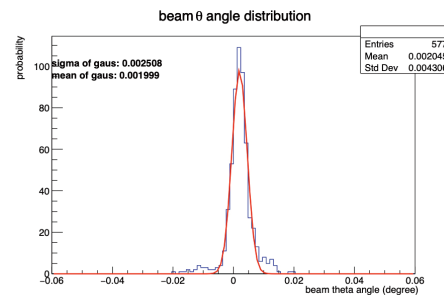


Fig. 4. Beam spot distribution of INTT Test beam.

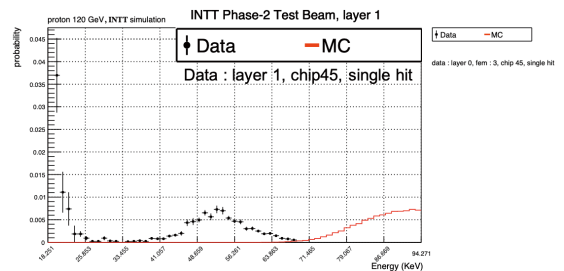


Fig. 5. Real energy deposit distribution.

gle passes a threshold, as illustrated in the right panel of Fig. 3. The proton starts to fire multiple strips, and the pass length of the primary strip becomes shorter than in the perpendicular case. Consequently, the MIP peak of the MC shrinks and leads to better agreement with the data, as demonstrated in the left panel of Fig. 3. The beam information of the phase-2 beam test is recorded by three wire chambers, and the beam spot is in Fig. 4, the sigma is 0.0025 degree. Thus, the beam information is optimized.

The second step is to reproduce the most probable value (MPV) of energy deposit. The function to convert data from mV to KeV is $0.075 * mV = KeV$. The MPV ratio of the data and MC is 56.5%, the plot is shown in Fig. 5.

In conclusion, the simulation indicated that the beam was not injected at a perfectly perpendicular condition to the INTT modules. The next step is to feed the beam-spot distribution to a simulation with a different angle and to find the angle between the beam direction and modules. In the phase-3 INTT test beam, the gain and timing setting needs to be checked.

Reference

- 1) Conceptual Design Report of sPHENIX (2018).

*1 RIKEN Nishina Center
 *2 Brookhaven National Laboratory
 *3 National Central University
 *4 Nara Women's University
 *5 Japan Atomic Energy Agency
 *6 Tokyo Metropolitan Industrial Technology Research Institute
 *7 Purdue University

Development of high-resolution hard X-ray detector system by using transition-edge sensor for accelerator-based experiments

T. Isobe,^{*1} H. Kaori,^{*2} T. Okumura,^{*1} S. Okada,^{*1} S. Yamada,^{*3} H. Tatsuno,^{*3} D. A. Bennett,^{*4} J. A. B. Mates,^{*4} D. Yang,^{*4} D. S. Swetz,^{*4} and T. Hashimoto^{*5} for the HEATES collaboration

A transition-edge sensor (TES) is a type of low-temperature microcalorimeter that provides a much better energy resolution than semiconductor detectors by using a superconducting material as the temperature sensor at the superconducting-to-normal transition-edge. Recently, a detector system with TES was employed for accelerator-based experiments.¹⁾ For instance, a high-resolution X-ray measurement of a Kaonic atom was successfully performed at J-PARC in spring 2018.²⁾ An energy resolution of 5.7 eV in FWHM was shown for the Co K α X-ray line (6.9257 keV) during the beam time, while a resolution of 5 eV in FWHM can be achieved for the same line with the beam off. As the next step of high-resolution X-ray spectroscopy with a TES detector system for accelerator-based science, we are constructing a new system by introducing a modern cryogenic system (HPD Co. Ltd. model 107 adiabatic demagnetization refrigerator, ADR, cryostat) and novel microwave readout system for TES. The model 107 cryostat has a helium-3-backed, single-stage ADR with an ADR base temperature of 30 mK and a 300-h no-load regulation at 100 mK. Figure 1(a) shows the inside of the new cryogenic system.

The sensitivity of the TES is expressed as $\Delta T = E/C$, where ΔT is the temperature change, E the energy of X-rays, and C the heat capacity of the TES. Thus, the size of the TES, which determines C , is limited for a target performance. Typically, the size of one pixel is $100 \times 100 \mu\text{m}^2$. In order to enlarge the acceptance of the detector, it is necessary to increase the number of TES pixels (readout channel). However, the number of electric connections to the cryostat is limited to less than ~ 100 due to the limitation in cooling power of the cryogenic system. Recently, a novel readout technique using a microwave resonator was developed.³⁾ By introducing such microwave readout, the number of readout channels is expected to be increased up to ~ 1000 per readout connection. Figures 1(b) and (c) show the transmitted power of the prototype resonator, which gives 64 tones, where one tone is used for one TES pixel readout.

After finishing the construction of the new detector system, we plan to execute online experimental projects for the precise measurement of hard X-ray

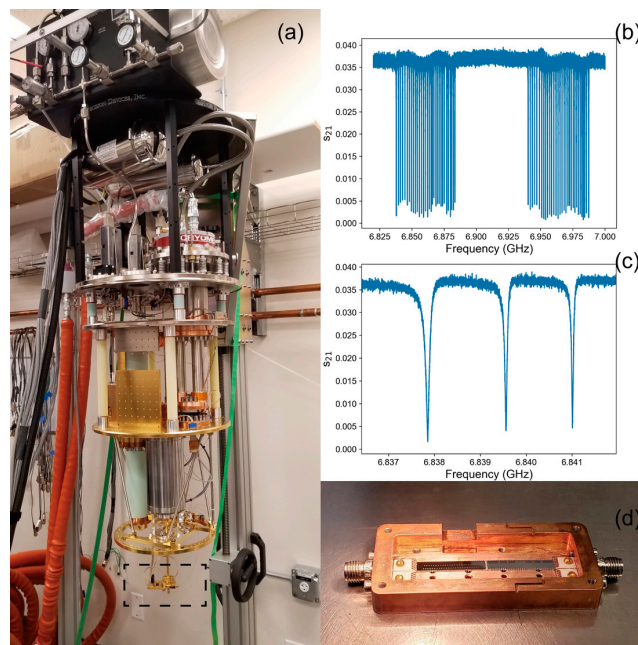


Fig. 1. (a) New cryogenic system to introduce the novel TES detector. The top plate is used for vacuum sealing. The other plates are used for shielding thermal radiation of 300 K, 3 K, and 300 mK from top to bottom. The TES detector is supposed to be mounted on the bottom part indicated by dashed square. (b) Transmitted power of the prototype resonator. Each tone corresponds to one channel (TES pixel). (c) Enlarged view of the X-axis of (b). (d) Prototype resonator mounted in model 107.

lines from atomic/nuclear excited states. For example, X-rays from a muonic atom will be measured for the validation of quantum electromagnetics. Furthermore, X-rays from the excited isomeric state of Th-229 are proposed to be measured. Currently, a molybdenum-gold bilayer TES microcalorimeter for X-rays in the range of 20 keV to 45 keV X-rays has been designed, and its prototype has been tested.

This work is supported by the Japanese MEXT KAKENHI under grant No. 18H05458 and No. 18H03713.

References

- 1) S. Okada *et al.*, Prog. Theor. Exp. Phys. **2016**, 091D01 (2016).
- 2) T. Hashimoto *et al.*, J. of Low Temp. Phys. **199**, 1018 (2020).
- 3) J. A. B. Mates *et al.*, Appl. Phys. Lett. **92**, 023514 (2008).

*1 RIKEN Nishina Center

*2 National Institute of Advanced Industrial Science and Technology (AIST)

*3 Graduate School of Science, Tokyo Metropolitan University

*4 National Institute of Standards and Technology (NIST)

*5 Japan Atomic Energy Agency (JAEA)

SAMURAI DAQ speed improvement

J. Gao,^{*1,*3} H. Baba,^{*1} M. Sasano,^{*1} and L. Stuhl^{*2}

In this contribution, we report the improvement of the SAMURAI DAQ speed. SAMURAI DAQ contains several VME subsystems. The typical dead time was about $200 \mu\text{s}$. It is necessary to improve the DAQ system to acquire sufficient data for recent studies.

The accurate measurement of dead time is critical for the performance improvement. Conventionally, we estimate the typical dead time by checking the width of busy signals using an oscilloscope. However the width can be different for events with different data sizes. Therefore we developed a new method to evaluate the dead time as a function of data size using saved data. This method helps us find the device that critically limits the DAQ speed.

The data size is easy to obtain from the data file, while the dead time can be extracted from event time-stamps. Let Δt be the time interval between neighboring events (see Fig. 1). If we acquire a large amount of data, we can expect some events to be accepted immediately after the dead time is finished (like event 3 in Fig. 1).

$$\text{dead time}(size = s) = \inf\{\Delta t_i | size_i = s\}.$$

With pairs $(size_i, \Delta t_i)$ of each event, where $size_i$ is the data size of the device of interest for event i and Δt_i is defined in Fig. 1, we can draw a 2D histogram. For example, Fig. 2 shows two plots generated from SAMURAI30 experiment¹⁾ data. In this example, the histogram for the proton drift chamber (PDC) has a linear edge, but that for the beam drift chamber (BDC) appears to have a plateau on the small data size side. This implies that BDC should wait for other device(s) to finish data saving when it has a small amount of data. We conclude that PDC is the bottleneck and should be improved. We can repeat these steps to optimize DAQ performance until all devices show a linear edge on the histograms or the dead time becomes low enough for the experiment.

This method is also useful for comparing the performance of different modules. For example, Fig. 3(a) and Fig. 3(b) show the results for two widely used TDCs,

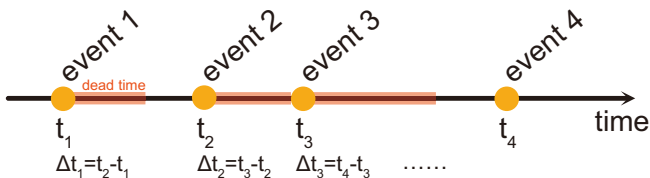


Fig. 1.: Definition of the time interval between neighboring events Δt .

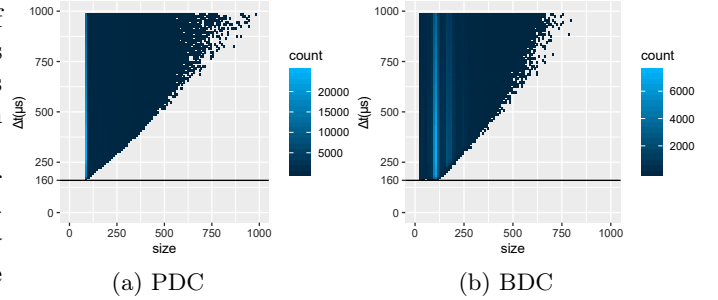


Fig. 2.: Plot of Δt versus data size for SAMURAI30 data. A comparison of the figures indicates that PDC limits the DAQ performance.

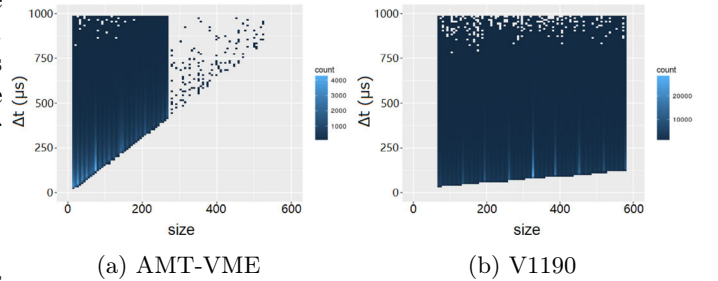


Fig. 3.: Plot of Δt versus data size for source test data. AMT-VME TDC has a larger slope, implying that its performance is worse.

AMSC AMT-VME TDC and CAEN V1190 TDC, respectively. We performed a source test for each TDC and plotted the resulting 2D histograms. The edge in the AMT-VME's histogram exhibits a sharper slope, which implies that the dead time of this module quickly increases when the data size increases. We emphasize here that it would be very difficult to recognize this performance difference through an oscilloscope measurement.

We applied this method to optimize DAQ for the SAMURAI 11 experiment.²⁾ According to the results shown in Fig. 3, the DAQ speed was limited by the TDC modules, rather than the detectors. Therefore in the experiment, all AMT-VME TDCs were replaced by V1190 TDCs. Combined with other optimizations, such as the disabling of unnecessary TDC headers, the typical dead time in SAMURAI 11 was about $50 \mu\text{s}$, and the accepted trigger rate was about 5 kHz. This is a large improvement over previous experiments in SAMURAI, which typically had a dead time of about $200 \mu\text{s}$ and accepted trigger rate of about 1 kHz.

(This work is funded by the China scholarship Council.)

References

- 1) L. Stuhl *et al.*, RIKEN Accel. Prog. Rep. **52**, 33 (2018).
- 2) M. Sasano *et al.*, in this report.

^{*1} RIKEN Nishina Center, Japan

^{*2} Center for Nuclear Study, University of Tokyo, Japan

^{*3} School of Physics, Peking University, China

High-stability high-voltage power supply for MRTOF[†]

P. Schury,^{*1} M. Wada,^{*1} H. Wollnik,^{*1,*2} J. -Y. Moon,^{*1,*3} T. Hashimoto,^{*1,*3} and M. Rosenbusch^{*1}

Achieving the highest possible mass resolving power in a multi-reflection time-of-flight (MRTOF) mass spectrograph requires very high-stability power supplies. To this end, we have developed a programmable high-voltage power supply that can achieve long-term stability on the order of parts-per-million. We have demonstrated that in the ≤ 1 Hz band the output stability is on the level of 1 part per million (ppm) during one hour, with only slightly more output variation across 3 days. We have further demonstrated that the output is largely free of noise in the 1 Hz–200 Hz band. We have also demonstrated settling to the ppm level within one minute following a 100 V step transition. Finally, we have demonstrated that when these power supplies are used to bias the electrodes of an MRTOF the measured time-of-flight is stable on the ppm-level for at least one hour.

In order to achieve a fast-settling, high-precision, long-term stable high-voltage power supply for driving our MRTOF, we have extended the concept laid out in the Voltage Multipliers, Inc, application note “AN-0300 - High Voltage Op-Amp Application Using Opto-Couplers,¹⁾” which describes the use of infrared LEDs and high-voltage photodiodes to emulate an operational amplifier with up to 15 kV power supply span. A conceptual circuit diagram of our design, separated into functional blocks, is given in Fig. 1.

A crate of 16 power supplies was built to bias the

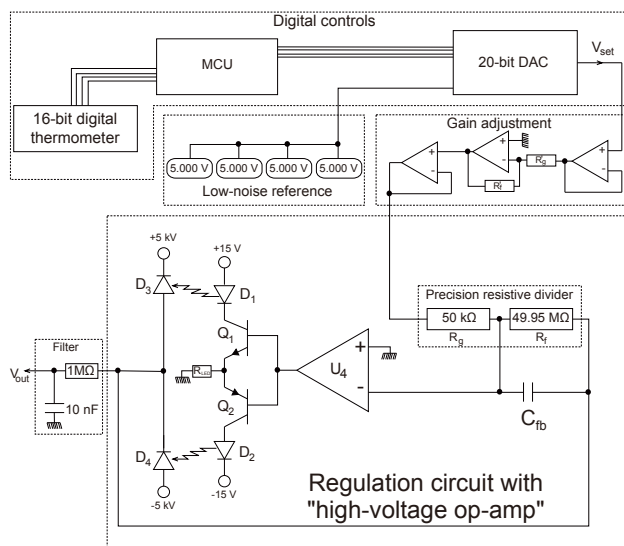


Fig. 1. Design of the high-voltage stabilization circuit.

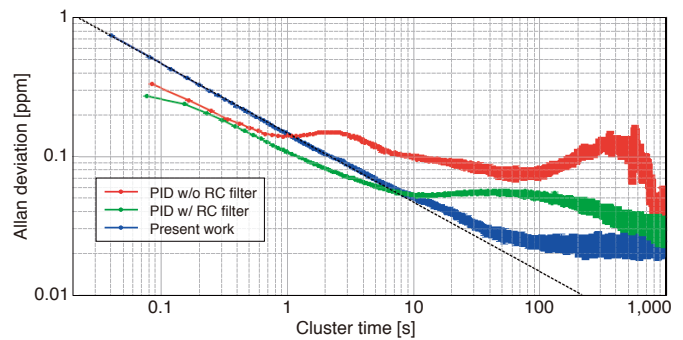


Fig. 2. Allan deviation from individual ion times-of-flight. The PID regulation without and with RC filter exhibit a slope approximating white noise to ≈ 1 s and ≈ 10 s, respectively. The dashed line indicates the trend expected for white noise. The Allan deviation curve switches to a flat line indicative of flicker noise at a level of ≈ 0.02 ppm, which coincides with the 0.1 ns raw bin width from the TDC.

electrodes of 50 cm MRTOF-MS in the E3 (KISS) vault. The voltages were adjusted until a time resolving power of $\frac{t}{\Delta t} \approx 250,000$ was achieved. Due to the lens voltage requiring a bias of 5 kV or more, we have thus far opted to use an NHR 42 60r high-precision ± 6 kV power supply from ISEG to bias this electrode.

Figure 2 shows the result of an analysis of time-of-flight data from a several-hours-long measurement using our newly developed power supplies with the MRTOF in E3 along with a similar analysis using pre-existing hours-long duration data from our full-size MRTOF-MS operated with a PID stabilization scheme. The data for the PID stabilization was obtained using a 30 ms cycle period, yielding a minimum Allan deviation²⁾ sampling period of ≈ 80 ms. The data for the present system was obtained using a 15 ms cycle period, yielding a minimum Allan deviation sampling period of ≈ 40 ms. These analyses shows that in terms of long-term stability the voltage stabilization circuit of the present work exceeds the performance of our RC filter enhanced PID regulation system. Using our new power supplies, the MRTOF exhibits white noise in the ion time-of-flight over a much wider duration than with the PID-based regulation systems.

References

- 1) “AN-0300 - High Voltage Op-Amp Application Using Opto-Couplers,” Voltage Multipliers, Inc, <http://www.voltagemultipliers.com/pdf/High-Voltage-Op-Amp-and-Linear-Regulator-App-Notes.pdf>.
- 2) N. El-Sheimy, H. Y. Hou, X. J. Niu, IEEE Trans. Instrum. Meas. **57**, 140–149 (2008).

[†] Condensed from Rev. Sci. Instrum. **91**, 014702 (2020)

^{*1} KEK Wako Nuclear Science Center

^{*2} New Mexico State University

^{*3} Institute for Basic Science

Eliminating mass-dependent inaccuracies in MRTOF-MS for the study of RI using arbitrary reference masses

M. Rosenbusch,^{*1} P. Schury,^{*1} M. Wada,^{*1} S. Imura,^{*2,*3} Y. Ito,^{*4} and H. Wollnik^{*5}

In high-precision mass spectrometry of radioactive isotopes, mass dependent inaccuracies are one of the major topics to be discussed, because the ionic mass (mass-to-charge ratio) of the rare isotopes to be studied can be distant from that of the reference ions used for calibration. In Penning-trap mass spectrometry, such effects have been studied extensively in the past using carbon cluster sources.¹⁾ For multi-reflection time-of-flight (MRTOF) mass spectrometry similar investigations are awaited, but are not completed yet. Other than in Penning traps, in electrostatic ion optics systems the trajectory of ions of equal energy but different mass is exactly the same, which comes from fundamental theorems. Following that, the detected TOF of any ion is obtained by $t_D = \alpha\sqrt{m/q}$, with the characteristic device constant α and m, q as mass and charge. The mass can be calculated by use of a reference ion with m_1, q_1 and TOF t_{D1} by:

$$m = q \frac{m_1}{q_1} \left(\frac{t_D - t_0}{t_{D1} - t_0} \right)^2, \quad (1)$$

with t_0 being the offset time of the measurement (start of the TDC). However, mass-dependent inaccuracies can come from the acceleration process of the ions, which has been investigated in a new theoretical framework.²⁾ The acceleration process of ions out of an ion trap happens with an electric field that is switched on with a transient in time with duration t_T , and induces a mass-dependent dynamic process. We have found a solution to include such a field transition, and to calibrate masses far away from the reference mass despite this effect, while having only one reference ion species available during the online measurement. To this end, the system can be pre-calibrated once using two stable ion species before the online measurement according to the new equation $t_D = \alpha\sqrt{m/q} + \beta\sqrt{q/m}$ having a second device constant β . During the online measurement, only one of the two reference species serves again as reference ion. Using a linear approximation of the acceleration field during the increase $\vec{E} = \vec{E}_{\max} \frac{t}{t_T}$, a new equation has been found for the mass of the ions:

$$m = q \left(\frac{\tilde{t}_D \tilde{t}_{D1}}{2\alpha \tilde{t}'_{D1}} + \sqrt{\left(\frac{\tilde{t}_D \tilde{t}_{D1}}{2\alpha \tilde{t}'_{D1}} \right)^2 - \frac{\beta}{\alpha}} \right)^2. \quad (2)$$

*1 Wako Nuclear Science Center (WNSC), IPNS, KEK

*2 RIKEN Nishina Center

*3 Osaka University

*4 Advanced Science Research Center, JAEA Ibaraki

*5 Department of Chemistry and Biochemistry, New Mexico State University

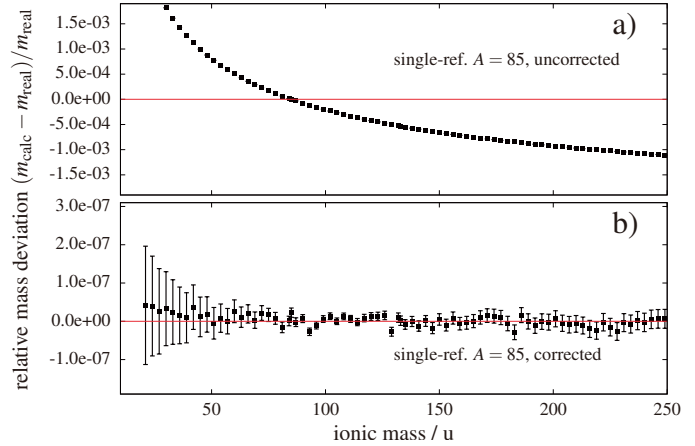


Fig. 1. Relative deviation from the real mass value (upon recalculation of the mass from the TOF data of the reflectron simulation) as a function of the mass number, using a transition time of 100 ns. a): Recalculation of masses using the usual approach without correction with mass $A = 85$ as reference ions. b): Recalculation with correction using Eq. (2). Note the different scales.

The times \tilde{t}_D , \tilde{t}'_{D1} , and \tilde{t}_{D1} are reduced detection times of the radioactive ion, the reference ion online, and the reference ion before the measurement, respectively. All times are reduced according to $\tilde{t}_D = t'_D - \frac{t_T}{2} - t_0$, where $t_T/2$ is a new correction for the switching transition emerging from the calculations. A simulation model for a simple TOF mass spectrometer with short TOF of only about $40 \mu\text{s}$ and a long switching time $t_T = 100 \text{ ns}$ has been written to show amplified effects. The TOF of ions has been simulated including dynamic acceleration, and over a broad mass range while assuming that our reference ions have mass $A = 85$. The results using the mass equation of the electrostatic problem and the newly derived mass formula is shown in Fig. 1. It can be seen that, in our constructed example, the impact of such dynamic ion acceleration can be very significant if the switching is not fully considered. For MRTOF-MS, however, this effect is usually very small because of the fast switches (20 ns) and the very long TOF of 6 ms. It will become important for measurements of super-heavy nuclei with large mass distances of reference to the SHE mass (depending on charge state), where the effects can become significant. The masses can then be accurately derived using the new correction.

References

- 1) A. Kellerbauer *et al.*, Eur. Phys. J. D **22**, 53 (2003).
- 2) M. Rosenbusch *et al.*, Int. J. Mass Spectrom., under review (2020).

On-line mass measurement using multi-reflection time-of-flight mass spectrograph (MRTOF-MS) at KISS

J. Y. Moon,^{*1} T. Hashimoto,^{*1} S. C. Jeong,^{*2} M. Wada,^{*2} P. Schury,^{*2} Y. X. Watanabe,^{*2} Y. Hirayama,^{*2} Y. Ito,^{*5} M. Rosenbusch,^{*3} T. Niwase,^{*4} H. Wollnik,^{*6} and H. Miyatake^{*2}

We report the first online measurement using a newly developed multi-reflection time-of-flight mass spectrograph (MRTOF-MS), which recently achieved a mass resolving power of, $\sim 120,000$ in an offline test. The detailed structure of the MRTOF-MS can be found in a previous report.¹⁾ As a calibrant for the $A \sim 200$ mass region, ^{85}Rb ions were chosen because the ^{198}Pt ions extracted from the gas cell cooler buncher (GCCB), were found more likely doubly charged.²⁾ The Rb ions existing in the ^{133}Cs ion source were filtered out by using the rear linear Paul trap mass filter and transported with significant intensity. During the online experiment using a ^{198}Pt target of 12.5 mg/cm^2 and ^{136}Xe beam of $10.75 \text{ MeV/nucleon}$, different target-like isotopes were produced in a multi-nucleon transfer reaction at KISS,³⁾ and among them, ^{194}Os ions were used to study the hyperfine structure.⁴⁾ At KISS, by adjusting the laser frequency, specific ions are selectively ionized by irradiating the ionization lasers in two steps and transported

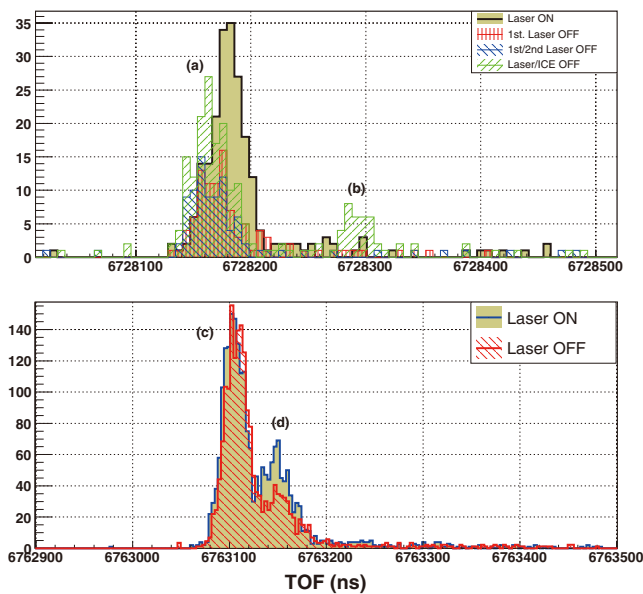


Fig. 1. Measured TOF spectra : ^{193}Os run (Upper) and ^{194}Os run (Lower). See the text for details.

^{*1} Institute for Basic Science, Rare Isotope Science Project
^{*2} Wako Nuclear Science Center (WNSC), Institute of Particle and Nuclear Studies (IPNS), High Energy Accelerator Research Organization (KEK)
^{*3} RIKEN Nishina Center
^{*4} Department of physics, Kyushu University
^{*5} Japan Atomic Energy Agency
^{*6} Department of Chem.&Bio.chem. New Mexico state university

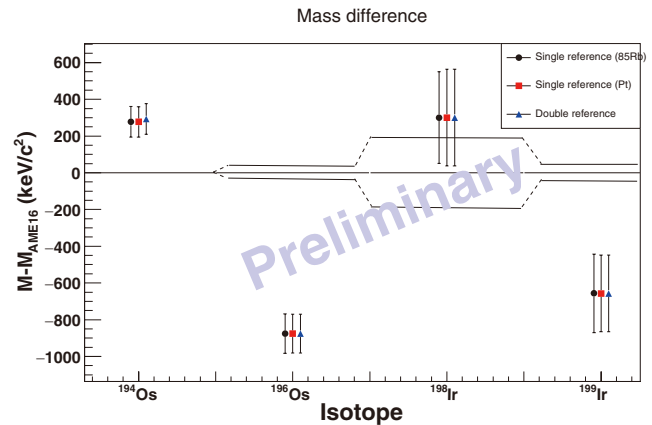


Fig. 2. Mass deviation from the AME2016 mass value. The solid line denotes the uncertainties from the AME2016.

with almost 100% purity. However, in most of the measurements, huge contaminants were observed, which seemed irrelevant to the ionization laser. As an example, Fig. 1 demonstrates the contaminants observed in the $^{193,194}\text{Os}$ runs, in which (a) and (c) are ^{193}Pt and ^{194}Pt ions, respectively, that survived from the elastic events emitted from the production target. The other contaminant near ^{194}Pt (d) is more likely a mixture of $A = 194$ isotopes (Ir, Au, and Hg). The contaminant (b), 6.5 micro-amu heavier than ^{193}Os , is not identified yet but sufficiently removed by the ion collection electrode (ICE). Fig. 2 demonstrates the accuracy and precision of each measurement of ^{194}Os ($T_{1/2} = 6 \text{ y}$), ^{196}Os ($T_{1/2} = 30 \text{ m}$), ^{198}Ir ($T_{1/2} = 8 \text{ s}$), and ^{199}Ir ($T_{1/2} = 6 \text{ s}$). Three different methods implemented to derive their masses, i.e., the single referencing method⁵⁾ using ^{85}Rb ions or Pt ions and the double referencing method,⁶⁾ were compared there. It should be noted that the large discrepancy of ^{194}Os is more likely due to the contaminant included in the ^{194}Os position, as previously described. The mass of ^{198}Ir has been directly measured for the first time, but it still needs more careful analysis.

References

- 1) J. Y. Moon *et al.*, RIKEN Accel. Prog. Rep. **52**, 138 (2019).
- 2) P. Schury *et al.*, in this report.
- 3) Y. Hirayama *et al.*, Nucl. Instrum. Methods Phys. Res. B **353**, 4 (2015).
- 4) Y. Hirayama *et al.*, in this report.
- 5) P. Schury *et al.*, Nucl. Instrum. Methods Phys. Res. B **335**, 39 (2014).
- 6) F. Wienholtz *et al.*, Nature **498**, 346 (2013).

Collinear laser spectroscopy of Ba^+ in $6s^2S_{1/2}$ - $6p^2P_{3/2}$ transition

Y. Sasaki,^{*1,*2} M. Tajima,^{*1} A. Takamine,^{*1} H. Iimura,^{*1,*3} M. Wada,^{*4} Y. Matsuo,^{*1,*2} and H. Ueno^{*1}

The nuclear electromagnetic properties in nuclear ground states and long-life isomeric states for a wide range of nuclides have been determined using collinear laser spectroscopy (CLS).¹⁾ We are developing a CLS apparatus for the slow RI beams that will be provided from the SLOWRI facility²⁾ in the near future, with the goal of realizing CLS for RIs that are difficult to obtain through the isotope separation on-line (ISOL) method. We have started off-line CLS test. As a first step, we selected stable Ba^+ isotope ions since their high intensity ion beams can be produced with a compact surface ionization source.

This report describes the off-line CLS experiment for the transition from the ground state $6s^2S_{1/2}$ to the excited state $6p^2P_{3/2}$. Tajima *et al.* report on the CLS test for the transition from $4d^2D_{5/2}$ to $6p^2P_{3/2}$ in this progress report.³⁾ The excitation wavelength for the $6s^2S_{1/2} \rightarrow 6p^2P_{3/2}$ transition for Ba^+ is 455 nm. We built an external cavity diode laser (ECDL), which was assembled with an anti-reflection-coated laser diode NDBA116T (peak wavelength range: 450 to 470 nm; manufactured by Nichia Corporation) and a 2400/mm holographic grating (Thorlabs GH13-24V) in a Littrow configuration. The wavelength of the ECDL was locked to a desired wavelength using a feedback system of a high-precision wavemeter (HighFines WS-U-10). The resulting time variation of the center frequency of the laser was narrowed to 4 MHz in full width at half maximum (Fig. 1).

The CLS test was performed using a home-built ECDL. Figure 2 shows a schematic of our CLS apparatus. Barium ions generated from the surface ionizer were accelerated by a high voltage of 10 to 20 keV. The accelerated ions were transported to an observation region after mass separation by a mass analyzing magnet.

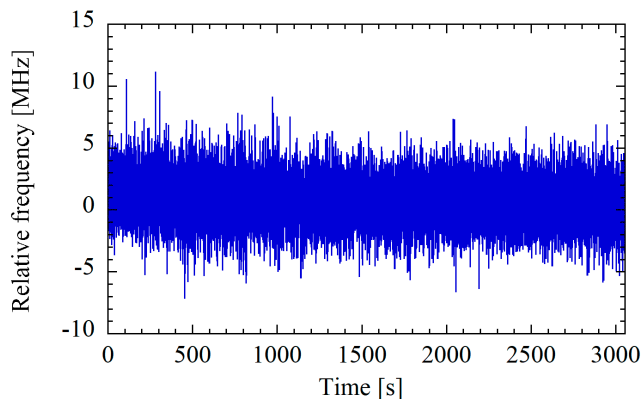


Fig. 1. Frequency locking result for our ECDL.

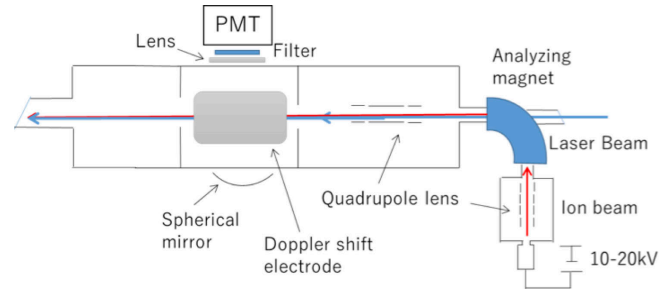


Fig. 2. Schematic diagram of our collinear laser spectroscopy apparatus.

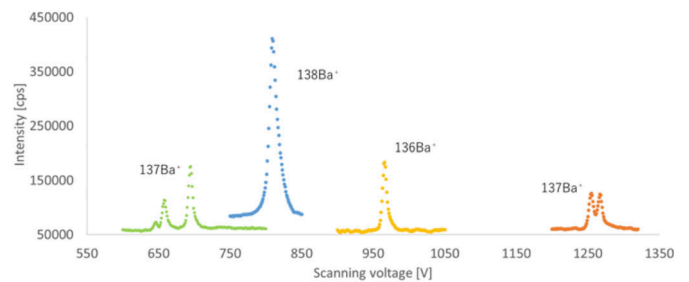


Fig. 3. Collinear laser spectroscopy spectra for $^{136-138}\text{Ba}^+$.

A series of electrodes to control the Doppler shift was placed around the observation region. Laser-induced fluorescence (LIF) from the ions was collected in a photomultiplier tube in front of the electrodes, as shown in Fig. 2. We observed resonance spectra while scanning the voltage of the electrodes to control the Doppler shift of the ions, instead of scanning the laser frequency. Figure 3 shows the observed spectra for $^{136,137,138}\text{Ba}^+$. At this time, the ions were accelerated to 10.51 keV, the laser frequency was locked to 658.372682 THz, and the laser power was 0.1 mW. The beam intensities were 200 pA, 350 pA, and 1.4 nA for $^{136}\text{Ba}^+$, $^{137}\text{Ba}^+$, and $^{138}\text{Ba}^+$, respectively. We successfully observed five resonance peaks for the transition between the hyperfine sublevels of $^{137}\text{Ba}^+$, and only the peaks for the $6s^2S_{1/2}$ state ($F = 1$) \rightarrow $6p^2P_{3/2}$ state ($F = 0, 1$) transition were not resolved, because the spacing is 32 MHz at most.

We continue systematic measurements under various experimental conditions such as different laser powers, acceleration voltages, and laser light path alignments for resolution improvement. We will also improve the sensitivity using a coincidence method,⁴⁾ aiming at the spectroscopy for low-yield nuclei obtained at online experiments.

References

- 1) P. Campbell *et al.*, Prog. Part. Nucl. Phys. **86**, 127 (2016).
- 2) M. Wada, Nucl. Instrum. Methods Phys. Res. B **317**, 450 (2013).
- 3) M. Tajima *et al.*, in this report.
- 4) D. A. Eastham *et al.*, Opt. Commun. **60**, 293 (1986).

*1 RIKEN Nishina Center

*2 Department of Advanced Science, Hosei University

*3 JAEA

*4 Wako Nuclear Science Center (WNSC), KEK

LIF observation of Rb atoms in superfluid helium by picosecond pulsed laser pumping

Y. Takeuchi,^{*1,*2} H. Kuramochi,^{*3} K. Imamura,^{*2} A. Takamine,^{*2} M. Doi,^{*1,*2} T. Yamamoto,^{*1,*2} Y. Matsuo,^{*1,*2} Y. Zempo,^{*4} T. Tahara,^{*3} and H. Ueno^{*2}

Our research group has been developing a laser spectroscopic method named OROCHI. The system uses superfluid helium (He II) as a trapping medium of atoms, and the interaction between the immersed atoms and the surrounding helium atoms leads to a unique property of the spectroscopic environment. In particular, the Stokes shift of the immersed atoms is important for understanding the dynamics of He II. In this study, we focus on the “atomic bubble” that causes the Stokes shift.

When atoms are introduced into He II, the surrounding helium atoms are pushed out by the exchange (Pauli) repulsion force.¹⁾ The resulting vacuum region is called an atomic bubble. When the shape of the outer electron orbit of the atom changes owing to a state transition such as excitation or absorption, the deformation of the atomic bubble follows. This cycle is repeated at each excitation (Fig. 1).

The absorption and emission occur within about 10^{-15} s, while it is estimated that the deformation of the bubble occurs on a timescale of a few picoseconds.¹⁾ However, this relaxation time has not been directly measured in the picosecond time scale so far. To clarify the dynamics of the atomic bubble system, we combined the laser spectroscopic technique in He II and an ultrafast laser spectroscopic technique.²⁾ In this research, we started with Rb as a target atom because its characteristics in He II has been well studied.^{3,4)} We here describe the current status of preparation for the first measurement of the relaxation time.

The wavelengths of atomic transitions in He II shift between absorption and emission owing to this deformation cycle.³⁾ In the excited state, a part of atoms in the observation area are expected to emit photons during the deformation process before the atomic bubble reaches its potential minimum of the excited state. Because the change of the emission wavelength corresponds to the degree of deformation, the relaxation time is mea-

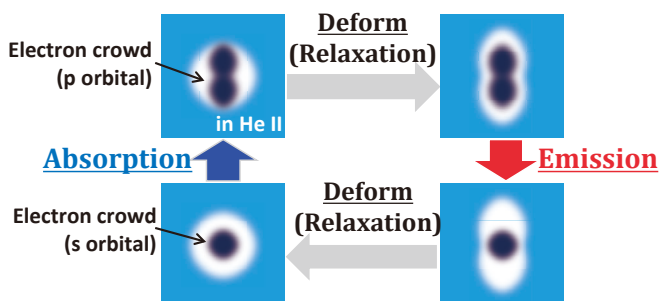


Fig. 1. Deformation cycle of an atomic bubble.

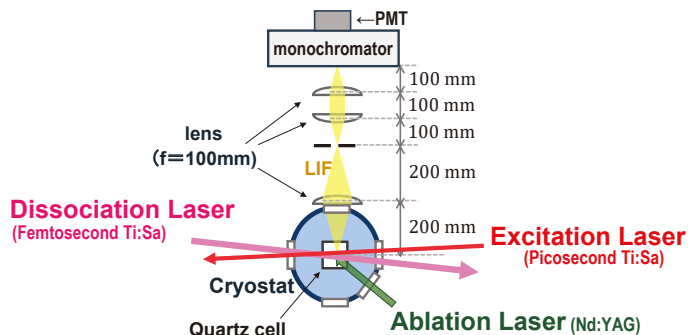


Fig. 2. Experimental setup of LIF detection.

sured by observing the time dependence of the emission wavelength.

For the observation, we plan to use a time-correlated single photon counting (TCSPC) system with a detector of high time resolution. The TCSPC records the time between the input of the excitation pulse laser signal and the detection of the laser-induced fluorescence (LIF) photon to obtain the time dependence of the LIF intensity. The typical time resolution of the system is 80 ps.

In this method, the pulse width of the excitation laser must be shorter than the relaxation time. Therefore, a picosecond mode-locked Ti: sapphire laser was introduced. The typical pulse width of the laser is 1.6 ps. Since the LIF of atoms in He II with ultrashort pulse lasers has not been observed, we conducted a laser performance evaluation experiment.

The observation was performed using the picosecond laser (laser power: 103 mW, repetition rate: 80 MHz) and an offline experiment setup and a laser sputtering method to introduce atoms. We used a monochromator and a photomultiplier tube for the fluorescence detection system. First, the LIF was measured by a wavelength sweep of the excitation laser. We obtained a spectrum that showed a peak in the fluorescence intensity at a laser wavelength of approximately 778 nm. This wavelength corresponds to the D1 excitation of Rb atoms in He II. Next, by fixing the laser wavelength fixed at the peak position, a wavelength sweep of the monochromator was performed. We observed an LIF spectrum centered at 794 nm, which is the D1 emission wavelength in He II.

In summary, we successfully observed the LIF of atoms in He II using the picosecond laser. We are planning to conduct an experiment of the relaxation time measurement by the TCSPC system.

References

- 1) B. Tabbert *et al.*, *J. Low Temp. Phys.* **109**, 653 (1997).
- 2) D. Mandal *et al.*, *Chem. Phys. Lett.* **359**, 77 (2002).
- 3) Y. Takahashi *et al.*, *Phys. Rev. Lett.* **71**, 1035 (1993).
- 4) T. Furukawa *et al.*, *Hyperfine Interact.* **196**, 191 (2010).

*1 Department of Advanced Sciences, Hosei University

*2 RIKEN Nishina Center

*3 Molecular Spectroscopy Laboratory, RIKEN

*4 Department of Computer and Information Science, Hosei University

Measurement of stopping-position width of highly energetic Rb ion beams in liquid nitrogen

M. Nishimura,^{*1,*2} K. Imamura,^{*2} A. Takamine,^{*2} K. Tsubura,^{*1,*2} A. Gladkov,^{*2} Y. Takeuchi,^{*1,*2} M. Doi,^{*1,*2} T. Yamamoto,^{*1,*2} M. Tajima,^{*2} T. Asakawa,^{*1,*2} Y. Sasaki,^{*1,*2} K. Doi,^{*1,*2} K. Kawata,^{*2,*3} H. Nishibata,^{*2,*4} Y. Ichikawa,^{*2} H. Ueno,^{*2} and Y. Matsuo^{*1,*2}

We are developing a laser spectroscopy technique named optical RI-atom observation in conduced helium as ion catcher (OROCH) for the study of nuclear properties of unstable nuclei. In this method, highly energetic ion beams are stopped in superfluid helium (He II) and neutralized, following which atoms are subjected to in-situ laser spectroscopy. The combination of optical pumping and the laser radiofrequency (RF) of microwave (MW) double-resonance methods enables us to determine the Zeeman and hyperfine splittings of atoms, from which the nuclear spin and moment are deduced. The method is promising particularly for low-yield nuclei because the stopping efficiency of He II is nearly 100%. We have successfully observed laser-induced fluorescence (LIF) from ^{85}Rb atoms of about 200 pps injected into He II as a 66 AMeV beam in the RIKEN RIPS beamline.¹⁾

However, the above energy beams could just reach the center of the optical cryostat after travelling for several millimeters in He II. In order to apply this method to heavier elements such as Ag, Cs, and Au, a beamline of higher energy is necessary to transport beams to the LIF observation region ($\phi 2 \text{ mm} \times 5 \text{ mm}$).

As the first step, we plan to apply this method to

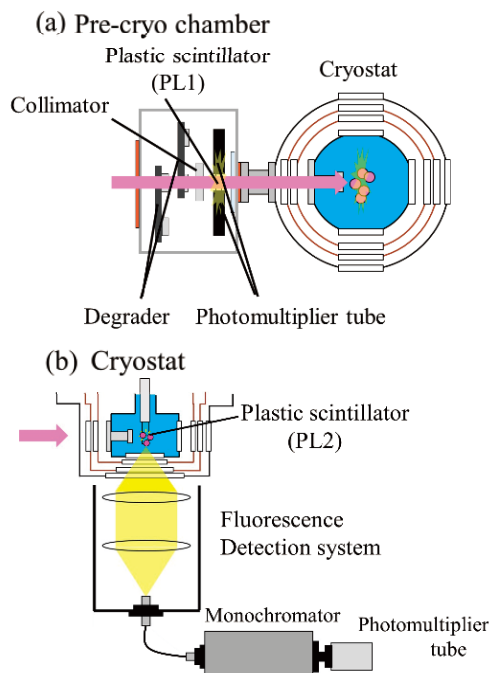


Fig. 1. Schematic of (a) the pre-cryo and (b) the cryostat chambers.

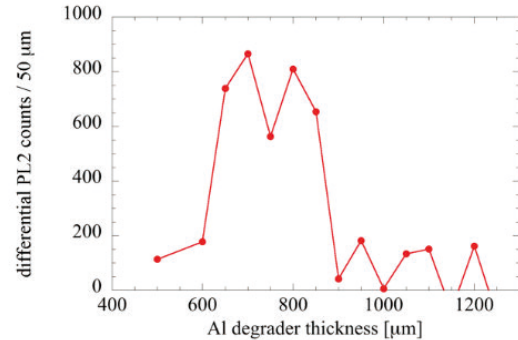


Fig. 2. Differential PL2 counts as a function of the Al degrader thickness.

radioactive Rb isotopes provided by the HIMAC SB2 beamline at NIRS. To verify the feasibility of an online experiment, we investigated beam yields and beam profile using a ^{84}Rb beam produced from a primary ^{84}Kr beam on a Be target of 350 AMeV. We observed photons from plastic scintillators to estimate the number of ^{84}Rb ions stopped in the LIF observation region. Liquid nitrogen was used as a stopper instead of superfluid helium in this experiment.

Figure 1 shows the schematics of the “pre-cryo” and cryostat chambers where two plastic scintillators PL1 and PL2 are placed. Details of the apparatus and measurement method are described elsewhere²⁾ in this progress report.

The result of the PL1 counts acquired to investigate the transverse beam profile is reported in Ref. 2). In order to measure the longitudinal stopping position of the beam, we counted the PL2 photons as a function of the thickness of aluminum energy degrader. The degrader thickness was changed in steps of $50 \mu\text{m}$. Figure 2 shows the differential counts between neighboring thicknesses, which correspond to the number of stopped ions. That is, the differential counts indicate the range distribution for the beam if the stopper material is regarded as aluminum. We found that the optimal degrader thickness was $\sim 750 \mu\text{m}$. The beam was stopped within a longitudinal width of 0.3 mm in aluminum. From this result, we roughly determined that the beams were stopped in a width of 1 mm in liquid nitrogen. If we convert this value to the stopping-position width in He II, the beams are estimated to be stopped in a width of 6 mm, considering the material density of He II. Further analysis to estimate the ^{84}Rb atom yields in the LIF observation region combined with the transverse beam profile is in progress.

References

- 1) K. Imamura *et al.*, Appl. Phys. Express **12**, 016502 (2019).
- 2) K. Tsubura *et al.*, in this report.

^{*1} Department of Advanced Sciences, Hosei University

^{*2} RIKEN Nishina Center

^{*3} Center for Nuclear Study(CNS), Tokyo University

^{*4} Department of Physics, Kyusyu University

Investigation of the secondary rubidium beam profile at HIMAC towards laser spectroscopy in an optical cryostat

K. Tsubura,^{*1,*2} K. Imamura,^{*2} A. Takamine,^{*2} M. Nishimura,^{*1,*2} A. Gladkov,^{*2} Y. Takeuchi,^{*1,*2} M. Doi,^{*1,*2} T. Yamamoto,^{*1,*2} M. Tajima,^{*2} T. Asakawa,^{*1,*2} Y. Sasaki,^{*1,*2} K. Doi,^{*1,*2} K. Kawata,^{*2,*3} H. Nishibata,^{*2,*4} Y. Ichikawa,^{*2} H. Ueno,^{*2} and Y. Matsuo^{*1,*2}

We are developing a laser spectroscopy technique named Optical RI-atom Observation in Condensed Helium as Ion-catcher (OROCHI) for the study of nuclear spins and moments. In the OROCHI experiment, we catch highly energetic ion beams in superfluid helium (He II) in our cryostat to neutralize them and conduct in-situ laser spectroscopy. We irradiate the neutralized atoms with circularly polarized laser light to produce spin polarization and measure the atomic Zeeman and hyperfine splitting of the atoms using the laser-radio-frequency and laser-microwave (mw) double resonance method.

In the previous online experiment,¹⁾ our group observed the laser-rf double resonance spectra for $^{84-87}\text{Rb}$ ion beams. It was reported that the atoms in superfluid helium shows a hyperfine structure constant slightly larger than that of a free atom by $\sim 1\%$.^{2,3)} Now, based on our interest in the hyperfine anomalies of the atoms in superfluid helium, we plan to measure the hyperfine splitting of the radioactive Rb, Ag, Cs, and Au isotopes, to which this method has not been applied.

We plan to apply this method to radioactive Rb isotopes provided by the HIMAC SB2 beam line at NIRS in FY 2020. As a prerequisite online experiment, we measured the beam yields of a ^{84}Rb beam produced in proton pickup reactions by a ^{84}Kr beam of 350 A MeV on a Be target of 12 mm thickness to investigate the beam profile of ^{84}Rb ions stopped in a laser-induced fluorescence (LIF) observation region ($\phi 2 \text{ mm} \times 5 \text{ mm}$).

The beam yields were counted with two plastic scintillation counters. One plastic scintillator (“PL1”: 30 mm square \times 0.1 mm thickness) was placed in a chamber, which we call the “pre-cryo chamber,” in front of the cryostat. Another plastic scintillator (“PL2”: 10 mm square \times 0.5 mm thickness) was placed at the center of the cryostat. A variable energy degrader system was placed upstream of PL1, and one of the collimators having various diameters can be set just upstream of PL1 in the pre-cryo chamber. A figure for the setup and the role of PL2 is described in the report by M. Nishimura *et al.*⁴⁾ in this progress report.

We measured the beam yields using PL1 as a function of the collimator diameter in order to investigate the transverse beam profile. The coincidence pulses

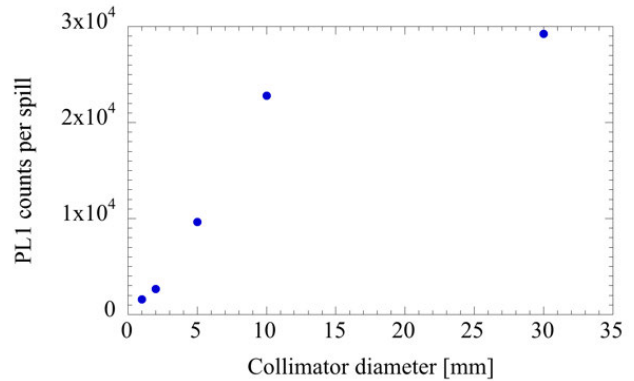


Fig. 1. Collimator diameter dependence of the yield of the secondary beam.

of two photomultipliers mounted at the left and right sides of PL1 were counted by a multichannel scaler (Techno AP APG7400A USB-MCA4) with a dead time of 1.5 μs . Figure 1 shows the collimator diameter dependence of PL1 counts. The primary beam intensity was 2×10^8 particles per spill (the repetition cycle of the beam spill was 3.3 s) for this measurement. Because the beam purity was $\sim 40\%$, which was evaluated from the particle identification, we found that ^{84}Rb beams of 3.8×10^4 particles per spill were provided from the HIMAC SB2 line at the full primary beam intensity of 5.9×10^8 particles per spill with a dead-time correction. This value agrees with a LISE++ calculation result. Currently, we are carefully analyzing the data and evaluating the beam profiles of ^{84}Rb and impurity ^{82}Kr , assuming the beam profiles follow a Gaussian distribution.

In summary, we evaluated the secondary beam yield variations by changing the collimator size to investigate the transverse profile of the beam. Combined with the results for the longitudinal distribution of the stopped atoms in the cryostat using PL2 counts,⁴⁾ the estimation of the yield and profile of ^{84}Rb atoms in the LIF observation region is in progress. We will verify the feasibility of the hyperfine structure constant measurements for various Rb and Ag isotopes at the HIMAC SB2 beam line.

References

- 1) X. F. Yang *et al.*, Phys. Rev. A **90**, 052516 (2014).
- 2) Y. Takahashi *et al.*, Z. Phys. B **98**, 391 (1995).
- 3) T. Furukawa, Ph.D. thesis, Osaka University (2007).
- 4) M. Nishimura *et al.*, in this report.

*1 Department of advanced science, Hosei University

*2 RIKEN Nishina Center

*3 CNS, University of Tokyo

*4 Department of Physics, Kyushu University

Degrader system for ZD-MRTOF

J. J. Liu,^{*1,*2} S. Chen,^{*1,*2} S. Imura,^{*3} M. Wada,^{*2} H. Ishiyama,^{*3} A. Takemaine,^{*3} M. Rosenbusch,^{*2} D. S. Hou,^{*4} and P. Schury^{*2}

After the successful experience with gas-cell techniques and the multi-reflection time-of-flight mass spectrograph (MRTOF-MS) at SLOWRI and GARIS-II, parasite experiments for commissioning the cryogenic He gas cell and MRTOF-MS using the ZeroDegree spectrometer have been proposed. A gutter RF carpet gas cell will be installed at the downstream side of F11 to stop heavy ions and extract them to the MRTOF-MS. Since the maximum stopping power of the gas cell is ~ 0.7 MeV/nucleon¹⁾ ions dumped from ZeroDegree that have an energy higher than 100 MeV/nucleon need to be slowed down before entering the gas cell. A degrader system will be installed. Additionally, as the commissioning will be run symbiotically with other ZeroDegree experiments, an independent data acquisition (DAQ) system for particle identification (PID) should be developed.

A movable flat Pb-glass degrader with a thickness of 7.1 mm was combined with a step motor rotating in the vertical direction from 0° to 90° , which is mounted in front of the gas-cell window. The step motor has a high resolution of 0.0072° per step enabling the fine tuning of the effective degrader thickness. The maximum effective thickness of the degrader is 10.04 mm when the degrader rotates to 45° , while there is no degrader at 90° . An online PID DAQ system with shared beam signals from ZeroDegree is developed independently for the BigRIPS DAQ, which will not be in conflict to other experiments. The PID could be performed by the ΔE - ΔE method using a multi-sampling ion chamber at F11 and Si detectors. Moreover, the ΔE -TOF- $B\rho$ method for PID could be applied using the multi-sampling ion chamber at F11, time of flight from F8 to F11 and F10 PPAC position information. With the selection of specified ions, the degrader angle can be optimized by measuring beam energy loss in the Si array. After fixing the angle of the degrader, the Si array will be removed and ions will be transported to the gas-cell.

The degrader system has been tested in an online experiment. A ^{238}U primary beam with an energy of 345 MeV/nucleon was incident on a 4-mm thick ^9Be target. Fragmentation around ^{80}Zn was produced and selected by BigRIPS and ZeroDegree spectrometers, where a wedge-shaped degrader at F10 was utilized so as to mono-energetically focus particles on F11 by adopting the LAA-monoionic optical mode. The PID has been performed by the ΔE - ΔE , as shown

*1 Department of Physics, the University of Hong Kong

*2 Wako Nuclear Science Center, KEK

*3 RIKEN Nishina Center

*4 Institute of Modern Physics

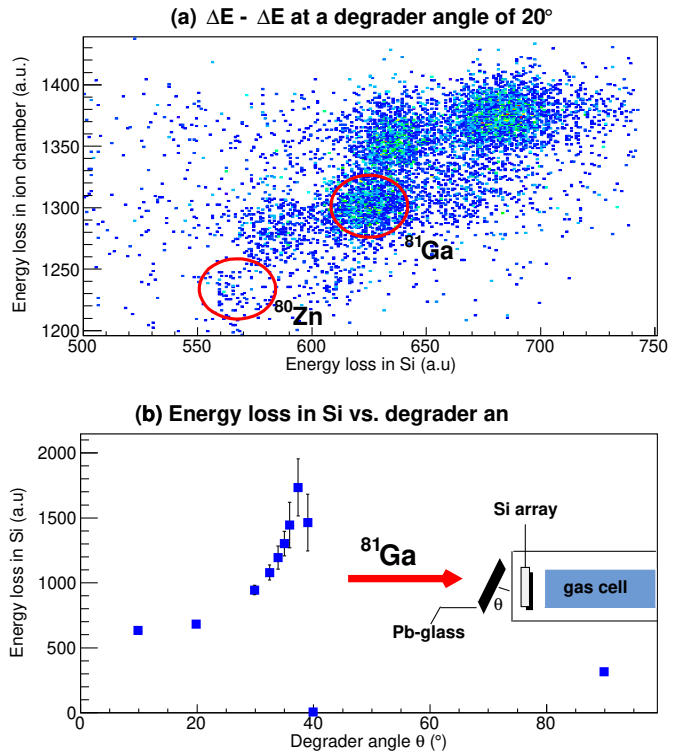


Fig. 1. (a) Particle identification using the ΔE - ΔE method by a multi-sampling ion chamber at F11 and Si detector; (b) energy loss in the Si detector as a function of the degrader angle

in Fig. 1(a), with a reasonable resolution. By scanning the degrader angle θ from 0° to 90° and gating on ^{81}Ga , the energy loss in Si as a function θ was obtained as shown in Fig. 1(b). By fine tuning of θ from 39° to 40° , ^{81}Ga was expected to be caught by the gas cell. This result is consistent with LISE++ calculation.

A real-time PID trigger is under construction within the PID DAQ system, and it can be possible to stop a single ion in the gas cell. With selected particle information from the DAQ, a pulse will be generated to turn off the DC field in the gas cell for a half life of the selected ion. In such a condition, the β -delayed neutron emission probability of the ion can be determined by counting daughter nuclei distinguished using MRTOF-MS.

Reference

- 1) M. Wada *et al.*, Nucl. Instrum. Methods Phys. Res. B **204**, 570–581 (2003)

First test of graphenic carbon vacuum windows with heavy ions

S. Purushothaman,^{*1} H. Haba,^{*2} E. Haettner,^{*1} S. Ishikawa,^{*3} K. Itahashi,^{*2} S. Y. Matsumoto,^{*2,*4}
Y. Miyake,^{*2} A. Sakaue,^{*4} R. Sekiya,^{*4} Y. K. Tanaka,^{*1,*5} and M. Tomut^{*6}

Currently, one of the main concerns in experiments involving high-luminosity hadron beams is the limitations imposed by the materials directly interacting with the beam. Beam windows are essential components in every accelerator and many experimental systems, and they experience enhanced radiation damage, high operation temperatures, and high thermal and transient stresses, adding to pressure differences between the beam vacuum and atmosphere. Graphenic carbon membranes are an excellent replacement for conventionally used window materials such as steel, beryllium, aluminum, or Inconel alloys because of their low atomic number and excellent thermomechanical properties. The excellent mechanical properties and molecular impermeability of suspended graphenic carbon membranes^{1,2)} make them an ideal vacuum window material with an extremely low window thickness that meets the mechanical stability requirements.

Due to the ultrahigh electron transmissivity in a wide electron energy range, high electrical conductivity, and high chemical stability of suspended graphenic carbon membranes, their use as a vacuum window material is currently being explored, and they are being implemented in fields such as electron microscopy and X-ray photoelectron spectroscopy. In a recent development, a novel x-ray transmission window based on polycrystalline graphene or graphenic carbon (GC) has been developed^{1,2)} as a replacement for the beryllium transmission windows in X-ray detectors. A maximum burst pressure of about 0.5–0.6 MPa at a window thickness of 1 μm and a diameter of 7.5 mm has been reported in Ref. 2).

The work outlined here aims intended to explore the outstanding mechanical properties demonstrated by the above-mentioned GC X-ray window within the context of hadron beams. As the first step, different aspects of irradiation-induced damage in the material were investigated in detail using 200 particle nA, 5 MeV/nucleon ^{20}Ne ion beam from the AVF accelerator at RIKEN. GC samples were placed at the E7B target position and irradiated. The total dose of each irradiation procedure was quantified by measuring the beam current with an accuracy of 5%. A collimator slit of a 3 mm width was used to limit the beam size on the samples. A Faraday cup downstream of the collimator was used to quantify the fluence.

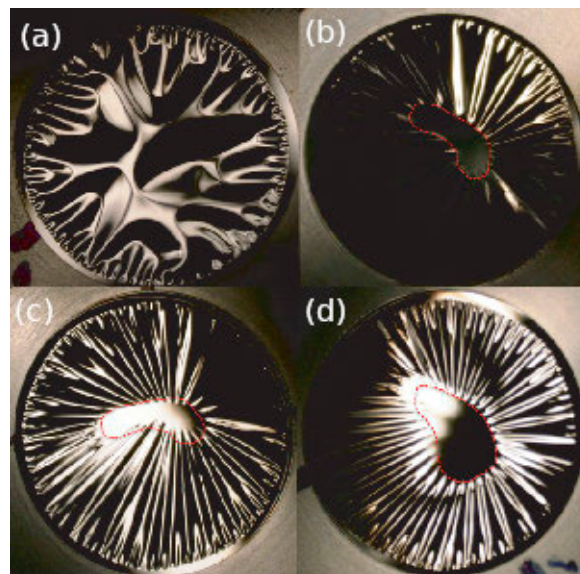


Fig. 1. (a) Non-irradiated sample. Foil irradiated at 200 particle nA for (b) 1 h 51 min at a total fluence of 9.7×10^{16} particles/cm², (c) 3 h 30 min at a total fluence of 2.1×10^{17} particles/cm², and (d) 10 h at a total fluence of 2.1×10^{17} particles/cm². Although the beam was collimated using a 3 mm collimator slit, the obtained beam spot was “comma” shaped with a non-uniform intensity distribution. This is reflected in the shape of the beam-induced compaction (marked with red dotted curves).

Five graphenic carbon samples of thickness 1 μm and diameter 7.5 mm were irradiated for different time intervals (fluences ranging from 9.7×10^{16} particles/cm² to 9.7×10^{17} particles/cm²) to study the evolution of irradiation-induced structural change.

The foil could mechanically withstand a 200 particle nA DC beam up to 10 h. A detailed investigation of the effects of irradiation-induced damage in the material is ongoing at the University of Münster and at GSI using Raman spectroscopy, scanning and transmission electron microscopy, and nanoindentation.

The next step will be to evaluate the performance under pressure during the irradiation under a differential helium pressure of 0.2 MPa across the membranes while monitoring the evolution of helium leakage. This will check the feasibility of the GC vacuum window as a candidate for hadronic ion beams.

References

- 1) S. Huebner *et al.*, MRS Adv. **1.20**, 1441 (2016).
- 2) S. Huebner *et al.*, IEEE Trans. Nucl. Sci. **62.2**, 588 (2015).

*1 GSI Helmholtzzentrum für Schwerionenforschung

*2 RIKEN Nishina Center

*3 Tohoku University

*4 Kyoto University

*5 RIKEN CPR

*6 University of Münster

Heavy-ion irradiation test of radiochromic films

T. Kambara,*¹ A. Yoshida,*¹ Y. Hayashi,*¹ K. Ishii,*¹ and T. Abe*¹

The heavy-ion irradiation of biological or industrial samples requires the dose-distribution measurement of a beam spot 5–10 cm in diameter. A radiochromic film changes its color according to the absorbed dose of ionizing radiation and enables two-dimensional high-resolution dose-distribution measurements. It is easy to handle and portable, and a personal computer can capture its image with an inexpensive and common image scanner and convert the numerical data of the image to optical density (OD) as a function of the absorbed dose.¹⁾ Radiochromic films are widely used in radiotherapy for dosimetry of high-energy photons.

In order to assess the usefulness of radiochromic films in our high-energy heavy-ion irradiation, we tested two types of films, GAFCHROMIC™ HD-V2 for a higher dose and EBT-3 for a lower dose,²⁾ using heavy ions with a wide range of linear energy transfer (LET). The irradiation targets were 4 cm × 5 cm rectangular segments of vendor-supplied 25 cm × 20 cm sheets of the films. The HD-V2 targets were irradiated by C ions with LETs of 22.5 and 179 keV/μm, Ar ions with LETs of 184 and 673 keV/μm, and Fe ions with LETs of 637 and 1061 keV/μm with dose ranging from 1 to 400 Gy, and the EBT-3 targets were irradiated by C ions with LET of 22.5 keV/μm, Ar ions with LET of 184 keV/μm, and Fe ions with LET of 637 keV/μm with dose ranging from 0.2 to 10 Gy.

The targets were irradiated at the E5B beamline of the RIKEN Ring Cyclotron where the LET was adjusted by Al-plate degraders.³⁾ The beam was collimated by a 20-mm-diameter aperture on a 10-mm-thick brass plate about 153 mm upstream of the target.

Before and after the irradiation, the target was scanned by an image scanner and converted to a 24-bit 75-dpi bitmap file. The numerical values of the three primary colors (RGB) of each pixel were converted to OD values following the procedure described in Ref. 1). Although each of the RGB colors can yield OD distributions, we show in the following the results for green, which is the most sensitive.

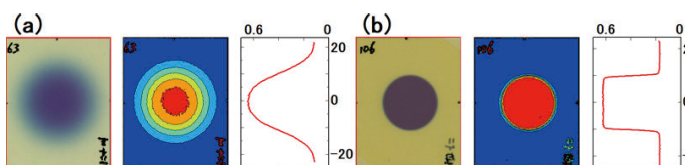


Fig. 1. Images, the corresponding OD distributions and one-dimensional vertical distributions through the center of films irradiated by (a) C ions after an 18.6-mm-thick degrader and (b) Ar ions without a degrader.

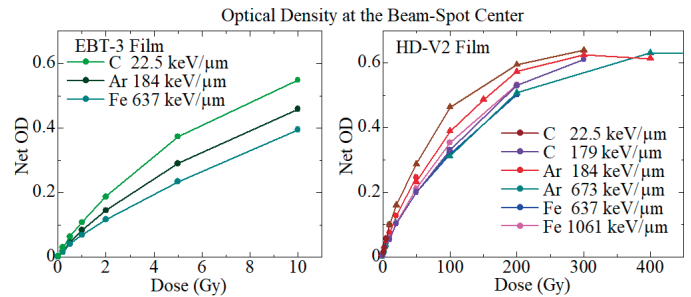


Fig. 2. OD of the films irradiated by heavy ions with different LETs as functions of the absorbed dose.

Figure 1 shows examples of images of the irradiated targets, the corresponding two-dimensional OD distributions, and its one-dimensional distribution along a vertical line through the center: (a) an HD-V2 film irradiated by 200 Gy of 179-keV/μm C ions and (b) an EBT-3 film irradiated by 10 Gy of 184-keV/μm Ar ions. The image in (a) is blurred since the C ions passed through an 18.6-mm-thick degrader before the target. The image in (b) is clear; its OD distribution is flat in the beam spot and drops sharply within about 1 mm at the edge since the Ar ions did not pass through a degrader.

We obtained the net OD distribution of a target as the difference between the distributions before and after the irradiation, and we took the OD value at the center of the beam spot. Figure 2 compares the dose dependence of the net OD value for different irradiation conditions and films.

The dose dependence of OD has a common feature: it first increases linearly and finally saturates above 200 Gy for HD-V2, but it does not saturate up to 10 Gy for EBT-3. It is higher for lighter ions and lower LETs but does not strongly depend on the ion and LET, remaining within $\pm 30\%$ overall, although the atomic number of the ions is different by more than 4 and the LET is different by nearly 50.

As a whole, the radiochromic films can be useful for various heavy ions with a wide range of LETs to evaluate doses between 0.2 and 200 Gy and to measure the two-dimensional dose distribution with a spatial resolution of about 1 mm. The films may also be useful for the comparison of irradiation dose between distant irradiation facilities since they are easily transported and treated.

References

- 1) T. Agematsu, H. Hanaya, T. Kojima, *Radioisotopes* **57**, 87 (2008) (Japanese).
- 2) <http://www.gafchromic.com/>.
- 3) H. Ryuto, T. Abe, N. Fukunishi, M. Kase, Y. Yano, J. Biomed, *Nanotechnol.* **2**, 1 (2006).

*¹ RIKEN Nishina Center

Computing and network environment at the RIKEN Nishina Center

T. Ichihara,*¹ Y. Watanabe,*¹ and H. Baba*¹

We are operating Linux cluster systems¹⁾ at the RIKEN Nishina Center (RNC).

Figure 1 shows the current configuration of the Linux servers at the RNC. The host *RIBF.RIKEN.JP* is used as the mail server, the NFS server of the user home directory, and the NIS master server. This is the core server for the RIBF Linux cluster. A new ssh login server *RIBF02.RIKEN.JP* with the CentOS 8.0 operating system (OS) was installed in November 2019.

For the mailing list service, we have been using the Majordomo²⁾ mailing list software at the host *RIBF.RIKEN.JP* for a long time. Since the maintenance of Majordomo was terminated several years ago, we have changed the mailing list software to Mailman.³⁾ Mailman has several functions addressing Domain-based Message Authentication Reporting

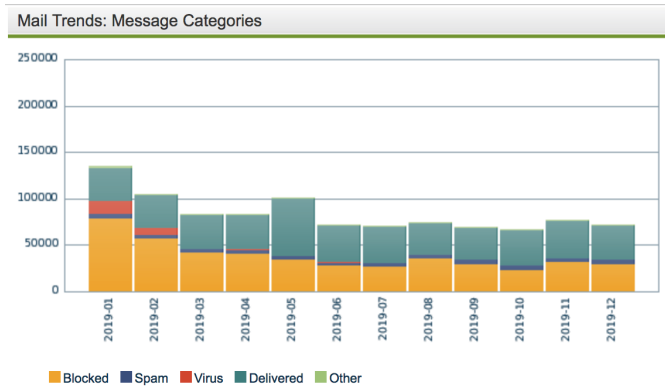


Fig. 2. Mail trends: message categories in 2019.

and Conformance (DMARC)⁴⁾ which has been introduced recently at the Federal Agencies⁵⁾ in US together with Sender Policy Framework (SPF) and DomainKeys Identified Mail (DKIM).

The hosts *RIBFSMTP1/2* are the mail gateways, which are used for tagging spam mails and isolating virus-infected mails. The latest version of Sophos Email Protection-Advanced (PMX 6.4.8) has been installed. Figure 2 shows the mail trends in 2019. Approximately 50% of the incoming mails were blocked by the PMX ip-blocker.

The host *RIBFUSER* has been used for the RIBF User Group registration and election of Users Executive Committee (UEC) members. Since twelve years had passed since the installation of this server, we replaced it with a new server, HP-DL20G9 with SL7.4 OS, in January 2019.

The host *RIBFWEB1* has been used as the Web server in RNC. Because seven years had passed since the installation of this server, we replaced it with a new server, HP-DL20G10 with CentOS 8.0 OS, in November 2019. With a virtual host function of the Apache http server, eight multi-host Web contents have been served at the server simultaneously

An anonymous ftp server, *FTP.RIKEN.JP*, is managed and operated at the RNC. Major Linux distributions, including Scientific Linux, Ubuntu, and CentOS, are mirrored daily for the convenience of their users and for facilitating high-speed access.

References

- 1) T. Ichihara *et al.*, RIKEN Accel. Prog. Rep. **52**, 159 (2019).
- 2) <http://old.greatcircle.com/majordomo/>.
- 3) <https://www.list.org/>.
- 4) <https://en.wikipedia.org/wiki/DMARC>.
- 5) <https://cyber.dhs.gov/bod/18-01/>.

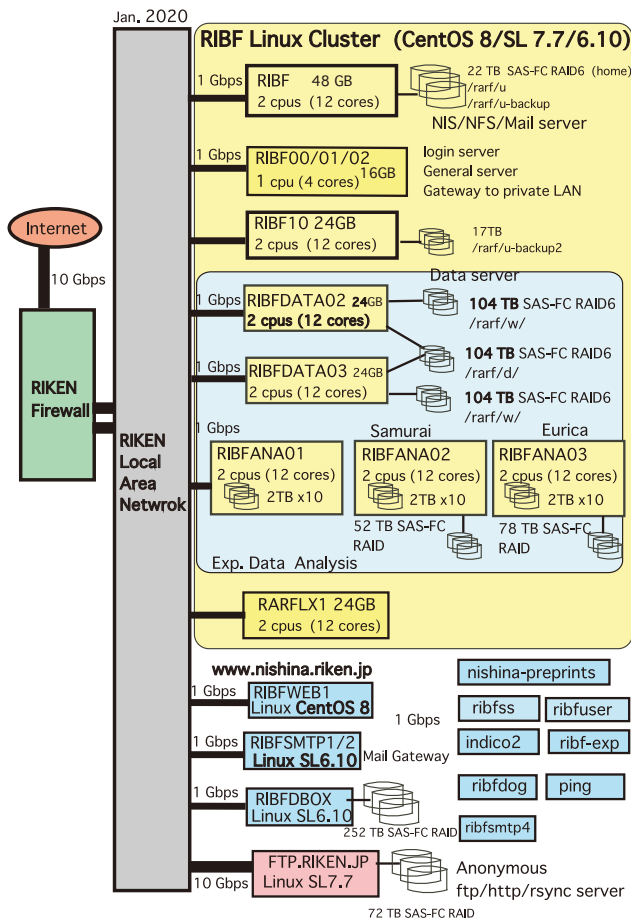


Fig. 1. Configuration of the RIBF Linux cluster.

*¹ RIKEN Nishina Center

CCJ operations in 2019

S. Yokkaichi,^{*1} H. En'yo,^{*1} T. Ichihara,^{*1} W. Nakai,^{*1} and Y. Watanabe^{*1}

Overview

The RIKEN Computing Center in Japan (CCJ)¹⁾ commenced operations in June 2000 as the largest off-site computing center for the PHENIX²⁾ experiment being conducted at RHIC. Since then, CCJ has been providing numerous services as a regional computing center in Asia. We have transferred several hundred TBs of raw data files and nDST^{a)} files from the RHIC Computing Facility (RCF)³⁾ to CCJ.

Many analysis and simulation projects are being conducted at CCJ, which are listed on the web page <http://ccjsun.riken.go.jp/ccj/proposals/>. As of December 2019, CCJ has contributed to 43 published papers and 44 doctoral theses.

Computing hardware and software

The network configuration and the computing hardware (nodes) and software (OS, batch queuing systems, database engine, etc.) are almost the same as described in the previous APR.¹⁾ We have two login servers, one main server (users' home directory, NIS, DNS, and NTP), and two disk servers the disk sizes of which are 13 and 26 TB. The main server has an external SAS RAID (21 TB) for the home and work regions of users as well as system usage. Moreover, the server has a RAID with built-in disks (13 TB) that can be used temporarily by users and the system.

We operate 26 computing nodes, of which 16 nodes were purchased in Mar. 2009 and 10 nodes were purchased in Mar. 2011. Thus, in total, 368 (= 8 × 16 nodes + 24 × 10 nodes) jobs can be processed simultaneously by these computing nodes using a batch queuing system, LSF 9.1.3.⁴⁾ The LSF license contract in CCJ is for 358 in total in JFY 2019, after the transfer of 80 licenses from the RIBF cluster. Table 1 lists the number of malfunctioning SATA or SAS disks in the HP servers, namely, computing nodes and NFS/AFS servers.

One database (postgreSQL⁵⁾) server and one AFS⁶⁾ server are operated in order to share the PHENIX computing environment. It should be noted that only the SL5⁷⁾ environment is shared by the computing nodes, which have approximately 0.9 TB of library files. We started two new data-transfer servers, which have a 10 G Ethernet I/F and 12 TB SATA RAID with built-in disks. Data transfer of the order of 100 TB from J-PARC will start in 2020 and also from BNL in the future. In addition, we operate two dedicated servers

Table 1. Number of malfunctioning HDDs in HP servers during 2011–2019.

Type(Size)	total	19	18	17	16	15	14	13	12	11
SATA (1 TB)	192	8	16	18	8	14	11	16	20	9
SATA (2 TB)	120	10	2	10	2	10	0	2	5	4
SATA (4 TB)	10	0	0	-	-	-	-	-	-	-
SAS (146 GB)	38	6	3	1	5	3	2	0	1	1
SAS (300 GB)	26	2	0	1	0	1	1	0	0	1

for the RHICf group⁸⁾ and two servers for the J-PARC E16 group,⁹⁾ in order to keep their dedicated compilation and library environments along with some data. Three 10-KVA UPSs are operated as power supply for these CCJ nodes, should be replaced in 2020.

Joint operation with ACCC/HOKUSAI

CCJ and the RIKEN Integrated Cluster of Clusters (RICC) have been jointly operated since July 2009. In April 2015, a new system named “HOKUSAI Greatwave” was launched by RIKEN ACCC,¹⁰⁾ and the joint operation with CCJ continued, with the inclusion of a new hierarchical archive system in which approximately 900 TB of CCJ data are stored. As of Nov. 2019, 886 TB is used, with the inclusion of 749 TB of PHENIX official data, 25 TB of KEK/J-PARC data, 3 TB of RHICf data, and 109 TB of user-level archive data. Subsequently, the “HOKUSAI BigWaterFall” IA cluster, which has 840 nodes/33600 CPU cores, was launched in 2017 by ACCC. CCJ has not started to use the cluster, because it lacks support for NFS to share the computing environment of PHENIX, unlike RICC. In autumn in 2020, ACCC will start a charging system to users for their usage of CPU-time and storage capacity. Thus we are discussing the optimal ratio of purchasing new machines to paying to ACCC.

References

- 1) S. Yokkaichi *et al.*, RIKEN Accel. Prog. Rep. **51**, 188 (2018).
- 2) <http://www.phenix.bnl.gov/>.
- 3) <https://www.racf.bnl.gov/>.
- 4) https://www.ibm.com/support/knowledgecenter/en/SSETD4_9.1.3/lsf_welcome.html.
- 5) <http://www.postgresql.org/>.
- 6) <http://www.openafs.org/>.
- 7) <http://www.scientificlinux.org/>.
- 8) Y. Itow *et al.*, arXiv:1409.4860 (Proposal).
- 9) S. Yokkaichi, in this report.
- 10) <http://accc.riken.jp/>.

^{*1} RIKEN Nishina Center

^{a)} term for a type of summary data files in PHENIX

III. RESEARCH ACTIVITIES II

(Material Science and Biology)

1. Atomic and Solid State Physics (Ion)

Control of electrical conductivity in diamond by boron implantation —application of high-temperature and high-pressure annealing

H. Yamazaki,^{*1} T. Minamidate,^{*2} M. Kidera,^{*1} A. Yamamoto,^{*3} R. Kato,^{*2} and H. Ueno^{*1}

Diamond is an excellent electrical insulator with a large band gap of 5.5 eV. Interestingly, it becomes a semiconductor when doped with a small amount of boron (for *p*-type) or phosphorus (for *n*-type). Ekimov *et al.* reported that B-doped diamond, when doped beyond the metal-to-insulator transition at $n_B \sim 3 \times 10^{20}$ B/cm³, shows superconductivity in samples grown by high-pressure and high-temperature synthesis.¹⁾ Theoretically, the superconducting critical temperature T_c can be increased substantially by reducing the effects of disorder in the B-doping processes.²⁾ For a higher T_c , more subtle control of doping using CVD and/or MBE methods is required, whereas a different method based on ion implantation is also worth investigating, since it enables selective ion doping in a controlled manner.

We attempted to control the electrical conductivity in diamond by means of the ion-implantation technique with the use of RILAC at RIKEN. In our study, for *n*- and *p*-type semiconductors (and possibly superconductors), nitrogen and boron ions are implanted into diamond, respectively. By changing the beam intensity and irradiation time, the concentration of nitrogen or boron was controlled. Note that achieving an *n*-type semiconductor, and needless to say an *n*-type superconductor, by the nitrogen-doping of diamond is challenging, since nitrogen behaves as a deep donor in diamond and does not contribute to conductivity.³⁾ The electrical conductivity observed in the nitrogen-implanted diamonds (*e.g.*, at $n_N \sim 7.5 \times 10^{21}$ N/cm³) is, therefore, most likely explained in terms of the carbon atoms connected via the *sp*² bonding produced by radiation damage. The Raman spectra support this scenario.

In this fiscal year, we mainly investigated boron-

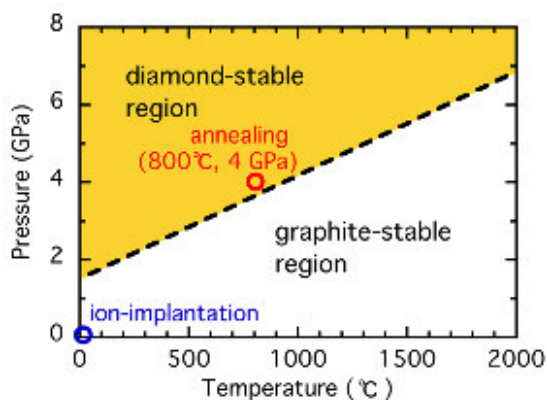


Fig. 1. Phase diagram of carbon. The annealing condition in this work is indicated by a red circle.

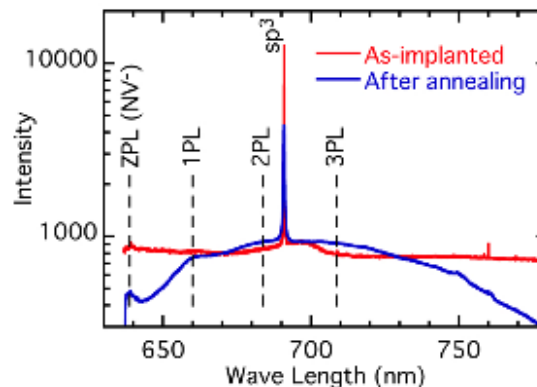


Fig. 2. Laser Raman spectra (632.8 nm excitation) of the as-implanted and annealed samples for $n_B \sim 6.8 \times 10^{22}$ B/cm³. The broken lines indicate the fluorescence emission of the zero-phonon line (ZPL) and *n*-phonon lines (*n*PLs; “phonon side band”) due to negatively charged nitrogen-vacancy (NV⁻) defect centers.

implanted diamonds. Boron ions were implanted into diamond crystals (each size is $1 \times 1 \times 0.3$ mm³) at 5 keV (implantation depth: ~ 10 nm) using an ECR ion source.⁴⁾ We prepared ten samples of different concentrations ranging from $n_B \sim 4.9 \times 10^{20}$ to 6.8×10^{22} B/cm³. Measurements of the magnetization and electrical resistivity show that the as-implanted diamond samples do not exhibit superconducting transitions, even though n_B values are nominally beyond the metal-to-insulator transition at 3×10^{20} B/cm³. In order to reduce the lattice damage produced during the implantation, we attempted annealing treatments after implantation. As the phase diagram of carbon (Fig. 1) shows, diamond is not stable at low pressures; we annealed the samples at 800°C and 4 GPa (in the diamond-stable region) for one hour. The annealed samples, however, indicate no sign of superconductivity. Rather, the annealing treatment degraded the diamond crystals: the (222) peak at a higher angle in x-ray diffraction measurement disappeared after annealing, whereas the (111) peak remained. Figure 2 shows a typical change in the Raman spectra after annealing. The fluorescence emission due to NV⁻ defect centers is clear, suggesting that the annealing treatment promotes the NV formation process, where nitrogen ions have been embedded in the Ib-type diamond as impurities. Hereafter, we must also consider the effect of the NV⁻ centers on the electrical conductivity in the implanted diamonds.

References

- 1) E. A. Ekimov *et al.*, Nature **428**, 542 (2004).
- 2) T. Shirakawa *et al.*, J. Phys. Soc. Jpn. **76**, 014711 (2007).
- 3) S. J. Sque *et al.*, Phys. Rev. Lett. **92**, 017402 (2004).
- 4) M. Kidera *et al.*, Eur. J. Mass Spectrom. **13**, 239 (2007).

^{*1} RIKEN Nishina Center

^{*2} Condensed Molecular Materials Laboratory, RIKEN

^{*3} Graduate School of Engineering and Science, Shibaura Institute of Technology

Superconducting proximity effect in epitaxial Nb(110)/Au(111)/Nb(110) trilayers

H. Yamazaki,^{*1} N. Shannon,^{*2} and H. Takagi^{*3}

Superconducting electronics, in which currents are carried by superconducting pairs of electrons, have great potential for future application in quantum computing. An essential element of superconducting circuits is the π junction, in which the phase of a superconducting wave function is inverted. One promising approach to building such a junction is to exploit the interplay between superconductivity and magnetism in superconductor (SC)/ferromagnet (FM)/SC heterostructures. Such multilayer structures are widely believed to achieve a Fulde-Ferrell-Larkin-Ovchinnikov (FFLO) state, in which the superconducting proximity effect drives a superconducting order with oscillating phase within the FM layer.¹⁾ However, this approach suffers from a serious drawback that the ferromagnetic elements tend to suppress superconductivity, forcing devices to operate at lower temperatures and with lower critical current densities.

In this study, we show that, in epitaxial Nb(110)/Au(111)/Nb(110) trilayers, the equilibrium superconducting state presents strong evidence of $0-\pi$ state transitions as a function of the Au-layer thickness (t_{Au}). Through the analysis of experimental data, we make a reasonable argument that a form of order-parameter oscillation, similar to the FFLO-like state in FM for SC/FM/SC junctions, is intrinsic to the proximity-induced Cooper pairs in the Au(111) layer. We tentatively ascribe this effect to the spin-orbit coupling (SOC) within the Au layer. Where SOC lifts the degeneracy between “up” and “down” spin electrons, electron pairs can form with a non-zero momentum. This leads to FFLO-like oscillations of the superconducting order parameter in real space. In the fcc lattice of Au, inversion symmetry is broken in the direction perpendicular to the (111) plane because of the ABCABC... stacking sequence of atomic planes, and the lack of inversion symmetry leads to the emergence of SOC.

We prepared a series of Nb(110)/Au(111)/Nb(110)

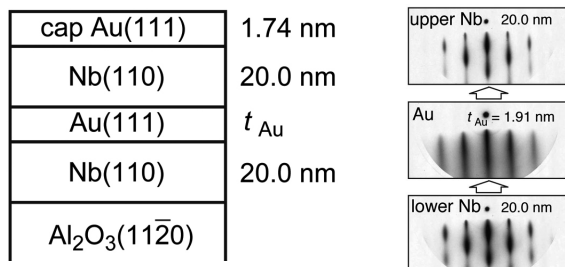


Fig. 1. Schematic diagram of a vertical section of the sample and the reversal images of RHEED patterns obtained in the growth process (right).

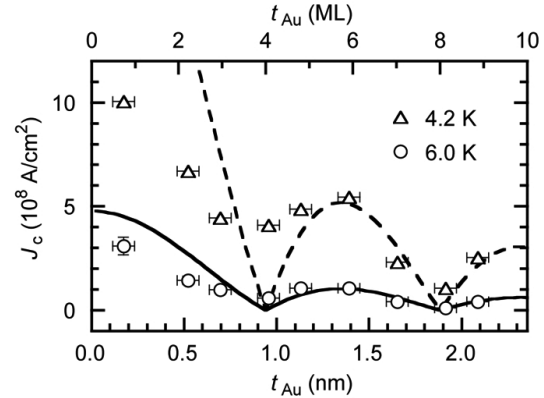


Fig. 2. Critical current density J_c of the Nb/Au[t_{Au}]/Nb trilayers at 4.2 K and 6.0 K (ML: atomic monolayer).

trilayers on single crystals of $\text{Al}_2\text{O}_3(11\bar{2}0)$ using MBE method. The sample structure is shown in Fig. 1. We will focus on single-domain samples ($0 < t_{\text{Au}} \leq 2.10$ nm), the superconducting properties of which are uniquely determined by t_{Au} . The superconducting critical current density J_c in zero magnetic field was estimated from the width of the M-H hysteresis curve for $H//$ sample plane by using a Bean model.²⁾ The data in Fig. 2 appear exactly like those for FM/SC multilayers, which have been confirmed to exhibit the $0-\pi$ state transitions as a function of t_{FM} .³⁾ Following previous articles,^{3,4)} we used the equation:

$$J_c = J_c^0 |\sin y| / y, \quad \text{where } y = 2\pi E_{\text{ex}}^{\text{eff}} t_{\text{Au}} / hV_f^{\text{Au}}. \quad (1)$$

The solid and dashed lines in Fig. 2 show theoretical fits to the data for 6.0 K and 4.2 K, respectively. Fits are obtained as a function of $E_{\text{ex}}^{\text{eff}}$ ($= 84.6$ meV) for $\nu_f^{\text{Au}} = 1.39 \times 10^6$ m/s and the ratio $J_c^0(4.2 \text{ K})/J_c^0(6.0 \text{ K}) = 5.0$, where $E_{\text{ex}}^{\text{eff}}$ is an effective parameter characterizing the order-parameter oscillations in the Au layer, ν_f^{Au} the Fermi velocity of Au, and J_c^0 the overall scale for J_c .

The value of $E_{\text{ex}}^{\text{eff}}$ ($= 84.6$ meV) is consistent with the SOC strength (120 meV) of conduction electrons in Au. A pairing state should occur between two electrons on the SOC-induced split parts of the Fermi surface. One might refute this argument on the grounds that a difference of 84.6 meV in energy between the spin-split bands is too large for the electrons to form a pair since the superconducting gap is no more than 1.40 meV in Nb. However, this is not the case with regard to the proximity effects.⁵⁾ Clearly, a theory is needed that treats the SOC effect on the proximity-induced Cooper pairs in a SC/normal metal/SC system.

References

- 1) A. I. Buzdin *et al.*, JETP Lett. **35**, 178 (1982).
- 2) E. M. Gyorgy *et al.*, Appl. Phys. Lett. **55**, 283 (1989).
- 3) Y. Blum *et al.*, Phys. Rev. Lett. **89**, 187004 (2002).
- 4) A. I. Buzdin, Rev. Mod. Phys. **77**, 935 (2005).
- 5) T. Kontos *et al.*, Phys. Rev. Lett. **86**, 304 (2001).

^{*1} RIKEN Nishina Center

^{*2} Okinawa Institute of Science and Technology Graduate University

^{*3} Max-Planck-Institute for solid state research

Simultaneous cluster dissociation and optical pumping of Ag in superfluid helium using a single UV laser

T. Yamamoto,^{*1,*2} K. Imamura,^{*1} A. Takamine,^{*1} W. Kobayashi,^{*2} Y. Takeuchi,^{*1,*2} M. Doi,^{*1,*2} H. Ueno,^{*1} and Y. Matsuo^{*1,*2}

We have been developing a laser spectroscopy method for atoms introduced into superfluid helium (He II). We generate spin polarization by the optically pumping the atoms and perform laser-radiofrequency and laser-microwave (MW) double resonance. This method enables us to determine the nuclear spins and electromagnetic moments through measurements of Zeeman splitting and hyperfine structure (HFS) splitting. Moreover, because HFSs in He II shift slightly from the value in vacuum, we are studying such an interaction between He II and atoms.

We have successfully measured HFSs of alkali atoms such as stable $^{85,87}\text{Rb}$ and ^{133}Cs in He II and observed small differences from those in vacuum.^{1,2)} Currently, we are attempting to apply this method to group 11 atoms to verify whether a similar difference appears in atoms other than alkali metal elements. The HFS transition of the stable isotope ^{197}Au atom in He II was observed using this technique.³⁾ To discuss the differential hyperfine anomalies between isotopes, it is necessary to measure the HFSs of at least two isotopes. Silver is a good candidate with two stable isotopes, ^{107}Ag and ^{109}Ag , the natural abundance ratio of which is almost 1:1.

In offline experiments, atoms have been introduced into He II using a two-step laser sputtering method, namely, by laser ablation and laser dissociation. As the first step, a metal sample placed above the He II surface is ablated by the second-harmonic pulse of a Nd:YAG laser (wavelength: 532 nm, repetition rate: 10 Hz, pulse width: 8 ns, pulse energy: ~ 5 mJ). Only clusters generated by the ablation process can be immersed in He II. Subsequently, atoms are supplied by the dissociation process for the spectroscopy of atoms in He II. Although a femtosecond Ti:Sa laser (wavelength: 800 nm, repetition rate: 500 Hz, pulse width: ~ 120 fs, pulse energy: ~ 200 μJ) has been efficient in the dissociation for various atomic species, we found this is not the case for Ag clusters.⁴⁾ Inspired by a report that Ag clusters in He II droplets show absorption in the range of 330–360 nm instead of 800 nm,⁵⁾ our group applied the third-harmonic pulse of Nd:YAG laser (wavelength: 355 nm, repetition rate: 20 Hz, pulse width: 5 ns, pulse energy: 8 mJ) to the dissociation process. The dissociation of Ag clusters was clearly confirmed by the generation of spin polarization of Ag atoms in He II through optical pumping.⁶⁾

For further study of Ag atoms using the laser-RF/MW double resonance method, it is indispensable to increase laser induced fluorescence (LIF) photon counts.

In particular, increasing the power of the pumping

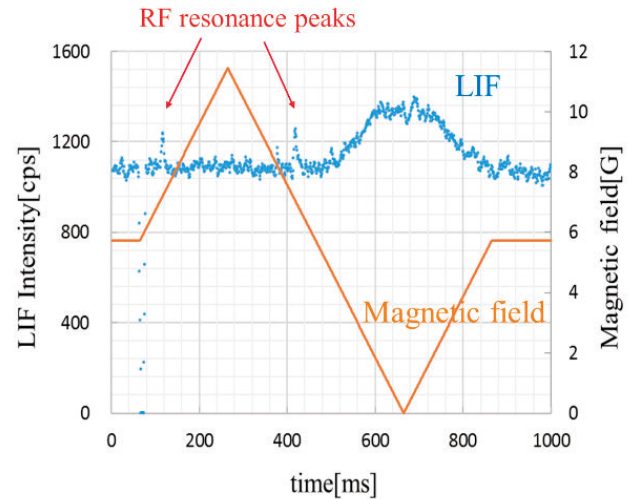


Fig. 1. Variation of LIF intensity with a magnetic field.

laser is promising because the LIF intensity is proportional to the pumping laser power for atoms in superfluid helium.⁷⁾ This approach should also be effective if the pumping laser simultaneously function as the dissociation laser.

Herein, we report the introduction of the fourth harmonics of a new DPSS laser (wavelength: 335 nm, repetition rate: 20 kHz, pulse width: ~ 20 ns, pulse energy: 5 μJ). The wavelength of the laser matches the wavelength for both Ag cluster dissociation and Ag atomic excitation in He II. Since the output power of the laser is greater than 100 mW on average, it is expected that the laser pulses can dissociate Ag clusters.

Figure 1 shows the result of increase and decrease in LIF intensity when a magnetic field (0–11.5 G) and an RF field (10.0 MHz) were applied to Ag atoms in He II. When a sufficient magnetic field is applied, spin polarization is achieved, and the LIF intensity decreases. In addition, when a constant RF is applied, the LIF intensity increases at the magnetic field that provides the Zeeman splitting energy corresponding to the resonant RF. We confirmed that the single laser can efficiently perform as both the dissociation and pumping laser for Ag atoms. In the next step, we will measure the HFS splitting of Ag atoms in He II by using this laser system.

References

- 1) T. Furukawa, Doctoral thesis, Osaka University (2007).
- 2) K. Imamura *et al.*, *Hyperfine Interact.* **230**, 73 (2014).
- 3) T. Fujita *et al.*, *RIKEN Accel. Prog. Rep.* **47**, 212 (2014).
- 4) T. Fujita *et al.*, *RIKEN Accel. Prog. Rep.* **50**, 196 (2014).
- 5) E. Loginov *et al.*, *Phys. Rev. Lett.* **106**, 233401 (2011).
- 6) W. Kobayashi *et al.*, *RIKEN Accel. Prog. Rep.* **52**, 19 (2019).
- 7) K. Imamura *et al.*, *Appl. Phys. Express.* **12**, 016502 (2019).

*1 RIKEN Nishina Center

*2 Department of Advanced Sciences, Hosei University

Baseline correction system for precision measurement of the hyperfine structure of Rb atoms in superfluid helium

M. Doi,^{*1,*2} K. Imamura,^{*2} A. Takamine,^{*2} Y. Takeuchi,^{*1,*2} T. Yamamoto,^{*1,*2} H. Ueno,^{*2} and Y. Matsuo^{*1,*2}

We have been developing a laser spectroscopic method for the atoms injected into superfluid helium (He II) with the objective of studying the nuclear structure of unstable nuclei with low production yields and short lifetimes. In this method, laser-induced fluorescence (LIF) is observed by applying the laser-radiofrequency (RF)/microwave (MW) double resonance method to atoms in He II to measure Zeeman splitting and hyperfine structure (HFS). It enables us to determine the nuclear magnetic moments and nuclear spins that reflect nuclear structure.

One of the effective ways to introduce atoms to He II is a two-step laser sputtering method. In a previous experiment, we successfully measured the hyperfine structure of ^{133}Cs atoms in He II with an uncertainty of 10^{-5} via the laser-microwave double resonance method.¹⁾ In order to discuss the hyperfine anomaly of atoms in He II, it is necessary to measure hyperfine structure splittings for at least two isotopes. We attempted to show the feasibility of deducing hyperfine splittings with an accuracy and a precision of 10^{-6} for Rb, which has two stable isotopes. However, it has been difficult to realize measurement with a sufficiently high precision owing to the fluctuation of the number of observed photons when we use the two-step laser sputtering method to supply atoms to He II. To overcome this difficulty, a baseline correction system to cancel the fluctuation of the number of atoms was developed.²⁾

The baseline correction system consists of an electro-optic modulator (EOM) to switch the polarization of the excitation laser quickly and a multichannel scaler (MCS) equipped with multi-channel inputs to count photons for circular and linear polarizations. It has been successfully demonstrated by observing the LIF count difference between spin-polarized and unpolarized atoms that the

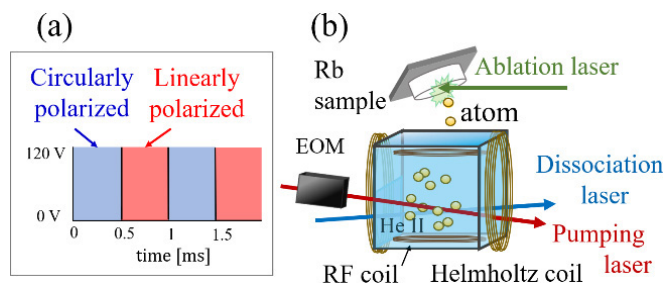


Fig. 1. (a) Switching of the polarization of the excitation laser by EOM. (b) Schematic of the experimental setup in a cryostat.

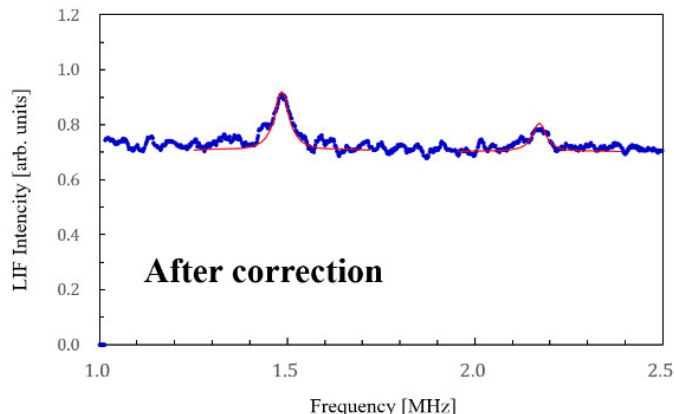


Fig. 2. Laser RF double-resonance spectrum of $^{85,87}\text{Rb}$ obtained using the baseline correction system.

baseline correction system works properly.²⁾

Next, we applied this system to a double-resonance experiment. With circularly polarized laser light irradiation, we expect to observe fluorescence from atoms only when the RF/MW frequency is resonant with the Zeeman splitting or hyperfine structure while scanning the RF/MW frequency. On the other hand, when the laser light is linearly polarized, all the atoms are excited; thus, the observed number of photons was proportional to the number of atoms.

We performed an RF double-resonance experiment for Rb atoms injected into He II using the baseline correction system. Rb atoms were irradiated with a 120-mW Ti:Sa laser (wavelength: 780 nm, laser diameter: 2 mm) of either circular or linear polarization. Figure 2 shows the spectrum obtained when we swept the RF frequency. We observed two fluorescence peaks. The peaks on the left and right correspond to resonance for the Zeeman splitting of ^{85}Rb and ^{87}Rb , respectively. The center frequencies of both peaks were consistent with the resonance frequencies estimated from our experimental condition. This result indicates that the baseline correction system works well in the double-resonance experiment as well as the previous work.³⁾

In the future, the present research will be extended by measuring the hyperfine structure of Rb with the baseline correction system to evaluate the hyperfine anomaly of Rb isotopes in He II, which requires a MW double-resonance experiment with a long sweep time and, hence, an increased fluctuation in the number of atoms.

References

- 1) K. Imamura *et al.*, *Hyperfine Interact.* **230**, 73 (2015).
- 2) M. Sanjo *et al.*, *RIKEN Accel. Prog. Rep.* **52**, 153 (2019).
- 3) T. Fujita *et al.*, *RIKEN Accel. Prog. Rep.* **47**, 212 (2014).

*1 Department of Advanced Sciences, Hosei University

*2 RIKEN Nishina Center

Profile measurement of laser microbeam produced by glass capillaries: tilt dependence

M. Mori,^{*1,*2} T. Ikeda,^{*2} Y. Hikima,^{*1,*2} S. Kawamura,^{*1,*2} and W. -G. Jin^{*1}

Tapered glass capillaries can simultaneously produce ion and laser microbeams with diameters of several tens of μm .^{1,2)} In the irradiation experiments at the RIKEN Pelletron facility, for example, H and He ions with energies of a few MeV are used. Their ranges are only about 100 μm in water at most. Since it is difficult to confirm incidence on the target by using detectors, the use of a μm -order laser sight system prior to the ion irradiation plays an important role in avoiding mis-shootings.³⁾ The μm -order laser sight through a capillary was demonstrated with visible light and then extended to UV in 2018.⁴⁾ This may be applicable to shorter wavelengths such as X-rays. Moreover, a multi-quantum beam (laser + ion) or (laser + laser) transmission through a capillary will be feasible. However, the transmission property is different between lasers and ions. Here, a laser beam bending along the tilted capillary axis is reported, which is known as the guiding effect for keV-energy ion microbeams through the capillaries without any magnetic field.

Figure 1 shows the experimental setup. A UV laser 375 nm in wavelength was extracted from a semiconductor laser source (THORLABS L375P70MLD; max.70 mW), and it entered a capillary mounted on a precise stage after reflection on two mirrors. The power of the laser microbeam was measured at a photodiode (OPHIR PD300) after a slit, which shields the scattered light from the taper part of the capillary. The microbeam was cut by a knife edge attached on a motorized stage (SURUGA SEIKI XYCV620-G-N) with a scan length and minimal step of 2 mm and 0.5 μm , respectively. The knife edge was located 3 mm downstream of the capillary outlet, of which the corresponding distance from the center of the tilting (θ) was 72 mm for a capillary with an outlet of 18 $\mu\text{m}\phi$.

The profiles were obtained by differentiating the beam power as a function of the knife-edge position. The peak shift according to θ is shown in Fig. 2. A steeper decrease for the $\theta(+)$ tilting, *i.e.*, an asymmetry of the profiles in the $\theta(+)$ and $\theta(-)$ tilting, can be found and may be attributed to the slightly asymmetric shape of capillaries. Satellite peaks are due to higher-order rings of the Fraunhofer pattern.¹⁾ The angles reconstructed

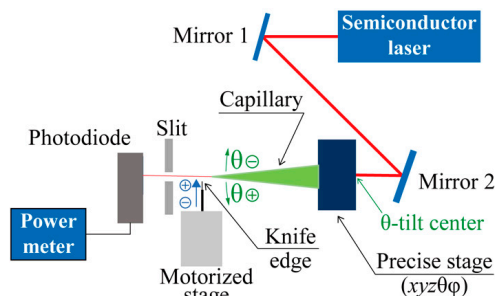


Fig. 1. Experimental setup with the knife-edge method.

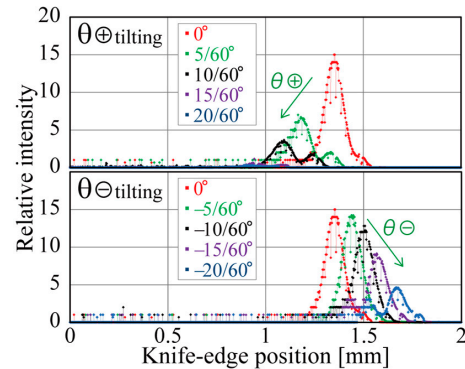


Fig. 2. Laser microbeam profiles measured by tilting the capillary in the $\theta(+)$ and $\theta(-)$ directions.

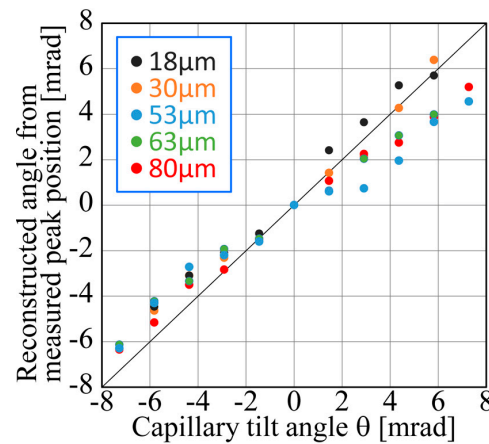


Fig. 3. Reconstructed angles as a function of θ .

from the measured peak positions are summarized for five outlet sizes, as shown in Fig. 3. The reconstructed angle is found to be nearly proportional to θ . The solid line shows $y = x$ as a guide to the eye. Most of the reconstructed angles are less than the tilting angles, especially for the outlets of 53, 63, and 80 $\mu\text{m}\phi$. Such a phenomenon is not found in ion experiments.^{5,6)} This is considered a result of different transmission mechanisms of ions and light in capillaries. Because ions lose their energies during scattering at the inner wall, they cannot penetrate the capillary window, and only those parallel to the capillary axis contribute to the output beam. However, light does not lose its energy during scattering and always contributes to the output beam. We concluded that the knife-edge method is capable of measuring the laser microbeam profile. Further, laser light is possibly guided by the capillary tilting. The next step will be to test the dependence on the divergence of the initial laser beam.

References

- 1) K. Sato *et al.*, RIKEN Accel. Prog. Rep. **51**, 21 (2018).
- 2) T. Ikeda *et al.*, Quantum Beam Sci. **4**, 22 (2020).
- 3) T. Ikeda *et al.*, RIKEN Accel. Prog. Rep. **51**, 245 (2018).
- 4) S. Kawamura *et al.*, J. Phys. Soc. Jpn. **89**, 055002 (2020).
- 5) M. Ikekame *et al.*, RIKEN Accel. Prog. Rep. **52**, 164 (2019).
- 6) T. Ikeda *et al.*, Nucl. Instrum. Methods Phys. Res. B **470**, 42 (2020).

^{*1} Department of Physics, Toho University

^{*2} RIKEN Nishina Center

2. Atomic and Solid State Physics (Muon)

Study on magnetism of defective reduced graphene oxides

R. Asih,^{*1,*2} D. P. Sari,^{*3,*2} M. A. Baqiya,^{*1} Darminto,^{*1} and I. Watanabe^{*2}

The origin of magnetism in graphene-based materials has been determined to be related with the presence of defects in their sheets.¹⁻³⁾ A graphene-derived material that has a significant amount of defects is reduced graphene oxide (rGO). The magnetic state of rGO has been reported to vary depending on the defect state and, thus, on the preparation history. Paramagnetic,⁴⁾ super-paramagnetic,⁵⁾ and even room-temperature ferromagnetic states^{1,2)} have been reported to coexist in rGO.⁶⁾ A magnetic ordering is expected to appear in the presence of a sufficient amount of defects in rGO.³⁾ In this study, we investigate the presence of possible room-temperature magnetic ordering in rGO prepared using the green-synthesized method⁷⁾ by means of muon-spin relaxation (μ SR).

The investigation of the Raman spectra of the synthesized rGO revealed the presence of a significant amount of defects and that the amount of defects can be enhanced by thermal reduction.⁷⁾ In addition to sp^2 carbon hybridization (C = C), the main functional group, the presence of different types of oxygen functionalities was observed in the synthesized rGO.^{7,8)} The magnetization at 300 K was found to increase with an increasing amount of defects, and the enhancement was not attributed to magnetic impurities.⁷⁾ Moreover, a divergence in $\chi(T)$ was observed under field cooling (FC) and zero-field cooling (ZFC) conditions, which might indicate that the blocking temperature is noticeable at 300 K. Thus, the μ SR experiment was subsequently performed to microscopically investigate magnetism in rGO at 300 K.

The inset in Fig. 1 shows the zero-field (ZF) time spectrum of the synthesized rGO at 300 K. An appreciable muon-spin precession on top of the decaying signal was observed in the spectrum, which is somehow similar to that observed in as-prepared graphene.⁹⁾ The spectrum can be well fitted by a single precession component and a Lorentzian decay. The fitting results in a hyperfine field of about 6 G. Such coherent muon-spin precession could indicate the presence of long-range magnetic ordering and/or the formation of a muonium (Mu)-H entangled state.⁹⁾ Meanwhile, the Lorentzian decay signifies muon diffusion through a carbon surface.¹⁰⁾ Under the assumption of the Mu-H dipolar interaction, a dipolar field of approximately 5 G is obtained which is equal to a Mu-H internuclear distance of 1.344 ± 0.005 . Furthermore, a longitudinal-field (LF) was applied to decouple the muon spin from the electron spin. The LF dependence of the muon-spin repolarization fraction is

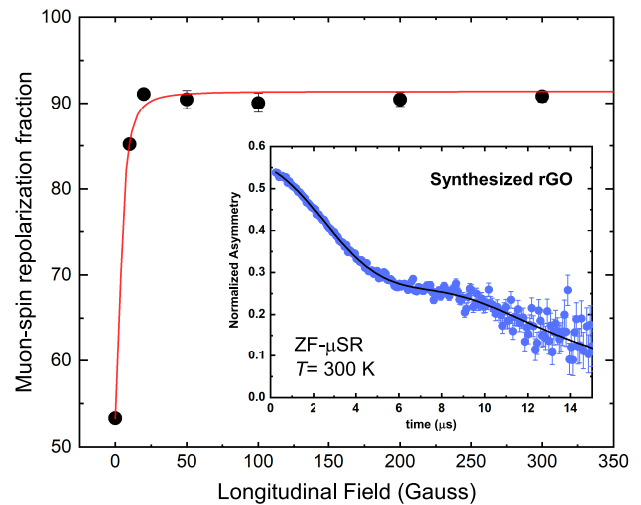


Fig. 1. Field dependence of the muon-spin repolarization fraction of the synthesized rGO at 300 K fitted by a simple model for the muonium radical (Eq. (1)). Inset: zero-field (ZF) μ SR spectrum (at 300 K) of the synthesized rGO fitted by the summation of Lorentzian decay and a single precession component, as described in the text.

displayed in Fig. 1, which can be well fitted by a simple model for isotropic muonium with the function described in Eq. (1).¹⁰⁾

$$P_{exp} = P_{dia} + A_{rad}[x^2/(x^2 + 1)], \quad (1)$$

where $x = B/B_{hyp}$. B_{hyp} is the hyperfine field for free muonium. P_{dia} and A_{rad} are the diamagnetic fraction and the amplitude of the radical fraction, respectively. The obtained B_{hyp} is about 4.35 ± 0.24 G, which is almost as large as that procured from the ZF spectrum. This B_{hyp} value corresponds to a hyperfine frequency of 12(1) MHz, which is close to the instrument cut-off of 13 MHz. This can be the reason why $\sim 45\%$ of the implanted muons were not observed in the ZF spectrum. Furthermore, a more detailed analysis in conjunction with first-principles calculations is required to confirm that the observed muon-spin precession originates from Mu-H interaction to form the CHMu group as suggested for hydrogenated graphene.⁹⁾

References

- 1) S. Qin *et al.*, Carbon **78**, 559 (2014).
- 2) G. Khurana *et al.*, Nanoscale **5**, 3346 (2013).
- 3) J. Tücek *et al.*, Chem. Soc. Rev. **47**, 3899 (2018).
- 4) M. Sepioni *et al.*, Phys. Rev. Lett. **105**, 207205 (2010).
- 5) S. K. Sarkar *et al.*, Physica E **64**, 78 (2014).
- 6) P. Z. Sun *et al.*, Nano Res. **7**, 1507 (2014).
- 7) D. Darminto *et al.*, IEEE Trans. Mag. **54**, 1 (2018).
- 8) R. Asih *et al.*, Mat. Sci. Forum **966**, 290 (2019).
- 9) M. Riccò *et al.*, Nano Lett. **11**, 4919 (2011).
- 10) M. Gaboardi *et al.*, J. Mater. Chem. A **2**, 1039 (2014).

^{*1} Department of Physics, Institut Teknologi Sepuluh Nopember, Indonesia

^{*2} RIKEN Nishina Center

^{*3} Department of Regional Environment Systems, Shibaaura Institute of Technology

Magnetic ground state of $J_{\text{eff}} = 0$ Mott insulator $\text{Ag}_3\text{LiRu}_2\text{O}_6$ under pressure

T. Takayama,^{*1,*2} M. Blankenhorn,^{*1,*2} A. Krajewska,^{*1,*2} D. P. Sari,^{*3,*4} I. Watanabe,^{*4} and H. Takagi^{*1,*2,*5}

The interplay of strong spin-orbit coupling (SOC) and electron correlation in heavy transition-metal oxides has been found to give rise to unprecedented electronic phases. Among such oxides, Mott insulators with a d^4 (t_{2g}^4) configuration are expected to exhibit exotic magnetism. In the d^4 systems, Hund's coupling produces an $S = 1$ and $L_{\text{eff}} = 1$ state. SOC thus yields a spin-orbit-entangled $J_{\text{eff}} = 0$ ground state. Although the $J_{\text{eff}} = 0$ state is non-magnetic, it may interact magnetically with each other through the excited $J_{\text{eff}} = 1$ levels separated by SOC. It was proposed that the system undergoes magnetic ordering when the energy gain by magnetic interactions overcomes the energy cost of the $J_{\text{eff}} = 0$ to 1 excitation, which is dubbed excitonic magnetism.¹⁾ Particularly, when the $J_{\text{eff}} = 0$ state is arranged on a honeycomb lattice, exotic magnetic ground states such as a spin-nematic phase or magnetic triplon liquid, are expected to emerge.

The $J_{\text{eff}} = 0$ honeycomb lattice may be realized in Ru^{4+} ($4d^4$) oxides. However, a honeycomb ruthenate Li_2RuO_3 is known to display spin-singlet dimerization accompanying orbital ordering.²⁾ In the dimerized state, the spin and orbital degrees of freedom are quenched, and spin-orbit coupling is inactive. In order to suppress the dimerization and realize the $J_{\text{eff}} = 0$ state, we employed an ion-exchange reaction and obtained the silver-intercalated compound $\text{Ag}_3\text{LiRu}_2\text{O}_6$.³⁾ The crystal structure at room temperature shows no appreciable distortion in the Ru honeycomb lattice, indicating the disappearance of dimerization.

The magnetic susceptibility $\chi(T)$ of $\text{Ag}_3\text{LiRu}_2\text{O}_6$ increases on cooling from room temperature and shows saturation below 100 K. Interestingly, no magnetic order is observed down to 0.3 K. From inelastic neutron scattering and ^7Li -NMR measurements, $\text{Ag}_3\text{LiRu}_2\text{O}_6$ was found to have a gapped magnetic excitation of ~ 35 meV, as expected for the $J_{\text{eff}} = 0$ -type singlet ground state.⁴⁾ The singlet ground state suggests that the magnetic exchange interactions are not strong enough to drive excitonic magnetism. We thus investigated the magnetic properties under high pressures as an attempt to enhance magnetic interactions. Indeed, under a pressure above 0.4 GPa, $\chi(T)$ shows a broad peak below room temperature, indicating the appearance of a pressure-induced electronic phase transition. However, the nature of the magnetic ground state under pressure remains un-

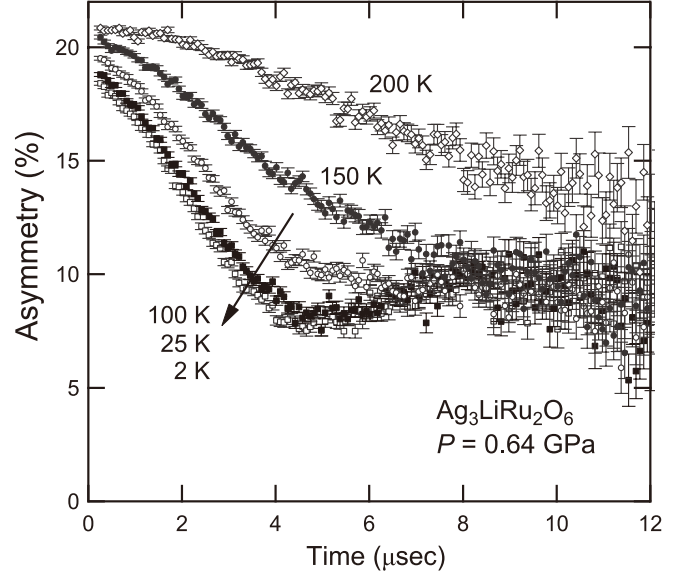


Fig. 1. Zero-field time spectra of muon asymmetry for $\text{Ag}_3\text{LiRu}_2\text{O}_6$ under a pressure of 0.64 GPa.

clear.⁴⁾

In order to understand the magnetic ground state under pressure, we performed a muon spin rotation measurement on $\text{Ag}_3\text{LiRu}_2\text{O}_6$ under pressure by using ARGUS, ISIS. At ambient pressure, the time dependence of muon asymmetry at low temperatures only shows a monotonic decrease, which is consistent with the nonmagnetic singlet ground state. As shown in Fig. 1, the time dependence of muon asymmetry did not show any pronounced change down to 2 K even at a pressure of 0.64 GPa, while $\chi(T)$ showed a broad peak at approximately 150 K at that pressure. This suggests that the broad peak observed in $\chi(T)$ under pressure is not associated with a magnetic ordering but represents another electronic phase transition while retaining the nonmagnetic ground state.

The nature of the pressure-induced nonmagnetic phase, revealed by the μSR measurement, remains elusive. The x -ray diffraction under pressure excluded the restored dimerization in this pressure range. The candidates of possible ground states include a spin-orbit triplon liquid, molecular orbital formation, or fluctuating dimers. We are currently attempting to determine the nature of this phase in combination with other spectroscopic probes.

References

- 1) G. Khaliullin, Phys. Rev. Lett. **111**, 197201 (2013).
- 2) Y. Miura *et al.*, J. Phys. Soc. Jpn. **76**, 033705 (2007).
- 3) S. A. J. Kimber *et al.*, J. Mater. Chem. **20**, 8021 (2010).
- 4) T. Takayama *et al.*, in preparation.

*1 Max Planck Institute for Solid State Research

*2 Institute for Functional Matter and Quantum Technologies, University of Stuttgart

*3 Graduate School of Engineering and Science, Shibaura Inst. of Tech.

*4 RIKEN Nishina Cente

*5 Department of Physics, University of Tokyo

Non-magnetic ground state of $\text{In}_2\text{Ru}_2\text{O}_7$ probed by muon spin rotation

T. Takayama,^{*1,*2} A. Krajewska,^{*1,*2} I. Watanabe,^{*3} D. P. Sari,^{*3,*4} and H. Takagi^{*1,*2,*5}

The interplay of charge, spin, and orbital degrees of freedom in correlated systems gives rise to a variety of exotic electronic states. Among these materials, ruthenium oxides containing Ru^{4+} cations (d^4 electron count), which host orbital degeneracy, display a variety of spin-orbital ordering phenomena such as spin singlet dimer formation in Li_2RuO_3 ¹⁾ and La_2RuO_5 .²⁾ A particularly interesting situation may be found when Ru^{4+} cations are placed on a frustrated lattice, for example, in pyrochlore ruthenate $\text{Tl}_2\text{Ru}_2\text{O}_7$, which displays a metal-to-insulator transition with a spin-singlet ground state.³⁾ The spin-singlet state is discussed to originate from the formation of 1D zig-zag Haldane chains and is potentially the first example of such a system emerging in a 3D lattice. While there is still discussion on the plausibility of the Haldane-chain scenario, the origin of this unique state and behavior distinct from those of other pyrochlore ruthenates remains unclear. Pyrochlore ruthenates appear to be an interesting playground for novel electronic states.

We discovered a new pyrochlore ruthenate $\text{In}_2\text{Ru}_2\text{O}_7$ which adopts a weakly distorted pyrochlore structure at 300 K. $\text{In}_2\text{Ru}_2\text{O}_7$ is an insulator and shows Curie-Weiss behavior at high temperatures. At $T_m \sim 220$ K, a sharp drop in magnetic susceptibility $\chi(T)$, similar to those of other spin-singlet ruthenate compounds,¹⁻³⁾ is observed. To elucidate the nature of the ground state of $\text{In}_2\text{Ru}_2\text{O}_7$ and the absence of a long-range magnetic ordered state, the temperature dependence of zero-field muon spin rotation (ZF- μ SR) is necessary. In this report, we present the result of a ZF- μ SR experiment performed on CHRONUS at ISIS, UK. We recorded the time evolution of ZF- μ SR spectra of $\text{In}_2\text{Ru}_2\text{O}_7$ from 300 K down to 10 K (Fig. 1(a)). No oscillation down to the lowest temperature was observed, excluding the presence of long-range antiferromagnetic order and pointing to a non-magnetic spin singlet state. The data over the whole studied temperature range were fitted to a “stretched” exponential:

$$P_z(t) = e^{-(\lambda t)^\beta}, \quad (1)$$

where $P_z(t)$ is the asymmetry, t is the time, λ is the relaxation rate, and β is the shape parameter. We observed a cross-over from a Gaussian-like to a Lorentzian-like damping with decreasing temperature (Figs. 1(a) and (b)). The high-temperature and low-temperature response can be explained by the slowing behaviour of the fluctuations of dilute Ru spins, which originate from

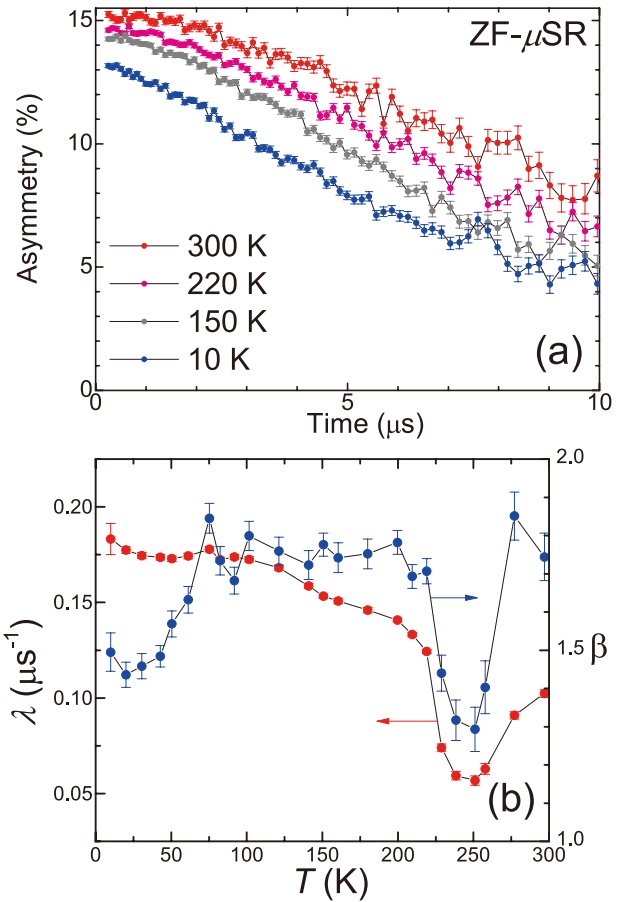


Fig. 1. (a) Time evolution of ZF- μ SR spectrum of $\text{In}_2\text{Ru}_2\text{O}_7$ powder sample at various temperatures. (b) Temperature dependence of λ and β fitted using equation (1).

the defects present in the system, or by the appearance of slowly fluctuating quasi-particle spins excited from the spin-singlet state induced by injected muons. Such a response was reported in other materials hosting a spin-singlet ground state.^{5,6)} In addition, a sharp change in λ and β is observed at T_m (Fig. 1(b)). The enhancement of λ below T_m would point to the opening of a gap.

In this report, the ground state of $\text{In}_2\text{Ru}_2\text{O}_7$ was investigated with ZF- μ SR. No evidence of long-range magnetic order was found; hence, the non-magnetic ground state was confirmed. The temperature dependence of the relaxation rate implies the opening of a gap. Other techniques such as resonant inelastic x-ray scattering could aid the determination of the gap size.

References

- 1) Y. Miura *et al.*, J. Phys. Soc. Jpn. **76**, 033705 (2007).
- 2) H. Wu *et al.*, Phys. Rev. Lett. **96**, 256402 (2006).
- 3) S. Lee *et al.*, Nat. Mat. **5** (2006).
- 4) K. Kojima *et al.*, Phys. Rev. Lett. **74**, 3471 (1995).
- 5) S. J. Blundell *et al.*, Phys. Rev. B **77**, 094424 (2008).
- 6) M. Miyazaki *et al.*, Phys. Rev. B **75**, 09440 (2007).

^{*1} Max Planck Institute for Solid State Research

^{*2} Institute for Functional Matter and Quantum Technologies, University of Stuttgart

^{*3} RIKEN Nishina Center

^{*4} Graduate School of Engineering and Science, Shibaura Institute of Technology

^{*5} Department of Physics, University of Tokyo

Short-range magnetic order in the frustrated antiferromagnet $\text{Cu}_5(\text{PO}_4)_3(\text{OH})_4$ (pseudomalachite)

H. Kikuchi,^{*1} Y. Fujii,^{*2} U. Widyaiswari,^{*3} and I. Watanabe^{*3}

Geometrically frustrated magnets have recently been attracting much interest, because they are expected to exhibit new physical states including spin liquid. Almost every frustrated magnet studied so far, *e.g.*, kagomé, triangular, and pyrochlore lattices, are based on triangular units. The spin frustrated effect, however, is not restricted to a triangle but appears if antiferromagnetic spins are on a polygon with odd-number edges such as a pentagon. A lattice containing pentagons as its unit can afford a new category for the spin frustration effect. $\text{Cu}_5(\text{PO}_4)_3(\text{OH})_4$ (mineral name: pseudomalachite) is an orthorhombic crystal¹⁾ with three crystallographically inequivalent sites of copper. Layers consisting of face-shared CuO_6 octahedrons extend in the *bc* plane and are separated by interlayer PO_4 tetrahedrons. A spin network in the *bc* plane formed by Cu^{2+} ions ($S = 1/2$) has a unique structure composed of triangles and pentagons.

We measured the magnetic susceptibility, specific heat, and high-field magnetization of pseudomalachite using natural mineral samples.²⁾ The sign of the Weiss temperature is found to be negative, indicating that the dominant interaction is antiferromagnetic. The specific heat $C(T)$ has a broad maximum at $T_f \approx 4.2$ K, where $\chi(T)$ shows a peak anomaly.

The relative change of $C(T)$ at T_f is very small if this transition is a long-range magnetic order.

The entropy change associated with the magnetic order was estimated to be approximately 5.5 J/(K·mol),

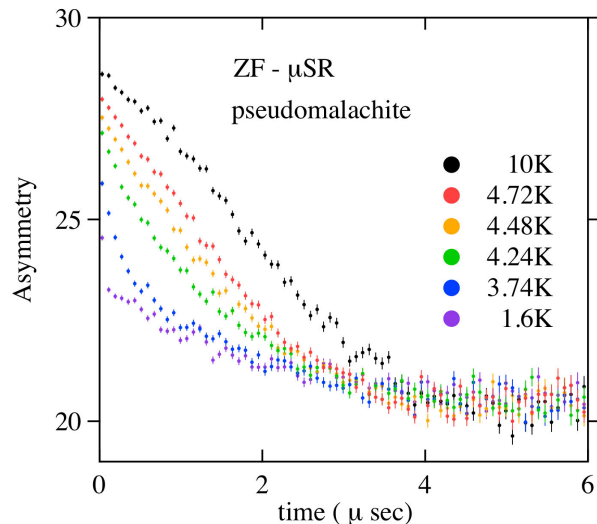


Fig. 1. ZF- μ SR spectra of pseudomalachite.

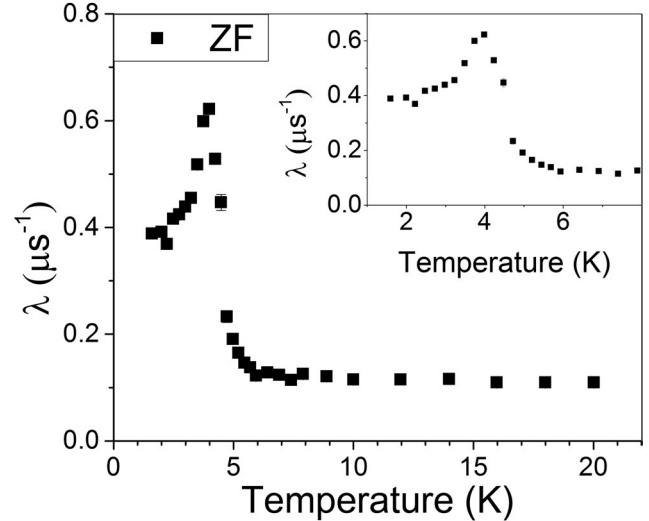


Fig. 2. Temperature dependence of the relaxation rate λ .

which is only one-fifth of the expected value $5R \ln 2 \approx 28.8$ J/(K·mol). In order to clarify the magnetic ordering transitions in this frustrated magnet, measurements using a microscopic and dynamic probe is highly desired.

Figure 1 shows the zero-field muon spin relaxation (ZF- μ SR) spectra measured down to 1.6 K. At relatively high temperatures, the spectra follow Gaussian curves.

Below approximately 4.2 K, the initial asymmetry begins to decrease, and the form of the spectra changes from the Gaussian to an exponential curve following $\exp(-\lambda/t)$, where λ is the relaxation rate. Figure 2 shows the temperature dependence of the relaxation rate obtained from a fit to the observed spectra. λ has a distinct peak at approximately 4 K, where the anomaly was observed in the specific-heat data. These observed results clearly indicate that the magnetic phase transition occurs at T_f .

The spectrum below T_f , however, does not show any spin rotation, suggesting that the internal field is dynamic, rather than static. Furthermore, even in the lowest-temperature spectrum, spin relaxation remains, and finite spin fluctuations seem to be present in the ordered phase. These findings are consistent with our macroscopic indication that the transition is not a long-range order but has the character of a short-range order, which originates from the geometrical spin frustration effect of the peculiar spin network of pseudomalachite.

References

- 1) G. L. Shoemaker *et al.*, *Am. Mineral.* **62**, 1042 (1977).
- 2) H. Kikuchi *et al.*, *J. Korean Phys. Soc.* **62**, 2037 (2013).

^{*1} Department of Applied Physics, University of Fukui

^{*2} FIR Center, University of Fukui

^{*3} RIKEN Nishina Center

μ SR investigation of spin liquid states in magnetic properties of MgTi_2O_4 sample

U. Widyaiswari,^{*1,*2} N. Hanasaki,^{*3} B. Kurniawan,^{*2} and I. Watanabe^{*1,*2}

The investigation of the geometrical frustration of strongly correlated systems is an interesting research field. These systems show various exotic physical properties such as spin ice,¹⁾ and spin liquid states.²⁾ In the spin liquid state, spins do not show magnetic ordering even at the ground state. The spin liquid state generally appears in triangular lattices and Kagome lattice systems, which show geometrical frustration of spin systems.²⁾ Materials with pyrochlore structures, such as pyrochlore oxides and spinel compounds, that have corner-sharing tetrahedral lattices are strong candidates to exhibit such exotic physical properties.

The spinel titanate, MgTi_2O_4 , has $3d^1$ electron ($S = 1/2$) within the Ti^{3+} ion and forms a pyrochlore lattice.³⁾ At room temperature, the lattice structure of MgTi_2O_4 is cubic, and it shows a structural transition to a tetragonal lattice at $T_{st} = 260$ K.⁴⁾ This structural phase transition is accompanied by a metal-insulator transition and changes in magnetic properties.⁴⁾ Isobe *et al.* proposed a spin-singlet insulator as the ground state, which did not form any magnetic ordering, suggesting the appearance of a spin liquid state.⁴⁾ At this moment, the spin state of MgTi_2O_4 in the ground state is still unclear and open for discussion. To explore the magnetic properties of MgTi_2O_4 , we performed microscopic measurements using muon-spin relaxation (μ SR) spectroscopy.

We measured the time evolution of the muon-spin polarization in the zero-field (ZF) condition at the RIKEN-RAL Muon Facility in the United Kingdom. Time spectra measured at several temperatures are shown in Fig. 1(a). No muon-spin precession was observed in the time spectrum, indicating that there was no long-range ordered state down to 6 K. We fitted the time spectra using Eq. (1).

$$A(t) = A_0 \exp(-\lambda t), \quad (1)$$

where A_0 is the initial asymmetry of the muon spin at $t = 0$ and λ is the muon-spin relaxation rate. The temperature dependence of λ is shown in Fig. 1(b). λ gradually increases with decreasing temperature below 250 K. The increase of λ indicates the appearance of a slowing down behavior of Ti^{3+} spin fluctuations. However, there is no critical slowing down behavior indicating the absence of a magnetic ordered state in the current ZF- μ SR study, as suggested in a previous study.⁴⁾ Accordingly, we plan to gather more detailed information on the spin dynamics by performing μ SR

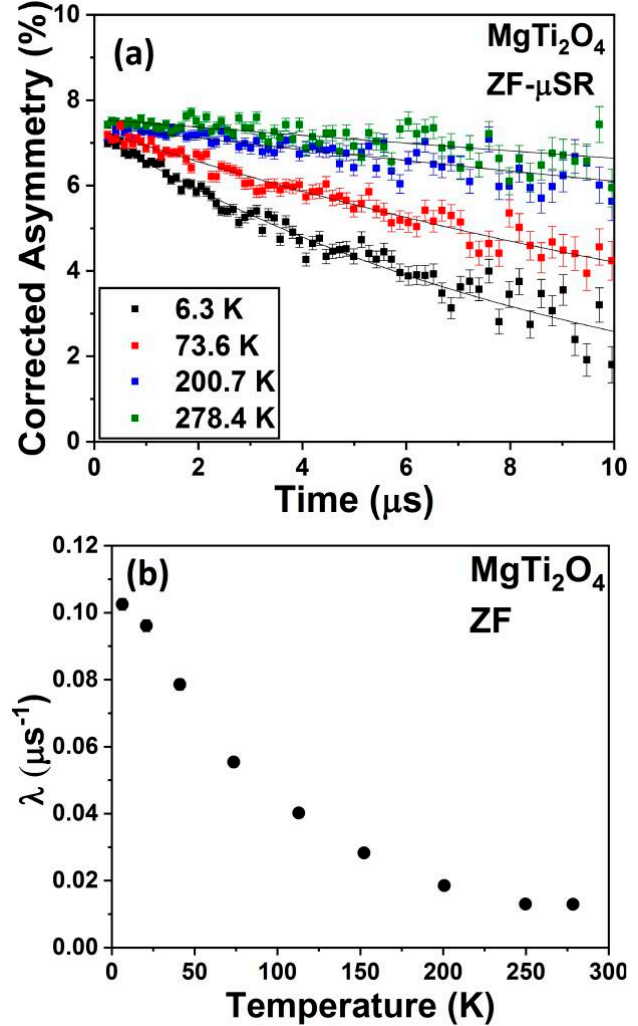


Fig. 1. (a) ZF- μ SR time spectra of MgTi_2O_4 and (b) temperature dependence of muon spin relaxation rate.

measurements in the longitudinal field (LF) condition.

References

- 1) M. J. Harris *et al.*, Phys. Rev. Lett. **79**, 2554 (1997).
- 2) L. Balents, Nature **464**, 199 (2010).
- 3) S. Torigoe *et al.*, Phys. Rev. B **98**, 134443 (2018).
- 4) M. Isobe, Y. Ueda, J. Phys. Soc. Jpn. **71**, 1848 (2002).

*1 RIKEN Nishina Center

*2 Department of Physics, Universitas Indonesia

*3 Department of Physics, Osaka University

Zero-point vibrational energy in the muon sites of La_2CuO_4

M. R. Ramadhan,^{*1,*3} M. I. Mohamed-Ibrahim,^{*2} S. Sulaiman,^{*2} and I. Watanabe^{*1,*2,*3}

La_2CuO_4 (LCO), the parent compound of high- T_C superconducting $\text{La}_{2-x}\text{Ba}_x\text{Sr}_x\text{CuO}_4$, is known to have antiferromagnetic long-range ordering (AF-LRO) due to its classification as a Mott insulator. One accurate experiment to prove the AF-LRO characteristic is the muon spin relaxation (μSR) technique. In this technique, the implanted muons that sense an internal magnetic field undergo Larmor precession. A previous study on bulk LCO showed that the muon's precession frequency is 5.5 MHz. Using the muon's gyromagnetic ratio, $\gamma_\mu = 135.538817 \text{ MHz/T}$, the internal field (B_μ^{exp}) felt by muons in bulk LCO was determined to be approximately 410 G.¹ A recent study on thin-film LCO showed that the implanted muons probe an additional internal field approximately 100–120 G.² While two clear precessions have been shown in the past, the exact location of the implanted muon is still unknown, which hinders the ability of the μSR technique to reveal more information and knowledge from the LCO system.

Our group has been developing a technique to precisely estimate the muon position by utilizing density functional theory (DFT) calculations. Generalized gradient approximation (GGA) was chosen for the exchange-correlation functional. The antiferromagnetic configuration of the Cu spin from Vaknin *et al.* is utilized for the non-collinear calculation.³ Because LCO is a Mott insulator, we need to include the Coulombic repulsion energy ($U_{\text{eff}} = 7.2 \text{ eV}$) in the DFT calculation. From our previous reports,^{4,5} we show the muon position from our DFT calculation and the muon's perturbation effect on the Cu-spin densities from a DFT perspective. However, even when using the distributed-spin model to calculate the internal field, the calculated internal field shows a 21% difference with that observed from the experimentally ($B_\mu^{\text{exp}} = 410 \text{ G}$, while $B_\mu^{\text{DFT}} = 498 \text{ G}$). We considered that this discrepancy originates from the zero-point vibrational motion (ZPVM) of the muon, which was not considered in our last report. As a fine quantum particle, the muon should fluctuate in its lowest-energy state. To include the ZPVM, we first evaluate the three-dimensional Hartree potential (V_μ^{Hartree}) around the implanted muon's position. Subsequently, we simply calculate the eigenvalues and eigenfunction for the ground state on those areas by using the following equation:

$$\left[\frac{\hbar^2}{2m_\mu} \nabla_i^2 + V_\mu^{\text{Hartree}}(r) \right] \Psi_\mu(r) = E_\mu \Psi_\mu(r), \quad (1)$$

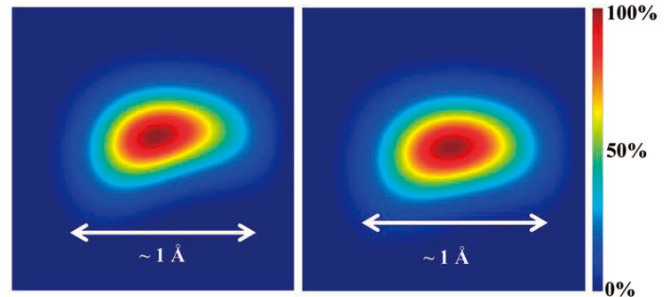


Fig. 1. Muon probability density map in the xz -plane for the (a) unperturbed LCO (b) perturbed LCO.

where m_μ denotes to the muon mass, and $|\Psi_\mu|^2(r)$ is the probability that the muon exists at each position r . This Schrödinger equation was using the finite-difference method. From our calculations, we conclude that the energy convergence is achieved by considering a $1.5 \times 1.5 \times 1.5 \text{ (Å)}$ area from the center of the muon position. The probability that the muon exists within this designated area is 100%.

As reported previously, the implanted muon only affects the local crystal and electronic structure of LCO. From our calculations, we obtained the ground-state energy as 0.82 eV for the unperturbed LCO and 0.89 eV for the perturbed LCO. The slight increase of the ground-state energy is very likely due to the local deformation of the crystal structure. However, the general description of the muon's distribution over the considered area is relatively the same as shown in Fig. 1. By using the muon probability density map of the perturbed LCO and the distributed-spin model from our previous reports^{4,5}, we successfully reduced the differences of the internal field to less than 1% ($B_\mu^{\text{exp}} = 410 \text{ G}$, while $B_\mu^{\text{DFT+ZPVM}} = 409 \text{ G}$). While this method shows a promising result for the LCO system, it still needs to be tested in other systems, in order to standardize this method to assist in μSR experiments.

References

- 1) J. I. Budnick *et al.*, Phys. Lett. A **124**, 103 (1987).
- 2) E. Stimp *et al.*, Phys. Rev. B **88**, 064419 (2013).
- 3) D. Vaknin *et al.*, Phys. Rev. Lett. **58**, 2802 (1987).
- 4) M. R. Ramadhan *et al.*, RIKEN Accel. Prog. Rep. **51**, 197 (2017).
- 5) M. R. Ramadhan *et al.*, RIKEN Accel. Prog. Rep. **52**, 173 (2018).

*1 Department of Physics, Universitas Indonesia

*2 School of Distance Education, Universiti Sains Malaysia

*3 RIKEN Nishina Center

Investigations of the quantum critical behavior of the $S = 1/2$ J_1 - J_2 square lattice antiferromagnets $\text{Sr}_2\text{Cu}(\text{Te}_{1-x}\text{W}_x)\text{O}_6$

S. Yoon,^{*1} W. -J. Lee,^{*1} S. Lee,^{*1,*2} C. H. Lee,^{*1} A. Berlie,^{*2} I. Watanabe,^{*3} and K. -Y. Choi^{*1}

The J_1 - J_2 square-lattice Heisenberg model offers a rich reservoir of exotic quantum phases. Depending on the ratio J_2/J_1 (the ratio of exchange interactions between a diagonal and a side of the square), the classical ground states encompass Néel, columnar antiferromagnetic, and disordered states. In particular, the B -site ordered double perovskites $\text{Sr}_2\text{Cu}(\text{Te}_{1-x}\text{W}_x)\text{O}_6$ ($B = \text{Cu}^{2+}$, $B'' = \text{Te}^{6+}$ or W^{6+}) with the tetragonal $I4/m$ structure are regarded as near-optimal realizations of the $S = 1/2$ Heisenberg model on a square lattice.¹⁻⁴ Notably, the magnetic ground state of $\text{Sr}_2\text{Cu}(\text{Te}_{1-x}\text{W}_x)\text{O}_6$ can be tuned from a Néel order ($x = 0$; $J_2/J_1 = 0.03$) through a quantum spin liquid to a columnar antiferromagnetic order ($x = 1$; $J_2/J_1 = 7.92$) by varying the B'' cation between Te^{6+} and W^{6+} ions.³ Owing to the similar sizes of the Te^{6+} and W^{6+} ions, $\text{Sr}_2\text{Cu}(\text{Te}_{1-x}\text{W}_x)\text{O}_6$ retains the isostructural crystal lattice.

Unlike the crystal structure, the magnetism is susceptible to a composition of the B'' cations that are involved in the magnetic exchange paths mediating the Cu^{2+} ions. W^{6+} ($5d^0$) hybridizes strongly with O $2p$, thereby enabling the magnetic exchange path Cu-O-W-O-Cu (J_2). This is in sharp contrast to the Te^{6+} ($4d^{10}$) ion, which is in favor of J_1 . The distinct role of the $\text{Te}^{6+}/\text{W}^{6+}$ ions in relation to the exchange interaction poses the question as to whether the theoretically predicted spin liquid phase can be achieved by controlling the composition of the B'' cations. Strikingly, there is tantalizing experimental evidence for a quantum disordered state in a wide composition range of $x \approx 0.1 - 0.7$.³ However, the observed wide range of the spin-liquid phase is not compatible with the theoretically predicted narrow composition range of $x \approx 0.23 \sim 0.33$. Recent theoretical calculations have proposed quenched disorders as a key ingredient to this discrepancy.^{3,4} To clarify the precise nature of the ground state, we focus on the compositions in the range of $x = 0.05 - 0.1$, which is at the boundary between the Néel antiferromagnetic order and the quantum disordered state.

Muon spin relaxation measurements were performed

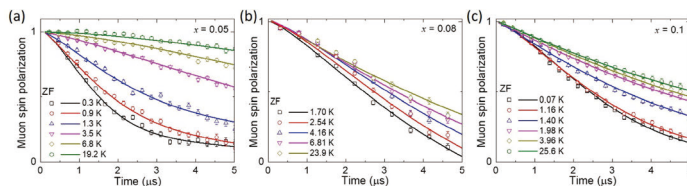


Fig. 1. Muon spin polarization data observed at zero field together with fitting curves (see the text for details) for $x = 0.05$, 0.08 , and 0.1 .

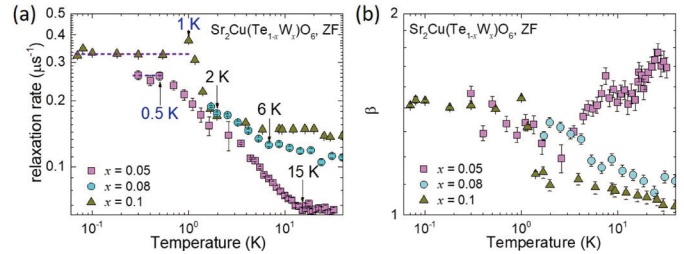


Fig. 2. Temperature dependences of the relaxation rate (a) and its stretch exponent (b) for $x = 0.05$, 0.08 , and 0.1 .

on ARGUS and CHRONUS spectrometers at RIKEN-RAL towards understanding the precise nature of the ground state and associated spin dynamics of the $x = 0.05$, 0.08 , and 0.1 compounds. Representative spectra are shown in Fig. 1. No spontaneous muon spin oscillation is observed, indicating the absence of long-range magnetic order. Moreover, all the observed μSR spectra are described by a stretched exponential function $\exp[-(\lambda t)^\beta]$, where λ is the muon relaxation rate and β is the exponent.

Temperature dependences of the muon spin relaxation rate, $\lambda(T)$, and its stretch exponent, $\beta(T)$, for $x = 0.05$, 0.08 , and 0.1 are plotted in Fig. 2. $\lambda(T)$ of $x = 0.05$ starts to increase on cooling below 15 K and subsequently becomes constant for temperatures below 0.5 K. In the $x = 0.08$ and 0.1 compounds, the crossover regime shrinks, and onset temperatures shift to 6 K and 2 K for $x = 0.08$ and 0.1 , respectively; on the other hand, a plateau appears at 1 K for $x = 0.1$. We comment that the $x = 0.05$ and 0.1 compounds reveal the persistent spin dynamics below $T = 0.5 - 1$ K, which is often observed in frustrated magnets.

In addition, the T -dependence of the stretching exponent, $\beta(T)$, of $x = 0.08$ and 0.1 resemble $\lambda(T)$ while increasing from 1 to 1.6 with decreasing temperature. In sharp contrast, $\beta(T)$ of $x = 0.05$ decreases from 1.8 to 1.3 on cooling to 25 K. Noticeably, the low- T $\beta(T)$ of the compounds is between those of Gaussian and Lorentzian relaxation functions. When we consider that a Gaussian-like distribution is expected for dense disordered systems or migrating unpaired spins in the matrix of singlet spins and that a Lorentzian-like distribution is expected for dilute systems, the ground state for $x = 0.05$, 0.08 , and 0.1 is largely compatible with the random singlet picture comprising resonating singlets and propagating orphan-like spins.

References

- 1) O. Mustonen *et al.*, Nat. Commun. **9**, 1085 (2018).
- 2) M. Watanabe *et al.*, Phys. Rev. B **98**, 054422 (2018).
- 3) O. Mustonen *et al.*, Phys. Rev. B **98**, 064411 (2018).
- 4) K. Uematsu, H. Kawamura, Phys. Rev. B **98**, 134427 (2018).

^{*1} Department of Physics, Chung-Ang university

^{*2} Science and Technology Facilities Council, ISIS-RAL

^{*3} RIKEN Nishina Center

Magnetic ordering and spin dynamics of $\text{Nd}_2\text{Ru}_2\text{O}_7$ studied by μSR

U. Widyaiswari,^{*1,*2} H. Sakai,^{*3} K. Inoue,^{*3} N. Hanasaki,^{*3} D. P. Sari,^{*4} B. Kurniawan,^{*2} and I. Watanabe^{*1,*2}

Pyrochlore ruthenate ($R_2\text{Ru}_2\text{O}_7$) is one of the systems that have a pyrochlore structure with the general formula $A_2B_2O_6O^*$, where A is a trivalent rare-earth ion and B is a tetravalent transition metal ion. This structure is composed of two corner-sharing tetrahedral lattices, which induce the magnetic frustration of spins on each corner of the tetrahedral lattices. Novel physical properties such as the spin-glass,¹⁾ spin-ice,²⁾ and metal-insulator transition accompanied by a magnetic transition,³⁻⁵⁾ are induced by this magnetically frustrated state. Those exotic properties originate from the competition and/or cooperation among the Coulomb interaction (U), spin-orbit coupling (SOC) effect, and exchange interaction between the rare-earth and transition metal ions.

The temperature dependence of the specific heat of $R_2\text{Ru}_2\text{O}_7$ shows a λ -type peak accompanied by a small cusp in the temperature dependence of magnetic susceptibility at the magnetic transition temperature, T_N .⁶⁻⁸⁾ T_N shifts to the higher temperature side from approximately 76 K to 160 K with increase in the ionic radius of R .⁶⁾ Ku *et al.* showed that three anomalies occur in $\text{Nd}_2\text{Ru}_2\text{O}_7$ at 146 K, 21 K, and 1.8 K.⁸⁾ At present, the origin of those anomalies is unclear. Accordingly, we investigated the magnetic properties of $\text{Nd}_2\text{Ru}_2\text{O}_7$ by the muon spin relaxation (μSR) method and compared the results with our previous results for $\text{Nd}_2\text{Ir}_2\text{O}_7$.^{4,5)}

The time evolution of the muon-spin polarization (μSR time spectrum) in zero field (ZF) was measured at several temperatures and analyzed by the following two-component relaxation function:

$$A(t) = A_1 \exp(-\lambda_1 t) + A_2 \exp(-\lambda_2 t). \quad (1)$$

The first and second components describe the fast and slow relaxation components, respectively. A_1 and A_2 are the asymmetry parameters while λ_1 and λ_2 are the muon relaxation rates of the two components.

We confirmed from the current study an ordered state of Ru spins below 146 K, showing a decrease in the initial asymmetry parameter accompanied by the appearance of a critical slowing down behavior of the Ru spin fluctuations.⁹⁾ Another anomaly of the muon relaxation rate was detected around 30 K as a broad dip in its temperature dependence.⁹⁾ This anomaly is unlikely to be due to the appearance of the magnetic ordering of Nd spins because no critical slowing down behavior was observed at lower temperatures in

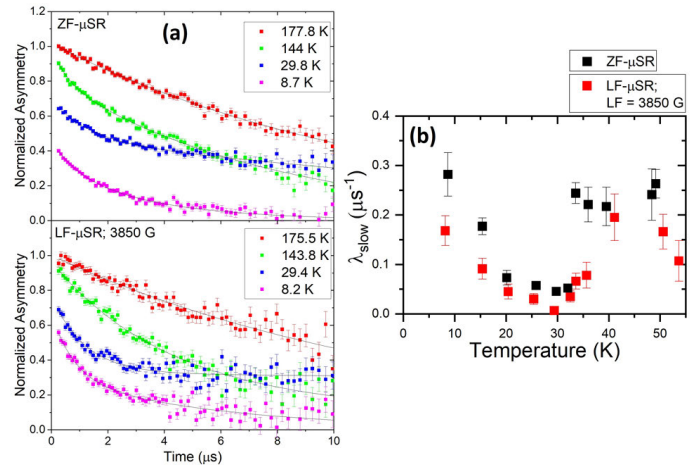


Fig. 1. (a) ZF- and LF- μSR time spectra of $\text{Nd}_2\text{Ru}_2\text{O}_7$ measured at various temperatures. An LF of 3850 G was applied for LF- μSR measurement. (b) Temperature dependences of the slow relaxation rate in both the ZF and LF condition.

$\text{Nd}_2\text{Ir}_2\text{O}_7$.^{4,5)}

In order to clarify the anomaly around 30 K, we measured μSR in the longitudinal-field (LF) condition under an applied field of 3850 G. Both ZF- and LF- μSR time spectra are shown in Fig. 1(a). We confirmed that the relaxation rate still showed the anomaly around 30 K in LF- μSR ,⁹⁾ but this anomaly was slightly smaller compared to the case of ZF- μSR . To obtain more information about the origin of the anomaly around 30 K, we are now planning to conduct further μSR measurements of the LF scan at several temperatures to investigate the change in spin dynamics.

References

- 1) J. G. Park *et al.*, Physica B **328**, 90 (2003).
- 2) M. J. Harris *et al.*, Phys. Rev. Lett. **79**, 2554 (1997).
- 3) K. Matsuhira *et al.*, J. Phys. Soc. Jpn. **80**, 094701 (2011).
- 4) R. Asih *et al.*, J. Phys. Soc. Jpn. **86**, 024705 (2017).
- 5) H. Guo *et al.*, Phys. Rev. B **88**, 060411(R) (2013).
- 6) M. Ito *et al.*, J. Phys. Chem. Solids **62**, 337 (2001).
- 7) N. Taira *et al.*, J. Solid State Chem. **152**, 441 (2000).
- 8) S. T. Ku *et al.*, J. Phys. Condens. Matt. **30**, 155601 (2018).
- 9) U. Widyaiswari *et al.*, to be published.

*1 RIKEN Nishina Center

*2 Department of Physics, Universitas Indonesia

*3 Department of Physics, Osaka University

*4 Graduate School of Engineering and Science, Shibaura Institute of Technology

Muon spin relaxation study of solute-vacancy interactions during natural aging of Al–Mg–Si–Cu alloys[†]

K. Nishimura,^{*1,*2} K. Matsuda,^{*1,*2} S. Lee,^{*1} I. Watanabe,^{*2} T. Matsuzaki,^{*2} S. Wenner,^{*3} and R. Holmestad^{*4}

Age-hardenable aluminum alloys are strengthened by nanometer-sized atomic clusters and precipitates that are coherent with the aluminum matrix. These are formed by the segregation of atoms (*e.g.*, Mg and Si) from a solid solution, where the solute atoms occupy substitutional sites in fcc-Al. Such a solid solution comprising a few at. % of alloying elements is achieved by solution heat treatment (SHT)—an annealing step at 770–870 K. The solid solution is highly unstable after quenching in ice water after SHT (SHTQ). During further heat treatments at a lower temperature (artificial aging) and even room-temperature storage (natural aging), vacancies and solute atoms co-diffuse and produce atomic clusters, with all atoms remaining at fcc-Al positions.^{1,2)} The most important techniques to detect and quantify precipitates in the Al–Mg–Si system have been transmission electron microscopy (TEM) and atom probe tomography (APT). However, small atomic clusters are difficult to detect in TEM, APT is unsuitable to investigate the crystallography of precipitates, and neither technique can map vacancies. Muon spin relaxation (μ SR) is one technique that can map vacancies, and it investigates short-range magnetic fields and the presence of point defects in solids. This work builds upon earlier literature on aluminum with trace elements and Al–Mg–Si alloys,^{3–7)} and it extends the analysis to the same alloys with Cu additions.

Figure 1 shows the zero-field μ SR spectra observed for Al-1.0%Mg₂Si-0.2%Cu-AQ (in the SHTQ condition) at measurement temperatures in the range of 20–280 K and for Al-1.0%Mg₂Si-0.2%Cu-350C (annealed at 623 K for 1000 min after SHTQ) at 280 K. The plot demonstrates that the muon spin depolarization rate depends heavily on temperature. Similar μ SR spectra were acquired for all samples. We have interpreted the measured μ SR spectra using a Monte Carlo simulation, in which four fitting parameters were employed: the dipolar width (Δ), trapping rate (ν_t), detrapping rate (ν_d), and fraction of

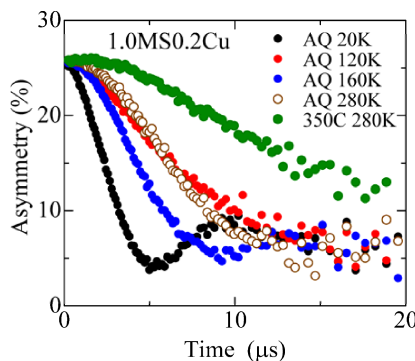


Fig. 1. Muon spin relaxation spectra for an as-quenched (AQ) Al-1.0%Mg₂Si-0.2%Cu sample at 20–280 K and a sample annealed at 623 K for 1000 min (350C) at 280 K.

[†] Condensed from the article in *Metall. Mater. Trans. A* **50**, 3446 (2019)

^{*1} Department of Materials Science and Engineering, U. Toyama
^{*2} RIKEN Nishina Center
^{*3} SINTEF Industry, Norway
^{*4} NTNU Norway

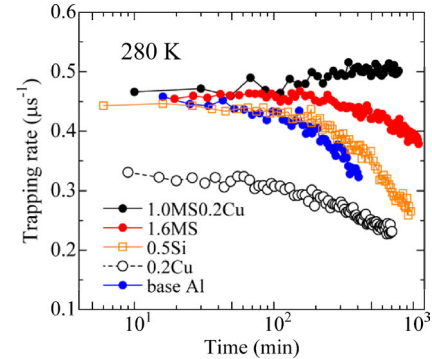


Fig. 2. Fitted trapping rates from isothermal relaxation spectra. Samples are quenched after SHT and kept at 280 K throughout the measurements. The trapping rates decrease with time for all alloys except the quaternary Al–Mg–Si–Cu alloy, the trapping rate for which increases with time.

initially trapped muons (P_0).^{3,8)}

From previous μ SR studies, muons are considered to be trapped by single vacancies or vacancy-solute pairs near room temperature.^{3–6)} Therefore, in most cases, the ν_t values decrease with time during natural aging because excess vacancies are lost at imperfections, such as grain boundaries, voids, and surfaces. The change in trapping rate during storage at 280 K after SHTQ was measured for Al-1.0%Mg₂Si-0.2%Cu, Al-1.6%Mg₂Si, Al-0.5%Si, Al-0.2%Cu, and base Al, as shown in Fig. 2. The horizontal axis denotes the time from SHTQ on a logarithmic scale. The ν_t values for the Cu-free samples decrease with time. The speed of the decrease is inversely correlated with the solute concentration, which is expected because muons have more defects to be trapped in and more time to undergo spin relaxation. The reason why the ν_t values of Al-0.2%Cu start out lower than in the other alloys is unclear. A surprising result from the isothermal experiment is that the ν_t values (black circles) for the Cu-added sample increase with time. If muons are trapped only at vacancy-associated sites, the result indicates that the number density of vacancies increases with time after quenching when all the elements Mg, Si, and Cu are present in the alloy composition. This suggests that new vacancies are continuously diffusing into the material and binding to solute atoms, shifting the equilibrium concentration of vacancies to higher levels than in the alloys with fewer elements. Further investigation to clarify this phenomenon using positron annihilation spectroscopy is in progress.

References

- 1) K. Matsuda *et al.*, *Mater. Trans.* **58**, 167 (2017).
- 2) M. Werinos *et al.*, *Mater. Design* **107**, 257 (2016).
- 3) S. Wenner *et al.*, *Phys. Rev. B* **86**, 104201 (2012).
- 4) S. Wenner *et al.*, *Acta. Mater.* **61**, 6082 (2013).
- 5) S. Wenner *et al.*, *Metall. Mater. Trans. A* **45**, 5777 (2014).
- 6) K. Nishimura *et al.*, *Arch. Metall. Mater.* **60**, 925 (2015).
- 7) K. Nishimura *et al.*, *J. Phys. Soc. Jpn. Conf.* **21**, 011030 (2018).
- 8) T. Hatano *et al.*, *Hyper. Inter.* **17**, 211 (1984).

Muon spin rotation study on the new organic spin liquid candidate λ -(STF)₂GaCl₄

T. Minamidate,^{*1,*2} D. P. Sari,^{*3} N. Matsunaga,^{*2} and I. Watanabe^{*3}

In recent research, some candidate quantum spin liquid (QSL) materials have been found in molecular conductors such as κ -(ET)₂Cu₂(CN)₃¹⁾ and EtMe₃Sb[Pd(dmit)₂]₂,²⁾ which have antiferromagnetic (AF) spin systems with a nearly regular triangular lattice. Recently, we found a new candidate QSL material, λ -(STF)₂GaCl₄, which can be located between the organic superconductor λ -(BETS)₂GaCl₄ and the antiferromagnet λ -(ET)₂GaCl₄ in the temperature-pressure phase diagram shown in Fig. 1. The AF phase in the ET salt is suppressed by a small pressure, and the STF salt shows neither the AF nor the superconducting transition down to 1.6 K. The STF salt shows a gradual peak structure in the temperature dependence of the static susceptibility, which is well described by the AF Heisenberg model with a regular triangular lattice.³⁾ In contrast to the good agreement of the susceptibility behavior, the calculated geometry of the spin interaction in λ -(STF)₂GaCl₄ is quite distorted from a regular triangle. Therefore, it can be a key material to investigate the stabilization mechanism of the QSL state. Hence we conducted a μ SR study to investigate the local spin dynamics of λ -(STF)₂GaCl₄.

We succeeded in synthesizing a high-quality sample of λ -(STF)₂GaCl₄, and in the 2017 beamtime, we conducted the first μ SR measurement. The μ SR time spectrum at 0.3 K started to decouple on applying a longitudinal field (LF) of 100 G, indicating that there is no AF long-range ordering. However, by comparing the time spectrum with that in an LF of 1000 G, for which the complete decoupling behavior was observed, we found that a slow relaxation remains, indicating that there are

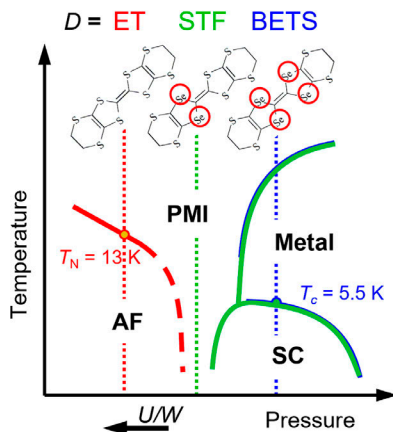


Fig. 1. Schematic temperature-pressure phase diagram of λ -D₂GaCl₄ (D = ET, STF, BETS).³⁾

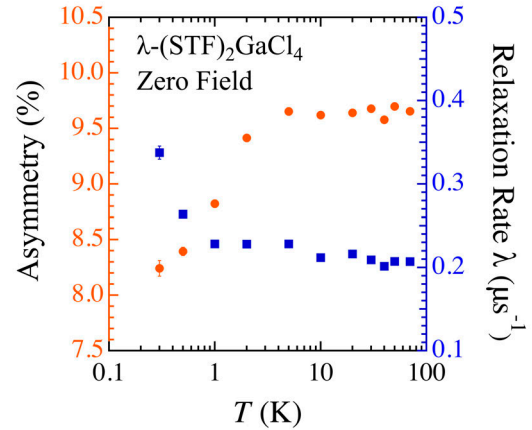


Fig. 2. Temperature dependence of the μ SR relaxation rate and total asymmetry under zero field in λ -(STF)₂GaCl₄.

some effects of fluctuating internal fields. This behavior is similar to that observed in the μ SR measurement of κ -(ET)₂Cu₂(CN)₃.⁴⁾

In the beamtime in July 2019, we conducted high-statistics μ SR measurement and improved the experimental setup. The total asymmetry was improved in comparison with the previous experiment in 2017, from 6% to 8.3% at 0.3 K. A reasonable asymmetry of about 10% is frequently observed in molecular conductors due to the formation of muonium. The time spectra can be fitted by a single exponential function. Figure 2 shows the temperature dependence of the total asymmetry and relaxation rate λ . The total asymmetry at a high temperature was 9.3% and started to decrease below 5 K. This decrease was not observed in the previous measurement due to unsatisfactory experimental conditions. In conjunction, we observed the increase of λ . We now suspect that these give evidence for the gradual growth of the local staggered moments in the short-range AF ordered region. The lack of the transition to the bulk AF state with the growth of the short-range order is considered to be due to static spin heterogeneity resulting from the disorder or due to the effect of the spin frustration. As the next step, it is important to measure the spin dynamics toward the lower-temperature region to elucidate whether the long-range AF order or the quantum critical point exists. Now, we have submitted a proposal for measurement using a ³He/⁴He dilution refrigerator. With the progress of this research, the microscopic spin dynamics in the QSL state and the stabilization mechanism of the QSL state in a disordered system can probably be clarified.

References

- 1) Y. Shimizu *et al.*, Phys. Rev. B **91**, 107001 (2003).
- 2) T. Itou *et al.*, Phys. Rev. B **77**, 104413 (2008).
- 3) T. Minamidate *et al.*, J. Phys. Soc. Jpn. **84**, 063704 (2015).
- 4) S. Nakajima *et al.*, J. Phys. Soc. Jpn. **81**, 063706 (2012).

*1 RIKEN Condensed Molecular Material Lab.

*2 Department of Physics, Hokkaido University.

*3 RIKEN Nishina Center

*4 Department of Physics, Sibaura Institute of Technology

Zero-field μ SR on single-crystal organic superconductor λ -(BETS) $_2$ GaCl $_4$

D. P. Sari,^{*1,*2} K. Hiraki,^{*3} T. Nakano,^{*4} Y. Nozue,^{*5} A. Hillier,^{*6} I. Watanabe,^{*2} and Y. Ishii^{*1}

Unconventional superconductivity is often realized in the vicinity of a magnetic ordered state, as observed in ruthenates, heavy fermions, cuprates, organic superconductors, and Fe-based superconductors.¹⁾ In the organic superconductor family κ -(ET) $_2X$ with the cation molecules ET = (CH $_2$) $_2$ S $_4$ C $_6$ S $_4$ (CH $_2$) $_2$ and anion molecules X , the superconducting state emerges on applying pressure to the long-range-ordered antiferromagnetic insulator at a low temperature below about 10 K, while at a high-temperature region, a crossover occurs from a metallic to a paramagnetic insulating state.²⁾ Therefore, it is suspected that the metallic-state spin correlations govern the superconductivity.

Powell and McKenzie³⁾ proposed that for the whole family of organic superconductors, which includes the systems with the β , β' , κ , and λ types of stacking cation molecules in the conducting plane, the metallic spin correlations, the spin fluctuations of which are maximum near the wave vector (π, π) , mediate superconductivity. In fact, two adjacent cation molecules form a dimer are considered as a site. Furthermore, electron hopping between a site and its nearest-neighbor sites in the transverse and longitudinal directions was described by the transfer integrals, t , and they create a type of square lattice. The second nearest neighbor sites were then determined by the diagonal transfer integral (from upper-right to lower-left corner of the square), t' . Then, the so-called anisotropic triangular lattice was characterized by the ratio, t'/t . Accordingly, the system reached frustration at $t'/t = 1$. The variation from a small t'/t (feature of the square lattice) passing through the frustration regime to a large t'/t (feature of quasi-one-dimensionality) changes the superconducting symmetry in the following manner. As the value of t'/t is varied, the superconducting symmetry change from “ $d_{x^2-y^2}$ ” for $t'/t < 0.93$, to “ $(s+d_{xy})+i(d_{x^2-y^2})$ ” for $t' \sim t$, to “ $s+d_{xy}$ ” for $t'/t \gtrsim 1.3$. It should be noticed that the “ $(s+d_{xy})+i(d_{x^2-y^2})$ ” state breaks time-reversal symmetry according to the momentum-dependence plot of the argument of the complex number of the superconducting gap for several cases of t'/t .

We focused on the study of the superconducting state in quasi-two-dimensional organic superconductor λ -(BETS) $_2$ GaCl $_4$ with BETS = (CH $_2$) $_2$ S $_2$ Se $_2$ C $_6$ S $_2$ S $_2$ (CH $_2$) $_2$ through muon spin relaxation (μ SR). By substituting Se with S, which yields a negative pressure, the superconducting state eventually changed to an antiferromagnetic state.^{4,5)} Our transverse-field μ SR study revealed that λ -

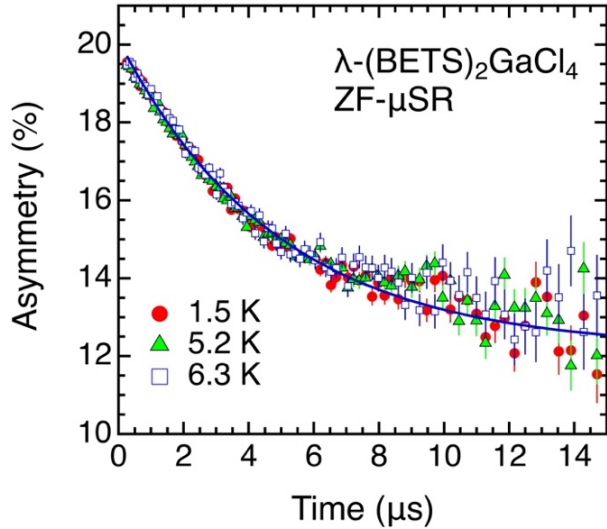


Fig. 1. Zero-field μ SR time spectra measured at several temperatures, below and above T_C of ~ 5.5 K. The solid line is a single exponential fitting model.

(BETS) $_2$ GaCl $_4$ has the characteristics both d -wave and s -wave pairing symmetry.⁶⁾ From our calculation on the basis of the density

functional theory of the transfer integral within BETS dimers, λ -(BETS) $_2$ GaCl $_4$ has two kinds of square lattices alternating in the a -direction. One has $t'/t \sim 0.8$, and the other has $t'/t \sim 0.2$.⁷⁾ Accordingly, the lattice is not simple, reflecting its superconducting pairing symmetry. In order to investigate the possibility of time-reversal symmetry breaking in λ -(BETS) $_2$ GaCl $_4$, we performed zero-field μ SR in the superconducting state, which can sensitively detect the spontaneous appearance of an internal field of the order of about 10^{-4} T.

We prepared ~ 130 mg single crystals of λ -(BETS) $_2$ GaCl $_4$ and oriented them all in the same direction. The polarized muon beam direction was nearly perpendicular to the conducting plane. Zero-field μ SR was conducted with high statistics up to 80 MEvents. Figure 1 shows the time spectra at several temperatures below and above the critical temperature, T_C , of ~ 5.5 K. The time spectra up to 10 μ s can fairly be analyzed using a single exponential function. No appreciable change of the relaxation rate was detected from the measurement at $T = 6.3$ K down to 1.5 K. We will perform similar measurements in different orientations of single crystals with respect to the muon beam direction in order to obtain complete and precise results.

References

- 1) G. R. Steward, Adv. In Phys. **66**, 75 (2017).
- 2) F. Kagawa, K. Miyagawa, K. Kanoda, Nature **436**, 534 (2005).
- 3) Powell and McKenzie, Phys. Rev. Lett. **98**, 027005 (2007).
- 4) Y. Saito *et al.*, J. Phys. Soc. Jpn. **87**, 013707 (2018).
- 5) T. Minamidate *et al.*, J. Phys. Soc. Jpn. **84**, 063704 (2015).
- 6) D. P. Sari, *et al.*, in preparation.
- 7) D. P. Sari, RIKEN Accel. Prog. Rep. **51**, 206 (2018).

^{*1} Graduate School of Engineering and Science, Shibaura Institute of Tech.

^{*2} RIKEN Nishina Center

^{*3} Department of Physics, Fukushima Medical University

^{*4} Graduate School of Science and Engineering, Ibaraki University

^{*5} Department of Physics, Osaka University

^{*6} ISIS Facility, STFC, United Kingdom

Relationship between the structure and electrical conductivity of 12-mer single-stranded polyadenine studied by scanning tunneling microscope†

H. Rozak,^{*1,*2} W. N. Zaharim,^{*2} I. Miyazaki,^{*3} N. E. Ismail,^{*2} S. N. Abu Bakar,^{*2} D. Kernain,^{*5} M. R. Samian,^{*4} K. Ichimura,^{*3} M. I. Mohamed-Ibrahim,^{*2} S. Sulaiman,^{*2} and I. Watanabe^{*1,*2,*3}

DNA has received much attention over the past few decades owing to their unique feature of π - π stacking interaction between neighboring bases. This feature provides an effective medium for the electron transport process in DNA.¹⁾ In biological phenomena, the electron transfer could be utilized to study the DNA damage and repair mechanism at the sub-atomic scale.²⁾

How can we differentiate the characteristics of electron motion in normal and damaged DNA? Furthermore, will damage in DNA affect the electron hopping rate and mechanism of electron motion? In order to answer these questions, firstly, we need to clarify whether DNA bases (A, C, G, and T) are conductive. Once strong baseline data of electron transfer in each base have been accumulated, the data could be used as a reference for normal and damaged DNA. A lot of studies have been conducted in the past to investigate the electronic properties of DNA.³⁾ Their findings vary from insulating to semi-conducting and metallic properties. In order to resolve this matter, two main techniques were used: scanning tunneling microscopy (STM) and muon spin relaxation spectroscopy (μ SR). Measurements were performed on 12-mer single-stranded (12-ss) adenine, cytosine, guanine, and thymine. But in this report, we only present the XRD and STM data of adenine (12-ssA).

XRD measurements were performed to characterize

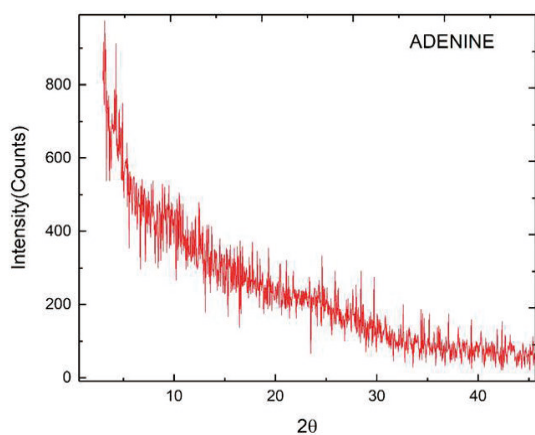


Fig. 1. XRD patterns of 12-ssA molecules measured at room temperature. The XRD patterns showed no sharp or enhanced diffraction peak, suggesting an amorphous state of the sample.

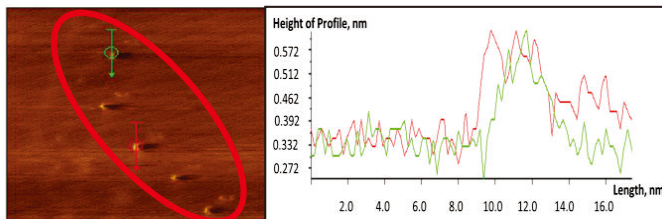


Fig. 2. The STM image of 12-ssA molecules that align in a one-dimensional chain structure and the analysis of the height profile of 12-ssA molecules.

the structure of a 12-ssA molecules at room temperature, however, no sharp diffraction peaks were observed in the XRD pattern, which indicated that the 12-ssA sample is not crystallized and it is in an amorphous state as shown in Fig. 1.

For the STM measurements, the molecular structure of the 12-ssA molecule was probed to measure the height profile between the tip to the sample molecule (h). This height profile represents the efficiency of the electron tunneling from the tip to the sample, which could be related to the conductivity of the sample. The relation between the height profile (h) and the efficiency of the tunneling current (I) could be expressed as follows:

$$I = V \times \exp[-2h^{-1}(2m\phi)^{1/2}h] \quad (1)$$

Where m is the electron rest mass and ϕ is the work function of the sample.⁴⁾ Based on Eq. (1), the current depends exponentially on the distance. If the distance between tip and sample surface increase, the tunneling current decreases.

In this study, the structure of 12-ssA molecules was found to be well observable on the graphite substrate as illustrated in Fig. 2. The structure of 12-ssA molecules was observed as bright spots in the red circle. The length of the molecule was about $4.3 \pm 1.6 \text{ \AA}$, and the side-by-side distance was $25 \pm 7.5 \text{ \AA}$. This figure indicates that 12-ssA was not perfectly insulating and had electrical conductivity because STM only probe the conductive sample.⁵⁾ The results of the height profile of 12-ssA molecules in Fig. 2 could be used to make a comparison with other samples (12-ssC, 12-ssG, and 12-ssT) in the future.

References

- 1) R. G. Endres *et al.*, *Rev. Mod. Phys.* **76**, 195 (2004).
- 2) M. A. Grodick *et al.*, *Biochemistry.* **54**, 962 (2015).
- 3) K. L. Jiménez-Monroy *et al.*, *J. Phys. Chem. A* **121**, 1182 (2017).
- 4) T. Ohshiro *et al.*, *Chem. Commun.* **46**, 2581 (2010).
- 5) B. Bhushan, H. Fuchs, *Applied Scanning Probe Methods II.* (Springer-Verlag Berlin Heidelberg, 2006).

† Condensed from the article in *Materials Science Forum.* **966**, Trans Tech Publications Ltd., (2019)

*1 RIKEN Nishina Center

*2 School of Distance Education, Universiti Sains Malaysia

*3 Department of Engineering, Hokaido University

*4 School of Biological Sciences, Universiti Sains Malaysia

*5 Institute of Research in Molecular Medicine, Universiti Sains Malaysia

Electron transfer in 12-mer double-stranded DNA by muon spectroscopy and scanning tunneling microscopy

H. Rozak,^{*1,*2} S. Sulaiman,^{*2} W. N. Zaharim,^{*2} N. E. Ismail,^{*2} S. N. Abu Bakar,^{*2} M. R. Samian,^{*4}
I. Miyazaki,^{*3} K. Ichimura,^{*3} and I. Watanabe^{*1,*2,*3}

Electron transport through DNA plays a pivotal role in biological systems. Processes that use electron transfer include scanning the damaged sites in DNA and DNA repair.^{1,2)} To understand these biological phenomena, it is necessary to investigate the electron transfer process in normal and damaged DNA at the microscopic level. The main questions of this study are: what is the difference in the characteristics of electron transfer between normal and damaged DNA, and how much the difference in the quantitative value for electron diffusion along the normal and damaged DNA helix.

In order to answer those questions, muon spin relaxation (μ SR) measurements were performed at the Argus spectrometer RIKEN RAL. This μ SR technique has been suggested as a good probe to study the motion of electron transfer in DNA because the muon spin relaxation could characterize or model the diffusion of electrons along the DNA helix via hyperfine interaction without producing any radiation effect on the sample.³⁾

In this study, 12-mer double-stranded synthetic DNA GC (12 mer-dsDNA GC) was used to portray the conditions for normal DNA. The measurements were performed at room temperature and the external longitudinal magnetic fields were applied up to



Fig. 1. STM image of 12 mer-dsDNA GC molecules aligned in one-dimensional chain structure.

*1 RIKEN Nishina Center

*2 School of Distance Education, Universiti Sains Malaysia

*3 Department of Engineering, Hokkaido University

*4 School of Biological Sciences, Universiti Sains Malaysia

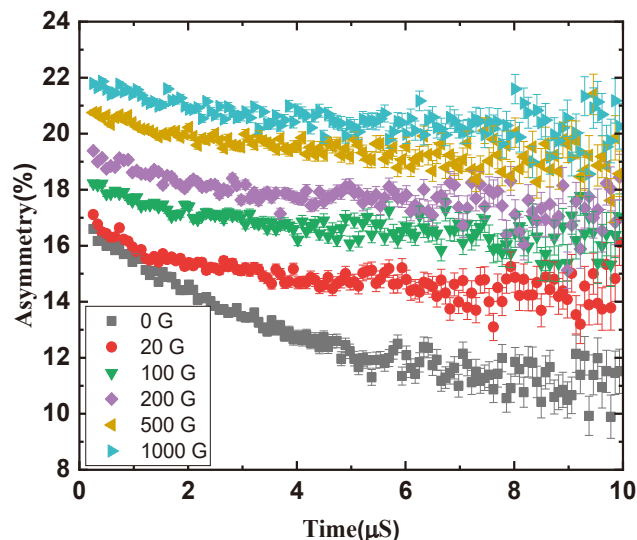


Fig. 2. Raw data of muon spin relaxation for 12-mer double-stranded synthetic DNA GC dependence over time.

3400 G. The 80 mg powder sample of 12 mer-dsDNA GC was wrapped in a thin silver foil with the diameter of 1.5 cm.

In addition, scanning tunneling microscopy (STM) measurements were conducted to probe the molecular structure of 12 mer-dsDNA GC. From the STM measurements, the images of 12 mer-dsDNA GC molecules were successfully observed as shown in Fig. 1. The image in Fig. 1, was taken in constant current mode at room temperature and it corresponds to the surface map of electron tunneling from HOMO tip to the LUMO of the sample.⁴⁾

Figure 2 shows the raw data of muon spin relaxation spectra dependence over time. The asymmetry is increased as the applied magnetic field increases. The muon spin relaxation becomes suppressed at the highest external magnetic fields. This result indicates that the spin relaxation of a muon is interacting with an electron that is rapidly diffusing along the molecule. At higher applied field, the muon-electron hyperfine coupling starts to be quenched. Accordingly, the muon spin relaxation is decreased, as illustrated in Fig. 2.

References

- 1) E. O'Brien *et al.*, *Science* **355**(6327), eaag1789 (2017).
- 2) M. A. Grodick *et al.*, *Biochemistry* **54**(4), 962 (2015).
- 3) M. Iain, *J. Phys. Chem. B* **123**(21), 4540 (2019).
- 4) R. Harison *et al.*, *Mater. Sci. Forum.* **966**, (2019).

μ SR study of the electron transfer mechanism of a blue copper protein, Pseudoazurin

A. D. Pant,^{*1,*2,*3} T. Yamaguchi,^{*1} K. Ishida,^{*3} and T. Kohzuma^{*1}

Electron transfer (ET) is an important phenomenon to understand biological processes such as photosynthesis and respiration systems. The study of ET in protein using positive muon was initiated by K. Nagamine's group with the cytochrome c protein.¹⁾ However, the electron transfer path/mechanism is not clearly understood yet. We aim to perform a systematic study to establish the application of muons to life science.

Since biological systems are complex in geometry and dynamic, we started studying the ET mechanism in a small and single active-site blue copper protein, rather than large systems. Copper proteins that contain single- or multi-copper sites in their prosthetic group work in a wide range of ET processes and biological energy conversion cycles.²⁾ The copper centers in these proteins play a main role in ET. However, there remain several obscure points in the ET pathway;³⁾ that is, there is no clear mechanism to understand the electron transfer. Blue copper protein (type: T1Cu) contains only a single copper-ion binding site that serves as an electron mediator between large proteins. Pseudoazurin (PAz), a member of T1Cu, functions in the electron transfer processes in several microorganisms. With the application of the muon spin rotation and relaxation (μ SR) method, we propose to probe the electron transfer mechanism in PAz, in which electron transfer occurs only from/to the copper center. The μ SR study on PAz will provide novel insight to understand the muon method for studies in life science.

In order to understand the ET mechanism and functions of copper proteins, we will perform μ SR measurements in reduced pseudoazurin (PAzCu¹⁺, diamagnetic) and oxidized pseudoazurin (PAzCu²⁺, paramagnetic) (Fig. 1) using surface muons (~ 4 MeV). For reference, a similar set of measurements will also be performed in buffer solution and pure water. The samples are prepared and purified (solution, concentration ~ 10 mM, volume ~ 700 μ L) in Kohzuma laboratory, Ibaraki University, Mito. The solution is filled in a sample cell (silicone rubber ring, $\phi 20$ mm, $t \sim 2$ mm, polyvinylidene chloride film ~ 15 μ m on both sides of the ring), which is masked by silver ring ($\phi 18$ mm, t 0.3 mm) so that the incident muon beam can be prevented from stopping in the rubber. The blue oxidized PAz changes to the reduced form using ascorbic acid. Indium sealing is used in a helium glove bag environment. The measurements will be performed at a transverse field of 2.3 G, zero field, and a longitudinal field

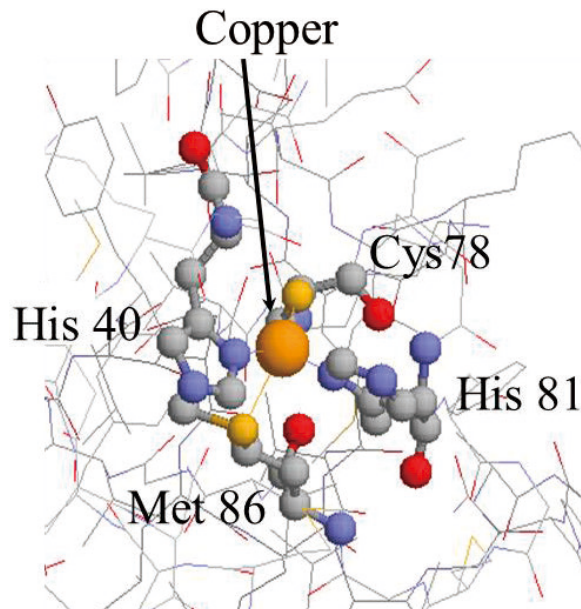


Fig. 1. Structure of pseudoazurin (PDB: 1BQK) with the coordinate scheme around Cu(II). Copper is an active site for electron transfer.

at different temperature ranges (20 K–300 K).

When a surface muon beam (\sim MeV) is incident on the sample solution, the beam energy is transferred to the solution until the end of the radiation track. A large fraction of incident muons will be found in the diamagnetic muon form and some in the muonium form (bound state of muon and an electron, $\text{Mu} = \mu^+e^-$). If low-energy muons are stopped around the copper center of reduced PAz, there is a possibility of electron transfer from the copper center to the muon to form Mu. The Mu formed by the former (in solution) and latter (by electron transfer) cases will be distinguished by their frequencies. Interactions will exist between muons and electrons as well as muons and nuclei. These behaviors are expected to be reflected in the time spectra. The relaxation of Mu depends on its interaction with the environment. For example, a small amount of oxygen will cause the fast relaxation of Mu.⁴⁾ The formation of Mu at different sites in the sample will provide information about the electron transfer mechanism.

References

- 1) K. Nagamine *et al.*, *Physica B* **289-290**, 631–635S (2000).
- 2) O. Farver, *Coord. Chem. Rev.* **255**, 757–773 (2011).
- 3) S. Wherland *et al.*, *Perspect. Sci.* **6**, 94–105 (2015).
- 4) A. D. Pant *et al.*, *J. Phys. Conf. Ser.* **551**, 012043 (2014).

*1 Institute of Quantum Beam Science, Ibaraki University

*2 IMSS, KEK

*3 Meson Science Laboratory, RIKEN Nishina Center

Temperature dependence of the total muonium emission yield from silica aerogel using μ SR method

K. Ishida,^{*1} K. Suzuki,^{*2} T. Mibe,^{*2} M. Iwasaki,^{1,*3} S. Kamal,^{*4} and J. Brewer^{*4}

We are developing thermal-energy muonium ($\text{Mu} = \mu^+ e^-$) production as a source of the cold muon beam for the muon g-2/EDM experiment planned at J-PARC.¹⁾ We observed at TRIUMF that the Mu emission rate from silica aerogel to vacuum is enhanced by surface ablation.^{2,3)} However, the present Mu yield measurement performed by tracking the muon decay positron is limited to a region away (~ 5 mm) from the surface owing to the large background from the muoniums decaying in aerogel. To enable measurement of the Mu emitted in vacuum including the region near the surface, where we are planning to shoot a Mu ionizing laser, we performed a new measurement using the Mu spin rotation (μ SR) method in the ARGUS spectrometer at the RIKEN-RAL Muon Facility. In μ SR, the precession of the muon spin can be detected by asymmetric emission of the muon decay positrons. Since the precession frequency of Mu is different from that of diamagnetic muon under an applied field, we can measure the fraction of muons forming the Mu state.

In the measurement, we added a gold foil to the downstream of the silica aerogel target. First, we set the muon-beam momentum so that the muons fully stop in the middle of the aerogel and measured the Mu spin relaxation intrinsic to the aerogel material. Then, we chose another momentum so that the muon stopping distribution peaked at the downstream surface of the aerogel. In this half-stopping condition, we observed an increase in the Mu spin relaxation rate.⁴⁾ This was interpreted as a result of Mu transfer to the gold foil after emission to vacuum. Once in gold, Mu changes its state to diamagnetic muon and cannot contribute to the Mu precession signal anymore.

Here, we report the first measurement of the temperature dependence of the Mu emission rate. In a naive model, where Mu is emitted after diffusion in spaces in the aerogel nano-structure, we expect that the Mu emission rate is proportional to the thermal Mu velocity, $v \propto T^{1/2}$, where T is the aerogel temperature.

Keys for the experiment are the cooling of the aerogel and the aerogel temperature measurement. Since the thermal conductivity of the silica aerogel is very low, we relied on cooling by thermal radiation emission. We designed a sample holder that covers all the faces of the aerogel and mounted it on the cryostat. In a cooling test conducted prior to the μ SR measurement, we used a K-type thermocouple directly inserted into the aero-

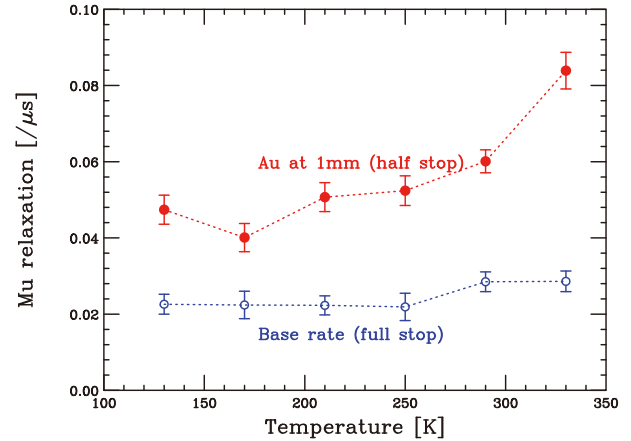


Fig. 1. Temperature dependence of the Mu relaxation rate with the muons stopped in the middle (full stop) and at the downstream edge of the silica aerogel (half stop).

gel in addition to the semiconductor thermometers on the cryostat and the sample holder. The thermocouple was chosen because of its small size and low heat mass. While cooling down from room temperature, the aerogel temperature initially followed that of the sample holder, though with some delay. Subsequently, the aerogel temperature was saturated at approximately 180 K and stabilized, however cold the sample holder was. This was understood as the effect of leakage of thermal radiation from the room-temperature surface through an opening used to insert the thermocouple. The saturation temperature was consistent with that expected with area fraction of the opening, which was about 10%. In the μ SR measurement, the thermocouple was removed, and the aerogel sample was completely surrounded by the cold surface. This ensured that the aerogel temperature reached equilibrium with that of the holder.

A preliminary result of the Mu relaxation rate measurement is shown in Fig. 1. The relaxation rate in the aerogel (full stop) did not change much with the temperature, while the rate in the half-stop condition was larger and showed some temperature dependence. We plan a detailed analysis to study whether it agrees with the diffusion model assuming the Mu velocity distribution equilibrated with the temperature.

References

- 1) M. Abe *et al.*, Prog. Theor. Exp. Phys. **2019**, 053C02 (2019).
- 2) P. Bakule *et al.*, Prog. Theor. Exp. Phys. **2013**, 103C01 (2013).
- 3) G. A. Beer *et al.*, Prog. Theor. Exp. Phys. **2014**, 091C01 (2014).
- 4) K. Ishida *et al.*, RIKEN Accel. Prog. Rep. **52**, 181 (2019).

*1 RIKEN Nishina Center

*2 IPNS, KEK

*3 Meson Science Laboratory, RIKEN

*4 University of British Columbia

3. Radiochemistry and Nuclear Chemistry

Relativistic density functional theory with the finite-light-speed correction for Coulomb interaction[†]

T. Naito,^{*1,*2} R. Akashi,^{*1} H. Z. Liang,^{*1,*2} and S. Tsuneyuki^{*1,*3}

The periodic table of elements is determined by the electronic configuration and represents the periodicity of fundamental atomic properties. However, the positions of super-heavy elements (SHEs) in the periodic table are tentative because their chemical properties have not been established. Owing to the short half-lives of SHEs, experimental measurements of their chemical properties are difficult. Thus, first-principles numerical simulations are complementary tools to such experimental measurements.

The first-principles calculation for SHEs requires proper treatment of the relativistic effect. The relativistic effect can modify the Coulomb interaction between the charged particles, which is significant in SHEs. The non-relativistic form is of the order $O(Z\alpha)$, whereas the second dominant contribution is of the order $O((Z\alpha)^2)$, which is called the Breit correction.¹⁾ Here, $\alpha \simeq 1/137$ is the fine-structure constant. The Breit correction is usually called the relativistic effect or finite-light-speed effect. The lowest order of relativistic effects incorporated using the Dirac equation is also $O((Z\alpha)^2) \sim O(1/c^2)$. Once the relativistic effects incorporated by the Dirac equation are considered, the Breit correction between two electrons should also be considered to keep consistency. Hereafter, we refer to both the Breit correction and effects incorporated using the Dirac equation as “relativistic effect” for simplicity.

So far, the electronic structure calculation with the relativistic effects in $O(1/c^2)$ has been performed based on wave-function theory. In contrast, density functional theory (DFT)^{2,3)} with the consistent inclusion of the relativistic effects up to the order $O(1/c^2)$ is unprecedented. Although the accuracy of DFT is lower than that of wave-function theory, DFT with the relativistic effects is highly desired, because DFT is applicable to larger systems such as molecules and coordination complex ions, the experimental syntheses of which are ongoing, and even solids.

In this paper, we formulate the Hartree-exchange-correlation functional for electron systems with the correction of $O(1/c^2)$. As a benchmark calculation, the all-electron calculation of atoms is performed.

We calculated the energy of the lawrencium atom with two electronic configurations, where one valence electron occupies the $6d$ orbital ($[\text{Rn}] 5f^{14} 6d^1 7s^2$) or $7p$ orbital ($[\text{Rn}] 5f^{14} 7s^2 7p^1$). For comparison, that of

Table 1. Total energies for lutetium and lawrencium atoms. All values are in the Hartree atomic unit.

	Outermost	Non-rel	SRel-CB
Lu	$5d^1$	– 13848.19912	– 14527.46807
	$6p^1$	–13848.12376	–14527.42700
Lr	$6d^1$	– 33551.48205	Unbound
	$7p^1$	–33551.38274	– 37331.31054

the lutetium atom is also calculated, where one valence electron occupies the $5d$ orbital ($[\text{Xe}] 4f^{14} 5d^1 6s^2$) or $6p$ orbital ($[\text{Xe}] 4f^{14} 6s^2 6p^1$). The energies calculated with these configurations in the non-relativistic (Non-rel) and the newly-developed relativistic (SRel-CB) schemes are listed in Table 1. The smaller values for the respective approximations in each atom are written in bold. In the lutetium atom, the outermost valence electron prefers to occupy the d orbital rather than the p orbital with all schemes. In contrast, in the lawrencium atom, the electron prefers to occupy the p orbital rather than the d orbital with the SRel-CB scheme, whereas it still prefers the d orbital in the Non-rel scheme, as in the lutetium case. The occupation of the p orbital could be the origin of the anomalous behavior of lawrencium.⁴⁾ This result is consistent with previous calculations using wave-function theory.^{5,6)} Note that we obtained the consistent results with far less computational cost than those previous calculations. It should also be noted that the p -block elements are defined as those in which the outer-most electrons occupy the p orbitals.⁷⁾ Lawrencium, thus, belongs to the p block, rather than d according to the definition. It seems, however, more appropriate to regard that the concept of “block” is ambiguous for the heavy and super-heavy elements, because the electronic configuration of lawrencium is almost the same as that of lutetium, and the only difference is in the outermost electron. Therefore, reconsideration of the classification appropriate for SHEs is mandatory.

References

- 1) G. Breit, Phys. Rev. **34**, 553 (1929). *ibid* **36**, 383 (1930).
- 2) P. Hohenberg, W. Kohn, Phys. Rev. **136**, B864 (1964).
- 3) W. Kohn, L. J. Sham, Phys. Rev. **140**, A1133 (1965).
- 4) T. K. Sato *et al.*, Nature **520**, 209 (2015).
- 5) E. Eliav, U. Kaldor, Y. Ishikawa, Phys. Rev. A **52**, 291 (1995).
- 6) X. Cao, M. Dolg, H. Stoll, J. Chem. Phys. **118**, 487 (2003).
- 7) F. A. Cotton, G. Wilkinson, P. L. Gaus, *Basic Inorganic Chemistry* (John Wiley & Sons, 1995).

[†] Condensed from the article in arXiv: 1911.10670

^{*1} Department of Physics, The University of Tokyo

^{*2} RIKEN Nishina Center

^{*3} Institute for Solid State Physics, The University of Tokyo

On-line anion-exchange experiment of Nb and Ta in HF/HNO₃ mixture solution for Db chemistry

S. Adachi,^{*1,*2} A. Toyoshima,^{*1,*3} K. Tsukada,^{*1,*4} H. Haba,^{*1} Y. Komori,^{*1} T. Yokokita,^{*1} Y. Shigekawa,^{*1} Y. Wang,^{*1} A. Kashihara,^{*1,*2} M. Kato,^{*1,*5} A. Nakajima,^{*1,*5} and K. Sueki^{*1,*6}

Superheavy elements with atomic number ≥ 104 are placed at the 7th period of the periodic table. Owing to the influence of strong relativistic effects caused by their large positive nuclear charge, these elements are expected to have chemical properties different from those of lighter homologues. However, because these elements have very short half-lives and low production rates in nuclear reactions, it is difficult to determine their chemical properties.

Few studies on the aqueous chemistry of Db, a group-5 superheavy element, have been performed together with the lighter homologues Nb and Ta and the pseudo-homologue Pa. In the anion exchange in 13.9 M HF solution, the distribution coefficient (K_d) of Db was reported to be smaller than those of Nb and Ta but larger than that of Pa.¹⁾ In 0.31 M HF/0.1 M HNO₃ solution, the adsorption of Db on the resin was showed to be clearly weaker than that of Ta and similar to those of Nb and Pa.²⁾ These studies suggest that Db would form [DbOF₄]⁻ like Nb or [PaOF₅]²⁻ and/or [PaF₇]²⁻ like Pa, but not [DbF₆]⁻ like Ta. Thus, the purpose of the present study is to investigate whether Db behaves like either Pa or Nb, particularly in high HF concentrations, which would enable us to deduce its chemical form: [DbOF₄]⁻ or [DbF₆]⁻. In this study, we performed on-line anion-exchange experiment of Nb and Ta in HF/HNO₃ mixture solution by using an automated rapid chemistry apparatus (ARCA) to determine the suitable experimental conditions for Db.

^{88g}Nb ($T_{1/2} = 14.5$ min) and ¹⁷⁰Ta ($T_{1/2} = 6.7$ min) were produced in the ^{nat}Ge(¹⁹F, nx) and ^{nat}Gd(¹⁹F, nx) reactions, respectively, using the RIKEN K70 AVF cyclotron. The reaction products transported by a He/KCl gas-jet system were deposited on a collection

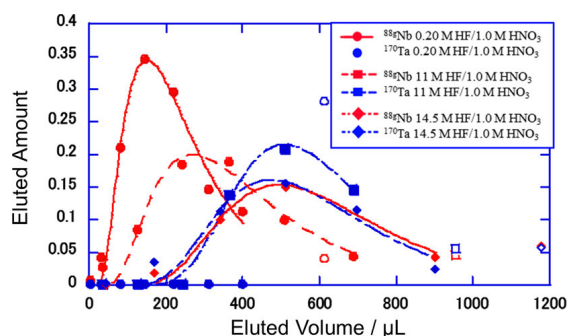


Fig. 1. Elution curves of ^{88g}Nb and ¹⁷⁰Ta in 0.20, 11, 14.5 M HF/1.0 M HNO₃ solutions.

*1 RIKEN Nishina Center

*2 Graduated school of Pure and Applied Sciences, Tsukuba University

*3 Institute for Radiation Sciences, Osaka University

*4 JAEA Advanced Science Research Center

*5 Science and Engineering, Tsukuba University

*6 Faculty of Pure and Applied Sciences, Tsukuba University

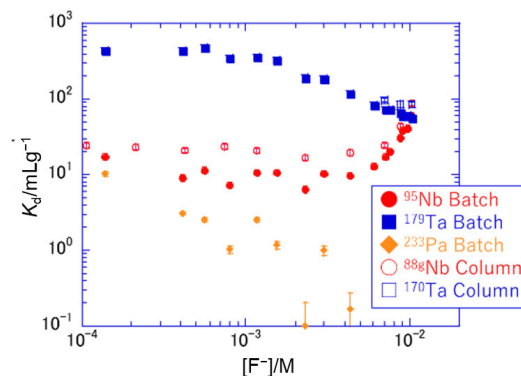


Fig. 2. Variation of the distribution coefficient, K_d , of Nb, Ta, and Pa as a function of $[F^-]$.

site of ARCA. Then, the products were dissolved in 0.1–14.5 M HF/1.0 M HNO₃ mixture solution. The solution was fed onto a small chromatographic column (1.6 mm *i.d.* \times 7 mm) filled with anion-exchange resin (MCI GEL CA08Y) at a flow rate of 1.0 mL/min. The effluent fractions were collected in 7 polypropylene tubes. The products remaining in the column were stripped with 0.015 M HF/6.0 M HNO₃ mixed solution and were collected in another PP tube. These fractions assayed by γ -ray spectrometry with a Ge detector to obtain elution curves for Nb and Ta.

Figure 1 shows, the elution curves of ^{88g}Nb and ¹⁷⁰Ta in 0.20, 11, and 14.5 M HF/1.0 M HNO₃ solutions. The eluted radioactivity $A(\nu)$ at effluent volume ν is expressed by the the following equation:

$$A(\nu) = A_{\max} \left\{ -N(\nu_p - \nu)^2 / (2\nu_p \nu) \right\} \quad (1)$$

where A_{\max} , N , and ν_p are maximum peak height, the number of theoretical plates, and the peak volume, respectively. The ν and ν_p values are corrected for the dead volume. The results of the fit are in good agreement with the experimental data. The K_d value based on the column chromatographic method is expressed as

$$K_d = \nu_p / m_r \quad (2)$$

where m_r is the mass of dry resin. The average m_r value was measured to be 5.7 ± 0.6 mg. The K_d values obtained through the online column chromatography and a batch experiment conducted separately are plotted in Fig. 2.

The K_d values in the on-line experiment are larger than those in the batch experiment. However, the overall trend of K_d values, such as a sudden increase in the K_d value of Nb at around $[F^-]_{eq} = 5 \times 10^{-3}$ M, was reproduced. This suggests that the anion-exchange kinetics of Db may be fast in the present mixed solution, and the K_d values of Db may be obtained under the present conditions. In the near future, we will perform online experiments of Db to determine its K_d value.

References

- 1) K. Tsukada *et al.*, Radiochim. Acta **97**, 83 (2009).
- 2) Y. Kasamatsu *et al.*, Chem. Lett. **38**, 1084 (2009).

Anion-exchange behaviour of Nb, Ta and Pa in H₂SO₄

M. Kato,^{*1,*2} K. Tsukada,^{*3} H. Haba,^{*1} Y. Komori,^{*1} T. Yokokita,^{*1} D. Mori,^{*1} S. Adachi,^{*1,*4}
A. Kashihara,^{*1,*4} and K. Sueki^{*1,*5}

Studies on the behavior of the group-4 elements Zr and Hf, which are homologous elements of Rf, have been conducted in H₂SO₄.¹⁾ It was found that the ion-exchange reaction of Zr and Hf is slow in H₂SO₄ and cannot reach equilibrium in current superheavy element studies. On the other hand, there are not many researches on the group-5 elements in H₂SO₄. Similarly to the group-4 elements, the ion-exchange reaction of the group-5 elements Nb and Ta, and their pseudo homologue Pa may be slow. To elucidate the behaviour of Db in H₂SO₄, it is necessary to clarify the behaviour of Nb, Ta and Pa in H₂SO₄.

⁹⁵Nb ($T_{1/2} = 35.0$ d) and ¹⁷⁹Ta ($T_{1/2} = 1.82$ y) were produced in the ^{nat}Zr(d, xn) and ^{nat}Hf(d, xn) reaction, respectively, by bombarding metallic ^{nat}Zr and ^{nat}Hf foils with a 24-MeV deuteron beam using the RIKEN AVF cyclotron.

Each target material was dissolved in 0.2 mL of concentrated HF solution in a PTFE beaker. After evaporation to dryness, the residue was dissolved with 0.2 mL of 1 M HF and then dried up. The residue was dissolved with 0.3 mL of 1 M HF and fed onto a chromatographic column filled with the anion-exchange resin (BIO RAD AG 1 × 8 100–200 mesh, F⁻ form 5 mm *i.d.* × 45 mm). After washing the column with 2.5 mL of 1 M HF, Zr and Hf were eluted from the column with 5 mL of the mixed solution of 9 M HCl/0.004 M HF. Then, Nb was eluted with 5 M HNO₃/0.2 M HF, while Ta was eluted with 4 M HCl.²⁾ ²³³Pa ($T_{1/2} = 27.0$ d) was chemically separated from ²³⁷Np ($T_{1/2} = 2.144 \times 10^6$ y). ²³⁷Np was dissolved with 0.2 mL of 9 M HCl, and fed onto the chromatographic column filled with the 100–150 mesh of the TK400 resin. Np was eluted with 20 mL of 9 M HCl, then Pa was eluted subsequently with 1.8 mL of 1 M HCl. The solution was evaporated to dryness to fume out HCl. Then, the residue was dissolved with pure water and evaporated to dryness 3 times. Then, radio tracers were stocked in a polypropylene vessel in 1 M H₂SO₄. For the batch experiments with low H₂SO₄ concentrations, the radiotracer was diluted to 0.2 M H₂SO₄ with pure water.

The anion-exchange resin used was the strongly basic anion exchanger, MCI GEL CA08Y supplied by Mitsubishi Chemical Corporation. The resin was washed with 2.0 M NaOH and 2.0 M H₂SO₄ alterna-

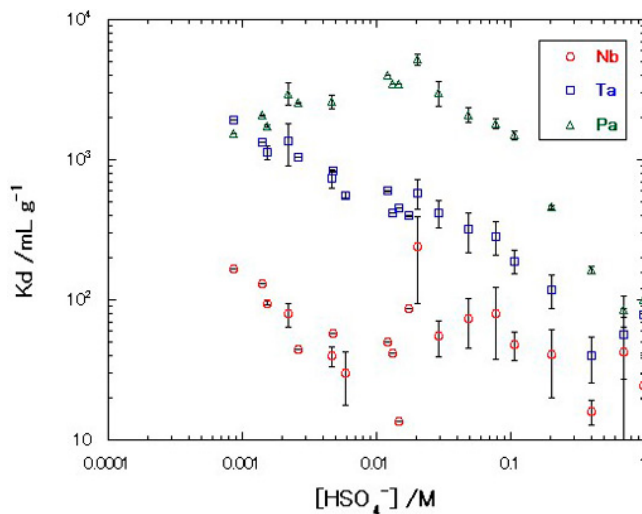


Fig. 1. Variation of the K_d values of ⁹⁵Nb, ¹⁷⁹Ta and ²³³Pa on the anion-exchanger CA08Y as a function of HSO₄⁻ concentration [HSO₄⁻].

tively 3 times to replace Cl⁻ ion in CA08Y with HSO₄⁻. Finally, the resin was washed with distilled water and dried up to a constant weight at 70°C in an oven.¹⁾

We determined the distribution coefficient (K_d) values of Nb, Ta, and Pa on CA08Y in H₂SO₄ at various concentrations. 5–25 mg of the resin and 3 mL of H₂SO₄ solutions with 50 μL of the radiotracer were placed in a polystyrene centrifuge tube and shaken for 120 min at 22°C. After centrifugation, a 1 mL of the solution was pipetted and subjected to γ -ray spectrometry with a Ge detector. The same treatment was conducted without the resin to determine the reference radioactivity. The radioactivity on the resin was determined by subtracting the solution radioactivity from the reference activity.

Figure 1 shows a variation of the K_d values of Nb, Ta, and Pa as a function of [HSO₄⁻]. Especially in the case of Nb, the K_d values varies greatly. Therefore, it's necessary to check the reproducibility of the data.

It was reported that the ion-exchange reaction of the group-4 elements is slow.¹⁾ However, we found that the reaction of the group-5 elements reach the equilibrium faster, within 20 s.

References

- 1) Z. J. Li *et al.*, Radiochim. Acta **100**, 157 (2012).
- 2) Y. Kasamatsu *et al.*, J. Nucl. Radiochem. Sci. **8**, 2 (2007).

*1 RIKEN Nishina Center

*2 Science and Engineering, University of Tsukuba

*3 JAEA, Advanced Science Research Center

*4 Graduated school of Pure and Applied Sciences, University of Tsukuba

*5 Faculty of Pure and Applied Sciences, University of Tsukuba

Anion exchange of Nb and Ta in HF/HCl mixture solution for Db chemistry

T. Yokokita*¹ and H. Haba*¹

Clarifying the chemical properties of superheavy elements with atomic number (Z) ≥ 104 is an intriguing and important subject. These elements are produced at accelerators using heavy-ion-induced nuclear reactions. The production rates of these elements are low, and their half-lives are short ($T_{1/2} \leq 1$ min). Thus, chemical studies on these elements are conducted on a single-atom basis.¹⁾

The fluoride ion is a very strong complexing agent for group-5 elements (Nb and Ta). The fluoride complex species of the heaviest group-5 element, dubnium (Db), is very interesting (Db forms oxyfluoride or fluoride complexes) because Nb and Ta form different fluoride complexes (Nb: $[\text{NbOF}_5]^{2-}$; Ta: $[\text{TaF}_7]^{2-}$) in 0.1–10 M HF ($[\text{F}^-] = 8.9 \times 10^{-3} - 1.9 \times 10^{-2}$ M).²⁾ To determine the fluoride complex species of Db, we plan to perform an ion-exchange study of Db. In this study, we performed an anion-exchange experiment on Nb and Ta in HF/HCl mixture solutions to determine the suitable experimental conditions and obtain comparable data for Db.

We produced ^{95}Nb and ^{179}Ta in the $^{\text{nat}}\text{Zr}(d, xn)$ and $^{\text{nat}}\text{Hf}(d, xn)^{179}\text{Ta}$ reactions (nat = natural isotopic abundance), respectively, by using the RIKEN AVF cyclotron. These radiotracers were purified by the anion-exchange method using the procedure reported in Ref. 3).

In the anion-exchange experiments, the anion-exchange resin (MCI GEL CA08Y) was added to 0.25 mL of an HF/HCl mixture solution containing both ^{95}Nb and ^{179}Ta in a PP tube, and the mixture was shaken using a mixer. Next, the resin was removed by centrifugation. Subsequently, the filtrate was pipetted into another tube, weighed, and subjected to γ -ray spectrometry using a Ge detector. The concentration of HF and HCl was determined by titration with a standardized NaOH solution before the experiments. In all anion-exchange experiments, control experiments without the resin were performed. The K_d values were determined from the

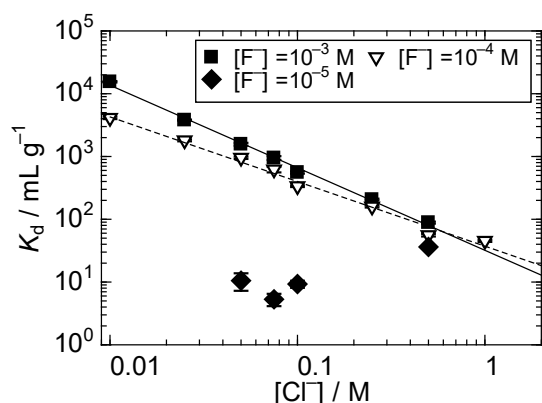


Fig. 1. K_d values of Nb in anion exchange as a function of Cl^- concentration.

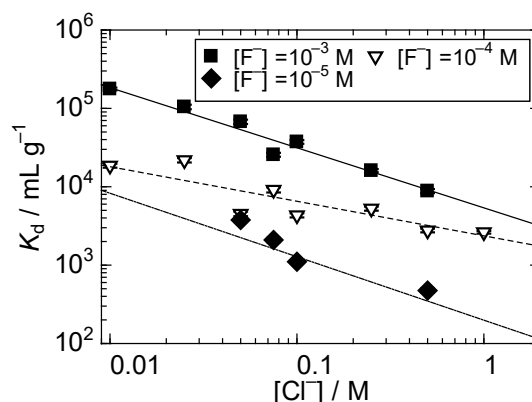


Fig. 2. K_d values of Ta in anion exchange as a function of Cl^- concentration.

following equation:

$$K_d = A_r V_s / A_s w_r = (A_c - A_s) V_s / A_s w_r, \quad (1)$$

where A_r and A_s are the radioactivities on the resin and in the solution, respectively; V_s is the volume (mL) of the solution; and w_r is the mass (g) of the dry resin. A_c denotes the radioactivity of the control solution.

The K_d values of Nb and Ta as a function of Cl^- concentration in the anion-exchange experiment are shown in Figs. 1 and 2, respectively. The values of Nb and Ta linearly decrease with increasing Cl^- concentration, except for Nb in $[\text{F}^-] = 10^{-5}$ M. These results suggest that Nb and Ta form anionic complexes in $[\text{F}^-] \geq 10^{-4}$ and $\geq 10^{-5}$ M, respectively. The slope values between $\log K_d$ and $\log [\text{Cl}^-]$ of Nb are -1.1 ± 0.1 and -1.3 ± 0.1 in $[\text{F}^-] = 10^{-4}$ and 10^{-3} M, respectively. These results indicate that the net charge of the adsorbed Nb species is -1 . For Ta, the slope values between $\log K_d$ and $\log [\text{Cl}^-]$ are -0.8 ± 0.1 , -0.4 ± 0.1 , and -0.8 ± 0.4 in $[\text{F}^-] = 10^{-5}$, 10^{-4} , and 10^{-3} M, respectively. These results indicate that the net charge of the adsorbed Ta species is -1 at $[\text{F}^-] = 10^{-5}$ and 10^{-3} M. However, at $[\text{F}^-] = 10^{-4}$ M, the net charge of the adsorbed Ta species cannot be determined.

We also obtained the K_d values of Nb and Ta as a function of F^- concentration in $[\text{HCl}] = 0.1$ M. We also obtained those of Pa in our previous study.⁴⁾ The sequence of the K_d values is $\text{Ta} > \text{Nb} > \text{Pa}$, and it is consistent with that in the HF/ HNO_3 mixture system.^{2,3)} This point suggests that the effect of the chloride ion is small for the complexation agent. On the other hand, another study is needed to check the effect of chloride ion.

References

- 1) A. Türler, V. Pershina, Chem. Rev. **113**, 1273 (2013).
- 2) Y. Kasamatsu *et al.*, J. Radioanal. Nucl. Chem. **279**, 371 (2009).
- 3) Y. Kasamatsu *et al.*, J. Nucl. Radiochem. Sci. **8**, 69 (2007).
- 4) T. Yokokita, H. Haba, RIKEN Accel. Prog. Rep. **52**, 186 (2019).

*¹ RIKEN Nishina Center

Anion exchange of element 104, Rf, at 0.11 M H₂SO₄ by using batch-type solid-liquid extraction apparatus, AMBER

T. Yokokita,^{*1} Y. Kasamatsu,^{*2} E. Watanabe,^{*2} Y. Komori,^{*1} Y. Shigekawa,^{*1} Y. Wang,^{*1} D. Mori,^{*1} H. Ninomiya,^{*2} S. Hayami,^{*2} K. Tonai,^{*2} K. Ghosh,^{*1} A. Shinohara,^{*2} and H. Haba^{*1}

The relativistic effect of orbital electrons is relatively more pronounced for heavy elements. In particular, the chemical properties of superheavy elements (SHEs) with atomic number $Z \geq 104$ are expected deviate from the periodicity of their lighter homologues in the periodic table. Thus, it is important and interesting to investigate the chemical properties of these elements. Thus far, ion-exchange experiments on SHEs have been conducted to determine the distribution coefficients (K_d), which are defined as the ratio of the elemental concentrations of the two phases.¹⁾ However, those values at equilibrium have not been obtained in most studies. To obtain the K_d values for Rf at equilibrium, a batch-type solid-liquid extraction apparatus called AMBER was developed,²⁾ and the equilibrium K_d values on the chloride complexation of Rf were successfully obtained in an Aliquat 336/HCl system.³⁾

To study the sulfate complexation of Rf, we plan to perform anion-exchange experiments with Rf and its homologous elements. By using AMBER, we have already performed online anion-exchange experiments with Zr and Hf in H₂SO₄ as the model experiments for Rf and determined the anion-exchange experimental condition of Rf as 0.1–0.7 M H₂SO₄.⁴⁾ In this work, we performed online anion-exchange experiments with Rf and Hf at 0.11 M H₂SO₄ by using AMBER to examine the equilibrium time for the distribution of the elements and determine their K_d values.

In the online anion exchange of Rf and Hf, we simultaneously produced ²⁶¹Rf and ¹⁶⁹Hf ($T_{1/2} = 3.24$ min) by the bombardment of a mixture of ²⁴⁸Cm and ^{nat}Gd mixture with ¹⁸O beams delivered by the K70 AVF cyclotron at RIKEN. The products were transported to a chemistry room by a He/KCl gas-jet system. The transported products were deposited on the collection site of AMBER's dissolution equipment for ~3 min and were dissolved with 0.24 mL of 0.11 M H₂SO₄. The solution sample was injected into a chemical reaction container containing the anion-exchange resin (MCI GEL CA08Y). After shaking the container with a shaker for 10, 30, and 90 s, only the solution phase was discharged from the container, after being passed through a PTFE filter by compressed air for 10 s. The discharged solution was collected in a Ta disk on the round table of an automated rapid α /SF detection system⁵⁾ and evaporated quickly to dryness using hot He gas and a halogen heat lamp. Subsequently, using the detection system's robot arm, the Ta disk was sub-

jected to rapid γ -ray measurement with a Ge detector to monitor ¹⁶⁹Hf. We also performed control experiments with 10-s shaking without the resin to determine the standard radioactivity of the solution sample. The K_d values were determined from the radioactivities in the resin and solution phases, the volume of the solution phase, and the mass of the dry resin.

We conducted 327 anion-exchange and 135 control cycles, and observed a total of 96 α events from the decay of ²⁶¹Rf and its daughter nuclide ²⁵⁷No ($T_{1/2} = 24.5$ s), including 14 time-correlated α - α correlations. The event ratios of ²⁶¹Rf between the resin and solution phases were estimated from the α events. The K_d values of Hf were constant in all the time ranges studied (10–90 s), indicating that equilibrium in the anion exchange of Hf was accomplished within 10 s. Those of Rf were also constant in all the time ranges studied, yielding values of approximately 10 mL g⁻¹. This indicates that Rf is not adsorbed on the resin. In turn, this is considered to suggest that Rf does not form an anionic sulfate complex at 0.11 M H₂SO₄, though there is a possibility that counter ions of HSO₄⁻ and SO₄²⁻ are preferentially adsorbed on the resin. It should be noted that that we cannot exclude the possibility that the kinetics of Rf is significantly slower than that of Zr and Hf. The K_d values at 0.1 M H₂SO₄ follow the order of Zr > Hf \gg Rf, and this sequence is consistent with the trend predicted by theoretical calculation.⁶⁾ Furthermore, in a cation-exchange study in H₂SO₄/HNO₃, the sequence of the K_d values was reported to be Rf > Hf \geq Zr.⁷⁾ These results indicate that the sulfate complexation of Rf is weaker than those of lighter homologues.

From the present work, we found that Rf is not adsorbed on the anion-exchange resin at 0.11 M H₂SO₄ within 10–90 s. However, it is not clear whether Rf avoids forming the anionic sulfate complex in this studied condition. We need additional anion-exchange experiments of Rf at a lower counter-ion concentration.

References

- 1) Y. Nagame *et al.*, Nucl. Phys. A **944**, 614 (2015).
- 2) Y. Kasamatsu *et al.*, Radiochim. Acta **103**, 513 (2015).
- 3) T. Yokokita *et al.*, Dalton Trans. **45**, 18827 (2016).
- 4) T. Yokokita *et al.*, RIKEN Accel. Prog. Rep. **52**, 187 (2019).
- 5) H. Haba *et al.*, RIKEN Accel. Prog. Rep. **45**, 204 (2012).
- 6) V. Pershina *et al.*, Radiochim. Acta **94**, 407 (2006).
- 7) Z. J. Li *et al.*, Radiochim. Acta **100**, 157 (2012).

^{*1} RIKEN Nishina Center

^{*2} Graduate School of Science, Osaka University

Anion exchange of Zr, Hf, and Th by the automated extraction apparatus: toward the chemical study of ^{104}Rf in HNO_3

E. Watanabe,^{*1} T. Yokokita,^{*2} Y. Kasamatsu,^{*1} S. Hayami,^{*1} K. Tonai,^{*1} Y. Shigekawa,^{*2} H. Haba,^{*2} and A. Shinohara^{*1}

Chemical elements with $Z \geq 104$ are called super-heavy elements (SHEs). The chemical properties of SHEs are almost unknown because they must be synthesized by heavy-ion-induced nuclear reactions using accelerators with very low cross sections and have very short half-lives ($T_{1/2} \leq 1$ min). There are some chemical experiments on ^{104}Rf in solution chemistry; however, its chemical properties are not sufficiently understood due to limited experimental methods. Further systematic experimental studies are needed. In our previous work, we developed the automated batch-type solid-liquid extraction apparatus (AMBER) and investigated the anion-exchange behavior of Rf in HCl and H_2SO_4 to obtain the distribution coefficients (K_d) of Rf under chemical equilibrium conditions.^{1,2)}

In this study, we focus on the formation of the Rf nitrate complexes. Indeed, the clear difference between the complexation of Th (pseudo homologue of Rf) and those of Zr and Hf (homologues) in HNO_3 is known; Th forms an anionic complex with large coordination numbers of 10 and/or 12, while Zr and Hf do not. We previously found that anion-exchange reactions using Adogen 464 resin (anion exchanger) in HNO_3 reach the chemical equilibrium in 60 s for Th, and this resin is promising for ^{261}Rf ($T_{1/2} = 68$ s) experiments. Toward the anion-exchange experiments of Rf in HNO_3 using AMBER, herein, we determined the experimental conditions for washing the resin and its repetitive use.

We produced the ^{88}Zr and ^{175}Hf isotopes in the $^{89}\text{Y}(d, 3n)$ and $^{nat}\text{Lu}(d, xn)$ reactions, respectively, by using the RIKEN AVF cyclotron. ^{234}Th was separated from ^{238}U (α -decay mother nuclide). These radionuclides were purified by an anion-exchange method.

0.3 mL of 8 M HNO_3 including ^{88}Zr , ^{175}Hf , and ^{234}Th was injected into the chemical reaction container in AMBER, containing 3 mg of the Adogen 464 resin, and the container was shaken for 60 s (anion-exchange part). After only the solution phase was discharged from the container passing through a PTFE filter with compressed air, the Zr, Hf, and Th adsorbed on the resin were washed out by injecting 0.1 M HNO_3 or 0.1 M HCl into the container (back extraction part). In the same manner as above, the washing solution was discharged from the container. This part was repeated until all of Zr, Hf, and Th were excluded from the resin. The recovery rate until the m -th back extraction was determined from the following equation:

$$R(m) = \frac{\sum_i^m A_i}{\sum_i^n A_i}, \quad (1)$$

^{*1} Graduate school of Science, Osaka University

^{*2} RIKEN Nishina Center

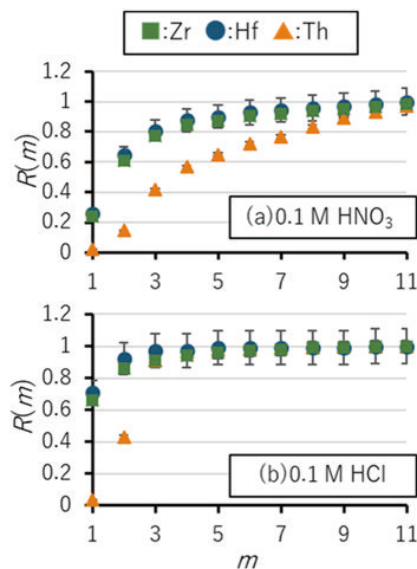


Fig. 1. Recovery rate $R(m)$ of Zr, Hf, and Th using 0.1 M HNO_3 and 0.1 M HCl as the back extractant.

where A_i is the radioactivity of the solution in the i -th back extraction, and n is the total number of back extraction.

Figure 1 shows the behavior of $R(m)$ as a function of m . This graph shows that 9 or 10 times of back extractions are required to wash out all of the Zr, Hf, and Th adsorbed on the resin in 0.1 M HNO_3 (a), while 3 or 4 times are enough in 0.1 M HCl (b). This difference results in different experimental times for one cycle (the total time of anion-exchange part, back extraction part, and conditioning part); 5 min for 0.1 M HNO_3 (9 back extractions), and 3 min for 0.1 M HCl (3 back extractions). We decided to use 0.1 M HCl as the solution for back-extraction since the experiments for ^{261}Rf should be performed in shorter cycles.

We performed about 100 cycles of the following sequence; 60 s of anion exchange with 8 M HNO_3 , followed by 4 back extractions with 0.1 M HCl , and then 2 iterations of conditioning with 8 M HNO_3 . The K_d values of Zr, Hf, and Th in the anion exchange were constant in 100 consecutive runs using AMBER, and this result indicates that the Adogen 464 resin has sufficient durability to conduct a repetitive anion-exchange experiment of ^{261}Rf .

In the near future, an on-line experiment of Zr and Hf will be conducted as a model experiment for Rf under the experimental conditions determined in this study.

References

- 1) T. Yokokita *et al.*, Dalton Trans. **45**, 18827 (2016).
- 2) T. Yokokita *et al.*, RIKEN Accel. Prog. Rep. **52**, 187 (2019).

^{99}Ru and ^{57}Fe Mössbauer spectroscopic studies of $\text{Na}_2\text{Ru}_{1-x}\text{Fe}_x\text{O}_3$ of sodium-ion battery electrode

K. Hamano,^{*1,*2} Y. Kobayashi,^{*1,*2} H. Haba,^{*2} and H. Ueno^{*2}

Sodium-ion batteries have attracted attention as the next generation of batteries after Li-ion batteries for large-scale applications owing to the abundance and low cost of sodium.^{1–3} The use of Na-excess metal oxides, Na_2MO_3 (M: transition metals), as cathode materials may realize large capacities through an additional oxygen redox reaction. Among Na-excess metal oxides, Na_2RuO_3 is expected to be the leading cathode material. In this study, we demonstrate the oxidation states and coordination environments of Ru ions in Na_2RuO_3 and $\text{Na}_2\text{Ru}_{1-x}\text{Fe}_x\text{O}_3$ ($x = 0.01$ and 0.05) after repeating the charge/discharge processes by means of ^{99}Ru and ^{57}Fe Mössbauer spectroscopy, XRD, and electrochemical measurements. Mössbauer spectroscopy is a powerful tool to understand the oxidation states of Ru ions. However, the measurements of ^{99}Ru Mössbauer spectra can only be performed at low temperatures because the Mössbauer transition energy is relatively high ($E_\gamma = 89.8$ keV).^{4,5} A ^{57}Fe -doped sample of $\text{Na}_2\text{Ru}_{1-x}\text{Fe}_x\text{O}_3$ was prepared to estimate the temperature dependence of the oxidation states of Ru sites by ^{57}Fe Mössbauer spectroscopy.

Na_2RuO_3 has a layered structure in which the first layer is composed of Na^+ and the second layer contains Na^+ and Ru^{4+} in the ratios 1:3 and 2:3, respectively. It is known that Na_2RuO_3 has two phases, namely, *ordered* and *disordered* arrangements, which correspond to sintering times of 48 h and 12 h, respectively. Ordered Na_2RuO_3 has honeycomb-type cation ordering in the $[\text{Na}_{1/3}\text{Ru}_{2/3}]\text{O}_2$ layers, whereas *disordered* Na_2RuO_3 has a random distribution of Na^+ and Ru^{4+} in the $[\text{Na}_{1/3}\text{Ru}_{2/3}]\text{O}_2$ layers. The two polymorphs exhibit significant differences in electrochemical properties.³

A sample of *disordered* $\text{Na}_2\text{Ru}_{0.99}\text{Fe}_{0.01}\text{O}_3$ was prepared through a solid-state reaction. A stoichiometric mixture of RuO_2 , NaHCO_3 , and Fe_2O_3 was pressed and sintered at 850°C for 12 h in an Ar atmosphere. The $\text{Na}_2\text{Ru}_{0.99}\text{Fe}_{0.01}\text{O}_3$ sample was confirmed to be in a single phase by XRD. For ^{99}Ru Mössbauer spectroscopy, the source nuclide ^{99}Rh ($T_{1/2} = 15.0$ d) was produced through the $^{99}\text{Ru}(p,n)^{99}\text{Rh}$ reaction at the AVF Cyclotron. ^{99}Ru Mössbauer spectra were obtained by a conventional arrangement, but both the source and absorbers were maintained at 4.2 K in a liquid He cryostat during the measurements.

The ^{57}Fe Mössbauer spectrum of *disordered* $\text{Na}_2\text{Ru}_{0.99}\text{Fe}_{0.01}\text{O}_3$ shows a doublet peak, as shown in Fig. 1. The doublet was analyzed with the distribu-

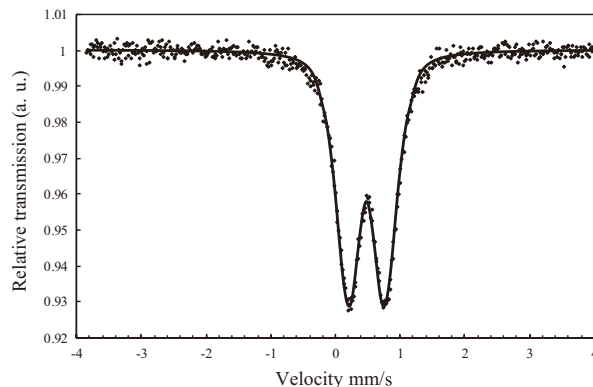


Fig. 1. ^{57}Fe Mössbauer spectrum of *disordered* $\text{Na}_2\text{Ru}_{0.99}\text{Fe}_{0.01}\text{O}_3$ measured at 15.0 K.

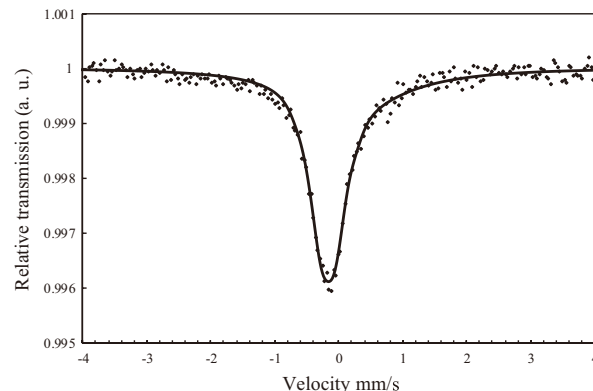


Fig. 2. ^{99}Ru Mössbauer spectrum of *disordered* $\text{Na}_2\text{Ru}_{0.99}\text{Fe}_{0.01}\text{O}_3$ measured at 5.0 K.

tion of quadrupole splitting (ΔE_Q) because Fe ions were randomly present at on Na and Ru sites. The mean values of the obtained distributions of the isomer shift (δ) and ΔE_Q were $0.48(1)$ mm/s and 0.64 mm/s, respectively. Fe ions were in a trivalent state in the $[\text{Na}_{1/3}\text{Ru}_{2/3}]\text{O}_2$ layers. The ^{99}Ru Mössbauer spectrum shows a broadened and asymmetric single line, as shown in Fig. 2. The isomer shift was $-0.30(1)$ mm/s, and the Ru ion was in a typical Ru^{4+} state. It is speculated that the line broadening is caused by an increase in the oxidation state of a part of the Ru ions from Ru^{4+} to Ru^{5+} and a significant distortion of the octahedron of RuO_6 with the introduction of a Fe^{3+} ion.

References

- 1) K. M. Mogare *et al.*, *Z. Anorg. Allg. Chem.* **630**, 547 (2004).
- 2) M. Tamaru *et al.*, *Electrochem. Commun.* **33**, 23 (2013).
- 3) B. M. de Boisse *et al.*, *Nature Commun.* **7**, 11397 (2016).
- 4) K. Takahashi *et al.*, *RIKEN Accel. Prog. Rep.* **48**, 242 (2015).
- 5) Y. Kobayashi *et al.*, *J. Phys.* **217**, 012023 (2010).

*1 Dep. of Eng. Sci., University of Electro-Commun.

*2 RIKEN Nishina Center

Development of an RF-carpet gas cell for the chemistry of superheavy elements

Y. Shigekawa,^{*1} A. Yamaguchi,^{*2} N. Sato,^{*1} A. Takamine,^{*1} M. Wada,^{*3} and H. Haba^{*1}

The chemical investigation of superheavy elements (SHEs), with atomic number $Z \geq 104$, is intriguing because of the strong relativistic effects on atomic electrons.¹⁾ In previous studies, the gas-phase chemical properties of SHEs up to Hs ($Z = 108$) and those of Cn ($Z = 112$), Nh ($Z = 113$), and Fl ($Z = 114$) have been measured¹⁾ with the help of the He gas-jet system, which allows the deceleration and rapid transport of produced SHEs to gas chromatographic apparatus. However, for the heaviest elements such as Cn, Nh, and Fl, reliable experimental data with sufficient statistics have not been obtained, because of their short half-lives (~ 1 s), which are shorter than the transportation time of the He gas-jet system (~ 3 s). The RF-carpet gas-cell system, currently used for precise mass measurements of transfermium elements,^{2,3)} allows the rapid deceleration and transportation (< 100 ms) of SHE ions separated with a gas-filled recoil ion separator (GARIS-II). In this study, we developed a cryogenic RF-carpet gas cell, placed after GARIS or GARIS-II and connected to a gas chromatographic apparatus, for the gas-phase chemistry of short-lived SHEs (< 3 s).

Figure 1 shows a schematic view and photograph of the constructed gas cell, which is similar to the one being used in the SHE-Mass-II.³⁾ A gas-cell chamber, where He gas for decelerating SHE ions is introduced, is supported by a cryocooler inside a vacuum chamber. The cryocooler can cool the gas cell to ~ 70 K, freezing gaseous impurities and preventing SHE ions from reacting with impurities. A DC cylinder and an RF carpet are placed inside the gas-cell chamber. The DC cylinder, consisting of 45 electrodes connected by low-outgas surface-mount resistors, produces a drift field of up to ~ 9 V/cm for transporting SHE ions to the RF carpet. The RF carpet consists of many concentric-ring electrodes with $60\text{-}\mu\text{m}$ width and $100\text{-}\mu\text{m}$ spacing. It has a $\Phi 0.32\text{-mm}$ hole at the center for extracting SHE ions. The hole diameter is less than that of SHE-Mass-II ($\Phi 0.74$ mm), allowing a lower pressure in the vacuum chamber and lower loss rate of He gas from the gas-cell chamber. A quadrupole

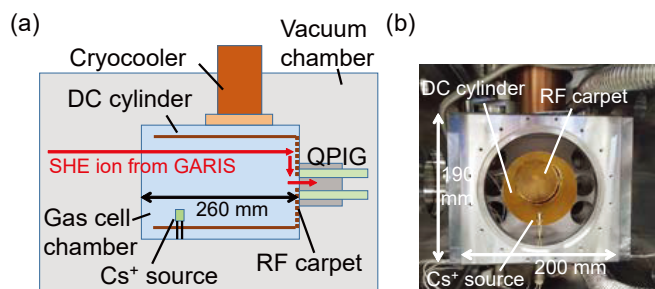


Fig. 1. (a) Schematic view and (b) photograph of the developed cryogenic RF carpet gas cell.

^{*1} RIKEN Nishina Center

^{*2} Quantum Metrology Laboratory, RIKEN

^{*3} Wako Nuclear Science Center (WNSC), IPNS, KEK

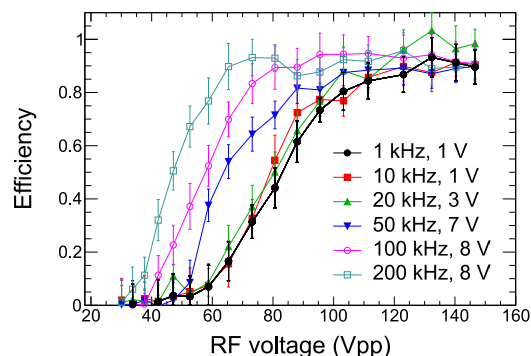


Fig. 2. Transportation efficiency of Cs^+ ions as a function of the RF voltage for combinations of the AF frequency and voltage with a drift field of 6.7 V/cm at a He pressure of 100 mbar and a gas-cell temperature of approximately 75 K.

ion guide (QPIG) is placed close to the hole of the RF carpet to transport extracted ions.

As an evaluation of the apparatus, we measured the transportation efficiency of Cs^+ ions from the surface of the RF carpet to the central hole of the carpet by using a Cs ion source placed inside the gas-cell chamber. First, the current of Cs^+ ions that reached the RF carpet was measured using the carpet as the Faraday cup. Next, Cs^+ ions were transported towards the carpet hole by applying RF fields, on which audio frequency (AF) fields were superimposed,⁴⁾ to the carpet. The current of Cs^+ ions extracted through the hole was measured using the QPIG as the Faraday cup. The transportation efficiency was obtained by dividing the current at the QPIG by that at the RF carpet.

Figure 2 shows an example of the measured transportation efficiency as a function of the RF voltage. For each AF frequency, the AF voltage was fixed to the value that could maximize the transportation efficiency. In Fig. 2, the transportation efficiency is saturated with high RF voltages, indicating that sufficient RF voltages can be applied to the RF carpet with our setup. High maximum transportation efficiencies (more than 80%) were successfully obtained; hence, the constructed gas cell would be applicable to experiments with SHE isotopes at low production rates. Higher AF frequencies are preferable in that lower RF voltages can saturate the efficiency (Fig. 2), and that faster transportation is expected.⁵⁾

We will measure the transportation efficiency through the QPIG with Cs ions and also with radioisotopes offline and online. In parallel, we will develop the gas chromatographic apparatus connected to the gas cell.

References

- 1) A. Türler, V. Pershina, Chem. Rev. **113**, 1237 (2013).
- 2) Y. Ito *et al.*, Phys. Rev. Lett. **120**, 152501 (2018).
- 3) M. Wada *et al.*, RIKEN Accel. Prog. Rep. **52**, 136 (2019).
- 4) F. Arai *et al.*, Int. J. Mass Spectrom. **362**, 56 (2014).
- 5) G. Bollen, Int. J. Mass Spectrom. **299**, 131 (2011).

An attempt to modify the membrane degasser (MDG)

Y. Komori,^{*1} K. Ooe,^{*2} T. Yokokita,^{*1} Y. Shigekawa,^{*1} and H. Haba^{*1}

We have been developing a rapid solvent extraction apparatus coupled to the GARIS gas-jet system for aqueous chemistry studies of element 106, Sg, and element 107, Bh.^{1,2)} This apparatus consists of a continuous dissolution apparatus called a membrane degasser (MDG), a flow solvent extractor (FSE), and liquid scintillation detectors. In the MDG, nuclear reaction products transported by the gas-jet method are continuously mixed and dissolved with an aqueous solution. The gas is removed through a hydrophobic membrane, and the solution is injected to the FSE. In our previous studies, we fabricated the MDG and studied the dissolution efficiencies of $^{90\text{m}}\text{Nb}$ ($T_{1/2} = 18.8$ s), $^{90\text{g}}\text{Nb}$ (14.6 h), and $^{178\text{a}}\text{Ta}$ (2.36 h) produced in the $^{\text{nat}}\text{Zr}(d, x)^{90\text{m, g}}\text{Nb}$ and $^{\text{nat}}\text{Hf}(d, x)^{178\text{a}}\text{Ta}$ reactions.¹⁾ We found that the dissolution efficiency of the short-lived $^{90\text{m}}\text{Nb}$ isotope is as low as approximately 50%, though those for the long-lived $^{90\text{g}}\text{Nb}$ and $^{178\text{a}}\text{Ta}$ isotopes are greater than 80%. We considered that the reason for the difference in dissolution efficiencies between the short-lived and long-lived isotopes is as follows: (i) the gas-jet-transported products are not mixed well with the aqueous solution and (ii) the long-lived isotopes accumulate in the MDG. In this work, we fabricated a miniaturized MDG to reduce the accumulation of the reaction products in the MDG. A major modification is the reduction of the inner volume of the MDG from 23 μL to 1.8 μL . We measured the dissolution efficiencies of $^{90\text{m}}\text{Nb}$, $^{90\text{g}}\text{Nb}$, and $^{178\text{a}}\text{Ta}$ using the miniaturized MDG and compared the results with those obtained with the conventional MDG. We also studied the dissolution efficiencies of ^{144}Eu ($T_{1/2} = 10.2$ s), ^{143}Sm (68 s), and ^{143}Eu (2.59 min) using the conventional MDG. The ^{144}Eu with a half-life of 10 s is favorable because its dissolution efficiency is less influenced by the accumulation in the MDG than that of the long-lived isotopes.

$^{90\text{m, g}}\text{Nb}$ and $^{178\text{a}}\text{Ta}$ were produced in the same reactions as mentioned above. Two $^{\text{nat}}\text{Zr}$ foils with a thickness of 2.4 μm and four $^{\text{nat}}\text{Hf}$ foils with a thickness of 4.4 μm were irradiated with a 24 MeV deuteron beam supplied by the RIKEN AVF cyclotron. The beam currents were 4.6 and 1.5 μA . The reaction products were transported by the He/KCl gas-jet system to the miniaturized or conventional MDG in the chemistry laboratory. The flow rate of the He carrier gas was 1.5 L/min. Before entering the MDG, nuclear reaction products were continuously mixed with 1 M HCl at a flow rate of 1 mL/min inside a PTFE capillary of 0.75 mm inner diameter (*i. d.*) and 5 cm length. Effluents from the MDG were collected for 30 or 60 s with polypropylene tubes and were subjected to γ -ray spectrometry with a Ge detector. The dissolution efficiencies were determined by

Table 1. Summary of the dissolution efficiencies obtained with the miniaturized and conventional MDGs.

Nuclide (Half-life)	Dissolution efficiency [%]	
	Miniaturized MDG	Conventional MDG
$^{90\text{m}}\text{Nb}$ (18.81 s)	35 \pm 2	36 \pm 5
$^{178\text{a}}\text{Ta}$ (2.36 h)	53 \pm 3	71 \pm 7
$^{90\text{g}}\text{Nb}$ (14.6 h)	60 \pm 20	81 \pm 10
^{144}Eu (10.2 s)	—	43 \pm 5
^{143}Sm (68 s)	—	74 \pm 8
^{143}Eu (2.59 min)	—	78 \pm 12

comparing the radioactivity in the effluents with that directly collected on a glass fiber filter. We also produced ^{144}Eu , ^{143}Sm , and ^{143}Eu through the $^{\text{nat}}\text{Sm}(d, x)$ reaction. Six $^{144}\text{SmF}_3$ targets deposited on Ti foils, each with a thickness of 495 $\mu\text{g}/\text{cm}^2$ were irradiated with a 24 MeV deuteron beam of 3.9 μA . The dissolution efficiencies of these nuclides were determined with the conventional MDG using almost the same procedures as for $^{90\text{m, g}}\text{Nb}$ and $^{78\text{a}}\text{Ta}$.

The dissolution efficiencies of $^{90\text{m, g}}\text{Nb}$ and $^{178\text{a}}\text{Ta}$ obtained with the miniaturized and conventional MDGs are summarized in Table 1. Those of ^{144}Eu , ^{143}Sm , and ^{143}Eu with the conventional MDG are also listed in Table 1. The dissolution efficiency of the short-lived $^{90\text{m}}\text{Nb}$ obtained with the miniaturized MDG is the same as that obtained with the conventional MDG. The efficiencies of the long-lived $^{178\text{a}}\text{Ta}$ and $^{90\text{g}}\text{Nb}$ with the miniaturized MDG are almost 20% lower than those with the conventional MDG. This might be the result of a decrease in the accumulation of the long-lived isotopes due to the smaller inner volume in the miniaturized MDG. The lower dissolution efficiency of the short-lived nuclides such as $^{90\text{m}}\text{Nb}$ and ^{144}Eu might be due to the insufficient mixing of the gas-jet-transported products with the aqueous solution. At this moment, we expect that a dissolution efficiency of $\sim 40\%$ is attainable for $^{265}\text{Sg}^{a, b}$ ($T_{1/2} = 8.5$ s, 14.4 s)³⁾ and ^{266}Bh ($T_{1/2} = 10.7$ s) using this MDG.⁴⁾ To increase the dissolution efficiency of these short-lived nuclides, more rapid and efficient mixing of the gas with the aqueous solution is necessary. We will improve the mixing unit of the MDG in the future.

References

- 1) Y. Komori *et al.*, RIKEN Accel. Prog. Rep. **49**, 29 (2016).
- 2) Y. Komori *et al.*, RIKEN Accel. Prog. Rep. **50**, 247 (2017).
- 3) H. Haba *et al.*, Phys. Rev. C **85**, 024611 (2012).
- 4) H. Haba *et al.*, EPJ Web Conf. **131**, 07006 (2016).

^{*1} RIKEN Nishina Center

^{*2} Osaka University Graduate School of Medicine

Preparation of Gd targets for in-beam fission measurements as a step towards the handling of ^{243}Am targets with ultra-thin backings

T. Tanaka,^{*1,*2} D. J. Hinde,^{*1,*2} H. Haba,^{*2} M. Dasgupta,^{*1,*2} S. Battison,^{*1} A. C. Berriman,^{*1} L. T. Bezzina,^{*1} J. Buete,^{*1} I. P. Carter,^{*1} K. J. Cook,^{*1} E. Graham,^{*1} J. Heighway,^{*1} T. D. Hume,^{*1} D. Y. Jeung,^{*1} Y. Komori,^{*2} P. McGlynn,^{*1} D. Mori,^{*2} S. A. Parker-Steele,^{*1} C. Sengupta,^{*1} C. Simenel,^{*1} E. C. Simpson,^{*1} M. A. Stoyer,^{*1,*3} B. M. A. Swinton-Bland,^{*1} Y. Wang,^{*2} W. Wojtaczka,^{*1} and T. Yokokita^{*2}

The study of in-beam fission characteristics is of fundamental importance in understanding heavy-ion induced fusion reactions and the shell structure of fissioning nuclei. Characteristic information is extracted from the measured velocities of the fission fragments. Since the fragments lose kinetic energy when passing through the target and/or backing to reach the detectors, thinner targets and backings are favored for studies to decrease the systematic error. Additionally, safe handling and survival of radioactive isotope (RI) targets in beam are important factors. Since thinner targets and backings are fragile, the optimization of the backing material, thickness and preparation procedures are key for studies with RI targets.

In order to find the optimum backing, a variety of backings with different material, thickness, and substrate, were prepared, as indicated in Table 1. As the thin backings are too thin for electrodeposition of the RI target, a substrate such as Cu is used to support the backing during electrodeposition, and is subsequently removed. The Ti and Cr materials were evaporated using an evaporator at ANFF. ^{a)} The Cu substrates were dissolved by a solution made by combining 4 grams of trichloroacetic acid (TCA), 20-mL 30% NH_3 solution and 20-mL deionized water, resulting in 40-mL of 9.3% TCA solution, similar to that described in Refs. 1–3). The success ratios for dissolving the Cu without breaking the backing materials were more than 80% for Ti backing material and less than 50% for Cr backing material. Attempts to release the Ti-backings from KI-coated glass by dissolving potassium iodide in water were not successful because the backings were broken.

As a backing test, the backings, 200-nm Ti, 300-nm Ti, and 300-nm Cr (once removed from the Cu sub-

Table 1. Combinations of backing material, thickness and substrate.

Backing material	Thickness	Substrate
Ti	200 nm	Cu
	300 nm	(3.6–4.7 μm)
	300 nm	KI-coated glass
Cr	300 nm	Cu (3.8–4.4 μm)
Al	740 nm	self-supporting

^{*1} Department of Nuclear Physics, The Australian National University

^{*2} RIKEN Nishina Center

^{*3} Lawrence Livermore National Laboratory

^{a)} Australian National Fabrication Facility, ANU node

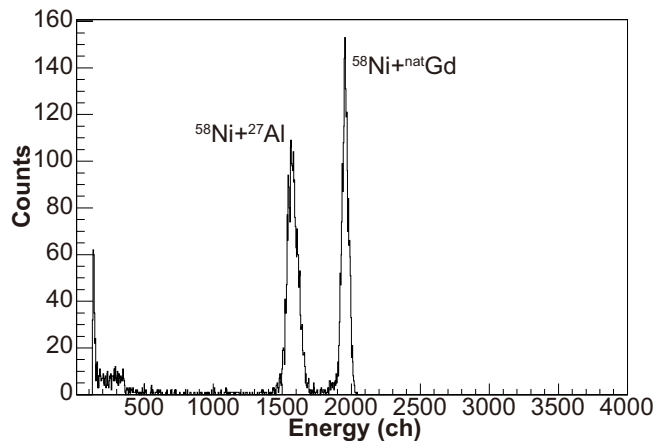


Fig. 1. Energy spectrum measured by a Si detector from the reaction of $^{58}\text{Ni} + ^{\text{nat}}\text{Gd}$ with Al backing.

strates), were irradiated by a 170 MeV $^{58}\text{Ni}^{12+}$ beam of 1 mm diameter, which was provided by the Heavy Ion Accelerator Facility of the Australian National University. The 300-nm Ti backing survived beam irradiation of 1.5 enA for more than one hour.

Gd target material, instead of RI ^{243}Am , was successfully deposited on Ti-backing and Al-backing by electrodeposition utilizing the Hot-Lab of RIKEN Nishina Center. The detailed procedures are similar to that described in Ref. 4). The thicknesses of 1.6-mm-diameter (5-mm-diameter) Gd targets were between 130 and 190 (40 and 120) $\mu\text{g}/\text{cm}^2$.

The Gd targets on 300-nm-Ti/740-nm-Al backings were tested with the same conditions as the backing test. An energy spectrum measured by a Si detector, which was mounted 15 cm downstream of the target at 18° with respect to the beam axis, is indicated in Fig. 1. The clear peaks indicate the elastic scattering from the reactions of $^{58}\text{Ni} + ^{\text{nat}}\text{Gd}$ and $^{58}\text{Ni} + ^{27}\text{Al}$, which demonstrate the uniformity and quality of the target and backing.

The safety of all of procedures for handling the target, as well as the uniformity and quality of the target, have been confirmed. The ^{243}Am target will be prepared using the same procedures as the Gd targets.

References

- 1) G. T. J. Arnison, Nucl. Instrum. Methods Phys. Res. **53**, 357 (1967).
- 2) B. Lommel *et al.*, Nucl. Instrum. Methods Phys. Res. A **655**, 44 (2011).
- 3) M. A. Stoyer *et al.*, LLNL-TR-752862 (2018).
- 4) Y. Kudou *et al.*, RIKEN Accel. Prog. Rep. **42**, 265 (2009).

Preparation of [^{211}At]-labeled sodium astatide (NaAt) by reducing with ascorbic acid for the treatment of thyroid cancer[†]

Y. Shirakami,^{*1} K. Kaneda,^{*1} A. Toyoshima,^{*1,*2} T. Watabe,^{*3} K. Ooe,^{*1,*3} A. Shinohara,^{*4} and J. Hatazawa^{*4}

Iodine-131 (^{131}I)-labeled sodium iodide, [^{131}I]-NaI, has been used in clinics as the standard medication for patients with thyroid cancer. NaI can be transferred into cancer cells via sodium-iodide symporters (NIS), resulting in cell death owing to β^- particles emitted from the ^{131}I atoms. The agent has some limitations: i) [^{131}I]-NaI does not work in some patients, even though the agent accumulates in tumor lesions, and ii) the patients treated with the drug require isolated hospitalization within a week.

[^{211}At]-NaAt is expected to be a novel therapeutic agent for patients with thyroid cancer as an alternative to [^{131}I]-NaI because the linear energy transfer (LET) of ^{211}At is much higher than that of ^{131}I . Several papers have proven the efficacy of the drug in animals and humans.^{1,2} The drug, however, has not been well evaluated in humans yet. One of the major problems of the agent is the difficulty in the chemical identification of NaAt due to the lack of a stable isotope of astatine. The aim of our study is to develop methods for the quality control of the drug.

Bismuth-209 was irradiated with helium-4 (α) at 29 MeV, and ^{211}At was produced through the $^{209}\text{Bi}(\alpha, 2n)^{211}\text{At}$ reaction. The target was placed in a quartz tube and heated up to 850°C under a mixture of helium and oxygen gas flow (30 mL/min and 10 mL/min, respectively). Dry-distilled ^{211}At was collected in a teflon tube cooled in an ice-water bath. Through the tube, 100 μL of distilled water was passed, and an aqueous solution of ^{211}At (bulk solution) was collected in a micro PFA vial.

An aqueous solution of [^{211}At]-NaAt was prepared using the following procedures. An aliquot of the bulk solution was transferred to a glass vial containing an aqueous solution of 7 w/v% sodium hydrogen carbonate. Subse-

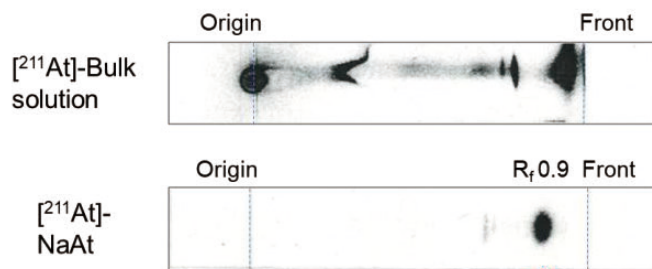


Fig. 1. TLC profiles of the [^{211}At] bulk solution and [^{211}At]-NaAt. Plate: Silica gel, Solvent: acetonitrile/water (2/1).

[†] Condensed from the article in *J. Nucl. Med.* **60**, 1301 (2019)

^{*1} Institute for Radiation Sciences, Osaka University

^{*2} RIKEN Nishina Center

^{*3} Graduate School of Medicine, Tracer Kinetics and Nuclear Medicine, Osaka University

^{*4} Research Center for Nuclear Physics, Osaka University

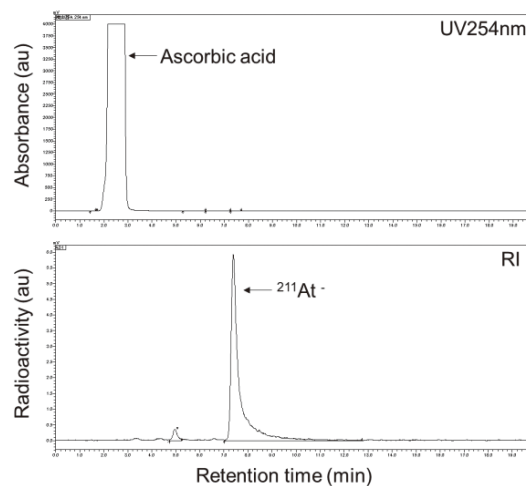


Fig. 2. HPLC profiles of [^{211}At]-NaAt. Column: reversed phase C-18 (Nakarai Tesque, Kyoto). Solvent: 20 mmol/L tetrabutylammonium chloride/acetonitrile (7 : 3). Upper: UV trace, Bottom: RI trace.

quently, an aqueous solution of 3 w/v% ascorbic acid was added to the vial. The mixture solution was kept for 1 h at room temperature. The radioactivity of the solution was adjusted to 10 MBq/mL.

Representative TLC profiles of the [^{211}At] bulk solution and [^{211}At]-NaAt are shown in Fig. 1. The [^{211}At] bulk solution was comprised of several radioactive spots having irregular shapes (Fig. 1, upper). This result indicated that the bulk solution is a mixture of several chemical species of ^{211}At , including the higher oxidation states of astatine (At^+ and/or At^{3+}) as well as astatide ion (At^-). The radioactive species were converged on a single component (relative to front (R_f) = 0.9, radiochemical purity (RCP) > 90%) after the addition of ascorbic acid (Fig. 1, bottom). The component was also presented as the major radioactive peak (retention time (R_t) = 7.42 min, RCP > 90%) by high-performance liquid chromatography (HPLC) analysis, as shown in Fig. 2. The component was estimated to be [^{211}At]-NaAt.

In thyroid cancer cells, the solution of [^{211}At]-NaAt was accumulated in cells specifically via NIS. The solution also inhibited tumor growth in mice with thyroid cancer.

These results suggest that ascorbic acid is efficient for the preparation of [^{211}At]-NaAt having high radiochemical purity. In conclusion, it is proved that [^{211}At]-NaAt is a promising agent for the treatment of patients with thyroid cancer.

References

- 1) J. G. Hamilton *et al.*, *Exp. Biol. Med.* **86**, 366 (1954).
- 2) S. Carlin *et al.*, *J. Nucl. Med.* **44**, 1827 (2003).

Development of radioimmunotherapy with astatine-211-conjugated antibodies

H. Takashima,^{*1,*2} Y. Koga,^{*1,*2} K. Onuki,^{*3} S. Manabe,^{*4,*5} R. Tsumura,^{*1} T. Anzai,^{*1} N. Iwata,^{*1} M. Yasunaga,^{*1} Y. Wang,^{*2} T. Yokokita,^{*2} Y. Komori,^{*2} D. Mori,^{*2} H. Haba,^{*2} H. Fujii,^{*3} and Y. Matsumura^{*1}

Macromolecules and macroproteins hardly extravasate from blood vessels at a normal organ site due to their large molecular weight. By contrast, since the permeability of blood vessels at tumor sites is higher than that at normal organs, macromolecules and macroproteins can extravasate from tumor vessels. Moreover, due to the poor lymphatic drainage system at tumor sites, macromolecules and macroproteins are retained for a prolonged time after extravasation. As a result, macromolecules and macroproteins selectively and efficiently accumulate in tumors. This phenomenon is the enhanced permeability and retention (EPR) effect,¹⁾ which is the rationale of drug delivery systems for cancer treatment. Antibodies such as immunoglobulin G (IgG), the molecular weight of which is approximately 150 kDa, accumulate in tumors via the EPR effect. In addition to the EPR effect, antigen-antibody interaction with target molecules expressed in tumors enhances the tumor accumulation of antibodies.²⁾

We successfully produced several types of monoclonal antibodies (mAbs) that recognize target molecules highly or specifically expressed in tumors, and applied mAbs to drug carriers. The antibody-drug conjugate (ADC) is composed of an mAb that recognizes target molecules in tumors and low-molecular weight anticancer agents, and it is an example of armed antibodies. Previously, using our mAbs, we prepared ADCs and demonstrated that they showed potent antitumor effects in cancer xenograft models.³⁻⁵⁾

Alpha particles are characterized by higher linear energy transfer (LET) and shorter range in tissue than other types of radiation, resulting in efficient deoxyribonucleic acid (DNA) double-strand breaks in accumulated cells with minor effects on adjacent cells. Accordingly, since the successful delivery of alpha emitters to tumor sites is expected to yield efficient antitumor effects with mild toxicity, we focus on the development of radioimmunotherapy (RIT) with an alpha-emitter-conjugated antibody.

In this study, we labeled antibodies with astatine-211, one of the most promising alpha emitters for cancer treatment, and evaluated the binding activities and *in vitro* cytotoxic effects of the radioactive antibodies.

We synthesized astatine-211 in the $^{209}\text{Bi}(\alpha, 2n)^{211}\text{At}$ reaction using the RIKEN Azimuthally Varying Field

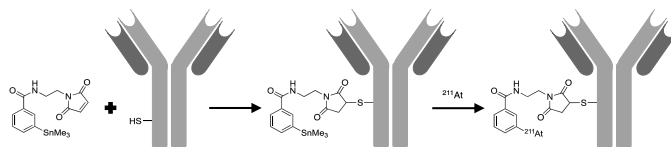


Fig. 1. Flowchart to prepare astatine-211-conjugated antibodies.

(AVF) cyclotron.

Figure 1 shows a flowchart to prepare astatine-211-conjugated antibodies. First, we reduced the interchain disulfide bonds of mAbs^{4,5)} and attached a trimethylstannyl benzoate linker to an mAb with reactive sulfhydryl groups via a thioether bond between the sulfhydryl and maleimide groups. Then, we labeled like-antibody complexes with astatine-211 via a halogen-exchange reaction. Subsequently, the astatine-211-conjugated antibodies were purified away from unconjugated astatine-211 using a PD-10 desalting column (GE Healthcare Life Sciences, Chicago, IL, USA). To increase the labeling efficiency, we optimized the procedure to purify astatine-211 from bismuth and calculated the labeling rate by dividing the radioactivities of immunoconjugates by those of astatine-211 that was initially applied to the reaction solution (100 MBq); the labeling rate was approximately 60%. We successfully prepared astatine-211-conjugated antibodies using both mAbs newly developed by us and trastuzumab, a clinically available mAb for patients with breast or gastric cancer.

We evaluated the affinity of astatine-211-conjugated antibodies by flow cytometry. The radioactive antibodies bound to cancer cells depending on the expression level of target molecules on the cell membrane, and the specific affinity of immunoconjugates was comparable to the corresponding mAbs. As a result, astatine-211-conjugated antibodies exerted *in vitro* cytotoxic effects on cancer cells depending on the expression of target molecules on the cell membrane.

In conclusion, we synthesized astatine-211 using the RIKEN AVF cyclotron and succeeded in constructing astatine-211-conjugated antibodies. The present data warrant further basic studies for future clinical development.

References

- 1) Y. Matsumura *et al.*, *Cancer Res.* **46**, 6387 (1986).
- 2) H. Takashima *et al.*, *Sci. Rep.* **7**, 12341 (2017).
- 3) Y. Koga *et al.*, *Int. J. Cancer.* **137**, 1457 (2015).
- 4) R. Tsumura *et al.*, *J. Control. Release.* **284**, 49 (2018).
- 5) H. Fuchigami *et al.*, *Sci. Rep.* **8**, 14211 (2018).

^{*1} Developmental Therapeutics, Exploratory Oncology Research & Clinical Trial Center (EPOC), National Cancer Center

^{*2} RIKEN Nishina Center

^{*3} Division of Functional Imaging, EPOC, National Cancer Center

^{*4} Synthetic Cellular Chemistry Laboratory, RIKEN

^{*5} Research Center for Pharmaceutical Development, Tohoku University

Anti-cancer effect of ^{211}At -labeled antibody on xenografted mice with intravenous injection

Y. Kanayama,^{*1} K. Sakamoto,^{*2} R. Zochi,^{*1} Y. Wang,^{*3} T. Yokokita,^{*3} Y. Komori,^{*3} D. Mori,^{*3} H. Haba,^{*3} and Y. Watanabe^{*1}

Astatine-211 is a promising α emitter for targeted α therapy because of its simple decay scheme, which can avoid undesirable radiation from daughter nuclides. In a previous study, we investigated the radiolabeling method of ^{211}At on monoclonal antibodies using a stannyl compound (*m*-MeATE). The synthesis of ^{211}At -labeled IgG was successful, but we observed the detachment of ^{211}At 24 h after intravenous (IV) injection. To overcome the deastatination, the use of decaborane, a boron cluster compound, is a possible solution because its binding to astatine is more stable *in vivo*.¹⁾ However, as we have previously reported,²⁾ the ^{211}At -decaborate moiety may increase hydrophobicity, which probably causes its poor bioavailability, resulting in the low tumor uptake by IV injection. In the present study, we introduced a PEG linker between decaborate and IgG to decrease the hydrophobicity. By using this conjugate, we investigated the anti-cancer effect of ^{211}At -labeled trastuzumab on HER2-positive cancer xenografted mice with IV injection.

The ^{211}At -decaborate (B10)-PEG5-trastuzumab was obtained through the 3-step synthesis (Fig. 1). We used 46 MBq of ^{211}At produced in the $^{209}\text{Bi}(\alpha, n)^{211}\text{At}$ reaction at the RIKEN AVF cyclotron for labeling 40 μg of the antibody-linker conjugate, and the mixture after the reaction was applied to filtration with G50 DNA-grade gel to remove free ^{211}At and replace it with physiological saline. The radioactivity yield was 65% (30.2 MBq was retained on the antibody), with the protein recovery rate being 64%. The specific radioactivity was 1.08 MBq/ μg .

We first investigated the bio-distribution of the ^{211}At -labeled trastuzumab in xenografted mice 3, 24, and 48 h after IV injection. Figure 2 shows that ^{211}At -trastuzumab was in the blood at significant levels (around 15%ID/g) for 48 h and progressively accumulated in the target A431 tumor region (up to approximately 20%ID/g) during the same period. On the other hand, the control C6 tumor region did not show a significant accumulation from 24 to 48 h. This result was consistent with the typical outcome of a PET imaging

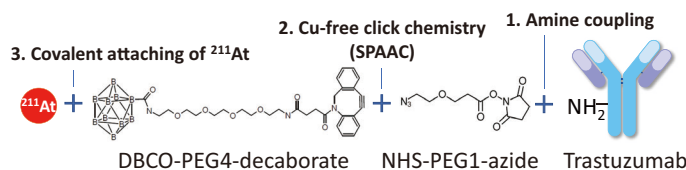


Fig. 1. Synthesis of ^{211}At -B10-PEG5-trastuzumab.

^{*1} Laboratory for Pathophysiological and Health Science, RIKEN
^{*2} Laboratory for Nonnatural Amino Acid Technology, RIKEN
^{*3} RIKEN Nishina Center

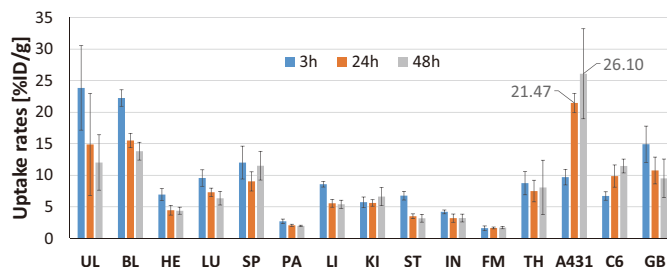


Fig. 2. Biodistribution in xenografted mice ($n = 4$). A431, HER2 positive; C6, HER2 negative.

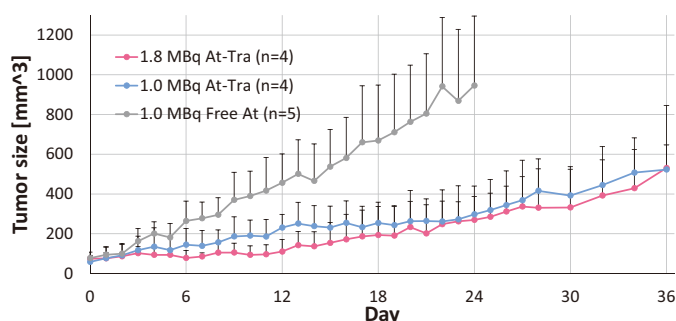


Fig. 3. Average tumor size of the mice after IV injection of ^{211}At -B10-PEG5-trastuzumab.

study using ^{64}Cu -labeled trastuzumab.

Subsequently, we proceeded to examine the anti-cancer effect of ^{211}At -trastuzumab via IV injection. Two groups of mice were administered 1.8 or 1.0 MBq of ^{211}At -trastuzumab (1.7 μg), while the control group was administered 1.0 MBq of free ^{211}At . The changes in the body weight and tumor size, as well as the survival rate were observed up to 36 days after the IV injection (Day 0) (the tumor size is shown in Fig. 3).

A larger dose (1.8 MBq) of ^{211}At -Trastuzumab caused a severe decrease in the body weight within a week, implying a serious side effect of the injection, and led to the euthanization of a mouse. The ^{211}At -trastuzumab in either dose successfully suppressed the growth of the tumor in size with only one shot of the IV injection, and no mice died because of the tumor. No adverse effects were observed in the 1.0 MBq At-Tra group. In contrast, the tumor grew much more rapidly in the control group, with no mice alive until Day 36. Thus, we successfully demonstrated the favorable anti-tumor effect of ^{211}At -B10-labeled trastuzumab conjugated with a PEG linker, which was probably supported by the improved biodistribution.

References

- 1) F. Guerard *et al.*, Cancer Biother. Radiopharm. **28**, 1 (2013).
- 2) K. Fujiki *et al.*, Chem. Sci. **10**, 1936 (2019).

Dispersion rates of astatine-211 from aqueous solutions and chloroform[†]

A. Toyoshima,^{*1,*2,*3} K. Nagata,^{*2,*3} K. Ooe,^{*1,*3,*4} Z. Zhang,^{*2,*3} T. Ikeda,^{*3} S. Ichimura,^{*3} H. Obata,^{*3} T. Yoshimura,^{*2,*3} and A. Shinohara^{*2,*3}

Airborne concentrations of radioactive materials are crucial for the evaluation of human exposure and radiation protection protocols. An important factor influencing airborne radioactivity concentration is the dispersal rate from a radioactive solid or liquid sample, which depends on the chemical forms of the radioactive materials. Therefore, to evaluate the airborne concentration, it is indispensable to experimentally determine the dispersal rates under various conditions. Recently, targeted alpha therapy using a short-lived radioisotope emitting α particles was developed.¹⁾ ^{211}At with a half-life of 7.2 h is a promising α -emitter for the therapy.²⁾ However, because of the lack of long-lived At isotopes, its dispersion has been rarely studied.³⁾ For realistic and effective clinical use of ^{211}At , the evaluation of its airborne concentration is necessary. Herein, we investigated the dispersal rates of ^{211}At in aqueous acidic, neutral, and alkaline solutions and in chloroform.

^{211}At was produced in the $^{209}\text{Bi}(\alpha, n)^{211}\text{At}$ reaction using the AVF cyclotron at the Research Center of Nuclear Physics, Osaka University. ^{211}At was also supplied from RIKEN through the Supply Platform of Short-lived Radioisotopes. ^{211}At was then separated from the irradiated Bi target by dry distillation. The experimental setup to measure the dispersal rate of ^{211}At is shown in Fig. 1. Details of the setup can be found in the full article. A plastic cylinder was connected to a filter holder in which a glass-fiber filter paper, charcoal-impregnated filter paper, and two charcoal cartridges were placed. The inside of the cylinder was covered with a thin polyethylene terephthalate sheet to catch dispersed ^{211}At on its surface. An air pump for ventilation was connected to the top of the holder. To a 100 mL beaker, 0.010 mL of the ^{211}At stock solution was added to 20 mL of the aqueous solutions and chloroform. To a 1.5 mL microtube, 0.002 mL of the ^{211}At solution was pipetted into 0.50 mL of the aqueous solutions. The radioactivity of ^{211}At used in a single run was 0.4–2 MBq at the start of the experiment. The interior of the system was ventilated at an air flow rate of 30 L/min. The solution was stirred with a magnetic stirrer during ventilation for 60 min. Subsequently, the characteristic 79 keV X-ray of Po attributed to the electron capture (EC) decay of ^{211}At in/on the sample solution, vessel, filter papers, cartridges, etc. was measured using a Ge detector.

Under all the studied conditions, the recovered yields

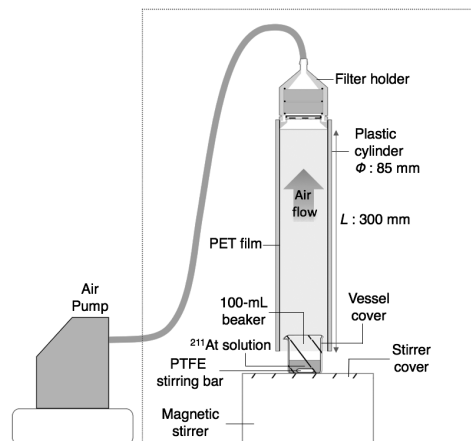


Fig. 1. Experimental setup for the measurement of dispersal rates of ^{211}At .

of ^{211}At were 100% within the error. This indicates that dispersed ^{211}At was completely collected using the setup. For the 100 mL beaker data, the dispersal rate of ^{211}At depended on the solution acidity, where 13% and 16% of ^{211}At dispersed moderately in the acidic and basic solutions, respectively, and 30% dispersed in the neutral buffer. In contrast, for the microtube, the dispersal rates of ^{211}At were much smaller (2–4%) than those from the beaker and were largely unchanged among the studied conditions. These results clearly show that ^{211}At dispersion was suppressed in the microtube because of the much smaller liquid surface area and was not strongly influenced by solution conditions. Upon the addition of ascorbic acid (AA) to the neutral buffer, the dispersal rate of ^{211}At was remarkably suppressed because of the reduction of the originally present At species to the monovalent ionic At^- .⁴⁾ In our previous clinical study with Na^{211}At ,⁵⁾ AA was required to be admixed at 1.2 weight/volume% to ^{211}At -stocked distilled water as a stabilizer in vivo. Thus, for the actual use of Na^{211}At , the dispersal rate of ^{211}At can be extremely low. In chloroform as well, a very low dispersal rate of ^{211}At was observed.

In conclusion, the dispersal rates of ^{211}At were found to vary depending on the solution conditions, with the maximum dispersion observed at pH 7. In the neutral solution containing AA, the dispersion rate of ^{211}At was quite low, suggesting that the dispersion of ^{211}At should be negligible in future clinical studies with Na^{211}At .

[†] Condensed from the article in *Radiat. Saf. Manage.* **18**, 16 (2019)

^{*1} RIKEN Nishina Center

^{*2} Institute for Radiation Sciences, Osaka University

^{*3} Graduate School of Science, Osaka University

^{*4} Osaka University Graduate School of Medicine

References

- 1) M. R. McDevitt *et al.*, *Eur. J. Nucl. Med.* **25**, 1341 (1998).
- 2) F. Guérard *et al.*, *Cancer Biother. Radiopharm.* **28**, 1 (2013).
- 3) U. Lindencrona *et al.*, *Appl. Radiat. Isotopes* **62**, 395 (2005).
- 4) J. Champion *et al.*, *J. Phys. Chem.* **117**, 1983 (2013).
- 5) T. Watabe *et al.*, *J. Nucl. Med.* **60**, 355 (2019).

Usability of ^{67}Cu as a therapeutic radioisotope for peptide receptor radionuclide therapy

Y. Fujisawa,^{*1} H. Haba,^{*2} Y. Magata,^{*3} and Y. Iida^{*1}

Copper-67 is an attractive radionuclide for nuclear medicine therapy, which has an emitted β -particle energy suitable for applying to small tumors and a physical half-life of 61.8 hours long enough to damage them. Recently, radiolabeled somatostatin (SST) analogues targeting SST receptor-2 are useful for diagnosis and therapy of neuroendocrine tumors (NETs). And peptide receptor radionuclide therapy (PPRT) has become one of the most promising treatments for patients with well to moderately differentiated unresectable or metastatic NETs. High energy β -particle-emitting ^{90}Y (2.28 MeV) becomes available for this therapy and shows high efficacy, but its application is limited by adverse effects.¹⁾ ^{67}Cu emits middle energy β -particles (0.39–0.58 MeV), and its maximal tolerated activity dose is much higher than ^{90}Y . So, ^{67}Cu may have an advantage in treating relatively small tumor masses.²⁾

In this study, we prepared a novel SST derivative, ToDBTTATE, labeled with ^{67}Cu (Fig. 1), and evaluated its potential for cancer therapy in mice bearing AR42J rat pancreatic tumor cells. ToDBTTATE has a ligand, diacetyl-bis (N^4 -methylthiosemicarbazone) (ATSM), which releases a copper in hypoxic condition such as tumor in its structure and the copper will remain at the site.³⁾

The ligand which was synthesized from 4-Methyl-3-thiosemicarbazide according to the procedure reported by Paterson *et al.*⁴⁾ was bound to TATE, a most frequently used SST analog in clinical practice and ^{67}Cu -ToDBTTATE was obtained from reaction with ^{67}Cu with microwave synthesis system. Tumor-bearing mice were prepared by implantation of AR42J tumor cells (5×10^6 cells) in 0.1 mL PBS into the flanks of nude mice (BALB/c-nu/nu, male). Biodistribution experiments were performed by intravenously administering

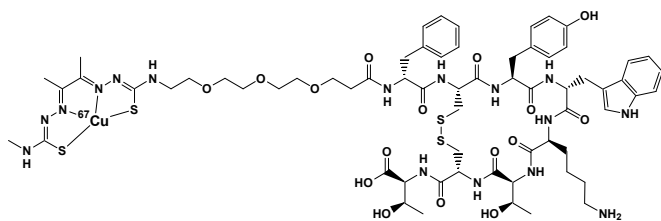


Fig. 1. Chemical structure of ^{67}Cu -ToDBTTATE.

^{*1} Faculty of Pharmaceutical Sciences, Suzuka University of Medical Science

^{*2} RIKEN Nishina Center

^{*3} Department of Molecular Imaging, Hamamatsu University School of Medicine

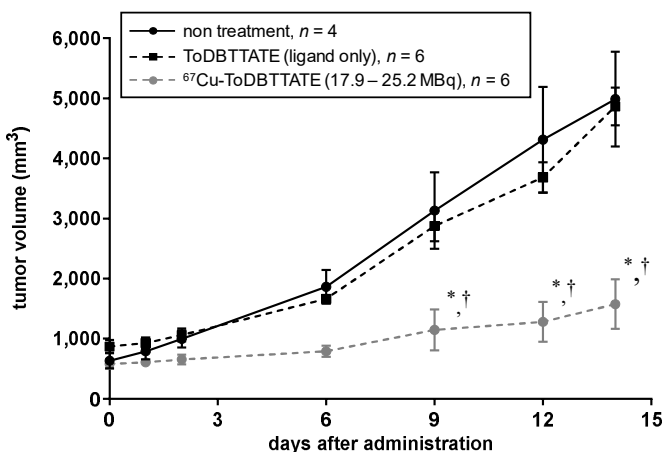


Fig. 2. Therapeutic studies of ^{67}Cu -ToDBTTATE. *, † Differences between the group of ^{67}Cu -ToDBTTATE and non-treatment (*)/ligand only (†) were determined at $p < 0.05$ by using Graph Pad PRISM ver. 6.05 (ANOVA followed by Tukey's test).

^{67}Cu -ToDBTTATE. The mice were killed at 1, 24 and 48 h after administration, and tissue of interest were excised and weighed after which their radioactivity was measured. For therapeutic studies, AR42J tumors were grown in BALB/c mice in the same way. Mice were intravenously administered with 17.9–25.2 MBq of ^{67}Cu -ToDBTTATE. Untreated mice were used as a control. Mice were weighed and tumor diameters were recorded regularly. The diameters of tumors were measured with a caliper, and tumor volumes were determined using the following formula: (longer diameter) \times (shorter diameter)²/2.

^{67}Cu -ToDBTTATE showed high accumulation in the tumor, 2.62 ± 0.46 , 1.75 ± 1.20 and $1.80 \pm 0.44\%$ ID/g at 1, 24 and 48 h after administration, respectively. Substantial tumor size reduction was observed in all mice treated with ^{67}Cu -ToDBTTATE (Fig. 2). As this result, ^{67}Cu -ToDBTTATE is a promising agent for the treatment of NETs and ^{67}Cu is expected to be suitable for treatment of relatively small tumor. The use of ^{67}Cu for cancer therapy has also potential for efficient tailor-made therapy.

References

- 1) G. A. Wiseman *et al.*, *Eur. J. Nucl. Med.* **27**, 766 (2000).
- 2) E. B. van Dieren *et al.*, *Int. J. Radiat. Oncol. Biol. Phys.* **36**, 197 (1996).
- 3) F. Dehdashti *et al.*, *Eur. J. Nucl. Med. Mo. Imaging* **307**, 844 (2003).
- 4) B. M. Paterson *et al.*, *Inorg. Chem.* **49**, 1884 (2010).

Quality evaluation of RIKEN ^{67}Cu for labeling peptide compound

S. Oshikiri,^{*1} H. Kato,^{*1} D. Mori,^{*1} A. Hino,^{*2} and H. Haba^{*1}

Copper-67 (^{67}Cu) with a half-life of 2.58 days is one of the promising RIs for both diagnosis and therapy in nuclear medicine. We have been developing a technology for producing ^{67}Cu via the $^{70}\text{Zn}(d, \alpha n)^{67}\text{Cu}$ reaction using the RIKEN AVF cyclotron and distributing purified ^{67}Cu products (RIKEN ^{67}Cu) to the general public through the Japan Radioisotope Association.¹⁾ In this work, we investigated the availability of RIKEN ^{67}Cu for radiolabeling a peptide compound.

DOTA-Substance P (DOTA-SP) is DOTA-peptide that has been studied as a candidate radiopharmaceutical for glioblastoma.^{2,3)} In the present study, we selected DOTA-SP as a model compound.

The labeling method of ^{67}Cu -DOTA-SP is as follows.

- Step 1: RIKEN ^{67}Cu chloride (2.6 MBq) was dissolved in 0.05 M hydrochloric acid to prepare a ^{67}Cu -stock solution (80 MBq/mL). The radioactivity of ^{67}Cu was determined using a germanium semiconductor detector.
- Step 2: DOTA-SP was dissolved in 0.75 M sodium acetate buffer at pH5.0 to prepare 14×10^{-5} , 4.6×10^{-5} , and 0.92×10^{-5} M DOTA-SP solutions.
- Step 3: 2.0 μL of the ^{67}Cu -stock solution was added to 1.0 μL of each DOTA-SP solution. The mixture of the ^{67}Cu -stock solution and DOTA-SP solutions of 14×10^{-5} , 4.6×10^{-5} , and 0.92×10^{-5} M resulted in 1.2, 3.5, and 17 MBq/nmol solutions, respectively.
- Step 4: The mixture in Step 3 was heated at 97°C for 10 min and kept at a room temperature for 5 min.
- Step 5: Labeling yields of ^{67}Cu -DOTA-SP were determined using the thin-layer chromatography (TLC) method with a C18 reversed-phase TLC plate (NAGEL PR-18W/UV254) and eluted with a mixture of acetonitrile, 0.5 M ammonium acetate, methanol, and tetrahydrofuran in a volume ratio of 4:3:2:1.

Figure 1 shows the labeling yield (%) as a function of the specific radioactivity of ^{67}Cu -DOTA-SP. RIKEN ^{67}Cu was used to label DOTA-SP with the highest yield at 1.2 MBq/nmol. The yield decreased with an increase of the specific radioactivity.

In previous research using another DOTA-peptide, DOTA-TATE, the labeling yield with ^{64}Cu was reported to be 97% at a specific radioactivity of 7 MBq/nmol.⁴⁾ ^{64}Cu is a radionuclide with a half-life of 12.7 h. We can convert thereported specific radioac-

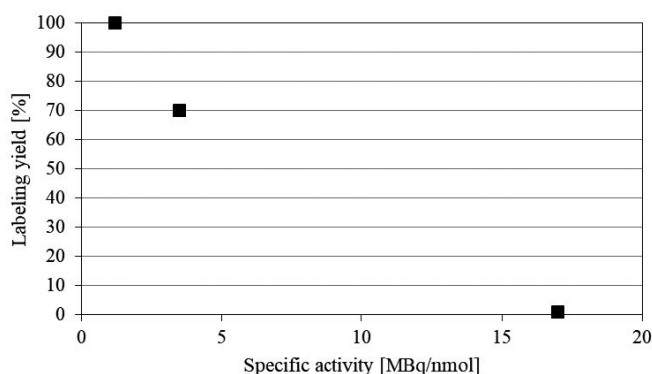


Fig. 1. Relation between specific activity (MBq/nmol) and labeling yield (%) of ^{67}Cu -DOTA-SP.

tivity of 7 MBq/nmol for ^{64}Cu into 1.4 MBq/nmol for ^{67}Cu . This is comparable with our result at 1.2 MBq/nmol in DOTA-SP and might be applicable to other compounds with such a specific radioactivity of RIKEN ^{67}Cu . This specific radioactivity was considered to be sufficient for use in studies such as *in vitro/in vivo* studies to examine candidate radiopharmaceuticals.

In this study, we evaluated the quality of RIKEN ^{67}Cu through DOTA-SP labeling and revealed that RIKEN ^{67}Cu has a high and sufficient quality to label compounds such as DOTA-peptides for studies on radiopharmaceuticals.

References

- 1) S. Yano *et al.*, RIKEN Accel. Prog. Rep. **49**, 22 (2016).
- 2) A. Majkowska-Pilip *et al.*, Molecules **23**, 2542 (2018).
- 3) L. Królicki *et al.*, Eur. J. Nucl. Med. Mol. Imaging **46**, 614 (2019).
- 4) S. N. Rylova *et al.*, PLoS One **13**, e0195802 (2018).

^{*1} RIKEN Nishina Center

^{*2} RI Research Department, FUJIFILM Toyama Chemical Co., Ltd.

Simultaneous imaging of Na^+/K^+ by semiconductor Compton camera GREI†

S. Motomura,*¹ I. Kii,*^{1,*2} H. Haba,*³ H. Yakushiji,*¹ Y. Watanabe,*¹ and S. Enomoto*⁴

Various metal elements exist in a living body and are used as essential factors for maintaining life. For example, sodium (Na) and potassium (K) are homologous alkali metals that are clearly distinguished by some biomolecules and used for forming a membrane potential required for nerve activity. Since various metal elements in a living body are controlled by specific biomolecules, it is expected that the behavior of these metal elements changes in diseased tissues.

We are exploring the possibility of a new concept of diagnostic imaging that diagnoses the function of a living organism by non-invasive visualization of the dynamics of associated metal elements in vivo. In particular, a nuclear medicine imaging technique, which takes the images of the radioisotopes (RIs) of the metal elements to be traced, enables the visualization of the dynamics of a deep part of a living body by administering a small amount of RIs. As for Na and K, ^{24}Na , ^{42}K , and ^{43}K have suitable half-lives for administration to a living body: 15, 12, and 22 h, respectively. However, since these are not positron-emitting nuclides, they cannot be imaged by PET, and the gamma-ray energies of the nuclides are too high for use in SPECT.

Therefore, we are studying the imaging of ^{24}Na , ^{42}K , and ^{43}K using a semiconductor Compton camera called GREI^{1,2)} to visualize the dynamics of Na^+ and K^+ in a living body. We have already obtained various results in the simultaneous imaging of multiple nuclides that emit gamma rays from about 200 KeV to 2 MeV by using GREI equipped with germanium semiconductor detectors as gamma-ray sensors. In addition, it is possible to create three-dimensional images simply by taking an image from one direction with a single imaging head

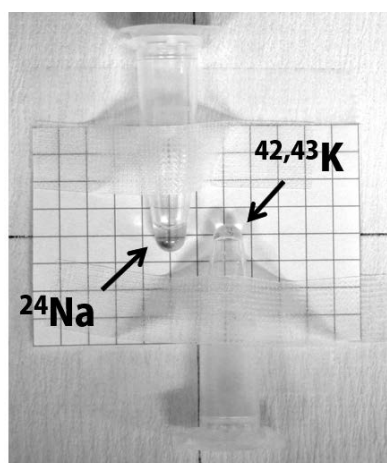


Fig. 1. RI solutions of ^{24}Na and $^{42,43}\text{K}$ collected in micro tubes. The gap between the tips of the micro tubes was 1 cm.

† Presented at The 14th Annual meeting of Japanese society for molecular imaging, May 23–24, (2019)

*¹ RIKEN Center for Biosystems Dynamics Research

*² Compass to Healthy Life Research Complex Program, RIKEN

*³ RIKEN Nishina Center for Accelerator-Based Science

*⁴ RIKEN Center for Life Science Technologies

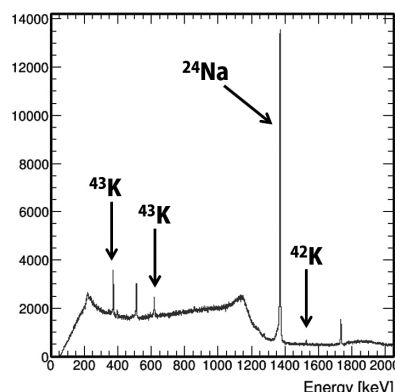


Fig. 2. Gamma-ray energy spectrum measured by GREI.

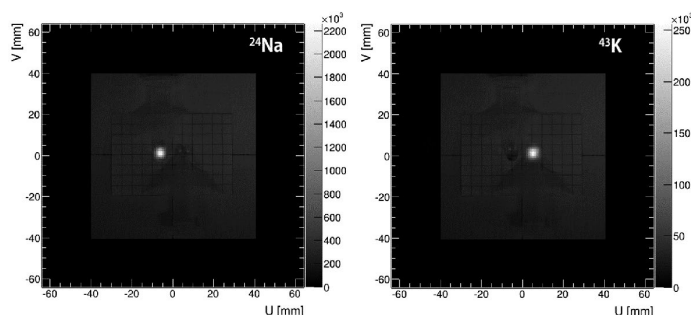


Fig. 3. Gamma-ray images of ^{24}Na and $^{42,43}\text{K}$ simultaneously measured by GREI.

without arranging a large number of sensors around the imaging target or rotating the imaging head.

Since FY2018, the use of these nuclides has been made possible at the Molecular Imaging Facility at RIKEN Kobe campus, and a series of protocols for manufacturing and preparing ^{24}Na , ^{42}K , and ^{43}K in-house and conducting GREI imaging experiments have been established. To demonstrate the feasibility of simultaneous imaging of these nuclides by GREI, we performed a test imaging experiment by using RI solutions.

RI solutions of ^{24}Na and $^{42,43}\text{K}$ were collected at the tips of two micro tubes separately (Fig. 1). ^{42}K and ^{43}K were not separated, because they are chemically identical. The radio-activities of ^{24}Na , ^{42}K , and ^{43}K were 2.1 MBq, 910 kBq, and 76 kBq, respectively. The tubes were placed under the GREI imaging head 3.5 cm away from the front detector. The GREI imaging was performed for 1 h.

Figure 2 shows the gamma-ray spectrum obtained in the GREI imaging experiment. We were able to clearly identify the gamma-ray peaks of each nuclide. By setting energy windows on the peaks of each nuclide, we performed three-dimensional image reconstruction on the recorded data. As a result, we succeeded in taking the images of ^{24}Na and $^{42,43}\text{K}$ simultaneously.

References

- 1) S. Motomura *et al.*, *J. Anal. At. Spectrom.* **28**, 934 (2013).
- 2) T. Ida *et al.*, *Jpn. J. Appl. Phys.* **58**, 016002 (2019).

Research progress on double-photon-emission coincidence imaging with cascade gamma-ray-emitting nuclide

M. Uenomachi,^{*1} Z. Zhong,^{*1} K. Shimazoe,^{*1} H. Takahashi,^{*1} D. Mori,^{*2} T. Yokokita,^{*2} Y. Komori,^{*2} and H. Haba^{*2}

Positron emission tomography (PET) and single-photon-emission computed tomography (SPECT) are important nuclear medicine modalities that have been widely used for clinical diagnosis. PET detects the coincidence of annihilation gamma-rays from a positron-emitting nuclide. SPECT uses a collimator to restrict the incident direction of gamma-rays. Therefore, nuclides for PET imaging are limited to positron-emitting nuclides and there is a theoretical spatial resolution limit derived from the positron range. The sensitivity of SPECT is relatively low because of its use of a collimator, and it is difficult to image multiple nuclides simultaneously. To realize highly sensitive multi-nuclide imaging, we proposed a double-photon-emission coincidence imaging method.¹⁾

For SPECT imaging, single-photon-emitting nuclides are preferable. Among them, there are nuclides that emit two photons in cascade decay. For example, ¹¹¹In, which is widely used in SPECT imaging, emits two gamma-rays at 171 keV and 245 keV. Using two gamma-rays, the position of nuclides can be determined with higher sensitivity. One of the methods using two gamma-rays is double-photon-emission computed tomography (DPECT).^{1,2)} This method can drastically increase the signal-to-noise (SN) ratio of Compton imaging³⁾ by coincidence detection for cascade gamma-rays with multiple Compton cameras, which is based on Compton scattering kinetics. Conventional Compton imaging can obtain only the angle information of incident gamma-rays, and drawing many Compton cones results in a low SN ratio. However, DPECT can limit the nuclide position from a Compton cone to an overlap of two Compton cones. We previously demonstrated DPECT using ¹³⁴Cs and ⁶⁰Co for application to fuel debris imaging²⁾ with GAGG-SiPM Compton cameras.⁴⁾ In the present research, we developed small GAGG-SiPM Compton cameras for application to nuclear medicine and demonstrated double-photon-emission coincidence methods using ⁴³K, which is one of the promising double-photon-emitting nuclides because of its short decay time and suitable gamma-ray

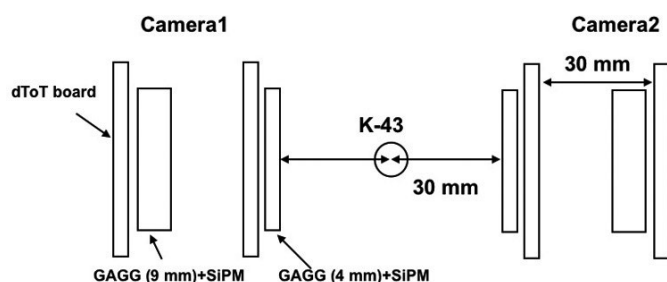


Fig. 1. Experimental setup of DPECT for ⁴³K.

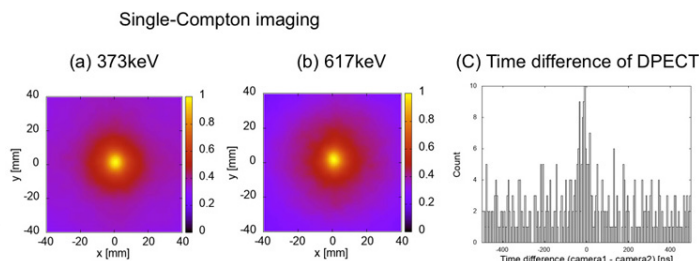


Fig. 2. Single-photon Compton imaging at (a) 373 keV and (b) 617 keV. (c) Time difference of DPECT (camera1-camera2).

energies.

⁴³K was produced in the ⁴³Ca(*d*, 2*p*)⁴³K reaction at the RIKEN AVF cyclotron. After chemical separation, 2 (6) MBq of ⁴³K in 6 (18) μ L H₂O was placed in a vial as a gamma-ray source. Figure 1 shows the experimental setup of DPECT for ⁴³K. ⁴³K mainly emits cascade gamma-rays at 617 keV and 373 keV. A Compton camera consists of a scatter layer and an absorber layer. Each layer consists of an 8 \times 8 GAGG array coupled to an 8 \times 8 SiPM array. The thicknesses of the GAGG arrays is 4 mm and 9 mm for scatterers and absorbers, respectively. The pixel size of the GAGG arrays is 2.5 mm \times 2.5 mm, and each crystal is separated by BaSO₄ reflectors. The signal from SiPM is processed by the dynamic time over threshold (dToT) method⁵⁾ to extract the energy. The distance from the ⁴³K source to a scatterer was 30 mm, and two Compton cameras were placed in opposite directions.

Figures 2(a) and 2(b) show images reconstructed through back projection. Figure 2(a) shows a single-photon Compton image at 373 keV and (b) shows an image at 617 keV. We succeeded in obtaining images of single-photon Compton imaging with our small Compton cameras. Figure 2(c) shows a histogram of time difference of double Compton coincidence events at 373 keV and 617 keV. However, the number of coincidence events that can be used for DPECT with Compton scattering energy windows was only 12. After this experiment, we increased the number of Compton cameras to detect double Compton coincident events efficiently and repeated the experiment with eight modules. The result is under analysis.

References

- 1) Y. Yoshihara *et al.*, Nucl. Instrum. Methods Phys. Res. A **873**, 51 (2017).
- 2) M. Uenomachi *et al.*, Nucl. Instrum. Methods Phys. Res. A **954**, 161682 (2020).
- 3) R. W. Todd *et al.*, Nature **251**, 132 (1974).
- 4) J. Jiang *et al.*, J. Nucl. Sci. Technol. **53**, 1067 (2015).
- 5) K. Shimazoe *et al.*, IEEE Trans. Nucl. Sci. **59**, 3213 (2012).

^{*1} Department of Engineering, The University of Tokyo

^{*2} RIKEN Nishina Center

Production of Np-236 in the $^{232}\text{Th} + ^7\text{Li}$ reaction for standard material in accelerator mass spectrometry

Y. Hayakawa,^{*1,*2} A. Yokoyama,^{*1,*3} A. Sakaguchi,^{*1,*4} K. Teranishi,^{*1,*2} R. Morita,^{*1,*2} N. Matsumura,^{*1,*3}
A. Nakajima,^{*1,*4} D. Mori,^{*1} Y. Komori,^{*1} T. Yokokita,^{*1} Y. Wang,^{*1} and H. Haba^{*1}

Neptunium-236 can be a useful tracer in the determination of ^{237}Np , an isotope of minor-actinide Np, which exists in tiny quantities in the environment owing to its release from nuclear facilities. Such determination is of practical use in various earth science fields such as surface material circulation and environmental pollution assessment.¹⁾ The measurement of ^{237}Np is expected to be quantified by accelerator mass spectrometry (AMS), although an internal standard method for Np needs an appropriate spike. Tracers for several elements are available now, but the spike for neptunium has not been developed yet. We aim to devise an efficient method for the production of ^{236}Np in the ground state of half-life 1.54×10^5 y as a candidate for the spike nuclide.

In this study, ^{236}Np tracer production was implemented in the reaction of $^{232}\text{Th} + ^7\text{Li}$ to measure ^{237}Np . In the beginning of the project, the excitation functions of Np isotopes and by-products were measured using target stacks of Th metal foils. We irradiated the targets with 42 MeV ^7Li ions from the RIKEN AVF cyclotron while integrating the beam current with a Faraday cup in the irradiation course. Chemical procedures were performed to isolate Np atoms from the target. The target material was dissolved in a mixed acidic solution of 0.027 M HF and 3 M HNO_3 , and the sample was dried by heating. Then, the residue was adjusted to 4 mL of 3 M HNO_3 solution, reduced with ascorbic acid and Fe

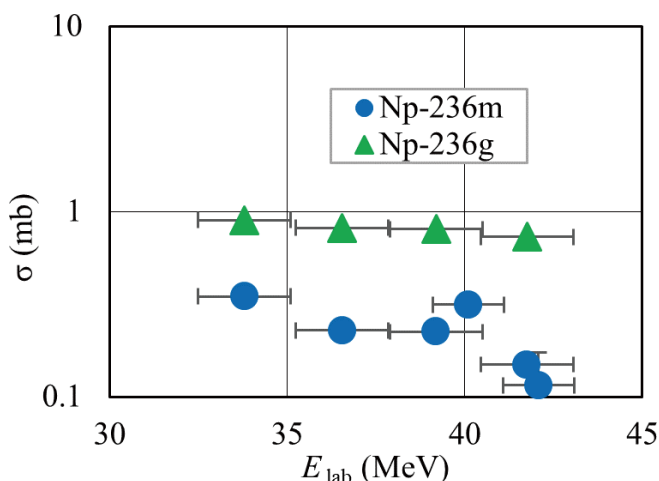


Fig. 1. Excitation functions of the production of Np-236m and Np-236g isomers.

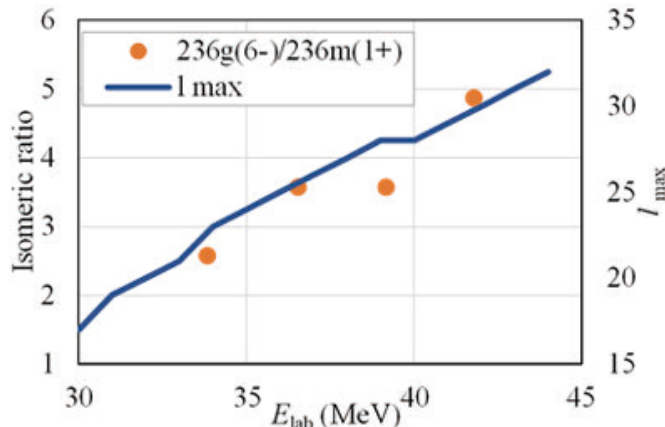


Fig. 2. Isomeric ratios of ^{236}Np and angular momenta transferred into targets.

ions and introduced into a TEVA resin column; subsequently, it was treated with 3 M HNO_3 and 10 M HCl for purification and finally with 0.1 M HCl for the elution of Np. To remove Pa, another process with a TK 400 column was performed. To determine the yields of Np isotopes and by-products, γ -ray spectrometry was conducted for the effluents with a Ge detector. For the Np-236g measurement, samples for AMS and ICP-MS were prepared through purification with UTEVA resin after waiting for Np-236m to decay out, and they were brought to the VERA facility in the University of Vienna, with which this project is in collaboration.

Figure 1 shows the excitation functions of the production of Np-236m and Np-236g. The yield in the ground state (6-) was found to be larger than that in the excited state (1+) in the studied energy range, although the former data are preliminarily taken.

Isomeric yields of the product are thought to be correlated with angular momentum in the composite system if their spins substantially differ from each other. The maximum orbital angular momenta transferred to the nuclear system were estimated using the ALICE code²⁾ and compared to the isomeric ratios of ^{236}Np in Fig. 2. The figure shows the correlation of observation to angular momenta. The analysis of the result is in progress, and additional experiments including mass spectrometry are in planning to confirm the precision and reproducibility of the data.

*1 RIKEN Nishina Center

*2 Graduate School of Natural Science and Technology, Kanazawa University

*3 Institute and College of Science and Engineering, Kanazawa University

*4 Center for Research in Isotopes and Environmental Dynamics, University of Tsukuba

References

- 1) W. Rund, G. S. Goff, in *Radionuclides in the Environment*, edited by D. A. Atwood (Wiley, 2013).
- 2) M. Blann, "CODE ALICE/85/300," UCID-20169 (September 1984).

Excitation function measurement of the $\text{Tl}(d, \alpha)^{203}\text{Hg}$ reaction for carrier-free ^{203}Hg tracer production

Y. Takahashi,^{*1} S. Goto,^{*1} D. Mori,^{*2} T. Yokokita,^{*2} Y. Komori,^{*2} Y. Wang,^{*2} and H. Haba^{*2}

The influence of relativistic effects on orbital electrons is notable in the superheavy elements with the atomic number $Z \geq 104$. It is predicted that the influence is maximum in the group-12 element $_{112}\text{Cn}$ according to a theoretical calculation.¹⁾ In order to confirm this prediction, we are planning chemical experiments on Hg as basic research for a chemical investigation of Cn. ^{203}Hg ($T_{1/2} = 46.594$ d) is a suitable radionuclide to conduct off-line experiments because it has a relatively long half-life and emits measurable γ -rays. A carrier-free ^{203}Hg tracer can be produced with the $^{\text{nat}}\text{Tl} + d$ reaction, but only the excitation functions of Pb and Tl isotopes obtained with that reaction were measured in previous studies.²⁻⁴⁾ In this study, we measured the excitation function of the $^{205}\text{Tl}(d, \alpha)^{203}\text{Hg}$ reaction.

The production cross sections of ^{203}Hg were measured by means of a stacked foil technique. $^{\text{nat}}\text{Tl}_2\text{O}_3$ pellets (96.5 mg cm^{-2} thick) were covered with 0.01 -mm-thick Al foil. These pellets and $^{\text{nat}}\text{Ti}$ foils (0.02 mm thick) were alternately stacked as a target. The $^{\text{nat}}\text{Ti}$ foils were used for monitoring the beam current and as an energy degrader. The target, fixed in a target holder, was irradiated with a 24 -MeV deuteron beam supplied from the RIKEN AVF cyclotron for 2.5 h in He gas. The beam current was measured with a Faraday cup connected to the target holder, and the average current was about 90 nA. The deuteron energies in the individual pellets and foils were calculated with LISE++ ver. 11.2.⁵⁾ After irradiation, the produced nuclides were identified and quantified by γ -ray spectrometry using Ge detectors.

Table 1 lists the identified nuclides and their nuclear data.

When each of ^{203}Pb and ^{203}Hg disintegrates, γ -rays of 279 keV are emitted. The radioactivity of each nu-

Table 1. Measured nuclides and their nuclear data.⁶⁻⁹⁾

Nuclide	Half-life	E_γ/keV	$I_\gamma/\%$
$^{204\text{m}}\text{Pb}$	66.93 min	899.15	99.144
^{203}Pb	51.92 h	279.1952	80.9
$^{202\text{m}}\text{Pb}$	3.54 h	422.12	84.108
$^{201\text{g}}\text{Pb}$	9.33 h	311.15	76.90
^{202}Tl	12.31 d	439.51	91.5
^{201}Tl	3.0421 d	167.43	10.00
^{203}Hg	46.594 d	279.1952	81.56

^{*1} Graduate school of science and technology, Niigata University

^{*2} RIKEN Nishina Center

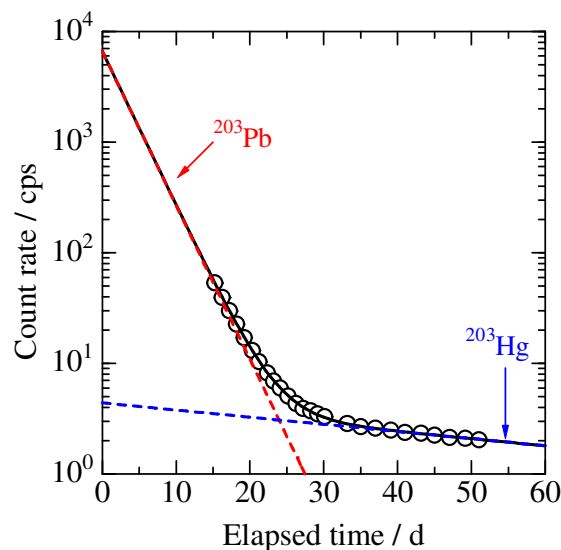


Fig. 1. Count rates of the 279 keV peak for one of the pellets. The solid curve indicates a fit of the experimental values based on Eq. (1). The dashed lines indicate the components of ^{203}Pb and ^{203}Hg .

clides can be determined by analyzing the change of the count rate of the 279 keV peak against elapsed time because their half-lives are quite different. The obtained count rates of the 279 keV peak are shown in Fig. 1.

The data in Fig. 1 can be fitted with the following equation:

$$C_{\text{tot}} = C_{0,\text{Pb}} \exp(-\lambda_{\text{Pb}} t) + C_{0,\text{Hg}} \exp(-\lambda_{\text{Hg}} t). \quad (1)$$

where $C_{0,X}$ and λ_X are the initial count rates and decay constant of a nuclide X of interest, respectively, and t is the elapsed time from the end of bombardment. The result of this analysis indicated that ^{203}Hg was certainly produced. The analysis is performed for all Tl pellets, and the determination of production cross sections of ^{203}Hg is in progress.

References

- 1) A. Türler *et al.*, Chem. Rev. **113**, 1237 (2013).
- 2) R. Adam Rebeles *et al.*, Nucl. Instrum. Methods Phys. Res. B **288**, 94 (2012).
- 3) R. Adam Rebeles *et al.*, J. Korean Phys. Soc. **59**, 1975 (2011).
- 4) J. W. Blue *et al.*, J. Med. Phys. **5**, 532 (1978).
- 5) O. B. Tarasov *et al.*, Nucl. Instrum. Methods Phys. Res. B **266**, 4657 (2008).
- 6) C. J. Chiara *et al.*, Nuclear Data Sheets **111**, 141 (2010).
- 7) F. G. Kondev, Nuclear Data Sheets **105**, 1 (2005).
- 8) S. Zhu *et al.*, Nuclear Data Sheets **109**, 699 (2008).
- 9) F. G. Kondev, Nuclear Data Sheets **108**, 365 (2007).

Activation cross sections of alpha-induced reactions on natural tungsten for ^{186}Re and ^{188}Re production

N. Ukon,^{*1,*2} M. Aikawa,^{*3,*4,*2} M. Saito,^{*4,*2} T. Murata,^{*4,*2} Y. Komori,^{*2} H. Haba,^{*2} and S. Takács^{*5}

Radioisotopes (RI) are used for diagnosis and therapy in nuclear medicine. ^{186}Re is a β^- emitter with a half-life of 3.72 days. Its maximum β^- energy of 1.07 MeV has average penetration ranges of 1.1 mm in soft tissue and 0.5 mm in bone. It decays with the emission of γ -rays at 137 keV ($I_\gamma = 9.47\%$). ^{188}Re is also a β^- emitter with a half-life of 17 h and a maximum β^- energy of 2.12 MeV, and it decays with γ -ray emission at 155 keV ($I_\gamma = 15.61\%$).^{1,2} Both isotopes can be used for theranostics investigations (therapy and diagnosis). We focused on processes to produce $^{186,188}\text{Re}$ through alpha-induced reactions on natural tungsten because only one previous work with one data point for both isotopes has been reported at an incident energy of 43 MeV.³ Therefore, we investigated the excitation function of the $^{\text{nat}}\text{W}(\alpha, x)^{186,188}\text{Re}$ reactions up to 51 MeV.

The excitation functions of the $^{\text{nat}}\text{W}(\alpha, x)^{186,188}\text{Re}$ reactions were measured using the stacked-foil technique, activation method, and high-resolution γ -ray spectroscopy. $^{\text{nat}}\text{W}$ foils (purity: 99%, Goodfellow Co., Ltd., UK) were stacked with $^{\text{nat}}\text{Ti}$ foils (purity: 99%, Goodfellow Co., Ltd., UK) for monitoring the beam parameters and degrading the beam energy. The average thicknesses of the W and Ti foils were 29.99 and 2.29 mg/cm², respectively. The irradiation was performed at the RIKEN AVF cyclotron. The target was irradiated by an alpha-particle beam of 51 MeV with an average intensity of 189.1 pA for 2 h. The incident beam energy was determined by the time-of-flight method using plastic scintillator monitors.⁴ The energy loss of the beam in the stacked target was calculated using the SRIM code available online.⁵ The γ -ray spectra of the activated foils were measured using a high-purity germanium (HPGe) detector. Nuclear decay data were taken from the online NuDat 2.7 database.⁶

From the net peak areas of the 137.16- and 155.04-keV γ -rays, the activation cross sections for the $^{\text{nat}}\text{W}(\alpha, x)^{186,188}\text{Re}$ reaction were deduced using the standard activation formula

$$\sigma = \frac{T_\gamma \lambda}{\varepsilon_d \varepsilon_\gamma \varepsilon_t N_t N_b (1 - e^{-\lambda t_b}) e^{-\lambda t} c (1 - e^{-\lambda t_m})},$$

where N_t denotes the surface density of target atoms, N_b the number of bombarding particles per unit time,

*1 Advanced Clinical Research Center, Fukushima Medical University

*2 RIKEN Nishina Center

*3 Faculty of Science, Hokkaido University

*4 Graduate School of Biomedical Science and Engineering, Hokkaido University

*5 Institute for Nuclear Research, Debrecen, (ATOMKI)

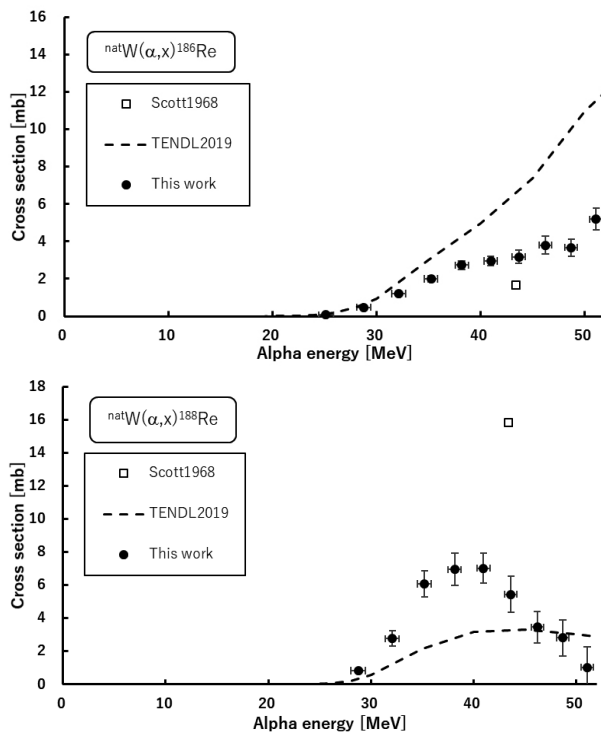


Fig. 1. Excitation functions of the $^{\text{nat}}\text{W}(\alpha, x)^{186,188}\text{Re}$ reactions. The results are compared with a previous study³⁾ and TENDL-2019.⁷⁾

T_γ the number of counts in the photo-peak, ε_d the detector efficiency, ε_γ the γ -ray abundances, ε_t the measurement dead time, λ the decay constant, t_b the bombarding time, t_c the cooling time, and t_m the acquisition time.

We found that the only previous data point obtained by Scott *et al.*³⁾ for the $^{\text{nat}}\text{W}(\alpha, x)^{186}\text{Re}$ reaction is approximately half of our data. In contrast, for the $^{\text{nat}}\text{W}(\alpha, x)^{188}\text{Re}$ reactions, the only data point of Scott *et al.*³⁾ is more than double our result. The TENDL-2019⁷⁾ predictions deviate considerably from the experimental data.

References

- 1) A. M. Denis-Bacelar *et al.*, Eur. J. Nucl. Med. Mol. Imaging **44**, 620 (2017).
- 2) I. G. Finlay *et al.*, Lancet Oncol. **6**, 392 (2005).
- 3) N. E. Scott *et al.*, Nucl. Phys. A **119**, 131 (1968).
- 4) T. Watanabe *et al.*, Proc. 5th Int. Part. Accel. Conf., (2014), p. 3566.
- 5) J. F. Ziegler *et al.*, SRIM: the Stopping and Range of Ions in Matter, <http://www.srim.org/>.
- 6) National Nuclear Data Center: the NuDat2 database, <http://www.nndc.bnl.gov/nudat2/>.
- 7) A. J. Koning *et al.*, TENDL-2019 nuclear data library, https://tendl.web.psi.ch/tendl_2019/tendl2019.html

Activation cross sections of alpha particle-induced reactions on natural hafnium up to 50 MeV[†]

S. Takács,^{*1} M. Aikawa,^{*2,*3,*4} M. Saito,^{*2,*3} T. Murata,^{*2,*3} N. Ukon,^{*5,*3} Y. Komori,^{*3} and H. Haba^{*3}

The $^{178\text{m}}\text{Ta}$ ($T_{1/2} = 9.31$ min) radioisotope is suitable for therapeutic applications owing to the high ionization capability of $K_{\alpha 1}$ and $K_{\alpha 2}$ radiation it emits (60%). The distribution of the injected isotope in the human body can be tracked using a positron emission tomography (PET) camera by utilizing its partial positron decay mode (total β^+ decay: 1.24%). An alternative production route for the medically interesting $^{178\text{m}}\text{Ta}$ radioisotope is the $^{178}\text{W}/^{178\text{m}}\text{Ta}$ generator system. To explore this possibility, activation cross sections of the $^{\text{nat}}\text{Hf}(\alpha, x)^{178}\text{W}$ ($T_{1/2} = 21.6$ d) reaction were investigated up to 50 MeV.

The experiment was performed at the RIKEN AVF cyclotron. The stacked-foil activation technique and high-resolution γ -ray spectrometry were applied. The stacked-foil target was assembled using pure metallic foils of $^{\text{nat}}\text{Hf}$ and $^{\text{nat}}\text{Ti}$ from Nilaco Corp., Japan with average thicknesses of 10.34 and 5.34 μm , respectively. Both the Hf and the Ti foils were inserted into the stack in pairs to compensate for the activity loss due to the recoil effect. The target was irradiated with a 51.0-MeV α -particle beam for 1 h. The incident beam energy was measured using the time-of-flight method.¹⁾ The energy loss of the bombarding alpha particles was calculated using the semi-empirical formula of Andersen and Ziegler.²⁾ The average beam intensity measured using a Faraday cup was cross checked with the $^{\text{nat}}\text{Ti}(\alpha, x)^{51}\text{Cr}$ monitor reaction. The experimentally determined cross sections for the $^{\text{nat}}\text{Ti}(\alpha, x)^{51}\text{Cr}$ monitor reaction agreed perfectly with their recommended value³⁾; therefore, the primary beam parameters were accepted in further data analysis. The γ -ray spectra of each irradiated foil were recorded using a high-resolution high-purity germanium (HPGE) detector without chemical separation. Five series of gamma-ray measurements were performed with increasing cooling times to observe the decay of the reaction products. Reaction and decay data for the data analysis were taken from the NuDat 2.7 database.⁴⁾

The production of tungsten isotopes from ^{173}W to ^{184}W was possible with the used alpha-particle parameters on a natural hafnium target. Due to limitation of the used experimental technique and the decay parameters of those isotopes cross sections were derived only for the $^{176}, ^{177}, ^{178}\text{W}$ radionuclides in our experiments. As the radionuclide ^{178}W can be produced on all the six stable isotopes of hafnium with the applied 51 MeV

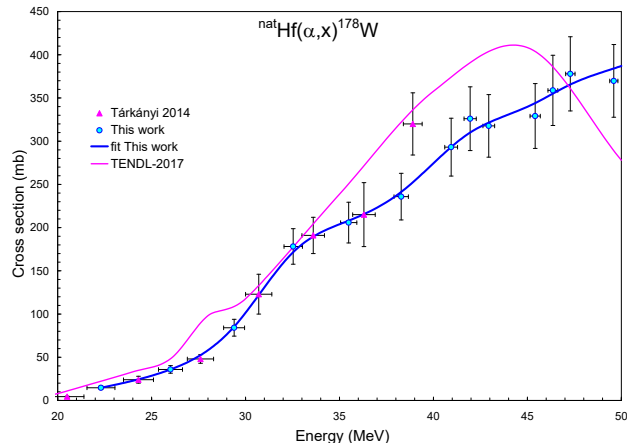


Fig. 1. Excitation function of the $^{\text{nat}}\text{Hf}(\alpha, x)^{178}\text{W}$ reaction in comparison with previous experimental data and the result of the model calculation taken from the TENDL-2017 database.⁵⁾

alpha-particle beam, the resulting excitation function has a complex shape. The practical threshold energy of this process is approximately 20 MeV because the very low yield of the $^{174}\text{Hf}(\alpha, \gamma)^{178}\text{W}$ reaction did not provide a measurable contribution. Since no gamma emission follows the decay of ^{178}W the $E_{\gamma} = 1340.85$ and $E_{\gamma} = 1350.55$ keV gamma lines of $^{178\text{m}}\text{Ta}$ and its decay product were used in the data analysis. The applied cooling time ensured the complete decay of the directly produced $^{178\text{m}}\text{Ta}$ and equilibrium between the decaying ^{178}W and $^{178\text{m}}\text{Ta}$.

The experimental data are in good agreement with each other, while the TENDL-2017⁵⁾ prediction follows the tendency of the experimental data up to 44 MeV.

In addition to the obtained cross sections of the $^{\text{nat}}\text{Hf}(\alpha, x)^{178}\text{W}$ reaction, cross sections for the $^{\text{nat}}\text{Hf}(\alpha, x)^{176}, ^{177}\text{W}$, $^{\text{nat}}\text{Hf}(\alpha, x)^{175}, ^{176}, ^{177}, ^{178\text{g}}, ^{180\text{g}}, ^{182\text{g}}, ^{183}\text{Ta}$, and $^{\text{nat}}\text{Hf}(\alpha, x)^{173}, ^{175}, ^{179\text{m}2}, ^{180\text{m}}, ^{181}\text{Hf}$ processes were determined. The results can contribute to develop the $^{178}\text{W}/^{178\text{m}}\text{Ta}$ generator system and to estimate the expected radio-impurity due to the co-production of other radionuclides.

This work was conducted in the framework of a Japanese - Hungarian Research Cooperative Program between JSPS and HAS.

References

- 1) T. Watanabe *et al.*, Proc. 5th Int. Part. Accel. Conf. (IPAC2014), (2014), p. 3566.
- 2) H. H. Andersen, J. F. Ziegler, *Helium Stopping Powers and Ranges in all Elements*, (Pergamon, Oxford, 1997).
- 3) A. Hermanne *et al.*, Nucl. Data Sheets **148**, 338 (2018).
- 4) National Nuclear Data Center, The NuDat 2.7 database, <http://www.nndc.bnl.gov/nudat2/>.
- 5) A. J. Koning *et al.*, Nucl. Data Sheets **155**, 1 (2019).

[†] Condensed from the article in Nucl. Instrum. Methods Phys. Res. B **459**, 50 (2019)

^{*1} Institute for Nuclear Research, Hungarian Academy of Sciences

^{*2} Graduate School of Biomedical Science and Engineering, Hokkaido University

^{*3} RIKEN Nishina Center

^{*4} Faculty of Science, Hokkaido University

^{*5} Advanced Clinical Research Center, Fukushima Medical University

Activation cross sections of alpha-induced reactions on natural ytterbium up to 50 MeV[†]

M. Saito,^{*1,*2} M. Aikawa,^{*1,*2,*3} T. Murata,^{*1,*2} N. Ukon,^{*4,*2} Y. Komori,^{*2} H. Haba,^{*2} and S. Takács^{*5}

Many radioisotopes can be used for medical diagnosis and therapy. One candidate radioisotope is $^{177\text{g}}\text{Lu}$ ($T_{1/2} = 6.647$ d).¹⁾ This radioisotope decays with emissions of a β -particle and γ -rays, which are useful for therapy and diagnosis. For practical use of $^{177\text{g}}\text{Lu}$, the best production reaction should be selected. Among the possible production reactions, we focused on the $^{\text{nat}}\text{Yb}(\alpha, x)^{177\text{g}}\text{Lu}$ reaction in this study. Only one experimental study on this reaction was found in a literature survey.²⁾ The study reported the production cross sections of $^{177\text{g}}\text{Lu}$ up to 37.7 MeV. We investigated the cross sections of the reaction up to 50 MeV.

The experiment was performed at the RIKEN AVF cyclotron. The stacked foil activation method and high resolution γ -ray spectrometry were used. The stacked target consisted of pure metallic foils of $^{\text{nat}}\text{Yb}$ (99% purity, Goodfellow Co., Ltd., UK) and $^{\text{nat}}\text{Ti}$ (99.6% purity, Nilaco Corp., Japan). The sizes and weights of the Yb (3 pieces of 25×25 mm²) and Ti (1 piece of 50×100 mm²) foils were measured for determination of the target thicknesses. The average thicknesses of the foils were found to be 16.60, 16.32, and 17.11 mg/cm² for the Yb foils and 2.40 mg/cm² for the Ti foil. The foils were cut into small pieces of 8×8 mm² to fit a target holder that also served as a Faraday cup. The target was irradiated with a 51.0-MeV α beam for 2 hours. The incident beam energy was measured by the time-of-flight method.³⁾ Energy degradation in the target was calculated by the SRIM code.⁴⁾ The average beam intensity measured by the Faraday cup was 414 nA. The γ -ray spectra of each irradiated foil were measured by a high-resolution HPGe detector without chemical separation. Reaction and decay data were taken from NuDat 2.7 for the data analysis.⁵⁾

The excitation function of the $^{\text{nat}}\text{Ti}(\alpha, x)^{51}\text{Cr}$ monitor reaction was derived from measurements of the 320.08-keV γ rays emitted after decay of ^{51}Cr ($T_{1/2} = 27.7025$ d). The derived cross sections were compared with the IAEA recommended values.⁶⁾ According to the comparison, the adopted beam intensity was 379 nA, a decrease of 8.4% from the measured value.

Production cross sections of $^{177\text{g}}\text{Lu}$ ($T_{1/2} = 6.647$ d) were derived from measurements of the γ line at 208.37 keV ($I_{\gamma} = 10.36\%$) after a cooling time of 3.1

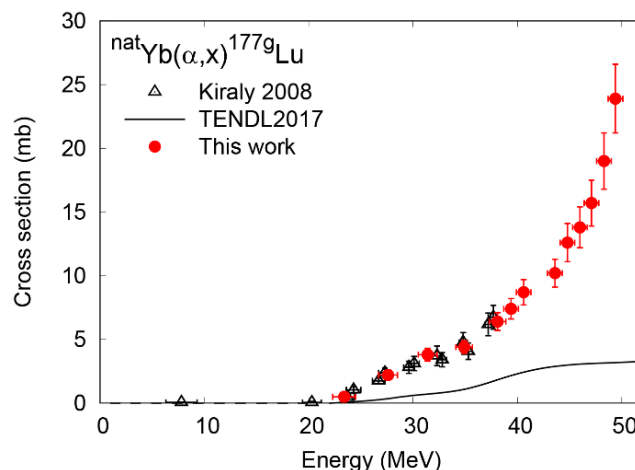


Fig. 1. Excitation function of the $^{\text{nat}}\text{Yb}(\alpha, x)^{177\text{g}}\text{Lu}$ reaction in comparison with previous experimental data²⁾ and the TENDL-2017 data prediction.⁷⁾

days. Its parent radionuclide ^{177}Yb ($T_{1/2} = 1.911$ h) decayed during the cooling time. The contribution of $^{177\text{m}}\text{Lu}$ ($T_{1/2} = 160.44$ d) was estimated using the measurement series after a cooling time of 143 days and was found to be negligibly small. The cumulative cross sections of the $^{\text{nat}}\text{Yb}(\alpha, x)^{177\text{g}}\text{Lu}$ reaction were derived and compared with the previous study²⁾ and the TENDL-2017 data,⁷⁾ as shown in Fig. 1. The experimental data are in good agreement with each other, but the TENDL-2017 data are much lower than the previous and our experimental ones.

In addition to $^{177\text{g}}\text{Lu}$, production cross sections of co-produced radionuclides $^{170, 171, 172, 173, 175}\text{Hf}$, $^{171\text{g}, 172\text{g}, 173}\text{Lu}$, and $^{169\text{g}}\text{Yb}$ were determined. The results are useful to evaluate radionuclidic impurities of $^{177\text{g}}\text{Lu}$ for its practical application.

This work was supported by Hokkaido University Nishino School Advanced Program Research Grant and JSPS KAKENHI Grant Number 17K07004.

References

- 1) K. Rahbar *et al.*, *J. Nucl. Med.* **58**, 85 (2017).
- 2) B. Király *et al.*, *Nucl. Instrum. Methods Phys. Res. B* **266**, 3919 (2008).
- 3) T. Watanabe *et al.*, *Proc. 5th Int. Part. Accel. Conf. (IPAC2014)*, (2014) p. 3566.
- 4) J. F. Ziegler *et al.*, *Nucl. Instrum. Methods Phys. Res. B* **268**, 1818 (2010).
- 5) National Nuclear Data Center, The NuDat 2.7 database, <http://www.nndc.bnl.gov/nudat2/>.
- 6) A. Hermanne *et al.*, *Nucl. Data Sheets* **148**, 338 (2018).
- 7) A. J. Koning *et al.*, *Nucl. Data Sheets* **155**, 1 (2019).

[†] Condensed from the article in *Nucl. Instrum. Methods Phys. Res. B* **453**, 15 (2019)

^{*1} Graduate School of Biomedical Science and Engineering, Hokkaido University

^{*2} RIKEN Nishina Center

^{*3} Faculty of Science, Hokkaido University

^{*4} Advanced Clinical Research Center, Fukushima Medical University

^{*5} Institute for Nuclear Research

Measurement of excitation functions for $^{165}\text{Ho}(\alpha, xn)^{165-168}\text{Tm}$ reactions

A. R. Usman,^{*1,*2} M. U. Khandaker,^{*1,*3} H. Haba,^{*1} N. Otuka,^{*1,*4} and M. Murakami^{*1}

Currently, therapeutic radioisotopes are predominantly produced via the (n, γ) reactions routes. However, charged-particle-induced nuclear reactions serve as good alternatives to produce these radioisotopes with high specific activities. The irradiation of holmium (Ho) with alpha-particle beams leads to the production of several important thulium (Tm) radioisotopes for applications in nuclear medicine. In addition to the use of ^{167}Tm as a skeletal imaging agent, the radioisotope was reported to be useful for studying bone and tumour.¹⁾ Furthermore, the Auger electrons as well as low-energy γ - and X-rays emitted from the moderately long-lived ^{167}Tm (9.25 days) are suitable for radiotherapy.^{2,3)} On the other hand, ^{165}Tm (1.25 days) has been considered as a potential replacement of the popular ^{167}Tm owing to its desirable decay characteristics.

A comprehensive analysis of all previous measurements of alpha-particle-induced reactions on holmium shows large and unacceptable discrepancies. In this work, new measurements have therefore been made with a relatively large number of holmium foils to explore the excitation functions at various energy points.

The overall procedure employed in the present work is similar to that of our previous studies.⁴⁻⁶⁾ The stacked target foils were irradiated with a beam of alpha-particles, and the foils were subjected to gamma-ray spectrometry to determine the production cross sections. Thin metallic holmium foils (purity: 99%, thickness: 12.29 μm , supplier: Goodfellow, UK) served as the target. There is only one isotope, ^{165}Ho (100%), in natural holmium. Natural copper foils and natural titanium foils served as degraders of the beam energy and were used for

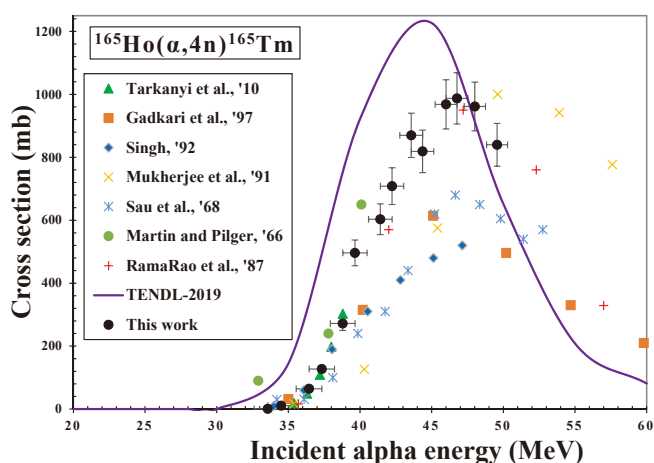


Fig. 1. Excitation function of the $^{165}\text{Ho}(\alpha, 4n)^{165}\text{Tm}$ reaction.

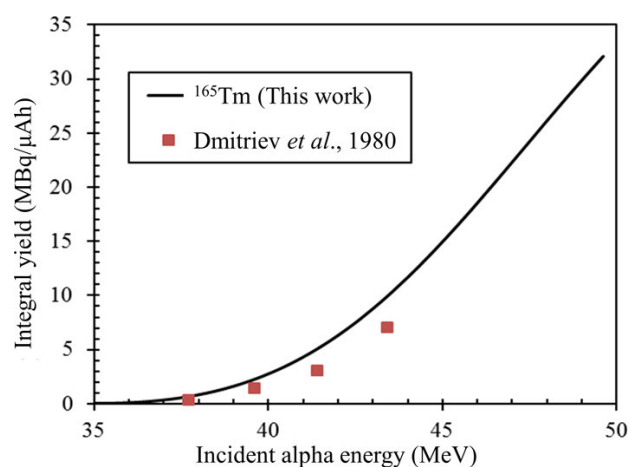


Fig. 2. Integral thick target yield for ^{165}Tm .

monitoring of beam the intensity. A 50.4 MeV beam extracted from the RIKEN AVF cyclotron was focused on target foils of 9-mm diameter. The stack was irradiated for 2.0 h with a beam intensity of 5.45×10^{11} alphas/s. The beam intensity was determined from the activities of ^{51}Cr produced from the $^{nat}\text{Ti}(\alpha, x)^{51}\text{Cr}$ monitor reaction, for which the cross section recommended by the IAEA ($\sigma = 26.4$ mb at $E_\alpha = 50$ MeV) was adopted. The measured production cross sections were calculated using the well-known activation equation.⁶⁾

Owing to space constraints, only the excitation function of ^{165}Tm and its thick target yield are presented in this report. ^{165}Tm is populated through the $^{165}\text{Ho}(\alpha, 4n)^{165}\text{Tm}$ reaction. ^{165}Tm (30.06 hours) decays via the EC + β^+ (100%) process to ^{165}Er . The cross sections of this radioisotope were measured via its relatively intense gamma line of $E_\gamma = 242.917$ keV ($I_\gamma = 35.5\%$).

The physical thick target yield has been calculated for the investigated radioisotope using the interpolation of the measured production cross sections by spline fits as well as the stopping power calculated using SRIM code.

In conclusion, new cross sections have been investigated for the $^{165}\text{Ho}(\alpha, 4n)^{165}\text{Tm}$, $^{165}\text{Ho}(\alpha, 3n)^{166}\text{Tm}$, $^{165}\text{Ho}(\alpha, 2n)^{167}\text{Tm}$, and $^{165}\text{Ho}(\alpha, n)^{168}\text{Tm}$ reactions, but in this short report, only the results for ^{165}Tm have been presented.

References

- 1) R. Chandra *et al.*, Radiol. **100**, 687 (1971).
- 2) F. Tárkányi *et al.*, Appl. Radiat. Isot. **68**, 404 (2010).
- 3) M. Sadeghi *et al.*, J. Radioanal. Nucl. Chem. **291**, 731 (2012).
- 4) A. R. Usman *et al.*, Nucl. Instrum. Methods Phys. Res. B **368**, 112 (2016).
- 5) A. R. Usman *et al.*, Nucl. Instrum. Methods Phys. Res. B **399**, 34 (2017).
- 6) A. R. Usman, *et al.*, Appl. Radiat. Isot. **114**, 104 (2016).

*1 RIKEN Nishina Center

*2 Department of Physics, Umaru Musa Yar'adua University

*3 Center for Biomedical Physics, Sunway University

*4 Nuclear Data Section, International Atomic Energy Agency

Production cross sections of (d, x) reactions on natural erbium[†]

M. U. Khandaker^{*1,*2} and H. Haba^{*2}

Nowadays, radionuclides find wide applications in various field such as medicine, industry, agriculture etc. The production of such radionuclides is performed via a number of processes, mostly via the use of particle accelerators and nuclear reactors. Although the use of particle accelerators show some advantages over the nuclear reactors, however the production of radionuclides via former process is still not well practiced. The nuclear reaction cross-sections play a key role in optimization of production parameters for radionuclide of interest via the use of particle accelerators. Present study concerns the measurement of production cross-sections of residual radionuclides via deuteron irradiation on natural erbium target in the energy range of 4.59–23.06 MeV. This rare earth metal can also be used as a potential material for the production of some medically important thulium and erbium radionuclides. As an example, the production of the ^{167}Tm finds applications as a tracer for tumor and bone studies by using both the Anger/gamma camera and the rectilinear scanner.¹⁾ Furthermore, it's relatively long half-life ($T_{1/2} = 9.25$ d) and emission of γ -ray ($E_{\gamma} = 207.801$ keV, $I_{\gamma} = 42\%$) and Auger electrons (Auger $L = 5.5$ keV, 114%) made it suitable for applications in radionuclide therapy.²⁾ Note that considering the common drawbacks of (n, γ) production route (carrier added and low specific activity production), several authors³⁾ studied the production possibility of thulium radionuclides via light-charged particles-induced reactions on several targets. However, since a search of literature shows that the status of deuteron-induced reaction cross-sections on erbium

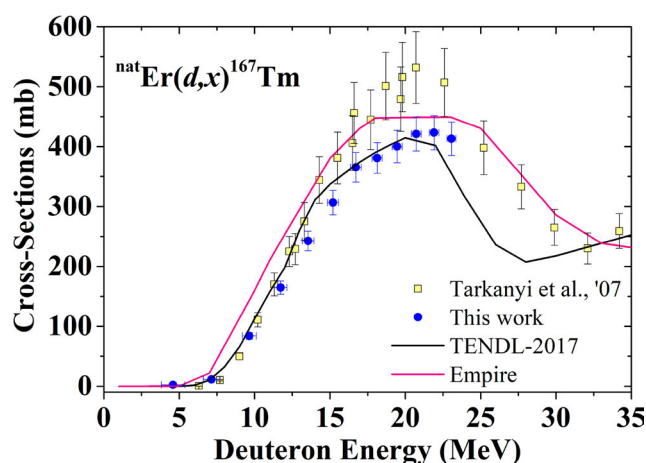


Fig. 1. Excitation function of the $^{\text{nat}}\text{Er}(d, x)^{167}\text{Tm}$ reaction.

[†] Condensed from Nucl. Instrum. Methods Phys. Res. B **470**, 1 (2020)

^{*1} Centre for Biomedical Physics, Sunway University

^{*2} RIKEN Nishina Center

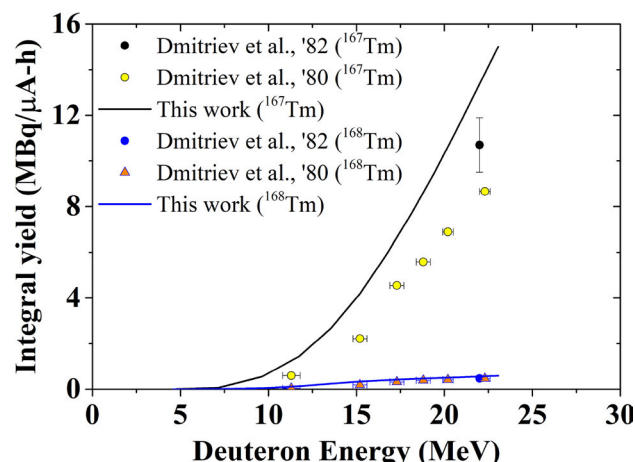


Fig. 2. Thick target integral yields (physical) for $^{167, 168}\text{Tm}$ radionuclides.

is not satisfactory, further study on such processes may find great significance in various respect.

In these circumstances, this study forms an interest to measure the production cross-sections of $^{\text{nat}}\text{Er}(d, x)^{163, 165, 166, 167, 168}\text{Tm}$ and $^{\text{nat}}\text{Er}(d, x)^{171}\text{Er}$ nuclear processes from their respective thresholds up to 23.06 MeV by using the AVF cyclotron of the RIKEN RI Beam Factory, Wako, Japan. Details on the irradiation technique, radioactivity determination, and data evaluation procedures are available in Ref. 4) Owing to the space limitation of this report, we present only the $^{\text{nat}}\text{Er}(d, x)^{167}\text{Tm}$ cross sections and the deduced yield in Figs. 1 and 2, respectively. Measured cross sections with an overall uncertainty of better than 33% are listed in Ref. 4). The cross-sections were normalized by using the $^{\text{nat}}\text{Ti}(d, x)^{48}\text{V}$ monitor cross sections recommended by IAEA. Measured data were critically compared with the available literature data, and an overall good agreement was found. However, only partial agreements were obtained with the data extracted from the TENDL-2017 library and Empire-3.2.2 code.

The deduced thick-target yields indicate that a low amount of no-carrier-added radioactivity of ^{167}Tm (4.2 MBq/ $\mu\text{A-h}$) could be obtained by irradiating an enriched ^{167}Er target with 15-MeV deuteron energy from a cyclotron.

References

- 1) D. G. Medvedev, L. F. Mausner, G. A. Greene, A. L. Hanson, Appl. Radiat. Isot. **66**, 1300 (2008).
- 2) H. Uusijarvi, P. Bernhardt *et al.*, J. Nucl. Med. **47**, 807 (2006).
- 3) F. Tarkanyi, A. Hermanne, F. Ditroi, S. Takacs, Appl. Radiat. Isot. **135**, 67 (2018).
- 4) M. U. Khandaker, H. Haba *et al.*, Nucl. Instrum. Methods Phys. Res. B **470**, 1 (2020).

Activation-cross-section measurement of alpha-induced reactions on natural dysprosium

T. Murata,^{*1,*2} M. Aikawa,^{*1,*2,*3} M. Sakaguchi,^{*1,*2} H. Haba,^{*2} Y. Komori,^{*2} Z. Szűcs,^{*4} F. Ditrói,^{*4} and S. Takács^{*4}

Holmium-166 can be used for a liver-cancer treatment called radioembolization.¹⁾ It is worthwhile to investigate the most efficient method for ^{166}Ho production by comparing possible production reactions. The alpha-induced reaction on dysprosium is one of them. However, there are no available experimental data for this reaction. Thus, we were motivated to perform an experiment for the $^{\text{nat}}\text{Dy}(\alpha, x)^{166}\text{Ho}$ reaction.

The experiment was performed using the AVF cyclotron at the RIKEN Beam Factory (Wako, Saitama, Japan). The stacked-foil activation technique and high-resolution γ -ray spectrometry were used to measure the cross sections of generated radionuclides. The stacked-foil target consisted of natural dysprosium (99% purity, Goodfellow Co., Ltd., UK) and natural titanium (99.6% purity, Nilaco Corp., Japan). The sizes and weights of both foils were measured, and the derived average thicknesses of the natural dysprosium and natural titanium foils were $23.6\ \mu\text{m}$ and $5.1\ \mu\text{m}$, respectively. Both foils were cut into pieces of $8 \times 8\ \text{mm}^2$ size and inserted into the target holder, which served as a Faraday cup. The target was irradiated with a 50.6-MeV alpha beam. The measured beam intensity was 103.8 pA. The beam energy was measured using the time-of-flight (TOF) method.²⁾ The energy degradation in the target was calculated using the stopping powers obtained from SRIM code.³⁾

After one-hour irradiation, the target was removed from the target holder for off-line γ -ray spectrometry

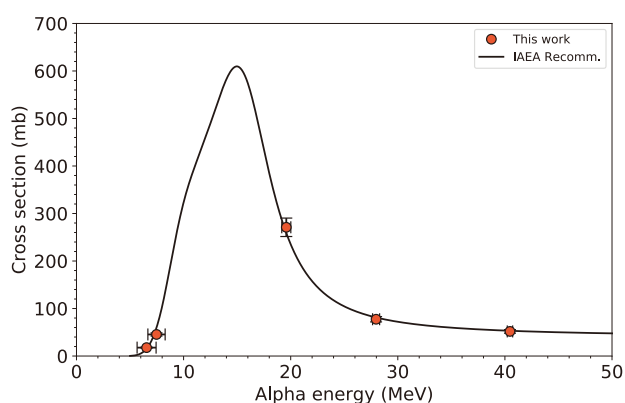


Fig. 1. Comparison of the excitation function of the $^{\text{nat}}\text{Ti}(\alpha, x)^{51}\text{Cr}$ monitor reaction with IAEA's recommended values.⁴⁾

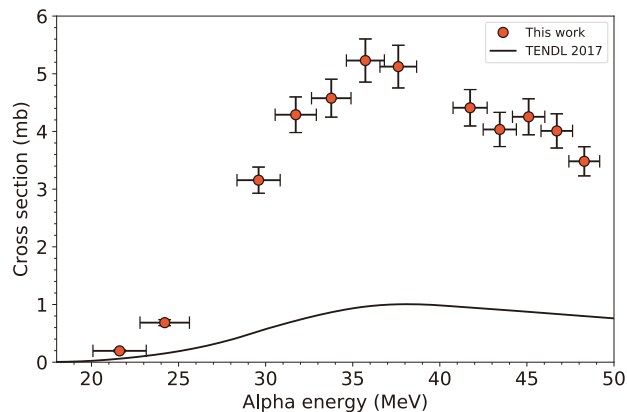


Fig. 2. Comparison of the excitation function of the $^{\text{nat}}\text{Dy}(\alpha, x)^{166}\text{Ho}$ reaction with the TENDL-2017 data.⁵⁾

using a high-purity germanium (HPGe) detector. The 320.08-keV γ -line ($T_{1/2} = 27.704\ \text{d}$, $I_{\gamma} = 9.91\%$) was used to derive the cross sections of the $^{\text{nat}}\text{Ti}(\alpha, x)^{51}\text{Cr}$ monitor reaction.

Because the cross sections of the monitor reaction were significantly different from IAEA's recommended values,⁴⁾ an elemental analysis of the dysprosium foil was conducted via scanning electron microscopy with energy dispersive spectroscopy (SEM-EDS) using JSM-6610LA with JED-2300, JEOL Ltd. at Hokkaido Research Organization. The foil was found to contain 4.27% oxygen by mass. The stopping power of natural dysprosium was modified by considering the oxygen compounds. Consequently, the excitation function of the $^{\text{nat}}\text{Ti}(\alpha, x)^{51}\text{Cr}$ reaction showed good agreement with the recommended values⁴⁾ as shown in Fig. 1. The beam intensity was corrected by -4% from the measured one.

The γ -line of 80.576 keV ($T_{1/2} = 26.824\ \text{h}$, $I_{\gamma} = 6.56\%$) was used to derive the excitation function of the $^{\text{nat}}\text{Dy}(\alpha, x)^{166}\text{Ho}$ reaction. The result is shown in Fig. 2 with the TENDL-2017 data.⁵⁾ It was found that the TENDL-2017 data⁵⁾ significantly underestimate the cross sections of this reaction.

The production of the radioactive by-products, such as ^{167}Ho ($T_{1/2} = 3.003\ \text{h}$), is being analyzed. The results will be published in a forthcoming paper.

References

- 1) M. Reinders *et al.*, *Semin. Nucl. Med.* **49**, 237 (2019).
- 2) T. Watanabe *et al.*, *Proc. 5th Int. Part. Accel. Conf. (IPAC2014)*, (2014), p. 3566.
- 3) J. F. Ziegler *et al.*, *Nucl. Instrum. Methods Phys. Res. B* **268**, 1818 (2010).
- 4) A. Hermanne *et al.*, *Nucl. Data Sheets* **148**, 338 (2018).
- 5) A. J. Koning *et al.*, *Nucl. Data Sheets* **113**, 2841 (2012).

*1 Graduate School of Biomedical Science and Engineering, Hokkaido University

*2 RIKEN Nishina Center

*3 Faculty of science, Hokkaido University

*4 Institute for Nuclear Research, Hungarian Academy of Sciences (ATOMKI)

Production cross sections of ^{157}Dy in alpha-particle-induced reactions on natural gadolinium

D. Ichinkhorloo,^{*1,*2,*3} M. Aikawa,^{*1,*4,*3} Ts. Zolbadral,^{*4,*2,*3} T. Murata,^{*4,*3} M. Sakaguchi,^{*4,*3}
Y. Komori,^{*3} T. Yokokita,^{*3} and H. Haba^{*3}

The radioisotope dysprosium-157 ($T_{1/2} = 8.14$ h) can be used for bone scanning (skeletal imaging).¹⁾ This radionuclide can be produced through charged-particle-induced reactions on natural gadolinium. In this work, the production cross sections of ^{157}Dy in the alpha-particle-induced reactions on natural gadolinium were studied. No previous experimental data were found in a literature survey. The results were compared with TENDL-2017 data.²⁾

The experiment was performed at the RIKEN AVF cyclotron. In the experiment, we used the stacked foil technique, the activation method, and high-resolution γ -ray spectrometry to determine the activation cross sections.

The stacked target consisted of 8×8 mm² foils cut from a larger Gd foil (25 μm , 50×50 mm², 99.9% purity, Nilaco Corp., Japan) and Ti foils (5 μm , 50×100 mm², 99.6% purity, Nilaco Corp., Japan). The isotopic composition of the natural Gd target is ^{152}Gd (0.2%), ^{154}Gd (2.2%), ^{155}Gd (14.8%), ^{156}Gd (20.5%), ^{157}Gd (15.7%), ^{158}Gd (24.8%), and ^{160}Gd (21.8%).

The sizes and weights of the larger foils were measured to derive the average thickness. The thickness of the Gd and Ti foils were found to be 25.4 and 2.29 mg/cm², respectively. The Ti foils were used to assess beam parameters and target thicknesses using the $^{nat}\text{Ti}(\alpha, x)^{51}\text{Cr}$ monitor reaction. The cut foils were stacked in a target holder, which also served as a Faraday cup.

The alpha-particle beam was accelerated to 51.1 MeV by the RIKEN AVF cyclotron. The beam energy was measured using the time-of-flight method.³⁾ The stacked target was irradiated for 60 min with an average beam intensity of 257.6 nA. The beam intensity was measured using the Faraday cup. Energy degradation in the stacked target was calculated using SRIM code.⁴⁾

The γ -rays emitted from the irradiated foils were measured using a high-resolution high-purity germanium (HPGe) detector. The γ -ray spectra were analyzed using the software Gamma Studio (SEIKO EG&G). The γ -rays at 326.3 keV ($I_\gamma = 93\%$) emitted after the decay of ^{157}Dy ($T_{1/2} = 8.14$ h) was measured to derive the cross sections of the $^{nat}\text{Gd}(\alpha, x)^{157}\text{Dy}$

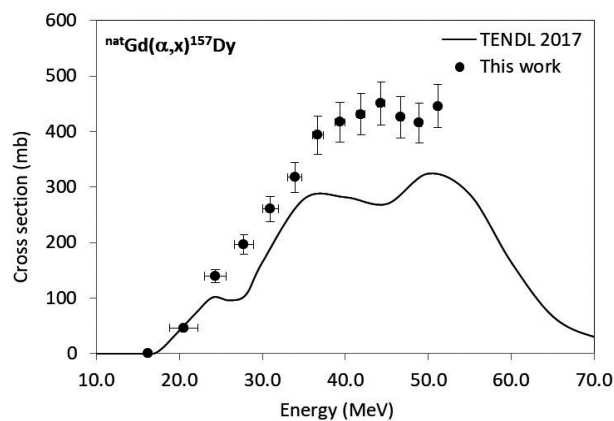


Fig. 1. Excitation function of the $^{nat}\text{Gd}(\alpha, x)^{157}\text{Dy}$ reaction.

reaction. The measurements were performed after a cooling time of 15 h.

The total uncertainties (8.8%) were estimated from the square root of the quadratic summation of each component: statistical uncertainty (1.5%), target thickness (2%), target purity (1%), beam intensity (5%), detector efficiency (6%), and γ -ray intensity (3.2%).

The cross sections derived from the activity of ^{157}Dy are presented in comparison with TENDL-2017 data²⁾ in Fig. 1. The TENDL-2017 data underestimate our experimental cross sections.

In summary, we have performed an experiment to measure the activation cross sections of alpha-particle-induced reactions on ^{nat}Gd up to 51 MeV at the RIKEN AVF cyclotron. In this work, the production cross sections of ^{157}Dy were determined, and the results were compared with the prediction of TALYS-based model calculation, for which data were taken from the TENDL-2017 online database.

This work was supported by JSPS KAKENHI Grant Number 17K07004.

References

- 1) G. Subramanian *et al.*, J. Nucl. Med. **12**, 558 (1971).
- 2) A. J. Koning *et al.*, Nucl. Data Sheets **155**, 1 (2019).
- 3) T. Watanabe *et al.*, Proc. 5th Int. Part. Accel. Conf. (IPAC 2014), 3566 (2014).
- 4) J. F. Ziegler *et al.*, SRIM: the Stopping and Range of Ions in Matter, <http://www.srim.org>.

*1 Faculty of Science, Hokkaido University

*2 Nuclear Research Center, National University of Mongolia

*3 Nishina Center for Accelerator-Based Science, RIKEN

*4 Graduate School of Biomedical Science and Engineering, Hokkaido University

*5 School of Science, Hokkaido University

Activation cross sections of alpha-particle induced nuclear reactions on natural palladium[†]

M. Aikawa,^{*1,*2} M. Saito,^{*3,*2,*4} Y. Komori,^{*2} H. Haba,^{*2} S. Takács,^{*5} F. Ditrói,^{*5} and Z. Szücs^{*5}

Production cross sections of radioactive isotopes (RI) are fundamental information for medical applications such as therapy and diagnostics. One of the medical RI is ^{103}Pd ($T_{1/2} = 16.991$ d), which is used for brachytherapy¹⁾ and targeted radionuclide therapy as part of the $^{103}\text{Pd}/^{103\text{m}}\text{Rh}$ *in vivo* generator.²⁾ In addition to the direct production of ^{103}Pd , the contribution from the decay of its parent, $^{103\text{g}}\text{Ag}$, is worthy of investigation. There are several charged-particle-induced reactions to produce ^{103}Ag . In a literature survey, only one experimental study of $^{103\text{g}}\text{Ag}$ production cross sections of α -induced reactions on $^{\text{nat}}\text{Pd}$ was found.³⁾ The incident energy of the previous study is limited to below 37 MeV and even lower than that at the peak of the cross sections. Therefore, we are motivated to perform an experiment to determine the excitation function of the $^{\text{nat}}\text{Pd}(\alpha, x)^{103\text{g}}\text{Ag}$ reaction up to 50 MeV.

The experiment was performed at the RIKEN AVF cyclotron. The stacked-foil activation technique and high-resolution γ -ray spectrometry were used. Thin metallic foils of $^{\text{nat}}\text{Pd}$ (99.95% purity, Nilaco Corp., Japan) and $^{\text{nat}}\text{Ti}$ (99.9% purity, Goodfellow Co., Ltd., UK) were purchased to fabricate a target. The size and weight of the large foils were measured. The average thicknesses of the Pd and Ti foils were found to be 9.70 and 4.85 mg/cm² from the measurement, respectively. The foils were cut into small pieces of 10 × 10 mm² to fit a target holder. The stacked target consisted of 12 sets of the group of Pd-Pd-Ti-Ti foils. The target was irradiated for 2 h by a 51.2-MeV α beam with an average intensity of 111.4 nA. The intensity was measured using a Faraday cup. The initial beam energy was determined using the time-of-flight method.⁴⁾ The energy degradation of the beam in the target was calculated using the polynomial approximation of stopping-power data.⁵⁾ Gamma-ray spectra from each irradiated foil were measured four times to follow the decay of the reaction products with half-lives between 50 min and 460 days. Nuclear-decay data were taken from NuDat 2.7.⁶⁾

The 118.74-keV γ rays ($I_{\gamma} = 31.2\%$) emitted with the decay of $^{103\text{g}}\text{Ag}$ ($T_{1/2} = 65.7$ min) were measured after a cooling time of 3.6 h. There are minor contributions to the photo-peak area from co-produced isotopes,

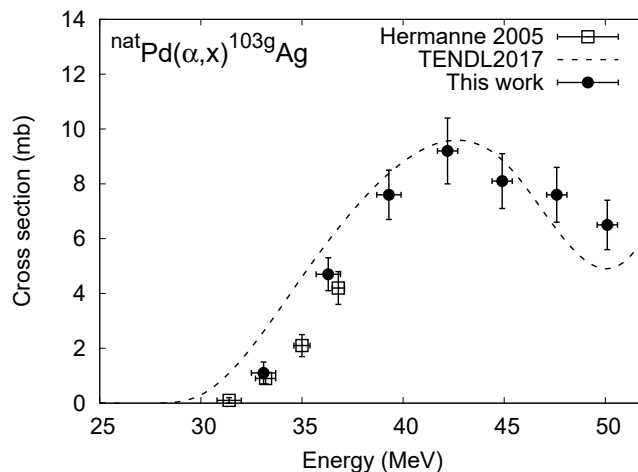


Fig. 1. Cumulative cross sections of the $^{\text{nat}}\text{Pd}(\alpha, x)^{103\text{g}}\text{Ag}$ reaction.

^{100}Pd and $^{111\text{m}}\text{Pd}$, but their total contribution is negligibly small. The measured counts are used to determine the excitation function of the $^{\text{nat}}\text{Pd}(\alpha, x)^{103\text{g}}\text{Ag}$ reaction. In addition to the direct production, there are contributions from the decay of its isomeric state ($T_{1/2} = 5.7$ s) and ^{103}Cd ($T_{1/2} = 7.3$ min). Therefore, cumulative cross sections are derived in this work. The result is shown in Fig. 1 in comparison with the experimental data obtained earlier³⁾ and the TENDL-2017 data.⁷⁾ Our result is slightly higher than the previous experimental data. The TENDL-2017 data provides an excitation function with a consistent tendency.

Our result extends cross-section data to the higher energy region and covers the peak. It enriches nuclear reaction databases and is available for development of theoretical calculation models.

This work is supported by the Japan - Hungary Research Cooperative Program, JSPS and HAS and by JSPS KAKENHI Grant Number 17K07004.

References

- 1) S. Nag *et al.*, *Int. J. Radiat. Oncol. Biol. Phys.* **44**, 789 (1999).
- 2) Z. Szücs *et al.*, *Radiochim. Acta* **92**, 215 (2004).
- 3) A. Hermanne *et al.*, *Nucl. Instrum. Methods Phys. Res. B* **229**, 321 (2005).
- 4) T. Watanabe *et al.*, *Proc. 5th Int. Part. Accel. Conf. (IPAC2014)*, (2014), p. 3566.
- 5) J. F. Ziegler *et al.*, *SRIM: the Stopping and Range of Ions in Matter* (2008).
- 6) National Nuclear Data Center, The NuDat 2.7 database, <http://www.nndc.bnl.gov/nudat2/>.
- 7) A. J. Koning *et al.*, *Nucl. Data Sheets* **113**, 2841 (2012).

[†] Condensed from the article in *Nucl. Instrum. Methods Phys. Res. B* **449**, 99 (2019)

^{*1} Faculty of Science, Hokkaido University

^{*2} RIKEN Nishina Center

^{*3} Graduate School of Science, Hokkaido University

^{*4} Present address: Graduate School of Biomedical Science and Engineering, Hokkaido University

^{*5} Institute for Nuclear Research, Hungarian Academy of Sciences (ATOMKI)

Excitation function measurement for zirconium-89 and niobium-90 production using alpha-induced reactions on yttrium-89†

T. Murata,^{*1,*2} M. Aikawa,^{*1,*2,*3} M. Saito,^{*1,*2} H. Haba,^{*2} Y. Komori,^{*2} N. Ukon,^{*4,*2} S. Takács,^{*5} and F. Ditrói^{*5}

Zirconium-89 ($T_{1/2} = 78.41$ h) and niobium-90 ($T_{1/2} = 14.6$ h) are expected to be used for immuno-PET.^{1,2)} From the viewpoint of radionuclide production, the investigation of effective production reactions is valuable. We focused on the α -induced reactions on the monoisotopic element ^{89}Y to produce the two radionuclides. Five experimental studies on these reactions^{3–5)} were found in a literature survey. However, significant discrepancies exist among the experimental data. Therefore, we were motivated to investigate α -induced reactions on ^{89}Y . The cross sections of co-produced radionuclides other than ^{89}Zr and ^{90}Nb were also determined.

The experiment was performed at the RIKEN AVF cyclotron. The stacked foil activation technique and high-resolution γ -ray spectrometry, which are well-established methods, were adopted for the experiment. The target was composed of pure metallic foils of ^{89}Y (99% purity, Goodfellow Co., Ltd., UK), $^{\text{nat}}\text{Ti}$ (99.6% purity, Nilaco Corp., Japan), and ^{27}Al (> 99% purity, Nilaco Corp., Japan). The sizes and weights of the foils were measured to determine their average thicknesses, which were found to be 24.2, 5.1, and 5.5 μm for Y, Ti, and Al, respectively. The three foils were cut into a small size of 1 cm \times 1 cm to fit a target holder, which also served as a Faraday cup. The stacked target was irradiated with a 50.9 ± 0.1 -MeV M-beam for 1 h. The incident energy of the beam was measured using the time-of-flight method.⁶⁾ The energy degradation in the target was calculated using stopping powers obtained from the Stopping and Range of Ions in Matter (SRIM) code.⁷⁾ The average beam intensity was measured as 411 nA using the Faraday cup. The irradiated stacks were dismantled for the off-line γ -ray spectrometry using HPGe detectors. The dead time was kept under 10% by adjusting the distances between the measured foil and HPGe detector. Reaction and decay data for the γ -ray spectrometry were taken from NuDat 2.7.⁸⁾

The beam parameters were verified using the $^{27}\text{Al}(\alpha, x)^{22}\text{Na}$ and $^{\text{nat}}\text{Ti}(\alpha, x)^{51}\text{Cr}$ monitor reactions in comparison with the IAEA recommended values.⁹⁾ Based on the comparison, the beam intensity was decreased by 4% from the measured value. The corrected intensity of 398 nA was adopted to derive cross sections.

The excitation function of the $^{89}\text{Y}(\alpha, x)^{89\text{g}}\text{Zr}$ reaction

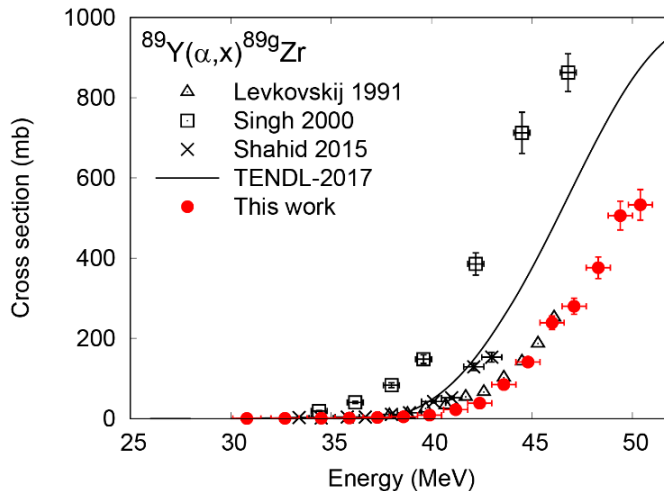


Fig. 1. Comparison of cumulative cross sections of the $^{89}\text{Y}(\alpha, x)^{89\text{g}}\text{Zr}$ reaction with previously reported data^{3–5)} and TENDL-2017 data.¹⁰⁾

was determined. The measurement of the 909.15-keV γ -rays ($T_{1/2} = 78.41$ h, $I_\gamma = 99.04\%$) was performed after a cooling time of 10 days, which was long enough for complete decay of the parent nuclei $^{89\text{g,m}}\text{Nb}$ and $^{89\text{m}}\text{Zr}$. The cumulative cross sections of $^{89\text{g}}\text{Zr}$ were obtained and compared with three previous studies^{3–5)} and TENDL-2017 data¹⁰⁾ in Fig. 1. One of the three experimental data sets³⁾ agree with our result. However, the others^{4,5)} deviate from ours.

In addition to $^{89\text{g}}\text{Zr}$, the production cross sections of ^{90}Nb and other co-produced radionuclides were determined and compared with previous studies and the TENDL-2017 data. Our results are reasonably consistent with some of the previous studies.

This work was supported by JSPS KAKENHI Grant Number 17K07004.

References

- 1) M. A. Deri *et al.*, Nucl. Med. Biol. **40**, 3 (2013).
- 2) V. Radchenko *et al.*, Radiochim. Acta **102**, 433 (2014).
- 3) V. N. Levkovski, Cross Sections of Medium Mass Nuclide Activation ($A = 40$ – 100) by medium energy protons and alpha particles ($E = 10$ – 50 MeV) (Inter-Vesi, Moscow, USSR, 1991).
- 4) N. L. Singh *et al.*, Phys. Scr. **61**, 550 (2000).
- 5) M. Shahid *et al.*, Nucl. Instrum. Methods Phys. Res. B **358**, 160 (2015).
- 6) T. Watanabe *et al.*, Proc. 5th Int. Part. Accel. Conf. (IPAC2014), 3566 (2014).
- 7) J. F. Ziegler *et al.*, Nucl. Instrum. Methods Phys. Res. B **268**, 1818 (2010).
- 8) National Nuclear Data Center, The NuDat 2.7 database, <http://www.nndc.bnl.gov/nudat2/>.
- 9) A. Hermanne *et al.*, Nucl. Data Sheets **148**, 338 (2018).
- 10) A. J. Koning *et al.*, Nucl. Data Sheets **155**, 1 (2019).

† Condensed from the article in Nucl. Instrum. Methods Phys. Res. B **458**, 21 (2019)

*1 Graduate School of Biomedical Science and Engineering, Hokkaido University

*2 RIKEN Nishina Center

*3 Faculty of Science, Hokkaido University

*4 Advanced Clinical Research Center, Fukushima Medical University

*5 Institute for Nuclear Research, Hungarian Academy of Sciences

Production cross sections of ^{68}Ga via deuteron-induced reactions on natural zinc

Ts. Zolbadral,^{*1,*2} M. Aikawa,^{*1,*3,*2} D. Ichinkhorloo,^{*3,*2} Kh. Tegshjargal,^{*4} N. Javkhlantugs,^{*4} Y. Komori,^{*2} and H. Haba^{*2}

^{68}Ga ($T_{1/2} = 68$ min), a positron emitter, is a valuable medical isotope used for positron emission tomography (PET). One of the production routes of this radionuclide is the deuteron-induced reaction on zinc. In a literature survey, only two datasets of the experimental cross sections of the $^{\text{nat}}\text{Zn}(d,x)^{68}\text{Ga}$ reaction were found,^{1,2)} and these data show a remarkable discrepancy. It is necessary to obtain reliable cross sections to investigate the best production route for practical use. Therefore, we measured the production cross sections of ^{68}Ga via the deuteron-induced reaction on natural zinc.

The stacked-foil activation method and γ -ray spectrometry were used. The stacked target was composed of metallic foils of $^{\text{nat}}\text{Zn}$ (17.64 mg/cm², 99.9% purity) and $^{\text{nat}}\text{Ti}$ (9.13 mg/cm², 99.6% purity). The target was irradiated for 22 min by a 24-MeV deuteron beam from the RIKEN AVF cyclotron. The incident beam energy was measured using the time-of-flight method. The energy degradation in the stacked foils was calculated using SRIM code.³⁾ The beam intensity was measured using a Faraday cup and cross-checked using the $^{\text{nat}}\text{Ti}(d,x)^{48}\text{V}$ monitor reaction.⁴⁾ By referring to the cross sections of the monitor reaction, the beam intensity was increased 6.6% from the measured value and thereby corrected to 102.4 nA. The γ -ray spectra of the irradiated foils were measured using a high-resolution HPGe detector (ORTEC

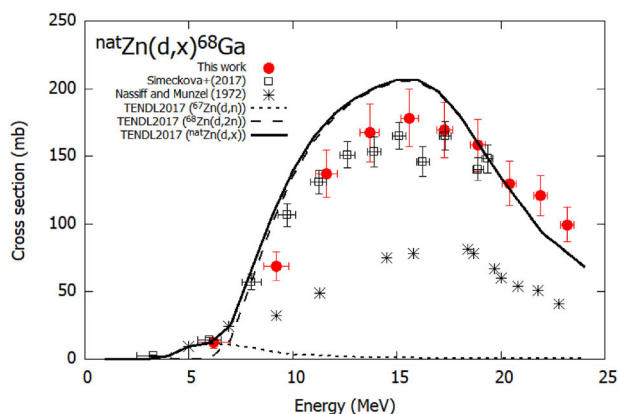


Fig. 1. Excitation function of the $^{\text{nat}}\text{Zn}(d,x)^{68}\text{Ga}$ reaction.

^{*1} Graduate School of Biomedical Science and Engineering, Hokkaido University

^{*2} RIKEN Nishina Center

^{*3} Faculty of Science, Hokkaido University

^{*4} School of Engineering and Applied Sciences, National University of Mongolia

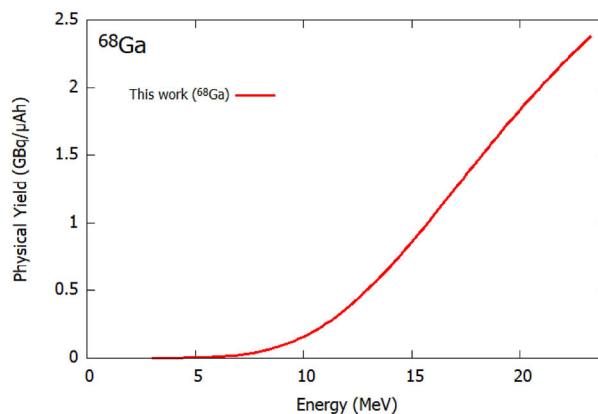


Fig. 2. Integral yield of ^{68}Ga .

GMX30P4-70) without chemical separation. The detector was calibrated using a standard mixed multiple γ -ray-emitting point source. The distance between the detector and foils was chosen to keep the dead time less than 7%.

The cross sections of the $^{\text{nat}}\text{Zn}(d,x)^{68}\text{Ga}$ reaction were derived from the measurements of the 1077.34-keV γ -line ($I_{\gamma} = 3.22\%$) associated with the ^{68}Ga decay. The excitation function of the reaction is shown in Fig. 1 in comparison with previous data^{1,2)} and the theoretical estimation of TENDL-2017.⁵⁾ Our result is consistent with the data reported by Šimečková *et al.*²⁾ but inconsistent with those reported by Nassiff and Münzel¹⁾ in the whole investigated energy region. The TENDL-2017 data overestimate the experimental data around the peak in the energy range of 8–18 MeV.

The physical yield of ^{68}Ga was deduced from the measured cross sections. The derived yield is shown in Fig. 2. The physical yield of ^{68}Ga via the deuteron-induced reaction on zinc is reported for the first time.

This work is supported by JSPS KAKENHI Grant Number 17 K07004. Ts.Z. was granted a scholarship by the M-JEED project (Mongolian-Japan Engineering Education Development Program, J11B16).

References

- 1) S. J. Nassiff, H. Münzel, *Radiochem. Radioanal. Lett.* **12**, 353 (1972).
- 2) E. Šimečková *et al.*, *EPJ Web Conf.* **146**, 11034 (2017).
- 3) J. F. Ziegler *et al.*, *Nucl. Instrum. Methods Phys. Res. B* **268**, 1818 (2010).
- 4) A. Hermanne *et al.*, *Nucl. Data Sheets* **148**, 338 (2018).
- 5) A. J. Koning *et al.*, *Nucl. Data Sheets* **155**, 1 (2019).

Production cross sections of ^{45}Ti via deuteron-induced reaction on ^{45}Sc

Ts. Zolbadral,^{*1,*2} M. Aikawa,^{*1,*3,*2} D. Ichinkhorloo,^{*3,*2} Kh. Tegshjargal,^{*4} Y. Komori,^{*2} H. Haba,^{*2} S. Takács,^{*5} F. Ditrói,^{*5} and Z. Szücs^{*5}

The radionuclide ^{45}Ti ($T_{1/2} = 184.8$ min) is a positron emitter ($E_{\beta^+} = 439$ keV, $I_{\beta^+} = 84.8\%$) suitable for positron emission tomography (PET). This radioisotope can be produced in the deuteron-induced reaction on a scandium-45 target at cyclotrons. However, the quality of experimental data on the cross sections of the $^{45}\text{Sc}(d,2n)^{45}\text{Ti}$ reaction is not satisfactory. The main purpose of this study is, therefore, to measure the cross sections of the $^{45}\text{Sc}(d,2n)^{45}\text{Ti}$ reaction for ^{45}Ti production. In addition, the physical yield is derived from the measured cross sections.

The stacked-foil activation technique and γ -ray spectrometry were adopted to determine the cross sections. The stacked target consisted of metallic foils of ^{45}Sc (thicknesses of 7.71 mg/cm² and 76.0 mg/cm² with a purity of 99.0%), ^{27}Al (4.99 mg/cm², 99.6%), and $^{\text{nat}}\text{Ti}$ (9.13 mg/cm², 99.6%). The target was irradiated for 30 min with a 24-MeV deuteron beam from the RIKEN AVF cyclotron. The incident beam energy was measured by the time-of-flight method. The energy degradation in the stacked target was calculated using the SRIM code.¹⁾ The beam intensity was measured using a Faraday cup and cross-checked with the $^{\text{nat}}\text{Ti}(d,x)^{48}\text{V}$ monitor reaction.²⁾ According to the cross checking, the intensity (175.2 nA) was corrected by a decrease of 3% from the measured value (180.3 nA). The γ -ray spectra of the irradiated foils were measured by a high-resolution and high-purity germanium (HPGe) detector. The detector was calibrated by a standard mixed γ -ray point source. The dead time was kept below 7% in the measurements.

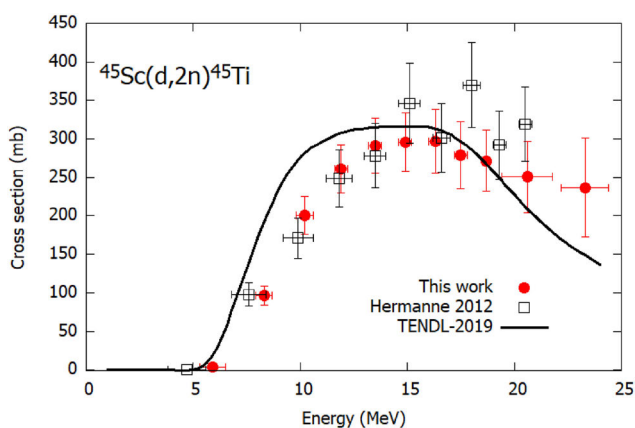


Fig. 1. Excitation function of the $^{45}\text{Sc}(d,2n)^{45}\text{Ti}$ reaction.

*1 Graduate School of Biomedical Science and Engineering, Hokkaido University

*2 RIKEN Nishina Center

*3 Faculty of Science, Hokkaido University

*4 School of Engineering and Applied Sciences, National University of Mongolia

*5 Institute for Nuclear Research (ATOMKI), Hungary

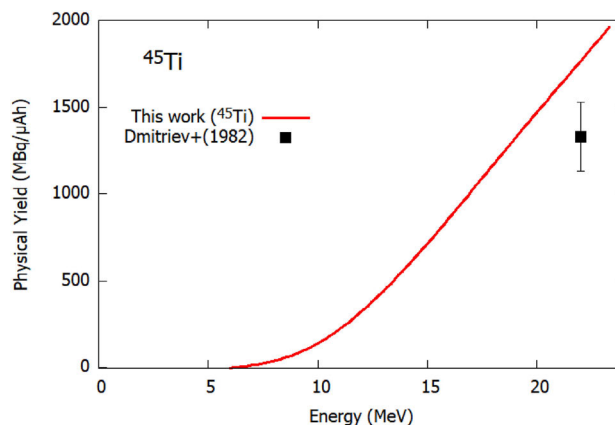


Fig. 2. Physical yield of ^{45}Ti .

The cross sections of the $^{45}\text{Sc}(d,2n)^{45}\text{Ti}$ reaction were derived from the measurement of the 719.6-keV γ -line ($I_{\gamma} = 0.154\%$) associated with the ^{45}Ti decay. The excitation function of the $^{45}\text{Sc}(d,2n)^{45}\text{Ti}$ reaction is shown in Fig. 1 in comparison with previous experimental data³⁾ and the theoretical estimation from TENDL-2017.⁴⁾ The derived excitation function of the $^{45}\text{Sc}(d,2n)^{45}\text{Ti}$ reaction is consistent with the data reported by Hermanne *et al.*³⁾ The peak position of the TENDL-2017 data is slightly shifted to a lower energy.

The physical yield of ^{45}Ti was deduced from a spline fitted curve of the measured excitation function and stopping power calculated from the SRIM code.¹⁾ The derived yield is shown in Fig. 2. The present yield curve of ^{45}Ti is slightly higher than the experimental data measured by Dmitriev *et al.*⁵⁾ at 22 MeV. We confirmed that no radioactive impurities of titanium are produced in the energy range below 15 MeV, which is the threshold energy of ^{44}Ti production. Above 15 MeV and up to 24 MeV, the physical yield of ^{44}Ti is seven or more orders of magnitude less than that of ^{45}Ti and negligibly small. Thus, this reaction with chemical separation allows the production of high-specific-activity ^{45}Ti in this energy range.

This work is supported by JSPS KAKENHI Grant Number 17 K07004. Ts.Z was granted a scholarship by the M-JEED project (Mongolian-Japan Engineering Education Development Program, J11B16).

References

- 1) J. F. Ziegler *et al.*, Nucl. Instrum. Methods Phys. Res. B **268**, 1818 (2010).
- 2) A. Hermanne *et al.*, Nucl. Data Sheets **148**, 338 (2018).
- 3) A. Hermanne *et al.*, Nucl. Instrum. Methods Phys. Res. B **270**, 106 (2012).
- 4) A. J. Koning *et al.*, Nucl. Data Sheets **155**, 1 (2019).
- 5) P. P. Dmitriev *et al.*, INDC (CCP)-210, 1 (1983).

Present status of ^{211}At production at the RIKEN AVF cyclotron

Y. Wang,^{*1} N. Sato,^{*1} Y. Komori,^{*1} T. Yokokita,^{*1} D. Mori,^{*1} S. Usuda,^{*1} and H. Haba^{*1}

^{211}At is one of the most promising radionuclides for targeted alpha radiotherapy owing to its suitable half-life of $T_{1/2} = 7.214$ h and high alpha-particle emission probability of 100%.¹⁾ We have been producing ^{211}At via the $^{209}\text{Bi}(\alpha, 2n)^{211}\text{At}$ reaction at the RIKEN AVF cyclotron.^{2,3)} In this paper, we report improved production technologies of ^{211}At , which could reduce the separation time from 2 h to 1 h and yield a neutral dry ^{211}At product instead of the confused ^{211}At species in the solution.

Figure 1 shows the production process for dry ^{211}At . A metallic ^{209}Bi target ($> 99.999\%$, 20 mg/cm^2) was prepared through vacuum evaporation on an Al plate (thickness: 1 mm). As shown in Fig. 1(a), the Bi target was placed at an angle of 15° with respect to the beam axis. The target was cooled with water (10°C , 1.5 L/min) and He gas (30 L/min) during the irradiation. An alpha beam with an energy of $29.0 \pm 0.2\text{ MeV}$ was delivered from the RIKEN AVF cyclotron. The precise beam energy was measured using a time-of-flight detector.⁴⁾ A beam-wobbling system was used to rotate the beam spot on the target and to prevent heat concentration. After the beam passed through a Be window ($18.1\text{ }\mu\text{m}$) and He cooling gas (65 mm , 1.1 bar), the beam energy on the target was $28.0 \pm 0.2\text{ MeV}$, as calculated with LISE (ver. 11.0.72). The beam intensity ($4\text{--}32\text{ }\mu\text{A}$) and irradiation time (2 to 8 h) was varied to meet the users' requirements. Subsequently, ^{211}At was separated from the Bi target by using a dry distillation technique (see Fig. 1(b)). The irradiated Bi target was placed on a copper tray in a quartz tube and heated up to 850°C in 10 min, following which it was kept for another 15 min and finally cooled down naturally. ^{211}At sublimated from the target was transported from the quartz tube through a quartz capillary (*i.d.* = 2 mm , length = 13 cm) to a PFA cold trap (*i.d.* = 1 mm , length = 100 cm) by oxygen gas (10 mL/min). The PFA cold trap was cooled to -96°C to collect the gaseous ^{211}At . As shown in Fig. 1(c), after the distillation, the capillary and the PFA trap tube were washed with chloroform (FUJIFILM Wako Pure Chemical Corporation, Cat. No.: 033-15721, Infinity Pure, $200\text{--}400\text{ }\mu\text{L}$). The eluate collected in a 1-mL V-shaped glass vial was then dried up by dry N_2 gas (100 mL/min) at room temperature (see Fig. 1(d)). The chemical yields of the dry ^{211}At products were determined by measuring the $687\text{ keV } \gamma$ -ray ($I_\gamma = 0.261\%$) with a Ge detector. The chemical purity of the products and the decontamination factor of ^{209}Bi from ^{211}At were evaluated with chemical analysis using inductively coupled plasma mass spec-

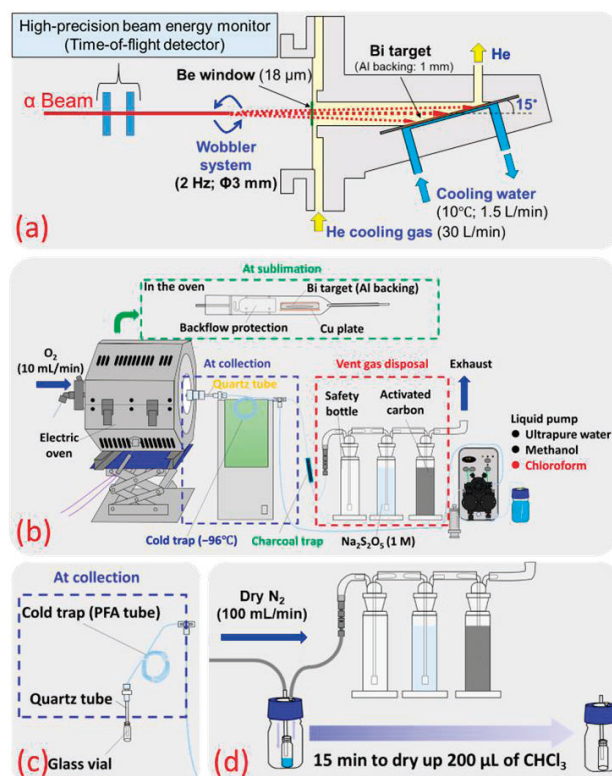


Fig. 1. Production process of dry ^{211}At .

trometry (ICP-MS).

We confirmed that the radioactivities of ^{211}At produced in the targets agreed well with those estimated from thick target yields in the literature.⁵⁾ The atomic ratio $^{210}\text{At}/^{211}\text{At}$ was determined to be less than 2.1×10^{-6} at the end of bombardment (EOB), which satisfied the medical requirement of $< 1 \times 10^{-3}$ at EOB.⁴⁾ The typical chemical yield was 80%. The chemical impurities ($> 1\text{ ng}$) in $200\text{ }\mu\text{L}$ of chloroform were Cu (43.84 ng), Al (38.90 ng), Zn (23.55 ng), and Bi (6.70 ng). The decontamination factor of ^{209}Bi for dry ^{211}At was determined to be 8.3×10^{-8} .

By using the current production technology of ^{211}At , 1 GBq of ^{211}At can be produced through 1.5-h irradiation with a $32\text{-}\mu\text{A}$ alpha beam (27.8 MeV on target). Dry ^{211}At can be prepared 4 h after EOB. We have been distributing ^{211}At to 14 users in Japan for the research and development of nuclear medicine.

References

- 1) M. Zalutsky *et al.*, *Curr. Radiopharm.* **4**, 177 (2011).
- 2) S. Yano *et al.*, *RIKEN Accel. Prog. Rep.* **50**, 263 (2017).
- 3) N. Sato *et al.*, *RIKEN Accel. Prog. Rep.* **50**, 262 (2017).
- 4) T. Watanabe *et al.*, *Proc. 12th Annual Meeting of Particle Accelerator Society of Japan*, (2015), p. 1198.
- 5) A. Hermanne *et al.*, *Appl. Radiat. Isot.* **63**, 1 (2005).

^{*1} RIKEN Nishina Center

Decontamination of Po in the $^{211}\text{Rn}/^{211}\text{At}$ generator system

K. Aoi,^{*1,*2} K. Kawasaki,^{*1,*2} S. Maruyama,^{*1,*2} M. Higashi,^{*1,*3} K. Washiyama,^{*4} A. Yokoyama,^{*1,*3}
I. Nishinaka,^{*5} D. Mori,^{*1} Y. Wang,^{*1} and H. Haba^{*1}

The short path length and high linear energy transfer of α particles are expected to enable targeted alpha therapy for the treatment of tumor. A promising nuclide among various α emitters is ^{211}At with a half-life of 7.21 h, which has gained popularity owing to its appropriate life and potential to synthesize labeled compounds as a halogen element. This has been the motivation behind several preclinical studies on At chemistry.¹⁾ To improve the availability of ^{211}At , the development of a $^{211}\text{Rn}/^{211}\text{At}$ generator would be useful for expanding nuclide production away from accelerator facilities because ^{211}Rn , which has a half-life of 14.6 h, is the parent nuclide of ^{211}At .²⁾ However, Po isotopes such as ^{207}Po and ^{206}Po , which are known to be harmful to the human body, may contaminate the At sample owing to decay from the Rn products. We aim to study the wet chemistry processes by using adsorption chromatography resins for an At solution free from Po contamination.

In this study, ^{211}At was produced via the $^{209}\text{Bi}(\alpha, 2n)$ reaction at the RIKEN AVF cyclotron and delivered to Kanazawa University. The irradiated Bi target was dissolved in 2 mL of 6 M HNO_3 and mixed with 10 mL of H_2O to prepare a 1 M HNO_3 solution, 2 mL of which was used to extract the ^{211}At nuclide into 18 mL of dodecane solvent.

Aliquots of the dodecane solution were subjected to back extractions into several solutions of various HCl concentrations. 2 mL of each solution was fed to adsorption chromatography columns filled with either a cation-exchange resin, DGA resin, or TEVA resin through a conditioning process in advance. The eluted solution from the column and the eluent due to additional washing with 2 mL of two solutions with the same HCl concentration were subjected to liquid scintillation counter (LSC) measurement to determine the ^{211}At radioactivity.

The results of the measurement of ^{211}At radioactivity after purification with adsorption chromatography columns demonstrate that the recoveries for DGA resin and cation-exchange resin were ca. 50% at most at 0.01 M HCl and were better than that for TEVA resin. This suggests that the species of At may have

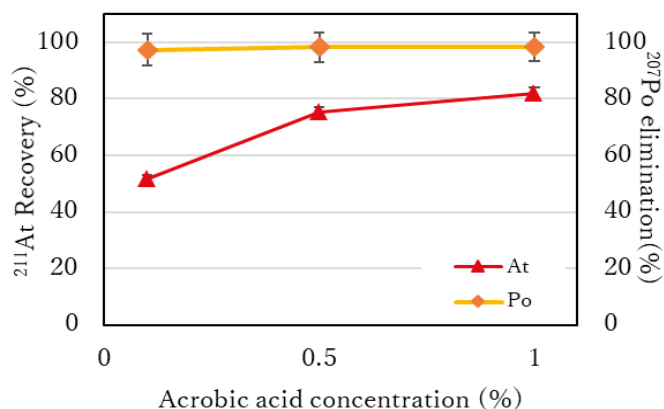


Fig. 1. Recovery of ^{211}At radioactivity and elimination of Po depending on the ascorbic-acid concentration.

a variety of oxidation states that affect adsorption in columns. Therefore, another experiment was performed to change their oxidation states by using a reductant agent and to confirm the effect of reduction with cation-exchange resin.

Similarly to the experiment described above, aliquots of the dodecane solution were subjected to back extractions into 0.01 M HCl solution, which had been adjusted to the solutions with 0.01, 0.1, and 1% ascorbic acid. The HCl solutions were fed to a column filled with cation-exchange resin that was conditioned well in advance. The eluent from the column was collected and subjected to the LSC measurement in the same manner as above.

The recovery of ^{211}At radioactivity with ascorbic acid as a reductant agent is shown in Fig. 1 together with Po elimination data taken with the Po activity produced in the JAEA tandem accelerator. It was found that the ^{211}At recoveries are improved to 80%, and the elimination of Po was successful under the same condition.

References

- 1) F. Guérard, J. -F. Gustin, M. W. Brechbiel, *Cancer Biother. Radiopharm.* **28**, 1 (2013).
- 2) E. Maeda *et al.*, *J. Radioanal. Nucl. Chem.* **303**, 1465 (2015).

*1 Graduate School of Natural Science and Technology, Kanazawa University

*2 Institute and College of Science and Engineering, Kanazawa University

*3 Fukushima Global Medical Science Center, Fukushima Medical University

*4 Quantum Beam Science Research Directorate, National Institutes for Quantum and Radiological Science and Technology

*5 RIKEN Nishina Center

Separation and purification of ^{139}Ce tracer for metallofullerene synthesisK. Akiyama,^{*1,*2} K. Amekura,^{*1} and H. Haba^{*2}

Recently, clinical tests have been conducted on radionuclides of group 3 elements including lanthanides, and some radionuclides were newly approved as radiopharmaceuticals. Metallofullerenes encapsulating lanthanide elements are attractive for application in electronic devices and pharmaceuticals. In particular, it is expected that rich π electrons on a metallofullerene surface enable the production of various metallofullerene derivatives by the addition of various functional groups and that the encapsulation of radionuclides by these derivatives could be applied as radiopharmaceuticals. For such applications, excellent radionuclides, such as ^{139}Ce , emitting monochromatic γ rays and have a half-life of several months are required. In this paper, we report the separation and purification of a ^{139}Ce tracer from its target material for metallofullerene synthesis.

Cerium-139 was produced from the $^{139}\text{La}(d, 2n)^{139}\text{Ce}$ reaction using a ^{nat}La target irradiated with $5\ \mu\text{A}$ of 24 MeV deuterons for 5 h at the RIKEN AVF cyclotron. After the irradiation, the La target containing ^{139}Ce was dissolved in nitric acid. For the separation and purification of ^{139}Ce from La, the solvent extraction method was employed and was executed according to the procedure shown in the Fig. 1. The solution samples obtained in a series of this extraction procedure were measured using a Ge semiconductor detector to check the remaining ^{139}Ce radioactivity in each sample.

The remaining amounts of the target material La and oxidant Cr were determined by optical absorption measurement and were found to be 2.1% and 3.9%, respectively.

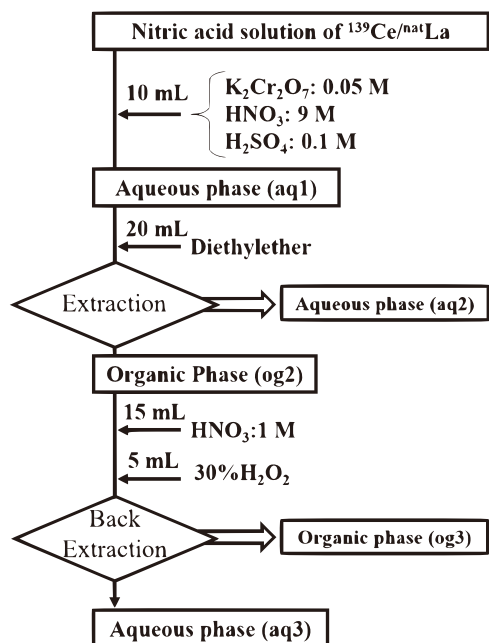


Fig. 1. Schematic diagram of ^{139}Ce separation from a La target.

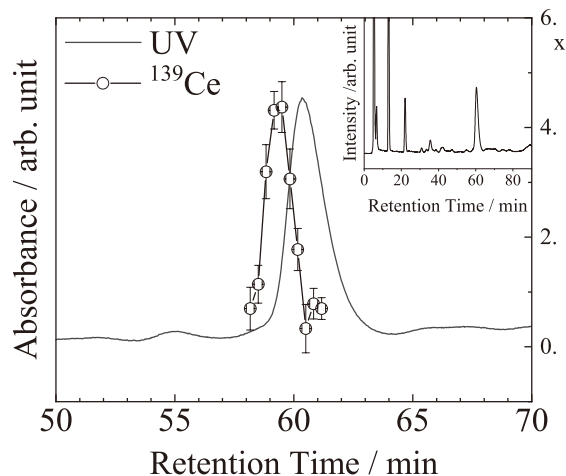


Fig. 2. HPLC elution behavior of ^{139}Ce metallofullerene together with UV-monitored chromatogram of metallofullerenes produced in this study.

tively. The amount of remaining La in a single separation process is still much larger than the amount of the ^{139}Ce tracer. However, it has been found that by repeating this separation procedure, it would be possible to obtain a sufficiently purified ^{139}Ce tracer.

As mentioned above, the separated ^{139}Ce tracer still includes large amounts of La and Cr. However, if the amounts of these impurities are sufficiently small relative to that of the added carrier element and do not affect the fullerene production, the purity of ^{139}Ce can be said to be sufficient in this experiment. To confirm this, Tb_4O_7 was added to a ^{139}Ce tracer solution, and this solution was employed for the metallofullerene production under the same conditions as those previously reported.¹⁾ In Fig. 2, the high-performance liquid chromatography (HPLC) elution behavior of ^{139}Ce metallofullerene (open circles) on a Buckyprep column (Nacalai Tesque, Inc., effluent: toluene) is shown together with a chromatogram acquired using UV absorption (gray solid line). The most dominant elution peak found in both chromatograms are due to $\text{M}@\text{C}_{82}$.²⁾ It is reported that the HPLC retention time of $\text{M}@\text{C}_{82}$ on a buckyprep column increases as the atomic number of the encapsulated lanthanide atom increased.³⁾ The observed UV-monitored HPLC elution peak around 60 min occurs after that of Ce metallofullerene and is considered to be derived from $\text{Tb}@\text{C}_{82}$ because no HPLC elution peak with sufficient intensity and faster retention time than that of $\text{Ce}@\text{C}_{82}$ is observed. In conclusion, the observed elution peak is derived from $\text{Tb}@\text{C}_{82}$ and the amount of the remaining La with this separation method is found to be sufficiently small.

References

- 1) K. Akiyama *et al.*, RIKEN Accel. Prog. Rep. **49**, 243 (2016).
- 2) H. Shinohara *et al.*, Rep. Prog. Phys. **63**, 843 (2000).
- 3) D. Fuchs *et al.*, J. Phys. Chem. **100**, 725 (1996).

^{*1} Department of Chemistry, Tokyo Metropolitan University

^{*2} RIKEN Nishina Center

Separation of ^{121m}Te from antimony without redox reaction

T. Kubota,^{*1,*2} S. Fukutani,^{*1} T. Takahashi,^{*1} H. Haba,^{*2} D. Mori,^{*2} and S. Takahashi^{*1}

Radioactive tellurium isotopes, such as ^{129}Te , ^{131}Te , and ^{132}Te , were released in the Fukushima Dai-ichi nuclear accident and are regarded as significant for the evaluation of exposure dose during 2011. Owing to their short half-life, radioactive materials derived from the accident have already decayed out; thus, the evaluation requires some laboratory experiments. In experiments where radio nuclides are added to plant and animal samples, carrier-free and high-purity tracers should be employed to avoid undesirable chemical effects. The production of a suitable tracer had been investigated in previous reports where radioactive tellurium generated by the bombardment of Sb_2O_3 with deuterium at an energy of 24 MeV was purified through a redox reaction.^{1,2)} However, this method generates toxic chlorine gas. More moderate methods, therefore, should be developed.

We found that tellurium is separated as a cation from anionic antimony through anion exchange chromatography. Chemical species of both elements were calculated under several conditions, following which tellurium was separated using the calculation results.

Tellurium and antimony exist as chloro-complex anions in a high-concentration HCl solution. With increasing pH, Te(IV) is converted into TeOOH^+ , while Sb(III) forms a precipitate. Through this precipitation, a large part of tellurium is co-precipitated. We considered that tellurium can be purified with careful control of the pH and HCl concentration, and we investigated the optimal conditions using Medusa-Hydra chemical equilibrium software for Windows.³⁾ The calculation results are shown below. Te(IV) was converted into TeOOH^+ at $\text{pH} > -0.2$ and $[\text{HCl}] < 1.6 \text{ M}$. Sb(III) remained as a solution at $\text{pH} < -0.5$ and $[\text{HCl}] > 3.2 \text{ M}$ with $[\text{Sb}] = 200 \text{ mM}$, which is equivalent to 900 mg Sb_2O_3 dissolved in 30 mL HCl and to a concentration derived from ordinary production at one time. At this antimony concentration, tellurium cannot be purified. Based on the fact that the solubility of antimony depends on its concentration, the maximum concentration of antimony at $\text{pH} = -0.2$ without precipitation was calculated to be 7 mM. In order to ensure that the purification was conducted without precipitation, we applied a concentration of 5 mM Sb.

An irradiated Sb_2O_3 pellet was dissolved in concentrated HCl, following which insoluble antimony was removed by centrifugation. The supernatant was diluted with H_2O to 2.4 M HCl and 5 mM Sb solution. The solution was loaded onto anion exchange resin (AG1x8,

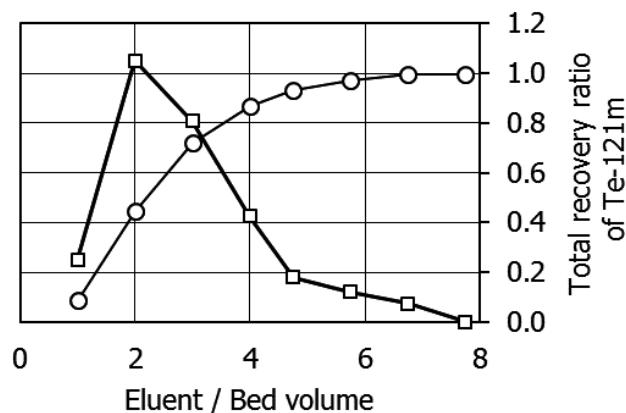


Fig. 1. Elution (□) and total recovery ratio (○) of tellurium from antimony (5 mM) with 1.6 M HCl.

Cl-form, 100–200 mesh, 10 mL), following which Te-121m was eluted with 1.6 M HCl.

Figure 1 shows the elution curve of Te-121m and the total recovery ratio of Te-121m. The total recovery ratio of Te-121m reached almost 100% with five bed volume eluent, while antimony was adsorbed onto the anion exchange resin without elution.

In this research, we investigated the purification of tellurium from matrix antimony with pH regulation. Its performance was satisfactory for a low antimony concentration. Further investigations are required to optimize the separation method for higher concentrations.

References

- 1) T. Kubota *et al.*, RIKEN Accel. Prog. Rep. **50**, 254 (2017).
- 2) T. Kubota *et al.*, RIKEN Accel. Prog. Rep. **52**, 205 (2019).
- 3) I. Puigdomenech, Chemical equilibrium diagrams: MEDUSA, (2010), <https://www.kth.se/che/medusa/downloads-1.386254> (accessed 2020-07-20).

^{*1} Institute for Integrated Radiation and Nuclear Science, Kyoto University

^{*2} RIKEN Nishina Center

Chemical separation of theranostic radionuclide ^{111}Ag produced in $^{\text{nat}}\text{Pd}(d, x)^{111}\text{Ag}$ reactions

K. Ooe,^{*1,*2} T. Watabe,^{*1,*2} Y. Shirakami,^{*2} D. Mori,^{*3} T. Yokokita,^{*3} Y. Komori,^{*3} H. Haba,^{*3} and J. Hatazawa^{*2,*4}

Silver-111 (^{111}Ag , $T_{1/2} = 7.45$ d) is a candidate radionuclide for theranostics (therapeutics + diagnosis). The nuclide emits β -particles (maximum β energy: 1036.8 keV), which can be applied to tumor therapy, and γ -rays with energies of 342 keV (branching ratio: 7%) and 245 keV (branching ratio: 1.33%), which can be used for imaging by single photon emission computed tomography (SPECT). However, ^{111}Ag has been rarely applied in the field of nuclear medicine. Toward the nuclear medical use of ^{111}Ag , we previously measured the production cross sections of $^{\text{nat}}\text{Pd}(d, x)^{111}\text{Ag}$ reactions.¹⁾ The energy at the peak of the excitation function of the $^{\text{nat}}\text{Pd}(d, x)^{111}\text{Ag}$ reactions was approximately 9 MeV with a cross section of approximately 40 mb, which is consistent with the reported results.²⁻⁴⁾ In this study, ^{111}Ag was chemically separated from a metallic $^{\text{nat}}\text{Pd}$ target through anion-exchange chromatography for future nuclear medical application of ^{111}Ag .

^{111}Ag was produced by irradiating a stack of 6 metallic $^{\text{nat}}\text{Pd}$ foils (purity: 99.95%, thickness: 0.10 mm, Nilaco Corp., Japan) with a 24-MeV deuteron beam from the RIKEN K70 AVF Cyclotron. The average beam intensity was approximately 200 nA, and the irradiation time was 30 min. After irradiation, one of the irradiated $^{\text{nat}}\text{Pd}$ targets was dissolved in a mixed HNO_3 and HCl solution. After evaporation to dryness, the residue was dissolved in 1 M HNO_3 solution and then fed into an anion exchange column (Muromac 1 \times 8, 200–400 mesh, NO_3^- form, $\Phi 10$ mm \times 11 cm). Firstly, ^{111}Ag was eluted by 1 M HNO_3 solution. According to the literature,⁵⁾ Ag shows no adsorption in 1 M HNO_3 solution on an anion-exchange resin, while Pd adsorbs on the resin. After the elution of ^{111}Ag , $^{\text{nat}}\text{Pd}$ was stripped by concentrated HNO_3 solution. Each eluted fraction (approximately 1 mL) was subjected to γ -ray spectrometry with a Ge detector for determining ^{111}Ag radioactivity by using the 342-keV γ peak of ^{111}Ag . Because this γ peak was partly overlapped by the 345-keV γ peak of ^{105}Ag ($T_{1/2} = 41.29$ d), which was simultaneously produced in the $^{\text{nat}}\text{Pd}(d, x)$ reactions, the area of the 342-keV γ peak of ^{111}Ag was calculated by Gaussian fitting. The elution behavior of $^{\text{nat}}\text{Pd}$ was checked using the 172-keV γ peak of $^{111\text{m}}\text{Pd}$ ($T_{1/2} = 5.5$ h), which was also produced in the $^{\text{nat}}\text{Pd}(d, x)$ reactions.

Figure 1 shows the elution curves of ^{111}Ag and

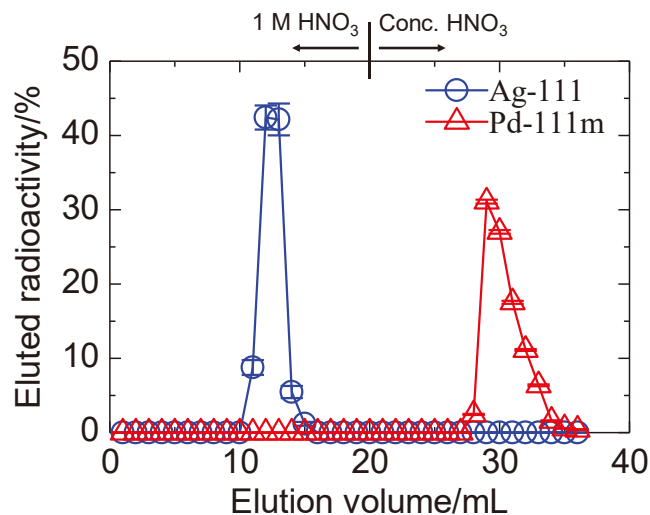


Fig. 1. Elution curves of ^{111}Ag and $^{111\text{m}}\text{Pd}$ in anion-exchange chromatography.

$^{111\text{m}}\text{Pd}$ obtained in this study. The elution of ^{111}Ag by 1 M HNO_3 solution started from fraction #11 and almost finished at fraction #16 before the start of elution of $^{111\text{m}}\text{Pd}$, showing the clear separation of ^{111}Ag from the $^{\text{nat}}\text{Pd}$ target. By changing the eluent to concentrated HNO_3 after fraction #20, the elution of $^{111\text{m}}\text{Pd}$ started from fraction #28. Very little ^{111}Ag and $^{111\text{m}}\text{Pd}$ radioactivities remained on the anion-exchange column after completion of the separation. The recovery yields of ^{111}Ag and $^{111\text{m}}\text{Pd}$ were approximately 99% and 98%, respectively. This high yield for ^{111}Ag is quite suitable for nuclear medical use, which requires large radioactivity for tumor therapy. Because many radioactive isotopes of Ag are produced in the $^{\text{nat}}\text{Pd}(d, x)$ reactions, the use of an enriched ^{110}Pd target is essential for the selective production of ^{111}Ag in the $^{110}\text{Pd}(d, 2n)^{111}\text{Ag}$ reactions. However, enriched ^{110}Pd targets are quite expensive, and it is important to recycle the ^{110}Pd target after the separation of ^{111}Ag . Therefore, the high recovery yield for $^{111\text{m}}\text{Pd}$ obtained in this study is also favorable for the separation of ^{111}Ag in medical use. The present results will lead to preclinical studies of therapeutic effects with ^{111}Ag .

References

- 1) K. Ooe *et al.*, RIKEN Accel. Prog. Rep. **52**, 195 (2019).
- 2) A. Hermanne *et al.*, Nucl. Instrum. Methods Phys. Res. B **217**, 193 (2004).
- 3) N. Ukon *et al.*, Nucl. Instrum. Methods Phys. Res. B **426**, 13 (2018).
- 4) F. Ditrói *et al.*, Nucl. Instrum. Methods Phys. Res. B **270**, 61 (2012).
- 5) J. P. Faris, R. F. Buchanan, Anal. Chem. **36**, 1157 (1964).

*1 Department of Nuclear Medicine and Tracer Kinetics, Osaka University Graduate School of Medicine

*2 Institute for Radiation Sciences, Osaka University

*3 RIKEN Nishina Center

*4 Research Center for Nuclear Physics, Osaka University

Preliminary investigation of nanoclay-gel-based fluorescent gel dosimeters under carbon-ion beam

T. Maeyama,^{*1,*2} A. Mochizuki,^{*1,*2} N. Fukunishi,^{*2} and K. L. Ishikawa^{*2,*3}

High-precision radiotherapy that focuses high doses of radiation on tumors and decreases the amount of damage to healthy tissues is becoming popular. To validate the complex dose distribution, tissue-equivalent dosimetry with high spatial resolution in three dimensions is required. Gel dosimetry has attracted attention for dose verification in advanced radiotherapy. A gel dosimeter is prepared from a radiation-sensitive compound and a gelling agent. After a radiation-induced chemical reaction, the gel retains the same spatial distribution, and the 3D dose distribution can be evaluated by 3D gel scanning. Gel dosimeters are categorized according to the characterization method used: the nuclear magnetic resonance (NMR) measurement method,¹⁻⁵⁾ absorptiometry (X-ray⁶⁾ or visible light^{7,8)}, and fluorometry. The sensitivity of detection by fluorometry⁹⁻¹¹⁾ is approximately 1,000 times greater than that by visible-light absorptiometry because fluorescence can be detected against a low background, isolated from excitation light. In contrast, absorptiometry measures transmitted light relative to high incident light levels at the same wavelength. The measurement methods using NMR and X-ray computed tomography (CT) also show limited detection sensitivity, and the dose of irradiation products must be at least several Gy for successful detection. In contrast, mGy-level dose can be detected by fluorometry. Thus, gel dosimeters employing fluorometry are expected to be the most highly sensitive type of gel dosimeter.

In a recent study, we reported a nanoclay-gel-based dosimeter that uses fluorescent dyes for X-ray irradiation. Although most gel dosimeters are prepared using organic gelling agents, such as gelatin, sensitivity can be enhanced by introducing inorganic nanosized clay as the gelling agent.⁹⁻¹¹⁾ There are two types of such agents. The first is nanoclay-based radio-fluorogenic gel (NC-RFG), in which a fluorescent dye is produced when a non-fluorescent dye, such as coumarin-3-carboxylic acid (CCA), reacts with radicals formed from the radiolysis of water. The second type of gel is nanoclay-based radio degradation fluorescence gel (NC-RDG), in which a non-fluorescent dye is produced when a fluorescent dye, such as rhodamine 6G (R6G) or 7-diethylamino-4-methylcoumarin (7D4MC), reacts with radicals. In this study, nanoclay-gel-based fluorescent gel dosimeters were applied to heavy-ion-beam irradiation for preliminary investigation.

Fluorescent gels were prepared using nanoclay as the gel, deionized water, and a fluorescence dye or probe. Two types of gel dosimeters prepared for this study. One was prepared from 2 μM 7D4MC and 2.5-wt% nanoclay as follows. First, clay dispersion stock was prepared by

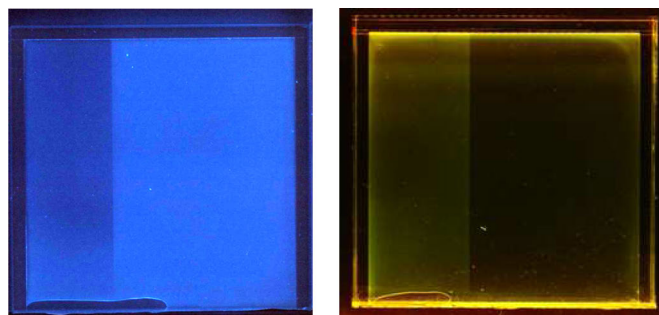


Fig. 1. Scanned image of fluorescent gel after irradiation with 135 MeV/nucleon $^{12}\text{C}^{6+}$ (entrance surface dose = 12 Gy).

mixing 23.35 g of ultra-pure water (Simplicity UV, Millipore Corp.) with 0.75 g of clay in a glass beaker at room temperature. A fluorescence probe stock solution (500 mL) was prepared by mixing 1.14 mg of 7D4MC with water. The clay dispersion stock (24.1 g) and fluorescence probe stock solution (5.9 mL) were then introduced to a 50 mL screw-capped glass vial and mixed using a rotation/revolution vacuum mixer (V-mini300, EME Corp., Japan) for 10 min at 1200/600 rpm and -90 hPa gauge pressure to obtain a uniform dispersion.

The other was prepared from 100 μM dihydrorhodamine 123 (DHR123) and 2.5-wt% nanoclay using a rotation/revolution vacuum mixer with the same procedure. Finally, prepared gels were enclosed in a $100 \times 100 \times 10$ mm plate. The prepared samples were irradiated using $^{12}\text{C}^{6+}$ -ion beams (135 MeV/nucleon) accelerated by the RI Beam Factory (RIBF) at RIKEN. The irradiated samples were scanned using a fluorescent gel scanner.

The irradiation changes in fluorescence intensity with irradiation were observed, as shown in Fig. 1. The left image shows the entrance surface. In 7D4MC fluorescent gel, the fluorescence intensity decreases with increasing dose, and in DHR123 fluorescent gel, the fluorescence intensity increases with increasing dose. The detailed results are currently being analyzed, and some results will be submitted.

References

- 1) T. Maeyama *et al.*, J. Radiat. Res. **57**, 318 (2016).
- 2) T. Maeyama *et al.*, J. Phys. Chem. B **121**, 4238 (2017).
- 3) T. Maeyama *et al.*, Radiat. Phys. Chem. **96**, 92 (2014).
- 4) T. Maeyama *et al.*, Radiat. Phys. Chem. **107**, 7 (2015).
- 5) T. Maeyama *et al.*, Radiat. Phys. Chem. **146**, 121 (2018).
- 6) E. Maynard *et al.*, Phys. Med. Biol. **63**, 075014 (2018).
- 7) K. I. Penev *et al.*, Med. Phys. **44**, 1948 (2017).
- 8) I. Kawamura *et al.*, Jpn. J. Appl. Phys. **58**, 0222003 (2019).
- 9) T. Maeyama *et al.*, J. Phys. Conf. Ser. **1305**, 012045 (2019).
- 10) T. Maeyama *et al.*, Sens. Actuators A **298**, 111435 (2019).
- 11) T. Maeyama *et al.*, Radiat. Phys. Chem. **151**, 42 (2018).

^{*1} Kitasato Univ

^{*2} RIKEN Nishina Center

^{*3} Univ. of Tokyo

4. Radiation Chemistry and Biology

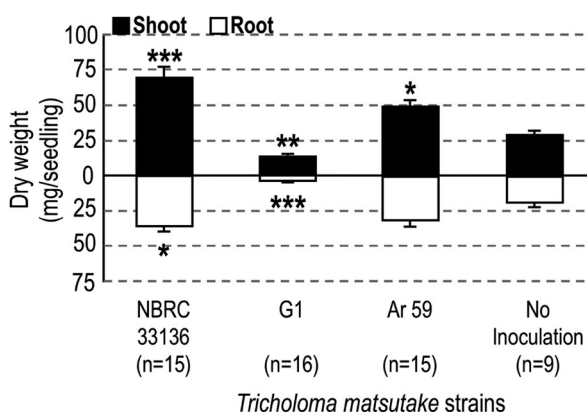
Mutants of the ectomycorrhizal mushroom *Tricholoma matsutake* that exert detrimental effects on its symbiotic partner *Pinus densiflora*[†]

H. Murata,^{*1} S. Nakano,^{*1} T. Yamanaka,^{*1} T. Abe,^{*2} H. Ichida,^{*2} Y. Hayashi,^{*2} T. Shimokawa,^{*1} K. Tahara,^{*1} and A. Ohta^{*3}

Tricholoma matsutake is an ectomycorrhizal fungus that produces the prized mushrooms “matsutake” in symbiotic association with conifers.¹⁾ In our attempts to induce mutants of *T. matsutake* that could be useful in artificial cultivation for fruiting by γ -ray irradiation at 500 Gy, we isolated a mutant, designated as G1, that grew better in substrates than the wild-type NBRC 33136.¹⁾ The phenotype of G1 on agar plates somewhat resembled that of Ar 59, which had been isolated by argon-ion-beam irradiation at 500 Gy; both mutants overproduced amylase and cellulase activities and exhibited a mycelial morphology different from the wild-type, forming a fuzzy cotton-ball-like colony, rather than a mycelial mat.^{1,2)} In the present study, we examined how G1 and Ar 59 influence the plant growth of *Pinus densiflora* seedlings in vitro.

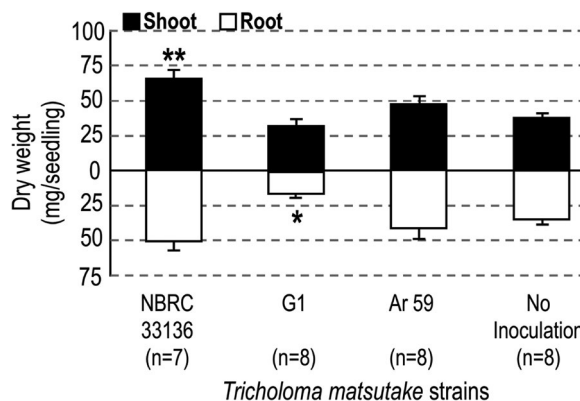
The inoculation was performed with two different methods. The first involved sterile 1-week-old *P. densiflora* seedlings, in which the seedlings were planted in a pumiceous soil substrate filled with *T. matsutake* mycelia and axenically co-cultured at 23°C for 120 days. The second involved sterile 1-month-old *P. densiflora* seedlings already grown in the pumiceous soil, in which *T. matsutake* mycelia were placed on the surface of the substrate where the shoot base emerged; they were axenically co-cultured at 23°C for 150 days.

In the first experiment, G1 exhibited a significant detrimental effect on both above- and below-ground organs; root systems were severely underdeveloped or collapsed, leading in turn to aboveground wilting (Fig. 1).



© Canadian Science Publishing

Fig. 1. Biomass measurements of 1-week-old *P. densiflora* seedlings co-cultured with *T. matsutake* strains for 120 days.



© Canadian Science Publishing

Fig. 2. Biomass measurements of 1-month-old *P. densiflora* seedlings co-cultured with *T. matsutake* strains for 150 days.

This result contrasts with the plant-growth-promoting effect of Ar 59, as well as NBRC 33136; the former allowed the seedlings to gain significantly higher above-ground and total biomasses than the control, while the latter allowed them to gain significantly higher above-ground, belowground, and total biomasses (Fig. 1).

In the second experiment, seedlings associated with G1 exhibited significant decreases in their belowground biomasses, and many lateral roots degenerated significantly, reducing their rhizosphere biomasses (Fig. 2). Seedlings associated with Ar 59, in contrast, exhibited neither plant-growth-promoting nor plant-growth-inhibiting effects (Fig. 2). Unlike these mutants, NBRC 33136 promoted plant growth; the aboveground and total biomasses significantly increased, but the below-ground biomass did not (Fig. 2).

Data suggest that there could be a regulatory region in the genome of *T. matsutake* that determines plant associating behaviors, depending upon where the mutations occur and what environment the fungus inhabits based on its endophytic association with non-host plants.³⁾ The overproduction of degrading enzymatic activities is not the cause of G1's trait of harming its symbiotic partner, because Ar 59 overproduced the same enzymatic activities without harming *P. densiflora* seedlings. Genomic and transcriptomic analyses of these mutants will allow us to unearth the unknown regulatory mechanisms involved in the ectomycorrhizal symbiosis of *T. matsutake*.

References

- 1) H. Murata *et al.*, *Botany* **97**, 463 (2019).
- 2) H. Murata *et al.*, *Mycorrhiza* **28**, 171 (2018).
- 3) H. Murata *et al.*, *Mycorrhiza* **23**, 235 (2013).

[†] Condensed from the article in *Botany* **97**, 463–474 (2019)

^{*1} Forest Research and Management Organization

^{*2} RIKEN Nishina Center

^{*3} Lake Biwa Environmental Research Institute

Effect of heavy-ion-beam irradiation on mycelial growth of medicinal mushrooms

M. Hatashita,*¹ K. Takagi,*¹ H. Ichida,*² and T. Abe*²

It is well known that β -D-glucans from fungi are effective initiators of cell-mediated immunity in humans.¹⁾ β -D-glucans isolated from various fungi differ in their chemical structures and, consequently, in their immunomodulatory activities. For example, schizophyllan, which is a β -D-glucan extracted from the fungus *Schizophyllum commune* and is classified as a medicine, stimulates the immune system.²⁾ We are aiming to establish beneficial mutants from several extremely rare fungi with immunostimulatory activities. We had already achieved the isolation of several *Cordyceps militaris* mutants with higher proliferative activity by the repeated propagation of expanding hyphal tips from the proton-beam irradiation of the fungus.³⁾ Heavy-ion beams have been accepted as an effective mutagen.⁴⁾ A small number of genes are expected to be disrupted in the mutant genomes because heavy-ion beams can induce mutations with a high frequency at relatively low doses. Such characteristics of heavy-ion irradiation are advantageous for mutation breeding. In the latest study, prior to mutant screening by ion-beam breeding, we examined the dose dependence of mycelial growth of two fungi against the irradiation of heavy-ion beams and compared the mycelial-growth effect of heavy-ion-beam irradiation to that of proton-beam irradiation.

The microbial strain *Fuscoporia obliqua* NBRC 8681 was obtained from the National Institute of Technology and Evaluation. It was inoculated on an agar plate (potato dextrose agar [PDA⁵⁾]) and incubated at 25°C. The microbial strain *Polyporus umbellatus* ATCC 60546 was purchased from the American Type Culture Collection. It was inoculated on an agar plate (yeast malt peptone agar [YM⁵⁾]) and incubated at 25°C. These samples were inoculated on fresh 6 cm plates 4 days before the irradiation and incubated in the dark at room temperature. The 200-MeV proton-beam irradiation (LET 0.5 keV/ μ m) on the culture plates was carried out by the Wakasa Wan Multi-purpose Accelerator with Synchrotron and Tandem at the Wakasa Wan Energy Research Center in the dose range of 100–2,000 Gy. The culture plates were irradiated with Ar ions (LET 180 keV/ μ m) and Fe ions (LET 640 keV/ μ m) in the dose range of 100–300 Gy at the RIKEN RI-beam factory.

For the growth-rate measurement, three loops of mycelia from the center of each irradiated plate were inoculated on each center of three fresh 9 cm plates and incubated at 25°C. The maximum and minimum diameters of the mycelial zone of each plate were measured using a vernier caliper 8 days later. The data from three irradiated plates were averaged and compared with the data from the control.

*¹ Res. and Develop. Dept., The Wakasa Wan Energy Research Center

*² RIKEN Nishina Center

Table 1. Effect of ion-beam irradiation on mycelial growth of medicinal mushrooms.

Strain	Ion	Dose (Gy)	Relative ratio of mycelium growth (%)
<i>F. obliqua</i>	H	0	100.0
		500	47.4
		1,000	23.7
		1,500	3.1
		2,000	0.0
	Ar	0	100.0
		150	67.6
		300	50.8
	Fe	0	100.0
		100	82.0
		200	60.7
		300	42.2
<i>P. umbellatus</i>		H	0
	500		85.7
	1,000		52.7
	1,500		6.2
	2,000		0.0
	Ar	0	100.0
		150	99.1
		300	5.3
	Fe	0	100.0
		100	94.2
		200	56.8
		300	2.3

Table 1 lists the relative ratio of the mycelial growth for two strains, which were irradiated with three kinds of ion beams, respectively. Under any irradiation condition, the mycelial growth rate decreased as the irradiation dose increased. For proton-beam irradiation, the results for irradiation doses of 100 and 300 Gy were almost the same as those of the control (data not shown), and the relative suppressions of mycelial growth were observed from 500 to 2,000 Gy. Relative ratios of mycelial growth of 50.8% and 42.2% were obtained with *F. obliqua* after irradiation with 300 Gy of Ar and Fe ions, respectively. Moreover, relative ratios of 5.3% and 2.3% were obtained with *P. umbellatus* after irradiation with 300 Gy of Ar and Fe ions, respectively. Heavy-ion beams showed a higher relative biological effectiveness (RBE) of mycelial growth inhibition than proton beams, regardless of the kind of fungi.

References

- 1) D. L. Williams, *Mediators Inflamm.* **6**, 247-50 (1997).
- 2) V. E. Ool, F. Liu, Liu, *Curr. Med. Chem.* **7**, 715-29 (2000).
- 3) S. K. Das *et al.*, *Lett. Appl. Microbiol.* **47**, 534-8 (2008).
- 4) Y. Kazama *et al.*, *Genes Genet. Syst.* **88**, 189-97 (2013).
- 5) A. Imtiaj *et al.*, *Mycobiology* **36**, 34–39 (2008).

Yield improvement of starch-degrading enzyme in fungi by ion-beam mutagenesis

H. Iwahara,^{*1} T. Matsui,^{*1} H. Ichida,^{*2} and T. Abe^{*2}

To improve the productivity of amylolytic enzymes in filamentous fungi that are widely used worldwide, various breeding processes have been conducted so far. In breeding by classical mutagenesis, chemical mutagen treatment, UV irradiation, and gamma-ray irradiation have been used for years on filamentous fungi; however, the range of mutation could be narrowed with the repeated use of the same conventional methods. Therefore, this study was conducted with the aim of investigating the possibility of heavy-ion beams as a new source of mutagenesis for breeding filamentous fungi.

The spores of *Aspergillus niger* that produce starch-degrading enzymes were dried on membrane filters (ADVANTEC, A020A025A), and these membranes, packed in Hybri-bags (Cosmo Bio), were irradiated with heavy-ion beams of carbon and iron (50 to 400 Gy). The LETs of C and Fe ions were 76 keV/ μm and 640 keV/ μm , respectively.

The mutants obtained from 200 Gy of C ions and 400 Gy of Fe ions with a survival rate of approximately 20% were examined for their enzyme productivity (Fig. 1).

Simultaneously, we also examined mutants that had been treated with N-methyl-N'-nitro-N-nitrosoguanidine (NTG) and UV irradiation on the same *A. niger* strain and compared them with those obtained using heavy-ion beams.

Among the mutagens used, NTG treatment yielded the most diversified morphology on the strain, and UV irradiation showed the least change in morphology. The morphology of mutants treated with heavy-

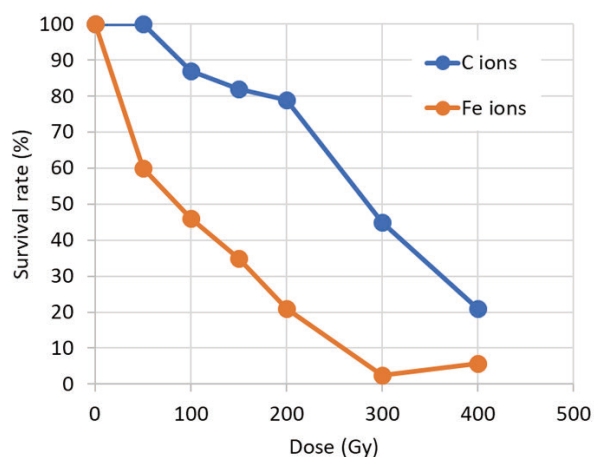


Fig. 1. Survival curves of fungi producing starch-degrading enzymes after C- and Fe-ion irradiation.

^{*1} Novozymes Japan

^{*2} RIKEN Nishina Center

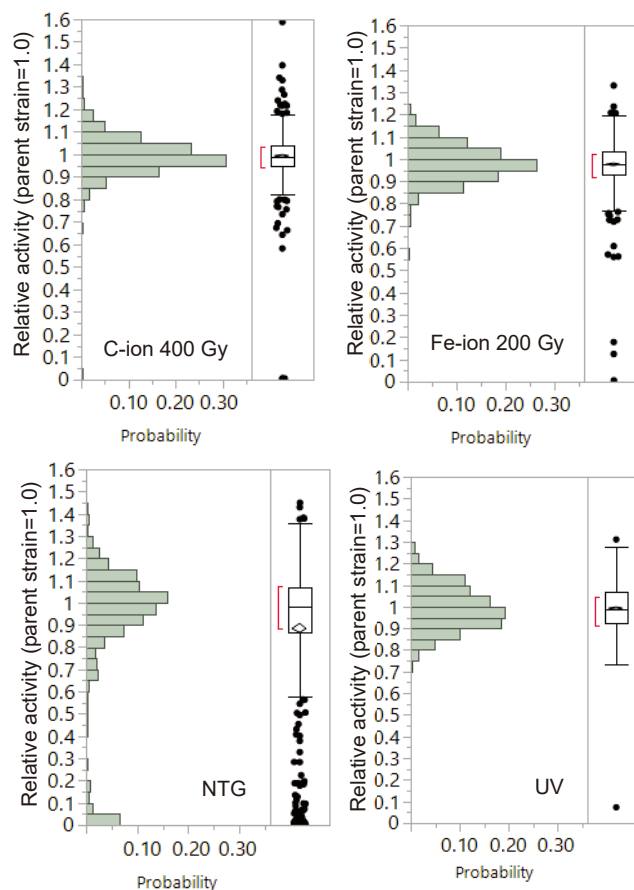


Fig. 2. Yield deviations of mutants treated with various mutagens.

ion beams was less diversified than that of NTG, but considerable diversity was still observed in the sporulation and the length of aerial hyphae.

In addition, 920 strains were randomly isolated from each mutagen group and cultivated in a liquid medium with 96-well microtiter plates, and their enzyme productivity was examined and compared with that of the parent strain (Fig. 2). The NTG mutant group showed the largest variation, but both the C-ion and Fe-ion mutants also showed a wide variation. In addition, several mutants from both the ion beams and NTG showed a higher productivity than the parent strain. These mutants will be further examined in larger-scale fermentation.

From these results, it was confirmed that the heavy-ion beam was effective against *A. niger* as a mutagenesis tool for improving productivity. We will continue to conduct screening on a larger scale with the aim of further improving enzyme productivity.

Mutation breeding of sake yeast using heavy-ion-beam irradiation

K. Baisho,^{*1} H. Tomioka,^{*1} Y. Furuki,^{*1} Y. Hayashi,^{*2} and T. Abe^{*2}

In recent years, the total sake consumption has been decreasing, although the consumption of fruity sake variants such as Ginjo-shu is increasing. Taste of fruity sake results from malic acid.¹⁾ Malic acid is produced by yeast during main fermentation (moromi).²⁾ The main objective of this study is to isolate a high-malic-acid-producing yeast strain through the irradiation of heavy-ion beams to develop high-value-added products.

The parent strain is an in-house yeast strain, T-66. It is isolated from Kyokai-kobo K-6 and tends to produce more organic acid more than K-6. T-66 was precultured in 5 mL of a koji extract medium (a Baumé degree of 6.0) at 30°C for 2 days. The cultured yeast cells were spread on YPD agar medium plates [20 g/L (w/v) glucose, 20 g/L (w/v) polypeptone, 10 g/L (w/v) yeast extract, and 18 g/L (w/v) agar]. We irradiated the plates with 500 Gy of Fe-ion beams (790 keV/ μm) at the RIKEN Nishina center in July 2018. After incubation at 30°C for 5 days, 88 mutant yeast strains were isolated from the plates.

As primary screening, the mutagenized yeast strains was precultured in 5 mL of *koji* extract medium. 3 mL of yeast culture was added to 20 mL of *koji* extract medium supplemented with 7 g alcohol-dehydrated *koji* and incubated at 20°C for 10 days.³⁾ Filtrated mediums were measured using an alcohol densitometer (Alcomate AL-2, Woodson Riken Keiki, Tokyo), and titratable acid-

Table 1. Analysis of mutant yeast strains.

Sample name	Alcohol content [%]	Titratable acidity [-]	Malic acid [mg/L]
Parent strain	19.7	4.5	639.2
P1-8	19.5	5.2	908.3
P2-11	18.9	4.8	624.8
P3-10	18.2	4.9	975.6
P4-3	16.6	4.8	797.8
P6-12	20.2	4.9	778.5
P6-9	20.0	4.8	725.7
P7-13	19.7	5.0	884.3
P7-6	20.1	4.8	1100.5

Table 2. Analysis of small-scale sake brewing.

Sample name	Sake meter value [-]	Alcohol content [%]	Titratable acidity [-]	Amino acid content [-]	Sensory evaluation
Parent strain	+4.6	17.1	2.9	0.8	3
P1-8	+4.1	16.8	3.6	0.8	2
P3-10	+1.8	16.6	3.6	0.8	1
P7-6	+9.1	17.3	3.4	0.7	2

^{*1} Akita Shurui Seizoh Co., Ltd.

^{*2} RIKEN Nishina Center

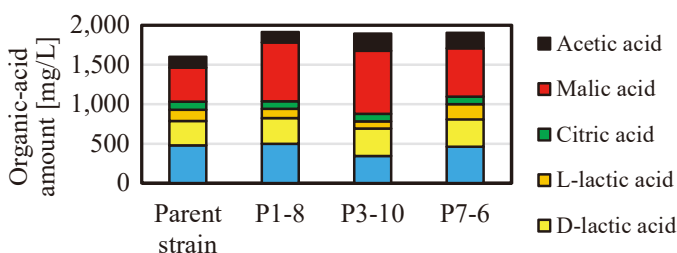


Fig. 1. Organic-acid production of isolated mutant yeast strains.

ity was measured using the official analysis method of the National Tax Agency. We selected 8 mutant yeast strains that produced more organic acids than the parent strain without producing any off-flavor. Next, the amount of organic acid (succinic acid, lactic acid, citric acid, malic acid, and acetic acid) was measured using an F-kit (J. K. International, Tokyo). Table 1 lists the results of primary screening. The malic-acid production amounts of P1-8, P3-10, and P7-6 strains were higher than those of the parent strains.

As secondary screening, the parent strain, T-66, and 3 selected mutant yeast strains were examined by small-scale sake brewing. After the filtration of fermentation mash, the sake meter value (SMV), an indicator of sweetness of sake; alcohol content; titratable acidity; and amino-acid content were measured using the official analysis method of the National Tax Agency. Additionally, we performed sensory evaluation (3-step rating: 1 is good and 3 is bad). Table 2 lists the results. The three selected mutant yeast strains produced more organic acid than the parent strain. While the SMVs are different, the three mutants show almost the same level of alcohol production as T-66. This result shows that the three mutant yeasts have good brewing ability. P3-10 scored the highest value in sensory evaluation. To verify the reason for this result, the amount of organic acid was measured using an F-kit (Fig. 1). P3-10 showed a higher malic-acid content and lower succinic-acid content than the other mutants, indicating that the sake brewed with this strain will have a light taste that matches the preference of recent consumers. It was shown that the P3-10 strain produces a lighter-tasting sake than the parent strain, T-66.

We isolated the high-malic-acid-producing yeast strain P3-10 derived from T-66. P3-10 produces not only more malic acid but also more acetic acid more than T-66. Because acetic acid produces an off-flavor for sake, we plan to improve on the P3-10 strain.

References

- 1) Y. Shimazu *et al.*, *J. Brew. Soc. Japan* **106**, 747 (2011).
- 2) M. Toyozawa *et al.*, *J. Ferment. Technol.* **38**, 342 (1960).
- 3) K. Saito *et al.*, *J. Brew. Soc. Japan* **87**, 915 (1992).

Isolation of morphological mutants in a bryophyte model *Marchantia polymorpha* using heavy-ion mutagenesis

S. Sakai,^{*1} C. Hirata,^{*1} Y. Sakai,^{*1} Y. Kazama,^{*2,*3} T. Abe,^{*2} and K. Ishizaki^{*1}

Since land plants emerged approximately 470 million years ago, their body plans have changed significantly during evolution through a transition from gametophyte-dominant to sporophyte-dominant life histories and the development of many specialized tissues and organs, such as stomata, vascular tissues, roots, leaves, seeds, and flowers. Bryophytes occupy a basal position in land-plant evolution, and the haploid (n) gametophyte is dominant over the diploid ($2n$) sporophyte in their life histories, while angiosperms (flowering plants), the last diverged group of land plants, have diploid ($2n$) sporophyte-dominant life histories. For better understanding of the evolution of body plan in land plants, the accumulation of knowledge about the molecular mechanism for the gametophytic organ development in bryophytes is needed. Forward-genetic approaches focusing on the gametophyte development in bryophytes are especially important.

The bryophyte *Marchantia polymorpha* is a classical but recently emerging model plant. Recently, powerful experimental tools for molecular genetics have been established in *M. polymorpha*, including high-frequency transformation techniques and genome-editing techniques using the CRISPR/Cas9 system,¹ in addition to the whole genome sequence information.² As it exhibits low genetic redundancy in most regulatory pathways,² *M. polymorpha* should be advantageous for forward-genetic approaches. Similar to other bryophytes, the spores are haploid; therefore, the effect of the induced mutations can be immediately observed in the first gametophyte generation developed from the spores.

In this study, we adopted a heavy-ion beam as the mutagen for screening mutants with altered gametophyte morphology in *M. polymorpha*. Spores, which are single

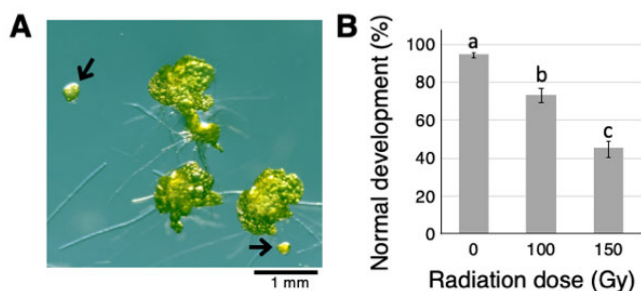


Fig. 1. Assessment of the mutagenicity of carbon-ion beams on the spores of *M. polymorpha*. Plants grown from the spores irradiated with carbon-ion beams were observed (A), and the ratio of normal thallus development was evaluated (B) ($N = 4$, $n = 69$ – 466 , bar = SD). Values accompanied by different letters are significantly different (Tukey's test, $p < 0.05$). Arrow, growth-arrested plants.

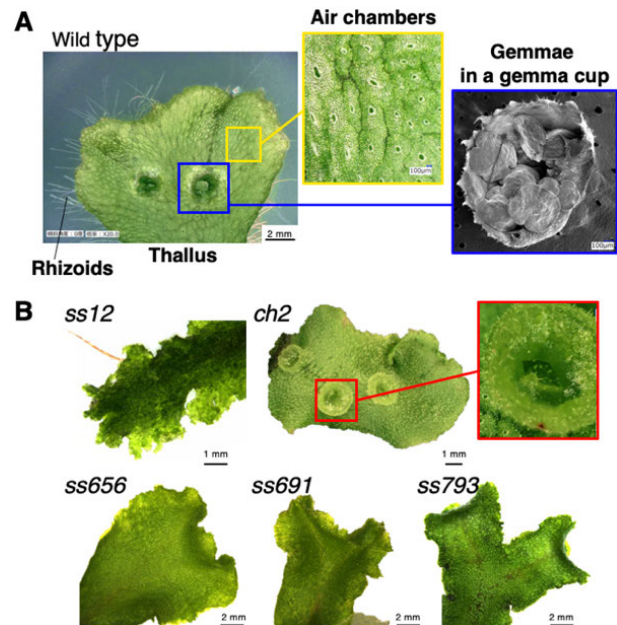


Fig. 2. Wild-type thallus (A) and isolated morphological mutants (B) of *M. polymorpha*.

cells and the start point of the development of the thallus (plant body) in *M. polymorpha*, were irradiated with a carbon-ion beam (LET: $30 \text{ keV}/\mu\text{m}$) at a dose of 100 Gy or 150 Gy. Carbon-ion irradiation decreased the ratio of the normal thallus development from the spores in a radiation-dose-dependent manner (Fig. 1A and B).

Subsequently, the plants developed from spores irradiated with carbon-ion beams were further cultured for several weeks to screen for mutants. To date, 19 mutants showing abnormal thallus development were successfully isolated among $\sim 9,000$ individuals. As shown in Fig. 2A, on the thallus surface of the wild-type plant, air chambers (yellow square) and gemma cups with clonal progenies, gemmae (blue square), are developed. Two of the 19 isolated mutants develop defective air chambers, 10 have abnormal gemmae and gemma cups, and 7 showed defects in both air-chamber and gemma-cup development. For example, a mutant *ss12* shows a marked decrease in the frequency of air-chamber formation and *ch2* has gemma cups with no gemma (red square), while *ss656*, *ss691*, and *ss793* are deficient in the development of gemma cups (Fig. 2B). We are currently conducting the detailed characterization of morphological phenotypes in these mutants, in parallel with the identification of the causal genes using next-generation sequencing (NGS). These mutants seem promising to reveal important factors functioning in the gametophytic organ development in the model basal land plant *M. polymorpha*.

References

- 1) K. Ishizaki *et al.*, *Plant Cell Physiol.* **57**, 262–270 (2016).
- 2) J. L. Bowman *et al.*, *Cell.* **171**, 287–305 (2017).

^{*1} Dep. Biol., Fac. Sci., Grad. Sch. Sci. Kobe Univ.

^{*2} RIKEN Nishina Center

^{*3} Fac. Biosci. Biotech., Fukui Pref. Univ.

Breeding of summer-autumn-flowering small-flowered spray-type chrysanthemums cultivar ‘Nagasaki SWC1’ by heavy-ion-beam irradiation

A. Hisamura,^{*1} J. Morooka,^{*2} T. Abe,^{*3} Y. Hayashi,^{*3} and T. Hirano^{*3,*4}

In Nagasaki Prefecture, the small-flowered spray-type chrysanthemums is promoted for planting in open fields because producers can cultivate it at low cost. It has a great demand during Obon (early in August) as a funeral flower in Japan. It is necessary to ship three colors of flowers (red, white, and yellow) simultaneously from the market. However, the shipment time is unstable because of bloom delays or bud departing at the early stage caused by high temperatures during the cultivation period. Therefore, the development of a new cultivar that enables a stable shipment time has been desired to meet the needs of the market. We conducted cross-breeding and selected a superior red lineage for which the blooming time can be controlled using long-day treatment under lighting (Fig. 2(a)). In this study, we irradiated this superior red lineage with a heavy-ion beam to obtain cultivars of different colors that have the same shipment time as the superior red lineage. It has been reported that the flower color of the original cultivar is important to obtain a wide mutation spectrum of the flower color in *Chrysanthemum*.¹⁾ This cultivar was thought to be suitable for inducing mutations of the flower color such as white or yellow. As a result, we succeeded in developing a new cultivar known as ‘Nagasaki SWC1’ with white flowers in 2018.

We irradiated 27 scions of the superior red lineage with C-ion beams (LET: 23 keV/ μm) at a dose of 5 Gy at RIKEN Nishina Center in January 2015. We planted and pinched the irradiated scions as a mother stock, following which we picked scions. We planted these scions in the field and obtained 984 candidate mutant plants, including 49 flower-color mutants. Some of these mutants were chimera. Therefore we isolated the plants with only white flowers in the first selection. We multiplied these plants and cultivated them in the field in 2016. Subsequently we selected a superior plant named ‘W1-1’ in the second selection. The third selection was performed in 2017 to confirm its stability of characteristics and flower color. The final experimental production of ‘W1-1’ was performed at the field of an agricultural center, and ‘W1-1’ gained high evaluation in a test of adaptability to local fields in 2018. We named this superior cultivar ‘Nagasaki SWC1’ and applied for the registration of this variety on March 18, 2019.

‘Nagasaki SWC1’ has a white (white-group 155-C on the R.H.S. color chart) single flower (Fig. 2(b)). It



Fig. 1. Original flower and the flower-color mutants.



Fig. 2. Original flower (a) and a new cultivar ‘Nagasaki SWC1’ (b).

blooms in the middle of July under natural long days. It is also possible to control blooming by long-day treatment under light culture and adjust the shipment time to the period of highest demand which is early August. Furthermore, ‘Nagasaki SWC1’ has a small unnecessary inferior branch. This characteristic provides a labor-saving plant shape which is suitable for bouquet making. These characteristics of ‘Nagasaki SWC1’ are inherited from the superior red lineage. Therefore, red and white flowers can be shipped simultaneously in the period of highest demand. This is a great advantage for producers, and an increase in their income can be expected. Presently, we are working on breeding a yellow flower line. Our aim is to breed a new cultivar for a set of three colors of small-flowered spray-type chrysanthemums.

Reference

1) K. Tamaki *et al.*, Hort. Res. (Japan) **16**, 117 (2017).

^{*1} Agriculture and Forestry Technical Development Center, Nagasaki Prefectural Government

^{*2} Shimabara Development Bureau

^{*3} RIKEN Nishina Center

^{*4} Faculty of Agriculture, University of Miyazaki

Mutation induction in strawberry of original Saitama cultivar by C-ion irradiation

H. Uchida,^{*1} H. Oda,^{*1} E. Kondo,^{*1} Y. Hayashi,^{*2} and T. Abe^{*2}

Agriculture in Saitama prefecture is in a poor situation owing to the aging of producers and the decrease in the number of new farmers. Strawberry is one of the important farm products of Saitama because of its high productivity per unit area. We have been working on the breeding of strawberry since 2008 to enhance the production of strawberry. We successfully produced our original cultivars “Saien I-1Go” and “Saien I-3Go”¹⁾ and registered them in February 2019. These cultivars have a rich taste with high sugar content and moderate acidity, as well as a good balance between sweetness and acidity. Therefore, the production of these cultivars is expected to expand in the near future. On the other hand, they have the disadvantages of a late harvest period and low yield compared to general main varieties. In addition, the peel color of “Saien I-3Go” darkens in the warm season, which results in a reduced evaluation of the fruit appearance. To solve these problems, we conducted mutation breeding by using heavy-ion beams and are in the process of developing promising lines with improved yield factors such as an increased number of fruit sets, an earlier harvesting season, and a desirable peel color.

We used “Saien I-1Go” and “Saien I-3Go” for irradiation from 2015 to 2018. The seedlings were irradiated with C-ion beams (LET 22.5 keV/ μm) at dose ranges of 10–30 Gy, 30–80 Gy, and 30–120 Gy in 2015–2016, 2017, and 2018, respectively. After irradiation, seedlings were grown by cuttings. The survival rate was measured after 4 to 5 weeks, and the growth and changes in peel color were observed after planting. Selected mutant lines were propagated in a runner plant, and the stability of mutant

Table 1. Survival rate of “Saien I-1Go” and “Saien I-3Go.”

Dose (Gy)	Survival rate (%)	
	Saien I-1Go	Saien I-3Go
0	100.0	100.0
30	90.7	93.2
40	92.8	-
60	78.3	61.9
80	60.0	-
90	-	26.4
120	-	4.4

“Saien I-1Go” in 2017, and “Saien I-3Go” in 2018

The number of surviving plants was counted 4 (“Saien I-1Go”) or 5 (“Saien I-3Go”) weeks after irradiation.

^{*1} Saitama Agricultural Technology Research Center

^{*2} RIKEN Nishina Center

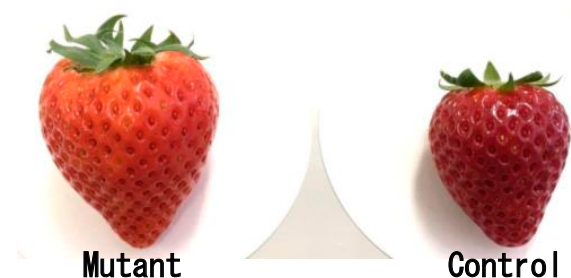


Fig. 1. Peel color of a mutant of “Saien I-3Go” irradiated at a dose of 30 Gy.



Fig. 2. High-branching mutant of “Saien I-1Go” irradiated at a dose of 80 Gy.

traits was confirmed in the next year.

According to the result, both “Saien I-1Go” and “Saien I-3Go” survived even at a dose of 80 Gy or more. A previous study showed that the lethal dose 50 of C-ion irradiation for apple and Japanese pear scions are 18 Gy and 13 Gy, respectively.²⁾ This suggests that the seedlings of strawberry may be a viable plant species even at high irradiation doses relative to those of other plants of the family Rosaceae (Table 1).

We obtained several mutant lines in this study. One of these mutant lines changed the peel color from dark red to light red (Fig. 1). Another line increased the number of branches and flowers owing to abnormal branching morphology (Fig. 2). We are currently investigating the other characteristics of these promising mutant lines, such as the grass shape, flowering time, and yield. We are also investigating whether the target trait is inherited in progeny and examining whether it is promising as a breeding stock.

The peel color of the mutant is lighter than that of the control.

The number of branches and flowers increased in the mutant.

References

- 1) H. Oda *et al.*, Bulletin of the Saitama Agricultural Technology Research Center. jpn. **17**, 7 (2018).
- 2) Y. Ito *et al.*, RIKEN Accel. Prog. Rep. **37**, 151 (2004).

Characteristics of heavy-ion mutagenesis in cultivated strawberry

T. Wada,*¹ T. Sueyoshi,*¹ K. Oku,*¹ K. Shimomura,*¹ and T. Abe*²

A cultivated strawberry cultivar “Fukuoka S6” has been a popular product in the Japanese strawberry market due to its high quality, which is attributed to desirable characteristics, such as large, deeply red, glossy and tasty fruits. However, this cultivar also has some disadvantages, such as late maturity and a soft fruit pericarp, which causes physical damage to the fruit while transporting. Ion-beam irradiation has attracted much attention as a novel technique for inducing spotted mutagenesis on plant genomes.¹⁾ This study developed mutants of strawberry, which show early flowering and high fruit firmness, by using heavy-ion-beam irradiation.

An experiment was performed in 2014 and 2015. In 2014, strawberry nursery seedlings (5 plants per treatment) propagated in a sterilized condition were exposed to a $^{12}\text{C}^{6+}$ ion-beam (1.62 GeV, LET 30 keV μm^{-1}) at the RIKEN Ring Cyclotron at doses of 0 (no treatment), 10, 15, 20, or 30 Gy. In 2015, seedlings were propagated similarly, separated, and filled up in a 50-ml falcon tube (at 7 g per tube). Eight tubes per treatment were exposed to a $^{12}\text{C}^{6+}$ ion-beam. Irradiated seedlings were transplanted and cultured on 1/2MS media at 20°C with a 16-h light regime, the weight of seedlings after 2 months from transplanting were measured, and the propagation ratio was calculated in comparison with the initial weight. The effect of each treatment was evaluated by comparing the propagation ratio to that achieved without treatment. Surviving seedlings were potted, acclimated, and transplanted in a greenhouse. The characteristics of mutants were examined using “Fukuoka S6” as a control.

The propagation ratio decreased with an increase in irradiation dose, but the propagation ratio at 30 Gy, which was the highest dosage, was 74% of that achieved without treatment (Fig. 1). Although many previous studies using cultivated strawberry adopted a dosage of approximately 10 Gy, such as 8 to 16 Gy,²⁾ 10 to 20 Gy,³⁾ and 0.5 to 2.5 Gy,⁴⁾ to obtain mutants in a practical breeding

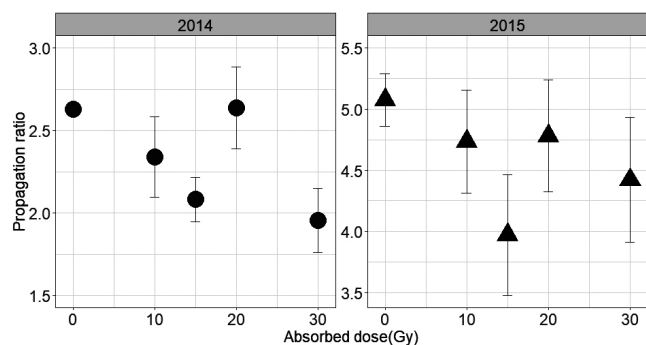


Fig. 1. Propagation ratio of strawberry seedlings mutated by carbon-ion beam irradiation.

*¹ Fukuoka Agric. Res. Cent.

*² RIKEN Nishina Center

Table 1. Characteristics of strawberry seedlings mutated by carbon-ion-beam irradiation.

Trait		Absorbed dose (Gy)				Total
		10	15	20	30	
Fruit color	Darkening	1	2	1	3	7
	Lightening	1	4	0	0	5
Fruit size	Upsizing	0	0	0	0	0
	Downsizing	12	23	10	15	61

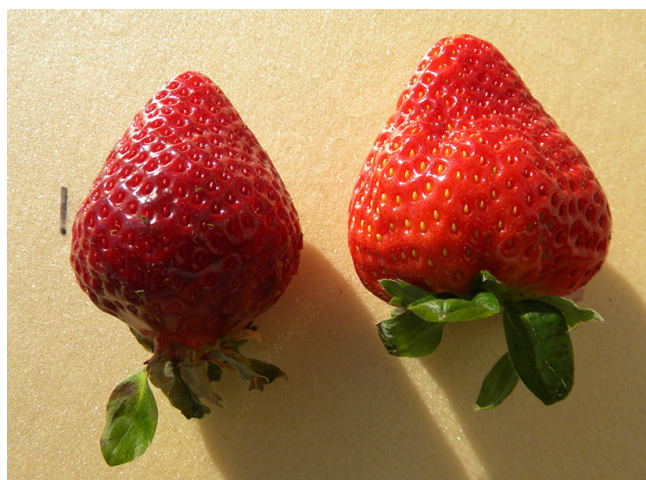


Fig. 2. Fruits of a mutant line developed from 15 Gy heavy-ion-beam irradiation (left) and “Fukuoka S6” (right). Bars = 1 cm.

program, the median lethal dose (LD₅₀) has not been detected. The survival ratio at 32 Gy of $^{12}\text{C}^{6+}$ ion-beam irradiation was 91%,²⁾ suggesting that the LD₅₀ of strawberry is greater than 30 Gy. Since the genome of strawberry was allo-octoploid ($2n = 8x = 56$), genes on a homoeologous genome might have compensated for the loss of functions of a certain gene. Summarizing those previous studies and this study, the practical and suitable dosage of $^{12}\text{C}^{6+}$ heavy-ion-beam irradiation to obtain mutants of cultivated strawberry efficiently should be further investigated.

Some surviving plants indicated characteristics different from “Fukuoka S6” in the forcing culture of the greenhouse (Table 1). The fruit-pericarp pigmentation of mutants varied widely from darker red to lighter red (Fig. 2), but the fruit size only showed downsizing; further, some mutants showed harder fruit firmness than the control.

References

- 1) A. Tanaka *et al.*, *Genes Genet. Syst.* **72**, 141 (1997).
- 2) N. Chiba *et al.*, *JAEA-Review* **2008-055**, 78 (2008).
- 3) T. Abe *et al.*, *Breed. Res.* **16**, 67 (2014).
- 4) M. Yotoriyama *et al.*, *JAEA-Review* **2010-065**, 71 (2011).

Improvement of the Brix content of the sweet potato “Anno-Beni” by mutation induced using heavy-ion-beam irradiation

T. Hashiguchi,^{*1} K. Yamane,^{*1} J. Nagai,^{*1} F. Tojima,^{*1} K. Ishii,^{*2} Y. Hayashi,^{*2} and T. Abe^{*2}

Heavy-ion-beam irradiation effectively induces plant mutations and is used for plant breeding.¹⁾ The sweet potato cultivar “Anno-Beni,” which has a high sugar content, is an important and special product in the Tanegashima island area. However, the weather can cause the sugar content to be unstable and the product to taste bad. Sugar is produced from starch by storage and heat, and it turns into sweetness. However, the dry-matter content and starch content change according to the harvest time, storage period, and tuber root position. Therefore, by inducing mutations through heavy-ion-beam irradiation, varieties and strains with a stable sugar content have been selected. In this study, we measured the dry-matter contents of selected mutants irradiated with a heavy-ion-beam, and in this report, we describe the effect of the irradiation on the sugar content.

Embryogenic callus derived from the stem apex of the “Anno-Beni” B1 line were irradiated with a C-ion-beam (LET 23 keV/ μm) at a dose of 5, 10, and 15 Gy in 2015. Regenerated plants that grew normally were obtained from the irradiated callus. Subsequently, we propagated 196 individual plantlets to 5 clone plants, respectively, and cultivated them in the field of KIAD * 1, Kumage Branch for line selection in 2016. We selected 31 lines that grew better and had higher dry-matter contents than the control (Table 1).

In the next year, the 31 selected lines were grown by vegetative propagation, and 5 individual plants per line were cultivated in the field. We investigated the plant growth and dry-matter contents in 2017. The root tubers of the 4 lines were steamed and, diluted with water in a 1 : 1 ratio, their Brix contents were measured. Brix is the sugar content of an aqueous solution. It is known that there is a correlation between the dry-matter rate and Brix percentage of tuberous roots in sweet potato.²⁾ Although the means of the dry-matter content in 4 mutant lines showed no significant difference, the Brix contents of 4 lines were higher than those of the control (Table 2).

Some root tubers produced by mutant lines had a higher Brix percentage and dry-matter rate than the control (Fig. 1). These results, obtained through the individual selection of mutant lines showing better growth and higher dry-matter contents than the control, suggest that high-Brix-content strains could be selected.

Table 1. Line selection by dry-matter ratio of mutants of the sweet potato “Anno-Beni” obtained by C-ion-beam irradiation.

Dose (Gy)	Number of regenerated shoots	Number of selected plants
5	107	25
10	70	5
15	19	1

Table 2. Dry matter and Brix content of 4 mutant lines of sweet potato.

Line name	Dose (Gy)	Tested root tubers	Mean of dry matter ratio (%)	Mean of brix (%)
No. 15	5	7	34.3	12.4
No. 17	5	7	34.1	12.7
No. 27	5	5	35.9	13.0
No. 34	10	5	36.0	13.2
Control (B1)	-	16	33.3	11.6

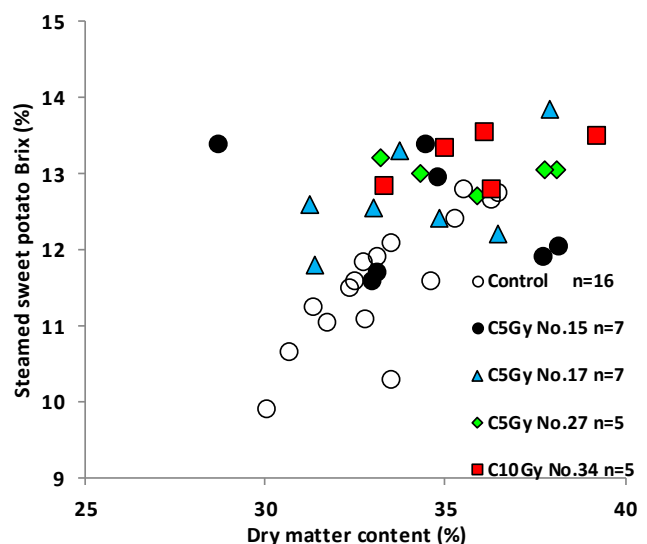


Fig. 1. Correlation between Brix content and dry-matter ratio in root tubers produced by 4 mutant lines.

References

- 1) T. Abe *et al.*, *Breed. Res.* **16**, 67 (2014).
- 2) M. Ouchida, K. Ueno, *Rep. Kyushu Br. Crop Sci. Soc. Japan* **80**, 22 (2014).

^{*1} Kagoshima Prefectural Institute for Agricultural Development (KIAD)

^{*2} RIKEN Nishina Center

Development of mutagenesis technique for leguminous crops using heavy-ion-beam irradiation and screening of useful mutants

P. Siviengkhek,^{*1} K. Ishii,^{*2} T. Sato,^{*2,*3} Y. Hayashi,^{*2} and T. Abe^{*2}

Leguminous crops (soybean, mungbean, and peanut) are important sources of lipid and protein for the human diet. In Lao PDR, mungbean and soybean productions are well suited to local soil and temperature conditions, which include both wet and dry seasons. However, soybean and mungbean productions are currently operated on a small scale and at a household level depending on the local farmers' skill. There are several factors hampering the expansion of the production area and yield for both crops. Mungbean has an indeterminate flowering habit, which implies that it does not have a defined flowering period and will continue flowering as long as adequate soil moisture is provided. Consequently, harvesting mungbean is costly because of its long cultivation period and loss of grains from early-matured pods. On the other hand, most varieties of soybean are sensitive to the photoperiod. It is necessary to cultivate suitable varieties depending on the locations or seasons; otherwise, some varieties flower early, resulting in a low production yield. To overcome these difficulties, productions of mungbean with a determinate flowering trait and soybean with a non/less photosensitive trait are desired. Some mutants of soybean have been obtained with carbon-ion-beam irradiation.¹⁻³ In this study, to determine an efficient condition for mutant induction, we irradiated mungbean and soybean with heavy-ion beams at various absorbed doses and observed the effects on plant growth.

Dry seeds of mungbean (*Vigna radiate* 'Pakse') and

Table 1. Germination and growth of soybean (ARC3) irradiated by C-ion and Ar-ion beams at different doses.

Ion	Dose (Gy)	Germination rate (%)	Survival rate (%) [*]	Growth Index ^{**}
Control	0	90.0	90.0	1.00
C	25	63.3	63.3	0.99
	50	70.0	70.0	0.91
	75	70.0	56.7	0.82
	100	80.0	63.3	0.73
	125	80.0	23.3	0.50
	150	80.0	43.3	0.68
	200	80.0	16.7	0.26
Ar	5	83.3	83.3	0.88
	10	90.0	83.3	0.80
	20	90.0	76.7	0.65
	30	63.3	26.7	0.39

^{*} Number of growing plants / 30 sown seeds

^{**} Plant height / average height of control plants

Table 2. Germination and growth of mungbean (Pakse) irradiated by C-ion and Ar-ion beams at different doses.

Ion	Dose (Gy)	Germination rate (%)	Survival rate (%) [*]	Growth Index ^{**}
Control	0	100.0	83.3	1.00
C	25	96.7	80.0	0.93
	50	93.3	83.3	0.98
	75	80.0	80.0	0.95
	100	96.7	86.7	0.97
	125	96.7	93.3	0.83
	150	96.7	70.0	0.86
Ar	5	86.7	83.3	1.00
	10	90.0	70.0	0.92
	20	86.7	73.3	0.91
	30	90.0	90.0	0.92
	40	83.3	83.3	0.66
	50	63.3	63.3	0.54

soybean (*Glycine max* L. Merr 'ARC3') are packed into a rectangular plastic box or into a plastic petri dish in which a cork sheet is bedded to lay seeds in a single layer. Seeds of mungbean and soybean packed into the rectangular plastic box were irradiated with C ions (135 MeV/n) at doses of 0–150 Gy and 0–200 Gy, respectively. The LET of C-ion beams was controlled to 30 keV/ μ m. Seeds packed into the plastic petri dish were irradiated with Ar ions (160 MeV/n) at doses of 0–50 Gy. The LET of C-ion beams was controlled to 188 keV/ μ m. After irradiation, the seeds were sowed at an experimental field.

Soybean showed sensitivity to both C-ion (in the range of 0–200 Gy) and Ar-ion (0–50 Gy) beams (Table 1). Although mungbean showed lower sensitivity, the growth rate was reduced to 0.83 after 125 Gy irradiation of a C-ion beam and to 0.54 after 50 Gy irradiation of an Ar-ion beam (Table 2). To optimize the mutation rate, we determined the minimal doses that yield a growth index appropriate for mutagenesis with heavy-ion beams. Therefore, we determined the appropriate absorbed doses for mutant selection as follows: for soybean, C-ion beams at 75 and 100 Gy, and Ar-ion beams at 10 and 20 Gy were used; for mungbean, C-ion beams at 125 and 150 Gy, and Ar-ion beams at 30 and 40 Gy were used. Among the irradiated soybean plants, some male sterile plants were found. The highest percentage of male sterile plants was 67% after Ar-ion-beam irradiation at 20 Gy, followed by 33%, 17%, and 17% after C-ion-beam irradiation at 150, 125 and 100 Gy, respectively. On the other hand, there were no male sterile plants among mungbean plants.

References

- 1) H. Kuribara *et al.*, RIKEN Accel. Prog. Rep. **43**, 286 (2010).
- 2) S. Arase *et al.*, Plant Biotech. **28**, 323 (2011).
- 3) R. Grasso *et al.*, PLoS One **11**, e0167998 (2016).

^{*1} Maize and Cash Crop Research Center, National Agriculture, Forestry and Rural Development Research Institute (NAFRI)

^{*2} RIKEN Nishina Center

^{*3} Graduate School of Agriculture, Tohoku University

Mutants of sorghum variety “WRAY” induced by heavy-ion irradiation

H. Cai,^{*1} N. Yuyama,^{*1} and T. Abe^{*2}

Sorghum [*Sorghum bicolor* (L.) Moench; $2n = 2x = 20$] is one of the most important cereals for food, forage, sugar, and biofuel worldwide.¹⁾ Sorghum, maize (*Zea mays*), rice (*Oryza sativa*), wheat (*Triticum aestivum*), and barley (*Hordeum vulgare*) are called the world’s five major food crops, and sorghum is the staple for more than 500 million people worldwide (<http://www.fao.org>). In this study, to induce mutations, dry seeds of sweet sorghum variety “WRAY” were treated using Ar- and C-ion beams in RIBF from 2015 to 2016.

The seeds were irradiated with Ar (290 keV/ μm) ions and C (30 keV/ μm) ions. The doses of the Ar and C ions were 5 to 50 Gy, and 50 to 125 Gy, respectively. Survival rates were estimated by counting M_1 plants surviving in the field. M_2 seeds were harvested separately from each self-pollinated M_1 plant. The mutants were identified from M_2 plants. Mutation rates were calculated based on the numbers of M_1 lines, which showed morphological mutants in M_2 generation. The highest rate of morphological mutants was observed at a C-ion irradiation dose of 75 Gy (Table 1). A total of 9 morphological mutants were identified from 374 lines, among which, 2 mutants were in Ar- treated plants and 7 mutants were in C- treated plants. The phenotypes of mutants were dwarf, yellow leaf, late heading and early heading (Fig. 1). *Ma3* is an important flowering-time gene that will be useful in sorghum breeding.²⁾ A next-generation sequencing and genetic analysis revealed that an early-heading mutant has a 1-bp deletion in *Ma3*. The genetic analysis of other mutants is ongoing.

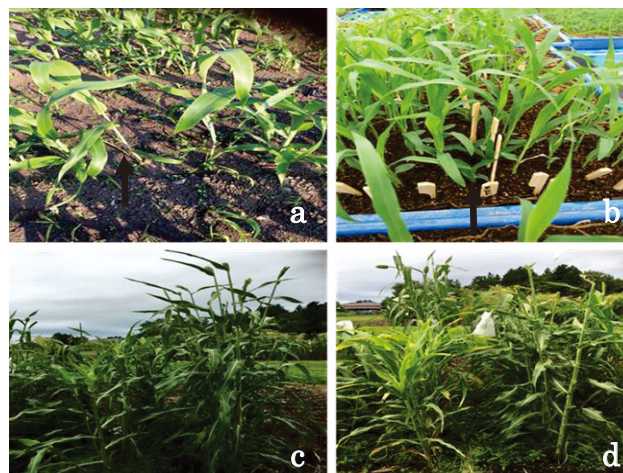


Fig. 1. Mutations induced by heavy-ion beams. (a) Early line, (b) dwarf line, (c) late line (left) and wild type (right) and (d) yellow leaf line (left) and semi-dwarf line.

References

- 1) A. H. Paterson *et al.*, *Nature* **457**, 551 (2009).
- 2) K. L. Childs *et al.*, *Plant Physiol.* **113**, 611 (1997).

Table 1. Effects of ion-beam irradiation on mutation induction.

Ions	Dose (Gy)	Survival rate (%)	No. of M_1 lines	No. of morphological mutants				Total	Mutation rate (%)
				yellow leaf	dwarf	late heading	early heading		
Control	0	80							
Ar	5	83	85	1				1	1.2
	10	48	49		1			1	2.0
	15	18	5					0	0
C	50	91							
	75	67	235	1	3	2	1	7	3.0
	100	21							
	125	15							

^{*1} Forage Crop Research Institute, JGAFSA

^{*2} RIKEN Nishina Center

Genetic analysis of an early flowering rice mutant induced by argon ions

R. Morita,^{*1} H. Ichida,^{*1} K. Ichinose,^{*1} Y. Shirakawa,^{*1} Y. Hayashi,^{*1} T. Sato,^{*1,*2} and T. Abe^{*1}

Heading date, also known as flowering time, is one of the important traits for a crop such as rice to achieve a high yield by making effective use of sunlight and temperature.¹⁾ Although numerous genes influencing the heading date have been identified and characterized in rice, it is necessary to identify novel genes that determine the heading date to understand the mechanism to control this trait. To identify a novel gene influencing the heading date, we isolated a rice mutant (Ar-G150) that exhibited an early flowering phenotype from a rice (*Oryza sativa* L. cv. Nipponbare) M₂ population derived from imbibed seeds irradiated with argon ions (2.5 Gy, 95 MeV/n, LET: 286 keV μ m⁻¹). To determine the mode of inheritance of the early flowering trait, we produced F₂ progenies derived from a cross between Ar-G150 and their original variety, Nipponbare. We grew Nipponbare, Ar-G150, and the F₂ progenies in a greenhouse under natural photoperiod conditions from June 17, 2016, and recorded the heading date of each plant. The heading date of Nipponbare were from September (Sept.) 2nd to Sept. 6th. The heading date of Ar-G150 were from August (Aug.) 23rd to Aug. 26th, approximately 10 days earlier than Nipponbare. Segregation for the early-flowering phenotype was observed in F₂ progenies, *i.e.*, seven F₂ plants showed normal flowering (the heading dates were from Sept. 2nd to Sept. 5th), and 23 F₂ plants showed early flowering (the heading dates were from Aug. 23rd to Aug. 27th). The segregation of normal- and early-flowering phenotypes in the F₂ progenies (7:23) showed a good fit to a 1:3 ratio (the two-tailed *p*-value from Fisher's exact test was 1.00), indicating that Ar-G150 possessed a single dominant mutated gene with an early-flowering trait. To characterize the mutated phenotype in detail or determine the causative gene of early flowering, the homozygous line for the mutated gene is needed. Thus, we cultivated 16 F₃ lines (approximately 20 plants per line) derived from the self-pollination of early-flowering F₂ plants to select the homozygous line using a paddy field in 2019. In 5 out of the 16 F₃ lines, all F₃ plants exhibited early flowering, indicating that the mutated gene in their parental plant was homozygous. In the remaining 11 lines, segregation for the early- and normal-flowering phenotype was observed in F₃ plants, indicating that the mutated gene in the parental plant was heterozygous. The number of homozygous F₂ and heterozygous F₂ (5:11) showed a good fit to a 1:2 ratio (the two-tailed *p*-value from Fisher's exact test was 1.00).

^{*1} RIKEN Nishina Center

^{*2} Graduate School of Agricultural Science, Tohoku University

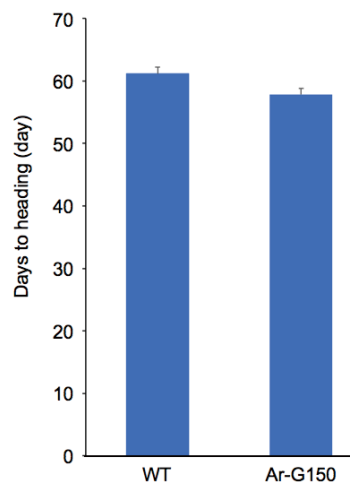


Fig. 1. Days to heading of WT and Ar-G150 grown under a short-day condition. Values are means \pm standard error ($n = 5$). Student's *t*-test was used to compare the two groups.

These results indicated that the early-flowering character was determined by a single gene.

Using the homozygous F₃ plants, we started to characterize the early-flowering phenotype of Ar-G150. First, we determined the days to heading under a controlled photoperiod condition using a growth chamber to reveal whether the mutated gene affects the photoperiod response. We grew Nipponbare and Ar-G150 plants under a short-day condition (10 h light/14 h dark), and measured the days to heading. Since rice is a short-day plant and the critical photoperiod of Nipponbare is estimated to be 15.6 h,²⁾ this condition prompts rice plants to develop flowers. Under this condition, the days to heading of Ar-G150 (57.8 \pm 1.0 d, average \pm standard error) was slightly less than the days to heading of Nipponbare (61.2 \pm 1.2 d), although no significant differences were observed between the days to heading of both lines ($p > 0.05$), suggesting that the mutated gene have little or no effect of promoting flowering under the short-day conditions (Fig. 1). We also started to perform the whole genome re-sequencing analysis of homozygous F₃ mutants to reveal the causative gene. The information of the causative gene will help us understand the mechanism to control the heading date of rice in more detail.

References

- 1) B. Wang, J. Li, *Plant Cell* **31**, 1416 (2019).
- 2) T. Horie, H. Nakagawa, *Jpn. J. Crop Sci.* **59**, 687 (1990).

Approach toward isolating early-heading mutants from Tana Toraja local aromatic rice “Pare Bau” irradiated with argon- and carbon-ion beams

A. M. Okasa,^{*1,*2,*3} M. Riadi,^{*1} T. Sato,^{*2,*3} K. Toriyama,^{*2} K. Ishii,^{*3} Y. Hayashi,^{*3} T. Abe,^{*3} and R. Sjahril^{*1,*4}

Tana Toraja is a mountainous area in the northern part of South Sulawesi, Indonesia. The area has been known as an aromatic-rice-producing area.¹⁾ The aromatic rice cultivar “Pare Bau” has good grain quality and fragrant aroma, making it relatively expensive in the market, but it has several disadvantages including late heading dates and long stems for modern farming systems. The heading date can be determined by the basic vegetative phase (BVP) and photoperiod sensitive phase (PSP).²⁾ Indonesian rice cultivated in mountain areas has a relatively short PSP and relatively long BVP. This study aims to isolate early heading mutant lines induced by heavy-ion-beam irradiation.

Dry seeds of Tana Toraja local aromatic rice cultivar (*Oryza sativa* L. “Pare Bau”) were irradiated with carbon ions (30 keV/ μm) and argon ions (300 keV/ μm) in the RI-beam factory, RIKEN Nishina Center, Japan. Owing to a limited range of Ar-ion beams, seeds for Ar-ion irradiation needed to be packed in a single layer. For this purpose, a sponge was bedded as a bottom plate in a plastic rectangular box (75 × 50 × 18 mm). The doses of Ar-ion and C-ion irradiation were 10 and 150 Gy, respectively.^{3,4)} We investigated the heading dates of Pare Bau lines irradiated with Ar and C ions (PB-A and PB-C, respectively).

In May 2016, M₁ seeds (1000 seeds of PB-A and 1000 seeds of PB-C) were germinated and sown in seedling pots and grown in a greenhouse for three weeks. The germination rates of M₁ seeds were 53% for PB-C and 49% for PB-A, while that of the wild-type control was 70%. The seedlings (94 PB-A and 79 PB-C plants) were transplanted in the paddy fields of Hasanuddin University (S: 5°7′53.50″ E: 119°28′57.97″; 20 m above sea level) in June 2016. Owing to poor establishment of seedlings, only small amounts of M₁ plants (13 PB-A and 13 PB-C plants) set more than 50 seeds in November 2016. In June 2017, 50 M₂ seedlings per line were transplanted in the paddy field of mountainous Enrekang Regency (S: 3°19′47.44″ E: 119°50′1.57″; 650 m above sea level) neighboring Tana Toraja Regency. Based on heading dates at least one week earlier (<119 days) than those of the wild-type control (>125 days), we selected 82 PB-A and 26 PB-C plants as mutant candidates. From these M₂ plants, we sampled M₃ seeds with relatively large grain weights per



Fig. 1. Phenotypes of early-heading mutants induced by heavy-ion-beam irradiation in the paddy field of Enrekang Regency.

panicle from 18 lines of PB-A and one line of PB-C in October 2017. In May 2018, 50 M₃ seedlings per line were transplanted in the paddy field of Enrekang Regency. Heading dates of the M₃ individual plants and wild-type control plants were recorded for the first 25 plants showing relatively early heading. The days to heading of the wild-type control was 126 to 130 days with an average of 128 days, while those of the following nine lines were 108 to 126 days with an average of 117 to 121 days, which were over one week less than that of the wild-type control (Fig. 1). These lines are PB-A.5.3.45, PB-A.6.1.9, PB-A.7.1.30, PB-A.12.2.4, PB-A.12.2.12, PB-A.14.2.14, PB-A.14.3.1, PB-A.14.4.3, and PB-C.20.1.49. We expect these lines to contain mutant candidates. Genetic analysis will be performed for M₄ lines and their hybrids with the wild type to investigate the mutated genes responsible for early heading.

Acknowledgements

The authors would like to express their deepest gratitude to the Directorate General of Resources for Science, Technology and Higher Education (DGRSTHE), the Ministry of Education and Culture for Enhancing International Publication Program through the PMDSU Scholarship.

References

- 1) H. Sahardi, F. Djufry, Proc. National Seminar on Genetic Resources of Agriculture, (2013) pp. 1.34–43.
- 2) B. S. Vergara, T. T. Chang, *The Flowering Response of the Rice Plant to Photoperiod: A Review of the Literature*, 4th Edition (IRRI, Philippines, 1985).
- 3) Y. Hayashi *et al.*, RIKEN Accel. Prog. Rep. **50**, 27 (2017).
- 4) Y. Hayashi *et al.*, RIKEN Accel. Prog. Rep. **51**, 238 (2018).

*1 Faculty of Agriculture, Hasanuddin University

*2 Graduate School of Agricultural Science, Tohoku University

*3 RIKEN Nishina Center

*4 Corresponding author

A novel domain of *LONG GRAIN 1* in rice possesses transcriptional activation activity

H. Abe,^{*1} R. Morita,^{*1} Y. Shirakawa,^{*1} Y. Hayashi,^{*1} H. Ichida,^{*1} and T. Abe^{*1}

We previously identified the gene *LONG GRAIN 1* (*LIN1*), which regulates seed development, and a mutation of the gene (*lin1*), which causes long grain size.¹⁾ The *lin1* mutant was obtained from rice (*Oryza sativa* L. ssp. *japonica* cv. Nipponbare) M₂ population derived from imbibed seeds irradiated with argon-ion beams (5 Gy, 95 MeV/nucleon, LET: 286 keV m⁻¹) in the RIKEN RI-beam factory.¹⁾ *LIN1* is predicted to encode the 412 amino acid protein, LIN1, with calculated MW 42,579 and pI 10.8. InterPro search of LIN1 revealed that LIN1 has no known functional domain and/or motif.

To gain more insight into LIN1 functions for seed development, we conducted yeast two-hybrid screening for isolation of LIN1 interaction proteins (LIPs).²⁾ We obtained several LIPs, and one LIP was MADS1, the transcription factor for floral organ development. During the course of the yeast two-hybrid assay for LIN1 and MADS1 interaction, we noticed that mutant *lin1* was more actively bound to MADS1 than full length LIN1 (Figs. 2.3 and 4). As sequence alignments of LIN1 homologs in rice and *Arabidopsis* revealed that LIN1 has 5 short stretch conserved domains (I~V) (Fig. 1.1), we divided LIN1 into several N- and C-terminal fragments, each containing several conserved domains, and performed yeast two-hybrid assays. Unexpectedly, yeast cells transformed with BD-fusion construct of N-terminal fragment of LIN1-M120 (Fig. 1.3) containing only conserved domain I were grown on a selection plate of SD/-Leu/-Trp/-His/-Ade not only in the presence of AD-MADS1 but also in an AD-empty construct (Figs. 2.6 and 7). On the contrary, the BD-

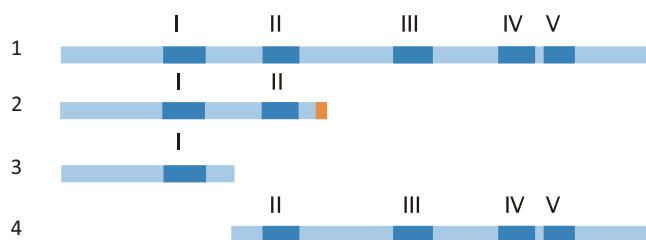


Fig. 1. Schematic diagram of LIN1, *lin1* and LIN1 fragment protein sequence. Dark blue color with Roman numerals (I~V) indicates positions of conserved domains. 1. Full length LIN1 protein (M1-G412). 2. Mutant *lin1* protein caused by 1 bp deletion of LIN1 gene. The frame shift mutation result for an extended sequence (orange color) and a premature stop codon. 3. N-terminal fragment of LIN1-M120 containing the domain I. 4. C-terminal fragment of P121-LIN1 without the N-terminal portion (3) of LIN1.

^{*1} RIKEN Nishina Center

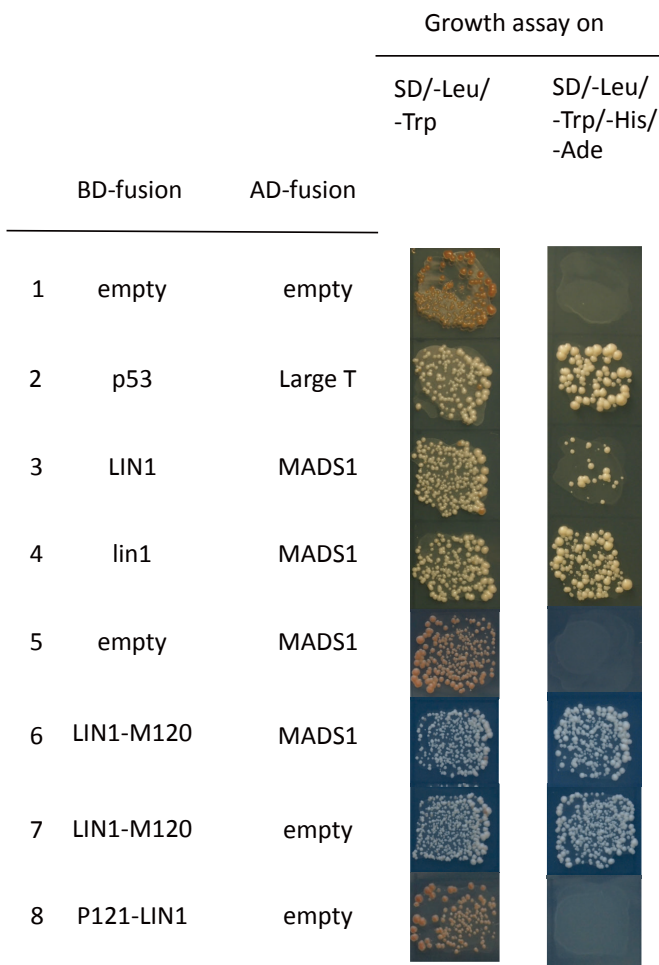


Fig. 2. Yeast two-hybrid assays. Combination of BD-fusion constructs and AD-fusion constructs are indicated (1-8). Both constructs were transformed into Y2H-Gold yeast competent cells, and growth assays on SD/-Leu/-Trp and SD/-Leu/-Trp/-His/-Ade plates were performed.

fusion construct of the C-terminal fragment of P121-LIN1 (Fig. 1.4) had no such activity (Fig. 2.8). These results indicate that the N-terminal fragment of LIN1-M120 had transcriptional activation activity for the reporter gene expression in yeast cells.

Considering the results, we hypothesize that LIN1 might be a novel transcription factor family protein with N-terminal transcriptional activation activity for regulating seed development. Elucidation of LIN1-regulated target genes should be provided for important information not only for understanding seed development but also for application of plant breeding.

References

- 1) R. Morita *et al.*, Mol. Breeding **39**, 135 (2019).
- 2) H. Abe *et al.*, unpublished.

Establishment of large mutant lines on rotifer using heavy-ion-beam irradiation

K. Tsuneizumi,*¹ M. Yamada,*¹ K. Ichinose,*¹ H. Ichida,*¹ and T. Abe*¹

In larviculture, rotifers (*Brachionus plicatilis* sensu stricto) are generally used as the initial feed for hatched larvae,¹⁾ while larger preys (e.g., *Artemia*) are needed with larval growth. The improper management of feed size and density results in mass mortality, a high incidence of morphologically abnormal development, and a substantial depletion of fish larvae.²⁾ To improve the survival and growth of fish larvae, prey of appropriate size between those of rotifer and *Artemia* is needed. The aim of this study was to apply heavy-ion-beam-based mutation breeding techniques^{3,4)} for the selection of rotifer mutants with larger body sizes.

The size distributions of the lorica length of rotifers are 170–320 μm in individuals carrying amictic eggs. The next food item *Artemia* nauplii has a body length of 400–1,000 μm , and thus, there is a large size gap (320–400 μm) between rotifer and *Artemia* nauplii. The rotifer strain is widely divided into two types, obligate and cyclically parthenogenesis, based on their life cycle.⁵⁾ In aquaculture facilities, the intensive mass culture of live food rotifers is performed via parthenogenetic reproduction to induce their rapid proliferation. The Notojima strain is known as the largest rotifer strain used in Japan and has obligate parthenogenesis. Based on these characteristics, this study used the Notojima strain as the raw material for ion-beam irradiation.

In our previous study, we measured the biological effect of heavy-ion-beam irradiation on rotifers under different conditions.⁶⁾ In this study, a large-scale screening method was developed, and mutant lines with increased body sizes were selected using the length of the lorica as indicators. Heavy-ion-beam irradiation was performed using carbon (C) (1.62 GeV, LET = 23 keV/ μm) at six irradiation doses of 100, 150, 200, 300, 400, and 600 Gy and argon (Ar) (3.8 GeV, LET = 312 keV/ μm) at six irradiation doses of 25, 50, 75, 100, 150, and 200 Gy. After irradiation, morphometric characteristics were compared with control groups without irradiation.

The results of categorising lorica lengths of the control and the 56 selected larger mutant strains are shown in Fig. 1. Strains were classified according to their average lorica length: Class I for 340–350 μm , Class II for 350–360 μm , and Class III for 360–370 μm . Class I corresponds to over 11% elongation, Class II to 15%, and Class III to 18% compared to the lorica length of the controls. The large mutant lines from 1968 rotifers irradiated with C-ion beams were categorized as follows: 30 lines to Class I, 19 lines to Class II, and 3 lines to Class III. In the large mutant lines from 1080 rotifers irradiated with Ar-ion beams, there were 3 lines in Class I

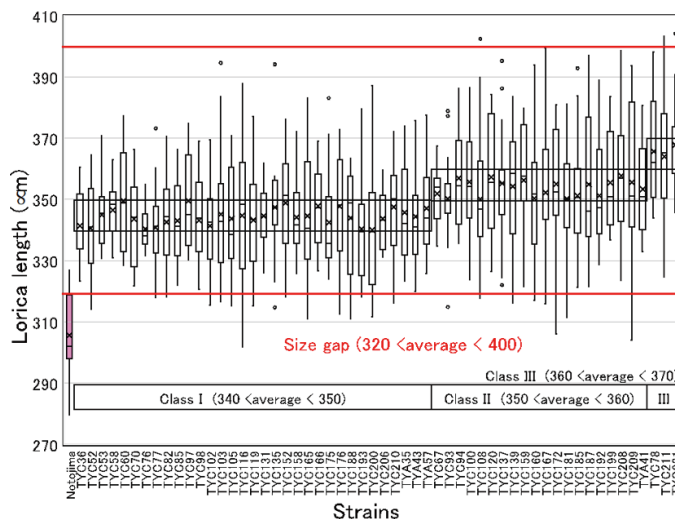


Fig. 1. Comparison of lorica lengths between large mutant strains and the control.

and 1 line in Class II (Fig. 1). Steel's multiple comparison tests showed a difference at 0.001 significance level in lorica lengths of all larger mutant strains from Class I to Class III compared with the control group ($305.6 \pm 3.0 \mu\text{m}$).

The size range of lorica length of the larger mutant strains was 320–400 μm , which is not covered by the size ranges of the wild-type rotifer and *Artemia* nauplii in seedling production (Fig. 1, red bars). Various larger mutant strains have been established by mutagenesis with heavy-ion-beam irradiation, and these strains may help reduce the mass mortality of domestic fish if used during the intermediate feeding stage between rotifers and *Artemia* nauplii.

The lorica lengths of all large mutant strains showed significant differences compared to the control group (Steel's multiple comparison tests, $p < 0.001$, $n = 20$). Boxplots indicate the lorica lengths of rotifers ($n = 20$). Strains were separated into classes according to the average lorica length.

References

- 1) S. Mills *et al.*, *Hydrobiologia* **796**, 39 (2017).
- 2) T. Kotani *et al.*, *J World Aquac. Soc.* **40**, 383 (2009).
- 3) T. Abe *et al.*, in *Plant Mutation Breeding and Biotechnology*, edited by Q. Y. Shu *et al.* (CABI, Oxfordshire, 2012), p. 99.
- 4) A. Tanaka *et al.*, *J. Radiat. Res.* **51**, 223 (2010).
- 5) T. Yoshinaga *et al.*, *Hydrobiologia* **412**, 103 (1999).
- 6) K. Tsuneizumi *et al.*, *RIKEN Accel. Prog. Rep.* **52**, 221 (2019).

*¹ RIKEN Nishina Center

Contribution of multiple DNA repair pathways in *Arabidopsis thaliana* dry seeds after heavy-ion-beam irradiation

K. Ishii,*¹ S. Ohbu,*¹ M. Yamada,*¹ and T. Abe*¹

Heavy-ion-beam irradiation induces DNA double-strand break (DSB) which is critical damage to cellular proliferation. DSB is repaired by two main pathways: homologous recombination (HR) repair, which is homology-dependent and error-free; canonical non-homologous end-joining (C-NHEJ), which is Ku-dependent and potentially error-prone and by a recently identified error-prone pathway, alternative non-homologous end-joining (A-NHEJ). Which pathway is chosen is dependent on the phase of cell cycle and the initiation of DNA end resection.¹⁾ HR is preferred during the S/G2 phase in the cell cycle because sister chromatids can be used as homologous templates. C-NHEJ functions through the cell cycle and especially in G1 and G2 phase. A-NHEJ functions when the key factors of C-NHEJ are absent, essentially in the S phase. Because most embryo cells in dried seeds are in the G1 phase,²⁾ it is possible that C-NHEJ will mainly function after heavy-ion-beam irradiation. In this study, we irradiated heavy-ion-beams on three different lines: a wild type, a C-NHEJ-deficient line, and a HR-deficient line, and we measured mutation rates to reveal how each DSB-repair pathway functions.

We obtained *Arabidopsis thaliana* seeds of SALK_123114 line with a T-DNA insertion in the *Ku70* gene (a *Ku70*($-/-$) mutant) and SALK_038057 line with that in the *Rad54* gene (a *Rad54*($-/-$) mutant) from Nottingham Arabidopsis Stock Centre (NASC) and used them as the C-NHEJ-deficient and HR-deficient lines, respectively. Dry seeds of Col-0 line (wild type), the *Ku70*($-/-$) mutant, and the *Rad54*($-/-$) mutant were irradiated with $^{12}\text{C}^{6+}$ (135 MeV/nucleon) ions at doses ranging from 0 to 600 Gy. The LET of C-ion beams were controlled to 30 keV/ μm . After the irradiation, flowering rate (number of flowering plants per total number of incubated seeds) were measured as survival rate, as previously described.³⁾ We also obtained seeds of CS16118 line with a T-DNA insertion in the *APG3* gene (an *APG3*($+/-$) mutant) from NASC. The *APG3*($+/-$) mutant was crossed with the *Ku70*($-/-$) and *Rad54*($-/-$) mutants to produce *Ku70*($-/-$)*APG3*($+/-$) and *Rad54*($-/-$)*APG3*($+/-$) mutants in the F₂ generations, respectively. Dry seeds of the *APG3*($+/-$) line (regarded as a wild type), *Ku70*($-/-$)*APG3*($+/-$) line, and *Rad54*($-/-$)*APG3*($+/-$) line were irradiated with $^{12}\text{C}^{6+}$ (135 MeV/nucleon) ions at 60 Gy. The LET of C-ion beams was controlled to 30 keV/ μm . After the irradiation, appearance ratio was measured as mutation rate, as previously described.⁴⁾

The flowering rates of un-irradiated control of the wild

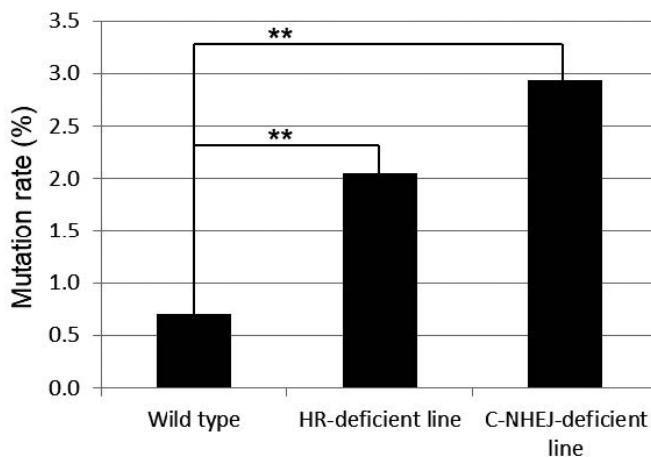


Fig. 1. Mutation rate after C-ion-beam irradiation at 60 Gy. **: $p < 0.01$.

type, C-NHEJ-deficient line, and HR-deficient line were not lower than 0.99. In the wild type, the flowering rate was 0.80 even after 600 Gy-irradiation, while in the *Rad54*($-/-$) mutant, the rate was reduced to 0.30. In the *Ku70*($-/-$) mutant, there was no individual flowered only after 120 Gy-irradiation. It is suggested that both C-NHEJ and HR pathways are involved in DNA repair after heavy-ion-beam irradiation and the C-NHEJ pathway has a greater contribution.

While the mutation rate of the wild type was 0.7%, those of the HR-deficient and C-NHEJ-deficient lines were significantly ($p < 0.01$) higher: 2.0% and 2.9%, respectively. It is possible that in the HR-deficient lines, DSBs usually repaired by the HR pathway are repaired by the C-NHEJ pathway. Although the difference between the HR-deficient and C-NHEJ-deficient lines was not significant, the C-NHEJ-deficient line showed higher mutation rate. It is suggested that when the C-NHEJ pathway is absent, DSBs are repaired not by the error-free HR pathway but by the error-prone A-NHEJ pathway, resulting in higher mutation rate.

In this study, it was suggested that DSBs induced in dry seeds of *A. thaliana* by heavy-ion beams are mainly but not entirely repaired by the C-NHEJ pathway. One possibility is that the embryo cells in the dry seeds are not uniform in the G1 phase. Another is that DSBs are not completely repaired in the G1 phase but in the following phase beyond the cell cycle check points.

References

- 1) C. S. Spampinato, Cell. Mol. Life Sci. **74**, 1693 (2017).
- 2) R. D. de Castro, H. W. M. Hilhorst, R. Bras. Fisiol. Veg. **12**, 105 (2000).
- 3) Y. Kazama *et al.*, Plant Biotechnol. **25**, 113 (2008).
- 4) Y. Kazama *et al.*, Plant Biotechnol. **29**, 441 (2012).

*¹ RIKEN Nishina Center

Ion-microbeam irradiation to damage DNA in RPE cell nucleus with tapered glass capillary optics at Pelletron facility

T. Ikeda,^{*1} M. Sakai,^{*2,*1} K. Takemoto,^{*2,*1} A. Shibata,^{*3} M. Izumi,^{*1} and M. Uesaka^{*2}

Cell irradiation experiments with ion microbeams have started at a new beamline of the RIKEN Pelletron accelerator facility in the Nishina R&D Building. The purpose of the experiments is to investigate the dynamics of the accumulation of restoration proteins after DNA double-strand breaks (DSB). The microbeam irradiation allows artificial DNA damage, which defines the time zero for the accumulation of repair proteins. To create DSB efficiently, ions with high linear energy transfer (LET) should be used. Figure 1 shows the LET in water for H and He ions with an energy E below 5 MeV. The H and He ions have maximum LETs of 80 and 240 keV/ μm , respectively, just before stopping. If we use He ions with an energy of 4.5 MeV, an LET of more than 100 keV/ μm is available through an ion range of 27 μm . The LET value is large enough to create DSB.

The irradiation was performed at the BL-W30 beamline employing a single tapered glass capillary optics at the beam port, where the microbeam was emitted in the horizontal direction. A He-ion beam was accelerated to 4.5 MeV with a tandem accelerator (Pelletron 5SDH-2, 1.7 MV max.), and it entered a glass capillary having an outlet diameter and end window thickness of 11.4 μm and 8.6 μm , respectively. The details of the capillary microbeam at an old beamline of our facility are reported elsewhere.^{1,2)} The target was nuclei of retinal pigment epithelial (RPE) cells cultivated in a liquid medium. The cells were fully confluent in petri dishes, the glass bottoms of which were marked to find irradiated cells for the fluorescence observation after the irradiation. As shown in Fig. 2(a), the petri dish was positioned at an angle of approximately 45° to the capillary axis. To maintain the cells in the dish filled with the medium, it was dripped onto the bottom of the dish at a speed controlled by a peristaltic pump. The microbeam intensity was set to approximately 15 ions/s, which was confirmed before and after the irradiation. The irradiation distance be-

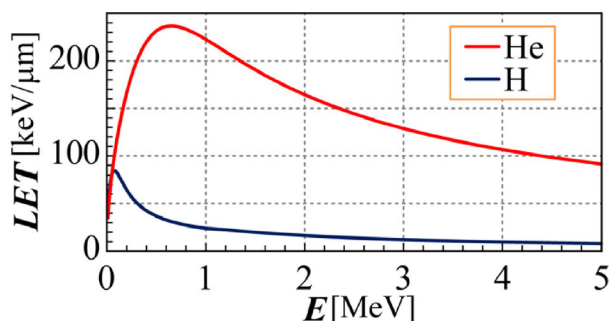


Fig. 1. Comparison of the LETs of H and He ions in water with an energy between 0 and 5 MeV.

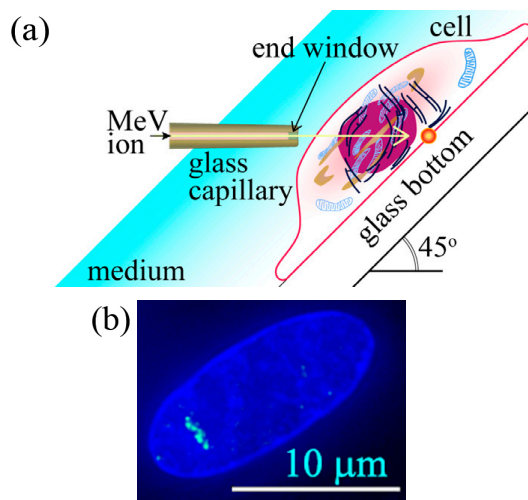


Fig. 2. (a) Cell irradiation with a glass capillary. The angle was set to approximately 45° with respect to the capillary axis. (b) Irradiated RPE cell nucleus with DSB points.

tween the capillary outlet and the cells was set to several micrometers. The distance was always monitored by a microscope above the irradiation point. Each dish was moved for 3–8 min to irradiate the cells on a line across the dish. The total number of dishes was four. After the irradiation, 30 min was spent for the repair process based on an enzymatic reaction. Subsequently, the cells were fixed with 3% paraformaldehyde (PFA)-2% sucrose in phosphate-buffered saline (PBS), followed by washing with PBS. Next, the dishes were filled with PBS for delivery to Gunma University for observation by an optical microscope with three-dimensional structured illumination, 3D-SIM, microscopy (DeltaVision OMX version 4, GE Healthcare).

Figure 2(b) shows a bottom view of one of the irradiated cells. The blue area corresponds to the cell nucleus labeled by DAPI. The bright blue points are DSB positions where phosphorylated histone H2AX was labeled with Alexa Fluor® 488 by the immunofluorescence method. The DSB points are clearly aligned on a line with extremely low background fluorescence. The line is expected to be a He ion track stopping at or penetrating the nucleus. The photo is one of the z -sliced photos with a slice step Δz of 0.25 μm .

The brightness information of each pixel in the images was stored as a 3D map. Using the map, the directions of all ion tracks and the density distributions of DSB and other restoration proteins were extracted. The time evolution of repair of DSB as a function of the distance from the ion track will be obtained in the next experiment by changing the time between irradiation and fixing.

References

- 1) V. Mäkel *et al.*, Rev. Sci. Instrum. **85**, 014302 (2014).
- 2) T. Ikeda *et al.*, Quantum Beam Sci. **4**, 22 (2020).

^{*1} RIKEN Nishina Center

^{*2} The Graduate School of Engineering, Univ. of Tokyo

^{*3} Gunma University Initiative for Advanced Research (GIAR), Gunma Univ.

IV. OPERATION RECORDS

Electric power consumption of RIKEN Nishina Center in 2019

E. Ikezawa,^{*1} Y. Watanabe,^{*1} H. Yamasawa,^{*1} and O. Kamigaito^{*1}

The average hourly electrical power consumption of the RIKEN Nishina Center (RNC) for each day in 2019 is shown in Fig. 1. The total electrical power consumption by RNC in 2019 was 56,928 MWh, which was 5% higher than that in 2018. When RI Beam Factory (RIBF) experiments using an uranium (^{238}U) beam

were conducted, the maximum commercial electrical power supply to the RIKEN Wako campus reached 20.05 MW with a cogeneration system (CGS) output of 6.0 MW on November 11, 2019, and the maximum electrical power consumption of RNC reached 15.8 MW on November 27, 2019.

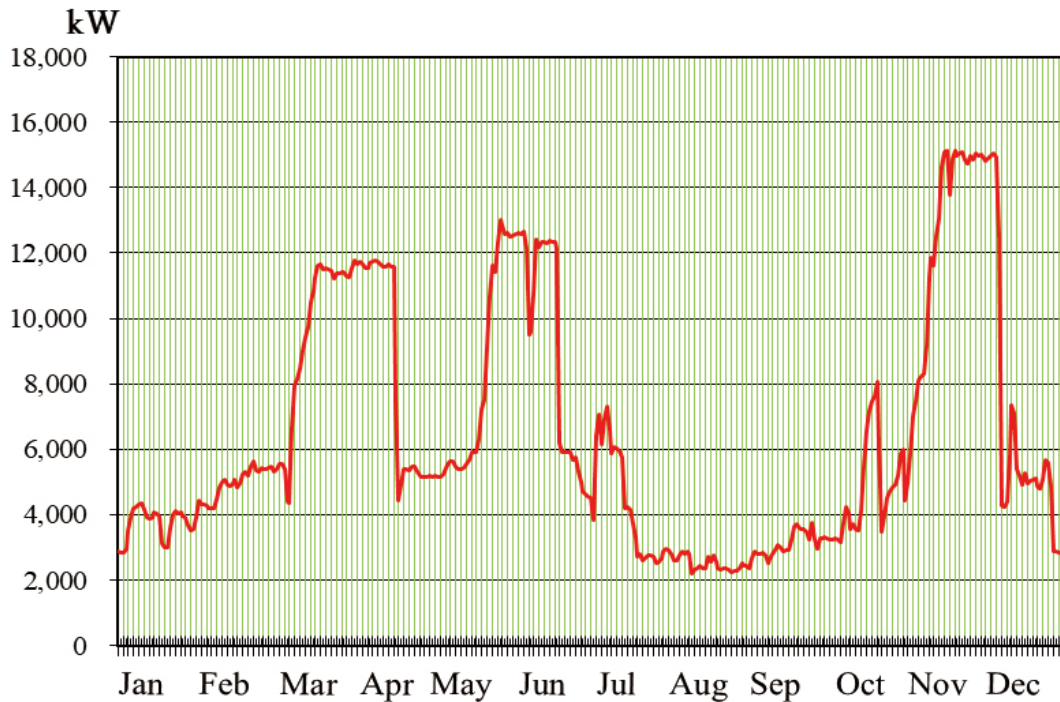


Fig. 1. Average hourly electrical power consumption of RNC for each day in 2019.

^{*1} RIKEN Nishina Center

Operation report of the ring cyclotrons in the RIBF accelerator complex

N. Tsukiori,^{*1} K. Ozeki,^{*2} T. Dantsuka,^{*2} M. Fujimaki,^{*2} T. Fujinawa,^{*2} N. Fukunishi,^{*2} S. Fukuzawa,^{*1}
 M. Hamanaka,^{*1} H. Hasebe,^{*2} Y. Higurashi,^{*2} E. Ikezawa,^{*2} H. Imao,^{*2} S. Ishikawa,^{*1} O. Kamigaito,^{*2}
 Y. Kanai,^{*2} M. Kase,^{*2} M. Kidera,^{*2} K. Kobayashi,^{*1} M. Komiyama,^{*2} R. Koyama,^{*1} K. Kumagai,^{*2} T. Maie,^{*2}
 M. Nagase,^{*2} T. Nagatomo,^{*2} T. Nakagawa,^{*2} M. Nakamura,^{*2} T. Nakamura,^{*1} M. Nishida,^{*1} M. Nishimura,^{*1}
 J. Ohnishi,^{*2} H. Okuno,^{*2} N. Sakamoto,^{*2} J. Shibata,^{*1} K. Suda,^{*2} A. Uchiyama,^{*2} S. Watanabe,^{*2}
 T. Watanabe,^{*2} Y. Watanabe,^{*2} K. Yadomi,^{*1} K. Yamada,^{*2} and H. Yamasawa^{*2}

The operation report of the ring cyclotrons in the RIBF accelerator complex from Jan. to Dec. 2019 is presented here. Table 1 presents a summary of the beams accelerated by these cyclotrons. The availability in the table is defined by the ratio of the actual beam time to the scheduled beam time, which is an index of the stable operation of accelerators. In calculating each availability, for beam times that were completed earlier than scheduled, the scheduled times are identified with the actual times. Multiple experiments supplying identical beams are shown as a block.

The total beam supply time (actual beam time) was 1581.8 h. The ratio of beam times between the experiments conducted in the old facility (RARF) and those conducted in the new facility (RIBF) was 8% and 92%.

In the RARF, the actual beam time was 128.0 h, and the availability was 105.6%. Beams were stably supplied as usual. In addition to the beams listed in Table 1, experiments for synthesizing the 119th element using a ⁵¹V beam were conducted as a closed beam time under the Nishina Center Director.

In the RIBF, three beam services were conducted. The total beam time was 1453.8 h, and the availability was 92.2%. For the supply of ²³⁸U beams, a maximum beam intensity of 94.2 particle nA was achieved, which was 1.3 times higher than the value of 72.0 particle nA in a previous beam time in Oct. 2018. A second high-temperature oven¹⁾ was added in the 28-GHz superconducting electron cyclotron resonance ion source, which has contributed to an increase in intensity and the stabilization of the uranium beam. Furthermore, the stabilization of the magnetic field of the IRC has also contributed to a stable beam intensity and an improvement in the transmission efficiencies for RRC and fRC.²⁾ For

the supply of ¹²⁴Xe beams, a maximum beam intensity of 173 particle nA was achieved, which was 1.7 times higher than the value of 102 particle nA in a previous beam time in Apr. 2016.

The improvement of the acceleration voltage by the upgrade of the RRC resonators³⁾ performed in 2018 has contributed to the remarkable enhancement in the intensity of beams delivered to the RIBF. In 18.25-MHz operations, both resonators were operated with an acceleration voltage of over 138 kV. Owing to an improvement of the shunt impedance, a significant reduction was achieved in the frequencies of the voltage breakdown by discharge and in the high-voltage trips of the vacuum tube. After all beam times scheduled in the first half of this fiscal year had been finished, a high-power test was performed. Both resonators achieved an acceleration voltage of 160 kV, which was twice that before the upgrade.

However, after the resonator upgrade of RRC, water leakages occurred in cooling water channels of the stems several times in 2018 and once in 2019. We spent 4–5 days repairing the leakage point by welding. Water leakage is a very serious problem that hinders the stable operation of RIBF. Therefore, during this summer maintenance period, an intensive investigation to find tiny leaks and the treatment of all the leaks found in the investigation were conducted. Since then, no degradations of vacuum occurred due to water leakage from the stems.

References

- 1) J. Ohnishi *et al.*, RIKEN Accel. Prog. Rep. **52**, 109 (2019).
- 2) R. Koyama *et al.*, in this report.
- 3) K. Yamada *et al.*, RIKEN Accel. Prog. Rep. **52**, 13 (2019).

Table 1. Summary of the accelerated beams in 2019.

Beam particle	Energy (MeV/nucleon)	Acceleration mode	Beam course	Beam intensity (particle nA)		Beam time (h)		Availability (%)
				Requested	Actual	Scheduled	Actual	
RARF								
¹² C	135	AVF-RRC	E5B (Biology)	1	483.3	39.0	28.5	100.0
¹⁴ N	135		E3B (RI production)	500	571.0	72.0	78.7	109.4
⁵⁶ Fe	90		E5B (Biology)	1	7.9	12.0	9.2	100.0
⁴⁰ Ar	160	AVF-RRC-IRC	E5B (Biology)	1	18.3	17.5	11.6	100.0
RIBF								
⁷⁸ Kr	345	RILAC2-RRC-fRC-IRC-SRC	BigRIPS/SAMURAI	> 300	272.2	672.0	649.0	96.6
¹²⁴ Xe			BigRIPS/ZDS	>80	165.4	516.0	372.6	72.2
²³⁸ U			BigRIPS/ZDS/F12	>60	94.2	388.9	432.2	111.1
Total						1717.4	1581.8	93.1

^{*1} SHI Accelerator Service Ltd.

^{*2} RIKEN Nishina Center

RILAC operation

E. Ikezawa,^{*1} T. Ohki,^{*2} M. Kase,^{*1} T. Nakagawa,^{*1} N. Sakamoto,^{*1} H. Okuno,^{*1} N. Fukunishi,^{*1} Y. Watanabe,^{*1} M. Komiyama,^{*1} A. Uchiyama,^{*1} T. Maie,^{*1} M. Nagase,^{*1} M. Fujimaki,^{*1} T. Watanabe,^{*1} H. Hasebe,^{*1} H. Imao,^{*1} K. Ozeki,^{*1} K. Suda,^{*1} Y. Higurashi,^{*1} K. Yamada,^{*1} S. Watanabe,^{*1} M. Kidera,^{*1} T. Nagatomo,^{*1} K. Kumagai,^{*1} T. Nishi,^{*1} H. Yamauchi,^{*2} K. Oyamada,^{*2} M. Tamura,^{*2} A. Yusa,^{*2} K. Kaneko,^{*2} and O. Kamigaito^{*1}

The RIKEN heavy-ion linac (RILAC) was operated in December 2019. Some statistics regarding the operation of RILAC from January 1 to December 31, 2019 are presented in Table 1.

Table 2 lists the beam service times in the standalone mode of RILAC in 2019.

The following works and tests to upgrade RILAC have been in progress at the LINAC building during the reporting period. The details are described elsewhere in this progress report.

- (1) Performance tests were conducted at the new 28-GHz superconducting electron cyclotron resonance ion source (SC 28-GHz ECR ion source). Table 3 lists the operation time of the performance tests in 2019.
- (2) The section after the A2 cavity was reconstituted. The necessary preparation for the installation of a superconducting RILAC (SRI-LAC), middle-energy beam transport (MEBT), and high-energy beam transport (HEBT) was conducted.

We performed the following maintenance works during the reporting period.

- (1) In the radio-frequency systems, DC high-voltage power supplies were subjected to annual inspection. The major components with mechanical parts were subjected to simple inspection.
- (2) The water pumps were subjected to simple inspection. All cooling towers were subjected to monthly inspection.

Table 1. Statistics of RILAC operation from January 1 to December 31, 2019.

Operation time of RILAC	43.7 h
Mechanical problem	0.0 h
Standalone RILAC	23.9 h
Injection into RRC	0.0 h
Total beam service time of RILAC	23.9 h

- (3) All turbomolecular pumps were subjected to simple inspection. Cryogenic pumps used for cavities 3, 4, and 6 and the standby units were overhauled.
- (4) All magnet power supplies were subjected to simple inspection.

Table 2. Beam service time of standalone RILAC in 2019.

Beam course	Total time (h)	%
In acceleration room	23.9	100.0
e2	0.0	0.0
e3	0.0	0.0
Total	23.9	0.0

Table 3. Operation time of the SC 28-GHz ECR ion source in 2019.

Ion	Mass	Total time (h)
Ar	40	463.4
Ca	40	650.6
V	51	403.0
Zn	70	1017.6
Total		2534.6

^{*1} RIKEN Nishina Center

^{*2} SHI Accelerator Service Ltd.

Operation report on the RIKEN AVF cyclotron for 2019

M. Hamanaka,^{*1} K. Suda,^{*2} M. Fujimaki,^{*2} N. Fukunishi,^{*2} S. Fukuzawa,^{*1} A. Goto,^{*2} H. Hasebe,^{*2} Y. Higurashi,^{*2} E. Ikezawa,^{*2} H. Imao,^{*2} S. Ishikawa,^{*1} O. Kamigaito,^{*2} K. Kaneko,^{*1} M. Kase,^{*2} M. Kidera,^{*2} K. Kobayashi,^{*1} M. Komiyama,^{*2} Y. Kotaka,^{*3} R. Koyama,^{*1} K. Kumagai,^{*2} T. Maie,^{*2} M. Nagase,^{*2} T. Nagatomo,^{*2} T. Nakagawa,^{*2} T. Nakamura,^{*1} M. Nishida,^{*1} M. Nishimura,^{*1} J. Ohnishi,^{*2} H. Okuno,^{*2} Y. Oshiro,^{*3} K. Ozeki,^{*2} N. Sakamoto,^{*2} J. Shibata,^{*1} N. Tsukiori,^{*1} A. Uchiyama,^{*2} S. Watanabe,^{*2} T. Watanabe,^{*2} Y. Watanabe,^{*2} K. Yadomi,^{*1} and K. Yamada^{*2}

The yearly report on the operation of the RIKEN AVF cyclotron (denoted as AVF hereafter) for the period January - December 2019 is presented here. AVF has four beam courses as stand-alone operations: C03 (RI production), E7A (CRIB), E7B (student experiment), and C12 (a new course for nuclear physics). The beam courses are shown schematically in Fig. 1. In addition, AVF is used as an injector of RRC. In this mode, there are three beam delivery schemes: RRC-RARF, RRC-IRC-E5, and RRC-SRC.

The yearly operation statistics and beams accelerated using AVF are summarized in Tables 1 and 2, respectively. The total operation time was 3603 h, of which 3166 h was dedicated to AVF stand-alone experiments and 437 h to operations as the injector of RRC. The latter decreased by 1114 h compared with that in the last year. New experiments were conducted at the C12 course in the E7 experimental hall. It is remarkable that there was no trouble in AVF during beam services in this year. The phase slit that leaked cooling water in the last year was replaced by a new one during a maintenance period in the summer. In the same period, the SC-ECR ion source operated for AVF since 2008 was removed owing to the difficulty of maintenance. As an alternative,

the 18 GHz ECR ion source used for RILAC to produce intense metallic ions was installed. At the end of 2019, the ion source became operational as an injector for AVF.

Table 1. Comparison of AVF operation statistics with that in the previous year.

AVF stand-alone operation	2018	2019
Tuning of AVF [h]	886	1314
Trouble of AVF [h]	6	0
C03 exp. [h]	2067	873
E7A exp. [h]	262	789
E7B exp. [h]	274	152
C12 exp. [h]	0	36
Sub total [h]	3489	3166
AVF operation as injector of RRC	2018	2019
Tuning of AVF [h]	132	117
Trouble of AVF [h]	1	0
RRC-RARF exp. [h]	600	239
RRC-IRC-E5 exp. [h]	820	81
Sub total [h]	1551	437
Total [h]	5042	3603

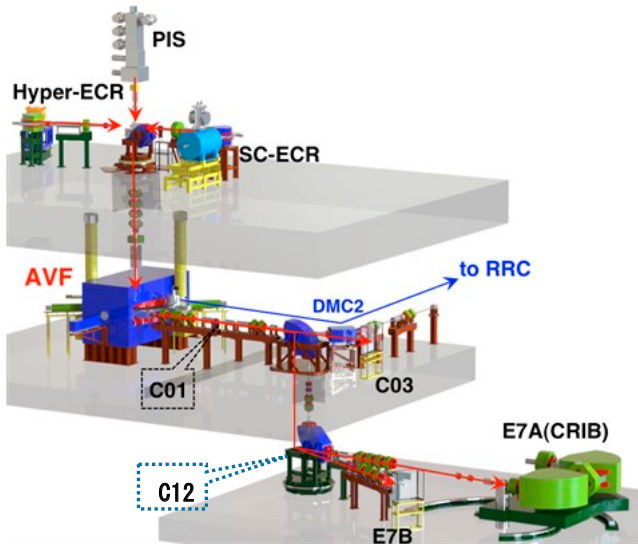


Fig. 1. Overview of the AVF cyclotron with ion sources, each experimental course, and the beam transport line to RRC.

Table 2. AVF beam list in 2019.

Particle	Energy [MeV/nucleon]	Course/Scheme
AVF stand-alone operation		
p	12	C03
d	12	C03
⁴ He	6.5	E7B
⁴ He	7.25	C03, E7B
⁴ He	12.5	C03
⁶ Li	11.2	E7A
⁷ Li	6	C03, E7B
¹⁰ B	7	E7A
¹⁸ O	6	C03
¹⁸ O	6	C03
¹⁸ O	6	C12
¹⁸ O	7	C12
¹⁹ F	6	C03
²⁰ Ne	5	E7B
²⁴ Mg	7	E7A
²⁴ Mg	8	E7A
AVF operation as injector of RRC		
¹² C	7	RRC-RARF
¹⁴ N	7	RRC-RARF
⁴⁰ Ar	5.19	RRC-IRC-E5
⁵⁶ Fe	5	RRC-RARF

*1 SHI Accelerator Service Ltd.

*2 RIKEN Nishina Center

*3 Center for Nuclear Study, the University of Tokyo

Present status of the liquid-helium supply and recovery system

T. Dantsuka,^{*1} H. Okuno,^{*1} M. Nakamura,^{*1} S. Tsuruma,^{*1} M. Takahashi,^{*1} M. Kuroiwa,^{*1} M. Ohshima,^{*2} H. Miura,^{*2} H. Shiraki,^{*2} H. Hirai,^{*2} K. Kimura,^{*2} M. Haneda,^{*2} A. Mikami,^{*2} M. Nagano,^{*2} and H. Hazama^{*2}

The liquid-helium supply and recovery system,¹⁾ which can produce liquid helium at a liquefaction rate of 200 L/h from pure helium gas, had been under stable operation since the beginning of April 2001. As operation failures due to aging-related deterioration has increased in recent years, a new liquefier was introduced in 2017. It can produce liquid helium at a liquefaction rate of 220 L/h from pure helium gas. In the summer of 2018, the older helium liquefier has failed. However, with the new helium liquefier, we can supply liquid helium without stoppage.

The volumes of liquid helium supplied each year from 2001 to 2018 are shown in Fig. 1. The supplied volume gradually increased from 20,000 L to 180,000 L. Owing to a malfunction, the supplied volume decreased in 2014.

The purity of helium gas recovered from the laboratories is gradually deteriorating. At present, the impurity concentration in the recovered gas is about 500 ppm. The impurity concentration does not affect the liquefaction operation, but it is necessary to observe the progress. The volumes of helium gas recovered from each building in Wako campus were measured. The recovery efficiency, which is defined as the ratio of the amount of recovered helium gas to the amount of supplied liquid helium, was calculated to be more than 85% for the buildings on the south side of Wako campus, namely, the Cooperation Center building of the Advanced Device Laboratory, Chemistry and Material Physics building, and Nanoscience Joint Laboratory building.

Reference

- 1) K. Ikegami *et al.*, RIKEN Accel. Prog. Rep. **34**, 349 (2001).

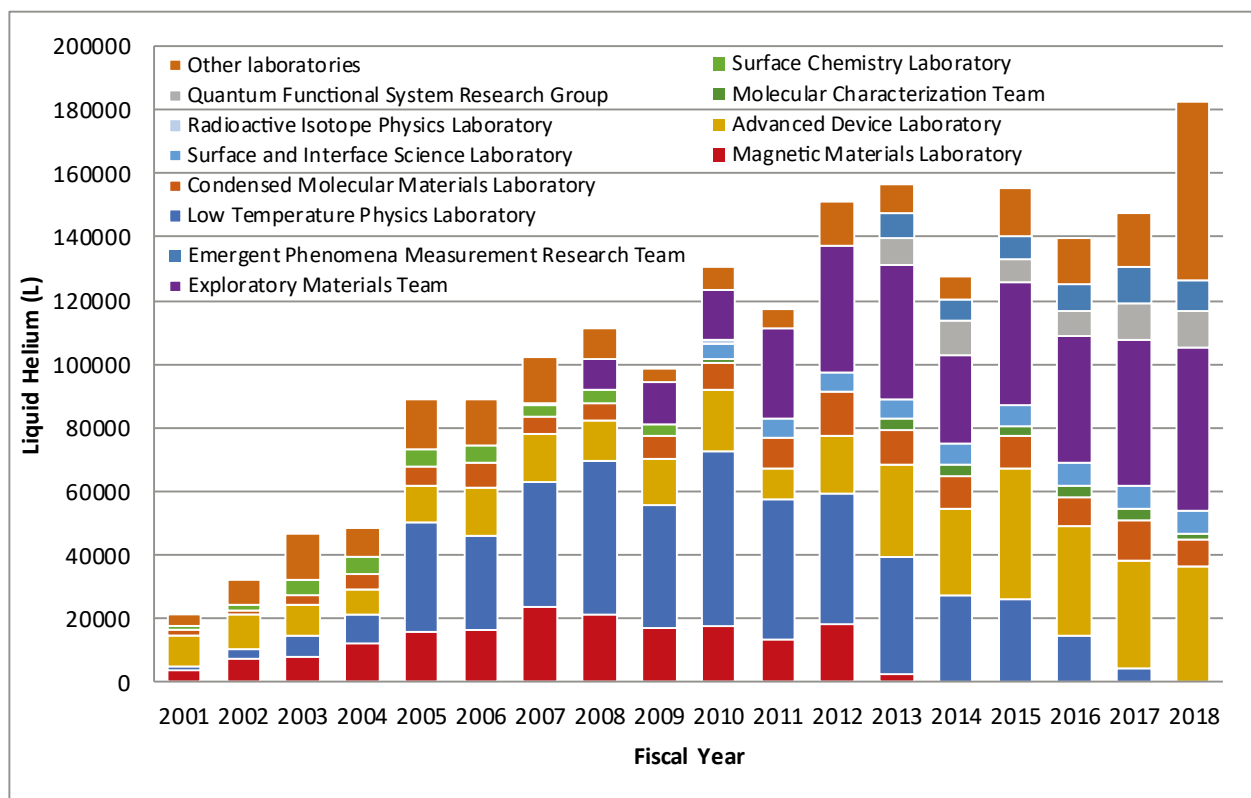


Fig. 1. Volumes of liquid helium supplied to the various laboratories for each fiscal year from 2001 to 2018.

^{*1} RIKEN Nishina Center

^{*2} Nippon Air Conditioning Service K.K.

Operation of the BigRIPS cryogenic plant

K. Kusaka,^{*1} M. Ohtake,^{*1} K. Yoshida,^{*1} M. Ohshima,^{*2} A. Mikami,^{*2} H. Hazama,^{*2} H. Miura,^{*2} H. Shiraki,^{*2} H. Hirai,^{*2} M. Haneda,^{*2} K. Kimura,^{*2} and M. Nagano^{*2}

We performed two continuous operations of the BigRIPS cryogenic plant in 2019. The first operation period was from March 1 to June 24, and the second was from October 23 to December 11. The total operation time of the compressor unit was 72,222 h.

During these continuous operations, we encountered two significant incidents. One incident was the failure of the compressor unit in June. We first noticed an unusual noise that was produced by the main motor of the compressor unit. Although the noise level gradually increased daily, we maintained the continuous operation while monitoring the vibrations of the main compressor and the motor unit. However, the compressor unit suddenly stopped on June 13. Though no interlock alarm event was recorded, we consider that the reason was the over current of the main motor unit because a sudden increase of the main motor current from 29.9 A to 32.6 A was recorded in the control system. We could restart the compressor unit and maintain the continuous operation till the end of the beam time.

The main motor unit was disassembled on site to investigate the origin of the unusual vibrations. In a bearing unit on the coupling side, damage was found on a surface of its inner ring and the bearing balls (Fig. 1). We also found that the size of the housing for the damaged bearing unit was 5 μm larger than its dimension standard (+0–25 μm). The motor unit was reassembled with new bearing units, and the housing was re-manufactured with a tolerance of +0.0 μm . After the regular maintenance of the whole compressor unit, a test operation was successfully performed, and no unusual noise was produced in the second operation period.

Figure 2 shows the vibration acceleration in the vertical and horizontal directions as a function of the total operation time. Two rapid increases of the vibration acceleration at operation times of 59,000 h and 71,000 h indicate the damage of the bearing unit occurred in Dec. 2016¹⁾ and in June 2019. The vibration acceleration re-



Fig. 1. Damaged bearing unit, disassembled from the coupling side of the motor unit.

^{*1} RIKEN Nishina Center

^{*2} Nippon Air Conditioning Services Co., Ltd.

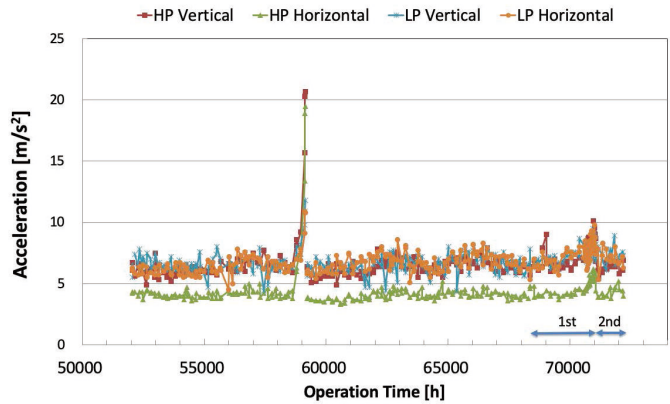


Fig. 2. Vibration acceleration of the compressor unit. Two operation periods are indicated by arrows.

mained less than 8 m/s^2 in the second operation period.

The other incident consisted of the failures of the first expansion turbine T1 in the refrigerator. The T1 turbine did not start rotation in the starting up of the refrigerator. The starting sequence of the refrigerator unit usually proceeds automatically as follows. The purge line valve opens for 30 s so that room-temperature helium gas flows into the gas-bearing cartridge of the expansion turbines T1 and T2. Subsequently the control valve CV3130 in the turbine inlet line gradually opens, and the inflow of the cold helium gas starts the rotation of T1 and T2 simultaneously. The opening of CV3130 increases up to 50% and the rotation speeds of T1 and T2 turbine increase beyond 3000 rps depending on the temperature of the inlet helium gas.

The first failure of T1 turbine occurred on June 13, when a sudden stop of the compressor caused refrigerator trip. After having the compressor unit restarted, we restarted the refrigerator operation. After the turbine trip caused by the low-temperature interlock of the inlet helium gas during the start up, T1 did not start rotation in the automatic starting sequence. We somehow started the refrigerator without the purging process and could proceed with the beam time till June 19. We stopped the refrigerator in the usual manner and visually checked T1 and T2 in the summer maintenance. Although no visual abnormality was found in the maintenance, the same failure occurred in the test operation on September 25. T1 did not work during start up.

Both turbine cartridges were sent to its manufacturer Linde and were disassembled. While T2 was not damaged, the gas bearing of T1 had problems. Scratches and particles were found on the lower axial bearing. After replacing the lower axial bearing with a new one and polishing the shaft, T1 turbine cartridge was reassembled. The repaired turbines were remounted on October 24, and the refrigerator successfully started on October 25. The origin of the scratches is under investigation.

Reference

- 1) K. Kusaka *et al.*, RIKEN Accel. Prog. Rep. **50**, 285 (2017).

Radiation safety management at RIBF

K. Tanaka,^{*1} Y. Uwamino,^{*1} H. Sakamoto,^{*1} R. Hirunuma-Higurashi,^{*1} H. Mukai,^{*2} A. Akashio,^{*1} T. Okayasu,^{*1} R. Suzuki,^{*3} M. Takekoshi,^{*3} Y. Yamauchi,^{*3} K. Igarashi,^{*1} S. Iizuka,^{*1} N. Usudate,^{*1} and Y. Shioda^{*1}

The results of radiation monitoring at RIBF, performed between the border of the facility and the radiation-controlled area, are reported. The residual doses along the accelerator setups are also presented. In 2019, a ^{238}U beam of about 345 MeV/nucleon was provided at an intensity of 70 particle nA in November and December. A ^{78}Kr beam of about 345 MeV/nucleon of 300 particle nA was used in March and April. Subsequently, ^{128}Xe beam of about 345 MeV/nucleon of 80 particle nA was used in May and June.

The dose rates at the boundary of the radiation-controlled area were monitored. Neutron and γ -ray monitors were used at three locations roofs of the RRC, IRC, and BigRIPS. Figure 1 shows the annual neutron dose at these positions. In 2019, even the highest annual dose of 60 $\mu\text{Sv}/\text{y}$ at the IRC roof was lower than the legal limit of 5.2 mSv/y.

The dose rates at the site boundary, where the legal limit is 1 mSv/y, were monitored. Neutron and γ -ray monitors were used, and the annual dose in 2019 was found to be lower than the detection limit after background correction. The detection limit of the neutron monitor is 2 $\mu\text{Sv}/\text{y}$ and that of the γ -ray monitor is 8 $\mu\text{Sv}/\text{y}$. Therefore, it was inferred that the annual dose at the boundary was less than 10 $\mu\text{Sv}/\text{y}$, which is considerably lower than the legal limit.

The residual radioactivity at the deflectors of the cyclotrons was measured just before maintenance work.

The residual dose depends on factors such as the beam intensity, accelerator operation time, and cooling time. The dose rates from 1986 are shown in Fig. 2. The dose rates for FRC, IRC, and SRC are shown for the years since 2006, when the RIBF operation started. For AVF, the dose rate increased in 2006 because the radioisotope production was started and the beam intensity increased.

The residual radioactivity along the beam lines was measured after almost every experiment. Figure 3 shows the locations of measurement points where high residual doses were observed. Table 1 lists the dose rates, beam conditions, and cooling time at the measurement points. The maximum dose was 46 mSv/h at point 23, which is in the vicinity of the beam dump of BigRIPS.

The radioactivity in the closed cooling system at BigRIPS was measured. The water for the F0 target, the exit beam dump, and the side-wall dump were sampled

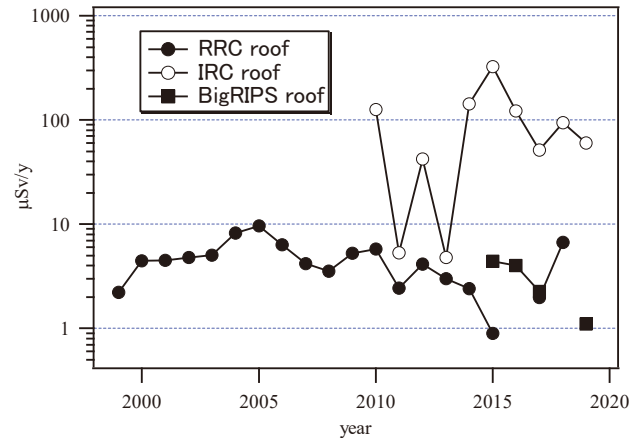


Fig. 1. Radiation dose at the boundary of the radiation-controlled area.

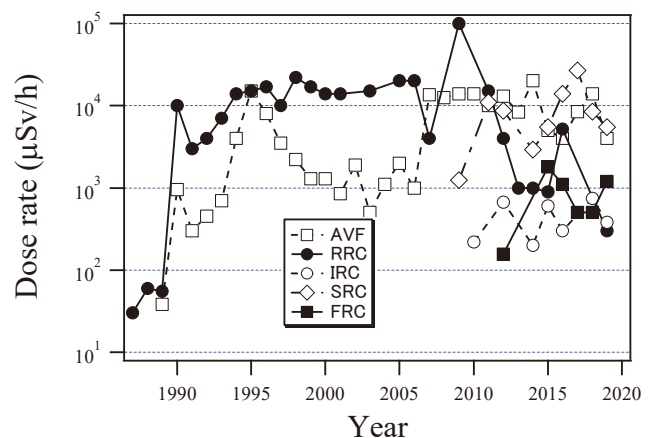


Fig. 2. Dose rates of residual radioactivity at the deflectors of 5 cyclotrons.

in June. The water in the closed cooling systems for the F0 target was not replaced in 2019. 1300 L of water for the exit beam dump was replaced in April 2018, following which 200 L and 130 L of water was supplied in March and October 2019, respectively. For the side-wall beam dump, all of the water was replaced in July 2018. The results are listed in Table 2. A liquid scintillation counter (LSC-7400, Hitachi Co. Ltd.) was used for low-energy γ ray of 18 keV from H-3 nuclide. A Ge detector (GC2019, Canberra Co. Ltd.) was also used for γ rays emitted from other radionuclides. The radionuclides, except for H-3, were already filtered by an ion exchange resin in the closed cooling systems. Although the overall value of contamination was less

*1 RIKEN Nishina Center

*2 Japan Environment Research Corporation

*3 Daiwa Atomic Engineering Corporation

than the legal limit for drain water, as summarized in Table 2, the water from the closed cooling system will be dumped into the drain tank before the next operation to prevent contamination in the room in the case of a water leakage.

The E-learning module, which can be accessed anytime and from anywhere (even from outside RIKEN), has been used for re-training the radiation workers at RIBF. About 670 radiation workers have completed the training in 2019.

As described above, radiation management to comply with laws and to keep the radiation level as low as possible has been conducted successfully.

Table 1. Dose rates measured at beam lines in 2019. Points 1–24 indicate the locations where measurements were taken as shown in Fig. 3.

Point	Dose rate (μSv/h)	Date (M/D)	Particle	Energy (MeV/u)	Intensity (pnA)	Cooling time (h)
1	300	12/27	O-18	6.0	1000	50
2	240	12/27	O-18	6.0	1000	50
3	100	12/27	O-18	6.0	1000	50
4	800	12/27	O-18	6.0	1000	50
5	90	7/29	α	7.25	5000	1014
6	400	7/29	V-51	6.0	1000	276
7	120	7/29	V-51	6.0	1000	276
8	120	12/27	U-238	10.75	2629	497
9	95	7/29	V-51	6.0	1000	291
10	110	7/29	N-14	135	142	355
11	2600	6/26	Xe-124	50	370	163
12	2800	12/18	U-238	50	508	286
13	150	12/18	U-238	50	508	286
14	315	12/18	U-238	345	94	284
15	33500	6/26	Xe-124	345	148	161
16	280	12/18	U-238	345	94	284
17	150	6/26	Xe-124	345	148	161
18	1100	6/26	Xe-124	345	148	161
19	250	6/26	Xe-124	345	148	161
20	790	6/26	Xe-124	345	148	161
21	1860	6/26	Xe-124	345	148	161
22	2800	6/26	Xe-124	345	148	161
23	46000	6/26	Xe-124	345	148	161
24	415	12/18	U-238	345	94	284

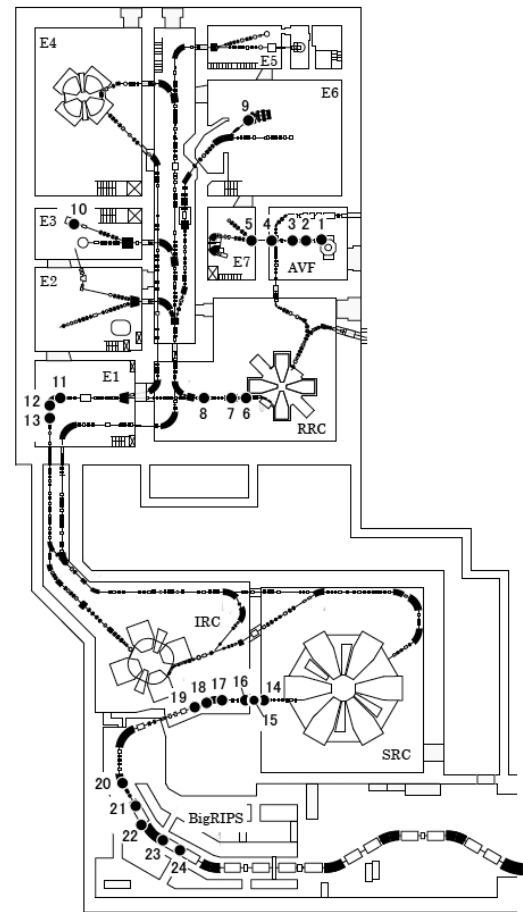


Fig. 3. Layout of the beam lines at RIBF. The measurement locations listed in Table 1 are indicated.

Table 2. Concentrations of radionuclide in the cooling water at BigRIPS, the allowable legal limits for drain water, and the ratios of concentration to the allowable limit.

Cooling water	Nuclide	Concentration[a] (Bq/cm ³)	Limit[b] (Bq/cm ³)	Ratio to limit [a/b]	
BigRIPS F0 target	H-3	3.2	60	5.3e-2	
	Mn-54	3.9e-4 ¹⁾	1.0	3.9e-4	
		summation		5.3e-2	
BigRIPS exit beam dump	H-3	7.6	60	1.3e-1	
	Be-7	1.4e-2	30	4.5e-4	
	Mn-54	5.1e-3	1	5.1e-3	
	Co-56	2.1e-3	0.3	6.9e-3	
	Co-57	5.1e-3	4	1.3e-3	
BigRIPS side-wall beam dump	Co-58	1.3e-2	1	1.3e-2	
	Co-60	2.2e-3	0.2	1.1e-2	
	summation			1.7e-1	
BigRIPS side-wall beam dump	H-3	8.4	60	1.4e-1	
	Be-7	8.5e-3	30	2.8e-4	
	Mn-54	1.5e-3	1	1.5e-3	
	Co-57	2.3e-3	4	5.6e-4	
	Co-58	1.3e-3	1	1.3e-3	
		Co-60	1.7e-3	0.2	8.6e-3
		summation		0.15	

1) read as 3.9×10^{-4}

Operation of the Pelletron tandem accelerator

T. Ikeda,^{*1} M. Hamagaki,^{*1} and H. Sato^{*1}

The tandem accelerator (Pelletron 5SDH-2, 1.7 MV max.) in the Nishina R&D Building, which is managed by the Detector Team of RNC, is joint-use equipment in Wako campus. Figure 1 shows the configuration of the beam elements. Two ion sources are employed. One is the RF charge-exchange ion source, called Alphatross, for experiments using He ion beams. The other is the Source of Negative Ions by Cesium Sputtering (SNICS), which is used for experiments with almost all other ions. Thus far, ion species of H, He, Li, B, C, N, O, Si, Ti, Ni, Cu, and Au have been accelerated at 0.5–1.7 MV.

The accelerator has four beam lines named BL-E/W nn (nn stands for the bending angle). BL-E45 is used for surface modification. BL-E15 is reserved for the analysis of Rutherford backscattering (RBS) spectrometry/elastic recoil detection analysis (ERDA). A micrometer-sized beam based on glass capillary optics with an end window is available at BL-W30 to irradiate the biological sample in air or solution.

During the annual reporting period from January 1 to December 31, 2019, the total machine time (MT) including a machine study was 20 days, where the condition test of the ion sources is not included. The ion species accelerated in 2019 were the light ions H⁺, He⁺ and He²⁺ with energies ranging from 1.0 to 4.8 MeV and Au ions with energies of 3 and 9 MeV, as summarized in Table 1. An experiment used both H and He ions on a day to compare the effects of different stopping powers. The topics (1–6) are listed with the number of days of machine time.

(1) Microbeam performance study with H ions using

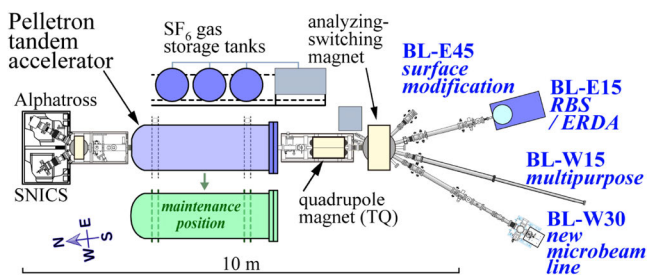


Fig. 1. Pelletron tandem accelerator and beamlines in the Nishina R&D Building.

Table 1. Beam conditions and experiments conducted in the tandem accelerator. A day for He²⁺ includes an MT for H⁺.

Ion	Energy [MeV]	Beam current [pA]	Experiment	Operation time [days]
H ⁺	1.0–3.0	0.001–160	Irradiation	8
He ^{+,2+}	3.0–4.8	0.018–200	Irradiation	12
Au ⁵⁺	3.0–9.0	0.1	Irradiation	1

^{*1} RIKEN Nishina Center

Table 2. Approved conditions at the RIKEN Pelletron.

Ion	Maximum Energy	Ion	Maximum Energy
H	3.4 MeV	B	10.2 MeV
He	5.1 MeV	C	12 MeV
Li/Be	6.8 MeV	other	0.6 MeV/u

* Z : 1 – 83 excluding deuterons

* Maximum intensity: 6.3×10^{12} ions / s (1 μ A)

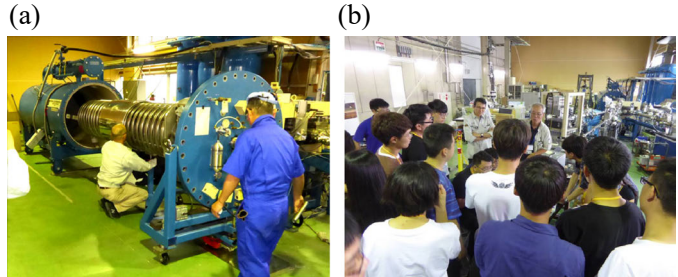


Fig. 2. (a) Overhaul of the Pelletron accelerator. (b) A school principal explaining the accelerator to students.

glass capillaries at BL-W30¹⁾ (7 days)

- (2) Microbeam (He ion) irradiation for single cells at BL-W30²⁾ (9 days including 1 day with He/H ions.)
- (3) RBS/ERDA experiments using carbon ions (0 day)
- (4) Educational experiment of proton capture by carbon/boron nucleus for Nishina School (2 days)
- (5) Development of charged-particle/gamma-ray detector to be used for RIBF experiments (2 days)
- (6) Other development using protons (0 day)

In this year, the regulation of the maximum energy of carbon ions was changed, as summarized in Table 2 with other ions. The charge state $^{12}\text{C}^{6+}$ is now available with the full acceleration voltage of 1.7 MV ($E_{\text{carbon}} = 11.9$ MeV). The approved maximum energy was 0.6 MeV/nucleon.

The acceleration tank was overhauled in May for the first time in 3 years (Fig. 2(a)). No serious deterioration was found at any essential parts for the operation. The pellet chains and inner wall of the tank were cleaned to avoid sudden voltage drops. In August, the experiment of the Nishina School was performed. 1- and 2-MeV protons were provided for the nuclear resonance reaction of $^{12}\text{C}(p, \gamma)^{13}\text{N}$, the reaction energies of which are 0.457 and 1.699 MeV, respectively. The energy spectra of the γ rays from the carbon and boron targets were obtained. Some known and unknown γ -ray peaks were discussed by the student participants.

References

- 1) T. Ikeda *et al.*, Nucl. Instrum. Methods Phys. Res. B **470**, 42 (2020).
- 2) T. Ikeda *et al.*, in this report.

Fee-based activities operated by the Industrial Application Research Team

A. Yoshida,^{*1} T. Kambara,^{*1} H. Haba,^{*1} and D. Mori^{*1}

The fee-based activities operated by the Industrial Application Research Team in 2019, which are the utilization of heavy-ion beams in the industry and the distribution of radioisotopes, are summarized below.

RIKEN Nishina Center allows the use of the AVF cyclotron, RILAC, and RIKEN Ring Cyclotron (RRC) by private companies in Japan for a fee.¹⁾ At present, the main users are semiconductor companies that irradiate space-use semiconductor devices with Ar, Kr, or Xe ions from the RRC to simulate single-event effects due to the heavy-ion components of cosmic radiation. Proposals for beam utilization are reviewed by a program advisory committee dedicated to industrial use (InPAC). In July 2019, InPAC held its 9th meeting, where it reviewed and approved two proposals. No fee-based beamtimes were executed in 2019.

Since 2007, RIKEN has distributed radioisotopes (RIs) to users in Japan for a fee in collaboration with the Japan Radioisotope Association²⁾ (JRIA). The nuclides are ^{65}Zn ($T_{1/2} = 244$ days), ^{109}Cd ($T_{1/2} = 463$ days), ^{88}Y ($T_{1/2} = 107$ days), ^{85}Sr ($T_{1/2} = 65$ days), and ^{67}Cu ($T_{1/2} = 61.8$ hours) produced by the Nuclear Chemistry Research Team (formerly RI Applications Team) at the AVF cyclotron. According to a material transfer agreement (MTA) drawn between JRIA and RIKEN, JRIA mediates the transaction of the RIs and distributes them to users. ^{65}Zn and ^{109}Cd are delivered approximately two weeks after the acceptance of an order. ^{85}Sr , ^{88}Y , and ^{67}Cu , which have short half-lives, are not stocked like ^{65}Zn and ^{109}Cd but are produced in a scheduled beamtime after an order is accepted. Therefore, they are delivered two months or more after an order. Details can be found on the online ordering system J-RAM³⁾ of JRIA.

In 2019, we delivered no ^{109}Cd , two shipments of ^{65}Zn with a total activity of 6.7 MBq, two of ^{88}Y with a total activity of 2 MBq, and one of ^{67}Cu with an activity of 5 MBq. The final recipients of the RIs were two universities, one research institute, and one medical research center.

Figure 1 shows the yearly trends in the number of orders and the amounts of distributed RIs. Compared with 2018, the amounts of distributed ^{65}Zn and ^{85}Sr decreased and that of distributed ^{88}Y remained the same. The shipment of ^{67}Cu is the first since we started its delivery in August 2018.

In the general trend, the demand for long-lived RIs has drastically decreased, whereas that for short-lived RIs is increasing.

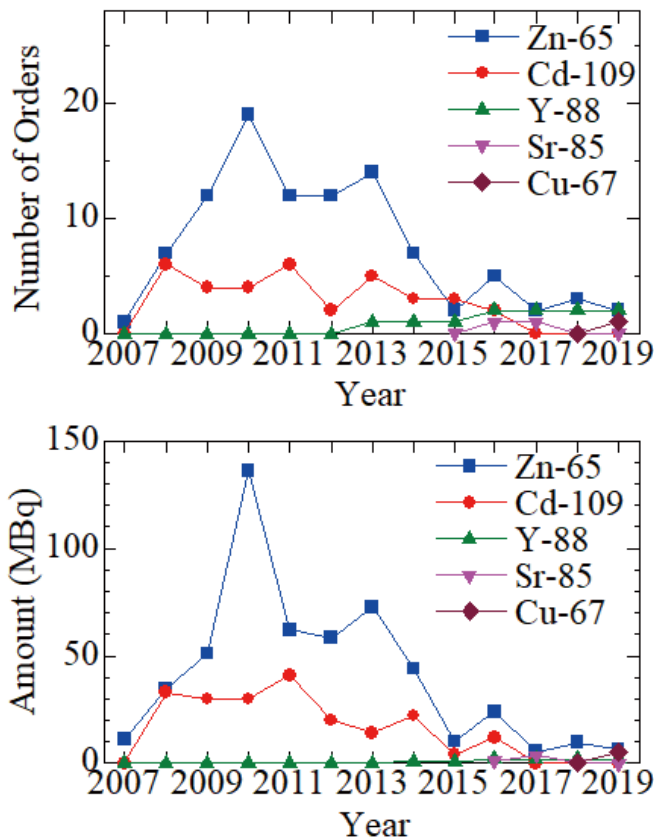


Fig. 1. Number of orders (upper) and amount (lower) of the RIs distributed yearly from 2007 to 2019. The distribution of ^{88}Y started in 2010, that of ^{85}Sr in 2015, and that of ^{67}Cu in 2018.

References

- 1) <http://ribf.riken.jp/sisetu-kyoyo/> (Japanese).
- 2) <http://www.jrias.or.jp/> (Japanese),
<http://www.jrias.or.jp/e/> (English).
- 3) <https://j-ram.org/> (Japanese).

^{*1} RIKEN Nishina Center

V. EVENTS

Nishina School 2019

H. Ishiyama,^{*1} T. Motobayashi,^{*1} and H. Ueno^{*2}

Nishina School aims at introducing nuclear physics research to Asian university students who are choosing their future field of study. In 2019, the 13th Nishina School was held from July 30 to August 9. This period was made slightly later than usual to make it easier for Japanese students to participate after their term-end examinations. Students and supervisors from Peking University (PKU), the University of Hong Kong (HKU), Seoul National University, Rikkyo University, and Tohoku University joined Nishina School this year. High-school students from Philips Exeter Academy, USA, along with their teacher, participated in most of the School programs. Figure 1 shows all 22 students and School staff members.

The School began with self-introductions of the students. The first week was dedicated mostly to lectures and training on a few subjects related to a nuclear reaction experiment that was performed in the second week of the School. The lectures were on a few basic topics for research, including overviews of nuclear physics and nuclear astrophysics, as well as methods of radiation measurements. Another lecture was dedicated to radiation safety. The training subjects were electronic-pulse propagation and radiation detection. The training covered the detectors, electronics, and data acquisition system to be used in the experiment in the following week.

The program in the second week focused on a reaction experiment using proton beams from the Pelletron accelerator at RIKEN Nishina Center. The students were divided into six groups, which oversaw six different types of measurements. They started to design the experiment by evaluating the feasibility of measurements (*i.e.*, estimation of γ -ray yields, etc.), following which they set the detectors around the reaction target and determined the conditions of beam exposure based on their considerations. After the experiment, they analyzed the experimental data obtained and finally made presentations on

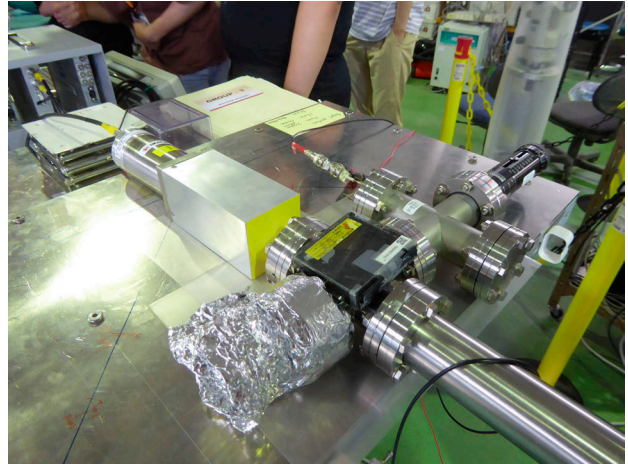


Fig. 2. Photograph of the experimental apparatus. The ^{12}C or BN target in the vacuum pipe at the center of photograph was irradiated with proton beams from the Pelletron accelerator. The NaI detector at upper side of the photograph detected γ -rays generated by the reactions.

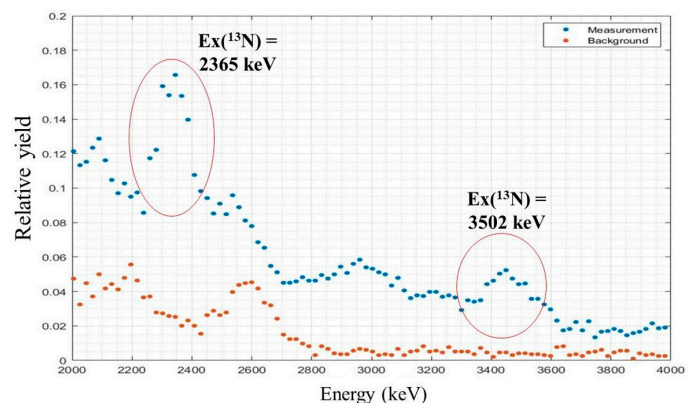


Fig. 3. Example of the γ -ray spectra obtained for the “in-beam” measurement of the $^{12}\text{C}(p, \gamma)^{13}\text{N}$ reaction with a 2-MeV proton beam.



Fig. 1. Participants of Nishina School 2019.

their results. They studied the low-energy $^{12}\text{C}(p, \gamma)^{13}\text{N}$ or $^{10}\text{B}(p, \alpha)^7\text{Be}$ reaction, which are related to nucleosynthesis in stars.

Figure 2 shows the experimental apparatus. Proton beams with an energy of 1 or 2 MeV bombarded a carbon or boron nitride target, which stopped the protons to provide a so-called thick target yield of those reactions. Two methods were employed to determine the resonance yield: the detection of “in-beam” γ -rays from ^{13}N or ^7Be excited states and the detection of 511-keV γ -rays from the β^+ decay of ^{13}N or ^7Be activities, which is known as the “activation” technique. Figure 3 shows an example of the obtained γ -ray spectrum for the “in-beam” measurement of the $^{12}\text{C}(p, \gamma)^{13}\text{N}$ reaction. Two distinct peaks of relevance in the experiment are clearly observed. The six teams could finally extract the reaction cross sections.

We thank all the staff members of the Nishina Center who participated and helped in Nishina School 2019.

^{*1} School Master

^{*2} Chair, Nishina School Steering Committee

Creation of superheavy elements highlighted at the closing ceremony of IYPT 2019[†]

H. En'yo,^{*1}

The year, 2019 was the International Year of the Periodic Table (IYPT). It marked the celebration of the 150th anniversary of Mendeleev's periodic table and the completion of the 7th row of the table. The opening ceremony took place on January 29th at the UNESCO HQ in Paris, and the closing ceremony took place on December 5th at the Tokyo Prince Hotel. The closing ceremony was hosted by the Chemical Society of Japan, Science Council of Japan, and RIKEN on behalf of UNESCO, IUPAC, and IUPAP.

The closing ceremony included an impressive list of exhibitions and sessions; it started with an opening session, followed by sessions titled "Introduction of IYPT activities" and "Discoveries and Creation of elements," and ended with a session titled "Periodic Table for Next Generations." The event also had musical performances, including one by an orchestra comprised of Japanese chemists. The entire program was recorded and can be viewed on the web page of IYPT of Japan.¹⁾

An important session for Nishina Center was the "Creation of Superheavy Elements," which started with the piano fantasy "Nihonium" played by a high school student Honoka Motai. Miss Motai is so devoted to the periodic table that the discovery of nihonium inspired her to compose the music she performed. Her beautiful music was accompanied by a screen showing the landscape of Nihonium Avenue stretching from Wako City Station to RIKEN.²⁾ This avenue is a "walk of fame" of about 15 min for the 118 elements from hydrogen to oganesson, which are displayed in paving stones and lead to the entrance of RIKEN, where a large monument dedicated to nihonium is installed.

After the piano performance, celebrated speeches were given with institutional introductory movies. This included Victor Matveev for the Joint Institute for Nuclear Research, Karlheinz Langanke for GSI Helmholtzzentrum für Schwerionenforschung, Roderick Clark for Lawrence Berkeley National Laboratory, Mark Stoyer for Lawrence Livermore National Laboratory, Krzysztof Rykaczewski for Oak Ridge National Laboratory, Kosuke Morita for RIKEN Nishina Center, and a final speech given by Yuri Oganessian representing all the discoverers. Lastly, the boards of 15 superheavy elements from Rf ($Z = 104$) to Og ($Z = 118$) are shown in line by M. Itkis (JINR), V. Matveev (JINR), R. Clark (LBNL), A. Yakushev (GSI), C. Duellmann (GSI, JGUM), M. Block (GSI, JGUM), K. Langanke (GSI), D. Ackermann (GANIL), J. Khuyagbaatar (GSI), M. Honoka (Tokyo Gakugei University Senior High School) with K. Morimoto (RIKEN), S. Dmitriev (FLNR, JINR), V. Utyonkov (FLNR, JINR), M. Stoyer (LLNL), K. Rykaczewski (ORNL), and A. Karpov (FLNR, JINR), respectively.

These scientists had participated in both this ceremony and the 4th International Symposium on Superheavy Elements (SHE2019), held from 1–5 December at Hakone. H. Haba (RIKEN) and K. Morita (Kyushu-U, RIKEN) jointly chaired the symposium.

References

- 1) <https://iypt.jp/>.
- 2) The video was created by N. Miya-uchi, RIKEN Nishina Center, and can be obtained upon request.



Fig. 1. The boards of 15 superheavy elements from Rf to Og displayed by discoverers.

[†] Condensed from the article in Nucl. Phys. News **30**, 1 (2020)

^{*1} RIKEN Nishina Center

The 3rd “Hodan-kai” meeting for the future of exotic nuclear physics

W. Horiuchi,^{*1,*2} Y. Ichikawa,^{*3,*4} K. Sekizawa,^{*5} and D. Suzuki^{*3} for the “Hodan-kai” meeting organizers

The third “Hodan-kai” meeting by young researchers was held from February 19 to 21, 2020 at the Integrated Innovation Building in Kobe campus of RIKEN, which is the same venue as for the previous Hodan-kai meetings. This Hodan-kai was the third in the meeting series organized by RIBF Theory Forum and RIKEN Nishina Center, and supported by RIKEN iTHEMS and JICFuS. The style of Hodan-kai is different from that of an ordinary workshop in which recent research works are presented by the respective research groups. This meeting aims to facilitate the exchange of new ideas among young researchers, including unmaturing ideas and dreams that are not feasible at present. Given the spirit of the meeting, the presentation files are disclosed to the public. Furthermore, the venue is located in a rather isolated place, which enables participants to concentrate on physics discussions. The meeting always exceeds the scheduled time owing to passionate discussions among the participants.

The first Hodan-kai was held from July 21 to August 2, 2017, and focused mainly on the latest theoretical research on nuclear physics. The number of participants was 49 with 23 presentations. The second meeting was held from February 18 to 20, 2019 and had 42 participants. While limiting the number of presentations to 25, the topic was extended: 6 presentations were made by theoretical nuclear physicists, 7 presentations by experimental nuclear physicists, and 12 presentations by researchers in other fields that may closely be re-



Fig. 1. Group photograph of the 3rd “Hodan-kai” meeting.

*1 Department of Physics, Hokkaido University

*2 RIBF Theory Forum

*3 RIKEN Nishina Center

*4 Department of Physics, Kyushu University

*5 Center for Transdisciplinary Research, Institute for Research Promotion, Niigata University



Fig. 2. Photograph of a panel discussion.

lated to nuclear physics. The program and summary of the first and second Hodan-kai were shared on their respective websites.^{1,2)}

In the third Hodan-kai, we had 43 participants and 17 presentations by young researchers including 6 and 7 presentations by theoretical and experimental nuclear physicists, respectively, and 4 presentations by researchers in other fields. In addition to these talks given in the regular Hodan-kai style, we newly organized two “panel discussion” sections to facilitate interaction among the participants. In the panel discussions, introductory talks on “New textbook for nuclear physics” and “What is cooling?” were given by the organizers, and 5–7 short talks were given by invited panelists. Though, as always, these exciting discussions easily exceeded the scheduled time, the meeting ended successfully while keeping the spirit of Hodan-kai. The full program and summary of the third Hodan-kai can be found on its website.³⁾ Figures 1 and 2 show some snapshots of the 3rd Hodan-kai. Attracting more students to this meeting is one of the key ingredients for the success of “Hodan-kai.” We plan to hold the next Hodan-kai in February 2021 and look forward to having more participants.

References

- 1) 1st Hodan-kai: <https://indico2.riken.jp/event/2509/>.
- 2) 2nd Hodan-kai: <https://indico2.riken.jp/event/2864/>.
- 3) 3rd Hodan-kai: <https://indico2.riken.jp/event/3157/>.

SHE2019—The 4th International Symposium on Superheavy Elements

H. Haba on behalf of the SHE2019 Local Organizing Committee*¹

The 4th International Symposium on Superheavy Elements (SHE2019) was held on December 1–5, 2019 at The Prince Hakone Lake Ashinoko in Hakone, Japan. Hakone is close to Tokyo, situated at the foot of Mount Fuji, and one of the most popular travel destinations among Japanese and foreign tourists. SHE2019 followed the previous symposiums at Texas A&M University, USA in 2013 and 2015 and Kazimierz Dolny, Poland in 2017. This symposium was jointly organized by the RIKEN Nishina Center, Research Center for Superheavy Elements, Kyushu University, and Advanced Science Research Center, Japan Atomic Energy Agency. It had 130 registrants from 16 countries. There were 2 plenary, 33 invited, and 27 oral talks, as well as 14 poster presentations.

SHE2019 covered all theoretical and experimental aspects of superheavy nuclei and atoms. SHE2019 started with two plenary talks titled “SHE2019 Symposium: experimental challenges” by Y. Oganessian and “Superheavy elements: theoretical challenge” by W. Nazarewicz of Michigan State University, USA on the evening of December 1. From the morning of December 2 till the evening of December 4, the following scientific sessions were conducted: 1) Reaction of Synthesis of the Heaviest and Neutron-rich Nuclei; 2) Status and Short-term Plans at SHE Facilities; 3) Nu-

cleosynthesis of SHE and Search in Nature; 4) Properties and Structure of the SHN; and Decays, 5) Heavy Atoms and Chemistry of SHE; 6) New Approaches and Setups; and 7) New Facilities, Setups, and Instrumentations. On the evening of December 2–4, Young Scientists sessions were held to give young scientists as many opportunities for oral presentation as possible.

The excursion of SHE2019 was conducted in the afternoon on December 4. The participants visited Hakone Lake to enjoy the scenery, Hakone Sekisho (checkpoint) to experience the history, and Hakone Shrine to explore the local culture and religion.

The year 2019 marked the 150th anniversary of the discovery of the periodicity of chemical elements by Dmitriy Ivanovich Mendelejev. Thus, the United Nations and UNESCO proclaimed 2019 as the “International Year of the Periodic Table of Chemical Elements (IYPT2019).” The Closing Ceremony of IYPT was held at The Tokyo Prince Hotel in Tokyo, Japan on December 5th, immediately after SHE2019. Most of the SHE2019 participants joined the Closing Ceremony of IYPT and celebrated the discoveries of elements 113, 115, 117, and 118—nihonium (Nh), moscovium (Mc), tennessine (Ts), and oganesson (Og), respectively—and the completion of the 7th period of the periodic table.



Fig. 1. Conference photo taken at a garden of The Prince Hakone Lake Ashinoko on December 4, 2019 (©Hideto En'yo).

*¹ RIKEN Nishina Center

RIKEN Symposium “Trends in ion-beam breeding over the last two decades and future research”

T. Abe,^{*1} Y. Hayashi,^{*1} H. Ichida,^{*1} K. Ishii,^{*1} R. Morita,^{*1} K. Tsuneizumi,^{*1} M. Izumi,^{*1} Y. Shirakawa,^{*1}
S. Ohbu,^{*1} M. Yamada,^{*1} H. Abe,^{*1} K. Ichinose,^{*1} and N. Asakawa^{*1}

The RIKEN Symposium on “Trends in ion-beam breeding over the last two decades and future research” was held on 23–24 Jan. 2020 at the RIKEN Wako Campus. It was the 9th RARF/RIBF User’s Meeting on Biology, which is held once every two years. The Beam Mutagenesis Group promotes various life-science applications of ion beams from the RI Beam Factory. In particular, this group develops new techniques to breed plants and microbes with the use of heavy-ion irradiation. We started collaborations with flower companies and public agricultural experimental stations in 1996 to investigate the potential uses of heavy-ion beams in applied plant breeding. As a result, two new flower varieties were obtained from irradiated samples in 1998. The former is a dahlia having large flowers and a novel color, and it has been sold in Hiroshima City since the autumn of 2001.¹⁾ The latter is a verbena, which is sterile, generating no seeds; produces flowers with a prolonged lifespan; and has been marketed since the spring of 2002.²⁾ We formed a consortium for ion-beam breeding. In 2019, it consisted of 184 domestic and 20 overseas user institutions. We have already produced 34 new plant varieties. This meeting was first convened in Jan. 2003 to spread ion-beam breeding technology, and it consisted of practical research, biology, and special lectures. Practical research is classified into research on flowers, food crops, microbes, and environmental-improving plants such as trees and moss depending on the irradiation samples. Figure 1 shows the change in the numbers of participants categorized by their specialization. The number of flower breeders has decreased since the early meetings. We found that ions with higher LETs, such as Fe, are effective for the mutation breeding of microbes.³⁾ Two new yeast strains created in 2010 are currently used by over 20 breweries to produce high-quality sake in Japan.⁴⁾ The number of microbe breeders has increased since 2011. NEXT and SIP programs were started from 2010 and 2014, respectively. We have been investigating the effects of LETs ranging from 23 to 640 keV/ μm on mutation induction. The highest mutation rate was observed at an LET of 30 keV/ μm (LETmax) in *Arabidopsis thaliana*⁵⁾ and rice.⁶⁾ The majority of mutations caused by LETmax irradiation were small deletions that were sufficient to disrupt a single gene.⁷⁾ We have been using high-throughput DNA sequencing technologies to analyze gene mutations. An increasing number of biologists have shown that mutants induced by LETmax irradiation have become more useful and important in modern

*1 RIKEN Nishina Center

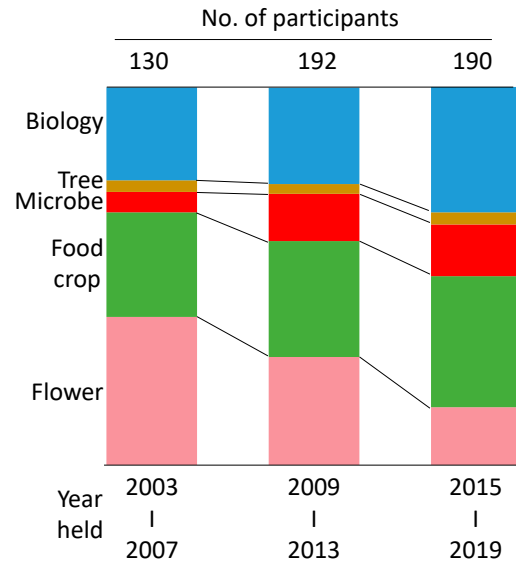


Fig. 1. Changes in the specializations of symposium participants from 2003 to 2019.

genetic studies, enabling the discovery of genes.^{8,9)}

The symposium began with the history over the last two decades of biology and practical research on flowers and food crops. In a special issue, Dr. Kang, who belongs to ARTI and KAERI and is the President of the Korean Society of Breeding Science, introduced “Current status and future prospect of mutation breeding research in Korea.” The next session was on the results of breeding microbe such as *Tricholoma matsutake*, baker’s yeast, and microalgae. Finally, we discussed avenues for research on biology and ion-beam breeding in the next decade. The targets of heavy-ion breeding have extended from flowers to crops such as grains and beans, which will contribute to solving the global problems of food supply and environmental stress. The next meeting will be held in Jan. 2022.

References

- 1) M. Hamatani *et al.*, RIKEN Accel. Prog. Rep. **34**, 169 (2001).
- 2) T. Kanaya *et al.*, Plant Biotech. **25**, 91 (2008).
- 3) H. Ichida *et al.*, Mut Res. **639**, 101 (2008).
- 4) M. Yokobori *et al.*, RIKEN Accel. Prog. Rep. **45**, xxiii (2012).
- 5) Y. Kazama *et al.*, Plant Biotech. **25**, 113 (2008).
- 6) Y. Hayashii *et al.*, RIKEN Accel. Prog. Rep. **50**, 27 (2017).
- 7) Y. Kazama *et al.*, BMC Plant Biol. **11**, 161 (2011).
- 8) Y. Koide *et al.*, Proc. Natl. Acad. Sci. USA **115**, E1955 (2018).
- 9) R. Morita *et al.*, Mol. Breed. **39**, 135 (2019).

RIKEN Open Day 2019

H. Haba*¹ and K. Takahashi*¹

RIKEN Open Day, on which many laboratories showcase their research activities and attractive experimental devices to the public, was held in the RIKEN Wako campus on April 20, 2019. In the Nishina Center, 17 research groups comprising more than 200 researchers participated in the event, as listed in Table 1. The cover page of the leaflet that introduced the exhibition content in the Nishina Center is shown in Fig. 1. The radiation controlled area in the RIBF building was opened to the public to display the world's largest superconducting cyclotron SRC, the in-flight RI separator BigRIPS, and other powerful experimental devices, along with the exhibition laboratories.

The year 2019 marked the 150th anniversary of the discovery of the periodicity of chemical elements by Dimitry Mendeleev. Thus, the United Nations and UNESCO proclaimed 2019 as the "International Year of the Periodic Table of Chemical Elements." Dr. Kosuke Morita, the director of the Superheavy Element Research Group, gave a scientific lecture titled "In search of further new elements" at the Suzuki Umetaro Hall. He presented the discovery of element 113, nihonium, and the research plan for the next new element, element 119, at RIBF. The weather on the open day was very pleasant. A total of 8,253 visitors came to the RIKEN Wako Campus. Among them, 3,013 visited RIBF.



Fig. 1. Cover of the leaflet provided by the Nishina Center for RIKEN Open Day 2019.

Table 1. List of the Nishina Center exhibitions on RIKEN Open Day 2019.

Laboratory / Group / Team	Exhibition theme	Number of staff
Accelerator Group	The World's Strongest Superconducting Ring Cyclotron	35
SLOWRI Team	Ion Trap and Ultra-Slow RI Production	4
BigRIPS Team	Superconducting RI Beam Separator BigRIPS	11
Rare RI-Ring Team	Precision Mass Measurement in 1 ms	8
Spin isospin Laboratory	Microscopes for Unstable Nuclei	13
SAMURAI Team	SAMURAI Magnetic Spectrometer	6
Nuclear Spectroscopy Laboratory	Tiny Magnets in Materials	12
Radioactive Isotope Physics Laboratory	Study on Origin of Elements at RIBF	9
	Glass Marble Shooting	10
Nishina Center	Nuclear Chart with LEGO Block	7
Nuclear Chemistry Research Team	Familiar RI and Useful RI	6
Ion Beam Breeding Team	Creating Amazing Plants	15
Superheavy Element Research Group	The Discovery of the New Element "Nihonium"	12
User Liaison Group	Let's Make Your Nihonium	7
SCRIT Team	Handmade Spectrometer	7
	See Radiation with Diffusion Cloud Chamber	
Radiation Laboratory	Enjoy Spinning a Variety of Tops	11
	Research Activities in the Experimental Hadron Physics	
Quantum Hadron Physics Laboratory	Elementary Particles, Nuclei and the Universe	13
High Energy Astrophysics Laboratory	In Space Now	40

*¹ RIKEN Nishina Center

Outreach activities outside the Wako campus

N. Miyauchi*¹

The year 2019 marks the 150th anniversary of the discovery of Mendeleev's periodic law. Further, in 2016, the names of the four elements up to the 118th, including the 113th element nihonium, were finalized, and the 7th period of the periodic table was completed. To commemorate these events, the United Nations General Assembly and UNESCO declared 2019 as the International Year of Periodic Table (IYPT2019). Accordingly, various events related to the periodic table were held globally. In Japan, "the Japan Chemical Society, International Year of Periodic Table 2019 Executive Committee" organized special traveling exhibitions at about 20 locations across the country to familiarize people with the periodic table. The User Liaison Group held workshops at two locations in these traveling exhibitions.

JST Science Agora in Daiba, Tokyo on Nov. 16–17

The workshop aimed to build a model of the 113th element, nihonium. The first workshop was held at a traveling exhibition booth organized by the Executive Committee of the International Periodic Table at the Science Agora¹⁾ venue on November 16 and 17, 2019 (the Science Agora itself was held for three days, from November 15 to 17). Specifically, we asked participants to make a three-dimensional nihonium model using small beads, which are a children's toy, and helped them gain an understanding of the nucleus and how nihonium was discovered. Although the nucleus is never visible to the naked eye, the workshop was an attempt to make people feel the existence of the nucleus by making a model using the actual number of protons and neutrons.

This time, owing to the limited size of our booth, only a few participants could be taught by a researcher. As a result, the total number of participants was only 44 over two days. Although the workshop had the disadvantage of not being able to handle a large number of people, it was well received because the participants were able to talk with actual researchers owing to the face-to-face seating style.

Ehime Prefectural Science Museum on Jan. 18–19

The next nihonium workshop was held at another traveling exhibition booth organized by the Executive Committee at the Ehime Prefectural Science Museum²⁾ on January 18 and 19, 2020 (we were invited for two days to the traveling exhibition that was conducted from December 14, 2019 to January 26, 2020). The workshop was a great success because Mr. Yoji Hisamatsu (of this Science Museum), who directed all the traveling exhibitions, took care of us. More than 100 participants made



Fig. 1. Workshop to make a nihonium model using small beads.



Fig. 2. Brief lecture on atomic nuclei and nihonium.

their own models of nihonium over the two days of the workshop.

RIKEN Osaka Campus Open Day 2019

Apart from the above two traveling exhibitions, we participated in the open house of RIKEN's Osaka campus on November 23, 2019. Various RIKEN Centers from all over Japan also participated in the event to introduce their research to people in the Osaka area. We introduced research at the RNC by using a small 3D nuclear chart produced by a 3D printer, in addition to poster panels. We had a large audience including children. The exhibition was very successful.

References

- 1) <https://www.jst.go.jp/sis/scienceagora/en/reports/2019/>.
- 2) <http://www.i-kahaku.jp/index.html>.

*¹ RIKEN Nishina Center

VI. ORGANIZATION AND ACTIVITIES OF RIKEN NISHINA CENTER

(Activities, Members, Publications & Presentations)

1. Organization

1.1 Organization Chart as of March 31, 2020 (End of FY2019)

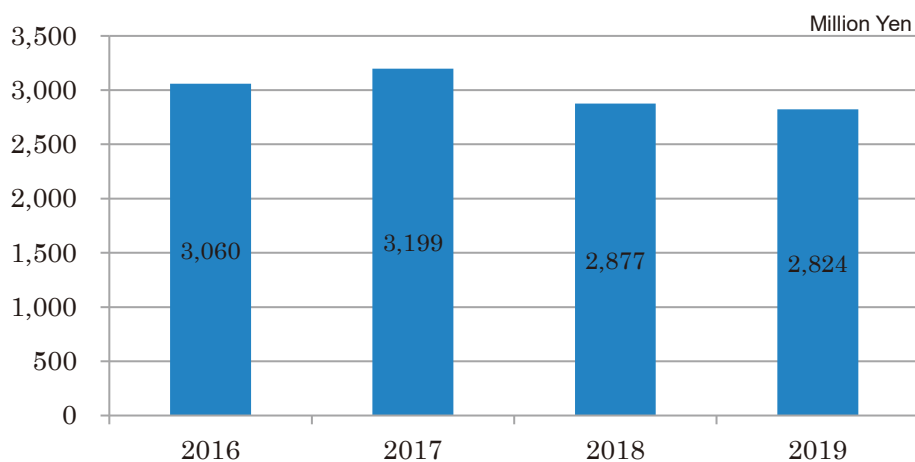


1.2 Topics in FY2019

Year	Date	Topics in Management
2019	Apr. 1	Newly appointed: Deputy Director of RIKEN BNL Research Center: David MORRISON
2019	Apr. 1	Newly appointed: Team Leader of Plant Genome Evolution Research Team: Tomoko ABE

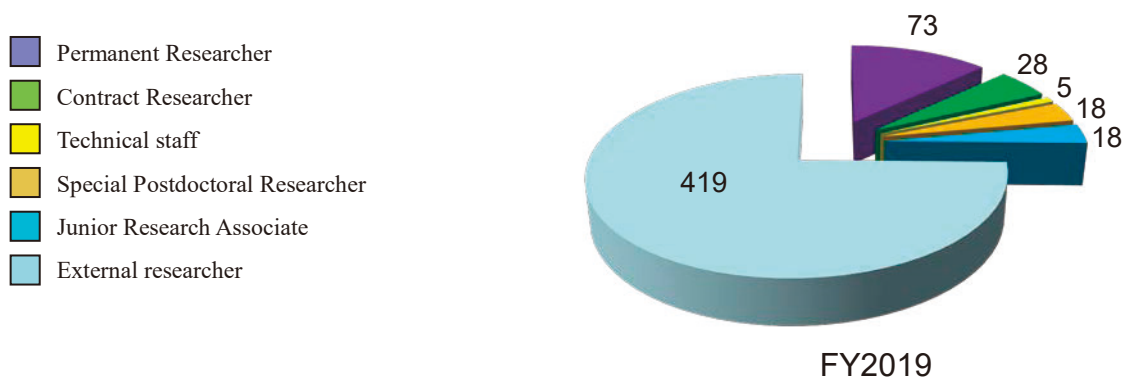
2. Finances

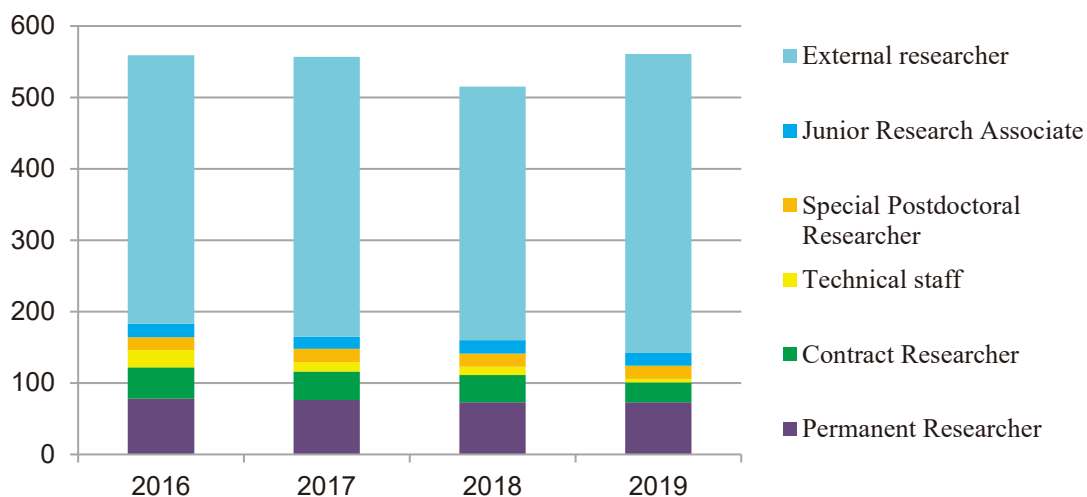
A transition of the RNC budget for the past four years is shown in following graph.



3. Staffing

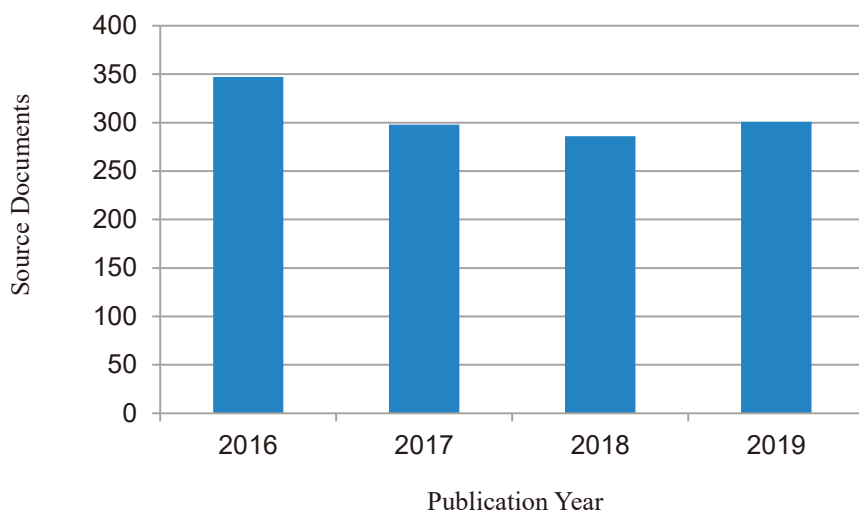
At the start of FY 2019, there were 142 personnel affiliated with RNC and 419 researchers visiting RNC for research purpose. The following graphs show a breakdown of personnel into six categories as of April 1, 2019, and a transition of the number of each category.





4. Research publication

The number of papers published annually from RNC is shown graphically using the data obtained from Clarivate Analytics' Web of Science Documents.



Citation analysis for the past four years

As of April 2020

Indicators \ Year	2016	2017	2018	2019
Total number of papers	347	298	286	301
Percentage of papers in top 10%	15.85	16.78	20.63	9.63
Percentage of papers in top 1%	1.44	2.68	4.20	1.00

5. Management

Headed by the RNC Director Hideto En'yo, the RIKEN Nishina Center for Accelerator-Based Science (RNC) consists of:

- 9 Laboratories
- 10 Groups with 27 Teams
- 2 overseas research centers with 3 Groups

as of the end of FY2019. There are also two 'Partner Institutes' which conduct research in the laboratories set up in RNC. RNC is managed by its Director who takes into consideration the majority decision of the RNC Coordination Committee. The management of RNC is supported by the following committees:

- Program Advisory Committee
- Safety Review Committee
- RIBF Machine Time Committee
- Public Relations Committee

There are also committees to support the President of RIKEN and/or the Director of RNC such as:

- Nishina Center Advisory Council with three subcommittees:
 - RBRC Scientific Review Committee (SRC)
 - International Advisory Committee for the RIKEN-RAL Muon Facility
 - RBRC Management Steering Committee (MSC)

Nishina Center for Accelerator-based Science

Executive Members (as of March 31, 2020)

Hideto EN'YO	Director
Hiroyoshi SAKURAI	Deputy Director (Nuclear Science and Transmutation Research Division)
Osamu KAMIGAITO	Deputy Director (Research Facility Development Division)
Tomoko ABE	Deputy Director (Accelerator Application Division)
Yasushige YANO	Senior Advisor
Tohru MOTOBAYASHI	Senior Advisor
Hideyuki SAKAI	Senior Advisor

RNC Coordination Committee

The following subjects relevant to the RNC management are deliberated under the chairmanship of the RNC Director:

- Establishment of the new organization or reorganization in RNC
- Personnel management of RNC researchers
- Research themes and research budget
- Approval of the Partner Institutes
- Evaluation of the management of RNC and the response to the recommendations by external evaluation

The RNC Coordination Committee is held monthly.

Members (as of March 31, 2020)

Hideto EN'YO	Director, RNC; Director, Radiation Laboratory
Hiroyoshi SAKURAI	Deputy Director, RNC; Director, Radioactive Isotope Physics Laboratory and Nuclear Transmutation Data Research Group; Team Leader, Muon Date Team
Osamu KAMIGAITO	Deputy Director, RNC; Director, Accelerator Group and High-Intensity Accelerator R&D Group; Team Leader, Infrastructure Management Team
Tomoko ABE	Deputy Director, RNC; Director, Beam Mutagenesis Group; Team Leader, Ion Beam Breeding Team and Plant Genome Evolution Research Team
Yasushige YANO	Senior Advisor, RNC
Tohru MOTOBAYASHI	Senior Advisor, RNC
Hideyuki SAKAI	Senior Advisor, RNC
Tomohiro UESAKA	Director, Spin Isospin Laboratory and Research Instruments Group
Hideki UENO	Director, Nuclear Spectroscopy Laboratory and User Liaison Group; Team Leader, Outreach Team
Toru TAMAGAWA	Director, High Energy Astrophysics Laboratory
Kosuke MORITA	Director, Superheavy Element Research Group
Yuko MOTIZUKI	Director, Astro-Glaciology Research Group
Hiroki OKUNO	Deputy Group Director, Accelerator Group; Team Leader, Accelerator R&D Team, Cryogenic Technology Team, and High-Power Target R&D Team

Nobuhisa FUKUNISHI	Deputy Group Director, Accelerator Group; Team Leader, Beam Dynamics & Diagnostics Team
Masanori WAKASUGI	Director, Instrumentation Development Group; Team Leader, Rare RI-Ring Team and SCRIT Team
Hironobu HABA	Director, RI Application Research Group; Team Leader, RI Application Team and Superheavy Element Production Team
Tetsuo HATSUDA	Director, Quantum Hadron Physics Laboratory
Emiko HIYAMA	Director, Strangeness Nuclear Physics Laboratory
Masahiko IWASAKI	Director, Meson Science Laboratory
Kanenobu TANAKA	Director, Safety Management Group
Koji MORIMOTO	Team Leader, Superheavy Element Device Development Team
Hideaki OTSU	Team Leader, SAMURAI Team and Fast RI Data Team
Toshiyuki SUMIKAMA	Team Leader, Slow RI Data Team
Naruhiko SAKAMOTO	Team Leader, Cyclotron Team and High-Gradient Cavity R&D Team
Takahide NAKAGAWA	Team Leader, Ion Source Team
Eiji IKEZAWA	Team Leader, RILAC Team
Hironobu ISHIYAMA	Team Leader, SLOWRI Team
Koichi YOSHIDA	Team Leader, BigRIPS Team
Hidetada BABA	Team Leader, Computing and Network Team
Hiromi SATO	Team Leader, Detector Team
Atsushi YOSHIDA	Team Leader, Industrial Application Research Team
Ken-ichiro YONEDA	Team Leader, RIBF User Liaison Team
Yasuyuki AKIBA	Group Leader, Experimental Group, RIKEN BNL Research Center
Taku IZUBUCHI	Group Leader, Computing Group, RIKEN BNL Research Center
Tsukasa TADA	Vice Chief Scientist, Quantum Hadron Physics Laboratory
Yutaka WATANABE	Deputy Team Leader, Infrastructure Management Team
Yasushi WATANABE	Deputy Team Leader, RIBF User Liaison Team
Koichi ABE	Director, Nishina Center and iTHEMS Promotion Office

Program Advisory Committee

The Program Advisory Committee reviews experimental proposals submitted by researchers and reports the approval/disapproval of the proposals to the RNC Director. The Committee also reports to the RNC Director the available days of operation at RIBF or the Muon Facility at RAL allocated to researchers. The Committee is divided into three categories according to the research field.

- Nuclear Physics Experiments at RIBF (NP-PAC): academic research in nuclear physics
- Materials and Life Science Researches at RNC (ML-PAC): academic research in materials science and life science
- Industrial Program Advisory Committee (In-PAC): non-academic research

Program Advisory Committee for Nuclear Physics Experiments at RI Beam Factory (NP-PAC)

The 20th NP-PAC was held on December 16–18, 2019 at RIBF.

Members (as of March 31, 2020)

Robert V.F. JANSSENS (Chair)	University of North Carolina at Chapel Hill
Dieter ACKERMANN	GANIL
Nori AOI	Osaka University
Maria J.G. BORGE	Consejo Superior de Investigaciones Científicas
Robert CHARITY	Washington University in St. Louis
Augusto O. MACCHIAVELLI	Lawrence Berkeley National Laboratory
Gabriel MARTINEZ-PINEDO	Technische Universität Darmstadt, GSI Helmholtzzentrum für Schwerionenforschung
Iain MOORE	University of Jyväskylä
David J. MORRISSEY	Michigan State University
Hitoshi NAKADA	Chiba University
Alexandre OBERTELLI	Technische Universität Darmstadt
Takehiko SAITO	RIKEN Cluster for Pioneering Research
Kimiko SEKIGUCHI	Tohoku University
Philip J. WOODS	University of Edinburgh
Andrea VITTURI	Università di Padova
Xiaohong ZHOU	Institute of Modern Physics, CAS

Program Advisory Committee for Materials and Life Science Researches at RIKEN Nishina Center (ML-PAC)

The 18th and 19th ML-PAC was held on June 28, 2019 and January 24, 2020 at RIBF, respectively.

Members (as of March 31, 2020)

Adrian HILLIER (Chair)	ISIS, RAL (UK)
Philippe MENDELS	Laboratoire de Physique des Solides, Université Paris (SUD)
Zhi QIN	Institute of Modern Physics, CAS
Toshiyuki AZUMA	RIKEN Cluster for Pioneering Research
Ryosuke KADONO	Institute of Materials Structure Science (KEK)

Atsushi KAWAMOTO	Hokkaido University
Shigeyuki KAWANO	The University of Tokyo
Kenya KUBO	International Christian University
Hiroyuki YAMASE	Research Center for Functional Materials, NIMS
Xu-Guang ZHENG	Saga University
Robert V.F. JANSSENS	University of North Carolina at Chapel Hill

Industrial Program Advisory Committee (In-PAC)

The 9th In-PAC was held on July 10, 2019 at RNC.

Safety Review Committee

The Safety Review Committee is composed of two sub committees, the Safety Review Committee for Accelerator Experiments and the Hot-Lab Safety Review Committee. These Committees review the safety regarding the usage of radiation generating equipment based on the proposal submitted to the RNC Director from the spokesperson of the approved experiment.

Safety Review Committee for Accelerator Experiments

Members (as of March 31, 2020)

Hiromi SATO (Chair)	Team Leader, Detector Team
Kouji MORIMOTO	Team Leader, Superheavy Element Device Development Team
Eiji IKEZAWA	Team Leader, RILAC Team
Hiromitsu HABA	Team Leader, RI Application Team
Atsushi YOSHIDA	Team Leader, Industrial Cooperation Team
Koichi YOSHIDA	Team Leader, BigRIPS Team
Naoki FUKUDA	Technical Scientist, BigRIPS Team
Naruhiko SAKAMOTO	Team Leader, Cyclotron Team
Daisuke SUZUKI	Research Scientist, Radioactive Isotope Physics Laboratory
Masaki SASANO	Senior Research Scientist, Spin Isospin Laboratory
Yuichi ICHIKAWA	Senior Research Scientist, Nuclear Spectroscopy Laboratory

External members

Shinichiro MICHIMASA	Assistant Professor, Center for Nuclear Study, University of Tokyo
Hidetoshi YAMAGUCHI	Lecturer, Center for Nuclear Study, University of Tokyo
Yutaka WATANABE	Associate Professor, High Energy Accelerator Research Organization, KEK

Ex officio members

Kanenobu TANAKA	Director, Safety Management Group
Hisao SAKAMOTO	Technical Scientist, Safety Management Group

Hot-Lab Safety Review Committee

Members (as of March 31, 2020)

Kazuya TAKAHASHI (Chair)	Senior Research Scientist, Nuclear Chemistry Research Team
Kanenobu TANAKA	Director, Safety Management Group
Hisao SAKAMOTO	Technical Scientist, Safety Management Group
Hiroki MUKAI	Technical Staff I, Safety Management Group
Eriko HIGURASHI	Technical Scientist, Safety Management Group
Hiromitsu HABA	Team Leader, RI Application Team
Tetsuya OHNISHI	Senior Research Scientist, SCRIT Team

RIBF Machine Time Committee

Upon request of the RNC Director, the RIBF Machine Time Committee deliberates on the machine time schedule of RIBF and reports the results to the Director.

Members (as of March 31, 2020)

Hideki UENO (Chair)	Director, User Liaison Group and Nuclear Spectroscopy Laboratory
Osamu KAMIGAITO	Director, Accelerator Group
Masanori WAKASUGI	Director, Instrumentation Development Group
Tomohiro UESAKA	Director, Research Instruments Group and Spin Isospin Laboratory
Nobuhisa FUKUNISHI	Deputy Group Director, Accelerator Group
Hiroki OKUNO	Deputy Group Director, Accelerator Group
Hiroyoshi SAKURAI	Director, Radioactive Isotope Physics Laboratory
Tomoko ABE	Director, Beam Mutagenesis Group

Hirimitsu HABA	Director, RI Application Research Group
Kanenobu TANAKA	Director, Safety Management Group
Ken-ichiro YONEDA	Team Leader, RIBF User Liaison Team
Kouji MORIMOTO	Team Leader, Superheavy Element Research Device Development Team
Koichi YOSHIDA	Team Leader, BigRIPS Team

External members

Kentaro YAKO	Associate Professor, Center for Nuclear Study, University of Tokyo
Hidetoshi YAMAGUCHI	Lecturer, Center for Nuclear Study, University of Tokyo
Yutaka WATANABE	Associate Professor, High Energy Accelerator Research Organization, KEK

Observers

Hideto EN'YO	Director, RNC
Susumu SHIMOURA	Director, Center for Nuclear Study, University of Tokyo
Michiharu WADA	Director, KEK Wako Nuclear Science Center
Kosuke MORITA	Director, Superheavy Element Research Group
Hideaki OTSU	Team Leader, SAMURAI Team
Atsushi YOSHIDA	Team Leader, Industrial Cooperation Team
Tohru MOTOBAYASHI	Senior Advisor, RNC
Hideyuki SAKAI	Senior Advisor, RNC
Kathrin WIMMER	Lecturer, University of Tokyo; Chair, The RIBF Users Executive Committee (RIBF-UEC)
Yasuhiro SAKEMI	Professor, Center for Nuclear Study, University of Tokyo
Koichi ABE	Director, Nishina Center and iTHEMS Promotion Office
Kazushige FUKUSHIMA	Manager, Nishina Center and iTHEMS Promotion Office

Public Relations Committee

Upon request of the RNC Director, the Public Relations Committee deliberates and coordinates the following matters:

- Creating public relations system for RNC
- Prioritization of the public relations activities for RNC
- Other general and important matters concerning the public relations of RNC

Members (as of March 31, 2020)

Koichi ABE (Chair)	Director, Nishina Center and iTHEMS Promotion Office
Hiro Yoshi SAKURAI	Deputy Director, RNC; Director, Radioactive Isotope Physics Laboratory
Osamu KAMIGAITO	Deputy Director, RNC; Director, Accelerator Group
Tomoko ABE	Deputy Director, RNC; Director, Beam Mutagenesis Group
Tetsuo HATSUDA	Director, Quantum Hadron Physics Laboratory
Masahiko IWASAKI	Director, Meson Science Laboratory
Tomohiro UESAKA	Director, Spin Isospin Laboratory and Research Instruments Group
Hideki UENO	Director, Nuclear Spectroscopy Laboratory and User Liaison Group
Toru TAMAGAWA	Director, High Energy Astrophysics Laboratory
Emiko HIYAMA	Director, Strangeness Nuclear Physics Laboratory
Kosuke MORITA	Director, Superheavy Element Research Group

RBRC Management Steering Committee (MSC)

RBRC MSC is set up according to the Memorandum of Understanding between RIKEN and BNL concerning the collaboration on the Spin Physics Program at the Relativistic Heavy Ion Collider (RHIC). The 25th MSC was held on May 24, 2019.

Members (as of May 24, 2019)

Motoko KOTANI	Executive Director, RIKEN
Tetsuo HATSUDA	Program Director, RIKEN Interdisciplinary Theoretical and Mathematical Sciences Program
Shoji NAGAMIYA	Senior Visiting Scientist, RNC
Robert TRIBBLE	Deputy Director for Science and Technology, BNL
Dmitori DENISOV	Deputy Associate Laboratory Director for High Energy Physics, BNL
Berndt MUELLER	Associate Laboratory Director for Nuclear and Particle Physics, BNL

6. International Collaboration

Country	Partner Institute	Objects	RNC contact person
---------	-------------------	---------	--------------------

Austria	Stefan Meyer Institute for Subatomic Physics	Framework	Masahiko IWASAKI, Director, Meson Science Laboratory
China	China Nuclear Physics Society	Creation of the council for China -Japan research collaboration on nuclear physics	Hiroyoshi SAKURAI, Director, Radioactive Isotope Physics Laboratory
	Peking University	Nuclear Science	Hiroyoshi SAKURAI, Director, Radioactive Isotope Physics Laboratory
	Institute of Modern Physics, Chinese Academy of Science	Physics of heavy ions	Hiroyoshi SAKURAI, Director, Radioactive Isotope Physics Laboratory
	School of Nuclear Science and Technology, Lanzhou University	Framework	Masahiko IWASAKI, Director, Meson Science Laboratory
	School of Physics, Nanjing University	Framework	Emiko HIYAMA, Director, Strangeness Nuclear Physics Laboratory
	Department of Physics, Faculty of Science, The University of Hong Kong	Experimental and educational research collaboration in experimental nuclear physics	Hiroyoshi SAKURAI, Director, Radioactive Isotope Physics Laboratory
	School of physics, Nankai University	Framework	Emiko HIYAMA, Director, Strangeness Nuclear Physics Laboratory
Finland	University of Jyvaskyla	Basic nuclear physics and related instrumentation	Hironobu ISHIYAMA, Team Leader, SLOWRI Team
France	National Institute of Nuclear Physics and Particle Physics (IN2P3)	Physics of heavy ions	Tomohiro UESAKA, Director, Spin Isospin Laboratory
	Normandy University	Framework	Tomohiro UESAKA, Director, Spin Isospin Laboratory
Germany	Technische Universität München	Nuclear physics, hadron physics, nuclear astrophysics	Emiko HIYAMA, Director, Strangeness Nuclear Physics Laboratory
	GSI	Physics of heavy ions and accelerator	Hiroyoshi SAKURAI, Director, Radioactive Isotope Physics Laboratory
	Department of Physics, Technische Universität Darmstadt	Framework	Emiko HIYAMA, Director, Strangeness Nuclear Physics Laboratory
Hungary	The Institute of Nuclear Research of the Hungarian Academy of Sciences (ATOMKI)	Nuclear physics, Atomic Physics	Tomohiro UESAKA, Director, Spin Isospin Laboratory
Indonesia	ITB, UNPAD, ITS, UGM, UI	Material science using muons at the RIKEN-RAL muon facility	Masahiko IWASAKI, Director, Meson Science Laboratory
	Hasanuddin University	Agricultural science and related fields involving heavy-ion beam mutagenesis using Indonesian crops	Tomoko ABE, Director, Beam Mutagenesis Group
Italy	Applied Physics Division, National Institute for New Technologies, Energy and Environment (ENEA)	Framework	Hiroyoshi SAKURAI, Director, Radioactive Isotope Physics Laboratory
	European Center for Theoretical Studies in Nuclear Physics and Related Areas (ECT*)	Theoretical physics	Tetsuo HATSUDA, Director, Quantum Hadron Physics Laboratory
	Istituto Nazionale di Fisica Nucleare (INFN)	Physics of heavy ions	Hiroyoshi SAKURAI, Director, Radioactive Isotope Physics Laboratory
Country	Partner Institute	Objects	RNC contact person
Korea	Seoul National University	Nishina School	Hiroyoshi SAKURAI, Director, Radioactive Isotope Physics Laboratory
	College of Natural Science, Ewha Women's University	Framework	Tomohiro UESAKA, Director, Spin Isospin Laboratory
	College of Natural Sciences, INHA University	Framework	Emiko HIYAMA, Director, Strangeness Nuclear Physics Laboratory
Malaysia	Universiti Sains Malaysia	Muon Science	Masahiko IWASAKI, Director, Meson Science Laboratory
Norway	Faculty of Mathematics and Natural Science, University of Oslo (UiO MN)	Framework	Hiroyoshi SAKURAI, Director, Radioactive Isotope Physics Laboratory

Poland	The Henryk Niewodniczanski Institute of Nuclear Physics, Polish Academy of Sciences(IFPAN)	Framework	Hiroyoshi SAKURAI, Director, Radioactive Isotope Physics Laboratory
Romania	“Horia Hulubei” National Institute of Physics and Nuclear Engineering Bucharest-Magurele, Romania	Framework	Tomohiro UESAKA, Director, Spin Isospin Laboratory
	University of Bucharest	Framework	Tomohiro UESAKA, Director, Spin Isospin Laboratory
Russia	Joint Institute for Nuclear Research (JINR)	Framework	Tomohiro UESAKA, Director, Spin Isospin Laboratory
	Russian Research Center “Kurchatov Institute”	Framework	Hiroyoshi SAKURAI, Director, Radioactive Isotope Physics Laboratory
Switzerland	Paul Scherrer Institute	Improve the performance and reliability of accelerator systems	Osamu KAMIGAITO, Director, Accelerator Group
USA	Columbia University	The development of QCDCQ	Hideto EN’YO, Director, Radiation Laboratory
	Michigan State University	Comprehensive The use of TPC (Time Projection Chamber)	Tomohiro UESAKA, Director, Spin Isospin Laboratory
Vietnam	Vietnam Atomic Energy Commission	Framework	Hiroyoshi SAKURAI, Director, Radioactive Isotope Physics Laboratory
Europe	European Nuclear Science and Application Research2	Framework	Tomohiro UESAKA, Director, Spin Isospin Laboratory
	The European Organization for Nuclear Research (CERN)	R&D and application of micro-pattern gas detectors (MPGD) technology (RD51 Collaboration)	Hideto EN’YO, Director, Radiation Laboratory
	The European Organization for Nuclear Research (CERN)	Collaboration in the ALICE Experiment	Hideto EN’YO, Director, Radiation Laboratory

7. Awards

Awardee, Laboratory / Team	Award	Organization	Date
Emiko HIYAMA, Director, Strangeness Nuclear Physics Laboratory	The FY 2019 Prize for Science and Technology, the Commendation for Science and Technology by the Minister of Education, Culture, Sports, Science and Technology	The Minister of Education, Culture, Sports, Science and Technology	Apr. 17
Daiki MORI, Technical Staff, Nuclear Chemistry Research Team	Young Scientist Oral Presentation Award at 56th Annual Meeting on Radioisotopes and Radiation Researchers	Japan Radioisotope Association	Jul. 4
Nozomi SATO, Research Part-time Worker, Nuclear Chemistry Research Team	IUPAC Periodic Table of Younger Chemists	IUPAC	Jul. 8
Yasushi ABE, Visiting Scientist, Instrumentation Development Group	The 16th PASJ Annual Award for poster presentation	Particle Accelerator Society of Japan	Aug. 3
Akio TOMIYA, Special Postdoctoral Researcher, Computing Group	The 13th Particle Physics Medal (FY2019): Young Scientist Award in Theoretical Particle Physics	Particle Theory Committee	Sep. 19
Kosuke MORITA, Director, Superheavy Element Research Group	The 2019 Kimura Award	The Japan Society of Nuclear and Radiochemical Sciences (JNRS)	Sep. 25

Koichi YOSHIDA, Team Leader, BigRIPS Team	The Saitama prefecture High-pressure Gas Chairman Commendation	The Saitama prefecture High-pressure Gas Committee	Oct. 23
A joint research group of RNC's Safety Management Group and the Neutron Beam Technology Team of RIKEN Center for Advanced Photonics	2019 Symposium on Nuclear Data Poster Presentation Award	Atomic Energy Society of Japan Nuclear Data Division	Nov.28
Tomoya NAITO, Student Trainee, Quantum Hadron Physics Laboratory	2020 CAEN Best Young Speaker Award	Organizing Comettee of "Vth Topical Workshop on Modern Aspects in Nuclear Structure"	Feb. 8
Hirimitsu HABA, Director, the RI Application Group	Open Innovation Prize (President of Science Council of Japan Prize)	Cabinet Office, Government of Japan	Feb. 27

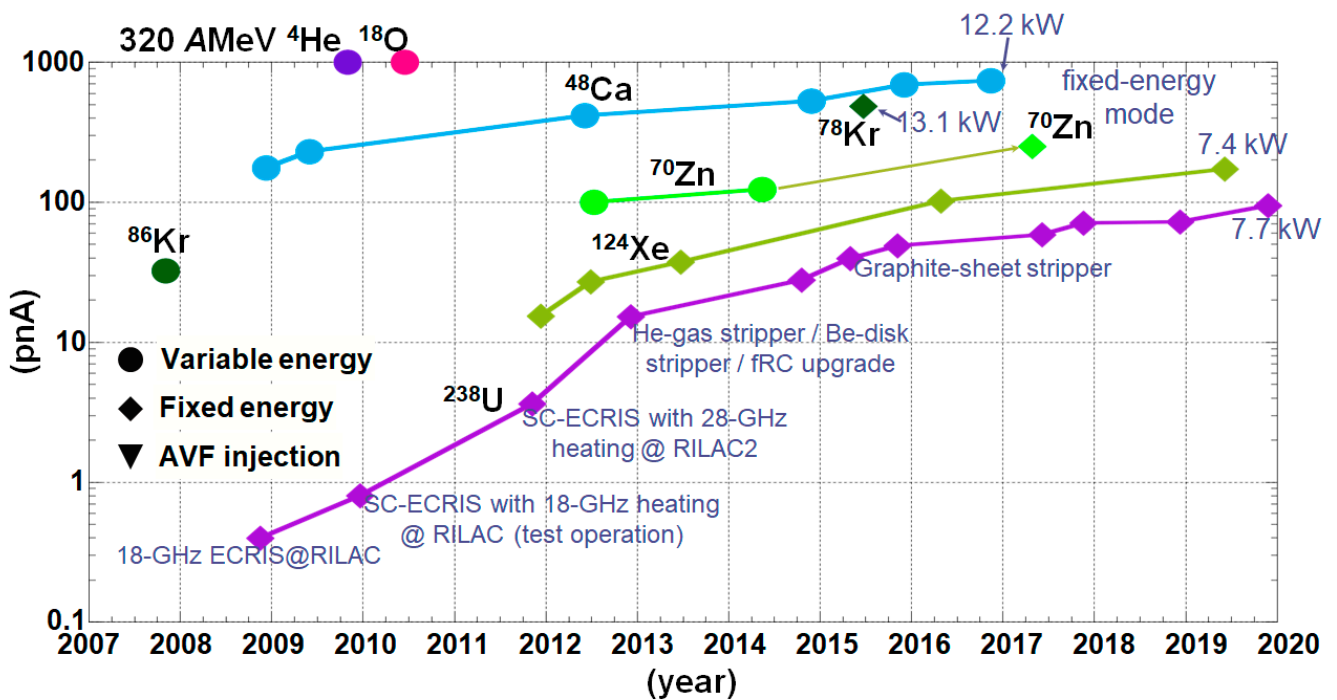
8. Brief overview of the RI Beam Factory

Intensity of Primary Beams

Achieved beam intensities (as of March 2019)

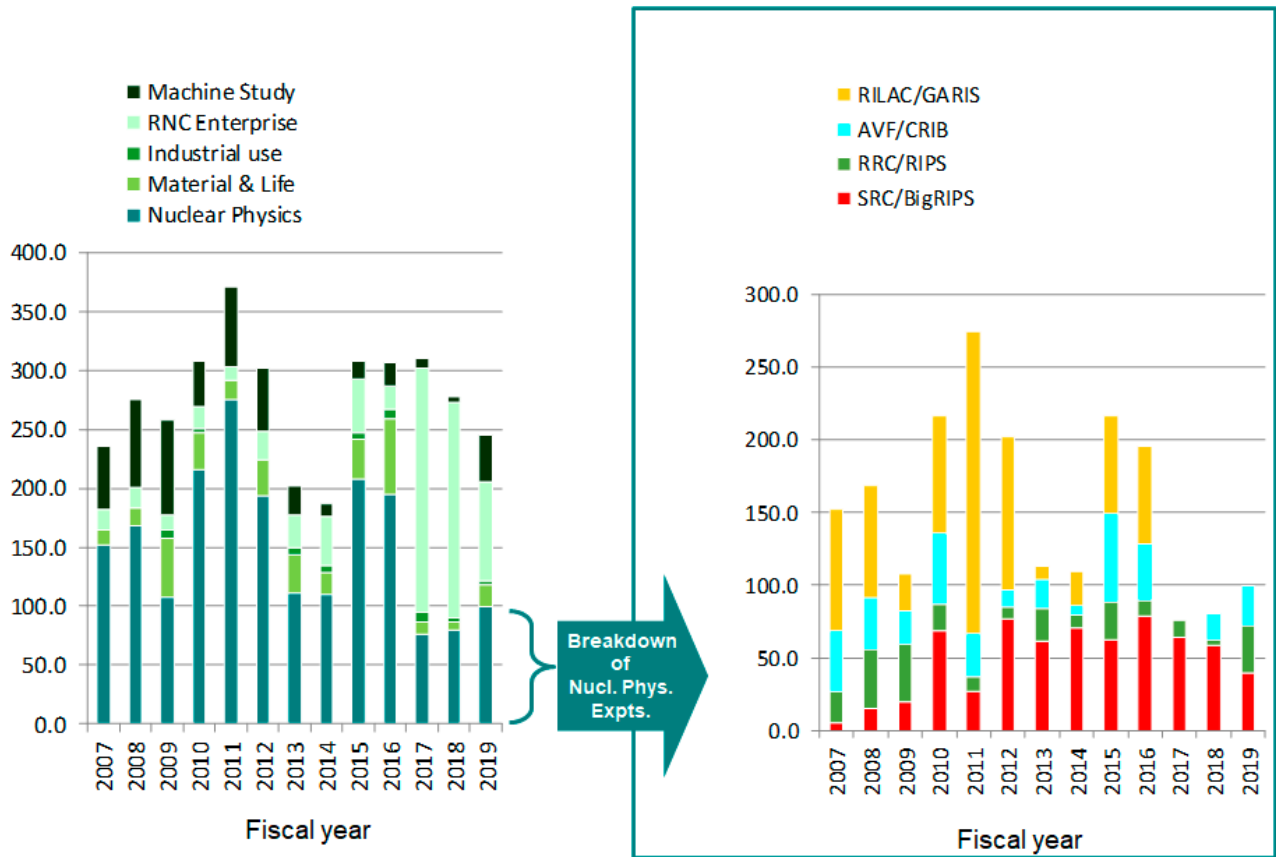
^{238}U	94 pnA (345 MeV/nucleon, Nov. 2019)
^{124}Xe	173 pnA (345 MeV/nucleon, Jun. 2019)
^{86}Kr	30 pnA (345 MeV/nucleon, Nov. 2007)
^{78}Kr	486 pnA (345 MeV/nucleon, May. 2015)
^{70}Zn	250 pnA (345 MeV/nucleon, May 2017)
^{48}Ca	730 pnA (345 MeV/nucleon, Nov. 2016)
^{18}O	1000 pnA (345 MeV/nucleon, Jun. 2010)
^{14}N	400 pnA (250 MeV/nucleon, Oct. 2010)
^4He	1000 pnA (250 MeV/nucleon, Oct. 2009)
d	1000 pnA (250 MeV/nucleon, Oct. 2010)
pol. d	120 pnA, $P\sim 80\%$ (250 MeV/nucleon, May 2015)

History of Beam Intensity Upgrade



Beam energies of the beams without explicitly indicated are 345 AMeV.

Total beam time for experiments



Total beam time allocated to BigRIPS experiments



Nuclear Science and Transmutation Research Division Radioactive Isotope Physics Laboratory

1. Abstract

This Laboratory works as one of core research groups conducting programs at the world-premiere heavy-ion accelerator facility of RIKEN “RI Beam Factory (RIBF).” The Laboratory explores exotic nuclear structures and dynamics in exotic nuclei that have never been investigated before, such as those with largely imbalanced proton and neutron numbers. Our aim is to develop new experimental techniques utilizing fast radioactive isotope (RI) beams at RIBF, to discover new phenomena and properties in exotic nuclei. The Laboratory is focusing three major subjects; shell evolution of very neutron-rich nuclei, the r-process path and equation-of-state in asymmetric nuclear matter. The Laboratory has initiated international collaborations for in-beam gamma spectroscopy, decay spectroscopy and heavy-ion induced reactions, and has formed a discussion forum for next generation gamma-ray detectors.

2. Major Research Subjects

- (1) Study of structure and dynamics of exotic nuclei through developments of new tools in terms of reaction- and technique-based methodology
- (2) Research on EOS in asymmetric nuclear matter via heavy-ion induced reactions
- (3) Detector developments for spectroscopy and reaction studies

3. Summary of Research Activity

(1) In-beam gamma spectroscopy

In the medium and heavy mass region explored at RIBF, collective natures of nuclei are one of important subjects, which are obtained through production and observation of high excited and high spin states. To populate such states, heavy-ion induced reactions such as fragmentation, fission are useful. So far, we have developed two-step fragmentation method as an efficient method to identify and populate excited states, and lifetime measurements to deduce transition strength.

Devices utilized for the in-beam gamma spectroscopy are ZeroDegree Spectrometer (ZDS) and a NaI array DALI2. Since the end of 2008, the first spectroscopy on nuclei island-of-inversion region was performed, we have explored step-by-step new and unknown regions in the nuclear chart. The second campaign in 2009 was organized to study background components originating from atomic processes in a heavy target. Neutron-rich nuclei at $N = 20$ to 28 were studied in 2010. In 2011–2013, we conducted experiment programs for Ca-54, Ni-78, neutron-rich nuclei at $N = 82$ and neutron-deficient nuclei at $Z = 50$.

A multitude of data obtained with inelastic, nucleon knock-out, fragmentation channels have been analyzed and published. In 2011–2013, collective natures of Mg-36, 38 and Si-42 were both published in PRL. Excited states firstly observed in Ca-54 were reported in Nature to demonstrate a new nuclear magic number of 34. Fragmentation reaction has been found efficient for nuclei with $A > 100$ and low-lying excited state in Pd-126 has been successfully observed and reported in PRC. In 2019, results of the first spectroscopy of ^{40}Mg was published in PRL, to demonstrate the exotic structure which is very different from in other neutron-rich Mg isotopes.

To further strengthen the in-beam gamma spectroscopy at RIBF, we have proposed a new setup of MINOS + DALI2 to search for the 1st excited states in even-even neutron-rich nuclei with $Z \sim 20$ to 40. The program was submitted to the PAC 2013 as a new category of proposal, “proposal for scientific program” and was S-ranked. A dedicated collaboration “SEASTAR” has been established as a subset of in-beam gamma collaboration “SUNFLOWER.” The three campaigns were organized in 2014, 2015 and 2017 to study very neutron-rich isotopes, and were very productive to access very neutron-rich nuclei such as Ar-52, Ca-56, Ni-78, Kr-100, Zr-110. In 2019, the result of the first spectroscopy was published in Nature.

A new project of high resolution gamma spectroscopy with fast beams “HiCARI” has been proposed at PAC 2018 and the campaign programs are scheduled in 2020. MINIBALL and several Ge tracking detectors from Japan, Europe, the USA and Korea are being combined to form an array of germanium detectors. The new setup aims to accelerate researches of the nuclear structure by observing gamma-lines in even-odd nuclei and measuring lifetimes of excited states. The two workshops were organized in 2019, and the machine time of 43.5 days in total was approved at PAC 2019.

Concerning a next generation detector, a discussion forum has been established to write up a white paper on tracking germanium detectors and high-efficient crystal detectors such LaBr₃ and GAGG.

(2) Decay spectroscopy

Beta- and isomer-spectroscopy is an efficient method for studying nuclear structure, especially for non-yrast levels. We had accumulated experimental techniques at the RIPS facility to investigate nuclear structure in light mass region via beta-gamma and beta-p coincidence. Concerning the medium and heavy mass region available at RIBF, we have developed two position-sensitive active-stoppers, strip-silicon detectors and a cylindrical active stopper called CAITEN, to achieve a low-background measurement by taking correlation between heavy ion stop position and beta-ray emission position. A site of decay-spectroscopy at the new facility of RIBF is the final focal plane of ZDS, where high precision of TOF in particle identification is obtained due to a long flight path from BigRIPS to ZDS.

At the end of 2009, the first decay spectroscopy was organized with a minimum setup of four clover gamma detectors and silicon strip detectors, to study neutron-rich nuclei with $A \sim 110$. The first campaign was found successful and efficient to publish four letter articles in 2011, two PRL’s and two PLB’s. One of the PRL papers is associated to the r-process path where half-lives for 18

neutron-rich nuclei were determined for the first time. The other PRL paper reported a finding of deformed magic number 64 in the Zr isotopes.

The success of the first decay-spectroscopy campaign stimulated to form a new large-scale collaboration “EURICA,” where a twelve Euroball cluster array is coupled with the silicon-strip detectors to enhance gamma efficiency by a factor of 10. A construction proposal of “EURICA” was approved in the PAC 2011, and the commissioning was successfully organized in spring 2012. Since then, physics runs had been conducted for programs approved to survey nuclei of interest as many as possible, such as Ni-78, Pd-128, Sn-100. The EURICA collaboration finished its physics programs in summer 2016. So far, 54 papers including 14 PRL’s and 13 PLB’s were published. One of the highlights is discovery of a seniority isomer in Pd-128, of which cascade gamma decay gives the energy of first excited state and robustness of $N = 82$ magic number, and the other is a half-life measurement for 110 neutron-rich nuclei across the $N = 82$ shell gap, which shows implications for the mechanism and universality of the r-process path.

Beta-delayed neutron emission probability of medium and heavy neutron-rich nuclei is important to understand nuclear structure and the r-process path. In 2013, a new collaboration “BRIKEN” has been established to form a He-3 detector array. A present design of the array has neutron efficiency as high as 70% up to 3 MeV. The array was coupled with the AIDA silicon strip system. A construction proposal was approved at the PAC 2013 and three physics proposals have been approved. The commissioning run was conducted in autumn 2016. The major physics runs were conducted in 2017–2019.

The CAITEN detector was successfully tested with fragments produced with a Ca-48 beam in 2010.

(3) Equation-of-state via heavy-ion central collisions

Equation-of-state in asymmetric nuclear matter is one of major subjects in physics of exotic nuclei. Pi-plus and pi-minus yields in central heavy ion collisions at the RIBF energy are considered as one of EOS sensitive observables at the RIBF energy. To observe charged pions, a TPC for the SAMURAI spectrometer is being constructed under an international collaboration “S π RIT,” Construction proposal was submitted at the PAC 2012, and physics proposals were approved at the PAC 2012 and 2013. The physics runs were successfully conducted in spring 2016. The data analysis is in progress to produce the first physics results.

An international symposium “NuSYM” on nuclear symmetry energy was organized at RIKEN July 2010 to invite researchers in three sub-fields, nuclear structure, nuclear reaction and nuclear astrophysics, and to discuss nuclear symmetry energy together. Since then, the symposium series have been held every year and been useful to encourage theoretical works and to strengthen the collaboration.

(4) Nucleon correlation and cluster in nuclei

Nucleon correlation and cluster in nuclei are matters of central focus in a “beyond mean-field” picture. The relevant programs with in-beam gamma and missing-mass techniques are to depict nucleon condensations and correlations in nuclear media as a function of density as well as temperature. Neutron-halo and –skin nuclei are objects to study dilute neutron matter at the surface. By changing excitation energies in neutron-rich nuclei, clustering phenomena and role of neutrons are to be investigated.

In 2013, two programs were conducted at the SAMURAI spectrometer. One is related to proton-neutron correlation in the C-12 nucleus via p-n knockout reaction with a carbon target. The other is to search for a cluster state in C-16, which was populated via inelastic alpha scattering. The data is being analyzed.

In 2018, a new project based on missing mass spectroscopy was launched to investigate an exotic cluster state in a very proton-rich nucleus. The experiment was organized at GANIL with combination of RIKEN liquid hydrogen target CRYPTA and the MUST2 detector array in 2018.

Members

Group Director

Hiro Yoshi SAKURAI (Deputy Director, RNC)

Special Temporary Research Scientist

Takashi ICHIHARA

Research/Technical Scientists

Yoichi NAKAI (Senior Research Scientist)
Tadaaki ISOBE (Senior Research Scientist)
Akihisa KOHAMA (Senior Research Scientist)

Pieter Christiaan DOORNENBAL (Senior Research Scientist)
Shunji NISHIMURA (Senior Research Scientist)
Daisuke SUZUKI (Research Scientist)

Research Consultants

Akitsu IKEDA
Masayasu ISHIHARA

Kenichi MATSUYANAGI
Hiroyuki MURAKAMI

Special Postdoctoral Researcher

Browne FRANK

Visiting Researcher

Alejandro ALGORA (JSPS)
Benoit J. C. MAUSS (JSPS)

Byul MOON (Nat'l Res. Foundation)

Junior Research Associates

Hideki SHIMIZU (Univ. of Tokyo)

Takuma KOIWAI (Univ. of Tokyo)

International Program Associates

Juan SAIZ LOMAS (Univ. of York)

Xiaohui SUN (Peking Univ.)

Senior Visiting Scientists

Koichiro ASAH (Tokyo Tech)
Shigeru KUBONO (Univ. of Tokyo)

Kengo OGAWA (Chiba Univ.)

Visiting Scientists

Nori AOI (Osaka Univ.)
Giordano CERIZZA (Michigan State Univ.)
Jin-hee CHANG (Michigan State Univ.)
Silvio CHERUBINI (Univ. of Catania)
Martha Liliana CORTES SUA (INFN)
Mitsunori FUKUDA (Osaka Univ.)
Byungsik HONG (Korea Univ.)
Kazuo IEKI (Rikkyo Univ.)
Kei IIDA (Kochi Univ.)
Natsumi IKENO (Tottori Univ.)
Takuji IZUMIKAWA (Niigata Univ.)
Takashi KISHIDA (Aoyama Gakuin Univ.)
Gabor KISS (ATOMKI)
Khiem LE (Vietnam Academy of Sci. and Tech.)
Hiu Ching LEE (The Univ. of Hong Kong)
Giuseppe LORUSSO (Nat'l Phys. Lab.)
Alan MCINTOSH (Texas A & M Univ.)
Yoshiharu MORI (Kyoto Univ.)
Tetsuya MURAKAMI (Kyoto Univ.)

Megumi NIIKURA (Univ. of Tokyo)
Evgueni NIKOLSKI (Kurchatov Inst.)
Daiki NISHIMURA (Tokyo City Univ.)
Takashi OHTSUBO (Niigata Univ.)
Hooi Jin ONG (Osaka Univ.)
Akira ONO (Tohoku Univ.)
Naohiko OTSUKA (IAEA)
Kazuhiro OYAMATSU (Aichi Shukutoku Univ.)
Clementine Angelique Marie-Th SANTAMARIA (Berkeley Lab)
Paer-Anders SOEDERSTROEM (TU Darmstadt)
Maya TAKECHI (Niigata Univ.)
Ryo TANIUCHI (Univ. of York)
Rensheng WANG (Soochow Univ.)
Hiroshi WATANABE (Beihang Univ.)
Kathrin WIMMER (Inst.o de Estructura de la Materia, Consejo Superior de Investigaciones Cientias, CSIC)
Jin WU (Argonne Nat'l Lab.)
Yasutaka YAMAMOTO (Osaka Univ.)

Visiting Technicians

Jorge AGRAMUNT ROS (Valencia city hall)
Hilde DE WITTE (KU Leuven)

Herbert E. HESS (Univ. of Cologne)
Ivan KOJOUHAROV (GSI)

Student Trainees

Takamichi AOKI (Univ. of Tokyo)
Takumi AOKI (Univ. of Tokyo)
Yusei BANDO (Univ. of Tokyo)
Jonathan BARNEY (Michigan State Univ.)
Linh BUI (Vietnam Atomic Energy Inst.)
Justin B. ESTEE (Michigan State Univ.)
Hiroaki FUKUSHIMA (Rikkyo Univ.)
Shinnosuke KANAYA (Osaka Univ.)
Masanori KANEKO (Kyoto Univ.)
Jiseok KIM (Korea Univ.)
Asahi KOHDA (Osaka Univ.)

Kei KOKUBUN (Univ. of Tokyo)
Shunpei KOYAMA (Univ. of Tokyo)
Jung Woo LEE (Korea Univ.)
Thomas G. PARRY (Univ. of Surrey)
Takeshi SAITO (Univ. of Tokyo)
Hidaka TANABE (Tsukuba Univ.)
Chun Yuen TSANG (Michigan State Univ.)
Phong VI (VNU Univ. of Sci.)
Ryo WAKABAYASHI (Osaka Univ.)
Tik Tsun YEUNG (The Univ. of Hong Kong)
Naoya YOSHIDA (Univ. of Tokyo)

Part-time Worker

Kiyomi ARAI (Research Part-time Worker I)
Mie DOI (Research Part-time Worker I)
Masanori KANEKO (Research Part-time Worker I)
Miki KANOU (Research Part-time Worker I)

Noriko OKAYASU (Research Part-time Worker I)
Tsuneyo SUZUKI (Research Part-time Worker I)
Misuzu KANOU (Research Part-time Worker II)
Eiko MIZUMOTO (Research Part-time Worker II)

List of Publications & Presentations

Publications

[Original papers]

- T. Lokotko, S. Leblond, J. Lee, P. Doornenbal, A. Obertelli, A. Poves, F. Nowacki, K. Ogata, K. Yoshida, G. Authelet, H. Baba, D. Calvet, F. Chateau, S. Chen, A. Corsi, A. Delbart, J. Gheller, A. Gillibert, T. Isobe, V. Lapoux, M. Matsushita, S. Momiyama, T. Motobayashi, M. Niikura, H. Otsu, C. Peron, A. Peyaud, E. Pollacco, J. Rousse, H. Sakurai, C. Santamaria, Z. Xu, M. Sasano, Y. Shiga, S. Takeuchi, R. Taniuchi, T. Uesaka, H. Wang, V. Werner, F. Browne, L. Chung, Z. Dombradi, S. Franchoo, F. Giacoppo, A. Gottardo, K. Hadynska-Klek, Z. Korkulu, S. Koyama, Y. Kubota, M. Lettmann, C. Louchart, R. Lozeva, K. Matsui, T. Miyazaki, S. Nishimura, L. Olivier, S. Ota, Z. Patel, E. Sahin, C. Shand, P. Soderstrom, I. Stefan, D. Steppenbeck, T. Sumikama, D. Suzuki, Z. Vajta, and J. Wu, “Shell structure of the neutron-rich isotopes $^{69,71,73}\text{Co}$,” *Phys. Rev. C* **101**, 034314 (2020).
- Y. Sun, A. Obertelli, P. Doornenbal, C. Barbieri, Y. Chazono, T. Duguet, H. Liu, P. Navratil, F. Nowacki, K. Ogata, T. Otsuka, F. Raimondi, V. Soma, Y. Utsuno, K. Yoshida, N. Achouri, H. Baba, F. Browne, D. Calvet, F. Chateau, S. Chen, N. Chiga, A. Corsi, M. Cortes, A. Delbart, J. M. Gheller, A. Giganon, A. Gillibert, C. Hilaire, T. Isobe, T. Kobayashi, Y. Kubota, V. Lapoux, T. Motobayashi, I. Murray, H. Otsu, V. Panin, N. Paul, W. Rodriguez, H. Sakurai, M. Sasano, D. Steppenbeck, L. Stuhl, Y. Togano, T. Uesaka, K. Wimmer, K. Yoneda, O. Aktas, T. Aumann, L. Chung, F. Flavigny, S. Franchoo, I. Gasparic, R. B. Gerst, J. Gibelin, K. Hahn, D. Kim, T. Koiwai, Y. Kondo, P. Koseoglou, J. Lee, C. Lehr, B. Linh, T. Lokotko, M. MacCormick, K. Moschner, T. Nakamura, S. Park, D. Rossi, E. Sahin, D. Sohler, P. A. Soderstrom, S. Takeuchi, H. Tornqvist, V. Vaquero, V. Wagner, S. Wang, V. Werner, X. Xu, H. Yamada, D. Yan, Z. Yang, M. Yasuda, and L. Zanetti, “Restoration of the natural $E(1/2_1^+) - E(3/2_1^+)$ energy splitting in odd-K isotopes towards $N = 40$,” *Phys. Lett. B* **802**, 135215 (2020).
- V. Vaquero, A. Jungclaus, T. Aumann, J. Tscheuschner, E. Litvinova, J. Tostevin, H. Baba, D. Ahn, R. Avigo, K. Boretzky, A. Bracco, C. Caesar, F. Camera, S. Chen, V. Derya, P. Doornenbal, J. Endres, N. Fukuda, U. Garg, A. Giaz, M. Harakeh, M. Heil, A. Horvat, K. Ieki, N. Imai, N. Inabe, N. Kalantar-Nayestanaki, N. Kobayashi, Y. Kondo, S. Koyama, T. Kubo, I. Martel, M. Matsushita, B. Million, T. Motobayashi, T. Nakamura, N. Nakatsuka, M. Nishimura, S. Nishimura, S. Ota, H. Otsu, T. Ozaki, M. Petri, R. Reifarh, J. Rodriguez-Sanchez, D. Rossi, A. Saito, H. Sakurai, D. Savran, H. Scheit, F. Schindler, P. Schrock, D. Semmler, Y. Shiga, M. Shikata, Y. Shimizu, H. Simon, D. Steppenbeck, H. Suzuki, T. Sumikama, D. Symochko, I. Syndikus, H. Takeda, S. Takeuchi, R. Taniuchi, Y. Togano, J. Tsubota, H. Wang, O. Wieland, K. Yoneda, J. Zenihiro, and A. Zilges, “Fragmentation of single-particle strength around the doubly magic nucleus ^{132}Sn and the position of the $0f_{5/2}$ proton-hole state in ^{131}In 131,” *Phys. Rev. Lett.* **124**, 022501 (2020).
- M. Cortes, W. Rodriguez, P. Doornenbal, A. Obertelli, J. Holt, S. Lenzi, J. Menendez, F. Nowacki, K. Ogata, A. Poves, T. Rodriguez, A. Schwenk, J. Simonis, S. Stroberg, K. Yoshida, L. Achouri, H. Baba, F. Browne, D. Calvet, F. Chateau, S. Chen, N. Chiga, A. Corsi, A. Delbart, J. M. Gheller, A. Giganon, A. Gillibert, C. Hilaire, T. Isobe, T. Kobayashi, Y. Kubota, V. Lapoux, H. Liu, T. Motobayashi, I. Murray, H. Otsu, V. Panin, N. Paul, H. Sakurai, M. Sasano, D. Steppenbeck, L. Stuhl, Y. Sun, Y. Togano, T. Uesaka, K. Wimmer, K. Yoneda, O. Aktas, T. Aumann, L. Chung, F. Flavigny, S. Franchoo, I. Gasparic, R. B. Gerst, J. Gibelin, K. Hahn, D. Kim, T. Koiwai, Y. Kondo, P. Koseoglou, J. Lee, C. Lehr, B. Linh, T. Lokotko, M. MacCormick, K. Moschner, T. Nakamura, S. Park, D. Rossi, E. Sahin, D. Sohler, P. A. Soderstrom, S. Takeuchi, H. Tornqvist, V. Vaquero, V. Wagner, S. Wang, V. Werner, X. Xu, H. Yamada, D. Yan, Z. Yang, M. Yasuda, and L. Zanetti, “Shell evolution of $N = 40$ isotones towards ^{60}Ca : First spectroscopy of ^{62}Ti ,” *Phys. Lett. B* **800**, 135071 (2020).
- M. Tanaka, M. Takechi, A. Homma, M. Fukuda, D. Nishimura, T. Suzuki, Y. Tanaka, T. Moriguchi, D. Ahn, A. Aimaganbetov, M. Amano, H. Arakawa, S. Bagchi, K. Behr, N. Burtebayev, K. Chikaato, H. Du, S. Ebata, T. Fujii, N. Fukuda, H. Geissel, T. Hori, W. Horiuchi, S. Hoshino, R. Igosawa, A. Ikeda, N. Inabe, K. Inomata, K. Itahashi, T. Izumikawa, D. Kamioka, N. Kanda, I. Kato, I. Kenzihina, Z. Korkulu, Y. Kuk, K. Kusaka, K. Matsuta, M. Mihara, E. Miyata, D. Nagae, S. Nakamura, M. Nassurlla, K. Nishimuro, K. Nishizuka, K. Ohnishi, M. Ohtake, T. Ohtsubo, S. Omika, H. Ong, A. Ozawa, A. Prochazka, H. Sakurai, C. Scheidenberger, Y. Shimizu, T. Sugi-hara, T. Sumikama, H. Suzuki, S. Suzuki, H. Takeda, Y. Tanaka, I. Tanihata, T. Wada, K. Wakayama, S. Yagi, T. Yamaguchi, R. Yanagihara, Y. Yanagisawa, K. Yoshida, and T. Zholdybayev, “Swelling of doubly magic ^{48}Ca core in Ca isotopes beyond $N = 28$,” *Phys. Rev. Lett.* **124**, 102501 (2020).
- G. Zhang, H. Watanabe, G. Dracoulis, F. Kondev, G. Lane, P. Regan, P. A. Soderstrom, P. Walker, K. Yoshida, H. Kanaoka, Z. Korkulu, P. Lee, J. Liu, S. Nishimura, J. Wu, A. Yagi, D. Ahn, T. Alharbi, H. Baba, F. Browne, A. Bruce, M. Carpenter, R. Carroll, K. Chae, C. Chiara, Z. Dombradi, P. Doornenbal, A. Estrade, N. Fukuda, C. Griffin, E. Ideguchi, N. Inabe, T. Isobe, S. Kanaya, I. Kojouharov, T. Kubo, S. Kubono, N. Kurz, I. Kuti, S. Lalkovski, T. Lauritsen, C. Lee, E. Lee, C. Lister, G. Lorusso, G. Lotay, E. McCutchan, C. B. Moon, I. Nishizuka, C. Nita, A. Odahara, Z. Patel, V. Phong, Z. Podolyak, O. Roberts, H. Sakurai, H. Schaffner, D. Seweryniak, C. Shand, Y. Shimizu, T. Sumikama, H. Suzuki, H. Takeda, S. Terashima, Z. Vajta, J. Valiente-Dobon, Z. Xu, and S. Zhu, “Interplay of quasiparticle and vibrational excitations: First observation of isomeric states in ^{168}Dy and ^{169}Dy ,” *Phys. Lett. B* **799**, 135036 (2019).
- L. Sinclair, R. Wadsworth, J. Dobaczewski, A. Pastore, G. Lorusso, H. Suzuki, D. Ahn, H. Baba, F. Browne, P. Davies, P. Doornenbal, A. Estrade, Y. Fang, N. Fukuda, J. Henderson, T. Isobe, D. Jenkins, S. Kubono, Z. Li, D. Lubos, S. Nishimura, I. Nishizuka, Z. Patel, S. Rice, H. Sakurai, Y. Shimizu, P. Schury, H. Takeda, P. Soderstrom, T. Sumikama, H. Watanabe, V. Werner, J. Wu, and Z. Xu, “Half-lives of ^{73}Sr and ^{76}Y and the consequences for the proton dripline,” *Phys. Rev. C* **100**, 044311 (2019).
- K. Nakano, Y. Watanabe, S. Kawase, H. Wang, H. Otsu, H. Sakurai, S. Takeuchi, Y. Togano, T. Nakamura, Y. Maeda, D. S. Ahn, M. Aikawa, S. Araki, S. Chen, N. Chiga, P. Doornenbal, N. Fukuda, T. Ichihara, T. Isobe, S. Kawakami, T. Kin, Y. Kondo, S. Koyama, T. Kubo, S. Kubono, M. Uesaka, A. Makinaga, M. Matsushita, T. Matsuzaki, S. Michimasa, S. Momiyama, S. Nagamine, M. Niikura, T. Ozaki, A. Saito, T. Saito, Y. Shiga, M. Shikata, Y. Shimizu, S. Shimoura, T. Sumikama, P. A. Soderstrom, H. Suzuki, H. Takeda, R. Taniuchi, J. Tsubota, Y. Watanabe, K. Wimmer, T. Yamamoto, and K. Yoshida, “Isotope production in proton-, deuteron-, and carbon-induced reactions on ^{93}Nb at 113 MeV/nucleon,” *Phys. Rev. C* **100**, 044605 (2019).
- S. Chen, J. Lee, P. Doornenbal, A. Obertelli, C. Barbieri, Y. Chazono, P. Navratil, K. Ogata, T. Otsuka, F. Raimondi, V. Soma, Y. Utsuno, K. Yoshida, H. Baba, F. Browne, D. Calvet, F. Chateau, N. Chiga, A. Corsi, M. Cortes, A. Delbart, J. Gheller, A. Giganon, A. Gillibert,

- C. Hilaire, T. Isobe, J. Kahlbow, T. Kobayashi, Y. Kubota, V. Lapoux, H. Liu, T. Motobayashi, I. Murray, H. Otsu, V. Panin, N. Paul, W. Rodriguez, H. Sakurai, M. Sasano, D. Steppenbeck, L. Stuhl, Y. Sun, Y. Togano, T. Uesaka, K. Wimmer, K. Yoneda, N. Achouri, O. Aktas, T. Aumann, L. Chung, F. Flavigny, S. Franchoo, I. Gasparic, R. Gerst, J. Gibelin, K. Hahn, D. Kim, T. Koiwai, Y. Kondo, P. Koseoglou, C. Lehr, B. Linh, T. Lokotko, M. MacCormick, K. Moschner, T. Nakamura, S. Park, D. Rossi, E. Sahin, D. Sohler, P. Soderstrom, S. Takeuchi, H. Tornqvist, V. Vaquero, V. Wagner, S. Wang, V. Werner, X. Xu, H. Yamada, D. Yan, Z. Yang, M. Yasuda, and L. Zanetti, “Quasifree neutron knockout from ^{54}Ca corroborates arising $N = 34$ Neutron magic number,” *Phys. Rev. Lett.* **123**, 142501 (2019).
- R. Yokoyama, R. Grzywacz, B. Rasco, N. Brewer, K. Rykaczewski, I. Dillmann, J. Tain, S. Nishimura, D. Ahn, A. Algora, J. Allmond, J. Agramunt, H. Baba, S. Bae, C. Bruno, R. Caballero-Folch, F. Calvino, P. Coleman-Smith, G. Cortes, T. Davinson, C. Domingo-Pardo, A. Estrade, N. Fukuda, S. Go, C. Griffin, J. Ha, O. Hall, L. Harkness-Brennan, J. Heideman, T. Isobe, D. Kahl, M. Karny, T. Kawano, L. Khiem, T. King, G. Kiss, A. Korgul, S. Kubono, M. Labiche, I. Lazarus, J. Liang, J. Liu, G. Lorusso, M. Madurga, K. Matsui, K. Miernik, F. Montes, A. Morales, P. Morrall, N. Nepal, R. Page, V. Phong, M. Piersa, M. Prydderch, V. Pucknell, M. Rajabali, B. Rubio, Y. Saito, H. Sakurai, Y. Shimizu, J. Simpson, M. Singh, D. Stracener, T. Sumikama, R. Surman, H. Suzuki, H. Takeda, A. Tarifeno-Saldivia, S. Thomas, A. Tolosa-Delgado, M. Wolinska-Cichocka, P. Woods, and X. Xu, “Strong one-neutron emission from two-neutron unbound states in β decays of the r -process nuclei $^{86,87}\text{Ga}$,” *Phys. Rev. C* **100**, 031302 (2019).
- V. Phong, G. Lorusso, T. Davinson, A. Estrade, O. Hall, J. Liu, K. Matsui, F. Montes, S. Nishimura, A. Boso, P. Regan, R. Shearman, Z. Xu, J. Agramunt, J. Allmond, D. Ahn, A. Algora, H. Baba, N. Brewer, C. Bruno, R. Caballero-Folch, F. Calvino, M. Wolinska-Cichocka, G. Cortes, I. Dillmann, C. Domingo-Pardo, A. Gargano, S. Go, C. Griffin, R. Grzywacz, L. Harkness-Brennan, T. Isobe, A. Jungclaus, D. Kahl, L. Khiem, G. Kiss, A. Korgul, S. Kubono, K. Miernik, A. Morales, N. Nepal, M. Piersa, S. Podolyak, B. Rasco, K. Rykaczewski, H. Sakurai, Y. Shimizu, D. Stacener, T. Sumikama, H. Suzuki, H. Takeda, J. Tain, A. Tarifeno-Saldivia, A. Tolosa-Delgado, V. Vaquero, P. Woods, R. Yokoyama, and C. Yuan, “Observation of a μs isomer in $^{134}_{49}\text{In}_{85}$: Proton-neutron coupling “south-east” of $^{132}_{50}\text{Sn}_{82}$,” *Phys. Rev. C* **100**, 011302 (2019).
- V. Vaquero, A. Jungclaus, J. Rodriguez-Sanchez, J. Tostevin, P. Doornenbal, K. Wimmer, S. Chen, E. Nacher, E. Sahin, Y. Shiga, D. Steppenbeck, R. Taniuchi, Z. Xu, T. Ando, H. Baba, F. Bello Garrote, S. Franchoo, A. Gargano, K. Hadynska-Klek, A. Kusoglu, J. Liu, T. Lokotko, S. Momiyama, T. Motobayashi, S. Nagamine, N. Nakatsuka, M. Niikura, R. Orlandi, T. Saito, H. Sakurai, P. Soderstrom, G. Tveten, Z. Vajta, and M. Yalcinkaya, “Inclusive cross sections for one- and multi-nucleon removal from Sn, Sb, and Te projectiles beyond the $N = 82$ shell closure,” *Phys. Lett. B* **795**, 356–361 (2019).
- K. Wimmer, P. Doornenbal, W. Korten, T. Arici, P. Aguilera, A. Algora, T. Ando, H. Baba, B. Blank, A. Boso, S. Chen, A. Corsi, P. Davies, G. de Angelis, G. de France, D. Doherty, J. Gerl, R. Gernhauser, D. Jenkins, S. Koyama, T. Motobayashi, S. Nagamine, M. Niikura, A. Obertelli, D. Lubos, B. Rubio, E. Sahin, T. Saito, H. Sakurai, L. Sinclair, D. Steppenbeck, R. Taniuchi, R. Wadsworth, and M. Zielinska, “Discovery of ^{68}Br in secondary reactions of radioactive beams,” *Phys. Lett. B* **795**, 266–270 (2019).
- D. Lubos, J. Park, T. Faestermann, R. Gernhauser, R. Krucken, M. Lewitowicz, S. Nishimura, H. Sakurai, D. Ahn, H. Baba, B. Blank, A. Blazhev, P. Boutachkov, F. Browne, I. Celikovic, G. de France, P. Doornenbal, Y. Fang, N. Fukuda, J. Giovinazzo, N. Goel, M. Gorska, S. Ilieva, N. Inabe, T. Isobe, A. Jungclaus, D. Kameda, Y. Kim, I. Kojouharov, T. Kubo, N. Kurz, Y. Kwon, G. Lorusso, K. Moschner, D. Murai, I. Nishizuka, Z. Patel, M. Rajabali, S. Rice, H. Schaffner, Y. Shimizu, L. Sinclair, P. Soderstrom, K. Steiger, T. Sumikama, H. Suzuki, H. Takeda, Z. Wang, N. Warr, H. Watanabe, J. Wu, and Z. Xu, “Improved value for the gamow-teller strength of the ^{100}Sn beta decay,” *Phys. Rev. Lett.* **122**, 222502 (2019).
- Z. Chen, Z. Li, H. Hua, H. Watanabe, C. Yuan, S. Zhang, G. Lorusso, S. Nishimura, H. Baba, F. Browne, G. Benzoni, K. Chae, F. Crespi, P. Doornenbal, N. Fukuda, G. Gey, R. Gernhauser, N. Inabe, T. Isobe, D. Jiang, A. Jungclaus, H. Jung, Y. Jin, D. Kameda, G. Kim, Y. Kim, I. Kojouharov, F. Kondev, T. Kubo, N. Kurz, Y. Kwon, X. Li, J. Lou, G. Lane, C. Li, D. Luo, A. Montaner-Piza, K. Moschner, C. Niu, F. Naqvi, M. Niikura, H. Nishibata, A. Odahara, R. Orlandi, Z. Patel, Z. Podolyak, T. Sumikama, P. Soderstrom, H. Sakurai, H. Schaffner, G. Simpson, K. Steiger, H. Suzuki, J. Taprogge, H. Takeda, Z. Vajta, H. Wang, J. Wu, A. Wendt, C. Wang, H. Wu, X. Wang, C. Wu, C. Xu, Z. Xu, A. Yagi, Y. Ye, and K. Yoshinaga, “Proton shell evolution below ^{132}Sn : first measurement of low-lying β -emitting isomers in $^{123,125}\text{Ag}$,” *Phys. Rev. Lett.* **122**, 212502 (2019).
- R. Taniuchi, C. Santamaria, P. Doornenbal, A. Obertelli, K. Yoneda, G. Authalet, H. Baba, D. Calvet, F. Chateau, A. Corsi, A. Delbart, J. M. Gheller, A. Gillibert, J. Holt, T. Isobe, V. Lapoux, M. Matsushita, J. Menendez, S. Momiyama, T. Motobayashi, M. Niikura, F. Nowacki, K. Ogata, H. Otsu, T. Otsuka, C. Peron, S. Peru, A. Peyaud, E. Pollacco, A. Poves, J. Y. Rouse, H. Sakurai, A. Schwenk, Y. Shiga, J. Simonis, S. Stroberg, S. Takeuchi, Y. Tsunoda, T. Uesaka, H. Wang, F. Browne, L. Chung, Z. Dombardi, S. Franchoo, F. Giacoppo, A. Gottardo, K. Hadynska-Klek, Z. Korkulu, S. Koyama, Y. Kubota, J. Lee, M. Lettmann, C. Louchart, R. Lozeva, K. Matsui, T. Miyazaki, S. Nishimura, L. Olivier, S. Ota, Z. Patel, E. Sahin, C. Shand, P. A. Soderstrom, I. Stefan, D. Steppenbeck, T. Sumikama, D. Suzuki, Z. Vajta, V. Werner, J. Wu, and Z. Xu, “ ^{78}Ni revealed as a doubly magic stronghold against nuclear deformation,” *Nature* **569**, 53–58 (2019).
- N. Paul, A. Obertelli, C. Bertulani, A. Corsi, P. Doornenbal, J. Rodriguez-Sanchez, G. Authalet, H. Baba, D. Calvet, F. Chateau, S. Chen, A. Delbart, J. Gheller, A. Giganon, A. Gillibert, T. Isobe, V. Lapoux, M. Matsushita, S. Momiyama, T. Motobayashi, M. Niikura, H. Otsu, C. Peron, A. Peyaud, E. Pollacco, J. Rouse, H. Sakurai, C. Santamaria, M. Sasano, Y. Shiga, D. Steppenbeck, S. Takeuchi, R. Taniuchi, T. Uesaka, H. Wang, K. Yoneda, T. Ando, T. Arici, A. Blazhev, F. Browne, A. Bruce, R. Carroll, L. Chung, M. Cortes, M. Dewald, B. Ding, Z. Dombardi, F. Flavigny, S. Franchoo, F. Giacoppo, M. Gorska, A. Gottardo, K. Hadynska-Klek, Z. Korkulu, S. Koyama, Y. Kubota, A. Jungclaus, J. Lee, M. Lettmann, B. Linh, J. Liu, C. Liu, C. Lizarazo, C. Louchart, R. Lozeva, K. Matsui, T. Miyazaki, K. Moschner, S. Nagamine, N. Nakatsuka, C. Nita, S. Nishimura, C. Nobs, L. Olivier, S. Ota, Z. Patel, Z. Podolyak, M. Rudigier, E. Sahin, T. Saito, C. Shand, P. Soderstrom, I. Stefan, T. Sumikama, D. Suzuki, R. Orlandi, V. Vaquero, Z. Vajta, V. Werner, K. Wimmer, J. Wu, and Z. Xu, “Prominence of Pairing in Inclusive ($p, 2p$) and (p, pn) Cross Sections from Neutron-Rich Nuclei,” *Phys. Rev. Lett.* **122**, 162503 (2019).
- H. Watanabe, H. Wang, G. Lorusso, S. Nishimura, Z. Xu, T. Sumikama, P. A. Soderstrom, P. Doornenbal, F. Browne, G. Gey, H. Jung, J. Taprogge, Z. Vajta, J. Wu, A. Yagi, H. Baba, G. Benzoni, K. Chae, F. Crespi, N. Fukuda, R. Gernhauser, N. Inabe, T. Isobe,

- A. Jungclaus, D. Kameda, G. Kim, Y. Kim, I. Kojouharov, F. Kondev, T. Kubo, N. Kurz, Y. Kwon, G. Lane, Z. Li, C. B. Moon, A. Montaner-Piza, K. Moschner, F. Naqvi, M. Niikura, H. Nishibata, D. Nishimura, A. Odahara, R. Orlandi, Z. Patel, Z. Podolyak, H. Sakurai, H. Schaffner, G. Simpson, K. Steiger, Y. Sun, H. Suzuki, H. Takeda, A. Wendt, and K. Yoshinaga, “New isomers in $^{125}\text{Pd}_{79}$ and $^{127}\text{Pd}_{81}$: Competing proton and neutron excitations in neutron-rich palladium nuclides towards the $N = 82$ shell closure,” *Phys. Lett. B* **792**, 263–268 (2019).
- S. Michimasa, J. Hwang, K. Yamada, S. Ota, M. Dozono, N. Imai, K. Yoshida, Y. Yanagisawa, K. Kusaka, M. Ohtake, M. Matsushita, D. S. Ahn, O. Beliuskina, N. Chiga, K. Chikaato, N. Fukuda, S. Hayakawa, E. Ideguchi, K. Iribe, C. Iwamoto, S. Kawase, K. Kawata, N. Kitamura, S. Masuoka, H. Miyatake, D. Nagae, R. Nakajima, T. Nakamura, K. Nakano, S. Omika, H. Otsu, H. Sakurai, P. Schrock, H. Shimizu, Y. Shimizu, T. Sumikama, X. Sun, D. Suzuki, H. Suzuki, M. Takaki, M. Takechi, H. Takeda, S. Takeuchi, T. Teranishi, R. Tsunoda, H. Wang, Y. Watanabe, Y. X. Watanabe, K. Wimmer, K. Yako, H. Yamaguchi, L. Yang, H. Yoshida, and S. Shimoura, “OEDO, the energy-degrading beamline at RI Beam Factory,” *PTEP* **2019**, 043D01 (2019).
- J. Hwang, S. Michimasa, S. Ota, M. Dozono, N. Imai, K. Yoshida, Y. Yanagisawa, K. Kusaka, M. Ohtake, D. S. Ahn, O. Beliuskina, N. Fukuda, C. Iwamoto, S. Kawase, K. Kawata, N. Kitamura, S. Masuoka, H. Otsu, H. Sakurai, P. Schrock, T. Sumikama, H. Suzuki, M. Takaki, H. Takeda, R. Tsunoda, K. Wimmer, K. Yako, and S. Shimoura, “Angle-tunable wedge degrader for an energy-degrading RI beamline,” *PTEP* **2019**, 043D02 (2019).
- K. Wimmer, F. Recchia, S. Lenzi, S. Riccetto, T. Davinson, A. Estrade, C. Griffin, S. Nishimura, F. Nowacki, V. Phong, A. Poves, P. A. Soderstrom, O. Aktas, M. Al-Aqeel, T. Ando, H. Baba, S. Bae, S. Choi, P. Doornenbal, J. Ha, L. Harkness-Brennan, T. Isobe, P. John, D. Kahl, G. Kiss, I. Kojouharov, N. Kurz, M. Labiche, K. Matsui, S. Momiyama, D. Napoli, M. Niikura, C. Nita, Y. Saito, H. Sakurai, H. Schaffner, P. Schrock, C. Stahl, T. Sumikama, V. Werner, W. Witt, and P. Woods, “First spectroscopy of ^{61}Ti and the transition to the Island of Inversion at $N = 40$,” *Phys. Lett. B* **792**, 16–20 (2019).
- A. Tolosa-Delgado *et al.* [BRIKEN Collaboration], “Commissioning of the BRIKEN detector for the measurement of very exotic β -delayed neutron emitters,” *Nucl. Instrum. Methods Phys. Res. A* **925**, 133–147 (2019).
- X. Xu, J. H. Liu, C. X. Yuan, Y. M. Xing, M. Wang, Y. H. Zhang, X. H. Zhou, Yu. A. Litvinov, K. Blaum, R. J. Chen, X. C. Chen, C. Y. Fu, B. S. Gao, J. J. He, S. Kubono, Y. H. Lam, H. F. Li, M. L. Liu, X. W. Ma, P. Shuai, M. Si, M. Z. Sun, X. L. Tu, Q. Wang, H. S. Xu, X. L. Yan, J. C. Yang, Y. J. Yuan, Q. Zeng, P. Zhang, X. Zhou, W. L. Zhan, S. Litvinov, G. Audi, S. Naimi, T. Uesaka, Y. Yamaguchi, T. Yamaguchi, A. Ozawa, B. H. Sun, K. Kaneko, Y. Sun, and F. R. Xu “Masses of ground and isomeric states of ^{101}In and configuration-dependent shell evolution in odd- A Indium isotopes,” *Phys. Rev. C* **100**, 051303(R) (2019).
- N. T. Zhang, X. Y. Wang, D. Tudor, B. Bucher, I. Burducea, H. Chen, Z. J. Chen, D. Chesneau, A. I. Chilug, L. R. Gasques, D. G. Ghita, C. Gomoiu, K. Hagino, S. Kubono, Y. J. Li, C. J. Lin, W. P. Lin, R. Margineanu, A. Pantelica, I. C. Stefanescu, M. Straticiu, X. D. Tang, L. Trache, A. S. Umar, W. Y. Xin, S. W. Xu, and Y. Xu, “Constraining the $^{12}\text{C}+^{12}\text{C}$ astrophysical S-factors with the $^{12}\text{C}+^{13}\text{C}$ measurements at very low energies,” *Phys. Lett. B* **801**, 135170 (2020).
- B. Elman, A. Gade, R. V. F. Janssens, A. D. Ayangeakaa, D. Bazin, J. Belarge, P. C. Bender, B. A. Brown, C. M. Campbell, M. P. Carpenter, H. L. Crawford, B. P. Crider, P. Fallon, A. M. Forney, J. Harker, S. N. Liddick, B. Longfellow, E. Lunderberg, C. J. Prokop, J. Sethi, R. Taniuchi, W. B. Walters, D. Weisshaar, and S. Zhu, “Probing the role of proton cross-shell excitations in ^{70}Ni using nucleon knockout reactions,” *Phys. Rev. C* **100**, 034317 (2019).
- Y. Ichikawa, H. Nishibata, A. Takamine, K. Imamura, T. Fujita, T. Sato, Y. Shimizu, D. S. Ahn, K. Asahi, H. Baba, D. L. Balabanski, F. Boulay, J. M. Daugas, N. Fukuda, A. Gladkov, N. Inabe, Y. Ishibashi, Y. Ohtomo, T. Otsuka, T. Sumikama, H. Suzuki, H. Takeda, L. C. Tao, H. Ueno, and H. Yamazaki, “Interplay between nuclear shell evolution and shape deformation revealed by the magnetic moment of ^{75}Cu ,” *Nat. Phys.* **15**, 321–325 (2019).
- A. Sakurai, B. K. Sahoo, K. Asahi, and B. P. Das, “Relativistic many-body theory of the electric dipole moment of ^{129}Xe and its implications for probing new physics beyond the standard model,” *Phys. Rev. A* **100**, 020502 (R) (2019).
- F. Boulay, G. S. Simpson, Y. Ichikawa, S. Kisiov, D. Bucurescu, A. Takamine, D. S. Ahn, K. Asahi, H. Baba, D. L. Balabanski, T. Egami, T. Fujita, N. Fukuda, C. Funayama, T. Furukawa, G. Georgiev, A. Gladkov, M. Hass, K. Imamura, N. Inabe, Y. Ishibashi, T. Kawaguchi, T. Kawamura, W. Kim, Y. Kobayashi, S. Kojima, A. Kusoglu, R. Lozeva, S. Momiyama, I. Mukul, M. Niikura, H. Nishibata, T. Nishizaka, A. Odahara, Y. Ohtomo, D. Ralet, T. Sato, Y. Shimizu, T. Sumikama, H. Suzuki, H. Takeda, L. C. Tao, Y. Togano, D. Tominaga, H. Ueno, H. Yamazaki, X. F. Yang, and J. M. Daugas, “ g Factor of the ^{99}Zr ($7/2^+$) isomer: monopole evolution in the shape-coexisting region,” *Phys. Rev. Lett.* **124**, 112501 (2020).
- T. Sonoda, I. Katayama, M. Wada, H. Iimura, V. Sonnenschein, S. Iimura, A. Takamine, M. Rosenbusch, T. M. Kojima, D. S. Ahn, N. Fukuda, T. Kubo, S. Nishimura, Y. Shimizu, H. Suzuki, H. Takeda, M. Tanigaki, H. Tomita, K. Yoshida, and H. Ishiyama, “Conceptual study on parasitic low-energy RI beam production with in-flight separator BigRIPS and the first stopping examination for high-energy RI beams in the parasitic gas cell,” *Prog. Theor. Exp. Phys.* **2019**, 113D02 (2019).
- G. Häfner, K. Moschner, A. Blazhev, P. Boutachkov, P. J. Davies, R. Wadsworth, F. Ameil, H. Baba, T. Bäck, M. Dewald, P. Doornenbal, T. Faestermann, A. Gengelbach, J. Gerl, R. Gernhäuser, S. Go, M. Górská, H. Grawe, E. Gregor, H. Hotaka, T. Isobe, D. G. Jenkins, J. Jolie, H. S. Jung, I. Kojouharov, N. Kurz, M. Lewitowicz, G. Lorusso, R. Lozeba, E. Merchan, F. Naqvi, H. Nishibata, D. Nishimura, S. Nishimura, N. Pietralla, H. Scaffner, P. -A. Söderström, K. Steiger, T. Sumikama, J. Taprogge, P. Thöle, H. Watanabe, N. Warr, V. Werner, Z. Y. Xu, A. Yagi, K. Yoshinaga, and Y. Zhu, “Properties of γ -decaying isomers in the ^{100}Sn region populated in fragmentation of a ^{124}Xe beam,” *Phys. Rev. C* **100**, 024302 (2019).
- R. Yokoyama, M. Singh, R. Grzywacz, A. Keeler, T. T. King, J. Agramunt, N. T. Brewer, S. Go, J. Heideman, J. Liu, S. Nishimura, P. Parkhurst, V. H. Phong, M. M. Rajabali, B. C. Rasco, K. P. Rykaczewski, D. W. Stracener, J. L. Tain, A. Tolosa-Delgado, K. Vaigneur, and M. Wolińska-Cichocka, “Segmented YSO scintillation detectors as a new β -implant detection tool for decay spectroscopy in fragmentation facilities,” *Nucl. Instrum. Methods Phys. Res. A* **937**, 93–97 (2019).
- J. W. Lee *et al.* [SPIRIT Collaboration], “Charged particle track reconstruction with πRIT Time Projection Chamber,” *Nucl. Instrum. Methods Phys. Res. A* **965**, 163840 (2020).

C. Y. Tsang *et al.* [SPiRIT Collaboration], “Space charge effects in the Σ RIT time projection chamber,” *Nucl. Instrum. Methods Phys. Res. A* **959**, 163477 (2019).

J. Estee *et al.* [SPiRIT Collaboration], “Extending the dynamic range of electronics in a Time Projection Chamber,” *Nucl. Instrum. Methods Phys. Res. A* **944**, 162509 (2019).

[Review articles]

谷内稜, 櫻井博儀, 「2重魔法数とその破れ: ニッケル 78 のガンマ線分光が解明した閉殻性」, 「物理科学, この1年 2020」, パリティ 2020 年 1 月号, pp.86–89, 丸善出版, (2020).

R. Taniuchi and Pieter Doornenbal, “A new Frontier of unstable doubly magic nuclei,” *AAPPS BULLETIN* **29**, 13–18 (2019).

[Proceedings]

J. Giovinozzo, T. Goigoux, B. Blank, P. Ascher, M. Gerbaux, S. Grevy, T. Kurtukian-Nieto, C. Magron, P. Doornenbal, N. Fukuda, N. Inabe, G. Kiss, T. Kubo, S. Kubono, S. Nishimura, H. Sakurai, Y. Shimizu, C. Sidong, P. Soderstrom, T. Sumikama, H. Suzuki, H. Takeda, P. Vi, J. Wu, D. Ahn, J. Agramunt, A. Algora, V. Guadilla, A. Montaner-Piza, A. Morales, S. Orrigo, B. Rubio, Y. Fujita, M. Tanaka, W. Gelletly, P. Aguilera, F. Molina, F. Diel, D. Lubos, G. de Angelis, D. Napoli, C. Borcea, A. Boso, R. Cakirli, E. Ganioglu, J. Chiba, D. Nishimura, H. Oikawa, Y. Takei, S. Yagi, K. Wimmer, G. de France, S. Go, and B. Brown, “Two-proton Radioactivity: the Interesting Case of ^{67}Kr and Further Studies,” *Acta Phys. Pol. B* **51**, 577 (2020).

A. Vitéz-Sveicz, A. Algora, A. I. Morales, B. Rubio, G. G. Kiss, G. D. Angelis, F. Recchia, S. Nishimura, J. Agramunt, V. Guadilla, A. Montaner-Pizá, S. E. A. Orrigo, A. Horváth, D. Napoli, S. Lenzi, A. Boso, V. H. phong, J. Wu, P. -A. Söderström, T. Sumikama, H. Suzuki, H. Takeda, D. S. Ahn, H. Baba, P. Doornenbal, N. Fukuda, N. Inabe, T. Isobe, T. Kubo, S. Kubono, H. Sakurai, Y. Shimizu, S. Chen, B. Blank, P. Acher, M. Gerbaux, T. Goigoux, J. Giovinozzo, S. Grévy, T. Kurtukián Nieto, C. Magron, W. Gelletly, Dz. Dombrádi, Y. Fujita, M. Tanaka, P. Aguilera, F. Molina, J. Eberth, F. Diel, D. Lubos, C. Borcea, E. Ganioglu, D. Nishimura, H. Oikawa, Y. Takei, S. Yagi, W. Korten, G. de France, P. Davies, J. Liu, J. Lee, T. Lokotko, I. Kojouharov, N. Kurz, and H. Schaffner, “Studying the exotic decay $^{70}\text{Kr} \rightarrow ^{70}\text{Br}^*$,” *Acta Phys. Pol. B* **51**, 587–594 (2020).

B. Ding, Z. Liu, X. Liu, P. Doornenbal, A. Obertelli, S. Lenzi, P. Walker, L. Chung, B. Linh, G. Authelet, H. Baba, D. Calvet, F. Chateau, A. Corsi, A. Delbart, J. Gheller, A. Gillibert, T. Isobe, V. Lapoux, M. Matsushita, S. Momiyama, T. Motobayashi, M. Niikura, F. Nowacki, H. Otsu, C. Peron, A. Peyaud, E. Pollacco, J. Rousse, H. Sakurai, M. Sasano, Y. Shiga, S. Takeuchi, R. Taniuchi, T. Uesaka, H. Wang, K. Yoneda, X. Tang, Y. Lam, T. Huang, M. Sun, W. Zhang, H. Lu, D. Hou, F. Browne, Z. Dombradi, S. Franchoo, F. Giacoppo, A. Gottardo, K. Hadynska-Klek, Z. Korkulu, S. Koyama, Y. Kubota, J. Lee, M. Lettmann, R. Lozeva, K. Matsui, T. Miyazaki, S. Nishimura, C. Louchart, L. Olivier, S. Ota, Z. Patel, E. Sahin, C. Santamaria, C. Shand, P. Soderstrom, G. Stefan, D. Steppenbeck, T. Sumikama, D. Suzuki, Z. Vajta, V. Werner, J. Wu, Z. Xu, X. Zhou, Y. Zhang, H. Xu, and F. Zhang, “Spectroscopic study in neutron-rich Mn isotopes around the $N = 40$ “Island of Inversion,”” *EXON-2018 Proceedings of the International Symposium on Exotic Nuclei “Exotic Nuclei,”* 22–34 (2019)

A. Tolosa-Delgado, J. Agramunt, D. Ahn, A. Algora, H. Baba, S. Bae, N. Brewer, C. Bruno, R. Caballero Folch, F. Calvino, P. Coleman-Smith, G. Cortes, T. Davinson, I. Dillmann, C. Domingo-Pardo, A. Estrade, N. Fukuda, S. Go, C. Griffin, R. Grzywacz, J. Ha, O. Hall, L. Harkness-Brennan, T. Isobe, D. Kahl, M. Karny, L. Khiem, G. Kiss, M. Kogimtzis, S. Kubono, M. Labiche, I. Lazarus, J. Lee, J. Liang, J. Liu, G. Lorusso, K. Matsui, K. Miernik, F. Montes, B. Moon, A. Morales, N. Nepal, S. Nishimura, R. Page, V. Phong, Z. Podolyak, V. Pucknell, B. Rasco, P. Regan, A. Riego, B. Rubio, K. Rykaczewski, Y. Saito, H. Sakurai, Y. Shimizu, J. Simpson, P. Soderstrom, D. Stracener, T. Sumikama, H. Suzuki, J. Tain, M. Takechi, H. Takeda, A. Tarifeno-Saldivia, S. Thomas, P. Woods, X. Xu, and R. Yokoyama, “Improving nuclear data input for r-process calculations around $A \sim 80$,” *Springer Proc. Phys.* **219**, 453–456 (2019)

F. Recchia, K. Wimmer, S. Lenzi, S. Riccetto, T. Davinson, A. Estrade, C. Griffin, S. Nishimura, F. Nowacki, V. Phong, A. Poves, P. A. Soderstrom, O. Aktas, M. Alaqueel, T. Ando, H. Baba, S. Bae, S. Choi, P. Doornenbal, J. Ha, L. Harkness-Brennan, T. Isobe, P. John, D. Kahl, G. Kiss, M. Labiche, K. Matsui, S. Momiyama, D. Napoli, M. Niikura, C. Nita, Y. Saito, H. Sakurai, P. Schrock, C. Stahl, T. Sumikama, V. Werner, and W. Witt, “Isomer spectroscopy in odd-even Ti isotopes: approaching $N = 40$,” *Acta Phys. Pol. B* **50**, 669 (2019).

Y. Watanabe, J. Suwa, K. Nakano, S. Kawase, H. Wang, H. Otsu, H. Sakurai, D. Ahn, M. Aikawa, T. Ando, S. Araki, S. Chen, N. Chiga, P. Doornenbal, N. Fukuda, T. Isobe, S. Kawakami, T. Kin, Y. Kondo, S. Koyama, S. Kubono, Y. Maeda, A. Makinaga, M. Matsushita, T. Matsuzaki, S. Michimasa, S. Momiyama, S. Nagamine, T. Nakamura, M. Niikura, T. Ozaki, A. Saito, T. Saito, Y. Shiga, M. Shikata, Y. Shimizu, S. Shimoura, T. Sumikama, P. Soderstrom, H. Suzuki, H. Takeda, S. Takeuchi, R. Taniuchi, Y. Togano, J. Tsubota, M. Uesaka, Y. Watanabe, K. Wimmer, T. Yamamoto, and K. Yoshida, “Isotopic production cross sections of residual nuclei in proton- and deuteron-induced reactions on $^{91,92}\text{Y}$, $^{92,93}\text{Zr}$, and $^{93,94}\text{Nb}$ around 100 MeV/nucleon,” *CERN Proc.* **1**, 139–144 (2019).

X. Sun, H. Wang, H. Otsu, H. Sakurai, D. Ahn, M. Aikawa, P. Doornenbal, N. Fukuda, T. Isobe, S. Kawakami, S. Koyama, T. Kubo, S. Kubono, G. Lorusso, Y. Maeda, A. Makinaga, S. Momiyama, K. Nakano, M. Niikura, Y. Shiga, P. A. Soderstrom, H. Suzuki, H. Takeda, S. Takeuchi, R. Taniuchi, Y. Watanabe, Y. Watanabe, H. Yamasaki, and K. Yoshida, “Cross section measurements in the reactions of ^{136}Xe on proton, deuteron and carbon at 168 MeV/u,” *CERN Proc.* **1**, 153–158 (2019).

S. Kubono, T. Kawabata, N. Iwasa, J. J. He, and S. Q. Hou, “Experimental Challenge to the Cosmological Li Problem,” *Proc. Int. Conference on Nuclei in the Cosmos XV*, ed. A. Formicola, *et al.*, Springer Proceedings in Physics **219**, 45–52 (2019).

S. Hayakawa, K. Abe, O. Beliuskina, S. M. Cha, K. Y. Chae, S. Cherubini, P. Figuera, Z. Ge, M. Gulino, J. Hu, A. Inoue, N. Iwasa, D. Kahl, A. Kim, D. H. Kim, G. G. Kiss, S. Kubono, M. La Cognata, L. Lamia, M. Lattuada, E. J. Lee, J. Y. Moon, Sara Palmerini, C. Parascandolo, S. Y. Park, D. Pierrousakou, Rosario Gianluca Pizzone, G. G. Rapisarda, S. Romano, H. Shimizu, C. Spitaleri, Xiaodong Tang, O. Trippella, Aurora Tumino, P. Vi, H. Yamaguchi, L. Yang, and N. T. Zhang “Cross section measurements of the $^7\text{Be}(n, p)^7\text{Li}$ and the $^7\text{Be}(n, \alpha)^4\text{He}$ reactions covering the big-bang nucleosynthesis energy range by the trojan horse method at CRIB,” *Proc. Int. Conference on Nuclei in the Cosmos XV*, ed. A. Formicola, *et al.*, Springer Proceedings in Physics **219**, 33–38 (2019).

- L. Lamia, C. Spitaleri, M. Mazzocco, S. Hayakawa, C. A. Bertulani, A. Boiano, C. Boiano, Carlo Brogini, Antonio Cacioli, Rosanna Depalo, F. Galtarossa, G. L. Guardo, M. Gulino, S. Kubono, M. La Cognata, M. La Commara, G. La Rana, M. Lattuada, Roberto Menegazzo, A. Pakou, C. Parascandolo, D. Piatti, D. Pierroutsakou, Rosario Gianluca Pizzone, S. Romano, G. G. Rapisarda, M. L. Sergi, O. Sgouros, F. Soramel, V. Soukeras, E. Strano, D. Torresi, Aurora Tumino, H. Yamaguchi, F. L. Villante, and G. L. Zhang “The Cosmologically Relevant ${}^7\text{Be}(n, \alpha){}^4\text{He}$ Reaction in View of the Recent THM Investigations,” Proc. Int. Conference on Nuclei in the Cosmos XV, ed. A. Formicola, *et al.*, Springer Proceedings in Physics **219**, 53–56 (2019).
- H. Shimizu, D. Kahl, H. Yamaguchi, K. Abe, O. Beliuskina, S. M. Cha, K. Y. Chae, A. A. Chen, Z. Ge, S. Hayakawa, N. Imai, N. Iwasa, A. Kim, D. H. Kim, M. J. Kim, S. Kubono, M. S. Kawag, J. Liang, J. Y. Moon, S. Nishimura, S. Oka, S. Y. Park, A. Psaltis, T. Teranishi, Y. Ueno, and L. Yang, “Study on ${}^{26m}\text{Al}(p, \gamma)$ reaction at the SNe temperature,” JPS Conf. Proc. **31**, 011073 (2020).
- S. Hayakawa, M. La Cognata, L. Lamia, H. Shimizu, L. Yang, H. Yamaguchi, K. Abe, O. Beliuskina, S. M. Cha, K. Y. Chae, S. Cherubini, P. Figuera, Z. Ge, M. Gulino, J. Hu, A. Inoue, N. Iwasa, D. Kahl, A. Kim, D. H. Kim, G. Kiss, S. Kubono, M. La Commara, M. Lattuada, E. J. Lee, J. Y. Moon, S. Palmerini, C. Parascandolo, S. Y. Park, D. Pierroutsakou, R. G. Pizzone, G. G. Rapisarda, S. Romano, C. Spitaleri, X. D. Tang, O. Trippella, A. Tumino, P. Vi, and N. T. Zhang, “Experimental study on the ${}^7\text{Be}(n, p){}^7\text{Li}$ and the ${}^7\text{Be}(n, \alpha){}^4\text{He}$ reactions for cosmological lithium problem,” JPS Conf. Proc. **31**, 011036 (2020).

Presentations

[International conferences/workshops]

- H. Sakurai (invited), “In-flight radioactive isotope beam facilities and nuclear physics at RIKEN,” The First African Nuclear Physics Conference (ANPC), Kruger, South Africa, July 1–5, 2019.
- S. Nishimura (invited), “r-process studies at RIBF,” Nuclear and astrophysics aspects for the rapid neutron capture process in the era of multimessenger observations, ECT*, Trento, Italy, July 1–5, 2019.
- S. Nishimura (invited), “Decay properties of exotic nuclei” China-Japan Collaboration Workshop on Nuclear Mass and Life for Unraveling Mysteries of R-process, ITP-CAS, Beijing, China, October 9–13, 2019.
- S. Nishimura (invited), “Ukakuren” JINA-CEE IReNA/NAOJ Workshop, National Astronomy Observation of Japan, Mitaka, Japan, December 3–4 (2019).
- T. Isobe (poster), “Measurement of Th-229 low lying isomeric state with MRTOF+TES system at RIKEN-RIBF,” 18th International Workshop on Low Temperature Detectors (LTD18), Milano, Italy, July 22–26, 2019.
- T. Isobe (invited), “Latest update on RIKEN facilities,” 9th International Symposium on Nuclear Symmetry Energy (NuSym2019), Danan, Vietnam, September 30–October 4, 2019.
- T. Isobe (oral), “Experimental study of hydrogen isotopes production in Sn+Sn RI collisions at 270 AMeV,” 9th International Symposium on Nuclear Symmetry Energy (NuSym2019), Danan, Vietnam, September 30–October 4, 2019.
- P. Doornenbal (invited), “Structure of exotic Calcium and Nickel isotopes,” 14th Asia Pacific Physics Conference, Kuching, Malaysia, November 17–22, 2019.
- P. Doornenbal (invited), “Exploring the terra incognita of exotic nuclei at RIKEN: past achievements and future endeavors,” VINANST-13, Reu Island, Vietnam, August 7–9, 2019.
- P. Doornenbal (invited), “Towards high-resolution in-beam Gamma-ray spectroscopy at the RIBF,” 27th International Nuclear Physics Conference (INPC), Glasgow, UK, July 29–August 2, 2019.
- P. Doornenbal (invited), “In-beam gamma-ray spectroscopy at RIKEN,” 1st African Nuclear Physics Conference (ANPC), Kruger National Park, South Africa, July 1–5, 2019.
- P. Doornenbal (oral), “High resolution spectroscopy of ${}^{78}\text{Ni}$,” High Resolution Gamma-ray Spectroscopy at the RIBF Workshop, Darmstadt, Germany, April 10–12, 2019.
- P. Doornenbal (oral), “Technical Considerations,” High Resolution Gamma-ray Spectroscopy at the RIBF Workshop, Darmstadt, Germany, April 10–12, 2019.
- D. Suzuki (invited), “Present and future of in-beam spectroscopy at RIBF,” Workshop on RI-beam Spectroscopy by Innovative Gaseous Active Targets, Osaka, Japan, December 19–20, 2019.
- D. Suzuki (invited), “Present and future of in-beam spectroscopy at RIBF,” Workshop on RI-beam Spectroscopy by Innovative Gaseous Active Targets, Osaka, Japan, December 19–20, 2019.
- D. Suzuki (oral), “Coulomb and quantum bubbles in heavy nuclei,” High Resolution Gamma-Ray Spectroscopy at the RIBF, Darmstadt, Germany, April 10–12, 2019.
- D. Suzuki (oral), “rp-process study at OEDO,” OEDO collaboration workshop, Wako, Japan, September 2, 2019.
- D. Suzuki (oral), “Recent results from SUNFLOWER and future perspectives,” JSPS/NRF/NSFC A3 Foresight Program “Nuclear Physics in the 21st Century” Joint Kickoff Meeting, Kobe, Japan, December 6–7, 2019.
- D. Suzuki (invited), “Present and future of in-beam spectroscopy at RIBF,” Workshop on RI-beam Spectroscopy by Innovative Gaseous Active Targets, Osaka, Japan, December 19–20, 2019.
- D. Suzuki (invited), “Present and future of in-beam spectroscopy at RIBF,” Workshop on RI-beam Spectroscopy by Innovative Gaseous Active Targets, Osaka, Japan, December 19–20, 2019.
- D. Suzuki (oral), “Coulomb and quantum bubbles in heavy nuclei,” High Resolution Gamma-Ray Spectroscopy at the RIBF, Darmstadt, Germany, April 10–12, 2019.
- D. Suzuki (oral), “rp-process study at OEDO,” OEDO collaboration workshop, Wako, Japan, September 2, 2019.
- W. Horiuchi, S. Hatakeyama, A. Kohama (oral), “Nuclear “diffuseness” probed by proton-nucleus diffraction,” The 27th International

- Nuclear Physics Conference (INPC 2019), Glasgow, UK, July 29–August 2, 2019. (INPC 2019)
- S. Kubono (invited), “Heavy element synthesis under explosive burning on neutron stars,” The 10th European Summer School on Experimental Nuclear Astrophysics Catania, INFN-LNS, June 16–23, 2019.
- S. Kubono (invited), “Experimental approach to explosive H-burning in X-ray bursts and SNeII,” Workshop on origin of Elements and Cosmic Evolution: From Big-Bang to Supernovae and Mergers, Beihang University, China, November 27–29, 2019.
- K. Asahi (invited), “Experiment on nuclear EDMs,” KEK Workshop on Nucleon EDMs and Spin Structure 2020, KEK Tokai Campus, Tokai, Ibaraki, Japan, January 11, 2020.
- R. Taniuchi (oral), “Approaching the fifth island of inversion from the north” High Resolution Gamma-Ray Spectroscopy at the RIBF, TU Darmstadt, Germany, April 10–12, 2019.
- R. Taniuchi (oral), “In-beam gamma-ray spectroscopy of ^{78}Ni reveals its doubly magic character,” 27th International Nuclear Physics Conference (INPC 2019), Glasgow, United Kingdom, July 29–August 2, 2019.
- R. Taniuchi (oral), “Quest for shell quenching of $N = 50$ in doubly magic ^{78}Ni ” 8th SUNFLOWER Workshop/HiCARI Workshop, Osaka, September 26–28, 2019.
- V. Phong (oral), “ β -decay measurements of very neutron-rich isotopes around Mass $A = 130$ within the BRIKEN project at RIBF,” 15th International Symposium on Origin of Matter and Evolution of Galaxies (OMEG15), Kyoto, Japan, July 2–5, 2019.
- V. Phong (oral), “Measurement of very neutron-rich beta delayed neutron emitters around mass $A = 130$ relevant to the astrophysical r-process,” 9th International Symposium on Nuclear Symmetry Energy (NuSYM2019), Danang, Vietnam, September 30–October 4, 2019.
- H. Shimizu (poster), “Study on $^{26m}\text{Al}(p, \gamma)$ reaction at the SNe temperature,” Symposium on Origin of Matter and Evolution of Galaxies (OMEG15), Kyoto, Japan, July 2–5, 2019.
- H. Shimizu (poster), “Isomeric ^{26}Al beam production with CRIB,” Nuclear Physics School For Young Scientists (NUSYS-2019), Lanzhou, China, August 12–17, 2019.
- T. Koiwai (oral), “Single-particle structure of ^{55}Ti and ^{57}Ti ,” Workshop on high-resolution gamma-ray spectroscopy at the RIBF, Darmstadt, Germany, April 2019
- T. Koiwai (oral), “In-beam γ -ray spectroscopy of ^{55}K and ^{55}Ca via nucleon knockout reactions,” International Nuclear Physics Conference (INPC 2019), Glasgow, UK, July–August 2019
- T. Koiwai (oral), “ $N = 34$ beyond ^{54}Ca : Single-particle structure of $^{55,57}\text{Ti}$,” 8th SUNFLOWER Workshop and HiCARI Workshop (JSPS A3Foresight), Osaka, Japan, August 2019.

[Domestic conferences/workshops]

- 櫻井博儀 (招待講演), 「RIBFでの核物理研究」, 研究会「シミュレーションによる宇宙の基本法則と進化の解明に向けて (QUCS2019)」, 京都大学基礎物理学研究所, 京都, 2019年12月.
- 西村俊二 (口頭発表), 「rプロセスの研究: 実験的検証と挑戦」, 研究会「原子核物理でつむぐrプロセス」, 京都大学基礎物理学研究所, 京都, 2019年5月22–24日.
- P. Doornenbal (invited), “Recent results from SUNFLOWER and future plans,” RIBF Week, Wako, Japan, September 2–4, 2019.
- P. Doornenbal (invited), “Results from SEASTAR III,” SAMURAI Workshop, Tokyo, Japan, August 30–31, 2019.
- P. Doornenbal (oral), “Sunflower Status,” SUNFLOWER/HiCARI Workshop, Osaka, Japan, August 26–28, 2019.
- P. Doornenbal (invited), “Probing the Nuclear Shell Closures far off Stability with In-Beam Gamma-Ray Spectroscopy,” JPS Spring Meeting, Kyushu, Japan, March 14–17, 2019.
- 横口雄仁 (口頭発表), 堀内渉, 小濱洋央, 「反陽子-原子核散乱による希薄核密度領域の探索」, 日本物理学会第75回年次大会, 名古屋大学東山キャンパス, 名古屋, 2020年3月16日–20日.
- F. Browne (oral), “Coulomb excitation study of Se isotopes beyond $N = 50$,” 8th SUNFLOWER Workshop/HiCARI Workshop (JSPS A3Foresight), Osaka, Japan, August 26–28, 2019.
- 谷内稜 (招待講演), 「核変形に対して二重閉殻を堅持する ^{78}Ni 」, 日本物理学会第75回年次大会, 名古屋大学 (オンライン開催), 2020年3月16–19日.
- 旭 耕一郎 (招待講演), 「原子の EDM と時間反転対称性の破れ—反磁性原子の EDM を中心に」, 電子 EDM 研究会, 東京大学駒場キャンパス, 目黒, 2019年12月11日.

[Seminars]

- T. Isobe, “Overview of the RI Beam Facility (RIBF),” CNS Summer School 2019 (CNSSS19), Nishina Hall Riken Wako, August 21–27, 2019.
- T. Isobe, “Experimental study of asymmetric dense nuclear matter Equation Of State by using heavy RI collisions at RIBF-S π RIT,” CNS Summer School 2019 (CNSSS19), Nishina Hall Riken Wako, August 21–27, 2019.
- S. Kubono, “Special lectures on nuclear astrophysics,” Department of Physics, Hong Kong University, April 15–18, 2019.
- K. Asahi, “Electric dipole moments of diamagnetic atoms—Present status of experiments,” CNS Seminar, Hongo, Tokyo, Japan, June 13, 2019.
- R. Taniuchi, “ ^{78}Ni revealed as a doubly magic stronghold against nuclear deformation,” 276th RIKEN RIBF Nuclear Physics Seminar, Saitama, Japan, May 28, 2019.
- R. Taniuchi, “In-beam gamma-ray spectroscopy of ^{78}Ni revealed its double magicity and shape-coexistence,” The RIBF Users Group Thesis Award lecture, RIBF Week 2019, Saitama, September 3, 2019.

Awards

- P. Doornenbal, RIKEN BAIHO Award 2020, Achievement: In-beam γ -ray spectroscopy of the neutron-rich doubly-magic nucleus ^{78}Ni
- R. Taniuchi, The RIBF Users Group Thesis Award, September 3, 2019.
谷内稜, 第 14 回 (2020 年) 日本物理学会若手奨励賞, 2020 年 3 月 18 日.
谷内稜, 第 26 回原子核談話会 新人賞, 2020 年 3 月 18 日.
- V. Phong, ANPhA (and AAPPS DNP) award for Young Scientists at 9th International Symposium on Nuclear Symmetry Energy (NuSYM2019): 2nd prize.

Press releases

- 「魔法数研究に金字塔—ついに中性子過剰なニッケル原子核の二重魔法性に結論—」, 2019 年 5 月 2 日.
「新魔法数 34 の新たな証拠—中性子ノックアウト反応で探るカルシウム-54 の閉殻構造—」, 2019 年 10 月 18 日.
「急激に膨れる原子核—カルシウム同位体で見つかった異常な核半径増大現象—」, 2020 年 3 月 13 日.

Outreach activities

- 櫻井博儀, 「元素の進化と変換」, 2019 年度芦屋公民館サイエンス講座, 2019 年 4–6 月.
磯部忠昭, 「科学者になるという事～世界最先端の研究と未来～」, 細田学園講演会, 細田学園高等学校, 志木, 2019 年 6 月 24 日.

Others**[Software package]**

- A. Kohama, K. Iida, K. Oyamatsu, H. Iwase, Release of “kurotama0” update (ver. 3.0), Contribution of PHITS update to ver. 3.20, March 2020.

Nuclear Science and Transmutation Research Division

Spin isospin Laboratory

1. Abstract

The Spin Isospin Laboratory pursues research activities putting primary focus on interplay of spin and isospin in exotic nuclei. Understanding nucleosyntheses in the universe, especially those in r- and rp-processes is another big goal of our laboratory.

Investigations on isospin dependences of nuclear equation of state, spin-isospin responses of exotic nuclei, occurrence of various correlations at low-densities, evolution of spin-orbit coupling are main subjects along the line. We are leading a mass measurement project with the Rare RI Ring project, too. Through the experimental studies, we will be able to elucidate a variety of nuclear phenomena in terms of interplay of spin and isospin, which will in turn, lead us to better understanding of our universe.

2. Major Research Subjects

- (1) Direct reaction studies of neutron-matter equation of state
- (2) Study of spin-isospin responses with RI-beams
- (3) R-process nucleosynthesis study with heavy-ion storage ring
- (4) Application of spin-polarization technique to RI-beam experiments and other fields
- (5) Development of special targets for RI-beam experiments

3. Summary of Research Activity

(1) Direct reaction studies of neutron matter equation of state

Direct reactions induced by light-ions serve as powerful tools to investigate various aspects of nuclei. We are advancing experimental programs to explore equation of state of neutron matter, via light-ion induced reactions with RI-beams.

(1-1) Determination of a neutron skin thickness by proton elastic scattering

A neutron skin thickness is known to have strong relevance to asymmetry terms of nuclear equation of state, especially to a term proportional to density. The ESPRI project aims at determining density distributions in exotic nuclei precisely by proton elastic scattering at 200–300 MeV/nucleon. An experiment for ^{132}Sn that is a flagship in this project has been successfully performed.

(1-2) Asymmetry terms in nuclear incompressibility

Nuclear incompressibility represents stiffness of nuclear matter. Incompressibility of symmetric nuclear matter is determined to be 230 ± 20 MeV, but its isospin dependence still has a large uncertainty at present. A direct approach to the incompressibility of asymmetric nuclear matter is an experimental determination of energies of isoscalar giant monopole resonances (GMR) in heavy nuclei. We have developed, in close collaboration with Center for Nuclear Study (CNS) of University of Tokyo, an active gas target for deuteron inelastic scattering experiments to determine GMR energies. The active gas target has been already tested with oxygen and xenon beams at HIMAC and finally has been applied to a ^{132}Sn experiment at RIBF.

(1-3) Multi-neutron and α -cluster correlations at low densities

Occurrences of multi-neutron and α -cluster correlations are other interesting aspects of nuclear matter and define its low-density behavior. The multi-neutron and α -cluster correlations can be investigated with the large-acceptance SAMURAI spectrometer. The SAMURAI has been already applied to experiments to explore light neutron-rich nuclei close to the dripline. We plan to reinforce experimental capabilities of the SAMURAI by introducing advanced devices such as MINOS (Saclay) and NeuLAND (GSI).

(1-4) Fission barrier heights in neutron-rich heavy nuclei

The symmetry energy has a strong influence on fission barrier heights in neutron-rich nuclei. Knowledge on the fission barrier heights, which is quite poor at present, is quite important for our proper understanding on termination of the r-process. We are planning to perform, in collaboration with the TU Munich group, ($p, 2p$)-delayed fission experiments at the SAMURAI to determine the fission barrier heights in neutron-rich nuclei in Pb region.

(2) Study of spin-isospin responses with RI-beams

The study of spin-isospin responses in nuclei forms one of the important cores of nuclear physics. A variety of collective states, for example isovector giant dipole resonances, isobaric analogue states, Gamow-Teller resonances, have been extensively studied by use of electromagnetic and hadronic reactions from stable targets.

The research opportunities can be largely enhanced with light of availabilities of radioactive isotope (RI) beams and of physics of unstable nuclei. There are three possible directions to proceed. The first direction is studies of spin-isospin responses of unstable nuclei via inverse-kinematics charge exchange reactions. A neutron-detector array WINDS has been constructed, under a collaboration of CNS, Tokyo and RIKEN, for inverse kinematics (p, n) experiments at the RI Beam Factory. We have already applied WINDS to the (p, n) experiments for ^{12}Be , ^{132}Sn and plan to extend this kind of study to other exotic nuclei.

The second direction is studies with RI-beam induced charge exchange reaction. RI-beam induced reactions have unique properties which are missing in stable-beam induced reactions and can be used to reach the yet-to-be-discovered states. We have constructed the SHARAQ spectrometer and the high-resolution beam-line at the RI Beam Factory to pursue the capabilities of RI-beam induced reactions as new probes to nuclei. One of the highlights is an observation of β^+ type isovector spin monopole resonances (IVSMR) in ^{208}Pb and ^{90}Zr via the ($t, ^3\text{He}$) reaction at 300 MeV/nucleon.

The third direction is studies of neutron- and proton-rich nuclei via stable-beam induced charge exchange reactions, which is conducted under collaboration with Research Center for Nuclear Physics (RCNP), Osaka University. We have performed the double

charge exchange $^{12}\text{C}(^{18}\text{O}, ^{18}\text{Ne})^{12}\text{Be}$ reaction at 80 MeV/nucleon to investigate structure of a neutron-rich ^{12}Be nucleus. Peaks corresponding to ground and excited levels in ^{12}Be have been clearly observed. Another double charge exchange reaction, ($^{12}\text{C}, ^{12}\text{Be}(0_2^+)$) are being used to search for double Gamow-Teller resonances.

(3) R-process nucleosynthesis study with heavy-ion storage ring

Most of the r-process nuclei become within reach of experimental studies for the first time at RI Beam Factory at RIKEN. The Rare RI Ring at RIBF is the unique facility with which we can perform mass measurements of r-process nuclei. Construction of the Rare RI Ring started in FY2012 in collaboration with Tsukuba and Saitama Universities. A major part of the ring has been completed and the commissioning run is planned in FY2014.

We are planning to start precise mass measurements of r-process nuclei soon. A series of experiments will start with nuclei in the $A = 80$ region and will be extended to heavier region.

(4) Application of spin-polarization technique to RI-beam experiments and other fields

A technique to produce nuclear polarization by means of electron polarization in photo-excited triplet states of aromatic molecules can open new applications. The technique is called "Triplet-DNP." A distinguished feature of Triplet-DNP is that it works under a low magnetic field of 0.1–0.7 T and temperature higher than 100 K, which exhibits a striking contrast to standard dynamic nuclear polarization (DNP) techniques working in extreme conditions of several Tesla and sub-Kelvin.

We have constructed a polarized proton target system for use in RI-beam experiments. Recent experimental and theoretical studies have revealed that spin degrees of freedom play a vital role in exotic nuclei. Tensor force effects on the evolution of shell and possible occurrence of p - n pairing in the proton-rich region are good examples of manifestations of spin degrees of freedom. Experiments with the target system allow us to explore the spin effects in exotic nuclei. It should be noted that we have recently achieved a proton polarization of 40% at room temperature in a pentacene- d_{14} doped p-terphenyl crystal.

Another interesting application of Triplet-DNP is sensitivity enhancement in NMR spectroscopy of biomolecules. We started a new project to apply the Triplet-DNP technique to study protein-protein interaction via two-dimensional NMR spectroscopy, in close collaboration with biologists and chemists.

(5) Development of special targets for RI-beam experiments

For the research activities shown above, we are developing and hosting special targets for RI-beam experiments listed below:

- (a) Polarized proton target (described in (4))
- (b) Thin solid hydrogen target
- (c) MINOS (developed at Saclay and hosted by the Spin Isospin Laboratory)

Members

Director

Tomohiro UESAKA

Research/Technical Scientists

Masaki SASANO (Senior Research Scientist)

Ken-ichiro YONEDA (Senior Research Scientist)

Juzo ZENIHIRO (Senior Research Scientist)

Sarah NAIMI (Research Scientist)

Contract Researchers

Takeshi INOUE

Kenichiro TATEISHI

Postdoctoral Researcher

Junki TANAKA

Junior Research Associates

Tomoya HARADA

Shoichiro MASUOKA

International Program Associates

Siwei HUANG (Peking Univ.)

Alexandra-Ionela STEFANESCU (Univ. of Bucharest)

Ionut-Catalin STEFANESCU (Univ. of Bucharest)

Hongfu LI (IMP, CAS)

Research Consultants

Harutaka SAKAGUCHI (Osaka Univ.)

Yasuyuki SUZUKI (Niigata Univ.)

Kazuko TANABE (Otsuma Women's Univ.)

Senior Visiting Scientist

Hiroyuki SAGAWA (Univ. of Aizu)

Visiting Scientists

Hidetoshi AKIMUNE (Konan Univ.)
 Didier BEAUMEL (CNRS IPN Orsay)
 Konstanze BORETZKY (GSI)
 Christoph CAESAR (GSI)
 Anna CORSI (CEA Saclay)
 Zsolt DOMBRADI (ATOMKI)
 Zoltan ELEKES (ATOMKI)
 Zsolt FULOP (ATOMKI)
 Tatsuya FURUNO (Osaka Univ.)
 Igor GASPARIĆ (Rudjer Boskovic Inst.)
 Zhuang GE (IMP, CAS)
 Alain GILLIBERT (CEA Saclay)
 Valdir GUIMARAES (Inst. de Fisica da Univ. de Sao Paulo)
 Zoltan HALASZ (ATOMKI)
 Matthias HOLL (TRIUMF)
 Kaori KAKI (Shizuoka Univ.)
 Takahiro KAWABATA (Kyoto Univ.)
 Yuma KIKUCHI (NIT, Tokuyama College)
 Yosuke KONDO (Tokyo Tech.)
 Zeren KORKULU (ATOMKI)
 Attila KRASZNAHORKAY (ATOMKI)
 Dorottya KUNNE SOHLER (ATOMKI)
 Istvan KUTI (ATOMKI)
 Valerie LAPOUX (CEA Saclay)
 Yury LITVINOV (GSI)
 Hongna LIU (TU Darmstadt)

Yohei MATSUDA (Tohoku Univ.)
 Kenjiro MIKI (Tohoku Univ.)
 Tetsuaki MORIGUCHI (Tsukuba Univ.)
 Momo MUKAI (Tsukuba Univ.)
 Takashi NAKAMURA (Tokyo Tech.)
 Alexandre OBERTELLI (TU Darmstadt)
 Kazuyuki OGATA (Osaka Univ.)
 Valerii PANIN (CEA Saclay)
 Emanuel POLLACCO (CEA Saclay)
 Kimiko SEKIGUCHI (Tohoku Univ.)
 Haik SIMON (GSI)
 Laszlo STUHL (ATOMKI)
 Baohua SUN (Beihang Univ.)
 Yelei SUN (TU Darmstadt)
 Shinji SUZUKI (Chinese Academy of Sci.)
 Satoru TERASHIMA (Beihang Univ.)
 Hans Toshihide TOERNQVIST (TU Darmstadt)
 Yasuhiro TOGANO (Rikkyo Univ.)
 Takashi WAKUI (QST)
 He WANG (Tokyo Tech.)
 Takayuki YAMAGUCHI (Saitama Univ.)
 Nobuhiro YANAI (Kyushu Univ.)
 Zaihong YANG (Osaka Univ.)
 Juzo ZENIHIRO (Kyoto Univ.)
 Yuhu ZHANG (Chinese Academy of Sci.)

Visiting Technicians

Gilles AUTHÉLET (CEA Saclay)
 Denis CALVET (CEA Saclay)
 Alain DELBART (CEA Saclay)
 Jean-Marc GHELLER (CEA Saclay)
 Arnaud GIGANON (CEA Saclay)

Clement HILAIRE (CEA Saclay)
 Daniel KOERPER (GSI)
 Cedric PERON (CEA Saclay)
 Jean-Yves ROUSSE (CEA Saclay)
 Olivier TELLIER (CEA Saclay)

Student Trainees

Paul E. ANDRE (CEA Saclay)
 Takanobu DOI (Kyoto Univ.)
 Wenbo DOU (Saitama Univ.)
 Naoki EBINA (Tokyo Tech.)
 Shiyo EN'YO (Kyoto Univ.)
 Yuuki FUJII (Tokyo Tech.)
 Yuki FUJIKAWA (Kyoto Univ.)
 Saiya FUJIWARA (Kyushu Univ.)
 Jian GAO (Peking Univ.)
 Daiki HAMAKAWA (Saitama Univ.)
 Yuya HAMANO (Kyushu Univ.)
 Yuto HIJIKATA (Kyoto Univ.)
 Yuma HIRAI (Kyushu Univ.)
 Shun HOSOI (Saitama Univ.)
 Nancy Anne Paul HUPIN (Univ. of Paris-Saclay)
 Kento INABA (Kyoto Univ.)
 Yasuto INADA (Saitama Univ.)
 Daiki INOMOTO (Kyushu Univ.)
 Minami INOUE (Tohoku Univ.)
 Shunya ISHIDA (Tohoku Univ.)
 Leo KAGESAWA (Tsukuba Univ.)
 Daisuke KAJIKI (Saitama Univ.)
 Hina KASAHARA (Kyushu Univ.)
 Kenta KAWAHARA (Tohoku Univ.)
 Yusuke KAWASHIMA (Kyushu Univ.)

Sho KITAYAMA (Tohoku Univ.)
 Shuhei KIYOTAKE (Univ. of Miyazaki)
 Hironori KOUNO (Kyushu Univ.)
 Taishi KUBO (Kyushu Univ.)
 Atsushi KURIHARA (Tokyo Tech.)
 Hayato KUROSAWA (Tohoku Univ.)
 Christopher LEHR (TU Darmstadt)
 Pengjie LI (The Univ. of Hong Kong)
 Zanetti LORENZO (TU Darmstadt)
 Ryu MAEDA (Tohoku Univ.)
 Riku MATSUMURA (Saitama Univ.)
 Hareru MIKI (Tokyo Tech.)
 Midori MIWA (Saitama Univ.)
 Motoki MURATA (Kyoto Univ.)
 Anna NAKAGAWA (Tohoku Univ.)
 Shinnosuke NAKAI (Tohoku Univ.)
 Mio NISHIMURA (Rikkyo Univ.)
 Toui NISHIMURA (Univ. of Miyazaki)
 Kotaro NONAKA (Univ. of Miyazaki)
 Kyoko NOSAKA (Tohoku Univ.)
 Shintaro OKAMOTO (Kyoto Univ.)
 Su-yeon PARK (Ewha Womans Univ.)
 Atsumi SAITO (Tokyo Tech.)
 Yuko SAITO (Tohoku Univ.)
 Daisuke SAKAI (Tohoku Univ.)

Shigehito SAKAKI (Kyushu Univ.)
 Kosuke SAKANASHI (Osaka Univ.)
 Akane SAKAUE (Kyoto Univ.)
 Mamoru SAKAUE (Saitama Univ.)
 Tetsuro SHIMADA (Tokyo Tech.)
 Dora SZALKAI (Eotvos Lorand Univ.)
 Kohei TAKAHASHI (Tokyo Tech.)
 Yuta UTSUKI (Tohoku Univ.)

Vadim WAGNER (TU Darmstadt)
 Atomu WATANABE (Tohoku Univ.)
 Kohei YAMAMOTO (Tohoku Univ.)
 Shinpei YAMANAGA (Univ. of Miyazaki)
 Akira YASUDA (Tokyo Tech.)
 Kenjiro YOKOTA (Saitama Univ.)
 Yuuki YOSHITOME (Tokyo Tech.)
 Jianwei ZHAO (Beihang Univ.)

Interns

Maruf ALI (Univ. of Surrey)
 Richard CRANE (Univ. of Surrey)

George W. G. W. HUDSON-CHANG (Univ. of Surrey)

Assistants

Emiko ISOGAI
 Asako TAKAHASHI

Yuri TSUBURAI

List of Publications & Presentations

Publications

[Original papers]

- Z. Elekes, Á. Kriepkó, D. Sohler, K. Sieja, K. Ogata, K. Yoshida, P. Doornenbal, A. Obertelli, G. Authelet, H. Baba, D. Calvet, F. Château, A. Corsi, A. Delbart, J. -M. Gheller, A. Gillibert, T. Isobe, V. Lapoux, M. Matsushita, S. Momiyama, T. Motobayashi, H. Otsu, C. Péron, A. Peyaud, E. C. Pollacco, J. -Y. Roussé, H. Sakurai, C. Santamaria, Y. Shiga, S. Takeuchi, R. Taniuchi, T. Uesaka, H. Wang, K. Yoneda, F. Browne, L. X. Chung, Zs. Dombrádi, F. Flavigny, S. Franchoo, F. Giacoppo, A. Gottardo, K. Hadyńska-Klęk, Z. Korkulu, S. Koyama, Y. Kubota, J. Lee, M. Lettmann, C. Louchart, R. Lozeva, K. Matsui, T. Miyazaki, M. Niikura, S. Nishimura, L. Olivier, S. Ota, Z. Patel, E. Sahin, C. Shand, P. -A. Söderström, I. Stefan, D. Steppenbeck, T. Sumikama, D. Suzuki, Zs. Vajta, V. Werner, J. Wu, and Z. Xu, “Nuclear structure of ^{76}Ni from the $(p, 2p)$ reaction,” *Phys. Rev. C* **99**, 014312 (2019).
- A. I. Chilug, V. Panin, D. Tudor, L. Trache, I. C. Stefanescu, A. E. Spiridon, A. Saastamoinen, Z. Halasz, T. Motobayashi, T. Uesaka, K. Yoneda, H. Otsu, “Study of the 9C breakup through NP1412-SAMURAI29R1 experiment,” *AIP Conf. Proc.* **2076**, 060001 (2019).
- Z. H. Yang, F. M. Marqués, N. L. Achouri, D. S. Ahn, T. Aumann, H. Baba, D. Beaumel, M. Böhmer, K. Boretzky, M. Caamaño, S. Chen, N. Chiga, M. L. Cortés, D. Cortina, P. Doornenbal, C. A. Douma, F. Dufter, J. Feng, B. Fernández-Domínguez, Z. Elekes, U. Forsberg, T. Fujino, N. Fukuda, I. Gašparić, Z. Ge, R. Gernhäuser, J. M. Gheller, J. Gibelin, A. Gillibert, B. M. Godoy, Z. Halász, T. Harada, M. N. Harakeh, A. Hirayama, S. W. Huang, N. Inabe, T. Isobe, J. Kahlbow, N. Kalantar-Nayestanaki, D. Kim, S. Kim, M. A. Knösel, T. Kobayashi, Y. Kondo, P. Koseoglou, Y. Kubota, I. Kuti, C. Lehr, P. J. Li, Y. Liu, Y. Maeda, S. Masuoka, M. Matsumoto, J. Mayer, H. Miki, M. Miwa, I. Murray, T. Nakamura, A. Obertelli, N. Orr, H. Otsu, V. Panin, S. Park, M. Parlog, S. Paschalis, M. Potlog, S. Reichert, A. Revel, D. Rossi, A. Saito, M. Sasano, H. Sato, H. Scheit, F. Schindler, T. Shimada, Y. Shimizu, S. Shimoura, I. Stefan, S. Storck, L. Stuhl, H. Suzuki, D. Symochko, H. Takeda, S. Takeuchi, J. Tanaka, Y. Togano, T. Tomai, H. T. Törnqvist, J. Tscheuschner, T. Uesaka, V. Wagner, K. Wimmer, H. Yamada, B. Yang, L. Yang, Y. Yasuda, K. Yoneda, L. Zanetti, and J. Zenihiro, “Study of multi-neutron systems with SAMURAI spectrometer,” *Springer Proc. Phys.* **238**, 529–534 (2020).
- V. P. Ladygin, A. V. Averyanov, E. V. Chernykh, D. Enache, Yu. V. Gurchin, A. Yu. Isupov, M. Janek, J. -T. Karachuk, A. N. Khrenov, D. O. Krivenkov, P. K. Kurilkin, N. B. Ladygina, A. N. Livanov, O. Mezhenka, S. M. Piyadin, S. G. Reznikov, Ya. T. Skhomenko, A. A. Terekhin, A. V. Tishevsky, and T. Uesaka (DSS Collaboration), “Energy dependence of the vector A_y and tensor A_{yy} and A_{xx} analyzing powers in deuteron-proton elastic scattering at large scattering angles,” *EPJ Web of Conferences* **204**, 01019 (2019).
- O. Mezhenka, A. V. Averyanov, E. V. Chernykh, D. Enache, Yu. V. Gurchin, A. Yu. Isupov, M. Janek, J. -T. Karachuk, A. N. Khrenov, D. O. Krivenkov, P. K. Kurilkin, V. P. Ladygin, N. B. Ladygina, A. N. Livanov, S. M. Piyadin, S. G. Reznikov, Ya. T. Skhomenko, A. A. Terekhin, A. V. Tishevsky, T. Uesaka, and J. Urban (DSS Collaboration), “Study of the deuteron analyzing powers in dp elastic scattering at the energy of 800 MeV,” *EPJ Web Conf.* **204** (2019) 10001(2019).
- N. Paul, A. Obertelli, C. A. Bertulani, A. Corsi, P. Doornenbal, J. L. Rodriguez-Sanchez, G. Authelet, H. Baba, D. Calvet, F. Château, S. Chen, A. Delbart, J. -M. Gheller, A. Giganon, A. Gillibert, T. Isobe, V. Lapoux, M. Matsushita, S. Momiyama, T. Motobayashi, M. Niikura, H. Otsu, C. Péron, A. Peyaud, E. C. Pollacco, J. -Y. Roussé, H. Sakurai, C. Santamaria, M. Sasano, Y. Shiga, D. Steppenbeck, S. Takeuchi, R. Taniuchi, T. Uesaka, H. Wang, K. Yoneda, T. Ando, T. Arici, A. Blazhev, F. Browne, A. M. Bruce, R. Carroll, L. X. Chung, M. L. Cortés, M. Dewald, B. Ding, Zs. Dombrádi, F. Flavigny, S. Franchoo, F. Giacoppo, M. Górska, A. Gottardo, K. Hadyńska-Klęk, Z. Korkulu, S. Koyama, Y. Kubota, A. Jungclaus, J. Lee, M. Lettmann, B. D. Linh, J. Liu, Z. Liu, C. Lizarazo, C. Louchart, R. Lozeva, K. Matsui, T. Miyazaki, K. Moschner, S. Nagamine, N. Nakatsuka, C. Nita, S. Nishimura, C. R. Nobs, L. Olivier, S. Ota, Z. Patel, Zs. Podolyák, M. Rudigier, E. Sahin, T. Y. Saito, C. Shand, P. -A. Söderström, I. G. Stefan, T. Sumikama, D. Suzuki, R. Orlandi, V. Vaquero, Zs. Vajta, V. Werner, K. Wimmer, J. Wu, and Z. Xu, “Prominence of pairing in inclusive $(p, 2p)$ and (p, pn) cross sections from neutron-rich nuclei,” *Phys. Rev. Lett.* **122**, 162503 (2019).
- X. Xu, M. Wang, K. Blaum, J. D. Holt, Yu. A. Litvinov, A. Schwenk, J. Simonis, S. R. Stroberg, Y. H. Zhang, H. S. Xu, P. Shuai, X. L. Tu, X. H. Zhou, F. R. Xu, G. Audi, R. J. Chen, X. C. Chen, C. Y. Fu, Z. Ge, W. J. Huang, S. Litvinov, D. W. Liu, Y. H. Lam, X. W. Ma, R. S. Mao, A. Ozawa, B. H. Sun, Y. Sun, T. Uesaka, G. Q. Xiao, Y. M. Xing, T. Yamaguchi, Y. Yamaguchi, X. L. Yan, Q. Zeng, H. W. Zhao, T. C. Zhao, W. Zhang, and W. L. Zhan, “Masses of neutron-rich $^{52-54}\text{Sc}$ and $^{54,56}\text{Ti}$ nuclides: The $N = 32$ subshell closure in scandium,” *Phys. Rev. C* **99**, 064303 (2019).

- X. Xu, J. H. Liu, C. X. Yuan, Y. M. Xing, M. Wang, Y. H. Zhang, X. H. Zhou, Yu. A. Litvinov, K. Blaum, R. J. Chen, X. C. Chen, C. Y. Fu, B. S. Gao, J. J. He, S. Kubono, Y. H. Lam, H. F. Li, M. L. Liu, X. W. Ma, P. Shuai, M. Si, M. Z. Sun, X. L. Tu, Q. Wang, H. S. Xu, X. L. Yan, J. C. Yang, Y. J. Yuan, Q. Zeng, P. Zhang, X. Zhou, W. L. Zhan, S. Litvinov, G. Audi, S. Naimi, T. Uesaka, Y. Yamaguchi, T. Yamaguchi, A. Ozawa, B. H. Sun, K. Kaneko, Y. Sun, and F. R. Xu, “Masses of ground and isomeric states of ^{101}In and configuration-dependent shell evolution in odd-A indium isotopes,” *Phys. Rev. C* **100**, 051303 (2019).
- A. Corsi, Y. Kubota, J. Casal, M. Gomez-Ramos, A. M. Moro, G. Authelet, H. Baba, C. Caesar, D. Calvet, A. Delbart, M. Dozono, J. Feng, F. Flavigny, J. -M. Gheller, J. Gibelin, A. Giganon, A. Gillibert, K. Hasegawa, T. Isobe, Y. Kanaya, S. Kawakami, D. Kim, Y. Kiyokawa, M. Kobayashi, N. Kobayashi, T. Kobayashi, Y. Kondo, Z. Korkulu, S. Koyama, V. Lapoux, Y. Maeda, F. M. Marques, T. Motobayashi, T. Miyazaki, T. Nakamura, N. Nakatsuka, Y. Nishio, A. Obertelli, A. Ohkura, N. A. Orr, S. Ota, H. Otsu, T. Ozaki, V. Panin, S. Paschalis, E. C. Pollacco, S. Reichert, J. -Y. Rousse, A. T. Saito, S. Sakaguchi, M. Sako, C. Santamaria, M. Sasano, H. Sato, M. Shikata, Y. Shimizu, Y. Shindo, L. Stuhl, T. Sumikama, Y. L. Sun, M. Tabata, Y. Togano, J. Tsubota, T. Uesaka, Z. H. Yang, J. Yasuda, K. Yoneda, and J. Zenihiro, “Structure of ^{13}Be probed via quasi-free scattering,” *Phys. Lett. B* **797**, 134843 (2019).
- S. Chen, J. Lee, P. Doornenbal, A. Obertelli, C. Barbieri, Y. Chazono, P. Navrátil, K. Ogata, T. Otsuka, F. Raimondi, V. Som’*a*, Y. Utsuno, K. Yoshida, H. Baba, F. Browne, D. Calvet, F. Château, N. Chiga, A. Corsi, M. L. Cortés, A. Delbart, J. -M. Gheller, A. Giganon, A. Gillibert, C. Hilaire, T. Isobe, J. Kahlbow, T. Kobayashi, Y. Kubota, V. Lapoux, H. N. Liu, T. Motobayashi, I. Murray, H. Otsu, V. Panin, N. Paul, W. Rodriguez, H. Sakurai, M. Sasano, D. Steppenbeck, L. Stuhl, Y. L. Sun, Y. Togano, T. Uesaka, K. Wimmer, K. Yoneda, N. Achouri, O. Aktas, T. Aumann, L. X. Chung, F. Flavigny, S. Franchoo, I. Gašparić, R. -B. Gerst, J. Gibelin, K. I. Hahn, D. Kim, T. Koiwai, Y. Kondo, P. Koseoglou, C. Lehr, B. D. Linh, T. Lokotko, M. MacCormick, K. Moschner, T. Nakamura, S. Y. Park, D. Rossi, E. Sahin, D. Sohler, P. -A. Söderström, S. Takeuchi, H. Törnqvist, V. Vaquero, V. Wagner, S. Wang, V. Werner, X. Xu, H. Yamada, D. Yan, Z. Yang, M. Yasuda, and L. Zanetti, “Quasifree neutron knockout from ^{54}Ca corroborates arising $N = 34$ Neutron magic number,” *Phys. Rev. Lett.* **123**, 142501 (2019).
- V. Ladygin, A. Averyanov, E. Chernykh, D. Enache, Y. Gurchin, A. Isupov, M. Janek, J. -T. Karachuk, A. Khrenov, D. Krivenkov, P. Kurilkin, N. Ladygina, A. Livanov, O. Mezhenska, S. Piyadin, S. Reznikov, Y. Skhomenko, A. Terekhin, A. Tishevsky, and T. Uesaka, “Spin studies of the short-range correlations with polarized beams at JINR-nuclotron,” *JPS Conf. Proc.* **26**, 023023 (2019).
- M. L. Cortés, W. Rodriguez, P. Doornenbal, A. Obertelli, J. D. Holt, S. M. Lenzi, J. Menéndez, F. Nowacki, K. Ogata, A. Poves, T. R. Rodríguez, A. Schwenk, J. Simonis, S. R. Stroberg, K. Yoshida, L. Achouri, H. Baba, F. Browne, D. Calvet, F. Château, S. Chen, N. Chiga, A. Corsi, A. Delbart, J. -M. Gheller, A. Giganon, A. Gillibert, C. Hilaire, T. Isobe, T. Kobayashi, Y. Kubota, V. Lapoux, H. N. Liu, T. Motobayashi, I. Murray, H. Otsu, V. Panin, N. Paul, H. Sakurai, M. Sasano, D. Steppenbeck, L. Stuhl, Y. L. Sun, Y. Togano, T. Uesaka, K. Wimmer, K. Yoneda, O. Aktas, T. Aumann, L. X. Chung, F. Flavigny, S. Franchoo, I. Gašparić, R. -B. Gerst, J. Gibelin, K. I. Hahn, D. Kim, T. Koiwai, Y. Kondo, P. Koseoglou, J. Lee, C. Lehr, B. D. Linh, T. Lokotko, M. MacCormick, K. Moschner, T. Nakamura, S. Y. Park, D. Rossi, E. Sahin, D. Sohler, P. -A. Söderström, S. Takeuchi, H. Toernqvist, V. Vaquero, V. Wagner, S. Wang, V. Werner, X. Xu, H. Yamada, D. Yan, Z. Yang, M. Yasuda, L. Zanetti, “Shell evolution of $N = 40$ isotones towards ^{60}Ca : First spectroscopy of ^{62}Ti ,” *Phys. Lett. B* **800**, 135071 (2020).
- H. N. Liu, A. Obertelli, P. Doornenbal, C. A. Bertulani, G. Hagen, J. D. Holt, G. R. Jansen, T. D. Morris, A. Schwenk, R. Stroberg, N. Achouri, H. Baba, F. Browne, D. Calvet, F. Château, S. Chen, N. Chiga, A. Corsi, M. L. Cortés, A. Delbart, J. -M. Gheller, A. Giganon, A. Gillibert, C. Hilaire, T. Isobe, T. Kobayashi, Y. Kubota, V. Lapoux, T. Motobayashi, I. Murray, H. Otsu, V. Panin, N. Paul, W. Rodriguez, H. Sakurai, M. Sasano, D. Steppenbeck, L. Stuhl, Y. L. Sun, Y. Togano, T. Uesaka, K. Wimmer, K. Yoneda, O. Aktas, T. Aumann, L. X. Chung, F. Flavigny, S. Franchoo, I. Gašparić, R. -B. Gerst, J. Gibelin, K. I. Hahn, D. Kim, T. Koiwai, Y. Kondo, P. Koseoglou, J. Lee, C. Lehr, B. D. Linh, T. Lokotko, M. MacCormick, K. Moschner, T. Nakamura, S. Y. Park, D. Rossi, E. Sahin, D. Sohler, P. -A. Söderström, S. Takeuchi, H. Törnqvist, V. Vaquero, V. Wagner, S. Wang, V. Werner, X. Xu, H. Yamada, D. Yan, Z. Yang, M. Yasuda, and L. Zanetti, “How robust is the $N = 34$ subshell closure? first spectroscopy of ^{52}Ar ,” *Phys. Rev. Lett.* **122**, 072502 (2019).
- J. Tanaka, C. Bertulani, and S. Typel, “Post-formation in alpha emission from nuclei,” *EPJ Web Conf.* **227**, 01001 (2020).
- T. Matsumoto, J. Tanaka, and K. Ogata, “Borromean feshbach resonance in ^{11}Li studied via $^{11}\text{Li} (p, p')$,” *Prog. Theor. Exp. Phys.* **12**, 123D02 (2019).
- S. Bagchi, R. Kanungo, W. Horiuchi, G. Hagen, T. D. Morris, S. R. Stroberg, T. Suzuki, F. Ameil, J. Atkinson, Y. Ayyad, D. Cortina-Gil, I. Dillmann, A. Estradé, A. Evdokimov, F. Farinon, H. Geissel, G. Guastalla, R. Janik, S. Kaur, R. Knöbel, J. Kurcewicz, Y. A. Litvinov, M. Marta, M. Mostazo, I. Mukha, C. Nociforo, H. J. Ong, S. Pietri, A. Prochazka, C. Scheidenberger, B. Sitar, P. Strmen, M. Takechi, J. Tanaka, Y. Tanaka, I. Tanihata, S. Terashima, J. Vargas, H. Weick, and J. S. Winfield, “Neutron skin and signature of the $N = 14$ shell gap found from measured proton radii of $^{17-22}\text{N}$,” *Phys. Lett. B* **790**, 251–256 (2019).
- S. Bagchi, R. Kanungo, W. Horiuchi, G. Hagen, T. D. Morris, S. R. Stroberg, T. Suzuki, F. Ameil, J. Atkinson, Y. Ayyad, D. Cortina-Gil, I. Dillmann, A. Estradé, A. Evdokimov, F. Farinon, H. Geissel, G. Guastalla, R. Janik, S. Kaur, R. Knöbel, J. Kurcewicz, Y. Litvinov, M. Marta, M. Mostazo, I. Mukha, C. Nociforo, H. J. Ong, S. Pietri, A. Prochazka, C. Scheidenberger, B. Sitar, P. Strmen, M. Takechi, J. Tanaka, Y. Tanaka, I. Tanihata, S. Terashima, J. Vargas, H. Weick, and J. Stuart Winfield, “Measurement of proton-distribution radii of neutron-rich nitrogen isotopes,” *EPJ Web Conf.* **223**, 01003 (2019).
- H. Kouno, Y. Kawashima, K. Tateishi, T. Uesaka, N. Kimizuka, and N. Yanai, “Non-pentacene polarizing agents with improved air-stability for triplet dynamic nuclear polarization at room temperature,” *J. Phys. Chem. Lett.* **10**, 2208–2213 (2019).
- K. Nishimura, H. Kouno, K. Tateishi, T. Uesaka, K. Ideta, N. Kimizuka, and N. Yanai, “Triplet dynamic nuclear polarization of nanocrystals dispersed in water at room temperature,” *Phys. Chem. Chem. Phys.* **21**, 16408–16412 (2019).
- K. Tateishi, M. Negoro, H. Nonaka, A. Kagawa, S. Sando, S. Wada, M. Kitagawa, and T. Uesaka, “Dynamic nuclear polarization with photo-excited triplet electrons using 6,13-diphenylpentacene,” *Phys. Chem. Chem. Phys.* **21**, 19737–19741 (2019).
- H. Kouno, K. Orihashi, K. Nishimura, Y. Kawashima, K. Tateishi, T. Uesaka, N. Kimizuka, and N. Yanai, “Triplet dynamic nuclear polarization of crystalline ice using water-soluble polarizing agents,” *Chem. Commun.* **56**, 3717–3720 (2020).

- L. Stuhl, M. Sasano, J. Gao, Y. Hirai, K. Yako, T. Wakasa, D. S. Ahn, H. Baba, A. I. Chilug, S. Franchoo, Y. Fujino, N. Fukuda, J. Gibelin, I. S. Hahn, Z. Halasz, T. Harada, M. N. Harakeh, D. Inomoto, T. Isobe, H. Kasahara, D. Kim, G. G. Kiss, T. Kobayashi, Y. Kondo, Z. Korkulu, S. Koyama, Y. Kubota, A. Kurihara, H. N. Liu, M. Matsumoto, S. Michimasa, H. Miki, M. Miwa, T. Motobayashi, T. Nakamura, M. Nishimura, H. Otsu, V. Panin, S. Park, A. T. Saito, H. Sakai, H. Sato, T. Shimada, Y. Shimizu, S. Shimoura, A. Spiridon, I. C. Stefanescu, X. Sun, Y. L. Sun, H. Suzuki, E. Takada, Y. Togano, T. Tomai, L. Trache, D. Tudor, T. Uesaka, H. Yamada, Z. Yang, M. Yasuda, K. Yoneda, K. Yoshida, J. Zenihiro, and N. Zhang, “Study of spin-isospin responses of radioactive nuclei with the background-reduced neutron spectrometer, PANDORA,” *Nucl. Instrum. Methods Phys. Res. B* **463**, 189–194 (2020).
- Y. Kubota, M. Sasano, T. Uesaka, M. Dozono, M. Itoh, S. Kawase, M. Kobayashi, C. S. Lee, H. Matsubara, K. Miki, H. Miya, Y. Ono, S. Ota, K. Sekiguchi, T. Shima, T. Taguchi, T. L. Tang, H. Tokieda, T. Wakasa, T. Wakui, J. Yasuda, and J. Zenihiro, “Development of a neutron detector with a high position resolution at intermediate energies,” *Nucl. Instrum. Methods Phys. Res. A* **914**, 32–41 (2019).

[Books]

- H. Sagawa, N. Yoshida, 「量子コンピュータ」, 量子情報理論 第3版, 1–300 (2019).

[Proceedings]

- T. Yamaguchi, N. Tadano, Y. Abe, M. Amano, Z. Ge, D. Kamioka, T. Moriguchi, D. Nagae, S. Naimi, A. Ozawa, F. Suzuki, S. Suzuki, T. Suzuki, T. Uesaka, M. Wakasugi, K. Wakayama, and Y. Yamaguchi, “Development of a new in-ring beam monitor in the Rare-RI Ring,” *Nucl. Instrum. Methods Phys. Res. B* **463**, 241–243 (2019).

Presentations**[International conferences/workshops]**

- H. Sagawa (invited), “Recent progress on single and double spin-isospin excitations,” Neutrino Nuclear Response 2019 (NNR19), RCNP, Osaka, Japan, May 8–9, 2019.
- H. Sagawa (Oral), “Single and double charge exchange excitations of spin-isospin mode,” Nuclear Structure and Dynamics (NSD2019), Venice, Italy, May 13–17, 2019.
- H. Sagawa (invited), “Three-body model for nuclei near and beyond drip line,” Theoretical Nuclear Physics in Padova, Italy, May 20–21, 2019.
- S. Naimi (Oral), “First mass measurements with the rare-RI ring at RIBF/RIKEN for nuclear astrophysics,” 27th International Nuclear Physics Conference 2019, Glasgow, UK, July 29–August 2, 2019.
- S. Huang, Z. Yang, and M. Marques (poster), “Experimental study of $4n$ with $^8\text{He}(p, 2p)$ reaction,” International Nuclear Physics Conference Glasgow, UK, July 29–August 2, 2019.
- J. Tanaka (invited), “Clear evidence of α clusters in the ground state of heavy nuclei,” The 27th International Nuclear Physics Conference Glasgow, UK, July 29–August 2, 2019.
- S. Naimi, D. Nagae, Y. Abe, Y. Yamaguchi, S. Omika, K. Inomata, H. Arakawa, S. Hosoi, Y. Inada, W. B. Dou, D. Kajiki, K. Nishimuro, T. Kobayashi, T. Yamaguchi, D. Hamakawa, M. Mukai, T. Moriguchi, R. Kagesawa, D. Kamioka, A. Ozawa, F. Suzuki, S. Suzuki, Z. Ge, C. Y. Fu, Q. Wang, M. Wang, S. Ota, S. Michimasa, N. Kitamura, S. Masuoka, D. S. Ahn, H. Suzuki, N. Fukuda, H. Takeda, Y. Shimizu, Yu. A. Litvinov, G. Lorusso, P. Walker, Zs. Podolyk, M. Wakasugi, and T. Uesaka (Poster), “Mass measurement of neutron-rich ^{122}Rh , $^{123,124}\text{Pd}$ and ^{125}Ag nuclides with rare-RI ring at RIBF in RIKEN,” 28th International Nuclear Physics Conference 2019, Glasgow, UK, July 29–August 2, 2019.
- H. Sagawa (Oral), “Single and double charge exchange excitations of spin-isospin mode,” EPJ Web Conf. **223**, 01053 (2019).
- H. Sagawa (invited), “EoS from terrestrial experiments: static and dynamic polarizations of nuclear density+B12,” 9th International Symposium on Nuclear Symmetry Energy (Nusym2019), Da Nang City, Vietnam, September 30–October 4, 2019.
- J. Tanaka (invited), “Direct evidence of α clusters in the ground state of heavy nuclei,” The 4th International Workshop on Quasi-Free Scattering with Radioactive-Ion Beams, October 13–18, 2019.
- T. Uesaka, “Possibility of LOREX at RIBF,” LOREX Workshop, GSI, Germany, December 12–13, 2019.
- H. Sagawa (invited), “Recent topics of single and double phonon spin-isospin excitations,” Vth Topical Workshop on Modern Aspects in Nuclear Structure, Bormio, Italy, February 4–9, 2019.
- S. En'yo, “A large solid hydrogen target for the proton elastic scattering with high intensity RI beams,” CLUSHIQ2020, Beppu, Japan, January 23–24, 2020.

[Domestic conferences/workshops]

- 立石健一郎, 上坂友洋 (招待講演), 「光励起電子スピンをういた動的核偏極—超偏極溶液 NMR に向けて」, 第 58 回 NMR 討論会 (NMR 討論会・SEST 2019 連合大会), 川崎コンベンションホール, 川崎, 2019 年 11 月 7–9 日.
- 高田秀佐, 上坂友洋, 立石健一郎, 吉岡瑞樹, 大竹淑恵, 若林泰生, NOPTREX コラボレーション (口頭発表), 「Triplet-DNP による陽子偏極を利用した中性子スピフィルターの開発—小型中性子源 RANS での性能評価—」, 日本物理学会 2019 年秋季大会, 山形大学, 山形, 2019 年 9 月 17–20 日.
- 松村理久 (ポスター発表), 「核分裂生成核種 Sr-90 の陽子および重陽子誘起反応に関する研究」, 日本物理学会第 75 回年次大会, 名古屋大学, 名古屋, 2020 年 3 月 16–19 日.
- 上坂友洋 (口頭発表), 「超偏極が拓く科学技術～フェムト・テクノロジーの未来に向けて～」, 理研-九大-福岡市-ISIT 連携シンポジウム, 理研和光キャンパス, 和光, 2019 年 5 月 22 日.
- 上坂友洋 (口頭発表), 「Triplet-DNP enhanced NMR is just around the corner」, DSB プロジェクト年次報告会, 理研横浜キャンパス, 鶴見, 2019 年 11 月 13 日.

原田知也 (口頭発表), 「不安定核 ^{132}Sn の逆運動学陽子弾性散乱測定」, 日本物理学会第 75 回年次大会, 名古屋大学, 名古屋, 2020 年 3 月 16–19 日.

延與紫世 (口頭発表), 「大強度 RI ビーム実験のための固体水素標的の開発」, 日本物理学会第 75 回年次大会, 名古屋大学, 名古屋, 2020 年 3 月 16–19 日.

土方佑斗 (口頭発表), 「大強度不安定核ビームの粒子識別のための Xe ガス検出器の開発」, 日本物理学会第 75 回年次大会, 名古屋大学, 名古屋, 2020 年 3 月 16–19 日.

[Seminar]

上坂友洋 (口頭発表), 「核物質の多様性」, 物理学第二教室原子核ハドロン研究室セミナー京都大学, 京都, 2019 年 11 月 29 日.

Nuclear Science and Transmutation Research Division

Nuclear Spectroscopy Laboratory

1. Abstract

The research group has conducted nuclear-physics studies utilizing stopped/slowed-down radioactive-isotope (RI) beams mainly at the RIBF facility. These studies are based on the technique of nuclear spectroscopy such as β -ray-detected NMR (β -NMR), γ -PAD (Perturbed Angular Distribution), laser, and Mössbauer among other methods that takes advantage of intrinsic nuclear properties such as nuclear spins, electromagnetic moments, and decay modes. In particular, techniques and devices for the production of spin-controlled RI beams have been developed and combined to the spectroscopic studies, which enable high-sensitivity measurements of spin precessions/resonances through a change in the angular distribution of radiations. Anomalous nuclear structures and properties of far unstable nuclei are investigated from thus determined spin-related observables. The group also aims to apply such techniques to interdisciplinary fields such as fundamental physics and materials science by exploiting nuclear probes.

2. Major Research Subjects

- (1) Nuclear spectroscopy utilizing spin-oriented fast RI beams
- (2) Nuclear/Atomic laser spectroscopy & SLOWRI R&D
- (3) Application of RI probes to materials science
- (4) Fundamental physics: Study of symmetry

3. Summary of Research Activity

(1) Nuclear spectroscopy utilizing spin-oriented fast RI beams

Measurements of static electromagnetic nuclear moments over a substantial region of the nuclear chart have been conducted for structure studies on the nuclei far from the β -decay stability. Utilizing nuclear spin orientation phenomena of RIs created in the projectile-fragmentation reaction, ground- and excited-state electromagnetic nuclear moments been determined by means of the β -ray-detected nuclear magnetic resonance (β -NMR) and the γ -ray time differential perturbed angular distribution (γ -TDPAD) methods. In particular, a new method developed for controlling spin in a system of rare RIs, taking advantage of the mechanism of the two-step projectile fragmentation reaction combined with the momentum-dispersion matching technique, has been developed and employed making fully use of world's highest intensity rare RIBs delivered from BigRIPS for rare isotopes.

(2) Nuclear/Atomic laser spectroscopy & SLOWRI R&D

The group has been conducting system development for nuclear laser spectroscopy from the following two approaches in order to realize experiments for rare isotopes at RIBF. One is collinear laser spectroscopy for a large variety of elements using slowed-down RI beams produced via a projectile-fragmentation reaction, which can be achieved only by the universal low-energy RI-beam delivery system, SLOWRI, under installation in collaboration with the SLOWRI Team. This slowed-down RI-beam scheme enables to perform high-precision laser spectroscopy even with fast-fragmentation-based RIBs without the elemental limitation problematic in the ISOL-based RIBs.

The other approach is a new method utilizing superfluid helium (He II) as a stopping medium of energetic RI beams, in which the characteristic atomic properties of ions surrounded by superfluid helium enables us to perform unique nuclear laser spectroscopy. RI ions trapped in He II are known to exhibit a characteristic excitation spectrum significantly blue-shifted compared with the emission one. Consequently, the background derived from the excitation-laser stray light, which often causes serious problems in measurements, can be drastically reduced.

(3) Application of RI probes to materials science

The application of RI and heavy ion beams as a probe for condensed matter studies is also conducted by the group. The microscopic material dynamics and properties have been investigated through the deduced internal local fields and the spin relaxation of RI probes based on various spectroscopies utilizing RI probes such as β -NMR/NQR spectroscopy, Mössbauer spectroscopy, the γ -ray time differential perturbed angular correlation (γ -TDPAC) spectroscopy. Furthermore, studies on the control of electrical conductivity of diamond by boron and nitrogen implantation are ongoing.

Provided that highly spin-polarized RI probes are produced independently of their element properties and doped into a substance as an impurity, the constituent particle of the substance can be substituted by the same element RI probe without changing the material structure. This scheme provides a new opportunity for materials-science researches, but a key technology, production of element-independent highly spin-polarized RI beams, has not yet been achieved. In this subject, the group has conducted R&D studies to realize an ultra-slow & highly-spin-polarized RI beams, based on the technique of the atomic beam resonance.

(4) Fundamental physics: Study of symmetry

The nuclear spins of stable and unstable isotopes sometimes play important roles in fundamental physics research. New experimental methods and devices have been developed for studies of the violation of time reversal symmetry (T-violation) using spin-polarized nuclei. These experiments aim to detect the small frequency shift in the spin precession arising from new mechanisms beyond the Standard Model.

Members

Director

Hideki UENO

Research/Technical Scientists

Hiroki YAMAZAKI (Senior Research Scientist)

Yuichi ICHIKAWA (Senior Research Scientist)

Aiko TAKAMINE (Research Scientist)

Research & Development Scientist

Tetsu SONODA

Special Postdoctoral Researcher

Hiroki NISHIBATA

Postdoctoral Researcher

Minori TAJIMA

Research Associate

Aleksey GLADKOV

Junior Research Associate

Keita KAWATA (Univ. of Tokyo)

Senior Visiting Scientists

Yukari MATSUO (Hosei Univ.)

Hideyuki SAKAI (Univ. of Tokyo)

Takaharu OTSUKA (Univ. of Tokyo)

Visiting Scientists

Dimiter Loukanov BALABANSKI (IHIN)

Georgi GEORGIEV (CNRS-IN2P3)

Kei IMAMURA (Okayama Univ.)

Yoko ISHIBASHI (Tohoku Univ.)

Yoshio KOBAYASHI (Univ. of Electro-Commun.)

Kenya KUBO (Int'l Christian Univ.)

Kensaku MATSUTA (Osaka Univ.)

Jun MIYAZAKI (Hokuriku Univ.)

Takamasa MOMOSE (The Univ. of British Columbia)

Jiro MURATA (Rikkyo Univ.)

Jin NAKAMURA (Univ. of Electro-Commun.)

Hiroki NISHIBATA (Kyushu Univ.)

Naoki NISHIDA (Tokyo Univ. Sci)

Tomoya SATO (Tokyo Tech)

Wataru SATO (Kanazawa Univ.)

Andrew E. STUCHBERY (The Australian Nat'l Univ.)

Satoshi TSUTSUI (Japan Synchrotron Radiation Res. Inst.)

Yasuhiro YAMADA (Tokyo Univ. Sci)

Deyan T. YORDANOV (Inst. de Phys.Nucl. d'Orsay)

Akihiro YOSHIMI (Okayama Univ.)

Student Trainees

Shota AMAGASA (Tokyo Univ. Sci)

Takumi ASAKAWA (Hosei Univ.)

Kazuho DOI (Hosei Univ.)

Miru DOI (Hosei Univ.)

Takumi FUNABASHI (Tokyo Univ. Sci)

Timothy J. GRAY (The Australian Nat'l Univ.)

Kentaro HAMANO (Univ. of Electro-Commun.)

Kazuki HAMAZAKI (Tokyo Univ. Sci)

Kyouichi IZUOKA (Tokyo Univ. Sci)

Masato KII (Univ. of Electro-Commun.)

Naoki KOSHIKAWA (Tokyo Univ. Sci)

Masaki NISHIMURA (Hosei Univ.)

Shinichi OKAMURA (Univ. of Ferrara)

David PELLETIER (ENSICAEN)

Yusuke SASAKI (Hosei Univ.)

Ryo TAKEMURA (Tokyo Univ. Sci)

Yuika TAKEUCHI (Hosei Univ.)

Kenta TSUBURA (Hosei Univ.)

Tomoaki YADA (Hosei Univ.)

Takumi YAMAMOTO (Hosei Univ.)

Fumiya YOKOSUKA (Aoyama Gakuin Univ.)

Interns

Chengyu GUO (Peking Univ.)

Chan HEO (The Univ. of Hong Kong)

Meng Chit HO (The Univ. of Hong Kong)

Ziyao HU (Peking Univ.)

Min Young KIM (Seoul Nat'l Univ.)

Minju KUM (Seoul Nat'l Univ.)

Euijoon KWON (Seoul Nat'l Univ.)

Joo Hyun LEE (Seoul Nat'l Univ.)

Pak Yi LI (The Univ. of Hong Kong)

Fumiya OURA (Tohoku Univ.)

Shoko TAKESHIGE (Rikkyo Univ.)

Masashi TAWARA (Rikkyo Univ.)

Hao WANG (Peking Univ.)

Sau Hei WONG (The Univ. of Hong Kong)

Seungbum WOO (Seoul Nat'l Univ.)

Lisheng YANG (Peking Univ.)

Ryan W. YEUNG (The Univ. of Hong Kong)

Zhenxiang ZHOU (Peking Univ.)

Temporary Staffing

Emiko FUJINO

Naoko YUASA

Assistant

Izumi YOSHIDA

List of Publications & Presentations**Publications****[Original papers]**

- M. Tajima, N. Kuroda, C. Amsler, H. Breuker, C. Evans, M. Fleck, A. Gligorova, H. Higaki, Y. Kanai, B. Kolbinger, A. Lanz, M. Leali, V. Mäkel, C. Malbrunot, V. Mascagna, Y. Matsuda, D. Murtagh, Y. Nagata, A. Nanda, B. Radics, M. Simon, S. Ulmer, L. Venturelli, E. Widmann, M. Wiesinger, and Y. Yamazaki, “Antiproton beams with low energy spread for antihydrogen production,” *J. Instrum.* **14**, P05009 (2019).
- L. C. Tao, Y. Ichikawa, C. X. Yuan, Y. Ishibashi, A. Takamine, A. Gladkov, T. Fujita, K. Asahi, T. Egami, C. Funayama, K. Imamura, J. L. Lou, T. Kawaguchi, S. Kojima, T. Nishizaka, T. Sato, D. Tominaga, X. F. Yang, H. Yamazaki, Y. L. Ye, H. Ueno, Y. Yanagisawa, and K. Yoshida, “Negative parity states in ^{39}Cl configured by crossing major shell orbits,” *Chin. Phys. Lett.* **36**, 062101-1–4 (2019).
- D. S. Ahn, N. Fukuda, H. Geissel, N. Inabe, N. Iwasa, T. Kubo, K. Kusaka, D. J. Morrissey, D. Murai, T. Nakamura, M. Ohtake, H. Otsu, H. Sato, B. M. Sherrill, Y. Shimizu, H. Suzuki, H. Takeda, O. B. Tarasov, H. Ueno, Y. Yanagisawa, and K. Yoshida, “Location of the neutron dripline at fluorine and neon,” *Phys. Rev. Lett.* **123**, 212501-1–6 (2019). [Featured in Physics] [Editors’ Suggestion]
- S. Tsutsui, M. Mizumaki, and Y. Kobayashi, “Electronic and atomic dynamics in Sm and Eu cage-structured intermetallics,” *Hyperfine Interact.* **240**, 84-1–16 (2019).
- T. Funabashi, Y. Kobayashi, and Y. Yamada, “Metastable iron carbide thin films produced by pulsed laser deposition of iron in methane atmosphere,” *Hyperfine Interact.* **240**, 121-1–8 (2019).
- F. Boulay, G. S. Simpson, Y. Ichikawa, S. Kisyov, D. Bucurescu, A. Takamine, D. S. Ahn, K. Asahi, H. Baba, D. L. Balabanski, T. Egami, T. Fujita, N. Fukuda, C. Funayama, T. Furukawa, G. Georgiev, A. Gladkov, M. Hass, K. Imamura, N. Inabe, Y. Ishibashi, T. Kawaguchi, T. Kawamura, W. Kim, Y. Kobayashi, S. Kojima, A. Kusoglu, R. Lozeva, S. Momiyama, I. Mukul, M. Niikura, H. Nishibata, T. Nishizaka, A. Odahara, Y. Ohtomo, D. Ralet, T. Sato, Y. Shimizu, T. Sumikama, H. Suzuki, H. Takeda, L. C. Tao, Y. Togano, D. Tominaga, H. Ueno, H. Yamazaki, X. F. Yang, and J. M. Daugas, “ g -Factor of the ^{99}Zr ($7/2^+$) isomer: Monopole evolution in shape coexisting region,” *Phys. Rev. Lett.* **124**, 112501-1–6 (2020).
- K. Hamazaki, Y. Kobayashi, and Y. Yamada, “Iron nitride films produced by arc deposition of iron in a nitrogen atmosphere,” *Hyperfine Interact.* **241**, 4-1–10 (2020).
- Y. Yamada, Y. Sato, Y. Kobayashi, T. Ando, N. Takahama, K. Some, M. Sato, M. Mihara, M. K. Kubo, W. Sato, J. Miyazaki, T. Nagatomo, J. Kobayashi, A. Okazawa, S. Sato, and A. Kitagawa, “In-beam Mössbauer spectra for ^{57}Mn implanted sulfur hexafluoride,” *Hyperfine Interact.* **241**, 15-1–15 (2020).
- T. Otsuka, Y. Tsunoda, T. Abe, N. Shimizu, and P. Van Duppen, “Underlying structure of collective bands and self-organization in quantum systems,” *Phys. Rev. Lett.* **123**, 222502 (2019).
- S. Sels, T. Day Goodacre, B. A. Marsh, A. Pastore, W. Ryssens, Y. Tsunoda, N. Althubiti, B. Andel, A. N. Andreyev, D. Atanasov, A. E. Barzakh, M. Bender, J. Billowes, K. Blaum, T. E. Cocolios, J. G. Cubiss, J. Dobaczewski, G. J. Farooq-Smith, D. V. Fedorov, V. N. Fedosseev, K. T. Flanagan, L. P. Gaffney, L. Ghys, P.-H. Heenen, M. Huyse, S. Kreim, D. Lunney, K. M. Lynch, V. Manea, Y. Martinez Palenzuela, T. M. Medonca, P. L. Molkanov, T. Otsuka, J. P. Ramos, R. E. Rossel, S. Rothe, L. Schweikhard, M. D. Seliverstov, P. Spagnoletti, C. Van Beveren, P. Van Duppen, M. Veinhard, E. Verstraelen, A. Welker, K. Wendt, F. Wienholtz, R. N. Wolf, and A. Zadvornaya, “Shape staggering of mid-shell mercury isotopes from in-source laser spectroscopy compared with density functional theory and Monte Carlo shell model calculations,” *Phys. Rev. C* **99**, 044306 (2019).
- F. Flavigny, J. Elseviers, A. N. Andreyev, C. Bauer, V. Bildstein, A. Blazhev, B. A. Brown, H. De Witte, J. Diriken, V. N. Fedosseev, S. Franchoo, R. Gernhäuser, M. Huyse, S. Ilieva, S. Klupp, Th. Kröll, R. Lutter, B. A. Marsh, D. Mücher, K. Nowak, T. Otsuka, J. Pakarinen, N. Patronis, R. Raabe, F. Recchia, P. Reiter, T. Roger, S. Sambi, M. Seidlitz, M. D. Seliverstov, B. Siebeck, Y. Tsunoda, P. Van Duppen, M. Vermeulen, M. Von Schmid, D. Voulot, N. Warr, F. Wenander, and K. Wimmer, “Microscopic structure of coexisting 0^+ states in ^{68}Ni probed via two-neutron transfer,” *Phys. Rev. C* **99**, 054332 (2019).
- L. Xie, X. F. Yang, C. Wraith, C. Babcock, J. Bieroń, J. Billowes, M. L. Bissell, K. Blaum, B. Cheal, L. Filippin, K. T. Flanagan, R. F. Garcia Ruiz, W. Gins, G. Gaigalas, M. Godefroid, C. Gorges, L. K. Grob, H. Heylen, P. Jönsson, S. Kaufmann, M. Kowalska, J. Krämer, S. Malbrunot-Ettenauer, R. Neugart, G. Neyens, W. Nörtershäuser, T. Otsuka, J. Papuga, R. Sánchez, Y. Tsunoda, and D. T. Yordanov, “Nuclear charge radii of $^{62-80}\text{Zn}$ and their dependence on cross-shell proton excitations,” *Phys. Lett. B* **797**, 134805 (2019).
- C. Hornung, D. Amanbayev, I. Dedes, G. Kripko-Koncz, I. Miskun, N. Shimizu, S. Ayet San Andrés, J. Bergmann, T. Dickel, J. Dudek, J. Ebert, H. Geissel, M. Górska, H. Grawe, F. Greiner, E. Haettner, T. Otsuka, W. R. Plaß, S. Purushothaman, A.-K. Rink, C. Scheidenberger, H. Weick, S. Bagchi, A. Blazhev, O. Charviakova, D. Curien, A. Finlay, S. Kaur, W. Lippert, J.-H. Otto, Z. Patyk, S. Pietri, Y. K. Tanaka, Y. Tsunoda, and J. S. Winfield, “Isomer studies in the vicinity of the doubly-magic nucleus ^{100}Sn : Observation of a new low-lying isomeric state in ^{97}Ag ,” *Phys. Lett. B* **802**, 135200 (2019).
- T. Otsuka, A. Gade, O. Sorlin, T. Suzuki, and Y. Utsuno, “Evolution of shell structure in exotic nuclei,” *Rev. Mod. Phys.* **92**, 015002 (2020).
- T. Miyagi, T. Abe, M. Kohno, P. Navratil, R. Okamoto, T. Otsuka, N. Shimizu, and S. R. Stroberg, “Ground-state properties of doubly magic nuclei from the unitary-model-operator approach with the chiral two- and three-nucleon forces,” *Phys. Rev. C* **100**, 034310

(2019).

- B. Abromeit, V. Tripathi, H. L. Crawford, S. N. Liddick, Y. Utsuno, P. C. Bender, B. P. Crider, R. Dungan, P. Fallon, K. Kravvaris, N. Larson, R. S. Lubna, A. O. Macchiavelli, T. Otsuka, C. J. Prokop, A. L. Richard, N. Shimizu, S. L. Tabor, A. Volya, and S. Yoshida, “Beta decay of $T_z = +11/2$ isotopes ^{37}Al and ^{39}Si understanding Gamow Teller strength distribution in neutron rich nuclei,” *Phys. Rev. C* **100**, 014323 (2019).
- A. Matta, W. N. Catford, N. A. Orr, J. Henderson, P. Ruotsalainen, G. Hackman, A. B. Garnsworthy, F. Delaunay, R. Wilkinson, G. Lotay, N. Tsunoda, T. Otsuka, A. J. Knapton, G. C. Ball, N. Bernier, C. Burbadge, A. Chester, D. S. Cross, S. Cruz, C. Aa. Diget, T. Domingo, T. E. Drake, L. J. Evitts, F. H. Garcia, S. Hallam, E. MacConnachie, M. Moukaddam, D. Muecher, E. Padilla-Rodal, O. Paetkau, J. Park, J. L. Pore, U. Rizwan, J. Smallcombe, J. K. Smith, K. Starosta, C. E. Svensson, J. Williams, and M. Williams, “Shell evolution approaching the $N = 20$ island of inversion: Structure of ^{29}Mg ,” *Phys. Rev. C* **99**, 044320 (2019).
- Y. L. Sun, A. Obertelli, P. Doornenbal, C. Barbieri, Y. Chazono, T. Duguet, H. N. Liu, P. Navrátil, F. Nowacki, K. Ogata, T. Otsuka, F. Raimondi, V. Somà, Y. Utsuno, K. Yoshida, N. Achouri, H. Baba, F. Browne, D. Calvet, F. Château, S. Chen, N. Chiga, A. Corsi, M. L. Cortés, A. Delbart, J. -M. Gheller, A. Giganon, A. Gillibert, C. Hilaire, T. Isobe, T. Kobayashi, Y. Kubota, V. Lapoux, T. Motobayashi, I. Murray, H. Otsu, V. Panin, N. Paul, W. Rodriguez, H. Sakurai, M. Sasano, D. Steppenbeck, L. Stuhl, Y. Togano, T. Uesaka, K. Wimmer, K. Yoneda, O. Aktas, T. Aumann, L. X. Chung, F. Flavigny, S. Franchoo, I. Gašparić, R. -B. Gerst, J. Gibelin, K. I. Hahn, D. Kim, T. Koiwai, Y. Kondo, P. Koseoglou, J. Lee, C. Lehr, B. D. Linh, T. Lokotko, M. MacCormick, K. Moschner, T. Nakamura, S. Y. Park, D. Rossi, E. Sahin, D. Sohler, P. -A. Söderström, S. Takeuchi, H. Törnqvist, V. Vaquero, V. Wagner, S. Wang, V. Werner, X. Xu, H. Yamada, D. Yan, Z. Yang, M. Yasuda, and L. Zanetti, “Restoration of the natural $E(1/2_1^+) - E(3/2_1^+)$ energy splitting in odd- k isotopes towards $N = 40$,” *Phys. Lett. B* **802**, 135215 (2020).
- S. Chen, J. Lee, P. Doornenbal, A. Obertelli, C. Barbieri, Y. Chazono, P. Navrátil, K. Ogata, T. Otsuka, F. Raimondi, V. Somà, Y. Utsuno, K. Yoshida, H. Baba, F. Browne, D. Calvet, F. Château, N. Chiga, A. Corsi, M. L. Cortés, A. Delbart, J.-M. Gheller, A. Giganon, A. Gillibert, C. Hilaire, T. Isobe, J. Kahlbow, T. Kobayashi, Y. Kubota, V. Lapoux, H. N. Liu, T. Motobayashi, I. Murray, H. Otsu, V. Panin, N. Paul, W. Rodriguez, H. Sakurai, M. Sasano, D. Steppenbeck, L. Stuhl, Y. L. Sun, Y. Togano, T. Uesaka, K. Wimmer, K. Yoneda, N. Achouri, O. Aktas, T. Aumann, L. X. Chung, F. Flavigny, S. Franchoo, I. Gašparić, R.-B. Gerst, J. Gibelin, K. I. Hahn, D. Kim, T. Koiwai, Y. Kondo, P. Koseoglou, C. Lehr, B. D. Linh, T. Lokotko, M. MacCormick, K. Moschner, T. Nakamura, S. Y. Park, D. Rossi, E. Sahin, D. Sohler, P.-A. Söderström, S. Takeuchi, H. Törnqvist, V. Vaquero, V. Wagner, S. Wang, V. Werner, X. Xu, H. Yamada, D. Yan, Z. Yang, M. Yasuda, and L. Zanetti, “Quasifree neutron knockout from corroborates arising neutron magic number,” *Phys. Rev. Lett.* **123**, 142501 (2020).
- F. Diel, Y. Fujita, H. Fujita, F. Cappuzzello, E. Ganioglu, E.-W. Grewe, T. Hashimoto, K. Hatanaka, M. Honma, T. Itoh, J. Jolie, B. Liu, T. Otsuka, K. Takahisa, G. Susoy, B. Rubio, and A. Tamii, “High-resolution study of the Gamow-Teller (GT-) strength in the $^{60}\text{Zn}(^3\text{He}, t)^{64}\text{Ge}$ reaction,” *Phys. Rev. C* **99**, 054322 (2019).

[Review article]

- Y. Ichikawa, “Nuclear shell evolution with shape deformation—Structure of exotic nuclei investigated by the magnetic moment—(「変形しながら殻進化—磁気モーメントで探るエキゾチック核の『中身』」),” *Isotope News* **765**, 26–29 (2019).

Presentations

[International conferences/workshops]

- H. Ueno (invited), “Nuclear-physics research based on RI spin orientation technique,” XXXVI Mazurian Lakes Conference on Physics, Piaski, Poland, September 1–7, 2019.
- A. Takamine (invited), “Recent progress in the development of gas cells, SHE results combining GARIS with GASCELL+MRTOF,” Expert Meeting on Next-Generation Fragment Separators 2019, Darmstadt, Germany, September 30–October 3, 2019.
- Y. Ichikawa (invited), “Magnetic-moment measurement of exotic nuclei using spin-oriented RI beams at RIBF,” 14th Asia-Pacific Physics Conference (APPC 2019), Sarawak, Malaysia, November 17–22, 2019.
- T. Otsuka (invited), “Self-organization of quantum systems and the structure of heavy nuclei,” Workshop Physics between lead and uranium: In preparation of new experimental campaigns at ISOLDE, Leuven, Belgium, April 16–18, 2019.
- T. Otsuka (invited), “Alpha clustering in nuclei and the shell model,” Theoretical Nuclear Physics in Padova: A Meeting in Honor of Prof. Andrea Vitturi, Padova, Italy, May 20–21 2019.
- T. Otsuka (invited), “Self-organization in nuclear structure and its impact to heavy nuclei—A challenge to Bohr-Mottelson’s picture and a future prospect—,” LXIX International Conference on Nuclear Spectroscopy and Nuclear Structure “Fundamental Problems of Nuclear Physics, Nuclei at Borders of Nucleon Stability, High Technologies,” (Nucleus-2019), Dubna, Russia, July 1–5, 2019.
- T. Otsuka (invited), “Nuclear matrix elements with advanced shell model methods,” Workshop on Progress and Challenges in Neutrinoless Double Beta Decay, Trento, Italy, July 15–19, 2019.
- T. Otsuka (invited), “Ab initio studies on the drip line of the Island-of-Inversion nuclei,” Workshop on Ab initio Nuclear Theory from Breakthroughs to Applications, Guildford, UK, July 24–26, 2019.
- T. Otsuka (oral), “Self-organization in atomic nuclei and nuclear collectivity,” 27th International Nuclear Physics Conference (INPC 2019), Glasgow, UK, July 29–August 2, 2019.
- T. Otsuka (invited), “Precision nuclear structure via the Monte-Carlo shell model,” ESNT Workshop Laser Spectroscopy as a Tool for Nuclear Theories, Saclay, France, October 7–11, 2019.
- T. Otsuka (invited), “Evolution of shape and shell of atomic nuclei and the self-organization,” 2XVII International Meeting on “Selected topics in nuclear and atomic physics,” Fiera di Primiero, Italy, September 30–October 4, 2019.
- T. Otsuka (invited), “Olaf gets into shapes,” Symposium on “Particles, photons, and fields: Messengers of violent events from the nucleus,

through the sky, to the cosmos,” Groningen, the Netherlands, November 21, 2019.

- T. Otsuka (invited), “Self-organization of quantum systems and nuclear collectivity,” International Symposium on Clustering as a Window on the Hierarchical Structure of Quantum Systems (CLUSHIQ2020), Beppu, Japan, January 23–24, 2020.
- T. Otsuka (invited), “Self-organization in nuclear collective bands,” Fifth Topical Workshops on Modern Aspects of Nuclear Structure, Bormio, Italy, February 4–9, 2020.
- T. Otsuka (invited), “Nuclear matrix elements of neutrinoless double beta decay calculated by Monte Carlo shell model for ^{76}Ge and ^{136}Xe ,” International Conference on Neutrino and Nuclear Physics 2020 (CNNP2020), Cape Town, South Africa, February 24–28, 2020.
- T. Otsuka (invited), “Structure of F-Ne-Na-Mg isotopes and new mechanism of driplines,” Workshop on Progress in Ab Initio Techniques in Nuclear Physics, Vancouver, Canada, March 3–6, 2020.

[Domestic conferences/workshops]

- 市川雄一, 「原子核励起状態の磁気モーメント測定」, 2019 年度「物質階層原理研究」 & 「ヘテロ界面研究」合同春合宿, 御殿場, 2019 年 5 月 10–11 日.
- 上野秀樹, “Highly Spin-polarized RI beams and the application to nuclear and condensed-matter physics,” 新学術領域「宇宙観測検出器と量子ビームの出会い。新たな応用への架け橋。」第 1 回領域全体会議, 東京大学 Kavli IPMU, 柏市, 2019 年 7 月 15–16 日.
- 高峰愛子, “Development of an RF ion guide gas cell for universal ultra slow RI beams,” 新学術領域「宇宙観測検出器と量子ビームの出会い。新たな応用への架け橋。」第 1 回領域全体会議, 東京大学 Kavli IPMU, 柏, 2019 年 7 月 15–16 日.
- 今井康貴, 藤枝亮, 植竹智, 笹尾登, 吉村太彦, 吉村浩司, 吉見彰洋, 宮本祐樹, 増田孝彦, 原秀明, 今村慧, 上垣外修一, 中川孝秀, 金井保之, 市川雄一, 長友傑, 本田洋介, 坂上和之, 「量子イオンビーム (QIB) 分光に向けた Yb ドープファイバーを用いた 987 nm 光の増幅」, 日本物理学会 2019 年秋季大会, 岐阜大学柳戸キャンパス, 岐阜, 2019 年 9 月 10–13 日.
- 今井伸明, 堂園昌伯, 道正新一郎, 炭竈聡之, 大田晋輔, J. W. Hwang, 岩本ちひろ, 川瀬頌一郎, 川田敬太, 北村徳隆, 増岡翔一郎, 中野敬太, P. Schrock, 鈴木大介, 角田理恵子, K. Wimmer, for ImPACT17-02-02 collaboration, 「逆運動学 $^{79}\text{Se}(d, p)$ 反応による中性子捕獲反応断面積の評価」, 日本物理学会 2019 年秋季大会, 山形大学小白川キャンパス, 山形, 2019 年 9 月 17–20 日.
- 川田敬太, 大田晋輔, 堂園昌伯, 銭廣十三, 岩本ちひろ, 北村徳隆, 酒井英行, 笹野匡紀, 増岡翔一郎, 道正新一郎, 横山輪, 矢向謙太郎, Laszlo STUHL, 坂口治隆, 原田知也, 寺嶋知, 西畑洗希, 角田理恵子, 今井伸明, Ningtao Zhang, Jongwon Hwang, 遠藤史隆, 「入射核破砕反応による ^{52}Fe 周辺核の高スピンアイソマーの生成」, 日本物理学会 2019 年秋季大会, 山形大学小白川キャンパス, 山形, 2019 年 9 月 17–20 日.
- 庭瀬暁隆, 和田道治, P. Schury, 伊藤由太, 木村創太, 加治大哉, M. Rosenbusch, 渡辺裕, 平山賀一, 宮武宇也, J. Y. Moon, 石山博恒, 森本幸司, 羽場宏光, 田中泰貴, 石澤倫, 高峰愛子, 森田浩介, H. Wollnik, 「MRTOF-MS を用いた ^{207}Ra の精密質量—崩壊特性測定」, 日本物理学会 2019 年秋季大会, 山形大学小白川キャンパス, 山形, 2019 年 9 月 17–20 日.
- 宇都野穰, 市川隆敏, 清水則孝, 大塚孝治, 「 ^{42}Ca における非軸対称超変形状態と多重変形共存」, 日本物理学会 2019 年秋季大会, 山形大学小白川キャンパス, 山形, 2019 年 9 月 17–20 日.
- 角田佑介, 大塚孝治, 清水則孝, 「モンテカルロ殻模型による Sm 同位体の形状変化の研究」, 日本物理学会 2019 年秋季大会, 山形大学小白川キャンパス, 山形, 2019 年 9 月 17–20 日.
- 阿部喬, P. Maris, 大塚孝治, 清水則孝, 角田佑介, 宇都野穰, J. P. Vary, 吉田亨, 「モンテカルロ殻模型による第一原理計算からのアルファクラスター構造の研究」, 日本物理学会 2019 年秋季大会, 山形大学小白川キャンパス, 山形, 2019 年 9 月 17–20 日.
- 上野秀樹, 「核整列 RI ビームを用いた β -NMR 測定法」, 新学術領域「クラスター階層」 & 「量子ビーム応用」合同検出器ワークショップ, 東北大学青葉山キャンパス, 仙台, 2019 年 9 月 20–21 日.
- 大塚孝治 (招待講演), 「原子核物理のパラダイムシフトと京コンピュータ」, 研究会 シミュレーションによる宇宙の基本法則と進化の解明に向けて, 京都, 2019 年 12 月 16–19 日.
- 小澤直也, 長濱弘季, 早水友洋, 中村圭佑, 小高康照, 田中香津生, 大塚未来, 小森有希子, 市川雄一, 羽場宏光, 上野秀樹, 酒見泰寛, 「フロンシウム原子の電気双極子能率探索のための表面電離イオン源の開発」, 日本物理学会第 75 回年次大会, 名古屋 (名古屋大学現地開催中止), 2020 年 3 月 16–19 日.
- 横須賀文哉, 高峰愛子, 田島美典, 岡野泰彬, 佐々木悠輔, 浅河拓光, 飯村秀紀, 和田道治, H. A. Schuessler, 松尾由賀利, 上野秀樹, 前田はるか, 「コリニアレーザー分光を使った Zr 同位体の核構造研究に向けたレーザー光源開発」, 日本物理学会第 75 回年次大会, 名古屋 (名古屋大学現地開催中止), 2020 年 3 月 16–19 日.
- 西村昌輝, 今村慧, 高峰愛子, 螺良健太, Aleksey Gladkov, 竹内由衣花, 土居三瑠, 山本匠, 田島美典, 浅河拓光, 佐々木悠輔, 土井一步, 川田敬太, 西畑洗希, 市川雄一, 上野秀樹, 松尾由賀利, 「液体窒素環境下における高速 Rb イオンビームの停止位置制御」, 日本物理学会第 75 回年次大会, 名古屋 (名古屋大学現地開催中止), 2020 年 3 月 16–19 日.
- 螺良健太, 今村慧, 高峰愛子, 西村昌輝, Aleksey Gladkov, 竹内由衣花, 土居三瑠, 山本匠, 田島美典, 浅河拓光, 佐々木悠輔, 土井一步, 川田敬太, 西畑洗希, 市川雄一, 上野秀樹, 松尾由賀利, 「核モーメント測定法開発のための光学用クライオスタットにおける Rb の収量測定」, 日本物理学会第 75 回年次大会, 名古屋 (名古屋大学現地開催中止), 2020 年 3 月 16–19 日.

Press releases

“Zirconium isotopes are suddenly deformed even in the excited state (「ジルコニウム同位体は励起状態でも突然変形する」),” press release from RIKEN, March 17, 2020.

RIKEN HP: https://www.riken.jp/press/2020/20200317_2/index.html.

“Basic principles of nuclear shape and self-organization in quantum systems (「原子核の形の基本原理と量子系での自己組織化」),” joint press-release from the University of Tokyo and RIKEN, November 26, 2019.

The Univ. of Tokyo HP: <https://www.s.u-tokyo.ac.jp/ja/press/2019/6629/>.

RIKEN HP: https://www.riken.jp/press/2019/20191126_1/index.html.

“Research group lead by RIKEN and the University of Tokyo succeeded in measuring excited-state nuclear magnetic moment of a neutron-rich copper isotope (「理研と東大など、中性子過剰な銅同位体原子核の励起状態の磁気モーメント測定に成功」),” Nikkei Shinbun Newspaper Online, January 30, 2019.

“New structural aspects of copper isotopes unveiled through the nuclear magnetic moment—Successful measurement by maximizing spin alignment of the RI beam— (「磁気モーメントから分かる銅同位体の新たな姿—極限までスピン整列度を高めた RI ビームを駆使して測定に成功—」),” joint press-release from RIKEN and the University of Tokyo, January 30, 2019.

RIKEN HP: https://www.riken.jp/press/2019/20190130_2/.

The Univ. of Tokyo HP: <https://www.s.u-tokyo.ac.jp/ja/info/6251/>.

JICFuS HP: <https://www.jicfus.jp/jp/190130pressrelease/>.

Outreach activities

H. Ueno, Special Exhibition of the International Year of the Periodic Table 2019 (国際周期表年特別展 2019 「理化学研究所のニホニウム模型をつくろう」), Ehime Prefectural Science Museum, January 18–19, 2020.

A. Takamine, Interactive Event “RIKEN DAY: Let’s talk with researchers!” (理研 DAY : 研究者と話そう! 「原子核を捕まえて光でみる」), Tokyo Science Museum, December 15, 2019.

H. Ueno, RIKEN Osaka Campus Open Day 2019, Suita, November 23, 2019.

H. Ueno, Kagakudo 100 Books 2019 Selection Committee (科学道 100 冊 2019 選書委員会).

Nuclear Science and Transmutation Research Division High Energy Astrophysics Laboratory

1. Abstract

In the immediate aftermath of the Big Bang, the beginning of our universe, only hydrogen and helium existed. However, nuclear fusion in the interior of stars and the explosion of supernovae in the universe over 13.8 billion years led to the evolution of a world brimming with the many different elements we have today. By using scientific satellites or balloons to observe X-rays and gamma-rays emitted from celestial objects, we are observing the synthesis of the elements at their actual source. Our goal is to comprehensively elucidate the scenarios for the formation of the elements in the universe, together with our research on sub-atomic physics through the use of an accelerator.

2. Major Research Subjects

- (1) Nucleosynthesis in stars, supernovae, and neutron star mergers
- (2) Plasma and vacuum in extremely strong magnetism and gravity
- (3) Research and development of innovative X-ray and gamma-ray detectors

3. Summary of Research Activity

High Energy Astrophysics Laboratory started in April 2010. The goal of our research is to reveal the mechanism of nucleosynthesis and the evolution of elements in the universe, and to observe/discover exotic physical phenomena in extremely strong magnetic and/or gravitational fields. We have observed supernova remnants, strongly magnetized neutron stars, pulsars, black holes and galaxies with X-ray astronomical satellites, balloons and ground-based telescopes.

(1) Nucleosynthesis in the universe

(1-1) XRISM

We have contributed to the XRISM (X-ray imaging and spectroscopy mission) mission for the launch in 2022. XRISM is the recovery mission of the ASTRO-H/Hitomi satellite, which was launched in February 2016 but lost by an accident one month after the launch. Hitomi carried four X-ray and gamma-ray detectors covering the 0.3–600 keV energy range. We, in collaboration with JAXA (Japan Aerospace Exploration Agency), Tokyo Metropolitan University, Kanazawa University, Saitama University, NASA/GSFC etc., contributed to the soft X-ray spectrometer (SXS), which achieves unprecedented energy resolution (<7 eV) in the 0.3–12 keV energy band with a low temperature micro calorimeter. We hoped to use SXS to discover many previously-unknown elemental lines in the universe and to measure the abundance of these elements, but this was not possible with Hitomi. The XRISM satellite carries almost identical X-ray detectors as the Hitomi satellite, and is expected to carry out scientific observations that were not done with the Hitomi mission.

(1-2) MAXI

From April 2018, High Energy Astrophysics Laboratory hosts MAXI (Monitor of All-sky X-ray Image) onboard International Space Station (ISS), which was attached on ISS in 2009. MAXI is a RIKEN-lead project collaborating with JAXA and other universities. Since MAXI scans X-ray all-sky in 90 minutes, many transient objects including neutron star or blackhole binaries are found. All of the data are going to public soon after they are taken, and almost all of the groups in high-energy phenomena rely on the MAXI data. In 2018, we issued 34 alerts as ATEL (Astronomer's Telegram) and 5 new blackhole candidates were found. To detect counterparts of neutron star merger events (*i.e.* gravitational wave events), we have prepared an automatic searching system and keep watching all-sky.

(1-3) Astrophysical Data Analysis

In parallel with the mission development/operations, we performed data analysis.

- We proved that the abundance ratios of the iron-peak elements in the Perseus cluster were consistent with the solar abundance. In previous studies, overabundance of Cr, Mn, and Ni are reported, but Hitomi's high spectroscopic data denied the overabundance. The inter-galactic medium of the nearby cluster has similar abundance pattern of our galaxy.
- We have detected a mysterious hump in the spectrum of the neutronstar low-mass X-ray binary, Aquila X-1. The hump can be interpreted as a recombination-edge of heavy elements (Cd) which were possibly produced by rp-process in X-ray bursts on the neutron star surface.

(2) Extremely strong magnetism and gravity

We have contributed to the NASA's world-first X-ray polarimeter mission IXPE (Imaging X-ray Polarimeter Explorer). High Energy Astrophysics Laboratory is responsible for providing the gas electron multipliers (GEMs) to the IXPE mission: the GEM is a key device of the X-ray polarimeter and produced based on our patent for space use. The IXPE satellite will be launched in the second half of 2021. We have already provided the flight qualified GEMs to the project in FY2018, and have contributed to the detector calibrations in FY2019.

By using the IXPE mission, we aim to proof the strong magnetism of Magnetars, which are one of the species of neutron stars which have ultra-strong magnetic field $B > 10^{11}$ T. In such ultra-strong magnetic field, higher-order diagrams, $O(eB/m^2)$, $O(eB/m^2)^2$ etc., never eliminated in the QED perturbation theory. As the results, we observe newly-emerging phenomenon such as vacuum polarization, vacuum birefringence, etc. If such exotic phenomena are detected, we sure that Magnetars have really ultra-strong

magnetic field.

(3) Innovative X-ray and gamma-ray detectors

In collaboration with NASA Goddard Space Flight Center, we have developed and tested a hard X-ray polarimeter with a Time Projection Chamber technique. This TPC polarimeter is one of candidates of the future satellite XPP (X-ray polarimeter Probe mission) planned with an international consortium.

As an successor of the MAXI mission, we are also verifying the principle of a new concept, multiplexing lobster-eye (MuLE) optics, to monitor the entire sky with a wide field-of-view for detecting and immediate reporting transient objects such as a neutron star merger.

Members

Group Director

Toru TAMAGAWA

Research/Technical Scientist

Tatehiro MIHARA (Senior Research Scientist)

Contract Researcher

Takao KITAGUCHI

Visiting Researcher

Asami HAYATO (JSPS Fellow)

Visiting Scientists

Aya BAMBA (Univ. of Tokyo)

Teruaki ENOTO (Kyoto Univ.)

Naohisa INADA (NIT, Nara College)

Satoru KATSUDA (Saitama Univ.)

Tomoki KIMURA (Tohoku Univ.)

Motohide KOKUBUN (ISAS/JAXA)

Toru MISAWA (Shinshu Univ.)

Ikuyuki MITSUISHI (Nagoya Univ.)

Yujin NAKAGAWA (JAMSTEC)

Toshio NAKANO (JTEC Corporation)

Hirofumi NODA (Osaka Univ.)

Hirokazu ODAKA (Univ. of Tokyo)

Yuki OKURA (NAOJ/Nat'l Inst. of Natural Sci.)

Rohta TAKAHASHI (NIT, Tomakomai College)

Yoko TAKEUCHI (TIRI)

Yukikatsu TERADA (Saitama Univ.)

Harufumi TSUCHIYA (JAEA)

Masaki WAKABAYASHI (Jakulin Commercial Company LC)

Shin'ya YAMADA (Tokyo Metropolitan University)

Student Trainees

Miho OKUBO (Tokyo University of Science)

Tomoshi TAKEDA (Tokyo University of Science)

Marina TSUTSUMI (Tokyo University of Science)

Keisuke UCHIYAMA (Tokyo University of Science)

Yuto YOSHIDA (Tokyo University of Science)

Yuuki WADA (Univ. of Tokyo)

List of Publications & Presentations

Publications

[Original papers]

- T. Ebisuzaki, J. Katori, J. Makino, A. Noda, H. Shinkai, and T. Tamagawa, "INO: Interplanetary network of optical lattice clocks," *Int. J. Mod. Phys. D* **29**, id.1940002 (2020).
- S. Oda, M. Shidatsu, S. Nakahira, T. Tamagawa, Y. Moritani, R. Itoh, Y. Ueda, H. Negoro, K. Makishima, N. Kawai, and T. Mihara, "X-ray and optical observations of the black hole candidate MAXI J1828-249," *Publ. Astron. Soc. Jpn.* **71**, id.108 (2019).
- T. Kitaguchi, K. Black, T. Enoto, A. Hayato, J. Hill, W. Iwakiri, P. Kaaret, T. Mizuno, and T. Tamagawa, "A convolutional neural network approach for reconstructing polarization information of photoelectric X-ray polarimeters," *Nucl. Instrum. Methods Phys. Res. A* **942**, id.162389 (2019).
- M. Kubota, T. Tamagawa, K. Makishima, T. Nakano, W. Iwakiri, M. Sugizaki, and K. Ono, "An enigmatic hump around 30 keV in Suzaku spectra of Aquila X-1 in the hard state," *Publ. Astron. Soc. Jpn.* **71**, id.33 (2019).
- C. Hu, T. Mihara, M. Sugizaki, Y. Ueda, and T. Enoto, "Monitoring the superorbital period variation and spin period evolution of SMC X-1," *Astrophys. J.* **885**, id.123 (2019).
- E. Gotthelf, J. Halpern, J. Alford, T. Mihara, H. Negoro, N. Kawai, S. Dai, M. Lower, S. Johnston, M. Bailes, S. Osłowski, F. Camilo, H. Miyasaka, and K. Madsen, "The 2018 x-ray and radio outburst of magnetar XTE J1810-197," *Astrophys. J. Lett.* **874**, id.L25 (2019).
- Q. Abarr, M. Baring, B. Beheshtipour, M. Beilicke, G. de Geronimo, P. Dowkontt, M. Errando, V. Guarino, N. Iyer, F. Kislak, M. Kiss, T. Kitaguchi, H. Krawczynski, J. Lanzi, S. Li, L. Lisalda, T. Okajima, M. Pearce, L. Press, B. Rauch, D. Stuchlik, H. Takahashi, J. Tang, N. Uchida, A. West, P. Jenke, H. Krimm, A. Lien, C. Malacaria, J. Miller, and C. Wilson-Hodge, "Observations of a GX 301-2 apastron flare with the x-calibur hard x-ray polarimeter supported by NICER, the swift XRT and BAT, and fermi GBM," *Astrophys. J.* **891**, id.70 (2020).
- M. Ohno, *et al.*, "Event-selection technique for the multi-layer Si -CdTe Compton camera onboard Hitomi," *Nucl. Instrum. Methods Phys. Res. A* **924**, 327-331 (2019).

Presentations

[International conferences/workshops]

- Y. Takeuchi (Oral), "Development and properties of 100 mm-square size LTCC-GEM," The 6th International Conference on Micro Pattern Gaseous Detectors (MPGD19), La Rochelle, France, May 5–10, 2019.
- T. Kitaguchi (Poster), "A machine learning approach for reconstructing X-ray polarization information acquired with micro-pattern gas polarimeters," The 6th International Conference on Micro Pattern Gaseous Detectors (MPGD19), La Rochelle, France, May 5–10, 2019.
- K. Uchiyama (Poster), "Irradiation test with heavy ions of fine-pitch LCP-GEMs for the IXPE satellite mission," The 6th International Conference on Micro Pattern Gaseous Detectors (MPGD19), La Rochelle, France, May 5–10, 2019.

[Domestic conferences/workshops]

- 三原建弘 (口頭発表), 「全天 X 線監視装置 MAXI の 10 年」, 日本物理学会秋季大会, 山形大学, 山形, 2019 年 9 月 17–20 日.
- 齋藤耀 (口頭発表), 「小型衛星搭載を目指したガンマ線バースト偏光度検出器の開発」, 日本物理学会秋季大会, 山形大学, 山形, 2019 年 9 月 17–20 日.
- 高橋弘充 (口頭発表), 「硬 X 線集光偏光計 XL-Calibur 気球実験の 2021 年フライトへ向けた準備状況」, 日本物理学会秋季大会, 山形大学, 山形, 2019 年 9 月 17–20 日.
- 會澤優輝 (口頭発表), 「CMOS イメージャを用いた X 線偏光撮像システムの開発 III」, 日本物理学会秋季大会, 山形大学, 山形, 2019 年 9 月 17–20 日.
- 郡司修一 (口頭発表), 「偏光 X 線観測衛星 IXPE の進捗状況とシミュレーションへの取り組み」, 日本物理学会第 75 回年次大会, 名古屋大学, オンライン開催, 名古屋, 2020 年 3 月 16–19 日.
- 内山慶祐 (口頭発表), 「IXPE 衛星搭載 GEM の宇宙線重イオンへの耐性試験」, 日本物理学会第 75 回年次大会, 名古屋大学, オンライン開催, 名古屋, 2020 年 3 月 16–19 日.
- 春日知明 (口頭発表), 「CMOS イメージャを用いた X 線偏光撮像システムの開発 IV」, 日本物理学会第 75 回年次大会, 名古屋大学, オンライン開催, 名古屋, 2020 年 3 月 16–19 日.
- 玉川徹 (口頭発表), 「X 線偏光観測衛星 IXPE への参加現状 (5)」, 日本天文学会 2020 年春季年会, 筑波大学, オンライン開催, つくば, 2020 年 3 月 16–19 日.
- 山口友洋 (口頭発表), 「X 線偏光観測衛星 IXPE 搭載 X 線望遠鏡用受動型熱制御素子サーマルシールドの開発 (6)」, 日本天文学会 2020 年春季年会, 筑波大学, オンライン開催, つくば, 2020 年 3 月 16–19 日.
- 山本龍哉 (口頭発表), 「シミュレーションを用いた IXPE 衛星による広がった天体の X 線偏光解析手法の研究」, 日本天文学会 2020 年春季年会, 筑波大学, オンライン開催, つくば, 2020 年 3 月 16–19 日.
- 畠内康輔 (口頭発表), 「CMOS イメージセンサを用いた硬 X 線撮像偏光計の開発 II」, 日本天文学会 2020 年春季年会, 筑波大学, オンライン開催, つくば, 2020 年 3 月 16–19 日.
- 高橋弘充 (口頭発表), 「硬 X 線偏光観測実験 XL-Calibur 気球の 2021 年フライトへ向けた準備状況」, 日本天文学会 2020 年春季年会, 筑波大学, オンライン開催, つくば, 2020 年 3 月 16–19 日.
- 澤野達哉 (口頭発表), 「重力波源 X 線対応天体探査計画 Kanazawa-SAT3 フライトモデルの分光性能評価」, 日本天文学会 2020 年春季年会, 筑波大学, オンライン開催, つくば, 2020 年 3 月 16–19 日.
- 石崎欣尚 (口頭発表), 「X 線分光撮像衛星 XRISM 搭載 Resolve の開発の現状 V」, 日本天文学会 2020 年春季年会, 筑波大学, オンライン開催, つくば, 2020 年 3 月 16–19 日.
- 三原建弘 (口頭発表), 「MAXI/GSC による 銀河系ハローの BH 連星 MAXI J0637-430 の発見と, 2019 年度後半の突発現象」, 日本天文学会 2020 年春季年会, 筑波大学, オンライン開催, つくば, 2020 年 3 月 16–19 日.
- 浅井和美 (口頭発表), 「中性子星との低質量 X 線連星の長期変動について II」, 日本天文学会 2020 年春季年会, 筑波大学, オンライン開催, つくば, 2020 年 3 月 16–19 日.
- 高嶋聡 (口頭発表), 「「すざく」衛星による降着中性子星 SMC X-1 の広がった鉄輝線の解析とその軌道・超軌道位相依存性」, 日本天文学会 2020 年春季年会, 筑波大学, オンライン開催, つくば, 2020 年 3 月 16–19 日.
- 玉川徹 (口頭発表), 「X 線偏光観測衛星 IXPE への参加現状 (4)」, 日本天文学会 2019 年秋季年会, 熊本大学, 熊本, 2019 年 9 月 11–13 日.
- 三石郁之 (口頭発表), 「X 線偏光観測衛星 IXPE 搭載 X 線望遠鏡用受動型熱制御素子サーマルシールドの開発 (5)」, 日本天文学会 2019 年秋季年会, 熊本大学, 熊本, 2019 年 9 月 11–13 日.
- 山本龍哉 (口頭発表), 「シミュレーションを用いた IXPE 衛星による X 線偏光解析手法の研究」, 日本天文学会 2019 年秋季年会, 熊本大学, 熊本, 2019 年 9 月 11–13 日.
- 北口貴雄 (口頭発表), 「機械学習を用いた飛跡画像処理による光電子追跡型 X 線偏光計の感度向上および IXPE 衛星データへの応用」, 日本天文学会 2019 年秋季年会, 熊本大学, 熊本, 2019 年 9 月 11–13 日.
- 石崎欣尚 (口頭発表), 「X 線分光撮像衛星 XRISM 搭載 Resolve の開発の現状 IV」, 日本天文学会 2019 年秋季年会, 熊本大学, 熊本, 2019 年 9 月 11–13 日.
- 小高裕和 (口頭発表), 「CMOS イメージセンサを用いた硬 X 線撮像偏光計の開発」, 日本天文学会 2019 年秋季年会, 熊本大学, 熊本, 2019 年 9 月 11–13 日.
- 大久保美穂 (口頭発表), 「シンクロトロン放射光を用いた高エネルギー X 線偏光計の性能評価」, 日本天文学会 2019 年秋季年会, 熊本大学, 熊本, 2019 年 9 月 11–13 日.
- 高橋弘充 (口頭発表), 「硬 X 線偏光観測実験 X(L)-Calibur 気球の 2018 年の観測結果と 2021 年フライトへ向けた準備状況」, 日本天文学会 2019 年秋季年会, 熊本大学, 熊本, 2019 年 9 月 11–13 日.

- 武田朋志 (口頭発表), 「APV25/SRS を利用した TPC X 線偏光計の開発と偏光観測に最適な APV 25 設定の調査」, マイクロパターンガス検出器 & アクティブ媒質 TPC 合同研究会, 理化学研究所, 和光, 2019 年 12 月 6-7 日.
- 吉田勇登・佐藤宏樹 (口頭発表), 「超小型衛星搭載用 GEM X 線検出器の開発」, マイクロパターンガス検出器 & アクティブ媒質 TPC 合同研究会, 理化学研究所, 和光, 2019 年 12 月 6-7 日.
- 周圓輝 (ポスター発表), 「撮像素子の数を大幅に削減する多重化ロブスターアイ X 線 光学系の開発実証」, JAXA 宇宙科学研究所, 相模原, 2020 年 1 月 8-9 日.
- 郡司修一 (ポスター発表), 「IXPE 衛星による広がった天体の観測シミュレーション」, JAXA 宇宙科学研究所, 相模原, 2020 年 1 月 8-9 日.
- 三石郁之 (ポスター発表), 「X 線偏光観測衛星 IXPE 搭載に向けた望遠鏡用サーマル シールドの開発」, JAXA 宇宙科学研究所, 相模原, 2020 年 1 月 8-9 日.
- 高橋弘充 (ポスター発表), 「硬 X 線集光偏光計 X(L)-Calibur 気球実験の 2018 年フライトと将来計画」, JAXA 宇宙科学研究所, 相模原, 2020 年 1 月 8-9 日.
- 玉川徹 (ポスター発表), 「X 線偏光観測衛星 IXPE」, JAXA 宇宙科学研究所, 相模原, 2020 年 1 月 8-9 日.
- 石崎欣尚 (ポスター発表), 「X 線分光撮像衛星 (XRISM) 搭載 Resolve の開発状況」, JAXA 宇宙科学研究所, 相模原, 2020 年 1 月 8-9 日.

Nuclear Science and Transmutation Research Division Superheavy Element Research Group

1. Abstract

The elements with their atomic number $Z > 103$ are called as trans-actinide or superheavy elements. This group has been studying the physical and chemical properties of superheavy elements. They must be produced by artificially for the scientific study utilizing the accelerators in RIBF. Two teams lead the study of the superheavy elements. Superheavy Element Production Team studies various methods of efficient production of the superheavy elements and their physical and chemical properties. Superheavy Element Device Development Team develops the main experimental device, *i.e.*, the gas-filled recoil ion separator, GARIS.

The synthesis of elements having atomic numbers over 119 will be attempted with the aim of establishing nuclear synthesis technology that reaches the “island of stability” where the lifetime of atomic nuclei is expected to be prolonged significantly. With the aim of constructing an ultimate nuclear model, maximum utilization will be made of key experimental devices which become fully operational in order to conduct research for the syntheses of element 119 and 120.

2. Major Research Subjects

Superheavy Element Production Team

- (1) Searching for new elements
- (2) Spectroscopic study of the nucleus of heavy elements
- (3) Chemistry of superheavy elements
- (4) Study of a reaction mechanism for fusion process

Superheavy Element Device Development Team

- (5) Maintenance of GARIS, GARIS-II and development of new gas-filled recoil ion separator GARIS-III
- (6) Maintenance and development of detector and DAQ system for GARIS, GARIS-II and GARIS-III
- (7) Maintenance and development of target system for GARIS, GARIS-II and GARIS-III

3. Summary of Research Activity

(1) Searching for new elements

To expand the periodic table of elements and the nuclear chart, we will search for new elements.

(2) Spectroscopic study of the nucleus of heavy elements

Using the high sensitivity system for detecting the heaviest element, we plan to perform a spectroscopic study of nuclei of the heavy elements.

(3) Chemistry of superheavy elements

Study of chemistry of the trans-actinide (superheavy element) has just started world-wide, making it a new frontier in the field of chemistry. Relativistic effects in chemical property are predicted by many theoretical studies. We will try to develop this new field.

(4) Study of a reaction mechanism for fusion process

Superheavy elements have been produced by complete fusion reaction of two heavy nuclei. However, the reaction mechanism of the fusion process is still not well understood theoretically. When we design an experiment to synthesize nuclei of the superheavy elements, we need to determine a beam-target combination and the most appropriate reaction energy. This is when the theory becomes important. We will try to develop a reaction theory useful in designing an experiment by collaborating with the theorists.

(5) Research Highlight

The discovery of a new element is one of the exciting topics both for nuclear physicists and nuclear chemists. The elements with their atomic number $Z > 103$ are called as trans-actinides or superheavy elements. The chemical properties of those elements have not yet been studied in detail. Since those elements do not exist in nature, they must be produced by artificially, by using nuclear reactions for the study of those elements. Because the production rate of atoms of those elements is extremely small, an efficient production and collection are key issues of the superheavy research. In our laboratory, we have been trying to produce new elements, studying the physical and chemical properties of the superheavy elements utilizing the accelerators in RIKEN.

Although the Research Group for Superheavy element has started at April 2013, the Group is a renewal of the Superheavy Element Laboratory started at April 2006, based on a research group which belonged to the RIKEN accelerator research facility (RARF), and had studied the productions of the heaviest elements. The main experimental apparatus is a gas-filled recoil ion separator GARIS. The heaviest elements with their atomic numbers, 107 (Bohrium), 108 (Hassium), 109 (Meitnerium), 110 (Darmstadtium), 111 (Roentgenium), and 112 (Copernicium) were discovered as new elements at Helmholtzzentrum für Schwerionenforschung GmbH (GSI), Germany by using ^{208}Pb or ^{209}Bi based complete fusion reactions, so called “cold fusion” reactions. We have made independent confirmations of the productions of isotopes of 108th, 110th, 111th, and 112th elements by using the same reactions performed at GSI. After these work, we observed an isotope of the 113th element, $^{278}\text{113}$, in July 2004, in April, 2005, and in August 2012. The isotope, $^{278}\text{113}$, has both the largest atomic number, ($Z = 113$) and atomic mass number ($A = 278$) which have determined experimentally among the isotopes which have been produced by cold fusion reactions. We could show the world highest sensitivity for production and detection of the superheavy elements by these observations. Our results that related to $^{278}\text{113}$ has been recognized as a discovery

of new element by a Joint Working Party of the International Union of Pure and Applied Chemistry (IUPAC) and International Union of Pure and Applied Physics (IUPAP). Finally, we named the 113th element as “Nihonium.”

We decided to make one more recoil separator GARIS-II, which has an acceptance twice as large as existing GARIS, in order to realize higher sensitivity. The design of GARIS-II has finished in 2008. All fabrication of the separator will be finished at the end of fiscal year 2008. It has been ready for operation after some commissioning works.

Preparatory work for the study of the chemical properties of the superheavy elements has started by using the gas-jet transport system coupled to GARIS. The experiment was quite successful. The background radioactivity of unwanted reaction products has been highly suppressed. Without using the recoil separator upstream the gas-jet transport system, large amount of unwanted radioactivity strongly prevents the unique identification of the event of our interest. This new technique makes clean and clear studies of chemistry of the heaviest elements promising.

The spectroscopic study of the heaviest elements has started by using alpha spectrometry. New isotope, ^{263}Hs ($Z = 108$), which has the smallest atomic mass number ever observed among the Hassium isotopes, had discovered in the study. New spectroscopic information for ^{264}Hs and its daughters have obtained also. The spectroscopic study of Rutherfordium isotope ^{261}Rf ($Z = 104$) has done and 1.9-s isomeric state has directly produced for the first time.

Preparatory works for the study of the new superheavy elements with atomic number 119 and 120 have started in 2013. We measured the reaction products of the ^{248}Cm ($^{48}\text{Ca}, xn$) $^{296-x}\text{Lv}$ ($Z = 116$) previously studied by Frelov Laboratory of Nuclear Reaction, Russia, and GSI. We observed 5 isotopes in total which tentatively assigned to ^{293}Lv , and ^{292}Lv .

Member

Director

Kosuke MORITA

List of Publications & Presentations

Publications

[Original papers]

T. Tanaka, K. Morita, K. Morimoto, D. Kaji, H. Haba, R. A. Boll, N. T. Brewer, S. Van Cleve, D. J. Dean, S. Ishizawa, Y. Ito, Y. Komori, K. Nishio, T. Niwase, B. C. Rasco, J. B. Roberto, K. P. Rykaczewski, H. Sakai, D. W. Stracener, and K. Hagino, “Study of quasielastic barrier distributions as a step towards the synthesis of superheavy elements with hot fusion reactions,” *Phys. Rev. Lett.* **124**, 052502-1–052502-6 (2020).

Presentations

[International conferences/workshops]

K. Morita (invited), “Superheavy element search at RIKEN,” The 4th International Symposium on Superheavy Elements (SHE2019), Hakone, Japan, December 1–5, 2019.
S. Sakaguchi (oral), “Perspective in the super heavy element research,” Joint Kickoff Meeting of JSPS/NRF/NSFC A3 Foresight Program “Nuclear physics in the 21st century,” Kobe, Japan, December 6–7, 2019.

Awards

森田浩介, 「113 番元素の発見による放射化学への貢献」, 第 63 回日本放射化学, 木村賞.

Others

森田浩介, 理化学研究所 一般公開, 理化学研究所 梅太郎ホール, 和光, 2019 年 04 月 20 日.
森田浩介, 核化学夏の学校, 由布院 由布トピア, 由布, 2019 年 09 月 13 日.
森田浩介, 「新元素の探索」, 錯体化学討論会市民講座, 名古屋大学, 名古屋, 2019 年 09 月 21 日.
森田浩介, 「113 番元素の発見による放射化学への貢献」, 日本放射化学学会, いわき, 2019 年 09 月 25 日.
森田浩介, 「サイエンスカフェ in SAGA」, 産業労働部 ものづくり産業課, 科学館, 鳥栖, 2019 年 09 月 28 日.
森田浩介, 「新元素の探索」, 埼玉大学 (理学部) むつめ祭, 埼玉 埼玉大学理学部, さいたま, 2019 年 11 月 02 日.
森田浩介, IYPT 閉会式, 東京 東京プリンスホテル, 東京, 2019 年 12 月 05 日.
森田浩介, 「新元素の探索」, 大分県試験研究機関, 大分県立図書館, 大分, 2019 年 11 月 16 日.
森田浩介, 「福井サイエンスフェスタ」, 福井県教育庁, 福井市 AOSSA, 福井, 2019 年 02 月 11 日.
森田浩介, 「日本のすごい科学者」, 朝日小学生新聞, 2019 年 10 月 07 日.
森田浩介, 「113 番・119 番元素への思い」, 毎日新聞, 2019 年 08 月 22 日.

Nuclear Science and Transmutation Research Division

Superheavy Element Research Group

Superheavy Element Production Team

1. Abstract

The elements with atomic number $Z \geq 104$ are called as trans-actinide or superheavy elements (SHEs). Superheavy Element Production Team investigates synthesis mechanisms of SHEs, nuclear properties of SHE nuclei, and chemical properties of SHEs mainly in collaboration with Superheavy Element Devise Development Team and Nuclear Chemistry Research Team of RIKEN Nishina Center.

2. Major Research Subjects

- (1) Search for new superheavy elements
- (2) Decay spectroscopy of the heaviest nuclei
- (3) Study of reaction mechanisms for production of the heaviest nuclei
- (4) Study of chemical properties of the heaviest elements

Summary of Research Activity

(1) Search for new superheavy elements

In November, 2016, the 7th period of the periodic table was completed with the official approval of four new elements, nihonium (Nh, atomic number $Z = 113$), moscovium (Mc, $Z = 115$), tennessine (Ts, $Z = 117$), and oganesson (Og, $Z = 118$) by International Union of Pure and Applied Chemistry (IUPAC). We have started to search for new elements to expand the chart of the nuclides toward the island of stability and the periodic table of the elements toward the 8th period of the periodic table. Since June, 2017, RIKEN heavy-ion Linear ACcelerator (RILAC) has been shut down for its upgrade until the end of 2019. During this long-term break, to continue SHE studies at RIBF, we moved GAS-filled Recoil Ion Separator II (GARIS II) from the irradiation room of RILAC to the E6 room of RIKEN Ring Cyclotron (RRC). In December 2017, the RRC + GARIS II setup became ready for SHE studies. We first conducted the commissioning of the RRC + GARIS II setup in the $^{nat}\text{La} + ^{51}\text{V}$, $^{159}\text{Tb} + ^{51}\text{V}$, and $^{208}\text{Pb} + ^{51}\text{V}$ reactions. Then, we started to search for new element, element 119 in the $^{248}\text{Cm} + ^{51}\text{V}$ reaction in January, 2018. In 2019, we continued to search for element 119 in the $^{248}\text{Cm} + ^{51}\text{V}$ reaction. We also developed the new separator GARIS III on the beam line of the upgraded RILAC, *i.e.* Superconducting RIKEN heavy-ion Linear ACcelerator (SRILAC). The SRILAC + GARIS III setup will be ready for the SHE experiments in 2020.

(2) Decay spectroscopy of the heaviest nuclei

We developed a novel detector, referred to as an “ α -TOF detector,” for correlated measurements of atomic masses and decay properties of low-yield, short-lived radioactive isotopes using a multi-reflection time-of-flight mass spectrograph. By correlating measured time-of-flight signals with decay events, it can suppress background events and obtain accurate, high-precision mass and half-life values even in cases of very low event rates. An offline test of the α -TOF detector showed that the time-of-flight detection efficiency for 5.48 MeV α -particles is more than 90% and yields a time resolution of 250.6(68) ps and an α -energy resolution of 141.1(9) keV.

(3) Study of reaction mechanisms for production of the heaviest nuclei

SHE nuclei have been produced by complete fusion reactions of two heavy nuclei. However, the reaction mechanism of the fusion process is still not well understood both theoretically and experimentally. We measured excitation functions for the quasielastic scattering of the $^{248}\text{Cm} + ^{22}\text{Ne}$, $^{248}\text{Cm} + ^{26}\text{Mg}$, and $^{238}\text{U} + ^{48}\text{Ca}$ reactions using GARIS at RILAC. The quasielastic barrier distributions were successfully extracted for these systems, and compared with coupled-channels calculations. It was found that the results can be utilized to locate the optimal energy for the future searches for undiscovered superheavy nuclei.

(4) Study of chemical properties of the heaviest elements

Chemical characterization of newly-discovered SHEs is an extremely interesting and challenging subject in modern nuclear and radiochemistry. In collaboration with Nuclear Chemistry Research Team of RIKEN Nishina Center, we are developing SHE production systems as well as rapid single-atom chemistry apparatuses for chemistry studies of SHEs. We installed a gas-jet transport system to the focal plane of GARIS at RILAC. This system is a promising approach for exploring new frontiers in SHE chemistry: the background radiations from unwanted products are strongly suppressed, the intense primary heavy-ion beam is absent in the gas-jet chamber, and hence the high gas-jet extraction yield is attained. Furthermore, the beam-free conditions make it possible to investigate new chemical systems. In 2019, we continued to develop an ultra-rapid gas-chromatograph apparatus at the focal plane of GARIS for the gas chemistry of SHEs. This apparatus consists of an RF carpet gas cell and a cryo-gas-chromatograph column with a Si detector array. For the aqueous chemistry, we also developed a flow solvent extraction apparatus which consisted of a continuous dissolution apparatus, a flow extraction apparatus, and a liquid scintillation counter.

Members

Team Leader

Hiromitsu HABA

Research & Development Scientist

Daiya KAJI

Special Postdoctoral Researcher

Tomohiro HAYAMIZU

Visiting Scientists

Satoshi ADACHI (Kyushu Univ.)	Minghui HUANG (Inst. of Modern Phys.)
Marc ASFARI (Inst. Pluridisciplinaire Hubert Curien)	Hiroyuki KOURA (JAEA)
Mahananda DASGUPTA (Australian Nat'l Univ.)	Daisuke NAGAE (Kyushu Univ.)
Olivier DORVAUX (Strasbourg Univ.)	Satoshi SAKAGUCHI (Kyushu Univ.)
Benoit Jean-Paul GALL (Strasbourg Univ./Inst. Pluridisciplinaire Hubert Curien)	Mirei TAKEYAMA (Yamagata Univ.)
Zaiguo GAN (Inst. of Modern Phys.)	Masaomi TANAKA (Kyushu Univ.)
Shintaro GO (Kyushu Univ.)	Taiki TANAKA (The Australian Nat'l Univ.)
David HINDE (The Australian Nat'l Univ.)	Huabin YANG (Inst. of Modern Phys.)
	Zhiyuan ZHANG (Inst. of Modern Phys.)

Student Trainees

Masato HIGASHI (Kyushu Univ.)	Natsuki NAITO (Kyushu Univ.)
Tamito KAI (Kyushu Univ.)	Mako OSADA (Kyushu Univ.)
Kieran KESSACI (IPHC Strasbourg/Strasbourg Univ.)	Kazuya SHIRASAKA (Kyushu Univ.)
Ikuto MURAKAMI (Kyushu Univ.)	Yoshihide SUEKAWA (Kyushu Univ.)
Yuto NAGATA (Kyushu Univ.)	

List of Publications & Presentations

Publications

[Original papers]

- S. Ahmed, E. Altieri, T. Andalib, M. J. Barnes, B. Bell, C. P. Bidinosti, Y. Bylinsky, J. Chak, M. Das, C. A. Davis, F. Fischer, B. Franke, M. T. W. Gericke, P. Giampa, M. Hahn, S. Hansen-Romu, K. Hatanaka, T. Hayamizu, B. Jamieson, D. Jones, K. Katsika, S. Kawasaki, T. Kikawa, W. Klassen, A. Konaka, E. Korkmaz, F. Kuchler, L. Kurchaninov, M. Lang, L. Lee, T. Lindner, K. W. Madison, J. Mammei, R. Mammei, J. W. Martin, R. Matsumiya, E. Müller, T. Momose, R. Picker, E. Pierre, W. D. Ramsay, Y. -N. Rao, W. R. Rawnsley, L. Rebenitsch, W. Schreyer, S. Sidhu, S. Vanbergen, W. T. H. van Oers, Y. X. Watanabe, and D. Yosifov, “Fast-switching magnet serving a spallation-driven ultracold neutron source,” *Phys. Rev. Accel. Beams* **22**, 102401-1–16 (2019).
- T. Tanaka, K. Morita, K. Morimoto, D. Kaji, H. Haba, R. A. Boll, N. T. Brewer, S. Van Cleve, D. J. Dean, S. Ishizawa, Y. Ito, Y. Komori, K. Nishio, T. Niwase, B. C. Rasco, J. B. Roberto, K. P. Rykaczewski, H. Sakai, D. W. Stracener, and K. Hagino, “Fusion dynamics for hot fusion reactions to synthesize superheavy nuclei revealed in quasielastic barrier distributions,” *Phys. Rev. Lett.* **124**, 052502-1–96 (2020).
- Y. Wang, Y. Wittwer, J. Zhang, J. Yang, H. Haba, Y. Komori, T. Yokokita, S. Cao, F. Fan, R. Eichler, A. Türler, and Z. Qin, “Mass spectrometric speciation of metal-carbonyls in the gas phase,” *PSI Annual Report 2018, Laboratory of Radiochemistry*, 13–14 (2019).
- Y. Kasamatsu, N. Kondo, K. Nakamura, Y. Kuboki, H. Ninomiya, Y. Shigekawa, E. Watanabe, Y. Yasuda, K. Toyomura, M. Nagase, T. Yokokita, Y. Komori, H. Haba, T. Yoshimura, H. Itabashi, and A. Shinohara, “Solvent extraction of Zr and Hf from HCl by Aliquat 336 using a flow-type extraction apparatus toward online chemical studies of element 104, rutherfordium,” *Solv. Extr. Ion Exch* **38**, 318–327 (2020).
- T. Niwase, M. Wada, P. Schury, H. Haba, S. Ishizawa, Y. Ito, D. Kaji, S. Kimura, H. Miyatake, K. Morimoto, K. Morita, M. Rosenbusch, H. Wollnik, T. Shanley, and Y. Benari, “Development of an “ α -TOF” detector for correlated measurement of atomic masses and decay properties,” *Nucl. Instrum. Methods Phys. Res. A* **953**, 163198-1–8 (2020).
- Y. Sakemi, H. Nagahama, T. Hayamizu, N. Ozawa, K. S. Tanaka, K. Harada, A. Uchiyama, and J. Tsutsumi, “Present status of fundamental symmetry experimental project with laser cooled heavy elements,” *CNS Annual Report* **2018**, 23–24 (2020).
- N. Ozawa, H. Nagahama, T. Hayamizu, J. Tsutsumi, K. S. Tanaka, K. Harada, A. Uchiyama, and Y. Sakemi, “Development of a novel surface ionizer for the electron EDM measurement using francium,” *CNS Annual Report* **2018**, 25–26 (2020).

[Review articles]

- H. Haba, “The rewards and challenges of expanding the periodic table,” *Chem. Eng. News*, August 5, 36–37 (2019).
- 羽場宏光, 「第 8 周期の新元素を求めて」, *放射化学* **40**, 14–20 (2019).
- 羽場宏光, 「日本の研究者による新元素の探索と周期表の開拓—ニッポニウム, 93 番元素, ニホニウム。さらなる新元素を求めて—」, *化学と工業* **72**, 944–945 (2019).

[Books]

豊嶋厚史, 羽場宏光, 「超重元素化学—溶液化学」, in 「フロンティアシリーズ 2 超重元素化学の最前線」, 永目論一郎 (編著), pp. 41–48, 日本放射化学会, 2019 年 9 月 1 日.

[Proceedings]

H. Haba for RIKEN SHE Collaboration, “Present status and perspectives of SHE researches at RIKEN,” in Proceedings of the International Symposium on Exotic Nuclei, Petrozavodsk, Russia, 10–15 September 2018, Yu. E. Penionzhkevich, Yu. G. Sobolev (Eds.), (World Scientific Publishing Co. Pte. Ltd., 2020), pp. 192–199.

Presentations

[International conferences/workshops]

- H. Haba (invited), “Production and applications of radioisotopes at RIKEN RI Beam Factory,” SHE Science Symposium, Oak Ridge, USA, May 30, 2019.
- H. Haba (invited), “Synthesis and chemistry of new elements at RIKEN,” 9th European Chemistry Congress, Berlin, Germany, June 17–18, 2019.
- A. Yakushev, L. Lens, Ch. E. Düllmann, M. Asai, M. Block, H. Brand, H. M. David, J. Despotopulos, A. Di Nitto, K. Eberhardt, U. Forsberg, P. Golubev, M. Götz, S. Götz, H. Haba, L. Harkness-Brennan, W. Hartmann, R. -D. Herzberg, D. Hinde, J. Hoffmann, A. Hübner, E. Jäger, M. Jourdan, D. Judson, J. Khuyagbaatar, B. Kindler, Y. Komori, J. Konki, J. V. Kratz, J. Krier, N. Kurz, M. Laatiaoui, S. Lahiri, B. Lommel, M. Maiti, A. Mistry, Ch. Mokry, K. Moody, Y. Nagame, J. P. Omtvedt, P. Papadakis, V. Pershina, T. Reich, D. Rudolph, J. Runke, L. Samiento, T. K. Sato, M. Schädel, P. Scharrer, B. Schausten, D. Shaughnessy, J. Steiner, P. Thörle-Pospiech, A. Toyoshima, N. Trautmann, K. Tsukada, J. Uusitalo, K. -O. Voss, A. Ward, M. Wegrzecki, N. Wiehl, E. Williams, and V. Yakusheva (invited), “Chemical studies of superheavy elements at a recoil separator, with a focus on Fl,” 6th International Conference on the Chemistry and Physics of the Transactinide Elements (TAN19), Wilhelmshaven, Germany, August 25–30, 2019.
- M. Götz, Ch. E. Düllmann, A. Yakushev, M. Asai, J. Ballof, A. Di Nitto, K. Eberhardt, S. Götz, H. Haba, E. Jäger, Y. Kaneya, Y. Komori, J. V. Kratz, J. Krier, B. Lommel, A. Mitsukai, Y. Nagame, T. K. Sato, A. Toyoshima, K. Tsukada, V. Wolter, and V. Yakusheva (poster), “In-situ synthesis of volatile transition metal carbonyl complexes with short-lived radioisotopes,” 6th International Conference on the Chemistry and Physics of the Transactinide Elements (TAN19), Wilhelmshaven, Germany, August 25–30, 2019.
- Z. Qin, Y. Wang, S. Cao, J. Zhang, J. Yang, H. Haba, F. Fan, Y. Komori, T. Yokokita, K. Morimoto, D. Kaji, Y. Wittwer, R. Eichler, and A. Türler (poster), “The study of rhenium pentacarbonyl complexes using single-atom chemistry in gas phase,” 6th International Conference on the Chemistry and Physics of the Transactinide Elements (TAN19), Wilhelmshaven, Germany, August 25–30, 2019.
- Y. Wang, Y. Wittwer, J. Zhang, J. Yang, H. Haba, Y. Komori, T. Yokokita, S. Cao, F. Fan, R. Eichler, A. Türler, and Z. Qin (oral), “The species identification of Mo, W, and Re carbonyl complexes with laserablation time-of-flight mass-spectrometry,” 6th International Conference on the Chemistry and Physics of the Transactinide Elements (TAN19), Wilhelmshaven, Germany, August 25–30, 2019.
- L. Lens, A. Yakushev, Ch. E. Düllmann, M. Asai, M. Block, H. Brand, M. Dasgupta, H. M. David, J. Despotopulos, A. Di Nitto, K. Eberhardt, M. Götz, P. Golubev, S. Götz, H. Haba, L. Harkness-Brennan, F. P. Heßberger, R. -D. Herzberg, D. Hinde, J. Hoffmann, A. Hübner, E. Jäger, D. Judson, J. Khuyagbaatar, B. Kindler, Y. Komori, J. Konki, J. V. Kratz, J. Krier, N. Kurz, M. Laatiaoui, S. Lahiri, B. Lommel, M. Maiti, A. K. Mistry, C. Mokry, K. Moody, Y. Nagame, J. P. Omtvedt, P. Papadakis, V. Pershina, A. Roth, D. Rudolph, J. Runke, L. Sarmiento, M. Schädel, P. Scharrer, T. Sato, D. Shaughnessy, B. Schausten, J. Steiner, P. Thörle-Pospiech, N. Trautmann, K. Tsukada, J. Uusitalo, A. Ward, M. Wegrzecki, E. Williams, N. Wiehl, and V. Yakusheva (poster), “Optimizations of the TASCACOMPACT setup towards chemical studies of nihonium (element 113),” 6th International Conference on the Chemistry and Physics of the Transactinide Elements (TAN19), Wilhelmshaven, Germany, August 25–30, 2019.
- T. Niwase, M. Wada, P. Schury, Y. Ito, S. Kimura, D. Kaji, M. Rosenbusch, Y. Watanabe, Y. Hirayama, H. Miyatake, J. Y. Moon, H. Ishiyama, K. Morimoto, H. Haba, T. Tanaka, S. Ishizawa, A. Takamine, K. Morita, and H. Wollnik (poster), “Development and first results from a novel “ α -ToF” detector used with a multi-reflection time-of-flight mass spectrograph,” 6th International Conference on the Chemistry and Physics of the Transactinide Elements (TAN19), Wilhelmshaven, Germany, August 25–30, 2019.
- T. Tanaka, K. Morita, K. Morimoto, D. Kaji, H. Haba, R. A. Boll, N. T. Brewer, S. V. Cleve, D. J. Dean, S. Ishizawa, Y. Ito, Y. Komori, K. Nishio, T. Niwase, B. C. Rasco, J. B. Roberto, K. Rykaczewski, H. Sakai, D. W. Stracener, and K. Hagino (oral), “Fusion dynamics for hot fusion reactions revealed in quasielastic barrier distributions,” 6th International Conference on the Chemistry and Physics of the Transactinide Elements (TAN19), Wilhelmshaven, Germany, August 25–30, 2019.
- M. Wada, P. Schury, H. Miyatake, Y. X. Watanabe, Y. Hirayama, H. Wollnik, S. Kimura, S. Ishizawa, T. Niwase, M. Rosenbusch, D. Kaji, K. Morimoto, H. Haba, I. Takamine, T. Tanaka, H. Ishiyama, Y. Ito, J. Y. Moon, and K. Morita (invited), “SHE-Mass-II setup for direct mass measurement of hot-fusion superheavy nuclides,” 6th International Conference on the Chemistry and Physics of the Transactinide Elements (TAN19), Wilhelmshaven, Germany, August 25–30, 2019.
- Y. Ito, P. Schury, M. Wada, F. Arai, H. Haba, Y. Hirayama, S. Ishizawa, D. Kaji, S. Kimura, H. Koura, M. McCormick, H. Miyatake, J. -Y. Moon, K. Morimoto, K. Morita, M. Mukai, I. Murray, T. Niwase, K. Okada, A. Ozawa, M. Rosenbusch, A. Takamine, T. Tanaka, Y. Watanabe, H. Wollnik, and S. Yamaki (oral), “Direct mass measurements of mendelevium isotopes in the vicinity of the $N = 152$ deformed shell-closure,” 6th International Conference on the Chemistry and Physics of the Transactinide Elements (TAN19), Wilhelmshaven, Germany, August 25–30, 2019.
- H. Haba (invited), “Present status and perspectives of superheavy element researches at RIKEN,” XXXVIth Mazurian Lakes Conference on Physics, Piaski, Poland, September 1–7, 2019.
- H. Haba (invited), “RI production—Chemistry of new elements to diagnosis and treatment of cancer—,” Tsukuba Conference 2019, Tsukuba, Japan, October 2–4, 2019.
- Y. Kasamatsu, H. Ninomiya, S. Hayami, M. Nagase, E. Watanabe, Y. Shigekawa, N. Kondo, H. Haba, T. Yokokita, Y. Komori, D. Mori, Y. Wang, K. Ghosh, M. Kaneko, and A. Shinohara (poster), “Cocprecipitation of nobelium with samarium hydroxide,” The 4th Interna-

tional Symposium on Superheavy Elements (SHE2019), Hakone, Japan, December 1–5, 2019.

- Z. Qin, Y. Wang, S. W. Cao, J. C. Zhang, F. L. Fang, J. Yang, H. Haba, Y. Komori, T. Yokokita, K. Morimoto, D. Kaji, Y. Wittwer, R. Eichler, and A. Türler (invited), “Towards the bohrium carbonyl complexes in gas phase,” The 4th International Symposium on Superheavy Elements (SHE2019), Hakone, Japan, December 1–5, 2019.
- Y. Wang, Y. Wittwer, J. Zhang, S. Cao, Y. Komori, T. Yokokita, Y. Shigekawa, F. Fan, J. Yang, H. Haba, R. Eichler, A. Türler, and Z. Qin (oral), “Species identification of Re carbonyls using laser-ablation time-of-flight mass-spectrometer,” The 4th International Symposium on Superheavy Elements (SHE2019), Hakone, Japan, December 1–5, 2019.
- T. Yokokita, Y. Kasamatsu, E. Watanabe, Y. Komori, H. Ninomiya, Y. Wang, D. Mori, K. Ghosh, A. Shinohara, and H. Haba (oral), “Anion exchange of Rf, Zr, Hf, and Th in H₂SO₄,” The 4th International Symposium on Superheavy Elements (SHE2019), Hakone, Japan, December 1–5, 2019.
- T. Niwase, M. Wada, P. Schury, Y. Ito, S. Kimura, D. Kaji, M. Rosenbusch, Y. X. Watanabe, Y. Hirayama, H. Miyatake, J. Y. Moon, H. Ishiyama, K. Morimoto, H. Haba, T. Tanaka, S. Ishizawa, A. Takamine, K. Morita, and H. Wollnik (oral), “Correlation measurement of precision mass and decay properties of nuclei via MRTOF-MS with α -ToF detector,” The 4th International Symposium on Superheavy Elements (SHE2019), Hakone, Japan, December 1–5, 2019.
- M. Rosenbusch, M. Wada, P. Schury, S. Iimura, H. Haba, Y. Hirayama, H. Ishiyama, S. Ishizawa, Y. Ito, D. Kaji, S. Kimura, H. Miyatake, J. Y. Moon, K. Morimoto, T. Tanaka, T. Niwase, A. Takamine, K. Morita, Y. X. Watanabe, and H. Wollnik (oral), “Dynamic ejection-field correction for MR ToF mass spectrometry of SHE using arbitrary mass references,” The 4th International Symposium on Superheavy Elements (SHE2019), Hakone, Japan, December 1–5, 2019.
- H. Haba (plenary), “Production and applications of radioisotopes at RIKEN RI Beam Factory—Search for new elements through diagnosis and therapy of cancer—,” The 10th International Conference on Isotopes (10ICI), Kuala Lumpur, Malaysia, February 3–7, 2020.
- H. Haba (invited), “Present status and perspectives of superheavy element chemistry at RIKEN,” The 10th International Conference on Isotopes (10ICI), Kuala Lumpur, Malaysia, February 3–7, 2020.

[Seminars]

- H. Haba, “Production of radioisotopes for application Studies at RIKEN RI Beam Factory,” Seminar at Institute of Modern Physics (IMP), Lanzhou, China, August 12, 2019.
- H. Haba, “Production of radioisotopes for application Studies at RIKEN RI Beam Factory,” IFIN-HH Seminar at Horia Hulubei National Institute for R&D in Physics and Nuclear Engineering, Bucharest, Rumania, October 21, 2019.
- H. Haba, “Production of radioisotopes for application studies at RIKEN RI Beam Factory,” Seminar at Sunway University, Selangor, Malaysia, February 10, 2020.

[Domestic conferences/workshops]

- 羽場宏光 (招待講演), 「新元素化学の展望」, 日本物理学会 2019 年秋季大会, 山形, 2019 年 9 月 17–20 日.
- 庭瀬暁隆, 和田道治, P. Schury, 伊藤由太, 木村創太, 加治大哉, M. Rosenbusch, 渡辺裕, 平山賀一, 宮武宇也, J. Y. Moon, 石山博恒, 森本幸司, 羽場宏光, 田中泰貴, 石澤倫, 高峰愛子, 森田浩介, H. Wollnik (口頭発表), 「MRTOF-MS を用いた ²⁰⁷Ra の精密質量-崩壊特性測定」, 日本物理学会 2019 年秋季大会, 山形, 2019 年 9 月 17–20 日.
- 早川優太, 坂口綾, 村田真優, 松村夏紀, 藤沼修平, 中島朗久, 笠松良崇, 篠原厚, 小森有希子, 横北卓也, 森大輝, 矢納慎也, 羽場宏光, 横山明彦 (口頭発表), 「U+p 及び Th+Li 反応による Np 同位体励起関数の作成」, 日本放射化学会第 63 回討論会 (2019), いわき, 2019 年 9 月 24–26 日.
- 横北卓也, 笠松良崇, 渡邊瑛介, 小森有希子, 二宮秀美, 王洋, 森大輝, ゴーシュコースタブ, 篠原厚, 羽場宏光 (口頭発表), 「硫酸系における Rf の陰イオン交換」, 日本放射化学会第 63 回討論会 (2019), いわき, 2019 年 9 月 24–26 日.
- 速水翔, 二宮秀美, 渡邊瑛介, 重河優大, 永瀬将浩, 笠松良崇, 近藤成美, 羽場宏光, 横北卓也, 小森有希子, 森大輝, 王洋, ゴーシュコースタブ, 佐藤隆, 篠原厚 (口頭発表), 「水酸化サマリウム共沈法を用いた 102 番元素ノーベリウムの沈殿実験」, 日本放射化学会第 63 回討論会 (2019), いわき, 2019 年 9 月 24–26 日.
- 庭瀬暁隆, 和田道治, P. Schury, 伊藤由太, 木村創太, 加治大哉, M. Rosenbusch, 渡辺裕, 平山賀一, 宮武宇也, J. Y. Moon, 石山博恒, 森本幸司, 羽場宏光, 田中泰貴, 石澤倫, 高峰愛子, 森田浩介, H. Wollnik (口頭発表), 「MRTOF + α -TOF を用いた ²⁰⁷Ra の質量-崩壊特性測定」, 日本放射化学会第 63 回討論会 (2019), いわき, 2019 年 9 月 24–26 日.
- 安達サディア, 末木啓介, 豊嶋厚史, 塚田和明, 羽場宏光, 小森有希子, 横北卓也, 森大輝 (ポスター発表), 「HF/HNO₃ 水溶液中における Nb, Ta, Pa の陰イオン交換実験~Db フッ化物錯体の推定に向けて~」, 日本放射化学会第 63 回討論会 (2019), いわき, 2019 年 9 月 24–26 日.
- 森田涼雅, 早川優太, 小森有希子, 横北卓也, 森大輝, 羽場宏光, 笠松良崇, 篠原厚, 横山明彦 (ポスター発表), 「²³⁹Np 複合核系における核分裂断面積測定による軌道角運動量の推定」, 日本放射化学会第 63 回討論会 (2019), いわき, 2019 年 9 月 24–26 日.
- 羽場宏光 (招待講演), 「新元素を探そう!」, 日本化学会 君たちの将来と化学の未来 東大で過ごす化学な週末, 文京, 2019 年 10 月 20 日.
- 羽場宏光 (招待講演), 「113 番ニホニウムの発見」, 国際周期表年 2019 特別展オープニングイベント, 山形, 2019 年 11 月 3 日.
- 羽場宏光 (招待講演), 「元素をつくろう!」, サイエンスアゴラ国際周期表年特別企画 元素検定 2019@東京, 江東, 2019 年 11 月 16 日.
- 羽場宏光 (招待講演), 「ラジオアイソトープの製造と応用—新元素の探索からがんの診断・治療まで—」, 2019 年度日本アイソトープ協会シンポジウム「PET・イメージング研究の最前線~ライフサイエンスと理工学の融合~」, 川崎, 2019 年 11 月 22 日.
- 羽場宏光 (招待講演), 「理研におけるラジオアイソトープの製造と応用~新元素の探索からがんの診断・治療まで~」, 第 75 回放射線計測研究会, 和光市, 2020 年 1 月 18 日.
- 小澤直也, 長濱弘季, 早水友洋, 中村圭佑, 小高康熙, 田中香津生, 大塚未来, 小森有希子, 市川雄一, 羽場宏光, 上野秀樹, 酒見泰寛 (口

頭発表), 「フランシウム原子の電気双極子能率探索のための表面電離イオン源の開発」, 日本物理学会第 75 回年次大会 (2020 年), 名古屋, 2020 年 3 月 16-19 日.

庭瀬暁隆, 和田道治, P. Schury, 伊藤由太, 木村創大, 加治大哉, M. Rosenbusch, 渡辺裕, 平山賀一, 宮武宇也, J. Y. Moon, 石山博恒, 森本幸司, 羽場宏光, 田中泰貴, 石澤倫, 飯村俊, 高峰愛子, 森田浩介, H. Wollnik (口頭発表), 「MRTOF+ α -TOF を用いた短寿命 α 崩壊核種の質量-崩壊特性測定」, 日本物理学会第 75 回年次大会 (2020 年), 名古屋, 2020 年 3 月 16-19 日.

Nuclear Science and Transmutation Research Division Superheavy Element Research Group Superheavy Element Device Development Team

1. Abstract

A gas-filled recoil ion separator has been used as a main experimental device for the study of superheavy elements. This team is in charge of maintaining, improving, developing, and operating the separators and related devices. In the RIBF facility, three gas-filled recoil ion separators are installed at RILAC and RRC facility. One is GARIS that is designed for a symmetric reaction such as cold-fusion reaction, and the other two are developed for an asymmetric reaction such as hot-fusion reaction, GARIS-II and GARIS-III. New elements $^{278}113$ were produced by $^{70}\text{Zn} + ^{209}\text{Bi}$ reaction using GARIS. Further the new element search $Z > 118$ is currently in progress by using GARIS-II and GARIS-III.

2. Major Research Subjects

- (1) Maintenance of GARIS, GARIS-II and development of new separator GARIS-III
- (2) Maintenance and development of detector and DAQ system for superheavy element research
- (3) Maintenance and development of target system for GARIS, GARIS-II and GARIS-III

3. Summary of Research Activity

The GARIS-II and III are newly developed which has an acceptance twice as large as existing GARIS, in order to realize higher transmission. A new element search program aiming to element 119 was started using GARIS-II. And new separator GARIS-III was developed and installed into the RILAC experimental hall. It will be ready for operation in the physical year 2020 after some commissioning works. We will also offer user-support if a researcher wishes to use the devices for his/her own research program.

Members

Team Leader

Kouji MORIMOTO

Research/Technical Scientists

Masaki FUJIMAKI (concurrent: Senior Technical Scientist) Daiya KAJI (Technical Scientist)

Postdoctoral Researchers

Pierre BRIONNET Sota KIMURA

Junior Research Associates

Satoshi ISHIZAWA Toshitaka NIWASE

Visiting Scientists

Shin-ichi GOTO (Niigata Univ.) Katsuhisa NISHIO (JAEA)
Eiji IDEGUCHI (Osaka Univ.) Fuyuki TOKANAI (Yamagata Univ.)
Yuta ITO (JAEA)

Student Trainees

Hayato NUMAKURA (Yamagata Univ.) Hiroki TSUNODA (Niigata Univ.)
Yoshiki TAKAHASHI (Niigata Univ.)

List of Publications & Presentations

Publications

[Original papers]

- S. Ishizawa, K. Morimoto, D. Kaji, T. Tanaka, and F. Tokanai, "Improvement of the detection efficiency of a time-of-flight detector for superheavy element search," *Nucl. Instrum. Methods Phys. Res. A* **960**, 163614 (2020).
- T. Niwase, M. Wada, P. Schury, H. Haba, S. Ishizawa, Y. Ito, D. Kaji, S. Kimura, H. Miyatake, K. Morimoto, K. Morita, M. Rosenbusch, H. Wollnik, T. Shanley, and Y. Benari, "Development of an α -TOF" detector for correlated measurement of atomic masses and decay properties," *Nucl. Instrum. Methods Phys. Res. A*, **953**, 163198 (2020).
- H. Numakura, K. Morimoto, D. Kaji, K. Kosugi, C. Horikawa, S. Ishizawa, M. Takeyama, and F. Tokanai, "Evaluation of a back-illuminated solid state detector with thin dead layer for super heavy element research," *Jpn. J. Appl. Phys.* **59**, 066004 (2020).

[Review articles]

庭瀬暁隆, 和田道治, P. Schury, 伊藤由太, 木村創大, 加治大哉, M. Rosenbusch, 渡辺裕, 平山賀一, 宮武宇也, J. Y. MOON, 石山博恒, 森本幸司, 羽場宏光, 田中泰貴, 石澤倫, 高峰愛子, 森田浩介, H. Wollnik, 「MRTOF+ α -TOF を用いた ^{207}Ra の質量-崩壊特性測定」, *放射化学* 第 41 号 2020 年 3 月.

Presentations

[International conferences/workshops]

- K. Morimoto (invited), “The discovery of element 113,” TAN 19, Wilhelmshaven, Germany, August 2019.
- S. Ishizawa (oral), K. Morimoto, D. Kaji, T. Tanaka, and F. Tokanai, “Improvement of the detection efficiency of a time-of-flight detector for superheavy element search,” The 2019 IEEE Nuclear Science Symposium (NSS) and Medical Imaging Conference (MIC), Manchester, UK, October 26–November 5, 2019.
- P. Brionnet (oral), “First measurement of the reaction $^{51}\text{V}+^{159}\text{Tb} \rightarrow ^{210}\text{Ra}^*$ on GARIS-II,” The 4th International Symposium on Superheavy Elements (SHE2019), Hakone, Japan, December 1–5, 2019.
- T. Niwase (oral), M. Wada, P. Schury, Y. Ito, D. Kaji, M. Rosenbusch, Y. X. Watanabe, Y. Hirayama, J. Y. MOON, H. Ishiyama, T. Tanaka, A. Takamine, S. Kimura, K. Morimoto, H. Haba, S. Ishizawa, K. Morita, H. Miyatake, and H. Wollnik, “Correlation measurement of precision mass and decay properties of nuclei via MRTOF-MS with α -ToF detector,” The 4th International Symposium on Superheavy Elements (SHE2019), Hakone, Japan, December 1–5, 2019.
- S. Ishizawa (poster), K. Morimoto, D. Kaji, T. Tanaka, and F. Tokanai, “Improvement of the detection efficiency of a time-of-flight detector with a large effective area for superheavy element search,” The 4th International Symposium on Superheavy Elements (SHE2019), Hakone, Japan, December 1–5, 2019.
- T. Niwase (poster), M. Wada, P. Schury, Y. Ito, S. Kimura, D. Kaji, M. Rosenbusch, Y. X. Watanabe, Y. Hirayama, H. Miyatake, J. Y. Moon, H. Ishiyama, K. Morimoto, H. Haba, T. Tanaka, S. Ishizawa, A. Takamine, K. Morita, and H. Wollnik, “Development and first results from a novel “ α -TOF” detector used with a multi-reflection time-of-flight mass spectrograph,” TAN 19, Wilhelmshaven, Germany, August 2019.
- H. Numakura (poster), C. Horikawa, K. Morimoto, S. Ishizawa, M. Takeyama, and F. Tokanai, “Evaluation of dead-layer thickness of SSD for SHE research,” The 19th International Conference on Solid State Dosimetry (SSD19), Hiroshima, September 15–20, 2019.
- I. Murakami (poster), S. Sakaguchi, D. Kaji, K. Morimoto, T. Niwase, K. Morita *et al.*, “Development of MCP ToF Detectors at Kyushu University,” The 4th International Symposium on Superheavy Elements (SHE2019), Hakone, Japan, December 1–5, 2019.
- K. Morimoto (oral), “Discovery of Nh and search for element 119,” nSHE RG Collaboration Meeting. Oak Ridge National Laboratory and the University of Tennessee Knoxville, US, May 30–June 1, 2019.
- D. Kaji (oral), “GARIS-2/-3 performance,” nSHE RG Collaboration Meeting. Oak Ridge National Laboratory and the University of Tennessee Knoxville, US, May 30–June 1, 2019.
- P. Brionnet (oral), “Data analysis I,” nSHE RG Collaboration Meeting. Oak Ridge National Laboratory and the University of Tennessee Knoxville, US, May 30–June 1, 2019.
- S. Ishizawa (oral), “Optimization of ToF system,” nSHE RG Collaboration Meeting. Oak Ridge National Laboratory and the University of Tennessee Knoxville, US, May 30–June 1, 2019.
- S. Kimura (oral), “Determination of anchor via direct mass measurement with MR-TOF,” nSHE RG Collaboration Meeting. Oak Ridge National Laboratory and the University of Tennessee Knoxville, US, May 30–June 1, 2019.
- K. Morimoto (oral), “Present status and plans of GARIS, GARIS-II and GARIS-III,” SSRI-PNS Collaboration Meeting 2019, Nishina hall, Nishina Bldg. 2F, September 4, 2019.

[Domestic conferences/workshops]

- 庭瀬暁隆, 和田道治, P. Schury, 伊藤由太, 木村創大, 加治大哉, M. Rosenbusch, 渡辺裕, 平山賀一, 宮武宇也, J. Y. MOON, 石山博恒, 森本幸司, 羽場宏光, 田中泰貴, 石澤倫, 高峰愛子, 森田浩介, H. Wollnik, 「MRTOF-MS を用いた ^{207}Ra の精密質量-崩壊特性測定」, 日本物理学会 2019 年秋季大会, 山形大学, 山形, 2019 年 9 月.
- 庭瀬暁隆, 和田道治, P. Schury, 伊藤由太, 木村創大, 加治大哉, M. Rosenbusch, 渡辺裕, 平山賀一, 宮武宇也, J. Y. MOON, 石山博恒, 森本幸司, 羽場宏光, 田中泰貴, 石澤倫, 高峰愛子, 森田浩介, H. Wollnik, 「MRTOF+ α -TOF を用いた ^{207}Ra の質量-崩壊特性測定」, 日本放射化学会第 63 回討論会 (2019), いわき, 2019 年 9 月.
- 庭瀬暁隆, 和田道治, P. Schury, 伊藤由太, 木村創大, 加治大哉, M. Rosenbusch, 渡辺裕, 平山賀一, 宮武宇也, J. Y. MOON, 石山博恒, 森本幸司, 羽場宏光, 田中泰貴, 石澤倫, 飯村俊, 高峰愛子, 森田浩介, H. Wollnik, 「MRTOF+ α -TOF を用いた短寿命 α 崩壊核種の質量-崩壊特性測定」, 日本物理学会 第 75 回年次大会 (2020 年), 名古屋大学, 名古屋, 2020 年 3 月.

Awards

庭瀬暁隆, 日本放射化学会第 63 回討論会 (2019), 若手優秀発表賞 2019 年 9 月

Others

森本幸司, 理化学研究所仙台地区 一般公開, 「新元素「ニホニウム」の発見と新たな展開」, 理化学研究所 仙台地区, 2019 年 07 月 27 日.

Nuclear Science and Transmutation Research Division Astro-Glaciology Research Group

Summary of Research Activities

Our Astro-Glaciology Research Group promotes both experimental and theoretical studies to open up the new interdisciplinary research field of astro-glaciology, which combines astrophysics, astrochemistry, glaciology, and climate science.

On the experimental side, we measure isotopic and ionic concentrations in ice cores drilled at Dome Fuji station, Antarctica, in collaboration with the National Institute of Polar Research (NIPR, Tokyo). Here, the ice cores are time capsules which preserve atmospheric information of the past. In particular, the ice cores obtained around the Dome Fuji site are very unique, because they contain much more information on the stratosphere than any other ice cores obtained from elsewhere on Earth. This means that we have significant advantages in using Dome Fuji ice cores if we wish to study the Universe, since UV photons, gamma-rays, and high-energy protons emitted by astronomical phenomena affect the atmosphere of the stratosphere. Our principal aim is thus to acquire and interpret information preserved in ice cores regarding:

- Signatures of past volcanic eruptions and solar cycles;
- Relationships between climate change and volcanic activity, and climate change and solar activity as well;
- Traces of past supernovae in our galaxy, in order to understand better the rate of galactic supernova explosions.

Moreover, we are promoting experimental projects on:

- Development of an automated laser melting sampler for analyzing ice cores with high depth resolution and high through-put;
- Development of precise analytical techniques of high sensitivity for analyzing ice cores;
- The application of analytical methods to measure isotopes developed for ice cores to archaeological artifacts;
- The evolution of molecules in space.

On the theoretical side, we are simulating numerically:

- Chemical effects of giant solar flares and supernovae on the Earth's atmosphere;
- The explosive and the r-process nucleosynthesis in core-collapse supernovae.

Combining our experimental evidence and theoretical simulations, we are promoting the researches mentioned above. In particular, climate change is the most critical issue facing the world in the 21st century. It is also emphasized that the frequency of supernova explosions in our galaxy has not yet been fully understood, and this is a crucial key to understand of the r-process nucleosynthesis, one of the goals of the Nishina Center. We note that our subjects all will contribute to an understanding relationships between the Universe and Earth.

Members

Director

Yuko MOTIZUKI

Research/Technical Scientists

Kazuya TAKAHASHI (Senior Research Scientist)

Yoichi NAKAI (Senior Research Scientist)

Technical Staff I

Yu Vin SAHOO

Senior Visiting Scientists

Yasushige YANO (RIKEN/Nishina Memorial Foundation)

Kunihiko KODERA (Meteorological Res. Inst.)

Visiting Scientists

Hideharu AKIYOSHI (Nat'l Inst. for Environmental Studies)

Naoyuki KURITA (Nagoya Univ.)

Akira HORI (Kitami Inst. of Tech.)

Hideki MADOKORO (Mitsubishi Heavy Industries, Ltd.)

Kazuho HORIUCHI (Hirosaki Univ.)

Hideaki MOTOYAMA (Nat'l Inst. of Polar Res.)

Yoshinori IIZUKA (Hokkaido Univ.)

Kenji TANABE (Okayama Univ. of Sci.)

Visiting Technician

Junya HIROSE (Fusion Tech. Co., Ltd.)

Student Trainee

Hisashi HAYAKAWA (Osaka Univ.)

Part-time Worker

Satomi NEGISHI (Part-time Worker I)

List of Publications & Presentations

Publications

[Original papers]

T. Minami, K. Hatanaka, Y. Motizuki, Y. Nakai, and K. Takahashi, "A method of collecting trace amounts of vermilion from artifacts for source estimation by sulfur isotope ($\delta^{34}\text{S}$) analysis: use of sulfur-free adhesive," *Journal of Archaeological Science: Reports* **28**, 102027, (2019).

[Books]

望月優子, 「Newton ライト 2.0 周期表」 (協力), ニュートンプレス, 2019 年 12 月.

望月優子, 「ニュートン式超図解 最強に面白い!! 周期表」 (協力), ニュートンプレス, 2019 年 7 月.

Presentations

[International conferences/workshops]

Y. Motizuki (invited), "The oxygen isotopic variations in a Dome Fuji (Antarctica) ice core—Relationships of the temperature proxy with solar activity and oceanic variations," WCRP/SPARC SATIO-TCS joint workshop on Stratosphere-Troposphere Dynamical Coupling in the Tropics, Kyoto, February 21–25, 2020.

H. Akiyoshi, Y. Nakai, Y. Motizuki, T. Imamura, and Y. Yamashita, "Ozone change simulations of Halloween event and Carrington event using MIROC3.2 chemistry-climate model," WCRP/SPARC SATIO-TCS joint workshop on Stratosphere-Troposphere Dynamical Coupling in the Tropics, Kyoto, February 21–25, 2020.

Y. V. Sahoo, K. Takahashi, Y. Nakai, Y. Motizuki, and H. Motoyama, "Annually-resolved water isotope measurements in a shallow ice core (DFS10) for 60 meters depth," (A poster paper), The Tenth Symposium on Polar Science, Tachikawa, December 3–5, 2019.

S. Fujita, K. Goto-Azuma, M. Hirabayashi, A. Hori, Y. Iizuka, Y. Motizuki, H. Motoyama, K. Takahashi, H. Enomoto, K. Fukui, Y. Hoshina, F. Nakazawa, S. Sugiyama, and S. Surdyk, "Metamorphism of layered firn at Dome Fuji, Antarctica: Evolution of relations between Near-infrared reflectivity and the other textural/chemical properties," The Tenth Symposium on Polar Science, Tachikawa, December 3–5, 2019.

K. Kanzawa, F. Miyake, Y. Tada, K. Horiuchi, S. Otani, K. Sasa, Y. Motizuki, K. Takahashi, Y. Nakai, H. Motoyama, and H. Matsuzaki, "Variation of cosmogenic ^{10}Be for cosmic ray event in 5480 BC from Antarctic Dome Fuji ice core," The 8th East Asia Accelerator Mass Spectrometry Symposium, Nagoya, Japan, December 3–6, 2019.

Y. Motizuki (invited), "Women in Astronomy: A view from a gender-imbalanced country," IAU Symposium 358: "Astronomy for Equity, Diversity and Inclusion—a roadmap to action within the framework of IAU centennial anniversary," Tokyo, November 12–15, 2019.

Y. Motizuki (invited), "Historical supernova signatures in polar ice cores," International workshop on "Historical supernovae, novae and other transient events," Leiden, the Netherlands, October 14–18, 2019.

[Domestic conferences/workshops]

望月優子, 高橋和也, 中井陽一, Y. V. Sahoo, 本山秀明, 小寺邦彦, 「南極ドームふじアイスコアからさぐる気候変動と太陽活動との相関」, 日本天文学会 2020 年春季年会, つくば, 2020 年 3 月 16–19 日.

中井陽一, 日高宏, 渡辺直樹, 「低エネルギーイオンと低温氷表面との反応実験装置開発の現状」, 日本物理学会第 75 回年次大会, 名古屋, 2020 年 3 月 16 日–19 日.

菅澤佳世, 三宅美沙, 多田悠馬, 堀内一穂, 大谷昴, 笹公和, 高橋努, 松村真寿美, 落合悠太, 望月優子, 高橋和也, 中井陽一, 本山秀明, 松崎浩之, 「BC5480 年宇宙線イベントにおけるドームふじアイスコア中の ^{10}Be と ^{36}Cl 濃度の変動」, 第 67 回応用物理学会春季学術講演会, 東京, 2020 年 3 月 12–15 日.

三宅美沙, 堀内一穂, 櫻井敬久, 望月優子, 中井陽一, 高橋和也, 本山秀明, 松崎浩之, 「宇宙線生成核種を用いた紀元前 660 年頃の宇宙線イベント調査」, 第 67 回応用物理学会春季学術講演会, 東京, 2020 年 3 月 12–15 日.

望月優子 (招待講演), 「南極氷中の核種存在比から過去の気候変動をさぐる—宇宙との関連を視野に」, 埼玉大学理学部物理量子力学特別講義, さいたま, 2020 年 1 月 20 日.

高橋和也 (招待講演), 「極微量の硫黄同位体比分析による, 遺跡から出土した水銀朱の産地同定」, 第 370 回ガスクロマトグラフィー研究会特別講演会, 「科学と文化に貢献するガスクロマトグラフィー—人を知る, 地球を知る, 宇宙を知る」, 東京, 2019 年 11 月 22 日.

望月優子 (招待講演), 「ドームふじアイスコアから探る気候変動と太陽活動との関係」, 東京大学大学院理学系研究科 地球惑星科学専攻 佐藤研究室セミナー, 東京, 2019 年 10 月 8 日.

菅澤佳世, 三宅美沙, 多田悠馬, 堀内一穂, 大谷昴, 笹公和, 望月優子, 高橋和也, 中井陽一, 本山秀明, 松崎浩之, 「ドームふじアイスコア中 ^{10}Be と ^{36}Cl 濃度の測定による BC5480 年宇宙線イベントの調査」, 日本物理学会 2019 年秋季大会, 山形, 2019 年 9 月 17–20 日.

中井陽一, 日高宏, 渡部直樹, 「星間塵表面を模擬した低温氷表面と低エネルギーイオンとの反応実験装置の開発」 (ポスター発表), 原子衝突学会第 44 回年会, 調布, 2019 年 9 月 5 日.

望月優子 (招待講演), 「南極の氷からひもとく宇宙と地球の歴史」, 公益財団法人山田長満奨学会 30 周年記念講演会, 川崎, 2019 年 7 月 20 日.

Press releases

高橋和也, 望月優子, 南武志, 「超微量硫黄同位体比分析を考古学に応用する—京田遺跡の出土品から赤色顔料を精密分析—」, 2019 年 11 月 26 日. https://www.riken.jp/press/2019/20191126_2/

K. Takahashi and Y. Motizuki, “Sticky tape: A key ingredient for mapping artifact origins,” March 9, 2020. https://www.riken.jp/en/news_pubs/research_news/pr/2019/20191126_2/

RIKEN Science News blog; It Ain't Magic, “Tape and vermilion: ingredients for mapping artifact origins,” by Adam Phillips, March 9, 2020. <https://itaintmagic.riken.jp/hot-off-the-press/tape-and-vermilion-ingredients-for-mapping-artifact-origins/>

望月優子 (個別取材受), 「サイエンス View: 地球最古の氷 掘削せよ」読売新聞記事, 2019 年 5 月 26 日.

Outreach activities

望月優子 (招待講演), 「南極の氷からひもとく宇宙と地球の歴史と研究環境を皆で整えていくことの大切さ」, 高松第一高等学校 (香川県) 理研団体見学, 和光, 2019 年 7 月 29 日.

Y. V. Sahoo (Invited talk), “Studying and pursuing research positions in Japan,” Sakura Science High School Program promoted by Department of Japan-Asia Youth Exchange Program in Science, Japan Society and Technology Agency, Wako, June 11, 2019.

望月優子 (招待講演), 「南極の氷からひもとく宇宙と地球の歴史」, KEK-TYL スクール理系女子キャンプ 2019, つくば, 2019 年 4 月 3-4 日.

Others

K. Takahashi, “Detecting traces of sulfur in ice cores—An advanced isotope-measuring system can reveal insights about past environments in shorter time,” RIKEN RESEARCH, SUMMER 2019, November 2019.

Nuclear Science and Transmutation Research Division Nuclear Transmutation Data Research Group

1. Abstract

The nuclear waste problem is an inevitable subject in nuclear physics and nuclear engineering communities. Since the Chicago Pile was established in 1942, nuclear energy has become one of major sources of energy. However, nowadays the nuclear waste produced at nuclear power plants has caused social problems. Minor actinide components of the waste have been studied well as a fuel in fast breeder reactors or ADS. Long-lived fission products (LLFP) in waste, on the other hand, have not been studied extensively. A deep geological disposal has been a policy of several governments, but it is difficult to find out location of the disposal station in terms of security, sociology and politics. To solve the social problem, a scientific effort is necessary for nuclear physics community to find out efficient methods for reduction of nuclear waste radioactivity. In the world-wide situation above, our Group aims to obtain reaction data of LLFP at RIBF and other muon facilities for muon capture data. These data are necessary to design an accelerator-based system for transmutation, and also may lead to a new discovery and invention for peaceful use of nuclear power and the welfare of humanity.

2. Major Research Subjects

The Group is formed by three research teams. The first two Teams, “Fast RI Data Team” and “Slow RI Data Team,” are in charge of proton- and deuteron-induced reaction data of LLFP in inverse kinematics at RIBF. The third Team “Muon Data Team” is to obtain muon capture data of LLFP at muon facilities. All of the teams are focusing to obtain high-quality data which are essentially necessary to establish reliable reaction models. Each team has its own subjects and promotes LLFP reaction programs based on their large experiences, techniques and skills.

3. Summary of Research Activity

In 2014, all the teams polished up experimental strategies, formed collaboration and prepared experiments. Physics runs for spallation reaction were successfully organized at RIBF in 2015–2017. The muon program started at RCNP, Osaka University in spring 2016 and the data for Pd isotopes were successfully obtained in 2017–2019 via in-beam method with DC beams at RCNP, and via activation method with pulsed beams at J-PARC and ISIS-RAL/RIKEN facilities.

The reaction data obtained with both fast and energy-degraded beams at RIBF encouraged the nuclear data group of JAEA, and a new database called “JENDLE/ImPACT-2018” has been released. The new database has been generated by a newly developed reaction model “DEURACS” which treats deuteron-induced reactions. DEURACS reproduces very well cross section data, and much better than other reaction models. A simulation code “PHITS” has been re-coordinated to use the database information.

In December 2018, the Team leader, Hideaki Otsu, was invited to join Technical Meeting of IAEA, entitled “Novel Multidisciplinary Applications with Unstable Ion Beams and Complementary Techniques.” Our activity has been demonstrated and recognized internationally.

Member

Group Director

Hiroyoshi SAKURAI (concurrent: Director, RI Physics Lab.)

List of Publications & Presentations

Publications

[Original papers]

H. Okuno, H. Sakurai, Y. Mori, R. Fujita, and M. Kawashima, *Proceedings of the Japan Academy, Series B* **95**, 430–439 (2019).

Presentations

[International conferences/workshops]

H. Sakurai (invited), “A program for accelerator-based transmutation system for LLFP,” Fourth International Workshop on Technology and Components of Accelerator-Driven Systems (TCADS-4), Antwerp, Belgium, October 14–17, 2019.

Press releases

「核のゴミ」問題解決に必要な加速器の概念を提案—既存の300倍の高出力重陽子ビームの加速が可能に—, 2019年8月9日.

Patents

Outreach activities

櫻井博儀, 「核のゴミ」をめぐる元素変換への挑戦, 三鷹ネットワーク大学, 2019年9月19日.

Nuclear Science and Transmutation Research Division

Nuclear Transmutation Data Research Group

Fast RI Data Team

1. Abstract

Fast RI team aims at obtaining and accumulating the cross section data for long lived fission products (LLFPs) in order to explore the possibility of using accelerator for nuclear transmutation.

LLFPs as nuclear waste have been generated continuously in nuclear power plants for wealth for human lives, while people noticed the way of disposal has not necessarily been established, especially after the Fukushima Daiichi power plant disaster. One of the ways to reduce the amount of LLFP or to recover them as recycled resources is nuclear transmutation technique.

RIBF facility has a property to generate such LLFP as a secondary beam and the beam species are identified by event by event. Utilizing the property, absolute values of the cross section of various reactions on LLFPs are measured and accumulated as a database.

2. Major Research Subjects

- (1) Measurement of reaction products by the interaction of LLFPs with proton, deuteron, and photon to explore candidate reactions for the transmutation of LLFPs.
- (2) Evaluation of the cross section data for the neutron induced reactions from the obtained data.

3. Summary of Research Activity

- (1) Acting as a collaboration hub on many groups which plan to take data using fast RI beams in RIBF facility.
- (2) Concentrating on taking data for proton and deuteron induced spallation reactions with inverse kinematics.
- (3) Accumulating the cross section data and evaluating them as evaluated nuclear data.
- (4) Evaluating cross section of neutron induced reaction on LLFP by collaborating with the nuclear model calculation and evaluation group.

Members

Team Leader

Hideaki OTSU (Concurrent: Team Leader, SAMURAI Team)

Visiting Scientists

Takashi TERANISHI (Kyushu Univ.)

Student Trainees

Keita NAKANO (Kyushu Univ.)

List of Publications & Presentations

Publications

[Original papers]

- H. Wang, H. Otsu, N. Chiga *et al.*, "Enhancement of element production by incomplete fusion reaction with weakly bound deuteron," *Commun. Phys.* **2**, 78 (2019).
- K. Nakano, Y. Watanabe, S. Kawase, H. Otsu *et al.*, "Isotope production in proton-, deuteron-, and carbon-induced reactions on ^{93}Nb at 113 MeV/nucleon," *Phys. Rev. C* **100**, 044605 (2019).
- S. Michimasa, J. Hwang, K. Yamada, H. Otsu *et al.*, "OEDO, the energy-degrading beamline at RI Beam Factory," *Prog. Theor. Exp. Phys.* **4**, 043D01 (2019).
- J. Hwang, S. Michimasa, S. Ota, H. Otsu *et al.*, "Angle-tunable wedge degrader for an energy-degrading RI beamline," *Prog. Theor. Exp. Phys.* **4**, 043D02 (2019).
- S. Takeuchi, T. Nakamura, M. Shikata, H. Otsu *et al.*, "Coulomb breakup reactions of $^{93,94}\text{Zr}$ in inverse kinematics," *Prog. Theor. Exp. Phys.* **1**, 013D02 (2019).

[Proceedings]

- X. Sun, H. Wang, H. Otsu, H. Sakurai *et al.*, "Cross section measurements in the reactions of ^{136}Xe on proton, deuteron and carbon at 168 MeV/u," *Proc. of the 15th Internat. Conf. on Nuclear Reaction Mechanisms, CERN-Proceedings-2019-001* (CERN, Geneva, 2019), pp. 153–157.
- Yu. Watanabe, J. Suwa, K. Nakano, H. Otsu *et al.*, "Isotopic production cross sections of residual nuclei in proton- and deuteron-induced reactions on $^{91,92}\text{Y}$, $^{92,93}\text{Zr}$, and $^{93,94}\text{Nb}$ around 100 MeV/nucleon," *Proc. of the 15th Internat. Conf. on Nuclear Reaction Mechanisms, CERN-Proceedings-2019-001* (CERN, Geneva, 2019), pp. 139–144.

Presentations**[International conferences/workshops]**

- H. Otsu, “Cross section measurements for LLFP nuclei at RIBF,” Fourth International Workshop on Technology and Components of Accelerator-Driven Systems (TCADS-4), Antwerp, Belgium, October 14–16, 2019.
- H. Wang, “Spallation reaction study for long-lived fission products in nuclear waste,” International Nuclear Physics Conference 2019 (INPC2019), Glasgow, UK, July 29–August 2, 2019.
- H. Wang, “Spallation reaction study for long-lived fission products in nuclear waste,” International conference on nuclear data and technology (ND2019), Beijing, China, May 19–24, 2019.
- K. Nakano, “Isotope-production Cross Sections of Residual Nuclei in Proton- and Deuteron-induced Reactions on ^{93}Zr at 50 MeV/u,” International conference on nuclear data and technology (ND2019), Beijing, China, May 19–24, 2019.
- X. Sun, “Cross-section Measurement in the Reactions of ^{136}Xe on Proton, Deuteron and Carbon,” International conference on nuclear data and technology (ND2019), Beijing, China, May 19–24, 2019.
- Y. Togano *et al.*, “Status report of dipole strength measurement performed in S09 and ImPACT,” SAMURAI International Collaboration Workshop, Rikkyo University, Japan, August 30–31, 2019.

[Domestic conferences/workshops]

大津秀暁 他 4 名, ImPACT-RIBF Collaboration, 「核変換による高レベル放射性廃棄物の大幅な低減・資源化 (4-1), “LLFP の断面積測定とそのエネルギー依存性”」, 日本原子力学会, 水戸, 2019 年 3 月.

Press releases

ワン・ヘ (Wang He), 大津秀暁, 櫻井博儀, 「重陽子による元素変換確率の増大—そのまま融合するか, 分裂してから一部だけ融合するか—」, 理化学研究所, 2019 年 7 月 5 日.

Doctor theses

中野敬太, “Study of Isotope Production in Proton- and Deuteron-Induced Spallation Reactions on ^{93}Nb and ^{93}Zr ,” 九州大学 大学院総合理工学府.

Bachelor theses

松村理久, 「核分裂生成核種 ^{90}Sr の陽子および重陽子誘起反応に関する研究」, 東邦大学 理学部.

西津美咲, 「Se-79 の核破砕反応データ取得に向けた二次ビームの粒子識別」, 九州大学 総合理工学部.

Nuclear Science and Transmutation Research Division

Nuclear Transmutation Data Research Group

Slow RI Data Team

1. Abstract

This team is in charge of the development of low-energy RI beams of long-lived fission fragments (LLFP) from the ^{238}U by means of degrading the energy of beams produced by the BigRIPS fragment separator.

2. Major Research Subjects

Studies of the slowing down and purification of RI beams are the main subjects of the team. Developments of devices used for the slowing down of RI beams are also an important subject.

- (1) Study and development of the slowed-down methods for LLFP.
- (2) Development of the devices used for the slowing down.
- (3) Operation of the BigRIPS separator and supply the low energy LLFP beam to the experiment in which the cross sections of LLFP are measured at the low energy.
- (4) Development of the framework to seamlessly handle device, detector, DAQ, and analysis for the easy control of the complicated slowed-down RI beam production and its development.

3. Summary of Research Activity

A new OEDO beam line, designed for the slowed-down RI beams, was constructed under the collaboration with CNS, the University of Tokyo. Our group was responsible for the construction of the infrastructure such as the cooling water and the electrical equipment, and the movement and alignment of existing vacuum chambers, quadrupole magnets. The power supply for the Superconducting Triplet Quadrupoles (STQ) was made, which had a stability also under the low current condition.

Slowed-down ^{93}Zr beams with 20 or 50 MeV/nucleon were successfully developed at June 2016 for the first time. The methods to obtain the narrow energy, position, and angle distribution were developed. The methods of the energy adjustment and the particle identification at 50 MeV/nucleon were developed. The ^{93}Zr and ^{107}Pd beams with 50 MeV/nucleon were produced for the nuclear-transmutation experiments using proton or deuteron targets at October 2016. The commissioning experiment of the OEDO beam line was successfully performed at June 2017. The first transmutation experiments using OEDO beam line were performed with ^{93}Zr , ^{107}Pd , and ^{79}Se around 20 MeV/nucleon.

With our developments, the slowed-down RI beams became ready for the transmutation experiments. On the other hand, the procedure to make the slowed-down RI beams became highly specialized. In order to easily produce the slowed-down RI beam, the framework is under the development to seamlessly handle the device, detector, DAQ, and analysis.

Members

Team Leader

Toshiyuki SUMIKAMA

Student Trainee

SungHan BAE (Seoul Nat'l Univ.)

List of Publications & Presentations

Publications

[Original papers]

- S. Takeuchi *et al.*, "Coulomb breakup reactions of $^{93,94}\text{Zr}$ in inverse kinematics," Prog. Theor. Exp. Phys. **2019**, 013D02 (2019).
 S. Michimasa *et al.*, "OEDO, the energy degrading beamline at RI Beam Factory," Prog. Theor. Exp. Phys. **2019**, 043D01 (2019).
 H. Jongwon *et al.*, "Angle-tunable wedge degrader for an energy-degrading RI beamline," Prog. Theor. Exp. Phys. **2019**, 043D02 (2019).

Nuclear Science and Transmutation Research Division

Nuclear Transmutation Data Research Group

Muon Data Team

1. Abstract

Dr. Yoshio Nishina observed muons in cosmic rays in 1937. The muon is an elementary particle similar to electron and classified to lepton group. The muon has positive or negative electric charge, and the lifetime is $2.2 \mu\text{sec}$. The negative muon (μ^-) is 207 times heavier than the electron and behaves as a “heavy electron” in materials. The negative muon is captured by atomic orbits of nuclei to form a muonic atom and cascades down to the 1 s orbit to make muon nuclear capture. The muon is combined with a proton in the nucleus to convert to a neutron and a neutrino. The muon nuclear capture reaction on a nucleus (A_ZN) with the atomic number Z and mass number A generates the isotopes of ${}^{A-x}_{Z-1}N$ ($x = 0, 1, 2, 3, 4$) by emitting some neutrons in the reaction. The phenomenon is called “muon nuclear transmutation.” The reaction branching ratio of ${}^A_ZN(\mu^-, xn\nu)_{Z-1}^{A-x}N$ reactions ($x = 0, 1, 2, 3, 4$) is one of important factors toward various applications with nuclear transmutation technique. From a viewpoint of the nuclear physic, the muon nuclear capture reaction is very unique and interesting. A high-energy compound nuclear state is suddenly generated in the nuclei associated with a weak conversion process of proton to neutron and neutrino. Many experimental results have been so far reported, however, the reaction mechanism itself is not well clarified. The research team aims at obtaining the experimental data to investigate the reaction mechanism of muon nuclear capture, and also at theoretical understanding on the nuclear capture reaction.

2. Major Research Subjects

- (1) Experimental clarification on the mechanism of nuclear muon capture reaction
- (2) Theoretical understanding on the nuclear muon capture reaction
- (3) Interdisciplinary applications with the nuclear transmutation technique

3. Summary of Research Activity

There are two experimental methods to study the muon nuclear capture reaction. The first one is “muon in-beam spectroscopy method.” The neutron and γ -ray emissions from the excited states of ${}^{A-x}_{Z-1}N$ nuclei are prompt events and are observed by the “muon in-beam spectroscopy method” with a DC muon beam. The reaction branching ratio is directly determined by measuring the neutron multiplicity in the reaction. The DC muon beam is available at the MuSIC (Muon Science Innovative Channel) muon facility in the Research Center for Nuclear Physics (RCNP) at Osaka University. The second one is “muon activation method” with the pulsed muon beam. The produced unstable nuclei ${}^{A-x}_{Z-1}N$ make $\beta^{+/-}$ decays. The γ -rays associated with $\beta^{+/-}$ decays to the daughter nuclei are observed in the experiment. The build-up curve of γ -ray yield at muon beam-on and the decay curve at beam-off are measured. Since the half-lives and decay branching ratios of $\beta^{+/-}$ - γ decays are known, the reaction branching ratios to the ${}^{A-x}_{Z-1}N$ nuclei are determined by the γ -ray yield curves. The pulsed muon beam is available at the RIKEN-RAL Muon Facility in the UK and J-PARC muon facility.

Muon nuclear capture reactions are studied on five isotope-enriched palladium targets (${}^{104,105,106,108,110}\text{Pd}$) and five isotope-enriched zirconium targets (${}^{90,91,92,94,96}\text{Zr}$) employing two experimental methods. By obtaining the experimental data on the Pd and Zr targets, the reaction mechanism is investigated experimentally, and the results are compared with appropriate theoretical calculations. The ${}^{107}\text{Pd}$ is classified to a long-lived fission product (LLFP) and is contained in a spent nuclear fuel. The study of muon nuclear capture on the Pd and Zr targets is aiming at exploring a possible reaction path to make the nuclear transmutation of the Pd and Zr metal extracted from the spent nuclear fuel without an isotope separation process. This research was funded by the ImpACT Program of Council for Science, Technology and Innovation (Cabinet Office, Government of Japan).

(1) Experiments with “muon in-beam spectroscopy method”

Muon nuclear capture reactions were investigated on five palladium targets (${}^{104,105,106,108,110}\text{Pd}$) by employing the DC muon beam at MuSIC. The γ -ray and neutron in the muon nuclear capture reaction were measured with the time information relative to muon beam arrival. The measured neutron multiplicity gives the reaction branching ratio of ${}^A_{46}\text{Pd}(\mu^-, xn\nu)_{45}^{A-x}\text{Rh}$ reactions, where $A = 104, 105, 106, 108, 110$ and $x = 0, 1, 2, 3, 4$.

Employing a newly built neutron spectrometer, the neutron was measured to obtain the reaction branching ratios of muon capture reactions on the Pd targets. We have constructed a neutron spectrometer named “Seamine”: Scintillator Enclosure Array for Muon Induced Neutron Emission. The spectrometer consists of 21 liquid scintillation counters, 2 Ge γ -ray detectors, 7 BaF₂ counters. The Pd target, muon beam counters and muon degraders are placed at the center of spectrometer. The neutron counter is a BC-501A liquid scintillation counter with 20 cm diameter and 5 cm depth and is connected to a 5” photo multiplication tube (H4144-01). The total neutron detection efficiency is estimated 5%, where the distance is 4 cm from the target to neutron counters. The Ge γ -ray detectors are placed at 10 cm from the target, and the typical detection efficiency is 0.5% for 200 keV γ -ray. The BaF₂ counters are located beneath the target to detect fast γ -rays emitted from the compound nucleus formed in the reactions. Signals from the liquid scintillation counters are processed in a CAEN V1730B waveform digitizer (16 channel, 14 bit, 500 M samplings/sec.). The neutron- γ discrimination is performed on-line during the experiment, and the detailed data analysis is conducted off-line after the experiment. The neutron energy spectrum is constructed in the digitizer. Signals from Ge detectors are also processed in the digitizer to obtain the energy and time spectrum of γ -rays associated with the reaction. Signals from the BaF₂ counters and muon beam counters are sent to the digitizer to make the fast timing signals.

We have established the muon in-beam spectroscopy method employing the “Seamine” spectrometer. The neutron data analysis

is in progress to obtain the multiplicity, the energy and the TOF spectrum using start signals given by γ -rays detected in the BaF₂ counters. The γ -ray data gives the energy spectrum of prompt γ -rays and muonic X-rays originated from the ^{104,105,106,108,110}Pd targets.

(2) Experiments with “muon activation method” at the RIKEN-RAL Muon Facility

We conducted the experiments on the muon nuclear capture employing the muon activation method at the RIKEN-RAL Muon Facility in the UK. The pulsed muon beam was irradiated on the ^{104,105,106,108,110}Pd targets. The γ -rays were detected by a Ge detector located at the downstream of the Pd targets to maximize the detection efficiency. The build-up and decay curves of γ -ray intensities were measured associated with $\beta^{+/-}$ decays of produced unstable nuclei to daughter nuclei. The γ -ray-yield curves give the absolute radiation activity produced by the reaction, and the reaction branching ratios are determined for ^A₄₆Pd(μ^- , $x\nu$)^{A-x}₄₅Rh reactions. The decay curves of γ -rays from the produced nuclei with long half-lives were measured under low γ -ray background at an experimental apparatus built in a separated room. The detailed off-line data analysis is in progress.

(3) Experiments with “muon activation method” at J-PARC muon facility

The experiments employing the muon activation method were performed at J-PARC muon facility. The five isotope-enriched Pd targets (^{104,105,106,108,110}Pd) were irradiated by the pulsed muon beam, and the build-up and decay curves of γ -ray intensities were measured.

In addition to the Pd targets, the experiments on five isotope-enriched Zr target (^{90,91,92,94,96}Zr) were conducted to obtain the reaction branching ratios of ^A₄₀Zr(μ^- , $x\nu$)^{A-x}₃₉Y reactions, where A = 90, 91, 92, 94, 96. The obtained reaction branching ratios on the Pd and Zr targets are important to understand the reaction mechanism of muon nuclear capture. The ⁹³Zr is one of the LLFP and is contained in a spent nuclear fuel. The experiment on the Zr targets is to explore a possibility to realize the nuclear transmutation of the Zr metal extracted from the spent nuclear fuel.

In order to obtain the reaction branching ratio of ¹⁰⁷₄₆Pd(μ^- , $x\nu$)^{107-x}₄₅Rh reactions, the muon activation experiment was performed employing a Pd target containing ¹⁰⁷Pd of 15.3%. The γ -ray intensities associated with $\beta^{+/-}$ decays of produced unstable nuclei were measured to obtain the build-up and decay curves. Once the branching ratios of the reactions on the ^{104,105,106,108,110}Pd targets are obtained, these contributions are extracted from the branching-ratio data obtained for the Pd target with ¹⁰⁷Pd. The reaction branching ratio of ¹⁰⁷₄₆Pd(μ^- , $x\nu$)^{107-x}₄₅Rh reactions is finally determined. The detailed off-line data analysis is in progress.

(4) Comparison with theory

The muon activation method gives the reaction branching ratios. The muon in-beam spectroscopy method gives the neutron multiplicity and the neutron energy spectrum. These experimental results are important to understand the compound nuclear state and neutron emission mechanism. The reaction branching ratios obtained by the muon activation method are compared with the results of neutron multiplicity measurements. The neutron energy spectrum is considered to be reflected by the energy distribution of compound nuclear state and neutron emission mechanism. The experimental results are compared with the appropriate calculations employing the neutron emission mechanisms due to an evaporation, a cascade and a direct emission processes with assuming the energy distribution at compound nuclear state.

Members

Team Leader

Hiroyoshi SAKURAI

Contract Researcher

Teiichiro MATSUZAKI

List of Publications & Presentations

Publications

[Original papers]

S. Wenner, C. D. Marioara, K. Nishimura, K. Matsuda, S. Lee, T. Namiki, I. Watanabe, T. Matsuzaki, and R. Holmestad, “Muon spin relaxation study of solute?vacancy interactions during natural aging of Al-Mg-Si-Cu alloys,” *Metall. Mater. Trans. A* **50**, 3446–3451 (2019).

[Proceedings]

R. Fujita, M. Kawashima, M. Ozawa, and T. Matsuzaki, “Reduction and resource recycling of high-level radioactive wastes through nuclear transmutation—overview and current progress—,” *Proceeding for the 13th International Conference on Nucleus-Nucleus Collisions (NN2018)*.

Presentations

[International conferences/workshops]

T. Saito, M. Niikura, T. Matsuzaki, and H. Sakurai for ImPACT muon collaboration, “Neutron emission property after nuclear muon capture of palladium,” *International Nuclear Physics Conference 2019, Scottish Event Campus, Glasgow, UK, July 29–August 2, 2019*.

Nuclear Science and Transmutation Research Division High-Intensity Accelerator R&D Group

1. Abstract

The High-Intensity Accelerator R&D group, consisting of two teams, develops elemental technology of high-power accelerators and high-power targets, aiming at future applications to nuclear transmutations of long-lived fission product into short-lived nuclides. The research subjects are superconducting rf cavities for low-velocity ions, design of high-power accelerators, high-power target systems and related technologies.

Nuclear transmutation with high-intensity accelerators is expected to reduce the high-level radioactive wastes and to recycle the precious resources such as rare-earth materials in future. This method is one of the important applications of the ion-accelerator technologies that have been developed at RIKEN for a long time. Under the framework of ImPACT Fujita Program, we have conducted R&D of elemental technology related to the high-power accelerators and high-power targets, from FY2014 to FY2018. We gained a lot of experiences in these R&Ds. Among them, the development of a superconducting rf cavity has become the basis of the upgrade program of the RILAC facility which started in 2016.

2. Major Research Subjects

- (1) R&D of elemental technology of high-power accelerators and high-power targets.

3. Summary of Research Activity

- (1) A high-gradient rf cavity has been constructed and tested based on the superconducting rf technology.
- (2) Several candidates for the high-power target have been proposed and their prototypes have been tested.
- (3) A high-current deuteron RFQ has been designed.

Member

Group Director

Osamu KAMIGAITO (concurrent: Group Director, Accelerator Group)

Nuclear Science and Transmutation Research Division

High-Intensity Accelerator R&D Group

High-Gradient Cavity R&D Team

1. Abstract

We develop new components for accelerators dedicated for low-beta-ions with very high intensity. Specifically, we are designing and constructing a cryomodule for superconducting linac efficient for acceleration of low-beta-ions. In parallel, we try to optimize an rf acceleration system by making computer simulations for acceleration of very high intensity beams.

2. Major Research Subjects

- (1) Development of high-gradient cavities for low beta ions
- (2) Development of power saving cryomodules

3. Summary of Research Activity

- Development of highly efficient superconducting accelerator modules

Members

Team Leader

Naruhiko SAKAMOTO

Research/Technical Scientists

Kazunari YAMADA

Yutaka WATANABE

Kazutaka OZEKI

Research & Development Scientist

Kenji SUDA

List of Publications & Presentations

Publications

[Proceedings]

N. Sakamoto, T. Dantsuka, M. Fujimaki, H. Imao, O. Kamigaito, K. Kusaka, H. Okuno, K. Ozeki, K. Suda, A. Uchiyama, T. Watanabe, Y. Watanabe, K. Yamada, E. Kako, H. Nakai, H. Sakai, K. Umemori, H. Hara, A. Miyamoto, K. Sennyu, and T. Yanagisawa, "Development of superconducting quarter-wave resonator and cryomodule for low-beta ion accelerators at RIKEN Radioactive Isotope Beam Factory," Proceedings of the 19th International Conference on RF Superconductivity (SRF2019), (2019), pp. 750–757.

Presentations

[International conferences/workshops]

N. Sakamoto, T. Dantsuka, M. Fujimaki, H. Imao, O. Kamigaito, K. Kusaka, H. Okuno, K. Ozeki, K. Suda, A. Uchiyama, T. Watanabe, Y. Watanabe, K. Yamada, E. Kako, H. Nakai, H. Sakai, K. Umemori, H. Hara, A. Miyamoto, K. Sennyu, and T. Yanagisawa (invited), "Development of superconducting quarter-wave resonator and cryomodule for low-beta ion accelerators at RIKEN Radioactive Isotope Beam Factory," 19th International Conference on RF Superconductivity (SRF2019), Dresden, Germany, June 30–July 5, 2019.

Nuclear Science and Transmutation Research Division
High-Intensity Accelerator R&D Group
High-Power Target R&D Team

1. Abstract

The subjects of this team cover R&D studies with respect to target technology for the transmutation of the LLFPs.

2. Major Research Subjects

- (1) Liquid lithium target for production of neutron or muon
- (2) Beam window without solid structure

3. Summary of Research Activity

- (1) Liquid lithium target for production of neutron or muon
(H. Okuno)
- (2) Beam window with solid structure
(H. Okuno)

Member**Team Leader**

Hiroki OKUNO

List of Publications & Presentations**Publications****[Original papers]**

H. Okuno, H. Sakurai, Y. Mori, R. Fujita, and M. Kawashima, "Proposal of a 1-ampere-class deuteron single-cell linac for nuclear transmutation," Proceedings of the Japan Academy, Series B **95**, 430–439 (2019).

Presentations**[International conferences/workshops]**

H. Okuno (oral), "Accelerator and target for transmutation of long-lived fission products in nuclear waste," Fourth International Workshop on Technology and Components of Accelerator-Driven Systems (TCADS-4), Antwerp, Belgium, October 14–17, 2019.

H. Okuno (oral), "Seeking for a novel fabrication technology to make a large-bore SRF-QWR cavity for 1-ampere class linac," TTC 2020, Genève, Switzerland, February 4–7, 2020.

Press releases

「核のゴミ」問題解決に必要な加速器の概念を提案—既存の 300 倍の高出力重陽子ビームの加速が可能に—, 理研プレスリリース, 2019 年 8 月 9 日.

Research Facility Development Division Accelerator Group

1. Abstract

The Accelerator Group, consisting of seven teams, pursues various upgrade programs on the world-leading heavy-ion accelerator facility, RI Beam Factory (RIBF), to enhance the accelerator performance and operation efficiency. The programs include the R&D of superconducting ECR ion source, charge stripping systems, beam diagnostic devices, radiofrequency systems, control systems, and beam simulation studies. We are also maintaining the large infrastructure to realize effective operation of the RIBF. Moreover, we are actively promoting the applications of the facility to various research fields.

Our primary mission is to supply intense, stable heavy-ion beams for the users through effective operation, maintenance, and upgrade of the RIBF accelerators and related infrastructure. The director members govern the development programs that are not dealt with by a single team, such as intensity upgrade and effective operation. We also discuss the future plans of RIBF along with other laboratories belonging to the RIBF research division.

Various improvements and developments have been carried out for the RIBF accelerators in order to upgrade the beam intensities and stability. Owing to the efforts, for example, the intensity of the uranium beam has increased by 70% in the last three years, resulting in the intensity of 94 pA (7.7 kW) at the exit of the superconducting ring cyclotron. The beam intensity of ^{124}Xe has increased to 173 pA, corresponding to the beam power of 7.4 kW.

In 2016, a supplemental budget was approved for the upgrade of RIBF aiming at synthesizing heavier new elements. A superconducting linac booster has been constructed at the RILAC facility with this budget under the collaboration with KEK researchers. We also constructed a new superconducting ECR ion source at RILAC. The beam commissioning with the upgraded RILAC, which has been named "SRILAC," was started in January 2020. Finally, the SRILAC facility passed the facility inspection by the Nuclear Regulatory Authority on the last day of FY2019. The accelerating cavities of the ring cyclotron, which had been suffered from the low accelerating voltage, were also modified with this supplemental budget. This modification played a key role in the increase of the beam intensities of uranium and xenon mentioned above. We also started providing intense vanadium beams for the synthesis of a new element [119] at GARIS II in 2017.

On the other hand, we have started a new project with RCNP, Osaka university, for the promotion of application research using short-lived radioisotopes since 2017. A high-power target for production of ^{211}At is under development with RI Application Research Group of RNC in the framework of this project. It will be installed and tested in the SRILAC facility in near future.

An upgrade plan of RIBF for further increasing heavy-ion beams, especially the uranium beam, has been continuously discussed. The plan proposed recently is based on a new idea of "charge-stripper ring (CSR)," which is used to improve the overall stripping efficiency of the uranium beam. This device recirculates and re-injects the uranium ions into the charge stripper until the ions become the charge state required for the succeeding acceleration, while the bunch structure is kept with its isometric orbit lengths for all the charge states. Design study of the whole CSR is under progress after intensive optical calculations for the circulating beam. The final goal of this plan is to increase the uranium beam intensity by 20 times of the present value, namely up to 2000 pA, at the exit of SRC.

2. Major Research Subjects

- (1) Intensity upgrade of RIBF accelerators (Okuno)
- (2) Effective and stable operation of RIBF accelerators (Fukunishi)
- (3) Commissioning of the upgraded RILAC (SRILAC) facility
- (4) Promotion of the future plan

3. Summary of Research Activity

- (1) The maximum intensities of the uranium and xenon beams reached 94 and 173 pA, respectively, at 345 MeV/nucleon.
- (2) The maximum intensity of the calcium beam reached 740 pA at 345 MeV/nucleon, which corresponds to 12.3 kW. That of the krypton beam reached 486 pA, corresponding to 13.4 kW.
- (3) The overall beam availability for the RIBF experiments averaged for 5 years from 2013 to 2017 was 92%. Although the availability fell down to 79% in 2018 because of several hardware troubles, it exceeded 92% in 2019.
- (4) A major upgrade of the accelerator facility has been conducted aiming at synthesizing heavier new elements. It includes construction of a superconducting linac booster of RILAC, construction of a new superconducting ECR ion source, and modification of the accelerating cavities of the ring cyclotron (RRC). The upgraded RILAC (SRILAC) facility passed the facility inspection by the Nuclear Regulatory Authority, as scheduled.
- (5) The large infrastructure was properly maintained based on a well-organized cooperation among the related sections.
- (6) An intensity-upgrade plan of the RIBF has been further investigated. Design study of the charge-stripper ring (CSR) is under progress.

Members

Group Director

Osamu KAMIGAITO

Deputy Group Directors

Hiroki OKUNO (for intensity upgrade)

Nobuhisa FUKUNISHI (for stable and efficient operation)

Junior Research Associate

Takahiro KARINO (Utsunomiya Univ.)

Kaori NAKAMURA (The University of Tokyo)

Research Part-time Worker I

Akira GOTO

Masayuki KASE

Research Consultants

Tadashi FUJINAWA

Toshiyuki HATTORI

Visiting Scientists

Eiji KAKO (KEK)

Taro KONOMI (KEK)

Hirotsuka NAKAI (KEK)

Noboru SASAO (Okayama Univ.)

Kensei UMEMORI (KEK)

Yasutaka IMAI (Okayama Univ.)

Hiroshi SAKAI (KEK)

Student Trainees

Akira FUJIEDA (Okayama Univ.)

Hiroyuki KAINO (Okayama Univ.)

Assistant

Karen SAKUMA

Administrative Part-time Worker II

Ryoko UMEZAKI

List of Publications & Presentations

Publications

[Original papers]

T. Karino, "Evaluation method of beam instability in laser ion source using solenoid," *Rev. Sci. Instrum.* **91**, 033316 (2020).

K. Nakamura, N. Nishiura, M. Okamura, T. Kanetsue, S. Ikeda, and A. Cannavo, "Feasibility study of a compact heavy ion source for investigation of laboratory magnetospheric plasma," *Rev. Sci. Instrum.* **91**, 033503 (2020).

[Proceedings]

O. Kamigaito, K. Ozeki, N. Sakamoto, K. Suda, and K. Yamada, "Measurement of mechanical vibration of SRILAC cavities," *Proceedings of the 19th International Conference on RF Superconductivity (SRF2019)*, (Dresden, Germany, TUP042, 2019), pp. 515.

O. Kamigaito, T. Dantsuka, M. Fujimaki, N. Fukunishi, H. Hasebe, Y. Higurashi, E. Ikezawa, H. Imao, M. Kidera, M. Komiyama, K. Kumagai, T. Maie, Y. Miyake, T. Nagatomo, T. Nakagawa, M. Nakamura, T. Nishi, J. Ohnishi, H. Okuno, K. Ozeki, N. Sakamoto, K. Suda, A. Uchiyama, T. Watanabe, Y. Watanabe, and K. Yamada, "Recent progress in RIKEN RI Beam Factory," *Proceedings of 22nd International Conference on Cyclotrons and their Applications (CYC2019)*, (Cape Town, South Africa, MOB01, 2019).

Presentations

[International conferences/workshops]

O. Kamigaito (invited), "Recent progress in RIKEN RI Beam Factory," *22nd International Conference on Cyclotrons and their Applications (CYC2019)*, Cape Town, South Africa, September 22–27, 2019.

T. Karino (oral), "Evaluation method of beam instability in laser ion source using solenoid," *The 18th International Conference on Ion Sources (ICIS2019)*, Lanzhou, China, September 1–6, 2019.

K. Nakamura (oral), "Feasibility study of a compact heavy ion source for investigation of laboratory magnetospheric plasma," *The 18th International Conference on Ion Sources (ICIS2019)*, Lanzhou, China, September 1–6, 2019.

A. Fujieda (oral), "Ba-ion spectroscopy experiment for high-intensity gamma-ray source using heavy ions," *The 12th International Workshop on Fundamental Physics Using Atoms (FPUA2020)*, Wako, Japan, January 9–10, 2020.

**Research Facility Development Division
Accelerator Group
Accelerator R&D Team**

1. Abstract

We are developing the key hardware in upgrading the RIBF accelerator complex. Our primary focus and research is charge stripper which plays an essential role in the RIBF accelerator complex. Charge strippers remove many electrons in ions and realize efficient acceleration of heavy ions by greatly enhancing charge state. The intensity of uranium beams is limited by the lifetime of the carbon foil stripper conventionally installed in the acceleration chain. The improvement of stripper lifetimes is essential to increase beam power towards the final goal of RIBF in the future. We are developing the low-Z gas stripper. In general gas stripper is free from the lifetime related problems but gives low equilibrium charge state because of the lack of density effect. Low-Z gas stripper, however, can give as high equilibrium charge state as that in carbon foil because of the suppression of the electron capture process. Another our focus is the upgrade of the world's first superconducting ring cyclotron.

2. Major Research Subjects

- (1) Development of charge strippers for high power beams (foil, low-Z gas)
- (2) Upgrade of the superconducting ring cyclotron
- (3) Maintenance and R&D of the electrostatic deflection/inflexion channels for the beam extraction/injection

3. Summary of Research Activity

(1) Development of charge strippers for high power beams (foil, low-Z gas)

(H. Hasebe, H. Imao, H. Okuno)

We are developing the charge strippers for high intensity heavy ion beams. We are focusing on the developments on carbon or berrilium foils and gas strippers including He gas stripper.

(2) Upgrade of the superconducting ring cyclotron

(J. Ohnishi, H. Okuno)

We are focusing on the upgrade of the superconducting ring cyclotron.

(3) Maintenance and R&D of the electrostatic deflection/inflexion channels for the beam extraction/injection

(J. Ohnishi, H. Okuno)

We are developing high-performance electrostatic channels for high power beam injection and extraction.

Members

Team Leader

Hiroki OKUNO

Research/Technical Scientists

Hiroshi IMAO (Senior Research Scientist)

Jun-ichi OHNISHI (Senior Technical Scientist)

Hiroo HASEBE (Technical Scientist)

Special Postdoctoral Researcher

Yasuto MIYAKE

Junior Research Associate

Naoya IKOMA

Visiting Scientists

Andreas ADELMANN (Paul Sherrer Inst.)

Noriyosu HAYASHIZAKI (Tokyo Tech)

Hironori KUBOKI (KEK)

Student Trainees

Taishi SASAKI (Nagaoka Univ. of Tech.)

Yoshiki SHIKUMA (Nagaoka Univ. of Tech.)

Part-time Workers

Taishi SASAKI (Research Part-time Worker II)

Yoshiki SHIKUMA (Research Part-time Worker II)

List of Publications & Presentations

Publications

[Original papers]

- N. Ikoma, Y. Miyake, M. Takahashi, H. Okuno, S. Namba, K. Takahashi, T. Sasaki, and T. Kikuchi, "Demonstration of plasma window with diameter of 20 mm and pressure separation for accelerator application," *Plasma Fusion Res.* **14**, 1206148 (2019).
- N. Ikoma, Y. Miyake, M. Takahashi, H. Okuno, S. Namba, K. Takahashi, T. Sasaki, and T. Kikuchi, "Characteristics of plasma window with various channel diameters for accelerator applications," *Review of Scientific Instruments* **91**, 053503 (2020).

Research Facility Development Division

Accelerator Group

Ion Source Team

1. Abstract

Our aim is to operate and develop the ECR ion sources for the accelerator-complex system of the RI Beam Factory. We focus on further upgrading the performance of the RI Beam Factory through the design and fabrication of a superconducting ECR ion source for production of high-intensity heavy ions.

2. Major Research Subjects

- (1) Operation and development of the ECR ion sources
- (2) Development of a superconducting ECR heavy-ion source for production of high-intensity heavy ion beams

3. Summary of Research Activity

(1) Operation and development of ECR ion sources

(T. Nakagawa, M. Kidera, Y. Higurashi, T. Nagatomo, Y. Kanai, and H. Haba)

We routinely produce and supply various kinds of heavy ions such as zinc and calcium ions for the super-heavy element search experiment as well as uranium ions for RIBF experiments. We also perform R&D's to meet the requirements for stable supply of high-intensity heavy ion beams.

(2) Development of a superconducting ECR ion source for use in production of a high-intensity heavy ion beam

(T. Nakagawa, J. Ohnishi, M. Kidera, Y. Higurashi, and T. Nagatomo)

The RIBF is required to supply heavy ion beams with very high intensity so as to produce RI's and for super-heavy element search experiment. We have designed and are fabricating an ECR ion source with high magnetic field and high microwave-frequency, since the existing ECR ion sources have their limits in beam intensity. The coils of this ion source are designed to be superconducting for the production of high magnetic field. We are also designing the low-energy beam transport line of the superconducting ECR ion source.

Members

Team Leader

Takahide NAKAGAWA

Research/Technical Scientists

Takashi NAGATOMO (Senior Technical Scientist)

Yoshihide HIGURASHI (Technical Scientist)

Masanori KIDERA (Technical Scientist)

Special Temporary Research Scientist

Yasuyuki KANAI

List of Publications & Presentations

Publications

[Original papers]

T. Nagatomo *et al.*, "High intensity vanadium beam for synthesis of new superheavy elements with well-controlled emittance by using "slit triplet"," Rev. Sci. Instrum. ICIS18, 023318 (2020).

A. Uchiyama *et al.*, "Control system for the new RIKEN 28-GHz superconducting electron cyclotron resonance ion source for SRILAC," Rev. Sci. Instrum. ICIS18, 025101 (2020).

[Proceedings]

T. Nagatomo *et al.*, "Development of RIKEN 28 GHz SC-ECRISs for synthesizing super-heavy elements," Proc. HIAT2018, doi:10.18429/JACoW-HIAT2018-TUZAA01.

Presentations

[International conferences/workshops]

Y. Higurashi (invited), "Status and perspective for high intensity uranium beams from the RIKEN 28 GHz ECRIS," ICIS2019, Lanzhou, China, September 1–6, 2019.

T. Nakagawa (oral), "Production of intense metal ion beam with RIKEN 28 GHz SC-ECRIS," ICIS2019, Lanzhou, China, September 1–6, 2019.

T. Nagatomo (oral), "Well-controlled emittance of the metallic ion beam extracted from the 28 GHz SC-ECRIS adopting the superconducting acceleration cavity for new super heavy elements research," ICIS2019, Lanzhou, China, September 1–6, 2019.

Research Facility Development Division

Accelerator Group

RILAC Team

1. Abstract

The operation and maintenance of the RIKEN Heavy-ion Linac (RILAC) have been carried out. There are two operation modes: one is the stand-alone mode operation and the other is the injection mode operation. The RILAC has been used especially as an injector for the RIKEN RI-Beam Factory accelerator complex. The RILAC is composed of the 28 GHz SC ECR ion source, the frequency-variable RFQ linac, the frequency-variable main linac, and the SC booster linac (SRILAC).

2. Major Research Subjects

- (1) The long term high stability of the RILAC operation.
- (2) Improvement of high efficiency of the RILAC operation.

3. Summary of Research Activity

The RILAC was started to supply ion beams for experiments in 1981. Thousands hours are spent in a year for delivering many kinds of heavy-ion beams to various experiments.

The RILAC has two operation modes: one is the stand-alone mode operation delivering low-energy beams directly to experiments and the other is the injection mode operation injecting beams into the RRC. In the first mode, the RILAC supplies a very important beam to the nuclear physics experiment of “the research of super heavy elements.” In the second mode, the RILAC plays a very important role as upstream end of the RIBF accelerator complex.

The maintenance of these devices is extremely important in order to keep the long-term high stability and high efficiency of the RILAC beams. Therefore, improvements are always carried out for the purpose of more stable and more efficient operation.

Members

Team Leader

Eiji IKEZAWA

Research/Technical Scientist

Yutaka WATANABE (Senior Technical Scientist)

List of Publications & Presentations

Publications

[Proceedings]

M. Tamura, E. Ikezawa, T. Ohki, H. Yamauchi, K. Oyamada, A. Yusa, K. Kaneko, Y. Watanabe, and O. Kamigaito, “Present status of RILAC,” Proceedings of the 16th Annual Meeting of Particle Accelerator Society of Japan, (2019), pp. 1263.

Presentations

[Domestic conferences]

田村匡史, 池沢英二, 大木智則, 山内啓資, 小山田和幸, 遊佐陽, 金子健太, 渡邊裕, 上垣外修一, (FSPI010), 「理研重イオンリニアックの現状報告」, 第16回日本加速器学会年会, 京都, 2019年7月31日-8月3日.

Research Facility Development Division Accelerator Group Cyclotron Team

1. Abstract

Together with other teams of Nishina Center accelerator division, maintaining and improving the RIBF cyclotron complex. The accelerator provides high intensity heavy ions. Our mission is to have stable operation of cyclotrons for high power beam operation. Recently stabilization of the rf system is a key issue to provide 10 kW heavy ion beam.

2. Major Research Subjects

- (1) RF technology for Cyclotrons
- (2) Operation of RIBF cyclotron complex
- (3) Maintenance and improvement of RIBF cyclotrons
- (4) Single turn operation for polarized deuteron beams
- (5) Development of superconducting cavity

3. Summary of Research Activity

- Development of the rf system for a reliable operation
- Development of highly stabilized low level rf system
- Development of superconducting cavity
- Development of the intermediate-energy polarized deuteron beams.

Members

Team Leader

Naruhiko SAKAMOTO

Research/Technical Scientists

Kazutaka OZEKI (Senior Technical Scientist)

Kenji SUDA (Technical Scientist)

List of Publications & Presentations

Publications

[Proceedings]

- K. Suda, O. Kamigaito, K. Ozeki, N. Sakamoto, Y. Watanabe, K. Yamada, E. Kako, H. Nakai, H. Sakai, K. Umemori, H. Hara, A. Miyamoto, K. Sennyu, and T. Yanagisawa, "Fabrication and performance of superconducting quarter-wavelength resonators for SRILAC," Proceedings of the 19th International Conference on RF Superconductivity, (2019), pp. 182–187.
- H. Imao, O. Kamigaito, N. Sakamoto, T. Watanabe, Y. Watanabe, K. Yamada, and K. Oyamada, "Non-evaporative getter-based differential pumping system for SRILAC at RIBF," Proceedings of the 19th International Conference on RF Superconductivity (2019), pp. 419–423.
- K. Yamada, T. Dantsuka, H. Imao, O. Kamigaito, K. Kusaka, H. Okuno, K. Ozeki, N. Sakamoto, K. Suda, T. Watanabe, Y. Watanabe, E. Kako, H. Nakai, H. Sakai, K. Umemori, H. Hara, A. Miyamoto, K. Sennyu, and T. Yanagisawa, "Construction of superconducting linac booster for heavy-ion linac at RIKEN Nishina Center," Proceedings of the 19th International Conference on RF Superconductivity, (2019), pp. 502–507.
- O. Kamigaito, K. Ozeki, N. Sakamoto, K. Suda, and K. Yamada, "Measurement of mechanical vibration of SRILAC cavities," Proceedings of the 19th International Conference on RF Superconductivity (2019), pp. 513–517.
- 月居憲俊, 福澤聖児, 濱仲誠, 石川盛, 小林清志, 小山亮, 仲村武志, 西田稔, 西村誠, 柴田順翔, 矢富一慎, 大関和貴, 段塚知志, 藤巻正樹, 藤縄雅, 福西暢尚, 長谷部裕雄, 日暮祥英, 池沢英二, 今尾浩士, 上垣外修一, 金井保之, 加瀬昌之, 木寺正憲, 込山美咲, 熊谷桂子, 真家武士, 長瀬誠, 長友傑, 中川孝秀, 中村仁音, 大西純一, 奥野広樹, 坂本成彦, 須田健嗣, 内山暁仁, 渡部秀, 渡邊環, 渡邊裕, 山田一成, 山澤秀行, 「理研 RIBF におけるリングサイクロトロン」の運転報告, 第 16 回日本加速器学会年会, 京都大学吉田キャンパス, (京都, 2019), pp.1193–1197.
- 濱仲誠, 福澤聖児, 石川盛, 小林清志, 小山亮, 仲村武志, 西田稔, 西村誠, 柴田順翔, 月居憲俊, 矢富一慎, 金子健太, 小山田和幸, 田村匡史, 遊佐陽, 須田健嗣, 藤巻正樹, 福西暢尚, 後藤彰, 長谷部裕雄, 日暮祥英, 今尾浩士, 加瀬昌之, 上垣外修一, 木寺正憲, 込山美咲, 熊谷桂子, 真家武士, 長瀬誠, 長友傑, 中川孝秀, 大西純一, 奥野広樹, 大関和貴, 坂本成彦, 内山暁仁, 渡部秀, 渡邊環, 渡邊裕, 山田一成, 小高康照, 大城幸光, 「理研 AVF サイクロトロン運転の現状報告」, 第 16 回日本加速器学会年会, 京都大学吉田キャンパス, (京都, 2019), pp. 1224–1228.

Presentations

[International conferences/workshops]

- K. Ozeki (oral), "Power couplers for RIKEN superconducting QWR," World Wide Fundamental Power Coupler meeting #5, Geneva, Switzerland, June 25–26, 2019.

- K. Suda, O. Kamigaito, K. Ozeki, N. Sakamoto, Y. Watanabe, K. Yamada, E. Kako, H. Nakai, H. Sakai, K. Umemori, H. Hara, A. Miyamoto, K. Sennyu, and T. Yanagisawa (poster), “Fabrication and performance of superconducting quarter-wavelength resonators for SRILAC,” 19th International Conference on RF Superconductivity (2019), Dresden, Germany, June 30–July 5, 2019.
- H. Imao, O. Kamigaito, N. Sakamoto, T. Watanabe, Y. Watanabe, K. Yamada, and K. Oyamada (poster), “Non-evaporative getter-based differential pumping system for SRILAC at RIBF,” 19th International Conference on RF Superconductivity (2019), Dresden, Germany, June 30–July 5, 2019.
- K. Yamada, T. Dantsuka, H. Imao, O. Kamigaito, K. Kusaka, H. Okuno, K. Ozeki, N. Sakamoto, K. Suda, T. Watanabe, Y. Watanabe, E. Kako, H. Nakai, H. Sakai, K. Umemori, H. Hara, A. Miyamoto, K. Sennyu, and T. Yanagisawa (poster), “Construction of superconducting linac booster for heavy-ion linac at RIKEN Nishina Center,” 19th International Conference on RF Superconductivity (2019), Dresden, Germany, June 30–July 5, 2019.
- O. Kamigaito, K. Ozeki, N. Sakamoto, K. Suda, and K. Yamada (poster), “Measurement of mechanical vibration of SRILAC cavities,” 19th International Conference on RF Superconductivity (2019), Dresden, Germany, June 30–July 5, 2019.

[Domestic conferences/workshops]

月居憲俊, 福澤聖児, 濱仲誠, 石川盛, 小林清志, 小山亮, 仲村武志, 西田稔, 西村誠, 柴田順翔, 矢富一慎, 大関和貴, 段塚知志, 藤卷正樹, 藤縄雅, 福西暢尚, 長谷部裕雄, 日暮祥英, 池沢英二, 今尾浩士, 上垣外修一, 金井保之, 加瀬昌之, 木寺正憲, 込山美咲, 熊谷桂子, 真家武士, 長瀬誠, 長友傑, 中川孝秀, 中村仁音, 大西純一, 奥野広樹, 坂本成彦, 須田健嗣, 内山暁仁, 渡部秀, 渡邊環, 渡邊裕, 山田一成, 山澤秀行 (ポスター発表), 「理研 RIBF におけるリングサイクロトロン」の運転報告, 第 16 回日本加速器学会年会, 京都大学吉田キャンパス, 京都, 2019 年 7 月 31 日–8 月 3 日.

濱仲誠, 福澤聖児, 石川盛, 小林清志, 小山亮, 仲村武志, 西田稔, 西村誠, 柴田順翔, 月居憲俊, 矢富一慎, 金子健太, 小山田和幸, 田村匡史, 遊佐陽, 須田健嗣, 藤卷正樹, 福西暢尚, 後藤彰, 長谷部裕雄, 日暮祥英, 今尾浩士, 加瀬昌之, 上垣外修一, 木寺正憲, 込山美咲, 熊谷桂子, 真家武士, 長瀬誠, 長友傑, 中川孝秀, 大西純一, 奥野広樹, 大関和貴, 坂本成彦, 内山暁仁, 渡部秀, 渡邊環, 渡邊裕, 山田一成, 小高康熙, 大城幸光 (ポスター発表), 「理研 AVF サイクロトロン」の運転の現状報告, 第 16 回日本加速器学会年会, 京都大学吉田キャンパス, 京都, 2019 年 7 月 31 日–8 月 3 日.

Research Facility Development Division

Accelerator Group

Beam Dynamics & Diagnostics Team

1. Abstract

Aiming at stable and efficient operation of the RIBF cascaded cyclotron system, Beam Dynamics and Diagnostics Team develops power supplies, beam instrumentation, computer control and beam dynamic studies. We have successfully increased the beam availability for user experiments to more than 90%. We have also established small-beam-loss operations. The latter strongly contributes to recent high-power operations at RIBF.

2. Major Research Subjects

- (1) More efficient and stable operations of the RIBF cascaded cyclotron system
- (2) Maintenance and developments of the beam instrumentation
- (3) Developments of computer control system for more intelligent and efficient operations
- (4) Maintenance and improvements of the magnet power supplies for more stable operations
- (5) Upgrade of the existing beam interlock system for high-power beams with few tens of kW

3. Summary of Research Activity

- (1) High-intensity heavy-ion beams such as 94-pnA uranium, 173-pnA xenon, 486-pnA krypton, and 740-pnA calcium beams have been obtained.
- (2) The world-first high-Tc SQUID beam current monitor has been developed.
- (3) The bending power of the fixed-frequency Ring Cyclotron has been upgraded to 700 MeV.
- (4) The world-most-intense V beams are stably supplied to super-heavy-element search experiments.
- (5) The RIBF control system has been operated stably by replacing legacy hardware controllers carried over from our old facility with new ones. Several useful operation tools are also developed.
- (6) The dated power supplies exciting the main coils of RIKEN Ring Cyclotron has been upgrade to a new one having a better long-term stability than the old ones.

Members

Team Leader

Nobuhisa FUKUNISHI

Research/Technical Scientists

Masaki FUJIMAKI (Senior Technical Scientist)

Keiko KUMAGAI (Senior Technical Scientist)

Tamaki WATANABE (Senior Technical Scientist)

Kazunari YAMADA (Senior Technical Scientist)

Akito UCHIYAMA (Technical Scientist)

Expert Technician

Misaki KOMIYAMA

Postdoctoral Researcher

Takahiro NISHI

Visiting Scientists

Shin-ichiro HAYASHI (Hiroshima Int'l Univ.)

Atsushi KAMOSHIDA (Nat'l Instruments Japan Corporation)

Takuya MAEYAMA (Kitasato Univ.)

Student Trainee

Anri MOCHIZUKI (Kitasato Univ.)

Part-time Worker

Makoto NAGASE (Research Part-time Worker I)

List of Publications & Presentations

Publications

[Original papers]

A. Uchiyama, T. Nagatomo, Y. Higurashi, J. Ohnishi, M. Komiyama, K. Kumagai, M. Fujimaki, H. Yamauchi, M. Tamura, K. Kaneko, N. Fukunishi, and T. Nakagawa, "Control system for the new RIKEN 28-GHz superconducting electron cyclotron resonance ion source for SRILAC," *Rev. Sci. Instrum.* **91**, 025101 (2020).

[Proceedings]

- T. Watanabe, H. Imao, O. Kamigaito, N. Sakamoto, N. Fukunishi, M. Fujimaki, K. Yamada, Y. Watanabe, T. Toyama, T. Miyao, A. Miura, K. Hanamura, T. Kawachi, R. Koyama, and A. Kamoshida, "Calibration of the beam energy and position monitor system for the RIKEN superconducting acceleration cavity," Proceedings of the 2019 International Beam Instrumentation Conference (IBIC2019), Pre-Release 1–3, Malmö, Sweden, September 8–12, 2019.
- K. Yamada *et al.*, "Construction of superconducting linac booster for heavy-ion linac at RIKEN Nishina Center," Proc. SRF2019, TUP037, Dresden, Germany, 2019-July, p. 504.
- R. Koyama, A. Uchiyama, H. Imao, and T. Watanabe, "Upgrade of gas stripper control system for system integration at RIBF," Proceedings of the 16th Annual Meeting of Particle Accelerator Society of Japan, 865–868, Kyoto, Japan, July 31–August 3, 2019.
- A. Uchiyama, M. Komiyama, K. Kumagai, E. Ikezawa, J. Ohnishi, H. Yamauchi, and M. Tamura, "Upgrade of electromagnet power supply control at RILAC," Proceedings of the 16th Annual Meeting of Particle Accelerator Society of Japan, 869–872, Kyoto, Japan, July 31–August 3, 2019.
- T. Watanabe, T. Toyama, K. Hanamura, H. Imao, O. Kamigaito, A. Kamoshida, T. Kawachi, R. Koyama, N. Sakamoto, N. Fukunishi, M. Fujimaki, A. Miura, T. Miyao, K. Yamada, and Y. Watanabe, "Mapping measurement for beam energy position monitor system for RIKEN superconducting acceleration cavity," Proceedings of the 16th Annual Meeting of Particle Accelerator Society of Japan, 1105–1108, Kyoto, Japan, July 31–August 3, 2009.

Presentations**[International conferences/workshops]**

- K. Yamada *et al.* (poster), "Construction of superconducting linac booster for heavy-ion linac at RIKEN Nishina Center," 19th International Conference on RF Superconductivity (SRF2019), Dresden, Germany, June 30–July 5, 2019.
- A. Uchiyama, T. Nagatomo, Y. Higurashi, J. Ohnishi, M. Komiyama, K. Kumagai, M. Fujimaki, H. Yamauchi, M. Tamura, K. Kaneko, N. Fukunishi, and T. Nakagawa (poster), "Control system for the new RIKEN 28-GHz superconducting electron cyclotron resonance ion source for SRILAC," The 18th International Conference on Ion Sources (ICIS2019), Lanzhou, China, September 1–6, 2019.
- T. Watanabe, H. Imao, O. Kamigaito, N. Sakamoto, N. Fukunishi, M. Fujimaki, K. Yamada, Y. Watanabe, T. Toyama, T. Miyao, A. Miura, K. Hanamura, T. Kawachi, R. Koyama, and A. Kamoshida, "Calibration of the beam energy and position monitor system for the RIKEN superconducting acceleration cavity," The 2019 International Beam Instrumentation Conference (IBIC2019), Malmö, Sweden, September 8–12.
- M. Komiyama *et al.* (poster), "Recent updates of the RIKEN RI Beam Factory control system," The 17th Biennial International Conference on Accelerator and Large Experimental Physics Control Systems (ICALEPCS 2019), New York, USA, October 5–11, 2019.
- K. Yamada (oral), "Cryomodule design, assembly and installation utilizing KOACH system," TESLA Technology Collaboration (TTC) Meeting 2020 at CERN, Geneva, Switzerland, February 4–7, 2020.

[Domestic symposium]

- M. Komiyama, A. Uchiyama, and K. Kumagai (poster), "Beam Interlock System of RIKEN RI Beam Factory," 7th Accelerator Facility Safety Symposium, Tokai, Ibaragi, Japan, January 23–24, 2020.

Research Facility Development Division
Accelerator Group
Cryogenic Technology Team

1. Abstract

We are operating the cryogenic system for the superconducting ring cyclotron in RIBF. We are operating the helium cryogenic system in the south area of RIKEN Wako campus and delivering the liquid helium to users in RIKEN. We are trying to collect efficiently gas helium after usage of liquid helium.

2. Major Research Subjects

- (1) Operation of the cryogenic system for the superconducting ring cyclotron in RIBF.
- (2) Operation of the helium cryogenic plant in the south area of Wako campus and delivering the liquid helium to users in Wako campus.

3. Summary of Research Activity

- (1) Operation of the cryogenic system for the superconducting ring cyclotron in RIBF
(H. Okuno, T. Dantsuka, M. Nakamura, T. Maie).
- (2) Operation of the helium cryogenic plant in the south area of Wako campus and delivering the liquid helium to users in Wako campus.
(T. Dantsuka, S. Tsuruma, M. Kuroiwa, M. Takahashi, H. Okuno).

Members

Team Leader

Hiroki OKUNO

Research/Technical Scientists

Masato NAKAMURA (Senior Technical Scientist)

Expert Technicians

Tomoyuki DANTSUKA

Takeshi MAIE

Part-time Workers

Mamoru TAKAHASHI (Research Part-time Worker I)
 Shizuho TSURUMA (Administrative Part-time Worker I)

Mayumi KUROIWA (Administrative Part-time Worker II)

Research Facility Development Division Accelerator Group Infrastructure Management Team

1. Abstract

Our team is in charge of operation, maintenance, and monitoring of research infrastructure of the whole RIBF, such as cooling water system, air conditioner system, building equipment, and so on. It is very important to keep these infrastructures working properly for the effective and efficient operation of RIBF.

We are also involved in the planning of the RIBF beam time, which is conducted by the RIBF User Liaison Team, through the estimation of the utility costs such as the electricity and the gas used for the power generator. Another important mission of our team is to coordinate large-scale repair works carried out by the RIKEN Facility Section so that the beam time can proceed smoothly.

In the last three years, there were big construction works related to the upgrade project of the RILAC facility. We carried out the design of the SRF test facility, took part in the design work of the new building for radioisotope purification, jointly designed the ion source room, and so on. The transfer work of GARIS II and the room-temperature cavities of the RILAC booster was conducted by our team.

2. Major Research Subjects

- (1) Operation, maintenance and monitoring of infrastructure of RI Beam Factory.
- (2) Participation in the beam time planning through utility cost estimation.
- (3) Coordination of large construction work and modification related to RI Beam Factory.

Members

Team Leader

Osamu KAMIGAITO (concurrent: Group Director, Accelerator Group)

Deputy Team Leader

Yutaka WATANABE (concurrent: Senior Technical Scientist, RILAC Team.)

Special Temporary Technical Scientist

Shu WATANABE

Special Temporary Employee

Hideyuki YAMASAWA

List of Publications & Presentations

Publications

[Proceedings]

- K. Suda, O. Kamigaito, K. Ozeki, N. Sakamoto, Y. Watanabe, K. Yamada, E. Kako, H. Nakai, H. Sakai, K. Umemori, H. Hara, A. Miyamoto, K. Sennyu, and T. Yanagisawa, "Fabrication and performance of superconducting quarter-wavelength resonators for SRILAC," Proceedings of the 19th International Conference on RF Superconductivity (SRF2019), Dresden, Germany, MOP055, 182 (2019).
- H. Imao, K. Yamada, N. Sakamoto, T. Watanabe, Y. Watanabe, O. Kamigaito, and K. Oyamada, "Non-evaporable getter-based differential pumping system for SRILAC at RIBF," Proceedings of the 19th International Conference on RF Superconductivity (SRF2019), Dresden, Germany, TUP013, 419 (2019).
- K. Yamada, T. Dantsuka, H. Imao, O. Kamigaito, K. Kusaka, H. Okuno, K. Ozeki, N. Sakamoto, K. Suda, T. Watanabe, Y. Watanabe, E. Kako, H. Nakai, H. Sakai, K. Umemori, H. Hara, A. Miyamoto, K. Sennyu, and T. Yanagisawa, "Construction of superconducting linac booster for heavy-ion linac at RIKEN Nishina Center," Proceedings of the 19th International Conference on RF Superconductivity (SRF2019), Dresden, Germany, TUP037, 504 (2019).
- N. Sakamoto, T. Dantsuka, M. Fujimaki, H. Imao, O. Kamigaito, K. Kusaka, H. Okuno, K. Ozeki, K. Suda, A. Uchiyama, T. Watanabe, Y. Watanabe, K. Yamada, E. Kako, H. Nakai, H. Sakai, K. Umemori, H. Hara, A. Miyamoto, K. Sennyu, and T. Yanagisawa, "Development of superconducting quarter-wave resonator and cryomodule for low-beta ion accelerators at RIKEN Radioactive Isotope Beam Factory," Proceedings of the 19th International Conference on RF Superconductivity (SRF2019), Dresden, Germany, WETEB1, 752 (2019).
- O. Kamigaito, T. Dantsuka, M. Fujimaki, N. Fukunishi, H. Hasebe, Y. Higurashi, E. Ikezawa, H. Imao, M. Kidera, M. Komiyama, K. Kumagai, T. Maie, Y. Miyake, T. Nagatomo, T. Nakagawa, M. Nakamura, T. Nishi, J. Ohnishi, H. Okuno, K. Ozeki, N. Sakamoto, K. Suda, A. Uchiyama, T. Watanabe, Y. Watanabe, and K. Yamada, "Recent progress in RIKEN RI Beam Factory," Proceedings of 22nd International Conference on Cyclotrons and their Applications (CYC2019), Cape Town, South Africa, MOB01, (2019).

- N. Tsukiori, K. Ozeki, S. Fukuzawa, M. Hamanaka, S. Ishikawa, K. Kobayashi, R. Koyama, T. Nakamura, M. Nishida, M. Nishimura, J. Shibata, K. Yadomi, T. Dantsuka, M. Fujimaki, T. Fujinawa, N. Fukunishi, H. Hasebe, Y. Higurashi, E. Ikezawa, H. Imao, O. Kamigaito, Y. Kanai, M. Kase, M. Kidera, M. Komiyama, K. Kumagai, T. Maie, M. Nagase, T. Nagatomo, T. Nakagawa, M. Nakamura, J. Ohnishi, H. Okuno, N. Sakamoto, K. Suda, A. Uchiyama, S. Watanabe, T. Watanabe, Y. Watanabe, K. Yamada, and H. Yamasawa, "Status Report on the Operation of RIBF Ring Cyclotron," Proceedings of the 16th Annual Meeting of Particle Accelerator Society of Japan (PASJ2019), July 31–August 3, 2019, Kyoto, Japan, FSPH002, 1193 (2019).
- M. Hamanaka, K. Suda, A. Goto, J. Ohnishi, Y. Oshiro, S. Fukuzawa, S. Ishikawa, R. Koyama, T. Nakamura, M. Nishida, M. Nishimura, J. Shibata, N. Tsukiori, K. Yadomi, K. Kaneko, K. Oyamada, M. Tamura, Akira Yusa, M. Fujimaki, N. Fukunishi, H. Hasebe, Y. Higurashi, H. Imao, M. Kase, O. Kamigaito, M. Kidera, M. Komiyama, K. Kumagai, T. Maie, M. Nagase, T. Nagatomo, T. Nakagawa, H. Okuno, K. Ozeki, N. Sakamoto, A. Uchiyama, S. Watanabe, T. Watanabe, Y. Watanabe, K. Yamada, and Y. Kotaka, "Status report on the operation of RIKEN AVF Cyclotron," Proceedings of the 16th Annual Meeting of Particle Accelerator Society of Japan (PASJ2019), July 31–August 3, 2019, Kyoto, Japan, FSPH010, 1224 (2019).

Research Facility Development Division Instrumentation Development Group

1. Abstract

This group develops core experimental installations at the RI Beam factory. Three projects are currently going on. SLOWRI is an experimental installations under testing and a common element enabling multiple-use. This will stop high-energy RI beams in a gas-catcher system and re-accelerates up to several-tenth keV, and the high-quality cold RI beam will be delivered to the users. SCRIT is the world first facility for an electron scattering off unstable nuclei, and has been constructed independently of the RIBF main facility. The first physic result was demonstrated in 2017, and the facility is now under upgrading of the electron beam power driving the RI beam production. Rare-RI Ring is an event-by-event operated heavy-ion storage ring aiming at the precision mass measurement for extremely rare exotic nuclei. This is now open for an experimental proposal application, and has already performed PAC-approved experiments, and an improvement for higher precise mass measurement is now going on. All instrumentations were designed to maximize the research potential of the world's most intense RI beams, and the exclusive equipment available at the RI Beam Factory makes experimental challenges possible. Technologies and experiences accumulated in this group will be able to provide opportunities of new experimental challenges and the foundation for future developments of RIBF.

2. Major Research Subjects

- (1) SCRIT Project
- (2) SLOWRI Project
- (3) Rear RI Ring Project
- (4) RUNBA project (Beam recycling development)

3. Summary of Research Activity

We are developing beam manipulation technology in carrying out above listed project. They are the high-quality slow RI beam production (SCRIT and SLOWRI), the beam cooling and stopping (SCRIT and SLOWRI), and the beam accumulation technology (Rare RI Ring) in a storage ring. The technological knowhow accumulated in our projects will play a significant role in the next generation RIBF. Status and future plan for each project is described in subsections. The electron scattering from ^{132}Xe isotopes has been successfully measured and the nuclear charge density distribution has been obtained in SCRIT. We are ready for the electrons scattering experiments for unstable nuclei. Rare RI Ring has been commissioned and the performances has been evaluated. We have demonstrated a mass-measurement capability of R3 and successfully started mass-measurements for unknown-mass nuclei in the experiments approved by PAC. Recently, we succeeded in measurement of masses of $^{74,76}\text{Ni}$, ^{122}Rh , and ^{124}Pd for the first time. SLOWRI is now under test experiments to establish a slow RI beam production using two types of gas cells. PALIS has been commissioned from 2015, and basic functions such as, for instance, the RI-beam stopping in Ar gas cell and the extraction from the gas cell have beam evaluated. RF ion-guide gas cell is now under testing and it will be online-commissioned in this year. Future plans for these projects are described in subsections.

We have started a new project from last year. According to the future plan of Nishina center, we are going to develop a beam re-cycling technique. A circulation of an RI beam in a storage ring equipped by a thin internal target is maintained until that some nuclear reaction happen at the target. The circulating beam losses the energy and the emittance grows up turn by turn because of existing internal target. In order to establish a beam re-cycling technique, the energy loss and growth of the energy-spread and the emittance have to be compensated by using a re-acceleration system and a beam-cooling or a fast feedback system. A beam re-cycling technique is supposed to greatly enhance an RI use efficiency in a nuclear physics study. As a first step for the development of these novel technique, we will construct a testbench consisting of a relatively small size of heavy-ion storage ring that will be connect to our ISOL (ERIS) in SCRIT facility. This ring named RUNBA (Recycled-Unstable-Nuclear Beam Accumulator) is equipped by acceleration devices and beam-cooling devices necessary in our R&D study. It was originally constructed as a beam cooler ring (s-LSR) at the Institute for Chemical Research (ICR), Kyoto University more than ten years ago. This has been already moved to RIBF in last year, and will be re-constructed by the SCRIT system in following year. Technical development for key devices required in RUNBA such as a charge breeder, an energy-spread compensator, and an internal target system have been already started under the research cooperation agreement with ICR Kyoto University.

Members

Director

Masanori WAKASUGI

Contract Researcher

Ryo OGAWARA

Visiting Scientists

Yasushi ABE (Nat'l Inst. of Radiological Sci.)
Akira OZAWA (Tsukuba Univ.)

Fumi SUZAKI (JAEA)

Student Trainees

So Sato (Rikkyo Univ.)

Shu TAKAGI (Kyoto Univ.)

Part-time Worker

Midori TAKEMON (Administrative Part-time Worker I)

List of Publications & Presentations

Publications and presentations are listed in subsections.

Research Facility Development Division Instrumentation Development Group SLOWRI Team

1. Abstract

SLOWRI is a universal low-energy RI-beam facility at RIBF that provides a wide variety of short-lived nuclei as high-purity and low-emittance ion beams or stored ions in a trap, including a parasitic operation mode. The SLOWRI team develops and manages the facility and performs high-precision spectroscopy experiments. The construction of the SLOWRI facility began in FY2013 and commissioning work is ongoing. From April 1st in FY2019, SLOWRI has been started to be co-operated under RNC and WNSC/KEK collaboration.

High-energy radioactive ion beams from the projectile fragment separator BigRIPS are thermalized in a large He gas catcher cell (RFC cell) or in a small Ar gas catcher cell (PALIS cell). From these gas cells, the low-energy ion beams will be delivered via mass separators and switchyards to various devices: such as an ion trap, a collinear fast beam apparatus, and a multi-reflection time of flight mass spectrograph. A multi-reflection time-of-flight mass spectrograph (MRTOF) has been also developed.

Two mass measurement projects using MRTOF mass spectrographs have been started: one is for trans uranium elements at the GARIS facility and the other is for r-process nuclides at SLOWRI facility. At GARIS-II, we installed second prototype SLOWRI combined with MRTOF, which is a medium-sized cryogenic RF-carpet He gas cell. Using second prototype SLOWRI, more than 80 nuclear masses have been measured including first mass measurements of Md and Es isotopes. In FY2019, the mass measurement for ^{257}Db has been successfully performed at GARIS-II, and the mass has been directly determined for the first time. At SLOWRI facility, third prototype SLOWRI is under construction, which is a 50-cm-long RF-carpet-type He gas cell combined with MRTOF. The third prototype will be installed at F11 of BigRIPS, downstream of ZeroDegree spectrometer, which can provide symbiotic measurements with other BigRIPS experiments.

Parallely, the on-line commissioning for PALIS has been continuously performed at F2 of BigRIPS. For the optimization of optical components on SLOWRI beam line, which connects between these gas cells installed at BigRIPS and an experimental room, a compact cesium ion source was installed at the upstream of the beam line in FY2019.

2. Major Research Subjects

- (1) Construction of the stopped and low-energy RI-beam facility, SLOWRI.
- (2) Development of a multi-reflection time-of-flight mass spectrograph for precision mass measurements of short-lived nuclei.
- (3) Development of collinear laser spectroscopy apparatus.
- (4) Development of a parasitic slow RI-beam production method using resonance laser ionization.
- (5) Commissioning for SLOWRI beam line.

3. Summary of Research Activity

(1) Construction of stopped and low-energy RI-beam facility (SLOWRI)

SLOWRI consists of two gas catchers (RF carpet gas cell and PALIS gas cell), mass separators a 50-m-long beam transport line, a beam cooler-buncher, an isobar separator, and a laser system. The RF carpet gas cell will be installed at the exit of the D5 dipole magnet of BigRIPS. The gas catcher contains a large cryogenic He gas cell with a large traveling wave rf-carpet. The PALIS gas cell is installed in the vicinity of the second focal plane slit of BigRIPS. It will provide parasitic RI-beams from those ions lost in the slits during other experiments. In this gas catcher, thermalized RI ions quickly become neutral and will be re-ionized by resonant laser radiations. Off- and on-line commissioning is underway.

Based on test experiments with the prototype setups, the RF-carpet gas cell contains a three stage rf-carpet structure: a gutter rf carpet (1st carpet) for the collection thermal ions in the cell into a small slit, a narrow (about 10 mm) traveling-wave rf-carpet (2nd carpet) for collection of ions from the gutter carpet and for transporting the ions towards the exit, and a small rf carpet for extraction from the gas cell. In FY2019, we modified the 1st carpet to have a finer pitch which was reduced by 20% compared with the previous version, in order to improve the transport efficiency. We tested the transport performance of the new 1st carpet using Cs^+ ions provided with a surface ionization ion source installed inside the gas cell. As the result, we have successfully achieved 80% transport efficiency in a He gas of 133 mbar. As combined with a transport efficiency on the 2nd carpet, we confirmed more than 70% extraction efficiency from the gas cell for the Cs^+ ions which were collected onto the RF carpets.

We will install the RF-carpet gas cell combined with MRTOF at F11 of BigRIPS at first, where the on-line commissioning and systematic mass measurements will be started from FY2020. At F11, symbiotic measurements with other BigRIPS experiments such as HiCARI projects can be performed.

(2) Development of a multi-reflection TOF mass spectrograph for short-lived nuclei

The atomic mass is one of the most important quantities of a nucleus and has been studied in various methods since the early days of modern physics. From among many methods we have chosen a multi-reflection time-of-flight (MRTOF) mass spectrometer. Slow RI beams extracted from the RF ion-guide are bunched and injected into the spectrometer with a repetition rate of ~ 100 Hz. A mass-resolving power of 170,000 has been obtained with a 2 ms flight time for ^{40}K and ^{40}Ca isobaric doublet. This mass-resolving power should allow us to determine ion masses with an accuracy of $\leq 10^{-7}$.

The MR-TOF mass spectrograph has been placed under the GARIS-II separator aiming at direct mass measurements of trans-

uranium elements. A medium-sized cryogenic He gas cell was placed at the focal plane of GARIS-II and a bunched low-energy heavy ion beam was transported to the trap of MRTOF. Mass measurements of more than 80 nuclides, including short-lived ($T_{1/2} = 10$ ms) isotopes of Ra and several isotopes of the trans-uranium elements Fm, Es, No and Md were performed in collaboration with Wako Nuclear Science Center (WNSC) of KEK and Super Heavy Element Synthesis team of RIKEN. In FY2019, the mass measurement of a super heavy element of ^{257}Db has been successfully performed, and the mass has been directly measured for the first time.

A new MRTOF has been assembled in FY2019 to be coupled with the third SLOWRI prototype gas cell, which will be installed at F11 of BigRIPS. Using an ion source of K^+ , the offline commissioning has been successfully performed. As the result, an impressive mass-resolving power of 570,000 has been achieved.

(3) Development of collinear fast beam apparatus for nuclear charge radii measurements

The root-mean-square charge radii of unstable nuclei have been determined exclusively by isotope shift measurements of the optical transitions of singly charged ions or neutral atoms by laser spectroscopy. Many isotopes of alkali, alkali-earth, and noble-gas elements in addition to several other elements have been measured by collinear laser spectroscopy since these ions all have good optical transitions and are available at conventional ISOL facilities. However, isotopes of other elements, especially refractory and short-lived ones, have not been investigated so far.

In SLOWRI, isotopes of all atomic elements will be provided as well collimated, mono-energetic ion beams. This should expand the range of nuclides available for laser spectroscopy. In the first years of the RIBF project, elements in the vicinity of Ni, such as Ni, Co, Fe, Cr, Cu, Ga, and Ge are planned to be investigated. They all have possible optical transitions in the ground states of neutral atoms with presently available laser systems. Some of them have so called recycling transitions, which enhance the detection probabilities noticeably. Furthermore, the multistep resonance ionization (RIS) method can be applied to the isotopes of Ni as well as those of some other elements. The required minimum intensity for this method can be as low as 10 atoms per second.

An off-line mass separator and a collinear fast beam apparatus with a large solid-angle fluorescence detector was built previously. A 617-nm transition of the metastable Ar^+ ion at 20 keV was measured with both collinear and anti-collinear geometry, which allowed determination of the absolute resonant frequency of the transition at rest with a relative accuracy better than 10^{-8} . A new setup is under preparation at the SLOWRI experiment area in collaboration with the Ueno nuclear spectroscopy laboratory.

(4) Development of parasitic slow RI-beam production scheme using resonance laser ionization

More than 99.9% of RI ions produced in projectile fission or fragmentation are simply dumped in the first dipole magnet and the slits. A new scheme, named PALIS, meant to rescue such precious RI using a compact gas catcher cell and resonance laser ionization, was proposed as a part of SLOWRI. The thermalized RI ions in a cell filled with Ar gas can be quickly neutralized and transported to the exit of the cell by gas flow. Irradiation of resonance lasers at the exit ionizes neutral RI atoms efficiently and selectively. The resonance ionization scheme itself can also be a useful method to perform hyperfine structure spectroscopy of RI of many elements.

In FY2019, we had two on-line experiments and a part of the experimental result was published in Prog. Theor. Exp. Phys. (See our publication list) Technical developments are under progress in on- and off-line commissioning.

(5) Commissioning for SLOWRI beam line

SLOWRI beam line composes of four dipole magnets, two focal plane chambers, 62 electrostatic quadrupole singlets, 11 electrostatic quadrupole quartets and 7 beam profile monitors. The hardware construction has been almost finished. In order to tune the optical components, a compact ion source, which can be used as a side-inserted type device, has been installed at the upstream of the beam line. We will start the tuning for the beam line using Cs^+ ions provided from the ion source in FY2020.

Members

Team Leader

Hironobu ISHIYAMA

Research/Technical Scientists

Takao KOJIMA (Senior Research Scientist)

Aiko TAKAMINE (Research Scientist)

Tetsu SONODA (Technical Scientist)

Expert Technician

Takeshi MAIE

Junior Research Associate

Shun IIMURA

Visiting Scientists

Hideki IIMURA (JAEA)

Kunihiro OKADA (Sophia Univ.)

Mikael REPONEN (Univ. of Jyväskylä)

Hans SCHUESSLER (Texas A&M Univ.)

Volker SONNENSCHNEIN (Nagoya Univ.)

Minoru TANIGAKI (Kyoto Univ.)

Hideki TOMITA (Nagoya Univ.)

Hermann WOLLNIK (Univ. of Giessen)

Student Trainees

Ryunosuke KODAMA (Univ. of Electro-Commun.)

Kento SUZUKI (Univ. of Electro-Commun.)

Part-time Workers

Ichirou KATAYAMA (Research Part-time Worker I)

Marco ROSENBUSCH (Research Part-time Worker I)

List of Publications & Presentations**Publications****[Original papers]**

- T. Sonoda, I. Katayama, M. Wada, H. Iimura, V. Sonnenschein, S. Iimura, A. Takamine, M. Rosenbusch, T. M. Kojima, D. S. Ahn, N. Fukuca, T. Kubo, S. Nishimura, Y. Shimizu, H. Suzuki, H. Takaeda, M. Tanigaki, H. Tomita, K. Yoshida, and H. Ishiyama, “Conceptual study on parasitic low-energy RI beam production with in-flight separator BigRIPS and the first stopping examination for high-energy RI beam in the parasitic gas cell,” *Progress of Theoretical and Experimental Physics*, **2019-11**, 113D02, (2019).
- M. Rosenbusch, M. Wada, P. Schury, Y. Ito, H. Ishiyama, S. Ishizawa, Y. Hirayama, S. Kimura, T. M. Kojima, H. Miyatake, J. Y. Moon, T. Niwase, T. Sonoda, A. Takamine, Y. X. Watanabe, and H. Wollnik, “A new multi-reflection time-of-flight mass spectrograph for the SLOWRI facility,” *Nucl. Instrum. Methods Phys. Res. B* **463**, 184–188 (2020).
- P. Aschere, N. Althubiti, D. Atanasov, K. Blaum, R. B. Cakirli, S. Grevy, F. Herfurth, S. Kreim, D. Lunney, V. Manea, D. Neidherr, M. Rosenbusch, L. Schweikhard, A. Welker, F. Wienholtz, R. N. Wolf, and K. Zuber, “Mass measurements of neutron-rich isotopes near $N = 20$ by in trap decay with the ISOLTRAP spectrometer,” *Phys. Rev. C* **100**, 014304 (2019).
- H. Wollnik, M. Wada, P. Schury, M. Rosenbusch, Y. Ito, and H. Miyatake, “Time-of-flight mass spectrographs of high mass resolving power,” *International Journal of Modern Physics A*, doi:10.1142/S0217751X19420016, (2019).
- T. Niwase, M. Wada, P. Schury, H. Haba, S. Ishizawa, Y. Ito, D. Kaji, S. Kimura, H. Miyatake, K. Morimoto, K. Morita, M. Rosenbusch, H. Wollnik, T. Shanley, and Y. Benari, “Development of an alpha-TOF detector for correlated measurement of atomic masses and decay properties,” *Nucl. Instrum. Methods Phys. Res. A* **953**, 163198 (2020).
- P. Schury, M. Wada, H. Wollnik, J. -Y. Moon, T. Hashimoto, and M. Rosenbusch, “High-stability, high-voltage power supplies for use with multi-reflection time-of-flight mass spectrographs,” *Rev. Sci. Instrum.* **91**, 014702 (2020)
- S. Sels, P. Fischer, H. Heylem, V. Lagaki, S. Lechner, F. M. Maier, P. Plattner, M. Rosenbusch, F. Wienholts, R. N. Wolf, W. Nortershauser, L. Schweikhard, and S. Malbrunot-Ettenauer, “First steps in the development of the multi ion reflection apparatus for collinear laser spectroscopy,” *Nucl. Instrum. Methods Phys. Res. B* **463**, 310–314 (2020).
- S. Lechner, P. Fischer, H. Heylen, V. Lagaki, F. Maier, P. Plattner, M. Rosenbusch, S. Sels, F. Wienholtz, R. N. Wolf, W. Nortershauser, L. Schweikhard, and S. Malbrunot-Ettenauer, “Fluorescence detection as a new diagnostics tool for electrostatic ion beam traps,” *Hyperfine Interactions* **240**, 95 (2019).
- Y. Hirayama, Y. X. Watanabe, M. Mukai, P. Schury, M. Ahmed, H. Ishiyama, S. C. Jeong, Y. Kakiguchi, S. Kimura, J. Y. Moon, M. Oyaizu, J. H. Park, M. Wada, and H. Miyatake, “Nuclear spectroscopy of r-process nuclei using KEK Isotope Separation System,” *Nucl. Instrum. Methods Phys. Res. A* **463**, 425–430 (2020).
- M. Mukai, Y. Hirayama, P. Schury, Y. X. Watanabe, M. Ahmed, H. Haba, H. Ishiyama, S. C. Jeong, Y. Kakiguchi, S. Kimura, J. Y. Moon, M. Oyaizu, A. Ozawa, J. H. Park, H. Ueno, M. Wada, and H. Miyatake, “Development of a multi-segmented proportional gas counter for beta-decay spectroscopy at KISS,” *Nucl. Instrum. Methods Phys. Res. B* **463**, 421–424 (2020).
- N. Kimura, R. Kodama, K. Suzuki, S. Oishi, M. Wada, K. Okada, N. Ohmae, H. Katori, and N. Nakamura, “Direct determination of the energy of the first excited fine structure level in Ba^{6+} ,” *Phys. Rev. A* **100**, 052508, (2019)

[Proceedings]

- Y. X. Watanabe, Y. Hirayama, P. Schury, Y. Kakiguchi, M. Oyaizu, M. Wada, M. Miyatake, M. Mukai, S. Kimura, H. Ishiyama, S. C. Jeong, J. Y. Moon, and J. H. Park, “Production of neutron-rich nuclei by multinucleon transfer reactions at KISS project” *Exotic Nuclei*, 486–491 (2019).
- Y. X. Watanabe, Y. Hirayama, M. Mukai, M. Ahmed, Y. Kakiguchi, H. Miyatake, M. Oyaizu, P. Schury, M. Wada, S. Kimura, H. Ishiyama, S. C. Jeong, J. Y. Moon, and J. H. Park, “Experimental studies of neutron-rich nuclei around $N = 126$ at KEK isotope separation system,” *EPJ Web Conf.* **223**, 01069 (2019).

Presentations**[International conferences/workshops]**

- H. Tomita, V. Sonnenschein, R. Terabayashi, M. Ohashi, S. Kato, S. Suzuki, K. Saito, Y. Matsui, T. Sakazaki, T. Iguchi, N. Nishizawa, T. Sonoda, H. Ishiyama, and K. Yoshida (poster), “Development of frequency comb based laser absorption/ionization spectroscopy of radioactive isotopes”, International Conference on Laser Probing (PLATAN 2019), Helmholtz Institute, Mainz, May 19–24, 2019.
- A. Takamine (invited), “Recent progress in the development of gas cells, and SHE results combining GARIS with GASCELL + MRTOF”, Expert Meeting on Next-Generation in-Flight Separators, GSI FAIR, Darmstadt, Germany, October 1, 2019.
- H. Ishiyama (invited), “Present status of SLOWRI”, RIBF Users Meeting 2019, RIKEN, Japan, September 4, 2019.
- H. Ishiyama (invited), “Present status of SLOWRI”, SSRI-PNS collaboration meeting 2019, RIKEN, Japan, September 4, 2019.
- S. Iimura, A. Takamine, J. Liu, S. Chen, M. Rosenbusch, M. Wada, and H. Ishiyama (poster), “Development of gas cell to stop and collect high energy RI beam, and extract radioactive ions with a high efficiency”, The ALL RIKEN Workshop 2019, RIKEN, Japan, December 5–6, 2019.

[Domestic conferences/workshops]

富田英生, V. Sonnenschein, 加藤弘太郎, 寺林稜平, 西澤典彦, 井口哲夫, M. Reponen, 園田哲, 石山博恒, 和田道治, 片山一郎, 竹田浩之, 鈴木浩, 清水陽平, 吉田光一, 飯村秀紀, 高峰愛子, M. Rosenbuch, 小島隆夫, 久保敏幸, K. Wendt (口頭発表), 「理化学研究所 RI ビームファクトリー低速 RI ビーム生成装置における共鳴イオン化レーザーイオン源の開発」, 次世代放射線シンポジウム 2019, 首都大学東京, 東京, 2019 年 8 月 8-9 日.

飯村俊 (口頭発表), 「理研 BigRIPS SLOWRI における RF カーペットガスセルの開発」, 京大複合研専門研究会「短寿命核 RI を用いた核分光と核物性研究 VI」兼「第 11 回停止・低速 RI ビームを用いた核分光研究会」, 京大複合研, 京都, 2020 年 1 月 16-17 日.

高峰愛子 (口頭発表), 「核・物質科学研究への応用を目指した高偏極 RI ビーム生成」, 京大複合研専門研究会「短寿命核 RI を用いた核分光と核物性研究 VI」兼「第 11 回停止・低速 RI ビームを用いた核分光研究会」, 京大複合研, 京都, 2020 年 1 月 16-17 日.

石山博恒 (口頭発表), 「放射性トレーサー ^8Li 法で固体電池界面のリチウム拡散は追跡可能か?」, 京大複合研専門研究会「短寿命核 RI を用いた核分光と核物性研究 VI」兼「第 11 回停止・低速 RI ビームを用いた核分光研究会」, 京大複合研, 京都, 2020 年 1 月 16-17 日.

Outreach activities

H. Ishiyama (school master), S. Iimura (school staff), and T. Kojima (school staff), Nishina School 2019, Riken, Wako, Japan, July 30–August 1, 2019.

Research Facility Development Division Instrumentation Development Group Rare RI-ring Team

1. Abstract

The aim of Rare-RI Ring (R3) is to measure the masses of short-lived unstable nuclei far from the beta-stability line. In particular, a high-precision mass measurement for nuclei located around the r-process pass (rare-RI) is required in nucleosynthesis point of view. The R3 completed the construction at the end of 2014, and has been performed commissioning experiments several times by 2017. Through the commissioning experiments, we confirmed the high ability of R3 as a storage ring capable of handling one event, and demonstrated that it is possible to perform the time-of-flight Isochronous Mass Spectrometry (IMS) in shorter than 1 ms. We have acquired an adequate efficiency to conduct the mass measurement experiments in the end of 2017. In 2018, we have successfully conducted the first mass measurement experiment for $^{74,76}\text{Ni}$, ^{122}Rh , $^{123,124}\text{Pd}$, and ^{125}Ag . The analysis is in progress for giving the new experimental mass values of $^{74,76}\text{Ni}$, ^{122}Rh , ^{124}Pd , and for improving the experimental mass values of ^{123}Pd , ^{125}Ag . The remaining issues as the R3 facility are further improvement of experimental efficiency and that of mass measurement precision. In 2019, we started efforts to resolve those issues.

2. Major Research Subjects

- (1) Further improvement of experimental efficiency and mass measurement precision
- (2) Precision mass measurement for rarely produced isotopes related to r-process

3. Summary of Research Activity

In the commissioning experiments up to 2017, we confirmed the unique performances of R3 and demonstrated the time-of-flight isochronous mass measurement method. The ring structure of R3 was designed with a similar concept of a separate-sector ring cyclotron. It consists of six sectors and straight sections, and each sector consists of four rectangular bending magnets. Two magnets at both ends of each sector are additionally equipped with ten trim coils to form a precise isochronous field. We have realized in forming the precise isochronous field of 5 ppm with wide momentum range of $\Delta p/p = \pm 0.5\%$. Another performance required for R3 is to efficiently seize hold of an opportunity of the mass measurement for rare-RIs produced unpredictably. It was realized by constructing the Isotope-Selectable Self-trigger Injection (ISSI) scheme which pre-identified rare-RI itself triggers the injection kicker magnets. Key device was an ultra-fast response kicker system that has been successfully developed. Full activation of the kicker magnetic field can be completed within the flight time of the rare-RI from an originating point (F3 focal point in BigRIPS) of the trigger signal to the kicker position in R3.

Since R3 accumulates, in principle, only one event, we fabricated high-sensitive beam diagnostic devices in the ring. They should be applicable even for one event circulation. One of them is a cavity type of Schottky pick-up installed in a straight section of R3. The Schottky pick-up successfully monitored a single $^{78}\text{Kr}^{36+}$ ion circulation with the measurement time of less than 10 ms in the first commissioning experiment. We also confirmed that it is useful for fine tuning of the isochronous field. Another is a timing monitor, which detects secondary electrons emitted from thin carbon foil placed on the circulation orbit. The thickness of the foil is $50 \mu\text{g}/\text{cm}^2$. This timing monitor is working well to observe first several tens turns for injected event.

We performed mass measurement in the third commissioning experiment by using unstable nuclei which masses are well-known. The masses of ^{79}As , ^{77}Ga , ^{76}Zn , and ^{75}Cu relative to ^{78}Ge were derived with the accuracy of less than 10 ppm. In addition, we have improved the extraction efficiency to 2% by considering the matching condition between the emittance of injection events and the acceptance of R3. This extraction efficiency was sufficient to conduct the accepted two proposals: mass measurements of Ni isotopes and mass measurements of Sn region.

In the beginning of 2018, we examined the feasibility of these two proposals in detail. Consequently, we decided to proceed with two proposals at the same period. In the beginning of November 2018, we have conducted the first experiment using the R3 to measure the masses for $^{74,76}\text{Ni}$ in 4 days. After that, we also measured the masses for ^{122}Rh , $^{123,124}\text{Pd}$, and ^{125}Ag in 4.5 days at the end of November 2018. These nuclei were successfully extracted from R3 with the efficiency of 1–2%. The masses of $^{74,76}\text{Ni}$, ^{122}Rh , and ^{124}Pd can be determined experimentally for the first time. On the other hand, the masses of ^{123}Pd and ^{125}Ag will be improved the precision compared with previous experimental values. These analyses are still in progress. Since each proposal has a machine time of several days to measure the masses of exotic nuclei, we will plan to conduct the mass measurements of the other Ni isotopes and nuclei of Sn region in 2020 or later.

With further improvements in experimental efficiency and mass measurement precision, the R3 enables mass measurement of extremely rare-RIs that are inaccessible for other techniques. In 2019, we started to add one more kicker magnet. More accurate injection and reliable extraction will be possible, the experimental efficiency will be improved about 10 times from the previous experiment. We plan to conduct a beam test in 2020.

Members

Team Leader

Masanori WAKASUGI

Research/Technical Scientist

Yoshitaka YAMAGUCHI (Technical Scientist)

Expert Technician

Takeshi MAIE

Visiting Scientists

Yasushi ABE (Nat'l Inst. of Radiological Sci.)

Fumi SUZAKI (JAEA)

List of Publications & Presentations

Publications

[Original papers]

- X. Xu, M. Wang, K. Blaum, J. D. Holt, Yu. A. Litvinov, A. Schwenk, J. Simonis, S. R. Stroberg, Y. H. Zhang, H. S. Xu, P. Shuai, X. L. Tu, X. H. Zhou, F. R. Xu, G. Audi, R. J. Chen, X. C. Chen, C. Y. Fu, Z. Ge, W. J. Huang, S. Litvinov, D. W. Liu, Y. H. Lam, X. W. Ma, R. S. Mao, A. Ozawa, B. H. Sun, Y. Sun, T. Uesaka, G. Q. Xiao, Y. M. Xing, T. Yamaguchi, Y. Yamaguchi, X. L. Yan, Q. Zeng, H. W. Zhao, T. C. Zhao, W. Zhang, and W. L. Zhan, "Masses of neutron-rich $^{52-54}\text{Sc}$ and $^{54,56}\text{Ti}$ nuclides: The $N = 32$ subshell closure in scandium," *Phys. Rev. C* **99**, 064303 (2019).
- X. Xu, J. H. Liu, C. X. Yuan, Y. M. Xing, M. Wang, Y. H. Zhang, X. H. Zhou, Yu. A. Litvinov, K. Blaum, R. J. Chen, X. C. Chen, C. Y. Fu, B. S. Gao, J. J. He, S. Kubono, Y. H. Lam, H. F. Li, M. L. Liu, X. W. Ma, P. Shuai, M. Si, M. Z. Sun, X. L. Tu, Q. Wang, H. S. Xu, X. L. Yan, J. C. Yang, Y. J. Yuan, Q. Zeng, P. Zhang, X. Zhou, W. L. Zhan, S. Litvinov, G. Audi, S. Naimi, T. Uesaka, Y. Yamaguchi, T. Yamaguchi, A. Ozawa, B. H. Sun, K. Kaneko, Y. Sun, and F. R. Xu, "Masses of ground and isomeric states of ^{101}In and configuration-dependent shell evolution in odd-A indium isotopes," *Phys. Rev. C* **100**, 051303(R) (2019).
- F. C. Ozturk, B. Akkus, D. Atanasov, H. Beyer, F. Bosch, D. Boutin, C. Brandau, P. Buehler, R. B. Cakirli, R. J. Chen, W. D. Chen, X. C. Chen, I. Dillmann, C. Dimopoulou, W. Enders, H. G. Essel, T. Faestermann, O. Forstner, B. S. Gao, H. Geissel, R. Gernhaeuser, R. E. Grisenti, A. Gumberidze, S. Hagmann, T. Heftrich, M. Heil, M. O. Herdrich, P. -M. Hillenbrand, T. Izumikawa, P. Kienle, C. Kraushofer, C. Kleffner, C. Kozuharov, R. K. Knoebel, O. Kovalenko, S. Kreim, T. Kuehl, C. Lederer-Woods, M. Lestinsky, S. A. Litvinov, Yu. A. Litvinov, Z. Liu, X. W. Ma, L. Maier, B. Mei, H. Miura, I. Mukha, A. Najafi, D. Nagae, T. Nishimura, C. Nociforo, F. Nolden, T. Ohtsubo, Y. Oktem, S. Omika, A. Ozawa, N. Petridis, J. Piotrowski, R. Reifarh, J. Rossbach, R. Sanchez, M. S. Sanjari, C. Scheidenberger, R. S. Sidhu, H. Simon, U. Spillmann, M. Steck, Th. Stoehlker, B. H. Sun, L. A. Susam, F. Suzuki, T. Suzuki, S. Yu. Torilov, C. Trageser, M. Trassinelli, S. Trotsenko, X. L. Tu, P. M. Walker, M. Wang, G. Weber, H. Weick, N. Winckler, D. F. A. Winters, P. J. Woods, T. Yamaguchi, X. D. Xu, X. L. Yan, J. C. Yang, Y. J. Yuan, Y. H. Zhang, X. H. Zhou, and the FRS-ESR, ILIMA, SPARC, and TBWD Collaborations, "New test of modulated electron capture decay of hydrogen-like ^{142}Pm ions: Precision measurement of purely exponential decay," *Phys. Lett. B* **797**, 134800 (2019).
- J. T. Zhang, K. Yue, H. X. Li, X. L. Tu, C. J. Shao, P. Ma, B. Mei, X. C. Chen, Y. Y. Yang, X. Q. Liu, Y. M. Xing, K. H. Fang, Z. Y. Sun, M. Wang, Yu. A. Litvinov, T. Yamaguchi, P. Egelhof, Y. H. Zhang, and X. H. Zhou, "The development of in-ring reaction measurements at the HIRFL-CSR," *Nucl. Instrum. Methods Phys. Res. A* **948**, 162848-1-5 (2019)

[Proceedings]

- Z. Ge, T. Uesaka, S. Naimi, D. Nagae, Y. Abe, S. Omika, F. Suzuki, T. Yamaguchi, Y. Yamaguchi, M. Wakusugi, H. Li, K. Wakayama, H. Arakawa, K. Inomata, K. Nishimuro, T. Kobayashi, A. Ozawa, S. Hosoi, Y. Inada, S. Suzuki, T. Moriguchi, M. Mukai, M. Amano, D. Kamioka, and Y. Yano, "Scheme of high-resolution identification and selection of secondary ions for mass measurements with the Rare-RI Ring," *Hyper. Int.* **240** 92/1-11 (2019).

Presentations

[International conferences/workshops]

- A. Ozawa (invited), "Mass measurements for Ni-isotopes in Rare-RI Ring, RIBF," China-Japan Collaboration Workshop on Nuclear Mass and Life for Unraveling Mysteries of R-process, Beijing, China, October 10-12, 2019.
- T. Yamaguchi (invited), "New experimental plan and detector R&D at the Rare-RI Ring facility," China-Japan Collaboration Workshop on Nuclear Mass and Life for Unraveling Mysteries of R-process, Beijing, China, October 10-12, 2019.

[Seminars]

- T. Yamaguchi, "Charge changing cross section measurement—A possible method to extract point-proton radii of radioactive isotopes," Beihang Univ., Beijing, China, October 14, 2019.

[Domestic conferences/workshops]

- 向井もも (口頭発表), 「薄膜を利用した飛行時間検出器の開発」, 日本物理学会 2019 年秋季大会, 山形大学, 山形, 2019 年 9 月 17-20 日.
- 稲田康人 (口頭発表), 「稀少 RI リングのためのファイバーシンチレーション検出器の開発」, 日本物理学会 2019 年秋季大会, 山形大学, 山形, 2019 年 9 月 17-20 日.

細井駿（口頭発表）、「稀少 RI リングのため薄膜を利用した位置検出器の開発」, 日本物理学会 2019 年秋季大会, 山形大学, 山形, 2019 年 9 月 17-20 日.

山口由高（招待講演）、「RIBF における重イオン蓄積リング」, 宇宙史研究センター構成員会議, 筑波大学, つくば, 2019 年 11 月 21 日.

長江大輔（口頭発表）、「稀少 RI リングでの粒子蓄積確認の為の飛行時間検出器」, 日本物理学会第 75 回年次大会, 現地開催中止, 2020 年 3 月 16-19 日.

Research Facility Development Division Instrumentation Development Group SCRIT Team

1. Abstract

The SCRIT Electron Scattering Facility has been constructed at RIKEN RIBF. This aims at investigation of internal nuclear structure for short-lived unstable nuclei by means of electron scattering. SCRIT (Self-Confining RI Ion Target) is a novel method to form internal targets in an electron storage ring. This is a unique method for making electron scattering experiments for unstable nuclei possible. Construction of the facility has been started in 2009. This facility consists of an electron accelerator (RTM), a SCRIT-equipped electron storage ring (SR2), an electron-beam-driven RI separator (ERIS), and a window-frame spectrometer for electron scattering (WiSES) which consists of a large window-frame dipole magnet, drift chambers and trigger scintillators. Installation of all components in the facility was completed in 2015. After the comprehensive test and tuning, the luminosity was reached to $3 \times 10^{27}/(\text{cm}^2\text{s})$ with the number of injected ions of 3×10^8 . In 2016, we successfully completed a measurement of diffraction of scattered electrons from ^{132}Xe nuclei and determined the charge density distribution for the first time. The facility is now under setting up to move the first experiment for unstable nuclei.

2. Major Research Subjects

Development of SCRIT electron scattering technique and measurement of the nuclear charge density distributions of unstable nuclei.

3. Summary of Research Activity

SCRIT is a novel technique to form internal target in an electron storage ring. Positive ions are three dimensionally confined in the electron beam axis by transverse focusing force given by the circulating electron beam and applied electrostatic longitudinal mirror potential. The created ion cloud composed of RI ions injected from outside works as a target for electron scattering. Construction of the SCRIT electron scattering facility has been started in 2009. The electron accelerators RTM and the storage ring SR2 were successfully commissioned in 2010. Typical accumulation current in SR2 is 250–300 mA at the energy range of 100–300 MeV that is required energy range in electron scattering experiment. The SCRIT device was inserted in the straight section of SR2 and connected to an ISOL named ERIS (Electron-beam-driven RI separator for SCRIT) by 20-m long low energy ion transport line. A buncher system based on RFQ linear trap named FRAC (Fringing-RF-field-Activated dc-to-pulse converter) was inserted in the transport line to convert the continuous beam from ERIS to pulsed beam, which is acceptable for SCRIT. The detector system WiSES consisting of a high-resolution magnetic spectrometer, drift chambers and trigger scintillators, was constructed, and it has a solid angle of 100 msr, energy resolution of 10^{-3} , and the scattering angle coverage of 25–55 degrees. A wide range of momentum transfer, 80–300 MeV/c, is covered by changing the electron beam energy from 150 to 300 MeV.

We successfully measured a diffraction pattern in the angular distribution of scattered electron from ^{132}Xe isotope at the electron beam energy of 150 MeV, 200 MeV, and 300 MeV, and derived the nuclear charge distribution by assuming two-parameters Fermi model for the first time. At this time, luminosity was reached to $3 \times 10^{27}/(\text{cm}^2\text{s})$ at maximum and the averaged value was $1.2 \times 10^{27}/(\text{cm}^2\text{s})$ with the number of injected target ions of 3×10^8 .

We are now under preparation for going to the experiments for unstable nuclei. There are some key issues for that. They are increasing the intensity of the RI beams from ERIS, efficient DC-to-pulse conversion at FRAC, improving the transmission efficiency from FRAC to SCRIT, and effective suppression of the background in measurement of scattered electrons. RI beam intensity will be improved by upgrading the electron beam power from 10 W to 60 W, increasing the contained amount of U in the target ion source, and some modifications in mechanical structure in the ion source. For upgrading the electron beam power, the RF system of RTM has been maintained intensively, and we will continue the development of RTM. For efficient DC-to-pulse conversion, we established the two-step bunching method, which is time compression at FRAC in combination with pre-bunching at the ion source using grid action. Furthermore, we will improve the conversion efficiency and the transmission efficiency from FRAC to the SCRIT device by cooling the trapped ions using minuscule amounts of a buffer gas. These improvements on FRAC were already confirmed in off-line test. Since one of significant contribution to the background for scattered electron is scattering from massive structural objects around the trapping region originated from halo components of the electron beam, we remodeled the SCRIT electrodes. The vacuum pump system at the SCRIT device has been upgraded to reduce the contribution of residual gases. Luminosity for radioactive Xe isotopes is expected to be more than $10^{26}/(\text{cm}^2\text{s})$ after these improvements. Then, we will be able to start experiments for unstable nuclei. When further upgrading in the RTM power planed to be 3 kW will be achieved, we can extend the measurements to more exotic nuclei.

In 2018, we developed several instruments. One is the introduction of the surface-ionization type ion source at ERIS in order to increase kinds of radioactive beam and to produce high intensity beam. Another development is the upgrading of the drift chamber located in front of the magnetic spectrometer of WiSES to improve the momentum resolution and angular acceptance. These developments help us to realize experiments for unstable nuclei.

In 2019, we installed a newly designed SCRIT electrodes. The main purpose of the replacement was to lower the background during the measurement due to the electron scattering from the SCRIT electrodes itself but not from the ion targets for the experiment. For that purpose, we employed thin metal wires to construct the electrodes rather than metal plates nor blocks. In addition, we modified the inside structure of the SCRIT chamber to symmetrize the electric ground potential affecting the potential curve inside the electrodes. Currently, we are adjusting the SR2 accelerator and ion source ERIS to be ready for the measurement by means of the new

SCRIT electrodes.

Members

Team Leader

Masanori WAKASUGI

Research/Technical Scientists

Masamitsu WATANABE (Senior Research Scientist)

Tetsuya OHNISHI (Senior Technical Scientist)

Expert Technician

Takeshi MAIE

Contract Researcher

Akitomo ENOKIZONO

Research Consultants

Takashi EMOTO

Shinichi ICHIKAWA

Masahiro HARA

Senior Visiting Scientist

Toshitada HORI (Hiroshima Univ.)

Visiting Scientists

Toshimi SUDA (Tohoku Univ.)

Yuki HONDA (Tohoku Univ.)

Tadaaki TAMAE (Tohoku Univ.)

Kazuyoshi KURITA (Rikkyo Univ.)

Kyo TSUKADA (Tohoku Univ.)

Shuo WANG (Shandong Univ.)

Student Trainees

Taihei AOYAGI (Tohoku Univ.)

Daisuke TAKI (Tohoku Univ.)

Syota TAKAYAMA (Tohoku Univ.)

Hikari WAUKE (Tohoku Univ.)

List of Publications & Presentations

Publications

[Proceedings]

- K. Tsukada, K. Adachi, A. Enokizono, T. Fujita, M. Hara, T. Hori, M. Hori, S. Ichikawa, K. Kasama, K. Kurita, K. Namba, T. Ohnishi, T. Suda, T. Tamae, M. Togasaki, M. Wakasugi, M. Watanabe, and K. Yamada, “Electron scattering from ^{208}Pb and ^{132}Xe ions at the SCRIT facility,” *Hyperfine interact* **240**, 1–120 (2019).

Presentations

[International conferences/workshops]

- T. Suda (invited), “Proton charge radius by low-energy electron scattering,” International Workshop on the Structure of the Proton, Yamagata, February 10–11, 2019.
- T. Suda (oral), “Nuclear physics with low-energy and high-intensity electron beam,” Neutrino Nuclear Response 2019 (NNR19), RCNP, Osaka, Japan, May 8–9, 2019.
- T. Suda (invited), “Electron scattering for short-lived nuclei,” Gordon Conference on “Exploring simple structural patterns and dynamics of nuclei,” New London US, June 16–21, 2019.
- T. Suda (invited), “Nuclear physics with electron beam,” Connecting Fundamental Physics, Chemistry and the Origins of Biomolecular Homochirality, National Observatory of Japan, June 26–27, 2019.
- S. Sato (oral), M. Wakasugi, T. Ohnishi, M. Watanabe, A. Enokizono, and K. Kurita, “Improvement of a dc-to-pulse conversion efficiency of FRAC,” The 13th International Conference on Stopping and Manipulation of Ions and related topics (SMI2019), Montreal, Canada, July 16–19, 2019.
- T. Suda (plenary/invited), “Electron scattering for short-lived nuclei,” International Nuclear Physics Conference (INPC2019), Glasgow UK, July 29–August 2, 2019.
- M. Watanabe (poster), A. Enokizono, M. Hara, Y. Honda, T. Hori, S. Ichikawa, K. Kasama, K. Kurita, M. Nakano, K. Namba, T. Oonishi, S. Sato, T. Suda, S. Takayama, T. Tamae, K. Tsukada, M. Wakasugi, and H. Wauke, “Fine optimization of SCRIT facility for short-lived nuclei experiment,” International Nuclear Physics Conference (INPC2019), Glasgow, UK, July 29–August 2, 2019.
- T. Suda (invited), “Proton radius,” The 11th Circum-Pan-Pacific Symposium on High Energy Spin Physics, Miyazaki Japan, August 27–30, 2019.
- H. Wauke (poster), T. Aoyagi, A. Enokizono, Y. Honda, T. Suda, S. Takayama, T. Tamae, K. Tsukada, T. Ohnishi, M. Wakasugi, and M. Watanabe, “Precise magnetic field measurement of electron spectrometer for the electron scattering off unstable nuclei experiment,” International school for Strangeness Nuclear Physics 2019, Tohoku Univ., Sendai, Japan, September 5–8, 2019.

- K. Tsukada (oral), T. Aoyagi, A. Enokizono, M. Hara, Y. Honda, T. Hori, S. Ichikawa, K. Kurita, T. Ohnishi, S. Sato, T. Suda, S. Takayama, T. Tamae, M. Wakasugi, and M. Watanabe, “Present status and future prospects of the SCRIT electron scattering facility,” 9th International Symposium on Nuclear Symmetry Energy (NuSYM2019), Danang City, Vietnam, September 30–October 4, 2019.
- T. Suda (invited), “Proton radius,” 14th Asia-Pacific Physics Conference (APPC2019), Kuching Malaysia, November 17–22, 2019.
- K. Tsukada (oral), T. Aoyagi, A. Enokizono, M. Hara, Y. Honda, T. Hori, S. Ichikawa, K. Kurita, T. Ohnishi, S. Sato, T. Suda, T. Tamae, M. Wakasugi, and M. Watanabe, “Present status of SCRIT electron scattering facility,” 14th Asia-Pacific Physics Conference (APPC2019), Sarawak, Malaysia, November 17–22, 2019.
- T. Suda (invited), “Electron-scattering activities in Japan for nucleon and nuclei,” KVI Seminar, KVI Groningen, Netherlands, January 8, 2019.
- T. Suda (invited), “ULQ2 project,” Collaborative Seminar by REIMEI, RCNP and Clusters, February 2020.
- T. Ohnishi (oral), A. Enokizono, M. Hara, T. Hori, S. Ichikawa, K. Kurita, R. Ogawara, S. Sato, T. Suda, S. Takayama, D. Taki, S. Takagi, T. Tamae, K. Tsukada, M. Wakasugi, M. Watanabe, and H. Wauke, “Electron scattering with unstable nuclei at the SCRIT electron scattering facility,” Vth Topical Workshop on Modern Aspects in Nuclear Structure—The Many Facets of Nuclear Structure, Bormio, Italy, February 4–9, (2020).

[Domestic conferences/workshops]

- 須田利美 (招待講演), 「ガンマ線ビームを用いた原子核・ハドロン物理の新局面と今後の展望」, 低エネルギー・大電流電子ビームと原子核物理, RCNP 研究会, 大阪, 2019 年 3 月 4–5 日.
- 須田利美 (招待講演), 「陽子のサイズがおかしい?」, 東京大学物理学教室コロキウム, 東京, 2019 年 11 月 8 日.
- 和宇慶ひかり (口頭発表), 「SCRIT 電子スペクトロメーターの 3 次元磁場測定」, 東北大学理学研究科 6 専攻+生命科学研究科合同シンポジウム 2020, 東北大学, 2020 年 2 月 14 日.
- 和宇慶ひかり (ポスター発表), 塚田暁, 青柳泰平, 須田利美, 高山祥太, 瀧大祐, 玉江忠明, 本多佑記, 「SCRIT 電子スペクトロメーターの 3 次元磁場測定」, ELPH シンポジウム, 東北大学 ELPH, 仙台, 2019 年 3 月 6 日.
- 佐藤蒼 (口頭発表), 榎園昭智, 大西哲也, 栗田和好, 須田利美, 塚田暁, 和宇慶ひかり, 若杉昌徳, 渡邊正満, 「SCRIT 実験のための高効率 RFQ クーラーバンチャーの開発」, 日本物理学会第 75 回年次大会, 名古屋大学, 名古屋, 2020 年 3 月 16–19 日.
- 和宇慶ひかり (口頭発表), 青柳泰平, 榎園昭智, 大西哲也, 栗田和好, 佐藤蒼, 須田利美, 高木周, 高山祥太, 瀧大祐, 玉江忠明, 塚田暁, 本多佑記, 若杉昌徳, 渡邊正満, 「SCRIT 電子スペクトロメーターの 3 次元磁場測定」, 日本物理学会第 75 回年次大会, 名古屋大学, 名古屋, 2020 年 3 月 16–19 日.
- 塚田暁 (口頭発表), 青柳泰平, 市川進一, 榎園昭智, 大西哲也, 栗田和好, 佐藤蒼, 須田利美, 高山祥太, 瀧大祐, 玉江忠明, 原雅弘, 堀利匡, 本多佑記, 和宇慶ひかり, 若杉昌徳, 渡邊正満, 「炭素標的を用いた SCRIT 実験用電子スペクトロメーターの性能評価」, 日本物理学会第 75 回年次大会, 名古屋大学, 名古屋, 2020 年 3 月 16–19 日.

[International seminars/lectures]

- T. Suda, Lectures: “Electron scattering for nucleon and nuclei,” Johannesburg, South Africa, October 19–November 3, 2019.
- T. Suda, Public lecture: “Nihonium: 113th element,” Johannesburg, South Africa, October 19–November 3, 2019.

[Domestic seminars/lectures]

- 須田利美, 「電子線核物理特論」, 大学院講義, 2019 年 10 月–2020 年 3 月.
- 須田利美, 「宇宙創生物理学概論」, GPPU 講義, 2019 年 6 月.
- 須田利美, 「元素について」, 熊谷高校訪問生への特別講義, 2019 年 8 月 26 日.
- 須田利美, “Physics Today,” 新潟大学集中講義, 2019 年 12 月 3–5 日.
- 須田利美, 「元素と原子核」, 熊谷高校特別授業, 2019 年 12 月 6 日.
- 須田利美, 「日本で発見された 113 番新元素ニホニウム」, 仙台青陵中等学校出前授業, 2019 年 12 月 10 日.

Awards

- H. Wauke, SNP School Incentive Prize, “Precise magnetic field measurement of electron spectrometer for the electron scattering off unstable nuclei experiment,” International school for Strangeness Nuclear Physics 2019, Tohoku Univ., Sendai, Japan, September 5–8, 2019.

Others

- T. Ohnishi, A. Enokizono, M. Hara, T. Hori, S. Ichikawa, K. Kurita, R. Ogawara, S. Sato, T. Suda, S. Takayama, D. Taki, S. Takagi, T. Tamae, K. Tsukada, M. Wakasugi, M. Watanabe, and H. Wauke, “The SCRIT project at RIKEN,” NUSTAR Annual Meeting 2020, GSI, Darmstadt, Germany, March 2–6, (2020).

Research Facility Development Division Research Instruments Group

1. Abstract

The Research Instruments Group is the driving force at RI Beam Factory (RIBF) for continuous enhancement of activities and competitiveness of experimental research. Consisting of four teams, we are in charge of the operation, maintenance, and improvement of the core research instruments at RIBF, such as the BigRIPS in-flight RI separator, ZeroDegree spectrometer and SAMURAI spectrometer, and the related infrastructure and equipment. We are also in charge of the production and delivery of RI beams using the BigRIPS separator. The group also conducts related experimental research as well as R&D studies on the research instruments.

2. Major Research Subjects

Design, construction, operation, maintenance, and improvement of the core research instruments at RIBF and related R&D studies. Experimental studies on exotic nuclei.

3. Summary of Research Activity

The current research subjects are summarized as follows:

- (1) Production and delivery of RI beams and related research
- (2) Design, construction, operation, maintenance, and improvement of the core research instruments at RIBF and their related infrastructure and equipment
- (3) R&D studies on the core research instruments and their related equipment at RIBF
- (4) Experimental research on exotic nuclei using the core research instruments at RIBF

Members

Director

Tomohiro UESAKA

Contract Researcher

Toshiyuki KUBO

Junior Research Associate

Rieko TSUNODA

Senior Visiting Scientist

Toshio KOBAYASHI (Tohoku Univ.)

Student Trainee

Fumitaka ENDO (Tohoku Univ.)

Research Facility Development Division

Research Instruments Group

BigRIPS Team

1. Abstract

This team is in charge of design, construction, development and operation of BigRIPS in-flight separator and its related research instruments at RI beam factory (RIBF). They are employed not only for the production of RI beams but also the experimental studies using RI beams.

2. Major Research Subjects

Design, construction, development and operation of BigRIPS in-flight separator, RI-beam transport lines, and their related research instruments

3. Summary of Research Activity

This team is in charge of design, construction, development and operation of BigRIPS in-flight separator, RI-beam transport lines, and their related research instruments such as ZeroDegree spectrometer at RI beam factory (RIBF). They are employed not only for the production of RI beams but also various kinds of experimental studies using RI beams. The research subjects may be summarized as follows:

- (1) General studies on RI-beam production using in-flight scheme.
- (2) Studies on ion-optics of in-flight separators, including particle identification of RI beams.
- (3) Simulation and optimization of RI-beam production.
- (4) Development of beam-line detectors and their data acquisition system.
- (5) Experimental studies on production reactions and unstable nuclei.
- (6) Experimental studies of the limits of nuclear binding.
- (7) Development of superconducting magnets and their helium cryogenic systems.
- (8) Development of a high-power production target system.
- (9) Development of a high-power beam dump system.
- (10) Development of a remote maintenance and remote handling systems.
- (11) Operation, maintenance and improvement of BigRIPS separator system, RI-beam transport lines, and their related research instruments such as ZeroDegree spectrometer and so on.
- (12) Experimental research using RI beams.

Members

Team Leader

Koichi YOSHIDA

Research/Technical Scientists

Yoshiyuki YANAGISAWA (Senior Research Scientist)

Naohito INABE (Senior Technical Scientist)

Kensuke KUSAKA (Senior Technical Scientist)

Masao OHTAKE (Senior Technical Scientist)

Naoki FUKUDA (Technical Scientist)

Hiroyuki TAKEDA (Technical Scientist)

Contract Researchers

Deuk Soon AHN

Yohei SHIMIZU

Hiroshi SUZUKI

Visiting Scientists

Alan Matthew AMTHOR (Bucknell Univ.)

Daniel P. BAZIN (Michigan State Univ.)

Alfredo ESTRADA VAZ (Central Michigan Univ.)

Michael FAMIANO (Western Michigan State Univ.)

Hans GEISSEL (GSI/Justus-Liebig Univ. Giessen)

Tuomas Arne Santeri GRAHN (Univ. of Jyvaskyla)

Kazuo IEKI (Rikkyo Univ.)

Naohito IWASA (Tohoku Univ.)

Yutaka MIZOI (Univ. of Electro-Commun.)

David MORRISSEY (Michigan State Univ.)

Mauricio PORTILLO (Michigan State Univ.)

Bradley M. SHERRILL (Michigan State Univ.)

Oleg TARASOV (Michigan State Univ.)

Student Trainee

Shunki ISHIKAWA (Tohoku Univ.)

Part-time Worker

Tetsuro KOMATSUBARA (Research Part-time Worker I)

List of Publications & Presentations**Publications****[Original papers]**

- Y. Ichikawa, H. Nishibata, Y. Tsunoda, A. Takamine, K. Imamura, T. Fujita, T. Sato, S. Momiyama, Y. Shimizu, D. S. Ahn, K. Asahi, H. Baba, D. L. Balabanski, F. Boulay, J. M. Daugas, T. Egami, N. Fukuda, C. Funayama, T. Furukawa, G. Georgiev, A. Gladkov, N. Inabe, Y. Ishibashi, T. Kawaguchi, T. Kawamura, Y. Kobayashi, S. Kojima, A. Kusoglu, I. Mukul, M. Niikura, T. Nishizaka, A. Odahara, Y. Ohtomo, T. Otsuka, D. Ralet, G. S. Simpson, T. Sumikama, H. Suzuki, H. Takeda, L. C. Tao, Y. Togano, D. Tominaga, H. Ueno, H. Yamazaki, and X. F. Yang, "Interplay between nuclear shell evolution and shape deformation revealed by the magnetic moment of ^{75}Cu ," *Nat. Phys.* **15**, 321 (2019).
- Z. Q. Chen, Z. H. Li, H. Hua, H. Watanabe, C. X. Yuan, S. Q. Zhang, G. Lorusso, S. Nishimura, H. Baba, F. Browne, G. Benzoni, K. Y. Chae, F. C. L. Crespi, P. Doornenbal, N. Fukuda, G. Gey, R. Gernhäuser, N. Inabe, T. Isobe, D. X. Jiang, A. Jungclaus, H. S. Jung, Y. Jin, D. Kameda, G. D. Kim, Y. K. Kim, I. Kojouharov, F. G. Kondev, T. Kubo, N. Kurz, Y. K. Kwon, X. Q. Li, J. L. Lou, G. J. Lane, C. G. Li, D. W. Luo, A. Montaner-Pizá, K. Moschner, C. Y. Niu, F. Naqvi, M. Niikura, H. Nishibata, A. Odahara, R. Orlandi, Z. Patel, Zs. Podolyák, T. Sumikama, P. -A. Söderström, H. Sakurai, H. Schaffner, G. S. Simpson, K. Steiger, H. Suzuki, J. Taprogge, H. Takeda, Zs. Vajta, H. K. Wang, J. Wu, A. Wendt, C. G. Wang, H. Y. Wu, X. Wang, C. G. Wu, C. Xu, Z. Y. Xu, A. Yagi, Y. L. Ye, and K. Yoshinaga, "Proton shell evolution below ^{132}Sn : first measurement of low-lying β -emitting isomers in $^{123,125}\text{Ag}$," *Phys. Rev. Lett.* **122**, 212502 (2019).
- D. Lubos, J. Park, T. Faestermann, R. Gernhäuser, R. Krücken, M. Lewitowicz, S. Nishimura, H. Sakurai, D. S. Ahn, H. Baba, B. Blank, A. Blazhev, P. Boutachkov, F. Browne, I. Čeliković, G. de France, P. Doornenbal, Y. Fang, N. Fukuda, J. Giovinazzo, N. Goel, M. Górska, S. Ilieva, N. Inabe, T. Isobe, A. Jungclaus, D. Kameda, Y. K. Kim, I. Kojouharov, T. Kubo, N. Kurz, Y. K. Kwon, G. Lorusso, K. Moschner, D. Murai, I. Nishizuka, Z. Patel, M. M. Rajabali, S. Rice, H. Schaffner, Y. Shimizu, L. Sinclair, P. -A. Söderström, K. Steiger, T. Sumikama, H. Suzuki, H. Takeda, Z. Wang, N. Warr, H. Watanabe, J. Wu, and Z. Xu, "Improved value for the gamow-teller strength of the ^{100}Sn beta decay," *Phys. Rev. Lett.* **122**, 222502 (2019).
- D. S. Ahn, N. Fukuda, H. Geissel, N. Inabe, N. Iwasa, T. Kubo, K. Kusaka, D. J. Morrissey, D. Murai, T. Nakamura, M. Ohtake, H. Otsu, H. Sato, B. M. Sherrill, Y. Shimizu, H. Suzuki, H. Takeda, O. B. Tarasov, H. Ueno, Y. Yanagisawa, and K. Yoshida, "Location of the neutron dripline at fluorine and neon," *Phys. Rev. Lett.* **123**, 212501 (2019).
- H. Watanabe, H. K. Wang, G. Lorusso, S. Nishimura, Z. Y. Xu, T. Sumikama, P. -A. Söderström, P. Doornenbal, F. Browne, G. Gey, H. S. Jung, J. Taprogge, Zs. Vajta, J. Wu, A. Yagi, H. Baba, G. Benzoni, K. Y. Chae, F. C. L. Crespi, N. Fukuda, R. Gernhäuser, N. Inabe, T. Isobe, A. Jungclaus, D. Kameda, G. D. Kim, Y. K. Kim, I. Kojouharov, F. G. Kondev, T. Kubo, N. Kurz, Y. K. Kwon, G. J. Lane, Z. Li, C. -B. Moon, A. Montaner-Pizá, K. Moschner, F. Naqvi, M. Niikura, H. Nishibata, D. Nishimura, A. Odahara, R. Orlandi, Z. Patel, Zs. Podolyák, H. Sakurai, H. Schaffner, G. S. Simpson, K. Steiger, Y. Sun, H. Suzuki, H. Takeda, A. Wendt, and K. Yoshinaga, "New isomers in $^{125}\text{Pd}_{79}$ and $^{127}\text{Pd}_{81}$: Competing proton and neutron excitations in neutron-rich palladium nuclides towards the $N = 82$ shell closure," *Phys. Lett. B* **792**, 263 (2019).
- A. Corsi, Y. Kubota, J. Casal, M. Gómez-Ramos, A. M. Moro, G. Authalet, H. Baba, C. Caesar, D. Calvet, A. Delbart, M. Dozono, J. Feng, F. Flavigny, J. -M. Gheller, J. Gibelin, A. Giganon, A. Gillibert, K. Hasegawa, T. Isobe, Y. Kanaya, S. Kawakami, D. Kim, Y. Kiyokawa, M. Kobayashi, N. Kobayashi, T. Kobayashi, Y. Kondo, Z. Korkulu, S. Koyama, V. Lapoux, Y. Maeda, F. M. Marqués, T. Motobayashi, T. Miyazaki, T. Nakamura, N. Nakatsuka, Y. Nishio, A. Obertelli, A. Ohkura, N. A. Orr, S. Ota, H. Otsu, T. Ozaki, V. Panin, S. Paschalis, E. C. Pollacco, S. Reichert, J. -Y. Rousse, A. T. Saito, S. Sakaguchi, M. Sako, C. Santamaria, M. Sasano, H. Sato, M. Shikata, Y. Shimizu, Y. Shindo, L. Stuhl, T. Sumikama, Y. L. Sun, M. Tabata, Y. Togano, J. Tsubota, T. Uesaka, Z. H. Yang, J. Yasuda, K. Yoneda, and J. Zenihiro, "Structure of ^{13}Be probed via quasi-free scattering," *Phys. Lett. B* **797**, 134843 (2019).
- G. X. Zhang, H. Watanabe, G. D. Dracoulis, F. G. Kondev, G. J. Lane, P. H. Regan, P. -A. Söderström, P. M. Walker, K. Yoshida, H. Kanaoka, Z. Korkulu, P. S. Lee, J. J. Liu, S. Nishimura, J. Wu, A. Yagi, D. S. Ahn, T. Alharbi, H. Baba, F. Browne, A. M. Bruce, M. P. Carpenter, R. J. Carroll, K. Y. Chae, C. J. Chiara, Zs. Dombradi, P. Doornenbal, A. Estrade, N. Fukuda, C. Griffin, E. Ideguchi, N. Inabe, T. Isobe, S. Kanaya, I. Kojouharov, T. Kubo, S. Kubono, N. Kurz, I. Kuti, S. Lalkovski, T. Lauritsen, C. S. Lee, E. J. Lee, C. J. Lister, G. Lorusso, G. Lotay, E. A. McCutchan, C. -B. Moon, I. Nishizuka, C. R. Nita, A. Odahara, Z. Patel, V. H. Phong, Zs. Podolyák, O. J. Roberts, H. Sakurai, H. Schaffner, D. Seweryniak, C. M. Shand, Y. Shimizu, T. Sumikama, H. Suzuki, H. Takeda, S. Terashima, Zs. Vajta, J. J. Valiente-Dóbon, Z. Y. Xu, and S. Zhu, "Interplay of quasiparticle and vibrational excitations: First observation of isomeric states in ^{168}Dy and ^{169}Dy ," *Phys. Lett. B* **799**, 135036 (2019).
- P. J. Davies, J. Park, H. Grawe, R. Wadsworth, R. Gernhäuser, R. Krücken, F. Nowacki, D. S. Ahn, F. Ameil, H. Baba, T. Bäck, B. Blank, A. Blazhev, P. Boutachkov, F. Browne, I. Čeliković, M. Dewald, P. Doornenbal, T. Faestermann, Y. Fang, G. de France, N. Fukuda, A. Gengelbach, J. Gerl, J. Giovinazzo, S. Go, N. Goel, M. Górska, E. Gregor, H. Hotaka, S. Ilieva, N. Inabe, T. Isobe, D. G. Jenkins, J. Jolie, H. S. Jung, A. Jungclaus, D. Kameda, G. D. Kim, Y. -K. Kim, I. Kojouharov, T. Kubo, N. Kurz, M. Lewitowicz, G. Lorusso, D. Lubos, L. Maier, E. Merchan, K. Moschner, D. Murai, F. Naqvi, H. Nishibata, D. Nishimura, S. Nishimura, I. Nishizuka, Z. Patel, N. Pietralla, M. M. Rajabali, S. Rice, H. Sakurai, H. Schaffner, Y. Shimizu, L. F. Sinclair, P. -A. Söderström, K. Steiger, T. Sumikama, H. Suzuki, H. Takeda, J. Taprogge, P. Thöle, S. Valder, Z. Wang, N. Warr, H. Watanabe, V. Werner, J. Wu, Z. Y. Xu, A. Yagi, K. Yoshinaga, and Y. Zhu, "Toward the limit of nuclear binding on the $N = Z$ line: Spectroscopy of ^{96}Cd ," *Phys. Rev. C* **99**, 021302(R) (2019).
- J. Park, R. Krücken, D. Lubos, R. Gernhäuser, M. Lewitowicz, S. Nishimura, D. S. Ahn, H. Baba, B. Blank, A. Blazhev, P. Boutachkov, F. Browne, I. Čeliković, G. de France, P. Doornenbal, T. Faestermann, Y. Fang, N. Fukuda, J. Giovinazzo, N. Goel, M. Górska,

- H. Grawe, S. Ilieva, N. Inabe, T. Isobe, A. Jungclaus, D. Kameda, G. D. Kim, Y. -K. Kim, I. Kojouharov, T. Kubo, N. Kurz, Y. K. Kwon, G. Lorusso, K. Moschner, D. Murai, I. Nishizuka, Z. Pate, M. M. Rajabali, S. Rice, H. Sakurai, H. Schaffner, Y. Shimizu, L. Sinclair, P. -A. Söderström, K. Steiger, T. Sumikama, H. Suzuki, H. Takeda, Z. Wang, H. Watanabe, and J. Wu, “New and comprehensive β - and $\beta\beta$ -decay spectroscopy results in the vicinity of ^{100}Sn ,” *Phys. Rev. C* **99**, 034313 (2019).
- V. H. Phong, G. Lorusso, T. Davinson, A. Estrade, O. Hall, J. Liu, K. Matsui, F. Montes, S. Nishimura, A. Boso, P. H. Regan, R. Shearman, Z. Y. Xu, J. Agramunt, J. M. Allmond, D. S. Ahn, A. Algora, H. Baba, N. T. Brewer, C. G. Bruno, R. Caballero-Folch, F. Calvino, M. Wolińska-Cichočka, G. Cortes, I. Dillmann, C. Domingo-Pardo, A. Gargano, S. Go, C. J. Griffin, R. K. Grzywacz, L. Harkness-Brennan, T. Isobe, A. Jungclaus, D. Kahl, L. H. Khiem, G. Kiss, A. Korgul, S. Kubono, K. Miernik, A. I. Morales, N. Nepal, M. Piersa, Zs. Podolyák, B. C. Rasco, K. P. Rykaczewski, H. Sakurai, Y. Shimizu, D. W. Stacener, T. Sumikama, H. Suzuki, H. Takeda, J. L. Tain, A. Tarifeño-Saldivia, A. Tolosa-Delgado, V. Vaquero, P. J. Woods, R. Yokoyama, and C. Yuan, “Observation of a μs isomer in $^{134}\text{In}_{85}$: Proton-neutron coupling “southeast” of $^{132}\text{Sn}_{82}$,” *Phys. Rev. C* **100**, 011302(R) (2019).
- R. Yokoyama, R. Grzywacz, B. C. Rasco, N. Brewer, K. P. Rykaczewski, I. Dillmann, J. L. Tain, S. Nishimura, D. S. Ahn, A. Algora, J. M. Allmond, J. Agramunt, H. Baba, S. Bae, C. G. Bruno, R. Caballero-Folch, F. Calvino, P. J. Coleman-Smith, G. Cortes, T. Davinson, C. Domingo-Pardo, A. Estrade, N. Fukuda, S. Go, C. J. Griffin, J. Ha, O. Hall, L. J. Harkness-Brennan, J. Heideman, T. Isobe, D. Kahl, M. Karny, T. Kawano, L. H. Khiem, T. T. King, G. G. Kiss, A. Korgul, S. Kubono, M. Labiche, I. Lazarus, J. Liang, J. Liu, G. Lorusso, M. Madurga, K. Matsui, K. Miernik, F. Montes, A. I. Morales, P. Morrall, N. Nepal, R. D. Page, V. H. Phong, M. Piersa, M. Prydderch, V. F. E. Pucknell, M. M. Rajabali, B. Rubio, Y. Saito, H. Sakurai, Y. Shimizu, J. Simpson, M. Singh, D. W. Stracener, T. Sumikama, R. Surman, H. Suzuki, H. Takeda, A. Tarifeño-Saldivia, S. L. Thomas, A. Tolosa-Delgado, M. Wolińska-Cichočka, P. J. Woods, and X. X. Xu “Strong one-neutron emission from two-neutron unbound states in β decays of the r-process nuclei $^{86,87}\text{Ga}$,” *Phys. Rev. C* **100**, 031302(R) (2019).
- L. Sinclair, R. Wadsworth, J. Dobaczewski, A. Pastore, G. Lorusso, H. Suzuki, D. S. Ahn, H. Baba, F. Browne, P. J. Davies, P. Doornenbal, A. Estrade, Y. Fang, N. Fukuda, J. Henderson, T. Isobe, D. G. Jenkins, S. Kubono, Z. Li, D. Lubos, S. Nishimura, I. Nishizuka, Z. Patel, S. Rice, H. Sakurai, Y. Shimizu, P. Schury, H. Takeda, P. -A. Söderström, T. Sumikama, H. Watanabe, V. Werner, J. Wu, and Z. Y. Xu, “Half-lives of ^{73}Sr and ^{76}Y and the consequences for the proton dripline,” *Phys. Rev. C* **100**, 044311 (2019).
- K. Nakano, Y. Watanabe, S. Kawase, H. Wang, H. Otsu, H. Sakurai, S. Takeuchi, Y. Togano, T. Nakamura, Y. Maeda, D. S. Ahn, M. Aikawa, S. Araki, S. Chen, N. Chiga, P. Doornenbal, N. Fukuda, T. Ichihara, T. Isobe, S. Kawakami, T. Kin, Y. Kondo, S. Koyama, T. Kubo, S. Kubono, M. Uesaka, A. Makinaga, M. Matsushita, T. Matsuzaki, S. Michimasa, S. Momiyama, S. Nagamine, M. Niikura, T. Ozaki, A. Saito, T. Saito, Y. Shiga, M. Shikata, Y. Shimizu, S. Shimoura, T. Sumikama, P. A. Söderström, H. Suzuki, H. Takeda, R. Taniuchi, J. Tsubota, Y. Watanabe, K. Wimmer, T. Yamamoto, and K. Yoshida, “Isotope production in proton-, deuteron-, and carbon-induced reactions on ^{93}Nb at 113 MeV/nucleon” *Phys. Rev. C* **100**, 044605 (2019).
- H. Wang, H. Otsu, N. Chiga, S. Kawase, S. Takeuchi, T. Sumikama, S. Koyama, H. Sakurai, Y. Watanabe, S. Nakayama, D. S. Ahn, H. Baba, S. D. Chen, K. Chikaato, M. L. Cortés, N. Fukuda, A. Hirayama, R. Hosoda, T. Isobe, S. Kawakami, Y. Kondo, S. Kubono, Y. Maeda, S. Masuoka, S. Michimasa, I. Murray, R. Nakajima, T. Nakamura, K. Nakano, M. Nishimura, T. Ozaki, A. Saito, T. Saito, H. Sato, Y. Shimizu, S. Shimoura, P. -A. Söderström, Y. Soudo, X. H. Sun, J. Suwa, D. Suzuki, H. Suzuki, H. Takeda, M. Takechi, Y. Togano, T. Tomai, H. Yamada, M. Yasuda, and K. Yoshida, “Enhancement of element production by incomplete fusion reaction with weakly bound deuteron,” *Commun. Phys.* **2**, 78 (2019).
- A. Tolosa-Delgado, J. Agramunt, J. L. Tain, A. Algora, C. Domingo-Pardo, A. I. Morales, B. Rubio, A. Tarifeño-Saldivia, F. Calvino, G. Cortes, N. T. Brewer, B. C. Rasco, K. P. Rykaczewski, D. W. Stracener, J. M. Allmond, R. Grzywacz, R. Yokoyama, M. Singh, T. King, M. Madurga, S. Nishimura, V. H. Phong, S. Go, J. Liu, K. Matsui, H. Sakurai, G. G. Kiss, T. Isobe, H. Baba, S. Kubono, N. Fukuda, D. S. Ahn, Y. Shimizu, T. Sumikama, H. Suzuki, H. Takeda, P. A. Soderstrom, M. Takechi, C. G. Bruno, T. Davinson, C. J. Griffin, O. Hall, D. Kahl, P. J. Woods, P. J. Coleman-Smith, M. Labiche, I. Lazarus, P. Morrall, V. F. E. Pucknell, J. Simpson, S. L. Thomas, M. Prydderch, L. J. Harkness-Brennan, R. D. Page, I. Dillmann, R. Caballero-Folch, Y. Saito, A. Estrade, N. Nepal, F. Montes, G. Lorusso, J. Liang, S. Bae, J. Ha, B. Moon, the BRIKEN collaboration, “Commissioning of the BRIKEN detector for the measurement of very exotic β -delayed neutron emitters,” *Nucl. Instrum. Methods Phys. Res. A* **925**, 133 (2019).
- S. Takeuchi, T. Nakamura, M. Shikata, Y. Togano, Y. Kondo, J. Tsubota, T. Ozaki, A. Saito, H. Otsu, H. Wang, H. Sakurai, Y. Watanabe, S. Kawase, D. S. Ahn, M. Aikawa, T. Ando, S. Araki, S. Chen, N. Chiga, P. Doornenbal, S. Ebata, N. Fukuda, T. Isobe, S. Kawakami, T. Kin, S. Koyama, S. Kubono, Y. Maeda, A. Makinaga, M. Matsushita, T. Matsuzaki, S. Michimasa, S. Momiyama, S. Nagamine, K. Nakano, M. Niikura, K. Ogata, T. Saito, Y. Shiga, Y. Shimizu, S. Shimoura, T. Sumikama, Pär-Anders Söderstrom, H. Suzuki, H. Takeda, R. Taniuchi, M. Uesaka, Y. Watanabe, K. Wimmer, T. Yamamoto, and K. Yoshida, “Coulomb breakup reactions of $^{93,94}\text{Zr}$ in inverse kinematics,” *Prog. Theor. Exp. Phys.* **2019**, 013D02 (2019).
- S. Michimasa, J. Hwang, K. Yamada, S. Ota, M. Dozono, N. Imai, K. Yoshida, Y. Yanagisawa, K. Kusaka, M. Ohtake, M. Matsushita, D. S. Ahn, O. Beliuskina, N. Chiga, K. Chikaato, N. Fukuda, S. Hayakawa, E. Ideguchi, K. Iribe, C. Iwamoto, S. Kawase, K. Kawata, N. Kitamura, S. Masuoka, H. Miyatake, D. Nagae, R. Nakajima, T. Nakamura, K. Nakano, S. Omika, H. Otsu, H. Sakurai, P. Schrock, H. Shimizu, Y. Shimizu, T. Sumikama, X. Sun, D. Suzuki, H. Suzuki, M. Takaki, M. Takechi, H. Takeda, S. Takeuchi, T. Teranishi, R. Tsunoda, H. Wang, Y. Watanabe, Y. X. Watanabe, K. Wimmer, K. Yako, H. Yamaguchi, L. Yang, H. Yoshida, and S. Shimoura, “OEDO, the energy-degrading beamline at RI Beam Factory,” *Prog. Theor. Exp. Phys.* **2019**, 043D01 (2019).
- J. Hwang, S. Michimasa, S. Ota, M. Dozono, N. Imai, K. Yoshida, Y. Yanagisawa, K. Kusaka, M. Ohtake, D. S. Ahn, O. Beliuskina, N. Fukuda, C. Iwamoto, S. Kawase, K. Kawata, N. Kitamura, S. Masuoka, H. Otsu, H. Sakurai, P. Schrock, T. Sumikama, H. Suzuki, M. Takaki, H. Takeda, R. Tsunoda, K. Wimmer, K. Yako, and S. Shimoura, “Angle-tunable wedge degrader for an energy-degrading RI beamline,” *Prog. Theor. Exp. Phys.* **2019**, 043D02 (2019).
- T. Sonoda, I. Katayama, M. Wada, H. Iimura, V. Sonnenschein, S. Iimura, A. Takamine, M. Rosenbusch, T. M. Kojima, D. S. Ahn, N. Fukuda, T. Kubo, S. Nishimura, Y. Shimizu, H. Suzuki, H. Takeda, M. Tanigaki, H. Tomita, K. Yoshida, and H. Ishiyama, “Conceptual study on parasitic low-energy RI beam production with in-flight separator BigRIPS and the first stopping examination for high-energy RI beams in the parasitic gas cell,” *Prog. Theor. Exp. Phys.* **2019**, 113D02 (2019).

[Proceedings]

- K. Kusaka, “Long term operation of the superconducting triplet quadrupoles with cryocoolers for BigRIPS in-flight separator at RIKEN,” 2019 IOP Conf. Ser.: Mater. Sci. Eng. **502**, 012103(2019).

Presentations**[International conferences/workshops]**

- H. Suzuki (oral), “Discovery of ^{72}Rb & production of proton-rich RI-beams at RIBF,” The International Conference on Proton-Emitting nuclei (PROCON2019), East Lansing, Michigan, USA, June 3–7, 2019.
- N. Fukuda (invited), “Observation of new isotopes at RIKEN RI Beam Factory,” XXXVI Mazurian Lakes Conference on Physics, Piaski, Poland, September 1–7, 2019.
- K. Kusaka (poster), “Long term operation of the superconducting triplet quadrupoles with cryocoolers,” EUCAS2019: 14th European Conference on Applied Superconductivity, SEC, Glasgow, UK, September 1–5, 2019.
- D. S. Ahn (invited), “Status of RI beam production at BigRIPS,” Expert meeting on Next-Generation Fragment Separators 2019, Darmstadt, Germany, September 30–October 2, 2019.
- H. Takeda(invited), “Development of various new ion-optics modes at BigRIPS,” Expert meeting on Next-Generation Fragment Separators 2019, Darmstadt, Germany, September 30–October 2, 2019.
- N. Fukuda (invited), “Observation of new isotopes at RIKEN RI Beam Factory,” 14th Asia Pacific Physics Conference, Sarawak, Malaysia, November 17–21, 2019.
- N. Fukuda (oral), “Present status of RI production at RIKEN RI Beam Factory and future prospects—RI Production at high energies—,” JSPS/NRF/NSFC A3 Foresight Program “Nuclear Physics in the 21st Century,” Joint Kickoff Meeting, Kobe, Japan, December 6–7, 2019.

[Domestic conferences/workshops]

- 松本翔汰 (口頭発表), 西隆博, 高木基伸, A. D. Soon, 馬場秀忠, 藤岡宏之, 福田直樹, 福西暢尚, H. Geissel, 稲辺尚人, 板橋健太, 日下健祐, 三木謙二郎, 三輪海彩, 永江知文, 阪上朱音, 清水陽平, 炭竈聡之, 鈴木宏, 竹田浩之, 田中良樹, 上坂友洋, 渡辺珠以, 矢向謙太郎, 柳澤善行, 吉田光一, 銭廣十三, 「BigRIPSにおける高精度パイ中間子原子分光・二重ガモフテラー巨大共鳴探索実験の現状」, 日本物理学会第72回年次大会, 九州大学, 福岡, 2019年3月14日–17日.
- S. Masuoka, S. Shimoura, M. Takaki, M. Dozono, C. Iwamoto, K. Kawata, N. Kitamura, M. Kobayashi, S. Michimasa, R. Nakajima, S. Ota, H. Tokieda, R. Yokoyama, D. S. Ahn, H. Baba, N. Fukuda, T. Harada, E. Ideguchi, N. Imai, N. Inabe, Y. Kondo, T. Kubo, Y. Maeda, F. M. Marques, M. Matsushita, T. Nakamura, N. Orr, H. Sakai, H. Sato, P. Schrock, L. Stuhl, T. Sumikama, H. Suzuki, H. Takeda, K. Taniue, T. Uesaka, K. Wimmer, K. Yako, Y. Yamaguchi, Y. Yanagisawa, K. Yoshida, and J. Zenihiro, 「二重荷電交換反応 $^4\text{He}(^8\text{He}, ^8\text{Be})$ 反応の再測定 II」, 日本物理学会第72回年次大会, 九州大学, 福岡, 2019年3月14日–17日.
- 三木晴瑠, 中村隆司 (口頭発表), 近藤洋介, N. L. Achouri, T. Aumann, 馬場秀忠, F. Delaunay, P. Doornenbal, 福田直樹, J. Gibelin, J. Hwang, 稲辺尚人, 磯部忠昭, 亀田大輔, 簡野大輝, S. Kim, 小林信之, 小林俊雄, 久保敏幸, S. Leblond, J. Lee, M. Marques, 南方亮吾, 本林透, 村井大地, 村上哲也, 武藤琴美, 中嶋丈嘉, 中塚徳継, A. Navin, 西征爾郎, 生越駿, N. A. Orr, 大津秀暁, 佐藤広海, 佐藤義輝, 清水陽平, 鈴木宏, 高橋賢人, 竹田浩之, 武内聡, 田中隆己, 梶野泰宏, A. G. Tuff, M. Vandebrouck, 米田健一郎, 「荷電交換反応を用いた中性子過剰非束縛核 ^{28}F の研究」, 日本物理学会第72回年次大会, 九州大学, 福岡, 2019年3月14日–17日.
- 富田瑞樹 (口頭発表), 武智麻郎, 大坪隆, 本間彰, 田中聖臣, 福田光順, 鈴木健, 西村太樹, 森口哲朗, 安得順, A. S. Aimaganbetov, 天野将道, 荒川裕樹, S. Bagchi, K. H. Behr, N. Burtbayev, 親跡和弥, 杜航, 藤井朋也, 福田直樹, H. Geissel, 堀太地, 星野寿春, 伊五澤涼, 池田彩夏, 稲辺尚人, 猪股玖美, 板橋健太, 泉川卓司, 上岡大起, 神田直人, 加藤郁磨, I. Kenzhina, Z. Korkulu, Ye. Kuk, 日下健祐, 三原基嗣, 宮田恵理, 長江大輔, 中村翔健, M. Nassurulla, 西室国光, 西塚賢治, 大甕舜一朗, 大西康介, 大竹政雄, 王恵仁, 小沢頭, A. Prochazka, 櫻井博儀, C. Scheidenberger, 清水陽平, 杉原貴信, 炭竈聡之, 鈴木伸司, 鈴木宏, 竹田浩之, 田中悠太郎, 田中良樹, 和田太郎, 若山清志, 八木翔一, 山口貴之, 柳原陸斗, 柳澤善行, 吉田光一, T. K. Zholdybayev, 「Sc 同位体の荷電変化断面積測定」, 日本物理学会第72回年次大会, 九州大学, 福岡, 2019年3月14日–17日.
- 堂園昌伯 (口頭発表), 今井伸明, 道正新一郎, 下浦享, 大田晋輔, 炭竈聡之, 千賀信幸, 大津秀暁, 入部弘太郎, 他 ImPACT17-02-01 コラボレーション, 「低速 RI ビームを用いた ^{107}Pd の陽子・重陽子誘起反応測定」, 日本物理学会第72回年次大会, 九州大学, 福岡, 2019年3月14日–17日.
- 入部弘太郎 (口頭発表), 堂園昌伯, 今井伸明, 道正新一郎, 下浦享, 大田晋輔, 炭竈聡之, 千賀信幸, 大津秀暁, 寺西高, 他 ImPACT17-02-01 コラボレーション, 「低速 RI ビームを用いた ^{93}Zr の陽子・重陽子誘起反応測定」, 日本物理学会第72回年次大会, 九州大学, 福岡, 2019年3月14日–17日.
- 栗原篤志 (口頭発表), 中村隆司, 近藤洋介, 武内聡, 斗米貴人, 齊藤敦美, 安田昌弘, 山田啓貴, 島田哲朗, 三木晴瑠, 松本真由子, N. L. Achouri, T. Aumann, 馬場秀忠, F. Delaunay, P. Doornenbal, 福田直樹, J. Gibelin, J. Hwang, 稲辺尚人, 磯部忠昭, 亀田大輔, S. KimD, 小林信之, 小林俊雄, 久保敏幸, S. Leblond, J. Lee, M. Marques, 本林透, 村井大地, 村上哲也, 武藤琴美, 中塚徳継, A. Navin, N. A. Orr, 大津秀暁, 佐藤広海, 佐藤義輝, 清水陽平, 鈴木宏, 高橋賢人, 竹田浩之, 梶野泰宏, A. G. Tuff, M. Vandebrouck, 米田健一郎, 「 ^{22}C のクーロン分解反応」, 日本物理学会第72回年次大会, 九州大学, 福岡, 2019年3月14日–17日.
- 吉留勇起, 近藤洋介 (口頭発表), 中村隆司, N. L. Achouri, T. Aumann, 馬場秀忠, F. Delaunay, P. Doornenbal, 福田直樹, J. Gibelin, J. Hwang, 稲辺尚人, 磯部忠昭, 亀田大輔, 簡野大輝, S. Kim, 小林信之, 小林俊雄, 久保敏幸, S. Leblond, J. Lee, M. Marques, 南方亮吾, 本林透, 村井大地, 村上哲也, 武藤琴美, 中嶋丈嘉, 中塚徳継, A. Navin, 西征爾郎, 生越駿, N. A. Orr, 大津秀暁, 佐藤広海, 佐藤義輝, 清水陽平, 鈴木宏, 高橋賢人, 竹田浩之, 武内聡, 田中隆己, 梶野泰宏, A. G. Tuff, M. Vandebrouck, 米田健一郎, 「 ^{25}O の不変質量核分光」, 日本物理学会第72回年次大会, 九州大学, 福岡, 2019年3月14日–17日.
- 三木晴瑠 (口頭発表), 近藤洋介, 中村隆司, N. L. Achouri, T. Aumann, 馬場秀忠, F. Delaunay, P. Doornenbal, 福田直樹, Julien Gibelin, J. Hwang, 稲辺尚人, 磯部忠昭, 亀田大輔, 簡野大輝, S. Kim, 小林信之, 小林俊雄, 久保敏幸, S. Leblond, J. Lee, M. Marques, 南方

亮吾, 本林透, 村井大地, 村上哲也, 武藤琴美, 中嶋丈嘉, 中塚徳継, A. Navin, 西征爾郎, 生越駿, N. A. Orr, 大津秀暁, 佐藤広海, 佐藤義輝, 清水陽平, 鈴木宏, 高橋賢人, 竹田浩之, 武内聡, 田中隆己, 榊野泰宏, A. G. Tuff, M. Vandebrouck, 米田健一郎, 「荷電交換反応を用いた非束縛核 ^{28}F の探索」, 日本物理学会 2019 年秋季大会, 山形大学, 山形, 2019 年 9 月 17 日-20 日.

吉留勇起 (口頭発表), 近藤洋介, 中村隆司, N. L. Achouri, T. Aumann, 馬場秀忠, F. Delaunay, P. Doornenbal, 福田直樹, J. Gibelin, J. Hwang, 稲辺尚人, 磯部忠昭, 亀田大輔, 簡野大輝, S. Kim, 小林信之, 小林俊雄, 久保敏幸, S. Leblond, J. Lee, M. Marques, 南方亮吾, 本林透, 村井大地, 村上哲也, 武藤琴美, 中嶋丈嘉, 中塚徳継, A. Navin, 西征爾郎, 生越駿, N. A. Orr, 大津秀暁, 佐藤広海, 佐藤義輝, 清水陽平, 鈴木宏, 高橋賢人, 竹田浩之, 武内聡, 田中隆己, 榊野泰宏, A. G. Tuff, M. Vandebrouck, 米田健一郎, 「 ^{25}O の不変質量核分光」 日本物理学会 2019 年秋季大会, 山形大学, 山形, 2019 年 9 月 17 日-20 日.

N. Fukuda (oral), “Current and near future BigRIPS DAQ,” RIBFDAQ workshop 2019, RIKEN, Wako, Japan, December 23, 2019.

Press releases

RIKEN プレス発表 (2019.11.19) フッ素とネオンの同位元素の存在限界を初めて決定—原子核の地図の境界線を 20 年ぶりに更新—
稲辺尚人, 福田直樹, 久保敏幸, 中村隆司

Research Facility Development Division

Research Instruments Group

SAMURAI Team

1. Abstract

In collaboration with research groups in and outside RIKEN, the team designs, develops and constructs the SAMURAI spectrometer and relevant equipment that are and will be used for reaction experiments using RI beams at RI Beam Factory. The SAMURAI spectrometer consists of a large superconducting dipole magnet and a variety of detectors to measure charged particles and neutrons. After the commissioning experiment in March 2012, the team prepared and conducted, in collaboration with researchers in individual experimental groups, the first series of experiments with SAMURAI in May 2012. Then, several numbers of experiments were well performed until now utilizing the property of SAMURAI. The team also provides a basis for research activities by, for example, organizing collaboration workshops by researchers who are interested in studies or plan to perform experiments with the SAMURAI spectrometer.

2. Major Research Subjects

Design, operation, maintenance and improvement of the SAMURAI spectrometer and its related research instruments. Support and management for SAMURAI-based research programs. Generate future plans for next generation instruments for nuclear reaction studies.

3. Summary of Research Activity

The current research subjects are summarized as follows:

- (1) Operation, maintenance and improvement of a large superconducting dipole magnet that is the main component of the SAMURAI spectrometer.
- (2) Design, development and construction of various detectors that are used for nuclear reaction experiments using the SAMURAI spectrometer.
- (3) Preparation for planning experiments using SAMURAI spectrometer.
- (4) Maintenance and improvement of the SAMURAI beam line.
- (5) Formation of a collaboration platform called SAMURAI collaboration.
- (6) Preparation for next generation spectrometer for nuclear reaction studies.

Members

Team Leader

Hideaki OTSU

Research & Development Scientist

Mizuki NISHIMURA

Junior Research Associate

Takato TOMAI

List of Publications & Presentations

Publications

[Original papers]

- A. Revel, O. Sorlin, F. M. Marqués, H. Otsu *et al.*, “Extending the Southern Shore of the Island of Inversion to ^{28}F ,” *Phys. Rev. Lett.* **124**, 152502 (2020).
- K. J. Cook, T. Nakamura, Y. Kondo, K. Hagino, H. Otsu *et al.*, “Halo Structure of the Neutron-Dripline Nucleus ^{19}B ,” *Phys. Rev. Lett.* **124**, 212503 (2020).
- M. L. Cortes, W. Rodriguez, P. Doornenbal, A. Obertelli, H. Otsu *et al.*, “Shell evolution of $N = 40$ isotones towards ^{60}Ca : first spectroscopy of ^{62}Ti ,” *Phys. Lett. B* **800**, 135071 (2020).
- Y. L. Sun, A. Obertelli, P. Doornenbal, H. Otsu *et al.*, “Restoration of the natural $E(1/2_1^+)$ - $E(3/2_1^+)$ energy splitting in odd-K isotopes towards $N = 40$,” *Phys. Lett. B* **802**, 135215 (2020).
- S. Chen, J. Lee, P. Doornenbal, A. Obertelli, H. Otsu *et al.*, “Quasifree Neutron Knockout from ^{54}Ca Corroborates Arising $N = 34$ Neutron Magic Number,” *Phys. Rev. Lett.* **123**, 142501 (2019).
- A. Corsi, Y. Kubota, J. Casal, H. Otsu *et al.*, “Structure of ^{13}Be probed via quasi-free scattering,” *Phys. Lett. B* **797**, 134843 (2019).
- Y. Kondo, T. Tomai, and T. Nakamura, “Recent progress and developments for experimental studies with the SAMURAI spectrometer,” *Nucl. Instrum. Methods Phys. Res. B* **463**, 173–178 (2020).
- L. Stuhl, M. Sasano, H. Otsu *et al.*, “Study of spin-isospin responses of radioactive nuclei with the background-reduced neutron” spectrometer, PANDORA,” *Nucl. Instrum. Methods Phys. Res. B* **463**, 189–194 (2020).

Y. Togano, T. Nakamura, Y. Kondo, H. Otsu *et al.*, “New γ -ray detector CATANA for in-beam γ -ray spectroscopy with fast RI beams,” Nucl. Instrum. Methods Phys. Res. B **463**, 195–197 (2020).

[Proceedings]

- M. Kurata-Nishimura *et al.*, “Experimental study of nuclear equation of state using heavy ion collisions at RIKEN-RIBF,” Proc. 15th Int. Symp. Origin of Matter and Evolution of Galaxies (OMEG15) JPS Conf. Proc. 31, (2020), p. 011023.
- J. Gibelin *et al.*, “Boron isotopes at the drip-line: ^{19}B ,” Proc. of the 22nd Int. Conf. on Few-Body Problems in Physics Springer Proceedings in Physics 238 (2020), p. 103.
- B. Monteagudo *et al.*, “Structure of Beryllium isotopes beyond the neutron dripline,” Proc. of the 22nd Int. Conf. on Few-Body Problems in Physics Springer Proceedings in Physics 238 (2020), p. 331.
- Z. H. Yang *et al.*, “Study of multi-neutron systems with the SAMURAI spectrometer,” Proc. of the 22nd Int. Conf. on Few-Body Problems in Physics Springer Proceedings in Physics 238 (2020), p. 529.
- A. I. Chilug, *et al.*, “Study of the ^9C breakup through NP1412-SAMURAI29R1 experiment,” Carpathian Summer School of Physics 2018 (CSSP18), Sinaia, Romania, AIP Conference Proceedings 2076, 060001 (2019).

Presentations

[International conferences/workshops]

- M. Kurata-Nishimura, “Experimental study of nuclear equation of state using heavy ion collisions at RIKEN-RIBF,” The 15th International Symposium on Origin of Matter and Evolution of Galaxies, Kyoto, July 2–5, 2019.
- M. Kurata-Nishimura, “Recent results of collective flow at neutron rich Sn+Sn collisions with 270 MeV/u,” 9th International Symposium on Nuclear Symmetry Energy (NuSYM 2019), Da Nang, Vietnam, October 2–5, 2019.
- T. Nakamura, “Recent progress of spectroscopic studies of nuclei near and beyond the neutron drip line,” Thirty Eighth International Workshop on Nuclear Theory, Rila Mountains, Bulgaria, June 23–29, 2019.
- Y. Kondo, “Spectroscopy of Oxygen isotopes beyond the neutron drip line,” Gordon Research Conference, “Exploring simple structural patterns and the dynamics of nuclei,” New London, NH, US, June 16–21, 2019.
- K. J. Cook, “Nuclear structure at the neutron drip-line: determining the halo nature of ^{19}B using coulomb breakup,” Gordon Research Conference, “Exploring simple structural patterns and the dynamics of nuclei,” New London, NH, US, June 16–21, 2019.
- Y. Kondo, “Spectroscopy of unbound nuclei towards the possible doubly magic nucleus ^{28}O ,” 27th International Nuclear Physics Conference, Glasgow, UK, July 29–August 2, 2019.
- T. Nakamura, “Spectroscopy of neutron-drip-line nuclei using SAMURAI at RIBF,” 27th International Nuclear Physics Conference, Glasgow, UK, July 29–August 2, 2019.
- T. Tomai, “Observation of excited states of ^{31}Ne using nuclear breakup reaction,” 27th International Nuclear Physics Conference, Glasgow, UK, July 29–August 2, 2019.
- T. Nakamura, “SAMURAI at RIBF: recent progress and near-future perspectives,” RIBF USERS Meeting 2019, RIKEN, Wako, Japan, September 3–4, 2019.
- T. Nakamura, “Multi-neutron clusters,” 4th International Workshop on Quasi-Free Scattering with Radioactive-Ion Beams, Maresias, Brazil, October 9–13, 2019.
- T. Nakamura, “Study of nuclear structure with radioactive beams,” WE-Heraeus Summer School on: Nuclear Physics in Astrophysics, Heidelberg, Germany, September 9–16, 2019.
- T. Nakamura, “Exploration of neutron drop line nuclei at RIBF,” 14th Asia-Pacific Physics Conference, Borneo Convention Centre Kuching, Sarawak, Malaysia, November 17–22, 2019.
- T. Nakamura, “Experiments on neutron-rich nuclei at SAMURAI at RIBF for astrophysics,” Workshop on “Origin of elements and cosmic evolution: From big-bang to supernovae and mergers,” Beihang University, Beijing China, November 27–29, 2019.
- T. Nakamura, “Exotic nuclei for investigating hierarchical structure of matter,” International Symposium on Clustering as a Window on the Hierarchical Structure of Quantum Systems (CLUSHIQ2020), Beppu, Japan, January 23–24, 2020.
- T. Nakamura, “Coulomb breakup of halo nuclei,” Japan-France Joint Workshop Clusters in Quantum Systems: From Atoms to Nuclei and Hadrons, Fukuoka, Japan, January 27–31, 2020.
- T. Nakamura, “Study of exotic nuclei along the neutron drip line and beyond,” Vth Topical Workshop on Modern Aspects of Nuclear Structure, Bormio, Italy, February 4–9, 2020.
- N. A. Orr, “High-energy direct reaction studies of light, nuclei beyond the neutron dripline,” 27th International Nuclear Physics Conference, Glasgow, UK, July 29–August 2, 2019.
- N. A. Orr, “Direct reaction studies with high-energy radioactive beams of light nuclei beyond the neutron dripline,” Workshop on Challenges in Direct Nuclear Reactions, Beijing, China, August 19–21, 2019.
- N. A. Orr, “Direct reaction studies of light neutron-rich nuclei beyond the dripline,” CENuM-RULiC Joint Workshop on Extreme Nuclear States and Reactions, Daejeon, South Korea, October 31–November 2, 2019.
- F. M. Marqués, “Probing nuclei with (too) many neutrons,” Gordon Research Conference, “Exploring simple structural patterns and the dynamics of nuclei,” New London, NH, US, June 16–21, 2019.
- F. M. Marqués, “The extremes of neutron richness,” Pisa Summer School—Rewriting Nuclear Physics Textbooks: One More Step Forward, Pisa, Italy, July 22–26, 2019.
- F. M. Marqués, “Exotic structures in exotic nuclei,” 24th European Conference on Few-Body Problems in Physics, Guildford, UK, 2–6

September 2019.

- F. M. Marqués, “Two-neutron emission and related phenomena,” Workshop GDR RESANET—Nuclear Structure under Extreme Conditions, Caen, France, December 9–10, 2019.
- J. Gibelin, “Neutron-rich boron isotopes at and beyond the drip line,” Japan-France Joint Workshop Clusters in Quantum Systems: From Atoms to Nuclei and Hadrons, Fukuoka, Japan, January 27–31, 2020.
- C. Lenain, “Search for Hydrogen 7 and its 4 neutron decay at SAMURAI,” Japan-France Joint Workshop Clusters in Quantum Systems: From Atoms to Nuclei and Hadrons, Fukuoka, Japan, January 27–31, 2020.
- M. Duer, “Study of the ${}^8\text{He}(p, p\alpha)4n$ reaction,” International Workshop on Quasi-free Scattering with Radioactive Beams Maresias, Brazil, QFS-RB19, October 13–18, 2019.
- M. Knösel, “Precise measurement of the neutron-neutron scattering length,” International Workshop on Quasi-free Scattering with Radioactive Beams QFS-RB19, Maresias, Brazil, October 13–18, 2019.
- C. Lehr, “Results from NeuLAND @ SAMURAI and the low-energy dipole response of ${}^6,8\text{He}$,” NUSTAR Annual Meeting, GSI Darmstadt, Germany, March 2–6, 2020,
- [SAMURAI International Collaboration Workshop 2019, Rikkyo University, Tokyo, Japan, August 30–31, 2019.]

- Y. L. Sun *et al.*, “STRASSE: a silicon tracker project for quasi free scattering at RIBF.”
- T. Nakamura *et al.*, “Development of high-granularity neutron detector array HIME.”
- T. Aumann *et al.*, “Status of TUDa funding application for construction of HIME and future experiments at SAMURAI.”
- D. Rossi *et al.*, “Invariant-mass spectroscopy at the low-Z shore of the island of inversion.”
- H. Chae *et al.*, “Study of unbound nuclei ${}^{33}\text{Ne}$ via one-proton knockout reactions.”
- Sonja Storck, *et al.*, “Analysis update on the lifetime measurement of the ${}^{26}\text{O}$ g.s. at SAMURAI.”
- M. Duer, *et al.*, “Analysis of the ${}^8\text{He}(p, p\alpha)4n$.”
- Z. Yang, *et al.*, “Quasi-free (p,pn) reaction with Borromean nuclei ${}^{11}\text{Li}$, ${}^{14}\text{Be}$, and ${}^{17}\text{B}$.”
- V. Panin *et al.*, “Status report of S24 experiment: investigation of unbound states in neutron-deficient ${}^{66}\text{Se}$.”
- H. Otsu *et al.*, “HI- α invariant mass spectroscopy.”
- S. Kim *et al.*, “Study of unbound excited states in ${}^{17}\text{C}$.”
- Y. Hirai *et al.*, “Study of Gamow-Teller transition in neutron-rich ${}^{11}\text{Li}$.”
- T. Pohl *et al.*, “Analysis status of S31: probing isospin dependence of nucleon correlations using (p, pN) reaction.”
- T. Motobayashi *et al.*, “Nuclear breakup and coulomb dissociation of ${}^9\text{C}$ nucleus studied at RIBF RIKEN.”
- T. Isobe *et al.*, “Experimental study of density dependent symmetry energy at RIBF-SPIRIT.”
- Z. H. Yang *et al.*, “Status report of s034: study of ${}^7\text{H}$ and the tetra-neutron using ${}^8\text{He}(p, 2p)$ reaction.”
- P. Li *et al.*, “Cluster structure of neutron-rich Beryllium isotopes investigated by cluster quasi-free scattering reaction.”
- Y. Togano *et al.*, “Status report of dipole strength measurement performed in S09 and ImPACT.”
- C. Lehr *et al.*, “Analysis update on the low-energy dipole response of the halo nuclei ${}^6,8\text{He}$.”
- J. Tanaka *et al.*, “Search for preformed-alpha particles via alpha-knockout reaction from alpha-decay nuclei.”
- N. A. Orr *et al.*, “Status of NEBULA-Plus and possible future experiments.”
- Y. KONDO *et al.*, “Status report of the SAMURAI21 experiment.”
- H. Wang *et al.*, “Study on tensor correlation in neutron-rich nuclei via (p, pd) reaction.”

[Domestic conferences/workshops]

- 中村隆司, 「エキゾチック核子多体系で紐解く物質の階層構造」, 第二回クラスター階層領域研究会, 東京工業大学, 東京, 2019年5月31–6月1日.
- 安田聖, 「ダイニュートロン探索のための高精細中性子検出器の開発-II」, 2019年秋季大会, 山形大学, 山形, 2019年9月17–20日.
- 三木晴瑠, 「荷電交換反応を用いた非束縛核 28F の探索」, 2019年秋季大会, 山形大学, 山形, 2019年9月17–20日.
- 島田哲朗, 「中性子過剰非束縛核 30F の核分光」, 日本物理学会 2019年秋季大会, 山形大学, 山形, 2019年9月17–20日.
- 吉留勇起, 「 ${}^{25}\text{O}$ の不変質量核分光」, 日本物理学会 2019年秋季大会第75回年次大会, 山形大学, 山形, 2019年9月17–20日.
- 中村隆司, 「多中性子クラスター探索のための反跳陽子検出器 CATANA/STRASSE」, 新学術領域「クラスター階層」量子ビーム応用」合同検出器ワークショップ, 東北大学, 仙台, 2019年9月20–21日.
- 安田聖, “Development of the neutron detector array with high granularity (HIME) for dineutron correlation measurement,” 新学術領域研究「量子クラスターで読み解く物質の階層構造」スクール, 理化学研究所, 和光, 2020年3月2–4日.
- 海老名直樹, 「不安定核の準弾性散乱測定用陽子検出器の開発」, 新学術領域研究「量子クラスターで読み解く物質の階層構造」スクール, 理化学研究所, 和光, 2020年3月2–4日.
- 高橋康平, 「高分解能中性子検出器 HIME の開発」, 新学術領域研究「量子クラスターで読み解く物質の階層構造」スクール, 理化学研究所, 和光, 2020年3月2–4日.
- 斗米貴人, 「変形誘引型ハロー核 31Ne の非束縛励起状態の探索」, 新学術領域研究「量子クラスターで読み解く物質の階層構造」スクール, 理化学研究所, 和光, 2020年3月2–4日.
- 齊藤敦美, 「中性子過剰ヘリウム同位体のクーロン分解反応」, 新学術領域研究「量子クラスターで読み解く物質の階層構造」スクール, 理化学研究所, 和光, 2020年3月2–4日.
- 齊藤敦美, 「中性子過剰ヘリウム同位体のクーロン分解反応」, 日本物理学会第75回年次大会, 名古屋大学, 名古屋, 2020年03月

16–19 日.

[Poster presentation]

S. Storck, “Lifetime measurement of the ^{26}O g.s. at SAMURAI,” International Nuclear Physics Conference, Glasgow, UK, INPC2019, July 29–August 2, 2019.

Awards

J. Kahlbow, Giersch Award for Outstanding Doctoral Thesis 2019, 2019.

Press releases

O. Sorlin and F. M. Marqués, “L’oxygène-28 n’aurait pas la stabilité que la théorie lui prédit,” IN2P3-CNRS: Actualités - April 27, 2020, <https://in2p3.cnrs.fr/fr/cnrsinfo/loxygene-28-naurait-pas-la-stabilite-que-la-theorie-lui-predit>.

Doornenbal Pieter, 櫻井博儀, 「新魔法数 34 の新たな証拠—中性子ノックアウト反応で探るカルシウム-54 の閉殻構造—」, 理化学研究所, 和光, 2019 年 10 月 18 日.

Doctor theses

B. Monteagudo, “Structure and neutron decay of the unbound Beryllium isotopes $^{15,16}\text{Be}$,” Université de Caen Normandie, November 2019.

J. Kahlbow, “The low-Z shore of the island of inversion: invariant-mass spectroscopy of the heavy fluorine isotopes $^{29}\text{F}^*$ & ^{30}F at SAMURAI with NeuLAND,” Technische Universität Darmstadt, 2019.

Master theses

M. Knösel, “Investigation of the dineutron system via quasi-free He-4-knockout reactions at He-6,” Technische Universität Darmstadt, 2019.

三木晴瑠, 「荷電交換反応を用いた非束縛核 ^{28}F の研究」, 東京工業大学理学院物理学系.

島田哲朗, 「中性子過剰な非束縛フッ素同位体の研究」, 東京工業大学理学院物理学系.

栗原篤志, 「 ^{22}C のクーロン分解反応」, 東京工業大学理学院物理学系.

Bachelor theses

高橋康平, 「高分解能中性子検出器 HIME の開発」, 東京工業大学.

海老名直樹, 「不安定核の準弾性散乱測定用陽子検出器の開発」, 東京工業大学.

Research Facility Development Division

Research Instruments Group

Computing and Network Team

1. Abstract

This team is in charge of development, management and operation of the computing and network environment, mail and information servers and data acquisition system and management of the information security of the RIKEN Nishina Center.

2. Major Research Subjects

- (1) Development, management and operation of the general computing servers
- (2) Development, management and operation of the mail and information servers
- (3) Development, management and operation of the data acquisition system
- (4) Development, management and operation of the network environment
- (5) Management of the information security

3. Summary of Research Activity

This team is in charge of development, management and operation of the computing and network environment, mail and information servers and data acquisition system and management of the information security. The details are described elsewhere in this progress report.

(1) Development, management and operation of the general computing servers

We are operating Linux/Unix NIS/NFS cluster system for the data analysis of the experiments and general computing. This cluster system consists of eight computing servers with 64 CPU cores and totally 200 TB RAID of highly-reliable Fibre-channel interconnection. Approximately 700 user accounts are registered on this cluster system. We are adopting the latest version of the Scientific Linux (X86_64) as the primary operating system, which is widely used in the accelerator research facilities, nuclear physics and high-energy physics communities in the world.

(2) Development, management and operation of the mail and information servers

We are operating RIBF.RIKEN.JP server as a mail/NFS/NIS server. This server is a core server of RIBF Linux cluster system. Postfix has been used for mail transport software and dovecot has been used for imap and pop services. These software packages enable secure and reliable mail delivery. Sophos Email Security and Control (PMX) installed on the mail front-end servers which tags spam mails and isolates virus-infected mails. The probability to identify the spam is approximately 95–99%. We are operating several information servers such as Web servers, Integrated Digital Conference (INDICO) server, Wiki servers, Groupware servers, Wowza streaming servers. We have been operating approximately 70 units of wireless LAN access points in RNC. Almost the entire radiation-controlled area of the East Area of RIKEN Wako campus is covered by wireless LAN for the convenience of experiments and daily work.

(3) Development, management and operation of the data acquisition system

We have developed the standard data-acquisition system named as RIBFDAQ. This system can process up to 40 MB/s data. By using crate-parallel readout from front-end systems such as CAMAC and VME, the dead time could be minimized. To synchronize the independent DAQ systems, the time stamping system has been developed. The resolution and depth of the time stamp are 10 ns and 48 bits, respectively. This time stamping system is very useful for beta decay experiments such as EURICA, BRIKEN and VANDLE projects. One of the important tasks is the DAQ coupling, because detector systems with dedicated DAQ systems are transported to RIBF from foreign facilities. In case of SAMURAI Silicon (NSCL/TUM/WUSTL), the readout system is integrated into RIBFDAQ. The projects of MUST2 (GANIL), MINOS (CEA Saclay), NeuLAND (GSI) and TRB3 (TUM) cases, data from their DAQ systems are transferred to RIBFDAQ and merged online. For SPIRIT (RIKEN/GANIL/CEA Saclay/NSCL), RIBFDAQ is controlled from the NARVAL-GET system that is a large-scale signal processing system for the time projection chamber. EURICA (GSI), BRIKEN (GSI/Univ. Liverpool/IFIC), VANDLE (UTK) and OTPC (U. Warsaw) projects, we adopt the time stamping system to apply individual trigger for each detector system. In this case, data are merged in offline. In addition, we are developing intelligent circuits based on FPGA. General Trigger Operator (GTO) is an intelligent triggering NIM module. Functions of “common trigger management,” “gate and delay generator,” “scaler” are successfully implemented. The trigger system in BigRIPS DAQ is managed by 5 GTO modules. To improve the data readout speed of VME system, we have successfully developed the MPV system which is a parallel readout extension of the VME system. Data readout sequence is completely parallelized that helps to improve the DAQ deadtime. Thanks to the MPV system, now the DAQ system in RIBF is 10 times faster than in 2007.

(4) Development, management and operation of the network environment

We have been managing the network environment collaborating with Information Systems Division in RIKEN. All the Ethernet ports of the information wall sockets are capable of the Gigabit Ethernet connection (10/100/1000 BT). In addition, some 10 Gbps networks port has been introduced to RIBF experimental area. Approximately 70 units of wireless LAN access points have been installed to cover the almost entire area of Nishina Center.

(5) Management of the information security

It is essential to take proper information security measures for information assets. We are managing the information security of Nishina Center collaborating with Information Systems Division in RIKEN.

Members**Team Leader**

Hidetada BABA

Research/Technical Scientist

Yasushi WATANABE (Senior Research Scientist)

Junior Research Associate

Fumiya GOTO

Special Temporary Research Scientist

Takashi ICHIHARA

List of Publications & Presentations**Presentations****[International Conferences/Workshops]**

H. Baba, "MOCO and MPV/computing infrastructure at RIBF, HOKUSAI and U-Tokyo/current and near future BigRIPS DAQ," RIBF-DAQ Workshop, Wako, Japan, December 23, 2019.

[Domestic Conferences/Workshops]

H. Baba, "RIBF DAQ," SAMURAI International Collaboration Workshop, Toshima, Japan, August 30–31, 2019.

後藤文也 (オンライン発表), 「MTV 実験の報告 2」, 日本物理学会第 75 回年次大会, 名古屋大学, 名古屋, 2020 年 3 月 16–19 日.

馬場秀忠 (オンライン発表), 「並列化 VME バスによる DAQ の高速化」, 日本物理学会第 75 回年次大会, 名古屋大学, 名古屋, 2020 年 3 月 16–19 日.

Research Facility Development Division

Research Instruments Group

Detector Team

1. Abstract

This team is in charge of development, fabrication, and operation of various detectors used for nuclear physics experiments at RIBF. Our current main mission is maintenance and improvement of detectors which are used at BigRIPS separator and its succeeding beam lines for beam diagnosis and particle identification of RI beams. We are also engaged in R&D of new detectors that can be used for higher-intensity RI beams. In addition, we are doing the R&D which uses the pelletron accelerator together with other groups.

2. Major Research Subjects

Development, fabrication, and operation of various detectors for nuclear physics experiments, including beam-line detectors which are used for the production and delivery of RI beams (beam diagnosis and particle identification). R&D which uses the pelletron accelerator.

3. Summary of Research Activity

The current research subjects are summarized as follows:

- (1) Maintenance and improvement of the beam-line detectors which are used at BigRIPS separator and its succeeding beam lines.
- (2) Development of new beam-line detectors with radiation hardness and tolerance for higher counting rates.
- (3) Management of the pelletron accelerator and R&D which uses the pelletron.

Members

Team Leader

Hiroshi SATO

Research/Technical Scientist

Tokihiro IKEDA (Senior Research Scientist)

Special Temporary Employee

Manabu HAMAGAKI

Visiting Scientist

Takeshi KOIKE (Tohoku University)

Student Trainees

Shunya KAWAMURA (Toho University)

Masaya SAKAI (University of Tokyo)

Kento TAKEMOTO (University of Tokyo)

Yuka HIKIMA (Toho University)

Mitsumasa MORI (Toho University)

List of Publications & Presentations

Publications

[Original papers]

- D. S. Ahn, N. Fukuda, H. Geissel, N. Inabe, N. Iwasa, T. Kubo, K. Kusaka, D. J. Morrissey, D. Murai, T. Nakamura, M. Ohtake, H. Otsu, H. Sato, B. M. Sherrill, Y. Shimizu, H. Suzuki, H. Takeda, O. B. Tarasov, H. Ueno, Y. Yanagisawa, and K. Yoshida, "Location of the neutron dripline at fluorine and neon," *Phys. Rev. Lett.* **123**, 212501 (2019).
- H. Wang, H. Otsu, N. Chiga, S. Kawase, S. Takeuchi, T. Sumikama, S. Koyama, H. Sakurai, Y. Watanabe, S. Nakayama, D. S. Ahn, H. Baba, S. D. Chen, K. Chikaato, M. L. Cortes, N. Fukuda, A. Hirayama, R. Hosoda, T. Isobe, S. Kawakami, Y. Kondo, S. Kubono, Y. Maeda, S. Masuoka, S. Michimasa, I. Murray, R. Nakajima, T. Nakamura, K. Nakano, M. Nishimura, T. Ozaki, A. Saito, T. Saito, H. Sato, Y. Shimizu, S. Shimoura, P. -A. Söderström, Y. Soudo, X. H. Sun, J. Suwa, D. Suzuki, H. Suzuki, H. Takeda, M. Takechi, Y. Togano, T. Tomai, H. Yamada, M. Yasuda, and K. Yoshida, "Enhancement of element production by incomplete fusion reaction with weakly bound deuteron," *Commun. Phys.* **2**, 78 (2019).
- A. Corsi, Y. Kubota, J. Casal, M. Gomez-Ramos, A. M. Moro, G. Authelet, H. Baba, C. Caesar, D. Calvet, A. Delbart, M. Dozono, J. Feng, F. Flavigny, J. -M. Gheller, J. Gibelin, A. Giganon, A. Gillibert, K. Hasegawa, T. Isobe, Y. Kanaya, S. Kawakami, D. Kim, Y. Kiyokawa, M. Kobayashi, N. Kobayashi, T. Kobayashi, Y. Kondo, Z. Korkulu, S. Koyama, V. Lapoux, Y. Maeda, F. M. Marques, T. Motobayashi, T. Miyazaki, T. Nakamura, N. Nakatsuka, Y. Nishio, A. Obertelli, A. Ohkura, N. A. Orr, S. Ota, H. Otsu, T. Ozaki, V. Panin, S. Paschalis, E. C. Pollacco, S. Reichert, J. -Y. Rousse, A. T. Saito, S. Sakaguchi, M. Sako, C. Santamaria, M. Sasano, H. Sato, M. Shikata, Y. Shimizu, Y. Shindo, L. Stuhl, T. Sumikama, Y. L. Sun, M. Tabata, Y. Togano, J. Tsubota, T. Uesaka, Z. H. Yang, J. Yasuda, K. Yoneda, and J. Zenihiro, "Structure of ^{13}Be probed via quasi-free scattering," *Phys. Lett. B* **797**, 134843 (2019).

[Proceedings]

- M. Ohno, T. Irimatsugawa, Y. Miura, H. Takahashi, T. Ikeda, C. Otani, M. Sakama, and N. Matsufuji, “Calorimetry of heavy charged particle by superconducting transition-edge sensor,” *Journal of Low Temperature Physics* **193**, 1222–1227 (2018).
- R. Smith, M. Ohno, Y. Miura, N. Nakada, Y. Mitsuya, H. Takahashi, T. Ikeda, C. Otani, M. Sakama, N. Matsufuji, T. Irimatsugawa, S. Kohjiro, H. Yamamori, and F. Hirayama, “Microcalorimetry of carbon ion beam for medical treatment by transition edge sensor,” *Journal of Low Temperature Physics* **199**, 1012–1017 (2020).
- T. Ikeda, M. Ikekame, Y. Hikima, M. Mori, S. Kawamura, T. Minowa, and W. -G. Jin, “Profile measurements of MeV ion microbeams in atmosphere extracted from single tapered glass capillaries with an end window,” *Nucl. Instrum. Methods Phys. Res. B* **470**, 42–47 (2020).
- T. Sumikama, T. Kubo, N. Fukuda, D. S. Ahn, H. Takeda, Y. Shimizu, H. Suzuki, N. Inabe, D. Murai, H. Sato, K. Kusaka, Y. Yanagisawa, M. Ohtake, and K. Yoshida, “First success of RI-beam separation and particle identification for nuclei with atomic number $Z > 82$ at RIKEN RI beam factory,” *Nucl. Instrum. Methods Phys. Res. B* **463**, 237–240 (2020).

Presentations

[International conferences/workshops]

- T. Ikeda, M. Ikekame, Y. Hikima, M. Mori, T. Kawamura, T. Minowa, and W. -G. Jin (oral), “Profile measurements of MeV ion microbeams in atmosphere extracted from single tapered glass capillary with an end window,” 13th European Conference on Accelerators in Applied Research and Technology (ECAART13), Split, Croatia, May 5–10, 2019.
- M. Mori, T. Kawamura, T. Ikeda, T. Minowa, and W. -G. Jin (poster), “Profile measurement of laser microbeam produced by glass capillaries : tilting dependence,” 24th Optoelectronics and Communications Conference/International Conference on Photonics in Switching and Computing 2019 (OECC/PSC 2019), Fukuoka, Japan, July 7–11, 2019.
- R. Smith, M. Ohno, Y. Miura, N. Nakada, H. Takahashi, Y. Mitsuya, N. Matsufuji, M. Sakama, T. Ikeda, T. Irimatsugawa, S. Koujiro, H. Yamamori, F. Hirayama, and C. Otani (poster), “Microcalorimetry of carbon ion beam for medical treatment by transition edge sensor,” 18th International Workshop on Low Temperature Detectors (LTD-18), Milano, Italy, July 22–26, 2019.
- T. Ikeda, M. Ikekame, Y. Hikima, M. Mori, T. Kawamura, T. Minowa, and W. -G. Jin (poster), “Measurement of proton microbeam profiles in atmosphere produced by single tapered glass capillary optics with an end window,” International Conference on Photonic, Electronic and Atomic Collisions (ICPEAC2019), Deauville, France, July 23–30, 2019.
- T. Kawamura, T. Ikeda, M. Mori, and W. -G. Jin (poster), “Development of UV-laser microbeam cell irradiation system by glass capillary optics : estimation of density enhancement,” 16th International Congress of Radiation Research (ICRR2019), Manchester, UK, August 25–29, 2019.
- Y. Hikima, T. Ikeda, M. Ikekame, M. Mori, T. Kawamura, and W. -G. Jin (poster), “Fine structure evaluation by pattern recognition for ion microbeam extracted from tapered glass capillary optics,” 23rd International Workshop on Inelastic Ion-Surface Collisions (IISC-23), Matsue, Japan, November 17–22, 2019.

[Domestic conferences/workshops]

- 池田時浩, 浜田学, 佐藤広海 (口頭発表), 「理化学研究所におけるタンデム加速器の現状 (2018–2019 年度)」, 第 32 回タンデム加速器及びその周辺技術の研究会, 神戸大学, 神戸, 2019 年 7 月 5–6 日.
- 酒井雅哉, 池田時浩, 柴田淳史, 竹本健人, 上坂充 (ポスター), 「 α 線治療のための He イオンビーム DNA 照射分析の基礎研究」, 第 16 回日本加速器学会年会, 京都大学, 京都, 2019 年 7 月 31 日–8 月 3 日.
- 池田時浩 (口頭発表), 「フタ付ガラスキャピラリーによる MeV イオンマイクロビーム照射で生じた細胞核内イオントラックの解析」, 日本物理学会 2019 年秋季大会, 岐阜大学, 岐阜, 2019 年 9 月 10–13 日.
- 酒井雅哉, 池田時浩, 柴田淳史, 竹本健人, 上坂充 (口頭発表), 「 α 線治療のための He イオンマイクロビーム DNA 照射分析の基礎研究」, 日本原子力学会 2019 年秋の大会, 富山大学, 富山, 2019 年 9 月 11–13 日.
- 三木晴瑠, 近藤洋介, 中村隆司, Nadia Lynda Achouri, Thomas Aumann, 馬場秀忠, Franck Delaunay, Pieter Doornenbal, 福田直樹, Julien Gibelin, Jongwon Hwang, 稲辺尚人, 磯部忠昭, 亀田大輔, 簡野大輝, Sunji Kim, 小林信之, 小林俊雄, 久保敏幸, Sylvain Leblond, Jenny Lee, Miguel Marques, 南方亮吾, 本林透, 村井大地, 村上哲也, 武藤琴美, 中嶋丈嘉, 中塚徳継, Alahari Navin, 西征爾郎, 生越駿, Nigel Andrew Orr, 大津秀暁, 佐藤広海, 佐藤義輝, 清水陽平, 鈴木宏, 高橋賢人, 竹田浩之, 武内聡, 田中隆己, 梅野泰宏, Adam Garry Tuff, Marine Vandebrouck, 米田健一郎 (口頭発表), 「荷電交換反応を用いた非束縛核 ^{28}F の探索」, 日本物理学会 2019 年秋季大会, 山形大学, 山形, 2019 年 9 月 17–20 日.
- 吉留勇起, 近藤洋介, 中村隆司, Nadia Lynda Achouri, Thomas Aumann, 馬場秀忠, Franck Delaunay, Pieter Doornenbal, 福田直樹, Julien Gibelin, Jongwon Hwang, 稲辺尚人, 磯部忠昭, 亀田大輔, 簡野大輝, Sunji Kim, 小林信之, 小林俊雄, 久保敏幸, Sylvain Leblond, Jenny Lee, Miguel Marques, 南方亮吾, 本林透, 村井大地, 村上哲也, 武藤琴美, 中嶋丈嘉, 中塚徳継, Alahari Navin, 西征爾郎, 生越駿, Nigel Andrew Orr, 大津秀暁, 佐藤広海, 佐藤義輝, 清水陽平, 鈴木宏, 高橋賢人, 竹田浩之, 武内聡, 田中隆己, 梅野泰宏, Adam Garry Tuff, Marine Vandebrouck, 米田健一郎 (口頭発表), 「 ^{25}O の不変質量核分光」, 日本物理学会 2019 年秋季大会, 山形大学, 山形, 2019 年 9 月 17–20 日.
- 池田時浩, 佐藤広海 (口頭発表), 「タンデム加速器によるキャピラリーマイクロビームの生成と応用」, 第 80 回応用物理学会秋季学術講演会, 北海道大学, 札幌, 2019 年 9 月 18–21 日.
- スミスライアン, 大野雅史, 高橋浩之, 三津谷有貴, 三浦義隆, 中田直樹, 松藤成弘, 坂間誠, 池田時浩 (口頭発表), 「超伝導転移端センサによる治療用炭素重粒子カロリメトリ」, 第 80 回応用物理学会秋季学術講演会, 北海道大学, 札幌, 2019 年 9 月 18–21 日.
- 大野雅史, スミスライアン, 三浦義隆, 中田直樹, 三津谷有貴, 高橋浩之, 池田時浩, 坂間誠, 松藤成弘 (口頭発表), 「超伝導転移端センサによる重粒子ビーム精密計測」, 第 80 回応用物理学会秋季学術講演会, 北海道大学, 札幌, 2019 年 9 月 18–21 日.
- 池田時浩, 引間有花, 森光正, 河村俊哉, 金衛国 (口頭発表), 「フタ付ガラスキャピラリーで生成された MeV イオンマイクロビームの CR-39 によるスポット構造評価」, 第 62 回放射線化学討論会, 福井大学附属国際原子力工学研究所, 敦賀, 2019 年 9 月 23–25 日.

酒井雅哉, 池田時浩, 柴田淳史, 泉雅子, 竹本健人, 上坂充 (口頭発表), 「 α 線治療のための He イオンマイクロビーム DNA 照射分析の基礎研究」, 日本原子力学会 2020 年春の年会, 福島大学, 福島, 2020 年 3 月 16-18 日.

本林透, 池田時浩, 石山博恒, ピーター ドーネンバル, 佐藤広海, 上野秀樹 (口頭発表), 「仁科スクール—原子核反応実験を中心とした学部学生向け国際プログラム」, 日本物理学会第 75 回年次大会 (2020 年), 名古屋大学, 名古屋, 2020 年 3 月 16-19 日.

池田時浩, 酒井雅哉, 竹本健人, 柴田淳史, 泉雅子, 上坂充 (口頭発表), 「ガラスキャピラリーで生成されたイオンマイクロビームによる RPE 細胞の DNA 損傷誘発実験」, 日本物理学会第 75 回年次大会 (2020 年), 名古屋大学, 名古屋, 2020 年 3 月 16-19 日.

引間宥花, 池田時浩, 浜垣学, 金衛国 (口頭発表), 「ガラスキャピラリー光学系によるイオンマイクロビームの照射距離とスポットサイズの相関」, 日本物理学会第 75 回年次大会 (2020 年), 名古屋大学, 名古屋, 2020 年 3 月 16-19 日.

Awards

河村俊哉, JSRC Young Scientist Award for 16th International Congress of Radiation Research (ICRR2019), 日本放射線化学会, 2019 年 7 月 12 日.

Accelerator Applications Research Division Beam Mutagenesis Group

1. Abstract

This group promotes biological applications of ion beams from RI Beam Factory (RIBF). Ion Beam Breeding Team studies various biological effects of fast heavy ions and develops new technology to breed plants and microbes by heavy-ion irradiations. Plant Genome Evolution Research Team studies the effect of chromosomal rearrangements on plant genomes and phenotypes.

2. Major Research Subjects

- (1) Biological effects of fast heavy ions
- (2) Molecular nature of DNA alterations induced by heavy-ion irradiation
- (3) Research and development of heavy-ion breeding
- (4) Identification of plant sex-determining genes using mutants and their evolutionary study

3. Summary of Research Activity

Summary of research activities of the two teams are given in the sections of each team.

Member

Director

Tomoko ABE

List of Publications & Presentations

Publications and presentations for each research team are listed in subsections.

Accelerator Applications Research Division

Beam Mutagenesis Group

Ion Beam Breeding Team

1. Abstract

Ion beam breeding team studies various biological effects of fast heavy ions. It also develops new technique to breed plants and microbes by heavy-ion irradiations. Fast heavy ions can produce dense and localized ionizations in matters along their tracks, in contrast to photons (X rays and gamma rays) which produce randomly distributed isolated ionizations. These localized and dense ionization can cause double-strand breaks of DNA which are not easily repaired and result in mutation more effectively than single-strand breaks. A unique feature of our experimental facility at the RIKEN Ring Cyclotron (RRC) is that we can irradiate living tissues in atmosphere since the delivered heavy-ion beams have energies high enough to penetrate deep in matter. This team utilizes a dedicated beam line (E5B) of the RRC to irradiate microbes, plants and animals with beams ranging from carbon to iron. Its research subjects cover study of ion-beam radiation mutagenesis, genome-wide analyses of mutation, and development of new plants and microbial varieties by heavy-ion irradiation. Thirty new varieties have already been brought to the market.

2. Major Research Subjects

- (1) Study on the biological effects by heavy-ion irradiation
- (2) Study on the molecular nature of DNA alterations induced by heavy-ion irradiation
- (3) Innovative applications of heavy-ion beams

3. Summary of Research Activity

We study biological effects of fast heavy ions from the RRC using ^{135}A MeV C, N, Ne ions, ^{95}A MeV Ar ions, ^{90}A MeV Fe ions and from the IRC using ^{160}A MeV Ar ions. We also develop breeding technology of microbes and plants. Main subjects are:

(1) Study on the biological effects by heavy-ion irradiation

Heavy-ion beam deposits a concentrated amount of dose at just before stop with severely changing the linear energy transfer (LET). The peak of LET is achieved at the stopping point and known as the Bragg peak (BP). Adjusting the BP to target malignant cells is well known to be effective for cancer therapy. On the other hand, a uniform dose distribution is a key to the systematic study for heavy-ion mutagenesis, thus to the improvement of the mutation efficiency. Plants and microbes therefore, are irradiated using ions with stable LET. We investigated the effect of LET ranging from 23 to $640\text{ keV}/\mu\text{m}$, on mutation induction using dry seeds of the model plants *Arabidopsis thaliana* and rice (*Oryza sativa* L.). The most effective LET (LET_{max}) was $30\text{ keV}/\mu\text{m}$ in *Arabidopsis* and rice dry seeds. LET_{max} irradiations showed the same mutation rate as that by chemical mutagens, which typically cause high mutation rate. The LET_{max} of imbibed rice seeds and dry wheat (*Triticum monococcum*) seeds were shown to be $50\text{--}63\text{ keV}/\mu\text{m}$ and $50\text{ keV}/\mu\text{m}$, respectively. In the case of microbe, filamentous fungus (*Neurospora crassa*), the Ar ions at $290\text{ keV}/\mu\text{m}$ demonstrated higher mutagenic activity than the Fe-ions at $640\text{ keV}/\mu\text{m}$. Thus, the LET is an important factor to be considered in heavy-ion mutagenesis.

(2) Study on the molecular nature of DNA alterations induced by heavy-ion irradiation

We analyzed the DNA alterations corresponding to morphological mutants in *Arabidopsis* and rice. In the mutants from C- and Ar-ions irradiations, the majority of the induced mutations were deletions. The proportion of large deletions (>100 bp) increased with increasing LET. We concluded that the size of deletions generated by heavy-ion beam irradiation increased with increasing LET. Whole-genome analysis by high-throughput sequencing is a powerful tool used to characterize the nature of induced mutations. We also developed a new pipeline named the Automated Mutation Analysis Pipeline (AMAP), for the rapid detection of whole-genome mutations in *Arabidopsis*. We comprehensively characterized the mutation effects of ion beams of C ($30\text{ keV}/\mu\text{m}$) and Ar ($290\text{ keV}/\mu\text{m}$) by whole-genome mutational analysis on eight morphological mutants with AMAP. C ions at a dose of 400 Gy mainly induced single-nucleotide variants (SNVs) and small insertions and deletions (InDels) at a rate of 57 sites per mutant genome. LET_{max} irradiation is effective for breeding because of its very high mutation frequency. Most mutations are SNV and small deletions which are capable of disrupting a single gene. Thus, irradiation can efficiently generate knockout mutants of a target gene and can be applied to reverse genetics. On the other hand, irradiation with Ar ions at a dose of 50 Gy showed a mutation spectrum different from that at LET_{max}. The proportion of SNVs and small InDels was low at a rate of 28 sites per mutant genome, while that of large deletions and chromosomal rearrangements was high (10 sites per mutant genome). As such, higher LET irradiation is promising as a new mutagen suitable for the functional analysis of tandem duplicated genes.

(3) Innovative application of heavy-ion beams

In 1999, we formed a consortium for ion-beam breeding consisting of 24 groups. In 2019, the consortium grew to 184 groups from Japan and 20 from overseas. Previously, the ion-beam breeding procedures were carried out using mainly flowers and ornamental plants. We have recently put a new non-pungent and tearless onion, 'Smile ball,' on the market along with 'Kiku Meigetsu,' an edible late flowering chrysanthemum. In addition, a new project was launched to expand the cultivation area of this variety of chrysanthemum in Yamagata prefecture. Beneficial variants have been cultivated for various plant species, such as high yield sea weeds, lipids-hyperaccumulating unicellular alga, large marine plankton and lettuce with a low browning property as a cut vegetable. We collaborate

with Miyagi prefectural government and Tohoku University to breed salt-resistant lines in the more delicious commercial rice varieties, 'Hitomebore' and 'Manamusume.' Imbibed seeds were irradiated with the LETmax (C-ions) on 16 April, 2011. We have isolated a candidate line of salt-resistant mutant from 719 M₂ progenies grown in the saline paddy field in 2012. This line grew well after transplantation and had high yield in common paddy field as well. By broadening the target of heavy-ion breeding extending from flowers to crops such as grains, the technology will contribute to solving the global problems of food shortage and environmental destruction.

Members

Team Leader

Tomoko ABE

Research/Technical Scientists

Tokihiro IKEDA (Senior Research Scientist)
Masako IZUMI (Senior Research Scientist)
Teruyo TSUKADA (Senior Research Scientist)

Kazuhide TSUNEIZUMI (Senior Research Scientist)
Ryouhei MORITA (Technical Scientist)

Research & Development Scientist

Hiroyuki ICHIDA

Technical Staff I

Yoriko HAYASHI

Yuki SHIRAKAWA

Technical Staff II

Sumie OHBU

Mieko YAMADA

Special Temporary Technical Scientists

Hiroshi ABE

Katsunori ICHINOSE

Research Consultant

Masahiro MII (Chiba Univ.)

Visiting Scientists

Ayumi DEGUCHI (Chiba Univ.)
Makoto FUJIWARA (Sophia Univ.)
Eitaro FUKATSU (Forestry and Forest Products Res. Inst.)
Tomonari HIRANO (Univ. of Miyazaki)
Akiko HOKURA (Tokyo Denki Univ.)
Yutaka MIYAZAWA (Yamagata Univ.)
Kazumitsu MIYOSHI (Chiba Univ.)
Toshikazu MORISHITA (Nat'l Agriculture and Food Res. Org.)
Koji MURAI (Fukui Prefectural Univ.)

Kyosuke NIWA (Tokyo Univ. of Marine Sci. and Tech.)
Norihiro OHTSUBO (Kyoto Prefectural Univ.)
Tadashi SATO (Tohoku Univ.)
Yoichi SATO (Riken Food Co., Ltd.)
Kenichi SUZUKI (Suntory Flowers Co., Ltd.)
Hinako TAKEHISA (Nat'l Inst. of Agrobiological Sci.)
Masanori TOMITA (Central Res. Inst. of Electric Power Industry)
Masao WATANABE (Tohoku Univ.)
Takeshi YAMAKI (Riken Vitamin Co., Ltd.)

Visiting Technicians

Yukiko KANAZAWA (Nippon Beet Sugar Manufacturing Co., Ltd.)
Miho MOGAMIYA (Riken Food Co., Ltd.)

Daisuke SAITO (Riken Food Co., Ltd.)
Takuji YOSHIDA (Takii & Co., Ltd.)

Research Fellow

Hironari UCHIDA (Saitama Agricultural Tech. Res. Center)

Student Trainee

Yuta HARUNARI (Tokyo Denki Univ.)

Part-time Worker

Haruka WATANABE (Administrative Part-time Worker II)

List of Publications & Presentations

Publications

[Original papers]

- T. Kashiwabara, K. Tanoi, N. Kitajima, A. Hokura, T. Abe, T. Nakanishi, and I. Nakai, “Comparative *in vivo* imaging of arsenic and phosphorus in *Pteris vittata* gametophyte by synchrotron μ -XRF and radioactive tracer techniques,” *Chem. Lett.* **48**, 319–321 (2019).
- Y. Hayashi, S. Ishii, T. Hirano, K. Ichinose, Y. Kazama, and T. Abe, “New ornamental cherry cultivars induced by heavy-ion beam irradiation,” *Acta Hort.* **1235**, 99–103 (2019).
阿部知子, 市田裕之, 森田竜平, 大野豊, 長谷純宏, 高城啓一, 畑下昌範, 村井耕二, 「ミュータゲノミクスと変異統合データベースの構築」, *JATAFF ジャーナル* **7**, 19–23 (2019).
- M. Krasovec, Y. Kazama, K. Ishii, T. Abe, and D. A. Filatov, “Immediate dosage compensation is triggered by the deletion of Y-linked genes in *Silene latifolia*,” *Current Biol.* **29**, 2214–2221 (2019).
- H. Kawamoto, K. Yamanaka, A. Koizumi, K. Ishii, Y. Kazama, T. Abe, and S. Kawano, “An asexual flower of *Silene latifolia* and *Microbotryum lychnidis-dioicae* promotes sex-organ development,” *PLoS One* **14**, e0217329 (2019).
- H. Ichida and T. Abe, “An improved and robust method to efficiently deplete repetitive elements from complex plant genomes,” *Plant Sci.* **280**, 455–60 (2019).
- H. Murata, S. Nakano, T. Yamanaka, T. Shimokawa, T. Abe, H. Ichida, Y. Hayashi, K. Tahara, and A. Ohta, “Conversion from mutualism to parasitism: a mutant of the ectomycorrhizal agaricomycete *Tricholoma matsutake* that induces stunting, wilting, and root degeneration in seedlings of its symbiotic partner, *Pinus densiflora*, *in vitro*,” *Botany* **97**, 463–474 (2019).
- H. Ichida, R. Morita, Y. Shirakawa, Y. Hayashi, and T. Abe, “Targeted exome sequencing of unselected heavy-ion beam-irradiated populations reveals less-biased mutation characteristics in the rice genome,” *Plant J* **98**, 301–314 (2019).
- R. Morita, H. Ichida, K. Ishii, Y. Hayashi, H. Abe, Y. Shirakawa, K. Ichinose, K. Tsuneizumi, T. Kazama, K. Toriyama, T. Sato, and T. Abe, “*LONG GRAIN 1*: a novel gene that regulates grain length in rice,” *Mol. Breed.* **39**, 135–142 (2019).
- Y. Sawada, M. Sato, M. Okamoto, J. Masuda, S. Yamaki, M. Tamari, Y. Tanokashira, S. Kishimoto, A. Ohmiya, T. Abe, and M. Y. Hirai, “Metabolome-based discrimination of chrysanthemum cultivars for the efficient generation of flower color variations in mutation breeding,” *Metabolomics* **15**, 118–129 (2019).

Presentations

[International conferences/workshops]

- H. Ichida (invited), R. Morita, Y. Shirakawa, Y. Hayashi, and T. Abe, “A less-biased approach to characterize carbon-ion beam-induced mutations by whole exome sequencing of unselected M2 populations in rice,” *Rice Functional Genomics Workshop in XXVII Plant & Animal Genome Conference*, San Diego, USA, January 12–16, 2019.
- K. Niwa (poster), T. Abe, and A. Kobiyama, “Possibility of polyploidy breeding using cryptic species in the marine crop *Pyropia yezoensis* (Bangiales, Rhodophyta),” *23rd International Seaweed Symposium*, Jeju, Korea, April 28–May 3, 2019.
- T. Abe (invited), H. Ichida, Y. Hayashi, Y. Shirakawa, K. Ishii, and R. Morita, “Ion-beam radiation mutagenesis and plant mutation breeding,” *14th Conference of Society for the Advancement of the Breeding Research in Asia and Oceania*, Gwangju, Korea, July 2–5, 2019.
- H. Murata (oral), S. Nakano, T. Yamanaka, T. Shimokawa, T. Abe, H. Ichida, Y. Hayashi, K. Tahara, and A. Ohta, “Radiation mutagenesis of the ectomycorrhizal fungus *Tricholoma matsutake*,” *The 10th International Workshop on Edible Mycorrhizal Mushrooms*, Nagano, Japan, October 23, 2019.
- T. Hioki (oral), H. Kunitake, T. Abe, and T. Hirano, “Analysis of petal size regulatory mechanisms in flower mutant of *Arabidopsis thaliana*,” *The 14th JKTC Seminar*, Qingdao, China, October 18–21, 2019.

[Domestic conferences/workshops]

- 阿部知子 (招待講演), 林依子, 市田裕之, 「Ion Beam Mutagenesis とイオンビーム品種改良プラットフォーム」, 第 1 回 重・クラスターイオンビーム利用による微生物由来高生産性エネルギー 環境シンポジウム, 筑波大学, つくば, 2019 年 1 月 29 日.
- 上田純平 (口頭発表), 風間裕介, 阿部知子, 村井耕二, 「一粒系コムギ DV92 系統における花成遅延変異体 late-heading 2~5 (lh2~5) の同定」, 日本育種学会 第 135 回講演会, 千葉大学, 千葉, 2019 年 3 月 16–17 日.
- 市田裕之 (口頭発表), 阿部知子, 「効率的な反復配列除去技術の開発とコムギ全ゲノム解析への応用」, 日本育種学会 第 135 回講演会, 千葉大学, 千葉, 2019 年 3 月 16–17 日.
- 二羽恭介 (口頭発表), 阿部知子, 小檜山篤志, 「スサビノリと隠蔽種の交雑実験」, 日本藻類学会第 43 回大会, 京都大学, 京都, 2019 年 3 月 17 日.
- 阿部知子 (招待講演), 「イオンビーム育種技術で夢の植物を創る」, 第 6 回ミニシンポ「機能性バイオ」(TIA かけはし研究「機能性バイオ」グループ), 東京大学, 柏, 2019 年 3 月 18 日.
- 村田宗謙 (口頭発表), 渡川友里恵, 林依子, 阿部知子, 國武久登, 平野智也, 「重イオンビーム照射雄性配偶子が重複受精と胚発生に及ぼす影響」, 園芸学会平成 31 年度春季大会, 明治大学, 川崎, 2019 年 3 月 23–24 日.
- 常泉和秀 (口頭発表), 山田美恵子, 一瀬勝紀, 市田裕之, 金禎珍, 萩原篤志, 川田実季, 片山貴士, 崎山一孝, 手塚信弘, 小磯雅彦, 阿部知子, 「重イオンビーム照射によるシオミズツボワムシ大型変異系統の育種」, 日本農芸化学会 2019 年度大会, 東京農業大学, 世田谷, 2019 年 3 月 26–27 日.
- 村田仁 (口頭発表), 仲野翔太, 山中高史, 下川知子, 阿部知子, 市田裕之, 林依子, 田原恒, 太田明, 「二員培養系で共生パートナーのアカマツ実生苗を枯らすマツタケ変異体の作出」, 日本農芸化学会 2019 年度大会, 東京農業大学, 世田谷, 2019 年 3 月 26–27 日.

- 阿部知子 (口頭発表), 石井公太郎, 風間裕介, 平野智也, 「重イオンビーム照射により誘発したシロイヌナズナ変異の特徴」, 基礎物理解学研究所研究会「放射線の生体影響解明への分野横断による挑戦」, 京都大学, 京都, 2019年5月23-25日.
- 石井公太郎 (口頭発表), 市田裕之, 阿部知子, 「イネの品種特異的高精度リファレンス配列作製手法の開発」, 日本育種学会第136回講演会, 近畿大学, 奈良, 2019年9月6-7日.
- 久村麻子 (口頭発表), 諸岡淳司, 阿部知子, 林依子, 平野智也, 「重イオンビーム照射による夏秋小ギク品種「長崎 SWC1」の育成」, 日本育種学会第136回講演会, 近畿大学, 奈良, 2019年9月6-7日.
- 泉雅子 (ポスター発表), 阿部知子, 「重粒子線により誘発される DNA 二本鎖切断の修復機構の解析」, 第42回日本分子生物学会大会, 福岡国際会議場 マリンメッセ福岡, 福岡, 2019年12月3-6日.
- 阿部知子 (招待講演), 「イオン育種の現状とそれぞれの施設の特徴」, 福井イオンビーム育種研究会, 若狭湾エネルギー研究センター, 敦賀, 2019年12月13日.
- 藤田悠生 (口頭発表), 市田裕之, 風間智彦, 阿部知子, 鳥山欽哉, 「indica 品種 Lebed に台中 65 号を戻し交雑して得られた雄性不稔性の解析」, 国立遺伝学研究所 イネ属近縁種研究会「Oryza 属ゲノム情報を活用した遺伝的多様性研究の推進」, 国立遺伝学研究所, 三島, 2019年12月12-13日.

Press releases

- 市田裕之, 阿部知子, 「効率的な反復配列除去技術の開発とコムギ全ゲノム解析への応用」, 日本育種学会 2019 年春季大会 (135 回) 千葉大学 記者発表, 2019 年 3 月 7 日.
- 静岡県, 「新品種「S1200」への期待」, 静岡県農林技術研究所, 研究所ニュース 58, 2019 年 8 月.
- 久村麻子, 諸岡淳司, 阿部知子, 林依子, 平野智也, 「重イオンビーム商社による夏秋小ギク品種「長崎 SWC1」の育成」, 日本育種学会 2019 年秋季大会 (136 回), 近畿大学 記者発表, 2019 年 9 月 3 日.

Patents

- 阿部知子, 森田竜平, 林依子, 市田裕之, 安部弘, 佐藤雅志, 「種子のサイズが増大した植物の製造方法」, 特許出願番号 2019-000749, 出願日 2019 年 1 月 7 日.
- 阿部知子, 常泉和秀, 市田裕之, 萩原篤志, キム・ヒジン, 阪倉良孝, 菅向志郎, 小磯雅彦, 手塚信弘, 川田実季, 小林敬典, 「ワムシの変異系統の作出方法, ワムシの変異系統, および重イオンビームの判定方法」特許出願番号 2019-015899, 出願日 2019 年 1 月 31 日.
- 久村麻子, 諸岡淳司, 阿部知子, 林依子, 平野智也, 「キク品種「長崎 SWC1」」, 品種登録出願番号 33790, 出願日 2019 年 3 月 18 日.
- 落合成光, 阿部知子, 林依子, 「ハイビスカス品種「マザーオレンジ」」, 品種登録出願番号 33885, 出願日 2019 年 4 月 22 日.

Outreach activities

- 阿部知子, 市田裕之, 山田美恵子, 「重イオンビームに陸上養殖, 「ワカメの革新」進む」日本の縁深き海藻, その歴史と現在 (後編), <https://jbpress.ismedia.jp/articles/-/55473>, 漆原次郎 (記者), 現代ビジネス, 食の研究所, 2019 年 2 月 15 日. <https://www.foods-ch.com/shokuhin/1556092438588/>, フーズチャンネル, 2019 年 4 月 25 日 (転載)
- We established the “Asagao (Morning glory) Club” to deepen the understanding of our technology of mutation breeding. The club distributes the morning glory seeds irradiated with C-ion on request, and collects and compiles the observation reports of their growth. Some reports have been featured in the booklet issued by the club every two years.

**Accelerator Applications Research Division
Beam Mutagenesis Group
Plant Genome Evolution Research Team**

1. Abstract

Established in May 2018, the plant genome evolution research team studies the effect of heavy-ion induced mutations on plant phenotypes. Chromosome rearrangements including translocation, inversion, and deletion are thought to play an important role in evolution and have a great potential to provide large phenotypic changes. However, this potential has not been fully investigated because of the lack of an effective method to induce rearrangements. We recently found that chromosomal rearrangements are frequently induced after heavy-ion irradiations with high valence numbers such as Fe ions or Ar ions. This frequency is 30 times higher than that of the previous techniques and allows characterization of the effect of chromosomal rearrangements. We develop and optimize molecular and bioinformatics techniques based on the recent progress on genome sequencing technology, to efficiently identify and analyse genomic mutations from model and non-model plant species. We also utilise this heavy-ion's unique capability for plant breeding and evolution studies.

2. Major Research Subjects

- (1) Study on the effect of chromosomal rearrangements on plant genomes and phenotypes
- (2) Identification of the plant sex-determining genes and their evolutionary study

3. Summary of Research Activity

(1) Study on the effect of chromosomal rearrangements on plant genomes and phenotypes

In order to investigate the effect of chromosome rearrangements on plant phenotypes, we analysed the Arabidopsis mutant Ar55-as1, which were originally induced by Ar-beam irradiation at a dose of 50 Gy with an LET of 290 keV/ μm . This mutant has no homozygous mutation in any genes but has chromosomal rearrangements in the genome. This mutant shows a clear morphological mutant phenotype in which the petiole is shorter than wild-type plants. As a result of the investigation of the trait of each individual and the presence or absence of chromosome rearrangements in the M3 generation of the mutant, we found that the inversion of chromosome 2 is responsible for the phenotype. In addition, this inversion was found to be a dominant mutation. From this finding, we showed that a chromosome rearrangement can dominantly affect the plant phenotype. We are currently investigating the effect of this inversion on gene expression.

We also attempted to induce a chromosome rearrangement at a target position by using genome editing technology, because this technique will be necessary when the functional analysis of chromosomal rearrangements will be performed in the future. There has been no report in which a large chromosomal rearrangement was induced in *A. thaliana* by the genome editing. However, we expected that if it is a proven chromosomal region where chromosome rearrangement has occurred by heavy-ion irradiation, it can be induced even when using genome editing. As a result, 760-kb inversion or deletion was successfully induced by genome editing.

(2) Identification of the plant sex-determining genes and their evolutionary study

A dioecious plant, *Silene latifolia*, has heteromorphic sex chromosomes (X and Y). We previously identified sex changing mutants of *S. latifolia* by heavy-ion mutagenesis. The sex-changing mutants include hermaphroditic mutants and asexual mutants. The former has both stamens and gynoecium, while the latter have no reproductive organs. By whole-genome analysis and RNA seq analysis, we have identified a gene that is deleted in all 14 of the 14 hermaphroditic mutants. This gene could be a candidate of sex determinant gene with gynoecium suppressing function.

Members

Team Leader

Tomoko ABE

Contract Researcher

Kotaro ISHII

Visiting Scientists

Ali FERJANI (Tokyo Gakugei Univ.)

Yusuke KAZAMA (Fukui Prefectural Univ.)

Student Trainees

Andi M. OKASA (Tohoku Univ.)

Part-time Worker

Yukako ABE (Part-time Worker)

List of Publications & Presentations

Publications

[Original papers]

- N. Fujita, Y. Kazama, N. Yamagishi, K. Watanabe, S. Ando, H. Tsuji, S. Kawano, N. Yoshikawa, and K. Komatsu, “Development of the VIGS system in the dioecious plant *Silene latifolia*,” *Int. J. Mol. Sci.* **20**, 1031 (2019).
- M. Krasovec, Y. Kazama, K. Ishii, T. Abe, and D. A. Filatov, “Immediate dosage compensation is triggered by the deletion of Y-linked genes in *Silene latifolia*,” *Current Biol.* **29**, 2214–2221 (2019).
- R. Morita, H. Ichida, K. Ishii, Y. Hayashi, H. Abe, Y. Shirakawa, K. Ichinose, K. Tsuneizumi, T. Kazama, K. Toriyama, T. Sato, and T. Abe, “*LONG GRAIN 1*: a novel gene that regulates grain length in rice,” *Mol. Breed.* **39**, 135 (2019).
- H. Kawamoto, K. Yamanaka, A. Koizumi, K. Ishii, Y. Kazama, T. Abe, and S. Kawano, “An asexual flower of *Silene latifolia* and *Microbotryum lychnidis-dioicae* promotes sex-organ development,” *PLoS One* **14**, e0217329 (2019).

Presentations

[International conferences/workshops]

- K. Ishii, Y. Kazama, T. Hirano, T. Takeshita, S. Kawano, and T. Abe (poster), “Development of a pipeline for whole-genome mutational analysis and its application on heavy-ion mutagenesis,” Rice Functional Genomics Workshop in XXVII Plant & Animal Genome Conference, San Diego, USA, January 12–16, 2019.
- T. Abe (invited), H. Ichida, Y. Hayashi, Y. Shirakawa, K. Ishii, and R. Morita, “Ion-beam radiation mutagenesis and plant mutation breeding,” 14th Conference of Society for the Advancement of the Breeding Research in Asia and Oceania, Gwangju, Korea, July 2–5, 2019.

[Domestic conferences/workshops]

- 風間裕介 (招待講演), “Study of plant sex chromosome by using heavy-ion induced mutants,” 第1回重・クラスターイオンビーム利用による微生物由来高生産性エネルギー、環境シンポジウム、筑波大学、つくば、2019年1月29日。
- 上田純平、風間裕介、阿部知子、村井耕二 (口頭発表), 「一粒系コムギ DV92 系統における花成遅延変異体 late-heading 2~5 (lh2~5) の同定」, 日本育種学会 第135回講演会、千葉大学、千葉市、2019年3月16–17日。
- 阿部知子、石井公太郎、風間裕介、平野智也 (口頭発表), 「重イオンビーム照射により誘発したシロイヌナズナ変異の特徴」, 基礎物理研究所研究会「放射線の生体影響解明への分野横断による挑戦」, 京都大学、京都、2019年5月23–25日。
- 石井公太郎、市田裕之、阿部知子 (ポスター発表), 「イネの品種特異的高精度リファレンス配列作製手法の開発」, 日本育種学会第136回講演会、近畿大学、奈良、2019年9月6–7日。
- 風間裕介、M. Krasovec、石井公太郎、阿部知子、D. A. Filatov (口頭発表), 「雌雄異株植物ヒロハノマンテマで発見した性染色体の即時遺伝子量補正」, 日本遺伝学会 91 回大会、福井大学、福井、2019年9月11–14日。
- 橋本佳澄、西浦愛子、上田純平、風間裕介、市田裕之、阿部知子、村井耕二 (ポスター発表), 「重イオンビームによって作出された超極早生コムギ変異体 extra early-flowering 4 における原因遺伝子の同定」, 日本遺伝学会 91 回大会、福井大学、福井、2019年9月11–14日。
- 酒井嵩人、平田千穂、風間裕介、阿部知子、三村徹郎、深城英弘、石崎公康 (ポスター発表), 「重イオンビーム照射胞子を用いたゼニゴケ配偶体形態形成変異体のスクリーニングと解析」, 日本植物学会 83 回大会、東北大学、仙台市、2019年9月15–17日。
- 渡邊遥、大部澄江、阿部知子、風間裕介 (ポスター発表), 「ゲノム編集によるシロイヌナズナへの染色体再編成の導入」, 日本植物学会 83 回大会、東北大学、仙台、2019年9月15–17日。
- 風間裕介 (口頭発表), 「染色体再編成: その誘発と表現型に与える影響」, 第12回北陸合同バイオシンポジウム、清風荘、あわら、2019年10月25–26日。
- 上田純平、風間裕介、阿部知子、市田裕之、村井耕二 (ポスター発表), 「一粒系コムギ (*Triticum monococcum*) KU104-2 および DV92 系統から作出した花成遅延変異体 late-heading 1, 2 (lh1, 2) の解析」, 第14回ムギ類研究会、鳥取大学乾燥地研究センター、鳥取、2019年11月2–3日。
- 橋本佳澄、西浦愛子、上田純平、風間裕介、阿部知子、市田裕之、村井耕二 (ポスター発表), 「重イオンビーム照射によって作出された超極早生コムギ変異体 extra early-flowering 4 における原因遺伝子の同定」, 第14回ムギ類研究会、鳥取、鳥取大学乾燥地研究センター、2019年11月2–3日。
- 高城啓一、石井公太郎、畑下昌範、阿部知子 (ポスター発表), 「ATM/ATR 機能欠損シロイヌナズナ根端における X 線照射後の γ -H2AX の時間空間分布」, 日本放射線影響学会 第62回大会、京都大学、京都、2019年11月14–16日。
- 風間裕介 (招待講演), 「福井県立大学におけるイオン育種の展望—園芸植物の染色体再編研究」, 福井イオンビーム育種研究会、若狭湾エネルギー研究センター、敦賀、2019年12月13日。

Accelerator Applications Research Division

RI Application Research Group

1. Abstract

RI Application Research Group promotes industrial applications of radioisotopes (RI) and ion beams at RIKEN RI Beam Factory (RIBF). Nuclear Chemistry Research Team develops production technologies of useful RIs for application studies in nuclear and radiochemistry. The team also develops technologies of mass spectrometry for trace-element and isotope analyses and apply them to the research fields such as cosmochemistry, environmental science, archaeology, and so on. Industrial Application Research Team promotes industrial applications of the accelerator facility and its related technologies.

2. Major Research Subjects

- (1) Research and development of RI production technologies at RIBF
- (2) RI application researches
- (3) Development of trace element analyses using accelerator techniques and its application to geoscience and archaeological research fields
- (4) Development of chemical materials for ECR ion sources of the RIBF accelerators
- (5) Development of technologies on industrial utilization and novel industrial applications of RIBF
- (6) Support of industrial utilization of the heavy-ion beams at RIBF
- (7) Support of some materials science experiments
- (8) Fee-based distribution of RIs produced at RIBF

3. Summary of Research Activity

See the subsections of Nuclear Chemistry Research Team and Industrial Application Research Team.

Members

Director

Hiromitsu HABA

Team Leaders

Hiromitsu HABA

Atsushi YOSHIDA

List of Publications & Presentations

See the subsections of Nuclear Chemistry Research Team and Industrial Application Research Team

Accelerator Applications Research Division

RI Application Research Group

Nuclear Chemistry Research Team

1. Abstract

The Nuclear Chemistry Research Team develops production technologies of unique radioisotopes (RIs) at RIKEN RI Beam Factory (RIBF) and applies them in the research fields of physics, chemistry, biology, engineering, medicine, pharmaceutical and environmental sciences. The purified RIs such as ^{65}Zn , ^{67}Cu , ^{85}Sr , ^{88}Y , and ^{109}Cd are delivered to universities and institutes through Japan Radioisotope Association. We also develop new technologies of mass spectrometry for the trace-element analyses using accelerator technology and apply them to the research fields such as cosmochemistry, environmental science, archaeology, and so on. We perform various isotopic analyses on the elements such as S, Pd, and Pb using ICP-MS, TIMS, and IRMS. We also develop chemical materials for ECR ion sources of the heavy-ion accelerators at RIBF.

2. Major Research Subjects

- (1) Research and development of RI production technologies at RIBF
- (2) RI application researches
- (3) Development of trace element analyses using accelerator techniques and its application to geoscience and archaeological research fields
- (4) Development of chemical materials for ECR ion sources of the heavy-ion accelerators at RIBF

3. Summary of Research Activity

(1) Research and development of RI production technologies at RIBF and RI application researches

Due to its high sensitivity, the radioactive tracer technique has been successfully applied for investigations of the behavior of elements in the fields of chemistry, biology, engineering, medicine, pharmaceutical and environmental sciences. We have been developing production technologies of useful radiotracers at RIBF and conducting their application studies in collaboration with many researchers in various fields. With 30-MeV proton, 24-MeV deuteron, and 50-MeV alpha beams from the AVF cyclotron, we presently produce about 100 radiotracers from ^7Be to ^{211}At . Among them, ^{65}Zn , ^{67}Cu , ^{85}Sr , ^{88}Y , and ^{109}Cd are delivered to Japan Radioisotope Association for fee-based distribution to the general public in Japan. Our RIs are also distributed to researchers under the Supply Platform of Short-lived Radioisotopes for Fundamental Research, supported by MEXT KAKENHI. On the other hand, radionuclides of a large number of elements are simultaneously produced from metallic targets such as $^{\text{nat}}\text{Ti}$, $^{\text{nat}}\text{Ag}$, $^{\text{nat}}\text{Hf}$, ^{197}Au , and ^{232}Th irradiated with a 135-MeV $\text{nucl.}^{-1}\text{ }^{14}\text{N}$ beam from the RIKEN Ring Cyclotron. These multitracers are also supplied to universities and institutes as collaborative researches.

In 2019, we developed production technologies of radioisotopes such as ^{24}Na , $^{42,43}\text{K}$, $^{44\text{m}}\text{Sc}$, ^{48}Cr , ^{111}Ag , ^{186}Re , ^{211}At , ^{224}Ra , ^{212}Pb , and ^{225}Ac which were strongly demanded but lack supply sources in Japan. We also investigated the excitation functions for the $^{\text{nat}}\text{V}(p, x)$, $^{\text{nat}}\text{Cr}(p, x)$, $^{\text{nat}}\text{La}(p, x)$, $^{169}\text{Tm}(p, x)$, $^{\text{nat}}\text{Ta}(p, x)$, $^{45}\text{Sc}(d, x)$, $^{\text{nat}}\text{Tl}(d, x)$, $^{\text{nat}}\text{Ca}(\alpha, x)$, $^{\text{nat}}\text{Ni}(\alpha, x)$, $^{\text{nat}}\text{Sb}(\alpha, x)$, $^{\text{nat}}\text{Nd}(\alpha, x)$, $^{\text{nat}}\text{Gd}(\alpha, x)$, and $^{\text{nat}}\text{Dy}(\alpha, x)$ reactions to quantitatively produce useful RIs. We used radiotracers of $^{42,43}\text{K}$, $^{44\text{m}}\text{Sc}$, ^{111}Ag , ^{186}Re , ^{211}At , ^{224}Ra , ^{212}Pb , and ^{225}Ac for application studies in chemistry, ^{24}Na , $^{42,43}\text{K}$, $^{44\text{m}}\text{Sc}$, ^{67}Cu , ^{186}Re , ^{211}At , and ^{225}Ac in nuclear medicine. We also produced ^{65}Zn , ^{67}Cu , and ^{88}Y for our scientific researches on a regular schedule and supplied the surpluses through Japan Radioisotope Association to the general public. In 2019, we accepted 2 orders of ^{65}Zn with a total activity of 6.7 MBq, 1 order of ^{67}Cu with 5 MBq, and 2 orders of ^{88}Y with 2 MBq. We also distributed $^{44\text{m}}\text{Sc}$ (2 MBq \times 3), ^{88}Zr (1 MBq \times 1 and 2 MBq \times 1), ^{95}Nb (1 MBq \times 2 and 2 MBq \times 1), ^{124}Sb (2 MBq \times 1), ^{141}Ce (9 kBq \times 1 and 13 kBq \times 1), ^{175}Hf (1 MBq \times 1 and 2 MBq \times 1), and ^{211}At (5 MBq \times 4, 50 MBq \times 6, 100 MBq \times 11, and 120 MBq \times 1) under the Supply Platform of Short-lived Radioisotopes for Fundamental Research.

(2) Superheavy element chemistry

Chemical characterization of newly-discovered superheavy elements (SHEs, atomic numbers $Z \geq 104$) is an extremely interesting and challenging subject in modern nuclear and radiochemistry. We are developing SHE production systems as well as rapid single-atom chemistry apparatuses at RIBF. Using heavy-ion beams from RILAC and AVF, ^{261}Rf ($Z = 104$), ^{262}Db ($Z = 105$), ^{265}Sg ($Z = 106$), and ^{266}Bh ($Z = 107$) are produced in the $^{248}\text{Cm}(^{18}\text{O}, 5n)^{261}\text{Rf}$, $^{248}\text{Cm}(^{19}\text{F}, 5n)^{262}\text{Db}$, $^{248}\text{Cm}(^{22}\text{Ne}, 5n)^{265}\text{Sg}$, and $^{248}\text{Cm}(^{23}\text{Na}, 5n)^{266}\text{Bh}$ reactions, respectively, and their chemical properties are investigated.

We installed a gas-jet transport system to the focal plane of the gas-filled recoil ion separator GARIS at RILAC. This system is a promising approach for exploring new frontiers in SHE chemistry: the background radiations from unwanted products are strongly suppressed, the intense primary heavy-ion beam is absent in the gas-jet chamber, and hence the high gas-jet extraction yield is attained. Furthermore, the beam-free condition makes it possible to investigate new chemical systems. To realize aqueous chemistry studies of Sg and Bh, we have been developing a continuous and rapid solvent extraction apparatus which consists of a continuous dissolution apparatus Membrane DeGasser (MDG), a Flow Solvent Extractor (FSE), and a liquid scintillation detector for α /SF-spectrometry. On the other hand, we have a gas-jet coupled target system and a safety system for a radioactive ^{248}Cm target on the beam line of AVF. In 2019, the distribution coefficients of ^{261}Rf on the anion-exchange resin in the H_2SO_4 system were measured with the AutoMated Batch-type solid-liquid Extraction apparatus for Repetitive experiments of transactinides (AMBER) which was developed by the research group of Osaka University. The distribution coefficients of ^{262}Db on the anion-exchange resin in the mixed HF/HNO_3

system were also measured with the Automated Rapid Chemistry Apparatus (ARCA) of Japan Atomic Energy Agency. We produced radiotracers of ^{88}Zr , ^{95}Nb , $^{95\text{m}}\text{Tc}$, ^{175}Hf , $^{177,179}\text{Ta}$, and ^{183}Re at AVF and conducted model experiments for aqueous chemistry studies on Rf, Db, and Bh. In 2019, we developed a cryogenic RF-carpet gas cell, which will be placed on the focal plane of GARIS and connected to a gas chromatographic apparatus, for the future gas-phase chemistry of the short-lived SHEs (<3 s).

(3) Development of trace element analyses using accelerator techniques and its application to geoscience and archaeological research fields

We have been developing the ECR Ion Source Mass Spectrometer (ECRIS-MS) for trace element analyses. In 2019, we renovated the detection system of ECRIS-MS and evaluated its sensitivity and mass resolution power. We equipped a laser-ablation system with an ion source and a pre-concentration system to achieve high-resolution analyses for noble gases such as Kr and Xe.

Using the conventional ICP-MS, TIMS, IRMS, and so on, we analyzed sediments such as a ferro-manganese nodule in the Pacific Ocean to elucidate its growth history concerning the environmental changes in the ocean. We also studied Pb and S isotope ratios on cinnabar and asphalt samples from ancient ruins in Japan to elucidate the distribution of goods in the archaic society and to reveal the establishment of the Yamato dynasty in the period from Jomon to Tumulus. We established a sampling technique for pigment without any damages on the artifacts or wall paintings, using a S-free adhesive tape. Then, we applied the technique to the analyses of the pigment from Roman ruins in Badalona, Spain. We also applied the technique to the analyses of the red-color substances on the artifacts such as Kyoden remains (Izumo-city, Shimane prefecture), Renpeijou-ato (Zentuji-city, Kagawa prefecture) and so on. We also investigated the transmutation of the long-lived ^{107}Pd to the stable Pd isotopes by the deuteron-induced nuclear reaction.

(4) Development of chemical materials for ECR ion sources of the heavy-ion accelerators at RIBF

In 2019, we prepared metallic ^{238}U rods and $^{238}\text{UO}_2$ on a regular schedule for ^{238}U -ion accelerations with the 28-GHz ECR of RILAC II.

Members

Team Leader

Hiromitsu HABA

Research/Technical Scientist

Kazuya TAKAHASHI (Senior Research Scientist)

Research & Development Scientist

Hiroo HASEBE

Contract Researcher

Yukiko KOMORI

Special Postdoctoral Researcher

Yudai SHIGEKAWA

Postdoctoral Researchers

Yang WANG

Takuya YOKOKITA

Technical Staff I

Daiki MORI

Research Consultant

Hisaaki KUDO (Niigata Univ.)

Visiting Scientists

Masayuki AIKAWA (Hokkaido Univ.)

Kazuhiko AKIYAMA (Tokyo Metropolitan Univ.)

Ferenc DITRÓI (ATOMKI)

Osuke FUJIMOTO (Fujifilm Toyama Chemical Co., Ltd.)

Takahiro HIRAKI (Okayama Univ.)

Hayato IKEDA (Tohoku Univ.)

Noriko ISHIOKA (QST)

Masamichi KAJITA (Fujifilm Toyama Chemical Co., Ltd.)

Hiroshi KATO (Fujifilm Toyama Chemical Co., Ltd.)

Mayeen U. KHANDAKER (Sunway Univ.)

Hidetoshi KIKUNAGA (Tohoku Univ.)

Yoshikatsu KOGA (Nat'l Cancer Center)

Shoko KUBOTA (Fujifilm Toyama Chemical Co., Ltd.)

Takumi KUBOTA (Kyoto Univ.)

Susanta Kumar LAHIRI (Saha Inst. of Nucl. Phys.)

Takahiko MASUDA (Okayama Univ.)

Toshimitsu MOMOSE (Int'l Univ. of Health and Welfare)

Akio NAGANO (Fujifilm Toyama Chemical Co., Ltd.)

Eri NAKAMURA (Fujifilm Toyama Chemical Co., Ltd.)

Kenichiro OGANE (Int'l Univ. of Health and Welfare)

Miki OHTSUKA (Waseda Univ.)

Kazuhiro OOE (Osaka Univ.)

Shinobu OSHIKIRI (Fujifilm Toyama Chemical Co., Ltd.)

Yasutaka SAITO (Fujifilm Toyama Chemical Co., Ltd.)

Aya SAKAGUCHI (Univ. of Tsukuba)

Miho SATAKE (Fujifilm Toyama Chemical Co., Ltd.)

Yuki SATO (Fujifilm Toyama Chemical Co., Ltd.)

Kenji SHIMAZOE (Univ. of Tokyo)

Keisuke SUEKI (Univ. of Tsukuba)
 Kentaro SUZUKI (Fujifilm Toyama Chemical Co., Ltd.)
 Zoltán SZŰCS (ATOMKI) Sándor TAKÁCS (ATOMKI)
 Hiroyuki TAKAHASHI (Univ. of Tokyo)
 Miho TAKAHASHI (Tokyo Univ. of Marine Sci. and Tech.)
 Miwako TAKAHASHI (Nat'l Inst. of Radiological Sci.)
 Yuichi TAKAKU (Inst. for Environmental Sci.)
 Hiroki TAKASHIMA (Nat'l Cancer Center)
 Kazuo TANAKA (Tohoku Univ.)
 Masayoshi TODA (Tokyo Univ. of Marine Sci. and Tech.)

Atsushi TOYOSHIMA (Osaka Univ.)
 Takashi UI (Fujifilm Toyama Chemical Co., Ltd.)
 Naoyuki UKON (Fukushima Medical Univ.)
 Ahmed R. USMAN (Umaru Musa Yar'adua Univ.)
 Shigeki WATANABE (QST)
 Chunli YANG (Inst. of Modern Phys.)
 Akihiko YOKOYAMA (Kanazawa Univ.)
 Zenko YOSHIDA (ATOX Co., Ltd.)
 Koji YOSHIMURA (Okayama Univ.)

Visiting Technicians

Hideyuki ARAI (Metal Tech. Co. Ltd.)
 Hiroshi ARATA (Metal Tech. Co. Ltd.)
 Hidehiro HASHIMOTO (Metal Tech. Co. Ltd.)
 Yoshiyuki IIZUKA (ATOX Co., Ltd.)
 Akimitsu KANDA (Japan Radioisotope Association)
 Shota KIMURA (Japan Radioisotope Association)
 Yukiyoshi KON (Osaka Univ.)
 Takashi KURIHARA (Metal Tech. Co. Ltd.)

Takahiro MIKAMOTO (Japan Radioisotope Association)
 Hiroki SHIBAHARA (ATOX Co., Ltd.)
 Yuki TAKEMURA (ATOX Co., Ltd.)
 Yasutaka TAKEUCHI (ATOX Co., Ltd.)
 Shusaku TAZAWA (ATOX Co., Ltd.)
 Yuichirou WAKITANI (Japan Radioisotope Association)
 Mami YUKI (ATOX Co., Ltd.)

Student Trainees

Sadia ADACHI (Univ. of Tsukuba)
 Kjeld A. A. G. BEEKS (Vienna Univ. of Tech.)
 Desheng CHEN (Univ. of Chinese Academy of Sci.)
 Wei Seng FOONG (Univ. of Tokyo)
 Yuta HAYAKAWA (Kanazawa Univ.)
 Sho HAYAMI (Osaka Univ.)
 Xuan HOU (Univ. of Tokyo)
 Ayuna KASHIHARA (Univ. of Tsukuba)
 Mizuho KATO (Univ. of Tsukuba)
 Cheonghun KIM (Univ. of Tokyo)
 Mariko KOBAYASHI (Univ. of Tokyo)
 Masaharu KURINO (Univ. of Tokyo)
 Natsuki MATSUMURA (Kanazawa Univ.)
 Ryoga MORITA (Kanazawa Univ.)
 Tomohiro MURATA (Hokkaido Univ.)

Akihisa NAKAJIMA (Univ. of Tsukuba)
 Kaito NISHIZUKA (Univ. of Tsukuba)
 Koichi OKAI (Okayama Univ.)
 Moemi SAITO (Hokkaido Univ.)
 Michiya SAKAGUCHI (Hokkaido Univ.)
 Kaori SHIRAI (Niigata Univ.)
 Hayato SUZUKI (Ibaraki Univ.)
 Yusuke SUZUKI (Univ. of Tsukuba)
 Kakeru TERANISHI (Kanazawa Univ.)
 Katsuyuki TOKOI (Ibaraki Univ.)
 Katsuma TONAI (Osaka Univ.)
 Mizuki UENOMACHI (Univ. of Tokyo)
 Eisuke WATANABE (Osaka Univ.)
 Yuki YASUDA (Osaka Univ.)
 Zhihong ZHONG (Univ. of Tokyo)

Part-time Workers

Michiko KITAGAWA (Research Part-time Worker I)
 Nozomi SATO (Research Part-time Worker I)

Sachiko USUDA (Research Part-time Worker I)
 Minako OSANAI (Research Part-time Worker II)

List of Publications & Presentations

Publications

[Original papers]

- M. Aikawa, M. Saito, Y. Komori, H. Haba, S. Takács, F. Ditrói, and Z. Szűcs, "Activation cross sections of alpha-particle induced nuclear reactions on natural palladium," *Nucl. Instrum. Methods Phys. Res. B*, **449**, 99–104 (2019).
- E. Corniani, F. Ditrói, S. Takács, H. Haba, Y. Komori, M. Aikawa, M. Saito, and T. Murata, "Study of secondary implantation of radioisotopes during alpha-particle irradiation," *J. Radioanal. Nucl. Chem.* **320**, 813–822 (2019).
- M. Saito, M. Aikawa, T. Murata, N. Ukon, Y. Komori, H. Haba, and S. Takács, "Activation cross sections of alpha-induced reactions on natural ytterbium upto 50 MeV," *Nucl. Instrum. Methods Phys. Res. B* **453**, 15–21 (2019).
- M. Ebihara, Y. Oura, N. Shirai, Y. Nagakawa, N. Sakurai, H. Haba, H. Matsuzaki, H. Tsuruta, and Y. Moriguchi, "A new approach for reconstructing the ¹³¹I-spreading due to the 2011 Fukushima nuclear accident by means of measuring ¹²⁹I in airborne particulate matters," *J. Environ. Radio.* **208-209**, 106000-1–9 (2019).
- T. Masuda, A. Yoshimi, A. Fujieda, H. Fujimoto, H. Haba, H. Hara, T. Hiraki, H. Kaino, Y. Kasamatsu, S. Kitao, K. Konashi, Y. Miyamoto, K. Okai, S. Okubo, N. Sasao, M. Seto, T. Schumm, Y. Shigekawa, K. Suzuki, S. Stellmer, K. Tamasaku, S. Uetake, M. Watanabe, T. Watanabe, Y. Yasuda, A. Yamaguchi, Y. Yoda, T. Yokokita, M. Yoshimura, and K. Yoshimura, "X-ray pumping of the ²²⁹Th nuclear clock isomer," *Nature* **573**, 238–242 (2019).
- M. Saito, M. Aikawa, M. Sakaguchi, N. Ukon, Y. Komori, and H. Haba, "Production cross sections of ytterbium and thulium radioisotopes in alpha-induced nuclear reactions on natural erbium," *Appl. Radiat. Isot.* **154**, 108874-1–6 (2019).

- Y. Shigekawa, Y. Kasamatsu, E. Watanabe, H. Ninomiya, S. Hayami, N. Kondo, Y. Yasuda, H. Haba, and A. Shinohara, "Observation of internal-conversion electrons emitted from $^{229\text{m}}\text{Th}$ produced by beta decay of ^{229}Ac ," *Phys. Rev. C* **100**, 044304-1–7 (2019).
- A. Yamaguchi, H. Muramatsu, T. Hayashi, N. Yuasa, K. Nakamura, M. Takimoto, H. Haba, K. Konashi, M. Watanabe, H. Kikunaga, K. Maehata, N. Y. Yamasaki, and K. Mitsuda, "Energy of the ^{229}Th nuclear clock isomer determined by absolute γ -ray energy difference," *Phys. Rev. Lett.* **123**, 222501-1–6 (2019).
- T. Murata, M. Aikawa, M. Saito, H. Haba, Y. Komori, N. Ukon, S. Takács, and F. Ditrói, "Excitation function measurement for zirconium-89 and niobium-90 production using alpha-induced reactions on yttrium-89," *Nucl. Instrum. Methods Phys. Res. B* **458**, 21–27 (2019).
- S. Takács, M. Aikawa, M. Saito, T. Murata, N. Ukon, Y. Komori, and H. Haba, "Activation cross sections of alpha particle-induced reactions on natural hafnium up to 50 MeV," *Nucl. Instrum. Methods Phys. Res. B* **459**, 50–58 (2019).
- D. Ichinkhorloo, M. Aikawa, T. Zolbadral, Y. Komori, and H. Haba, "Activation cross sections of dysprosium-157, 159 and terbium-160 radioisotopes from the deuteron-induced reactions on terbium-159 up to 24 MeV," *Nucl. Instrum. Methods Phys. Res. B* **461**, 102–104 (2019).
- T. Minami, K. Hatanaka, Y. Motizuki, Y. Nakai, and K. Takahashi, "A method of collecting trace amounts of vermilion from artifacts for source estimation by sulfur isotope ($\delta^{34}\text{S}$) analysis: Use of sulfur-free adhesive tape to minimize damage to the artifact body during sampling," *J. Archaeol. Sci. Rep.* **28**, 102027-1–5 (2019).
- A. R. Usman, M. U. Khandaker, H. Haba, N. Otuka, and M. Murakami, "Production cross sections of thulium radioisotopes for alpha-particle induced reactions on holmium," *Nucl. Instrum. Methods Phys. Res. B* **469**, 42–48 (2020).
- M. Okamura, E. Beebe, S. Ikeda, T. Kanesue, D. Raparia, T. Karino, and H. Haba, " ^{96}Zr beam production for isobar experiment in relativistic heavy ion collider," *Rev. Sci. Instrum.* **91**, 013319-1–5 (2020).
- T. Tanaka, K. Morita, K. Morimoto, D. Kaji, H. Haba, R. A. Boll, N. T. Brewer, S. Van Cleve, D. J. Dean, S. Ishizawa, Y. Ito, Y. Komori, K. Nishio, T. Niwase, B. C. Rasco, J. B. Roberto, K. P. Rykaczewski, H. Sakai, D. W. Stracener, and K. Hagino, "Fusion dynamics for hot fusion reactions to synthesize superheavy nuclei revealed in quasielastic barrier distributions," *Phys. Rev. Lett.* **124**, 052502-1–96 (2020).
- M. U. Khandaker, H. Haba, Y. Komori, and N. Otuka, "Excitation functions of deuteron-induced nuclear reactions on erbium in the energy range of 4–24 MeV," *Nucl. Instrum. Methods Phys. Res. B* **470**, 1–9 (2019).
- Y. Wang, Y. Wittwer, J. Zhang, J. Yang, H. Haba, Y. Komori, T. Yokokita, S. Cao, F. Fan, R. Eichler, A. Türler, and Z. Qin, "Mass spectrometric speciation of metal-carbonyls in the gas phase," *PSI Annual Report 2018, Laboratory of Radiochemistry*, 13–14 (2019).
- M. Sakaguchi, M. Aikawa, M. Saito, N. Ukon, Y. Komori, and H. Haba, "Production cross sections of ^{89}Zr by deuteron-induced reactions on ^{89}Y ," *JAEA-Conf 2019-001*, 185–188 (2019).
- T. Fukuchi, H. Haba, and H. Kikunaga, "Phantom production for a multiple-isotope β -ray imaging system," *ELPH Annual Report, Tohoku University 2018*, 105–106 (2019).
- M. Saito, M. Aikawa, T. Murata, Y. Komori, H. Haba, S. Takács, F. Ditrói, and Z. Szűcs, "Production cross sections of ^{169}Yb by the proton-induced reaction on ^{169}Tm ," *Nucl. Instrum. Methods Phys. Res. B* **471**, 13–16 (2020).
- Y. Kasamatsu, N. Kondo, K. Nakamura, Y. Kuboki, H. Ninomiya, Y. Shigekawa, E. Watanabe, Y. Yasuda, K. Toyomura, M. Nagase, T. Yokokita, Y. Komori, H. Haba, T. Yoshimura, H. Itabashi, and A. Shinohara, "Solvent extraction of Zr and Hf from HCl by Aliquat 336 using a flow-type extraction apparatus toward online chemical studies of element 104, rutherfordium," *Solv. Extr. Ion Exch* **38**, 318–327 (2020).
- Z. Tsoodol, M. Aikawa, I. Dagvadorj, T. Khishigjargal, N. Javkhlantugs, Y. Komori, and H. Haba, "Production cross sections of ^{68}Ga and radioactive by-products in deuteron-induced reactions on natural zinc," *Appl. Radiat. Isot.* **159**, 109095-1–8 (2020).
- M. Sakaguchi, M. Aikawa, M. Saito, N. Ukon, Y. Komori, and H. Haba, "Activation cross section measurement of the deuteron-induced reaction on yttrium-89 for zirconium-89 production," *Nucl. Instrum. Methods Phys. Res. B* **472**, 59–63 (2020).
- T. Niwase, M. Wada, P. Schury, H. Haba, S. Ishizawa, Y. Ito, D. Kaji, S. Kimura, H. Miyatake, K. Morimoto, K. Morita, M. Rosenbusch, H. Wollnik, T. Shanley, and Y. Benari, "Development of an " α -TOF" detector for correlated measurement of atomic masses and decay properties," *Nucl. Instrum. Methods Phys. Res. A* **953**, 163198-1–8 (2020).
- J. Grund, M. Asai, K. Blaum, M. Block, S. Chenmarev, Ch. E. Düllmann, K. Eberhardt, S. Lohse, Y. Nagame, Sz. Nagy, P. Naubereit, J. J. W. van de Laar, F. Schneider, T. K. Sato, N. Sato, D. Simonovski, K. Tsukada, and K. Wendt, "First online operation of TRIGA-TRAP," *Nucl. Instrum. Methods Phys. Res. A* **972**, 164013-1–8 (2020).
- Y. Shigekawa, Y. Kasamatsu, Y. Yamakita, Y. Yasuda, E. Watanabe, N. Kondo, H. Haba, and A. Shinohara, "Development of a retarding-field type magnetic bottle spectrometer for studying the internal-conversion process of $^{235\text{m}}\text{U}$," *Nucl. Instrum. Methods Phys. Res. A* **976**, 164207-1–10 (2020).

[Review articles]

- H. Haba, "The rewards and challenges of expanding the periodic table," *Chem. Eng. News*, August 5, 36–37 (2019).
- 羽場宏光, 「第 8 周期の新元素を求めて」, **40**, 14–20 (2019).
- 羽場宏光, 「日本の研究者による新元素の探索と周期表の開拓—ニッポニウム, 93 番元素, ニホニウム. さらなる新元素を求めて—」, *化学と工業* **72**, 944–945 (2019).
- 羽場宏光, 「理研における核医学治療用ラジオアイソトープの製造」, *Drug Delivery Syst.* **35**, 114–120 (2020).
- 海野弘行, 笠松良崇, 重河優大, 羽場宏光, 平木貴宏, 増田孝彦, 山口敦史, 横北卓也, 吉見彰洋, 吉村浩司, 「高輝度 X 線を用いた核共鳴散乱技術による原子核 ^{229}Th アイソマー状態の人工生成」, *Isotope News No.* 768, 2–6 (2020).

[Books]

- 佐藤望, 工藤久昭, 「超重元素の合成」, in 「フロンティアシリーズ 2 超重元素化学の最前線」, 永目諭一郎 (編著), pp. 6–13, 日本放

射化学会, 2019年9月1日.

豊嶋厚史, 羽場宏光, 「超重元素化学—溶液化学」, in 「フロンティアシリーズ 2 超重元素化学の最前線」, 永目論一郎 (編著), pp. 41–48, 日本放射化学会, 2019年9月1日.

南武志, 高橋和也, 「京田遺跡 4 区出土遺物付着水銀朱の硫黄同位体分析」, in 「出雲市の文化財報告 39 京田遺跡 4 区 発掘調査報告書」, 出雲市教育委員会, pp. 165–168, 2019年3月.

羽場宏光 (分担執筆), 「アイソトープ手帳 12 版」, 日本アイソトープ協会 (編集・発行), 丸善出版株式会社, 2020年3月30日.

[Proceedings]

H. Haba for RIKEN SHE Collaboration, “Present status and perspectives of SHE researches at RIKEN,” in “Proceedings of the international symposium on exotic nuclei, Petrozavodsk, Russia, 10–15 September 2018,” Yu. E. Penionzhkevich, Yu. G. Sobolev (Eds.), World Scientific Publishing Co. Pte. Ltd., pp. 192–199 (2020).

Presentations

[International conferences/workshops]

- A. R. Usman, M. U. Khandaker, H. Haba, and N. Otuka (poster), “Cyclotron production cross sections of ^{61}Cu radionuclide from $^{nat}\text{Ni}(d, x)^{61}\text{Cu}$ nuclear reaction,” 2019 International Conference on Nuclear Data for Science and Technology (ND2019), Beijing, China, May 19–24, 2019.
- A. R. Usman, M. U. Khandaker, H. Haba, and N. Otuka (poster), “Towards formation of IAEA database for all metallic properties useful in radionuclides production: effect of varied titanium densities on excitation functions,” 2019 International Conference on Nuclear Data for Science and Technology (ND2019), Beijing, China, May 19–24, 2019.
- H. Haba (invited), “Production and applications of radioisotopes at RIKEN RI Beam Factory,” SHE Science Symposium, Oak Ridge, USA, May 30, 2019.
- H. Haba (invited), “Synthesis and chemistry of new elements at RIKEN,” 9th European Chemistry Congress, Berlin, Germany, June 17–18, 2019.
- H. Kanda, T. Nakano, N. Aoi, M. H. Fukuda, T. Yorita, T. Suzuki, N. Takahashi, A. Shinohara, H. Haba, S. Kamigaito, H. Kikunaga, H. Hama, T. Muto, H. Ikeda, H. Watabe, M. Itoh, H. Kawamura, Y. Sakemi, M. R. Zhang, K. Nagatsu, and H. Suzuki (oral), “Short-lived radioisotope supplying platform in Japan,” 39th Annual Conference of the Canadian Nuclear Society and 43rd Annual CNS/CNA Student Conference, Ottawa, Canada, June 23–26, 2019.
- T. Zolbadral, M. Aikawa, D. Ichinkhoroloo, K. Tegshjargal, N. Javkhlantugs, Y. Komori, and H. Haba (poster), “Production cross sections of ^{68}Ga and radioactive by-products in deuteron-induced reactions on natural zinc,” The 7th GI-CoRE Medical Science and Engineering Symposium FLASH, MBA, & 4DRT, Hokkaido, Japan, August 18–19, 2019.
- A. Yakushev, L. Lens, Ch. E. Düllmann, M. Asai, M. Block, H. Brand, H. M. David, J. Despotopoulos, A. Di Nitto, K. Eberhardt, U. Forsberg, P. Golubev, M. Götz, S. Götz, H. Haba, L. Harkness-Brennan, W. Hartmann, R. -D. Herzberg, D. Hinde, J. Hoffmann, A. Hübner, E. Jäger, M. Jourdan, D. Judson, J. Khuyagbaatar, B. Kindler, Y. Komori, J. Konki, J. V. Kratz, J. Krier, N. Kurz, M. Laatiaoui, S. Lahiri, B. Lommel, M. Maiti, A. Mistry, Ch. Mokry, K. Moody, Y. Nagame, J. P. Omtvedt, P. Papadakis, V. Pershina, T. Reich, D. Rudolph, J. Runke, L. Samiento, T. K. Sato, M. Schädel, P. Scharrer, B. Schausten, D. Shaughnessy, J. Steiner, P. Thörle-Pospiech, A. Toyoshima, N. Trautmann, K. Tsukada, J. Uusitalo, K. -O. Voss, A. Ward, M. Wegrzecki, N. Wiehl, E. Williams, and V. Yakusheva (invited), “Chemical studies of superheavy elements at a recoil separator, with a focus on Fl,” 6th International Conference on the Chemistry and Physics of the Transactinide Elements (TAN19), Wilhelmshaven, Germany, August 25–30, 2019.
- M. Götz, Ch. E. Düllmann, A. Yakushev, M. Asai, J. Ballof, A. Di Nitto, K. Eberhardt, S. Götz, H. Haba, E. Jäger, Y. Kaneya, Y. Komori, J. V. Kratz, J. Krier, B. Lommel, A. Mitsukai, Y. Nagame, T. K. Sato, A. Toyoshima, K. Tsukada, V. Wolter, and V. Yakusheva (poster), “In-situ synthesis of volatile transition metal carbonyl complexes with short-lived radioisotopes,” 6th International Conference on the Chemistry and Physics of the Transactinide Elements (TAN19), Wilhelmshaven, Germany, August 25–30, 2019.
- Z. Qin, Y. Wang, S. Cao, J. Zhang, J. Yang, H. Haba, F. Fan, Y. Komori, T. Yokokita, K. Morimoto, D. Kaji, Y. Wittwer, R. Eichler, and A. Türler (poster), “The study of rhenium pentacarbonyl complexes using single-atom chemistry in gas phase,” 6th International Conference on the Chemistry and Physics of the Transactinide Elements (TAN19), Wilhelmshaven, Germany, August 25–30, 2019.
- Y. Wang, Y. Wittwer, J. Zhang, J. Yang, H. Haba, Y. Komori, T. Yokokita, S. Cao, F. Fan, R. Eichler, A. Türler, and Z. Qin (oral), “The species identification of Mo, W, and Re carbonyl complexes with laserablation time-of-flight mass-spectrometry,” 6th International Conference on the Chemistry and Physics of the Transactinide Elements (TAN19), Wilhelmshaven, Germany, August 25–30, 2019.
- L. Lens, A. Yakushev, Ch. E. Düllmann, M. Asai, M. Block, H. Brand, M. Dasgupta, H. M. David, J. Despotopoulos, A. Di Nitto, K. Eberhardt, M. Götz, P. Golubev, S. Götz, H. Haba, L. Harkness-Brennan, F. P. Heßberger, R. -D. Herzberg, D. Hinde, J. Hoffmann, A. Hübner, E. Jäger, D. Judson, J. Khuyagbaatar, B. Kindler, Y. Komori, J. Konki, J. V. Kratz, J. Krier, N. Kurz, M. Laatiaoui, S. Lahiri, B. Lommel, M. Maiti, A. K. Mistry, C. Mokry, K. Moody, Y. Nagame, J. P. Omtvedt, P. Papadakis, V. Pershina, A. Roth, D. Rudolph, J. Runke, L. Sarmiento, M. Schädel, P. Scharrer, T. Sato, D. Shaughnessy, B. Schausten, J. Steiner, P. Thörle-Pospiech, N. Trautmann, K. Tsukada, J. Uusitalo, A. Ward, M. Wegrzecki, E. Williams, N. Wiehl, V. Yakusheva (poster), “Optimizations of the TASCA-COMPACT setup towards chemical studies of nihonium (element 113),” 6th International Conference on the Chemistry and Physics of the Transactinide Elements (TAN19), Wilhelmshaven, Germany, August 25–30, 2019.
- T. Niwase, M. Wada, P. Schury, Y. Ito, S. Kimura, D. Kaji, M. Rosenbusch, Y. Watanabe, Y. Hirayama, H. Miyatake, J. Y. Moon, H. Ishiyama, K. Morimoto, H. Haba, T. Tanaka, S. Ishizawa, A. Takamine, K. Morita, and H. Wollnik (poster), “Development and first results from a novel “ α -ToF” detector used with a multi-reflection time-of-flight mass spectrograph,” 6th International Conference on the Chemistry and Physics of the Transactinide Elements (TAN19), Wilhelmshaven, Germany, August 25–30, 2019.
- T. Tanaka, K. Morita, K. Morimoto, D. Kaji, H. Haba, R. A. Boll, N. T. Brewer, S. V. Cleve, D. J. Dean, S. Ishizawa, Y. Ito, Y. Komori,

- K. Nishio, T. Niwase, B. C. Rasco, J. B. Roberto, K. Rykaczewski, H. Sakai, D. W. Stracener, and K. Hagino (oral), “Fusion dynamics for hot fusion reactions revealed in quasielastic barrier distributions,” 6th International Conference on the Chemistry and Physics of the Transactinide Elements (TAN19), Wilhelmshaven, Germany, August 25–30, 2019.
- M. Wada, P. Schury, H. Miyatake, Y. X. Watanabe, Y. Hirayama, H. Wollnik, S. Kimura, S. Ishizawa, T. Niwase, M. Rosenbusch, D. Kaji, K. Morimoto, H. Haba, I. Takamine, T. Tanaka, H. Ishiyama, Y. Ito, J. Y. Moon, and K. Morita (invited), “SHE-Mass-II setup for direct mass measurement of hot-fusion superheavy nuclides,” 6th International Conference on the Chemistry and Physics of the Transactinide Elements (TAN19), Wilhelmshaven, Germany, August 25–30, 2019.
- Y. Ito, P. Schury, M. Wada, F. Arai, H. Haba, Y. Hirayama, S. Ishizawa, D. Kaji, S. Kimura, H. Koura, M. Maccormick, H. Miyatake, J. -Y. Moon, K. Morimoto, K. Morita, M. Mukai, I. Murray, T. Niwase, K. Okada, A. Ozawa, M. Rosenbusch, A. Takamine, T. Tanaka, Y. Watanabe, H. Wollnik, and S. Yamaki (oral), “Direct mass measurements of mendelevium isotopes in the vicinity of the $N = 152$ deformed shell-closure,” 6th International Conference on the Chemistry and Physics of the Transactinide Elements (TAN19), Wilhelmshaven, Germany, August 25–30, 2019.
- M. Okamura (oral), E. Beebe, S. Ikeda, T. Kanetsue, D. Raparia, and H. Haba, “ ^{96}Zr beam production for isobar experiment in RHIC,” The 18th International Conference on Ion Sources (ICIS’19), Lanzhou, China, September 1–6, 2019.
- H. Haba (invited), “Present status and perspectives of superheavy element researches at RIKEN,” XXXVIth Mazurian Lakes Conference on Physics, Piaski, Poland, September 1–7, 2019.
- H. Haba (invited), “RI production—Chemistry of new elements to diagnosis and treatment of cancer—,” Tsukuba Conference 2019, Tsukuba, Japan, October 2–4, 2019.
- T. Fukuchi, M. Shigeta, H. Haba, S. Yamamoto, and Y. Watanabe (poster), “Imaging performance evaluation of a multiple-isotope PET with $^{44\text{m}}\text{Sc}$ tracer,” 2019 IEEE Nuclear Science Symposium (NSS) and Medical Imaging Conference (MIC), Manchester, UK, October 26–November 2, 2019.
- T. Zolbadral, M. Aikawa, D. Ichinkhoroloo, T. Khishigjargal, Y. Komori, H. Haba, S. Takács, F. Ditrói, and Z. Szűcs (poster), “Production cross sections of ^{45}Ti via deuteron-induced reaction on scandium,” 2019 Symposium on Nuclear Data, Fukuoka, Japan, November 28–30, 2019.
- M. Saito, M. Aikawa, T. Murata, Y. Komori, H. Haba, S. Takács, F. Ditrói, and Z. Szűcs (poster), “Production of ^{169}Yb by the proton-induced reaction on ^{169}Tm ,” 2019 Symposium on Nuclear Data, Fukuoka, Japan, November 28–30, 2019.
- Y. Kasamatsu, H. Ninomiya, S. Hayami, M. Nagase, E. Watanabe, Y. Shigekawa, N. Kondo, H. Haba, T. Yokokita, Y. Komori, D. Mori, Y. Wang, K. Ghosh, M. Kaneko, and A. Shinohara (poster), “Coprecipitation of nobelium with samarium hydroxide,” The 4th International Symposium on Superheavy Elements (SHE2019), Hakone, Japan, December 1–5, 2019.
- E. Watanabe, S. Hayami, K. Tonai, H. Ninomiya, K. Ouchi, Y. Kasamatsu, Y. Kitagawa, M. Nakano, Y. Shigekawa, T. Yokokita, and A. Shinohara (poster), “Anion-exchange Experiment of Zr, Hf, and Th in HNO_3 ,” The 4th International Symposium on Superheavy Elements (SHE2019), Hakone, Japan, December 1–5, 2019.
- Z. Qin, Y. Wang, S. W. Cao, J. C. Zhang, F. L. Fang, J. Yang, H. Haba, Y. Komori, T. Yokokita, K. Morimoto, D. Kaji, Y. Wittwer, R. Eichler, and A. Türler (invited), “Towards the bohrium carbonyl complexes in gas phase,” The 4th International Symposium on Superheavy Elements (SHE2019), Hakone, Japan, December 1–5, 2019.
- Y. Wang, Y. Wittwer, J. Zhang, S. Cao, Y. Komori, T. Yokokita, Y. Shigekawa, F. Fan, J. Yang, H. Haba, R. Eichler, A. Türler, and Z. Qin (oral), “Species identification of Re carbonyls using laser-ablation time-of-flight mass-spectrometer,” The 4th International Symposium on Superheavy Elements (SHE2019), Hakone, Japan, December 1–5, 2019.
- T. Yokokita, Y. Kasamatsu, E. Watanabe, Y. Komori, H. Ninomiya, Y. Wang, D. Mori, K. Ghosh, A. Shinohara, and H. Haba (oral), “Anion exchange of Rf, Zr, Hf, and Th in H_2SO_4 ,” The 4th International Symposium on Superheavy Elements (SHE2019), Hakone, Japan, December 1–5, 2019.
- T. Niwase, M. Wada, P. Schury, Y. Ito, S. Kimura, D. Kaji, M. Rosenbusch, Y. X. Watanabe, Y. Hirayama, H. Miyatake, J. Y. Moon, H. Ishiyama, K. Morimoto, H. Haba, T. Tanaka, S. Ishizawa, A. Takamine, K. Morita, and H. Wollnik (oral), “Correlation measurement of precision mass and decay properties of nuclei via MRTOF-MS with α -ToF detector,” The 4th International Symposium on Superheavy Elements (SHE2019), Hakone, Japan, December 1–5, 2019.
- M. Rosenbusch, M. Wada, P. Schury, S. Iimura, H. Haba, Y. Hirayama, H. Ishiyama, S. Ishizawa, Y. Ito, D. Kaji, S. Kimura, H. Miyatake, J. Y. Moon, K. Morimoto, T. Tanaka, T. Niwase, A. Takamine, K. Morita, Y. X. Watanabe, and H. Wollnik (oral), “Dynamic ejection-field correction for MR ToF mass spectrometry of SHE using arbitrary mass references,” The 4th International Symposium on Superheavy Elements (SHE2019), Hakone, Japan, December 1–5, 2019.
- H. Haba (plenary), “Production and applications of radioisotopes at RIKEN RI Beam Factory—Search for new elements through diagnosis and therapy of cancer—,” The 10th International Conference on Isotopes (10ICI), Kuala Lumpur, Malaysia, February 3–7, 2020.
- H. Haba (invited), “Present status and perspectives of superheavy element chemistry at RIKEN,” The 10th International Conference on Isotopes (10ICI), Kuala Lumpur, Malaysia, February 3–7, 2020.
- Y. Komori, M. Murakami, and H. Haba (oral), “Measurements of excitation functions for the $^{nat}\text{W}(d, x)$ reactions based on new half-lives of rhenium isotopes,” The 10th International Conference on Isotopes (10ICI), Kuala Lumpur, Malaysia, February 3–7, 2020.

[Seminars]

- H. Haba, “Production of radioisotopes for application Studies at RIKEN RI Beam Factory,” Seminar at Institute of Modern Physics (IMP), Lanzhou, China, August 12, 2019.
- H. Haba, “Production of radioisotopes for application Studies at RIKEN RI Beam Factory,” IFIN-HH Seminar at Horia Hulubei National Institute for R&D in Physics and Nuclear Engineering, Bucharest, Rumania, October 21, 2019.
- Y. Komori, “Aqueous chemistry of superheavy elements at RIKEN,” IFIN-HH Seminar at Horia Hulubei National Institute for R&D in

Physics and Nuclear Engineering, Bucharest, Rumania, October 21, 2019.

H. Haba, "Production of radioisotopes for application studies at RIKEN RI Beam Factory", Seminar at Sunway University, Selangor, Malaysia, February 10, 2020.

Y. Komori, "Excitation function measurements in RIKEN", Seminar at Sunway University, Selangor, Malaysia, February 10, 2020.

[Domestic conferences/workshops]

福地知則, 重田美香, 羽場宏光, 山本誠一, 渡辺恭良, 榎本秀一 (口頭発表), 「陽電子-ガンマ線放出核 ^{44}Sc を用いた複数トレーサー PET イメージング」, 日本分子イメージング学会第 14 回総会・学術集会, 札幌, 2019 年 5 月 23-24 日.

藤井博史, 大貫和信, 高島大輝, 古賀宣勝, 津村遼, 松村保広, 羽場宏光, Wang Yang, Kaustab Ghosh, 小森有希子, 横北卓也, 森大輝, 眞鍋史乃 (ポスター発表), 「医療施設での α 線放出核種 ^{211}At の測定系の構築」, 日本分子イメージング学会第 14 回総会・学術集会, 札幌, 2019 年 5 月 23-24 日.

本村信治, 喜井勲, 羽場宏光, 薬師寺秀樹, 渡辺恭良, 榎本秀一 (口頭発表), 「半導体コンプトンカメラ GREI による Na^+/K^+ の同時イメージング」, 日本分子イメージング学会第 14 回総会・学術集会, 札幌, 2019 年 5 月 23-24 日.

森大輝, 横北卓也, 小森有希子, 玉洋, 羽場宏光, 神田晃充, 脇谷雄一郎, 松本幹雄, 木村俊夫 (口頭発表), 「理研における頒布用精製 $^{42,43}\text{K}$ および $^{44\text{m}}\text{Sc}$ の製造技術開発」, 第 56 回アイソトープ・放射線研究発表会, 文京, 2019 年 7 月 3-5 日.

重河優大 (口頭発表), 「 $^{235\text{m}}\text{U}$ と $^{229\text{m}}\text{Th}$ の内部転換過程に対する化学効果」, 第 58 回核化学夏の学校, 由布, 2019 年 9 月 11-14 日.

小森有希子 (口頭発表), 「理研の核化学研究環境」, 第 58 回核化学夏の学校, 由布, 2019 年 9 月 11-14 日.

齋藤萌美, 合川正幸, 坂口理哉, 右近直之, 小森有希子, 羽場宏光, タカチサンドール (口頭発表), 「荷電粒子入射反応における医療用放射性核種 ^{169}Yb 生成断面積測定実験」, 日本原子力学会 2019 年秋の大会, 富山, 2019 年 9 月 11-13 日.

村田朋大, 合川正幸, 坂口理哉, 羽場宏光, 小森有希子, タカチサンドール, フェレンチデイトロイ, ブーチゾルタン (口頭発表), 「Dy 標的へのアルファ粒子照射による ^{166}Ho の励起関数測定」, 日本原子力学会 2019 年秋の大会, 富山, 2019 年 9 月 11-13 日.

坂口理哉, 合川正幸, 齋藤萌美, 右近直之, 小森有希子, 羽場宏光 (口頭発表), 「 ^{89}Zr 生成を目的とした ^{89}Y 箔への重陽子照射における生成断面積の測定」, 日本原子力学会 2019 年秋の大会, 富山, 2019 年 9 月 11-13 日.

I. Dagvadorj, M. Aikawa, T. Zolbadral, Y. Komori, H. Haba (口頭発表), 「Production cross sections of dysprosium radioisotopes in deuteron-induced reactions on natural terbium up to 24 MeV」, 日本原子力学会 2019 年秋の大会, 富山, 2019 年 9 月 11-13 日.

羽場宏光 (招待講演), 「新元素化学の展望」, 日本物理学会 2019 年秋季大会, 山形, 2019 年 9 月 17-20 日.

庭瀬暁隆, 和田道治, P. Schury, 伊藤由太, 木村創太, 加治大哉, M. Rosenbusch, 渡辺裕, 平山賀一, 宮武宇也, J. Y. Moon, 石山博恒, 森本幸司, 羽場宏光, 田中泰貴, 石澤倫, 高峰愛子, 森田浩介, H. Wollnik (口頭発表), 「MRTOF-MS を用いた ^{207}Ra の精密質量-崩壊特性測定」, 日本物理学会 2019 年秋季大会, 山形, 2019 年 9 月 17-20 日.

増田孝彦, Kjeld Beeks, 羽場宏光, 原秀明, 平木貴宏, 藤枝亮, 藤本弘之, 鈴木健太, 海野弘行, 笠松良崇, 北尾真司, 小無健司, 宮本祐樹, 岡井晃一, 笹尾登, 佐藤帯子, Thorsten Schumm, 瀬戸誠, 重河優大, Simon Stellmer, 玉作賢治, 植竹智, 渡部信, 渡部司, 山口敦史, 安田勇輝, 依田芳卓, 吉見彰洋, 吉村浩司, 吉村太彦 (口頭発表), 「トリウム ^{229}Th 原子核異性体からの真空紫外光観測の現状」, 日本物理学会 2019 年秋季大会, 山形, 2019 年 9 月 17-20 日.

渡邊瑛介, 速水翔, 東内克馬, 笠松良崇, 北河康隆, 重河優大, 横北卓也, 中野雅由, 篠原厚 (ポスター発表), 「硝酸中における Zr, Hf および Th の錯形成に関する実験・理論研究—超重元素 Rf の化学研究に向けて—」, 第 13 回分子科学討論会 2019 名古屋, 名古屋, 2019 年 9 月 17-20 日.

早川優太, 坂口綾, 村田真優, 松村夏紀, 藤沼修平, 中島朗久, 笠松良崇, 篠原厚, 小森有希子, 横北卓也, 森大輝, 矢納慎也, 羽場宏光, 横山明彦 (口頭発表), 「U+p 及び Th+Li 反応による Np 同位体励起関数の作成」, 日本放射化学会第 63 回討論会 (2019), いわき, 2019 年 9 月 24-26 日.

小森有希子, 村上昌史, 羽場宏光 (口頭発表), 「 $^{nat}\text{W}(d, x)$ 反応による Re 同位体の励起関数と半減期の測定」, 日本放射化学会第 63 回討論会 (2019), いわき, 2019 年 9 月 24-26 日.

Y. Wang, N. Sato, Y. Komori, T. Yokokita, D. Mori, S. Usuda, H. Haba (口頭発表), 「Production of At-211 at RIKEN」, 日本放射化学会第 63 回討論会 (2019), いわき, 2019 年 9 月 24-26 日.

横北卓也, 笠松良崇, 渡邊瑛介, 小森有希子, 二宮秀美, 玉洋, 森大輝, ゴーシュコースタフ, 篠原厚, 羽場宏光 (口頭発表), 「硫酸系における Rf の陰イオン交換」, 日本放射化学会第 63 回討論会 (2019), いわき, 2019 年 9 月 24-26 日.

渡邊瑛介, 速水翔, 東内克馬, 二宮秀美, 笠松良崇, 北河康隆, 重河優大, 横北卓也, 中野雅由, 篠原厚 (口頭発表), 「Zr, Hf, Th の硝酸錯体形成に関する実験および理論研究 Rf の化学に向けて」, 日本放射化学会第 63 回討論会 (2019), いわき, 2019 年 9 月 24-26 日.

速水翔, 二宮秀美, 渡邊瑛介, 重河優大, 永瀬将浩, 笠松良崇, 近藤成美, 羽場宏光, 横北卓也, 小森有希子, 森大輝, 玉洋, ゴーシュコースタフ, 佐藤望, 篠原厚 (口頭発表), 「水酸化サマリウム共沈法を用いた 102 番元素ノーベリウムの沈殿実験」, 日本放射化学会第 63 回討論会 (2019), いわき, 2019 年 9 月 24-26 日.

重河優大, 笠松良崇, 山北佳宏, 金子政志, 渡邊雅之, 渡邊瑛介, 安田勇輝, 近藤成美, 篠原厚 (口頭発表), 「酸化物・フッ化物・塩化物系における U-235m の半減期および内部転換電子エネルギースペクトルの測定」, 日本放射化学会第 63 回討論会 (2019), いわき, 2019 年 9 月 24-26 日.

重河優大, 笠松良崇, 渡邊瑛介, 安田勇輝, 近藤成美, 二宮秀美, 速水翔, 羽場宏光, 篠原厚 (口頭発表), 「Ac-229 の β 線—電子同時計数測定による Th-229m の内部転換電子の観測」, 日本放射化学会第 63 回討論会 (2019), いわき, 2019 年 9 月 24-26 日.

庭瀬暁隆, 和田道治, P. Schury, 伊藤由太, 木村創太, 加治大哉, M. Rosenbusch, 渡辺裕, 平山賀一, 宮武宇也, J. Y. Moon, 石山博恒, 森本幸司, 羽場宏光, 田中泰貴, 石澤倫, 高峰愛子, 森田浩介, H. Wollnik (口頭発表), 「MRTOF + α -TOF を用いた ^{207}Ra の質量-崩壊特性測定」, 日本放射化学会第 63 回討論会 (2019), いわき, 2019 年 9 月 24-26 日.

雨倉啓, 秋山和彦, 羽場宏光, 久富木志郎 (口頭発表), 「ランタノイド内包フラーレン ($\text{Ln}^{3+}@\text{C}_{82}^{3-}$) における内包金属原子が炭素ケージに及ぼす振動的影響」, 日本放射化学会第 63 回討論会 (2019), いわき, 2019 年 9 月 24-26 日.

青井景都, 新裕貴, 川崎康平, 東美里, 鷺山幸信, 西中一郎, 羽場宏光, 森大輝, Yang Wang, 横山明彦 (ポスター発表), 「Rn-211/At-211

- ジェネレータシステムに必要な ^{207}Po 除去法の検討, 日本放射化学会第 63 回討論会 (2019), いわき, 2019 年 9 月 24–26 日.
- 安達サディア, 末木啓介, 豊嶋厚史, 塚田和明, 羽場宏光, 小森有希子, 横北卓也, 森大輝 (ポスター発表), 「HF/HNO₃ 水溶液中における Nb, Ta, Pa の陰イオン交換実験~Db フッ化物錯体の推定に向けて~」, 日本放射化学会第 63 回討論会 (2019), いわき, 2019 年 9 月 24–26 日.
- 森田涼雅, 早川優太, 小森有希子, 横北卓也, 森大輝, 羽場宏光, 笠松良崇, 篠原厚, 横山明彦 (ポスター発表), 「 ^{239}Np 複合核系における核分裂断面積測定による軌道角運動量の推定」, 日本放射化学会第 63 回討論会 (2019), いわき, 2019 年 9 月 24–26 日.
- 横北卓也 (口頭発表), 「新規ガンマ線イメージング用プローブ K-42, K-43 及び Sc-44m の製造」, 第二回 Chemical Probe 合同合宿セミナー, 嵐山町, 2019 年 10 月 8–9 日.
- 小森有希子 (ポスター発表), 「有用 RI プローブ製造に向けた核反応励起関数の測定」, 第二回 Chemical Probe 合同合宿セミナー, 嵐山町, 2019 年 10 月 8–9 日.
- Y. Wang (ポスター発表), 「Production of a therapeutic isotope, astatine-211 at RIBF」, 第二回 Chemical Probe 合同合宿セミナー, 嵐山町, 2019 年 10 月 8–9 日.
- 羽場宏光 (招待講演), 「新元素を探そう!」, 日本化学会 君たちの将来と化学の未来 東大で過ごす化学な週末, 文京, 2019 年 10 月 20 日.
- 羽場宏光 (招待講演), 「113 番ニホニウムの発見」, 国際周期表年 2019 特別展オープニングイベント, 山形, 2019 年 11 月 3 日.
- 花岡宏史, 大島康宏, 鈴木博元, 佐々木一郎, 渡辺茂樹, 羽場宏光, 荒野泰, 石岡典子, 対馬義人 (口頭発表), 「At-211 標識 α メチルフェニルアラニンを用いた内用放射線療法」, 日本核医学会第 61 回学術総会, 松山, 2019 年 11 月 4–6 日.
- 羽場宏光 (招待講演), 「元素をつくろう!」, サイエンスアゴラ国際周期表年特別企画元素検定 2019@東京, 江東, 2019 年 11 月 16 日.
- 羽場宏光 (招待講演), 「ラジオアイソトープの製造と応用—新元素の探索からがんの診断・治療まで—」, 2019 年度日本アイソトープ協会シンポジウム「PET・イメージング研究の最前線~ライフサイエンスと理工学の融合~」, 川崎, 2019 年 11 月 22 日.
- 高橋和也 (基調講演), 「極微量の硫黄同位体比分析による, 遺跡から出土した水銀朱の産地同定」, 日本分析化学会 第 370 回ガスクロマトグラフィー研究会特別講演会, 北, 2019 年 11 月 22 日.
- 羽場宏光 (招待講演), 「多光子ガンマ線放出核種の製造」, 「多光子ガンマ線時間/空間相関型断層撮像法の研究」ワークショップ, 港, 2019 年 12 月 6 日.
- 高島大輝, 古賀宣勝, 大貫和信, 眞鍋史乃, 津村遼, 安西高廣, 岩田望, Wang Yang, 横北卓也, 小森有希子, 森大輝, 羽場宏光, 藤井博史, 松村保広 (ポスター発表), 「アルファ線放出核種アスタチン-211 を用いた放射免疫療法の開発」, 第 5 回 AMED がん若手研究者ワークショップ, 千代田, 2020 年 1 月 9 日.
- 羽場宏光 (招待講演), 「理研におけるラジオアイソトープの製造と応用~新元素の探索からがんの診断・治療まで~」, 第 75 回放射線計測研究会, 和光, 2020 年 1 月 18 日.
- 高橋浩之, 島添健次, 鎌田圭, 羽場宏光, 百瀬敏光 (口頭発表), 「多光子ガンマ線時間・空間相関型イメージング法の研究 1 (概要)」, 2020 年第 67 回応用物理学会春季学術講演会, 千代田, 2020 年 3 月 12–15 日.
- 鎌田圭, 金敬鎮, 吉野将生, 庄子育宏, 山路晃弘, 黒澤俊介, 横田有為, 大橋雄二, 島添健次, 高橋美和子, 羽場宏光, 百瀬敏光, 高橋浩之, 吉川彰 (口頭発表), 「多光子ガンマ線時間・空間相関型イメージング法の研究 2 (シンチレータ開発)」, 2020 年第 67 回応用物理学会春季学術講演会, 千代田, 2020 年 3 月 12–15 日.
- 羽場宏光, 森大輝, 小森有希子, 横北卓也, 王洋, 高橋浩之, 島添健次, 鎌田圭, 百瀬敏光, 高橋美和子 (口頭発表), 「多光子ガンマ線時間・空間相関型イメージング法の研究 3 (RI 製造)」, 2020 年第 67 回応用物理学会春季学術講演会, 千代田, 2020 年 3 月 12–15 日.
- 大鐘健一郎, 井下敏孝, 岡崎紀雄, 古山桂太郎, 高橋美和子, 百瀬敏光, 高橋浩之, 島添健次, 鎌田圭, 羽場宏光 (口頭発表), 「多光子ガンマ線時間・空間相関型イメージング法の研究 4 (医療応用)」, 2020 年第 67 回応用物理学会春季学術講演会, 千代田, 2020 年 3 月 12–15 日.
- 上ノ町水紀, Zhong Zhihong, 大鐘健一郎, 島添健次, 高橋浩之, 鎌田圭, 羽場宏光, 高橋美和子, 百瀬敏光 (口頭発表), 「多光子ガンマ線時間・空間相関型イメージング法の研究 5 (システム開発)」, 2020 年第 67 回応用物理学会春季学術講演会, 千代田, 2020 年 3 月 12–15 日.
- 小澤直也, 長濱弘季, 早水友洋, 中村圭佑, 小高康熙, 田中香津生, 大塚未来, 小森有希子, 市川雄一, 羽場宏光, 上野秀樹, 酒見泰寛 (口頭発表), 「フランシウム原子の電気双極子能率探索のための表面電離イオン源の開発」, 日本物理学会第 75 回年次大会 (2020 年), 名古屋, 2020 年 3 月 16–19 日.
- 坂東佑星, 青木匠, 櫻井博儀, 新倉潤, 鈴木大介, 羽場宏光 (口頭発表), 「放射化法による多中性子原子核の探索」, 日本物理学会第 75 回年次大会 (2020 年), 名古屋, 2020 年 3 月 16–19 日.
- 海野弘行, 羽場宏光, 原秀明, 平木貴宏, 藤枝亮, 藤本弘之, 笠松良崇, 北尾真司, 小無健司, 増田孝彦, 宮本祐樹, 岡井晃一, 笹尾登, Kjeld Beeks, Thorsten Schumm, 瀬戸誠, 重河優大, A. Simon Stellmer, 玉作賢治, 植竹智, 渡部信, 渡部司, 山口敦史, 安田勇輝, 依田芳卓, 吉見彰洋, 吉村浩司, 吉村太彦 (口頭発表), 「トリウム 229 アイソマー準位からの真空紫外光の探索」, 日本物理学会第 75 回年次大会 (2020 年), 名古屋, 2020 年 3 月 16–19 日.
- 庭瀬暁隆, 和田道治, P. Schury, 伊藤由太, 木村創大, 加治大哉, M. Rosenbusch, 渡辺裕, 平山賀一, 宮武宇也, J. Y. Moon, 石山博恒, 森本幸司, 羽場宏光, 田中泰貴, 石澤倫, 飯村俊, 高峰愛子, 森田浩介, H. Wollnik (口頭発表), 「MRTOF+ α -TOF を用いた短寿命 α 崩壊核種の質量-崩壊特性測定」, 日本物理学会第 75 回年次大会 (2020 年), 名古屋, 2020 年 3 月 16–19 日.

Awards

- 森大輝, 「理研における頒布用精製 $^{42,43}\text{K}$ および ^{44m}Sc の製造技術開発」, 第 56 回アイソトープ・放射線研究発表会 若手優秀講演賞, 2019 年 7 月 4 日.
- N. Sato, “Awards the Element NIHONIUM”, Periodic Table of Younger Chemists, International Union of Pure and Applied Chemistry,

July 8, 2019.

中野貴志, 東達也, 羽場宏光, 齊藤直人, 松原雄二, 「先導的な量子ビーム応用によるスマートな健康長寿社会の創出」, 内閣府 第2回日本オープンイノベーション大賞日本学術会議会長賞, 2020年2月15日.

Press releases

自然界で最小の励起エネルギーをもつ原子核状態の人工的生成に成功—超精密「原子核時計」実現に大きく前進—, 理化学研究所, 2019年9月11日. https://www.riken.jp/press/2019/20190912_1/.

トリウム原子核の精密レーザー分光実現へ重要な一歩—トリウム 229 アイソマー状態のエネルギーを決定—, 理化学研究所, 2019年11月29日. https://www.riken.jp/press/2019/20191129_2/.

Accelerator Applications Research Division

RI Application Research Group

Industrial Application Research Team

1. Abstract

Industrial application research team handles non-academic activities at RIBF corresponding mainly to industries.

2. Major Research Subjects

- (1) Support of industrial utilization of the RIBF accelerator beam.
- (2) Development of technologies related to the industrial utilization and novel industrial applications.
- (3) Fee-based distribution of radioisotopes produced at RIKEN AVF Cyclotron.
- (4) Development of real-time wear diagnostics of industrial material using RI beams.

3. Summary of Research Activity

(1) Support of Industrial Utilization of RIBF

RNC promote facility-sharing program “Promotion of applications of high-energy heavy ions and RI beams.” In this program, RNC opens a part of the RIBF facility, which includes the AVF cyclotron, RILAC, RIKEN Ring Cyclotron and experimental instruments, to non-academic proposals from users including private companies. The proposals are reviewed by a program advisory committee, industrial PAC (IN-PAC). The proposals which have been approved by the IN-PAC are allocated with beam times and the users pay RIKEN the beam time fee. The intellectual properties obtained by the use of RIBF belong to the users. In order to encourage the use of RIBF by those who are not familiar with utilization of ion beams, the first two beam times of each proposal can be assigned to trial uses which are free of beam time fee.

In July 2019, the ninth IN-PAC met and approved two fee-based proposals from new users. In January 2019, IN-PAC held a mail review and approved one fee-based proposal from a continuously using private company. In January and February 2019, four fee-based beam times were performed with Kr-84 (70 MeV/nucleon) and Ar-40 (95 MeV/nucleon) beams at the E5A beamline. The client used the beam to simulate single-event effects of space-use semi-conductors by heavy-ion components of cosmic rays.

(2) Development of technologies related to the industrial utilization and novel industrial applications

We develop technologies to assess and improve the beam quality. Before each beam time, we measure the properties of the beam; the dependence of the beam energy on the degrader thickness, the beam LET-distribution at a certain depth of an irradiated sample calculated with the energy-loss code (SRIM), and the relation between the beam flux and the reading of a transmission-type detectors. Since the beam is extracted to the atmosphere and passes through materials, it can be contaminated with secondary nuclides produced by nuclear reactions in the materials. We study the beam impurity using radiochemical measurements and compared the results with simulations by the PHITS code. We tested radiochromic films as a new method of two-dimensional dose distribution measurement. We have irradiated two types of radiochromic films using C, Ar, and Fe ions and measured the change of optical density as a function of the dose. We conclude that radiochromic films can be useful to measure the dose distribution of heavy-ion irradiations with a spatial resolution of about 1 mm.

(3) Fee-based distribution of radioisotopes produced at RIKEN AVF Cyclotron

We have been handling fee-based distribution of radioisotopes since 2007. The radionuclides are Zn-65 ($T_{1/2} = 244$ days), Cd-109 (463 days), Y-88 (107 days), Sr-85 (65 days) and Cu-67 (2.58 days) which are produced at the AVF cyclotron by the nuclear chemistry research team. According to a material transfer agreement (MTA) drawn between Japan Radioisotope Association (JRIA) and RIKEN, JRIA mediates the transaction of the RIs and distributes them to users. Details can be found on the online ordering system J-RAM home page of JRIA.

In 2019, we delivered no Cd-109, two shipments of Zn-65 with a total activity of 6.7 MBq, two of Y-88 with a total activity of 2 MBq, and one of Cu-67 with an activity of 5 MBq. The final recipients of the RIs were two universities, one research institute and one medical research center.

(4) Development of real-time wear diagnostics of industrial material using RI beams

We are developing a method to determine the spatial distribution of gamma-ray emitting RIs on periodically-moving objects, named “GIRO” (Gamma-ray Inspection of Rotating Object), that is based on the same principle as the medical PET imaging but is simpler and less expensive. Two pairs of detectors were employed to obtain 3D image data. We also performed single-photon emission computer tomography (SPECT) mode measurement. GIRO can obtain SPECT-mode data together with PET-mode data. This method can be used for real-time inspection of a closed system in a running machine. In 2019, we are developing a portable size GIRO system in order to bring and demonstrate it for private companies.

Members

Team Leader

Atsushi YOSHIDA

Contract Researcher

Tadashi KAMBARA

Technical Staff I

Daiki MORI

List of Publications & Presentations

Presentations

[Domestic conferences/workshops]

吉田敦 (口頭発表), 「加速器施設で発生するイオンビームの非生物系産業利用」, 福井イオンビーム育種研究会, 福井県若狭湾エネルギー研究センター, 敦賀, 2019 年 12 月 13 日.

吉田敦 (口頭発表), 「宇宙時代到来～半導体でも重イオン照射～」, 理研シンポジウム「重イオンビーム育種技術の実用化 20 年」, 和光, 2020 年 1 月 23 日.

Subnuclear System Research Division Quantum Hadron Physics Laboratory

1. Abstract

Atomic nuclei are made of protons and neutrons bound by the exchange of pion and other mesons. Also, protons and neutrons are made of quarks bound by the exchange of gluons. These strong interactions are governed by the non-Abelian gauge theory called the quantum chromodynamics (QCD). On the basis of theoretical and numerical analyses of QCD, we study the interactions between the nucleons, properties of the dense quark matter realized at the center of neutron stars, and properties of the hot quark-gluon plasma realized in the early Universe. Strong correlations common in QCD and cold atoms are also studied theoretically to unravel the universal features of the strongly interacting many-body systems. Developing perturbative and non-perturbative techniques in quantum field theory and string theory are of great importance not only to solve gauge theories such as QED and QCD, but also to find the theories beyond the standard model of elementary particles. Various theoretical approaches along this line have been attempted.

2. Major Research Subjects

- (1) Perturbative and non-perturbative methods in quantum field theories
- (2) Theory of spontaneous symmetry breaking
- (3) Lattice gauge theory
- (4) QCD under extreme conditions
- (5) Nuclear and atomic many-body problems

3. Summary of Research Activity

(1) Perturbative and non-perturbative methods in quantum field theories

(1-1) Theory of the Anomalous Magnetic Moment of the Electron

The anomalous magnetic moment of the electron a_e measured in a Penning trap occupies a unique position among high precision measurements of physical constants in the sense that it can be compared directly with the theoretical calculation based on the renormalized quantum electrodynamics (QED) to high orders of perturbation expansion in the fine structure constant α , with an effective parameter α/π . Both numerical and analytic evaluations of a_e up to $(\alpha/\pi)^4$ were firmly established. The coefficient of $(\alpha/\pi)^5$ has been obtained recently by an extensive numerical integration. The contributions of hadronic and weak interactions have also been estimated. The sum of all these terms leads to $a_e(\text{theory}) = 1\,159\,652\,181.606(11)(12)(229) \times 10^{-12}$, where the first two uncertainties are from the tenth-order QED term and the hadronic term, respectively. The third and largest uncertainty comes from the current best value of the fine-structure constant derived from the cesium recoil measurement: $\alpha^{-1}(\text{Cs}) = 137.035\,999\,046(27)$. The discrepancy between $a_e(\text{theory})$ and $a_e(\text{experiment})$ is 2.4σ . Assuming that the standard model is valid so that $a_e(\text{theory}) = a_e(\text{experiment})$ holds, we obtained $\alpha^{-1}(a_e) = 137.035\,999\,1496(13)(14)(330)$, which is nearly as accurate as $\alpha^{-1}(\text{Cs})$. The uncertainties are from the tenth-order QED term, hadronic term, and the best measurement of a_e , in this order.

(1-2) Optimized perturbation theory and its relation to anti-Stokes lines

We discussed fundamental properties of the fastest apparent convergence (FAC) condition which is used as a variational criterion in optimized perturbation theory (OPT). We examine an integral representation of the FAC condition and a distribution of the zeros of the integral in a complex artificial parameter space on the basis of theory of Lefschetz thimbles. We find that the zeros accumulate on a certain line segment known as an anti-Stokes line in the limit $K \rightarrow \infty$, where K is a truncation order of a perturbation series. This phenomenon gives an underlying mechanism that physical quantities calculated by OPT can be insensitive to the choice of the artificial parameter.

(1-3) Perturbative static quark potential in Maximal Abelian gauge

One of the most interesting features of QCD is its peculiar behavior at low energies, where it displays confinement. Among the many explanations proposed for this phenomenon, one of the more interesting approaches utilizes its similarity to the behavior of a magnetic field in a type II superconductor. The magnetic field cannot penetrate the superconductor except for narrow flux tubes, much like the chromoelectric field extends only between confined particles, and if there existed elementary magnetic charges, they would be confined inside a superconductor much like quarks in the vacuum. We calculated the static quark potential for an SU(N) gauge theory in the Maximal Abelian gauge as well as its Abelian projection up to two loops in perturbation theory, and we discussed its renormalization properties.

(1-4) Lorentzian conformal field theories through sine-square deformation

In quantum field theories, symmetry plays an essential and exceptional role. Focusing on some proper symmetry and delving into its meaning have been proven to be one of the most fruitful strategies. We reexamined two-dimensional Lorentzian conformal field theory using the formalism previously developed in a study of sine-square deformation of Euclidean conformal field theory. We construct three types of Virasoro algebra. One of them reproduces the result by Lüscher and Mack, while another type exhibits the divergence in the central charge term. The other leads the continuous spectrum and contains no closed time-like curve in the system.

(2) Theory of spontaneous symmetry breaking

(2-1) Effective Lagrangian for Nambu-Goldstone modes in nonequilibrium open systems

We developed the effective field theory of diffusive Nambu-Goldstone (NG) modes associated with spontaneous internal symmetry breaking taking place in nonequilibrium open systems. The effective Lagrangian describing semi-classical dynamics of the NG modes

is derived and matching conditions for low-energy coefficients are also investigated. Due to new terms peculiar to open systems, the associated NG modes show diffusive gapless behaviors in contrast to the propagating NG mode in closed systems. We demonstrate two typical situations relevant to the condensed matter physics and high-energy physics, where diffusive type-A or type-B NG modes appear.

(2-2) Spontaneous symmetry breaking and Nambu-Goldstone modes in open classical and quantum systems

Spontaneous symmetry breaking (SSB) in Hamiltonian systems is a universal and widely observed phenomena in nature, *e.g.*, the electroweak and chiral symmetry breakings, superconductors, ferromagnets, solid crystals, and so on. It is also known that the SSB occurs even in dissipative systems such as reaction diffusion system and active matters. We discussed spontaneous symmetry breaking of open classical and quantum systems. When a continuous symmetry is spontaneously broken in an open system, a gapless excitation mode appears corresponding to the Nambu-Goldstone mode. Unlike isolated systems, the gapless mode is not always a propagation mode, but it is a diffusion one. Using the Ward-Takahashi identity and the effective action formalism, we establish the Nambu-Goldstone theorem in open systems, and derive the low-energy coefficients that determine the dispersion relation of Nambu-Goldstone modes. Using these coefficients, we classify the Nambu-Goldstone modes into four types: type-A propagation, type-A diffusion, type-B propagation, and type-B diffusion modes.

(3) Lattice gauge theory

(3-1) $N\Omega$ dibaryon from lattice QCD near the physical point

The nucleon(N)-Omega(Ω) system in the S-wave and spin-2 channel was studied from the (2+1)-flavor lattice QCD with nearly physical quark masses. The time-dependent HAL QCD method is employed to convert the lattice QCD data of the two-baryon correlation function to the baryon-baryon potential and eventually to the scattering observables. The potential, obtained under the assumption that its couplings to the D-wave octet-baryon pairs are small, is found to be attractive in all distances and to produce a quasi-bound state near unitarity. Including the extra Coulomb attraction, the binding energy of becomes 2.5 MeV. Such a spin-2 state could be searched through two-particle correlations in p-p, p-nucleus and nucleus-nucleus collisions.

(3-2) $\Lambda\Lambda$ and $N\Xi$ interactions from lattice QCD near the physical point

The S-wave $\Lambda\Lambda$ and $N\Xi$ interactions were studied on the basis of the (2+1)-flavor lattice QCD simulations close to the physical point. Lattice QCD potentials in four different spin-isospin channels are extracted by using the coupled-channel HAL QCD method and are parametrized by analytic functions to calculate the scattering phase shifts. The $\Lambda\Lambda$ interaction at low energies shows only a weak attraction, which does not provide a bound or resonant dihyperon. The $N\Xi$ interaction in the spin-singlet and isospin-singlet channel is most attractive and lead the $N\Xi$ system near unitarity. Relevance to the strangeness = -2 hypernuclei as well as to two-baryon correlations in proton-proton, proton-nucleus and nucleus-nucleus collisions was also discussed.

(3-3) Stress tensor around static quark-anti-quark from Yang-Mills gradient flow

The spatial distribution of the stress tensor around the quark-anti-quark pair in SU(3) lattice gauge theory was studied. The Yang-Mills gradient flow plays a crucial role to make the stress tensor well-defined and derivable from the numerical simulations on the lattice. The resultant stress tensor with a decomposition into local principal axes shows, for the first time, the detailed structure of the flux tube along the longitudinal and transverse directions in a gauge invariant manner. The linear confining behavior of the potential at long distances is derived directly from the integral of the local stress tensor.

(4) QCD under extreme conditions

(4-1) Finite density QCD based on complex Langevin method

The complex Langevin method (CLM) is one of a promising approach to overcome the sign problem. The central idea of this approach is that the stochastic quantization does not require the probabilistic interpretation of the Boltzmann weight e^{-S} even when the action takes complex values. Although the equivalence between CLM and the familiar path integral quantization is quite nontrivial, it is pointed out that the probability distribution of the drift term can judge the correctness of the CLM. This enable us to perform lattice simulation of QCD based on CLM in the finite density region in a self-contained manner. We discussed the applicability of the CLM with four-flavor staggered fermions on a $8^3 \times 16$ lattice with quark mass $m = 0.01$. In particular, we focus on the behavior of the eigenvalue distribution of the fermion mass matrix which is closely related to the appearance of the singular drift problem.

(4-2) Non-equilibrium quantum transport of chiral fluids from kinetic theory

We introduced the quantum-field-theory (QFT) derivation of chiral kinetic theory (CKT) from the Wigner-function approach, which manifests side jumps and non-scalar distribution functions associated with Lorentz covariance and incorporates both background fields and collisions. The formalism is utilized to investigate second-order responses of chiral fluids near local equilibrium. Such non-equilibrium anomalous transport is dissipative and affected by interactions. Contributions from both quantum corrections in anomalous hydrodynamic equations (EOM) of motion and those from the CKT and Wigner functions (WF) are considered in a relaxation-time approximation (RTA). Anomalous charged Hall currents engendered by background electric fields and temperature/chemical-potential gradients are obtained. Furthermore, chiral magnetic/vortical effects (CME/CVE) receive viscous corrections as non-equilibrium modifications stemming from the interplay between side jumps, magnetic-moment coupling, and chiral anomaly.

(4-3) Hadron-quark crossover in cold and hot neutron stars

We presented a much improved equation of state for neutron star matter, QHC19, with a smooth crossover from the hadronic regime at lower densities to the quark regime at higher densities. We now use the Togashi *et al.* equation of state, a generalization of the Akmal-Pandharipande-Ravenhall equation of state of uniform nuclear matter, in the entire hadronic regime; the Togashi equation of state consistently describes nonuniform as well as uniform matter, and matter at beta equilibrium without the need for an interpolation between pure neutron and symmetric nuclear matter. We describe the quark matter regime at higher densities with the Nambu-Jona-

Lasinio model, now identifying tight constraints on the phenomenological universal vector repulsion between quarks and the pairing interaction between quarks arising from the requirements of thermodynamic stability and causal propagation of sound. The resultant neutron star properties agree very well with the inferences of the LIGO/Virgo collaboration, from GW170817, of the pressure versus baryon density, neutron star radii, and tidal deformabilities. The maximum neutron star mass allowed by QHC19 is 2.35 MS, consistent with all neutron star mass determinations.

(5) Nuclear and atomic many-body problems

(5-1) Renormalized random-phase approximation

A fully self-consistent renormalized random-phase approximation was constructed based on the self-consistent Hartree-Fock mean field plus exact pairing solutions (EP). This approach exactly conserves the particle number and restores the energy-weighted sum rule, which is violated in the conventional renormalized particle-hole random-phase approximation for a given multipolarity. The numerical calculations are carried out for several light-, medium-, and heavy-mass nuclei such as O22, Ni60, and Zr90 by using the effective MSk3 interaction. To study the pygmy dipole resonance (PDR), the calculations are also performed for the two light and neutron-rich O24,28 isotopes, whose PDRs are known to be dominant. The results obtained show that the inclusion of ground-state correlations beyond the random-phase approximation (RPA) by means of the occupation numbers obtained from the EP affects the RPA solutions within the whole mass range, although this effect decreases with increasing the mass number. At the same time, the antipairing effect is observed via a significant reduction of pairing in neutron-rich nuclei. The enhancement of PDR is found in most neutron-rich nuclei under consideration within our method.

(5-2) Ab initio covariant density functional theory for nuclear structure

Nuclear structure models built from phenomenological mean fields, the effective nucleon-nucleon interactions (or Lagrangians), and the realistic bare nucleon-nucleon interactions were presented. The success of covariant density functional theory (CDFT) to describe nuclear properties and its influence on Brueckner theory within the relativistic framework are focused upon. The challenges and ambiguities of predictions for unstable nuclei without data or for high-density nuclear matter, arising from relativistic density functionals, are discussed. The basic ideas in building an ab initio relativistic density functional for nuclear structure from ab initio calculations with realistic nucleon-nucleon interactions for both nuclear matter and finite nuclei are presented. The current status of fully self-consistent relativistic Brueckner-Hartree-Fock (RBHF) calculations for finite nuclei or neutron drops (ideal systems composed of a finite number of neutrons and confined within an external field) is reviewed. The guidance and perspectives towards an ab initio covariant density functional theory for nuclear structure derived from the RBHF results are provided.

(5-3) QCD-like phase diagram with Efimov trimers and Cooper pairs

We investigated color superfluidity and trimer formation in resonantly interacting SU(3) Fermi gases with a finite interaction range. The finite range is crucial to avoid the Thomas collapse and treat the Efimov effect occurring in this system. Using the Skorniakov-Ter-Martirosian equation with medium effects, we show the effects of the atomic Fermi distribution on the Efimov trimer energy at finite temperature. We show the critical temperature of color superfluidity within the many-body T-matrix approximation. In this way, we can provide a first insight into the phase diagram as a function of the temperature T and the chemical potential μ . This phase diagram consists of trimer, normal, and color-superfluid phases, and is similar to that of quantum chromodynamics at finite density and temperature.

(5-4) Superfluid phase transitions in asymmetric nuclear matter

We investigated superfluid phase transitions of asymmetric nuclear matter at finite temperature (T) and density (ρ) with a low proton fraction ($Y_p \leq 0.2$), which is relevant to the inner crust and outer core of neutron stars. A strong-coupling theory developed for two-component atomic Fermi gases is generalized to the four-component case, and is applied to the system of spin-1/2 neutrons and protons. The phase shifts of neutron-neutron (nn), proton-proton (pp) and neutron-proton (np) interactions up to $k = 2 \text{ fm}^{-1}$ are described by multi-rank separable potentials. We show that the critical temperature T_{nn}^C of the neutron superfluidity at $Y_p = 0$ agrees well with Monte Carlo data at low densities and takes a maximum value $T_{nn}^C = 1.68 \text{ MeV}$ at $\rho/\rho_0 = 0.14$ with $\rho_0 = 0.17 \text{ fm}^{-3}$. Also, the critical temperature T_{nn}^C of the proton superconductivity for $Y_p \leq 0.2$ is substantially suppressed at low densities due to np-pairing fluctuations, and starts to dominate over T_{nn}^C only above $\rho/\rho_0 = 0.70(0.77)$ for $Y_p = 0.1(0.2)$, and (iii) the deuteron condensation temperature T_d^C is suppressed at $Y_p \leq 0.2$ due to a large mismatch of the two Fermi surfaces.

(5-5) One-dimensional Bose and Fermi gases with contact interactions

One-dimensional spinless Bose and Fermi gases with contact interactions have the close relationship via Girardeau's Bose-Fermi mapping, leading to the correspondences in their energy spectra and thermodynamics. However, correlation functions are in general not identical between these systems. We derive in both systems the universal relations for correlation functions, which hold for any energy eigenstate and any statistical ensemble of the eigenstates. These relations include the large-momentum tails of static structure factors and of momentum distributions as well as energy relations, which connect the sums of kinetic and interaction energies to the momentum distributions. The relations involve two- and three-body contacts, which measure local two- and three-body correlations, respectively. We clarified how the relations for bosons and fermions differ and are connected with each other. In particular, we found that the three-body contact makes no contribution to the bosonic energy relation, but it plays a crucial role in fermionic one.

Members**Director**

Tetsuo HATSUDA

Vice Chief Scientist

Tsukasa TADA

Research/Technical Scientists

Takumi DOI (Senior Research Scientist)

Yoshimasa HIDAKA (Senior Research Scientist)

Pascal Raphaël Gabriel NAIDON (Senior Research Scientist)

Haozhao LIANG (Senior Research Scientist)

Senior Scientist

Makiko NIO

Contract Researcher

Dang NGUYEN DINH

Special Postdoctoral Researchers

Tomoya HAYATA

Matthias W.G. BERWEIN

Takahiro DOI

Shinya GONGYO

Kazuya MAMEDA

Enrico RINALDI

Shoichiro TSUTSUI

Postdoctoral Researcher

Christiane Heike SCHMICKLER

Research Consultant

Takeo INAMI (Sungkyunkwan Univ. (SKKU))

Visiting Scientists

Shinya AOKI (Kyoto Univ.)

Tatsumi AOYAMA (KEK)

Gergely P. FEJOS (Eotvos Lorand Univ.)

Kenji FUKUSHIMA (Univ. of Tokyo)

Hideki HAMAGAKI (Nagasaki Inst. of Applied Sci.)

Koji HASHIMOTO (Osaka Univ.)

Masashi HAYAKAWA (Nagoya Univ.)

Tomoya HAYATA (Keio Univ.)

Yoichi IKEDA (Kyushu Univ.)

Takashi INOUE (Nihon Univ.)

Noriyoshi ISHII (Osaka Univ.)

Yoichi KAZAMA (Univ. of Tokyo)

Ivan KOSTOV (Inst. de Phys. Theorique)

Tetsuo MATSUI (The Open Univ. of Japan)

Takayuki MATSUKI (Tokyo Kasei Univ.)

Takaya MIYAMOTO (NEC Corporation)

Kenji MORITA (QST)

Masaki MURATA (Japan Univ. Economics)

Atsushi NAKAMURA (Hiroshima Univ.)

Takashi NAKATSUKASA (Tsukuba Univ.)

Hung NGUYEN (Duy Tan Univ.)

Yoji OHASHI (Keio Univ.)

RHINE KUMAR ARAYAKKANDI KEECH (Cochin Univ. of
Sci. and Tech.)

Norisuke SAKAI (Keio Univ.)

Kenji SASAKI (Kyoto Univ.)

Shoichi SASAKI (Tohoku Univ.)

Hiroshi SUZUKI (Kyushu Univ.)

Motoi TACHIBANA (Saga Univ.)

Sachiko TAKEUCHI (Japan College of Social Work)

Makoto TAKIZAWA (Showa Pharmaceutical Univ.)

Hiroshi TOKI (Osaka Univ.)

Di-Lun YANG (Keio Univ.)

Visiting Researchers

Yuta SEKINO (JSPS)

Hiroyuki TAJIMA (Kochi Univ.)

Student Trainees

Yutaro AKAHOSHI (Kyoto Univ.)

Asahi CHIKAOA (Univ. of Tokyo)

Yixin GUO (Univ. of Tokyo)

Xun LIU (Univ. of Tokyo)

Yan LYU (Peking Univ.)

Kotaro MURAKAMI (Kyoto Univ.)

Tomoya NAITO (Univ. of Tokyo)

Hikaru SAKAKIBARA (Univ. of Tokyo)

Ziting SUN (Univ. of Sci. and Tech. of China)

Hui TONG (Peking Univ.)

Zhenyu WANG (Nankai Univ.)

Tingyu ZHANG (Univ. of Sci. and Tech. of China)

Subnuclear System Research Division Strangeness Nuclear Physics Laboratory

1. Abstract

We proposed accurate calculation method called ‘Gaussian Expansion Method using infinitesimally shifted Gaussian lobe basis function.’ When one proceeds to four-body systems, calculation of the Hamiltonian matrix elements becomes much laborious. In order to make the four-body calculation tractable even for complicated interactions, the infinitesimally-shifted Gaussian lobe basis function has been proposed. The GEM with the technique of infinitesimally-shifted Gaussians has been applied to various three-, four- and five-body calculations in hypernuclei, the four-nucleon systems, and cold-atom systems. As results, we succeeded in extracting new understandings in various fields.

2. Major Research Subjects

- (1) Hypernuclear structure from the view point of few-body problem
- (2) Structure of exotic hadron system
- (3) quantum atomic system and ultra cold atomic system
- (4) Equation of state for neutron star

3. Summary of Research Activity

- (1) With use of ΞN interaction based on HAL Lattice QCD, we predict to have a bound state for $NN\Xi$ four-body system which would be the lightest bound Ξ hypernucleus. We also propose how to produce this hypernucleus.
- (2) Several compact ssscc-bar pentaquark resonances are predicted quark model, that is, $J^{\pi} = 1/2^{-}$ ($E = 5180$ MeV, $\Gamma = 20$ MeV), $5/2^{-}$ (5645 MeV, 30 MeV), $5/2^{-}$ (5670 MeV, 50 MeV), and $1/2^{+}$ (5360 MeV, 80 MeV). These are the candidates of compact pentaquark resonance states from the current best quark model, which should be confirmed either by experiments or lattice QCD calculations.
- (3) Mixtures of two kinds of fermions, such as spin up and down electrons in materials, are well-known to lead to pairing and superconductivity. In this project, study mixtures of three different kinds of fermions were studied. In these systems, in addition to pairing, a new kind of clustering by three can appear due the Efimov effect. We obtained the phase diagram of these systems and showed that it is similar to that of QCD, where the hadron phase is the analogue of the phase of Efimov clusters of three fermions.

Members

Director

Emiko HIYAMA

Research/Technical Scientists

Pascal NAIDON (Senior Research Scientist)

Special Postdoctoral Researcher /Contract Researcher

Yasuhiro YAMAGUCHI

Special Postdoctoral Researcher

Kadir Utku CAN Takuma YAMASHITA

Postdoctoral Researcher

Christiane H. SCHMICKLER

Senior Visiting Scientist

Makoto OKA (JAEA)

Visiting Scientists

Masayuki ASAKAWA (Osaka Univ.)
 Kadir Utku CAN (The Univ. of Adelaide)
 Jaume CARBONELL (CNRS/IN2P3, IJCLab)
 Lorenzo CONTESSI (Hebrew Univ. of Jerusalem)
 Jiwei CUI (Xidian Univ.)
 Akinobu DOTE (KEK)
 Shimpei ENDO (Tohoku Univ.)
 Tomokazu FUKUDA (Univ. of Electro-Commun.)
 Yasuro FUNAKI (Kanto Gakuin Univ.)
 Takenori FURUMOTO (Yokohama Nat'l Univ.)
 Philipp GUBLER (JAEA)

Satoru HIRENZAKI (Nara Women's Univ.)
 Atsushi HOSAKA (Osaka Univ.)
 Jinniu HU (Nankai Univ.)
 Tetsuo HYODO (Tokyo Metropolitan Univ.)
 Kiyomi IKEDA (Niigata Univ.)
 Masahiro ISAKA (Hosei Univ.)
 Souichi ISHIKAWA (Hosei Univ.)
 Daisuke JIDO (Tokyo Tech)
 Hyun-Chul KIM (Inha Univ.)
 Kei KOTAKE (Fukuoka Univ.)
 Toshio MOTOPA (Univ. of Electro-Commun.)

Takayuki MYO (Osaka Inst. of Tech.)
 Satoshi NAKAMURA (Tohoku Univ.)
 Kazuma NAKAZAWA (Gifu Univ.)
 Hidekatsu NEMURA (Osaka Univ.)
 Jean-Marc RICHARD (Univ. Lyon)
 Thomas RIJKEN (Univ. Of Nijmegen)
 Hans-Josef SCHULZE (INFN)
 Shoji SHINMURA (Gifu Univ.)
 Jirina STONE (Univ. of Tennessee)
 Hajime TOGASHI (Kyushu Univ.)
 Atsushi UMEYA (Nippon Inst. of Tech.)

Shin WATANABE (NIT, Gifu College)
 Wolfram WEISE (TU Munich)
 Chengjun XIA (Zhejiang Univ.)
 Masanobu YAHIRO (Kyushu Univ.)
 Ulugbek YAKHSHIEV (Inha Univ.)
 Taiichi YAMADA (Kanto Gakuin Univ.)
 Yasuo YAMAMOTO (Tsuru Univ.)
 Takuma YAMASHITA (Tohoku Univ.)
 Ying ZHANG (Tianjin Univ.)
 Xian-Rong ZHOU (East China Normal Univ.)

Student Trainees

Kongyi HU (Nankai Univ.)
 Jehee LEE (Tokyo Tech)
 Jie LIU (Nanjing Univ.)

Qi MENG (Nanjing Univ.)
 Qian WU (Nanjing Univ.)

Part-time Worker

Yoko FUJITA (Administrative Part-time Worker I)

List of Publications & Presentations

Publications

[Original papers]

- J. Lee, Q. Wu, Y. Funaki, and E. Hiyama, “Three-Body structure of $\Lambda^9\text{Be}$ with $\alpha\alpha\Lambda$ cluster model,” *Few-Body Syst.* **60**, 30 (2019).
 R. Lazauskas, E. Hiyama, and J. Carbonell, “Ab initio calculation of ^5H resonant states,” *Phys. Lett. B* **791**, 335 (2019).
 J. Lee, N. Yamanaka, and E. Hiyama, “Effect of the Pauli exclusion principle in the electric dipole moment of ^9Be with $|\mathcal{A}S| = 1$ interactions,” *Phys. Rev. C* **99**, 055503 (2019).
 E. Hiyama, R. Lazauskas, F. M. Marques, and J. Carbonell, “Modeling ^{19}B as a ^{17}B -n-n three-body system in the unitary limit,” *Phys. Rev. C* **100**, 011603(R) (2019).
 T. -W. Wu, M. -Z. Liu, L. -S. Geng, E. Hiyama, and M. P. Valderrama, “DK, DDK and DDDK molecules-understanding the nature of the D_{s0}^* (2317),” *Phys. Rev. D* **100**, 034209 (2019).
 E. Hiyama, K. Sasaki, T. Miyamaoto, T. Doi, T. Hatsuda, Y. Yamamoto, and T. Rijken, “Possible lightes Ξ hypernucleus with Modern ΞN interaction,” *Phys. Rev. Lett.* **124**, 092501 (2020).
 Y. Shimizu, Y. Yamaguchi, and M. Harada, “Heavy quark spin multiplet structure of $\text{Pc}(4312)$, $\text{Pc}(4440)$, and $\text{Pc}(4457)$,” arXiv:1904.00587 [hep-ph] (2019).
 Y. Yamaguchi, H. G.- Tecocoatz, A. Giachino, A. Hosaka, E. Santopinto, S. Takeuchi, and M. Takizawa, “Pc pentaquarks with chiral tensor and quark dynamics,” *Phys. Rev. D* **101**, 091502 (2020).
 Y. Yamaguchi and N. Yamanaka, “Large electric dipole moment of charged leptons in the standard model,” arXiv:2003.08195 [hep-ph] (2020).
 Q. Meng, E. Hiyama, K. U. Can, P. Gubler, M. Oka, A. Hosaka, and H. Zong, “Compact sssc pentaquark states predicted by a quark model,” *Phys. Lett. B* **798**, 135028 (2019).
 P. Froelich, T. Yamashita, Y. Kino, S. Jonsell, E. Hiyama, and K. Piszczatowski, “Four-body treatment of the antihydrogen-positronium system: binding, structure, resonant states and collisions,” *Hyperfine Interact.* **240**, 46 (2019).

[Review articles]

- Y. Yamaguchi, A. Hosaka, S. Takeuchi, and M. Takizawa, “Heavy hadronic molecules with pion exchange and quark core couplings: a guide for practitioners,” *J. Phys. G* **47**, 053001 (2020).

[Proceedings]

- Y. Yamaguchi, “pi J/ψ - $\text{D}\bar{\text{D}}\text{bar}^*$ potential described by the quark exchange diagram,” *EPJ Web Conf.* **204**, 01007 (2019).
 Y. Yamaguchi, “Short range interaction in pi J/ψ - $\text{D}\bar{\text{D}}\text{bar}^*$ channel,” *Int. J. Mod. Phys. Conf. Ser.* **49**, 1960005 (2019).
 Y. Yamaguchi, “Short range pi J/ψ - $\text{D}\bar{\text{D}}\text{bar}^*$ potential described by the quark exchange diagram,” *Springer Proc. Phys.* **238**, 629 (2020).

Presentations

[International conferences/workshops]

- E. Hiyama (invited), “Five-body structure of sssc.c,” The 1st CENuM Workshop for Hadron Physics, Incheon, Korea, June 17–18, 2019.
 E. Hiyama (invited), “Structure of light Ξ hypernuclei with modern ΞN interaction,” International workshop on “Nuclear structure at the crossroads” (INT 19-2a), Seattle, U.S.A., July 1–August 2, 2019.
 E. Hiyama (invited), “Five-body structure of sssc.c,” International Workshop on Perspectives in Hadron Physics, Quy Nhon, Vietnam, September 22–28, 2019.

- P. Naidon (Invited), “A bubble of polarons,” 2nd workshop “Clusters in quantum systems: from atoms to nuclei and hadrons,” Fukuoka, Japan, January 27–31, 2020.
- Y. Yamaguchi (oral), “Role of the tensor force in the heavy hadronic molecules,” The 18th International Conference on Hadron Spectroscopy and Structure (HADRON2019), Guilin, China, August 16–21, 2019.
- Y. Yamaguchi (oral), “Tensor force in heavy hadronic molecules,” Workshop on Chiral and heavy quark symmetries in quark-hadron physics, Osaka, Japan, August 25, 2019.
- Y. Yamaguchi (oral), “Hadronic molecules of heavy hadrons with tensor force,” The 24th European conference on few-body problems in physics (EFB24), Guirford, UK, September 2–6, 2019.
- Y. Yamaguchi (oral), “Heavy hadronic molecules: pion exchange and coupling to multiquark states,” Workshop on “Physics of heavy-quark and exotic hadrons,” Tokai, Ibaraki, Japan, January 27–29, 2020.
- Y. Yamaguchi (oral/poster), “Tensor force in the heavy hadronic molecules,” REIMEI Workshop on Universal Features of Quantum Flows with Spin, Orbital and Tensor Correlations, Tokai, Ibaraki, Japan, February 17–19, 2020.
- K. U. Can (oral), “Structure of the charmed baryons through an electromagnetic perspective,” 15th Rencontres du Vietnam Perspectives in Hadron Physics, ICISE, Quy Nhon, Vietnam, September 22–28, 2019.
- T. Yamashita, Y. Kino, E. Hiyama, S. Jonsell, and P. Froelich (poster), “Inelastic resonant scattering of positronium by (anti)hydrogen atom,” XX International Workshop on Low-Energy Positron and Positronium Physics & XXI International Symposium on Electron-Molecule Collisions and Swarms, Belgrade, Serbia, July 18–20, 2019.
- T. Yamashita, Y. Kino, E. Hiyama, K. Piszczatowski, S. Jonsell, and P. Froelich (oral, hot topic), “Towards prediction of the rates of antihydrogen positive ion production in antihydrogen-excited positronium reaction,” XXXIst International Conference on Photonic, Electronic, and Atomic Collisions (ICPEAC), Deauville, France, July 23–30, 2019.
- M. Niyama, T. Yamashita, and Y. Kino (poster), “Four-body calculation of energy levels of muonic molecule $d\mu e$ in muon catalyzed fusion,” XXXIst International Conference on Photonic, Electronic, and Atomic Collisions, Deauville, France, July 23–30, 2019.
- T. Yamashita, M. Umair, Y. Kino, and E. Hiyama (poster), “Coupled rearrangement channel calculation of dipole resonance states of positronic helium atom,” XXXIst International Conference on Photonic, Electronic, and Atomic Collisions, Deauville, France, July 23–30, 2019.
- C. H. Schmickler (oral), “Universal few-body physics of charged particles,” REIMEI Workshop on “Universal features of quantum flows with spin, orbital and tensor correlations,” Tokai, Ibaraki, Japan, February 17–19, 2020.

[Domestic conferences/workshops]

- 山口康宏 (口頭発表), 「パイオン交換力とハドロン分子状態」, 研究会「クォーク模型からみたエキゾチックハドロン研究の進展と QCD の新展開」, 和光, 2019 年 7 月 6 日.
- 山口康宏 (口頭発表), 「2 メソン系におけるヘビーフレーバー交換相互作用」, 日本物理学会 2019 年秋季大会, 山形, 2019 年 9 月 17–20 日.
- 山口康宏 (口頭発表), 「電子の電気双極子モーメントにおけるハドロンループの寄与」, Flavor Physics Workshop 2019, 富田林, 2019 年 11 月 19–22 日.

[Seminars]

- Y. Yamaguchi, “Heavy hadronic molecules: pion exchange and coupling to compact states,” Tokyo Institute of Technology, Tokyo, December 13, 2019.
- Y. Yamaguchi, “Heavy hadronic molecules: pion exchange and coupling to compact states,” Nagoya University, Nagoya, Aichi, Japan, December 17, 2019.
- T. Yamashita and Y. Kino (oral), “For analysis of fundamental muonic atom process: development of few-body calculation method and related topics on relativistic effects of exotic atoms,” Seminar on fundamental theories for negative muon experiments at J-PARC and its application to elemental analysis, Tokai, Ibaraki, Japan, April 18, 2019.

Awards

- 肥山詠美子, 科学技術分野の文部科学大臣表彰 科学技術賞 (研究部門) 「量子少数多体系の厳密計算理論の確立とその応用研究」, 2019 年 4 月 17 日.

Press releases

- 肥山詠美子室長, 土井琢身専任研究員, 数理創造プログラムの初田哲男プログラムディレクターらの国際共同研究グループ, 新たなハイパー原子核「グザイ・テトラバリオン」—グザイ粒子の振る舞いを精密計算で解き明かす—, 2020 年 3 月 5 日.

Subnuclear System Research Division Radiation Laboratory

1. Abstract

Nucleons, such as protons and neutrons, are a bound state of constituent quarks glued together with gluons. The detail structure of nucleons, however, is not well understood yet. Especially the mechanism to build up the spin of proton, which is $1/2$, is a major problem in physics of the strong force. The research goal of Radiation Laboratory is to solve this fundamental question using the world first polarized-proton collider, realized at RHIC in Brookhaven National Laboratory (BNL) in USA. RHIC stands for Relativistic Heavy Ion Collider, aiming also to create Quark Gluon Plasma, the state of Universe just after the Big Bang, and study its property. RIKEN-BNL Research Center (RBRC) also directed by H. En'yo carries our core team at BNL for those exciting researches using the PHENIX detector and its upgraded sPHENIX detector in preparation. We have observed that the proton spin carried by gluons is finite and indeed sizable. We also identified W bosons in the electron/positron decay channel and in the muon decay channel, with which we showed how much anti-quarks carry the proton spin. Other than the activities at RHIC we are preparing and starting new experiments at J-PARC and Fermilab to study the nature of hadron and preparing for the electron-ion collider (EIC). We are also performing technical developments such as novel ion sources, fine-pitch silicon pixel detectors and high-performance trigger electronics.

2. Major Research Subjects

- (1) Spin physics with relativistic polarized-proton collisions at RHIC
- (2) Study of nuclear matter at high temperature and/or at high density
- (3) Technical developments on radiation detectors and accelerators

3. Summary of Research Activity

(1) Experimental study of spin structure of proton using RHIC polarized proton collider

[See also RIKEN-BNL Research Center Experimental Group for the activities at BNL]

The previously published central neutral pion double spin asymmetries at the highest collision energies at RHIC of 510 GeV have been augmented with the publication of the complementary charged pion double spin asymmetries at the same collision energy. The ordering of the three pion asymmetries allows a direct determination of the sign of the gluon polarization which has been found to be nonzero. These results will be included in future global fits of all the existing experimental data in the world and will improve the sensitivity of quark and gluon spin contributions to the total spin of the nucleon. Additionally, the first double spin asymmetry results for direct photons and jets are being prepared by PHENIX. Both are in principle cleaner probes since no fragmentation functions are involved. The direct photon probe also restricts the initial, hard interaction to be predominantly between a quark and a gluon thus further increasing the sensitivity to the gluon spin.

While orbital angular momentum cannot be directly accessed at RHIC, several transverse spin phenomena have been observed which relate to orbital angular momentum and the three-dimensional structure of the nucleon. These phenomena by themselves have become a major field of research as the dynamics of the strong interaction. During the 2015 RHIC operation, collisions of transversely polarized protons with Au and Al nuclei were provided for the first time. Two rather surprising results have been discovered here. First, the single transverse spin asymmetries for J/Ψ particles which are found to be consistent with zero to even higher precisions, show distinctly nonzero asymmetries in proton-Au collisions at the lowest transverse momenta both if detected at slightly forward or backward regions with respect to the polarized beam. Also charged hadron single spin asymmetries have been observed in all three colliding systems. While a previously known nonzero forward asymmetry for positive hadrons was confirmed, a substantial reduction of these asymmetries for $p + \text{Al}$ and $p + \text{Au}$ collisions was observed. Such a reduction was predicted by several theoretical models describing the non-linear effects of high gluon densities in nuclei suggested by the so-called color-glass-condensate. While the kinematic region does not reach into the range where the color-glass-condensate is expected, this reduction in asymmetries has been met with interest by the theory community. The results have now been published. When moving to more central rapidities, the left-right asymmetries are known to be very small for neutral pions. Since then they have been confirmed to be small also for eta mesons and, for the first time, also for direct photons. The direct photon asymmetries are again very important here as they are only sensitive to the transverse spin effects in the initial state and not the fragmentation. Both results are being prepared for publication.

In June of 2017, an electro-magnetic calorimeter was installed in the most forward area of the STAR experiment and took polarized proton collision data for neutral particle production (neutron, photon, neutral pion). The cross-section measurement will give us new inputs to develop high-energy particle-collision models which are essential to understand air-shower from ultra-high energy cosmic rays. The asymmetry measurement will enable us to understand the hadron collision mechanism based on QCD. An unexpectedly large neutral pion asymmetry has been found using this data that may connect to the large pion asymmetries at smaller rapidities and higher transverse momenta. The results have been accepted for publication in PRL.

Some of us are participating in the Fermilab SeaQuest experiment as a pilot measurement of muon pairs from Drell-Yan process using a 120-GeV unpolarized proton at Fermilab. After finishing unpolarized measurements in 2017 to study the quark spin-orbit effect, a new measurement with a polarized proton target will start in 2020 to study the sea-quark orbit effect of the polarized proton in the target.

For many jet related measurements fragmentation functions are necessary to gain spin and or flavor sensitivity. Those are currently extracted by some of us using the KEK-Belle data. In addition to using the fragmentation results with RHIC measurements, they will also provide the basis for most of the key measurements to be performed at the electron-ion collider. In 2019, transverse momentum

dependent cross sections of pions, kaons and protons were published as a function of fractional energy and event topology. These measurements relate to essentially all transverse spin or momentum dependent measurements at RHIC, semi-inclusive DIS and the EIC.

As the Electron-Ion Collider is becoming a reality, many of us are participating in the various community efforts to define the physics goals of the EIC and how they inform on the choices of collisions energies, luminosities and detector components. While the accelerator efforts are naturally led by the two main Nuclear physics laboratories in the US, BNL and JLAB, a large EIC user group of more than 1000 members from all around the world is working on making the EIC a reality. Within this group, we are participating in various functions from the steering committee, the conference and talks committee to various physics or detector related topical groups.

(2) Experimental study of quark-gluon plasma using RHIC heavy ion collider

[See also RIKEN-BNL Research Center Experimental Group for the activities at BNL]

We have completed several key measurements in the study of quark-gluon plasma at RHIC. As the top of them, we lead the analysis of the first thermal photon measurement in heavy ion collisions. The measurement indicates that the initial temperature reached in the central Au + Au collision at 200 GeV is about 350 MeV, far above the expected transition temperature $T_c \sim 170$ MeV, from hadronic phase to quark-gluon plasma. This work was rewarded by Nishina Memorial Prize given to Y. Akiba in 2011. We also measured direct photons in $d + Au$ and direct photon flow strength v_2 and v_3 in Au + Au.

We lead measurement of heavy quark (charm and bottom) using VTX, a 4-layer silicon vertex tracker which we jointly constructed with US DOE. The detector was installed in PHENIX in 2011. PHENIX recorded approximately 10 times more data of Au+Au collisions in the 2014 run than the 2011 run. PHENIX recorded high statistics $p + p$ and $p + A$ data in 2015, and the doubled the Au + Au in 2016. PHENIX concluded its data taking in the 2016 run.

The results of the 2011 run was published in Physical Review C (Phys. Rev. C **93**, 034904 (2016)). This is the first publication from VTX. The result showed that the electrons from bottom quark decay is suppressed for $p_T > 4$ GeV/c, but the suppression factor is smaller than that of charm decay electrons for $3 < p_T < 4$ GeV/c. This is the first observation of bottom electron suppression in heavy ion collisions, and the first result that shows the bottom and charm suppression is different. The results of $b \rightarrow e$ and $c \rightarrow e$ measurement in the 2015 $p + p$ run has been published in Physical Review D99, 092003 (2019). The centrality dependence of the suppression $b \rightarrow e$ and $c \rightarrow e$ from the 2014 Au+Au data is in preparation.

PHENIX published measurements of flow strength in $p + Au$, $d + Au$, and $^3\text{He} + Au$ (Nature Physics **15**, 214 (2019)). The results provide strong evidence for formation of small droplet of quark gluon plasma in collisions of small systems at RHIC.

In Wako we are operating a cluster computer system (CCJ) specialized to analyze huge data sets taken with the PHENIX detector. It consists of 28 nodes (18 old nodes and 10 new nodes) each of which has two CPUs and 10 sets of local disks for data repository (old node: quad-core CPU, 1TB disk, new node: six-core CPU, 2 TB disk). There are 264 CPU cores and 380 TB disks in total. This configuration ensures the fastest disk I/O when each job is assigned to the node where the required data sets are stored. It is also important that this scheme doesn't require an expensive RAID system and network. Through this development we have established a fast and cost-effective solution in analyzing massive data.

The data of 0.9 Pbyte obtained by the PHENIX experiment is stored in a hierarchical storage system which is a part of HOKUSAI BigWaterfall/SailingShip supercomputer systems operated by the Head Office for Information Systems and Cybersecurity. In addition, we operate a dedicated server for the RHICf group and two servers for the J-PARC E16 group, to keep their dedicated compilation and library environments, and some data.

(3) Study of properties of mesons and exotic hadrons with domestic accelerators

Preparation of the experiment E16 at J-PARC Hadron experimental facility is underway with several Grant-in-Aids. This experiment aims to perform a systematic study of the spectral modification of low-mass vector mesons in nuclei to explore the physics of chiral symmetry breaking and restoration in dense nuclear matter, namely, the mechanism proposed by Nambu to generate most of hadron masses.

The Gas Electron Multiplier (GEM) technology is adopted for the two key detectors, GEM Tracker (GTR) and Hadron-blind Cherenkov detector (HBD). To improve electron-identification performance, lead-glass calorimeters (LG) are used in combination with HBD. We are in the production phase. The parts for six modules of GTR, four modules of HBD and six modules of LG are assembled and installed in the spectrometer magnet at J-PARC. Read-out electronics and trigger logic modules are also installed and tested. We have been a member of the CERN-RD51 collaboration to acquire the read-out technology for GEM. The MoU for RD51 was extended for the period of 2019–2023.

Due to the budgetary limitation, we aim to install a part of detectors at the beginning of the experiment, eight modules of GTR/HBD/LG out of 26 modules in the full installation. J-PARC PAC gave us a stage-2 approval on July 2017, to the commissioning run (Run 0), which will be performed when the beam line is completed. Although there is a significant delay from the originally planned date of March 2016, the construction of the beam line by KEK was completed finally in early 2020 to perform this experiment. We performed the 1st half of commissioning run (Run0a) in June 2020 successfully, and the 2nd half is planned in January 2021.

(4) Detector development for PHENIX experiment

The PHENIX experiment proposes substantial detector upgrades to go along the expected accelerator improvements, including the future electron-ion collider "EIC". The present PHENIX detector is repurposed to the sPHENIX (super PHENIX) detector which reuses the Babar solenoid magnet at SLAC and is covered by the hadronic calorimeter which was not available in the previous RHIC

experiments. The sPHENIX was approved for the Project Decision-2/3 (corresponds to DOE's Critical Decision-2/3) in May 2019. We RIKEN group have been developing the one of the tracking devices of sPHENIX detector, so called intermediate tracker (INTT) since 2015. The INTT provides the best timing resolution among the sPHENIX tracking system, in conjunction with a time projection chamber and a MAPS based vertex detectors. The R&D of INTT detector is almost in the last stage. The prototype detectors demonstrated satisfactory performance in the efficiency and position resolutions as designed in the last two beam tests at the Fermilab Test Beam Facility (FTBF) using 120 GeV proton beam in March 2018 and June 2019. The preparation for the production ladder assembly is ongoing both in Taiwan Silicon Detector Facility (TSiDF) and BNL.

We have been developing a plan to build a forward spectrometer to be added to the sPHENIX detector. With this addition, the fsPHENIX detector will have both hadronic and electromagnetic calorimetry as well as tracking in the forward rapidity region. This upgrade makes it possible to study forward jets and hadrons in jets which are of vital importance for the cold QCD program in polarized $p + p$ and $p + A$ collisions at RHIC. The fsPHENIX detector can be further upgraded to the ePHENIX detector to be used for electron-ion collisions at EIC. We are preparing test bench to perform R&D for the forward hadron calorimeter.

As the further investigation of the neutral pion production asymmetry discovered in the RHICf experiment, we started preparation for the next phase of the experiment, namely RHICf-II. The target year of physics data taking is 2024 as a part of sPHENIX experiment. The highlight of the upgraded experiment is the larger acceptance of the high position resolution part of the zero-degree calorimeter (ZDC). We found the detector technology developed for the FoCAL upgrade project of the ALICE experiment at LHC well satisfies the RHICf-II performance requirement. We thus resumed the associated membership of the ALICE collaboration and the RHICf-II detectors are to be developed together with the FoCAL collaboration. This new detector technology development is also a part of the R&D program for the essential ZDC detector for EIC.

Members

Director

Hideto EN'YO

Vice Chief Scientist

Yasuyuki AKIBA

Research/Technical Scientist

Yuji GOTO (Senior Research Scientist)

Itaru NAKAGAWA (Senior Research Scientist)

Seidl RALF (Senior Research Scientist)

Yasushi WATANABE (Senior Research Scientist)

Satoshi YOKKAICHI (Senior Research Scientist)

Contract Researcher

Tomonori TAKAHASHI

Special Postdoctoral Researcher

Koki KANNO

Research Associate

Wataru NAKAI

International Program Associates

Minho KIM (Korea Univ.)

Benard MULILO (Korea Univ.)

Senior Visiting Scientist

Toshiaki SHIBATA (Nihon Univ.)

Visiting Scientists

Kazuya AOKI (KEK)

Se Young HAN (Korea Univ.)

Shoichi HASEGAWA (JAEA)

Takashi KONDO (Tokyo Metropolitan Industrial Tech. Res. Inst.)

Shunzo KUMANO (KEK)

Tsutomu MIBE (KEK)

Yuhei MORINO (KEK)

Ken-ichi NAKANO (Tokyo Tech)

Megumi NARUKI (Kyoto Univ.)

Kyoichiro OZAWA (KEK)

Susumu SATO (JAEA)

Kenta SHIGAKI (Hiroshima Univ.)

Maya SHIMOMURA (Nara Women's Univ.)

Kiyoshi TANIDA (JAEA)

Student Trainees

Sakiko ASHIKAGA (Kyoto Univ.)

Ryohei FUJII (Kyoto Univ.)

Kaede KAMANO (Nara Women's Univ.)

Takehito KONDO (Hiroshima Univ.)

Yoko MINATO (Nara Women's Univ.)

Seiya MIYATA (Univ. of Tokyo)

Tomoki MURAKAMI (Univ. of Tokyo)

Satomi NAKASUGA (Kyoto Univ.)

Junsang PARK (Seoul Nat'l Univ.)

Kenta SATO (Nagoya Univ.)

Ayaka SUZUKI (Nara Women's Univ.)
Kazuki SUZUKI (Kyoto Univ.)

Yosuke UEDA (Hiroshima Univ.)
Jaehee YOO (Korea Univ.)

Intern

Ayaka SUZUKI (Nara Women's Univ.)

Assistant

Keiko SUZUKI

List of Publications & Presentations

Publications

[Original papers]

- C. Aidala *et al.* (PHENIX Collaboration), “Measurements of $\mu\mu$ pairs from open heavy flavor and Drell-Yan in $p + p$ collisions at $\sqrt{s_{NN}} = 200$ GeV,” *Phys. Rev. D* **99**, 072003 (2019).
- C. Aidala *et al.* (PHENIX Collaboration), “Nonperturbative-transverse-momentum broadening in dihadron angular correlations in $\sqrt{s_{NN}} = 200$ GeV proton-nucleus collisions,” *Phys. Rev. C* **99**, 044912 (2019).
- A. Adare *et al.* (PHENIX Collaboration), “Measurement of two-particle correlations with respect to second- and third-order event planes in Au + Au collisions at $\sqrt{s_{NN}} = 200$ GeV,” *Phys. Rev. C* **99**, 054903 (2019).
- C. Aidala *et al.* (PHENIX Collaboration), “Measurement of charm and bottom production from semileptonic hadron decays in $p + p$ collisions at $\sqrt{s_{NN}} = 200$ GeV,” *Phys. Rev. D* **99**, 092003 (2019).
- A. Adare *et al.* (PHENIX Collaboration), “Beam energy and centrality dependence of direct-photon emission from ultra-relativistic heavy-ion collisions,” *Phys. Rev. Lett.* **123**, 022301 (2019).
- C. Aidala *et al.* (PHENIX Collaboration), “Nuclear dependence of the transverse single-spin asymmetry in the production of charged hadrons at forward rapidity in polarized $p + p$, $p + \text{Al}$, and $p + \text{Au}$ collisions at $\sqrt{s_{NN}} = 200$ GeV,” *Phys. Rev. Lett.* **123**, 122001 (2019).
- U. A. Acharya *et al.* (PHENIX Collaboration), “ J/Ψ and $\Psi(2S)$ production at forward rapidity in $p + p$ collisions at $\sqrt{s_{NN}} = 510$ GeV,” *Phys. Rev. D* **101**, 052006 (2020).
- C. Aidala *et al.* (PHENIX Collaboration), “Nuclear-modification factor of charged hadrons at forward and backward rapidity in $p + \text{Al}$ and $p + \text{Au}$ collisions at $\sqrt{s_{NN}} = 200$ GeV,” *Phys. Rev. C* **101**, 034910 (2020).
- C. A. Aidala, Y. Goto, *et al.*, “The SeaQuest spectrometer at fermilab,” *Nucl. Instrum. Methods Phys. Res. A* **930**, 49–63 (2019).
- M. H. Kim, Y. Goto, I. Nakagawa, J. S. Park, R. Seidl, *et al.*, “Transverse single-spin asymmetry for very forward neutral pion production in polarized $p + p$ collisions at $\sqrt{s} = 510$ GeV,” *Phys. Rev. Lett.* **124**, 252501 (2019).
- M. Ichikawa *et al.*, “Trigger merging module for the J-PARC E16 experiment,” *IEEE Trans. Nucl. Sci.* **66**, 2022 (2019).

[Proceedings]

- A. Dote, Y. Goto, A. Hosaka, S. Kumano, and A. Monnai, “Proceedings, 8th international conference on quarks and nuclear physics (QNP2018),” *JPS Conf. Proc.* **26** (2019).
- A. Chen, Y. Goto, *et al.*, “Probing nucleon's spin structures with polarized Drell-Yan in the fermilab SpinQuest experiment,” *PoS SPIN2018*, 164 (2019).
- Y. Itow, Y. Goto, I. Nakagawa, R. Seidl, J. S. Park, M. H. Kim, *et al.*, “Recent results from the LHCf and RHICf experiments,” *EPJ Web Conf.* **208**, 05004 (2019).
- M. H. Kim, Y. Goto, I. Nakagawa, R. Seidl, J. S. Park, M. H. Kim, *et al.*, “Transverse single spin asymmetry for very forward π^0 production in polarized proton-proton collisions at $\sqrt{s} = 510$ GeV,” *EPJ Web Conf.* **208**, 05007 (2019).
- Y. Goto, “Asymmetry measurement of very forward neutral particle production in the RHICf experiment,” *Acta Phys. Polon. B Proc. Suppl.* **12**, 837 (2019).
- S. Ashikaga *et al.*, (J-PARC E16 Collaboration), “Measurement of vector meson mass in nuclear matter at J-PARC,” *JPS Conf. Proc.* **26**, 024005 (2019).

Presentations

[International conferences/workshops]

- Y. Goto (invited), “Nucleon structure study at RHIC and EIC,” YKIS2018b Symposium on Recent Developments in Quark-Hadron Sciences, Kyoto, Japan, June 12, 2018.
- Y. Goto (invited), “Asymmetry measurement of very forward neutral particle production in the RHICf experiment,” Diffraction and Low-x 2018, Reggio Calabria, Italy, August 29, 2018.
- Y. Goto (oral), “Very forward neutral particle measurement in the RHICf experiment,” 5th Joint Meeting of the APS Division of Nuclear Physics and the Physics Society of Japan, Hawaii, USA, October 26, 2018.
- Y. Goto (invite), “Electron-ion collider project,” Workshop on Progress on Hadron Structure Functions in 2018, Tsukuba, Japan, November 19, 2018.
- Y. Goto (invited), “Forward spin physics at PHENIX and sPHENIX,” International Workshop on Forward Physics and Forward Calorimeter Upgrade in ALICE, Tsukuba, Japan, March 7, 2019.
- Y. Goto (invited), “RHICf results,” Cold QCD Workshop, RHIC & AGS Annual Users' Meeting, Upton, New York, USA, June 4, 2019.

- Y. Goto (invited), “Plan for EIC (Electron-Ion Collider),” 14th ANPhA Board meeting and Symposium in Korea, Jeju Island, Korea, June 28, 2019.
- Y. Goto (invited), “Overview of future facilities for nucleon spin studies,” 11th Circum-Pan-Pacific Symposium on High Energy Spin Physics (Pacific Spin 2019), Miyazaki, Japan, August 30, 2019.
- Y. Goto (invited), “Physics and detector requirements at zero degree of EIC,” Workshop on Forward Physics and QCD at the LHC, the future Electron Ion Collider and Cosmic Ray Physics, Guanajuato, Mexico, November 19, 2019.
- S. Yokkaichi (invited), “Measurement of the spectral change of vector mesons in nuclei at the high-momentum beam line in J-PARC HEF,” J-PARC Symposium 2019, Tsukuba, Japan, September 23–26, 2019.
- S. Ashikaga, “Measurement of vector meson mass in nuclear matter at J-PARC,” The 8th International Conference on Quarks and Nuclear Physics (QNP2018), Tsukuba, Japan, November 13–17, 2018.
- M. Ichikawa, “Trigger merging module for the J-PARC E16 experiment,” 21st IEEE Real Time Conference RT2018 (RT2018), Williamsburg, VA, USA, June 12, 2018.

[Domestic conferences/workshops]

- 後藤雄二 (招待講演), 「Electron-Ion Collider (EIC) 計画」, 日本学術会議公開シンポジウム「素粒子物理・原子核物理分野の大型施設計画・大規模研究計画マスタープラン」, 東京, 2019年2月19日.
- 後藤雄二 (招待講演), “Progress on RHIC-spin physics,” Progress on QCD and Nucleon Structure in 2019, つくば, 2019年2月28日.
- 後藤雄二 (口頭発表), 「PHENIX 実験での偏極陽子 + 原子核衝突による最新の結果」, 日本物理学会 2019 年秋季大会, 山形大学, 山形, 2019年9月17日.
- 村上智紀 (口頭発表), 「J-PARC E16 実験に向けた飛跡検出器の開発および性能評価」, 日本物理学会第 74 回年次大会, 九州大学伊都キャンパス, 福岡, 2019年3月14–17日.
- 四日市悟 (招待講演), 「原子核中でのベクトル中間子の質量変化の測定」, ELPH 研究会 C023 「原子核中におけるハドロンの性質とカイラル対称性の役割」, 東北大学電子光理学研究センター, 仙台, 2018年9月11–12日.

Press releases

- 「陽子衝突からの左右非対称的な π 中間子の生成」, 理化学研究所, 東京大学宇宙線研究所, 名古屋大学, 日本原子力研究開発機構, 2020年6月23日.

Subnuclear System Research Division Meson Science Laboratory

1. Abstract

Particles like muons, pions, and kaons have finite life times, so they do not exist in natural nuclei or matters. By implanting these particles into nuclei/matters, exotic phenomena in various objects can be studied from new point of view.

For example, kaon is the second lightest meson, which has strange quark as a constituent quark. It is expected that if one embeds mesons into nuclei, the sizes of the nuclei become smaller and one can form a high-density object beyond the normal nuclear density. Study of this object could lead to better understanding of the origin of the mass of the matter, and may reveal the quark degree of freedom beyond the quark-confinement. The other example is the weak interaction in nuclear matter. It can only be studied by the weak decay of hypernuclei, which have Lambda particle in the nuclei.

Muon provides even wider scope of studies, covering condensed matter physics as well as nuclear and atomic physics, and we are trying to extend the application field further into chemical and biological studies. For instance, stopping positively charged muon in a material, we obtain information on the magnetic properties or the local field at the muon trapped site (μ SR). Injecting negatively charged muon to hydrogen gas, muonic hydrogen atom (μp) is formed. We are planning to measure μp hyperfine splitting energy to measure proton magnetic radius, which is complementary quantity to the proton charge radius and its puzzle. We are also interested in precision measurement of muon property itself, such as muon anomalous magnetic moment ($g - 2$).

In our research, we introduce different kind of impurities into nuclei/matters, and study new states of matter, new phenomena, or the object properties.

2. Major Research Subjects

- (1) Study of meson property and interaction in nuclei
- (2) Origin of matter mass/quark degree of freedom in nuclei
- (3) Condensed matter and material studies with muon
- (4) Nuclear and particle physics studies via muonic hydrogen
- (5) Development of ultra cold muon beam, and its application from material science to particle physics

3. Summary of Research Activity

(1) Hadron physics at J-PARC, RIKEN-RIBF, GSI and Spring-8

Kaon and pion will shed a new insight to the nuclear physics. The recent discovery of deeply bound pionic atom enables us to investigate the properties of mesons in nuclear matter. At RIKEN-RIBF, we are preparing precise experimental study of the pionic atom. Very lately, we succeeded to discover kaonic nuclear bound state, " K^-pp ," at J-PARC. The yield dependence on momentum-transfer shows that observed system is unexpectedly small. We extended our study on $\Lambda(1405)$ that could be $K - p$ bound state. By these experiments, we are studying the $\bar{K}N$ interaction, and clarify the nature of kaon in nuclei. At Spring-8 and at GSI, we are planning to study omega and η' nuclei. By these experiments, we aim to be a world-leading scientific research group using these light meta-stable particles.

(1-1) Deeply bound kaonic nuclei

J-PARC E15 experiment had been performed to explore the simplest kaonic nuclear bound state, " K^-pp ". Because of the strong attraction between $\bar{K}N$, the \bar{K} in nuclei may attract surrounding nucleons, resulting in forming a deeply bound and extremely dense object. Measurement of the kaon properties at such a high-density medium will provide precious information on the origin of hadron masses, if the standard scenario of the hadron-mass-generation mechanism, in which the hadron masses are depends on matter density and energy, is correct. Namely, one may study the chiral symmetry breaking of the universe and its partial restoration in nuclear medium.

The E15 experiment was completed to observe the " K^-pp " bound state by the in-flight ${}^3\text{He}(K^-, n)$ reaction, which allows us the formation via the invariant-mass spectroscopy by detecting decay particles from " K^-pp ". For the experiment, we constructed a dedicated spectrometer system at the secondary beam-line, K1.8BR, in the hadron hall of J-PARC.

With the Λ_{pn} final states obtained in the first stage experiment, we observed a kinematic anomaly in the Λp invariant mass near the mass threshold of $M(K^-pp)$ (total mass of kaon and two protons) at the lower momentum transfer q region. We conducted a successive experiment to examine the nature of the observed kinematical anomaly in the Λ_{pn} final state, and we confirmed the existence of the bound state below the mass threshold of $M(K^-pp)$ at as deep as the binding energy of 40 MeV. The momentum transfer q naturally prefers lower momentum for the bound state formation, but the observed event concentration extended having the form-factor parameter ~ 400 MeV/c. Based on the PWIA calculation, the data indicated that the " K^-pp " system could be as small as ~ 0.6 fm. It is astonishingly compact in contrast to the mean nucleon distance ~ 1.8 fm.

This observed signal shows that *a meson ($\bar{q}q$) forms a quantum state where baryons (qqq) exist as nuclear medium, i.e., a highly excited novel form of nucleus with a kaon, in which the mesonic degree-of-freedom still holds*. This is totally new form of nuclear system, which never been observed before.

(1-2) Precision X-ray measurement of kaonic atom

To study the $\bar{K}N$ interaction at zero energy from the atomic state level shift and width of kaon, we have performed an X-ray spectroscopy of atomic $3d \rightarrow 2p$ transition of negatively charged K-mesons captured by helium atoms. However, our first experiment is insufficient in energy resolution to see the K^- -nucleus potential. Aiming to provide a breakthrough from atomic level observation,

we introduce a novel X-ray detector, namely superconducting transition-edge-sensor (TES) microcalorimeter offering unprecedented high energy resolution, being more than one order of magnitude better than that achieved in the past experiments using conventional semiconductor detectors. The experiment J-PARC E62 aims to determine $2p$ -level strong interaction shifts of kaonic ${}^3\text{He}$ and ${}^4\text{He}$ atoms by measuring the atomic $3d \rightarrow 2p$ transition X-rays using TES detector with 240 pixels having about 23 mm^2 effective area and the average energy resolution of 7 eV (FWHM) at 6 keV. We carried out the experiment at J-PARC in June 2018 and successfully observed distinct X-ray peaks from both atoms. The data analysis is now ongoing.

Another important X-ray measurement of kaonic atom would be $2p \rightarrow 1s$ transition of kaonic deuteron (K^- -d). We have measured same transition of kaonic hydrogen (K^- -p), but the width and shift from electro-magnetic (EM) value reflect only isospin average of the $K^{\text{bar}}\text{N}$ interaction. We can resolve isospin dependence of the strong interaction by the measurements both for K^- -p and K^- -d. The experiment J-PARC E57 aims at pioneering measurement of the X-rays from K^- -d atoms. Prior to full (stage-2) approval of the E57 proposal, we performed a pilot run with hydrogen target in March 2019.

(1-3) Deeply bound pionic atoms and η' mesonic nuclei

We have been working on precision spectroscopy of pionic atoms systematically, which leads to understanding of the non-trivial structure of the vacuum and the origin of hadron masses. The precision data set stringent constraints on the chiral condensate at nuclear medium. We are presently preparing for the precision systematic measurements at RIBF. A pilot experiment performed in 2010 showed a unprecedented results of pionic atom formation spectra with finite reaction angles. The measurement of pionic ${}^{121}\text{Sn}$ performed in 2014 showed a very good performance of the system. We have been analyzing the data to achieve information on the pion-nucleus interaction based on the pionic atom spectroscopy.

We are also working on spectroscopy of η' mesonic nuclei in GSI/FAIR. Theoretically, peculiarly large mass of η' is attributed to UA(1) symmetry and chiral symmetry breaking. As a result, large binding energy is expected for η' meson bound states in nuclei (η' -mesonic nuclei). From the measurement, we can access information about gluon dynamics in the vacuum via the binding energy and decay width of η' -nuclear bound state.

(1-4) ${}^3_\Lambda\text{H}$ lifetime puzzle and our approach

Three recent heavy ion experiments (HypHI, STAR, and ALICE) announced surprisingly short lifetime for ${}^3_\Lambda\text{H}$ hyper-nucleus's *Mesonic Weak Decay* (MWD), which seems to be inconsistent with the fact that the ${}^3_\Lambda\text{H}$ is a very loosely bound system. It is very interesting to study this with a different experimental approach. We proposed a direct measurement of ${}^3_\Lambda\text{H}$ MWD lifetime with $\sim 20\%$ resolution at J-PARC hadron facility by using K^- meson beam at 1 GeV/c. As for the feasibility test, we also measure ${}^4_\Lambda\text{H}$ lifetime.

A Cylindrical Detector System (CDS) used in J-PARC E15/E31 experiment is employed to capture the delayed π^- as a weak decay product from ${}^{3,4}_\Lambda\text{H}$; a calorimeter is installed in the very forward region to tag fast π^0 meson emission at ~ 0 degree, which ensures that the Λ hyperon production with small recoil momentum. By this selection, we can improve the ratio between ${}^{3,4}_\Lambda\text{H}$ and quasi-free Λ and Σ background. A test beam for feasibility study with ${}^4\text{He}$ target has been conditionally approved by J-PARC PAC. We will conduct the experiment and to present the data in short.

(2) Muon science at RIKEN-RAL branch

The research area ranges over particle physics, condensed matter studies, chemistry and life science. Our core activities are based on the RIKEN-RAL Muon Facility located at the Rutherford-Appleton Laboratory (UK), which provides intense pulsed-muon beams. We have variety of important research activities such as particle/nuclear physics studies with muon's spin and condensed matter physics by muon spin rotation/relaxation/resonance (μSR).

(2-1) Condensed matter/materials studies with μSR

To improve our two μSR spectrometers, ARGUS (Port-2) and CHRNU (Port-4), we adjusted the threshold level of the muon-detector system for the zero-field condition. At this condition, we optimized the efficiency of the detector system and the counting rate was improved nearly 50% without any deformation of the time spectrum.

Among our scientific activities on μSR studies from year 2016 to 2019, following studies are most important subjects of material sciences at the RIKEN-RAL muon facility:

- (1) Deformed nodal superconducting gap state and asymmetric spin-fluctuation mediated Cooper pair in the quasi two-dimensional organic superconductor Λ -[BETS] $_2\text{GaCl}_4$
- (2) Multi magnetic transitions in the Ru-based pyrochlore systems, $\text{R}_2\text{Ru}_2\text{O}_7$.
- (3) Magnetic properties of the nano-cluster gold in the border of macro- and micro- scale.
- (4) Novel magnetic and superconducting properties of nano-size La-based high- T_C superconducting curates.
- (5) Determination of muon positions estimated from density functional theory (DFT) and dipole-field calculations.
- (6) Chemical muonic states in DNA molecules.

(2-2) Nuclear and particle physics studies via ultra-cold muon beam and muonic atoms

If we can improve muon beam emittance, timing and energy dispersion (so-called "ultra-cold muon"), then the capability of μSR studies will be drastically improved. The ultra-cold muon beam can stop in a thin foil, multi-layered materials and artificial lattices, so one can apply the μSR techniques to surface and interface science. The development of ultra-cold muon beam is also very important as the source of pencil-like small emittance muon beam for muon g-2 measurement.

Ultra-cold muon beam has been produced by laser ionization of muoniums in vacuum (bound system of μ^+ and electron). We are developing two key components, high efficiency muonium generator at room temperature and high intensity ionization laser. The study of muonium generator has been done in collaboration with TRIUMF. In 2013, we demonstrated at least 10 times increase of the muonium emission efficiency by fabricating fine laser drill-holes on the surface of silica aerogel. Further study was done in 2017 with more than 20 aerogel target having different surface conditions. We are analyzing the data to identify which condition most

contributed to increasing the muonium emission efficiency. We also developed a high power Lyman- α laser in collaboration with laser group at RIKEN. In this laser development, we succeeded to synthesize novel laser crystal Nd:YAG, which has an ideal wavelength property for laser amplification to generate Lyman- α by four-wave mixing in Kr gas cell. We already achieved 10 times increase of Lyman- α generation than before. However, in order to increase the intensity by one more order, we need a larger size crystal. So far we have inhomogeneity problem but we are trying to solve this problem.

Concerning the muonic atom, we are planning a new precise measurement of proton radius. A large discrepancy was found recently in the proton charge radius between the new precise value from muonic hydrogen atom at PSI and those from normal hydrogen spectroscopy and e-p scattering. We propose a precise measurement of Zemach radius (with charge and magnetic distributions combined) using the laser spectroscopy of hyperfine splitting energy in the muonic hydrogen atom. As a key parameter for designing the experiment, we need the quench rate of the muonic proton polarization due to collision with surrounding protons, for which only theoretical estimations are available. We successfully measured the quench rate of muonic deuterium polarization in deuterium gas, which confirmed the long lifetime consistent with the calculation. In this fiscal year, we carried out measurement on muonic proton in low pressure hydrogen gas.

Members

Director

Masahiko IWASAKI

Research Scientists

Kenta ITAHASHI (Senior Research Scientist)
Yue MA (Senior Research Scientist)
Haruhiko OUTA (Senior Research Scientist)

Fuminori SAKUMA (Senior Research Scientist)
Isao WATANABE (Senior Research Scientist)

Contract Researcher

Katsuhiko ISHIDA

Junior Research Associates

Julia ANGEL (Hokkaido Univ.)
Shun SEO (Univ. of Tokyo)

Muhamad UMAR (Hokkaido Univ.)

International Program Associates

Muhammad H.B. CHE LAH (Univ. Sains Malaysia)
Redo Muhammad RAMADHAN (Univ. Indonesia)
Harison B. ROZAK (Univ. Sains Malaysia)

Suci WINARSIH (Univ. Indonesia)
Utami WIDYAISWARI (Univ. Indonesia)

Research Consultant

Masayasu KAMIMURA

Senior Visiting Scientists

Hiroyuki NOUMI (Osaka Univ.)

Kazuhiro TANAKA (KEK)

Visiting Scientists

Tadashi ADACHI (Sophia Univ.)
Hiroko ARIGA (Hokkaido Univ.)
Retno ASIH (Inst. Teknologi Sepuluh Nopember)
Fahmi ASTUTI (Inst. Teknologi Sepuluh Nopember)
KwangYong CHOI (Chung-Ang Univ.)
Catalina Oana CURCEANU (INFN)
Zyun EZAWA (Tohoku Univ.)
Hiroyuki FUJIOKA (Tokyo Tech)
Takayuki GOTO (Sophia Univ.)
Maryam HASSANVAND (Isfahan Univ. of Tech.)
Wataru HIGEMOTO (JAEA)
Ko-ichi HIRAKI (Fukushima Medical Univ.)
Satoru HIRENZAKI (Nara Women's Univ.)
Koichi ICHIMURA (Hokkaido Univ.)
Yasuyuki ISHII (Shibaura Inst. of Tech.)
Ryosuke KADONO (KEK)
Takayuki KAWAMATA (Tohoku Univ.)
Seiko KAWAMURA (JAEA)
Takuya KOBAYASHI (Saitama Univ.)
Yoji KOIKE (Tohoku Univ.)

Seungwon LEE (Univ. of Toyama)
Kenji MATSUDA (Univ. of Toyama)
Mototsugu MIHARA (Osaka Univ.)
Yasuhiro MIYAKE (KEK)
Mohamed Ismail MOHAMED-IBRAHIM (Univ. Sains Malaysia)
Takehito NAKANO (Ibaraki Univ.)
Takahiro NAMIKI (Univ. of Toyama)
Katsuhiko NISHIMURA (Univ. of Toyama)
Yasuo NOZUE (Osaka Univ.)
Agustinus NUGROHO (Inst. Teknologi Bandung)
Kazuki OHISHI (Comprehensive Res. Org. for Sci. and Soc.)
Yu OISHI (KEK)
Atsushi OKAZAWA (Univ. of Tokyo)
Amba D. PANT (Ibaraki Univ.)
Dita PUSPITA SARI (Shibaura Inst. of Tech.)
Irwan RAMLI (Univ. Cokroaminoto Palopo)
Yuta SADA (Osaka Univ.)
Lusi SAFRIANI (Univ. Padjadjaran)
Naohito SAITO (KEK)

Ichiro SHIRAKI (Univ. of Yamanashi)
 Shukri SULAIMAN (Univ. Sains Malaysia)
 Ken SUZUKI (Stefan Meyer Inst.)
 Kensuke SUZUKI (Tohoku Univ.)
 Takao SUZUKI (Shibaura Inst. of Tech.)
 Tomohiro TAKAYAMA (Max Planck Inst.)
 Yoshiki TANAKA (GSI)
 Hiroshi TANIDA (Toyama Prefectural Univ.)

Andrea VACCHI (INFN)
 Eberhard WIDMANN (Stefan Meyer Inst.)
 Zhuan XU (Zhejiang Univ.)
 Ichihiro YAMAUCHI (Saga Univ.)
 Toshimitsu YAMAZAKI (Univ. of Tokyo)
 Masaru YOSOI (Osaka Univ.)
 Xu-Guang ZHENG (Saga Univ.)
 Johann ZMESKAL (Austrian Academy of Sci.)

Student Trainees

Irwan RAMLI (Hokkaido Univ.)
 Shu AIKAWA (Tokyo Tech)

Tanawat SAWASDEE (Suranaree Univ. of Tech.)

Part-time Worker

Mayumi YOSHIMURA (Administrative Part-time Worker II)

Assistants

Yoko FUJITA
 Kumiko TAKAHASHI

Mitsue YAMAMOTO

List of Publications & Presentations

Publications

[Original papers]

- M. Clemenza, *et al.*, “Muonic atom X-ray spectroscopy for non-destructive analysis of archaeological samples,” *Journal of Radioanalytical and Nuclear Chemistry* **322**, 1357–1363 (2019).
- B. V. Hampshire, K. Butcher, K. Ishida, G. Green, D. Paul, and A. Hillier, “Using negative muons as a probe for depth profiling silver Roman coinage,” *Heritage* **2**, 400–407 (2019).
- S. Asano, K. M. Suzuki, K. Kudo, I. Watanabe, A. Koda, R. Kadono, T. Noji, Y. Koike, T. Taniguchi, S. Kitagawa, K. Ishida, and M. Fujita, “Oxidation annealing effects on the spin-glass-like magnetism and appearance of superconductivity in T^{*}-type La_{1-x/2}Eu_{1-x/2}Sr_xCuO₄ (0.14 ≤ x ≤ 0.28),” *J. Phys. Soc. Jpn.* **88**, 084709/1-6 (2019).
- F. Astuti, M. Miyajima, T. Fukuda, M. Kodani, T. Nakano, T. Kambe, and I. Watanabe, “Anionogenic magnetism combined with lattice symmetry in alkali-metal superoxide RbO₂,” *J. Phys. Soc. Jpn.* **88**, 043701/1-5 (2019).
- M. A. Baqiya, T. Adachi, A. Takahashi, T. Konno, T. Ohgi, I. Watanabe, and Y. Koike, “Muon-spin relaxation study of the spin correlations in the overdoped regime of electron-doped high-T_C cuprate superconductors,” *Phys. Rev. B* **100**, 064514/1-5 (2019).
- S. Wenner, C. Marioara, K. Nishimura, K. Matsuda, S. Lee, T. Namiki, I. Watanabe, T. Matsuzaki, and R. Holmestad, “Muon spin relaxation study of solute-vacancy interactions during natural aging of Al-Mg-Si-Cu alloys,” *Metallurgical and Materials Transactions A* **50**, 3446–3451 (2019).
- T. Suzuki, K. Katayama, I. Watanabe, and H. Tanaka, “Spin-fluctuating ground state in the spin-1/2 kagome lattice (Rb_{1-x}Cs_x)₂Cu₃SnF₁₂ with x = 0.53 observed by muon spin relaxation,” *J. Phys. Soc. Jpn.* **89**, 074701 (2020).
- K. M. Suzuki, S. Asano, H. Okabe, A. Koda, R. Kadono, I. Watanabe, and M. Fujita, “Successive magnetic ordering sequence observed from muon spin rotation in T^{*}-structured R₂CuO₄ (R = Nd, Eu),” *Phys. Rev. B* (in press).
- H. Yamauchi, D. P. Sari, I. Watanabe, Y. Yasui, L. -J. Chang, K. Kondo, T. U. Ito, M. Ishikado, M. Hagihara, M. D. Frontzek, S. Chi, J. A. Fernandez-Baca, J. S. Lord, A. Berlie, A. Kotani, S. Mori, and S. Shamoto, “High-temperature short-range order in Mn₃RhSi,” *Commun. Mater.* (in press).
- K. Oinuma, N. Okano, H. Tsunakawa, S. Michimura, T. Kobayashi, H. Taniguchi, K. Satoh, J. Angel, I. Watanabe, Y. Ishii, H. Okamoto, and T. Itou, “Spin structure at zero magnetic field and field-induced spin reorientation transitions in a layered organic canted antiferromagnet bordered on a superconducting phase,” *Phys. Rev. B* (in press).
- M. Fujita, K. M. Suzuki, S. Asano, H. Okabe, A. Koda, R. Kadono, and I. Watanabe, “New aspects of magnetism in T^{*}-type Eu₂CuO₂ revealed by precise muon spin rotation/relaxation measurements,” *Phys. Rev. B* (in press).

[Review articles]

H. Ohnishi, F. Sakuma, and T. Takahashi, “Hadron physics at J-PARC,” *Prog. Part. Nucl. Phys.*, (in press)

[Books]

岩崎雅彦, 佐久間史典, 山我拓巳, 「最近の研究から : K 中間子と陽子 2 つからなる “奇妙な” 原子核」, *日本物理学会誌*, 2020 年 1 月号 第 75 巻第 1 号 (通巻 855 号) pp. 10–15.

[Proceedings]

- S. Kawasaki *et al.*, “A(1405) spectroscopy via the in-flight d(K⁻, n) reaction at the J-PARC K1.8BR,” *JPS Conf. Proc.* **26**, 022009 (2019).
- T. Yamaga *et al.*, “Results of KbarNN search via the (K⁻, n) reaction at J-PARC,” *JPS Conf. Proc.* **26**, 023008 (2019).
- T. Hashimoto *et al.*, “Kaonic atom experiments at J-PARC,” *JPS Conf. Proc.* **26**, 023013 (2019).

- H. Asano *et al.*, “Spectroscopic study of the $\Lambda(1405)$ resonance via the $d(K^-, n)$ reaction at J-PARC,” AIP Conf. Proc. **2130**, 040018 (2019).
- Y. K. Tanaka *et al.*, “Spectroscopy of η' -mesic nuclei with WASA at GSI/FAIR,” Acta Phys. Polon. B **51**, 39 (2020).

Presentations

[International conferences/workshops]

- F. Sakuma (invited), “ K^-pp bound system at J-PARC,” The 15th International Conference on Meson-Nucleon Physics and the Structure of the Nucleon (MENU-2019), Cohon University Center, Carnegie Mellon University, Pittsburgh Pennsylvania, June 2–7, 2019.
- K. Itahashi (invited), “Mesons in nuclei: review and perspectives,” 3rd Jagiellonian Symposium on Fundamental and Applied Subatomic Physics, Krakow, June 23–28, 2019.
- K. Itahashi (oral), “Precision spectroscopy of pionic atoms at RIBF,” The 27th International Nuclear Physics Conference (INPC 2019), Glasgow, UK, July 29–August 2, 2019.
- T. Yamaga (oral), “Result of KbarNN search via exclusive measurements of (K^-, n) reaction at J-PARC,” The 27th International Nuclear Physics Conference (INPC 2019), Glasgow, UK, July 29–August 2, 2019.
- S. Okada (oral), “Kaonic atom X-ray spectroscopy with superconducting detector,” The 27th International Nuclear Physics Conference (INPC 2019), Glasgow, UK, July 29–August 2, 2019.
- T. Hashimoto (oral), “Towards the X-ray measurement of kaonic deuterium at J-PARC,” The 27th International Nuclear Physics Conference (INPC 2019), Glasgow, UK, July 29–August 2, 2019.
- K. Ishida, “Status of the $g-2$ and EDM experiment at J-PARC,” FCCP2019, Anacapri, Italy, August 2019.
- K. Ishida, “Measurement of the proton Zemach radius from the hyperfine splitting in muonic hydrogen utilizing muon spin repolarization with laser: Principle and Method,” Proton Radius 2019, Veli Losinji, Croatia, September 2019.
- S. Kanda, “Measurement of the proton Zemach radius from the hyperfine splitting in muonic hydrogen utilizing muon spin repolarization with laser: Preparation Status,” Proton Radius 2019, Veli Losinji, Croatia, September 2019.
- K. Ishida, “Status of the $g-2$ and EDM experiment at J-PARC,” Proton Radius 2019, Veli Losinji, Croatia, September 2019.
- M. Iwasaki (invited), “Kaonic nuclear bound state “ K^-pp ” observation and possible future plan,” The 3rd J-PARC symposium (J-PARC2019), Tsukuba, September 23–26, 2019.
- K. Ishida *et al.*, “Laser spectroscopy of the $1s$ hyperfine splitting energy of muonic hydrogen for the determination of proton Zemach radius,” The 3rd J-PARC symposium (J-PARC2019), Tsukuba, Japan, September 23–26, 2019.
- M. Iwasaki (invited), “A novel and peculiar quantum system— K -meson and two protons bound state,” STRANEX: Recent progress and perspectives in STRANEX EXotic atoms studies and related topics ECT*, Trento, October 21–25, 2019.
- F. Sakuma (invited), “ $\Lambda(1405)pn$ Final State in the $K^- + {}^3\text{He}$ reaction,” STRANEX: Recent progress and perspectives in STRANEX EXotic atoms studies and related topics ECT*, Trento, October 21–25, 2019.

[Domestic conferences/workshops]

- 岩崎雅彦 (招待講演), 「 K^- 中間子と2つの陽子が束縛した奇妙な量子多体系」, 日本物理学会秋季大会, 山形大学, 山形, 2009年9月17–20日.
- O. Zhadyra (口頭発表), 「The physics E31 experiment to search the $\Lambda(1405)$ via the $d(K^-, \pi\Sigma)$ reaction at J-PARC K1.8BR」, 日本物理学会秋季大会, 山形大学, 山形, 2009年9月17–20日.
- 山我拓巳 (招待講演), 「反 K^- 中間子ビームを用いた反 K^- 中間子原子核の研究」, ELPH研究会 C024 「ハドロン構造における多粒子相関」, 東北大学電子光物理学研究センター, 仙台, 2019年10月16–17日.
- 関屋涼平, 「GSIにおける WASA 検出器を用いたハイパー核分光実験および η' 中間子原子核探索実験のためのプラスチックシンチレータパレルの開発 (II)」, 日本物理学会秋季大会, 山形大学, 山形, 2009年9月17–20日.
- 石田勝彦, 「英国理研 RAL ミュオン施設とミュオン利用分析」, 第2回文理融合シンポジウム 量子ビームで歴史を探る—加速器が紡ぐ文理融合の地平—, 大阪, 2019年12月.
- 松本翔汰 (口頭発表), 「高精度パイ中間子原子分光実験のための三面交替 MWDC の開発」, 日本物理学会年次大会, 2020年3月.

[Seminars]

- RIKEN Symposium, “International Workshop of Topological Quantum Materials,” Tainan, Taiwan, January 10–12, 2019.
- RIKEN Symposium, “The 5th International Symposium in Current Progress in Mathematics and Sciences,” Depok, Indonesia, July 9–10, 2019.

Awards

- S. Winarsih, RIKEN Summer School 2019, Poster Prize (in Physics).
- S. Winarsih, RIKEN Summer School 2019, Poster Prize (Best Presentation).
- S. Winarsih, RIKEN Exchange Meeting 2019, Poster Prize (Student Section), 理研栄峰賞 板橋健太 2020年3月.

Subnuclear System Research Division RIKEN BNL Research Center

1. Abstract

The RIKEN BNL Research Center was established in April 1997 at Brookhaven National Laboratory with Professor T. D. Lee of Columbia University as its initial Director. It is funded by the Rikagaku Kenkyusho (RIKEN, The Institute of Physical and Chemical Research) of Japan. The Center is dedicated to the study of strong interactions, including spin physics, lattice QCD and RHIC physics through the nurturing of a new generation of young physicists. Professor Lee was succeeded by BNL Distinguished Scientist, N. P. Samios, who served until 2013. Dr. S. H. Aronson led the Center from 2013. After strong and significant leadership for 4 years, S. Aronson stepped down from Director in March 31st 2017. Hideto En'yo succeeds from JFY 2017. Support for RBRC was initially for five years and has been renewed four times, and presently extends to 2023. The Center is located in the BNL Physics Department. The RBRC Theory Group activities are closely and intimately related to those of the Nuclear Theory, High Energy Theory, and Lattice Gauge Theory Groups at BNL. The RBRC Experimental Group works closely with Radiation Laboratory at RIKEN, Wako, the RHIC Spin Group at BNL, the RHIC Spin Physics community, and the PHENIX/sPHENIX collaboration. BNL provides office space, management, and administrative support. In addition, the Computational Science Initiative (CSI) and Information Technology Division (ITD) at BNL provide support for computing. The Deputy Director of RBRC is D. Morrison (BNL). D. Kharzeev (Stony Brook/BNL) is leader of the Theory Group. Y. Akiba (RIKEN) is Experimental Group leader. T. Izubuchi (BNL) is Computing Group leader.

2. Major Research Subjects

Major research subjects of the theory group are

- (1) Heavy Ion Collision
- (2) Perturbative QCD
- (3) Phenomenological QCD

Major research subjects of the computing group are

- (1) Search for new law of physics through tests for Standard Model of particle and nuclear physics
- (2) Dynamics of QCD and related theories
- (3) Theoretical and algorithmic development for lattice field theories, QCD machine design

Major research subject of the experimental group are

- (1) Experimental Studies of the Spin Structure of the Nucleon
- (2) Study of Quark-Gluon Plasma at RHIC
- (3) sPHENIX detector construction

3. Summary of Research Activity

Summary of Research Activities of the three groups of the Center are given in the sections of each group.

Members

Director

Hideto EN'YO

Deputy Director

David P. MORRISON

Administrative Staff

Kazushige FUKUSHIMA (Administration Manager, Nishina Center and iTHEMS Promotion Office)

Hiroshi ITO (Deputy Administration Manager, Nishina Center and iTHEMS Promotion Office)

Pamela ESPOSITO (Administrative Assistant)

Maureen MCNEIL-SHEA (Administrative Assistant)

**Subnuclear System Research Division
RIKEN BNL Research Center
Theory Group**

1. Abstract

The efforts of the RBRC theory group are concentrated on the major topics of interest in High Energy Nuclear Physics and strongly interacting Chiral Matter. This includes: understanding of the Quark-Gluon Plasma; the nature of dense quark matter; the initial state in high energy collisions, the Color Glass Condensate; its evolution through a Glasma; spin physics, as is relevant for polarized hadronic collisions; physics relevant to electron-hadron collisions and the Electron-Ion Collider; quantum transport and the Chiral Magnetic Effect.

Theory Group hosted many joint tenure track positions with universities in U.S. and Japan.

2. Major Research Subjects

- (1) Heavy Ion Collisions
- (2) Perturbative Quantum Chromo-Dynamics (QCD)
- (3) Phenomenological QCD
- (4) Chiral Matter

3. Summary of Research Activity

(1) Phase diagram of QCD

The heavy ion program at Relativistic Heavy Ion Collider (RHIC) at BNL is focused on the study of the properties of QCD matter at high energy densities and high temperatures. The RBRC Theory group performs research that supports and guides the experimental program at RHIC. In the past year, RBRC researchers had developed the theory of bulk viscosity's behavior near the critical point and investigated universality-driven analytic structure of QCD crossover (V. Skokov).

Y. Kikuchi (in collaboration with K. Kashiwa and A. Tomiya) have developed a novel approach to the phase transitions using the neural network. In collaboration with R. Kobayashi, K. Shiozaki, and S. Ryu, Y. Kikuchi has proven a new theorem with higher-form symmetry and applied it to the quantum dimer models.

(2) QCD Matter at High Energy Density and at small x

The RHIC experimental heavy ion program is designed to study the properties of matter at energy densities much greater than that of atomic nuclei. This includes the initial state of nucleus-nucleus collisions, the Color Glass Condensate, the intermediate state to which it evolves, the Glasma, and lastly the thermal state to which it evolves, the Quark-Gluon Plasma. Theorists at the RBRC have made important contributions to all of these subjects.

During the past year, D. Kharzeev and V. Skokov in their papers investigated the role of entanglement in gluon fields at small Bjorken x in generating the azimuthal anisotropy of hadrons produced in AA and pA collisions at RHIC. It has been found that the small x gluon distributions are directly related to the entanglement entropy. D. Kharzeev, in collaboration with T. Ullrich and Z. Tu, investigated the role of entanglement in explaining the LHC data on hadron multiplicity distributions, and proposed a program to study entanglement at the EIC.

Y. Hatta has investigated the photoproduction of J/ψ charmonium near the threshold and its link to the problem of the origin of the proton's mass. He has found that this process can be used to extract the proton mass distribution. Y. Hatta has also developed the theory of spin dependence of Pomeron and Odderon in elastic scattering, and proposed a mechanism for single spin asymmetry observed at RHIC. He has also made important contributions to developing the science program at the EIC.

Y. Mehtar-Tani has developed a theory of jet propagation through a dense QCD matter that properly takes into account the multiple scattering effects. He has also evaluated higher order QCD corrections to jet quenching, and proposed a dynamical grooming algorithm for QCD jets.

C. Shen has advanced the applications of hydrodynamics to the description of heavy ion collisions, and built a quantitative model for the Beam Energy Scan at RHIC. In collaboration with Kharzeev and others, he has implemented the effects of magnetic field on the hydrodynamical evolution.

The activity of RBRC members described above bridges the gap between fundamental theory and phenomenology of heavy ion collisions. This includes the lattice QCD studies, the analytical work on the dynamics of phase transitions, the development of hydrodynamical and kinetic theory approaches incorporating quantum anomalies, and phenomenology. Much of the current work in the field is based on the ideas originally developed by the RBRC theorists.

(3) Chiral Matter

Much of the work done at the RBRC Theory group has broad implications beyond the domain of Nuclear and High Energy physics. One example is the Chiral Magnetic Effect, originally proposed to occur in quark-gluon plasma, but discovered recently in condensed matter systems, so-called Dirac and Weyl semimetals (the original experimental observation of CME was made at BNL in $ZrTe_5$ in a paper co-authored by D. Kharzeev). It has become clear that RBRC can make a very substantial impact also on condensed matter physics, where the methods developed at RBRC can be applied to a new set of problems. Vice versa, some of the new theoretical developments in condensed matter physics can be utilized for the study of QCD matter. Because of this, the RBRC developed a new

initiative on Chiral Matter focusing on the studies of quantum behavior in strongly interacting matter containing chiral fermions – this includes the quark-gluon plasma, electroweak plasma, Dirac and Weyl semimetals, and topological insulators.

In the past year, the RBRC members within this new initiative obtained a number of new results. Some of them, with a direct relevance for the quark-gluon plasma, have been already described above; other results are of direct relevance for condensed matter physics. D. Kharzeev and his students have proposed a new chiral magnetic photocurrent that has been observed experimentally. Kharzeev in collaboration with Q. Li have developed a concept of a new type of “chiral qubit” based on Dirac and Weyl semimetals.

The Chiral Matter initiative has already broadened the impact of RBRC beyond the traditional domain of high-energy nuclear physics, and has extended the RBRC research into a new and extremely active area.

Members

Group Leader

Dmitri KHARZEEV

Deputy Group Leaders

Yoshitaka HATTA

RBRC Researchers

Jordy DE VRIES

Yuta KIKUCHI

Yacine MEHTAR-TANI

Chun SHEN

Vladimir SKOKOV

Visiting Scientists

Hiromichi NISHIMURA (Keio Univ.)

Yuya TANIZAKI (North Carolina State Univ.)

List of Publications & Presentations

Publications

[Original papers]

- D. E. Kharzeev and Y. Kikuchi, “Real-time chiral dynamics from a digital quantum simulation,” *Phys. Rev. Res.* **2**, 023342 (2020) doi:10.1103/PhysRevResearch.2.023342 [arXiv:2001.00698 [hep-ph]].
- S. Kaushik, D. E. Kharzeev, and E. J. Philip, “Transverse chiral magnetic photocurrent induced by linearly polarized light in symmetric weyl semimetals,” [arXiv:2006.04857 [cond-mat.mes-hall]].
- J. Garaud, M. N. Chernodub, and D. E. Kharzeev, “Vortices with magnetic field inversion in non-centrosymmetric superconductors,” [arXiv:2003.10917 [cond-mat.supr-con]].
- U. Gürsoy, D. Kharzeev, E. Marcus, K. Rajagopal, and C. Shen, “Charge-dependent flow induced by electromagnetic fields in heavy ion collisions,” [arXiv:2002.12818 [hep-ph]].
- A. S. Gorsky and D. E. Kharzeev, “Tensor supercurrent in QCD,” *Phys. Rev. D* **101**, 114002 (2020) doi:10.1103/PhysRevD.101.114002 [arXiv:2001.07638 [hep-th]].
- K. Hao, D. Kharzeev, and V. Korepin, “Bethe Ansatz for XXX chain with negative spin,” *Int. J. Mod. Phys. A* **34**, 1950197 (2019) doi:10.1142/S0217751X19501975 [arXiv:1909.00800 [hep-th]].
- G. Inghirami, M. Mace, Y. Hirono, L. Del Zanna, D. E. Kharzeev, and M. Bleicher, “Magnetic fields in heavy ion collisions: flow and charge transport,” *Eur. Phys. J. C* **80**, 293 (2020) doi:10.1140/epjc/s10052-020-7847-4 [arXiv:1908.07605 [hep-ph]].
- M. Chernodub, J. Garaud, and D. Kharzeev, [arXiv:1908.00392 [cond-mat.supr-con]].
- D. Kharzeev, E. Shuryak, and I. Zahed, “Baryogenesis and helical magnetogenesis from the electroweak transition of the minimal Standard Model,” [arXiv:1906.04080 [hep-ph]].
- Z. Tu, D. E. Kharzeev, and T. Ullrich, “Einstein-podolsky-rosen paradox and quantum entanglement at subnucleonic scales,” *Phys. Rev. Lett.* **124**, 062001 (2020) doi:10.1103/PhysRevLett.124.062001 [arXiv:1904.11974 [hep-ph]].
- X. G. Huang, D. E. Kharzeev, and H. Taya, “Real-time dynamics of axion particle production due to spontaneous decay of a coherent axion field,” *Phys. Rev. D* **101**, 016011 (2020) doi:10.1103/PhysRevD.101.016011 [arXiv:1904.08184 [hep-ph]].
- D. Kharzeev and J. Liao, *Nucl. Phys. News* **29**, 26–31 (2019) doi:10.1080/10619127.2018.1495479
- D. E. Kharzeev and Q. Li, “The chiral qubit: quantum computing with chiral anomaly,” [arXiv:1903.07133 [quant-ph]].
- S. Kaushik, D. E. Kharzeev, and E. J. Philip, “Chiral magnetic photocurrent in dirac and weyl materials,” *Phys. Rev. B* **99**, 075150 (2019) doi:10.1103/PhysRevB.99.075150 [arXiv:1810.02399 [cond-mat.mes-hall]].
- Y. Hatta, “ J/Ψ photo-production near threshold and the proton mass problem,” doi:10.1142/9789811214950_0035
- Y. Hatta and Y. Zhao, “Parton distribution function for the gluon condensate,” [arXiv:2006.02798 [hep-ph]].
- R. Boussarie and Y. Hatta, “QCD analysis of near-threshold quarkonium leptoproduction at large photon virtualities,” *Phys. Rev. D* **101**, 114004 (2020) doi:10.1103/PhysRevD.101.114004 [arXiv:2004.12715 [hep-ph]].
- Y. Hatta, “How EIC can help us to understand heavy-ion collisions,” [arXiv:2004.05336 [hep-ph]].
- Y. Hagiwara, Y. Hatta, R. Pasechnik, and J. Zhou, “Spin-dependent Pomeron and Odderon in elastic proton-proton scattering,” *Eur. Phys. J. C* **80**, 427 (2020) doi:10.1140/epjc/s10052-020-8007-6 [arXiv:2003.03680 [hep-ph]].

- C. A. Aidala, E. Aschenauer, F. Aslan, A. Bacchetta, I. Balitsky, S. Benic, S. Bhattacharya, M. Boglione, M. Burkardt, J. Cammarota, G. A. Chirilli, C. Cocuzza, A. Courtoy, D. de Florian, P. Di Nezza, A. Dumitru, S. Fucini, K. Fukushima, Y. Furletova, L. Gamberg, O. Garcia-Montero, F. Gelis, V. Guzey, Y. Hatta, F. Hautmann, T. J. Hobbs, T. Horn, E. Iancu, S. Joosten, Z. B. Kang, R. Kishore, Y. V. Kovchegov, P. Kroll, K. Kumerički, K. Kutak, T. Lappi, H. W. Lin, X. Liu, S. Liuti, C. Lorcé, H. Mäntysaari, C. Marquet, Y. Makris, K. A. Mamo, Y. Mehtar-Tani, A. Metz, Z. E. Meziani, G. A. Miller, J. Miller, A. Mukherjee, P. M. Nadolsky, F. I. Olness, B. Pasquini, B. Pire, C. Pisano, D. Pitonyak, M. V. Polyakov, A. Prokudin, J. W. Qiu, M. Radici, A. Rajan, S. Rajesh, M. Rinaldi, K. Roy, C. Royon, N. Sato, M. Schlegel, G. Schnell, P. Schweitzer, S. Scopetta, R. Seidl, K. Semenov-Tian-Shansky, A. Signori, D. Sokhan, A. M. Stasto, L. Szymanowski, A. Tarasov, D. Triantafyllopoulos, T. Ullrich, R. Venugopalan, I. Vitev, W. Vogelsang, A. Vossen, B. T. Wang, S. Wallon, K. Watanabe, C. Weiss, B. W. Xiao, H. U. Yee, and Y. Zhao, “Probing nucleons and nuclei in high energy collisions,” doi:10.1142/11684 [arXiv:2002.12333 [hep-ph]].
- R. Boussarie, Y. Hatta, L. Szymanowski, and S. Wallon, “Probing the Sivvers function with an unpolarized target: GTMD distributions and the Odderons,” *Phys. Rev. Lett.* **124**, 172501 (2020) doi:10.1103/PhysRevLett.124.172501 [arXiv:1912.08182 [hep-ph]].
- Y. Hatta, M. Strikman, J. Xu, and F. Yuan, “Sub-threshold J/ψ and Υ production in γA collisions,” *Phys. Lett. B* **803**, 135321 (2020) doi:10.1016/j.physletb.2020.135321 [arXiv:1911.11706 [hep-ph]].
- S. Benic, Y. Hatta, H. N. Li, and D. J. Yang, “Single-spin asymmetries at two loops,” *Phys. Rev. D* **100**, 094027 (2019) doi:10.1103/PhysRevD.100.094027 [arXiv:1909.10684 [hep-ph]].
- Y. Hatta, N. Mueller, T. Ueda, and F. Yuan, *Phys. Lett. B* **802**, 135211 (2020) doi:10.1016/j.physletb.2020.135211 [arXiv:1907.09491 [hep-ph]].
- Y. Hatta and X. Yao, “QCD evolution of the orbital angular momentum of quarks and gluons: Genuine twist-three part,” *Phys. Lett. B* **798**, 134941 (2019) doi:10.1016/j.physletb.2019.134941 [arXiv:1906.07744 [hep-ph]].
- Y. Hatta, A. Rajan, and D. L. Yang, “Near threshold J/ψ and Υ photoproduction at JLab and RHIC,” *Phys. Rev. D* **100**, 014032 (2019) doi:10.1103/PhysRevD.100.014032 [arXiv:1906.00894 [hep-ph]].
- R. Boussarie, Y. Hatta, and F. Yuan, “Proton spin structure at small- x ,” *Phys. Lett. B* **797**, 134817 (2019) doi:10.1016/j.physletb.2019.134817 [arXiv:1904.02693 [hep-ph]].
- X. Yao, Y. Hagiwara, and Y. Hatta, “Computing the gluon Sivvers function at small- x ,” *Phys. Lett. B* **790**, 361–366 (2019) doi:10.1016/j.physletb.2019.01.029 [arXiv:1812.03959 [hep-ph]].
- S. Benic and Y. Hatta, “Single spin asymmetry in forward pA collisions: Phenomenology at RHIC,” *Phys. Rev. D* **99**, 094012 (2019) doi:10.1103/PhysRevD.99.094012 [arXiv:1811.10589 [hep-ph]].
- B. Schenke, C. Shen, and P. Tribedy, “Running the gamut of high energy nuclear collisions,” [arXiv:2005.14682 [nucl-th]].
- A. Czajka, S. Hauksson, C. Shen, S. Jeon, and C. Gale, “Effects of the mean field on fluid dynamics in the relaxation time approximation,” [arXiv:2004.11920 [nucl-th]].
- B. Schenke, C. Shen, and D. Teaney, “Transverse momentum fluctuations and their correlation with elliptic flow in nuclear collision,” [arXiv:2004.00690 [nucl-th]].
- C. Shen and S. Alzhrani, “A collision geometry-based 3D initial condition for relativistic heavy-ion collisions,” [arXiv:2003.05852 [nucl-th]].
- C. Gale, J. F. Paquet, B. Schenke, and C. Shen, “Probing early-time dynamics and quark-gluon plasma transport properties with photons and hadrons,” [arXiv:2002.05191 [hep-ph]].
- J. F. Paquet *et al.* [JETSCAPE], “Revisiting Bayesian constraints on the transport coefficients of QCD,” [arXiv:2002.05337 [nucl-th]].
- A. Monnai, B. Schenke, and C. Shen, “QCD equation of state at finite densities for nuclear collisions,” [arXiv:2002.02661 [nucl-th]].
- C. Shen, “Studying QGP with flow: A theory overview,” [arXiv:2001.11858 [nucl-th]].
- B. Schenke, C. Shen, and P. Tribedy, “Bulk properties and multi-particle correlations in large and small systems,” [arXiv:2001.09949 [nucl-th]].
- Y. Tachibana, C. Shen, and A. Majumder, “Bulk medium evolution has considerable effects on jet observables!,” [arXiv:2001.08321 [nucl-th]].
- A. Kumar, A. Majumder, and C. Shen, “Energy and scale dependence of \hat{q} and the “JET puzzle”,” *Phys. Rev. C* **101**, 034908 (2020) doi:10.1103/PhysRevC.101.034908 [arXiv:1909.03178 [nucl-th]].
- B. Schenke, C. Shen, and P. Tribedy, “Hybrid Color Glass Condensate and hydrodynamic description of the Relativistic Heavy Ion Collider small system scan,” *Phys. Lett. B* **803**, 135322 (2020) doi:10.1016/j.physletb.2020.135322 [arXiv:1908.06212 [nucl-th]].
- G. Vujanovic, J. F. Paquet, C. Shen, G. S. Denicol, S. Jeon, C. Gale, and U. Heinz, “Exploring the influence of bulk viscosity of QCD on dilepton tomography,” *Phys. Rev. C* **101**, 044904 (2020) doi:10.1103/PhysRevC.101.044904 [arXiv:1903.05078 [nucl-th]].
- A. Monnai, B. Schenke, and C. Shen, “Equation of state at finite densities for QCD matter in nuclear collisions,” *Phys. Rev. C* **100**, 024907 (2019) doi:10.1103/PhysRevC.100.024907 [arXiv:1902.05095 [nucl-th]].
- A. Majumder, S. Cao, C. Shen, and G. Y. Qin, “Effects of drag induced radiation and multi-stage evolution on heavy quark energy loss,” *PoS HardProbes2018*, 130 (2019) doi:10.22323/1.345.0130 [arXiv:1902.02217 [nucl-th]].
- C. Gale, S. Jeon, S. McDonald, J. F. Paquet, and C. Shen, “Centrality dependence of the direct photon multiplicity in heavy ion collisions,” *PoS HardProbes2018*, 178 (2019) doi:10.22323/1.345.0178 [arXiv:1901.07019 [nucl-th]].
- B. Schenke, C. Shen, and P. Tribedy, “Multi-particle and charge-dependent azimuthal correlations in heavy-ion collisions at the Relativistic Heavy-Ion Collider,” *Phys. Rev. C* **99**, 044908 (2019) doi:10.1103/PhysRevC.99.044908 [arXiv:1901.04378 [nucl-th]].
- C. Gale, S. Jeon, S. McDonald, J. F. Paquet, and C. Shen, “Photon radiation from heavy-ion collisions in the $\sqrt{s_{NN}} = 19\text{--}200$ GeV regime,” *Nucl. Phys. A* **982**, 767–770 (2019) doi:10.1016/j.nuclphysa.2018.08.005 [arXiv:1807.09326 [nucl-th]].

- M. Singh, C. Shen, S. McDonald, S. Jeon, and C. Gale, “Hydrodynamic fluctuations in relativistic heavy-ion collisions,” *Nucl. Phys. A* **982**, 319–322 (2019) doi:10.1016/j.nuclphysa.2018.10.061 [arXiv:1807.05451 [nucl-th]].
- C. Shen and B. Schenke, “Dynamical initialization and hydrodynamic modeling of relativistic heavy-ion collisions,” *Nucl. Phys. A* **982**, 411–414 (2019) doi:10.1016/j.nuclphysa.2018.08.007 [arXiv:1807.05141 [nucl-th]].
- B. Schenke, C. Shen, and P. Tribedy, “Features of the IP-Glasma,” *Nucl. Phys. A* **982**, 435–438 (2019) doi:10.1016/j.nuclphysa.2018.08.015 [arXiv:1807.05205 [nucl-th]].
- S. Ryu, S. McDonald, C. Shen, S. Jeon, and C. Gale, “Effects of hadronic rescattering in mini-jet production and energy loss at the LHC,” *PoS High-pT2017*, 014 (2019) doi:10.22323/1.320.0014
- S. Cao, A. Majumder, G. Y. Qin, and C. Shen, “Drag induced radiation and multi-stage effects in heavy-flavor energy loss,” *Phys. Lett. B* **793**, 433–439 (2019) doi:10.1016/j.physletb.2019.05.020 [arXiv:1711.09053 [nucl-th]].
- B. Chakraborty, M. Honda, T. Izubuchi, Y. Kikuchi, and A. Tomiya, “Digital quantum simulation of the Schwinger model with topological term via adiabatic state preparation,” [arXiv:2001.00485 [hep-lat]].
- K. Kashiwa, Y. Kikuchi, and A. Tomiya, “Phase transition encoded in neural network,” *PTEP* **2019**, 083A04 (2019) doi:10.1093/ptep/ptz082 [arXiv:1812.01522 [cond-mat.dis-nn]].
- R. Kobayashi, K. Shiozaki, Y. Kikuchi, and S. Ryu, “Lieb-Schultz-Mattis type theorem with higher-form symmetry and the quantum dimer models,” *Phys. Rev. B* **99**, 014402 (2019) doi:10.1103/PhysRevB.99.014402 [arXiv:1805.05367 [cond-mat.stat-mech]].
- W. Dekens, J. de Vries, K. Fuyuto, E. Mereghetti, and G. Zhou, “Sterile neutrinos and neutrinoless double beta decay in effective field theory,” *J. High Energy Phys.* **06**, 097 (2020) doi:10.1007/JHEP06(2020)097 [arXiv:2002.07182 [hep-ph]].
- J. de Vries, E. Epelbaum, L. Girlanda, A. Gnech, E. Mereghetti, and M. Viviani, “Parity- and time-reversal-violating nuclear forces,” [arXiv:2001.09050 [nucl-th]].
- V. Cirigliano, W. Dekens, J. De Vries, M. Graesser, E. Mereghetti, S. Pastore, M. Piarulli, U. Van Kolck, and R. Wiringa, “Renormalized approach to neutrinoless double- β decay,” *Phys. Rev. C* **100**, 055504 (2019) doi:10.1103/PhysRevC.100.055504 [arXiv:1907.11254 [nucl-th]].
- J. de Vries, G. Falcioni, F. Herzog, and B. Ruijl, “Two- and three-loop anomalous dimensions of Weinberg’s dimension-six CP-odd gluonic operator,” [arXiv:1907.04923 [hep-ph]].
- V. Cirigliano, A. Crivellin, W. Dekens, J. de Vries, M. Hoferichter, and E. Mereghetti, “CP violation in higgs-gauge interactions: from tabletop experiments to the LHC,” *Phys. Rev. Lett.* **123**, 051801 (2019) doi:10.1103/PhysRevLett.123.051801 [arXiv:1903.03625 [hep-ph]].
- F. Oosterhof, B. Long, J. de Vries, R. Timmermans, and U. van Kolck, *Phys. Rev. Lett.* **122**, 172501 (2019) doi:10.1103/PhysRevLett.122.172501 [arXiv:1902.05342 [hep-ph]].
- J. Dragos, T. Luu, A. Shindler, J. de Vries, and A. Yousif, “Confirming the existence of the strong CP problem in lattice QCD with the gradient flow,” [arXiv:1902.03254 [hep-lat]].
- J. De Vries, M. Postma, and J. van de Vis, “The role of leptons in electroweak baryogenesis,” *J. High Energy Phys.* **04**, 024 (2019) doi:10.1007/JHEP04(2019)024 [arXiv:1811.11104 [hep-ph]].
- J. Kim, J. Dragos, A. Shindler, T. Luu, and J. de Vries, “Towards a determination of the nucleon EDM from the quark chromo-EDM operator with the gradient flow,” *PoS LATTICE2018*, 260 (2019) doi:10.22323/1.334.0260 [arXiv:1810.10301 [hep-lat]].
- J. de Vries, P. Draper, K. Fuyuto, J. Kozaczuk, and D. Sutherland, “Indirect signs of the peccei-quinn mechanism,” *Phys. Rev. D* **99**, 015042 (2019) doi:10.1103/PhysRevD.99.015042 [arXiv:1809.10143 [hep-ph]].
- W. Dekens, J. de Vries, M. Jung, and K. Vos, “The phenomenology of electric dipole moments in models of scalar leptoquarks,” *J. High Energy Phys.* **01**, 069 (2019) doi:10.1007/JHEP01(2019)069 [arXiv:1809.09114 [hep-ph]].
- J. Dragos, T. Luu, A. Shindler, J. de Vries, and A. Yousif, “Improvements to nucleon matrix elements within a θ vacuum from Lattice QCD,” *PoS LATTICE2018*, 259 (2019) doi:10.22323/1.334.0259 [arXiv:1809.03487 [hep-lat]].
- A. Connelly, G. Johnson, F. Rennecke, and V. Skokov, “Universal location of the Yang-Lee edge singularity in O(N) theories,” [arXiv:2006.12541 [cond-mat.stat-mech]].
- A. Connelly, G. Johnson, S. Mukherjee, and V. Skokov, “Universality driven analytic structure of QCD crossover: radius of convergence and QCD critical point,” [arXiv:2004.05095 [hep-ph]].
- C. P. Korthals Altes, H. Nishimura, R. D. Pisarski, and V. V. Skokov, “Free energy of a holonomous plasma,” *Phys. Rev. D* **101**, 094025 (2020) doi:10.1103/PhysRevD.101.094025 [arXiv:2002.00968 [hep-ph]].
- A. Dumitru, V. Skokov, and T. Stebel, “Subfemtometer scale color charge correlations in the proton,” *Phys. Rev. D* **101**, 054004 (2020) doi:10.1103/PhysRevD.101.054004 [arXiv:2001.04516 [hep-ph]].
- H. Duan, C. Akkaya, A. Kovner, and V. V. Skokov, “Entanglement, partial set of measurements, and diagonality of the density matrix in the parton model,” *Phys. Rev. D* **101**, 036017 (2020) doi:10.1103/PhysRevD.101.036017 [arXiv:2001.01726 [hep-ph]].
- C. P. Korthals Altes, H. Nishimura, R. D. Pisarski, and V. V. Skokov, “Conundrum for the free energy of a holonomous gluonic plasma at cubic order,” *Phys. Lett. B* **803**, 135336 (2020) doi:10.1016/j.physletb.2020.135336 [arXiv:1911.10209 [hep-th]].
- S. Schlichting and V. Skokov, “Saturation corrections to dilute-dense particle production and azimuthal correlations in the Color Glass Condensate,” *Phys. Lett. B* **806**, 135511 (2020) doi:10.1016/j.physletb.2020.135511 [arXiv:1910.12496 [hep-ph]].
- S. Mukherjee and V. Skokov, “Universality driven analytic structure of QCD crossover: radius of convergence in baryon chemical potential,” [arXiv:1909.04639 [hep-ph]].
- V. Skokov, “Measuring the Weizsäcker-Williams distribution of linearly polarized gluons at an electron-ion collider through dijet azimuthal asymmetries,” *PoS DIS2019*, 256 (2019) doi:10.22323/1.352.0256 [arXiv:1907.10334 [hep-ph]].

- M. Martinez, T. Schäfer, and V. Skokov, “Critical behavior of the bulk viscosity in QCD,” *Phys. Rev. D* **100**, 074017 (2019) doi:10.1103/PhysRevD.100.074017 [arXiv:1906.11306 [hep-ph]].
- R. D. Pisarski, V. V. Skokov, and A. Tselik, “A Pedagogical Introduction to the Lifshitz Regime,” *Universe* **5**, 48 (2019) doi:10.3390/universe5020048
- M. Mace, V. V. Skokov, P. Tribedy, and R. Venugopalan, “Initial state description of azimuthally collimated long range correlations in ultrarelativistic light-heavy ion collisions,” [arXiv:1901.10506 [hep-ph]].
- N. Armesto, F. Dominguez, A. Kovner, M. Lublinsky, and V. Skokov, “The Color Glass Condensate density matrix: Lindblad evolution, entanglement entropy and Wigner functional,” *J. High Energy Phys.* **05**, 025 (2019) doi:10.1007/JHEP05(2019)025 [arXiv:1901.08080 [hep-ph]].
- H. Nishimura, C. Korthals-Altes, R. D. Pisarski, and V. Skokov, “Thermal effective potential for the Polyakov loop to higher loop order,” *PoS Confinement2018*, 155 (2019) doi:10.22323/1.336.0155 [arXiv:1811.11736 [hep-th]].
- A. Dumitru, V. Skokov, and T. Ullrich, “Measuring the Weizsäcker-Williams distribution of linearly polarized gluons at an electron-ion collider through dijet azimuthal asymmetries,” *Phys. Rev. C* **99**, 015204 (2019) doi:10.1103/PhysRevC.99.015204 [arXiv:1809.02615 [hep-ph]].
- K. Dusling, M. Mace, V. V. Skokov, P. Tribedy, and R. Venugopalan, “Multiparticle correlations and collectivity in small systems from the initial state,” *Nucl. Phys. A* **982**, 495–498 (2019) doi:10.1016/j.nuclphysa.2018.09.051 [arXiv:1807.06032 [hep-ph]].
- M. Mace, V. V. Skokov, P. Tribedy, and R. Venugopalan, “Systematics of azimuthal anisotropy harmonics in proton–nucleus collisions at the LHC from the Color Glass Condensate,” *Phys. Lett. B* **788**, 161–165 (2019) doi:10.1016/j.physletb.2018.09.064 [arXiv:1807.00825 [hep-ph]].
- M. Mace, V. V. Skokov, P. Tribedy, and R. Venugopalan, “Hierarchy of azimuthal anisotropy harmonics in collisions of small systems from the Color Glass Condensate,” *Phys. Rev. Lett.* **121**, 052301 (2018) doi:10.1103/PhysRevLett.121.052301 [arXiv:1805.09342 [hep-ph]].
- R. D. Pisarski, V. V. Skokov, and A. M. Tselik, “Fluctuations in cool quark matter and the phase diagram of Quantum Chromodynamics,” *Phys. Rev. D* **99**, 074025 (2019) doi:10.1103/PhysRevD.99.074025 [arXiv:1801.08156 [hep-ph]].
- A. Dumitru, F. Gelis, T. Lappi, and Y. Mehtar-Tani, “Summary of week VII,” doi:10.1142/9789811214950.0057
- Y. Mehtar-Tani, A. Soto-Ontoso, and K. Tywoniuk, “Tagging boosted hadronic objects with dynamical grooming,” [arXiv:2005.07584 [hep-ph]].
- J. Barata and Y. Mehtar-Tani, “Improved opacity expansion at NNLO for medium induced gluon radiation,” [arXiv:2004.02323 [hep-ph]].
- Y. Mehtar-Tani, “Improved opacity expansion for medium-induced parton splitting,” [arXiv:2003.02884 [hep-ph]].
- C. A. Aidala, E. Aschenauer, F. Aslan, A. Bacchetta, I. Balitsky, S. Benic, S. Bhattacharya, M. Boglione, M. Burkardt, J. Cammarota, G. A. Chirilli, C. Cocuzza, A. Courtoy, D. de Florian, P. Di Nezza, A. Dumitru, S. Fucini, K. Fukushima, Y. Furlotova, L. Gamberg, O. Garcia-Montero, F. Gelis, V. Guzey, Y. Hatta, F. Hautmann, T. J. Hobbs, T. Horn, E. Iancu, S. Joosten, Z. B. Kang, R. Kishore, Y. V. Kovchegov, P. Kroll, K. Kumerički, K. Kutak, T. Lappi, H. W. Lin, X. Liu, S. Liuti, C. Lorcé, H. Mäntysaari, C. Marquet, Y. Makris, K. A. Mamo, Y. Mehtar-Tani, A. Metz, Z. E. Meziani, G. A. Miller, J. Miller, A. Mukherjee, P. M. Nadolsky, F. I. Olness, B. Pasquini, B. Pire, C. Pisano, D. Pitonyak, M. V. Polyakov, A. Prokudin, J. W. Qiu, M. Radici, A. Rajan, S. Rajesh, M. Rinaldi, K. Roy, C. Royon, N. Sato, M. Schlegel, G. Schnell, P. Schweitzer, S. Scopetta, R. Seidl, K. Semenov-Tian-Shansky, A. Signori, D. Sokhan, A. M. Stasto, L. Szymanowski, A. Tarasov, D. Triantafyllopoulos, T. Ullrich, R. Venugopalan, I. Vitev, W. Vogelsang, A. Vossen, B. T. Wang, S. Wallon, K. Watanabe, C. Weiss, B. W. Xiao, H. U. Yee, and Y. Zhao, “Probing nucleons and nuclei in high energy collisions,” doi:10.1142/11684 [arXiv:2002.12333 [hep-ph]].
- R. Boussarie and Y. Mehtar-Tani, “On gauge invariance of transverse momentum dependent distributions at small x ,” [arXiv:2001.06449 [hep-ph]].
- Y. Mehtar-Tani, A. Soto-Ontoso, and K. Tywoniuk, “Dynamical grooming of QCD jets,” *Phys. Rev. D* **101**, 034004 (2020) doi:10.1103/PhysRevD.101.034004 [arXiv:1911.00375 [hep-ph]].
- Y. Mehtar-Tani and K. Tywoniuk, “Improved opacity expansion for medium-induced parton splitting,” [arXiv:1910.02032 [hep-ph]].
- Y. Mehtar-Tani, A. Soto-Ontoso, and M. Verweij, “Background estimator for jet studies in $p + p$ and $A + A$ collisions,” *Phys. Rev. D* **100**, 114023 (2019) doi:10.1103/PhysRevD.100.114023 [arXiv:1904.12815 [hep-ph]].
- Y. Mehtar-Tani, “Gluon bremsstrahlung in finite media beyond multiple soft scattering approximation,” *J. High Energy Phys.* **07**, 057 (2019) doi:10.1007/JHEP07(2019)057 [arXiv:1903.00506 [hep-ph]].
- Y. Mehtar-Tani and K. Tywoniuk, “Higher-order corrections to jet quenching,” *PoS HardProbes2018*, 096 (2019) doi:10.22323/1.345.0096 [arXiv:1903.01302 [hep-ph]].
- K. Tywoniuk and Y. Mehtar-Tani, “Toward a unified description of jet and medium scales in heavy-ion collisions,” *Nucl. Phys. A* **982**, 631–634 (2019) doi:10.1016/j.nuclphysa.2018.12.003
- H. A. Andrews, L. Apolinario, R. A. Bertens, C. Bierlich, M. Cacciari, Y. Chen, Y. T. Chien, L. C. Mendez, M. Deak, D. d’Enterria, F. Dominguez, P. C. Harris, K. Kutak, Y. J. Lee, Y. Mehtar-Tani, J. Mulligan, M. Nguyen, C. Ning-Bo, D. Perepelitsa, G. Salam, M. Spusta, J. G. Milhano, K. Tywoniuk, M. Van Leeuwen, M. Verweij, V. Vila, U. A. Wiedemann, and K. C. Zapp, “Novel tools and observables for jet physics in heavy-ion collisions,” *J. Phys. G* **47**, 065102 (2020) doi:10.1088/1361-6471/ab7cbc [arXiv:1808.03689 [hep-ph]].

Subnuclear System Research Division
RIKEN BNL Research Center
Experimental Group

1. Abstract

RIKEN BNL Research Center (RBRC) Experimental Group studies the strong interactions (QCD) using RHIC accelerator at Brookhaven National Laboratory, the world first heavy ion collider and polarized $p + p$ collider. We have three major activities: Spin Physics at RHIC, Heavy ion physics at RHIC, and detector upgrades of PHENIX experiment at RHIC.

We study the spin structure of the proton using the polarized proton-proton collisions at RHIC. This program has been promoted by RIKEN's leadership. The first focus of the research is to measure the gluon spin contribution to the proton spin. Recent results from PHENIX π^0 measurement and STAR jet measurement has shown that gluons in the proton carry about 30% of the proton spin. This is a major milestone of RHIC spin program. The second goal of the spin program is to measure the polarization of anti-quarks in the proton using $W \rightarrow e$ and $W \rightarrow \mu$ decays. The results of $W \rightarrow e$ measurement was published in 2016. The final results of $W \rightarrow \mu$ was published in 2018.

The aim of Heavy ion physics at RHIC is to re-create Quark Gluon Plasma (QGP), the state of Universe just after the Big Bang. Two important discoveries, jet quenching effect and strong elliptic flows, have established that new state of dense matter is indeed produced in heavy ion collisions at RHIC. We are now studying the property of the matter. Recently, we have measured direct photons in Au + Au collisions for $1 < p_T < 3$ GeV/c, where thermal radiation from hot QGP is expected to dominate. The comparison between the data and theory calculations indicates that the initial temperature of 300 MeV to 600 MeV is achieved. These values are well above the transition temperature to QGP, which is calculated to be approximately 160 MeV by lattice QCD calculations.

We had major roles in detector upgrades of PHENIX experiment, namely, the silicon vertex tracker (VTX) and muon trigger upgrades. Both of the upgrade is now complete. The VTX is the main device to measure heavy quark (charm and bottom) production and the muon trigger is essential for $W \rightarrow \mu$ measurement. The results from the first run with VTX detector in 2011 was published. The results show that electrons from bottom quark decay is strongly suppressed at high p_T , but the suppression is weaker than that of charm decay electron for $3 < p_T < 4$ GeV/c. We have recorded 10 times as much Au + Au collisions data in each of the 2014 run and 2016 run. The large dataset will produce definitive results on heavy quark production at RHIC.

PHENIX completed its data taking in 2016. We are now working on R&D of intermediate silicon tracker INTT for sPHENIX, a new experiment at RHIC that will be installed in the PHENIX IR.

2. Major Research Subjects

- (1) Experimental Studies of the Spin Structure of the Nucleon
- (2) Study of Quark-Gluon Plasma at RHIC
- (3) PHENIX detector upgrades

3. Summary of Research Activity

We study the strong interactions (QCD) using the RHIC accelerator at Brookhaven National Laboratory, the world first heavy ion collider and polarized $p + p$ collider. We have three major activities: Spin Physics at RHIC, Heavy ion physics at RHIC, and detector upgrades of PHENIX experiment. From 2015, Y. Akiba (Experimental Group Leader) is the Spokesperson of PHENIX experiment.

(1) Experimental study of spin structure of proton using RHIC polarized proton collider

How is the spin of proton formed with 3 quarks and gluons? This is a very fundamental question in Quantum Chromodynamics (QCD), the theory of the strong nuclear forces. The RHIC Spin Project has been established as an international collaboration between RIKEN and Brookhaven National Laboratory (BNL) to solve this problem by colliding two polarized protons for the first time in history. This project also has extended the physics capabilities of RHIC.

The first goal of the Spin Physics program at RHIC is to determine the gluon contribution to proton spin. It is known that the spin of quark accounts for only 25% of proton spin. The remaining 75% should be carried either by the spin of gluons or the orbital angular momentum of quarks and gluons. One of the main goals of the RHIC spin program has been to determine the gluon spin contribution. Before the start of RHIC, there was little experimental constraint on the gluon polarization, ΔG .

PHENIX measures the double helicity asymmetry (A_{LL}) of π^0 production to determine the gluon polarization. Our most recent publication of $\pi^0 A_{LL}$ measurement at 510 GeV shows non-zero value of A_{LL} , indicating that gluons in the proton is polarized. Global analysis shows that approximately 30% of proton spin is carried by gluons.

RHIC achieved polarized $p + p$ collisions at 500 GeV in 2009. The collision energy increased to 510 GeV in 2012 and 2013. The main goal of these high energy $p + p$ run is to measure anti-quark polarization via single spin asymmetry A_L of the W production. We upgraded the muon trigger system to measure $W \rightarrow \mu$ decays in the forward direction. With the measurement of $W \rightarrow e$ and $W \rightarrow \mu$, we can cover a wide kinematic range in anti-quark polarization measurement. The 2013 run is the main spin run at 510 GeV. PHENIX has recorded more than 150/pb of data in the run. The final results of the A_L measurement in $W \rightarrow e$ channel in combined data of 2011 to 2013 was published in 2016. The paper on the final results of $W \rightarrow \mu$ was published in 2018. These high statistics results give strong constraints on the polarization of anti-quarks in the proton.

RHIC has the first polarized proton nucleus collision run in 2015. In this run, we discovered a surprisingly large nuclear dependence of single spin asymmetry of very forward neutron. The paper of this discovery was published in Physical Review Letters.

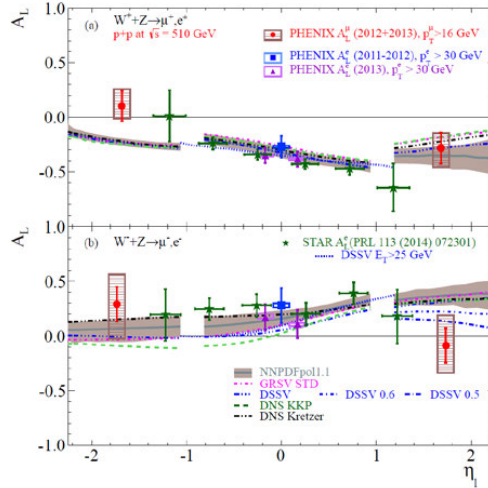


Fig. 1. Single spin asymmetry A_L of electrons from W and Z decays. The A_L is sensitive to the polarization of anti-quarks in the proton. The curves and the shaded region show theoretical calculations based on various polarized parton distribution (PDF) sets. The mid-rapidity points were published in Phys. Rev. D **93**, 051103(R) (2016). The forward/backward points were published in Phys. Rev. D **98**, 032007 (2018).

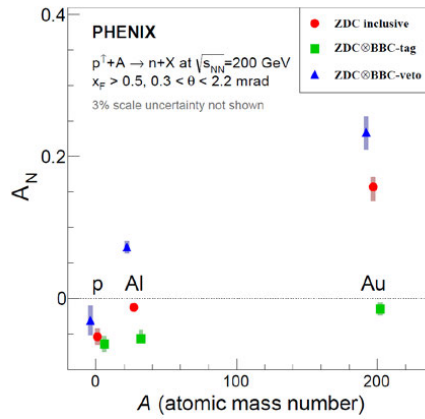


Fig. 2. Single spin asymmetry A_N of very forward neutron in $p + p$, $p + \text{Al}$, and $p + \text{Au}$ collision. Published in Phys. Rev. Lett. **120**, 022001 (2018).

(2) Experimental study of Quark-Gluon Plasma using RHIC heavy-ion collider

The goal of high energy heavy ion physics at RHIC is study of QCD in extreme conditions *i.e.* at very high temperature and at very high energy density. Experimental results from RHIC have established that dense partonic matter is formed in Au + Au collisions at RHIC. The matter is very dense and opaque, and it has almost no viscosity and behaves like a perfect fluid. These conclusions are primarily based on the following two discoveries:

- Strong suppression of high transverse momentum hadrons in central Au + Au collisions (jet quenching)
- Strong elliptic flow

These results are summarized in PHENIX White paper, which has approximately 2700 citations to date. The focus of the research in heavy ion physics at RHIC is now to investigate the properties of the matter. RBRC have played the leading roles in some of the most important results from PHENIX in the study of the matter properties. These include (1) measurements of heavy quark production from the single electrons from heavy flavor decay (2) measurements of J/Ψ production (3) measurements of di-electron continuum and (4) measurements of direct photons.

Our most important result is the measurement of direct photons for $1 < p_T < 5$ GeV/c in $p + p$ and Au + Au through their internal conversion to e^+e^- pairs. If the dense partonic matter formed at RHIC is thermalized, it should emit thermal photons. Observation of thermal photon is direct evidence of early thermalization, and we can determine the initial temperature of the matter. It is predicted that thermal photons from QGP phase is the dominant source of direct photons for $1 < p_T < 3$ GeV/c at the RHIC energy. We measured the direct photon in this p_T region from measurements of quasi-real virtual photons that decays into low-mass e^+e^- pairs. Strong enhancement of direct photon yield in Au + Au over the scaled $p + p$ data has been observed. Several hydrodynamical models can reproduce the central Au + A data within a factor of two. These models assume formation of a hot system with initial temperature of $T_{\text{init}} = 300$ MeV to 600 MeV. This is the first measurement of initial temperature of quark gluon plasma formed at RHIC. These

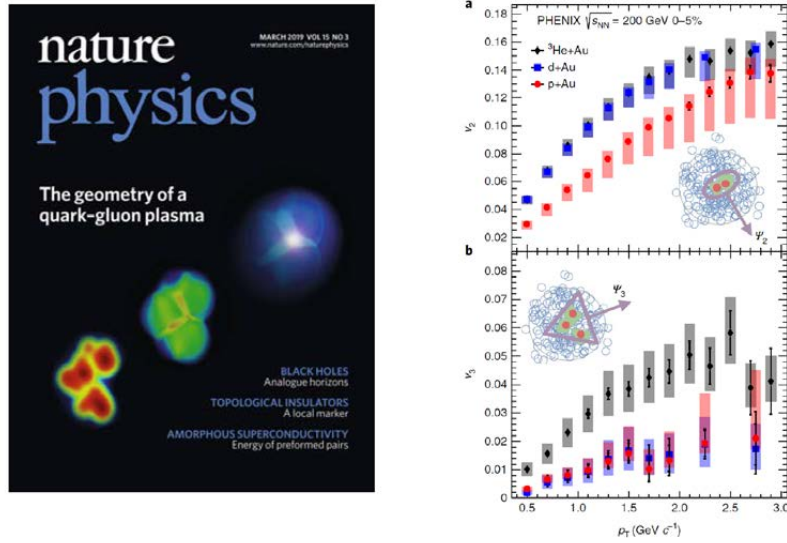


Fig. 3. Left: Cover of Nature Physics March 2019 issue featuring the PHENIX article reporting strong evidence of small QGP droplet formation. Right: Data of elliptic and triangular flow measured in p+Au, d+Au and $^3\text{He}+\text{Au}$ collisions.

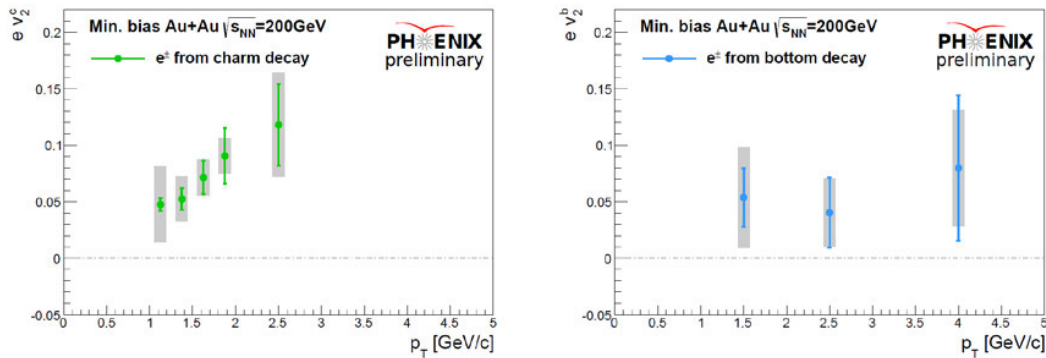


Fig. 4. Preliminary results of the elliptic flow strength v_2 of single electrons from charm and bottom decays.

results are recently published in Physical Review Letters. Y. Akiba is the leading person of the analysis and the main author of the paper. **He received 2011 Nishina memorial Prize mainly based on this work.**

PHENIX experiment measured the flow in small collision systems ($p + \text{Au}$, $d + \text{Au}$, and $^3\text{He} + \text{Au}$), and observed strong flow in all of these systems. Theoretical models that assume formation of small QGP droplets best describe the data. These results are published in Nature Physics in 2019.

(3) Detector upgrade

The group had major roles in several PHENIX detector upgrades, namely, the silicon vertex tracker (VTX) and muon trigger upgrades. VTX is a high precision charged particle tracker made of 4 layers of silicon detectors. It is jointly funded by RIKEN and the US DOE. The inner two layers are silicon pixel detectors and the outer two layers are silicon strip detectors. Y. Akiba is the project manager and A. Deshpande is the strip system manager. The VTX detector was completed in November 2010 and subsequently installed in PHENIX. The detector started taking data in the 2011 run. With the new detector, we measure heavy quark (charm and bottom) production in $p + p$, $A + A$ collisions to study the properties of quark-gluon plasma. The final result of the 2011 run was published. The result show that single electrons from bottom quark decay is suppressed, but not as strong as that from charm decay in low p_T region ($3 < p_T < 4$ GeV/c). This is the first measurement of suppression of bottom decay electrons at RHIC and the first observation that bottom suppression is smaller than charm. We have recorded 10 times as much Au + Au collisions data in each of the 2014 run and 2016 run. The large dataset will produce definitive results on heavy quark production at RHIC. A preliminary results on the elliptic flow strength v_2 of $b \rightarrow e$ and $c \rightarrow e$ has been presented in Quark Matter 2018 conference. The results of bottom/charm ratios in $p + p$ collisions at 200 GeV from the 2015 run was published (Phys. Rev. D99 092003 (2019)). A paper reporting measurements of the nuclear suppression factor R_{AA} of charm and bottom in Au+Au collisions from the 2014 data is in preparation.

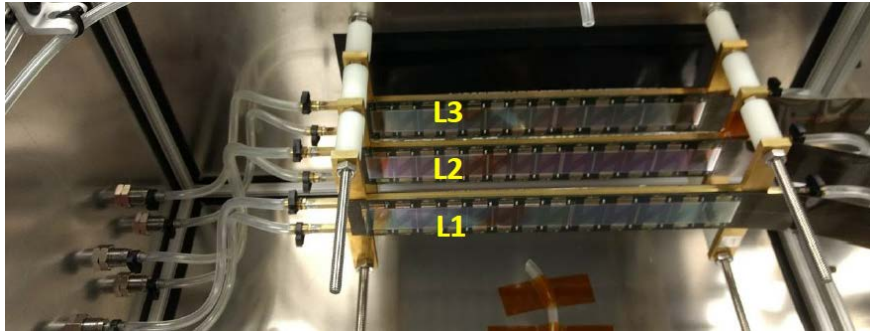


Fig. 5. Three ladder telescope made from INTT silicon tracker prototype. The prototype detector was tested in a beam test at FNAL in February 2018.

PHENIX completed its data taking in 2016. We are now working on R&D of intermediate silicon tracker INTT for sPHENIX, a new experiment at RHIC that will be installed in the PHENIX IR. A three ladder telescope of INTT prototype modules was tested in a beam test at FNAL. The prototype detector worked very well during the test.

Members

Group Leader

Yasuyuki AKIBA

RBRC Researchers

Jan C. BERNAUER

Megan CONNORS

Yuji GOTO

Takashi HACHIYA

Itaru NAKAGAWA

Seidl RALF

Atsushi TAKETANI

Takahito TODOROKI

Marta VERWEIJ

Yasushi WATANABE

Satoshi YOKKAICHI

Special Temporary Research Scientist

Takashi ICHIHARA

Visiting Scientists

Stefan BATHE (Baruch College Univ. of New York)

Gaku MITSUKA (KEK)

Rachid NOUICER (BNL)

Masahiro OKAMURA (BNL)

Takao SAKAGUCHI (BNL)

Takashi SAKO (Univ. of Tokyo)

Student Trainees

Kai-Yu Cheng (National Central U)

Anthony Hodges (Georgia State U)

Lihan Liu (Vanderbilt U)

Xiao Rui (Purdue U)

Cheng-Wei Shih (National Central U)

Cheuk-Ping Wong (Georgia State U)

List of Publications & Presentations

Publications

[Original papers]

- C. Aidala *et al.*, “Creation of quark-gluon plasma droplets with three distinct geometries,” *Nature Physics* **15**, 214 (2019).
- A. Adare *et al.*, “Beam energy and centrality dependence of direct-photon emission from ultrarelativistic heavy-ion collisions,” *Phys. Rev. Lett.* **123**, 022301 (2019).
- C. Aidala *et al.*, “Nuclear dependence of the transverse single-spin asymmetry in the production of charged hadrons at forward rapidity in polarized p+p, p+Al, and p+Au collisions at $\sqrt{s_{NN}} = 200$ GeV,” *Phys. Rev. Lett.* **123**, 122001 (2019).
- A. Adare *et al.*, “Multiparticle azimuthal correlations for extracting event-by-event elliptic and triangular flow in Au+Au collisions at $\sqrt{s_{NN}} = 200$ GeV,” *Phys. Rev. C* **99**, 024903 (2019).
- C. Aidala *et al.*, “Nonperturbative transverse momentum broadening in dihedron angular correlations in $\sqrt{s_{NN}} = 200$ GeV proton-nucleus collisions,” *Phys. Rev. C* **99**, 044912 (2019).
- A. Adare *et al.*, “Measurement of two-particle correlations with respect to second- and third- order event planes in Au+Au collisions at $\sqrt{s_{NN}} = 200$ GeV,” *Phys. Rev. C* **99**, 054903 (2019).
- C. Aidala *et al.*, “Measurements of $\mu\mu$ pairs from open heavy flavor and Drell-Yan in p+p collisions at $\sqrt{s} = 200$ GeV,” *Phys. Rev. D* **99**, 072003 (2019).

- C. Aidla *et al.*, “Measurement of charm and bottom production from semileptonic hadron decays in p+p collisions at $\sqrt{s_{NN}} = 200$ GeV,” *Phys. Rev. D* **99**, 092003 (2019).

Presentations

[International conferences/workshops]

- T. Hachiya (invited), “PHENIX heavy flavor highlights,” 8th International conference on new frontiers in physics (ICNFP 2019), Crete, Greece, August 21–29, 2019.
- M. Connors (invited), “PHENIX highlights,” 28th International conference on ultrarelativistic nucleus-nucleus collisions (Quark Matter 2019), Wuhan, China, November 4–9, 2019.
- T. Todoroki (oral), “Quark flavor dependence of particle flow in nucleus-nucleus collisions measured by PHENIX,” 28th International conference on ultrarelativistic nucleus-nucleus collisions (Quark Matter 2019), Wuhan, China, November 4–9, 2019.

Awards

- Megan Connors, CAREER award from the National Science Foundation.

Subnuclear System Research Division
 RIKEN BNL Research Center
 Computing Group

1. Abstract

The computing group founded in 2011 as a part of the RIKEN BNL Research Center established at Brookhaven National Laboratory in New York, USA, and dedicated to conduct researches and developments for large-scale physics computations important for particle and nuclear physics. The group was forked from the RBRC Theory Group.

The main mission of the group is to provide important numerical information that is indispensable for theoretical interpretation of experimental data from the first principle theories of particle and nuclear physics. Their primary area of research is lattice quantum chromodynamics (QCD), which describes the sub-atomic structures of hadrons, which allow us the ab-initio investigation for strongly interacting quantum field theories beyond perturbative analysis.

The RBRC group and its collaborators have emphasized the necessity and importance of precision calculations, which will precisely check the current understandings of nature, and will have a potential to find a physics beyond the current standard model of fundamental physics. We have therefore adopted techniques that aim to control and reduce any systematic errors. This approach has yielded many reliable results.

The areas of the major activities are R&D for high performance computers, developments for computing algorithms, and researches of particle, nuclear, and lattice theories. Since the inception of RBRC, many breakthroughs and pioneering works has carried out in computational forefronts. These are the use of the domain-wall fermions, which preserve chiral symmetry, a key symmetry for understanding nature of particle nuclear physics, the three generations of QCD devoted supercomputers, pioneering works for QCD calculation for Cabibbo-Kobayashi-Maskawa theory, QCD + QED simulation for isospin breaking, novel algorithm for error reduction in general lattice calculation. Now the chiral quark simulation is performed at the physical up, down quark mass, the precision for many basic quantities reached to accuracy of sub-percent, and the group is aiming for further important and challenging calculations, such as the full and complete calculation of CP violating $K \rightarrow \pi\pi$ decay and ϵ'/ϵ , or hadronic contributions to muon's anomalous magnetic moment $g - 2$. Another focus area is the nucleon's shape, structures, and the motion of quarks and gluon inside nucleon called parton distribution, which provide theoretical guidance to physics for sPHENIX and future Electron Ion Collider (EIC), Hyper Kamiokande, DUNE, or the origin of the current matter rich universe (rather than anti-matter). Towards finite density QCD, they also explore Quantum Computing to overcome the sign problem.

2. Major Research Subjects

- (1) Search for new law of physics through tests for Standard Model of particle and nuclear physics, especially in the framework of the Cabibbo-Kobayashi-Maskawa (CKM), hadronic contributions to the muon's anomalous magnetic moment ($g - 2$) for FNAL and J-PARC's experiments, as well as B physics at Belle II and LHCb.
- (2) Nuclear Physics and dynamics of QCD or related theories, including study for the structures of nucleons related to physics for Electron Ion Collider (EIC or eRHIC), Hyper Kamiokande, T2K, DUNE.
- (3) Theoretical and algorithmic development for lattice field theories, QCD machine (co-)design and code optimization.

3. Summary of Research Activity

In 2011, QCD with Chiral Quarks (QCDCQ), a third-generation lattice QCD computer that is a pre-commercial version of IBM's Blue Gene/Q, was installed as an in-house computing resource at the RBRC. The computer was developed by collaboration among RBRC, Columbia University, the University of Edinburgh, and IBM. Two racks of QCDCQ having a peak computing power of 2×200 TFLOPS are in operation at the RBRC. In addition to the RBRC machine, one rack of QCDCQ is owned by BNL for wider use for scientific computing. In 2013, 1/2 rack of Blue Gene/Q is also installed by US-wide lattice QCD collaboration, USQCD. The group has also used the IBM Blue Gene supercomputers located at Argonne National Laboratory and BNL (NY Blue), and Hokusai and RICC, the super computers at RIKEN (Japan), Fermi National Accelerator Laboratory, the Jefferson Lab, and others. From 2016, the group started to use the institutional cluster both GPU and Intel Knight Landing (KNL) clusters installed at BNL and University of Tokyo extensively.

Such computing power enables the group to perform precise calculations using up, down, and strange quark flavors with proper handling of the important symmetry, called chiral symmetry, that quarks have. The group and its collaborators carried out the first calculation for the direct breaking of CP (Charge Parity) symmetry in the hadronic K meson decay ($K \rightarrow \pi\pi$) amplitudes, ϵ'/ϵ , which provide a new information to CKM paradigm and its beyond. They also provide the hadronic contribution in muon's anomalous magnetic moment $(g - 2)_\mu$. These calculation for ϵ'/ϵ , hadronic light-by-light of $(g - 2)$, are long waited calculation in theoretical physics delivered for the first time by the group. The $K \rightarrow \pi\pi$ result in terms of ϵ'/ϵ currently has a large error, and deviates from experimental results by 2.1σ . To collect more information to decide whether this deviation is from the unknown new physics or not, the group continues to improve the calculation in various way to reduce their error. Hadronic light-by-light contribution to $(g - 2)_\mu$ is improved by more than two order of magnitudes compared to our previous results. As of 2019 summer, their calculation is among the most precise determination for the $g - 2$ hadronic vacuum polarization (HVP), and only one calculation in the world for the hadronic light-by-light (HLbL) contribution at physical point. These $(g - 2)_\mu$ calculations provide the first principle theoretical prediction for on-going new experiment at FNAL and also for the planned experiment at J-PARC. Other projects including flavor physics in the framework of the CKM theory for kaons and B mesons that include the new calculation of b-baryon decay, $\Lambda_b \rightarrow p$; the electromagnetic properties

of hadrons; the proton's and neutron's form factors and structure function including electric dipole moments; proton decay; nucleon form factors, which are related to the proton spin problem or neutrino-nucleon interaction; Neutron-antineutron oscillations; inclusive hadronic decay of τ leptons; nonperturbative studies for beyond standard model such composite Higgs or dark matter models from strong strongly interacting gauge theories; a few-body nuclear physics and their electromagnetic properties; QCD thermodynamics in finite temperature/density systems such as those produced in heavy-ion collisions at the Relativistic Heavy Ion Collider; Quantum Information, Quantum Computing; and applications of machine learning in field theories.

The RBRC group and its collaborators have emphasized the necessity and importance of precision calculations, which will provide stringent checks for the current understandings of nature, and will have a potential to find physics beyond the current standard model of fundamental physics. We have therefore adopted techniques that aim to control and reduce any systematic errors. This approach has yielded many reliable results, many of basic quantities are now computed within sub-percent accuracies.

The group also delivers several algorithmic breakthroughs, which speed up generic lattice gauge theory computation. These novel technique divides the whole calculation into frequent approximated calculations, and infrequent expensive and accurate calculation using lattice symmetries called All Mode Averaging (AMA), or a compression for memory needs by exploiting the local-coherence of QCD dynamics. Together with another formalism, zMobius fermion, which approximate chiral lattice quark action efficiently, the typical calculation is now improved by a couple of orders of magnitudes, and more than an order of magnitude less memory needs compared to the traditional methods. RBRC group and its collaborators also provide very efficient and generic code optimized to the state-of-arts CPU or GPU, and also improve how to efficiently generate QCD ensemble.

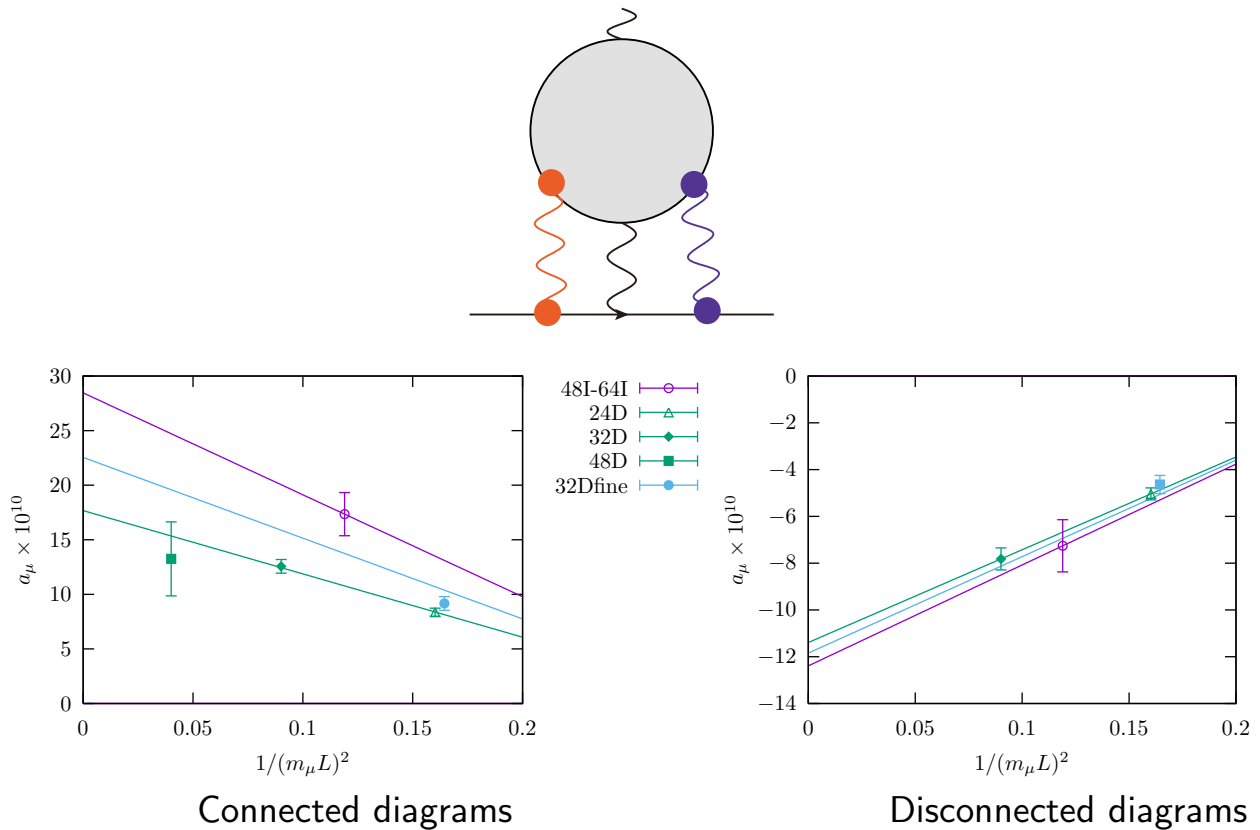


Fig. 1. The bottom plots are Hadronic Light-by-Light (HLbL) contributions to muon anomalous magnetic moment shown at top diagram.

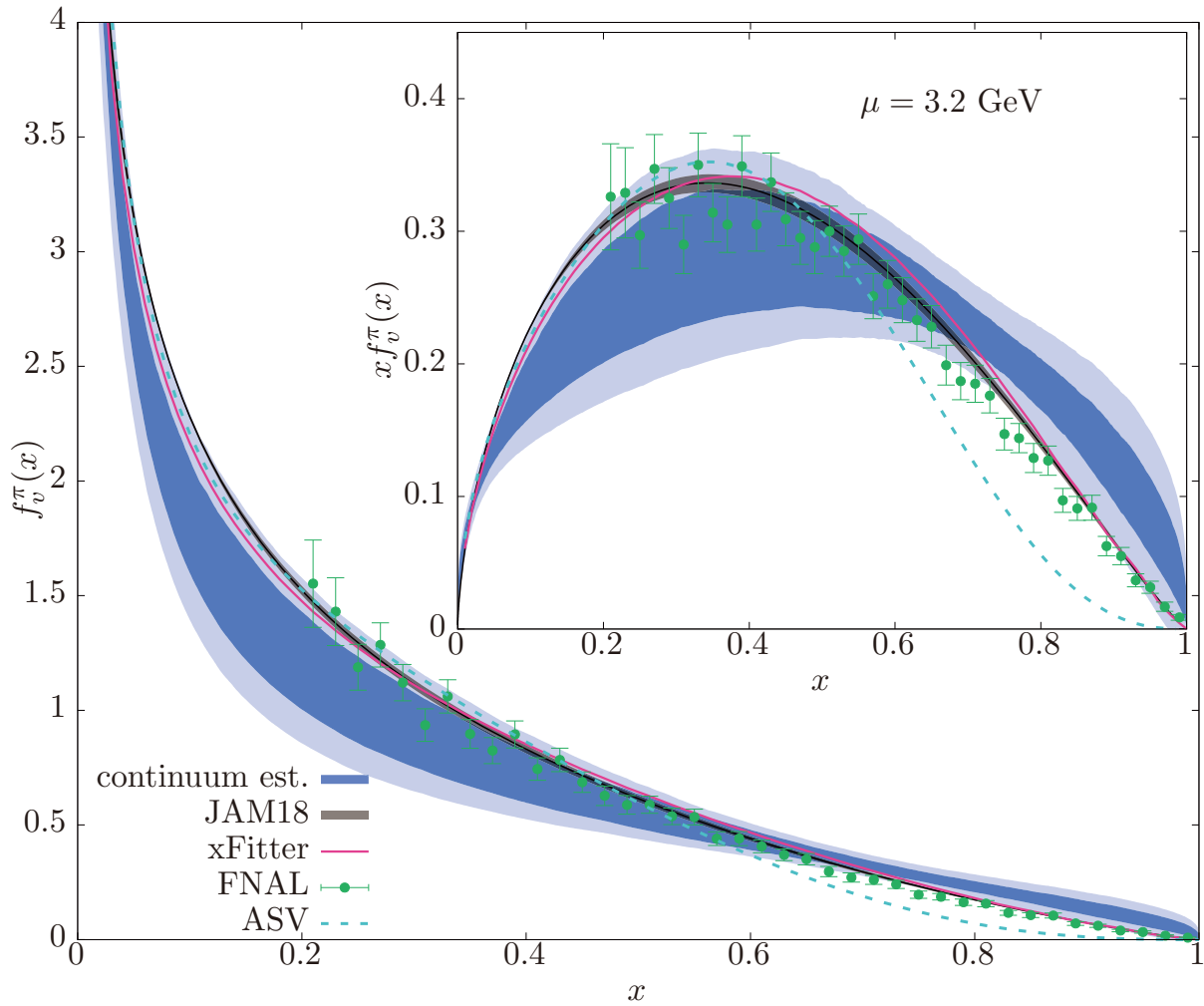


Fig. 2. Parton Distribution of pion as function of momentum fraction of valence quark, x , at factorization scale 3.2 GeV compared to phenomenological and experimental determinations. From arXiv:2007.06590

Members

Group Leader

Taku IZUBUCHI

Special Postdoctoral Researchers

Akio TOMIYA

Enrico RINALDI

RBRC Researchers

Yasumichi AOKI (RIKEN BNL Fellow, KEK)
 Ethan NEIL (RHIC Physics Fellow)
 Stefan MEINEL (RHIC Physics Fellow)

Sergey SYRITSYN (RHIC Physics Fellow)
 Luchang JIN (RHIC Physics Fellow)

Visiting Scientists

Thomas BLUM (Univ. of Connecticut)
 Chulwoo JUNG (BNL)
 Shigemi OHTA (KEK)
 Tomomi ISHIKAWA (Shanghai Jiao-Tong Univ.)
 Christoph LEHNER (BNL)

Meifeng LIN (BNL)
 Robert MAWHINNEY (Columbia Univ.)
 Hiroshi OKI (Nara Women’s Univ.)
 Christopher KELLY (Columbia Univ.)

List of Publications & Presentations

Publications

[Original papers]

- C. Y. Seng, X. Feng, M. Gorchtein, and L. C. Jin, “Joint lattice QCD–dispersion theory analysis confirms the quark-mixing top-row unitarity deficit,” *Phys. Rev. D* **101**, 111301 (2020). doi:10.1103/PhysRevD.101.111301 [arXiv:2003.11264 [hep-ph]].
- X. Feng, M. Gorchtein, L. C. Jin, P. X. Ma, and C. Y. Seng, “First-principles calculation of electroweak box diagrams from lattice QCD,” *Phys. Rev. Lett.* **124**, 192002 (2020). doi:10.1103/PhysRevLett.124.192002 [arXiv:2003.09798 [hep-lat]].
- T. Blum, N. Christ, M. Hayakawa, T. Izubuchi, L. Jin, C. Jung, and C. Lehner, “Hadronic light-by-light scattering contribution to the muon anomalous magnetic moment from lattice QCD,” *Phys. Rev. Lett.* **124**, 132002 (2020). doi:10.1103/PhysRevLett.124.132002 [arXiv:1911.08123 [hep-lat]].
- X. Feng, Y. Fu, and L. C. Jin, “Lattice QCD calculation of the pion charge radius using a model-independent method,” *Phys. Rev. D* **101**, 051502 (2020). doi:10.1103/PhysRevD.101.051502 [arXiv:1911.04064 [hep-lat]].
- X. Y. Tuo, X. Feng, and L. C. Jin, “Long-distance contributions to neutrinoless double beta decay $\pi^- \rightarrow \pi^+ ee$,” *Phys. Rev. D* **100**, 094511 (2019). doi:10.1103/PhysRevD.100.094511 [arXiv:1909.13525 [hep-lat]].
- G. Rendon, S. Meinel *et al.*, “ $I = 1/2$ S -wave and P -wave $K\pi$ scattering and the κ and K^* resonances from lattice QCD,” arXiv:2006.14035 [hep-lat]
- T. Blake, S. Meinel, and D. van Dyk. “Bayesian analysis of $b \rightarrow s\mu^+\mu^-$ Wilson coefficients using the full angular distribution of $\Lambda_b \rightarrow \Lambda(\rightarrow p\pi^-)\mu^+\mu^-$ Decays,” *Phys. Rev. D* **101**, 035023 (2020).
- R. Larsen, S. Meinel, S. Mukherjee, and P. Petreczky, “Excited bottomonia in quark-gluon plasma from lattice QCD,” *Phys. Lett. B* **800**, 135119 (2020).
- R. Larsen, S. Meinel, S. Mukherjee, and P. Petreczky, “Thermal broadening of bottomonia: Lattice nonrelativistic QCD with extended operators,” *Phys. Rev. D* **100**, 074506 (2019).
- J. R. Green, M. Engelhardt, N. Hasan, S. Krieg, S. Meinel, J. W. Negele, A. V. Pochinsky, and S. N. Syritsyn, “Excited-state effects in nucleon structure on the lattice using hybrid interpolators,” *Phys. Rev. D* **100**, 074510 (2019).
- L. Leskovec, S. Meinel, M. Pflaumer, and M. Wagner, “Lattice QCD investigation of a doubly-bottom $\bar{b}b\bar{u}u$ tetraquark with quantum numbers $I(J^P) = 0(1^+)$,” *Phys. Rev. D* **100**, 014503 (2019).
- N. Hasan, J. Green, S. Meinel, M. Engelhardt, S. Krieg, J. Negele, A. Pochinsky, and S. Syritsyn, “Nucleon axial, scalar, and tensor charges using lattice QCD at the physical pion mass,” *Phys. Rev. D* **99**, 114505 (2019).
- T. Izubuchi, S. Syritsyn *et al.*, “Valence parton distribution function of pion from fine lattice,” *Phys. Rev. D* **100**, 034516 (2019).
- E. Rinaldi, S. Syritsyn, *et al.* “Lattice QCD determination of neutron-antineutron matrix elements with physical quark masses,” *Phys. Rev. D* **99**, 074510 (2019).
- K. -Y. Kim, M. Nishida, M. Nozaki, M. Seo, Y. Sugimoto, and A. Tomiya, “Entanglement after quantum quenches in lifshitz scalar theories,” *J. Stat. Mech.* **1909**, 093104 (2019) arXiv:1904.01276 [hep-lat]
- B. Chakraborty, M. Honda, T. Izubuchi, Y. Kikuchi, and A. Tomiya, “Digital quantum simulation of the schwinger model with topological term via adiabatic state preparation,” arXiv:2001.00485 [hep-lat]

[Review articles]

- T. Aoyama, L. Jin, T. Blum, T. Izubuchi, C. Lehner *et al.*, “The anomalous magnetic moment of the muon in the standard model,” arXiv:2006.04822 [hep-ph]
- V. Cirigliano, Z. Davoudi, T. Izubuchi *et al.*, “The role of lattice QCD in searches for violations of fundamental symmetries and signals for new physics,” *Eur. Phys. J. A* **55**, 197 (2019).
- P. Gambino, S. Meinel, *et al.*, “Challenges in semileptonic B decays,” arXiv:2006.07287 [hep-ph]
- W. Detmold, S. Meinel, S. Syritsyn, *et al.* [USQCD Collaboration]. “Hadrons and nuclei,” *Eur. Phys. J. A* **55**, 193 (2019).
- C. Lehner, S. Meinel *et al.* [USQCD Collaboration]. “Opportunities for lattice QCD in quark and lepton flavor physics,” *Eur. Phys. J. A* **55**, 195 (2019).
- T. Izubuchi

[Books]

- K. Hashimoto, A. Tomiya *et al.*, “Physics uses machine learning (in Japanese),” Asakura, October 2019.
- K. Hashimoto, A. Tanaka, and A. Tomiya, “Deep Learning and physics (in Japanese),” Kodansha, June 2019.

[Proceedings]

- K. Maltman, T. Izubuchi, *et al.*, “Current status of inclusive hadronic τ determinations of $|V_{us}|$,” *SciPost Phys. Proc.* **1**, 006 (2019).
- M. Kawaguchi, S. Matsuzaki, and A. Tomiya, “Analysis on nonperturbative flavor violation at chiral crossover criticality in QCD,” arXiv:2005.07003 [hep-ph]
- M. Kawaguchi, S. Matsuzaki, and A. Tomiya, “Nonperturbative flavor breaking in topological susceptibility at Hot QCD criticality,” arXiv:2003.11375 [hep-ph]
- H. -T. Ding, S. -T. Li, S. Mukherjee, A. Tomiya, and X. -D. Wang, “Meson masses in external magnetic fields with HISQ fermions,” arXiv:2001.05322 [hep-lat]
- H. -T. Ding, O. Kaczmarek, F. Karsch, S. -T. Li, S. Mukherjee, A. Tomiya, and Y. Zhang, “Dirac Eigenvalue spectrum of $N_f = 2+1$ QCD

towards the chiral limit using HISQ fermions,” arXiv:2001.05217 [hep-lat]

A. Tomiya, H. -T. Ding, X. -D. Wang, Y. Zhang, S. Mukherjee, and C. Schmidt, “Phase structure of three flavor QCD in external magnetic fields using HISQ fermions,” arXiv:1904.01276 [hep-lat]

Presentations

[International conference/workshops]

- L. Jink (invited), “QED corrections to hadron masses,” χ QCD collaboration meeting at University of Kentucky, December 13, 2019.
- L. Jin (invited), “Status of Muon $g - 2$,” Brookhaven Forum 2019: Particle Physics and Cosmology in the 2020’s, September 26, 2019.
- L. Jin (invited), “Hadronic Light-by-Light RBC,” Hadronic contributions to $(g - 2) \mu$, INT Workshop INT-19-74W, September 11, 2019.
- L. Jin (invited, plenary) “QED_∞ in muon $g - 2$, hadron spectroscopy, and beyond,” 37th international conference on lattice field theory, June 20, 2019.
- A. Tomiya (invited), “Applications of machine learning to computational physics,” A.I. for nuclear physics (invited), Jefferson Laboratory, Virginia, USA, November 3, 2020.
- A. Tomiya, “Chiral condensate in Schwinger model by quantum computer,” International Workshop on “Theoretical Particle Physics 2019,” Tokyo, Japan, November 4, 2019.
- A. Tomiya, “Phase structure of three flavor QCD in external magnetic fields,” XQCD 2019, Tokyo, Japan, June 2019.
- A. Tomiya, “Phase structure of three flavor QCD in external magnetic fields,” Lattice 2019, Wuhan, China, June 2019.

[Domestic Conferences/Workshops]

- A. Tomiya, “Phase structure of three flavor QCD in external magnetic fields,” JPS meeting, Kyushu University, March 2019.
- A. Tomiya, “QCD phase transition under external magnetic field with improved staggered fermions,” JPS meeting, Tokyo University of Science, March 2018.

[Seminars]

- A. Tomiya, “Lattice gauge theory with quantum computers,” (Virtual) RIKEN Center for Computational Science, Japan, June 3, 2020.
- A. Tomiya, “Lattice gauge theory with quantum computers,” (Virtual) Osaka university, Japan, May 12, 2020.
- A. Tomiya, “An introduction to deep learning (lecture),” Jamstec (Japan Agency for Marine-Earth Science and Technology), Japan, January 13, 2019.
- A. Tomiya, “An introduction to lattice gauge theories (lecture),” Math club, Tokyo, Japan, December 28, 2019.
- A. Tomiya, “An introduction to deep learning (lecture),” Kochi Technological university, Kochi, Japan, December 13, 2019.
- A. Tomiya, “An introduction to Machine learning and science (lecture),” Kochi Technological university, Kochi, Japan, December 13, 2019.
- A. Tomiya, “An introduction to lattice gauge theories (lecture),” Jilin U, China, November 18, 2019.
- A. Tomiya, “An introduction to deep learning (lecture),” Waseda U (hpc-phys working group), Japan, November 7, 2019.
- A. Tomiya, “Phase transition in three flavor QCD with background magnetic field,” Jilin U, China, September 24, 2019.
- A. Tomiya, “Phase transition in three flavor QCD with background magnetic field,” Keio, Japan, July 10 2019.
- A. Tomiya, “Applications of machine learning to computational physics,” Brookhaven National Laboratory, NY, US, May 30, 2019.
- A. Tomiya, “Towards reduction of autocorrelation in HMC by machine learning,” Riken CCS, Kobe, Japan, March 29, 2019.
- A. Tomiya, “Deep Learning and Holographic QCD,” Riken, Wako, Japan, December 10, 2018.

Awards

- L. Jin and K. G. Wilson, “For his outstanding contributions to the calculation of the hadronic light-by-light scattering component of the anomalous magnetic moment of the muon,” Award for Excellence in Lattice Field Theory, 2019.
- L. Jin, “Lattice Calculation of the QED Correction to Meson Leptonic Decay,” U.S. Department of Energy (DOE), Early Career Research Program, Proposal 0000253629.
- S. Syritsyn, “Nucleon Structure, Fundamental Symmetries, and Lattice QCD,” U.S. National Science Foundation (NSF), Career Award
- A. Tanaka and A. Tomiya, “Particle Physics Medal, Young Scientist Award in Theoretical Particle Physics,” Japan Particle and Nuclear Theory Forum, 2019.
- A. Tanaka and A. Tomiya, “Journal of the Physical Society of Japan Most Cited Articles in 2018 from Vol.86 (2017),” Journal of the Physical Society of Japan, 2019.
- T. Izubuchi, BNL Science and Technology Award, 2020.

Press Releases

<https://www.bnl.gov/newsroom/news.php?a=117139>

May 5, 2020, RIKEN, Brookhaven National Laboratory, Columbia University, Universities of Connecticut, Nagoya, Regensburg, “Four Years of Calculations Lead to New Insights into Muon Anomaly”

Subnuclear System Research Division RIKEN Facility Office at RAL

1. Abstract

Our core activities are based on the RIKEN-RAL Muon Facility located at the ISIS Neutron & Muon Source at the Rutherford Appleton Laboratory (UK), which provides intense pulsed-muon beams. The RIKEN-RAL Muon Facility is a significant and long-standing collaboration between RIKEN and RAL in muon science—with 2020 being the 30th years of continuous agreements between RIKEN and RAL. The Facility enables muon science throughout Japan and other field—it continues to attract proposals from a wide variety of Japanese universities and institutions (with over 80 groups having now used the facility), and including industrial users such as Toyota, and has been instrumental in establishing scientific links with other Asian universities.

Muons have their own spins with 100% polarization, and can detect local magnetic fields and their fluctuations at muon stopping sites very precisely. The method to study the characteristics of materials by observing time dependent changes of muon spin polarization is called “Muon Spin Rotation, Relaxation and Resonance” (μ SR method), and is applied to study electro-magnetic properties of insulating, metallic, magnetic and superconducting systems. Muons reveal static and dynamic properties of the electronic state of materials in the zero-field condition, which is the ideal magnetic condition for research into magnetism. For example, we have carried out μ SR investigations on a wide range of materials including frustrated pyrochlore systems, which have variety of exotic ground states of magnetic spins, so the magnetism study of this system using muon is quite unique.

The ultra-cold muon beam can be stopped in thin foil, multi-layered materials and artificial lattices, which enables us to apply the μ SR techniques to surface and interface science. The development of an ultra-cold muon beam is also very important as a source of pencil-like small emittance muon beam for muon $g-2$ /EDM measurement. We have been developing muonium generators to create more muonium atoms in vacuum even at room temperature to improve beam quality compared with the conventional hot-tungsten muonium generator. We have demonstrated a strong increase in the muonium emission efficiency by fabricating fine laser drill-holes on the surface of silica aerogel. We are also developing a high power Lyman-alpha laser in collaboration with the Advanced Photonics group at RIKEN. The new laser will ionize muoniums 100 times more efficiently for slow muon beam generation.

Over the past 2–3 years, a significant development activity in muon elemental analysis has taken place, proton radius experiments have continued and been developed, and chip irradiation experiments have also continued.

2. Major Research Subjects

- (1) Materials science by muon-spin-relaxation method and muon site calculation
- (2) Development of elemental analysis using pulsed negative muons
- (3) Nuclear and particle physics studies via muonic atoms and ultra-cold muon beam
- (4) Other muon applications

3. Summary of Research Activity

(1) Material Science at the RIKEN-RAL Muon Facility

Muons have their own spins with 100% polarization, and can detect local magnetic fields and their fluctuations at muon stopping sites very precisely. The μ SR method is applied to studies of newly fabricated materials. Muons enable us to conduct (1) material studies under external zero-field condition, (2) magnetism studies with samples without nuclear spins, and (3) measurements of muon spin relaxation changes at wide temperature range with same detection sensitivity. The detection time range of local field fluctuations by μ SR is 10^{-6} to 10^{-11} second, which is an intermediate region between neutron scattering method (10^{-10} – 10^{-12} second) and Nuclear Magnetic Resonance (NMR) (longer than 10^{-6} second). At Port-2 and 4 of the RIKEN-RAL Muon Facility, we have been performing μ SR researches on strong correlated-electron systems, organic molecules, energy related materials and biological samples to study electron structures, superconductivity, magnetism, molecular structures and crystal structures.

Among our scientific activities on μ SR studies from year 2017 to 2020, following subjects of material sciences are most important achievements at the RIKEN-RAL muon facility:

- (1) Deformed nodal superconducting gap state and asymmetric spin-fluctuation mediated Cooper pair in the quasi two-dimensional organic superconductor λ -[BETS]₂GaCl₄
- (2) Multi magnetic transitions in the Ru-based pyrochlore systems, R₂Ru₂O₇.
- (3) Magnetic properties of the nano-cluster gold in the border of macro- and micro- scale.
- (4) Novel magnetic and superconducting properties of nano-size La-based high- T_C superconducting cuprates.
- (5) Determination of muon positions estimated from density functional theory (DFT) and dipole-field calculations.
- (6) Chemical muonic states in DNA molecules.

Result-1) We developed a novel method to determine deformed superconducting-gap structure with the density functional theory calculations. It was concluded that the two-dimensional organic superconductor λ -[BETS]₂GaCl₄ has a deformed nodal gap which has the steeper width rather than that of the d -wave state. Result-2) Doped hole effects on the magnetic properties of corner-shared magnetic moments on pyrochlore systems gave us new interpretations to understand exotic phenomena, like the quantum criticality of magnetic moments and a quasi-magnetic monopole state. Result-3) and 4) The nano-size effect show a new scheme of electronic properties of metallic element. We confirmed that the nano-gold cluster can have free electronic moment on one nano-cluster. The same nano-size effect was examined on the La-based high- T_C superconducting oxide changing the electronic state from insulating to superconducting. We confirmed the reduction in the magnetic interaction and the disappearance of the superconducting state leading

the increase in the ferromagnetic interaction within the wide-range of the hole concentration. Result-5) Well known and deeply investigated La_2CuO_4 has opened a new scheme of the Cu spin. Taking into account quantum effects to expand the Cu-spin orbital and muon positions, we have succeeded to explain newly found muon sites and hyperfine fields at those sites.

We have been continuing to develop muon-science activities in Asian countries. We enhanced international collaborations to organize new μSR experimental groups and to develop muon-site calculation groups using computational method. We are creating new collaborations with new teams in different countries and also continuing collaborations in μSR experiments on strongly correlated systems with researchers from Taiwan, Indonesia, China, Thailand and Malaysia including graduate students. We are starting to collaborate with the new Chinese muon group who are developing the Chinese Muon Facility and trying to develop more muon activities in the Asian area.

(2) Development of elemental analysis using pulsed negative muons

There has been significant development of elemental analysis using negative muons on Port 4 and Port 1 over the past couple of years. Currently, elemental analysis commonly uses X-ray and electron beams, which accurately measure surfaces. However a significant advantage of muonic X-rays over those of electronic X-rays is their higher energy due to the mass of the muon. These high energy muonic X-rays are emitted from the bulk of the samples without significant photon self-absorption. The penetration depth of the muons can be varied by controlling the muon momentum, providing data from a thin slice of sample at a given depth. This can be over a centimetre in iron, silver and gold or over 4 cm in less dense materials such as carbon.

Some techniques for elemental analysis are destructive or require the material under investigation to undergo significant treatment and some of the techniques are only sensitive to the surface. Therefore, negative muons offer a unique service in which they can measure inside, beyond the surface layer and completely non-destructively.

The areas of science that have used negative muons for elemental analysis have been very diverse. The largest area is the cultural heritage community as the non-destructive ability is particularly important and will become more so. This community have investigated swords from different eras, coins (Roman gold and silver, Islamic silver and from the Tudor Warship Mary Rose), miniature boats from Sardinia, reliefs on Baptist church gate, Bronze Age tools and cannon balls. In addition, energy materials (Li composition for hydrogen storage), bio-materials (search for iron to potentially help understand Alzheimer's), engineering alloys (manufacturing processes for new materials for jet engines), and functional materials (surface effects in piezo electrics) have also been investigated. The study was extended to see the difference by isotopes of silver and lead, which may give hint on the source of the material.

(3) Ultra-cold (low energy) Muon Beam Generation and Applications

Positive muon beam with thermal energy has been produced by laser ionization of muonium (bound system of μ^+ and electron) emitted from a hot tungsten surface with stopping surface muon beam at Port-3. The method generates a positive muon beam with acceleration energy from several 100 eV to several 10 keV, small beam size (a few mm) and good time resolution (less than 8 nsec). By stopping the ultra-cold muon beam in thin foil, multi-layered materials and artificial lattices, we can precisely measure local magnetic field in the materials, and apply the μSR techniques to surface and interface science. In addition, the ultra-cold muon is very important as the source of pencil-like small emittance muon beam for muon $g-2/\text{EDM}$ measurement. It is essential to increase the slow muon beam production efficiency by 100 times for these applications. There are three key techniques in ultra-cold muon generation: production of thermal muonium, high intensity Lyman-alpha laser and the ultra-cold muon beam line.

A high-power Lyman-alpha laser was developed in collaboration with the Advanced Photonics group at RIKEN. The new laser system is used at J-PARC U-line and, upon completion, will ionize muoniums 100 times more efficiently for slow muon beam generation. In this development, we succeeded to synthesize novel ceramic-based Nd:YAG crystal, which realized a highly efficient and stable laser system. However, larger size crystal than presently available is needed for full design power. We are working hard to improve the crystal homogeneity including the option of using slightly different material.

We also succeeded in developing an efficient muonium generator, laser ablated silica aerogel, which emits more muoniums into vacuum even at room temperature. Study has been done at TRIUMF utilizing positron tracking method of muon decay position. We demonstrated in 2013 at least 10 times increase of the muonium emission efficiency by fabricating fine laser drill-holes on the surface of silica aerogel. Further study was carried out in 2017 to find the optimum fabrication that will maximize the muonium emission. From the analysis, we found the emission has large positive correlation with the laser ablated area rather than with any other parameters. We also confirmed the muon polarization in vacuum. An alternative detection method for muonium emission using muonium spin rotation, which will be sensitive even to muoniums near the surface, was tested at RIKEN-RAL in 2018 and was found successful. The study was further applied the measurement of the temperature dependence.

In RIKEN-RAL Port 3, the ultra-cold muon beam line, which had been designed with hot tungsten, was completely rebuilt to use advantage of the new room temperature silica aerogel target. The equipment was tested with surface muon beam and basic data such as muon stopping in aerogel were taken. We are waiting the laser crystal development in order to proceed to ultra-cold muon generation. A similar target design will be adopted in the ultimate cold muon source planned for muon $g-2/\text{EDM}$ at J-PARC.

(4) Other Fundamental Physics Studies

A measurement of the proton radius using 2S-2P transition of muonic hydrogen at PSI revealed that the proton charge radius is surprisingly smaller than the radius measured using normal hydrogen spectroscopy and e-p scattering by more than 5 times their experimental precision. The muonic atom has larger sensitivity to the proton radius because the negative muon orbits closer to the proton, although there is no reason why these measurements can yield inconsistent results if there exists no exotic physics or unidentified phenomenon behind. The cause of the discrepancy is not understood yet, thus a new measurement with independent method is much anticipated.

We proposed the measurement of the proton radius by using the hyperfine splitting of the muonic hydrogen ground state. This hyperfine splitting is sensitive to the Zemach radius, which is a convolution of charge and magnetic-dipole distributions inside proton. We are planning to re-polarize the muonic hydrogen by a circularly polarized excitation laser (excites one of the $F = 1$ states and regenerates the muon spin polarization), and detect the recovery of the muon decay-asymmetry along the laser.

At RIKEN, we are developing dedicated laser system (mid-infrared high-power pulse laser system at around $6 \mu\text{m}$). We have tested the efficiency of our wavelength conversion scheme. We are going to test band-width narrowing using a seed laser of (Quantum Cascade Laser) and the laser reflection cavity. Preparation using muon beam is also in progress. We measured the muon stopping distribution in low-density hydrogen-gas cell, which gave us consistent results with beam simulation. Another key is the lifetime of the upper hyperfine state of the muonic hydrogen that will contribute the polarization. We successfully observed the clear muon spin precession of muonic deuterium atom in 2018 for the first time in the world. The measurement with muonic protium was carried out in 2019.

(5) Other topics

RIKEN and ISIS have signed a new collaboration agreement for the period 2018–2023. This is the fourth in a continuous series of agreements, the first being signed in 1990, resulting in a partnership which will have lasted over 30 years. Under the new agreement, ownership and operation of the facility was passed to ISIS, a refurbishment programme of the facility has started, a user programme for Japanese scientists continued under the partnership between RIKEN and ISIS. The RIKEN-RAL collaboration is regularly highlighted as a good example of UK-Japanese science partnership at the UK-Japan Joint Committee on Science and Technology (chaired by the UK Chief Scientific Advisor to Government and a counterpart from Japan)—for example, Dr. King and Dr. Watanabe presented RIKEN-RAL at the November 2016 meeting of the Committee. The RIKEN-RAL collaboration has also enabled the development of collaborative activity between RIKEN and other Asian universities, *e.g.* through several MoUs with Indonesian and Malaysian universities.

Members

Director

Philip KING

Research Scientist

Isao WATANABE (Senior Research Scientist)

Contract Researcher

Katsuhiko ISHIDA

List of Publications & Presentations

Publications

[Original papers]

- M. Abe *et al.* (J-PARC E34 collaboration), “A new approach for measuring the muon’s anomalous magnetic moment and electric dipole moment,” *Prog. Theor. Exp. Phys.* **2019**, 053C02 (2019).
- M. Clemenza *et al.*, “Muonic atom X-ray spectroscopy for non-destructive analysis of archaeological samples,” *Journal of Radioanalytical and Nuclear Chemistry* **322**, 1357–1363 (2019).
- B. V. Hampshire, K. Butcher, K. Ishida, G. Green, D. Paul, and A. Hillier, “Using negative muons as a probe for depth profiling silver Roman coinage,” *Heritage* **2**, 400–407 (2019).
- S. Asano, K. M. Suzuki, K. Kudo, I. Watanabe, A. Koda, R. Kadono, T. Noji, Y. Koike, T. Taniguchi, S. Kitagawa, K. Ishida, and M. Fujita, *J. Phys. Soc. Jpn.* **88**, 084709-1–6 (2019).
- F. Astuti, M. Miyajima, T. Fukuda, M. Kodani, T. Nakano, T. Kambe, and I. Watanabe, *J. Phys. Soc. Jpn.* **88**, 043701-1–5 (2019).
- M. A. Baqiya, T. Adachi, A. Takahashi, T. Konno, T. Ohgi, I. Watanabe, and Y. Koike, “Muon-spin relaxation study of the spin correlations in the overdoped regime of electron-doped high-TC cuprate superconductors,” *Phys. Rev. B* **100**, 064514-1–5 (2019).
- S. Wenner, C. Marioara, K. Nishimura, K. Matsuda, S. Lee, T. Namiki, I. Watanabe, T. Matsuzaki, and R. Holmestad, “Muon spin relaxation study of solute-vacancy interactions during natural aging of Al-Mg-Si-Cu alloys,” *Metallurgical and Materials Transactions A* **50**, 3446–3451 (2019).

Presentations

[International conferences/workshops]

- K. Ishida (oral), “Status of the g-2 and EDM experiment at J-PARC,” FCCP2019, Anacapri, Italy, August 29–31, 2019.
- K. Ishida (oral), “Measurement of the proton Zemach radius from the hyperfine splitting in muonic hydrogen utilizing muon spin repolarization with laser: Principle and Method,” Proton Radius 2019, Veli Losinj, Croatia, September 15–20, 2019.
- S. Kanda (oral), “Measurement of the proton Zemach radius from the hyperfine splitting in muonic hydrogen utilizing muon spin repolarization with laser: Preparation Status,” Proton Radius 2019, Veli Losinj, Croatia, September 15–20, 2019.
- K. Ishida (oral), “Status of the g-2 and EDM experiment at J-PARC,” Proton Radius 2019, Veli Losinj, Croatia, September 15–20, 2019.

- K. Ishida (oral), "Laser spectroscopy of the 1 s hyperfine splitting energy of muonic hydrogen for the determination of proton Zemach radius," The 3rd J-PARC symposium (J-PARC2019), Tsukuba, Japan, September 23–26, 2019.
- I. Watanabe (oral), The 1st International MIPAnet Conference on Science and Mathematics (IMC-SciMath 2019), Parapat, Indonesia, October 9–11, 2019.
- I. Watanabe (oral), 4th Padjadjaran International Physics Symposium (PIPS2019), Bandung, Indonesia, November 13–14, 2019.
- I. Watanabe (oral), International Conference on Magnetism and Its Application (IICMIA2019), Solo, Indonesia, November 20–21, 2019.

[Domestic conferences/workshops]

- 石田勝彦 (招待講演), 「英国理研 RAL ミュオン施設とミュオン利用分析」, 第 2 回文理融合シンポジウム 量子ビームで歴史を探る—加速器が紡ぐ文理融合の地平—, 大阪大学中之島センター, 大阪, 2019 年 12 月 25 日–26 日.
- 石田勝彦 (口頭発表), 「理研 RAL の現状と展望」, 第 10 回 「muon 科学と加速器研究」研究会, 理化学研究所, 和光, 2020 年 1 月 8 日–9 日.

[Seminars]

- RIKEN Symposium, "International workshop of topological quantum materials," Tainan, Taiwan, January 10–2, 2019.
- RIKEN Symposium, "The 5th international symposium in current progress in mathematics and sciences," Depok, Indonesia, July 9–10, 2019.

Awards

- S. Winarsih, RIKEN Summer School 2019, Poster Prize (in Physics)
- S. Winarsih, RIKEN Summer School 2019, Poster Prize (Best Presentation)
- S. Winarsih, RIKEN Exchange Meeting 2019, Poster Prize (Student Section)

Safety Management Group

1. Abstract

The RIKEN Nishina Center for Accelerator-Based Science possesses one of the largest accelerator facilities in the world, which consists of two heavy-ion linear accelerators and five cyclotrons. This is the only site in Japan where uranium ions are accelerated. The center also has electron accelerators of microtron and synchrotron storage ring. Our function is to keep the radiation level in and around the facility below the allowable limit and to keep the exposure of workers as low as reasonably achievable. We are also involved in the safety management of the Radioisotope Center, where many types of experiments are performed with sealed and unsealed radioisotopes.

2. Major Research Subjects

- (1) Safety management at radiation facilities of Nishina Center for Accelerator-Based Science
- (2) Safety management at Radioisotope Center
- (3) Radiation shielding design and development of accelerator safety systems

3. Summary of Research Activity

Our most important task is to keep the personnel exposure as low as reasonably achievable, and to prevent an accident. Therefore, we daily patrol the facility, measure the ambient dose rates, maintain the survey meters, shield doors and facilities of exhaust air and wastewater, replenish the protective supplies, and manage the radioactive waste. Advice, supervision and assistance at major accelerator maintenance works are also our task.

The interlock system for which is the part of the radiation control system developed for the RILAC upgrade was installed and started to operate. Access management system for the RILAC building, which was installed previous year, was improved to control

Minor improvements of the radiation safety systems were also done. The old UPS for radiation management system of Nishina building was replaced. Halogen sensitive filter for the exhaust system of Nishina building was newly installed.

Members

Director

Kanenobu TANAKA

Research/Technical Scientists

Rieko HIGURASHI (Technical Scientist)

Hisao SAKAMOTO (Technical Scientist)

Expert Technician

Atsuko AKASHIO

Technical Staff I

Hiroki MUKAI

Junior Research Associate

Kenta SUGIHARA

Visiting Scientists

Masayuki HAGIWARA (KEK)

Noriaki NAKAO (Shimizu Corporation)

Toshiya SANAMI (KEK)

Nobuhiro SHIGYO (Kyushu Univ.)

Hiroshi YASHIMA (Kyoto Univ.)

Student Trainees

Shougo IZUMITANI (Kyushu Univ.)

Eunji LEE (Kyushu Univ.)

Part-time Workers

Kimie IGARASHI (Administrative Part-time Worker I)

Satomi IIZUKA (Administrative Part-time Worker II)

Yukiko SHIODA (Administrative Part-time Worker II)

Naoko USUDATE (Administrative Part-time Worker II)

Temporary Staffing

Ryuji SUZUKI

Assistant

Tomomi OKAYASU

List of Publications & Presentations

Publications

[Proceedings]

田中鐘信, 「大規模加速器施設における, 事故時の円滑なジョ湯方伝達と避難の取り組み」, 日本放射線安全管理学会誌 **18**, 2 (2019).
向井弘樹, 田中鐘信, 上蓑義朋, 「RIBF 加速器施設の冷却水に関する放射線管理」, Isotope News **762**, 4 (2019).

Presentations

[International conferences/workshops]

- K. Tanaka (oral), “Recent trouble and measures in unsealed radioisotope handling at RIBF,” International Technical Safety Forum 2019, Lund, Sweden, May 13–17, 2019.
K. Tanaka (invited), “Radiation evaluation in RIBF,” Tsukuba, Japan, September 23–26, 2019.
K. Sugihara (poster), “Measurement of neutron energy spectra of 345 MeV/u ^{238}U Incidence on a Cu Target,” 2019 Symposium on Nuclear Data, Kasuga, Japan, November 28–30, 2019.
S. Izumitani (poster), “Production via the $^7\text{Li}(p, n) ^7\text{Be}$ reaction with 2.49 MeV proton injection,” 2019 Symposium on Nuclear Data, Kasuga, Japan, November 28–30, 2019.

[Domestic conference/workshops]

田中鐘信 (招待講演), 「RIBF のインターロックと運用」, 第 7 回加速器施設安全シンポジウム, 東海村, 2020 年 1 月 23–24 日.

Awards

[Excellent poster award]

- S. Izumitani, “Production via the $^7\text{Li}(p, n) ^7\text{Be}$ reaction with 2.49 MeV proton injection,” 2019 Symposium on Nuclear Data, Kasuga, Japan, November 28–30, 2019.

User Liaison Group

1. Abstract

The essential mission of the User Liaison Group is to maximize the research activities of RIBF by attracting users in various fields with a wide scope. The Group consists of two teams. The RIBF User Liaison Team provides various supports to visiting RIBF users through the RIBF Users Office. Managing RIBF beam time and organizing the Program Advisory Committee Meetings to review RIBF experimental proposals are also important mission of the Team in order to enhance collaborative-use of the RIBF. The Outreach Team has created various information materials, such as pamphlets, posters, and homepages, to introduce the research activities in the RNC. On the homepage, we provide information on usage of the RIBF facility. The team also participate in science introduction events hosted by public institutions. In addition, the User Liaison Group also takes care of laboratory tours for RIBF visitors from public. The numbers of visitors amounts to 2,300 per year.

Members

Director

Hideki UENO

Research Consultants

Ikuko HAMAMOTO (The Lund Univ.)

Munetake ICHIMURA (Univ. of Tokyo)

Assistants

Yu NAYA

Tomomi OKAYASU

Midori YAMAMOTO

User Liaison Group

RIBF User Liaison Team

1. Abstract

To enhance synergetic common use of the world-class accelerator facility, the Radioisotope Beam Factory (RIBF), it is necessary to promote a broad range of applications and to maximize the facility's importance. The facilitation and promotion of the RIBF are important missions charged to the team. Important operational activities of the team include: i) the organization of international Program Advisory Committee (PAC) meetings to review experimental proposals submitted by RIBF users, ii) RIBF beam-time operation management, and iii) promotion of facility use by hosting outside users through the RIBF Independent Users program, which is a new-user registration program begun in FY2010 at the RIKEN Nishina Center (RNC) to enhance the synergetic common use of the RIBF. The team opened the RIBF Users Office in the RIBF building in 2010, which is the main point of contact for Independent Users and provides a wide range of services and information.

2. Major Research Subjects

- (1) Facilitation of the use of the RIBF
- (2) Promotion of the RIBF to interested researchers

3. Summary of Research Activity

(1) Facilitation of the use of the RIBF

The RIBF Users Office, formed by the team in 2010, is a point of contact for user registration through the RIBF Independent User program. This activity includes:

- registration of users as RIBF Independent Users,
- registration of radiation workers at the RIKEN Wako Institute,
- provision of an RIBF User Card (a regular entry permit) and an optically stimulated luminescence dosimeter for each RIBF Independent User, and
- provision of safety training for new registrants regarding working around radiation, accelerator use at the RIBF facility, and information security, which must be completed before they begin RIBF research.

The RIBF Users Office is also a point of contact for users regarding RIBF beam-time-related paperwork, which includes:

- contact for beam-time scheduling and safety review of experiments by the In-House Safety Committee,
- preparation of annual Accelerator Progress Reports, and
- maintaining the above information in a beam-time record database.

In addition, the RIBF Users Office assists RIBF Independent Users with matters related to their visit, such as invitation procedures, visa applications, and the reservation of on-campus accommodation.

(2) Promotion of the RIBF to interested researchers

- The team has organized an international PAC for RIBF experiments; it consists of leading scientists worldwide and reviews proposals in the field of nuclear physics (NP) purely on the basis of their scientific merit and feasibility. The team also assists another PAC meeting for material and life sciences (ML) organized by the RNC Advanced Meson Laboratory. The NP and ML PAC meetings are organized twice a year.
- The team coordinates beam times for PAC-approved experiments and other development activities. It manages the operating schedule of the RIBF accelerator complex according to the decisions arrived at by the RIBF Machine Time Committee.
- To promote research activities at RIBF, proposals for User Liaison and Industrial Cooperation Group symposia/mini-workshops are solicited broadly both inside and outside of the RNC. The RIBF Users Office assists in the related paperwork.
- The team is the point of contact for the RIBF users' association. It arranges meetings at RNC headquarters for the RIBF User Executive Committee of the users' association.
- The Team conducts publicity activities, such as arranging for RIBF tours, development and improvement of the RNC official web site, and delivery of RNC news via email and the web.

Members

Team Leader

Ken-ichiro YONEDA

Contract Researcher

Tadashi KAMBARA

User Liaison Group Outreach Team

1. Abstract

The Outreach Team has created various information materials to introduce research activities in the RNC. For instance, the team makes brochures introducing the RNC and the RIBF accelerator facility, posters of symposia and the summer school hosted by RNC, the center homepage containing information such as details of RNC and the procedure for the use of the RIBF facility, and images of equipment and facilities available for researchers inside and outside RIKEN, among the others. Furthermore, the team also participates in science introduction events hosted by public institutions.

2. Major Work Contents

The major work contents of the Outreach Team is to promote the publicity of RNC, through the creation of various materials such as brochures, websites, posters, and videos, among the others. The arrangement of tours of the RIBF facility and the exhibition and introduction of the RIBF facility at science events are also conducted independently or in cooperation with RIKEN Public Relations Office.

3. Summary of Work Activity

The specific work contents performed by the team are as follows:

- [Website] The Team creates/manages the RNC official website (<http://www.nishina.riken.jp>), which introduces the organization and its research activities. This website plays an important role in providing information to researchers who visit RNC to conduct his/her own research.
- [Brochures] The Team has produced various brochures introducing the organization and the studies performed at RNC. The brochures named “Your body is made of star scraps” explaining element synthesis in the universe and “Introduction of RIBF Facility” in a cartoon style for children are among them.
- [Posters] Conference/Symposium posters connected with RNC were prepared on the request of organizers. For general purpose, a special poster featuring the nuclear chart has been prepared for distribution. In commemoration of the discovery of nihonium, brochures and posters dedicated to the ceremony were made.
- [RIBF Cyclopedica] In April 2012, the permanent exhibition hall (RIBF Cyclopedica) located at the entrance hall of the RIBF building was set up in cooperation with RIKEN Public Relations Office. Explanatory illustrations on nuclear science, research at RIBF, RIBF history, a 3D nuclear chart built with LEGO blocks, and a 1/6-size GARIS model are displayed to help understanding through visual means. The Team is also working on updating the exhibits.
- [RIBF facility tour] The Team arranges RIBF facility tour for over 2000 visitors per year. The tour is guided by a researcher.
- [Science event participation] In 2010, 2012, 2013, 2015, and 2016, the sub-team opened an exhibition booth of RNC to introduce the latest research activities on the occasion of the “Science Agora” organized by Japan Science and Technology Agency (JST). From time to time, the sub-team was invited to participate in scientific events by MEXT, Wako city, and Nissan global foundation.

One attraction targeting children is the hands-on work of assembling “Iron-beads” to create a nuclear chart or a shape of nihonium. In addition to the above-noted work contents, the Team conducts a variety of works, such as taking pictures of meetings organized by RNC, cooperation in the production of a 3D video to explain the accelerators and the research at RIBF, among the others.

Members

Team Leader

Hideki UENO

Deputy Team Leader

Yasushi WATANABE

Technical Staff I

Narumasa MIYAUCHI

List of Publications & Presentations

Outreach activities

Special Exhibition of the International Year of the Periodic Table 2019 (国際周期表年特別展 2019 「理化学研究所のニホニウム模型をつくろう」), Niihama (Ehime Prefectural Science Museum), January 18–19, 2020.

RIKEN Osaka Campus Open Day 2019, Suita, November 23, 2019.

Science Agora 2019 (an open forum organized by the Japan Science and Technology Agency), Tokyo (The National Museum of Emerging Science and Innovation), November 15–17, 2019.

Office of the Center Director

Summary of Research Activity

This office is in place from JFY2018 to support the center director in subjects which the promotion office is not able to cover. It also works as a home laboratory for research administrators and assistants with an indefinite term contract. This year's most important activity of the office was to support the International Symposium on Superheavy Elements (SHE2019) held at Hakone, Japan from 1st to 5th of December 2019. The Chair persons K. Morita and H. Haba run the symposium and were supported largely by this office; research administrator Narumasa MIYAUCHI and assistants Noriko ASAKAWA and Noriko KIYAMA. Miyachi also contributed largely to the International Year of Periodic table (IYPT2019), in the preparation of the travelling exhibitions and the preparation of the session "Creation of superheavy elements" in the IYPT2019 Closing Ceremony. His handmade video of "The Landscape of Nihonium Avenue" was greatly appreciated by the audience. Below is a list of activity of Nishina Center Director's Office, in public or semi-public events.

2019.03.01	NuPECC at Warsaw	Nishina Center is the associate member of (NuPECC: Nuclear Physics European Collaboration Committee, an Expert Committee of the European Science Foundation). The status report of Nishina Center was presented at their regular meeting at Warsaw, Poland. The minutes are available in http://www.nupecc.org/misc/min94.pdf
2019.03.11	RBRC SRC	Nishina Director participated in Scientific Review Committee of RIKEN-BNL Research Center.
2019.03.17	JPS meeting at Ito Campus, Kyushu University	As recommended by Nishina Center, Japan Physics Society organized a special joint session for IYPT2019 at the Ito Campus of Kyushu University with the Chemical Society of Japan at Kobe-Okamoto Campus of Konan University. K. Morita gave a plenary talk.
2019.04.17	Nishina Center, New-comers' Orientation	In the orientation for new comers in Nishina Center, introductory talk of "Researcher's Must Have" was given by Nishina Director.
2019.05.19	Completion Ceremony for Nihonium Avenue	Wako City held the Completion Ceremony of Nihonium Avenue in the RIKEN Wako Campus. The Mayor Matsumoto invited the donors and students to the Ceremony. The Nishina Director gave the presentation of "Welcome to the birthplace of 113 th element, nihonium (in Japanese)". Many of audience also attended the challenge exam for chemical elements, held together with the ceremony.
2019.05.29	ORNL visit	Nishina Director visited Oak Ridge National Laboratory to participate in the collaboration meeting for superheavy element search.
2019.06.11	Sakura Science High School Visit	Sakura Science High School, a government-driven virtual school for foreign exchange Students, visited RIKEN. Nishina Director gave a presentation of "Welcome to the birthplace of 113 th element, nihonium".
2019.06.24	NCAC	Nishina Center Advisory Committee was held. Nishina Director and the Center activities were reviewed for three days.
2019.06.28	ML-PAC	Nishina Director gave an introductory talk for ML-PAC (Program Advisory Committee for Materials and Life Science).
2019.07.10	IN-PAC	Nishina Director gave an introductory talk for In-PAC (Program Advisory Committee for Industrial usage), which was held in a closed session.
2019.07.27	Mendeleev 150	4 th International Conference on the Periodic Table (Mendeleev 150) was held at ITMO University in Saint Petersburg, Russian Federation (see https://mendeleev150.ifmo.ru/). Nishina Director gave a lecture titled "History of Nihonium" on behalf of Kosuke Morita. The talk was published in https://doi.org/10.1515/pac-2019-0810
2019.08.01	SCK-CEN visit	Nishina Director visited CNK-CEN which is the Belgian nuclear research centre, to seek for possible collaboration in MYRRHA (Multi-purpose hYbrid Research Reactor for High-tech Application).
2019.08.02	IUPAP-WG9	Nishina Director participated in the annual general meeting for IUPAP-WG9 (Working Group 9) held at University of Notre Dame in London, UK. Agenda is available at https://iupap.triumf.ca/icnp/meetings.html .
2019.08.21	NICT Visit	A delegation from NICT (National Institute of Information and Communication Technology) visited Nishina Center. Nishina Director made an introduction to them with a story of the first cyclotron made by Nishina was made on the Paulsen's arc converted which was developed for radio communication.
2019.08.26	TAN19	Tan19(6 th International Conference on the Chemistry and Physics of the Transactinide Elements) was held in Wilhelmshaven, Germany. Nishina Director was invited to give a lecture "Element Genesis over 13.8 Billion Universal Years" in a session dedicated to the International Year of Periodic Table: https://www-win.gsi.de/tan19/symposium.html .
2019.09.07	IYPT2019 Special Exhibition in Kyoto	Nishina Director gave a public lecture in the Special Exhibition in Kyoto for the International Year of Periodic Table, titled "13.8 billion years of element genesis, from Big-Bang to nihonium (in Japanese)".
2019.10.03	J. Soffer's Memorial	Nishina Director participated in a memorial symposium for J. Soffer, who was a leading theorist of perturbative QCD and the father of the RHIC spin project, at BNL, NY, USA.
2019.10.23	RAC	Nishina director gave a presentation in RIKEN Advisory Council.
2019.11.00	Chemistry and Chemical Industry	Nishina Director contributed a report of Mendeleev150 Symposium to the special contents for IYPT2019 in Chemistry and Chemical Industry, 940, Vol72-11, 2019.

2019.11.25	Event Myrrha	Nishina Director participated in Event MYRRHA (introduction of MYRRHA project to Japanese communities) held at Belgian Embassy at Tokyo, Japan
2019.12.05	IYPT2019 Closing Ceremony	Nishina director was a part of the organizing committee for the closing ceremony of IYPT2019, held in Tokyo, Japan. He produced and chaired a session named “Creation of superheavy elements” attended by many of actual discoverers. https://iypt.jp
2019.12.01	SHE2019	Director’s office fully supported the international Symposium on Superheavy Elements (SHE2019) held at Hakone, Japan from 1 st to 5 th of December 2019. The Chair persons are K. Morita and H. Haba. https://she2019.riken.jp
2019.12.16	NP-PAC	Nishina Director gave an introductory talk for NP-PAC (Program Advisory Committee for Nuclear Physics).
2020.01.24	ML-PAC	Nishina Director gave an introductory talk for ML-PAC (Program Advisory Committee for Materials and Life Science).
2020.01.00	Nuclear Physics News	Nishina Director reported “Superheavy Elements at the Closing Ceremony of IYPT” to Nuclear Physics News, Vol. 30, No. 1, 2020.
2020.01.27	Strategic review of Helmholtz Association	Nishina Director visited Helmholtz Association in Berlin, Germany, to review of the scientific field “MATTER” which includes GSI, DESY and other large-scale laboratories

Members

Director

Hideto EN’YO

Research Administrator

Narumasa MIYAUCHI (concurrently appointed to Outreach Team)

Assistants

Noriko ASAKAWA

Noriko KIYAMA

Yu NAYA (concurrently appointed to RIBF User Liaison Team)

Karen SAKUMA (concurrently appointed to Accelerator Group)

Asako TAKAHASHI (concurrently appointed to Spin Isospin Laboratory)

Mitsue YAMAMOTO (concurrently appointed to Meson Science Laboratory)

Izumi YOSHIDA (concurrently appointed to Nuclear Spectroscopy Laboratory)

List of Publications & Presentations

Publications

[Proceedings]

Hideto En’yo (invited), “History of nihonium,” Proceedings of Mendeleev 150, Pure and Applied Chemistry, **91**, 1941 (2019).

Presentations

[International conferences/workshops]

Hideto En’yo (invited), “History of nihonium,” 4th International Conference on the Periodic Table (Mendeleev 150), ITMO University in Saint Petersburg, Russian Federation, July 26–28, (2019).

Hideto En’yo (invited), “Element genesis over 13.8 billion Universal years,” Special Symposium for International Year of Periodic Table in the 6th International Conference on the Chemistry and Physics of the Transactinide Elements (TAN19), Wilhelmshaven, Germany, August 25–30, 2019.

Outreach activities

Hideto En’yo, “Welcome to the birthplace of 113th element, nihonium,” a lecture given to the Sakura Science High School, RIKEN-Wako, June 11, 2019.

Hideto En’yo *et al.* (invited), “Creation of superheavy elements,” The Closing Ceremony of IYPT2019, Tokyo, Japan, December 5, 2019.

Hideto En’yo, “Superheavy Elements at the Closing Ceremony of IYPT” contributed to Nuclear Physics News **30**, 39 2020.

延與秀人, 「ようこそ, 113 番元素ニホニウムの生誕地, 理研仁科センターへ」, ニホニウム通り完成記念式典 (和光市主催), 理研和光キャンパス, 和光, 2019 年 5 月 19 日.

延與秀人, 「元素創成の 138 億年: ビッグバンからニホニウムに至るまで」, 国際周期表年 2019 特別展, 京都大学, 京都, 2019 年 9 月 7 日.

Partner Institutions

The Nishina Center started research collaboration with universities and research institutes in 2008 under the “Research Partnership” agreement. This collaboration framework permits an external institute to develop its own projects at the RIKEN Wako campus in equal partnership with the Nishina Center. At present, two institutes, the Center for Nuclear Study (CNS), the University of Tokyo; and the Wako Nuclear Science Center (WNSC), Institute of Particle and Nuclear Studies (IPNS), High-energy Accelerator Research Organization (KEK) are conducting research activities under the “Research Partnership” agreement.

The CNS and the Nishina Center signed the partnership agreement in 2008. Until then, the CNS had collaborated in joint programs with RIKEN under the “Research Collaboration Agreement on Heavy Ion Physics” (collaboration agreement) signed in 1998. The partnership agreement redefines procedures related to the joint programs while keeping the spirit of the collaboration agreement. The joint programs include experimental nuclear-physics activities using CRIB, SHARAQ, and GRAPE at RIBF, accelerator development, and activities at RHIC PHENIX.

KEK started low-energy nuclear physics activity at RIBF in 2011 under the Research Partnership System. The joint experimental programs are based on KISS (KEK Isotope Separator). After the R&D studies on KISS, it became available for users from 2015.

The experimental proposals that request the use of the above-noted devices of the CNS and KEK together with the other RIBF key devices are screened by the Program Advisory Committee for Nuclear Physics experiments at RI Beam Factory (NP-PAC). The NP-PAC meetings are co-hosted together with the CNS and KEK.

The activities of the CNS and KEK are reported in the following pages.

Partner Institution
Center for Nuclear Study, Graduate School of Science
The University of Tokyo

1. Abstract

The Center for Nuclear Study (CNS) aims to elucidate the nature of nuclear system by producing the characteristic states where the Isospin, Spin and Quark degrees of freedom play central roles. These researches in CNS lead to the understanding of the matter based on common natures of many-body systems in various phases. We also aim at elucidating the explosion phenomena and the evolution of the universe by the direct measurements simulating nuclear reactions in the universe. In order to advance the nuclear science with heavy-ion reactions, we develop AVF upgrade, CRIB and SHARAQ facilities in the large-scale accelerators laboratories RIBF. The OEDO facility has been developed as an upgrade of the SHARAQ, where a RF deflector system has been introduced to obtain a good quality of low-energy beam. A new project for fundamental symmetry using heavy RIs has been starting to install new experimental devices in the RIBF. We promote collaboration programs at RIBF as well as RHIC-PHENIX and ALICE-LHC with scientists in the world, and host international meetings and conferences. We also provide educational opportunities to young scientists in the heavy-ion science through the graduate course as a member of the department of physics in the University of Tokyo and through hosting the international summer school.

2. Major Research Subjects

- (1) Accelerator Physics
- (2) Nuclear Astrophysics
- (3) Nuclear spectroscopy of exotic nuclei
- (4) Quark physics
- (5) Nuclear Theory
- (6) OEDO/SHARAQ project
- (7) Exotic Nuclear Reaction
- (8) Low Energy Nuclear Reaction Group
- (9) Active Target Development
- (10) Fundamental Physics

3. Summary of Research Activity

(1) Accelerator Physics

One of the major tasks of the accelerator group is the AVF upgrade project that included development of ion sources. In 2019, the operating time of the HyperECR was 2326 hours, which is 76% of the total operating time of the AVF cyclotron. The beam extraction system of the HyperECR is under development realize a high intensity and low emittance beam. For the pepper-pot emittance monitor used for the analysis of the beam injection transport system, we optimized the exposure time and gain of digital camera for a variety of thicknesses of fluorescent agent and was able to keep homogenized measurements despite of thickness. For the beam transport analysis of the beamline to CRIB, E7B, and EDM experiment from AVF cyclotron, we started developing 4D emittance monitor because the transverse components of beam are coupled and it is expected to measure high intensity beam in a few seconds.

(2) Nuclear Astrophysics

The main activity of the nuclear astrophysics group is to study astrophysical reactions and special nuclear clustering using the low-energy RI beam separator CRIB. Several experimental projects on big-bang nucleosynthesis (BBN) are currently under way. To give a solution to the cosmological ${}^7\text{Li}$ abundance problem, ${}^7\text{Be}(n, \alpha)/(n, p)$ astrophysical reactions were studied with the Trojan Horse method, and the rate of ${}^7\text{Be}(n, p_1)$, the (n, p) reaction with ${}^7\text{Li}$ excitation, is evaluated at the BBN temperature for the first time. ${}^7\text{Be}(d, p)$ measurement with a ${}^7\text{Be}$ -implanted target was carried out in 2018, in collaboration with RCNP, Osaka Univ. and JAEA. ${}^8\text{Li}(\alpha, n)$ reaction has been considered as responsible to the production of nuclei heavier than boron in some models of the BBN. To solve the discrepancy between the previous measurements of ${}^8\text{Li}(\alpha, n)$, a new experiment with γ -ray measurement was performed at CRIB in September 2018. To confirm the exotic linear-chain cluster structure in ${}^{14}\text{C}$ nucleus indicated in the previous ${}^{10}\text{Be} + \alpha$ resonant scattering measurement at CRIB, a new measurement was carried out at INFN-LNS, Catania, Italy, under the collaboration of CNS, INFN, Univ. Edinburgh and other institutes, in October 2018. A measurement on ${}^{25}\text{Al} + p$ resonant scattering was performed at CRIB in February 2019, to study the resonances relevant for the astrophysical ${}^{22}\text{Mg}(\alpha, p)$ reaction in X-ray bursters.

The main activity of the nuclear astrophysics group is to study astrophysical reactions and special nuclear clustering using the low-energy RI beam separator CRIB. As the first experiment of the INSPIRATION project, a measurement of the proton-halo ${}^8\text{B} + {}^{120}\text{Sn}$ system at energies around the Coulomb barrier was carried out in April 2019, under the collaboration of Japan and China. This was to study the reaction mechanism, including the break-up, of the system involving a weakly-bound nucleus, 8B. On the interest of nuclear clustering in the ${}^{14}\text{O}$ nucleus, a measurement of ${}^{10}\text{C} + \alpha$ elastic scattering was performed, under the collaboration of Belgium (ULB), Kyoto Univ., Osaka Univ., CNS, and other groups. We identified several peaks in the energy spectrum, which may show the existence of cluster states. Studies on big-bang nucleosynthesis (BBN) are currently under way. To give a solution to the cosmological ${}^7\text{Li}$ abundance problem, ${}^7\text{Be}(n, \alpha)/(n, p)$ astrophysical reactions were measured with the Trojan Horse method, and the first reliable evaluation of the rate of ${}^7\text{Be}(n, p_1)$, the (n, p) reaction with ${}^7\text{Li}$ excitation, at the BBN temperature, was made during 2019. To produce

RI beams at CRIB with higher intensity, a project to improve the heat capacity of the cryogenic gas target was initiated in 2019. We tested several materials for the sealing foils and the flanges, and a thermal monitoring with a thermography was introduced.

(3) Nuclear structure of exotic nuclei

The NUSPEQ (NUclear SPectroscopy for Extreme Quantum system) group studies exotic structures in high-isospin and/or high-spin states in nuclei. The CNS GRAPE (Gamma-Ray detector Array with Position and Energy sensitivity) is a major apparatus for high-resolution in-beam gamma-ray spectroscopy. Missing mass spectroscopy using the SHARAQ is used for another approach on exotic nuclei. The group plays a major role in the OEDO/SHARAQ project described below. In 2019, analysis of a new measurement of the ${}^4\text{He}({}^8\text{He}, {}^8\text{Be})4n$ reaction for better statistics and better accuracy has been proceeding.

(4) Quark Physics

Main goal of the quark physics group is to understand the properties of hot and dense nuclear matter created by colliding heavy nuclei at relativistic energies. The group has been involved in the PHENIX experiment at Relativistic Heavy Ion Collider (RHIC) at Brookhaven National Laboratory, and the ALICE experiment at Large Hadron Collider (LHC) at CERN. As for ALICE, the group has involved in the data analyses, which include the measurement of low-mass lepton pairs in Pb-Pb and p -Pb collisions, J/ψ measurements in p -Pb collisions, long range two particle correlations in p -Pb collisions, and searches for thermal photons in p -Pb collisions. The group has been involved in the ALICE-TPC upgrade using a Gas Electron Multiplier (GEM). Installation of GEM chambers in the TPC and commissioning of the TPC were carried out in 2019. The group has started working on the online space-charge distortion correction of the TPC by utilizing the GPUs and Machine learning technique.

(5) Nuclear Theory

The nuclear theory group participated in a project, "Priority Issue 9 to be tackled by using the Post-K Computer" and promotes computational nuclear physics utilizing supercomputers. We developed shell-model codes for the conventional Lanczos method and the Monte Carlo shell model for massively parallel computation. In FY2019, we performed the Monte Carlo shell model calculations of the Sm isotopes and revealed that the excited states of ${}^{154}\text{Sm}$ and ${}^{166}\text{Er}$ whose structures were considered to be β/γ vibration can be interpreted in view of shape coexistence.

(6) OEDO/SHARAQ project

The OEDO/SHARAQ group pursues experimental studies of RI beams by using the high-resolution beamline and the SHARAQ spectrometer. A mass measurement by TOF- $B\rho$ technique for very neutron-rich successfully reaches calcium isotopes beyond $N = 34$, ${}^{55,57}\text{Ca}$, and the preparation of publication is ongoing. The experimental study of 0^- strength in nuclei using the parity-transfer charge exchange (${}^{16}\text{O}, {}^{16}\text{F}$) is on progress and the data analysis is on the final stage. The OEDO beamline, which was an upgrade of the high-resolution beamline to produce low-energy RI beams, has started the operation in June and has successfully achieved the designed ion-optical performance. The first and second experiments were performed in October and November, and new data for nuclear transmutation of long lived fission products (LLFPs) were successfully obtained.

(7) Exotic Nuclear Reaction

The Exotic Nuclear Reaction group studies various exotic reactions induced by beams of unstable nuclei. One subject is inverse-kinematics (p, n) reaction. In 2017 a set of neutron counters PANDORA was used for the first time at HIMAC facility for the study of the ${}^6\text{He}(p, n)$ reaction. Candidate nuclei to study are high spin isomers such as ${}^{52}\text{Fe}(12^+)$. Development of isomer beam was carried out.

(8) Low Energy Nuclear Reaction Group

A recoil particle detector for missing mass spectroscopy, named TiNA, had been developed under the collaboration with RIKEN and RCNP. TiNA consists of 6 sector telescopes. Each of which as a stripped-type SSD and 2 CsI(Tl) crystals. After the test experiment at the tandem facility of Kyushu Univ., TiNA was employed at the physics experiment with OEDO. Development of the tritium target is still on-going. Several deuterium doped Ti targets were fabricated at the Toyama Univ. They were tested by using $d({}^{12}\text{C}, d)$ reaction at the tandem facility at Kyushu. The amount of deuterium was found to be scattered. The optimum condition to make the target will be sought for. The production cross section ${}^{178\text{m}2}\text{Hf}$ was evaluated for the mass production in the future. The digital signal processing devices for the GRAPE have been developed to measure the cascade transitions from the isomeric state. After chemical separation of Hf at the hot laboratory at RIBF. The week cascade decay was successfully measured.

(9) Active Target Development

Two types of gaseous active target TPCs called CAT's and GEM-MSTPC are developed and used for the missing mass spectroscopy. The CAT's are employed for the study of equation of state of nuclear matter. The measurement of giant monopole resonance in ${}^{132}\text{Sn}$ at RIBF with CAT-S and the data analysis is ongoing. In 2017, we developed a larger active target called CAT-M, which has 10-times larger active volume than that of CAT-S. The CAT-M was commissioned at HIMAC and the excitation energy spectrum of ${}^{136}\text{Xe}$ for proton scattering was measured. The GEM-MSTPC is employed for the nuclear astrophysics study. The data analysis of (α, p) reaction on ${}^{18}\text{Ne}$ and ${}^{22}\text{Mg}$ and the β -decay of ${}^{16}\text{Ne}$ followed by α emission are ongoing.

(10) Fundamental Physics

Although the Standard Model of particle physics is being steadily and successfully verified, the disappearance of the antimatter in the universe could not be sufficiently explained; a more fundamental framework is required and has to be studied. In order to

understand the mechanism of matter-antimatter symmetry violation, we are developing the next generation experiments employing ultracold atoms to search for the electron electric dipole moment (EDM) using heavy element francium (Fr) in an optical lattice at RIBF. In 2019, we developed a surface ionizer for production of a high intensity Fr ion beam. Using the surface ionizer, the 1st Fr production experiment was also conducted in 2019. At present, the development of a magneto-optical trap and an atomic interferometer are in progress.

Members

Director

Susumu SHIMOURA

Scientific Staff

Susumu SHIMOURA (Professor)
 Yasuhiro SAKEMI (Professor)
 Nobuaki IMAI (Associate Professor)
 Kentaro YAKO (Associate Professor)
 Taku GUNJI (Associate Professor)

Noritaka SHIMIZU (Project Associate Professor)
 Hidetoshi YAMAGUCHI (Lecturer)
 Shin'ichiro MICHIMASA (Assistant Professor)
 Shinsuke OTA (Assistant Professor)
 Hiroki NAGAHAMA (Assistant Professor)

Guest Scientists

Yutaka UTSUNO (Guest Professor)
 Daiki NISHIMURA (Guest Associate Professor)

Toshitaka KAJINO (Guest Post Doctoral Associate)

Technical Staff

Yasuteru KOTAKA

Technical Assistants

Yukimitsu OHSHIRO

Masayoshi YAGYU

Project Research Associates

Masanori DOZONO
 Seiya HAYAKAWA

Takashi ABE

Post Doctoral Associates

Shinichi HAYASHI
 Daiki SEKIHATA
 Keisuke NAKAMURA
 Keita KAMAKURA
 Jongwon HWANG
 Nanru MA

Yusuke TSUNODA
 Kota YANASE
 Laszlo STUHL
 Lei YANG
 Javier MENÉNDEZ

Assistant Teaching Staff

Yuko SEKIGUCHI

Academic Support Staff

Reiko KOJIMA

Chihiro IWAMOTO

Graduate Students

Shoichiro MASUOKA
 Noritaka KITAMURA
 Keita KAWATA
 Hideki SHIMIZU

Rieko TSUNODA
 Naoya OZAWA
 Shutaro HANAI
 Natsuki SHIMIZU

Administration Staff

Toshio OSUGI
 Ikuko YAMAMOTO

Takako ENDO
 Yukino KISHI

List of Publications & Presentations

Publications

[Original papers]

- K. Nakano, Y. Watanabe, S. Kawase, H. Wang, H. Otsu, H. Sakurai, S. Takeuchi, Y. Togano, N. Nakamura, M. Maeda, D. S. Ahn, M. Aikawa, S. Araki, S. Chen, N. Chiga, P. Doornenbal, N. Fukuda, T. Ichihara, T. Isobe, S. Kawakami, T. Kin, Y. Kondo, S. Koyama, T. Kubo, S. Kubono, M. Uesaka, A. Makinaga, M. Matsushita, T. Matsuzaki, S. Michimasa, S. Momiyama, S. Nagamine, M. Niikura, T. Ozaki, A. Saito, T. Saito, Y. Shiga, M. Shikata, Y. Shimizu, S. Shimoura, T. Sumikama, P. A. Söderström, H. Suzuki, H. Takeda, R. Taniuchi, J. Tsubota, Y. Watanabe, K. Wimmer, T. Yamamoto, and K. Yoshida, “Isotope production in proton-, deuteron-, and carbon-induced reactions on ^{93}Nb at 113 MeV/nucleon,” *Phys. Rev. C* **100**, 044605 (2019).
- A. Corsi, Y. Kubota, J. Casal, M. Gómez-Ramos, A. M. Moro, G. Authelet, H. Baba, C. Caesar, D. Calvet, A. Delbart, M. Dozono, J. Feng, F. Flavigny, J. -M. Gheller, J. Gibelin, A. Giganon, A. Gillibert, K. Hasegawa, T. Isobe, Y. Kanaya, S. Kawakami, D. Kim, Y. Kiyokawa, M. Kobayashi, N. Kobayashi, T. Kobayashi, Y. Kondo, Z. Korkulu, S. Koyama, V. Lapoux, Y. Maeda, F. M. Marques, T. Motobayashi, T. Miyazaki, T. Nakamura, N. Nakatsuka, Y. Nishio, A. Obertelli, A. Ohkura, N. A. Orr, S. Ota, H. Otsu, T. Ozaki, V. Panin, S. Paschalis, E. C. Pollacco, S. Reichert, J. - Y. Rousse, A. T. Saito, S. Sakaguchi, M. Sako, C. Santamaria, M. Sasano, H. Sato, M. Shikata, Y. Shimizu, Y. Shindo, L. Stuhl, T. Sumikama, Y. L. Sun, M. Tabata, Y. Togano, J. Tsubota, T. Uesaka, Z. H. Yang, J. Yasuda, K. Yoneda, and J. Zenihiro, “Structure of ^{13}Be probed via quasi-free scattering,” *Phys. Lett. B* **797**, 134843 (2019).
- M. Mazzocco, N. Keeley, A. Boiano, C. Boiano, M. La Commara, C. Manea, C. Parascandolo, D. Pierroutsakou, C. Signorini, E. Strano, D. Torresi, H. Yamaguchi, D. Kahl, L. Acosta, P. Di Meo, J. P. Fernandez-Garcia, T. Glodariu, J. Grebosz, A. Guglielmetti, Y. Hirayama, N. Imai, H. Ishiyama, N. Iwasa, S. C. Jeong, H. M. Jia, Y. H. Kim, S. Kimura, S. Kubono, G. La Rana, C. J. Lin, P. Lotti, G. Marquinez-Duran, I. Martel, H. Miyatake, M. Mukai, T. Nakao, M. Nicoletto, A. Pakou, K. Rusek, Y. Sakaguchi, A. M. Sanchez-Bentez, T. Sava, O. Sgouros, V. Soukeras, F. Soramel, E. Stiliaris, L. Stroe, T. Teranishi, N. Toniolo, Y. Wakabayashi, Y. X. Watanabe, L. Yang, Y. Y. Yang, and H. Q. Zhang, “Elastic scattering for the ^8B and $^7\text{Be} + ^{208}\text{Pb}$ systems at near-Coulomb barrier energies,” *Phys. Rev. C* **100**, 024602 (2019).
- H. Wang, H. Otsu, N. Chiga, S. Kawase, S. Takeuchi, T. Sumikama, S. Koyama, H. Sakurai, Y. Watanabe, S. Nakayama, D. S. Ahn, H. Baba, S. D. Chen, K. Chikaato, M. L. Cortés, N. Fukuda, A. Hirayama, R. Hosoda, T. Isobe, S. Kawakami, Y. Kondo, S. Kubono, Y. Maeda, S. Masuoka, S. Michimasa, I. Murray, R. Nakajima, T. Nakamura, K. Nakano, M. Nishimura, T. Ozaki, A. Saito, T. Saito, H. Sato, Y. Shimizu, S. Shimoura, P. A. Söderström, Y. Soudo, X. H. Sun, J. Suwa, D. Suzuki, H. Suzuki, H. Takeda, M. Takechi, Y. Togano, T. Tomai, H. Yamada, M. Yasuda, and K. Yoshida “Enhancement of element production by incomplete fusion reaction with weakly bound deuteron,” *Commun. Phys.* **2**, Article number 78 (2019).
- R. Taniuchi, C. Santamaria, P. Doornenbal, A. Obertelli, K. Yoneda, G. Authelet, H. Baba, D. Calvet, F. Chateau, A. Corsi, A. Delbart, J. -M. Gheller, A. Gillibert, J. D. Holt, T. Isobe, V. Lapoux, M. Matsushita, J. Menéndez, S. Momiyama, T. Motobayashi, M. Niikura, F. Nowacki, K. Ogata, H. Otsu, T. Otsuka, C. Peron, S. Peru, A. Peyaud, E. C. Pollacco, A. Poves, J. - Y. Rousse, H. Sakurai, A. Schwenk, Y. Shiga, J. Simonis, S. R. Stroberg, S. Takeuchi, Y. Tsunoda, T. Uesaka, H. Wang, F. Browne, L. X. Chung, Z. Dombradi, S. Franchoo, F. Giacoppo, A. Gottardo, K. Hadynska-Klek, Z. Korkulu, S. Koyama, Y. Kubota, J. Lee, M. Lettmann, C. Louchart, R. Lozeva, K. Matsui, T. Miyazaki, S. Nishimura, L. Olivier, S. Ota, Z. Patel, E. Sahin, C. Shand, P. -A. Söderström, I. Stefan, D. Steppenbeck, T. Sumikama, D. Suzuki, Z. Vajta, V. Werner, J. Wu, and Z. Y. Xu, “ ^{78}Ni revealed as a doubly magic stronghold against nuclear deformation,” *Nature* **569**, 53 (2019).
- N. Paul, A. Obertelli, C. A. Bertulani, A. Corsi, P. Doornenbal, J. L. Rodriguez-Sanchez, G. Authelet, H. Baba, D. Calvet, F. Chateau, S. Chen, A. Delbart, J. -M. Gheller, A. Giganon, A. Gillibert, T. Isobe, V. Lapoux, M. Matsushita, S. Momiyama, T. Motobayashi, M. Niikura, H. Otsu, C. Peron, A. Peyaud, E. C. Pollacco, J. -Y. Rousse, H. Sakurai, C. Santamaria, M. Sasano, Y. Shiga, D. Steppenbeck, S. Takeuchi, R. Taniuchi, T. Uesaka, H. Wang, K. Yoneda, T. Ando, T. Arici, A. Blazhev, F. Browne, A. M. Bruce, R. Carroll, L. X. Chung, M. L. Cortes, M. Dewald, B. Ding, Zs. Dombradi, F. Flavigny, S. Franchoo, F. Giacoppo, M. Gorska, A. Gottardo, K. Hadynska-Klek, Z. Korkulu, S. Koyama, Y. Kubota, A. Jungclaus, J. Lee, M. Lettmann, B. D. Linh, J. Liu, Z. Liu, C. Lizarazo, C. Louchart, R. Lozeva, K. Matsui, T. Miyazaki, K. Moschner, S. Nagamine, N. Nakatsuka, C. Nita, S. Nishimura, C. R. Nobs, L. Olivier, S. Ota, Z. Patel, Zs. Podolyak, M. Rudigier, E. Sahin, T. Y. Saito, C. Shand, P. -A. Söderström, I. G. Stefan, T. Sumikama, D. Suzuki, R. Orlandi, V. Vaquero, Zs. Vajta, V. Werner, K. Wimmer, J. Wu, and Z. Xu, “Prominence of Pairing in Inclusive (p , $2p$) and (p , pn) Cross Sections from Neutron-Rich Nuclei,” *Phys. Rev. Lett.* **122**, 162503 (2019).
- S. Michimasa, J. Hwang, K. Yamada, S. Ota, M. Dozono, N. Imai, K. Yoshida, Y. Yanagisawa, K. Kusaka, M. Ohtake, M. Matsushita, D. S. Ahn, O. Beliuskina, N. Chiga, K. Chikaato, N. Fukuda, S. Hayakawa, E. Ideguchi, K. Iribe, C. Iwamoto, S. Kawase, K. Kawata, N. Kitamura, S. Masuoka, H. Miyatake, D. Nagae, R. Nakajima, T. Nakamura, K. Nakano, S. Omika, H. Otsu, H. Sakurai, P. Schrock, H. Shimizu, Y. Shimizu, T. Sumikama, X. Sun, D. Suzuki, H. Suzuki, M. Takaki, M. Takechi, H. Takeda, S. Takeuchi, T. Teranishi, R. Tsunoda, H. Wang, Y. Watanabe, Y. X. Watanabe, K. Wimmer, K. Yako, H. Yamaguchi, L. Yang, H. Yoshida, and S. Shimoura, “OEDO, the energy-degrading beamline at RI Beam Factory,” *Prog. Theor. Exp. Phys.* **2019**, 043D01 (2019).
- J. Hwang, S. Michimasa, S. Ota, M. Dozono, N. Imai, K. Yoshida, Y. Yanagisawa, K. Kusaka, M. Ohtake, D. S. Ahn, O. Beliuskina, N. Fukuda, C. Iwamoto, S. Kawase, K. Kawata, N. Kitamura, S. Masuoka, H. Otsu, H. Sakurai, P. Schrock, T. Sumikama, H. Suzuki, M. Takaki, H. Takeda, R. Tsunoda, K. Wimmer, K. Yako, and S. Shimoura, “Angle-tunable wedge degrader for an energy-degrading RI beamline,” *Prog. Theor. Exp. Phys.* **2019**, 043D02 (2019).
- S. Takeuchi, T. Nakamura, M. Shikata, Y. Togano, Y. Kondo, J. Tsubota, T. Ozaki, A. Saito, H. Otsu, H. Wang, H. Sakurai, Y. Watanabe, S. Kawase, D. S. Ahn, M. Aikawa, T. Ando, S. Araki, S. Chen, N. Chiga, P. Doornenbal, S. Ebata, N. Fukuda, T. Isobe, S. Kawakami, T. Kin, S. Koyama, S. Kubono, Y. Maeda, A. Makinaga, M. Matsushita, T. Matsuzaki, S. Michimasa, S. Momiyama, S. Nagamine, K. Nakano, M. Niikura, K. Ogata, T. Saito, Y. Shiga, Y. Shimizu, S. Shimoura, T. Sumikama, P. A. Söderström, H. Suzuki, H. Takeda, R. Taniuchi, M. Uesaka, Y. Watanabe, K. Wimmer, T. Yamamoto, and K. Yoshida, “Coulomb breakup reactions of $^{93,94}\text{Zr}$ in inverse kinematics,” *Prog. Theor. Exp. Phys.* **2019**, 013D02 (2019).

- Z. Elekes, A. Kripko, D. Sohler, K. Sieja, K. Ogata, K. Yoshida, P. Doornenbal, A. Obertelli, G. Authelet, H. Baba, D. Calvet, F. Chateau, A. Corsi, A. Delbart, J. -M. Gheller, A. Gillibert, T. Isobe, V. Lapoux, M. Matsushita, S. Momiyama, T. Motobayashi, H. Otsu, C. Peron, A. Peyaud, E. C. Pollacco, J. -Y. Rousse, H. Sakurai, C. Santamaria, Y. Shiga, S. Takeuchi, R. Taniuchi, T. Uesaka, H. Wang, K. Yoneda, F. Browne, L. X. Chung, Zs. Dombradi, F. Flavigny, S. Franchoo, F. Giacoppo, A. Gottardo, K. Hadynska-Klek, Z. Korkulu, S. Koyama, Y. Kubota, J. Lee, M. Lettmann, C. Louchart, R. Lozeva, K. Matsui, T. Miyazaki, M. Niikura, S. Nishimura, L. Olivier, S. Ota, Z. Patel, E. Sahin, C. Shand, P. -A. Söderström, I. Stefan, D. Steppenbeck, T. Sumikama, D. Suzuki, Zs. Vajta, V. Werner, J. Wu, and Z. Xu, “Nuclear structure of ^{76}Ni from the (p,2p) reaction,” *Phys. Rev. C* **99**, 014312 (2019).
- S. Chen, J. Lee, P. Doornenbal, A. Obertelli, C. Barbieri, Y. Chazono, P. Navratil, K. Ogata, T. Otsuka, F. Raimondi, V. Soma, Y. Utsuno, K. Yoshida, H. Baba, F. Browne, D. Calvet, F. Chateau, N. Chiga, A. Corsi, M. L. Cortes, A. Delbart, J. M. Gheller, A. Giganon, A. Gillibert, C. Hilaire, T. Isobe, J. Kahlbow, T. Kobayashi, Y. Kubota, V. Lapoux, H. N. Liu, T. Motobayashi, I. Murray, H. Otsu, V. Panin, N. Paul, W. Rodriguez, H. Sakurai, M. Sasano, D. Steppenbeck, L. Stuhl, Y. L. Sun, Y. Togano, T. Uesaka, K. Wimmer, K. Yoneda, N. Achouri, O. Aktas, T. Aumann, L. X. Chung, F. Flavigny, S. Franchoo, I. Gasparic, R. -B. Gerst, J. Gibelin, K. I. Hahn, D. Kim, T. Koiwai, Y. Kondo, P. Koseoglou, C. Lehr, B. D. Linh, T. Lokotko, M. MacCormick, K. Moschner, T. Nakamura, S. Y. Park, D. Rossi, E. Sahin, D. Sohler, P. A. Söderström, S. Takeuchi, H. Tornqvist, V. Vaquero, V. Wagner, S. Wang, V. Werner, X. Xu, H. Yamada, D. Yan, Z. Yang, M. Yasuda, and L. Zanetti, “Quasifree neutron knockout from ^{54}Ca corroborates arising $N = 34$ neutron magic number,” *Phys. Rev. Lett.* **123**, 142501 (2019).
- L. Stuhl, M. Sasano, J. Gao, Y. Hirai, K. Yako, T. Wakasa, D. S. Ahn, H. Baba, A. I. Chilug, S. Franchoo, Y. Fujino, N. Fukuda, J. Gibelin, I. S. Hahn, Z. Halasz, T. Harada, M. N. Harakeh, D. Inomoto, T. Isobe, H. Kasahara, D. Kim, G. G. Kiss, T. Kobayashi, Y. Kondo, Z. Korkulu, S. Koyama, Y. Kubota, A. Kurihara, H. N. Liu, M. Matsumoto, S. Michimasa, H. Miki, M. Miwa, T. Motobayashi, T. Nakamura, M. Nishimura, H. Otsu, V. Panin, S. Park, A. T. Saito, H. Sakai, H. Sato, T. Shimada, Y. Shimizu, S. Shimoura, A. Spiridon, I. C. Stefanescu, X. Sun, Y. L. Sun, H. Suzuki, E. Takada, Y. Togano, T. Tomai, L. Trache, D. Tudor, T. Uesaka, H. Yamada, Z. Yang, M. Yasuda, K. Yoneda, K. Yoshida, J. Zenihiro, and N. Zhang, “Study of spin-isospin responses of radioactive nuclei with the background-free neutron spectrometer, PANDORA,” *Nucl. Instrum. Methods Phys. Res. B* **463**, 189–194 (2020).
- S. Michimasa, N. Imai, M. Dozono, J. W. Hwang, K. Yamada, S. Ota, K. Yoshida, Y. Yanagisawa, K. Kusaka, M. Ohtake, M. Matsushita, D. S. Ahn, O. Beliuskina, N. Chiga, K. Chikaato, N. Fukuda, S. Hayakawa, E. Ideguchi, K. Iribe, C. Iwamoto, S. Kawase, K. Kawata, N. Kitamura, S. Masuoka, H. Miyatake, D. Nagae, R. Nakajima, T. Nakamura, K. Nakano, S. Omika, H. Otsu, H. Sakurai, P. Schrock, H. Shimizu, Y. Shimizu, T. Sumikama, X. Sun, D. Suzuki, H. Suzuki, M. Takaki, M. Takechi, H. Takeda, S. Takeuchi, T. Teranishi, R. Tsunoda, H. Wang, Y. Watanabe, Y. X. Watanabe, K. Wimmer, K. Yako, H. Yamaguchi, L. Yang, H. Yoshida, and S. Shimoura, “New energy-degrading beamline for in-flight RI beams, OEDO,” *Nucl. Instrum. Methods Phys. Res. B* **463**, 143 (2020).
- M. L. Cortés, W. Rodriguez, P. Doornenbal, A. Obertelli, J. D. Holt, S. M. Lenzi, J. Menéndez, F. Nowacki, K. Ogata, A. Poves, T. R. Rodriguez, A. Schwenk, J. Simonis, S. R. Stroberg, K. Yoshida, L. Achouri, H. Baba, F. Browne, D. Calvet, F. Chateau, S. Chen, N. Chiga, A. Corsi, A. Delbart, J. -M. Gheller, A. Giganon, A. Gillibert, C. Hilaire, T. Isobe, T. Kobayashi, Y. Kubota, V. Lapoux, H. N. Liu, T. Motobayashi, I. Murray, H. Otsu, V. Panin, N. Paul, H. Sakurai, M. Sasano, D. Steppenbeck, L. Stuhl, Y. L. Sun, Y. Togano, T. Uesaka, K. Wimmer, K. Yoneda, O. Aktas, T. Aumann, L. X. Chung, F. Flavigny, S. Franchoo, I. Gasparic, R. -B. Gerst, J. Gibelin, K. I. Hahn, D. Kim, T. Koiwai, Y. Kondo, P. Koseoglou, J. Lee, C. Lehr, B. D. Linh, T. Lokotko, M. MacCormick, K. Moschner, T. Nakamura, S. Y. Park, D. Rossi, E. Sahin, D. Sohler, P. -A. Söderström, S. Takeuchi, H. Toernqvist, V. Vaquero, V. Wagner, S. Wang, V. Werner, X. Xu, H. Yamada, D. Yan, Z. Yang, M. Yasuda, and L. Zanetti, “Shell evolution of $N = 40$ isotones towards ^{60}Ca ; First spectroscopy of ^{62}Ti ,” *Phys. Lett. B* **800**, 135071 (2020).
- A. E. Barzakh, D. Atanasov, A. N. Andreyev, M. Al Monthery, N. A. Althubiti, B. Andel, S. Antalic, K. Blaum, T. E. Cocolios, J. G. Cubiss, P. Van Duppen, T. Day Goodacre, A. de Roubin, Yu. A. Demidov, G. J. Farooq-Smith, D. V. Fedorov, V. N. Fedosseev, D. A. Fink, L. P. Gaffney, L. Ghys, R. D. Harding, D. T. Joss, F. Herfurth, M. Huysse, N. Imai, M. G. Kozlov, S. Kreim, D. Lunney, K. M. Lynch, V. Manea, B. A. Marsh, Y. Martinez Palenzuela, P. L. Molkanov, D. Neidherr, R. D. Page, M. Rosenbusch, R. E. Rossel, S. Rothe, L. Schweikhard, M. D. Seliverstov, S. Sels, C. Van Beveren, E. Verstraelen, A. Welker, F. Wienholtz, R. N. Wolf, and K. Zuber, “Hyperfine anomaly in gold and magnetic moments of $I^\pi = 11/2^-$ gold isomers,” *Phys. Rev. C* **101**, 034308 (2020).
- K. B. Howard, U. Garg, M. Itoh, H. Akimune, S. Bagchi, T. Doi, Y. Fujikawa, M. Fujiwara, T. Furuno, M. N. Harakeh, Y. Hijikata, K. Inaba, S. Ishida, N. Kalantar-Nayestanaki, T. Kawabata, S. Kawashima, K. Kitamura, N. Kobayashi, Y. Matsuda, A. Nakagawa, S. Nakamura, K. Nosaka, S. Okamoto, S. Ota, S. Weyhmler, and Z. Yang, “Compression-mode resonances in the calcium isotopes and implications for the asymmetry term in nuclear incompressibility,” *Phys. Lett. B* **801**, 135185 (2020).
- T. Lokotko, S. Leblond, J. Lee, P. Doornenbal, A. Obertelli, A. Poves, F. Nowacki, K. Ogata, K. Yoshida, G. Authelet, H. Baba, D. Calvet, F. Chateau, S. Chen, A. Corsi, A. Delbart, J. M. Gheller, A. Gillibert, T. Isobe, V. Lapoux, M. Matsushita, S. Momiyama, T. Motobayashi, M. Niikura, H. Otsu, C. Peron, A. Peyaud, E. C. Pollacco, J. Y. Rousse, H. Sakurai, C. Santamaria, Z. Y. Xu, M. Sasano, Y. Shiga, S. Takeuchi, R. Taniuchi, T. Uesaka, H. Wang, V. Werner, F. Browne, L. X. Chung, Z. Dombradi, S. Franchoo, F. Giacoppo, A. Gottardo, K. Hadynska-Klek, Z. Korkulu, S. Koyama, Y. Kubota, M. Lettmann, C. Louchart, R. Lozeva, K. Matsui, T. Miyazaki, S. Nishimura, L. Olivier, S. Ota, Z. Patel, E. Sahin, C. Shand, P. -A. Söderström, I. Stefan, D. Steppenbeck, T. Sumikama, D. Suzuki, Z. Vajta, and J. Wu, “Shell structure of the neutron-rich isotopes $^{69,71,73}\text{Co}$,” *Phys. Rev. C* **101**, 034314 (2020).
- V. Vaquero, A. Jungclauss, T. Aumann, J. Tscheuschner, E. V. Litvinova, J. A. Tostevin, H. Baba, D. S. Ahn, R. Avigo, K. Boretzky, A. Bracco, C. Caesar, F. Camera, S. Chen, V. Derya, P. Doornenbal, J. Endres, N. Fukuda, U. Garg, A. Giaz, M. N. Harakeh, M. Heil, A. Horvat, K. Ieki, N. Imai, N. Inabe, N. Kalantar-Nayestanaki, N. Kobayashi, Y. Kondo, S. Koyama, T. Kubo, I. Martel, M. Matsushita, B. Million, T. Motobayashi, T. Nakamura, N. Nakatsuka, M. Nishimura, S. Nishimura, S. Ota, H. Otsu, T. Ozaki, M. Petri, R. Reifarh, J. L. Rodriguez-Sanchez, D. Rossi, A. T. Saito, H. Sakurai, D. Savran, H. Scheit, F. Schindler, P. Schrock, D. Semmler, Y. Shiga, M. Shikata, Y. Shimizu, H. Simon, D. Steppenbeck, H. Suzuki, T. Sumikama, D. Symochko, I. Syndikus, H. Takeda, S. Takeuchi, R. Taniuchi, Y. Togano, J. Tsubota, H. Wang, O. Wieland, K. Yoneda, J. Zenihiro, and A. Zilges, “Fragmentation of single-particle strength around the doubly magic nucleus ^{132}Sn and the position of the $0f_{5/2}$ proton-hole state in ^{131}In ,” *Phys. Rev. Lett.* **124**, 022501 (2020).

- A. Corsi, Y. Kubota, J. Casal, M. Gomez-Ramos, A. M. Moro, G. Authelet, H. Baba, C. Caesar, D. Calvet, A. Delbart, M. Dozono, J. Feng, F. Flavigny, J. -M. Gheller, J. Gibelin, A. Giganon, A. Gillibert, K. Hasegawa, T. Isobe, Y. Kanaya, S. Kawakami, D. Kim, Y. Kiyokawa, M. Kobayashi, N. Kobayashi, T. Kobayashi, Y. Kondo, Z. Korkulu, S. Koyama, V. Lapoux, Y. Maeda, F. M. Marques, T. Motobayashi, T. Miyazaki, T. Nakamura, N. Nakatsuka, Y. Nishio, A. Obertelli, A. Ohkura, N. A. Orr, S. Ota, H. Otsu, T. Ozaki, V. Panin, S. Paschalis, E. C. Pollacco, S. Reichert, J. -Y. Rousse, A. T. Saito, S. Sakaguchi, M. Sako, C. Santamaria, M. Sasano, H. Sato, M. Shikata, Y. Shimizu, Y. Shindo, L. Stuhl, T. Sumikama, Y. L. Sun, M. Tabata, Y. Togano, J. Tsubota, T. Uesaka, Z. H. Yang, J. Yasuda, K. Yoneda, and J. Zenihiro, "Structure of ^{13}Be probed via quasi-free scattering," *Phys. Lett. B* **797**, (2019).
- N. R. Ma, L. Yang, C. J. Lin, H. Yamaguchi, D. X. Wang, L. J. Sun, M. Mazzocco, H. M. Jia, S. Hayakawa, D. Kahl, S. M. Cha, G. X. Zhang, F. Yang, Y. Y. Yang, C. Signorini, Y. Sakaguchi, K. Abe, M. La Commara, D. Pierroutsakou, C. Parascandolo, E. Strano, A. Kim, K. Y. Chae, M. S. Kwag, G. L. Zhang, M. Pan, X. X. Xu, P. W. Wen, F. P. Zhong, H. H. Sun, and G. Guo, "Mita: A multilayer ionization-chamber telescope array for low-energy reactions with exotic nuclei," *Eur. Phys. J. A* **55**, 87 (2019).
- L. Lamia, M. Mazzocco, R. G. Pizzone, S. Hayakawa, M. L. Cognata, C. Spitaleri, C. A. Bertulani, A. Boiano, C. Boiano, C. Brogini, A. Caciolli, S. Cherubini, G. D'Agata, H. da Silva, R. Depalo, F. Galtarossa, G. L. Guardo, M. Gulino, I. Indelicato, M. L. Com-mara, G. L. Rana, R. Menegazzo, J. Mrazek, A. Pakou, C. Parascandolo, D. Piatti, D. Pierroutsakou, S. M. R. Puglia, S. Romano, G. G. Rapisarda, A. M. Sanchez-Benitez, M. L. Sergi, O. Sgouros, F. Soramel, V. Soukeras, R. Sparta, E. Strano, D. Torresi, A. Tu-mino, H. Yamaguchi, and G. L. Zhang, "Cross-section measurement of the cosmologically relevant $^7\text{Be}(n, \alpha)^4\text{He}$ reaction over a broad energy range in a single experiment," *The Astrophysical Journal* **879**, 23 (2019).
- B. Yang, Y. L. Ye, J. Feng, C. J. Lin, H. M. Jia, Z. H. Li, J. L. Lou, Q. T. Li, Y. C. Ge, X. F. Yang, H. Hua, J. Li, H. L. Zang, Q. Liu, W. Jiang, C. G. Li, Y. Liu, Z. Q. Chen, H. Y. Wu, C. G. Wang, W. Liu, X. Wang, J. J. Li, D. W. Luo, Y. Jiang, S. W. Bai, J. Y. Xu, N. R. Ma, L. J. Sun, D. X. Wang, Z. H. Yang, and J. Chen, "Investigation of the $^{14}\text{C}+\alpha$ molecular configuration in ^{18}O by means of transfer and sequential decay reaction," *Phys. Rev. C* **99**, 064315 (2019).
- L. J. Sun, X. X. Xu, S. Q. Hou, C. J. Lin, J. José, J. Lee, J. J. He, Z. H. Li, J. S. Wang, C. X. Yuan, F. Herwig, J. Keegans, T. Budner, D. X. Wang, X. Wang, H. Y. Wu, P. F. Liang, Y. Y. Yang, Y. H. Lam, P. Ma, F. F. Duan, Z. H. Gao, Q. Hu, Z. Bai, J. B. Ma, J. G. Wang, F. P. Zhong, C. G. Wu, D. W. Luo, Y. Jiang, Y. Liu, D. S. Hou, R. Li, N. R. Ma, W. H. Ma, G. Z. Shi, G. M. Yu, D. Patel, S. Y. Jin, Y. F. Wang, Y. C. Yu, Q. W. Zhou, P. Wang, L. Y. Hu, H. L. Zang, P. J. Li, Q. Q. Zhao, H. M. Jia, L. Yang, P. W. Wen, F. Yang, M. Pan, X. Y. Wang, Z. G. Hu, R. F. Chen, M. L. Liu, W. Q. Yang, and Y. M. Zhao, "Experimentally well-constrained masses of ^{27}P and ^{27}S : Implications for studies of explosive binary systems," *Phys. Lett. B* **802** 135213 (2020).
- M. D. Sun, Z. Liu, T. H. Huang, W. Q. Zhang, A. N. Andreyev, B. Ding, J. G. Wang, X. Y. Liu, H. Y. Lu, D. S. Hou, Z. G. Gan, L. Ma, H. B. Yang, Z. Y. Zhang, L. Yu, J. Jiang, K. L. Wang, Y. S. Wang, M. L. Liu, Z. H. Li, J. Li, X. Wang, A. H. Feng, C. J. Lin, L. J. Sun, N. R. Ma, W. Zuo, H. S. Xu, X. H. Zhou, G. Q. Xiao, C. Qi, and F. S. Zhang, "Fine structure in the α decay of ^{223}U ," *Phys. Lett. B* **800** 135096 (2020).
- W. Jiang, Y. L. Ye, C. J. Lin, Z. H. Li, J. L. Lou, X. F. Yang, Q. T. Li, Y. C. Ge, H. Hua, D. X. Jiang, D. Y. Pang, J. Li, J. Chen, Z. H. Yang, X. H. Sun, Z. Y. Tian, J. Feng, B. Yang, H. L. Zang, Q. Liu, P. J. Li, Z. Q. Chen, Y. Liu, Y. Zhang, J. Ma, H. M. Jia, X. X. Xu, L. Yang, N. R. Ma, and L. J. Sun, "Determination of the cluster-decay branching ratio from a near-threshold molecular state in ^{10}Be ," *Phys. Rev. C* **101**, 031304(R) (2020).
- L. J. Sun, X. X. Xu, C. J. Lin, J. Lee, S. Q. Hou, C. X. Yuan, Z. H. Li, J. José, J. J. He, J. S. Wang, D. X. Wang, H. Y. Wu, P. F. Liang, Y. Y. Yang, Y. H. Lam, P. Ma, F. F. Duan, Z. H. Gao, Q. Hu, Z. Bai, J. B. Ma, J. G. Wang, F. P. Zhong, C. G. Wu, D. W. Luo, Y. Jiang, Y. Liu, D. S. Hou, R. Li, N. R. Ma, W. H. Ma, G. Z. Shi, G. M. Yu, D. Patel, S. Y. Jin, Y. F. Wang, Y. C. Yu, Q. W. Zhou, P. Wang, L. Y. Hu, X. Wang, H. L. Zang, P. J. Li, Q. Q. Zhao, L. Yang, P. W. Wen, F. Yang, H. M. Jia, G. L. Zhang, M. Pan, X. Y. Wang, H. H. Sun, Z. G. Hu, R. F. Chen, M. L. Liu, W. Q. Yang, Y. M. Zhao, and H. Q. Zhang (RIBLL Collaboration), " β -decay spectroscopy of ^{27}S ," *Phys. Rev. C* **99**, 064312 (2019).
- P. F. Liang, L. J. Sun, J. Lee, S. Q. Hou, X. X. Xu, C. J. Lin, C. X. Yuan, J. J. He, Z. H. Li, J. S. Wang, D. X. Wang, H. Y. Wu, Y. Y. Yang, Y. H. Lam, P. Ma, F. F. Duan, Z. H. Gao, Q. Hu, Z. Bai, J. B. Ma, J. G. Wang, F. Zhong, C. G. Wu, D. W. Luo, Y. Jiang, Y. Liu, D. S. Hou, R. Li, N. R. Ma, W. H. Ma, G. Z. Shi, G. M. Yu, D. Patel, S. Y. Jin, Y. F. Wang, Y. C. Yu, Q. W. Zhou, P. Wang, L. Y. Hu, X. Wang, H. L. Zang, P. J. Li, Q. Q. Zhao, H. M. Jia, L. Yang, P. W. Wen, F. Yang, G. L. Zhang, M. Pan, X. Y. Wang, H. H. Sun, Z. G. Hu, R. F. Chen, M. L. Liu, W. Q. Yang, and Y. M. Zhao (RIBLL Collaboration), "Simultaneous measurement of β -delayed proton and γ emission of ^{26}P for the $^{25}\text{Al}(p, \gamma)^{26}\text{Si}$ reaction rate," *Phys. Rev. C* **101**, 024305 (2020).
- U. Acharya *et al.* (PHENIX Collaboration), " J/ψ and $\psi(2\text{S})$ production at forward rapidity in $p + p$ collisions at $\sqrt{s} = 510$ GeV," *Phys. Rev. D* **101**, 052006 (2020).
- S. Acharya *et al.* (ALICE Collaboration), "Evidence of rescattering effect in Pb-Pb collisions at the LHC through production of $\text{K}^*(892)^0$ and $\phi(1020)$ mesons," *Phys. Lett. B* **802**, 135225 (2020).
- S. Acharya *et al.* (ALICE Collaboration), "Measurement of electrons from heavy-flavour hadron decays as a function of multiplicity in p -Pb collisions at $\sqrt{s_{NN}} = 5.02$ TeV," *JHEP* **02**, 077 (2020).
- S. Acharya *et al.* (ALICE Collaboration), "Measurements of inclusive jet spectra in pp and central Pb-Pb collisions at $\sqrt{s_{NN}} = 5.02$ TeV," *Phys. Rev. C* **101**, 034911 (2020).
- S. Acharya *et al.* (ALICE Collaboration), "Studies of J/ψ production at forward rapidity in Pb-Pb collisions at $\sqrt{s_{NN}} = 5.02$ TeV," *JHEP* **02**, 041 (2020).
- S. Acharya *et al.* (ALICE Collaboration), "Multiplicity dependence of (multi-)strange hadron production in proton-proton collisions at $\sqrt{s} = 13$ TeV," *Eur. Phys. J. C* **80**, 167 (2020).
- S. Acharya *et al.* (ALICE Collaboration), " $3\Lambda\text{H}$ and anti- ΛH lifetime measurement in Pb-Pb collisions at $\sqrt{s_{NN}} = 5.02$ TeV via two-body decay," *Phys. Lett. B* **797**, 134905 (2019).
- S. Acharya *et al.* (ALICE Collaboration), "Measurement of $\text{Y}(1\text{S})$ elliptic flow at forward rapidity in Pb-Pb collisions at $\sqrt{s_{NN}} = 5.02$ TeV," *Phys. Rev. Lett.* **123**, 192301 (2019).

- C. Aidala *et al.* (PHENIX Collaboration), “Nuclear-modification factor of charged hadrons at forward and backward rapidity in $p+Al$ and $p+Au$ collisions at $\sqrt{s_{NN}} = 200$ GeV,” *Phys. Rev. C* **101**, 034910 (2020).
- S. Acharya *et al.* (ALICE Collaboration), “Measurement of prompt $D0$, $D+$, D^{*+} , and $Ds+$ production in p -Pb collisions at $\sqrt{s_{NN}} = 5.02$ TeV,” *JHEP* **12**, 092 (2019).
- S. Acharya *et al.* (ALICE Collaboration), “Multiplicity dependence of light (anti-)nuclei production in p -Pb collisions at $\sqrt{s_{NN}} = 5.02$ TeV,” *Phys. Lett. B* **800**, 135043 (2020).
- S. Acharya *et al.* (ALICE Collaboration), “Measurement of the inclusive isolated photon production cross section in pp collisions at $\sqrt{s} = 7$ TeV,” *Eur. Phys. J. C* **79**, 896 (2019).
- S. Acharya *et al.* (ALICE Collaboration), “Scattering Studies with Low-Energy Kaon-Proton Femtoscopy in Proton-Proton Collisions at the LHC,” *Phys. Rev. Lett.* **124**, 092301 (2020).
- S. Acharya *et al.* (ALICE Collaboration), “Charged-particle production as a function of multiplicity and transverse sphericity in pp collisions at $\sqrt{s} = 5.02$ and 13 TeV,” *Eur. Phys. J. C* **79**, 857 (2019).
- S. Acharya *et al.* (ALICE Collaboration), “Inclusive J/ψ production at mid-rapidity in pp collisions at $\sqrt{s} = 5.02$ TeV,” *JHEP* **10**, 084 (2019).
- S. Acharya *et al.* (ALICE Collaboration), “Study of the Λ - Λ interaction with femtoscopy correlations in pp and p -Pb collisions at the LHC,” *Phys. Lett. B* **797**, 134822 (2019).
- S. Acharya *et al.* (ALICE Collaboration), “Production of muons from heavy-flavour hadron decays in pp collisions at $\sqrt{s} = 5.02$ TeV,” *JHEP* **09**, 008 (2019).
- S. Acharya *et al.* (ALICE Collaboration), “Measurement of the production of charm jets tagged with $D0$ mesons in pp collisions at $\sqrt{s} = 7$ TeV,” *JHEP* **08**, 133 (2019).
- S. Acharya *et al.* (ALICE Collaboration), “Exploration of jet substructure using iterative declustering in pp and Pb-Pb collisions at LHC energies,” *Phys. Lett. B* **802**, 135227 (2020).
- S. Acharya *et al.* (ALICE Collaboration), “Measurement of charged jet cross section in pp collisions at $\sqrt{s} = 5.02$ TeV,” *Phys. Rev. D* **100**, 092004 (2019).
- S. Acharya *et al.* (ALICE Collaboration), “Measurement of jet radial profiles in Pb-Pb collisions at $\sqrt{s_{NN}} = 2.76$ TeV,” *Phys. Lett. B* **796**, 204–219 (2019).
- S. Acharya *et al.* (ALICE Collaboration), “First observation of an attractive interaction between a proton and a cascade baryon,” *Phys. Rev. Lett.* **123**, 112002 (2019).
- S. Acharya *et al.* (ALICE Collaboration), “Coherent J/ψ photoproduction at forward rapidity in ultra-peripheral Pb-Pb collisions at $\sqrt{s_{NN}} = 5.02$ TeV,” *Phys. Lett. B* **798**, 134926 (2019).
- S. Acharya *et al.* (ALICE Collaboration), “One-dimensional charged kaon femtoscopy in p -Pb collisions at $\sqrt{s_{NN}} = 5.02$ TeV,” *Phys. Rev. C* **100**, 024002 (2019).
- C. Aidala *et al.* (PHENIX Collaboration), “Nuclear dependence of the transverse single-spin asymmetry in the production of charged hadrons at forward rapidity in polarized $p + p$, $p+Al$, and $p+Au$ collisions at $\sqrt{s_{NN}} = 200$ GeV,” *Phys. Rev. Lett.* **123**, 122001 (2019).
- S. Acharya *et al.* (ALICE Collaboration), “Measurement of strange baryon-antibaryon interactions with femtoscopic correlations,” *Phys. Lett. B* **802**, 135223 (2020).
- S. Acharya *et al.* (ALICE Collaboration), “Investigations of anisotropic flow using multiparticle azimuthal correlations in pp , p -Pb, Xe-Xe, and Pb-Pb collisions at the LHC,” *Phys. Rev. Lett.* **123**, 142301 (2019).
- S. Acharya *et al.* (ALICE Collaboration), “Multiplicity dependence of (anti-)deuteron production in pp collisions at $\sqrt{s} = 7$ TeV,” *Phys. Lett. B* **794**, 50–63 (2019).
- S. Acharya *et al.* (ALICE Collaboration), “Calibration of the photon spectrometer PHOS of the ALICE experiment,” *J. Instrum.* **14**, P05025 (2019).
- C. Aidala *et al.* (PHENIX Collaboration), “Measurement of charm and bottom production from semileptonic hadron decays in $p + p$ collisions at $\sqrt{s_{NN}} = 200$ GeV,” *Phys. Rev. D* **99**, 092003 (2019).
- S. Acharya *et al.* (ALICE Collaboration), “Event-shape and multiplicity dependence of freeze-out radii in pp collisions at $\sqrt{s} = 7$ TeV,” *JHEP* **09**, 108 (2019).
- A. Kastberg, T. Aoki, B. K. Sahoo, Y. Sakemi, and B. P. Das, “An optical lattice based method for precise measurements of atomic parity violation,” *Phys. Rev. A* **100**, 050101(R) (2019).
- Y. Ichikawa, H. Nishibata, Y. Tsunoda, A. Takamine, K. Imamura, T. Fujita, T. Sato, S. Momiyama, Y. Shimizu, D. S. Ahn, K. Asahi, H. Baba, D. L. Balabanski, F. Boulay, J. M. Daugas, T. Egami, N. Fukuda, C. Funayama, T. Furukawa, G. Georgiev, A. Gladkov, N. Inabe, Y. Ishibashi, T. Kawaguchi, T. Kawamura, Y. Kobayashi, S. Kojima, A. Kusoglu, I. Mukul, M. Niikura, T. Nishizaka, A. Odahara, Y. Ohtomo, T. Otsuka, D. Ralet, G. S. Simpson, T. Sumikama, H. Suzuki, H. Takeda, L. C. Tao, Y. Togano, D. Tominaga, H. Ueno, H. Yamazaki, and X. F. Yang, “Interplay between nuclear shell evolution and shape deformation revealed by the magnetic moment of ^{75}Cu ,” *Nat. Phys.* **15**, 321 (2019).
- A. Gando, Y. Gando, T. Hachiya, M. Ha Minh, S. Hayashida, Y. Honda, K. Hosokawa, H. Ikeda, K. Inoue, K. Ishidoshiro, Y. Kamei, K. Kamizawa, T. Kinoshita, M. Koga, S. Matsuda, T. Mitsui, K. Nakamura, A. Ono, N. Ota, S. Otsuka, H. Ozaki, Y. Shibukawa, I. Shimizu, Y. Shirahata, J. Shirai, T. Sato, K. Soma, A. Suzuki, A. Takeuchi, K. Tamae, K. Ueshima, H. Watanabe, D. Chernykh, A. Kozlov, S. Obara, S. Yoshida, Y. Takemoto, S. Umehara, K. Fushimi, S. Hirata, B. E. Berger, B. K. Fujikawa, J. G. Learned, J. Maricic, L. A. Winslow, Y. Efremenko, H. J. Karwowski, D. M. Markoff, W. Tornow, T. O’Donnell, J. A. Detwiler, S. Enomoto, M. P. Decowski, J. Menéndez, R. Dvornický, and F. Šimkovic “Precision analysis of the ^{136}Xe two-neutrino double-beta spectrum in KamLAND-Zen and its impact on the quenching of nuclear matrix elements,” *Phys. Rev. Lett.* **122**, 192501 (2019).

- T. Otsuka, Y. Tsunoda, T. Abe, N. Shimizu, and P. Van Duppen, “Underlying structure of collective bands and self-organization in quantum systems,” *Phys. Rev. Lett.* **123**, 222502 (2019).
- I. Murray, M. MacCormick, D. Bazin, P. Doornenbal, N. Aoi, H. Baba, H. Crawford, P. Fallon, K. Li, J. Lee, M. Matsushita, T. Motobayashi, T. Otsuka, H. Sakurai, H. Scheit, D. Steppenbeck, S. Takeuchi, J. A. Tostevin, N. Tsunoda, Y. Utsuno, H. Wang, and K. Yoneda, “Spectroscopy of strongly deformed ^{32}Ne by proton knockout reactions,” *Phys. Rev. C* **99**, 011302(R) (2019).
- Md. S. R. Laskar, S. Saha, R. Palit, S. N. Mishra, N. Shimizu, Y. Utsuno, E. Ideguchi, Z. Naik, F. S. Babra, S. Biswas, S. Kumar, S. K. Mohanta, C. S. Palshetkar, P. Singh, and P. C. Srivastava, “ g -factor measurement of the 2738 keV isomer in ^{135}La ,” *Phys. Rev. C* **99**, 014308 (2019).
- H. Nishibata, S. Kanaya, T. Shimoda, A. Odahara, S. Morimoto, A. Yagi, H. Kanaoka, M. R. Pearson, C. D. P. Levy, M. Kimura, N. Tsunoda, and T. Otsuka, “Structure of ^{31}Mg : Shape coexistence revealed by beta-gamma spectroscopy with spin-polarized ^{31}Na ,” *Phys. Rev. C* **99**, 024322 (2019).
- S. Sels, T. Day Goodacre, B. A. Marsh, A. Pastore, W. Ryssens, Y. Tsunoda, N. Althubiti, B. Andel, A. N. Andreyev, D. Atanasov, A. E. Barzakh, M. Bender, J. Billowes, K. Blaum, T. E. Cocolios, J. G. Cubiss, J. Dobaczewski, G. J. Farooq-Smith, D. V. Fedorov, V. N. Fedosseev, K. T. Flanagan, L. P. Gaffney, L. Ghys, P. -H. Heenen, M. Huyse, S. Kreim, D. Lunney, K. M. Lynch, V. Manea, Y. Martinez Palenzuela, T. M. Medonca, P. L. Molkanov, T. Otsuka, J. P. Ramos, R. E. Rossel, S. Rothe, L. Schweikhard, M. D. Seliverstov, P. Spagnoletti, C. Van Beveren, P. Van Duppen, M. Veinhard, E. Verstraelen, A. Welker, K. Wendt, F. Wienholtz, R. N. Wolf, and A. Zadvornaya, “Shape staggering of midshell mercury isotopes from in-source laser spectroscopy compared with density-functional-theory and Monte Carlo shell-model calculations,” *Phys. Rev. C* **99**, 044306 (2019).
- A. Matta, W. N. Catford, N. A. Orr, J. Henderson, P. Ruotsalainen, G. Hackman, A. B. Garnsworthy, F. Delaunay, R. Wilkinson, G. Lotay, N. Tsunoda, T. Otsuka, A. J. Knapp, G. C. Ball, N. Bernier, C. Burbadge, A. Chester, D. S. Cross, S. Cruz, C. Aa. Diget, T. Domingo, T. E. Drake, L. J. Evitts, F. H. Garcia, S. Hallam, E. MacConnachie, M. Moukaddam, D. Muecher, E. Padilla-Rodal, O. Paetkau, J. Park, J. L. Pore, U. Rizwan, J. Smallcombe, J. K. Smith, K. Starosta, C. E. Svensson, J. Williams, and M. Williams, “Shell evolution approaching the $N = 20$ island of inversion: Structure of ^{29}Mg ,” *Phys. Rev. C* **99**, 044320 (2019).
- F. Flavigny, J. Elseviers, A. N. Andreyev, C. Bauer, V. Bildstein, A. Blazhev, B. A. Brown, H. De Witte, J. Diriken, V. N. Fedosseev, S. Franchoo, R. Gernhäuser, M. Huyse, S. Ilieva, S. Klupp, Th. Kröll, R. Lutter, B. A. Marsh, D. Muecher, K. Nowak, T. Otsuka, J. Pakarinen, N. Patronis, R. Raabe, F. Recchia, P. Reiter, T. Roger, S. Sambhi, M. Seidlitz, M. D. Seliverstov, B. Siebeck, Y. Tsunoda, P. Van Duppen, M. Vermeulen, M. Von Schmid, D. Voulot, N. Warr, F. Wenander, and K. Wimmer, “Microscopic structure of coexisting $0+$ states in ^{68}Ni probed via two-neutron transfer,” *Phys. Rev. C* **99**, 054332 (2019).
- T. Shizuma, M. Omer, R. Hajima, N. Shimizu, and Y. Utsuno, “Spin and parity determination of the 3.004 MeV level in ^{27}Al : Its low-lying multiplet structure,” *Phys. Rev. C* **100**, 014307 (2019).
- B. Abromeit, Vandana Tripathi, H. L. Crawford, S. N. Liddick, S. Yoshida, Y. Utsuno, P. C. Bender, B. P. Crider, R. Dungan, P. Fallon, K. Kravvaris, N. Larson, R. S. Lubna, T. Otsuka, C. J. Prokop, A. L. Richard, N. Shimizu, S. L. Tabor, and A. Volya, “ β -decay of $T_z = +11/2$ isotopes ^{37}Al and ^{39}Si ; Understanding Gamow-Teller strength distribution in neutron-rich nuclei,” *Phys. Rev. C* **100**, 014323 (2019).
- L. Kaya, A. Vogt, P. Reiter, M. Siciliano, N. Shimizu, Y. Utsuno, H. -K. Wang, A. Gargano, L. Coraggio, N. Itaco, K. Arnsward, D. Bazzacco, B. Birkenbach, A. Blazhev, A. Bracco, B. Bruyneel, L. Corradi, F. C. L. Crespi, G. de Angelis, M. Droste, J. Eberth, A. Esmaylzadeh, E. Farnea, E. Fioretto, C. Fransen, A. Gadea, A. Giaz, A. Görgen, A. Gottardo, K. Hadyńska-Klęk, H. Hess, R. Hirsch, P. R. John, J. Jolie, A. Jungclaus, V. Karayonchev, L. Kornwebel, W. Korten, S. Leoni, L. Lewandowski, S. Lunardi, R. Menegazzo, D. Mengoni, C. Michelagnoli, T. Mijatović, G. Montagnoli, D. Montanari, C. Müller-Gatermann, D. Napoli, Zs. Podolyák, G. Pollarolo, F. Recchia, J. -M. Régis, N. Saed-Samii, E. Şahin, F. Scarlassara, K. Schomacker, M. Seidlitz, B. Siebeck, P. -A. Söderström, A. M. Stefanini, O. Stezowski, S. Szilner, B. Szpak, E. Teruya, C. Ur, J. J. Valiente-Dobón, K. Wolf, K. Yanase, N. Yoshinaga, and K. O. Zell, “Isomer spectroscopy in ^{133}Ba and high-spin structure of ^{134}Ba ,” *Phys. Rev. C* **100**, 024323 (2019).
- T. Miyagi, T. Abe, M. Kohno, P. Navrátil, R. Okamoto, T. Otsuka, N. Shimizu, and S. R. Stroberg, “Ground-state properties of doubly magic nuclei from the unitary-model-operator approach with chiral two- and three-nucleon forces,” *Phys. Rev. C* **100**, 034310 (2019).
- Md. S. R. Laskar, R. Palit, S. N. Mishra, N. Shimizu, Y. Utsuno, E. Ideguchi, U. Garg, S. Biswas, F. S. Babra, R. Gala, C. S. Palshetkar, and Z. Naik, “Structure of the $11/2^-$ isomeric state in ^{133}La ,” *Phys. Rev. C* **101**, 034315 (2020).
- M. Hoferichter, P. Klos, J. Menéndez, and A. Schwenk, “Nuclear structure factors for general spin-independent WIMP-nucleus scattering,” *Phys. Rev. D* **99**, 055031 (2019).
- L. W. Iskra, R. Broda, R. V. F. Janssens, M. P. Carpenter, B. Fornal, T. Lauritsen, T. Otsuka, T. Togashi, Y. Tsunoda, W. B. Walters, and S. Zhu, “Revised $B(E3)$ transition rate and structure of the 3^- level in ^{96}Zr ,” *Phys. Lett. B* **788**, 396 (2019).
- L. Xie, X. F. Yang, C. Wraith, C. Babcock, J. Bieroń, J. Billowes, M. L. Bissell, K. Blaum, B. Cheal, L. Filippin, K. T. Flanagan, R. F. Garcia Ruiz, W. Gins, G. Gaigalas, M. Godefroid, C. Gorgesek, L. K. Grob, H. Heylen, P. Jönsson, S. Kaufman, M. Kowalska, J. Krämer, S. Malbrunot-Ettenauer, R. Neugart, G. Neyens, W. Nörtershäuser, T. Otsuka, J. Papuga, R. Sánchez, Y. Tsunoda, and D. T. Yordanov, “Nuclear charge radii of $^{62-80}\text{Zn}$ and their dependence on cross-shell proton excitations,” *Phys. Lett. B* **797**, 134805 (2019).
- E. A. Coello Perez, J. Menéndez, and A. Schwenk, “Two-neutrino double electron capture on ^{124}Xe based on an effective theory and the nuclear shell model,” *Phys. Lett. B* **797**, 134885 (2019).
- C. Hornung, D. Amanbayev, I. Dedes, G. Kripko-Koncz, I. Miskun, N. Shimizu, S. A. S. Andres, J. Bergmann, T. Dickel, J. Dudek, J. Ebert, H. Geissel, M. Gorska, H. Grawe, F. Greiner, E. Haettner, T. Otsuka, W. R. Plass, S. Purushothaman, A. -K. Rink, C. Scheidenberger, H. Weick, S. Bagchi, A. Blazhev, O. Charviakova, D. Curien, A. Finlay, S. Kaur, W. Lippert, J. -H. Otto, Z. Patyk, S. Pietri, Y. K. Tanaka, Y. Tsunoda, and J. S. Winfield, “Isomer studies in the vicinity of the doubly-magic nucleus ^{100}Sn ; observation of a new low-lying isomeric state in ^{97}Ag ,” *Phys. Lett. B* **802**, 135200 (2020).

- Y. L. Sun, A. Obertelli, P. Doornenbal, C. Barbieri, Y. Chazono, T. Duguet, H. N. Liu, P. Navrátil, F. Nowacki, K. Ogata, T. Otsuka, F. Raimondid, V. Somà, Y. Utsuno, K. Yoshida, N. Achouri, H. Baba, F. Browne, D. Calvet, F. Château, S. Cheng, N. Chiga, A. Corsi, M. L. Cortés, A. Delbart, J. -M. Gheller, A. Giganon, A. Gillibert, C. Hilaire, T. Isobe, T. Kobayashi, Y. Kubota, V. Lapoux, T. Motobayashi, I. Murray, H. Otsu, V. Panin, N. Paul, W. Rodriguez, H. Sakurai, M. Sasano, D. Steppenbeck, L. Stuhl, Y. Togano, T. Uesaka, K. Wimmer, K. Yoneda, O. Aktas, T. Aumann, L. X. Chung, F. Flavigny, S. Franchoo, I. Gašparić, R. -B. Gerst, J. Gibelin, K. I. Hahn, D. Kima, T. Koizumi, Y. Kondo, P. Koseoglou, J. Lee, C. Lehr, B. D. Linh, T. Lokotko, M. Ma, Cormick, K. Moschner, T. Nakamura, S. Y. Park, D. Rossi, E. Sahin, D. Sohler, P. -A. Söderström, S. Takeuchi, H. Törnqvista, V. Vaquero, V. Wagner, S. Wang, V. Werner, X. Xu, H. Yamada, D. Yan, Z. Yang, M. Yasuda, and L. Zanetti, “Restoration of the natural $E(1/2+)-E(3/2+)$ energy splitting in Odd-K isotopes towards $N = 40$,” *Phys. Lett. B* **802**, 135215 (2020).
- N. Shimizu, T. Mizusaki, Y. Utsuno, and Y. Tsunoda, “Thick-restart block Lanczos method for large-scale shell-model calculations,” *Comp. Phys. Comm.* **244**, 372 (2019).
- M. L. Cortés, W. Rodriguez, P. Doornenbal, A. Obertelli, J. D. Holt, S. M. Lenzi, J. Menéndez, F. Nowacki, K. Ogata, A. Poves, T. R. Rodríguez, A. Schwenk, J. Simonis, S. R. Stroberg, K. Yoshida, L. Achouri, H. Baba, F. Browne, D. Calvet, F. Château, S. Chens, N. Chiga, A. Corsi, A. Delbart, J. -M. Gheller, A. Giganon, A. Gillibert, C. Hilaire, T. Isobe, T. Kobayashi, Y. Kubota, V. Lapoux, H. N. Liu, T. Motobayashi, I. Murray, H. Otsu, V. Panin, N. Paul, H. Sakurai, M. Sasano, D. Steppenbeck, L. Stuhl, Y. L. Sun, Y. Togano, T. Uesaka, K. Wimmer, K. Yoneda, O. Aktas, T. Aumann, L. X. Chung, F. Flavigny, S. Franchoo, I. Gašparić, R. -B. Gerst, J. Gibelin, K. I. Hahn, D. Kima, T. Koizumi, Y. Kondo, P. Koseoglou, J. Lee, C. Lehr, B. D. Linh, T. Lokotko, M. MacCormick, K. Moschner, T. Nakamura, S. Y. Park, D. Rossi, E. Sahin, D. Sohler, P. -A. Söderström, S. Takeuchi, H. Toernqviste, V. Vaquero, V. Wagner, S. Wang, V. Werner, X. Xu, H. Yamada, D. Yan, Z. Yang, M. Yasuda, and L. Zanetti, “Shell evolution of $N = 40$ isotones towards ^{60}Ca ; First spectroscopy of ^{62}Ti ,” *Phys. Lett. B* **800**, 135071 (2020).
- V. Manea, J. Kartheim, D. Atanasov, M. Bender, K. Blaum, T. E. Cocolios, S. Eliseev, A. Herlert, J. D. Holt, W. J. Huang, Yu. A. Litvinov, D. Lunney, J. Menéndez, M. Mougeot, D. Neidherr, L. Schweikhard, A. Schwenk, J. Simonis, A. Welker, F. Wienholtz, and K. Zuber, First glimpse of the $N = 82$ shell closure below $Z = 50$ from masses of neutron-rich cadmium isotopes and isomers, *Phys. Rev. Lett.* **124**, 092502 (2020).
- M. Ciemala, S. Ziliani, F. C. L. Crespi, S. Leoni, B. Fornal, A. Maj, P. Bednarczyk, G. Benzoni, A. Bracco, C. Boiano, S. Bottoni, S. Brambilla, M. Bast, M. Beckers, T. Braunroth, F. Camera, N. Cieplicka-Orynczak, E. Clement, S. Coelli, O. Dorvaux, S. Erturk, G. de France, C. Fransen, A. Goldkuhle, J. Grebosz, M. N. Harakeh, L. W. Iskra, B. Jacquot, A. Karpov, M. Kicinska-Habior, Y. Kim, M. Kmiecik, A. Lemasson, S. M. Lenzi, M. Lewitowicz, H. Li, I. Matea, K. Mazurek, C. Michelagnoli, M. Matejska-Minda, B. Million, C. Muller-Gatermann, V. Nanal, P. Napiorkowski, D. R. Napoli, R. Palit, M. Rejmund, Ch. Schmitt, M. Stanoiu, I. Stefan, E. Vardaci, B. Wasilewska, O. Wieland, M. Zielinski, M. Zielinska, A. Atac, D. Barrientos, B. Birkenbach, A. J. Boston, B. Cederwall, L. Charles, J. Collado, D. M. Cullen, P. Desesquelles, C. Domingo-Pardo, J. Dudouet, J. Eberth, V. Gonzalez, J. Goupil, L. J. Harkness-Brennan, H. Hess, D. S. Judson, A. Jungclaus, W. Korten, M. Labiche, A. Lefevre, R. Menegazzo, D. Mengoni, J. Nyberg, R. M. Perez-Vidal, Zs. Podolyak, A. Pullia, F. Recchia, P. Reiter, F. Saillant, M. D. Salsac, E. Sanchis, O. Stezowski, Ch. Theisen, J. J. Valiente-Dobon, J. D. Holt, J. Menéndez, A. Schwenk, and J. Simonis, “Lifetime measurements of the second $2+$ state in neutron-rich ^{16}C and ^{20}O as a test of ab initio nuclear structure,” *Phys. Rev. C* **101** 021303 (2020).
- 角田佑介, “Ni 同位体における新奇な変形共存現象と核子配位に依存した殻進化の研究,” *原子核研究* 第 64 卷 1 号 25 頁 (2019).

[Books]

- T. Shibata, I. Tanihata, M. Fujiwara, T. Otsuka, and S. Shimoura: “Large-scale investigation of deposited radioactive materials,” *Environmental Contamination from the Fukushima Nuclear Disaster*, ed., Teruyuki Nakajima, Toshimasa Ohara, Mitsuo Uematsu and Yuichi Onda, CAMBRIDGE ENVIRONMENTAL CHEMISTRY SERIES, CAMBRIDGE, 2019, pp. 309–323.

[Proceedings]

- S. Hayakawa, K. Abe, O. Beliuskina, S. M. Cha, K. Y. Chae, S. Cherubini, P. Figuera, Z. Ge, M. Gulino, J. Hu, A. Inoue, N. Iwasa, D. Kahl, A. Kim, D. H. Kim, G. G. Kiss, S. Kubono, M. La Cognata, M. La Commara, L. Lamia, M. Lattuada, E. J. Lee, J. Y. Moon, S. Palmerini, C. Parascandolo, S. Y. Park, D. Pierroutsakou, R. G. Pizzone, G. G. Rapisarda, S. Romano, H. Shimizu, C. Spitaleri, X. Tang, O. Trippella, A. Tumino, P. Vi, H. Yamaguchi, L. Yang, and N. T. Zhang, “Cross section measurements of the $^7\text{Be}(n, p)^7\text{Li}$ and the $^7\text{Be}(n, \alpha)^4\text{He}$ reactions covering the Big-bang nucleosynthesis energy range by the Trojan horse method at CRIB,” *Nuclei in the Cosmos XV* (Springer International Publishing), 33–37 (2019).
- H. Yamaguchi, S. Hayakawa, L. Yang, H. Shimizu, D. Kahl, and CRIB collaboration, “Study on explosive nucleosynthesis with low-energy RI beams at CRIB,” *Nuclei in the Cosmos XV* (Springer International Publishing), 265–268 (2019).
- L. Lamia, C. Spitaleri, M. Mazzocco, S. Hayakawa, C. A. Bertulani, A. Boiano, C. Boiano, C. Brogini, A. Caciolli, R. Depalo, F. Galtarossa, G. L. Guardo, M. Gulino, S. Kubono, M. La Cognata, M. La Commara, G. La Rana, M. Lattuada, R. Menegazzo, A. Pakou, C. Parascandolo, D. Piatti, D. Pierroutsakou, R. G. Pizzone, S. Romano, G. G. Rapisarda, M. L. Sergi, O. Sgouros, F. Soramel, V. Soukera, E. Strano, D. Torresi, A. Tumino, H. Yamaguchi, F. L. Villante, and G. L. Zhang, “The cosmologically relevant $^7\text{Be}(n, \alpha)^4\text{He}$ reaction in view of the recent THM investigations,” *Nuclei in the Cosmos XV* (Springer International Publishing), 53–56 (2019).
- A. A. Oliva, L. Lamia, G. L. Guardo, C. Spitaleri, S. Cherubini, A. Cvetinovic, G. D’Agata, N. de Sereville, A. Di Pietro, P. Figuera, M. Gulino, F. Hammache, S. Hayakawa, I. Indelicato, M. La Cognata, M. La Commara, D. Lattuada, M. Lattuada, G. Manicò, M. Mazzocco, S. Messina, S. Palmerini, R. G. Pizzone, M. L. Pumo, G. G. Rapisarda, S. Romano, M. L. Sergi, N. Soic, R. Sparta, and A. Tumino, “Study of the neutron induced reaction $^{17}\text{O}(n, \alpha)^{14}\text{C}$ at astrophysical energies via the Trojan Horse Method,” *EPJ Web of Conferences* **227**, 02007 (2020).
- R. G. Pizzone, G. D’Agata, I. Indelicato, M. L. Cognata, P. Figuera, G. L. Guardo, S. Hayakawa, L. Lamia, M. Lattuada, M. Milin, G. G. Rapisarda, S. Romano, M. L. Sergi, N. Skukan, N. Soic, C. Spitaleri, and A. Tumino, “Fluorine destruction in stars studied via Trojan horse method,” *Proceedings of the 15th International Symposium on Origin of Matter and Evolution of Galaxies (OMEG15)*,

JPS Conf. Proc. 31, 011002 (2020).

- S. Ishikawa, N. Iwasa, S. Kubono, K. Asada, D. Guru, S. Hayakawa, K. Hirose, T. Kawabata, K. Kominato, H. Makii, M. Matsuda, S. Nishimura, K. Nishio, R. Orlandi, and T. Sakakibara, “Experimental study of the ${}^7\text{Be}(n, p){}^7\text{Li}^*$ reaction for the cosmological lithium problem,” Proceedings of the 15th International Symposium on Origin of Matter and Evolution of Galaxies (OMEG15), JPS Conf. Proc. 31, 011037 (2020).
- S. Palmerini, M. L. Cognata, L. Acosta, R. Alba, E. Chavez, S. Cherubini, G. D. Agata, A. D. Pietro, P. Figuera, K. D. L. Rios, G. L. Guardo, M. Gulino, S. Hayakawa, G. Kiss, M. L. Commara, L. Lamia, C. Maiolino, G. Manico, M. Mazzocco, J. Mrazek, C. Parascandolo, T. Petruze, D. Pierroutsakou, R. Pizzone, G. Rapisarda, S. Romano, D. Santonocito, R. Sparta, C. Spitaleri, and A. Tumino, “Measurement of the ${}^{27}\text{Al}(p, \alpha){}^{24}\text{Mg}$ reaction at astrophysical energies via the Trojan horse method,” Proceedings of the 15th International Symposium on Origin of Matter and Evolution of Galaxies (OMEG15), JPS Conf. Proc. 31, 011056 (2020).
- S. Hayakawa, M. L. Cognata, L. Lamia, H. Shimizu, L. Yang, H. Yamaguchi, K. Abe, O. Beliuskina, S. M. Cha, K. Y. Chae, S. Cherubini, P. Figuera, Z. Ge, M. Gulino, J. Hu, A. Inoue, N. Iwasa, D. Kahl, A. Kim, D. H. Kim, G. Kiss, S. Kubono, M. L. Commara, M. Lattuada, E. J. Lee, J. Y. Moon, S. Palmerini, C. Parascandolo, S. Y. Park, D. Pierroutsakou, R. G. Pizzone, G. G. Rapisarda, S. Romano, C. Spitaleri, X. D. Tang, O. Trippella, A. Tumino, P. Vi, and N. T. Zhang, “Experimental study on the ${}^7\text{Be}(n, p){}^7\text{Li}$ and the ${}^7\text{Be}(n, \alpha){}^4\text{He}$ reactions for cosmological lithium problem,” Proceedings of the 15th International Symposium on Origin of Matter and Evolution of Galaxies (OMEG15), JPS Conf. Proc. 31, 011036 (2020).
- H. Shimizu, D. Kahl, H. Yamaguchi, K. Abe, O. Beliuskina, S. M. Cha, K. Y. Chae, A. A. Chen, Z. Ge, S. Hayakawa, N. Imai, N. Iwasa, A. Kim, D. H. Kim, M. J. Kim, S. Kubono, M. S. Kawag, J. Liang, J. Y. Moon, S. Nishimura, S. Oka, S. Y. Park, A. Psaltis, T. Teranishi, Y. Ueno, and L. Yang, “Study on ${}^{26m}\text{Al}(p, \gamma)$, reaction at the SNe temperature,” Proceedings of the 15th International Symposium on Origin of Matter and Evolution of Galaxies (OMEG15), JPS Conf. Proc. 31, 011073 (2020).
- L. Yang, C. Lin, H. Jia, N. Ma, D. Wang, F. Yang, L. Sun, X. Xu, P. Wen, and F. Zhong, “Reactions with exotic nuclei at near and sub-barrier energies,” EPJ Web of Conferences 223, 01071 (2019).
- A. Uchiyama, K. Harada, T. Inoue, H. Kawamura, K. S. Tanaka, M. Itoh, T. Aoki, A. Hatakeyama, Y. Takahashi and Y. Sakemi, “Development of a dual isotope co-magnetometer using laser cooled rubidium toward electron electric dipole moment measurement using Francium,” Journal of Physics: Conf. Series 1206, 012008 (2019).
- M. Hoferichter, P. Klos, J. Menéndez, and A. Schwenk, “Dark-matter-nucleus scattering in chiral effective field theory,” Proceedings of the 9th International Workshop on Chiral Dynamics, PoS CD2018 (2019) 095.

Presentations

[International conferences/workshops]

- N. Imai (Oral), “Single particle structure coupled to the second $0+$ state in ${}^{32}\text{Mg}$,” High resolution gamma ray spectroscopy at RIBF, T. U. Darmstadt, Germany, April 10–12, 2019.
- N. Imai (Invited), “Controlling the motions of two kinds of fermions in a nucleus, a new energy degraded RI beam line OEDO,” Frontier Session of KPS meeting, Deajon, Korea, April 24–26, 2019.
- N. Imai (Oral), “Evaluation of the neutron capture reaction on ${}^{79}\text{Se}$ via a surrogate reaction of $d({}^{79}\text{Se}, p)$ reaction at OEDO,” The 15th International Symposium on Origin of Matter and Evolution of Galaxies, Kyoto, July 2–5, 2019.
- S. Michimasa (Oral), “Closed-shell nature in neutrons of ${}^{54}\text{Ca}$,” International Nuclear Physics Conference 2019 (INPC2019), Scottish Event Campus, Glasgow, UK, July 29–August 2, 2019.
- M. Dozono (Oral), “Proton-induced reactions on ${}^{107}\text{Pd}$ at around 30 MeV/nucleon: First result using slowed-down RI beams at OEDO,” International Nuclear Physics Conference 2019 (INPC2019), Scottish Event Campus, Glasgow, UK, July 29–August 2, 2019.
- J. Hwang (Oral), “Performance of the OEDO beamline,” International Nuclear Physics Conference 2019 (INPC2019), Scottish Event Campus, Glasgow, UK, July 29–August 2, 2019.
- N. Kitamura (Oral), “Structure of ${}^{30}\text{Mg}$ studied by in-beam gamma-ray spectroscopy via neutron knockout reactions,” International Nuclear Physics Conference 2019 (INPC2019), Scottish Event Campus, Glasgow, UK, July 29–August 2, 2019.
- N. Kitamura (Oral), “High-resolution spectroscopy of ${}^{95-98}\text{Kr}$,” 8th SUNFLOWER Workshop / HiCARI Workshop, Osaka University, Osaka, Japan, August 26–28, 2019.
- S. Michimasa (Invited), “OEDO status report and development,” OEDO collaboration meeting 2019, Nishina, Saitama, Japan, September 2, 2019.
- N. Imai (Invited), “Status report of ImPACT17-02-02,” OEDO collaboration meeting 2019, Nishina, Saitama, Japan, September 2, 2019.
- M. Dozono (Invited), “Status report of ImPACT17-02-01,” OEDO collaboration meeting 2019, Nishina, Saitama, Japan, September 2, 2019.
- J. Hwang (Invited), “Study of octupole deformation at OEDO,” OEDO collaboration meeting 2019, Nishina, Saitama, Japan, September 2, 2019.
- N. Imai (Invited), “Proposal of the surrogate reaction of ${}^{130}\text{Sn}(n, \gamma)$,” OEDO collaboration meeting 2019, Nishina, Saitama, Japan, September 2, 2019.
- S. Shimoura (Invited), “OEDO project—Slowing-down beam line in RIKEN RIBF,” XXIII International School on Nuclear Physics and Application (Varna2019), Varna, Bulgaria, September 23–27, 2019.
- S. Michimasa (Invited), “Present status of the OEDO-SHARAQ system,” Expert Meeting on Next-Generation Fragment Separators 2019, GSI, Germany, September 30–October 2, 2019.
- S. Shimoura (Invited), “Slowing-down beam line in RIKEN RIBF—OEDO,” 14th Asia-Pacific Physics Conference (APPC2019), Kuching, Malaysia, November 17–22, 2019.

- S. Michimasa (Oral), “Experimental study of neutron shell gap in Calcium-54,” 14th Asia-Pacific Physics Conference (APPC2019), Kuching, Malaysia, November 17–22, 2019.
- S. Ota (Oral), “Research of isoscalar giant monopole resonances using gaseous activetarget,” 14th Asia-Pacific Physics Conference (APPC2019), Kuching, Malaysia, November 17–22, 2019.
- N. Imai (Invited), “Shape coexistence of atomic nuclei,” Frontier Session of KPS meeting, KDJ Center, Gwangju, Korea, December 23–25, 2019.
- M. Dozono (Invited), “Nuclear astrophysics studies with OEDO,” JSPS/NRF/NSFC A3 Foresight Program “Nuclear Physics in the 21st Century” Joint Kickoff Meeting, Kobe, Hyogo, Japan, December 6–7, 2019.
- S. Ota (invited), “ K_τ from ISGMR measurements on and around ^{132}Sn ,” Gordon Research Conference, Nuclear Chemistry, “Exploring simple structure patterns and the dynamics of nuclei,” New London, NH, US, June 16–21, 2019.
- S. Ota (oral), “Giant resonances in Tin-region nuclei studied using gaseous active target,” Vth Topical Workshop on Modern Aspects in Nuclear Structure, Bormio, Italy, February 04–09, 2020.
- H. Yamaguchi (invited), “Studying astrophysical reactions and nuclear clusters with low-energy RI beams,” 2019 KPS Spring Meeting, Pioneering session: Low energy nuclear science for astrophysics, Daejeon, Korea, April 25, 2019.
- H. Yamaguchi (invited), “Experiments on astrophysical reactions with low-energy unstable nuclei beams at CRIB,” The 27th International Nuclear Physics Conference (INPC 2019), Glasgow, U.K., July 29–August 2, 2019.
- H. Yamaguchi (invited), “Nuclear astrophysics with low-energy RI beams,” Nuclear Physics School for Young Scientists (NUSYS-2019), Lanzhou, China, August 12–17, 2019.
- H. Shimizu (poster), “Isomeric ^{26}Al beam production with CRIB,” Nuclear physics School for Young Scientists (NUSYS-2019), Lanzhou, China, August 12–17, 2019.
- H. Yamaguchi (oral), “Activities at the low-energy RI beam separator CRIB,” RIBF Users Meeting 2019, Wako, Saitama, Japan, September 3–4, 2019.
- H. Yamaguchi (invited), “Nuclear astrophysics projects at CNS, the University of Tokyo,” International workshop on Origin of Elements and Cosmic Evolution: From Big-Bang to Supernovae and Mergers (OECE), Beijing, China, November 27–29, 2019.
- H. Yamaguchi (oral), “Active target for the TTIK method,” Workshop on RI-beam Spectroscopy by Innovative Gaseous Active Targets, Osaka, Japan, December 19–20, 2019.
- S. Hayakawa (invited), “Experimental study on the $^7\text{Be}(n, p)^7\text{Li}$ and the $^7\text{Be}(n, \alpha)^4\text{He}$ reactions for cosmological lithium problem,” The 15th International Symposium on Origin of Matter and Evolution of Galaxies (OMEG15), Kyoto, Japan, July 2–5, 2019.
- H. Shimizu (poster), “Study on $^{26m}\text{Al}(p, \gamma)$ reaction at the SNe temperature,” The 15th International Symposium on Origin of Matter and Evolution of Galaxies (OMEG15), Kyoto, Japan, July 2–5, 2019.
- T. Gunji for the ALICE Collaboration (oral), “Recent results in relativistic heavy-ion collisions with the ALICE experiment at the CERN-LHC,” 14th Asia-Pacific Physics Conference (APPC 2019), Kuching, Sarawak, Malaysia, November 17–22, 2019.
- D. Sekihata for the ALICE Collaboration (Oral), “Light neutral mesons production at the LHC measured by ALICE,” PHOTON 2019 International Conference on the Structure and the Interactions of the Photon, INFN-LNF, Frascati, Italy, 3–7 June 2019.
- D. Sekihata for the ALICE Collaboration (Poster), “Study of dielectron production in Pb-Pb collisions at $\sqrt{s_{NN}} = 5.02$ TeV with ALICE,” Quark Matter 2019 - the XXVIIIth International Conference on Ultra-relativistic Nucleus-Nucleus Collisions, Wuhan, China, November 3–9, 2019.
- Y. Sekiguchi for the ALICE collaboration (Oral), “Measurement of long-range two- and multi-particle correlations by ALICE,” the XXVIIIth International Conference on Ultra-relativistic Nucleus-Nucleus Collisions, Wuhan, China, November 3–9, 2019.
- Y. Sakemi(invited), “Fundamental physics with cold radioactive atoms,” 14th ASIA-PACIFIC PHYSICS CONFERENCE(APPC14), Kuching, Malaysia, November 20, 2019.
- Y. Sakemi(invited), “Fundamental physics with laser cooled atoms,” 36th Mazurian Lakes Conference on Physics (Probing fundamental laws of nature with exotic nuclei and atoms), Poland, Piaski, September-2, 2019.
- Y. Kotaka (Poster), “Development of the calculation method of injection beam trajectory of RIKEN AVF Cyclotron with 4D emittance measured by the developed pepper-pot emittance monitor,” 8th International Beam Instrumentation Conference, Malmö, Sweden, September 8–12, 2019.
- N. Shimizu (invited), “Configuration-interaction shell-model calculations for nuclear structure physics,” 11th Symposium on Discovery, Fusion, Creation of New Knowledge by Multidisciplinary Computational Sciences, Tsukuba International Congress Center, Tsukuba, Ibaraki, Japan, October 15, 2019.
- N. Shimizu (invited), “Level densities of pf-shell nuclei by large-scale shell-model calculations,” 7th Workshop on Nuclear Level Density and Gamma Strength, Oslo University, Oslo, Norway, May 28, 2019.
- T. Abe (oral), “Alpha-cluster structure of light nuclei from no-core Monte Carlo shell model,” RIBF Users Meeting, RIKEN RIBF, Saitama, Japan, September 3, 2019.
- T. Abe (oral), “Alpha-cluster structure from an ab-initio point of view,” RCNP Workshop on RI-beam Spectroscopy by Innovative Gaseous Active Targets, RCNP, Osaka University, Osaka, Japan, October 20, 2019.
- T. Abe (oral), “Intrinsic structure of light nuclei from no-core Monte Carlo shell model,” Pioneer Symposia on Various Manifestations of Nuclear Structure, KPS Fall Meeting 2019, Gwangju, Korea, October 20, 2019.
- K. Yanase (oral), “CP violation in atomic nuclei and Atomic EDM,” International workshop for graduate students and young physicists on nuclear physics, Peking, University, Beijing, China, November 22–25, 2019.
- K. Yanase (oral), “Atomic EDM and CP violation in atomic nuclei,” Nucleon electric dipole moments and spin structure in 2020, KEK,

Tokai, Japan, January 11, 2020.

- T. Abe (poster), "Alpha-cluster structure from the ab-initio Monte Carlo shell model," International Symposium on Clustering as a Window on the Hierarchical Structure of Quantum Systems (CLUSHIQ2020), Ryoutiku Bettei, Oita, Japan, January 23, 2020.
- J. Menéndez (invited), "Neutrinoless double-beta decay: novel insights on nuclear matrix elements," International Nuclear Physics Conference (INPC), Glasgow (United Kingdom), July 2019.
- J. Menéndez (invited), "Double-beta decay calculations: new tests and opportunities," the INT Program "Nuclear Structure at the Crossroads," Seattle (USA), July 2019
- J. Menéndez (invited), "Nuclear physics and double-beta decay," "Massive Neutrinos," the Wilhelm und Else Heraeus-Seminar Bad Honnef (Germany), July 2019.
- J. Menéndez (invited), "Relating double-beta decay to nuclear properties at hand," the workshop "Neutrino Nuclear Responses for Double Beta Decays and Astro Neutrinos (NNR19)," Osaka (Japan), May 2019.
- J. Menéndez (invited), "Beta decay in the nuclear shell model: capabilities, limitations, uncertainties," ECT*Workshop "Precise beta decay calculations for searches for new physics," Trento (Italy)
- Y. Tsunoda (poster), "Shapes of Sm isotopes studied by Monte Carlo shell model calculations," 11th Symposium on Discovery, Fusion, Creation of New Knowledge by Multidisciplinary Computational Sciences, Tsukuba International Congress Center, Tsukuba, Ibaraki, Japan, October 15, 2019.

[Domestic conferences/workshops]

- N. Imai (Oral), 「r-process 核の中性子捕獲反応実験について」, 基研研究会 "原子核物理で紡ぐ r-process" 京都, 2019 年 5 月 22 日-24 日.
- N. Imai (Oral), 「逆運動学 $^{79}\text{Se}(d, p)$ 反応による中性子捕獲反応断面積の評価」, 日本物理学会秋季大会, 山形大学, 山形, 2019 年 9 月 17 日-20 日.
- K. Kawata (Oral), 「入射核破碎反応による ^{52}Fe 周辺核の高スピンアイソマーの生成」, 日本物理学会秋季大会, 山形大学, 山形, 2019 年 9 月 17 日-20 日.
- R. Tsunoda (Oral), 「スズ同位体の励起状態と組んだアイソバリックアナログ共鳴状態」, 日本物理学会秋季大会, 山形大学, 山形, 2019 年 9 月 17 日-20 日.
- N. Kitamura (Oral), 「インビームガンマ線核分光で探る ^{30}Mg の核構造」, 日本物理学会秋季大会, 山形大学, 山形, 2019 年 9 月 17 日-20 日.
- N. Imai (Oral), 「Low-energy RI beam of versatile element; OEDO at RIBF」, ATTPC workshop, 大阪, 2019 年 12 月 19 日-20 日.
- 川田敬太ほか (口頭発表), 「入射核破碎反応による ^{52}Fe 周辺核の高スピンアイソマーの生成」, 日本物理学会 2019 年秋季大会, 山形大学, 山形, 2019 年 9 月 17 日-20 日.
- OEDO collaboration meeting 2019, 理化学研究所, 和光, 2019 年 9 月 2 日.
- 大田晋輔, 遠藤史隆 (口頭発表), 「大強度重イオンビーム照射用低圧ガスアクティブ標的 CAT の開発と現状」, マイクロパターンガス検出器 (MPGD)・アクティブ媒質 TPC 合同研究会, 理化学研究所, 和光, 2019 年 12 月 6-7 日.
- 遠藤史隆ほか (口頭発表), 「大強度重イオンビーム照射下でのアクティブ標的 CAT におけるイオンバックフローの抑制」, 日本物理学会第 75 回年次大会, 名古屋大学, 名古屋, 2020 年 3 月 16 日-19 日.
- 花井周太郎ほか (口頭発表), 「大強度 RI ビーム実験における高速応答飛跡検出器 SR-PPAC の性能評価」, 日本物理学会第 75 回年次大会, 名古屋大学, 名古屋, 2020 年 3 月 16 日-19 日.
- 堂園昌伯ほか (口頭発表), 「アイソマー同定のためのアクティブストッパーの開発」, 日本物理学会第 75 回年次大会, 名古屋大学, 名古屋, 2020 年 3 月 16 日-19 日.
- T. Gunji (oral), 「LHC-ALICE 実験における GEM-TPC 高度化の開発と現状」, 第 16 回マイクロパターンガス検出器 (MPGD) 第 3 回アクティブ媒質 TPC 合同研究会, 理化学研究所, 和光, 2019 年 12 月 6 日-7 日.
- T. Gunji (oral), 「ALICE 実験高度化における大型 GEM とトリガーレス DAQ の開発と実装」, 新学術領域「クラスター階層」量子ビーム応用 合同検出器ワークショップ, 東北大学, 仙台, 2019 年 9 月 20-21 日.
- T. Gunji (oral), 「高エネルギー重イオン衝突の物理: 基礎・最先端・課題・展望」, "将来展望," 理研シンポジウム チュートリアル研究会, 理化学研究所, 和光, 2019 年 8 月 19 日-21 日.
- T. Gunji (oral), 「Future ALICE upgrade beyond 2030」, 第 36 回拡大版 Heavy Ion Café, 上智大学, 千代田, 2019 年 6 月 22 日-23 日.
- D. Sekihata (oral), 「核子対あたり重心系エネルギー $\sqrt{s_{NN}} = 5.02$ TeV 陽子-陽子及び鉛-鉛原子核衝突における中性中間子と直接光子測定」, 日本物理学会秋季大会, 山形大学, 山形, 2019 年 9 月 17 日-20 日.
- D. Sekihata (Oral), 「QM2019 でのハードプローブの実験的まとめ」, 「ポスト QM2019」, 第 37 回 Heavy Ion Cafe 第 30 回 Heavy Ion Pub 合同研究会, 名古屋大学, 名古屋, 2019 年 12 月 22 日.
- D. Sekihata (Oral), 「ALICE 実験 TPC 検出器オンライン飛跡再構成に向けた機械学習による空間電荷効果の高速補正」, 日本物理学会第 75 回年次大会, 名古屋大学, 名古屋, 2020 年 3 月 16 日-19 日.
- 関口裕子 for the ALICE collaboration (Oral), 「小さい系における長距離 2 粒子相関測定」, 日本物理学会第 75 回年次大会, 名古屋大学, 名古屋, 2020 年 3 月 16 日-19 日.
- 関口裕子 for the ALICE collaboration (Oral), 「小さい系における方位角異方性のラピディティ依存性」, 日本物理学会秋季大会, 山形大学, 山形, 2019 年 9 月.
- 小高康熙 (Oral), 「理研 AVF サイクロトロン入射系のビーム軌道計算方法の評価と 4 次元エミッタンス測定器の改良」, 第 16 回日本加速器学会年会, 京都大学, 京都, 2019 年 7 月 31 日-8 月 3 日.
- 角田佑介 (招待講演), 「モンテカルロ殻模型によるベータ崩壊の研究」, 原子核物理でつむぐ r プロセス, 京都大学基礎物理学研究

所, 京都, 2019 年 5 月 22 日.

柳瀬宏太 (口頭発表), 「原子核における CP 対称性の破れと電気双極子モーメント」, 物理学会 2019 年秋季大会, 山形大学, 山形, 2019 年 9 月 18 日.

清水則孝 (口頭発表), 「現実的有効相互作用を用いた殻模型によるシッフモーメントの評価」, 物理学会 2019 年秋季大会, 山形大学, 山形, 2019 年 9 月 18 日.

角田佑介 (口頭発表), 「モンテカルロ殻模型による Sm 同位体の形状変化の研究」, 日本物理学会 2019 年秋季大会, 山形大学, 山形, 2019 年 9 月 18 日.

阿部喬 (口頭発表), 「Alpha-cluster structure from the ab-initio Monte Carlo shell model」, 日本物理学会 2019 年秋季大会, 山形大学, 山形, 2019 年 9 月 18 日.

阿部喬 (口頭発表), 「Alpha-cluster structure from ab-initio Monte Carlo shell model」, シミュレーションによる宇宙の基本法則と進化の解明に向けて (QUCS 2019), 京都大学基礎物理学研究所, 京都, 2019 年 12 月 18 日.

角田佑介 (口頭発表), 「モンテカルロ殻模型による中重核の構造の研究」, シミュレーションによる宇宙の基本法則と進化の解明に向けて (QUCS 2019), 京都大学基礎物理学研究所, 京都, 2019 年 12 月 18 日.

清水則孝 (口頭発表), 「原子核殻模型計算と多様な変形バンド」, シミュレーションによる宇宙の基本法則と進化の解明に向けて (QUCS 2019), 京都大学基礎物理学研究所, 京都, 2019 年 12 月 19 日.

柳瀬宏太 (ポスター発表), 「大規模殻模型計算による CP 耐用性を破る相互作用の探索」, シミュレーションによる宇宙の基本法則と進化の解明に向けて (QUCS 2019), 京都大学基礎物理学研究所, 京都, 2019 年 12 月 17 日.

[Seminars]

M. N. Harakeh, "Nuclear compression modes from stable to exotic nuclei," CNS + RIBF NP seminar # 267, RIBF Hall, February 3, 2020.

大城幸光 (Oral), 「CNS イオン源の現状」, 第 17 回 AVF 合同打ち合わせ, 放射線医学総合研究所, 千葉, 2019 年 6 月 27 日-28 日.

小高康熙 (Oral), 「理研 AVF の輸送系最適化の現状」, 第 17 回 AVF 合同打ち合わせ, 放射線医学総合研究所, 千葉, 2019 年 6 月 27 日-28 日.

大城幸光 (Oral), 「CNS イオン源の現状」, 第 18 回 AVF 合同打ち合わせ, 理化学研究所・CNS, 和光, 2020 年 2 月 18 日-19 日.

小高康熙 (Oral), 「理研 AVF のビーム輸送系最適化の現状」, 第 18 回 AVF 合同打ち合わせ, 理化学研究所・CNS, 和光, 2020 年 2 月 18 日-19 日.

森永晴彦先生を偲ぶ会, 記念講演会「21 世紀の物理学—宇宙・生命・サブアトム」, 学士会館, 千代田, 2019 年 6 月 2 日.

Awards

N. Kitamura, CNSSS18 Young scientist award, ANPhA/AAPPS-DNP award for young scientist for the presentation "characterization of a tritium target for two-neutron transfer reaction at TRIUMF."

Others

[External review]

External evaluation of CNS, Hongo Campus and CNS Building, January 30–31, 2020.

Partner Institution

Wako Nuclear Science Center, IPNS (Institute of Particle and Nuclear Studies)
KEK (High Energy Accelerator Research Organization)

1. Abstract

The Wako Nuclear Science Center (WNSC) of KEK aims to promote low-energy nuclear physics and nuclear astrophysics research as well as interdisciplinary studies using short-lived radioactive nuclei. WNSC operates the KEK Isotope Separation System (KISS) which is an electro-magnetic isotope separator featuring elemental selectivity from the use of resonance laser ionization in a gas catcher. The KISS facility provides various neutron-rich nuclei via multinucleon transfer reactions. Of particular significance is its provision of nuclei in the vicinity of the neutron magic number $N = 126$. Optical and β - γ spectroscopy have been applied to these neutron-rich nuclear beams, for nuclear structure and nuclear astrophysical studies. Several new developments—a rotating target, a donut-shaped gas cell, and in-jet laser ionization scheme—have been performed to improve the performance of KISS facility. The WNSC has also developed multi-reflection time of flight mass spectrographs (MRTOF-MS) for precision mass measurements of short-lived nuclei in collaboration with the RIKEN SLOWRI team and the Institute of Basic Science (IBS), Korea. After successful mass measurements in combination with the GARIS-II at RILAC, the existing MRTOF-MS setup has been renewed for use with the GARIS-II relocated after the ring cyclotron for high precision mass measurements of superheavy nuclides, and additional MRTOF-MS setups have been placed at KISS and at F11 of the ZeroDegree Spectrometer for comprehensive mass measurements of more than one thousand nuclides.

2. Major Research Subjects

- (1) Production and manipulation of radioactive isotope beams for nuclear experiments.
- (2) Explosive nucleosynthesis (r- and rp-process).
- (3) Heavy ion reaction mechanism for producing heavy neutron-rich nuclei.
- (4) Development of MRTOF mass spectrographs for short-lived nuclei.
- (5) Comprehensive mass measurements of short-lived nuclei including superheavy elements.

3. Summary of Research Activity

The Wako Nuclear Science Center (WNSC) provides low-energy short-lived radioactive ion beams to users from universities using the KEK isotope separator system (KISS). In FY2019, four experimental programs were carried out at KISS. In terms technical developments at KISS, an in-jet laser spectroscopy setup for high-precision laser spectroscopy and a multi-reflection time-of-flight mass spectrograph (MRTOF-MS) have been installed and tested online and applied to some physics cases. One was the hyperfine structure spectroscopy of ^{194}Os and ^{196}Os isotopes to determine their isotope shifts. Their half-lives (6 years and 35.9 minutes, respectively) are too long to reasonably determine the resonance wavelengths through decay measurement. However, the mass spectrograph allows us to use the ion counting method to identify the resonance by discriminating ions of specific isotope from an isobaric mixture in the time-of-flight spectrum. Another was $\beta - \gamma$ spectroscopy of $^{192\text{m}}\text{Os}$, $^{192\text{g}}, ^{192\text{m}}\text{Re}$ isotopes of nuclear astrophysical interest. In this experiment, the KISS beam was shared between the decay station and the MRTOF-MS. During the decay curve measurement at the decay station, the beam was transferred to the MRTOF-MS to determine the masses and the branching ratios of the isomeric states and the ground states. The same scheme was also used for the $\beta - \gamma$ spectroscopy studies of $^{186\text{g}}, ^{186\text{m}}, ^{187\text{g}}, ^{197}\text{Ta}$ isotopes.

For the interface between the KISS beams and the MRTOF-MS, a gas cell cooler-buncher (GCCB) plays an essential role. Singly-charged 20 keV ion beams from KISS enter the 30 cm-long gas cell through a 2-mm diameter aperture and are thermalized in 1 mbar He gas. The thermal ions are extracted by an RF-carpet and transported to a triplet RF quadrupole ion trap before injection into the MRTOF-MS. We discovered two important phenomena in the GCCB. One is that singly-charged ions are largely converted to doubly charged ions, which provides a significant gain in the mass resolving power. The other is molecular contaminants in the KISS beams are totally destroyed in the thermalization process. This feature can be a savior for all low-energy RI-beam facilities which have always suffered from these molecular contaminations.

In addition to the KISS MRTOF, two more MRTOF setups are presently operated by WNSC in collaboration with RIKEN SLOWRI team, one each at the GARIS-II and the BigRIPS facilities of RIKEN RIBF. These will be used for comprehensive mass measurements of short-lived nuclides including superheavy elements ($Z > 103$). In FY 2019, the first direct mass measurement of superheavy nuclide (^{257}Db , $Z = 105$) has been performed. This setup will be used for precision mass measurements of neutron-rich moscovium and nihonium isotopes for reliable determination of the atomic numbers as well as the mass numbers. The mass spectrograph at BigRIPS (ZD-MRTOF) is being installed at the end of the BigRIPS+ZeroDegree spectrometer and has already shown a highest mass resolving power of 570,000 with 9 ms flight time for $^{39}\text{K}^+$ ions in offline studies. First online commissioning experiment was scheduled using parasitic beams of in-beam γ experiments in the end of FY2019, however, it was cancelled due to spread of novel coronavirus disease.

Members

Group Leader

Michiharu WADA

Researchers

Yutaka WATANABE
Peter SCHURY
Sunchan Jeong

Yoshikazu HIRAYAMA
Hiroari MIYATAKE
Marco Rosenbusch

Technical Staff

Yutaka KAKIGUCHI

Michihiro OYAIZU

Visiting Researchers

Hermann WOLNICK (NMSU)
Jun-young MOON (IBS)
Sidong CHEN (HKU)
Wenduo XIAN (HKU)
Hirosi WATANABE (Beihan University)

Hyun-suk CHOI (Seoul National University)
Jiajian LIU (HKU)
Shuxiong YAN (Jinan University)
Dongsheng HOU (IMP)

Student Trainees

Toshitaka NIWASE (PhD. Student, Kyushu Univ.)

Shun IIMURA (PhD. Student, Osaka Univ.)

Assistant

Machiko IZAWA

List of Publications & Presentations

Publications

[Original papers]

- T. Niwase, M. Wada, P. Schury, H. Haba, S. Ishizawa, Y. Ito, D. Kaji, S. Kimura, H. Miyatake, K. Morimoto, K. Morita, B. M. Rosenbusch, H. Wollnik, T. Shanley, and Y. Benari, "Development of an " α -TOF" detector for correlated measurement of atomic masses and decay properties," *Nucl. Instrum. Methods Phys. Res. A* **953**, 163198 (2020).
- Y. Hirayama, Y. X. Watanabe, M. Mukai, P. Schury, M. Ahmed, H. Ishiyama, S. C. Jeong, Y. Kakiguchi, S. Kimura, J. Y. Moon, M. Oyaizu, J. H. Park, M. Wada, and H. Miyatake, "Nuclear spectroscopy of r-process nuclei using KEK Isotope Separation System," *Nucl. Instrum. Methods Phys. Res. B* **463**, 425–430 (2020).
- M. Rosenbusch, M. Wada, P. Schury, Y. Ito, H. Ishiyama, S. Ishizawa, Y. Hirayama, S. Kimura, T. M. Kojima, H. Miyatake, J. Y. Moon, T. Niwase, T. Sonoda, A. Takamine, Y. X. Watanabe, and H. Wollnik, "A new multi-reflection time-of-flight mass spectrograph for the SLOWRI facility," *Nucl. Instrum. Methods Phys. Res. B* **463**, 184–188 (2020).
- M. Mukai, Y. Hirayama, P. Schury, Y. X. Watanabe, M. Ahmed, H. Haba, H. Ishiyama, S. C. Jeong, Y. Kakiguchi, S. Kimura, J. Y. Moon, M. Oyaizu, A. Ozawa, J. H. Park, H. Ueno, M. Wada, and H. Miyatake, "Development of a multi-segmented proportional gas counter for β -decay spectroscopy at KISS," *Nucl. Instrum. Methods Phys. Res. B* **463**, 421–424 (2020).
- P. Schury, M. Wada, H. Wollnik, J. -Y. Moon, T. Hashimoto, and M. Rosenbusch, "High-stability, high-voltage power supplies for use with multi-reflection time-of-flight mass spectrographs," *Rev. Sci. Instrum.* **91**, 014702 (2020).
- S. Michimasa, N. Imai, M. Dozono, J. W. Hwang, K. Yamada, S. Ota, K. Yoshida, Y. Yanagisawa, K. Kusaka, M. Ohtake, M. Matsushita, D. S. Ahn, O. Beliuskina, N. Chiga, K. Chikaato, N. Fukuda, S. Hayakawa, E. Ideguchi, and S. Shimoura, "New energy-degrading beamline for in-flight RI beams, OEDO," *Nucl. Instrum. Methods Phys. Res. B* **463**, 143–147 (2020).
- N. Kimura, R. Kodama, K. Suzuki, S. Oishi, M. Wada, K. Okada, N. Ohmae, H. Katori, and N. Nakamura, "Direct determination of the energy of the first excited fine-structure level in Ba^{6+} ," *Phys. Rev. A* **100**, 052508 (2019).
- S. Ahmed, E. Altieri, T. Andalib, M. J. Barnes, B. Bell, C. P. Bidinosti, Y. Bylinsky, J. Chak, M. Das, C. A. Davis, F. Fischer, B. Franke, M. T. W. Gericke, P. Giampa, M. Hahn, S. Hansen-Romu, K. Hatanaka, T. Hayamizu, B. Jamieson, D. Jones, K. Katsika, S. Kawasaki, T. Kikawa, W. Klassen, A. Konaka, E. Korkmaz, F. Kuchler, L. Kurchaninov, M. Lang, L. Lee, T. Lindner, K. W. Madison, J. Mammei, R. Mammei, J. W. Martin, R. Matsumiya, E. Miller, T. Momose, R. Picker, E. Pierre, W. D. Ramsay, Y. -N. Rao, W. R. Rawnsley, L. Rebenitsch, W. Schreyer, S. Sidhu, S. Vanbergen, W. T. H. van Oers, Y. X. Watanabe, and D. Yosifov, "Fast-switching magnet serving a spallation-driven ultracold neutron source," *Phys. Rev. Accel. Beams* **22**, 102401 (2019).
- H. Wollnik, M. Wada, P. Schury, M. Rosenbusch, Y. Ito, and H. Miyatake, "Time-of-flight mass spectrographs of high mass resolving power," *International Journal of Modern Physics A* **34**, 36, 1942001 (2019).
- Y. Hirayama, M. Mukai, Y. X. Watanabe, M. Oyaizu, S. C. Jeong, Y. Kakiguchi, P. Schury, M. Wada, and H. Miyatake, "Efficient two-color two-step laser ionization schemes of $\lambda_1 \sim 250$ nm and $\lambda_2 = 307.9$ nm for heavy refractory elements-Measurements of ionization cross-sections and hyperfine spectra of tantalum and tungsten," *Rev. Sci. Instrum.* **90**, 115104 (2019).

- M. Mazzocco, N. Keeley, A. Boiano, C. Boiano, M. La Commara, C. Manea, C. Parascandolo, D. Pierroutsakou, C. Signorini, E. Strano, D. Torresi, H. Yamaguchi, D. Kahl, L. Acosta, P. Di Meo, J. P. Fernandez-Garcia, T. Glodariu, J. Grebosz, A. Guglielmetti, Y. Hirayama, N. Imai, H. Ishiyama, N. Iwasa, S. C. Jeong, H. M. Jia, Y. H. Kim, S. Kimura, S. Kubono, G. La Rana, C. J. Lin, P. Lotti, G. Marquinez-Durán, I. Martel, H. Miyatake, M. Mukai, T. Nakao, M. Nicoletto, A. Pakou, K. Rusek, Y. Sakaguchi, A. M. Sánchez-Benítez, T. Sava, O. Sgouros, V. Soukeras, F. Soramel, E. Stiliaris, L. Stroe, T. Teranishi, N. Toniolo, Y. Wakabayashi, Y. X. Watanabe, L. Yang, Y. Y. Yang, and H. Q. Zhang, “Elastic scattering for the ^8B and $^7\text{Be} + ^{208}\text{Pb}$ systems at near-Coulomb barrier energies,” *Phys. Rev. C* **100**, 024602 (2019).
- S. Ahmed, T. Andalib, M. J. Barnes, C. B. Bidinosti, Y. Bylinsky, J. Chak, M. Das, C. A. Davis, B. Franke, M. T. W. Gericke, P. Giampa, M. Hahn, S. Hansen-Romu, K. Hatanaka, B. Jamieson, D. Jones, K. Katsika, S. Kawasaki, W. Klassen, A. Konaka, E. Korkmaz, F. Kuchler, L. Kurchaninov, M. Lang, L. Lee, T. Lindner, K. W. Madison, J. Mammei, R. Mammei, J. W. Martin, R. Matsumiya, R. Picker, E. Pierre, W. D. Ramsay, Y. -N. Rao, W. R. Rawnsley, L. Rebenitsch, C. A. Remon, W. Schreyer, A. Sikora, S. Sidhu, J. Sonier, B. Thorsteinson, S. Vanbergen, W. T. H. vanOers, Y. X. Watanabe, and D. Yosifov, “A beamline for fundamental neutron physics at TRIUMF,” *Nucl. Instrum. Methods Phys. Res. A* **927**, 101–108 (2019).
- S. Ahmed, E. Altieri, T. Andalib, B. Bell, C. P. Bidinosti, E. Cudmore, M. Das, C. A. Davis, B. Franke, M. Gericke, P. Giampa, P. Gnyp, S. Hansen-Romu, K. Hatanaka, T. Hayamizu, B. Jamieson, D. Jones, S. Kawasaki, T. Kikawa, M. Kitaguchi, W. Klassen, A. Konaka, E. Korkmaz, F. Kuchler, M. Lang, L. Lee, T. Lindner, K. W. Madison, Y. Makida, J. Mammei, R. Mammei, J. W. Martin, R. Matsumiya, E. Miller, K. Mishima, T. Momose, T. Okamura, S. Page, R. Picker, E. Pierre, W. D. Ramsay, L. Rebenitsch, F. Rehm, W. Schreyer, H. M. Shimizu, S. Sidhu, A. Sikora, J. Smith, I. Tanihata, B. Thorsteinson, S. Vanbergen, W. T. H. van Oers, and Y. X. Watanabe, “First ultracold neutrons produced at TRIUMF,” *Phys. Rev. C* **99**, 025503 (2019).
- J. Surbrook, M. MacCormick, G. Bollen, M. Brodeur, M. Eibach, K. Gulyuz, A. Hamaker, C. Izzo, S. M. Lenzi, D. Puentes, M. Redshaw, R. Ringle, R. Sandler, S. Schwarz, P. Schury, N. Smirnova, C. Sumithrarachchi, A. A. Valverde, A. C. C. Villari, and I. T. Yandow, “Precision mass measurements of ^{44}V and $^{44\text{m}}\text{V}$ for nucleon-nucleon interaction studies,” *Hyperfine Interact* **240**, 65 (2019).
- N. Kimura, R. Kodama, K. Suzuki, S. Oishi, M. Wada, K. Okada, N. Ohmae, H. Katori, and N. Nakamura, “Direct wavelength measurement of the visible M1 transition in Ba^{7+} with a novel calibration method,” *Plasma and Fusion Research* **14**, 1201021 (2019).

[Proceedings]

- F. Galtarossa, L. Corradi, S. Szilner, E. Fioretto, G. Pollarolo, T. Mijatović, D. Montanari, D. Ackermann, D. Bourgin, S. Courtin, G. Fruet, A. Goasduff, J. Grebosz, F. Haas, D. Jelavić Malenica, S. C. Jeong, H. M. Jia, P. R. John, D. Mengoni, M. Milin, G. Montagnoli, F. Scarlassara, N. Skukan N. Soić A. M. Stefanini E. Strano, V. Tokić, C. A. Ur, J. J. Valiente-Dobón, and Y. X. Watanabe, “Light and heavy fragments mass correlation in the $^{197}\text{Au} + ^{130}\text{Te}$ transfer reaction,” *IL NUOVO CIMENTO* **42 C**, 2–3 (2019).

Presentations

[International conferences/workshops]

- M. Wada (invited), “Towards precise mass measurements of Nh and Mc isotopes,” 4th International Symposium on Superheavy Elements (SHE2019), Hakone, Japan, December 1–5, 2019.
- M. Wada (invited), “SHE-Mass-II setup for direct mass measurement of hot-fusion superheavy nuclides,” 6th International Conference on the Chemistry and Physics of the Transactinide Elements (TAN2019), Wilhelmshaven, Germany, August 25–31, 2019.
- M. Wada (invited), “Antiprotonic atoms with short-lived nuclei,” ECT* Antiproton-nucleus interactions and related phenomena, Trento, Italy, June 17–23, 2019.
- M. Wada (invited), “Towards comprehensive mass measurements with MRTOF mass spectrographs at RIKEN RIBF,” 2019 The Korean Physical Society Spring Meeting, Daejeon, Korea, April 24–26, 2019.
- M. Wada (invited), “Symbiotic mass measurement with ZD-MRTOF,” High Resolution Gamma-Ray Spectroscopy at the RIBF, Darmstadt, Germany, April 10–12, 2019.
- H. Miyatake (invited), “KISS Project,” 14th Asia-Pacific Physics Conference, Borneo, Indonesia, November 17–22, 2019.
- H. Miyatake (invited), “Recent progress of researches with KISS and MRTOF,” China-Japan Collaboration Workshop on “Nuclear mass and life for unraveling mysteries of r -process,” ITP/CAS, Beijing, China, October 9–13, 2019.
- H. Miyatake (invited), “Recent progress of researches with KISS and MRTOF,” The 15th International Symposium on Origin of Matter and Evolution of Galaxies (OMEG15), Kyoto, Japan, July 2–5, 2019.
- Y. Watanabe (invited), “RI production at low energies “Production of $N = 126$ nuclei and beyond using multinucleon transfer reactions,” JSPS/NRF/NSFC A3 Foresight Program—Nuclear Physics in the 21st Century,” Nuclear Structure & Nuclear Reaction Joint Kickoff Meeting, Kobe, Japan, December 6–7, 2019.
- Y. Watanabe (invited), “Recent experimental results of KEK Isotope Separation System (KISS),” 1-day workshop at GSI on new approaches to MNT reaction studies, Darmstadt, Germany, October 23, 2019.
- Y. Watanabe (invited), “Recent experimental results of KEK Isotope Separation System (KISS),” The 13th International Conference on Stopping and Manipulation of Ions and related topics (SMI-2019), Montreal, Canada, July 16–19, 2019.
- Y. Watanabe (invited), “Experimental studies of neutron-rich nuclei around $N = 126$ at KEK isotope separation system,” The IV International Conference on Nuclear Structure and Dynamics (NSD2019), Venice, Italy, May 13–17, 2019.
- Y. Watanabe (invited), “Production of $N = 126$ nuclei and beyond using multinucleon transfer reactions,” Physics between lead and uranium: in preparation of new experimental campaigns at ISOLDE, Leuven, Belgium, April 16–18, 2019.
- Y. Hirayama (invited), “Study of nuclear structure in the vicinity of nuclear structure in the vicinity of $N = 126$ at KISS,” Vth Topical Workshop on Modern Aspects in Nuclear Structure, Bormio, Italy, February 4–9, 2020.
- Y. Hirayama (poster), “Nuclear spectroscopy of r -process nuclei in the vicinity of $N = 126$ by using KISS,” 27th International Nuclear

Physics Conference (INPC 2019), Glasgow, UK, July 29–August 2, 2019.

- Y. Hirayama (invited), “Nuclear spectroscopy of r-process nuclei in the vicinity of $N = 126$ at KISS,” Physics between lead and uranium: in preparation of new experimental campaigns at ISOLDE, Leuven, Belgium, April 16–18, 2019. Hirayama P. Schury (invited), “Nuclear physics by multi-reflection time-of-flight mass spectroscopy at WNSC,” 27th International Nuclear Physics Conference (INPC 2019), Glasgow, UK, July 29–August 2, 2019.
- P. Schury (invited), “Present status and future plans for slow and stopped beams in RIKEN,” The 13th International Conference on Stopping and Manipulation of Ions and related topics (SMI-2019), Montreal, Canada, July 16–19, 2019.
- M. Rosenbusch (oral), “Dynamic ejection-field correction for MRTOF mass spectrometry of SHE using arbitrary mass references from reliable sources,” 4th International Symposium on Superheavy Elements (SHE2019), Hakone, Japan, December 1–5, 2019.
- T. Niwase (poster), “Development and first results from a novel “ α -TOF” detector used with a multi-reflection time-of-flight mass spectrograph,” 6th International Conference on the Chemistry and Physics of the Transactinide Elements (TAN2019), Wilhelmshaven, Germany, August 25–31, 2019.
- T. Niwase (oral), “Correlation measurement of precision mass and decay properties of nuclei via MRTOF-MS with α -ToF detector,” 4th International Symposium on Superheavy Elements (SHE2019), Hakone, Japan, December 1–5, 2019.

[Domestic conferences/workshops]

- 宮武宇也 (口頭発表), 「KISS での核分光研究」, 短寿命 RI を用いた核分光と核物性研究 VI, 京都大学複合原子力科学研究所, 大阪府熊取, 2020 年 1 月 16–17 日.
- 宮武宇也 (招待講演), 「第 7 周期元素科学: 超重元素の物理と化学」, 日本物理学会 2019 年秋季大会, 山形大学, 山形, 2019 年 9 月 17–25 日.
- 宮武宇也 (招待講演), 「第 3 ピークと終焉領域に対する実験的アプローチ」, 原子核でつむぐ r プロセス, 京都大学基礎物理学研究所, 京都, 2019 年 5 月 22–24 日.
- 渡邊裕 (招待講演), 「Present status of KISS」, RIKEN, RIBF Users Meeting2019, 理化学研究所, 和光, 2019 年 9 月 3–4 日.
- 渡邊裕 (招待講演), 「Nuclear researches relevant to r-process with KISS and MRTOF」, 宇宙における物質進化—原子核・原子・分子—第 1 回シンポジウム, 理化学研究所, 和光, 2019 年 8 月 1–2 日.
- 平山賀一 (口頭発表), 「KISS でのガスジェット内レーザー共鳴イオン化核分光」, 日本物理学会 2019 年秋季大会, 山形大学, 山形, 2019 年 9 月 17–25 日.
- P. Schury (口頭発表), 「Current status and ongoing strategy for MRTOF-MS at WNSC」, SSRI-PNS Collaboration Meeting 2019, 理化学研究所, 和光, 2019 年 9 月 4 日.
- 庭瀬暁隆 (口頭発表), 「Correlation measurement mass and decay properties of short-lived α -decay nuclei via MRTOF with α -TOF detector (MRTOF+ α -TOF を用いた短寿命 α 崩壊核種の質量-崩壊特性測定)」, 日本物理学会第 75 回年次大会, 名古屋大学, 名古屋, 2020 年 3 月 16–19 日.
- 庭瀬暁隆 (口頭発表), 「Correlation measurement of precision mass and decay properties of 207Ra with MRTOF+ α -TOF」. 日本放射化学会第 63 回討論会 (2020), いわき産業創造館, いわき, 2019 年 9 月 24–26 日.
- 庭瀬暁隆 (口頭発表), 「Correlation measurement of precision mass and decay properties of 207Ra with MRTOF-MS」, 日本物理学会 2019 年秋季大会, 山形大学, 山形, 2019 年 9 月 17–25 日.

Events (April 2019 — March 2020)

RNC

Apr. 20	Wako Open Campus
May. 24	The 25th RBRC Management Steering Committee (MSC)
Jun.24-26	The 5th Nishina Center Advisory Council (NCAC)
Jun. 28	The 18th Program Advisory Committee for Materials and Life Science Researches at RIKEN Nishina Center (ML-PAC)
Jul. 10	The 8th Industrial Program Advisory Committee (In-PAC)
Jul.31-Aug.9	Nishina School
Dec.16-18	The 20th Program Advisory Committee for Nuclear Physics Experiments at RI Beam Factory (NP-PAC)
Jan.24	The 19th Program Advisory Committee for Materials and Life Science Researches at RIKEN Nishina Center (ML-PAC)

CNS

Aug. 21-27	18th CNS International Summer School CNSSS19 https://indico2.cns.s.u-tokyo.ac.jp/event/65/
------------	---

Press Releases (April 2019–March 2020)

RNC		
May. 2	^{78}Ni revealed as a doubly magic stronghold against nuclear deformation	R. Taniuchi, P. Doornenbal, H. Sakurai, Radioactive Isotope Physics Laboratory
Jun. 15	Transverse momentum dependent production cross sections of charged pions, kaons and protons produced in inclusive e^+e^- annihilation at $\sqrt{s} = 10.58$ GeV	R. Seidl, Radiation Laboratory
Jun. 26	Gamma-ray Glow preceding Downward Terrestrial Gamma-ray Flash	Y. Wada, High Energy Astrophysics Laboratory
Jul. 5	Enhancement of element production by incomplete fusion reaction with weakly bound nucleus deuteron	W. He, H. Otsu, Fast RI Data Team, H. Sakurai, Nuclear Transmutation Data Research Group
Aug. 9	Proposal of a 1-ampere-class deuteron single-cell linac for nuclear transmutation	H. Okuno, High-Power Target R&D Team, H. Sakurai, Nuclear Transmutation Data Research Group
Sep. 12	X-ray pumping of the ^{229}Th nuclear clock isomer	H. Haba, RI Application Research Group
Oct. 18	Quasifree neutron knockout from ^{54}Ca corroborates arising $N = 34$ neutron magic number	P. Doornenbal, H. Sakurai, Radioactive Isotope Physics Laboratory
Nov. 19	Location of the neutron dripline at fluorine and neon	D.S. Ahn, N. Fukuda, N. Inabe, BigRIPS Team, T. Kubo, Research Instruments Group
Nov. 26	A method of collecting trace amounts of vermilion from artifacts for source estimation by sulfur isotope ($\delta^{34}\text{S}$) analysis: use of sulfur-free adhesive tape to minimize damage to the artifact body during sampling	K. Takahashi, Y. Motizuki, Astro-Glaciology Research Group
Nov. 26	Underlying structure of collective bands and self-organization in quantum systems	T. Otsuka, Nuclear Spectroscopy Laboratory
Nov. 29	Energy of the ^{229}Th nuclear clock isomer determined by absolute γ -ray energy difference	H. Haba, RI Application Research Group
Mar. 5	Possible lightest Ξ hypernucleus with modern ΞN interactions	E. Hiyama, Strangeness Nuclear Physics Laboratory, T. Doi, Quantum Hadron Physics Laboratory
Mar. 13	Swelling of doubly magic ^{48}Ca core in Ca isotopes beyond $N = 28$	M. Tanaka, Nuclear Spectroscopy Laboratory, M. Takechi, M. Fukuda, H. Sakurai, Radioactive Isotope Physics Laboratory
Mar. 17	g -Factor of the ^{99}Zr ($7/2^+$) isomer: monopole evolution in shape coexisting region	Y. Ichikawa, J.-M. Daugas, H. Ueno, Nuclear Spectroscopy Laboratory

VII. LIST OF PREPRINTS

List of Preprints (April 2019—March 2020)

RIKEN NC-NP

Not Applicable

RIKEN NC- AC

Not Applicable

RIKEN MP

Not Applicable

RIKEN QHP

411	Self-consistent random phase approximation based on the relativistic Hartree-Fock theory: Role of ρ -meson tensor coupling	Z. Wang <i>et al.</i>
412	Field-theoretical Derivation of the Negative Magnetoresistance with the Chiral Anomaly	K. Fukushima, Y. Hidaka
413	QCD-like phase diagram with Efimov trimers and Cooper pairs in resonantly interacting SU(3) Fermi gases	H. Tajima, P. Naidon
414	Non-relativistic expansion of Dirac equation with spherical scalar and vector potentials by similarity renormalization group	H. Liang, Y. Guo
415	$I = 2$ nn potential in the HAL QCD method with all-to-all propagators	Y. Akahoshi <i>et al.</i>
416	String confinement in 2-form lattice gauge theory	T. Hayata, A. Yamamoto
417	Spontaneous symmetry breaking and Nambu-Goldstone modes in open quantum and classical systems	Y. Minami, Y. Hidaka

CNS-REP

98	CNS Annual Report 2018	H. Nagahama
----	------------------------	-------------

KEK-REP

1904 .097 26	An inexpensive biasing system for use in electrostatic steering of ions	P. Schury, M. Wada
1904 .115 89	Development of an "a-TOF" detector for correlated measurement of atomic masses and decay properties	T. Niwase <i>et al.</i>
1910 .104 94	Accurately accounting for effects on times-of-flight caused by finite field-transition times during the ejection of ions from a storage trap: A study for TOF and MRTOF mass spectrometry	M. Rosenbusch <i>et al.</i>

Nishina Center Preprint server (not including Partner Institution) can be found at
<http://nishina-preprints.riken.jp/>

**VIII. LIST OF SYMPOSIA,
WORKSHOPS & SEMINARS**

List of Symposia & Workshops (April 2019–March 2020)

RNC			
1	Nishina School 2019	RIBF Conf. Hall, RIKEN Wako Campus	Jul. 30 - Aug. 9
2	8th SUNFLOWER workshop	Osaka University Nakanoshima Center	Aug. 26–28
3	New Trends in Integrable Systems 2019	Media Center, Osaka City University (Sugimoto campus)	Sep. 9–20
4	58th Nuclear Chemistry Summer School	Yufutopia, Oita Prefecture	Sep. 11–14
5	4th International Symposium on Superheavy Elements (SHE2019)	The Prince Hakone Lake Ashinoko	Dec. 1–5
6	International Symposium on Clustering as a Window on the Hierarchical Structure of Quantum Systems (CLUSHIQ2020)	Ryotiku Bettei, Oita Prefecture	Jan. 23–24
7	RIKEN Symposium "Practical application of Ion Beam Breeding in the past 20 years"	Suzuki Umetaro Hall	Jan. 23–24
8	Japan-France Joint Workshop on "Clusters in Quantum Systems: from Atoms to Nuclei and Hadrons"	Kyushu University	Jan. 27–31
9	18th AVF Liaison Meeting	Nishina Hall	Feb. 18–19
10	3rd RIBF Young Researchers' Discussion: Future of Physics of Exotic Nuclei	Integrated Innovation Building (IIB), RIKEN Kobe Campus	Feb. 19–21
11	Scientific Research on Innovative Areas "Clustering as a Window on the Hierarchical of Quantum Systems School"	Nishina Hall	Mar. 2–4

List of Seminars (April 2019–March 2020)

Nuclear Physics Monthly Colloquium

	Not held in 2019		
--	------------------	--	--

RIBF Nuclear Physics Seminar

1	Takaharu Otsuka (RNC)	Tin isotopes: Are they dull round nuclei? https://indico2.riken.jp/event/3022/	Apr. 9
2	Inoue Yoshiyuki (RIKEN)	Nature of coranae around supermassive black holes https://indico2.riken.jp/event/3040/	May 14
3	William B. Brinckerhoff (NASA)	Mass spectrometers to Mars and beyond https://indico2.riken.jp/event/3049/	May 16
4	Newcomers to Nishina Center in 2019	Newcomers' seminar https://indico2.riken.jp/event/3052/	May 21

5	Ryo Taniuchi (U. York)	^{78}Ni revealed as a doubly magic stronghold against nuclear deformation https://indico2.riken.jp/event/3069/	May 28
6	Koichi Sato (Osaka City U.)	Large-amplitude quadrupole shape mixing probed by the (p, p') reaction https://indico2.riken.jp/event/3081/	Jun. 11
7	Xing Fan (Harvard U.)	Towards an improved electron and positron magnetic moment measurement as a test of the Standard Model and CPT symmetry https://indico2.riken.jp/event/3100/	Jul. 8
8	Enrico Rinaldi (RIKEN, BNL)	The neutron lifetime with near-Exascale computing https://indico2.riken.jp/event/3092/	Jul. 9
9	Toshio Suzuki (Tohoku U.)	Is electron scattering useless to study neutron distribution in nuclei? https://indico2.riken.jp/event/3134/	Oct. 11
10	Masayuki Yamagami (U. Aizu)	Tetrahedral deformation in nuclei https://indico2.riken.jp/event/3147/	Oct. 15
11	Sohtaro Kanda (RNC)	Precision microwave spectroscopy of the ground-state hyperfine splitting in muonium atom https://indico2.riken.jp/event/3180/	Nov. 26
12	Kohl (Hampton U.)	The proton radius puzzle and its intersections https://indico2.riken.jp/event/3190/	Dec. 9
13	Andrea Vitturi (INFN)	The molecular cluster model for ^{12}C and the description of inelastic processes in ^{12}C induced by alpha particles https://indico2.riken.jp/event/3181/	Dec. 12
14	DeukSoon Ahn (RNC)	Location of the neutron dripline at fluorine and neon https://indico2.riken.jp/event/3309/	Jan. 14
15	Or Hen (MIT)	Short-range correlations and the quarks within https://indico2.riken.jp/event/3317/	Jan. 21
16	Muhsin N. Harakeh (KVI-CART, GANIL, GSI)	<i>Co-organized by CNS and RNC</i> Nuclear compression modes from stable to exotic nuclei https://indico2.riken.jp/event/3324/	Feb. 3

Seminar by Each Laboratory

Nuclear Science and Transmutation Research Division

1	José R. C. López-Urrutia (Max-Planck)	Hard-core atomic physics: highly charged ions https://indico2.riken.jp/event/3030/	Apr. 11
2	Roland Diehl (Max-Planck)	Gamma-ray spectroscopy from nuclei in the cosmos https://indico2.riken.jp/event/3103/	Jul. 9
3	Shigeki Fujiyama (RIKEN)	計算機を活用した固体 NMR の解析法 https://indico2.riken.jp/event/3105/	Jul. 24
4	Yugo Nagata (Tokyo U. Sci.)	静周期磁場によるポジトロニウム超微細構造の観測実験 https://indico2.riken.jp/event/3162/	Nov. 5
5	Takatoshi Aoki (U. Tokyo)	極低温 Fr 原子を用いたバリオン非保存効果誘起の光シフトの研究：標準模型を超えた新物理と核のアナポールモーメント https://indico2.riken.jp/event/3198/	Dec. 20
6	Yoichi Yatsu (Tokyo Tech)	超小型衛星による宇宙開発の実態 -成功と挫折の軌跡-	Jan. 28
7	Daiki Yamashita (RIKEN)	Er-implanted silica lasers based on Si nanobeam cavities https://indico2.riken.jp/event/3356/	Feb. 27

High Energy Astrophysics Lab. Seminar -> http://astro.riken.jp/wordpress/?page_id=65

Subnuclear System Research Division

1	Hirokazu Nishimura (RBRC)	QHP Seminar: Effective potential for the Polyakov loop to higher loop order	Apr. 1
2	Alex Kovner (U Connecticut)	NT / RIKEN seminar The Color Glass Condensate density matrix: Lindblad evolution, entanglement entropy and Wigner functional	Apr. 5
3	Tamura Hirokazu (Tohoku U.)	Nuclear physics with strange quarks --Recent results and future prospects at J-PARC-- https://indico2.riken.jp/event/3026/	Apr. 8
4	Paolo Bedaque (U. Maryland)	NT / RIKEN seminar: A Complex path around the sign problem	Apr. 12
5	Anatoly Radyushkin, (ODU/Jlab)	NT / RIKEN seminar: Parton distributions in Euclidean space	Apr. 19
6	Keh-Fei Liu (U. Kentucky)	RIKEN Lunch Seminar: Partons from the path-integral formalism of the hadronic tensor	Apr. 25
7	Gokce Basar (UIC)	RIKEN Lunch Seminar: Relativistic hydrodynamic fluctuations	May 3
8	Shoichiro Tsutsui (RIKEN)	QHP Seminar: Applicability of the complex Langevin method for QCD at finite density	May 8
9	Hirokazu Fujioaka (Tokyo Tech)	第4回「物質階層を横断する会」～ハドロン・原子核・原子・分子合同ミーティング ミハイベロン吸収によるダブルハイパー核フラグメント生成 https://indico2.riken.jp/event/3047/	May 10
10	Michael Strickland (Kent State U.)	NT / RIKEN seminar: The non-equilibrium attractor: Beyond hydrodynamics	May 10
11	Masashi Kaneta (Tohoku U.)	$\gamma d \rightarrow \Lambda K^+ n$ 反応での終状態相互作用を通じた Λn 間力測定実験計画 https://indico2.riken.jp/event/3070/	May 20
12	Enrico Rinaldi (RIKEN)	QHP Seminar: Composite Dark Matter	May 22
13	Semeon Valgushev (BNL)	RIKEN Lunch Seminar: Complex saddle points of path integrals	May 23
14	Shoichi Sasaki (Tohoku U.)	SNP Seminar: Nucleon form factors from lattice QCD at the physical point https://indico2.riken.jp/event/3042/	May 24
15	Henry Lamm (UMD)	NT / RIKEN seminar Pieces of the puzzle: Reaching QCD on quantum computers	May 24
16	Akio Tomiya (RBRC)	RIKEN Lunch Seminar: Applications of machine learning to computational physics	May 30
17	Kazuya Mameda (RIKEN)	QHP Seminar: Chiral kinetic theory with general relativity	Jun. 5
18	Hsiang-nan Li (NCTS)	NT / RIKEN seminar: D meson mixing via dispersion relation	Jun. 14
19	Nora Brambilla (TUM)	QHP Seminar: Nonrelativistic effective field theories for heavy quarkonium	Jun. 20
20	Minoru Tanaka (Osaka U.)	QHP Seminar: Search for new physics in isotope shifts of atomic spectra https://indico2.riken.jp/event/3091/	Jul. 10
21	Javad Shabani (NYU)	NT / RIKEN seminar: Topological superconducting qubits	Jul. 12
22	Paul Caucal (Saclay)	RIKEN Lunch Seminar: Deciphering the z_g distribution in ultrarelativistic heavy ion collisions	Jul. 25

23	Takafumi Niida (Tsukuba U.)	QHP Seminar: Global and local polarization in heavy-ion collisions	Jul. 31
24	Fabio Siringo (U. Catania)	NT / RIKEN seminar Perturbation Theory of Non-Perturbative QCD	Aug. 2
25	Jnanadeva Maharana (Inst. Physics, Bhubaneswar)	NT / RIKEN seminar: Topological Superconducting Qubits	Aug. 7
26	Kiminad Mamo (Stony Brook U.)	NT / RIKEN seminar DIS on a quantum extremal RN-AdS black hole: with application to DIS on a nucleus	Aug. 8
27	Ryo Karakida (AIST)	RIKEN Lunch Seminar: Mean field approach to the Fisher information matrix in deep neural networks	Aug. 15
28	Jean-Francois Paquet (Duke U.)	NT / RIKEN seminar: Effective and temperature-dependent viscosities in a hydrodynamically-expanding QCD plasma	Aug. 16
29	Daniel Harlow (MIT)	NT / RIKEN seminar: Symmetries in quantum field theory and quantum gravity	Aug. 23
30	Masazumi Honda (Cambridge)	RIKEN Lunch Seminar: Quantum black hole entropy from 4d supersymmetric Cardy formula	Aug. 29
31	Shailesh Chandrasekharan (Duke U.)	NT / RIKEN seminar: Qubit regularization of quantum field theories	Sep. 6
32	Andrey Tarasov (BNL)	RIKEN Lunch Seminar Deeply inelastic scattering structure functions on a hybrid quantum computer	Sep. 12
33	Derek Teaney (Stony Brook)	NT / RIKEN seminar: The bulk viscosity of QCD in the chiral limit	Sep. 19
34	Nodoka Yamanaka (Kyoto U.)	QHP Seminar: Nuclear electric dipole moment and the axions https://indico2.riken.jp/event/3115/	Sep. 25
35	Andrecia Ramnath (U. Jyvaskyla)	RIKEN Lunch Seminar: Rapidity correlators at unequal rapidity	Sep. 26
36	Giuliano Giacalone (IPhT – Saclay)	NT / RIKEN seminar: Observing the deformation of nuclei with relativistic nuclear collisions	Sep. 27
37	Adrien Florio (EPFL)	RIKEN Lunch Seminar Chiral charge dynamics in Abelian gauge theories at finite temperature	Oct. 3
38	Gerald Dunne (U. Connecticut)	NT / RIKEN seminar: Resurgence and non-perturbative physics	Oct. 4
39	Ming Li (U. Connecticut)	NT / RIKEN seminar JIMWLK equation from quantum-classical correspondence	Oct. 11
40	Rasmus Larsen (BNL)	RIKEN Lunch Seminar: Bottomonias in QGP from lattice QCD: Beyond the ground states	Oct. 17
41	Derek Teaney (Stony Brook U.)	NT/RIKEN Seminar: The bulk viscosity of QCD in the chiral limit	Oct. 18
42	Koichi Hattori (YITP)	QHP Seminar: Recent progress in relativistic magnetohydrodynamics	Oct. 23
43	Miguel A. Vazquez-Mozo (U. Salamanca)	QHP Seminar: Anomalous (super)fluids and differential geometry	Oct. 23
44	Sophia Han (Ohio U.)	NT/RIKEN Seminar: Detectability of phase transitions from multi-messenger observations	Oct. 25
45	Joseph Kapusta	Special NT/RIKEN Seminar: Relaxation time for strange quark spin in rotating quark-gluon plasma	Oct. 31

46	Alba S. Ontoso (BNL)	RIKEN Lunch Seminar: Revisiting the discovery potential of the isobar run at RHIC	Nov. 14
47	Paul Chesler (Harvard U.)	NT/RIKEN Seminar: Critical gravitational collapse and thermalization in small systems	Nov. 22
48	Savely Karshenboim (LMU)	QHP Seminar: New quantum SI units and fundamental constants	Nov. 26
49	Nicolas Wink (Heidelberg)	Special NT/RIKEN Seminar: Elementary correlation functions in QCD and their application	Dec. 4
50	Amit Kumar	NT/RIKEN Seminar Probing quark-gluon plasma at high resolution	Dec. 6
51	Florian Cougoulic	NT/RIKEN Seminar: Helicity-dependent generalization of the JIMWLK evolution and MV model	Dec. 13
52	Scott Lawrence	NT/RIKEN Seminar: From qubits to quarks: Parton physics on a quantum computer	Dec. 20
53	Kaushik Roy (Stony Brook U.)	RIKEN Lunch Seminar: NLO impact factor for inclusive photon+dijet production in $e + A$ DIS at small x	Jan. 23
54	Stefan Hoeche (Fermilab)	NT/RIKEN Seminar: Towards precision event simulation for collider experiments	Jan. 24
55	Dean Lee	NT/RIKEN Seminar New tools for the quantum many-body problem	Feb. 7
56	Xiangdong Ji	Special NT/RIKEN Seminar: Partonic structure of the proton from large momentum effective theory	Feb. 10
57	Greg Jackson (U. Bern)	RIKEN Lunch Seminar: Shedding light on photon and dilepton spectral functions	Feb. 13
58	Carlota A. Casas	NT/RIKEN Seminar: Solving the medium-induced gluon radiation spectrum for an arbitrary number of scatterings	Feb. 14
59	Eduardo Fraga	Special NT/RIKEN Seminar: Critical dynamics from small, noisy, fluctuating systems	Feb. 18
60	Leticia Palhares	Special NT/RIKEN Seminar: Infrared gluon mass and the Gribov-Zwanziger model of nonperturbative Yang-Mills theories	Feb. 19
61	Kazuki Ikeda (Osaka U.)	RIKEN Lunch Seminar: Phase transitions of quantum annealing and quantum chaos	Feb. 20
62	Duff Neill	NT/RIKEN Seminar: Soft fragmentation on the celestial sphere	Feb. 21
63	Tomoya Hayata (Keio U.)	QHP Seminar: Chiral magnetic/vortical effect of light	Feb. 26
64	Katerina Chatziioannou	NT/RIKEN Seminar: Studying supranuclear matter with gravitational waves from neutron star binaries	Feb. 28
65	Yong Zhao (BNL)	RIKEN Lunch Seminar: Nonperturbative Collins-Soper kernel from lattice QCD	Mar. 5
66	Abha Rajan (BNL)	RIKEN Lunch Seminar: Ioffe time behavior of PDFs and GPDs	Mar. 12

QHP Seminar -> <http://ribf.riken.jp/QHP/seminar.html>

SNP Seminar -> <http://snp.riken.jp/seminar.html>

RIKEN/BNL Lunch Time Talk -> <https://sites.google.com/site/rikenlunch/talks>

理化学研究所

埼玉県 和光市 広沢

RIKEN 2020-050